The Rational Design of Potent Ice Recrystallization Inhibitors for Use as Novel Cryoprotectants

Chantelle Capicciotti

B. Sc. Honours Biopharmaceutical Science, Medicinal Chemistry –
University of Ottawa, 2009

Thesis submitted to the
Faculty of Graduate and Postdoctoral Studies
in partial fulfillment of the requirements
for the Doctorate in Philosophy degree in Chemistry

Department of Chemistry
Faculty of Science
University of Ottawa

Candidate

Chantelle Capicciotti

Supervisor

Professor Robert N. Ben

© Chantelle Capicciotti, Ottawa, Canada, 2014

Dedicated to my love, Peter, my family, and the memory of
Peter (Yuri) Natis and Frank Peter Capicciotti

Anyone can give up, it's the easiest thing in the world to do. But to hold it together when everyone else would understand if you fell apart, that's true strength
-Anonymous.

So many of our dreams at first seem impossible, then they seem improbable, and then, when we summon the will, they soon become inevitable.
-Christopher Reeves

Acknowledgements

There are many people that I would like to acknowledge for their influence on this work and on my life within the past few years. First, I would like to thank Dr. Robert Ben, who took a chance on me five years ago as an undergraduate student and introduced me to the world of research and academia. I am truly appreciative of your constant support and guidance throughout the past five years, and for all of the opportunities you have provided for me. You are always willing to help and I am grateful for all of our discussions, both on research and on life. Thank you for making my time in your lab such a great experience.

I would also like to thank the Ben Lab members, both past and present, who have helped me throughout my graduate career. Anna Balcerzak and Jennie Briard, who have been excellent friends and colleagues, and who have been awesome "hotel-mates" at various conferences and research trips. To Dr. Roger Tam, Jackie Tokarew, Dr. Mathieu Leclère and Taz Cheema for initially welcoming me to the lab and teaching me invaluable research and life skills early in my graduate studies. To "honorary" Ben Lab member Francis Loiseau for late night lab discussions on research, chemistry and anything we thought worth discussing. To the excellent undergraduate students I was fortunate to work with, Ross Mancini, Jessica Poisson and Evan Perley-Robertson for your hard work and contribution to this thesis, which are highly appreciated. To all other Ben Lab members and Durst Lab members – Malay Doshi, Kyle McClymont, John Trant, Taline Boghossian, Thomas Charlton, Ibrahim Aboud, Sherif Kaldas and Oussama Talbi– for all of your positive contributions to the lab and making it a great place to work. Special thanks also goes to Stephanie Abraham for editing this thesis on a tight timeline.

I would like to thank Canadian Blood Services for funding in the last two years of my doctoral degree with a graduate fellowship program award. I would also like to thank Dr. Jason Acker and his excellent team of lab technicians Jayme Kurach, Tracey Turner and Adele Hansen at Canadian Blood Services in Edmonton, Alberta. All of your organization and perseverance on our intense, quick research trips to the blood labs have contributed more than I can say to this work. At some point, I am confident you will reach glycerol one thousand times. In addition, I would also like to acknowledge all other collaborators with this work including: Dr. Richard Payne at the University of Sydney;

Dr. Christopher Boddy at the University of Ottawa; Dr. Mark Taylor at the University of Toronto; Dr. James Harden at the University of Ottawa; Dr. David Bryce and Frédéric Perras at the University of Ottawa.

I owe a great amount to my mom, dad, and my family. Even through difficult times, you have provided constant encouragement to pursue my dreams. I am very lucky to have such a supportive and loving family to provide guidance throughout my life. Also, to Ciddy and Charlie, who have welcomed me into their family and who constantly look on the positive of everything, I am grateful for all you have done for me here in Ottawa. I would also like to thank my fantastic friends, Kara, Sarah and Kailey, who have always supported me and have been part of many memorable experiences of my time in Ottawa. You girls have always provided an escape from school or work when it was needed, and have always been available to talk and catch up, even when we have been thousands of miles away from each other.

Finally, to Peter. I am truly lucky to have such an amazing partner in life who supports me no matter what. I cannot express how grateful I am for all you have done for me, and for always being positive and encouraging me to follow my dreams.

Abstract

The development of effective methods to cryopreserve precious cell types has had tremendous impact on regenerative and transfusion medicine. Hematopoietic stem cell (HSC) transplants from cryopreserved umbilical cord blood (UCB) have been used for regenerative medicine therapies to treat conditions including hematological cancers and immodeficiencies. Red blood cell (RBC) cryopreservation in blood banks extends RBC storage time from 42 days (for hypothermic storage) to 10 years and can overcome shortages in blood supplies from the high demand of RBC transfusions. Currently, the most commonly utilized cryoprotectants are 10% dimethyl sulfoxide (DMSO) for UCB and 40% glycerol for RBCs. DMSO is significantly toxic both to cells and patients upon its infusion. Glycerol must be removed to <1% post-thaw using complicated, time consuming and expensive deglycerolization procedures prior to transfusion to prevent intravascular hemolysis. Thus, there is an urgent need for improvements in cryopreservation processes to reduce/eliminate the use of DMSO and glycerol.

Ice recrystallization during cryopreservation is a significant contributor to cellular injury and reduced cell viability. Compounds capable of inhibiting this process are thus highly desirable as novel cryoprotectants to mitigate this damage. The first compounds discovered that were ice recrystallization inhibitors were the biological antifreezes (BAs), consisting of antifreeze proteins and glycoproteins (AFPs and AFGPs). As such, BAs have been explored as potential cryoprotectants, however this has been met with limited success. The thermal hysteresis (TH) activity and ice binding capabilities associated with these compounds can facilitate cellular damage, especially at the temperatures associated with cryopreservation. Consequently, compounds that possess "custom-tailored" antifreeze activity, meaning they exhibit the potent ice recrystallization inhibition (IRI) activity without the ability to bind to ice or exhibit TH activity, are highly desirable for potential use in cryopreservation.

This thesis focuses on the rational design of potent ice recrystallization inhibitors and on elucidating important key structural motifs that are essential for potent IRI activity. While particular emphasis in on the development of small molecule IRIs, exploration into structural features that influence the IRI of natural and synthetic BAs and BA analogues is also described as these are some of the most potent inhibitors known to date. Furthermore, this thesis also investigates the use of small molecule IRIs for the cryopreservation of various different cell types to ascertain their potential as novel cryoprotectants to improve upon current cryopreservation protocols, in particular those used for the long-term storage of blood and blood products.

Through structure-function studies the influence of (glyco)peptide length, glycosylation and solution structure for the IRI activity of synthetic AFGPs and their analogues is described. This thesis also explores the relationship between IRI, TH and cryopreservation ability of natural AFGPs, AFPs and mutants of AFPs. While these results further demonstrated that BAs are ineffective as cryoprotectants, it revealed the potential influence of ice crystal shape and growth progression on cell survival during cryopreservation.

One of the most significant results of this thesis is the discovery of alkyl- and phenolic-glycosides as the first small molecule ice recrystallization inhibitors. Prior to this discovery, all reported small molecules exhibited only a weak to moderate ability to inhibit ice recrystallization. To understand how these novel small molecules inhibit this process, structure-function studies were conducted on highly IRI active molecules. These results indicated that key structural features, including the configuration of carbons bearing hydroxyl groups and the configuration of the anomeric center bearing the aglycone, are crucial for potent activity. Furthermore, studies on the phenolic-glycosides determined that the presence of specific substituents and their position on the aryl ring could result in potent activity. Moreover, these studies underscored the sensitivity of IRI activity to structural modifications as simply altering a single atom or functional group on this substituent could be detrimental for activity.

Finally, various IRI active small molecules were explored for their cryopreservation potential with different cell types including a human liver cell line (HepG2), HSCs obtained from human UCB, and RBCs obtained from human peripheral blood. A number of phenolic-glycosides were found to be effective cryo-additives for RBC freezing with significantly reduced glycerol concentrations (less than 15%). This is highly significant as it could drastically decrease the deglycerolization processing times that are required when RBCs are cryopreserved with 40% glycerol. Furthermore, it demonstrates the potential for IRI active small molecules as novel cryoprotectants that can improve upon current cryopreservation protocols that are limited in terms of the commonly used cryoprotectants, DMSO and glycerol.

Table of Contents

Acknowledgements……..ii
Abstract. ……iv
Table of Contents...…….vi
List of Figures……..xi
List of Tables…..……xvi
List of Schemes..……xvii
List of Abbreviations..…….xviii

Chapter 1: Introduction – Ice, Ice Recrystallization Inhibitors and Applications in Cryopreservation

1.1 Recrystallization of Ice…….…….. 1
1.1.1 Structure of Ice……..... 1
1.1.2 Mechanism of Ice Recrystallization…….. 3

1.2 Biological Antifreezes…… 4
1.2.1 Structures of Biological Antifreezes…….. 5
1.2.2 Antifreeze Activities: Thermal Hysteresis (TH) and Ice Recrystallization Inhibition (IRI) Activity…… 6
1.2.3 Thermal Hysteresis (TH) Activity – Mechanism of Action…….. 7
1.2.4 Important Structural Features For Ice Binding and TH Activity…….. 9
1.3 Ice Recrystallization Inhibitors…… 10
1.3.1 "Custom-Tailored" Peptide and Glycopeptide Analogues of Biological Antifreezes…… 10
1.3.2 Synthetic Polymers as Ice Recrystallization Inhibitors…… 13
1.3.3 Simple Carbohydrates - Moderate Ice Recrystallization Inhibitors…… 14
1.3.4 Summary and Conclusions of Current Ice Recrystallization Inhibitors…….. 17
1.4 Cryopreservation…… 18
1.4.1 Mechanisms of Cryoinjury During Cryopreservation…… 19
1.4.2 Cryoprotective Agents (CPAs)…… 20
1.4.3 Long-Term Storage of Blood and Blood Products…….. 21
1.4.4 Biological Antifreezes, Analogues of Biological Antifreezes and Carbohydrates as Cryoprotective Additives……... 23
1.4.5 Summary of Cryopreservation and its Limitations…….. 25

1.5 References…… 25

Chapter 2: Goals and Objectives

2.1 Introduction…… 36

2.2 Objective 1 - Determining the Important Structural Features for the IRI Activity of Native Synthetic AFGPs and AFGP Analogues Antifreezes…… 37

2.3 Objective 2 - Determining the Relationship between IRI, TH and Cryopreservation Ability of Natural Biological Antifreezes…… 39

2.4 Objective 3 - Determining the Important Structural Features for the IRI Activity of Simple Carbohydrates…… 40

2.5 Objective 4 - Determining the Influence of Hydrophobic Moieties for the IRI Activity of Simple Carbohydrates..... 41

2.6 Objective 5 - Determining the Influence of Aryl Moieties for the IRI Activity of Simple Carbohydrates..... 42

2.7 Objective 6 - Determining the Cryopreservation Potential of Small Molecule Ice Recrystallization Inhibitors..... 43

2.8 Summary of Goals and Objectives..... 44

2.9 References..... 44

Chapter 3: Elucidating the Structural Features Important for the IRI Activity of Native Synthetic AFGPs and AFGP Analogues

3.1 Introduction..... 48

3.2 The Relationship between IRI Activity, TH Activity, Glycopeptide Length and Structure for Synthetic AFGPs..... 50
3.2.1 Homogenous Synthetic AFGPs (synAFGPs)..... 50
3.2.2 Article: "Total Synthesis of Homogeneous Antifreeze Glycopeptides and Glycoproteins"..... 52
3.2.3 Results and Discussion of the Antifreeze Activity of synAFGPs..... 59
3.2.4 Summary and Conclusions for the IRI and TH Activity of synAFGPs..... 65

3.3 IRI and TH Activity of Peptide and Glycopeptide Analogues of AFGPs with Polyproline Type II (PPII) Helical Structure..... 66
3.3.1 Peptide and Glycopeptide AFGP Analogues with PPII Solution Structure.... 66
3.3.2 Article: "Synthesis of Peptides and Glycopeptides with Polyproline II Helical Topology as Potential Antifreeze Molecules"..... 68
3.3.3 Results and Discussion of Antifreeze Activity of Peptides and Glycopeptide AFGP Analogues with PPII Solution Structure..... 81
3.3.4 Summary and Conclusions for the IRI Activity of HyP AFGP Analogues.... 85

3.4 IRI and TH Activity of C-Linked Triazole AFGP Analogues..... 86
3.4.1 *C*-Linked Triazole AFGP Analogues..... 86
3.4.2 Article: "Synthesis and Evaluation of Linear CuAAC-Oligomerized Antifreeze Neo-Glycopeptides"..... 87
3.4.3 Results and Discussion of Antifreeze Activity of Triazole-Containing OGG-Gal Derivatives..... 96

3.5 Overall Summary and Conclusions for the IRI Activity of Peptide and Glycopeptide AFGP Analogues..... 97

3.6 References..... 98

Chapter 4: Modulating Antifreeze Activity and the Effect Upon Post-Thaw Cell Viability

4.1 Introduction..... 101

4.2 Conformational Analysis of LpAFPs …….. 103

4.3 Thermal Hysteresis (TH) Activity of the Biological Antifreezes…… 105

4.4 Ice Recrystallization Inhibition Activity of the Biological Antifreezes…….. 106

4.5 Investigating the Relationship between TH and IRI Activity…… 107

4.6 Cryopreservation Ability of BAs……... 111

4.7 The Relationship between Ice Crystal Growth Progression and Cryopreservation Ability…… 114

4.8 Summary and Conclusions for the TH, IRI, Ice Crystal Growth Habits and Cryopreservation Ability of Various Classes of Biological Antifreezes…….. 118

4.9 Experimental Section for Chapter 4…… 119

4.10 References…….. 122

Chapter 5: Small Carbohydrate-Based Molecules as Ice Recrystallization Inhibitors – Simple Mono- and Disaccharides and Complex Oligosaccharides

5.1 Introduction…… 126

5.2 Elucidating Key Structural Features Necessary for IRI Activity in Simple Monosaccharides and Monosaccharide Derivatives……... 128

5.2.1 Monosaccharides and Derivatives with Modifications to the C6 and C1 Positions…… 128

5.2.2 IRI Activity of C6-Modified Galactosides and Glucosides…….. 133

5.2.3 IRI Activity of C1-Modified Monosaccharides…… 135

5.3 Di-, Tri- and Oligosaccharides as Ice Recrystallization Inhibitors…… 137

5.3.1 Methylated and Reducing Di-, Tri- and Oligosaccharide Derivatives…….. 137

5.3.2 IRI Activity of Di-, Tri- and Oligosaccharide Derivatives…… 141

5.4 Summary and Conclusions for the IRI Activity of Simple Mono- and Disaccharides and Complex Oligosaccharides…… 144

5.5 Experimental Procedures and Compound Characterizations for Chapter 5…….. 145

5.6 References…… 156

5.7 NMR Spectra of Compounds in Chapter 5…….. 160

Chapter 6: Small Carbohydrate-Based Molecules as Ice Recrystallization Inhibitors – Carbohydrate-Based Surfactants and Hydrogelators

6.1 Introduction……... 172

6.2 Article: "Potent Ice Recrystallization Inhibition by Low Molecular Weight Carbohydrate-Based Surfactants and Hydrogelators"…….. 174

6.3 Carbohydrate Based-Surfactants and Hydrogelators as Potent Ice Recrystallization Inhibitors…….. 184
6.3.1 Synthesis of Carbohydrate-Based Surfactant and Hydrogelator Derivatives…… 184
6.3.2 IRI Activity of Carbohydrate-Based Surfactants…….. 188
6.3.3 IRI Activity of Carbohydrate-Based Hydrogelators…….. 191
6.3.4 Assessment of Ice Lattice Interactions…… 197
6.3.5 Characterization of Hydrogels and the Relationship with IRI Activity…… 201

6.4 Summary and Conclusions for the IRI Activity of Carbohydrate-Based Surfactants and Hydrogelators…… 203

6.5 Experimental Procedures and Compound Characterizations for Chapter 6…….. 205

6.6 References…….. 217

6.7 NMR Spectra of Compounds in Chapter 6…….. 221

Chapter 7: Small Carbohydrate-Based Molecules as Ice Recrystallization Inhibitors – Phenolic-Glycosides

7.1 Introduction…… 240

7.2 Phenolic-Glycosides as Ice Recrystallization Inhibitors…… 241
7.2.1 Structures and Synthesis of *Para*-Substituted Phenolic Glycosides…….. 241
7.2.2 IRI Activity of *Para*-Substituted Phenolic Glycosides…….. 244
7.2.3 Regioisomers of β-PMP-Glc, Modifications to the Glycosidic Linkage and Derivatives of β-PMP-Glc …… 251
7.2.4 IRI Activity of β-PMP-Glc Derivatives…… 257
7.2.5 β-linked PMP Containing Di- and Trisaccharide Derivatives…….. 261
7.2.6 IRI Activity of β-PMP-Di- and Trisaccharide Derivatives…….. 264

7.3 Quantifying the Relative Rates of Different IRI Active Small Molecules…….. 267

7.4 Summary and Conclusions for the IRI Activity of Phenolic-Glycosides…… 271

7.5 Experimental Procedures and Compound Characterizations for Chapter 7…….. 272

7.6 References…… 306

7.7 NMR Spectra of Compounds in Chapter 7…… 311

Chapter 8: Cryopreservation Ability of Novel IRI Active Carbohydrate-Based Small Molecules

8.1 Introduction…….. 366

8.2 Cytotoxic Effects and Cryopreservation Ability of Carbohydrate-Based Small Molecule IRIs with HepG2 Cells…… 369
8.2.1 Assessing Cytotoxicity of the Carbohydrate-Based Small Molecule IRIs… 369
8.2.2 Assessing Cryopreservation Ability of the Carbohydrate-Based Small Molecule IRIs with HepG2 Cells…….. 371
8.2.3 Summary and Conclusions for Cytotoxicity and Cryoprotective Ability of Small Molecule IRIs with HepG2 Cells…….. 374

8.3 Cryopreservation Ability of Carbohydrate-Based Small Molecule IRIs with UCB……. 374
8.3.1 Introduction – Cryopreservation of HSCs from UCB…… 374
8.3.2 Effect of Small Molecule IRIs for the Cryopreservation of UCB…… 375
8.3.3 Summary and Conclusions for UCB Cryopreservation with Small Molecule IRIs…… 380

8.4 Cryopreservation Ability of Carbohydrate-Based Small Molecule IRIs with RBCs….. 381
8.4.1 Introduction – Cryopreservation of RBCs…… 381
8.4.2 Article – "Small Molecule Inhibitors of Ice Recrystallization Enable Freezing of Human Red Blood Cells with Greatly Reduced Quantities of Glycerol"…… 384
8.4.3 Freezing of RBCs using β-PMP-Glc in the Presence of Reduced Glycerol Concentrations…… 392
8.4.4 Internalization and Cryomicroscopy Studies for the Freezing of RBCs in the Presence of β-PMP-Glc…….. 395
8.4.5 The Ability of Phenolic-Glycosides to Protect RBCs during Freezing with Reduced Glycerol Concentrations…… 400
8.4.6 Initial Deglycerolization of RBCs in the Presence of Glycerol and Phenolic-Glucosides…… 407
8.4.7 Osmotic Tolerance of RBCs after Treatment with Glycerol or Phenolic-Glucoside Solutions…… 415
8.4.8 Osmotic Tolerance of RBCs after Cryo-Solution Incubation and Treatment with Wash 1…….. 417
8.4.9 Osmotic Tolerance of RBCs after Treatment with Wash 2…… 419
8.4.10 Osmotic Tolerance of RBCs after Treatment with Wash 3…… 420
8.4.11 Attempted Deglycerolization after Analysis of RBC Osmotic Tolerances…….. 422
8.4.12 Summary and Conclusions for the Freezing of RBCs in the Presence of Phenolic-Glucoside IRIs with Reduced Glycerol Quantities…….. 426

8.5 Summary and Conclusions for the Cryopreservation Potential of Carbohydrate-Based Small Molecule IRIs…… 427

8.6 Experimental Procedures for Chapter 8…….. 428

8.7 References…….. 433

Conclusions…… 440

Contributions to Original Research…… 443

Publications and Patents…… 443

List of Figures

Chapter 1:

Figure 1.1 Schematic representation of the hexagonal ice 1_h lattice unit illustrating the a_1, a_2, a_3 and c axes and the basal, prism and bipyramidal planes…… 2
Figure 1.2 Representation of a liquid-layer (shaded) in a curved boundary between two ice grains…….. 3
Figure 1.3 Classification and structural differences between fish antifreeze proteins (AFPs) and antifreeze glycoproteins (AFGPs)…….. 6
Figure 1.4. Photographs illustrating dynamic ice shaping (DIS) and ice recrystallization inhibition (IRI) activity…….. 7
Figure 1.5. Formation of hexagonal bipyramidal crystals by inhibition of growth on the prism faces due to adsorption of BAs…….. 7
Figure 1.6. Illustrations of thermal hysteresis (TH) activity and the two models of ice growth inhibition…… 8
Figure 1.7. Important structural motifs on AFGPs for TH activity as determined by Nishimura and co-workers…… 9
Figure 1.8. Structure of first-generation lysine-based *C*-linked AFGP analogues……..... 11
Figure 1.9. Structures of potently IRI active *C*-Serine and OGG-Gal analogues…….. 11
Figure 1.10. Structures of OGG-Gal (**6**) analogues containing various monosaccharide moieties (**7**-**9**) and modifications to the side-chain linker between the carbohydrate moiety and polypeptide backbone (**10**-**16**)…… 12
Figure 1.11. Structures of synthetic polymers assessed for IRI activity…… 14

Chapter 2:

Figure 2.1 General structures of synAFGPs and HyP containing AFGP derivatives…… 38
Figure 2.2 Structures of the triazole-containing OGG-Gal derivatives…….. 39
Figure 2.3 General structures of C6- and C1-modified monosaccharide derivatives and di- and trisaccharide derivatives…….. 41
Figure 2.4 General structures of carbohydrate-based surfactants and hydrogelators…… 42
Figure 2.5 General structures of phenolic-glycosides…… 43
Figure 2.6 Structures of potently IRI active small molecules *N*-octyl-D-gluconamide (NOGlc), β-*para*-methoxyphenyl-D-glucopyranoside (β-PMP-Glc) and β-*para*-bromophenyl-D-glucopyranoside…… 44

Chapter 3:

Figure 3.1 Important structural motifs on synthetic AFGPs (synAFGPs) for TH activity as determined by Nishimura and co-workers…… 48
Figure 3.2 Structures of potently IRI active *C*-Serine and OGG-Gal analogues and the structural features crucial for the potent activity of OGG-Gal…… 49
Figure 3.3 Structures of synthetic homogeneous AFGPs assessed for antifreeze activity…… 51
***Figure 1. A)** Thermal hysteresis (TH) activity of homogeneous synthetic AFGPs and isolated AFGP-8 at 10 mg/mL. **B)** Ice crystal morphologies…… 60
***Figure 2.** Ice recrystallization inhibition (IRI) activity of isolated AFGP- 8, unglycosylated polypeptide $(ATA)_4$ (19), $AFGP_2$ (18), $AFGP_4$ (5), $AFGP_8$ (9), $AFGP_{12}$ (10), $AFGP_{16}$ (14), $AFGP_{32}$ (17)…… 61
***Figure 5.** CD spectra of synthetic AFGPs…… 63

*Asterisk indicates figures from articles provided within the text.

***Figure 6.** Circular dichroism spectra of synthetic AFGPs at variable temperature (-5 to 85 °C)…… 64
Figure 3.4 Structures of peptide and glycopeptide AFGP analogues with PPII helical solution structure…… 67
***Figure 5.** Ice crystal habit in the presence of HyP derivatives **1**-**10**…… 82
***Figure 6**. Ice recrystallization inhibition (IRI) activity of hydroxyproline derivatives **1–10**…….. 83
***Figure 3.** Circular dichroism (CD) spectra of peptides **1–10**…… 84
Figure 3.5 Structures of *C*-linked triazole-containing derivatives of OGG-Gal (**1**)…….. 86
***Figure 6** Ice crystal habit in the presence of **8b**, **10** and **11**…….. 96
***Figure 7** Ice recrystallization inhibition (IRI) activity of oligomers **8b**, **10** and **11**…… 96
Figure 3.6 Structural features crucial for the potent activity of OGG-Gal…… 97

Chapter 4:

Figure 4.1 Structure and CD Spectrum of WT and mutant *Lp*AFPs…… 104
Figure 4.2 TH activity of the BAs assayed at 1 mg/mL in water or 5 mg/mL in PBS…… 105
Figure 4.3 IRI activity of BAs assayed at concentrations ranging from 5.5 μM to 55 nM in PBS…… 107
Figure 4.4 Percent post-thaw cell viability and apoptosis of HepG2 cells cryopreserved with 1 mg/mL BA in 0% and 2% DMSO…… 112
Figure 4.5 Percent post-thaw cell viability and apoptosis of HepG2 cells cryopreserved with 1 mg/mL BA in 5% and 10% DMSO…… 113
Figure 4.6 TH activity of the BAs assayed at 1 mg/mL in water or 2% or 5% DMSO solutions…… 114
Figure 4.7 Ice crystal habits in the presence of BAs…… 115
Figure 4.8 Ice crystal growth patterns beginning at T_m, to temperatures within the TH gap and burst growth below T_f outside the TH gap…… 117

Chapter 5:

Figure 5.1 An illustration of the correlation between carbohydrate hydration and IRI activity…….. 127
Figure 5.2 Lowest energy conformers calculated for β-phenyl-D-galactopyranoside and β-phenyl-D-glucopyranoside and their singly hydrated states…… 129
Figure 5.3 Structures of C6-modified monosaccharides, anhydrosugars and inositols…… 130
Figure 5.4 Structures of α- and β-linked *C*-allyl and *O*-methyl galactosides, glucosides and mannosides…… 133
Figure 5.5 IRI activity of anhydrosugars **1** and **7**, C6-modified galactose and glucose derivatives **2**-**6** and **8**-**9** and inositols **10**-**12** at 22 mM in PBS…….. 134
Figure 5.6 IRI activity of monosaccharides and derivatives *C*-allylated at the C1 position (**24**-**28**) or *O*-methylated at the C1 (**29**-**33**) or C3 (**34**) position at 22 mM in PBS…… 135
Figure 5.7 IRI activity of monosaccharides and *O*-methylated monosaccharides **29**-**34** correlated to their respective hydration indices…….. 136
Figure 5.8 Structures of melibiose and disaccharide **35**…… 138
Figure 5.9 Structures of di- and trisaccharide derivatives containing β-(1,3)- and β-(1,6)-glycosidic bonds…… 139
Figure 5.10 Structures of lactose and human milk oligosaccharides **50-56**…… 141
Figure 5.11 IRI activity of di- and trisaccharide derivatives **35** and **41-46** at 22 mM in PBS……... 142
Figure 5.12 IRI activity of human milk oligosaccharides **50-56** at 22 mM in PBS…… 144

*Asterisk indicates figures from articles provided within the text.

Chapter 6:

Figure 6.1 Illustration of the formation of micelles and hydrogels in aqueous solution with surfactants and hydrogelators……..…… 172
Figure 6.2 Structures of carbohydrate-based surfactants n-octyl-β-D-gluco- and galactopyranoside **3** and **4** and hydrogelators *N*-octyl-D-glucon- and galactonamide **5** and **6**…… 173
***Fig. 2** The structures of non-ionic surfactants *n*-octyl-β-D-glucopyranoside (**3**), *n*-octyl-β-D-galactopyranoside (**4**), Brij58 and Triton X-100…… 184
***Fig. 4** The structures of D-sorbitol, D-dulcitol, low molecular weight hydrogelator derivatives NOGlc (**5**) and NOGal (**6**), *N*-methylated derivatives **7** and **8** and ether-linked derivatives **9** and **10**…… 184
Figure 6.3 Structures of β-Octyl-Gal derivative **17** and NOGlc derivatives **18-21**…….. 187
***Fig. 3** IRI activity of non-ionic surfactants **3**, **4**, Brij 58, Triton X-100 and anionic surfactant SDS…… 189
Figure 6.4 IRI activity of carbohydrate-based non-ionic surfactants **3** and **4** and β-Octyl-Gal derivative **17** at 22 mM in PBS…….. 190
Figure 6.5 Structures of potently IRI active lysine-based derivatives and truncated *C*-AFGP analogues that contain hydrophobic alkyl tails…… 191
***Fig. 5** IRI activity of D-sorbitol, D-dulcitol, **5** (NOGlc) and **6** (NOGal), *N*-methylated derivatives **7** and **8**, and ether-linked derivative **9**…… 192
Figure 6.6 Concentration dependence of the IRI activity of NOGlc (**5**)…….. 194
Figure 6.7 IRI activity of NOGlc derivatives NPrGlc (**18**), NHexGlc (**19**) and octyl-chain derivatives NOMan (**20**) and NOGul (**21**)…… 195
Figure 6.8 Numbering sequence of carbons on the carbohydrate head group of the *N*-octyl-aldonamides, identification of *syn*-1,3-hydroxyl groups and the conformation and flexibility of the carbohydrate head groups…….. 196
***Fig. 6** Ice crystal habits in the presence of **3**-**6** and AFGP-8 in water…… 197
***Fig. 7** Saturation recovery curves of frozen D_2O with AFPs or carbohydrate derivatives…. 200
***Fig. 8** STEM images of the hydrogels of NOGlc (**5**) and NOGal (**6**) in water and PBS…… 202
Figure 6.9 STEM image of the hydrogel of NOMan (**20**) in water…… 202
***Fig. 9** Dynamic shear moduli of the hydrogels of NOGlc (5) in water and PBS as a function of angular frequency ω…… 202

Chapter 7:

Figure 7.1 Structures of small molecule potent ice recrystallization inhibitors and the general structure of phenolic-glycosides…… 240
Figure 7.2 Structures of phenolic-glycosides β-PMP-Gal (**1**), β-PMP-Glc (**2**), β-PMP-Man (**3**), β-PMP-Xyl (**4**) and β-PMP-Arab (**5**)…… 242
Figure 7.3 Structures of various *para*-substituted phenolic-glucosides (**11**-**23**) and galactosides (**24**-**36**)…… 244
Figure 7.4 IRI activity of β-PMP-linked monosaccharides **1-5** at 22 mM in PBS…….. 245
Figure 7.5 IRI activity of *para*-substituted phenolic-glucosides **2** and **11**-**23**…… 247
Figure 7.6 IRI activity of *para*-substituted phenolic-galactosides **1** and **24-36**…….. 248
Figure 7.7 Hammett plots of the relationship between %MGS and the electronic effect of the *para*-substituent for phenolic-glucosides…… 250
Figure 7.8 Ice crystal habits in the presence of β-PMP-Glc (**2**) β-pBrPh-Glc (**11**)…… 251
Figure 7.9 Structures of β-PMP-Glc monosaccharide derivatives **37**-**52**…… 252
Figure 7.10 IRI activity of *para*-, *meta*- and *ortho*-substituted phenolic-glucosides **2**, **14**, **16** and **37**-**40**…….. 258

*Asterisk indicates figures from articles provided within the text.

Figure 7.11 IRI activity of α-linked phenolic-glycosides **41-46**…….. 259
Figure 7.12 IRI activity of *N*- and *S*-linked β-PMP-Glc derivatives **47** and **48**, β-PMB-Glc (**49**), C6-modified β-PMP-Glc derivatives **50** and **51** and C6-O-PMP-Glc (**52**)…….. 260
Figure 7.13 Structures of β-linked PMP-containing di- and trisaccharide derivatives **70-77**…… 261
Figure 7.14 Structures of dihydroxybenzene-linked disaccharides **83-86…**…… 264
Figure 7.15 IRI activity of β-PMP-linked di- and trisaccharides **70-77**…… 265
Figure 7.16 IRI activity of dihydroxybenzene-linked disaccharides **83-86**…… 267
Figure 7.17 Relationship between time and mean ice crystal area (in mm^2) for ice recrystallization in the presence of galactose and β-PMP-Glc (**2**) inhibitors…… 269

Chapter 8:

Figure 8.1 Structures of carbohydrate-based surfactants (**1**-**2**) and hydrogelators (**3**-**4**) phenolic-glycosides **5**-**8**…… 367
Figure 8.2 Percent cell viability of HepG2 cells treated with various concentrations of DMSO, β-Octyl-Gal (**1**) and NOGlc (**4**) following incubation for 18 h at 37°C as determined by MTT assay…… 370
Figure 8.3 Percent cell viability of HepG2 cells treated with various concentrations of β-PMP-Glc (**6**), β-pFPh-Glc (**7**) and β-pBrPh-Glc (**8**) following incubation for 18 h at 37°C as determined by MTT assay…… 371
Figure 8.4 Percent post-thaw cell viability and apoptosis of HepG2 cells cryopreserved with various concentrations of β-PMP-Glc (**6**), β-pFPh-Glc (**7**) and β-pBrPh-Glc (**8**) in DMSO cryoprotectant solutions…… 372
Figure 8.5 Percent post-thaw cell recoveries of HepG2 cells cryopreserved with various concentrations of β-PMP-Glc (**6**), β-pFPh-Glc (**7**) and β-pBrPh-Glc (**8**) in DMSO cryoprotectant solutions…… 373
Figure 8.6 Post-thaw % cell viability of HSCs ($CD34^+$ cells) cryopreserved with 220 mM galactose (Gal) or 220 mM sucrose (Suc) in DMSO cryoprotectant solutions…… 377
Figure 8.7 Post-thaw % cell viability of HSCs ($CD34^+$ cells) cryopreserved with 0.5, 1, and 2 mM NOGlc (**4**) in DMSO cryoprotectant solutions…… 379
Figure 8.8 Post-thaw % cell viability of HSCs ($CD34^+$ cells) cryopreserved with 110 mM β-PMP-Glc (**6**) in DMSO cryoprotectant solutions with or without 100 μg/mL catalase…….. 380
***Fig. 4** The effect of novel IRI active small molecules NOGlc (**4**), β-PMP-Glc (**6**) and sucrose in 20% glycerol on post-thaw RBC integrities…… 393
Figure 8.9 The effect of NOGlc (**4**), β-PMP-Glc (**6**) and sucrose without glycerol on post-thaw RBC integrities…… 393
***Fig. 5** The effect of β-PMP-Glc (**6**) on post-thaw RBC integrity (100 - % hemolysis) using reduced concentrations of glycerol…….. 395
***Fig. 6** The effect of 15% glycerol cryo-solutions with or without 110 mM β-PMP-Glc (**6**) on post-thaw RBC integrity…… 396
***Fig. 7** The effect of pre-incubation of cryo-solutions on post-thaw RBC integrity…… 398
Figure 8.10 RBC integrities after room temperature incubation for indicated time period with cryo-solutions without freezing…….. 399
***Fig. 9** Photographs illustrating the IRI activity of β-PMP-Glc (**6**) and the advancing ice-front during RBC freezing…….. 400
Figure 8.11 Post-thaw RBC integrities of RBC samples frozen with 15% glycerol solutions containing novel phenolic-glycoside additives **7**-**14**…… 402

*Asterisk indicates figures from articles provided within the text.

Figure 8.12 Post-thaw RBC integrities of RBC samples frozen with 15% glycerol solutions containing phenolic-glycoside additives **5**-**6**, **8**, or **14**-**16**…… 404
Figure 8.13 The effect of β-pBrPh-Glc (**8**) concentration in a 15% glycerol solution on post-thaw RBC integrity…….. 405
Figure 8.14 RBC integrities after room temperature incubation for indicated time period with 30 mM or 55 mM β-pBrPh-Glc (**8**) in 15% glycerol cryo-solutions without freezing…… 406
Figure 8.15 The effect of β-pBrPh-Glc (**8**) on post-thaw RBC integrity using reduced concentrations of glycerol…… 407
Figure 8.16 The effect of rapid freezing conditions on post-thaw RBC integrity using β-PMP-Glc (**6**) or β-pBrPh-Glc (**8**) in glycerol cryo-solutions…… 409
Figure 8.17 % Hgb lost in the deglycerolization process after rapid freezing to -80°C or -196°C with 15% glycerol, 110 mM β-PMP-Glc +15% glycerol, or 30 mM β-pBrPh-Glc +15% glycerol cryo-solutions…….. 411
Figure 8.18 % Hgb lost in washes 2 and 3 and total % RBC recoveries after rapid freezing to -80°C or -196°C with 15% glycerol, 110 mM β-PMP-Glc +15% glycerol, or 30 mM β-pBrPh-Glc +15% glycerol cryo-solutions…….. 414
Figure 8.19 Osmotic tolerance of RBCs incubated with SAGM or cryo-solutions…… 417
Figure 8.20 Osmotic tolerance of RBCs after wash 1…….. 418
Figure 8.21 Osmotic tolerance of RBCs after wash 2…… 420
Figure 8.22 Osmotic tolerance of RBCs after wash 3…… 421
Figure 8.23 % Hgb lost in the deglycerolization process optimized by osmotic tolerance studies…… 424
Figure 8.24 Total % RBC recoveries post-freeze-thaw-deglycerolization…… 426

List of Tables

Chapter 1:

Table 1.1. Isentropic molar compressibilities ($10^4K_2^o$(s), cm^3 mol^{-1} bar^{-1}) and hydration numbers of various monosaccharides and disaccharides…… 15

Chapter 4:

Table 4.1 Summary of quantified TH activity (ºC) and IRI activity (% MGS relative to PBS) for the BAs assessed in this study…….. 108

Chapter 5:

Table 5.1 Asymmetric dihydroxylation conditions to afford **16a** and **16b**…….. 132

Chapter 8:

Table 8.1 Summary of original deglycerolization wash conditions…… 410
Table 8.2 Measured osmolalities (mOsm/kg) of NaCl solutions…… 415
Table 8.3 Measured RBC MCVs and supernatant osmolalities (mOsm/kg) after incubation with cryo-solutions…….. 417
Table 8.4 Osmolalities of wash 1 solutions…….. 417
Table 8.5 Measured RBC MCVs and supernatant osmolalities (mOsm/kg) after incubation with wash 1…….. 418
Table 8.6 Measured RBC MCVs and supernatant osmolalities (mOsm/kg) after incubation with wash 2…….. 420

List of Schemes

Chapter 5:

Scheme 5.1 Synthesis of galactose derivatives **2**, **3** and **5** from the common galactose intermediate **14**……..... 131
Scheme 5.2 Synthesis of heptogalactose derivatives **6a** and **6b** by asymmetric dihydroxylations of **14** …… 132
Scheme 5.3 Synthesis of 6-deoxyheptoglucopyranose derivative **9**…… 132
Scheme 5.4 Synthesis of α-linked disaccharide **35** from galactosyl donor **38** and acceptor **14**…… 138
Scheme 5.5 General synthetic scheme for the preparation of β-1,3-linked disaccharides and β-1,3-/β-1,6-linked trisaccharides by Taylor *et al*…..…… 140

Chapter 6:

Scheme 6.1 Synthesis of carbohydrate-based non-ionic surfactants **3** and **4**…….. 185
Scheme 6.2 Preparation of carbohydrate-based hydrogelators **5** and **6** …….. 186
Scheme 6.3 Synthesis of *N*-methylated derivatives **7** and **8** …… 186
Scheme 6.4 Synthesis of ether-linked derivatives **9** and **10**…… 186
Scheme 6.5 Preparation of β-Octyl-Gal derivative **17** and NOGlc derivatives **18**-**21**…… 188

Chapter 7:

Scheme 7.1 Synthesis of β-PMP-Gal (**1**), β-PMP-Glc (**2**) and β-PMP-Xyl (**4**)…….. 242
Scheme 7.2 Synthesis of β-PMP-Man **(3)**…… 243
Scheme 7.3 A general synthetic scheme for the preparation of phenolic glycosides by Lewis acid catalyzed glycosidation…….. 244
Scheme 7.4 Preparation of meta-substituted phenolic glycosides **37** and **40**…….. 252
Scheme 7.5 Preparation of α-PMP-Glc (**43**) using Lemieux's halide ion catalyzed glycosidation conditions…… 253
Scheme 7.6 Preparation of α-linked phenolic-glucosides **41**-**44**…… 254
Scheme 7.7 Preparation of α-PMP-Gal (**45**) and α-PMP-Man (**46**)…… 255
Scheme 7.8 Preparation of *N*-linked derivative **47**, *S*-linked derivative **48** and β-PMB-Glc (**49**)…… 255
Scheme 7.9 Preparation of C6-modified β-PMP-Glc derivatives…… 256
Scheme 7.10 Synthesis of C6-*O*-PMP-Glc derivative **52**…… 257
Scheme 7.11 Preparation of β-PMP-melibiose (**70**), β-PMP-lactose (**73**) and β-PMP containing β-Gal-(1,3)-GalNAc (**74**)…… 262
Scheme 7.12 Preparation of β-PMP disaccharides **71** and **72**…….. 263
Scheme 7.13 Synthesis of dihydroxybenzene-linked disaccharides **83-86**…….. 264

List of Abbreviations

α	Alpha
β	Beta
γ	Gamma
δ	Delta
ε	Epsilon
^{1}H	Proton
^{13}C	Carbon
2D	Two-dimensional
3D	Three-dimensional
7-AAD	7-Aminoactinomycin D
Ac	Acetyl
Ac_2O	Acetic anhydride
AFGP(s)	Antifreeze glycoprotein (s)
AFGP-8	Antifreeze glycoprotein, fraction-8
AFP(s)	Antifreeze protein(s)
Ala	Alanine
Arab	Arabinose
All	Allyl
Atm	Atmospheres
Ax	Axial
BA(s)	Biological antifreeze(s)
$BF_3•OEt_2$	Boron trifluoride diethyl etherate
BM	Bone marrow
Bn	Benzyl
br	Broad
C-AFGP	*C*-linked antifreeze glycoprotein
C-linked	*Carbon*-linked
Cat.	Catalytic
CD	Circular dichroism
$CDCl_3$	Deuterated chloroform
CD_3OD	Deuterated methanol
cm^{-1}	Wavenumber
CPA	Cryoprotective agent
d	Doublet
D_2O	Deuterium oxide
dd	Doublet of doublets
DCM	Dichloromethane
DIPEA	Diisopropylethylamine
DIS	Dynamic ice shaping 2
DMF	Dimethyl formamide
DMSO	Dimethyl sulfoxide
dt	Doublet of triplets

ESI	Electrospray ionization
Et	Ethyl
Et_2O	Diethyl ether
EtOAc	Ethyl acetate
EtOH	Ethanol
eq	Equatorial
FITC	Fluorescein isothiocyanate
Fmoc	9-fluorenylmethyloxycarbonyl
Gal	Galactose
GalNAc	*N-acetyl-galactosamine*
Glc	Glucose
GlcNAc	*N-acetyl* glucosamine
Gly	Glycine
HCl	Hydrochloric Acid
Hct	Hematocrit
Hgb	Hemoglobin
HepG2	Human liver hepatocellular carcinoma cells
HI	Hydration Index
HPLC	High performance liquid chromatography
HSC(s)	Hematopoietic stem cell(s)
HyP	Hydroxyproline
IBF	Ice binding face
IR	Infrared
IR resin	Amberlite ion exchange resin
IRI	Ice recrystallization inhibition
IRIs	Ice Recrystallization Inhibitors
Lac	Lactose
LC	Leukocyte concentrate
*Lp*AFP	*Lolium perenne* antifreeze protein
Lys	Lysine
kDa	KiloDaltons
m	Multiplet
M	Molar
M+	Parent molecular ion
Man	Mannose
Me	Methyl
MeOH	Methanol
metHgb	Methemoglobin
MGS	Mean grain size
$MgSO_4$	Magnesium sulfate
MHz	Mega Hertz
mM	Millimolar
MS	Mass spectrometry
MS	Molecular sieves

MSC(s)	Mesenchymal stem cell(s)
NAc	*N-acetyl*
NaH	Sodium hydride
Na_2SO_4	Sodium sulfate
$NaHCO_3$	Sodium bicarbonate
NaOH	Sodium hydroxide
NaOMe	Sodium methoxide
NMO	N-Methylmorpholine
NOGlc	*N*-Octyl-gluconamide
NOGal	*N*-Octyl-galactonamide
NOGul	*N*-Octyl-gulonamide
NOMan	*N*-Octyl-Mannonamide
NHexGlc	*N*-Hexyl-gluconamide
NPrGlc	*N*-Propyl-gluconamide
OGG	Ornithine-glycine-glycine
OH	Hydroxyl
OMe	*O-Methoxy*
O/N	Overnight
OTf	Trifluoromethane sulfonate
PBS	Phosphate-buffered saline
pBrPh-	*para*-bromophenyl-
Pd/C	Palladium on carbon
$Pd(OH)_2$	Palladium hydroxide
PE	Phycoerythrin
pFPh-	*para*-fluorophenyl
PG	Protecting group
pKa	Acid dissociation constant
PMB	*para*-methoxybenzyl
PMP	*para*-methoxyphenyl
PMC	Partial molar compressibility
PMV	Partial molar volume
PPII	Polyproline type II
ppm	Parts per million
q	Quartet
QLL	Quasi-liquid layer
RBC(s)	Red blood cell(s)
Rf	Retention factor
RT	Room temperature
s	Singlet
Ser	Serine
SM	Starting material
SPPS	Solid-phase peptide synthesis
synAFGP	Synthetic antifreeze glycoproteins
t	Triplet

Tal	Talose
TBAF	Tetrabutylammonium fluoride
TBDMS	*tert*-butyldimethylsilyl
TEA	Triethylamine
TFA	Trifluoroacetic acid
TH	Thermal hysteresis
THF	Tetrahydrofuran
Thr	Threonine
TIS	Triisopropylsilane
TMS	Trimethylsilyl
TMSOTf	Trimethylsilyl trifluoromethane sulfonate
UCB	Umbilical cord blood
WT	Wild type

Chapter 1: Introduction – Ice, Ice Recrystallization Inhibitors and Applications in Cryopreservation

1.1 Recrystallization of Ice

Recrystallization is a phenomenon that is well documented in the geological and metallurgical literature and it also occurs in polycrystalline ice. [1-3] In ice, recrystallization is defined as the growth of large ice crystals (or ice grains) at the expense of small ones, and is a thermodynamically driven process that results in an overall reduction in the free energy of the system. Ice recrystallization is particularly problematic in the areas of frozen foods and cryopreservation of biological samples (cells, tissues etc.). Freezing of foods is a well-established process as it helps decrease the rates of deterioration. In the last 30 years, the frozen food industry has taken significant steps to improve the freezing and storage process of various food products, recognizing that all frozen food products have a finite shelf-life.[4,5] Changes in texture, taste and overall quality of a frozen food product are a direct result of the ice recrystallization process. It is well established that ice morphology is an important factor in determining food texture and quality. For example, ice cream containing small ice crystals has better texture and taste.[6]

In medicine, cryostorage is an important process to preserve biological materials or precious cell types such as stem cells (or other progenitors) as well as red blood cells. However, as with any cold storage practice, ice recrystallization remains a major problem and is a significant cause of cellular damage and cell death.[7,8] One way to overcome this problem lies in designing effective inhibitors of ice recrystallization. Many compounds have been discovered that have the ability to inhibit ice recrystallization, with the first and most prominently discussed being naturally occurring biological antifreezes. However, an understanding of the structure of polycrystalline ice and the mechanism of ice recrystallization is required prior to a discussion on the ability of compounds to inhibit this process.

1.1.1 Structure of Ice

Ice can exist in many different polymorphic forms. Individual water molecules in ice can possess different three-dimensional arrangements dependent upon temperature and pressure. The hexagonal ice I_h lattice unit is the most common form of ice below 0 °C and at atmospheric pressure.[9,10] It possesses a regular crystalline structure in which a single oxygen atom is hydrogen-bonded to two hydrogen atoms. The hexagonal ice I_h lattice unit is characterized by four axes, a_1, a_2, a_3 and c, and the surface of the hexagonal unit has eight faces.[9-12] Two of these faces are normal to the c-axis and are the basal faces, and the remaining six are prism faces. The

structure of hexagonal ice is shown in Figure 1.1. The arrangement of intermolecular hydrogen bonds influences the properties and phases of ice and at 0 °C and atmospheric pressure ice grows most rapidly along the *a*-axis to give hexagonal shaped crystals which grow as sheets.[9-11,13]

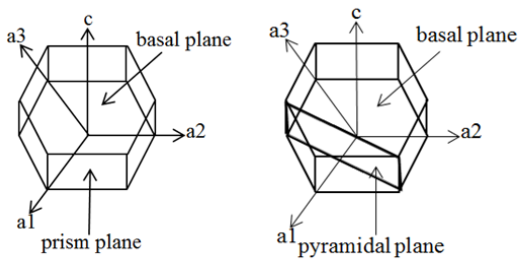

Figure 1.1 Schematic representation of the hexagonal ice 1_h lattice unit illustrating the a_1, a_2, a_3 and c axes and the basal, prism and bipyramidal planes.

Studies have indicated that when ice is in an aqueous solution, the interface between the ice lattice and the bulk water is not an abrupt transition. A semi-ordered layer called the quasi-liquid layer (QLL) exists in between the highly ordered ice lattice and the disordered bulk water phase surrounding ice crystals.[12,14-20] While a wide variety techniques have been used to study the QLL, its exact molecular nature and thickness has been debated throughout the literature.[20-34] Ellipsometric studies measuring the refractive index on the basal and prism faces of ice have suggested that the interface is more water-like in nature, rather than ice-like.[18-21,30,31] In contrast, other studies have suggested that the orientation and motion of water molecules in the QLL closely resembles that of ice.[22,24,33] The thickness of QLL between ice lattice and bulk water is approximately 10-15 Å.[16,17,35] However, this has been shown to be temperature dependent,[16,17,26,30,35] such that at temperatures approaching the melting point of ice (at -0.03 °C) the thickness was 15 nm, corresponding to approximately 40 monolayers water.[23] Below -10 °C the thickness was less than 0.3 nm, approximately one monolayer of water. In addition, the average density profile, thickness and orientational order and diffusion constants of water within the QLL interface also vary depending on the face of ice from which they are calculated and studies have suggested that the QLL is thicker on the basal and prism faces than on the pyramidal and secondary prism planes.[12,18,20] Light scattering techniques have also shown that ice crystals grow into the QLL and not into the bulk water layer.[36,37]

1.1.2 Mechanism of Ice Recrystallization

The recrystallization of ice in polycrystalline aqueous solutions is believed to occur through either grain boundary migration or Ostwald ripening. Grain boundary migration in ice is similar to grain boundary migration in metals and alloys[1-3] where large ice grains grow larger at the expense of small ice grains. An ice grain consists of the crystallographic orientation of the water molecules commonly observed in ice I_h (Figure 1.1). Grain boundaries are therefore the interfaces between different oriented ice grains.[38,39] Grain boundary migration occurs as individual molecules transfer from unfavorably oriented ice grains to favorably oriented ice grains. The boundaries of individual ice grains tend to be curved and the degree of curvature is proportional to the size of the grain. Boundaries of small ice crystals have a higher degree of curvature making them more convex (bulge outwards) and thus have a higher amount of surface energy. Large ice crystals have more concave grain boundaries and have a lower amount of surface energy. Grain boundaries migrate towards their center of curvature to reduce the overall degree of curvature, resulting in ice grains with concave boundaries (larger crystals) growing larger while those with convex boundaries (smaller crystals) decrease in size (depicted in Figure 1.2).[40,41] Thus, the driving force of grain boundary migration in ice arises from a reduction in grain boundary curvature, which results in an overall reduction in the energy of the system.

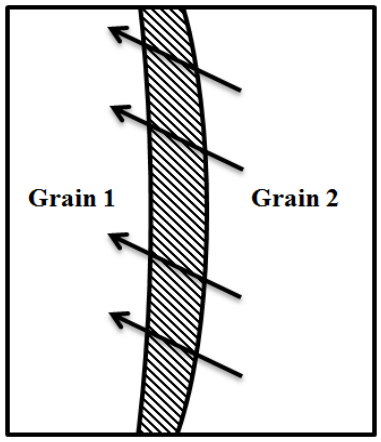

Figure 1.2 Representation of a liquid-layer (shaded) in a curved boundary between two ice grains. Large ice grains with concave boundaries (grain 2) grow larger while small grains with convex boundaries (grain 1) decrease in size to reduce the overall degree of grain boundary curvature. Arrows indicate the direction of boundary migration.

Grain boundary migration of polycrystalline ice assumes that water molecules are transferred directly from the shrinking ice grain to the growing grain. This assumption often neglects the presence of bulk-water or the QLL in between individual ice grains as the system is treated below

-10 °C.[40] However, Ostwald ripening of polycrystalline ice in an aqueous solution considers the whole ice crystal/liquid water system and thus accounts for the presence of bulk-water and the QLL. In ice, Ostwald ripening is the thermodynamically driven process whereby large ice crystals grow larger at the expense of small crystals, resulting in an overall reduction in energy of the ice crystal/bulk-water interface.[42-44] Throughout the Ostwald ripening process a constant ice volume is maintained. Smaller ice crystals have a higher surface area to volume ratio, giving them higher surface free energy since water molecules on the surface are less stable than the water molecules within the ice crystal.[42,43] However, larger ice crystals have a greater volume to surface area ratio and thus are thermodynamically more stable than small ice crystals. As the total overall volume of ice remains constant during the Ostwald ripening process, water molecules transfer from the surface of smaller ice crystals to bulk-water and then are transferred onto the surface of larger ice crystals. The net result is an increase in the average ice crystal size and a decrease in the total number of ice crystals at a constant total ice volume, resulting in an overall reduction in the free energy of the system.[44]

1.2 Biological Antifreezes

The first biological antifreezes were reported in the late 1950's and early 1960's when it was observed by Scholander and colleagues that marine teleost fish did not freeze during the winter despite the water temperature being -1.9 °C, over a degree below the freezing point of their blood serum.[45,46] DeVries and Wohlschlag later attributed their survival to the presence of circulating proteins and glycoproteins.[47-49] These proteins later became known as biological antifreezes (BAs), specifically antifreeze proteins (AFPs) and antifreeze glycoproteins (AFGPs). A variety of AFPs and AFGPs have since been identified in a number of different fish, insects, plants and bacteria.

Given their ability to prevent cryoinjury upon exposure to cold temperatures,[47-49] BAs have attracted a great deal of interest in the scientific and industrial communities.[5,50-53] BAs were the first compounds discovered that had the ability to inhibit ice recrystallization. However, they are a complex class of compounds with dramatically different structures, making it difficult to understand how they exhibit this property. Additionally, BAs also exhibit thermal hysteresis (TH) activity as a result of their ability to irreversibly bind to the surface of ice crystals.[54-58] While BAs do exhibit the highly desirable property of potent ice recrystallization inhibition, their use as cryoprotectants has been met with limited success. This is often attributed to the TH activity associated with these compounds, which is hypothesized to exacerbate cellular damage during the

cryopreservation process.[59-62] Nevertheless, this important class of compounds is the foundation upon which all "rationally designed" novel ice recrystallization inhibitors are based.[50-52,63-65]

1.2.1 Structures of Biological Antifreezes

There are four classes of structurally diverse fish AFPs that have been identified. These are type I,[11,66-75] type II,[76-84] type III,[76-80,85-90] and type IV AFPs.[91-93] The four types of fish AFPs have a wide variation in their size, which can range from 3-12 kDa, and in their secondary structures, which can be α-helices, β-rolls, random coils and globular structures. AFGPs are also present in fish, and are comprised of a tripeptide repeat of $(Ala\text{-}Ala\text{-}Thr)_n$, in which the secondary hydroxyl group of threonine is glycosylated with the disaccharide β-D-galactosyl-(1-3)-α-*N*-acetyl-D-galactosamine (structure shown in Figure 1.3).[13,49-51,94-98] In general, AFGPs have a homologous structure and have been separated into eight subclasses, AFGP 1-8, based on their molecular masses which range from 2.6 kDa (n = 4) to 33.7 kDa (n = 50).[49] Minor sequence variations have been identified in AFGPs where the first alanine residue is replaced by proline, or where the glycosylated threonine residue is occasionally replace by arginine.[99-104] The solution structure of AFGPs has been debated in the literature. Early circular dichroism (CD) and nuclear magnetic resonance (NMR) studies suggested AFGPs adopt an extended random coil structure.[105-110] However, studies have also suggested that they adopt an ordered helix similar to a PPII helix.[109,111-113] It has also been suggested that they adopt an amphipathic helical structure, with a hydrophilic face containing the exposed hydroxyl groups of the disaccharide moiety and a hydrophobic face containing the exposed methyl groups of the amino acid residues.[75] However, the most recent studies have indicated that AFGP 1-5 d o not possess long-range order and that AFGP-8 is predominantly random coil with short segments of localized order.[109-111] A brief summary of the key structural differences between fish AFPs and AFGPs is provided in figure 1.3.

A number of other AFPs have been identified in other organisms. Various insect AFPs have been identified such as those from the spruce budworm moth (*Choristoneura fumiferana*, *Cf*AFP),[114,115] the yellow mealworm beetle (*Tenebrio molitor*, *Tm*AFP),[116,117] the fire-coloured beetle (*Dendroides canadensis*, *Dc*AFP),[118] and the snow flea (sfAFP).[119] Plant AFPs have also been identified from carrot (*Daucus carrota*),[120] bittersweet nightshade (*Solanum dulcamara*),[121] perennial ryegrass (*Lolium perenne*),[122-124] Antarctic hair grass (*Deschampsia antartica*),[125] and several other species.[126,127] Additionally, AFPs have been identified in fungi and bacteria.[128-133] The secondary structures of the various AFPs from plants and insects are also diverse.[134,135] Regardless of where the AFPs are found or their secondary structure, they are all ice-binding

proteins that are crucial for the species survival in the harsh cold environments to which they are exposed.

Characteristic	AFGP	Type I AFP	Type II AFP	Type III AFP	Type IV AFP
Mass (kDa)	2.6 - 33	3.3 – 4.5	11 – 24	6.5	12
Key Properties	AAT repeat; disaccharide	Alanine-rich α-helix	Disulfide bonded	β-sandwich	Alanine rich; helical bundle
Representative Structure	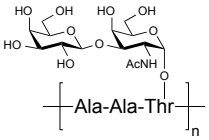	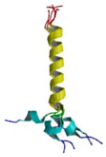			
Natural Source	Antarctic Notothenioids; northern cods	Right-eyed flounders; sculpins	Sea raven; smelt; herring	Ocean pout; wolfish; eel pout	Longhorn sculpin

Figure 1.3 Classification and structural differences between fish antifreeze proteins (AFPs) and antifreeze glycoproteins (AFGPs).

1.2.2 Antifreeze Activities: Thermal Hysteresis (TH) and Ice Recrystallization Inhibition (IRI) Activity

All BAs exhibit two types of antifreeze activities. The first and the most studied is thermal hysteresis (TH). This is defined as a selective depression of the freezing point of a solution relative to the melting point.[54-56] TH activity is the direct result of the binding of a BA to the surface of a seeded ice crystal.[57,58] The binding of the BA to the surface of ice facilitates a localized freezing point depression and induces a change in the ice crystal habit. This change in ice crystal habit is referred to as dynamic ice shaping (DIS) and is illustrated in Figure1.4A. The standard assay used to measure TH activity is nanolitre osmometry.[136] In this assay, a single ice crystal in an aqueous solution of the biological antifreeze is obtained, and the growth and behaviour of the crystal upon increasing/decreasing the temperature can be observed. TH activity is typically reported as the difference between the observed freezing and melting points in Kelvin or degrees Celsius.

The second type of antifreeze activity exhibited by biological antifreezes is their ability to inhibit ice recrystallization (referred to as ice recrystallization inhibition (IRI) activity).[39,137] An illustration of this process is shown in Figure 1.4B. Inhibiting ice recrystallization results in very small ice crystals within a frozen sample. While there are various methods for assessing IRI activity,[138-142] the most commonly used is the splat-cooling assay.[137] In the splat-cooling assay recrystallization can be observed by the change in size of individual ice grains and ice crystal size

can be quantified by measuring the mean ice grain area.[44,143] Thus, smaller ice crystal sizes represent greater IRI activity.

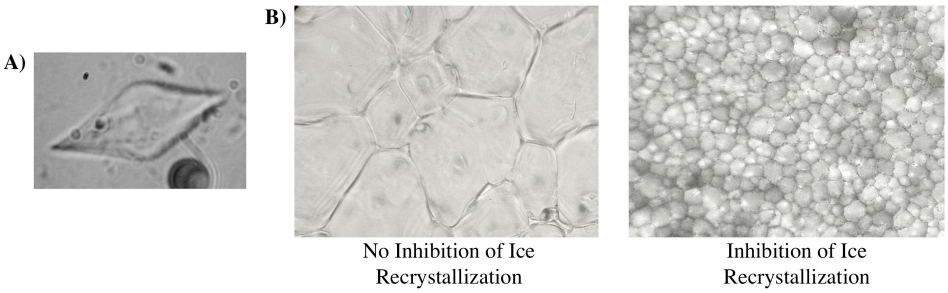

Figure 1.4. Photographs illustrating dynamic ice shaping (DIS) and ice recrystallization inhibition (IRI) activity. **A)** Ice crystal habit in the presence of 10 mg/mL AFGP-8. The binding of AFGP-8 to the surface of ice crystals induces a change in ice crystal habit, resulting in hexagonal bipyramidal (or spicule) ice crystal shapes. **B)** Photographs of annealed ice grains obtained from a splat-cooling assay. A compound that can inhibit ice recrystallization is able to maintain small ice crystals sizes within a frozen solution.

1.2.3 Thermal Hysteresis (TH) Activity - Mechanism of Action

The most widely accepted mechanism for thermal hysteresis (TH) involves an irreversible adsorption-inhibition process.[54-58] In this mechanism, BAs irreversibly bind to specific planes of a growing ice crystal. Preferential binding occurs on the prism faces of ice, thus inhibiting ice growth along the *a*-axis.[96,144-146] Ice crystal growth continues as the temperature of the solution is decreased below the hysteresis freezing point; however, it occurs along the *c*-axis, giving rise to the characteristic hexagonal bipyramidal (or spicule) crystal shapes (illustrated in Figure 1.5).[54,147] While it has been determined that BAs adsorb preferentially to the prism planes of a seeded ice crystal, various insect and plant AFPs adsorb to the basal planes, and it is postulated this results in the superior TH activity exhibited by these proteins.[134,135,148]

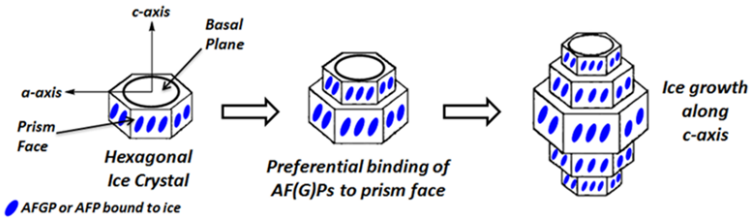

Figure 1.5. Formation of hexagonal bipyramidal crystals by inhibition of growth on the prism faces due to adsorption of BAs.

The irreversible binding of a BA to the surface of ice crystals results in a localized freezing point depression. This occurs *via* the Kelvin (or Gibbs-Thomson) Effect.[56] Given that ice growth cannot occur where the BA has adsorbed, growth occurs on the ice surfaces between adjacent BA

molecules, resulting in curved ice surfaces (shown in Figure 1.6). The energetic cost of adding a water molecule (freezing) to this curved surface is high and it becomes unfavourable for more water molecules to add to this surface, thus a localized freezing point depression is observed. This process does not affect the energetics of the melting process, hence only the freezing point is depressed while the melting point remains constant, resulting in a thermal hysteresis gap (Figure 1.6A).[56,146,149]

There are two proposed models that describe how BAs inhibit ice growth within the thermal hysteretic gap. The first (illustrated in Figure 1.6B) was proposed by Raymond and DeVries and is known as the step-pinning model. In this model, the growth of a step is inhibited by the BA which has pinned ice growth across the ice surface.[54] However, this model assumes that ice crystal growth occurs in steps advancing across the plane that the BA is adsorbed. The second model (illustrated in Figure 1.6C) is a three-dimensional model known as the mattress model and was proposed by Knight and DeVries. In this model, the adsorbed BA molecules exhibit inhibition by pinning ice growth normal (perpendicular) to the ice surface.[57]

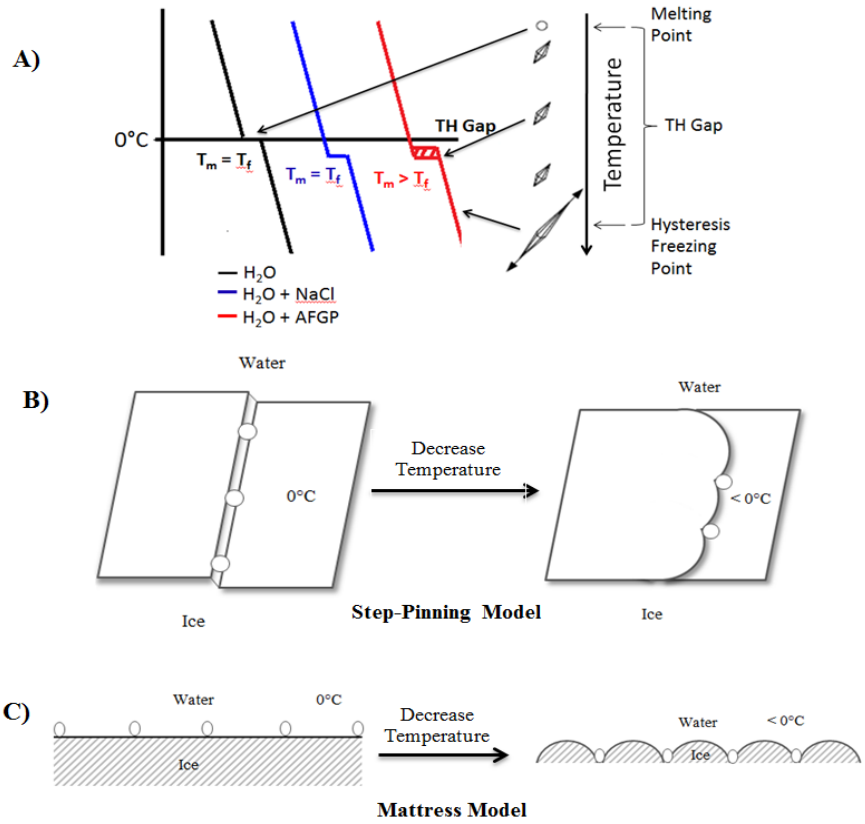

Figure 1.6. Illustrations of thermal hysteresis (TH) activity and the two models of ice growth inhibition.[13] **A)** BAs have the ability to depress the freezing point of ice crystals relative to the melting point, resulting in a thermal hysteresis gap. **B)** Step-pinning model and **C)** mattress model depicting the irreversible adsorption-inhibition mechanism of BAs

1.2.4 Important Structural Features For Ice Binding and TH Activity

It was originally proposed that adsorption of BAs to the surface of ice occurred through the hydrogen bonding of hydrophilic groups to the oxygen atoms in the ice lattice.[10,150] However, this is contradictory to the current mechanism of action for AFPs where the importance of hydrogen bonding between polar residues and ice has been questioned. Alternatively, it has been demonstrated that entropic and enthalpic contributions from hydrophobic residues are crucial for ice binding.[151-153] The importance of hydrophobic residues has been validated with a number of different AFPs through site-specific mutagenesis studies,[85,151,154,155] and in general it is believed that the ice-binding site of these AFPs is hydrophobic and has a discrete complementarity with the planes of ice to which it binds.[85,154-157]

In contrast to AFPs, the current hypothesis of how AFGPs bind to ice involves hydrogen bonding between the hydroxyl groups of the sugars and the ice lattice.[58] A landmark study conducted by Nishimura and co-workers investigated the key structural features of synthetic native AFGPs (synAFGPs) that were crucial for ice binding and TH activity.[158] In this study it was reported that three key motifs were required for TH activity (shown in Figure 1.7): 1) the *N*-acetyl group at the C2 position of the galactosamine; 2) the α-configuration of the *O*-glycosidic linkage between the disaccharide and the peptide chain; 3) the γ-methyl group of the threonyl residue. In addition, the TH activity of homogenous AFGPs is dependent upon the length of the glycoprotein segment.[158,159]

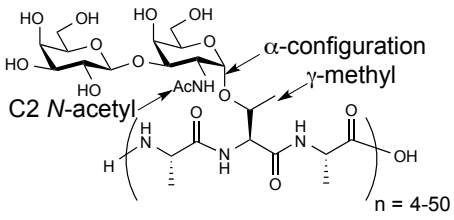

Figure 1.7. Important structural motifs for TH activity of synthetic AFGPs (synAFGPs) as determined by Nishimura and co-workers.[158]

It should be emphasized that the ability to bind to ice is believed to be a property unique to BAs. However, it has been reported that polyvinyl alcohol (PVA) can bind to ice and exhibit a small degree of thermal hysteresis.[160] Budke and Koop reported that PVA induces dynamic ice shaping capabilities and suggest this is occurring as the spacing of the PVA hydroxyl groups are closely matched to that of the prism planes of ice, allowing adsorption to these planes.[161] Furthermore, Inada and Lu have shown that PVA exhibits a small TH gap of 0.037 °C at 50 mg/mL, suggesting that an adsorption to ice is occurring.[160]

1.3 Ice Recrystallization Inhibitors

Despite the tremendous number of structure-function studies conducted on AFPs and AFGPs over the last three decades, TH is often the only antifreeze activity assessed and correlated to structural modifications. The ability of these analogues to inhibit ice recrystallization is typically overlooked and not assessed. Consequently, the structural features necessary for potent ice recrystallization inhibition (IRI) activity are currently not well understood. During the last several years considerable amount of progress has been made in discovering novel ice recrystallization inhibitors. The majority of this work has been based upon synthetic structural analogues of AFGPs. Many of these analogues are structurally very similar to AFGPs and while most have been IRI inactive, some have exhibited both types of antifreeze activity, TH and IRI activity.[50,51,158,162-166] However, a few derivatives with dramatic structural modifications relative to AFGPs have been discovered that possess "custom-tailored" antifreeze activity, meaning they have potent IRI activity but do not exhibit TH activity.[63,64] These compounds are thus ideally suited for applications as novel cryoprotectants as they do not exhibit the undesirable property of TH activity or ice binding capabilities that BAs exhibit. Furthermore, they are the first examples where the two properties of BAs that were thought to be correlated together, TH and IRI, were decoupled from each other.

1.3.1 "Custom-Tailored" Peptide and Glycopeptide Analogues of Biological Antifreezes

The first series of novel compounds reported by our laboratory that exhibited potent IRI activity were *carbon*-linked or *C*-linked AFGP analogues. These analogues did not possess the *O*-glycosidic linkage found in AFGPs, which is susceptible to hydrolysis under basic or acidic conditions. The first set of compounds reported were lysine-based *C*-linked AFGP derivatives (Figure 1.8).[167] In comparison to AFGPs, the terminal galactose unit and the *N*-acetyl group were removed leaving only an α-D-galactosyl unit that was conjugated to lysine residues. Lysine was used due to its structural similarity to an arginine residue, which is occasionally found in native AFGPs. [99-104] In addition, the alanine residues present in AFGPs were substituted with glycine residues to avoid racemization encountered during solid-phase synthesis.[167,168] The monomer tripeptide unit (**1**) and the analogue with three repeating tripeptide units (**2**, n = 3) did not exhibit IRI activity. However, the analogues with six and nine repeating tripeptide units (**3** and **4**, n = 6, n = 9) were both moderately IRI active. These derivatives (**3** and **4**) were also assessed for TH activity and both exhibited a small TH gap of 0.06 °C and induced the formation of hexagonal shaped ice crystals.

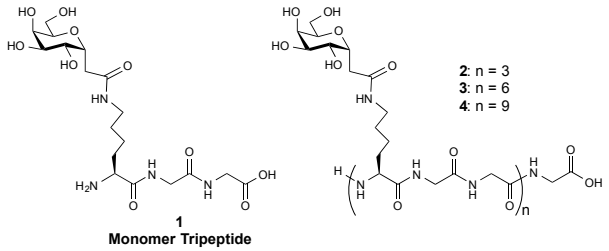

Figure 1.8. Structure of first-generation lysine-based *C*-linked AFGP analogues.[167]

Two other *C*-linked AFGP analogues have been reported that have maintained the potent IRI activity exhibited by AFGP-8 at equimolar concentrations but did not exhibit TH activity (Figure 1.9). One of these is a *C*-linked serine-based derivative which contains four tripeptide repeats and a *C*-linked galactosyl unit (**5**, *C*-serine analogue).[63] The other derivative also contains four tripeptide repeats, and is structurally similar to the lysine-based derivatives (Figure 1.8), however the *C*-linked α-D-galactosyl unit is conjugated to an ornithine residue (**6**, OGG-Gal analogue).[64] Both of these derivatives exhibited potent IRI activity at 5.5 μM and their activity was similar to that exhibited by AFGP-8 at 5.5 μM. Unlike AFGP-8, neither of these derivatives exhibited TH activity and while OGG-Gal (**6**) exhibited very weak dynamic ice shaping,[64] *C*-serine (**5**) did not exhibit any ice shaping capabilities.[63] This suggested that the exhibited IRI activity was not likely due to ice binding. These analogues were the first examples where the two properties of biological antifreezes, TH and IRI activity, were decoupled from each other. Additionally, these *C*-linked AFGP analogues were the first compounds that possessed "custom-tailored" antifreeze activity, meaning they exhibited potent IRI activity with little or no measureable TH activity.

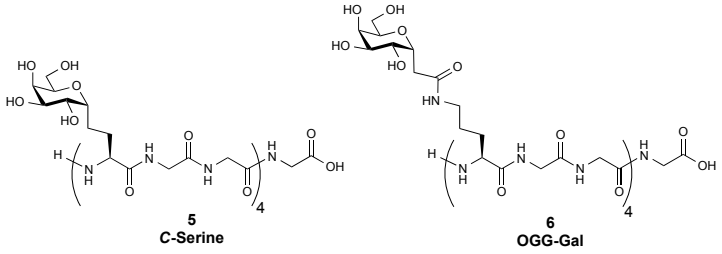

Figure 1.9. Structures of potently IRI active *C*-serine and OGG-Gal analogues.[63,64] These are the first compounds reported to exhibit "custom-tailored" antifreeze activity, meaning they exhibit potent IRI activity but not TH activity.

The first structure-function study conducted on OGG-Gal (**6**) examined the importance of the carbohydrate moiety.[64] The galactosyl moiety was substituted with three other monosaccharides: glucose, mannose and talose (**7**, **8** and **9**, respectively, Figure 1.10). Replacing the galactosyl unit with other monosaccharides was highly detrimental for IRI activity as the glucose analogue **7** exhibited weak activity, whereas the mannose and talose analogues (**8** and **9**) were inactive. These results indicated that the relative orientation of the hydroxyl groups on the carbohydrate

moiety on the polypeptide is highly influential on IRI activity. The configuration of the carbons bearing hydroxyl groups on simple carbohydrates (mono- and disaccharides) is known to influence the hydration of carbohydrates.[169-171] This led to the observation that carbohydrate hydration was important for IRI activity.[64] A more detailed discussion of carbohydrate hydration and its influence on IRI activity is provided in section 1.3.3. Briefly, carbohydrate hydration influences IRI activity by altering the ordering of bulk-water based on the compatibility of the carbohydrate within the three-dimensional hydrogen-bonded network of water.[64,172] The hydration of a carbohydrate is related to the compatibility of the sugar with the three-dimensional hydrogen-bond network of water.[169-171] Of the monosaccharides assessed, talose is the most compatible and is thought to have the best "fit" into this hydrogen-bond network, whereas galactose is the least compatible and has the worse "fit". It was hypothesized that a poorer "fit" of the carbohydrate into the hydrogen-bond network of bulk water resulted in a more disordered bulk water layer between the semi-ordered quasi-liquid layer and ordered ice crystal layer. Consequently, transferring water molecules from a more disordered bulk water layer to an ordered layer was energetically unfavorable. Thus, carbohydrates that are highly hydrated resulted in greater IRI activity.[172] While the overall hydration of the *C*-linked glycoconjugates **6**-**9** is not known, a more highly hydrated carbohydrate moiety conjugated on the glycopeptide (ie. galactose) proved significantly better for IRI activity than a less hydrated carbohydrate moiety.[64]

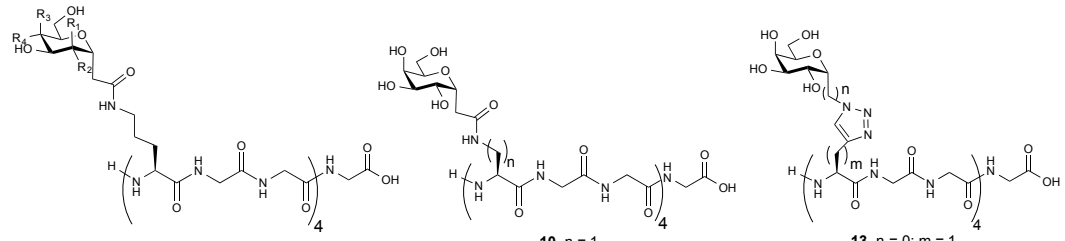

Figure 1.10. Structures of OGG-Gal (**6**) analogues containing various monosaccharide moieties (**7**-**9**)[64] and modifications to the side-chain linker between the carbohydrate moiety and polypeptide backbone (**10**-**16**).[166,173]

Various other structure-function studies on OGG-Gal (**6**) have been reported that have identified the structural features necessary for the potent IRI activity of this analogue. The influence of the side-chain linker between the carbohydrate residue and the polypeptide backbone has been explored in two studies. One study examined how the distance between the galactosyl moiety and the polypeptide backbone influenced activity by increasing or decreasing the distance between the carbohydrate and peptide backbone. The side chain linking the carbohydrate to the backbone was modified to contain a total of four, five, six or seven atoms in length (**10**, **11**, **6** and

12, respectively, Figure 1.10).[173] The second study examined the influence of the amide-bond within the side chain by replacing it with a suitable isostere, a triazole ring (**13**-**16**, Figure 1.10).[166] In all cases, analogues in which the side chain linking the carbohydrate to the peptide backbone was modified failed to exhibit IRI activity. These results indicated that the optimal length of linker between the carbohydrate and peptide backbone is six atoms for analogue **6**.[173] Furthermore, the amide bond within the side is crucial for potent activity as replacing it with a triazole-linker was detrimental to activity.[166]

1.3.2 Synthetic Polymers as Ice Recrystallization Inhibitors

Interest has also arisen in designing synthetic polymers that can inhibit ice recrystallization. Such compounds can be efficiently synthesized and would overcome the main limitation to using peptide and glycopeptide-based ice recrystallization inhibitors, which is that large-scale preparation of these compounds for *in vitro* or *in vivo* applications is problematic. The first polymer discovered to inhibit ice recrystallization was polyvinyl alcohol (PVA).[39] Extensive studies on the IRI activity of PVA have found its activity to be dependent on its molecular mass, with an increase in activity observed with higher molecular weight polymers of PVA.[174] Polymers with an average molecular weight of ~90 000 g/mol were found to exhibit comparable activity to a type I AFP from winter flounder at similar molar concentrations. However, due to the large difference in molecular weights between PVA and the AFP, the quantity of PVA required to exhibit this activity was significantly higher than that of the AFP. It has also been reported that PVA with an average molecular weight of ~115 500 has potent IRI activity at a concentration of 5 mg/mL.[52] It was suggested that the ability of PVA to inhibit ice recrystallization is attributed to its ability to interact with the ice crystal lattice because PVA induces dynamic ice shaping capabilities. This is suggested to occur from the spacing of the PVA hydroxyl groups, which are closely matched by the prism planes of ice, allowing adsorption to these planes.[161] Furthermore, PVA also exhibits a small TH gap of 0.037 °C at 50 mg/mL, suggesting that adsorption to ice is occurring.[160]

In addition to PVA, a number of other structurally diverse water-soluble polymers have also been investigated for their ability to inhibit ice recrystallization (Figure 1.11).[52,98] Polyacrylic acid (PAA, **17**), poly(2-aminoethyl methacrylate) (**18**), polyethylene glycol (PEG, **19**), poly-L-Lysine (**20**) and poly-L-glutamic acid (**21**) exhibited only weak IRI activity, and an increase in concentration did not improve activity for any of these polymers. Poly-L-hydroxyproline (**22**) was found to exhibit IRI activity and this activity was dependent on polymer concentration. Poly-L-hydroxyproline has a PPII helical secondary structure[175] similar to the structure suggested to be

adopted by AFGPs. However, it was suggested this secondary structure is not required for IRI activity as PVA and poly-L-hydroxyproline exhibited similar IRI activities, but PVA is largely unstructured in solution.[52] Two vinyl-derived glycopolymers were also assessed for their ability to inhibit ice recrystallization (**23** and **24**). The highest molecular weight glycopolymer with a glucose residue (**23**, at ~105000 g/mol) did exhibit a moderate ability to inhibit ice recrystallization. However, incorporating a different carbohydrate residue (**24**) failed to increase IRI activity.[52,98]

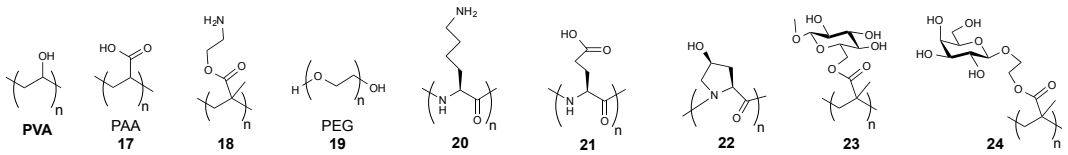

Figure 1.11. Structures of synthetic polymers assessed for IRI activity.[39,52,98,174]

1.3.3 Simple Carbohydrates - Moderate Ice Recrystallization Inhibitors

Despite the recent advances in the synthesis of peptides and glycopeptides, their synthesis still remains complex, time consuming and costly. Thus, the design of more simple small molecules that have the capacity to inhibit ice recrystallization would be ideally suited for the many medical, commercial and industrial applications. The first small molecules investigated for IRI were simple, commercially available mono- and disaccharides. This was reported in a study examining the correlation between carbohydrate hydration and ice recrystallization inhibition,[172] and arose from the observation that a more hydrated carbohydrate moiety was a contributing factor to the high IRI activity of a *C*-AFGP analogue (OGG-Gal, **6**).[64] Consequently, four monosaccharides and five disaccharides with known hydration parameters[169-171] were assessed for their ability to inhibit ice recrystallization. The structures of the mono- and disaccharides along with their corresponding hydration numbers, isentropic molar compressibility and partial molar volume values are shown in Table 1.1. At a concentration of 22 mM, D-galactose exhibited moderate IRI activity, D-glucose and D-mannose had weak activity while D-talose was inactive.[172] These results showed a strong linear correlation between the hydration number of the monosaccharides and their respective IRI activity, with monosaccharides having larger hydration numbers being more IRI active. The disaccharides examined also showed this strong linear correlation of their hydration number to IRI activity. Melibiose exhibited moderate IRI activity, while lactose and trehalose showed weak activity and maltose and sucrose were inactive.

Table 1.1. Isentropic molar compressibilities ($10^4K_2°(s)$, $cm^3\ mol^{-1}\ bar^{-1}$) and hydration numbers of various monosaccharides and disaccharides. Errors of molar compressibility values and hydration numbers are shown in parentheses.[170,172]

Carbohydrate	Molar Compressibility ($K_2°(s)x10^4$,$cm^3\ mol^{-1}\ bar^{-1}$)	Hydration Number	Carbohydrate	Molar Compressibility ($K_2°(s)x10^4$,$cm^3\ mol^{-1}\ bar^{-1}$)	Hydration Number
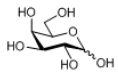 D-Galactose	-20.8 (0.5) -20.4 (0.4)	8.7 (0.2)	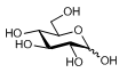 D-Glucose	-17.6 (0.3)	8.4 (0.2)
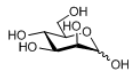 D-Mannose	-16.0 (0.5)	8.1 (0.2)	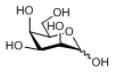 D-Talose	-11.9 (0.3)	7.7 (0.2)
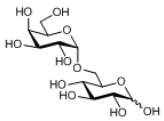 Melibiose	-31.2 (1.0)	15.5 (0.3)	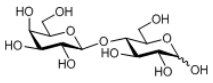 Lactose	-31.1 (0.2) -30.4 (1.0)	15.3 (0.3)
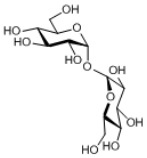 Trehalose	-30.2 (0.3)	15.3 (0.3)	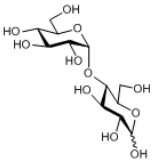 Maltose	-23.7 (1.0)	14.5 (0.3)
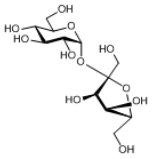 Sucrose	-17.8 (0.5)	13.9 (0.3)			

The hydration layer or hydration shell of a carbohydrate can be defined as the number of tightly bound water molecules that surround the carbohydrate in aqueous solution. The hydration of carbohydrates has been the focus of many studies, and hypotheses for rationalizing observed hydration characteristics include hydration numbers,[176-179] anomeric effect,[180] hydrophilic volume,[181] hydrophobic index,[182] the ratio of axial versus equatorial hydroxyl groups[183,184] and the compatibility with bulk-water based upon the position of the next-nearest-neighbor hydroxyl group.[185,186] In the early 1990's, Galema *et al*. studied key parameters thought to dictate hydration characteristics and these were correlated to carbohydrate stereochemistry. Using kinetic experiments and density ultrasound measurements, the partial molar volumes, isentropic partial molar compressibilities and hydration numbers were determined for many commercially available mono- and disaccharides.[169-171] The isentropic partial molar compressibility and partial molar volume values of the carbohydrates quantify their "compatibility" with the three-dimensional hydrogen-bond network of bulk-water as they are related to the size or volume the carbohydrate occupies upon hydration by water. Hydration numbers are calculated using isentropic coefficients

of compressibility and they predict the number of water molecules that are hydrogen-bonded to the carbohydrate.

It was observed that the compatibility of the carbohydrate with the three-dimensional hydrogen-bond network of bulk-water was directly related to the configuration of the C2- and C4 carbons of the carbohydrate. D-Talose, with axial hydroxyl groups on C2 and C4, had a higher isentropic molar compressibility value and a lower hydration number, and fit well into the three-dimensional hydrogen-bonded network of bulk-water. In contrast, D-galactose, with an axial hydroxyl group on C4 and equatorial hydroxyl group on C2, had a lower isentropic molar compressibility value and a higher hydration number, and had a poor fit into the three-dimensional hydrogen-bonded network of bulk-water. Thus, D-talose was the most compatible and caused the least disturbance on the hydrogen-bonded network of bulk-water, whereas D-galactose was the least compatible and caused a greater disturbance on the hydrogen-bonded network of bulk-water. The carbohydrates with an equatorial C4 hydroxyl and either an equatorial or axial C2 hydroxyl group (ie. D-glucose and D-mannose) had a moderate fit and caused a moderate disturbance of the three-dimensional hydrogen-bonded network of bulk-water.

With regards to the IRI activity of several mono- and disaccharides, a correlation was observed between IRI activity and carbohydrate hydration.[172] As none of the carbohydrates exhibited thermal hysteresis or dynamic ice shaping, it was unlikely that the IRI activity exhibited by the carbohydrates was due to an interaction with the ice lattice. This lead to an alternative proposed mechanism for the inhibition of ice recrystallization based upon the compatibility of a solute with bulk-water. A semi-ordered quasi-liquid layer (QLL) exists between the highly ordered ice lattice and bulk-water and for ice recrystallization to occur, bulk-water molecules transfer to the QLL, then subsequently from the QLL to the growing ice lattice.[36,37] It was suggested that the carbohydrates are concentrated at the bulk-water-QLL interface.[172] A carbohydrate that had a poor fit into bulk-water will cause a greater disturbance to its three-dimensional hydrogen-bonded network, increasing the energy associated with the transfer of bulk-water to the QLL. It was therefore hypothesized that the inhibition of ice recrystallization observed with carbohydrates occurred at the bulk-water-QLL interface as more highly hydrated carbohydrates, such as D-galactose, disrupted the pre-ordering of bulk-water making it energetically unfavourable for water molecules to transfer to the QLL. Less hydrated carbohydrates, such as D-talose, fit well into bulk-water and caused less of a disturbance to the pre-ordering of bulk-water, thus inhibition of ice recrystallization was not observed.

The disaccharides assessed in this study also showed a strong linear correlation of their IRI activity to their hydration numbers (values give in table 1.1).[172] However, the increase in

hydration numbers for disaccharides relative to monosaccharides was not reflected with an increase in IRI activity. For instance, melibiose has a hydration number of 15.5, yet it exhibited similar IRI activity to D-galactose, which has a hydration number of 8.7. Furthermore, D-galactose was significantly more IRI active than maltose, despite maltose having a much larger hydration number (8.7 for D-galactose and 14.5 for maltose). This was attributed to a difference in total steric volume between the monosaccharides (containing one carbohydrate unit) and disaccharides (containing two carbohydrate units). By dividing the carbohydrate hydration number by their partial molar volumes an indication of the degree of hydration per molar volume of carbohydrate was obtained. This value was referred to as the hydration index (HI) and it provided the degree of hydration of the substrate as a function of its size or volume. This metric was useful in justifying why highly hydrated monosaccharides exhibited similar IRI activity as highly hydrated disaccharides at 22 mM, despite hydration numbers for monosaccharides being almost half the value of disaccharides.[172] However, at higher carbohydrate concentrations, such as 220 mM, the disaccharides were twice as IRI active as the monosaccharides.[187] Thus, hydration numbers, not hydration indices, were better predictors of IRI activity at this concentration, but ultimately IRI activity still correlated with carbohydrate hydration.

1.3.4 Summary and Conclusions of Current Ice Recrystallization Inhibitors

Overall, this section has summarize that while the field of ice recrystallization inhibitors is expanding, only a few novel compounds have been identified as having potent activity. These potently IRI active derivatives have been large peptides, glycopeptides or high molecular weight polymers.[13,50-52,174] However, the large-scale preparation of these compounds can be problematic for the many medical and commercial applications of IRIs. Simple carbohydrates have been explored for their ability to inhibit ice recrystallization, but have only exhibit moderate activity. Consequently, the most potently IRI active molecules known to date are still the biological antifreezes (BAs).

A major application for potent IRIs is in the fields of cryobiology and cryopreservation. This is because a significant contributor to cellular injury and death during cryopreservation is ice recrystallization, and as such the ability to inhibit this process is highly desirable in a cryoprotectant.[188-192] This is described in greater detail in the next section (section 1.4). BAs are potent inhibitors of ice recrystallization, however they are often poor cryoprotectants due to their ice binding capabilities (described in section 1.4.4). Consequently, compounds that have "custom-tailored" antifreeze activity, such as the *C*-AFPGs developed by our laboratory are better candidates as novel cryoprotectants.[63,64] This is also described in more detail in the next section,

which describes how these compounds can function as beneficial cryoprotectants for a human embryonic liver cell line,[193] providing the rational to further design novel IRIs.

1.4 Cryopreservation

There are three main methods of cellular preservation, each of which offer their own unique advantages and limitations: hypothermic storage, vitrification and cryopreservation. Hypothermic storage is the process whereby cells are maintained at temperatures between 4 and 10 °C in the presence of an additive solution. Effectively at these temperatures biochemical events and metabolic processes are considerably slowed down to prevent the depletion of critical cellular metabolites and prevent injury.[194-198] However, alternate stress pathways involved in necrosis and apoptosis can be activated during hypothermic storage that can be detrimental to cell quality and viability.[8,199] In addition, hypothermic storage is limiting due to the short shelf-life of the preserved cells which can range from several days to weeks depending upon the cell type.[194,196-198]

Cryopreservation, the process whereby cells and tissues are stored at subzero temperatures (typically -80 °C or -196 °C) is very attractive for the long-term preservation of biological materials. At the temperatures associated with cryopreservation, all biochemical processes are effectively stopped, and cells can be stored for 10-20 years clinically depending upon the cell type. However, cryopreservation is a complex process during which careful attention to sample volume, cooling rates and cryoprotectants are extremely important to ensure cells survive the process.[196,198,200,201] The formation and recrystallization of both intra- and extracellular ice is also often detrimental to cells during the freezing and thawing processes of cryopreservation. While cryoprotectants are used to mitigate this damage, all cryoprotectants exhibit cytotoxicity and this complicates the cryopreservation process as they often must be removed after thawing. Vitrification is an alternative cryopreservation method that also mitigates damage caused by ice formation as it avoids crystallization altogether by freezing in an amorphous, glassy-solid state.[202-204] However, to vitrify a sample ultra-rapid cooling rates and very high concentrations of cryoprotectants must be used. In addition, the formation of ice crystals by devitrifcaiton can occur without proper storage of the sample or when slow warming rates are used, which can result in significant cellular damage.[203,205] Even with the complexity associated with the cryopreservation of various different cell types, it is the only method available and clinically approved for the long-term storage of precious cell types. Thus, there is an urgent need for new cryoprotectants and protocols to improve upon this process.

1.4.1. Mechanisms of Cryoinjury During Cryopreservation

Traditionally, there exist three characterized mechanisms of cell death that occur during cryopreservation. These are cell rupture due to damage to the external cell membrane, necrosis and cold induced apoptosis. Cell rupture is usually the result of osmotic imbalance causing a loss in membrane integrity.[8] Cell necrosis is characterized by cellular swelling (due to an increase in immune response), compromised cell membrane integrity, random DNA fragmentation by cellular endonucleases, cell lysis and the release of cytokines. Apoptosis (programmed cell death) is a highly complex and closely regulated biochemical pathway. It may appear at first that cell death due to apoptosis is not related to cryopreservation; however it has been demonstrated that cold-induced apoptosis is common in cryopreserved cells.[8,206]

The formation of ice under typical cryopreservation conditions is inevitable, but cooling rates become extremely important in mitigating the damage associated with ice formation. This is summarized by Mazur's two-factor hypothesis on the major forms of freezing damage.[207] For every cell type there is an optimal cooling and warming rate that is determined by the permeability of the cell membrane to water and the cryoprotectant. Hence, cryopreservation is performed with either slow or fast cooling rates depending on cell type. In most instances, ice will prefer to form outside of the cell.[192] Formation of extracellular ice creates an increased osmotic pressure across the cell membrane that intensifies as ice growth continues after the nucleation event. This occurs as all solutes are excluded from the ice lattice and are concentrated in the extracellular medium and causes an efflux of water from the cell.[208] Cells with less permeable membranes will rupture with increasing osmotic pressure if they cannot dehydrate fast enough. With optimal slow cooling rates for the cell type, the cell has time to respond by allowing intracellular and extracellular composition to be maintained near equilibrium by dehydration, volume reduction and an increase in intracellular solutes. As this process reduces the amount of intracellular water the chance for intracellular ice formation – a lethal process – is reduced. However, when slow cooling rates are not optimal for the cell type it has been shown that excessive cell shrinkage from dehydration and exposure to excessively high concentrations of electrolytes is also lethal to the cell and facilitates cell death.[188,209-212] This is commonly referred to as solute damage or the "solute effect" and it facilitates damage to the cell membrane that is irreparable.[188]

Cell permeability is also dependent upon temperature. Rapid cooling rates during cryopreservation traps water inside the cell as the formation of extracellular ice and the concentration of extracellular salts occur much faster than the rate at which water can leave the cell.[213] This results in an increase in the probability of intracellular ice formation as less

dehydration of the cell occurs and the intracellular compartment becomes increasingly supercooled below the freezing point.[214] The exact mechanism by which intracellular ice formation occurs and the mechanism by which it damages cells is not well understood.[215,216] However, it is believed that intracellular ice formation results in a significant amount of cell death. Hence, practical fast-freezing protocols must dehydrate cells prior to freezing in order to mitigate intracellular ice formation.[217] While the correlation between intracellular ice formation and cell death has been recognized, there is evidence to suggest that formation of intracellular ice does not directly kill cells.[192] Studies have shown that survival of cells post-cryopreservation is dependent upon the rate at which the cells are warmed during thawing and that cell death associated with intracellular ice formation is not caused by the initial nucleation of ice but by an alternate process during warming.[218,219] Possible mechanisms by which intracellular ice damages cells have been reviewed extensively in the literature and it has been concluded that a significant contributor to cell death is a result of ice recrystallization.[188,189]

1.4.2 Cryoprotective Agents (CPAs)

Two classes of cryoprotectants are commonly employed during cryopreservation depending upon the cooling rate: penetrating and nonpenetrating. Penetrating cryoprotectants, such as dimethyl sulfoxide (DMSO), glycerol and 1,2-propandiol, are able to readily cross the cell membrane and protect cells from injury during slow cooling by preventing excessive shrinkage and maintaining cell volumes.[220-223] They also protect cells by preventing or reducing the temperature at which the critical salt concentration is reached, when the cells are exposed to excessively high and lethal electrolyte concentrations during the slow cooling process. In addition, they reduce the amount of ice formed by depressing the freezing point and lowering the chemical potential of the solution.[190,224] The major problem with penetrating cryoprotectants is significant cytotoxicity due to the disruption of intracellular signaling.[225-228] This often results in the need to remove these cryoprotectants prior to the use of the cryopreserved cells. Furthermore, the addition of penetrating cryoprotectants must be done without exceeding the osmotic tolerance of the cells.[200]

Nonpenetrating cryoprotectants do not cross the cell membrane and hence remain outside the cell. Typical nonpenetrating cryoprotectants include starches such as hydroxyethyl starch (HES), polymers such as polyethylene glycol (PEG) and polyvinyl pyrrolidone (PVP) and certain sugars and sugar polymers such as trehalose, sucrose and dextran (molecular weights typically greater than 350-400 Da). They act by increasing the osmolality of the extracellular solution, which facilitates dehydration of the cell prior to freezing.[191,220,221] Thus, they protect cells during rapid

cooling by reducing the incidence of intracellular ice formation. They have also been hypothesized to protect during rapid cooling by stabilizing cell membranes.[229-231] Nonpenetrating cryoprotectants generally exhibit significantly less cytotoxic effects than penetrating cryoprotectants and their removal prior to use of the cryopreserved cells is not always necessary. However, the post-thaw cell survival using these cryoprotectants is typically not as high as penetrating cryorpotectants. Furthermore, a main drawback for their use is the rapid or ultra-rapid cooling rates that must be used during cryopreservation and the required storage in liquid nitrogen.

1.4.3 Long-Term Storage of Blood and Blood Products

The development of effective methods to preserve blood and blood products has had tremendous impact on regenerative and transfusion medicine over the past 50 years. Hematopoietic stem cells (HSCs) have been increasingly used for regenerative medicine therapies and their transplantation has been used to treat a number of different conditions including hematological cancers (leukemias, lymphomas), hematological diseases, anemias and immunodeficiencies.[232,233] The principal sources of HSCs are bone marrow (BM), mobilized peripheral blood stem cells (PBSCs) and umbilical cord blood (UCB). HSC transplantation from UCB offers advantages over BM and PBSCs including reduced risk of severe acute graft versus host diseases (GVHD), reduced risk of blood-borne infectious diseases, absence of risk to the donor, less stringent human leukocyte antigen-matching requirements and the units are rapid available.[234] This has resulted in a dramatic increase in UCB storage in public and private blood banks.

Clinical protocols for UCB cryopreservation involve the use of a 10% DMSO cryoprotectant solution and slow rate-controlled cooling 1-2 °C/min with storage in liquid nitrogen or its vapour (-196 °C or -150 °C, respectively). While these protocols are effective, resulting in high post-thaw viabilities of HSCs, there are significant drawbacks particularly with the use of DMSO as the cryoprotectant. DMSO is known to be toxic not only to cells, but also to patients upon re-infusion of thawed HSCs, and this toxicity is time, temperature and concentration dependent.[235,236] DMSO must be introduced to the HSCs at 4 °C for a short period of time (less than 10 minutes) prior to freezing. In addition, DMSO is not typically removed prior to re-infusion and adverse effects from patients receiving cryopreserved HSCs are well documented.[236,237] DMSO has been shown to have adverse effects on gastrointestinal, renal and hepatic systems, the central nervous system as well as cardiovascular and respiratory systems. Side effects from DMSO toxicity can be minor from nausea, abdominal cramping and shortness of breath, to major with cardiac or

respiratory arrest and neurological toxicity. Furthermore, studies have indicated that the extent of apoptosis in cryopreserved HSCs in DMSO can be close to 40% and these isolated HSCs have been demonstrated to have impaired engraftment capacity.[238,239] Thus, there is an urgent need for improvements in the cryopreservation protocols of UCB HSCs to significantly reduce or eliminate the use of DMSO cryoprotectant.

The most commonly used and preserved blood product in blood banks is red blood cells (RBCs). RBC transfusions are lifesaving by increasing RBC mass in patients with low oxygen-carrying capacity resulting from acute blood loss (traumatic/surgical haemorrhage), decreased RBC production in bone marrow (leukemias), or decreased RBC survival (hemolytic anemias).[196] Hypothermic preservation of RBCs has enabled blood banks to ensure a readily available and safe blood supply. However, this clinical biopreservation method is limited to a 42 day storage time period that can result in shortages of blood supplies when high numbers of emergency blood transfusions are required such as in the wake of a natural disaster.[195,240] In addition, while hypothermic storage slows down biochemical processes, cellular metabolism is not completely suppressed. This results in the occurrence of "hypothermic storage lessions" after a few weeks of storage, which reduce *in vivo* survival and RBC function.[194,196,241-245]

While cryopreservation of RBC units can extend storage time to 10 years, this preservation method is limited to rare blood phenotypes, autologous RBC storage and military applications for blood and blood product storage.[196,246,247] In Canada and the United States clinical cryopreservation conditions follow high glycerol/slow freeze protocols. High concentrations of the permeating cryoprotectant glycerol (> 40% v/v) are utilized along with slow cooling 1 °C/min and storage at -80 °C to ensure high recovery of RBCs after cryopreservation.[196,248] In Europe clinical cryopreservation protocols typically follow the low glycerol/rapid freeze conditions. In this method glycerol is utilized at 20% v/v and freezing is rapid (greater than 50 °C/min) in liquid nitrogen.[249] While this is an effective freezing method resulting in high RBC recoveries post-thaw, the main drawback is the use of liquid nitrogen for freezing and storage, which is very costly for large-scale preservation of RBC units and produces problems for the transport of frozen units.[196,246,247] One of the main reasons cryopreserved RBC units are not routinely used in transfusion medicine, regardless of the freezing method employed, is that current cryopreservation protocols do not permit the direct transfusion of RBCs immediately after thawing. Deglycerolization requires complicated and time consuming post-thaw deglycerolization procedures to ensure glycerol concentrations are reduced to less than 1% prior to transfusion to prevent post-transfusion intravascular hemolysis.[196,246,248,250,251] This process can also be damaging to RBCs and may result in up to a 20% loss of RBC volume after deglycerolization. Moreover,

these units must be transfused within 24 h imposing challenging logistics due to significant time and/or distance constraints on the transportation of cryopreserved RBCs.[252,253] However, while current cryopreservation methods are less than ideal for large-scale inventory management,[246] it remains the only technology that can readily deliver multiple units of pre-screened RBCs to patients with rare blood groups or complex alloimmunity, and for military applications where RBC units are required for casualty care in remote areas of the world.[194] Thus, improved cryopreservation methods using nontoxic cryoprotective additives and significantly reducing glycerol concentrations are urgently required.

1.4.4 Biological Antifreezes, Analogues of Biological Antifreezes and Carbohydrates as Cryoprotective Additives

Cellular damage due to ice recrystallization occurs during the storage and thawing cycles of cryopreservation. Given the ability of BAs to prevent cryo-injury in the organisms where they are found, it is not surprising that they have been investigated as cryoprotectants to increase cell viability post-thaw. In principle, BAs have the advantage of being relatively non-toxic compared to common cryoprotectants such as DMSO and glycerol. Several studies have reported benefits of using AFPs and AFGPs as cryoprotectants. Rubinsky and co-workers observed dramatically improved morphological integrity of immature oocytes and two-cell-stage embroys of mice and pigs that were subjected to vitrification in the presence of 40 mg/mL AFGPs.[254,255] Similar results were observed with mature mouse oocytes[256], bovine and ovine embryos at the morula/blastocyst stage,[257] ram spermatozoa,[258] chimpanzee spermatozoa[259] and porcine oocytes.[260] Additionally, post-thaw viabilities were increased in the presence of BAs with ram and chimpanzee spermatozoa and porcine oocytes however, cytotoxic effects during cooling were also observed.[258-260]

While there are reports of successful use of BAs as cryoprotectants, they often fail to protect mammalian cells from cryoinjury at temperatures outside of the TH gap and actually facilitate cellular damage during cryopreservation. For instance, no specific benefits were observed in survival rates of vitrified bovine blastocysts,[261] two-step-cryopreserved oyster oocytes[262] and equine embroys using various AFPs.[263] Freezing of red blood cells in the presence of glycerol with AFPs (at concentrations between 25 and 1000 μg/mL)[264] and AFGPs (at 40 μg/mL) has been reported to damage cells during cryopreservation.[265] A similar result was also observed during the cryopreservation of hematopoietic cells with AFPs in DMSO.[266] Additionally, cellular damage during cryopreservation with BAs has also been reported with spinach thylakoids,[267] intact rat heart (from cardiac explant)[268] and cardiomyocytes.[269] This damage has been attributed to the

change in ice crystal morphology that is induced in the presence of BAs (dynamic ice shaping capabilities).[265,269] Furthermore, it has been suggested that BAs may also increase the incidence of intracellular ice formation, thereby decreasing cell viabilities post-thaw.[270] Finally, reports have demonstrated both beneficial and detrimental effects with BAs during cryopreservation depending upon AFP concentration and type.[271] At low concentrations AFPs were reported to increase the survival rate of red blood cells however, at higher concentrations at which the ice recrystallization inhibition ability of the AFP was significantly enhanced, they decreased survival rates.[272,273]

In contrast to native biological antifreezes, the benefit of *C*-linked AFGP analogues possessing "custom-tailored" antifreeze activity for cryopreservation has been demonstrated. As described earlier, these analogues exhibit potent IRI activity but not TH activity (**5** and **6**, figure 1.9, section 1.3.1) and can function as effective cryoprotectants. Using a human embryonic liver cell line, 1.0-1.5 mg/mL of **5** or **6** doubled cell viability relative to the negative control (cell medium only).[274] The post-thaw viability was comparable to that obtained with a 2.5% DMSO solution. This effect was attributed to the IRI activity of these *C*-linked AFGP analogues. This conclusion was validated when it was demonstrated that IRI active carbohydrates exhibiting minimal cytotoxicity significantly increased cell viabilities post-thaw.[187] To date, these are the only examples where potent inhibitors of ice recrystallization not displaying thermal hysteresis activity or dynamic ice shaping capabilities have been successfully utilized as cryoprotectants.

Simple carbohydrates have been explored as cryoprotectants as alternatives to DMSO or glycerol as they exhibit little or no cytotoxicity. They resemble polyhydric alcohols such as glycerol or 1,2-propanediol, which influence the structure of surrounding water and ice formation.[275] However, conflicting results for the effectiveness of carbohydrates as cryoprotectants have been reported. Post-thaw cell viabilities have been increased with the use of carbohydrates,[276-279] which have been used in combinations with DMSO,[278,280-285] glycerol[286,287] and 1,2-propanediol.[288] This increase has been found to be dependent upon the structure of the carbohydrate used.[289-291] In contrast, the addition of carbohydrates to the cryoprotective media has failed to provide any added benefit or has been detrimental by significantly decreasing post-thaw cell viabilities.[292,293] Further complications arise as different cell types, various cooling rates and a wide range of carbohydrate concentrations are used in these studies. Additionally, carbohydrates are often added to cryopreservation solutions, but their effect is often not evaluated.[294,295]

1.4.5 Summary of Cryopreservation and its Limitations

Cryopreservation is currently the only technique available for the efficient long-term storage of precious cell types for regenerative medicine and transfusion medicine applications. While current conventional cryoprotectants such as DMSO and glycerol mitigate cellular damage and increase post-thaw cell viabilities, current cryopreservation protocols are significantly limited. This is mostly due to the significant toxic effects exhibited by conventional cryoprotectants both *in vitro* and in a clinical setting.[235-239] Thus, improvements in cryopreservation protocols are urgently required to reduce or eliminate the use of DMSO or glycerol cryoprotectants. As a major contributor to cellular injury and death during cryopreservation is attributed to the formation and growth of ice, compounds capable of inhibiting this process have tremendous potential as cryoprotectants. In particular, there is increasing interest in designing small molecule ice recrystallization inhibitors that can overcome the limitations of large peptides and glycopeptides that can be complicated and time consuming to produce. Overall, the design and study of novel IRI active compounds will facilitate a better understanding of how compounds inhibit this process, and will allow for the development of novel cryoprotectants that can improve upon current cryopreservation protocols that are limited in terms of the commonly used cryoprotectants, DMSO and glycerol.

1.5 References

1. Doherty, R.D.; Hughes, D.A.; Humphreys, F.J.; Jonas, J.J.; Jensen, D.J.; Kassner, M.E.; King, W.E.; McNelley, T.R.; McQueen, H.J.; Rollett, A.D. *Mater. Sci. Eng. A.* **1997**, *A238*, 219-274.

2. Rios, P.R.; Siciliano, F.J.; Sandim, H.R.Z.; Plaut, R.L.; Padilha, A.F. *Mater. Res.* **2005**, *8*, 225-238.

3. Gleiter, H. *Acta Metall.* **1969**, *17*, 565-573.

4. Goff, H.D. *Food Res. Int.* **1994**, *27*, 187-189.

5. Venketesh, S.; Dayananda, C. *Crit. Rev. Biotechnol.* **2008**, *28*, 57-82.

6. Petzold, G.; Aguilera, J.M. *Food Biophys.* **2009**, *4*, 378-396.

7. Baust, J.M.; Van Buskirk, R.; Baust, J.G. *In Vitro Cell. Dev. Biol. Anim.* **2000**, *36*, 262-270.

8. Baust, J.M. *Cell Preserv. Technol.* **2002**, *1*, 17-31.

9. Fletcher, N.H. Chapter 2 - Structure and Energry of Ordinary Ice. In: editor. The Chemical Physics of Ice (1st ed.). London: Cambridge University Press; 1970. p 23-48.

10. DeVries, A.L.; Lin, Y. *Biochim. Biophys. Acta.* **1977**, *495*, 388-392.

11. Harding, M.M.; Ward, L.G.; Haymet, A.D.J. *Eur. J. Biochem.* **1999**, *264*, 653-665.

12. Hayward, J.A.; Haymet, A.D.J. *J. Chem. Phys.* **2001**, *114*, 3713-3726.

13. Harding, M.M.; Anderberg, P.I.; Haymet, A.D.J. *Eur. J. Biochem.* **2003**, *270*, 1381-1392.

14. Fletcher, N.H. *Philos. Mag.* **1962**, *7*, 255-269.

15. Fletcher, N.H. *Philos. Mag.* **1968**, *18*, 1287 - 1300.

16. Karim, O.A.; Haymet, A.D.J. *Chem. Phys. Lett.* **1987**, *138*, 531-534.

17. Karim, O.A.; Haymet, A.D.J. *J. Chem. Phys.* **1988**, *89*, 6889-6896.

18. Furukawa, Y.; Yamamoto, M.; Kuroda, T. *J. Cryst. Growth.* **1987**, *82*, 665-677.

19. Furukawa, Y.; Ishikawa, I. *J. Cryst. Growth.* **1993**, *128*, 1137-1142.

20. Beaglehole, D.; Nason, D. *Surf. Sci.* **1980**, *96*, 357-363.

21. Döppenschmidt, A.; Butt, H.-J. *Langmuir.* **2000**, *16*, 6709-6714.

22. Dosch, H.; Lied, A.; Bilgram, J.H. *Surf. Sci.* **1996**, *366*, 43-50.

23. Sadtchenko, V.; Ewing, G.E. *J. Chem. Phys.* **2002**, *116*, 4686-4697.

24. Golecki, I.; Jaccard, C. *J. Phys. C Solid State.* **1978**, *11*, 4229-4237.

25. Kahan, T.F.; Reid, J.P.; Donaldson, D.J. *J. Phys. Chem. A.* **2007**, *111*, 11006-11012.

26. Kaverin, A.; Tsionsky, V.; Zagidulin, D.; Daikhin, L.; Alengoz, E.; Gileadi, E. *J. Phys. Chem. B.* **2004**, *108*, 8759-8762.

27. Güttinger, H.; Bilgram, J.H.; Känzig, W. *J. Phys. Chem. Solids.* **1979**, *40*, 55-66.

28. Brown, R.A.; Keizer, J.; Steiger, U.; Yeh, Y. *J. Phys. Chem.* **1983**, *87*, 4135-4138.

29. Bilgram, J.H. *Phys. Rep.* **1987**, *153*, 1-89.

30. Bluhm, H.; Ogletree, D.F.; Fadley, C.S.; Hussain, Z.; Salmeron, M. *J. Phys.: Condens. Matter.* **2002**, *14*, L227-L233.

31. Beaglehole, D.; Wilson, P. *J. Phys. Chem.* **1993**, *97*, 11053-11055.

32. Beaglehole, D.; Wilson, P. *J. Phys. Chem.* **1994**, *98*, 8096-8100.

33. Elbaum, M.; Lipson, S.G.; Dash, J.G. *J. Cryst. Growth.* **1993**, *129*, 491-505.

34. Gilpin, R.R. *J. Colloid Interface Sci.* **1980**, *77*, 435-448.

35. Karim, O.A.; Kay, P.A.; Haymet, A.D.J. *J. Chem. Phys.* **1990**, *92*, 4634-4635.

36. Halter, P.U.; Bilgram, J.H.; Känzig, W. *J. Chem. Phys.* **1988**, *89*, 2622-2629.

37. Bilgram, J.H. *Prog. Cryst. Growth Charact. Mater.* **1993**, *26*, 99-119.

38. Knight, C.A. *J. Appl. Phys.* **1966**, *37*, 568-574.

39. Knight, C.A.; Wen, D.; Laursen, R.A. *Cryobiology.* **1995**, *32*, 23-34.

40. Alley, R.B.; Perepezko, J.H.; Bentley, C.R. *J. Glaciol.* **1986**, *32*, 415-424.

41. Alley, R.B.; Perepezko, J.H.; Bentley, C.R. *J. Glaciol.* **1986**, *32*, 425-433.

42. Sutton, R.L.; Lips, A.; Piccirillo, G.; Sztehlo, A. *J. Food Sci.* **1996**, *61*, 741-745.

43. Hagiwara, T.; Hartel, R.; Matsukawa, S. *Food Biophys.* **2006**, *1*, 74-82.

44. Budke, C.; Heggemann, C.; Koch, M.; Sewald, N.; Koop, T. *J. Phys. Chem. B.* **2009**, *113*, 2865-2873.

45. Scholander, P.F.; van Dam, L.; Kanwisher, J.W.; Hammel, H.T.; Gordon, M.S. *J. Cell. Compar. Physiol.* **1957**, *49*, 5-24.

46. Gordon, M.S.; Amdur, B.H.; Scholander, P.F. *Biol. Bull.* **1962**, *122*, 52-62.

47. DeVries, A.L.; Wohlschlag, D.E. *Science.* **1969**, *163*, 1073-1075.

48. DeVries, A.L.; Komatsu, S.K.; Feeney, R.E. *J. Biol. Chem.* **1970**, *245*, 2901-2908.

49. DeVries, A.L. *Science*. **1971**, *172*, 1152-1155.

50. Garner, J.; Harding, M.M. *ChemBioChem*. **2010**, *11*, 2489-2498.

51. Peltier, R.; Brimble, M.A.; Wojnar, J.M.; Williams, D.E.; Evans, C.W.; DeVries, A.L. *Chem. Sci*. **2010**, *1*, 538-551.

52. Gibson, M.I.; Barker, C.A.; Spain, S.G.; Albertin, L.; Cameron, N.R. *Biomacromolecules*. **2009**, *10*, 328-333.

53. Capicciotti, C.J.; Doshi, M.; Ben, R.N. Ice Recrystallization Inhibitors: From Biological Antifreezes to Small Molecules. In: P. Wilson, editor. Recent Developments in the Study of Recrystallization ed.). New York: InTech; 2013. p 177-224.

54. Raymond, J.A.; DeVries, A.L. *Proc. Natl. Acad. Sci. U.S.A*. **1977**, *74*, 2589-2593.

55. Knight, C.A.; DeVries, A.L. *J. Cryst. Growth*. **1994**, *143*, 301-310.

56. Wilson, P.W. *Cryoletters*. **1993**, *14*, 31-36.

57. Knight, C.A.; Cheng, C.C.; DeVries, A.L. *Biophys. J*. **1991**, *59*, 409-418.

58. Knight, C.A.; Driggers, E.; DeVries, A.L. *Biophys. J*. **1993**, *64*, 252-259.

59. Carpenter, J.F.; Hansen, T.N. *Proc. Natl. Acad. Sci. U.S.A*. **1992**, *89*, 8953-8957.

60. Chao, H.; Davies, P.L.; Carpenter, J.F. *J. Exp. Biol*. **1996**, *199*, 2071-2076.

61. Rubinsky, B.; Arav, A.; DeVries, A.L. *Cryobiology*. **1992**, *29*, 69-79.

62. Wang, T.; Zhu, Q.; Yang, X.; Layne, J.R.J.; DeVries, A.L. *Cryobiology*. **1994**, *31*, 185-192.

63. Liu, S.; Ben, R.N. *Org. Lett*. **2005**, *7*, 2385-2388.

64. Czechura, P.; Tam, R.Y.; Dimitrijevic, E.; Murphy, A.V.; Ben, R.N. *J. Am. Chem. Soc*. **2008**, *130*, 2928-2929.

65. Capicciotti, C.J.; Leclère, M.; Perras, F.A.; Bryce, D.L.; Paulin, H.; Harden, J.; Liu, Y.; Ben, R.N. *Chem. Sci*. **2012**, *3*, 1408-1416.

66. Ewart, K.V.; Lin, Q.; Hew, C.L. *Cell. Mol. Life Sci*. **1999**, *55*, 271-283.

67. Jia, Z.; Davies, P.L. *Trends Biochem. Sci*. **2002**, *27*, 101-106.

68. Fletcher, G.L.; Hew, C.L.; Davies, P.L. *Annu. Rev. Physiol*. **2001**, *63*, 359-390.

69. Davies, P.L.; Sykes, B.D. *Curr. Opin. Struct. Biol*. **1997**, *7*, 828-834.

70. Hew, C.L.; Yang, D.S.C. *Eur. J. Biochem*. **1992**, *203*, 33-42.

71. Duman, J.G.; DeVries, A.L. *Comp. Biochem. Physiol. B: Comp. Biochem*. **1976**, *54*, 375-380.

72. Duman, J.G.; DeVries, A.L. *Nature*. **1974**, *247*, 237-238.

73. Ananthanarayanan, V.S.; Hew, C.L. *Biochem. Biophys. Res. Commun*. **1977**, *74*, 685-689.

74. Yang, D.S.C.; Sax, M.; Chakrabartty, A.; Hew, C.L. *Nature*. **1988**, *333*, 232-237.

75. Raymond, J.A.; Radding, W.; DeVries, A.L. *Biopolymers*. **1977**, *16*, 2575-2578.

76. Cheng, Y.; Yang, Z.; Tan, H.; Liu, R.; Chen, G.; Jia, Z. *Biophys. J*. **2002**, *83*, 2202-2210.

77. Baardsnes, J.; Davies, P.L. *Biochim. Biophys. Acta: Proteins Proteom*. **2002**, *1601*, 49-54.

78. Sönnichsen, F.D.; DeLuca, C.I.; Davies, P.L.; Sykes, B.D. *Structure*. **1996**, *4*, 1325-1337.

79. Madura, J.D.; Taylor, M.S.; Wierzbicki, A.; Harrington, J.P.; Sikes, C.S.; Sönnichsen, F. *J. Mol. Struct.-THEOCHEM*. **1996**, *388*, 65-77.

80. Miura, K.; Ohgiya, S.; Hoshino, T.; Nemoto, N.; Odaira, M.; Nitta, R.; Tsuda, S. *J. Biochem.* **1999**, *126*, 387-394.

81. Slaughter, D.; Fletcher, G.L.; Ananthanarayanan, V.S.; Hew, C.L. *J. Biol. Chem.* **1981**, *256*, 2022-2026.

82. Sönnichsen, F.D.; Sykes, B.D.; Davies, P.L. *Protein Sci.* **1995**, *4*, 460-471.

83. Ng, N.F.; Trinh, K.Y.; Hew, C.L. *J. Biol. Chem.* **1986**, *261*, 15690-15695.

84. Ng, N.F.; Hew, C.L. *J. Biol. Chem.* **1992**, *267*, 16069-16075.

85. DeLuca, C.I.; Davies, P.L.; Ye, Q.; Jia, Z. *J. Mol. Biol.* **1998**, *275*, 515-525.

86. Jia, Z.; Deluca, C.I.; Davies, P.L. *Protein Sci.* **1995**, *4*, 1236-1238.

87. Hew, C.L.; Slaughter, D.; Joshi, S.B.; Fletcher, G.L.; Ananthanarayanan, V.S. *J. Comp. Physiol. B.* **1984**, *155*, 81-88.

88. Schrag, J.D.; Cheng, C.-H.C.; Panico, M.; Morris, H.R.; DeVries, A.L. *Biochim. Biophys. Acta.* **1987**, *915*, 357-370.

89. Sönnichsen, F.D.; Sykes, B.D.; Chao, H.; Davies, P.L. *Science.* **1993**, *259*, 1154-1157.

90. Xue, Y.Q.; Sicheri, F.; Ala, P.; Hew, C.L.; Yang, D.S.C. *J. Mol. Biol.* **1994**, *237*, 351-352.

91. Deng, G.; Andrews, D.W.; Laursen, R.A. *FEBS Lett.* **1997**, *402*, 17-20.

92. Deng, G.; Laursen, R.A. *Biochim. Biophys. Acta.* **1998**, *1388*, 305-314.

93. Cheng, C.-H.C. *Curr. Opin. Genet. Dev.* **1998**, *8*, 715-720.

94. Komatsu, S.K.; DeVries, A.L.; Feeney, R.E. *J. Biol. Chem.* **1970**, *245*, 2909-2913.

95. DeVries, A.L.; Vandenheede, J.; Feeney, R.E. *J. Biol. Chem.* **1971**, *246*, 305-308.

96. Feeney, R.E.; Burcham, T.S.; Yeh, Y. *Annu. Rev. Biophys. Biophys. Chem.* **1986**, *15*, 59-78.

97. Bouvet, V.; Ben, R.N. *Cell Biochem. Biophys.* **2003**, *39*, 133-144.

98. Gibson, M.I. *Polym. Chem.* **2010**, *1*, 1141-1152.

99. Lin, Y.; Duman, J.G.; DeVries, A.L. *Biochem. Biophys. Res. Commun.* **1972**, *46*, 87-92.

100. Hew, C.L.; Slaughter, D.; Fletcher, G.L.; Joshi, S.B. *Can. J. Zool.* **1981**, *59*, 2186-2192.

101. Burcham, T.S.; Osuga, D.T.; Rao, B.N.; Bush, C.A.; Feeney, R.E. *J. Biol. Chem.* **1986**, *261*, 6384-6389.

102. Geoghegan, K.F.; Osuga, D.T.; Ahmed, A.I.; Yeh, Y.; Feeney, R.E. *J. Biol. Chem.* **1980**, *255*, 663-667.

103. O'Grady, S.M.; Schrag, J.D.; Raymond, J.A.; Devries, A.L. *J. Exp. Zool.* **1982**, *224*, 177-185.

104. Fletcher, G.L.; Hew, C.L.; Joshi, S.B. *Can. J. Zool.* **1982**, *60*, 348-355.

105. Franks, F.; Morris, E.R. *Biochim. Biophys. Acta.* **1978**, *540*, 346-356.

106. Bush, C.A.; Feeney, R.E.; Osuga, D.T.; Ralapati, S.; Yeh, Y.I.N. *Int. J. Pept. Protein Res.* **1981**, *17*, 125-129.

107. Ahmed, A.I.; Feeney, R.E.; Osuga, D.T.; Yeh, Y. *J. Biol. Chem.* **1975**, *250*, 3344-3347.

108. Berman, E.; Allerhand, A.; DeVries, A.L. *J. Biol. Chem.* **1980**, *255*, 4407-4410.

109. Lane, A.N.; Hays, L.M.; Crowe, L.M.; Crowe, J.H.; Feeney, R.E. *Protein Sci.* **1998**, *7*, 1555-1563.

110. Tsvetkova, N.M.; Phillips, B.L.; Krishnan, V.V.; Feeney, R.E.; Fink, W.H.; Crowe, J.H.; Risbud, S.H.; Tablin, F.; Yeh, Y. *Biophys. J.* **2002**, *82*, 464-473.

111. Bush, C.A.; Feeney, R.E. *Int. J. Pept. Protein Res.* **1986**, *28*, 386-397.

112. Bush, C.A.; Ralapati, S.; Matson, G.M.; Yamasaki, R.B.; Osuga, D.T.; Yeh, Y.; Feeney, R.E. *Arch. Biochem. Biophys.* **1984**, *232*, 624-631.

113. Rao, B.N.N.; Bush, C.A. *Biopolymers.* **1987**, *26*, 1227-1244.

114. Tyshenko, M.G.; Doucet, D.; Davies, P.L.; Walker, V.K. *Nat. Biotechnol.* **1997**, *15*, 887-890.

115. Hew, C.L.; Kao, M.H.; So, Y.-P.; Lim, K.-P. *Can. J. Zool.* **1983**, *61*, 2324-2328.

116. Graham, L.A.; Liou, Y.-C.; Walker, V.K.; Davies, P.L. *Nature.* **1997**, *388*, 727-728.

117. Schneppenheim, R.; Theede, H. *Comp. Biochem. Physiol. B: Comp. Biochem.* **1980**, *67*, 561-568.

118. Duman, J.G.; Li, N.; Verleye, D.; Goetz, F.W.; Wu, D.W.; Andorfer, C.A.; Benjamin, T.; Parmelee, D.C. *J. Comp. Physiol. B.* **1998**, *168*, 225-232.

119. Graham, L.A.; Davies, P.L. *Science.* **2005**, *310*, 461.

120. Smallwood, M.; Worrall, D.; Byass, L.; Elias, L.; Ashford, D.; Doucet, C.J.; Holt, C.; Telford, J.; Lillford, P.; Bowles, D.J. *Biochem. J.* **1999**, *340*, 385-391.

121. Huang, T.; Nicodemus, J.; Zarka, D.G.; Thomashow, M.F.; Wisniewski, M.; Duman, J.G. *Plant Mol. Biol.* **2002**, *50*, 333-344.

122. Sidebottom, C.; Buckley, S.; Pudney, P.; Twigg, S.; Jarman, C.; Holt, C.; Telford, J.; McArthur, A.; Worrall, D.; Hubbard, R.; Lillford, P. *Nature.* **2000**, *406*, 256.

123. Pudney, P.D.A.; Buckley, S.L.; Sidebottom, C.M.; Twigg, S.N.; Sevilla, M.-P.; Holt, C.B.; Roper, D.; Telford, J.H.; McArthur, A.J.; Lillford, P.J. *Arch. Biochem. Biophys.* **2003**, *410*, 238-245.

124. Kumble, K.D.; Demmer, J.; Fish, S.; Hall, C.; Corrales, S.; DeAth, A.; Elton, C.; Prestidge, R.; Luxmanan, S.; Marshall, C.J.; Wharton, D.A. *Cryobiology.* **2008**, *57*, 263-268.

125. John, U.P.; Polotnianka, R.M.; Sivakumaran, K.A.; Chew, O.; Mackin, L.; Kuiper, M.J.; Talbot, J.P.; Nugent, G.D.; Mautord, J.; Schrauf, G.E.; Spangenberg, G.C. *Plant Cell Environ.* **2009**, *32*, 336-348.

126. Hon, W.C.; Griffith, M.; Mlynarz, A.; Kwok, Y.C.; Yang, D. *Plant Physiol.* **1995**, *109*, 879-889.

127. Tremblay, K.; Ouellet, F.; Fournier, J.; Danyluk, J.; Sarhan, F. *Plant Cell Physiol.* **2005**, *46*, 884-891.

128. Duman, J.G.; Olsen, T.M. *Cryobiology.* **1993**, *30*, 322-328.

129. Hoshino, T.; Kiriaki, M.; Nakajima, T. *Cryoletters.* **2003**, *24*, 135-142.

130. Gilbert, J.A.; Davies, P.L.; Laybourn-Parry, J. *FEMS Microbiol. Lett.* **2005**, *245*, 67-72.

131. Sun, X.; Griffith, M.; Pasternak, J.J.; Glick, B.R. *Can. J. Microbiol.* **1995**, *41*, 776-784.

132. Yamashita, Y.; Nakamura, N.; Omiya, K.; Nishikawa, J.; Kawahara, H.; Obata, H. *Biosci. Biotechnol. Biochem.* **2002**, *66*, 239-247.

133. Kawahara, H.; Nakano, Y.; Omiya, K.; Muryoi, N.; Nishikawa, J.; Obata, H. *J. Biosci. Bioeng.* **2004**, *98*, 220-223.

134. Graether, S.P.; Kuiper, M.J.; Gagné, S.M.; Walker, V.K.; Jia, Z.; Sykes, B.D.; Davies, P.L. *Nature*. **2000**, *406*, 325-328.

135. Liou, Y.-C.; Tocilj, A.; Davies, P.L.; Jia, Z. *Nature*. **2000**, *406*, 322-324.

136. Chakrabartty, A.; Hew, C.L. *Eur. J. Biochem*. **1991**, *202*, 1057-1063.

137. Knight, C.A.; Hallett, J.; DeVries, A.L. *Cryobiology*. **1988**, *25*, 55-60.

138. Tomczak, M.M.; Marshall, C.B.; Gilbert, J.A.; Davies, P.L. *Biochem. Biophys. Res. Commun*. **2003**, *311*, 1041-1046.

139. Yu, S.O.; Brown, A.; Middleton, A.J.; Tomczak, M.M.; Walker, V.K.; Davies, P.L. *Cryobiology*. **2010**, *61*, 327-334.

140. Yagci, Y.E.; Antonietti, M.; Börner, H.G. *Macromol. Rapid Commun*. **2006**, *27*, 1660-1664.

141. Baruch, E.; Mastai, Y. *Macromol. Rapid Commun*. **2007**, *28*, 2256-2261.

142. Mastai, Y.; Rudloff, J.; Cölfen, H.; Antonietti, M. *ChemPhysChem*. **2002**, *3*, 119-123.

143. Jackman, J.; Noestheden, M.; Moffat, D.; Pezacki, J.P.; Findlay, S.; Ben, R.N. *Biochem. Biophys. Res. Commun*. **2007**, *354*, 340-344.

144. Wilson, P.W.; Beaglehole, D.; DeVries, A.L. *Biophys. J*. **1993**, *64*, 1878-1884.

145. Raymond, J.A.; Wilson, P.; DeVries, A.L. *Proc. Natl. Acad. Sci. U.S.A*. **1989**, *86*, 881-885.

146. Knight, C.A.; DeVries, A.L.; Oolman, L.D. *Nature*. **1984**, *308*, 295-296.

147. DeVries, A.L. *Comp. Biochem. Physiol. B: Comp. Biochem*. **1988**, *90*, 611-621.

148. Scotter, A.J.; Marshall, C.B.; Graham, L.A.; Gilbert, J.A.; Garnham, C.P.; Davies, P.L. *Cryobiology*. **2006**, *53*, 229-239.

149. Yeh, Y.; Feeney, R.E. *Chem. Rev*. **1996**, *96*, 601-618.

150. Wierzbicki, A.; Taylor, M.S.; Knight, C.A.; Madura, J.D.; Harrington, J.P.; Sikes, C.S. *Biophys. J*. **1996**, *71*, 8-18.

151. Chao, H.; Houston, M.E.; Hodges, R.S.; Kay, C.M.; Sykes, B.D.; Loewen, M.C.; Davies, P.L.; Sönnichsen, F.D. *Biochemistry*. **1997**, *36*, 14652-14660.

152. Haymet, A.D.J.; Ward, L.G.; Harding, M.M.; Knight, C.A. *FEBS Lett*. **1998**, *430*, 301-306.

153. Zhang, W.; Laursen, R.A. *J. Biol. Chem*. **1998**, *273*, 34806-34812.

154. Baardsnes, J.; Kondejewski, L.H.; Hodges, R.S.; Chao, H.; Kay, C.; Davies, P.L. *FEBS Lett*. **1999**, *463*, 87-91.

155. Marshall, C.B.; Daley, M.E.; Graham, L.A.; Sykes, B.D.; Davies, P.L. *FEBS Lett*. **2002**, *529*, 261-267.

156. Davies, P.L.; Baardsnes, J.; Kuiper, M.J.; Walker, V.K. *Philos. Trans. R. Soc. London, Ser. B*. **2002**, *357*, 927-935.

157. Doxey, A.C.; Yaish, M.W.; Griffith, M.; McConkey, B.J. *Nat. Biotechnol*. **2006**, *24*, 852-855.

158. Tachibana, Y.; Fletcher, G.L.; Fujitani, N.; Tsuda, S.; Monde, K.; Nishimura, S.-I. *Angew. Chem. Int. Ed*. **2004**, *43*, 856-862.

159. Wilkinson, B.L.; Stone, R.S.; Capicciotti, C.J.; Thaysen-Andersen, M.; Matthews, J.M.; Packer, N.H.; Ben, R.N.; Payne, R.J. *Angew. Chem. Int. Ed*. **2012**, *51*, 3606-3610.

160. Inada, T.; Lu, S.-S. *Chem. Phys. Lett*. **2004**, *394*, 361-365.

161. Budke, C.; Koop, T. *ChemPhysChem*. **2006**, *7*, 2601-2606.

162. Miller, N.; Williams, G.M.; Brimble, M.A. *Org. Lett*. **2009**, *11*, 2409-2412.

163. Peltier, R.; Evans, C.W.; DeVries, A.L.; Brimble, M.A.; Dingley, A.J.; Williams, D.E. *Cryst. Growth Des*. **2010**, *10*, 5066-5077.

164. Heggemann, C.; Budke, C.; Schomburg, B.; Majer, Z.; Wißbrock, M.; Koop, T.; Sewald, N. *Amino Acids*. **2010**, *38*, 213-222.

165. Norgren, A.S.; Budke, C.; Majer, Z.; Heggemann, C.; Koop, T.; Sewald, N. *Synthesis*. **2009**, *2009*, 488-494.

166. Capicciotti, C.J.; Trant, J.F.; Leclère, M.; Ben, R.N. *Bioconjugate Chem*. **2011**, *22*, 605-616.

167. Eniade, A.; Purushotham, M.; Ben, R.N.; Wang, J.B.; Horwath, K. *Cell Biochem. Biophys*. **2003**, *38*, 115-124.

168. Ben, R.N.; Eniade, A.A.; Hauer, L. *Org. Lett*. **1999**, *1*, 1759-1762.

169. Galema, S.A.; Engberts, J.B.F.N.; Hoeiland, H.; Foerland, G.M. *J. Phys. Chem*. **1993**, *97*, 6885-6889.

170. Galema, S.A.; Høiland, H. *J. Phys. Chem*. **1991**, *95*, 5321-5326.

171. Galema, S.A.; Howard, E.; Engberts, J.B.F.N.; Grigera, J.R. *Carbohydr. Res*. **1994**, *265*, 215-225.

172. Tam, R.Y.; Ferreira, S.S.; Czechura, P.; Chaytor, J.L.; Ben, R.N. *J. Am. Chem. Soc*. **2008**, *130*, 17494-17501.

173. Tam, R.Y.; Rowley, C.N.; Petrov, I.; Zhang, T.; Afagh, N.A.; Woo, T.K.; Ben, R.N. *J. Am. Chem. Soc*. **2009**, *131*, 15745-15753.

174. Inada, T.; Lu, S.-S. *Cryst. Growth Des*. **2003**, *3*, 747-752.

175. Horng, J.-C.; Raines, R.T. *Protein Sci*. **2006**, *15*, 74-83.

176. Stokes, R.H.; Robinson, R.A. *J. Phys. Chem*. **1966**, *70*, 2126-2131.

177. Suggett, A.; Ablett, S.; Lillford, P.J. *J. Solution Chem*. **1976**, *5*, 17-31.

178. Tait, M.J.; Suggett, A.; Franks, F.; Ablett, S.; Quickenden, P.A. *J. Solution Chem*. **1972**, *1*, 131-151.

179. Uedaira, H.; Uedaira, H. *J. Solution Chem*. **1985**, *14*, 27-34.

180. Kabayama, M.A.; Patterson, D.; Piche, L. *Can. J. Chem*. **1958**, *36*, 557-562.

181. Walkinshaw, M.D. *J. Chem. Soc. Perkin Trans. 2*. **1987**, 1903-1906.

182. Miyajima, K.; Machida, K.; Nakagaki, M. *Bull. Chem. Soc. Jpn*. **1985**, *58*, 2595-2599.

183. Franks, F. *Cryobiology*. **1983**, *20*, 335-345.

184. Suggett, A. *J. Solution Chem*. **1976**, *5*, 33-46.

185. Danford, M.D.; Levy, H.A. *J. Am. Chem. Soc*. **1962**, *84*, 3965-3966.

186. Warner, D.T. *Nature*. **1962**, *196*, 1055-1058.

187. Chaytor, J.L.; Tokarew, J.M.; Wu, L.K.; Leclère, M.; Tam, R.Y.; Capicciotti, C.J.; Guolla, L.; von Moos, E.; Findlay, C.S.; Allan, D.S.; Ben, R.N. *Glycobiology*. **2012**, *22*, 123-133.

188. Mazur, P. Life in the Frozen State - Principles of Cryobiology (Boca Baton, FL: CRC Press; 2004.

189. Acker, J.P.; McGann, L.E. *Cell Transplant*. **2002**, *11*, 563-571.

190. Mazur, P.C. *Science*. **1970**, *168*, 939-949.

191. Mazur, P. *Am. J. Physiol. - Cell Physiol*. **1984**, *247*, C125-C142.

192. Fowler, A.; Toner, M. *Ann. N.Y. Acad. Sci*. **2005**, *1066*, 119-135.

193. Leclère, M.; Kwok, B.K.; Wu, L.K.; Allan, D.S.; Ben, R.N. *Bioconjugate Chem*. **2011**, *22*, 1804-1810.

194. Holovati, J.L.; Hannon, J.L.; Gyongyossy-Issa, M.I.C.; Acker, J.P. *Transfus. Med. Rev*. **2009**, *23*, 25-41.

195. Kanias, T.; Acker, J.P. *FEBS J*. **2010**, *277*, 343-356.

196. Scott, K.L.; Lecak, J.; Acker, J.P. *Transfus. Med. Rev*. **2005**, *19*, 127-142.

197. Buskirk, R.G.V.; Baust, J.M.; Snyder, K.K.; Mathew, A.J.; Baust, J.G. *Bioprocess Int*. **2004**, *2*, 42-49.

198. Baust, J.G.; Gao, D.; Baust, J.M. *Organogenesis*. **2009**, *5*, 90-96.

199. Baust, J.M.; Buskirk, R.V.; Baust, J.G. *Cell Preserv. Technol*. **2002**, *1*, 63-80.

200. Meryman, H.T. *Transfusion*. **2007**, *47*, 935-945.

201. Bakhach, J. *Organogenesis*. **2009**, *5*, 119-126.

202. Fahy, G.M. *Cryobiology*. **2005**, *51*, 348-349.

203. Fahy, G.M.; Levy, D.I.; Ali, S.E. *Cryobiology*. **1987**, *24*, 196-213.

204. Fahy, G.M.; MacFarlane, D.R.; Angell, C.A.; Meryman, H.T. *Cryobiology*. **1984**, *21*, 407-426.

205. Macfarlane, D.R. *Cryobiology*. **1986**, *23*, 230-244.

206. Jurisicova, A.; Varmuza, S.; Casper, R.F. *Hum. Reprod. Update*. **1995**, *1*, 558-566.

207. Mazur, P.; Leibo, S.P.; Chu, E.H.Y. *Exp. Cell Res*. **1972**, *71*, 345-355.

208. Hobbs, P.V. Ice Physics (1st ed.). Oxford: Oxford University Press, USA; 1975.

209. Pegg, D.E.; Diaper, M.P. *Cryobiology*. **1991**, *28*, 18-35.

210. Pegg, D.E.; Diaper, M.P. *Biophys. J*. **1988**, *54*, 471-488.

211. Lovelock, J.E. *Proc. R. Soc. Lond. B. Biol. Sci*. **1957**, *147*, 427-433.

212. Leibo, S.P.; Mazur, P. *Cryobiology*. **1971**, *8*, 447-452.

213. Mazur, P. *J. Gen. Physiol*. **1963**, *47*, 347-369.

214. Karlsson, J.O.; Cravalho, E.G.; Borel Rinkes, I.H.; Tompkins, R.G.Y., M. L.; Toner, M. *Biophys. J*. **1993**, *65*, 2524-2536.

215. Toner, M.; Caravalho, E.G.; Karel, M. *J. Appl. Phys*. **1990**, *67*, 1582-1593.

216. Muldrew, K.; McGann, L.E. *Biophys. J*. **1990**, *57*, 525-532.

217. Mazur, P. *Cell Biophys*. **1990**, *17*, 53-92.

218. Fowler, A.; Toner, M. *Ann. N.Y. Acad. Sci*. **1998**, *858*, 245-252.

219. Farrant, J.; Molyneux, P.; Hasted, J.B.; Peares, P.; Echlin, P. *Philos. Trans. R. Soc. London B*. **1977**, *278*, 191-205.

220. McGann, L.E. *Cryobiology*. **1978**, *15*, 382-390.

221. Meryman, H.T. *Cryobiology*. **1971**, *8*, 173-183.

222. Lovelock, J.E. *Biochim. Biophys. Acta*. **1953**, *11*, 28-36.

223. Lovelock, J.E. *Biochem. J*. **1954**, *56*, 265-270.

224. Meryman, H.T. *Annu. Rev. Biophys. Bioeng*. **1974**, *3*, 341-363.

225. Song, Y.C.; Khirabadi, B.S.; Lightfoot, F.; Brockbank, K.G.M.; Taylor, M.J. *Nat. Biotechnol*. **2000**, *18*, 296-299.

226. Scheinkonig, C.; Kappicht, S.; Kolb, H.J.; Schleuning, M. *Bone Marrow Transplant*. **2004**, *34*, 531-536.

227. Topacoglu, H.; Karcioglu, O.; Ozsarac, M.; Oray, D.; Niyazi Ozucelik, D.; Tuncok, Y. *Vet. Hum. Toxicol*. **2004**, *46*, 138-140.

228. Hallare, A.V.; Köhler, H.R.; Triebskorn, R. *Chemosphere*. **2004**, *56*, 659-666.

229. Rapatz, G.; Sullivan, J.J.; Luyet, B. *Cryobiology*. **1968**, *5*, 18-25.

230. Anchordoguy, T.J.; Rudolph, A.S.; Carpenter, J.F.; Crowe, J.H. *Cryobiology*. **1987**, *24*, 324-331.

231. Crowe, J.H.; Crowe, L.M.; Carpenter, J.F.; Rudolph, A.S.; Wistrom, C.A.; Spargo, B.J.; Anchordoguy, T.J. *Biochim. Biophys. Acta*. **1988**, *947*, 367-384.

232. Hunt, C.J. *Transfus. Med. Hemoth*. **2011**, *38*, 107-123.

233. Harris, D.T. *Br. J. Haematol*. **2009**, *147*, 177-184.

234. Gluckman, E. *Br. J. Haematol*. **2009**, *147*, 192-199.

235. Davis, J.; Rowley, S.; Braine, H.; Piantadosi, S.; Santos, G. *Blood*. **1990**, *75*, 781-786.

236. Berz, D.; McCormack, E.M.; Winer, E.S.; Colvin, G.A.; Quesenberry, P.J. *Am. J. Hematol*. **2007**, *82*, 463-472.

237. Galmes, A.; Gutiérrez, A.; Sampol, A.; Canaro, M.; Morey, M.; Iglesias, J.; Matamoros, N.; Duran, M.A.; Novo, A.; Bea, M.D.; Galán, P.; Balansat, J.; Martínez, J.; Bargay, J.; Besalduch, J. *Haematologica*. **2007**, *92*, 986-989.

238. Greco, N.J.; Seetharaman, S.; Kurtz, J.; Lee, W.R.; Moroff, G. *Stem Cells Dev*. **2006**, *15*, 124-135.

239. Shim, J.-S.; Cho, B.; Kim, M.; Park, G.-S.; Shin, J.-C.; Hwang, H.-K.; Kim, T.-G.; Oh, I.-H. *Br. J. Haematol*. **2006**, *135*, 210-213.

240. Ramsey, G. *Transfusion*. **2008**, *48*, 2053-2055.

241. Högman, C.F. *Vox Sang*. **1998**, *74*, 177-187.

242. Högman, C.F.; Meryman, H.T. *Transfus. Med. Rev*. **1999**, *13*, 275-296.

243. Weinberg, J.A.; McGwin, G.J.; Vandromme, M.J.; Marques, M.B.; Melton, S.M.; Reiff, D.A.; Kerby, J.D.; Rue, L.W.I. *J. Trauma*. **2010**, *69*, 1427-1432.

244. Spinella, P.; Carroll, C.; Staff, I.; Gross, R.; Mc Quay, J.; Keibel, L.; Wade, C.; Holcomb, J. *J. Crit. Care*. **2009**, *13*, R151.

245. Valeri, C.R. *Vox Sang*. **2002**, *83*, 193-196.

246. Hess, J.R. *Transfus. Med*. **2004**, *14*, 1-8.

247. Hess, J.R.; Greenwalt, T.G. *Transfus. Med. Rev*. **2002**, *16*, 283-295.

248. American Association of Blood Banks Technical Manual (Bethesda, MD: American Association of Blood Banks; 2006.

249. Rowe, A.W.; Eyster, E.; Kellner, A. *Cryobiology*. **1968**, *5*, 119-128.

250. Meryman, H.T.; Hornblower, M. *Transfusion*. **1972**, *12*, 145-156.

251. Valeri, C.R.; Ragno, G.; Pivacek, L.E.; Srey, R.; Hess, J.R.; Lippert, L.E.; Mettille, F.; Fahie, R.; O'Neill, E.M.; Szymanski, I.O. *Transfusion*. **2001**, *41*, 933-939.

252. Lelkens, C.C.M.; Noorman, F.; Koning, J.G.; Truijens-de Lange, R.; Stekkinger, P.S.; Bakker, J.C.; Lagerberg, J.W.M.; Brand, A.; Verhoeven, A.J. *Transfusion*. **2003**, *43*, 157-164.

253. Bandarenko, N.; Cancelas, J.; Snyder, E.L.; Hay, S.N.; Rugg, N.; Corda, T.; Joines, A.D.; Gormas, J.F.; Pratt, G.P.; Kowalsky, R.; Rose, M.; Rose, L.; Foley, J.; Popovsky, M.A. *Transfusion*. **2007**, *47*, 680-686.

254. Rubinsky, B.; Arav, A.; DeVries, A.L. *Cryo-letters*. **1991**, *12*, 93-106.

255. Rubinsky, B.; Arav, A.; DeVries, A.L. *Cryobiology*. **1992**, *29*, 69-79.

256. O'Neil, L.; Paynter, S.J.; Fuller, B.J.; Shaw, R.W.; DeVries, A.L. *Cryobiology*. **1998**, *37*, 59-66.

257. Arav, A., Ramsbottom, G., Baguisi, A., Rubinsky, B., Roche, J. F., and Boland, M. P. *Cryobiology*. **1993**, *30*, 621-622.

258. Payne, S.R.; Oliver, J.E.; Upreti, G.C. *Cryobiology*. **1994**, *31*, 180-184.

259. Younis, A.I.; Rooks, B.; Khan, S.; Gould, K.G. *J. Androl*. **1998**, *19*, 207-214.

260. Chen, L.R.; Huang, W.Y.; Luoh, Y.S.; Wu, M.C. *J. Taiwan Livestock Res*. **1995**, *28*, 169-179.

261. Palasz, A.T., Gustafasson, H., Rodriguez-Martinez, H., Gusta, L., Larsson, B., and Mapletoft, R. J. *Cryobiology*. **1995**, *32*, 572-572.

262. Naidenko, T. *Cryo-letters*. **1997**, *18*, 375-382.

263. Lagneaux, D.; Huhtinen, M.; Koskinen, E.; Palmer, E. *Equine Vet. J*. **1997**, *29*, 85-87.

264. Pegg, D.E. *Cryobiology*. **1992**, *29*, 774.

265. Rubinsky, B.; DeVries, A.L. *Cryobiology*. **1989**, *26*, 580.

266. Hansen, T.N.; Smith, K.M.; Brockbank, K.G.M. *Transplant. Proc*. **1993**, *25*, 3182-3184.

267. Hincha, D.K.; DeVries, A.L.; Schmitt, J.M. *Biochim. Biophys. Acta*. **1993**, *1146*, 258-264.

268. Wang, T.; Zhu, Q.; Yang, X.; Layne, J.R.; DeVries, A.L. *Cryobiology*. **1994**, *31*, 185-192.

269. Mugano, J.A.; Wang, T.; Layne, J.R., Jr.,; DeVries, A.L.; Lee, R.E. *Cryobiology*. **1995**, 556-557.

270. Larese, A.; Acker, J.; Muldrew, K.; Yang, H.Y.; McGann, L. *Cryo-letters*. **1996**, *17*, 172-182.

271. Wang, J.H.; Bian, H.W.; Huang, C.N.; Ge, J.G. *Acta Biol. Exp*. **1999**, *32*, 271-276.

272. Carpenter, J.F.; Hansen, T.N. *Proc. Natl. Acad. Sci. U. S. A*. **1992**, *89*, 8953-7.

273. Chao, H.; Davies, P.L.; Carpenter, J.F. *J. Exp. Biol*. **1996**, *199*, 2071-6.

274. Leclère, M.; Kwok, B.K.; Wu, L.K.; Allan, D.S.; Ben, R.N. *Bioconj. Chem*. **2011**, *22*, 1804-1810.

275. Dashnau, J.L.; Vanderkooi, J.M. *J Food Sci*. **2007**, *72*, R001-10.

276. Tao, J.; Du, J.; Kleinhans, F.W.; Critser, E.S.; Mazur, P.; Critser, J.K. *J. Reprod. Fertil.* **1995**, *104*, 231-6.

277. Hossain, A.M.; Osuamkpe, C.O. *Arch. Androl.* **2007**, *53*, 99-103.

278. Eroglu, A.; Bailey, S.E.; Toner, M.; Toth, T.L. *Biol. Reprod.* **2009**, *80*, 70-78.

279. Mondal, B. *Cell Tissue Bank.* **2009**, *10*, 341-344.

280. Vicente, J.S.; Viudes-de-Castro, M.P. *Reprod. Nutr. Dev.* **1996**, *36*, 485-492.

281. Izadyar, F.; Matthijs-Rijsenbilt, J.J.; Den, O.K.; Creemers, L.B.; Woelders, H.; De Rooij, D.G. *J. Androl.* **2002**, *23*, 537-545.

282. Ma, W.; O'Shaughnessy, T.; Chang, E. *Neurosci. Lett.* **2006**, *403*, 84-89.

283. Santos, R.R.; Tharasanit, T.; Figueiredo, J.R.; van Haeften, T.; van den Hurk, R. *Cell Tissue Res.* **2006**, *325*, 523-531.

284. Cui, X.D.; Gao, D.Y.; Fink, B.F.; Vasconez, H.C.; Pu, L.L.Q. *Cryobiology.* **2007**, *55*, 269-278.

285. Petrenko, Y.A.; Jones, D.R.E.; Petrenko, A.Y. *Cryobiology.* **2008**, *57*, 195-200.

286. Gutierrez-Perez, O.; Juarez-Mosqueda, M.d.L.; Carvajal, S.U.; Ortega, M.E.T. *Cryobiology.* **2009**, *58*, 287-292.

287. Hu, J.H.; Li, Q.W.; Jiang, Z.L.; Yang, H.; Zhang, S.S.; Zhao, H.W. *Reprod. Domest. Anim.* **2009**, *44*, 571-575.

288. Coticchio, G.; De, S.L.; Rossi, G.; Borini, A.; Albertini, D.; Scaravelli, G.; Alecci, C.; Bianchi, V.; Nottola, S.; Cecconi, S. *Hum. Reprod.* **2006**, *21*, 1771-1776.

289. Si, W.; Wang, H.; Reid, C.; Hildebrandt, T.B.; Ji, W. *Am. J. Primatol.* **2006**, *68*, 103-108.

290. Yildiz, C.; Kaya, A.; Aksoy, M.; Tekeli, T. *Theriogenology.* **2000**, *54*, 579-85.

291. Yildiz, C.; Ottaviani, P.; Law, N.; Ayearst, R.; Liu, L.; McKerlie, C. *Reproduction.* **2007**, *133*, 585-595.

292. Son, J.H.; Kim, K.-H.; Nam, Y.-K.; Park, J.-K.; Kim, S.-K. *Biotechnol. Lett.* **2004**, *26*, 829-833.

293. Valente, S.S.; Pereira, R.M.; Baptista, M.C.; Marques, C.C.; Vasques, M.I.; Pereira, M.V.C.S.; Horta, A.E.M.; Barbas, J.P. *Anim. Reprod. Sci.* **2010**, *117*, 74-77.

294. Berthelot, F.; Venturi, E.; Cognie, J.; Furstoss, V.; Martinat-Botte, F. *Theriogenology.* **2007**, *68*, 178-185.

295. Borges, E.N.; Silva, R.C.; Futino, D.O.; Rocha-Junior, C.M.C.; Amorim, C.A.; Bao, S.N.; Lucci, C.M. *Cryobiology.* **2009**, *59*, 195-200.

Chapter 2: Goals and Objectives

2.1 Introduction

The development of effective preservation methods that maintain *ex vivo* cell viability and function has played an integral role in both regenerative and transfusion medicine. Currently, cryopreservation remains the only technique for the successful long-term preservation and storage of precious cell types such as HSCs from UCB and RBCs from peripheral for blood transfusions.[1-13] Cryoprotectants are necessary to ensure high cell recoveries and viabilities, with the most commonly used being penetrating cryoprotectants DMSO and glycerol. However, the toxicity of penetrating cryoprotectants, especially DMSO, has been well documented both *in vitro* and in a clinical setting.[14-18] While penetrating cryoprotectants can be removed prior to infusion of the cryopreserved cells, this process is time consuming, expensive, is damaging to the cells and ultimately means the thawed cells are not immediately available for use.[4,19-22] Thus, improvements in current cryopreservation protocols and in conventional cryoprotectants are therefore required to eliminate or reduce the quantity of DMSO or glycerol.

A significant contributor to cellular injury and death during cryopreservation is ice recrystallization.[5,10,11,23,24] Thus, compounds capable of inhibiting ice recrystallization have tremendous potential in the field of cryobiology and cryopreservation. Ice recrystallization inhibition (IRI) activity has largely been limited to biological antifreezes (BAs) such as antifreeze proteins and glycoproteins (AF(G)Ps).[25-36] Unfortunately, their use as cryoprotectants has ultimately been unsuccessful. This is attributed to the fact that BAs have the ability to bind to ice resulting in thermal hysteresis and a characteristic change in morphology (structure) of ice crystals.[37-42] This can exacerbate cellular damage incurred during cryopreservation an can significantly decrease post-thaw cell viabilities.

Despite the tremendous number of reports on the mechanism by which AF(G)Ps bind to ice and exhibit TH activity,[32,43-50] the mechanism by which IRI occurs is considerably less understood and is often overlooked and not assessed. There have been a number of reports on the rational design of compounds based on AFGPs, however only a few of these molecules have had the ability to inhibit ice recrystallization. Our laboratory has previously reported that *carbon*-linked (*C*-linked) AFGP analogues can exhibit "custom-tailored" antifreeze activity.[51,52] These analogues have potent IRI activity but do not possess TH activity associated with ice binding. Studies on these *C*-linked AFGP analogues have indicated that key structural features are important for the potent IRI activity exhibited by these molecules. In particular, they have highlighted the importance of the carbohydrate residue and the correlation between carbohydrate hydration and

IRI activity.[51,53] Furthermore, our laboratory has also demonstrated that these *C*-AFGPs are also effective cryoprotectants for a human embryonic liver cell line and result in similar post-thaw cell viabilities as a 2.5% DMSO solution.[54]

As only a few novel compounds have been identified as potent ice recrystallization inhibitors, the structural features necessary for potent IRI activity have not been definitively identified. Additionally, potent IRIs are currently limited to large peptide or glycopeptide-based molecules and the large-scale preparation of these compounds is problematic for *in vitro* and *in vivo* applications. As such, the overall goal of this thesis is to identify novel compounds that have the ability to potently inhibit ice recrystallization and to elucidate the structural features of these molecules that are required for this activity. This will provide a better understanding of ice recrystallization inhibition and will facilitate the rational design of IRIs for the many commercial and medical applications, particularly in cryopreservation. While large peptide and glycopeptide derivatives of native BAs are explored, considerable focus is on the discovery of small molecule ice recrystallization inhibitors as these have previously not been reported. Finally, the application of novel IRI active derivatives as cryoprotective additives will be explored to investigate if these molecules can successfully eliminate or reduce concentrations of DMSO or glycerol for the cryopreservation of UCB and RBCs. Thus, the overall focus and objectives of this thesis are as follows:

2.2 Objective 1 – Determining the Important Structural Features for the IRI Activity of Native Synthetic AFGPs and AFGP Analogues

The most potent inhibitors of ice recrystallization defined to date are the biological antifreezes, both AFPs and AFGPs. AFGPs have a homogeneous structure consisting of a tripeptide repeat of $(Ala\text{-}Ala\text{-}Thr)_n$, in which the secondary hydroxyl group of threonine is glycosylated with the disaccharide β-D-galactosyl-(1-3)-α-*N*-acetyl-D-galactosamine.[55] It has previously been demonstrated that certain structural modifications to AFGPs are detrimental for TH activity (section 1.2.4).[50,56] Furthermore, TH activity is also dependent upon the length of the glycoprotein segment and the number of tripeptide repeats.[50] Unfortunately, the influence that these structural modifications had on the IRI activity of these compounds was overlooked. Thus, it is unknown whether these same structural modifications to native AFGPs would have the same influence on IRI as TH activity. Furthermore, it was proposed these AFPGs adopted a polyproline type II (PPII) helical structure in solution and that their TH activity is strongly dependent upon this structure.[50] However, the correlation between PPII helical structure in solution and IRI activity has yet to be explored.

An understanding of the structural features important for the IRI activity of AFGPs and AFGP analogues (some of the most potent IRIs currently known) would provide valuable information for the rational design of novel "custom-tailored" ice recrystallization inhibitors that do not exhibit TH activity. As such, interest arose in examining the ability of synthetic native AFGPs (synAFGPs) and various other AFGPs analogues to inhibit ice recrystallization. The IRI and TH activity of a range of homogenous synAFGPs (general structure shown in figure 2.1) was quantified, and the relationship of both activities to glycopeptide length and solution structure was explored. This would determine if the structural features of AFGPs that are crucial for TH activity are also important for IRI. It would also elucidate if the ability of these compounds to inhibit ice recrystallization is influenced by glycopeptide length or solution structure, both of which have previously not been explored for their effect on AFGP IRI activity.

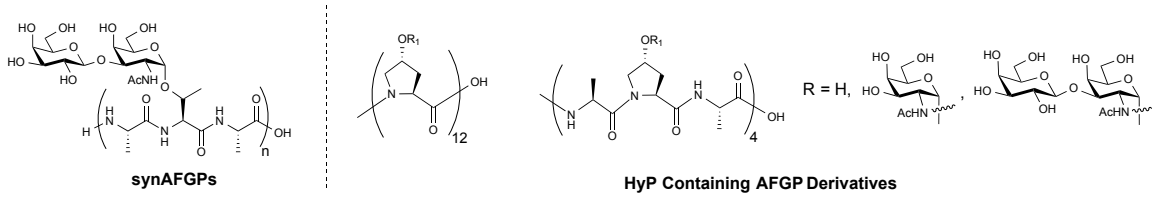

Figure 2.1 General structures of synAFGPs and HyP containing AFGP derivatives.

In addition to synAFGPs, we also sought to further investigate if the ability of molecules to adopt a PPII helical solution structure resulted in potent IRI activity. It was previously demonstrated that a contiguous hydroxyproline (HyP) nonapeptide and a galactosylated HyP nonaglycopeptide formed thermally stable PPII helical structures in solution.[57] Consequently, peptide and glycopeptide AFGP analogues containing hydroxyproline (HyP) residues were prepared and assessed for both TH and IRI (general structures shown in figure 2.1). This would determine if a correlation exists between PPII solution structure and IRI activity. Moreover, this could lead to the discovery of highly IRI active AFGP analogues since this class of compound (HyP containing derivatives) has not been explored for their ability to inhibit ice recrystallization.

Finally, structural derivatives of one of our laboratory's most IRI active analogue, OGG-Gal (figure 2.2), were also explored.[51] These analogues contained triazole rings within the polypeptide backbone. Prior results by our laboratory indicated that incorporating a triazole ring as a replacement for the amide bond in the side chain linking the carbohydrate moiety to the peptide backbone was detrimental for activity.[58] Incorporation of triazole rings within the backbone will reveal the importance of the glycine residues within the OGG-Gal glycopeptide for IRI activity, thus providing further information on the key structural features crucial for the potent activity of this molecule.

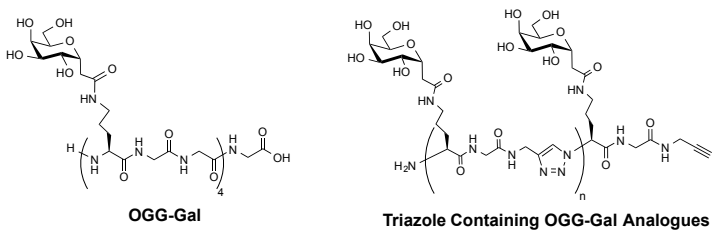

Figure 2.2 Structures of the triazole-containing OGG-Gal derivatives.

2.3 Objective 2 – Determining the Relationship between IRI, TH and Cryopreservation Ability of Natural Biological Antifreezes

As described previously, BAs are the most potent inhibitors of ice recrystallization known to date. Despite the tremendous number of studies on the TH activity of BAs,[32,43-49] there is a lack of information regarding their IRI activity. The relationship between TH and IRI activity has been debated throughout the literature. While some researchers argue that both antifreeze activities are tightly correlated and are derived by the ability of BAs to bind to ice,[25,26,35,59] others suggest there is little or no correlation between the two.[52,35,36] As our lab has interest in designing molecules that possess one type of antifreeze activity but not the other (IRI and not TH activity), we sought to explore the relationship between both antifreeze specific activities to determine if one could be modulated independently of the other. Towards this end, the TH and IRI activity of a range of natural biological antifreezes was assessed. This included AFGP-8 from *Gadus ogac* (rock cod),[60] a Type I AFP from *Pseudopleuronectes americanus* (winter flounder),[61] a Type III AFP from *Macrozoarces americanus* (ocean pout),[61] and wild-type (WT) and mutant plant AFPs from *Lolium perenne* (*Lp*AFP).[36,62,63] In addition to determining the correlation of the two activities within various classes of BAs, by studying the WT and mutant *Lp*AFPs we could determine if TH and IRI could be modulated independently within a single class of BA. This would support the hypothesis that potent IRI activity can be decoupled from TH activity and ice binding for the design of "custom-tailored" antifreeze analogues.

One of the overall goals of our laboratory is the use of the "custom-tailored" potent IRIs as novel cryoprotectants. Despite the potent IRI activity exhibited by BAs, they are generally poor cryoprotectants, and this is attributed to their ice binding capabilities and associated TH activity.[37-42] The BAs described above varied with their degree of exhibited TH and IRI activity, with some being highly IRI active but only weakly TH active. Consequently, we assessed the cryopreservation potential of these BAs with a human liver cell line (HepG2) to determine if varying degrees of TH and/or IRI alter cryopreservation outcome. This would elucidate if simply the ability to bind to ice is detrimental to cell survival during cryopreservation, or if other

contributing factors such as IRI, ice crystal shape or ice crystal growth progression affect the cryopreservation ability of these BAs.

2.4 Objective 3 – Determining the Important Structural Features for the IRI Activity of Simple Carbohydrates

Simple mono- and disaccharides have been previously demonstrated to exhibit a moderate ability to inhibit ice recrystallization.[53] This activity was ultimately correlated to hydration characteristics of these carbohydrates, and suggested that more highly hydrated carbohydrates and carbohydrate derivatives were more IRI active molecules.[51,53] Highly hydrated carbohydrates alter or disrupt the structure of bulk-water to a greater extent than poorly hydrated carbohydrates to allow for the sugar to "fit" within the three-dimensional structure of bulk-water.[64-66] Consequently, a mechanism for the inhibition of ice recrystallization exhibited by these mono- and disaccharides was proposed to be that the greater the molecule can disrupt the structure of bulk-water, the higher the observed IRI activity will be.[53]

The hydration of monosaccharides, and thus IRI activity, is suggested to be largely dictated by the configuration of the C2 and C4 positions of the pyranose ring.[53,65] The more IRI active and more hydrated monosaccharide was D-galactose, which possesses an axial C4-OH and an equatorial C2-OH (figure 2.3). Modifications to these position, such as altering C2 or C4 hydroxyl group configurations with D-glucose, D-mannose or D-talose, was detrimental and decreased IRI activity.[53] Similar results were also observed with monosaccharide derivatives and glycoprotein AFGP analogues, highlighting the sensitivity of IRI to these positions on the carbohydrate residue.[51,53]

To understand how simple small carbohydrates can inhibit ice recrystallization, we sought to explore the importance of the other hydroxyl group positions on the pyranose ring. Towards this end, the C6-OH group was modified to various other functional groups to determine its influence on activity (shown in figure 2.3). In addition, there was interest in investigating the importance of the C1 position for IRI as previous studies have suggested this position has little influence on carbohydrate hydration.[65] Consequently, small substituents were conjugated both α- and β-linked to this position (R = Me, Allyl, figure 2.3). This would provide valuable information with regards to the influence of substituents at this position and the configuration of the C1 position for the IRI activity of simple monosaccharide derivatives. Moreover, many monosaccharide derivatives with methyl groups at the C1-position have calculated hydration parameters,[65] thus the relationship between IRI and carbohydrate hydration could be further explored.

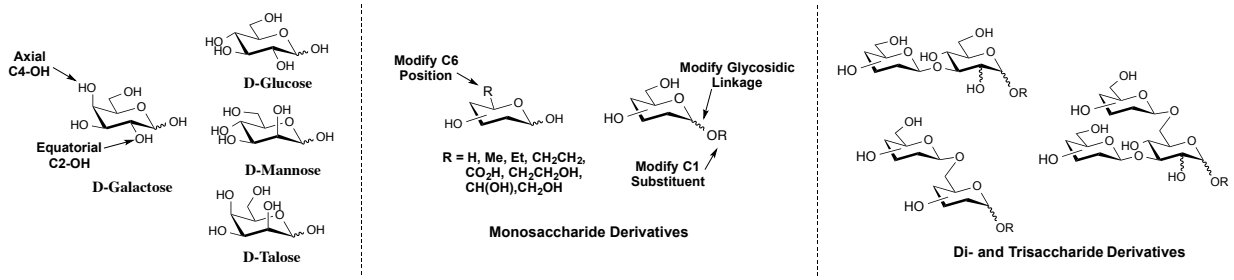

Figure 2.3 General structures of C6- and C1-modified monosaccharide derivatives and di- and trisaccharide derivatives.

Finally, various di-, tri- and oligosaccharides and their derivatives were explored as ice recrystallization inhibitors. Previous work by or laboratory demonstrated that disaccharides exhibited similar IRI activity as monosaccharides, despite the presence of the additional carbohydrate residue.[53] To determine if a cooperative effect due to an increase in the number of carbohydrate residues could increase activity, we sought to explore tri- and oligosaccharide derivatives for IRI (general structure shown in figure 2.3). This would also provide information with regards to the influence of the position and configuration of the glycosidic bond within these oligosaccharides and its important for IRI activity.

2.5 Objective 4 – Determining the Influence of Hydrophobic Moieties for the IRI Activity of Simple Carbohydrates

The IRI activity exhibited by simple mono- and disaccharides was attributed to their ability to disrupt or disorder the structure of bulk-water.[53] The greater the disruption on the three-dimensional hydrogen-bond network of water due to a poorer "fit" into this network resulted in more IRI active carbohydrates. These carbohydrates exhibited only weak to moderate IRI activity, and potently IRI active derivatives have been limited to large peptides, glycopeptides or high molecular weight polymers.[25-36,51,52,67-72] In an effort to design potently IRI active small molecules, interest arose in investigating carbohydrate-based molecules that were known to alter and/or sequester the structure of bulk-water for IRI activity. Such compounds included surfactants, organogelators and hydrogelators. These are amphiphilic molecules with a hydrophilic head and a hydrophobic tail that are able to self-assemble in water (or other solvents) to form micelles and/or hydrogels.[73,74]

Small molecule carbohydrate based surfactants and hydrogelators were explored as ice recrystallization inhibitors (general structures shown in figure 2.4). This would elucidate if amphiphilic molecules had the potential to be potent small molecule IRIs. In addition, as these molecules have specific self-assembling properties in aqueous solutions, the relationship between IRI and their ability to form either micelles or hydrogels could be explored. Finally, structure-

function studies were conducted to elucidate the importance of the carbohydrate head group and the hydrophobic tail. The influence of hydrophobic moieties has not been explored for ice recrystallization inhibition, and consequently by introducing these moieties potent IRI activity may be obtained on small carbohydrate based-molecules.

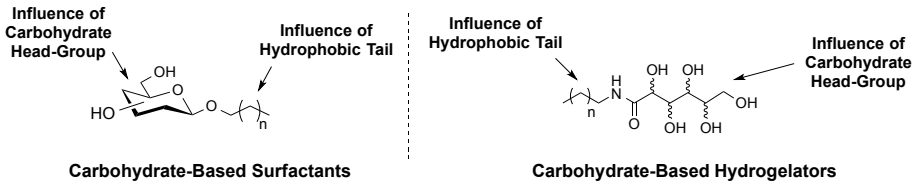

Figure 2.4 General structures of carbohydrate-based surfactants and hydrogelators.

2.6 Objective 5 – Determining the Influence of Aryl Moieties for the IRI Activity of Simple Carbohydrates

The hydrophobic moieties conjugated to the carbohydrate residues described in section 2.5 were long alkyl chains. It was determined that a few of these carbohydrate-based surfactants and hydrogelators could potently inhibit ice recrystallization, leading to the discovery of the first reported small molecule IRIs.[75] Structure-function studies on these derivatives uncovered the importance of hydrophobic moieties for potent activity. This has been demonstrated by our laboratory using other carbohydrate-based and lysine-based derivatives, where conjugation of long alkyl chains resulted in potent activity.[76,77]

A drawback to these novel derivatives however is that they possess surfactant-like characteristics that can be detrimental to cells and can solubilize cell membranes.[78-84] We therefore sought to explore if other hydrophobic moieties on carbohydrates could also result in potently IRI active small molecules. As such, we chose to employ an aryl ring as a hydrophobic moiety and various phenolic-glycosides were explored as ice recrystallization inhibitors to identify a second class of potent small molecule IRIs (figure 2.5). This would determine if an aryl ring could be an appropriate substitute for an alkyl chain and retain the potent IRI activity exhibited by the surfactants and hydrogelators. Furthermore, we could elucidate the influence of aryl-ring substituents and their regiochemistry, the relative orientation of hydroxyl groups on the carbohydrate ring, and the effect of the type of glycosidic bond (α- or β-linked) for the IRI activity of these phenolic-glycosides (figure 2.5). Finally, di- and trisaccharide phenolic-glycoside derivatives were also examined for their ability to inhibit ice recrystallization (figure 2.5). This would determine if a cooperative effect with increasing monosaccharide units could increase activity, and would also elucidate the importance of the glycosidic bond linkage and position for the IRI activity of these derivatives.

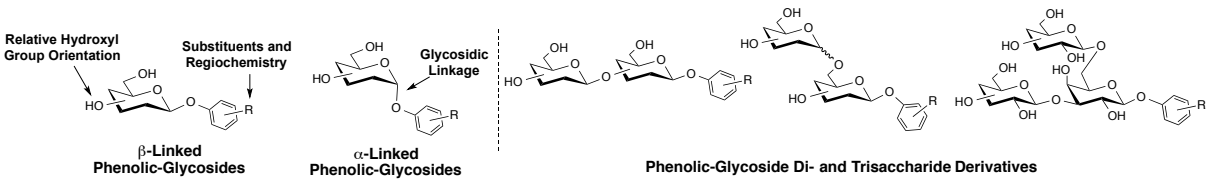

Figure 2.5 General structures of phenolic-glycosides.

2.7 Objective 6 – Determining the Cryopreservation Potential of Small Molecule Ice Recrystallization Inhibitors

A major application for ice recrystallization inhibitors is as novel cryoprotectants. This is attributed to the fact that a significant contributor to cellular injury and death during cryopreservation is ice recrystallization.[5,10,11,23,24] While current conventional cryoprotectants such as DMSO and glycerol mitigate cellular damage and increase post-thaw cell viabilities, current cryopreservation protocols are significantly limited. This is mostly due to the significant toxic effects exhibited by conventional cryoprotectants both *in vitro* and in a clinical setting.[14-18] Thus, improvements in cryopreservation protocols are urgently required to reduce or eliminate the use of DMSO or glycerol cryoprotectants.

Prior work by our laboratory has demonstrated that *C*-AFGPs exhibiting "custom-tailored" antifreeze activity can function as effective cryoprotectants for a human embryonic liver cell line.[54] Furthermore, our laboratory has also reported that at high concentrations (220 or 500 mM) IRI active carbohydrates exhibiting minimal cytotoxicity significantly increased cell viabilities post-thaw.[85] These studies demonstrated that compounds acting as "custom-tailored" ice recrystallization inhibitors were beneficial additives for cryopreservation and could increase cell viabilities and recoveries post-thaw.

Having identified a number of small molecule potent IRIs, such as those presented in figure 2.6, interest arose in exploring the cryopreservation potential of these molecules. Consequently, the cytotoxicity of these compounds and their effectiveness as cryo-additives for the cryopreservation of various different cell types was examined. The cell types explored were HepG2 cells (human liver hepatocellular carcinoma cells), hematopoietic progenitor (stem) cells (HSCs) obtained from human umbilical cord blood (UCB), and red blood cells (RBCs) obtained from human peripheral blood. HSCs from UCB and RBCs from peripheral blood are highly important for both regenerative and transfusion medicine, however there are significant drawbacks with their long-term storage by cryopreservation (as described in section 1.4.3). Thus, by exploring the cryopreservation potential of small molecule IRIs, this will determine if these compounds are effective as novel cryoprotectants or beneficial cryo-additives that reduce cellular damage post-thaw. In addition, it will elucidate if these molecules can be utilized either on their

own or in combination with reduced quantities of DMSO or glycerol to successfully cryopreserve various different cell types. Overall, these results will determine the potential small molecule IRIs have for improving upon current cryopreservation protocols that are limited in terms of the commonly used cryoprotectants, DMSO and glycerol.

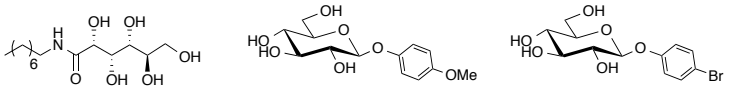

Figure 2.6 Structures of potently IRI active small molecules *N*-octyl-D-gluconamide (NOGlc), β-*para*-methoxyphenyl-D-glucopyranoside (β-PMP-Glc) and β-*para*-bromophenyl-D-glucopyranoside.

2.8 Summary of Goals and Objectives

With the goal of elucidating structural features necessary for potent ice recrystallization inhibition and identifying novel compounds, in particular small molecules, that are potent IRIs to be utilized as novel cryoprotectants, the overall objectives are as follows:

1. To elucidate the important structural features for the potent IRI activity of native synthetic AFGPs and AFGP analogues.
2. To determine the relationship between IRI, TH and cryopreservation ability of natural biological antifreezes, including AFPs and AFGPs.
3. To identify novel small molecule potent inhibitors of ice recrystallization and to elucidate the important structural features required for the IRI activity of these molecules and for simple carbohydrates.
4. To explore the cryopreservation potential of small molecule ice recrystallization inhibitors to identify novel cryoprotectants that can improve upon current cryopreservation protocols.

2.9 References

1. Meryman, H.T. *Transfusion*. **2007**, *47*, 935-945.

2. Baust, J.G.; Gao, D.; Baust, J.M. *Organogenesis*. **2009**, *5*, 90-96.

3. Bakhach, J. *Organogenesis*. **2009**, *5*, 119-126.

4. Scott, K.L.; Lecak, J.; Acker, J.P. *Transfus. Med. Rev*. **2005**, *19*, 127-142.

5. Fowler, A.; Toner, M. *Ann. N.Y. Acad. Sci*. **2005**, *1066*, 119-135.

6. Yang, H.; Acker, J.P.; Hannon, J.; Miszta-Lane, H.; Akabutu, J.J.; McGann, L.E. *Cytotherapy*. **2001**, *3*, 377-386.

7. Kanias, T.; Acker, J.P. *FEBS J*. **2010**, *277*, 343-356.

8. Valeri, C.R.; Ragno, G. *Transfusion Apheresis Sci*. **2006**, *34*, 271-287.

9. Hunt, C.J. *Transfus. Med. Hemoth*. **2011**, *38*, 107-123.

10. Mazur, P. *Am. J. Physiol. - Cell Physiol*. **1984**, *247*, C125-C142.

11. Mazur, P. Life in the Frozen State - Principles of Cryobiology (Boca Baton, FL: CRC Press; 2004.

12. Mazur, P. *Principles of cryobiology*. 2004. CRC Press LLC.

13. Holovati, J.L.; Hannon, J.L.; Gyongyossy-Issa, M.I.C.; Acker, J.P. *Transfus. Med. Rev.* **2009**, *23*, 25-41.

14. Davis, J.; Rowley, S.; Braine, H.; Piantadosi, S.; Santos, G. *Blood*. **1990**, *75*, 781-786.

15. Berz, D.; McCormack, E.M.; Winer, E.S.; Colvin, G.A.; Quesenberry, P.J. *Am. J. Hematol.* **2007**, *82*, 463-472.

16. Galmes, A.; Gutiérrez, A.; Sampol, A.; Canaro, M.; Morey, M.; Iglesias, J.; Matamoros, N.; Duran, M.A.; Novo, A.; Bea, M.D.; Galán, P.; Balansat, J.; Martínez, J.; Bargay, J.; Besalduch, J. *Haematologica*. **2007**, *92*, 986-989.

17. Greco, N.J.; Seetharaman, S.; Kurtz, J.; Lee, W.R.; Moroff, G. *Stem Cells Dev*. **2006**, *15*, 124-135.

18. Shim, J.-S.; Cho, B.; Kim, M.; Park, G.-S.; Shin, J.-C.; Hwang, H.-K.; Kim, T.-G.; Oh, I.-H. *Br. J. Haematol*. **2006**, *135*, 210-213.

19. Hess, J.R. *Transfus. Med*. **2004**, *14*, 1-8.

20. American Association of Blood Banks Technical Manual (Bethesda, MD: American Association of Blood Banks; 2006.

21. Meryman, H.T.; Hornblower, M. *Transfusion*. **1972**, *12*, 145-156.

22. Valeri, C.R.; Ragno, G.; Pivacek, L.E.; Srey, R.; Hess, J.R.; Lippert, L.E.; Mettille, F.; Fahie, R.; O'Neill, E.M.; Szymanski, I.O. *Transfusion*. **2001**, *41*, 933-939.

23. Acker, J.P.; McGann, L.E. *Cell Transplant*. **2002**, *11*, 563-571.

24. Mazur, P.C. *Science*. **1970**, *168*, 939-949.

25. Knight, C.A.; Hallett, J.; DeVries, A.L. *Cryobiology*. **1988**, *25*, 55-60.

26. Knight, C.A.; Wen, D.; Laursen, R.A. *Cryobiology*. **1995**, *32*, 23-34.

27. Knight, C.A.; DeVries, A.L.; Oolman, L.D. *Nature*. **1984**, *308*, 295-296.

28. Garner, J.; Harding, M.M. *ChemBioChem*. **2010**, *11*, 2489-2498.

29. Harding, M.M.; Anderberg, P.I.; Haymet, A.D.J. *Eur. J. Biochem*. **2003**, *270*, 1381-1392.

30. Harding, M.M.; Ward, L.G.; Haymet, A.D.J. *Eur. J. Biochem*. **1999**, *264*, 653-665.

31. Peltier, R.; Brimble, M.A.; Wojnar, J.M.; Williams, D.E.; Evans, C.W.; DeVries, A.L. *Chem. Sci*. **2010**, *1*, 538-551.

32. Davies, P.L.; Baardsnes, J.; Kuiper, M.J.; Walker, V.K. *Philos. Trans. R. Soc. London, Ser. B*. **2002**, *357*, 927-935.

33. Davies, P.L.; Hew, C.L. *FASEB J*. **1990**, *4*, 2460-2468.

34. Jia, Z.; Davies, P.L. *Trends Biochem. Sci*. **2002**, *27*, 101-106.

35. Yu, S.O.; Brown, A.; Middleton, A.J.; Tomczak, M.M.; Walker, V.K.; Davies, P.L. *Cryobiology*. **2010**, *61*, 327-334.

36. Pudney, P.D.A.; Buckley, S.L.; Sidebottom, C.M.; Twigg, S.N.; Sevilla, M.-P.; Holt, C.B.; Roper, D.; Telford, J.H.; McArthur, A.J.; Lillford, P.J. *Arch. Biochem. Biophys*. **2003**, *410*, 238-245.

37. Mugano, J.A.; Wang, T.; Layne, J.R., Jr.,; DeVries, A.L.; Lee, R.E. *Cryobiology*. **1995**, 556-557.

38. Rubinsky, B.; DeVries, A.L. *Cryobiology*. **1989**, *26*, 580.

39. Wang, T.; Zhu, Q.; Yang, X.; Layne, J.R.J.; DeVries, A.L. *Cryobiology*. **1994**, *31*, 185-192.

40. Rubinsky, B.; Arav, A.; DeVries, A.L. *Cryobiology*. **1992**, *29*, 69-79.

41. Carpenter, J.F.; Hansen, T.N. *Proc. Natl. Acad. Sci. U.S.A.* **1992**, *89*, 8953-8957.

42. Chao, H.; Davies, P.L.; Carpenter, J.F. *J. Exp. Biol.* **1996**, *199*, 2071-2076.

43. Chao, H.; Houston, M.E.; Hodges, R.S.; Kay, C.M.; Sykes, B.D.; Loewen, M.C.; Davies, P.L.; Sönnichsen, F.D. *Biochemistry*. **1997**, *36*, 14652-14660.

44. Haymet, A.D.J.; Ward, L.G.; Harding, M.M.; Knight, C.A. *FEBS Lett.* **1998**, *430*, 301-306.

45. Zhang, W.; Laursen, R.A. *J. Biol. Chem.* **1998**, *273*, 34806-34812.

46. Baardsnes, J.; Kondejewski, L.H.; Hodges, R.S.; Chao, H.; Kay, C.; Davies, P.L. *FEBS Lett.* **1999**, *463*, 87-91.

47. DeLuca, C.I.; Davies, P.L.; Ye, Q.; Jia, Z. *J. Mol. Biol.* **1998**, *275*, 515-525.

48. Marshall, C.B.; Daley, M.E.; Graham, L.A.; Sykes, B.D.; Davies, P.L. *FEBS Lett.* **2002**, *529*, 261-267.

49. Doxey, A.C.; Yaish, M.W.; Griffith, M.; McConkey, B.J. *Nat. Biotechnol.* **2006**, *24*, 852-855.

50. Tachibana, Y.; Fletcher, G.L.; Fujitani, N.; Tsuda, S.; Monde, K.; Nishimura, S.-I. *Angew. Chem. Int. Ed.* **2004**, *43*, 856-862.

51. Czechura, P.; Tam, R.Y.; Dimitrijevic, E.; Murphy, A.V.; Ben, R.N. *J. Am. Chem. Soc.* **2008**, *130*, 2928-2929.

52. Liu, S.; Ben, R.N. *Org. Lett.* **2005**, *7*, 2385-2388.

53. Tam, R.Y.; Ferreira, S.S.; Czechura, P.; Chaytor, J.L.; Ben, R.N. *J. Am. Chem. Soc.* **2008**, *130*, 17494-17501.

54. Leclère, M.; Kwok, B.K.; Wu, L.K.; Allan, D.S.; Ben, R.N. *Bioconjugate Chem.* **2011**, *22*, 1804-1810.

55. DeVries, A.L.; Komatsu, S.K.; Feeney, R.E. *J. Biol. Chem.* **1970**, *245*, 2901-2908.

56. Komatsu, S.K.; DeVries, A.L.; Feeney, R.E. *J. Biol. Chem.* **1970**, *245*, 2909-2913.

57. Owens, N.W.; Stetefeld, J.; Lattová, E.; Schweizer, F. *J. Am. Chem. Soc.* **2010**, *132*, 5036-5042.

58. Capicciotti, C.J.; Trant, J.F.; Leclère, M.; Ben, R.N. *Bioconjugate Chem.* **2011**, *22*, 605-616.

59. Hall, D.G.; Lips, A. *Langmuir*. **1999**, *15*, 1905-1912.

60. Bouvet, V.R.; Lorello, G.R.; Ben, R.N. *Biomacromolecules*. **2006**, *7*, 565-571.

61. Kao, M.H.; Fletcher, G.L.; Wang, N.C.; Hew, C.L. *Can. J. Zool.* **1986**, *64*, 578-582.

62. Middleton, A.J.; Brown, A.M.; Davies, P.L.; Walker, V.K. *FEBS Lett.* **2009**, *583*, 815-819.

63. Sidebottom, C.; Buckley, S.; Pudney, P.; Twigg, S.; Jarman, C.; Holt, C.; Telford, J.; McArthur, A.; Worrall, D.; Hubbard, R.; Lillford, P. *Nature*. **2000**, *406*, 256.

64. Galema, S.A.; Engberts, J.B.F.N.; Hoeiland, H.; Foerland, G.M. *J. Phys. Chem.* **1993**, *97*, 6885-6889.

65. Galema, S.A.; Høiland, H. *J. Phys. Chem.* **1991**, *95*, 5321-5326.

66. Galema, S.A.; Howard, E.; Engberts, J.B.F.N.; Grigera, J.R. *Carbohydr. Res.* **1994**, *265*, 215-225.

67. Eniade, A.; Purushotham, M.; Ben, R.N.; Wang, J.B.; Horwath, K. *Cell Biochem. Biophys.* **2003**, *38*, 115-124.

68. Inada, T.; Lu, S.-S. *Cryst. Growth Des.* **2003**, *3*, 747-752.

69. Inada, T.; Lu, S.-S. *Chem. Phys. Lett.* **2004**, *394*, 361-365.

70. Budke, C.; Koop, T. *ChemPhysChem.* **2006**, *7*, 2601-2606.

71. Gibson, M.I. *Polym. Chem.* **2010**, *1*, 1141-1152.

72. Gibson, M.I.; Barker, C.A.; Spain, S.G.; Albertin, L.; Cameron, N.R. *Biomacromolecules.* **2009**, *10*, 328-333.

73. Estroff, L.A.; Hamilton, A.D. *Chem. Rev.* **2004**, *104*, 1201-1218.

74. de Loos, M.; Feringa, B.L.; van Esch, J.H. *Eur. J. Org. Chem.* **2005**, *2005*, 3615-3631.

75. Capicciotti, C.J.; Leclère, M.; Perras, F.A.; Bryce, D.L.; Paulin, H.; Harden, J.; Liu, Y.; Ben, R.N. *Chem. Sci.* **2012**, *3*, 1408-1416.

76. Balcerzak, A.K.; Febbraro, M.; Ben, R.N. *RSC Adv.* **2013**, *3*, 3232-3236.

77. Trant, J.F.; Biggs, R.A.; Capicciotti, C.J.; Ben, R.N. *RSC Adv.* **2013**, *3*, 26005-26009.

78. de Almeida, M.V.; Le Hyaric, M. *Mini-Rev. Org. Chem.* **2005**, *2*, 283-297.

79. Lorber, B.; Bishop, J.B.; DeLucas, L.J. *Biochim. Biophys. Acta.* **1990**, *1023*, 254-265.

80. Michel, H.; Oesterhelt, D. *Proc. Natl. Acad. Sci. U.S.A.* **1980**, *77*, 1283-1285.

81. Harvie, P.; Wong, F.M.P.; Bally, M.B. *Biophys. J.* **1998**, *75*, 1040-1051.

82. Hildreth, J.E. *Biochem. J.* **1982**, *207*, 363-366.

83. Baron, C.; Thompson, T.E. *Biochim. Biophys. Acta.* **1975**, *382*, 276-285.

84. Plusquellec, D.; Chevalier, G.; Talibart, R.; Wróblewski, H. *Anal. Biochem.* **1989**, *179*, 145-153.

85. Chaytor, J.L.; Tokarew, J.M.; Wu, L.K.; Leclère, M.; Tam, R.Y.; Capicciotti, C.J.; Guolla, L.; von Moos, E.; Findlay, C.S.; Allan, D.S.; Ben, R.N. *Glycobiology.* **2012**, *22*, 123-133.

Chapter 3: Elucidating the Structural Features Important for the IRI Activity of Native Synthetic AFGPs and AFGP Analogues

3.1 Introduction

Antifreeze glycoproteins (AFGPs) are found in deep sea teleost fish in Arctic and Antarctic waters. They are comprised of a tripeptide repeat of $(Ala\text{-}Ala\text{-}Thr)_n$, in which the secondary hydroxyl group of threonine is glycosylated with the disaccharide β-D-galactosyl-(1-3)-α-*N*-acetyl-D-galactosamine).[1-9] AFGPs have been separated into eight subclasses, AFGP 1-8, based on their molecular masses which range from 2.6 kDa (n = 4) to 33.7 kDa (n = 50).[1] The solution structure of AFGPs has been debated in the literature and it has been suggested that they either adopt an extended random coil structure[10-15] or an ordered helix similar to a polyproline type II (PPII) helix (see section 1.2.1).[14,16-18] However, this structure is dependent upon the subclass of AFGP.[14-16]

It is well recognized that AFGPs exhibit both types of antifreeze activity: thermal hysteresis (TH) activity and potent ice recrystallization inhibition (IRI) activity. The structural features of AFGPs that are crucial for TH activity have been extensively studied. In 2004, a study conducted by Nishimura and co-workers identified three key motifs of synthetic native AFGPs (synAFGPs) that were required for TH activity (Figure 3.1): 1) the *N*-acetyl group at the C2 position of the galactosamine; 2) the α-configuration of the *O*-glycosidic linkage between the disaccharide and the peptide chain; 3) the γ-methyl group of the threonyl residue.[19] In addition, TH activity was also dependent upon the length of the glycoprotein and was increased as the number of tripeptide repeats increased. These synAFPGs were proposed to adopt a PPII helix in solution based on their CD spectra. However, in this study only TH and dynamic ice shaping (DIS) capabilities of the synAFGPs was assessed, and the IRI activity of these compounds was overlooked. Thus, it is unknown whether these same structural modifications to native AFGPs would have the same influence on IRI as TH activity. This is unfortunate as these biological antifreezes are some of the most potent ice recrystallization inhibitors discovered to date. An understanding of the structural features important for their IRI activity can provide valuable information for the rational design of "custom-tailored" antifreeze analogues possessing only potent IRI activity without TH activity.

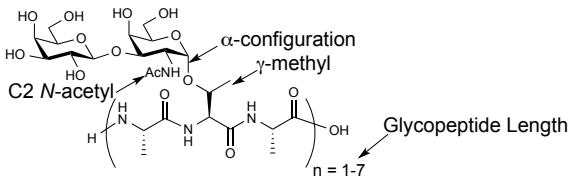

Figure 3.1. Important structural motifs on synthetic AFGPs (synAFGPs) for TH activity as determined by Nishimura and co-workers.[19]

Synthetic variants of AFGPs have been assessed for their ability to inhibit ice recrystallization. Analogues in which the native disaccharide was replaced with the monosaccharide α-*N*-acetyl-D-galactosamine were IRI active and induced the formation of hexagonal ice crystals, and this activity was dependent upon the length of the glycopeptide.[20] The incorporation of proline as a replacement for an alanine in the tripeptide repeat retained IRI activity. However, the irregular incorporation of proline for various alanine residues was detrimental to IRI.

Our laboratory previously reported that *carbon*-linked (*C*-linked) AFGP analogues with "custom-tailored" antifreeze activity (*C*-AFGP analogues *C*-serine and OGG-Gal, figure 3.2).[21,22] These compounds have IRI activity that is equipotent to AFGP 8 but they do not exhibit TH activity, suggesting that they are not binding to ice and that their mechanism of action differs from that of AFGPs. Additionally, our laboratory has reported that the potently IRI active OGG-Gal derivative is a beneficial additive for the cryopreservation of human embryonic liver cells and is as effective as a 2.5% DMSO solution.[23] Structure-function studies have indicated that key structural features of OGG-Gal are crucial for its potent activity (see section 1.3.1). The presence of a highly hydrated monosaccharide moiety, as well as the amide bond and six atoms in the side chain connecting the carbohydrate residue to the polypeptide backbone are beneficial for IRI activity.[22,24,25]

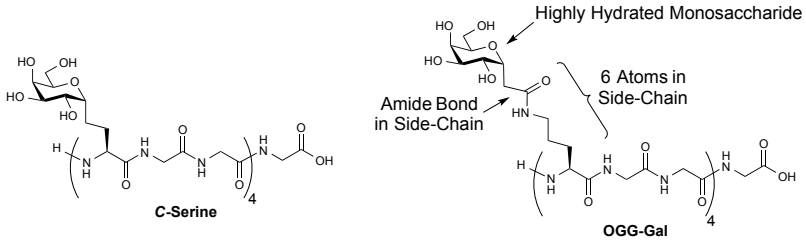

Figure 3.2. Structures of potently IRI active *C*-Serine and OGG-Gal analogues and the structural features crucial for the potent activity of OGG-Gal.

Only a few AFGP analogues have been reported that retain the potent IRI activity of AFGPs. This has made it difficult to understand the exact mechanism by which compounds inhibit ice recrystallization and to ascertain the structural requirements for potent activity. IRI activity is a highly desirable property, especially for effective cryoprotectants to negate cellular damage caused by ice recrystallization. Thus, we sought to elucidate the structural features important for the IRI activity of synthetic and native AFGPs and AFGP analogues as these are the most potently IRI active compounds reported to date. These studies will also facilitate the identification of novel compounds with "custom-tailored" antifreeze activity. IRI active compounds have potential as cryoprotectants, but TH activity and dynamic ice shaping capabilities are detrimental

properties for a cryoprotectant (section 1.4.4).[26-30] This chapter examines three different classes of glycopeptides for IRI and TH activity to address the following objectives:

1. We sought to explore the relationship between IRI and TH activity as a function of glycopeptide length and structure for homogenous synthetic AFGPs (synAFGPs). This would provide valuable insight on the structural requirements for the ice recrystallization inhibition of AFGPs. The results from this study are presented in section 3.2.
2. We also sought to investigate if AFGP analogues possessing a solution structure similar to a PPII helix could function as ice recrystallization inhibitors as it is suggested that synAFGPs adopt this structure in solution. Both peptides and glycopeptides that adopt a PPII helical structure in solution and were assessed for both TH and IRI activity to determine the influence of solution structure on these activities. These results are discussed in section 3.3.
3. Finally, derivatives of the potently IRI active *C*-AFGP analogue OGG-Gal previously reported by our laboratory were assessed for their ability to inhibit ice recrystallization. These derivatives **c**ontained triazole-linkages in the polypeptide backbone to further investigate the impact of this moiety on activity. The results from this study are described in section. 3.4.

3.2 The Relationship between IRI Activity, TH Activity, Glycopeptide Length and Structure for Synthetic AFGPs

3.2.1 Homogenous Synthetic AFGPs (synAFGPs)

As described previously (section 3.1), detailed structure-function studies have been conducted on synthetic AFGPs elucidating the key structural motifs crucial for TH activity.[19] However, the effect these structural modifications had on IRI activity was not assessed. To facilitate a more in-depth analysis on the relationship between both types of antifreeze activity, TH and IRI activity, a range of homogenous AFGPs were synthesized as assessed for both activities. The structures of these synAFGPs consist of a tripeptide repeat of $(Ala\text{-}Thr\text{-}Ala)_n$ glycosylated with the disaccharide β-D-galactosyl-(1-3)-α-*N*-acetyl-D-galactosamine on the threonine residues (figure 3.3).[31] This is very similar in structure to native AFGPs isolated from Atlantic, Arctic or Antarctic cod. The only differences are that the sequence of the tripeptide repeat in the native system is $(Ala\text{-}Ala\text{-}Thr)_n$ and the native system has two C-terminal alanine residues making it 14 amino acids in length for AFGP-8.[1,3-5,32] These studies will identify if structural features that are crucial for the TH activity of AFGPs are also important for the IRI activity of these glycopeptides.

Despite it being well recognized that AFGPs exhibit both types of antifreeze activity, this is the first study that directly establishes the relationship between AFGP structural modifications to both activities. Furthermore, these studies may help understand the structural requirements of these glycopeptides that contribute to their IRI activity, because AFGPs are among the biological antifreezes that exhibit the most potent inhibition of ice recrystallization. This will aide in the development of other ice recrystallization inhibitors that unlike AFGPs do not bind to ice and exhibit TH activity.

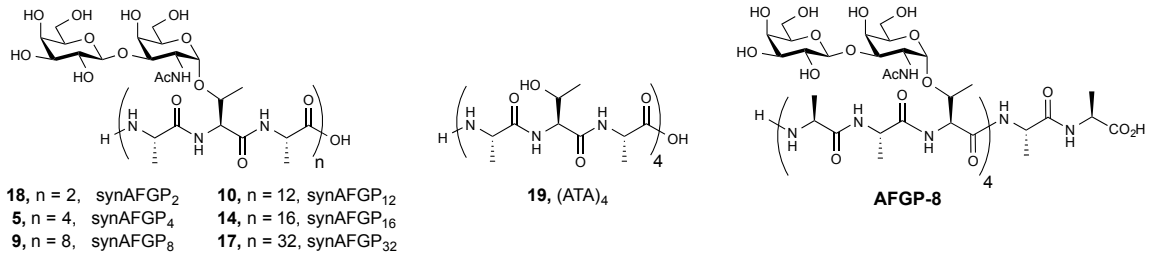

Figure 3.3 Structures of synthetic homogeneous AFGPs assessed for antifreeze activity.[31]

The synthesis and antifreeze specific activity (TH and IRI activity) of the synAFGPs assessed in this study was reported in an article published in 2012 in *Angewandte Chemie* from a collaboration between our laboratory and Dr. Richard J. Payne's laboratory in the school of chemistry at the University of Sydney. This article is provided in section 3.2.2 and a detailed discussion of the IRI and TH results and the relationship between glycopeptide length and solution structure for these activities is provided in section 3.2.3. All compounds, figures and schemes are numbered as they appear in the article and are reproduced with the same numbering schemes in section 3.2.3 to complement the discussion. The compound, figure and scheme numbers from this article discussing the synAFGPs are only for section 3.2 of this chapter.

Angewandte
Communications

Peptide Ligations

DOI: 10.1002/anie.201108682

Total Synthesis of Homogeneous Antifreeze Glycopeptides and Glycoproteins**

*Brendan L. Wilkinson, Robin S. Stone, Chantelle J. Capicciotti, Morten Thaysen-Andersen, Jacqueline M. Matthews, Nicolle H. Packer, Robert N. Ben, and Richard J. Payne**

Antifreeze glycoproteins (AFGPs) are a class of natural products found in deep sea teleost fish in Arctic and Antarctic waters. The physiological role of these biomolecules is to protect against cryoinjury in environments with subzero temperatures by preventing the growth of ice crystals in vivo.[1] Structurally, AFGPs are polymeric, mucin-type glycoproteins that consist of a single glycotripeptide repeat (Ala-Thr-Ala/Pro) in which each secondary hydroxy group on threonine is linked to the disaccharide β-D-galactosyl-(1→3)-α-*N*-acetyl-D-galactosamine (Scheme 1).[2] AFGPs range in molecular weight from approximately 2.6 kDa (4 repeat units) to 33.7 kDa (50 repeat units).

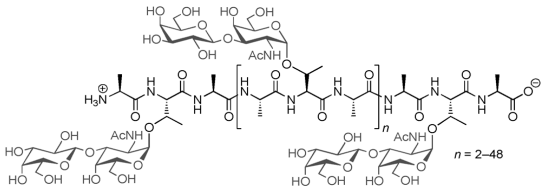

Scheme 1. Structure of native antifreeze glycoproteins (AFGPs).

The mechanism of action of AFGPs is proposed to occur through an adsorption-inhibition process in which the AFGP irreversibly binds to the surface of ice crystals, thus resulting in a localized freezing-point depression (through the Kelvin effect).[3] The difference between the depressed freezing point and the melting point of the ice crystal is termed thermal hysteresis (TH). The binding of AFGPs to ice results in a characteristic change in morphology from spherical to hexagonal-bipyramidal-shaped crystals.[3] AFGPs are also potent inhibitors of ice recrystallization, whereby they prevent the enthalpically driven growth of ice crystals, an activity known as ice recrystallization inhibition (IRI) activity.

The unique physicochemical properties of AFGPs have led to considerable interest in these molecules for applications in material science and medicine, including their use as cryoprotective agents for cells, tissues, and organs.[4] Such applications necessitate access to significant quantities of AFGPs in pure form, however, isolation and purification from natural sources is both labor-intensive and costly. An attractive alternative is the production of these biomolecules by chemical synthesis. To date, synthetic approaches have been limited to the preparation of small glycopeptides (≤ 14 amino acids in length) by using solid-phase peptide synthesis (SPPS).[5] However, a landmark study by Nishimura and co-workers enabled access to larger AFGPs (ca. 6–21 amino acids in length), bearing native and non-native glycans, through polymerization of tripeptide glycopeptides and subsequent extensive chromatographic purification of the polydisperse oligomers.[6] Importantly, this study facilitated the delineation of a number of structural features now known to be critical for antifreeze activity. To facilitate more in-depth structure–activity studies and to provide material with potential biomedical and industrial applications, it is essential to develop a convergent synthetic strategy that enables the efficient synthesis of a range of homogeneous and native AFGPs.[7] Towards this goal, we were interested in exploiting a native chemical ligation[8]–desulfurization approach[9] for the first convergent synthesis of native, homogeneous AFGPs ranging in size from 1.2 to 19.5 kDa. Specifically, we envisioned an iterative synthetic strategy based on three key reactions: 1) native chemical ligation between a glycopeptide bearing an N-terminal thiazolidine (Thz) residue and a C-terminal thioester moiety and a glycopeptide containing an N-terminal cysteine (Cys) residue, 2) conversion of the N-terminal Thz moiety to an N-terminal Cys residue, and 3) desulfurization of the Cys-containing glycopeptides to afford native and homogeneous AFGPs. Furthermore, unlike in previous studies, where only TH activity has been assessed, in the present study we were interested in evaluating both the TH and IRI activities of these synthetic homogeneous AFGPs.

Our synthetic strategy commenced with the synthesis of the key dodecaglycopeptide **1** bearing an N-terminal Thz residue by using Fmoc-SPPS strategy starting from 2-chlorotrityl chloride resin (**2**) preloaded with Fmoc-Ala-OH (see the

[*]

[**] We would like to thank the Australian Research Council for funding (ARC Discovery Project: 0986632) and the Canadian Blood Services for a GFP Award (C.J.C.).

Supporting information for this article is available on the WWW under http://dx.doi.org/10.1002/anie.201108682.

© 2012 Wiley-VCH Verlag GmbH & Co. KGaA, Weinheim

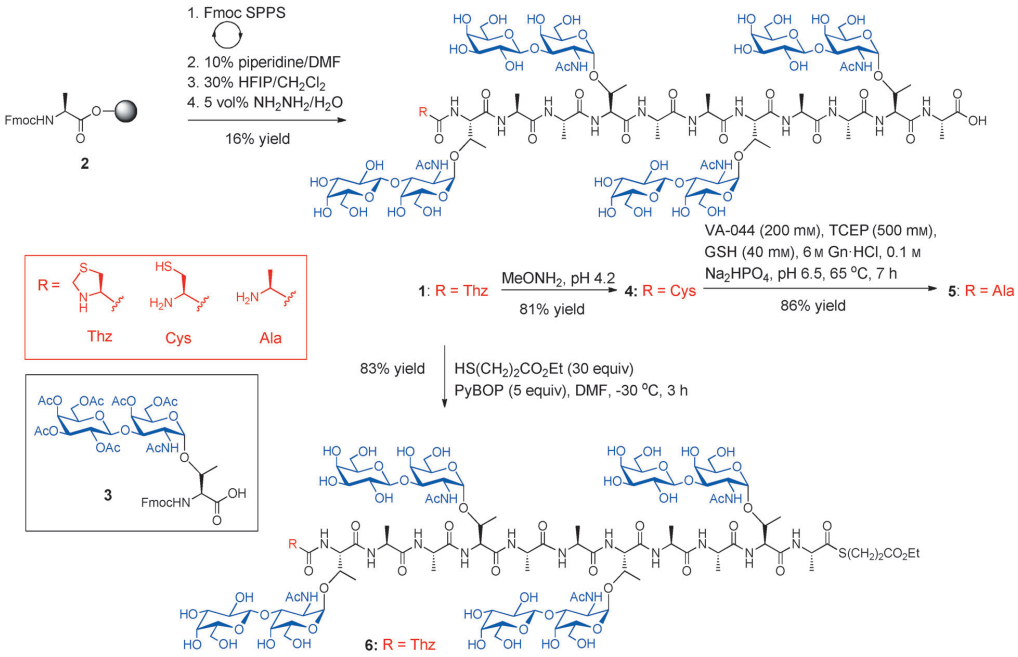

Scheme 2. Solid-phase synthesis of key dodecaglycopeptide **1**, $AFGP_4$ (**5**), and dodecaglycopeptide thioester **6**. One cycle of Fmoc SPPS includes the following steps: a) deprotection: 10% piperidine/DMF; b) coupling: Fmoc-Ala-OH or Fmoc-Thz-OH (4 equiv), PyBOP (4 equiv), NMM (8 equiv), DMF; for glycosylamino acid **3** (1.2 equiv), HATU (1.2 equiv), DIPEA (2.4 equiv), DMF; and c) capping: 9:1 v/v pyridine/Ac_2O. The yields given in the scheme are for the isolated products. Fmoc = 9-fluorenylmethoxycarbonyl, PyBOP = (1H-benzotriazol-1-yloxy)tris(pyrrolidino)-phosphonium hexafluorophosphate, NMM = *N*-methylmorpholine, HATU = O-(7-azabenzotriazol-1-yl)-*N*,*N*,*N*′,*N*′-tetra-methyluronium hexafluoro-phosphate, DIPEA = diisopropylethylamine, HFIP = 1,1,1,3,3,3-hexafluoro-2-propanol, Gn·HCl = guanidine hydrochloride, GSH = reduced gluta-thione.

Supporting Information and Scheme 2). After iterative assembly by Fmoc SPPS (which included the incorporation of preformed glycosylamino acid **3**), cleavage from the resin, and hydrazinolysis of the acetate protecting groups on the glycans,[10] **1** was isolated in 16% yield (based on original resin loading, see the Supporting Information for synthetic details). We reasoned that dodecaglycopeptide **1** could serve both as a precursor for the synthesis of the native antifreeze glycopeptide $AFGP_4$ and as a key intermediate for the preparation of the coupling partners that are necessary for the convergent assembly of larger oligomers through native chemical ligation. To gain access to the native $AFGP_4$ analogue and to demonstrate the feasibility of our synthetic approach, glycopeptide **1** was treated with a methoxyamine hydrochloride solution (0.2 M, final pH 4.2) to effect the conversion of the N-terminal Thz residue to glycopeptide **4**, now bearing an N-terminal Cys residue, which was isolated in 81% yield after HPLC purification. We then investigated conditions for desulfurization of the cysteinyl thiol of **4** to provide the native $AFGP_4$ (**5**). Here, we chose to use a modified version of the metal-free desulfurization procedure reported by Danishefsky and co-workers, which employs 2,2′-azobis-[2-(2-imidazolin-2-yl)propane] dihydrochloride (VA-044) as a radical initiator.[11] Reaction of **4** with VA-044 in the presence of tris(2-carboxyethyl)phosphine (TCEP) and reduced glutathione (GSH) at 65 °C[12] afforded $AFGP_4$ (**5**) in 86% yield after HPLC purification (see the Supporting Information and Scheme 2).

In addition to cysteine-containing glycopeptide **4**, access to C-terminal glycopeptide thioester **6** was also necessary for the proposed native chemical ligation assembly. As such, dodecaglycopeptide **1** was subjected to thioesterification reaction conditions described by Kajihara et al. (ethyl-3-mercaptopropionate (30 equiv), PyBOP (5 equiv) in DMF at −30 °C for three hours)[13] to provide the corresponding glycopeptide thioester **6** in 83% yield without any detectable epimerization of the C-terminal alanine residue (see the Supporting Information).[13]

After having successfully prepared glycopeptide **4** and glycopeptide thioester **6**, we examined the assembly of a larger AFGP oligomer, namely the 24-amino acid $AFGP_8$, by using the proposed native chemical ligation–desulfurization strategy. To this end, C-terminal glycopeptide thioester **6** was reacted with glycopeptide **4** in the presence of 4-mercaptophenylacetic acid (MPAA)[14] as a thiol additive (200 mM) and TCEP (20 mM) in 6 M Gn·HCl/0.2 M Na_2HPO_4 buffer at pH 7.2 and 25 °C (see the Supporting Information and Scheme 3). The ligation proceeded efficiently and reached completion within two hours (determined by LC–MS analysis). At this stage the reaction mixture was split to

 © 2012 Wiley-VCH Verlag GmbH & Co. KGaA, Weinheim

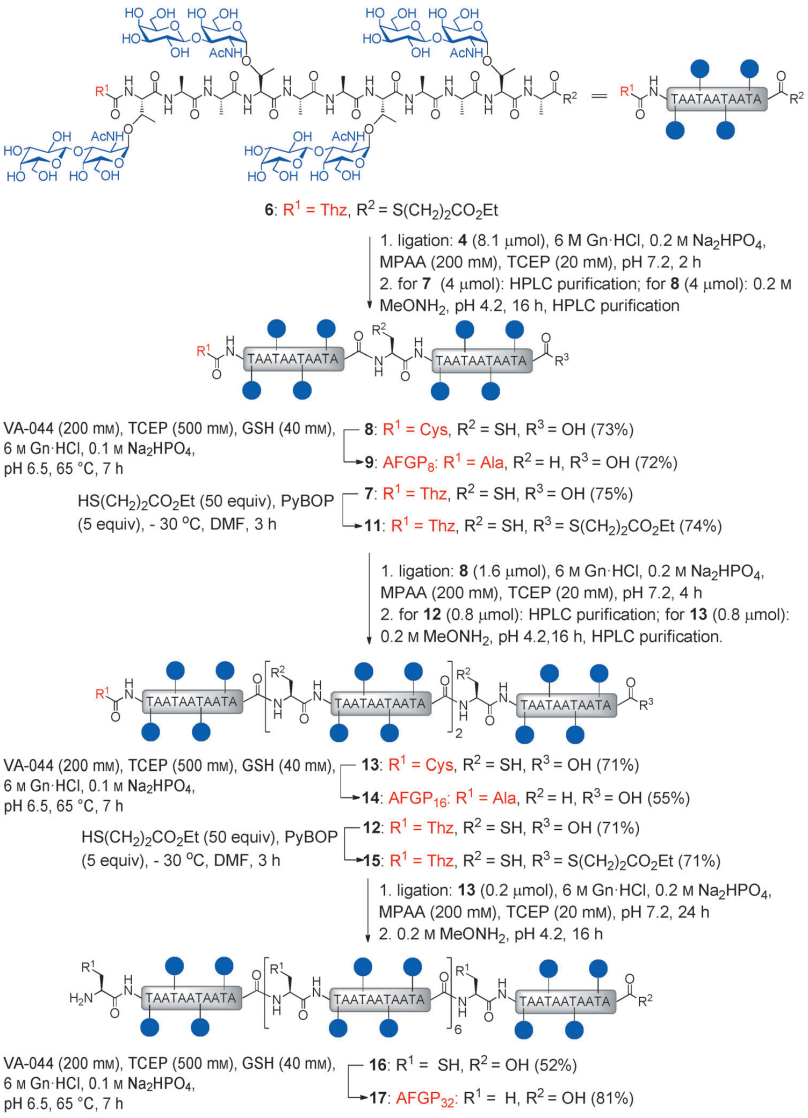

Scheme 3. Synthesis of homogeneous AFGP oligomers $AFGP_8$ (**9**), $AFGP_{16}$ (**14**), and $AFGP_{32}$ (**17**) through an iterative native chemical ligation–desulfurization strategy. A = alanine, T = threonine.

allow divergent access to $AFGP_8$ and the two coupling partners necessary for a subsequent ligation reaction. Direct HPLC purification of a portion of the crude ligation mixture (50%) provided the 24-amino acid glycopeptide **7**, possessing an N-terminal Thz moiety, in 75% yield. Direct treatment of the remaining portion of the ligation reaction with a solution of methoxyamine hydrochloride (0.2 M, final pH 4.2) led to conversion of the ligation product into glycopeptide **8**, bearing an N-terminal Cys residue, which was isolated in 73% yield after HPLC purification. Metal-free desulfurization of glycopeptide **8** by using the conditions described for $AFGP_4$ (**5**) provided the native $AFGP_8$ (**9**) in 72% yield after HPLC purification. Glycopeptide **8** was also reacted with dodecaglycopeptide thioester **6** by using the same native chemical ligation–desulfurization sequence described for the synthesis of $AFGP_8$ (**9**) to provide the 7.3 kDa 36-amino acid glycopeptide $AFGP_{12}$ (**10**; synthesis not shown, see the Supporting Information for synthetic details). After having successfully employed a protocol for the combination of native chemical ligation and Thz demasking to obtain glycopeptide **8**, we focused on the preparation of the 24-amino acid glycopeptide thioester **11** to serve as a coupling partner for the assembly of a 48-residue AFGP through native chemical ligation. This was achieved by treatment of **7** with a large excess of ethyl-3-mercaptopropionate (50 equiv) which provided the desired glycopeptide thioester **11** in 74% yield.

With 24-amino acid glycopeptide **8** and glycopeptide thioester **11** now in hand, the two fragments were next subjected to the native chemical ligation conditions employed above. On this occasion the reaction required four hours to reach completion (as determined by LC–MS analysis). A portion (50%) of the ligation mixture was directly purified by HPLC using a C4 column to afford glycopeptide **12** in 71% yield. The remaining ligation reaction mixture was subjected to the in situ Thz-demasking conditions to liberate glycopeptide **13**, bearing an N-terminal Cys residue, in 71% yield after HPLC purification using a C4 column. Metal-free desulfurization of glycopeptide **13** then provided the native 9.8 kDa 48-residue glycopeptide $AFGP_{16}$ (**14**) in 55% yield.

After successful preparation of the 48-amino acid $AFGP_{16}$ (**14**), we carried out one further ligation to access $AFGP_{32}$. Prior to the ligation event, the requisite C-terminal glycopeptide thioester **15** was prepared from **12** by using similar conditions as described for glycopeptide thioesters **6** and **11**, and **15** was isolated in good yield (71%). The 48-amino acid coupling partners **13** and **15** were next subjected to the

 © 2012 Wiley-VCH Verlag GmbH & Co. KGaA, Weinheim

reaction sequence of native chemical ligation, Thz demasking, and desulfurization. The ligation reaction proceeded smoothly and, upon completion, treatment of the crude reaction mixture with methoxyamine hydrochloride provided the 96-amino acid glycoprotein **16**, which was isolated in 52% yield after purification by HPLC using a C4 column. Finally, complete desulfurization of the eight sulfhydryl groups in **16** furnished the 19.5 kDa $AFGP_{32}$ glycoprotein **17** in excellent yield (81%) and purity after purification by HPLC using a C4 column.

With a range of native, synthetic AFGPs now in hand, we next examined the effect of glycopeptide/glycoprotein size on antifreeze activity. Specifically, the synthetic AFGPs were examined for thermal hysteresis (TH) activity by using nanoliter osmometry[15] and were assessed for ice recrystallization inhibition (IRI) activity by using a "splat cooling" assay (see the Supporting Information).[16] Synthetic AFGPs **9**, **10**, **14**, and **17** all displayed TH activity (Figure 1A) and dynamic ice shaping to produce hexagonal-bipyramidal ice crystals, thereby indicating that AFGP oligomers **5**, **9**, **10**, **14**, and **17** were binding to ice (Figure 1B,e–h). The same set of

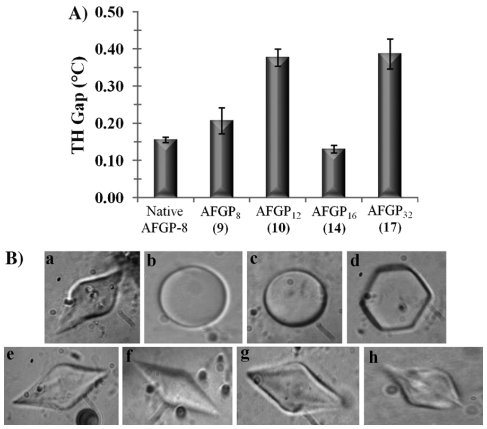

Figure 1. A) Thermal hysteresis (TH) activity of homogeneous synthetic AFGPs and isolated AFGP-8 at 10 mg mL^{-1}. B) Ice crystal morphology in the presence of: a) native AFGP-8; b) $AFGP_2$ (**18**); c) unglycosylated polypeptide $(ATA)_4$ (**19**; 5 mg mL^{-1}); d) $AFGP_4$ (**5**); e) $AFGP_8$ (**9**); f) $AFGP_{12}$ (**10**); g) $AFGP_{16}$ (**14**); h) $AFGP_{32}$ (**17**) at 10 mg mL^{-1}.

synthetic AFGPs also exhibited potent IRI activity at concentrations as low as 55 nM (Figure 2). The 24-amino acid $AFGP_8$ (**9**) possessed a significantly greater TH gap compared with AFGP-8 (a mixed fraction of isolated low-molecular-weight AFGPs) but similar TH activity to a reported AFGP with seven tripeptide repeats.[6] Interestingly, increasing the length of the synthetic AFGP in **10** ($AFGP_{12}$) led to a significant increase in both TH and IRI activities (Figures 1A and 2). However, further increasing the length of the glycopeptide in $AFGP_{16}$ (**14**) led to diminished TH and IRI activities. Specifically, the TH gap of **14** was approximately half of that exhibited by $AFGP_8$ (**9**; Figure 1A) but still exhibited similar IRI activity. The potent TH

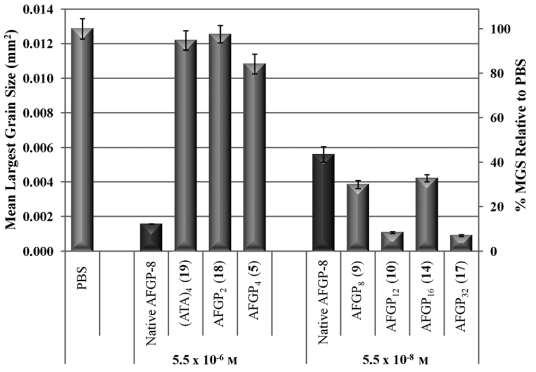

Figure 2. Ice recrystallization inhibition (IRI) activity of isolated AFGP-8, unglycosylated polypeptide $(ATA)_4$ (**19**), $AFGP_2$ (**18**), $AFGP_4$ (**5**), $AFGP_8$ (**9**), $AFGP_{12}$ (**10**), $AFGP_{16}$ (**14**), $AFGP_{32}$ (**17**) at the concentrations given in the figure. The %MGS (mean grain size) of ice crystals relative to the phosphate buffered saline (PBS) positive control is shown for all compounds.

and IRI activities displayed by $AFGP_{12}$ (**10**) is restored in the largest AFGP synthesized in this study, $AFGP_{32}$ (**17**). Specifically, this 19.5 kDa glycoprotein possessed the greatest TH gap (0.39 °C) and IRI activity (at 55 nM) of all the compounds synthesized. Although $AFGP_4$ (**5**) produced hexagonal ice crystals (Figure 1B,d), it did not exhibit a measureable TH gap at 10 mg mL^{-1} or IRI activity at 5.5 μM (Figure 2). This was a surprising result given that this synthetic construct[6,17] and the isolated mixed glycopeptide fraction AFGP-8,[18] have been shown to exhibit a TH gap in prior investigations. Hexaglycopeptide $AFGP_2$ (**18**) and unglycosylated peptide $(ATA)_4$ (**19**; see the Supporting Information for synthesis) did not exhibit thermal hysteresis or ice-structuring ability (Figure 1B,b,c), nor did they possess IRI activity (Figure 2), thus highlighting the importance of glycopeptide length and the necessity of the disaccharide moiety for antifreeze activity as has been highlighted previously.[6] To our knowledge, the present study represents the first investigation of both TH and IRI activities of homogenous synthetic AFGPs with larger chain lengths than seven repeating tripeptide units[6] and has revealed a number of previously unknown structure–activity relationships, which should prove useful for future design of synthetic antifreeze molecules.

Despite there being some debate about the precise conformation of AFGPs in solution,[18,19] several reports have suggested that the molecules adopt the secondary structure of a type II polyproline (PPII) helix in solution, as indicated by CD and NMR spectroscopic studies.[18–20] We were therefore interested in probing the temperature dependent (−5 to 85 °C) secondary structure of the synthetic homogeneous AFGPs in water by using far-UV CD spectroscopy to study correlations between secondary structure and antifreeze activity. At lower temperatures the CD spectra of all AFGPs ($AFGP_2$ (**18**), $AFGP_4$ (**5**), $AFGP_8$ (**9**), $AFGP_{12}$ (**10**), $AFGP_{16}$ (**14**), and $AFGP_{32}$ (**17**)) showed clear PPII helical structural features: a weak positive maximum at

 © 2012 Wiley-VCH Verlag GmbH & Co. KGaA, Weinheim

a wavelength of approximately 215 nm and a stronger negative minimum below 200 nm (see the Supporting Information).[21] In contrast to $AFGP_4$ (**5**), the unglycosylated analogue $(ATA)_4$ (**19**) has a spectrum that is characteristic of β-sheet structure (maximum at ca. 195 and minimum at ca. 220 nm). Notably, the main structural features of all AFGPs diminished with increasing temperature, thereby suggesting a loss of structure in favor of random-coil conformation (see the Supporting Information).[22] The spectral features of a PPII helix were most pronounced for $AFGP_4$ (**5**), which did not exhibit antifreeze activity in this study. The spectra for the smaller $AFGP_2$ (**17**) gave approximately 80% of the $AFGP_4$ (**5**) signal intensity, and the longer AFGPs showed a general trend of diminishing signal intensity with increasing size. Whilst heterogeneous, high-molecular-weight AFGPs that are derived from natural sources are thought to be highly flexible and to lack both short- and long-range order,[19a] we have shown for the first time, that PPII helical structure is retained in larger AFGPs as demonstrated for the 19.5 kDa $AFGP_{32}$ glycoprotein **17**. We note, however, that the secondary structure is not uniform in the analogues with different lengths. Potential differences in the overall structure of these synthetic AFGPs warrant further investigation and will be the focus of future research in our laboratories.

In summary, we have successfully employed a convergent native chemical ligation–desulfurization strategy for the preparation of homogeneous AFGPs ranging in size from 1.2 to 19.5 kDa. The synthetic strategy enabled the assembly of discretely sized AFGP oligomers previously unattainable by conventional synthetic routes. We have established, for the first time, important structure–activity relationships of homogeneous, high-molecular-weight AFGPs. In particular, we have determined the TH and IRI activities of a native 19.5 kDa AFGP which represents, to our knowledge, the highest-molecular-weight AFGP accessed in homogeneous form and one of the largest native glycoproteins prepared by total chemical synthesis to date.

Received: December 9, 2011
Revised: January 26, 2012
Published online: March 2, 2012

Keywords: antifreeze proteins · chemical ligation · glycopeptides · glycoproteins · thermal hysteresis

[1] A. L. DeVries, D. E. Wohlschlag, *Science* **1969**, *163*, 1073.
[2] A. L. DeVries, S. K. Komatsu, R. E. Feeney, *J. Biol. Chem.* **1970**, *245*, 2901.
[3] a) J. A. Raymond, A. L. DeVries, *Proc. Natl. Acad. Sci. USA* **1977**, *74*, 2589; b) C. A. Knight, C. C. Cheng, A. L. DeVries, *Biophys. J.* **1991**, *59*, 409; c) C. A. Knight, E. Driggers, A. L. DeVries, *Biophys. J.* **1993**, *64*, 252; d) C. A. Knight, A. L. DeVries, *J. Cryst. Growth* **1994**, *143*, 301; e) P. W. Wilson, *Cryo Lett.* **1993**, *14*, 31.
[4] M. M. Harding, P. I. Anderberg, A. D. J. Haymet, *Eur. J. Biochem.* **2003**, *270*, 1381.
[5] L. Nagel, C. Plattner, C. Budke, Z. Majer, A. L. DeVries, T. Berkemeier, T. Koop, N. Sewald, *Amino Acids* **2011**, *41*, 719.
[6] Y. Tachibana, G. L. Fletcher, N. Fujitani, S. Tsuda, K. Monde, S.-I. Nishimura, *Angew. Chem.* **2004**, *116*, 874; *Angew. Chem. Int. Ed.* **2004**, *43*, 856.
[7] a) J. Garner, M. M. Harding, *ChemBioChem* **2010**, *11*, 2489; b) R. Peltier, M. A. Brimble, J. M. Wojnar, D. E. Williams, C. W. Evans, A. L. DeVries, *Chem. Sci.* **2010**, *1*, 538.
[8] P. E. Dawson, T. W. Muir, I. Clark-Lewis, S. B. H. Kent, *Science* **1994**, *266*, 776.
[9] L. Z. Yan, P. E. Dawson, *J. Am. Chem. Soc.* **2001**, *123*, 526.
[10] a) B. L. Wilkinson, L. R. Malins, C. K. Y. Chun, R. J. Payne, *Chem. Commun.* **2010**, *46*, 6249; b) B. L. Wilkinson, S. Day, L. R. Malins, V. Apostolopoulos, R. J. Payne, *Angew. Chem.* **2011**, *123*, 1673; *Angew. Chem. Int. Ed.* **2011**, *50*, 1635.
[11] a) Q. Wan, S. J. Danishefsky, *Angew. Chem.* **2007**, *119*, 9408; *Angew. Chem. Int. Ed.* **2007**, *46*, 9248; b) J. Garner, K. A. Jolliffe, M. M. Harding, R. J. Payne, *Chem. Commun.* **2009**, 6925; c) K. S. A. Kumar, S. N. Bavikar, L. Spasser, T. Moyal, S. Ohayon, A. Brik, *Angew. Chem.* **2011**, *123*, 6261; *Angew. Chem. Int. Ed.* **2011**, *50*, 6137.
[12] C. Haase, H. Rohde, O. Seitz, *Angew. Chem.* **2008**, *120*, 6912; *Angew. Chem. Int. Ed.* **2008**, *47*, 6807.
[13] Y. Kajihara, A. Yoshihara, K. Hirano, N. Yamamoto, *Carbohydr. Res.* **2006**, *341*, 1333.
[14] E. C. B. Johnson, S. B. H. Kent, *J. Am. Chem. Soc.* **2006**, *128*, 6640.
[15] A. Chakrabartty, C. L. Hew, *Eur. J. Biochem.* **1991**, *202*, 1057.
[16] a) C. A. Knight, J. Hallett, A. L. DeVries, *Cryobiology* **1988**, *25*, 55; b) J. Jackman, M. Noestheden, D. Moffat, J. P. Pezacki, S. Findlay, R. N. Ben, *Biochem. Biophys. Res. Commun.* **2007**, *354*, 340.
[17] Y. Tachibana, N. Matsubara, F. Nakajima, T. Tsuda, S. Tsuda, K. Monde, S. I. Nishimura, *Tetrahedron* **2002**, *58*, 10213.
[18] A. N. Lane, L. M. Hays, R. E. Feeney, L. M. Crowe, J. H. Crowe, *Protein Sci.* **1998**, *7*, 1555.
[19] a) A. N. Lane, L. M. Hays, N. Tsvetkova, R. E. Feeney, L. M. Crowe, J. H. Crowe, *Biophys. J.* **2000**, *78*, 3195; b) V. R. Bouvet, G. R. Lorello, R. N. Ben, *Biomacromolecules* **2006**, *7*, 565; c) Y. Uda, S. Zepeda, F. Kaneko, Y. Matsuura, Y. Furukawa, *J. Phys. Chem. B* **2007**, *111*, 14355; d) F. Corzana, J. H. Busto, G. Jiménez-Osés, J. L. Asensio, J. Jiménez-Barbero, J. M. Peregrina, A. Avenoza, *J. Am. Chem. Soc.* **2006**, *128*, 14640; e) F. Corzana, J. H. Busto, G. Jiménez-Osés, M. García de Luis, J. L. Asensio, J. Jiménez-Barbero, J. M. Peregrina, A. Avenoza, *J. Am. Chem. Soc.* **2007**, *129*, 9458; f) F. Corzana, J. H. Busto, M. García de Luis, A. Fernández-Tejada, F. Rodríguez, J. Jiménez-Barbero, A. Avenoza, J. M. Peregrina, *Eur. J. Org. Chem.* **2010**, 3525; g) R. Y. Tam, C. N. Rowley, I. Petrov, T. Zhang, N. A. Afagh, T. K. Woo, R. N. Ben, *J. Am. Chem. Soc.* **2009**, *131*, 15745; h) S. S. Mallajosyula, A. D. MacKerell, Jr., *J. Phys. Chem. B* **2011**, *115*, 11215.
[20] C. A. Bush, R. E. Feeney, *Int. J. Pept. Protein Res.* **1986**, *28*, 386.
[21] J. Makowska, S. Rodziewicz-Motowidło, K. Bagińska, J. A. Vila, A. Liwo, L. Chmurzyński, H. A. Scheraga, *Proc. Natl. Acad. Sci. USA* **2006**, *103*, 1744.
[22] C. A. Bush, R. E. Feeney, D. T. Osuga, S. Ralapati, Y. Yeh, *J. Pept. Protein Res.* **1981**, *17*, 125.

 © 2012 Wiley-VCH Verlag GmbH & Co. KGaA, Weinheim

Circular Dichroism (CD) Spectropolarimetry

Far-UV CD spectra were recorded in 1-mm cells on a Jasco J-815 Spectropolarimeter equipped with a 6-position thermostatted Peltier MPTC-490S cell holder cooled by a Multitemp III waterbath (Pharmacia Biotech). Samples (0.1 mg/mL) in water were incubated at -5, 0, 10, 25, 40, 55, 70, 85 °C, as measured in the cell using a Digisense Thermometer (Exetech) equipped with a wire probe thermocouple. Data were collected in continuous scanning mode from 240–195 nm in 1 nm or 0.2 nm steps with a 1 nm bandwidth and 1 s digital integration time. Reported spectra are the average of 3 scans with buffer baseline correction and smoothing (3-point adjacent-averaging for 1-nm scans and 15-point adjacent-averaging for 0.2-nm scans).

Circular Dichroism Spectra

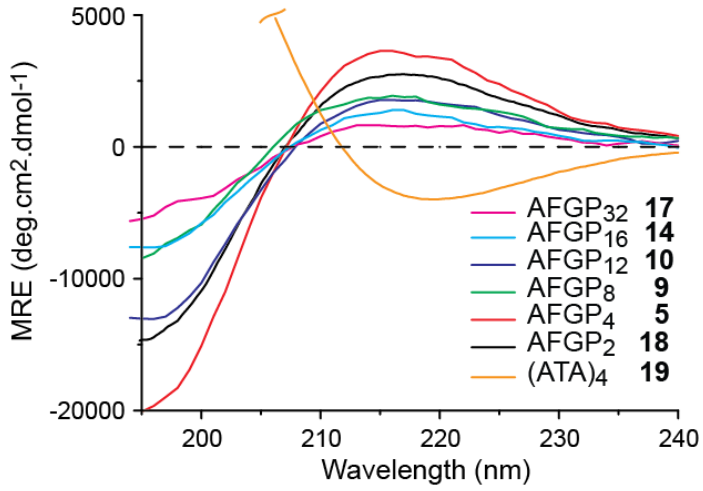

Figure 5. CD spectra of synthetic $AFGP_2$ (**18**), $AFGP_4$ (**5**), $AFGP_8$ (**9**), $AFGP_{12}$ (**10**), $AFGP_{16}$ (**14**) and $AFGP_{32}$ (**17**) and $(ATA)_4$ (**19**) at -5 ^{o}C (samples dissolved in distilled H_2O).

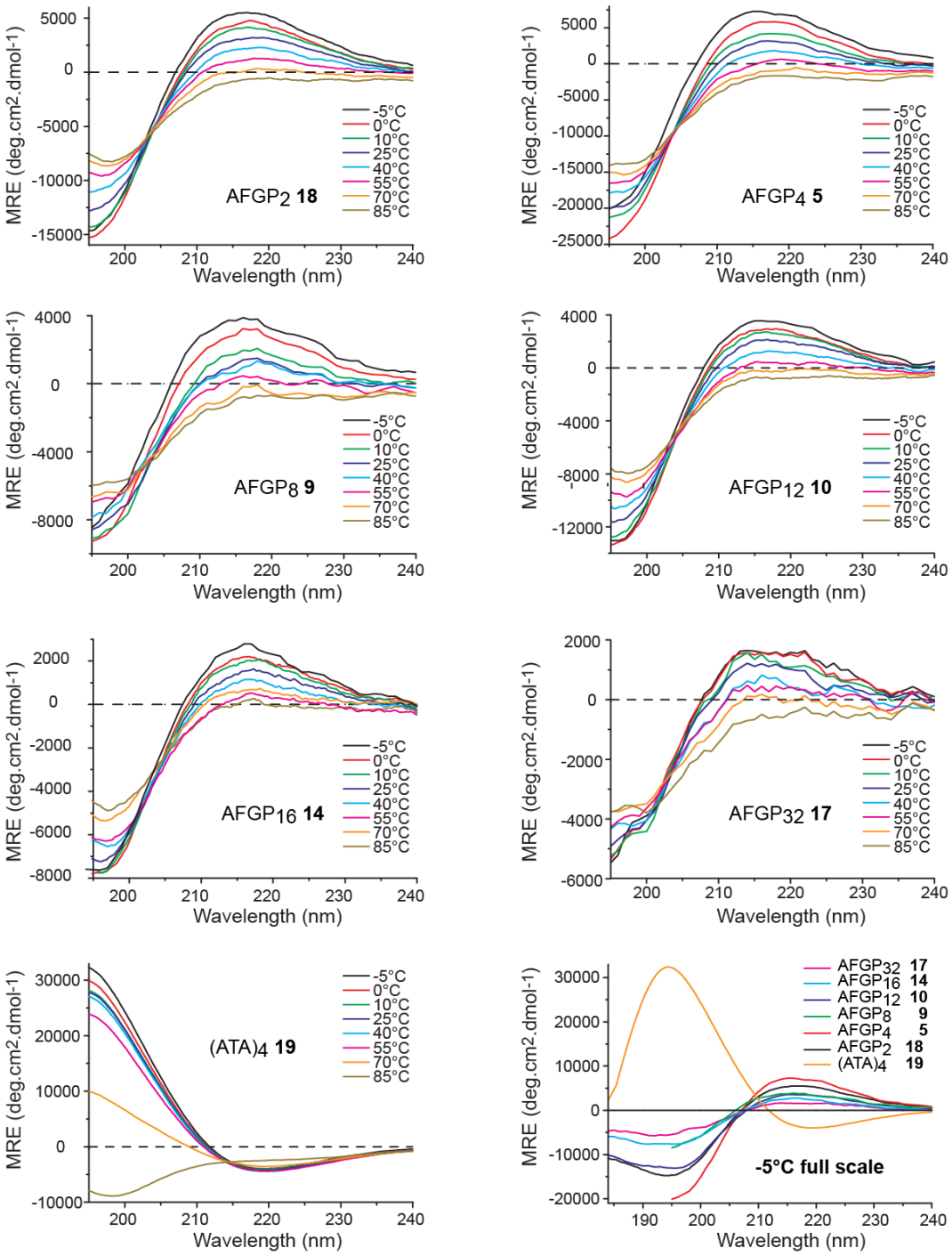

Figure 6. Circular dichroism spectra of synthetic AFGPs **5, 9, 10, 14, 17-19** and unglycosylated $(ATA)_4$ **19** at variable temperature (-5 ^{o}C to 85 ^{o}C).

3.2.3 Results and Discussion of the Antifreeze Activity of synAFGPs

The synthesis of the synAFGPs was completed by collaborators in Dr. Richard J. Payne's laboratory in the school of chemistry at the University of Sydney. Their strategy employed a convergent synthetic approach using native chemical ligation-desulfurization for the first synthesis of homogenous AFGPs ranging in size from 1.2 to 19.5 kDa (see schemes 2 and 3 in section 3.2.2).[31] The synthesis began with the preparation of a key dodecaglycopeptide containing an N-terminal thiazolidine (Thz) residue using Fmoc-SPPS (scheme 2). This dodecaglycopeptide was then utilized to employ key reactions to prepare the synAFGPs. The N-terminal Thz residue was converted to an N-terminal cysteine (Cys) residue in addition to the C-terminal end of the N-terminal Thz containing glycopeptide being converted to a thioester moiety (scheme 2). This would allow for native chemical ligation between the two glycopeptides for the preparation of the higher molecular weight synAFGPs (scheme 3). Desulfurization of the N-terminal Cys residues would then afford the N-terminal Ala residues on the synAFGPs (schemes 2 and 3).

With a range of synAFGPs, the effect of glycopeptide/glycoprotein size on antifreeze activity was examined. Specifically, the synAFGPs were examined for thermal hysteresis (TH) activity using nanoliter osmometry[33] and were assessed for ice recrystallization inhibition (IRI) activity using a "splat cooling" assay.[34,35] The TH activity and ice crystal habits of the synAFGPs, unglycosylated polypeptide $(ATA)_4$ (**19**) and native AFGP-8 is presented in Figure 1. The IRI activity of these compounds is presented in Figure 2. These figures are reproduced below, along with the structures of the synAFGPs within the figures.

$synAFGP_4$ (**5**) produced hexagonal ice crystals (Figure 1 B,d), however it did not exhibit a measureable TH gap at 10 mg/mL or IRI activity at 5.5 μm (Figure 2). At first, this was a surprising result given that native AFGP-8 with four repeating tripeptide units produces hexagonal-bipyramidal ice crystal shaping and a TH gap of 0.16 °C at 10 mg/mL. Additionally, a synthetic construct with the same tripeptide sequence $(Ala\text{-}Thr\text{-}Ala)_n$ repeated four times had been shown to exhibit a TH gap in prior investigations.[19,36] The previous chemical synthesis of $synAFGP_4$ by Nishimimura and co-workers in 2004 was achieved by polymerizing a triglycopeptide of (Ala-Thr-Ala) using diphenylphosphorylazide (DPPA) as a promoter.[19] Size-exclusion chromatography was then used to separate the product mixtures into homogenous fractions of specific chain lengths ranging from two to seven tripeptide repeats. However, it has recently been reported by Nishimura and co-workers in 2013 that a homogenous $synAFGP_4$ synthesized by microwave-assisted SPPS produced hexagonal ice crystal shapes and did not exhibit a TH gap.[37] It was therefore suggested that the products obtained from the polymerization protocol might be contaminated with macromolecular AFGPs even after size exclusion

chromatography, contributing to the observed enhanced activity for those products. A similar effect has been reported previously where the addition of higher molecular weight AFGPs (AFGP 1-5) to an AFGP-8 solution can enhance TH activity 2-8 fold.[38,39] Thus, this study validated the results obtained from our laboratory that synAFGP$_4$ (**5**) failed to exhibit any antifreeze specific activity.

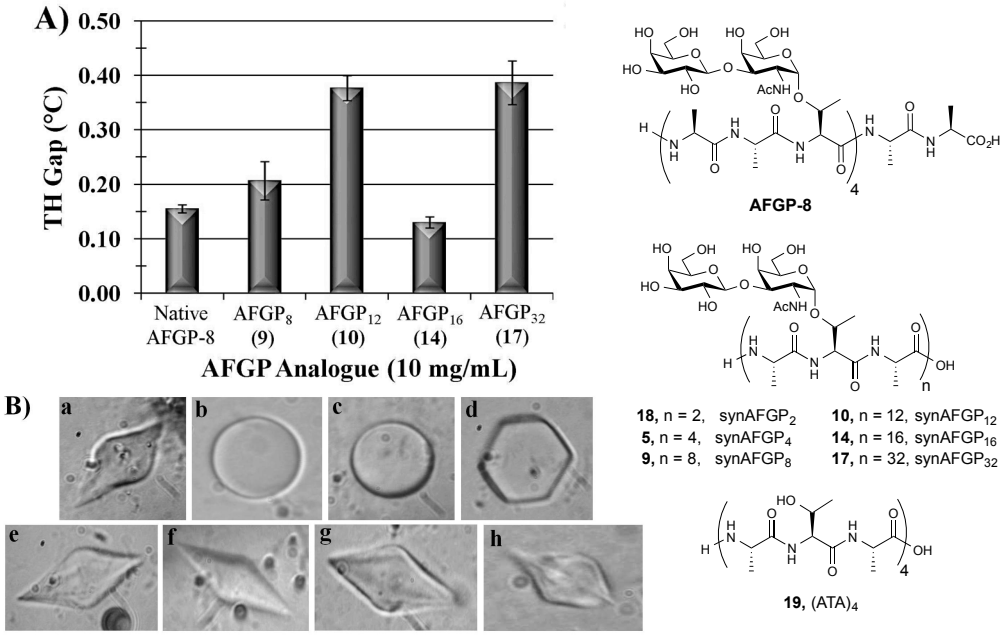

Figure 1. A) Thermal hysteresis (TH) activity of homogeneous synthetic AFGPs and isolated AFGP-8 at 10 mg/mL. **B)** Ice crystal morphology in the presence of: a) native AFGP-8; b) AFGP$_2$ (**18**); c) unglycosylated polypeptide (ATA)$_4$ (**19**; 5 mg/mL); d) AFGP$_4$ (**5**); e) AFGP$_8$ (**9**); f) AFGP$_{12}$ (**10**); g) AFGP$_{16}$ (**14**); h) AFGP$_{32}$ (**17**) at 10 mg/mL.

It is interesting to note that both synAFGP$_4$ (**5**) and native AFGP-8 contain four tripeptide repeats but a different sequence of amino acids. Native AFGP-8 consists of a tripeptide repeat of (Ala-Ala-Thr)$_n$ and bears two C-terminal Ala residues, whereas synAFGP$_4$ consists of a tripeptide repeat of (Ala-Thr-Ala)$_n$. However, only AFGP-8 exhibits antifreeze specific activity (Figures 1 and 2). It is suggested that the binding of AFGPs to ice involves hydrogen bonding between the hydroxyl groups of the sugars and the ice lattice.[40] Neither the X-ray crystal structure of AFGPs nor the definitive structure that AFGPs adopt in the presence of ice has yet been determined. The solution structure of AFGPs has been debated in the literature (see section 1.2.1), and while an ordered PPII helix has been suggested,[14,16-18] recent studies have suggested AFGP-8 is predominantly extended random coil with short segments of localized ordered structure.[10-16] This localized ordered structure is typically found in segments of the AFGP sequence where an alanine residue is replaced with a proline residue.[14,15] synAFGP$_4$ (**5**) was found to adopt a secondary structure in solution similar to a PPII helix as determined by far-UV CD spectroscopy (Figures 5

and 6).[31] The difference in the antifreeze activity exhibited by synAFGP$_4$ and AFGP-8 therefore might be attributed to the small variation in structures from the different sequences of amino acids in the tripeptide repeats. This could cause a change in the conformation adopted in solution, and even a small change could cause a drastic effect on the ability of the molecule to bind to ice and exhibit antifreeze activity.[19] However, further studies are still required to determine the influence of the sequence of amino acids in the tripeptide repeat on both antifreeze activity and solution conformation.

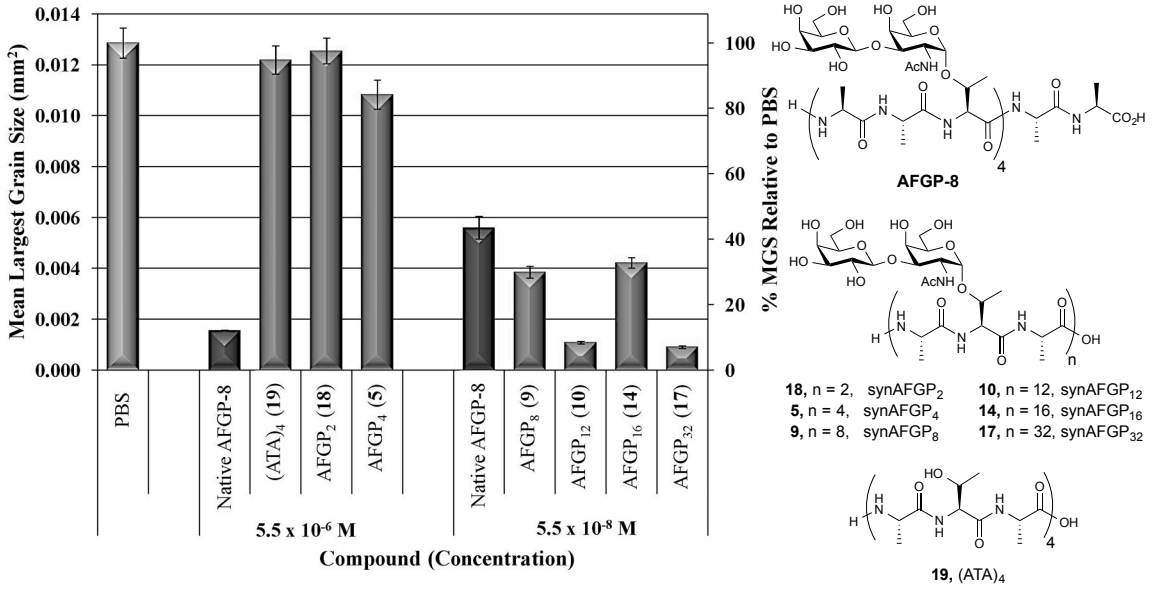

Figure 2. Ice recrystallization inhibition (IRI) activity of isolated AFGP- 8, unglycosylated polypeptide (ATA)$_4$ (**19**), AFGP$_2$ (**18**), AFGP$_4$ (**5**), AFGP$_8$ (**9**), AFGP$_{12}$ (**10**), AFGP$_{16}$ (**14**), AFGP$_{32}$ (**17**) at the concentrations given in the figure. The %MGS (mean grain size) of ice crystals relative to the phosphate buffered saline (PBS) positive control is shown for all compounds.

Hexaglycopeptide synAFGP$_2$ (**18**) and unglycosylated peptide (ATA)$_4$ (**19**) did not exhibit TH activity or dynamic ice shaping capabilities (Figure 1 B,b-c), nor did they inhibit ice recrystallization at 5.5 μm (Figure 2).[31] These results highlight the necessity of the disaccharide moiety and the impact of glycopeptide length for both activities. synAFGP$_8$, synAFGP$_{12}$, synAFGP$_{16}$ and synAFGP$_{32}$ (**9**, **10**, **14** and **17**, respectively) all displayed TH activity (Figure 1 A) and dynamic ice shaping capabilities to produce hexagonal-bipyramidal ice crystals, thereby indicating that these synAFGPs were binding to ice (Figure 1 B,e–h). The same set of synAFGPs also exhibited potent IRI activity at concentrations as low as 55 nm (Figure 2). These results emphasize the importance of glycopeptide length for antifreeze activity as has been described previously.[19] Nishimura and co-workers in 2013 synthesized a homogeneous synAFGP$_5$ derivative (five tripeptide repeats of (Ala-Thr-Ala)$_n$) utilizing a microwave-assisted SPPS

protocol, and this compound exhibited TH activity[37] suggesting that greater than four tripeptide repeats are required for activity when this sequence of amino acid is used for the tripeptide repeat. This current work with synAFGPs is the first investigation of both TH and IRI activities of homogenous synthetic AFGPs with chain lengths greater than four repeating tripeptide units. Additionally, the 19.5 kDa synAFGP$_{32}$ (**17**) is the highest molecular-weight AFGP chemically synthesized as assessed for antifreeze activity.

The 24-amino acid synAFGP$_8$ (**9**) possessed a greater TH gap compared with native AFGP-8, but similar TH activity to a reported synAFGP$_7$ with seven tripeptide repeats.[19] Increasing the length of the glycopeptide to twelve tripeptide repeats (synAFGP$_{12}$, **10**) increased TH and IRI activities (Figures 1A and 2). However, elongation to 16 tripeptide repeats (synAFGP$_{16}$, **14**) led to reduced TH and IRI activities. Additional elongation of the glycopeptide to 32 tripeptide repeats (synAFGP$_{32}$, **17**) restored the potent TH and IRI activities exhibited by these glycopeptides. synAFGP$_{32}$ had a TH gap of 0.39 ± 0.04 °C and IRI activity of 7.1 ± 0.41 % MGS relative to the PBS positive control (Figures 1A and 2). Interestingly, synAFGP$_{16}$ (**14**) exhibited almost half the TH activity (0.12 ± 0.01 °C) of synAFGP$_8$ (**9**, 0.21 ± 0.04 °C), yet synAFGP$_{16}$ (**14**) is double the length of synAFGP$_8$ (**9**) (Figure 1A). Moreover, these compounds both had similar IRI activities (approximately 30% MGS, Figure 2). Both synAFGP$_{12}$ (**10**) and synAFGP$_{32}$ (**17**) exhibited similar TH (0.38-0.39 °C) and IRI activities (7-8% MGS), despite synAFGP$_{32}$ (**17**) being almost three times the length of synAFGP$_{12}$ (**10**). Both of these synAFGPs were three times more IRI active than synAFGP$_8$ (**9**) and synAFGP$_{16}$ (**14**). However, TH activity was modulated differently as they were twice as TH active as synAFGP$_8$ (**9**) and almost four times as TH active as synAFGP$_{16}$ (**14**).

These results indicate that the magnitude of change in TH activity differed from the magnitude of change in IRI activity as the length of the homogenous synAFGPs was increased. This may suggest that the two types of antifreeze activities are not as tightly correlated as previously thought, and this hypothesis is discussed in more detail in Chapter 4. While further work is still required in this area to verify this hypothesis, studies on synthetic structural analogues of AFGPs have shown it is possible to decouple the two types of antifreeze activities from each other, resulting in compounds that exhibit "custom-tailored" antifreeze activity and are only IRI active and not TH active (see section 1.3.1).[21,22] The IRI and TH results of the synAFGPs also highlight the influence of glycopeptide length on both activities. While it was previously suggested that increasing the length of the glycopeptide would increase TH activity,[19] the results from our study indicate that there are optimal lengths and numbers of tripeptide repeats that result in the most

potent TH and IRI activities. Elongation of the synAFGP sequence does not always result in an increase in both activities.

The secondary structure adopted by the homogeneous synAFGPs in solution over a range of temperatures (-5 to 85 °C) was assessed using far-UV CD spectroscopy by Dr. Richard J. Payne's laboratory in the school of chemistry at the University of Sydney. All synAFGPs regardless of glycopeptide length showed PPII helical structural features at lower temperatures with a strong negative minimum around a wavelength of 195 nm and weak positive maximum at approximately 215 nm (Figures 5 and 6, reproduced below).[31] The unglycosylated $(ATA)_4$ (**19**) showed a spectrum characteristic of a β-sheet structure. As the temperature was increased the PPII structure began to diminish and the secondary structures of the synAFGPs had more random coil characteristics (Figure 6). The synAFGP$_4$ derivative (**5**) had the most defined PPII helical spectrum, and all other synAFGPs showed a decrease in signal intensity with an increase is synAFGP size (with constant temperature). This decrease in intensity could indicate that while significant PPII character is still observed, as the length of the synAFGPs was increased a distortion in the PPII conformation may be occurring making the glycopeptides more flexible.[41,42] This is consistent with the a lack of short- and long-range order in solution for heterogeneous native high molecular weight AFGPs.[43] However, other factors may be contributing to the observed decreased intensity such as changes in the hydration of the glycopeptides.[44]

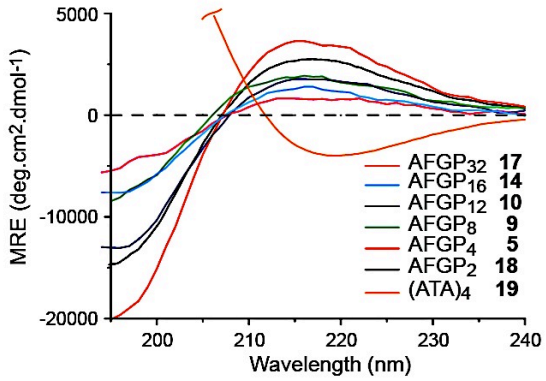

Figure 5. CD spectra of synthetic AFGP$_2$ (**18**), AFGP$_4$ (**5**), AFGP$_8$ (**9**), AFGP$_{12}$ (**10**), AFGP$_{16}$ (**14**), AFGP$_{32}$ (**17**) and $(ATA)_4$ (**19**) at -5 °C (samples dissolved in distilled H_2O).

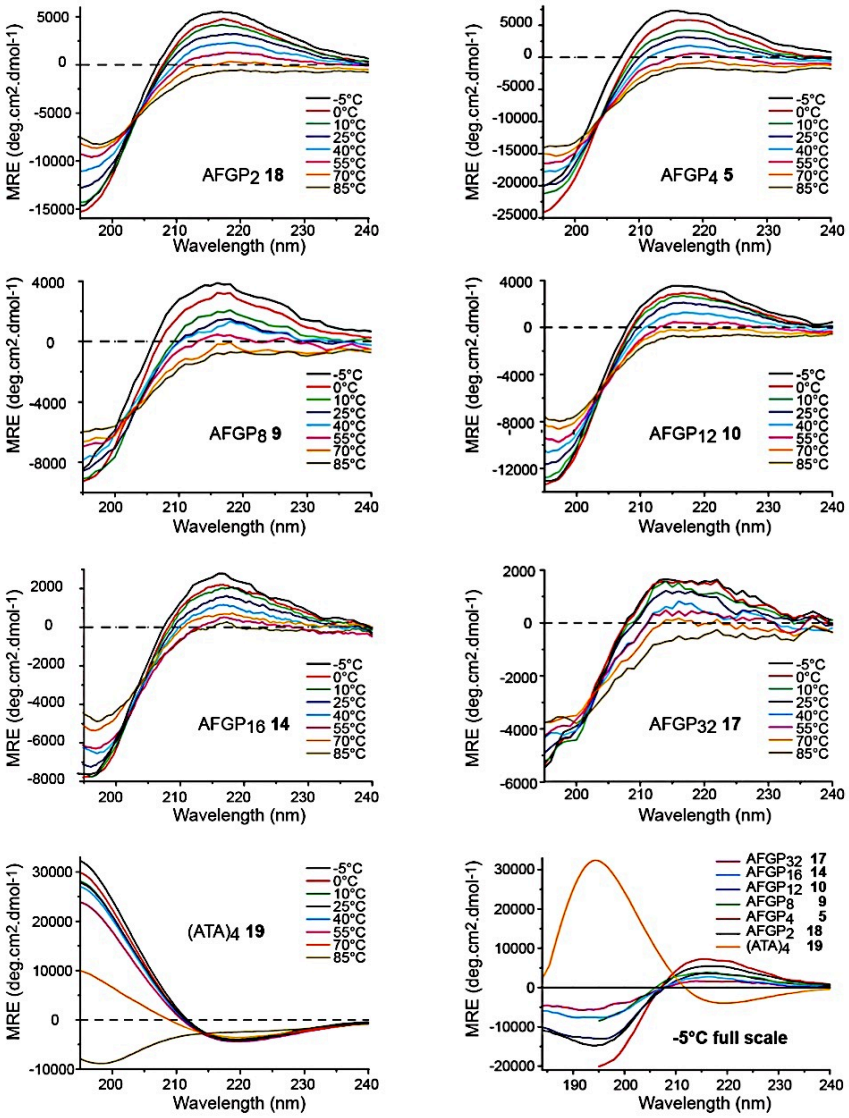

Figure 6. Circular dichroism spectra of synthetic AFGPs **5**, **9**, **10**, **14**, **17-18** and unglycosylated $(ATA)_4$ **19** at variable temperature (-5 to 85 °C).

Interestingly, the most defined PPII structure was observed for $synAFGP_4$ (**5**) and this derivative did not exhibit antifreeze activity. The higher molecular weight synAFGPs were also suggested to all adopt a PPII helical structure, yet the degree of antifreeze activity exhibited differed depending on the molecular weight of the glycoprotein. This suggests that a PPII helical structure may not be a requirement for the activity exhibited by these synAFGPs. This hypothesis is further supported by the fact that other AFGP derivatives that adopt a PPII helical structure in solution do not possess TH or IRI activity (see section 3.3). The exact cause for the difference in antifreeze activity observed for the elongated synAFGPs, and more specifically the decrease in activity observed with the $synAFGP_{16}$ (**14**) derivative, is not currently known. A plausible

explanation for this could be that cooperative effects may be occurring with the shorter synAFGPs (synAFGP$_8$ and synAFGP$_{12}$) such as aggregation, which has previously been demonstrated to enhance the TH activity of AFGP-8.[45] The largest synAFGP assessed in this study with 32 tripeptide repeats (synAFGP$_{32}$, **17**) may also be large enough to bind and cover a greater surface area of the ice crystals. This would decrease the surface area of exposed ice, thereby increasing the radius of curvature of the ice making it energetically unfavourable for ice growth to occur, consequently increasing activity (see section 1.2.3).[46,47] However, further studies are required to provide insight on the drastic difference in activities upon elongation of the synAFGP length. Nevertheless, this study has provided valuable insight into the important structural features and the dependence on size for both TH and IRI activity exhibited by AFGPs.

3.2.4 Summary and Conclusions for the IRI and TH Activity of synAFGPs

A range of homogenous synAFGPs varying in size from 1.2 – 19.5 kDa were assessed for their ability to inhibit ice recrystallization, to exhibit TH activity and dynamic ice shaping capabilities and were assessed for the structure they adopt in solution. This is the first study reported that has investigated the effect AFGP structural variations have on both TH and, more importantly, IRI activity. In addition, this is the first report of the chemical synthesis of high molecular weight AFGPs up to 32 tripeptide repeats (19.5 kDa glycoprotein) and of the antifreeze activity of homogenous high molecular weight AFGPs as the isolated higher molecular weight fractions (AFGPs 1-5) are mixtures of a variety of different sized glycopeptides.

The results from this study have highlighted the importance of the sequence of amino acids in the tripeptide repeat for both TH and IRI activity for the smallest native AFGP-8. Native isolated AFGP-8 consists of four tripeptide repeats of (Ala-Ala-Thr)$_n$ and bears two C-terminal alanine residues and it exhibits both activities. However, synAFGP$_4$ consists of four tripeptide repeats of (Ala-Thr-Ala)$_n$ and this compound did not exhibit either activity. This study has also emphasized the importance of glycosylation and glycopeptide length for both TH and IRI activity. Elongation of the synAFGPs to greater than four tripeptide repeats resulted in both activities. An increase in glycopeptide length did not always result in an increase in activity however, as the second longest glycopeptide assessed in this series with 16 tripeptide repeats (synAFGP$_{16}$) was less TH active than native AFGP-8. This synAFGP also exhibited half of the TH activity of synAFGP$_8$, which is half of its size, but these synAFGPs had similar IRI activity. These results suggest that IRI and TH activity can be modulated differently even within the biological antifreezes (discussed further in Chapter 4). This is significant as IRI activity was previously thought to be a direct result of TH activity, but potent IRI activity without TH activity is highly desirable for the application of ice

recrystallization inhibitors as cryoprotectants. Finally, while CD results have indicated that these synAFGPs adopt a PPII helical structure in solution, this structure is not a prerequisite for TH and IRI activity. synAFGP$_4$ showed the strongest PPII characteristics of the synAFGPs assessed in this study, yet this derivative did not exhibit either activity.

3.3 IRI and TH Activity of Peptide and Glycopeptide Analogues of AFGPs with Polyproline Type II (PPII) Helical Structure

3.3.1 Peptide and Glycopeptide AFGP Analogues with PPII Solution Structure

With the results of the synAFGP derivatives adopting a PPII helical structure in solution (section 3.2), interest arose in synthesizing derivatives of AFGPs that would possess more defined PPII structures to assess for both types of antifreeze activity. Towards this end, hydroxyproline (HyP) derivatives were explored as it had been previously demonstrated that a contiguous nonapeptide HyP and a galactosylated nonaglycopeptide HyP formed thermally stable PPII helical structures in solution.[44] Additionally, high molecular weight polymers of HyP with an average of 44 residues (HyP$_{44}$) were also found to exhibit moderate IRI activity and resulted in ice crystal sizes that were half the size of the PBS control.[48] We therefore sought to explore unglycosylated contiguous HyP derivatives **1**-**2** (figure 3.4), and glycosylated HyP derivatives **3**-**4** bearing an α-*N*-acetyl-D-galactosamine (α-GalNAc) as synAFGPs containing α-GalNAc residues in place of the native disaccharide retained TH activity.[19] (Glyco)peptides containing both a free N-terminal amine and an acetylated N-terminus we examined to determine the influence of the N-terminus on antifreeze activity. Furthermore, dodecapeptide derivatives with a tripeptide repeated of (Ala-HyP-Ala)$_4$ were prepared to investigate if HyP could be a suitable replacement for Thr found in native AFGPs. Thus, unglycosylated (**5**-**6**) and glycosylated derivatives with either an α-GalNAc monosaccharide (**7**-**8**) or the native β-D-galactosyl-(1-3)-α-*N*-acetyl-D-galactosamine (β-Gal-(1,3)-α-GalNAc) disaccharide (**9**-**10**) found in AFGPs were assessed for antifreeze specific activity (figure 3.4). This would provide valuable information with regards to the importance of a PPII solution structure for both IRI and TH activity and would further establish if these activities are influenced by this structure. Furthermore, this study would provide additional structure-function information on important features that are required not only for TH, but also for the IRI activity exhibited by AFGPs and synAFGPs as the IRI activity of biological antifreezes and their derivatives is often overlooked.

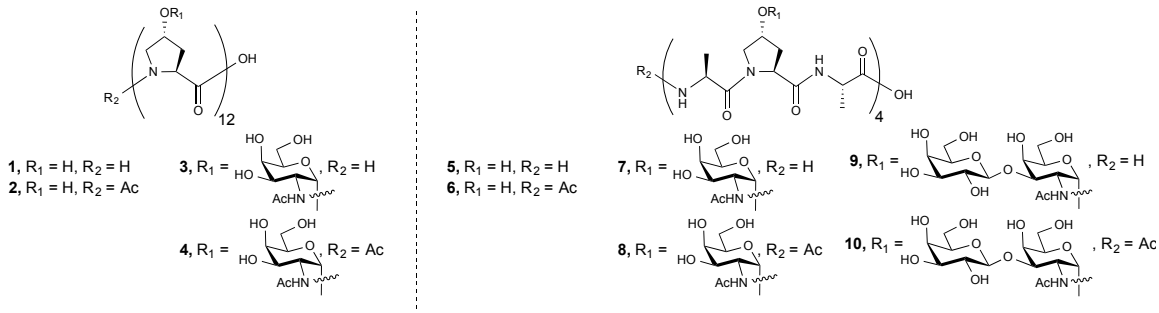

Figure 3.4 Structures of peptide and glycopeptide AFGP analogues with PPII helical solution structure.

The synthesis and antifreeze specific activity (TH and IRI activity) of the peptides and glycopeptides assessed in this study was reported in an article published in 2013 in *Bioorganic and Medicinal Chemistry* from a collaboration between our laboratory and Dr. Richard J. Payne's laboratory in the school of chemistry at the University of Sydney. This article is provided in section 3.3.2 and a detailed discussion of the IRI and TH results and the relationship between peptide and glycopeptide PPII solution structure for these activities is provided in section 3.3.3. All compounds, figures and schemes are numbered as they appear in the article and are reproduced with the same numbering schemes in section 3.2.3 to complement the discussion. The compound, figure and scheme numbers from this article discussing PPII peptides and glycopeptides are only for section 3.3 of this chapter.

3.3.2 Article: "Synthesis of Peptides and Glycopeptides with Polyproline II Helical Topology as Potential Antifreeze Molecules"

Bioorganic & Medicinal Chemistry 21 (2013) 3569–3581

Contents lists available at SciVerse ScienceDirect

Bioorganic & Medicinal Chemistry

journal homepage: www.elsevier.com/locate/bmc

Synthesis of peptides and glycopeptides with polyproline II helical topology as potential antifreeze molecules

Leo Corcilius [a], Gajan Santhakumar [a], Robin S. Stone [a], Chantelle J. Capicciotti [b], Soumya Joseph [c], Jacqueline M. Matthews [c], Robert N. Ben [b], Richard J. Payne [a,*]

ARTICLE INFO

Article history:
Available online 21 February 2013

Keywords:
Glycopeptides
Antifreeze glycoprotein
Carbohydrate
Hydroxyproline
Polyproline II helix

ABSTRACT

A library of peptides and glycopeptides containing (4*R*)-hydroxy-L-proline (Hyp) residues were designed with a view to providing stable polyproline II (PPII) helical molecules with antifreeze activity. A library of dodecapeptides containing contiguous Hyp residues or an Ala-Hyp-Ala tripeptide repeat sequence were synthesized with and without α-O-linked *N*-acetylgalactosamine and α-O-linked galactose-β-(1→3)-*N*-acetylgalactosamine appended to the peptide backbone. All (glyco)peptides possessed PPII helical secondary structure with some showing significant thermal stability. The majority of the (glyco)peptides did not exhibit thermal hysteresis (TH) activity and were not capable of modifying the morphology of ice crystals. However, an unglycosylated Ala-Hyp-Ala repeat peptide did show significant TH and ice crystal re-shaping activity suggesting that it was capable of binding to the surface of ice. All (glyco)peptides synthesized displayed some ice recrystallization inhibition (IRI) activity with unglycosylated peptides containing the Ala-Hyp-Ala motif exhibiting the most potent inhibitory activity. Interestingly, although glycosylation is critical to the activity of native antifreeze glycoproteins (AFGPs) that possess an Ala-Thr-Ala tripeptide repeat, this same structural modification is detrimental to the antifreeze activity of the Ala-Hyp-Ala repeat peptides studied here.

© 2013 Elsevier Ltd. All rights reserved.

1. Introduction

Antifreeze glycoproteins (AFGPs) are a class of natural products found in the body fluids of deep sea Teleost fish in Arctic and Antarctic waters.[1–6] The biological role of these molecules is to protect against cryoinjury in water temperatures colder than the equilibrium freezing point of blood and internal fluids, specifically through the prevention of ice crystal growth in vivo.[7] AFGPs possess two remarkable activities; (1) ice recrystallization inhibition (IRI) activity, whereby the molecules are capable of inhibiting the enthalpically driven reorganization of ice crystals and (2) thermal hysteresis (TH) activity, where the molecules possess the ability to suppress the freezing point of water below the melting point.[1–6] In addition, the binding of AFGPs to ice results in a characteristic change in morphology from spherical to hexagonal bipyramidal shaped ice crystals.[8–12] The mechanism of action of AFGPs is proposed to occur via an adsorption–inhibition process that results in the alteration of ice crystal morphology and a localized freezing point depression at the surface of the ice crystal through the Kelvin effect.[8–12]

AFGPs also possess intriguing structural features; they are mucin-type repeat glycoproteins consisting of a single glycotripeptide repeat (Ala-Ala-Thr), where each threonine is glycosylated to the disaccharide D-galactosyl-β-(1→3)-*N*-acetyl-D-galactosamine [Galβ-(1→3)GalNAc] through an α-glycosidic linkage (Fig. 1).[13] AFGPs range in molecular weight from approximately 2.6 kDa (four tripeptide repeat units) to 33.7 kDa (50 tripeptide repeat units).[1–6] Although the primary amino acid sequence of native AFGPs is highly conserved, Pro residues can often substitute Ala residues in the linear sequence to provide compounds with IRI and TH activity.[14,15] In addition, antifreeze activity can persist with a single GalNAc moiety, as demonstrated by the AFGP from *Pleagranna antarcticum*.[16]

Although there has been significant debate surrounding the precise conformation of native AFGPs in solution, a number of studies using circular dichroism (CD) spectropolarimetry and NMR, Raman and IR spectroscopy have demonstrated that native AFGPs of low molecular weight possess flexible left-handed helical structures similar to a polyproline II (PPII) helix.[17–19] The carbohydrate residues are thought to be aligned on one face of the helix generating a hydrophilic face, while the methyl side chains from the alanine and threonine residues make up the hydrophobic face. As a result, the AFGPs are believed to be amphipathic, with binding

0968-0896/$ - see front matter © 2013 Elsevier Ltd. All rights reserved.
http://dx.doi.org/10.1016/j.bmc.2013.02.025

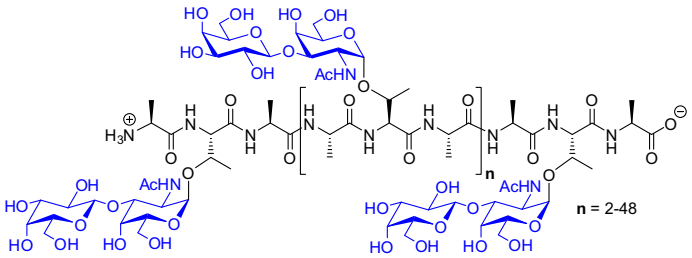

Figure 1. Structure of native antifreeze glycoproteins (AFGPs).

to the surface of ice occurring with the hydrophilic face.[20,21] Larger AFGPs are thought to possess more flexible random coil structures with high segmental mobility; however, recent CD studies with large synthetic AFGPs (up to 19.5 kDa) have shown that these structures do possess significant PPII structure in solution.[22]

The unique activity and structure of AFGPs has led to significant interest in these molecules for applications in material science and medicine.[23–27] A number of structure–activity studies have recently been conducted,[21,22,28–33] with the most extensive study reported by Nishimura and co-workers in 2004.[21] This study highlighted a number of key structural features that are essential for TH activity and for PPII helical structure; (1) the carbohydrate must be linked to the threonine residue with α-configuration, (2) the *N*-acetyl moiety must be present at the 2-position of the bridgehead sugar which must be galacto-configured, and (3) the γ-methyl group of threonine is essential (analogues with serine in place of threonine lost activity). This study has provided impetus for the rational design of AFGP analogues that possess antifreeze activity but are simpler to access.[34,45] Herein, we describe the synthesis of a library of peptides and glycopeptides incorporating unglycosylated or glycosylated (4*R*)-hydroxy-L-proline (Hyp). These (glyco)peptides were designed to possess more defined PPII helical secondary structures in solution when compared to native AFGPs, with a view to elucidating novel antifreeze molecules (Fig. 2).

2. Results and discussion

2.1. Design

Schweizer and co-workers have recently demonstrated that a nonapeptide of contiguous Hyp units bearing β-configured galactose at each Hyp residue was capable of forming thermally stable PPII helical structures in solution.[46] Molecular modeling suggested that this stability was owing to a regular network of glycan–glycan and glycan–peptide hydrogen bonds. Although PPII helical structure is by no means a prerequisite for antifreeze activity (other antifreeze peptides and proteins have different structures) it has been demonstrated to be one critical feature of native AFGPs vide supra.[17–19] This study provided us with inspiration to design a library of PPII helical peptides and glycopeptides possessing Hyp and glycosylated Hyp residues to elucidate novel antifreeze molecules. Although a recent study by Sewald and co-workers showed that incorporation of Hyp residues into AFGP–collagen hybrid peptides and glycopeptides was detrimental to antifreeze activity,[30] a collagen hydrolysate which contains significant Hyp content has been shown to inhibit ice recrystallization in frozen food[47] and simple collagen-based tetrapeptides have also exhibited potent antifreeze activity.[48] In addition, a recent study by Gibson et al. demonstrated that polymers of Hyp, specifically polyHyp$_{44}$, possessed moderate IRI activity.[38]

Our first targets included dodecapeptides **1** and **2**, and dodecaglycopeptides **3** and **4**, possessing contiguous unglycosylated Hyp and contiguous α-GalNAc-derived Hyp, respectively (Fig. 2). (Glyco)peptides possessing both a free N-terminal amine and an acetylated N-terminus were targeted to investigate the importance of the N-terminus on antifreeze activity.[49] It was anticipated that one of the two methylene carbons within the ring of Hyp could function as a substitute for the important methyl moiety of Thr in native AFGPs.[50] As such, a series of (glyco)peptides were also designed that possessed the native AFGP sequence but in which Thr was substituted with Hyp. This included dodecapeptides **5** and **6**, as well as dodecaglycopeptides **7** and **8** bearing α-linked GalNAc residues and **9** and **10**, bearing α-linked Gal-β-(1→3)-GalNAc, the carbohydrate present on native AFGPs. It was envisioned that this library would enable the importance of structure, amino acid sequence and glycosylation for antifreeze activity to be simultaneously evaluated.

2.2. Chemistry

2.2.1. Synthesis of glycosylamino acids

The synthesis of the proposed AFGP analogues began with the preparation of suitably protected glycosylhydroxyproline derivatives **11** and **12**, bearing α-linked GalNAc and α-linked Gal-β-(1→3)-GalNAc, respectively. Preparation of both analogues began from D-galactosamine hydrochloride salt **13** which was first treated with imidazole-based diazotransfer reagent **14**[51] to afford the corresponding 2-azido-2-deoxy sugar which was subsequently treated with acetic anhydride in pyridine in the presence of catalytic DMAP to effect global acetylation of the alcohol moieties and afford **15** in 68% yield over the two steps (Scheme 1). Selective anomeric deacetylation through treatment with ethylenediamine and acetic acid then provided hemiacetal **16** in quantitative yield. At this stage the hemiacetal was converted to the corresponding trichloroacetimidate **17** in 71% yield by treatment with trichloroacetonitrile and potassium carbonate which was now primed to serve as the donor in a Schmidt glycosylation reaction with a suitably protected Hyp acceptor. To this end, Fmoc-Hyp-O*t*Bu was reacted with **17** at −30 °C in a mixture of diethylether and dichloromethane using trimethylsilyl trifluoromethanesulfonate (TMSOTf) as the Lewis acid to provide glycosylamino acid **18** in 84% yield as an inseparable 3:1 mixture of α- and β-anomers. It is important to note that the use of diethylether as a co-solvent was critical to afford α-selectivity in the reaction. Reductive acetylation of the 2-azido moiety of **18** was effected by treatment with activated zinc and acetic anhydride in acetic acid. At this stage the α- and β-anomers could be separated by flash column chromatography which enabled isolation of the desired α-anomer **19** in 66% yield (88% yield based on combined isolated α- and β-anomers). It should be noted that NMR spectroscopic characterization of **19** showed it to be a 1:1 mixture of rotational isomers in the resulting spectra (see

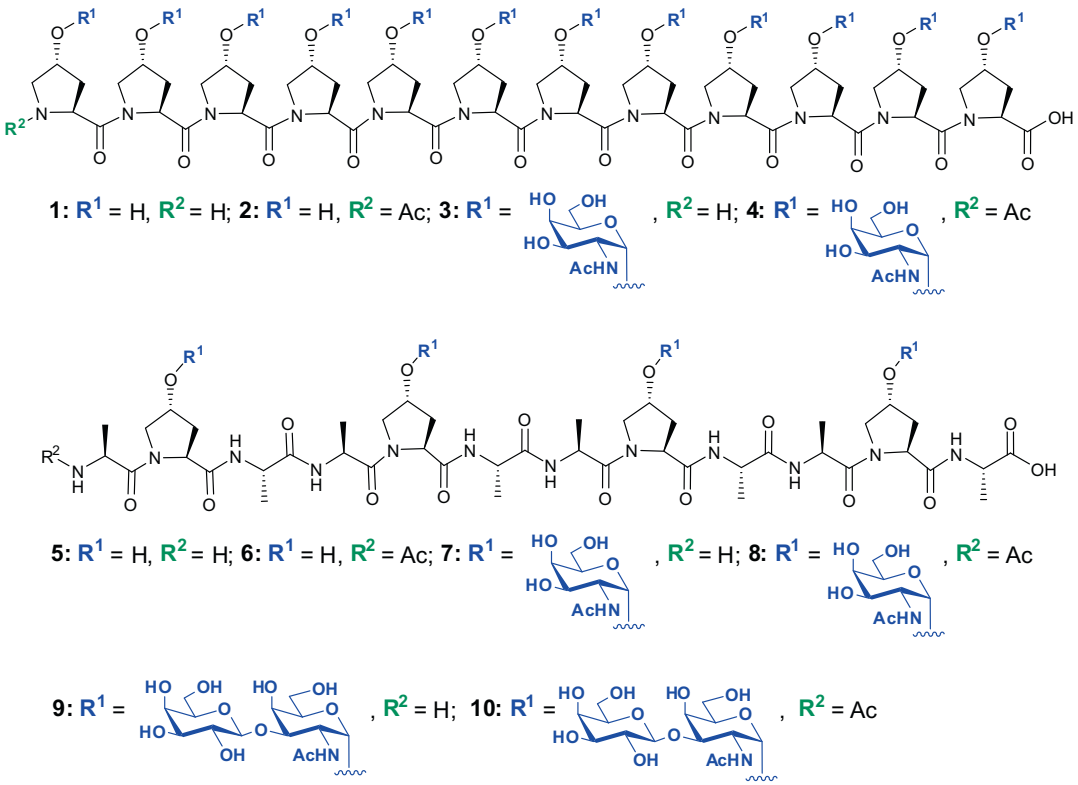

Figure 2. Proposed library of Hyp-based peptides and glycopeptides.

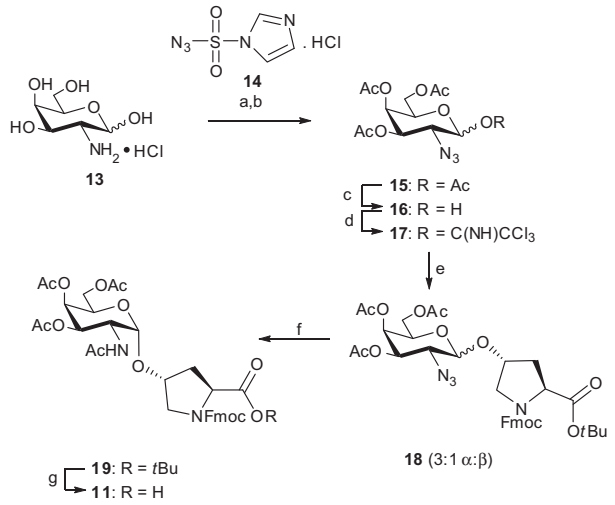

Scheme 1. Synthesis of monosaccharide-derived hydroxyproline building block **11**. Reagents and conditions: (a) imidazole-1-sulfonyl azide **14**,[51] $CuSO_4$, K_2CO_3, MeOH, rt, 18 h; (b) 1:6 v/v Ac_2O:pyridine, DMAP, rt, 18 h, 68% over two steps; (c) $H_2NCH_2CH_2NH_2$, AcOH, THF, rt, 24 h, quant.; (d) Cl_3CCN, K_2CO_3, DCM, rt, 14 h, 71%; (e) Fmoc-Hyp-O*t*Bu, TMSOTf, 1:1 v/v DCM/Et_2O, −30 °C, 1.5 h, 84%; (f) Ac_2O, AcOH, Zn, THF, rt, 18 h, 66%; (g) 95:5 v/v TFA:H_2O, rt, 30 min, 95%.

Supplementary data). Finally, acidolytic deprotection of the *tert*-butyl ester provided the desired glycosylamino acid building block **11** in 95% yield which was ready for incorporation into glycopeptide targets **3**, **4**, **7** and **8** via Fmoc-strategy SPPS.

Synthesis of the disaccharide containing glycosylamino acid building block **12** began from azide **18** prepared above (Scheme 2). Deacetylation under Zemplén conditions followed by treatment with benzaldehyde dimethylacetal in the presence of catalytic *p*-toluene sulfonic acid (*p*TsOH) under reduced pressure generated benzylidene acetal **20** which could be separated from the unwanted β-anomer via flash column chromatography in 61% yield over the two steps (80% based on isolated α- and β-anomers). Again, the NMR spectroscopic analysis of **20** showed a mixture of rotational isomers, confirmed by a saturation transfer experiment (see Supplementary data). Installation of the desired galactose moiety at the free C-3 hydroxyl was achieved by reaction with tetraacetyl galactose trichloroacetimidate **21** at −20 °C using TMSOTf as the Lewis acid promoter. As expected, the reaction proceeded with complete β-selectivity owing to neighboring group participation of the 2-acetyl group on the galactose moiety to provide **22** in 63% yield. From here, acidic deprotection of the benzylidene acetal followed by re-acetylation of the resulting alcohols at the 4- and 6-positions provided the peracetylated glycosylamino acid **23** in excellent yield. Reductive acetylation of the 2-azido functionality provided **24** which, following acidic cleavage of the *tert*-butyl ester provided the desired glycosylamino acid **12** in excellent yield over the two steps.

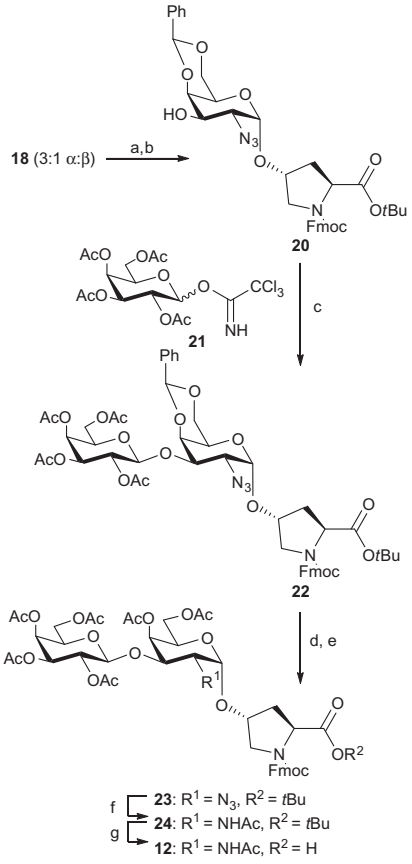

Scheme 2. Synthesis of disaccharide-derived hydroxyproline **12**. Reagents and conditions: (a) NaOMe, MeOH, pH 8–8.5, rt, 5 h; (b) benzaldehyde dimethylacetal, pTsOH, DMF, 120 mbar, 50 °C, 16 h, 61% over two steps; (c) TMSOTf, 4 Å MS, 1,2-DCE, −20 °C, 63%; (d) 4:1 v/v AcOH/H_2O, 50 °C, 20 h; (e) 1:9 v/v Ac_2O/pyridine, DMAP, rt, 18 h, 81% over two steps; (f) Ac_2O, AcOH, Zn, THF, rt, 18 h, 92%; (g) 95:5 v/v TFA, H_2O, rt, 30 min, 88%.

2.2.2. Solid-phase synthesis of (glyco)peptide targets 1–10

With glycosylamino acids **11** and **12** now in hand, attention turned to the synthesis of the proposed (glyco)peptide library (**1**–**10**). The first synthetic targets were the (glyco)peptides **1**–**4** possessing contiguous Hyp residues (Scheme 3). These were prepared via iterative Fmoc-strategy SPPS on 2-chlorotrityl-chloride resin. Briefly, Fmoc-deprotection of amino acids was carried out by treatment with 10 vol % piperidine in DMF while Fmoc-Hyp(O*t*Bu)-OH was coupled using benzotriazol-1-yl-oxytripyrrolidinophosphonium hexafluorophosphate (PyBOP, 4 equiv) and *N*-methylmorpholine (NMM, 8 equiv) in DMF. For the synthesis of glycopeptides **3** and **4**, glycosylamino acid **11** was coupled in only slight excess (1.2 equiv) with respect to the resin-bound (glyco)peptide using 2-(1*H*-7-Azabenzotriazol-1-yl)-1,1,3,3-tetramethyl uronium hexafluorophosphate (HATU, 1.2 equiv) as the coupling reagent and *N*,*N*-diisopropylethylamine as the base (2.4 equiv) for extended periods to ensure complete coupling. Following each amino acid or glycosylamino acid coupling the resin was treated with a capping solution comprising 10 vol % acetic anhydride in pyridine. Following the synthesis of the desired resin-bound (glyco)peptides by this iterative Fmoc-SPPS procedure, the two resulting resin-bound peptides were split and treated in one of two ways. The first batch was Fmoc-deprotection to afford resin-bound peptide **25** and resin-bound glycopeptide **26**. For the remaining resin, Fmoc-deprotection followed by treatment with acetic anhydride in pyridine afforded acetylated N-terminal resin-bound peptide **27** and glycopeptide **28**. Peptides **25** and **27** were next subjected to acidolytic deprotection of the *tert*-butyl ether groups and cleavage from the resin. Following reversed-phase HPLC purification peptides **1** and **2** were provided in 47% and 74% yield, respectively. In the case of resin-bound glycopeptides **26** and **28**, the carbohydrate moieties were first deacetylated by treating with 5 vol % hydrazine hydrate in DMF. Acidic cleavage from the resin followed by purification by reversed-phase HPLC then provided the desired glycopeptides **3** and **4** in 14% and 20% isolated yields, respectively. (Glyco)peptide targets **5**–**10** were synthesized via a similar Fmoc-SPPS protocol to that successfully employed for **1**–**4** (Scheme 4). Briefly, resin-bound (glyco)peptides **29**–**34** were initially synthesized by Fmoc-strategy SPPS in an identical manner to that described above. Glycosylamino acids **11** and **12** were coupled in slight excess (1.2 equiv) using HATU as the coupling reagent with extended reaction times to afford resin-bound **31** and **32**, containing four copies of the α-linked monosaccharide (GalNAc) moiety, and **33** and **34**, bearing four copies of the α-linked disaccharide [Gal-β-(1→3)GalNAc]. Acidolytic side chain deprotection and cleavage of **29** and **30** from the resin provided target dodecapeptides **5** and **6** in 52% and 68% yield, respectively. Carbohydrate deacetylation of **31**–**34** followed by acidic cleavage from the resin and reversed-phase HPLC purification provided the desired glycopeptides **7**–**10** in 17–26% isolated yields.

2.3. Circular dichroism (CD) studies

Having successfully prepared the (glyco)peptide library, we next investigated the secondary structures of **1**–**10**, specifically, whether the structures possessed PPII helical structure as per our design strategy. We initially used far-UV CD to assess the secondary structure of the (glyco)peptides in water at −5 °C (Fig. 3). The CD spectra of all 10 peptides showed clear PPII helical structural features—a weak positive maximum between wavelengths of 215 and 230 nm and a stronger negative minimum below 210 nm.[52] However, the (glyco)peptides displayed differences in the ampli-

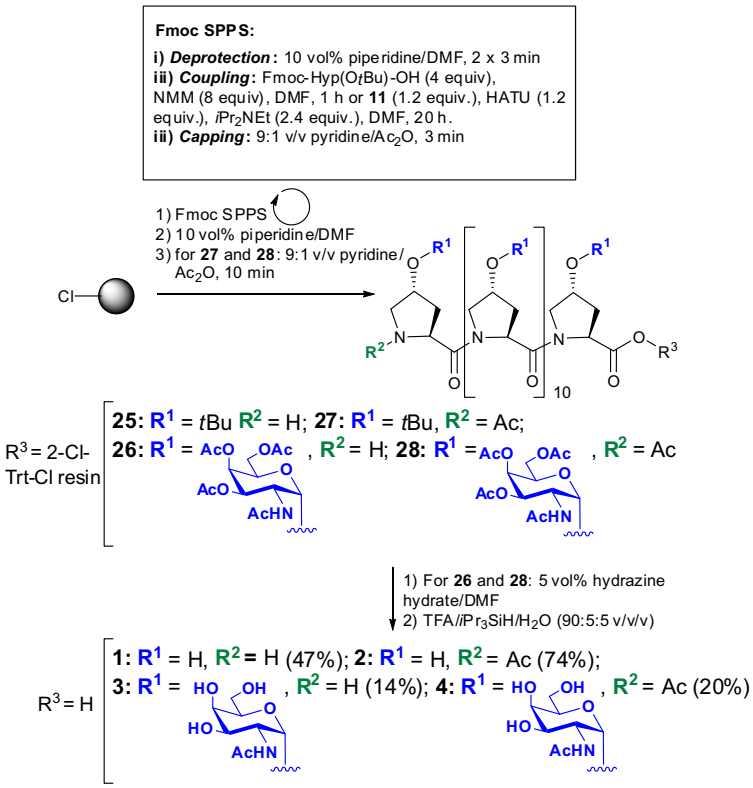

Scheme 3. Synthesis of contiguous Hyp-based (glyco)peptides **1**–**4** via Fmoc-SPPS.

tudes of minima and maxima at these wavelengths. The addition of an acetyl group can directly affect spectra as the extra amide bond may contribute to the far-UV CD spectrum and/or modify the structure (e.g., by removing the otherwise positive charge at the N-terminus). However, the spectra for the pair of $(Ala\text{-}Hyp\text{-}Ala)_4$ peptides (**5** and **6**) and GalNAc-derived $(Ala\text{-}Hyp\text{-}Ala)_4$ peptides (**7** and **8**) were identical. In contrast, the spectra of the acetylated variants from each of the other pairs of (glyco)peptides were of higher amplitude, but maintained the same spectral features. The contiguous Hyp peptides (**1**–**4**) gave rise to spectra with similar features, with minima at ~205 nm and maxima at ~225 nm. Notably, the non-glycosylated peptides from this series (**1** and **2**) gave rise to spectra that are most typical of polyproline peptides,[53] whereas the addition of the GalNAc moiety (**3** and **4**) resulted in an additional positive signal at wavelengths below 200 nm. The spectra of the $(Ala\text{-}Hyp\text{-}Ala)_4$ series of peptides (**5**–**10**), although very similar to each other were slightly different from the contiguous Hyp series (**1**–**4**), and are more typical of polylysine peptides,[53] with minima at wavelengths ~198 nm and maxima at ~220 nm. It is interesting to note the difference in structure between these $(Ala\text{-}Hyp\text{-}Ala)_4$ peptides, and the related $(ATA)_4$ peptides from our previous study.[22] Whereas the $(Ala\text{-}Hyp\text{-}Ala)_4$ peptides appear to possess similar PPII secondary structure regardless of the presence of α-O-linked glycosylation, only glycosylated forms of the $(AlaThrAla)_4$ peptide backbone possess PPII structure, indicating that the presence of the Hyp moiety is sufficient to induce PPII-like structure.

We also assessed the temperature-dependence (−5 °C to 85 °C) of the secondary structure for these (glyco)peptides. Observed spectral changes cluster within each $(Ala\text{-}Hyp\text{-}Ala)_4$ and $(Hyp)_{12}$ series (Fig. 4). All of the peptides display a gradual loss of PPII structure with increasing temperature. The contiguous Hyp (glyco)peptides (**1**–**4**) retained significant levels of PPII structure at 85 °C (as evidenced by positive signals at ~225 nm, Fig. 4). However, the addition of an α-linked GalNAc moiety in **3** and **4** (Fig. 4) did not further enhance the thermal stability compared to the unglycosylated counterparts (**1** and **2**, Fig. 4).[46] In a similar manner to synthetic $AFGP_4$, the $(Ala\text{-}Hyp\text{-}Ala)_4$ series (**5**–**10**) appear to completely lose PPII structure at higher temperatures. Similar to our previous studies of native synthetic AFGPs (e.g., $AFGP_4$, Fig. 4),[22] but notably in contrast to studies conducted on contiguous Hyp nonapeptides, thermal denaturation profiles that would indicate cooperative unfolding are not observed with **1**–**10**.[46]

2.4. Thermal hysteresis (TH), dynamic ice shaping ability and ice recrystallization inhibition (IRI) activity of 1–10

Having established the nature of the PPII helical structure of **1**–**10** in solution, we next examined whether changing the sequence from the native AFGPs in **1**–**10** would alter antifreeze activity. To this end, **1**–**10** were first examined for thermal hysteresis (TH) activity using nanoliter osmometry.[50] Unfortunately, the majority of the (glyco)peptides did not exhibit any measurable TH activity or the ability to induce ice crystal shaping at 10 mg/mL (Fig. 5A–J). The

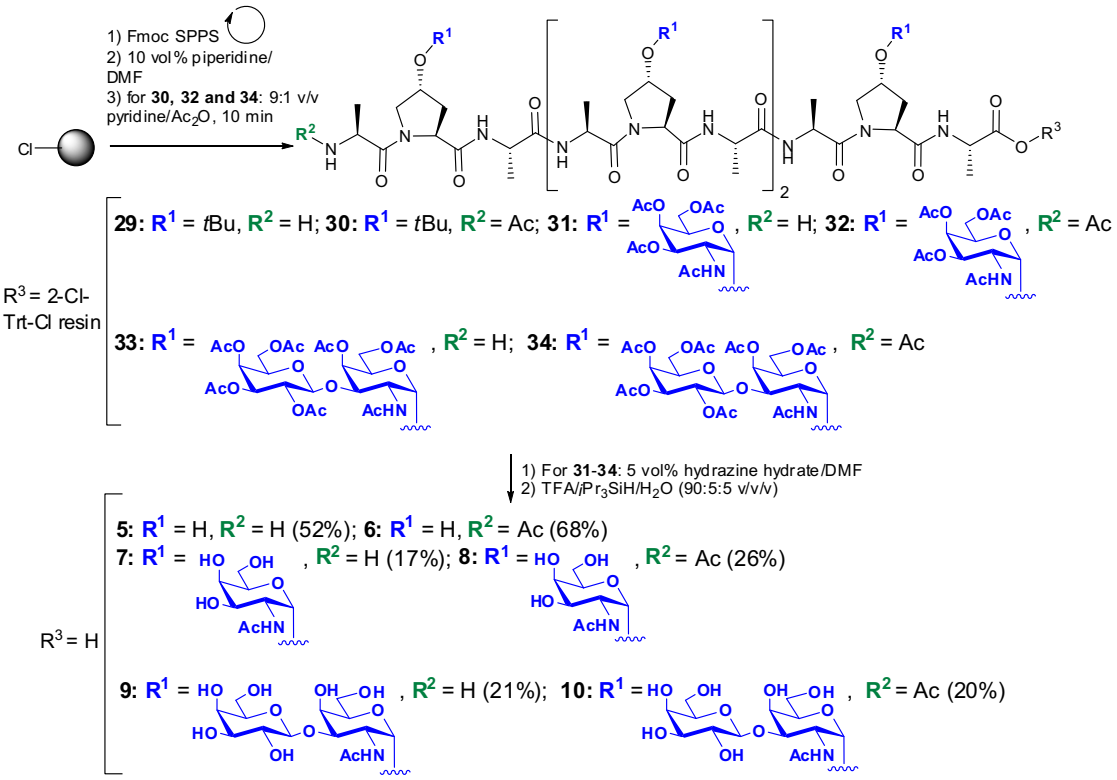

Scheme 4. Synthesis of (glyco)peptides **5**–**10** via Fmoc-SPPS.

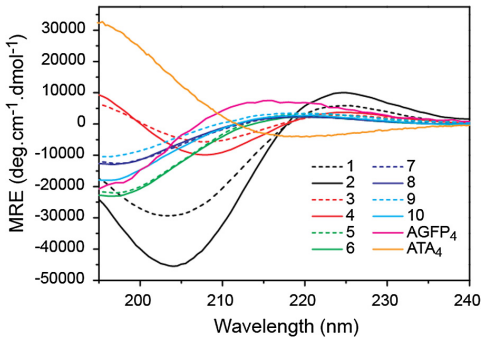

Figure 3. Circular dichroism (CD) spectra of peptides **1**–**10**, synthetic $AGFP_4$ and ATA_4 in water at −5 °C. Concentrations for each peptide were: **2**: 0.05 mg mL^{-1}; **1**, **5**, **6**, synthetic $AFGP_4$ and ATA_4: 0.1 mg mL^{-1}; **7**, **8**, and **10**: 0.2 mg mL^{-1}; **4**, and **9**: 0.4 mg mL^{-1}; **3**: 0.6 mg mL^{-1}. Data for $AGFP_4$ and ATA_4 have been reported previously.[22]

exception was peptide **6** which exhibited a small TH gap of 0.05 °C (±0.01 °C) at a concentration of 5 mg/mL (**6** could not be tested at higher concentrations due to insolubility). In addition, peptide **6** had dynamic ice shaping capabilities and induced oval ice crystal shapes (Fig. 5F). In comparison, a previously tested synthetic AFGP analogue ($synAFGP_4$) which is of analogous length to the Hyp-containing (glyco)peptides prepared here had no measurable TH gap but induced hexagonal ice crystal shapes (Fig. 5K).[22] The native AFGP fraction, AFGP-8 exhibits a TH gap of 0.15 °C and results in hexagonal bipyrimidal ice crystals at a concentration of 10 mg/mL (Fig. 5L).[22] These results suggest that the Hyp-containing (glyco)peptides assessed in this study are not interacting with the ice lattice except for unglycosylated N-terminally acetylated peptide **6**, which had a small TH gap of 0.05 °C (Fig. 5F). Interestingly, the absence of the terminal *N*-acetyl group (compound **5**) results in a loss of TH activity and ice shaping capability (Fig. 5E). Furthermore, while it has previously been reported that glycosylation of the polypeptide backbone is crucial for the TH activity of the isolated AFGP fraction, AFGP-8,[21,22] glycosylation of **6** with either GalNAc (**8**) or Gal-β-(1→3)-GalNAc (**10**) residues diminished activity.

(Glyco)peptides **1**–**10** were next assessed for ice recrystallization inhibition (IRI) activity using a 'splat-cooling' assay.[54,55] The majority of the (glyco)peptides showed a weak to moderate ability to inhibit ice recrystallization (Fig. 6). At a concentration of 7 mM the contiguous Hyp-based peptides **1** and **2** and glycopeptides **3** and **4** resulted in a mean ice crystal grain size (MGS) between 60% and 70% of that of the phosphate buffered saline (PBS) positive control, and were less IRI active than previously reported Hyp_{44} at 7 mM.[38] This suggests that the IRI activity of Hyp polymers may be dependent upon (glyco)peptide length, a result similar to that observed with polyvinyl alcohol[38,56] and synthetic homogenous AFGPs.[22] The presence or absence of an acetylated N-terminal residue did not have an effect on IRI activity. Furthermore, incorporating GalNAc residues to the contiguous Hyp backbone did not improve the IRI activity with glycopeptides **3** and **4** exhibiting sim-

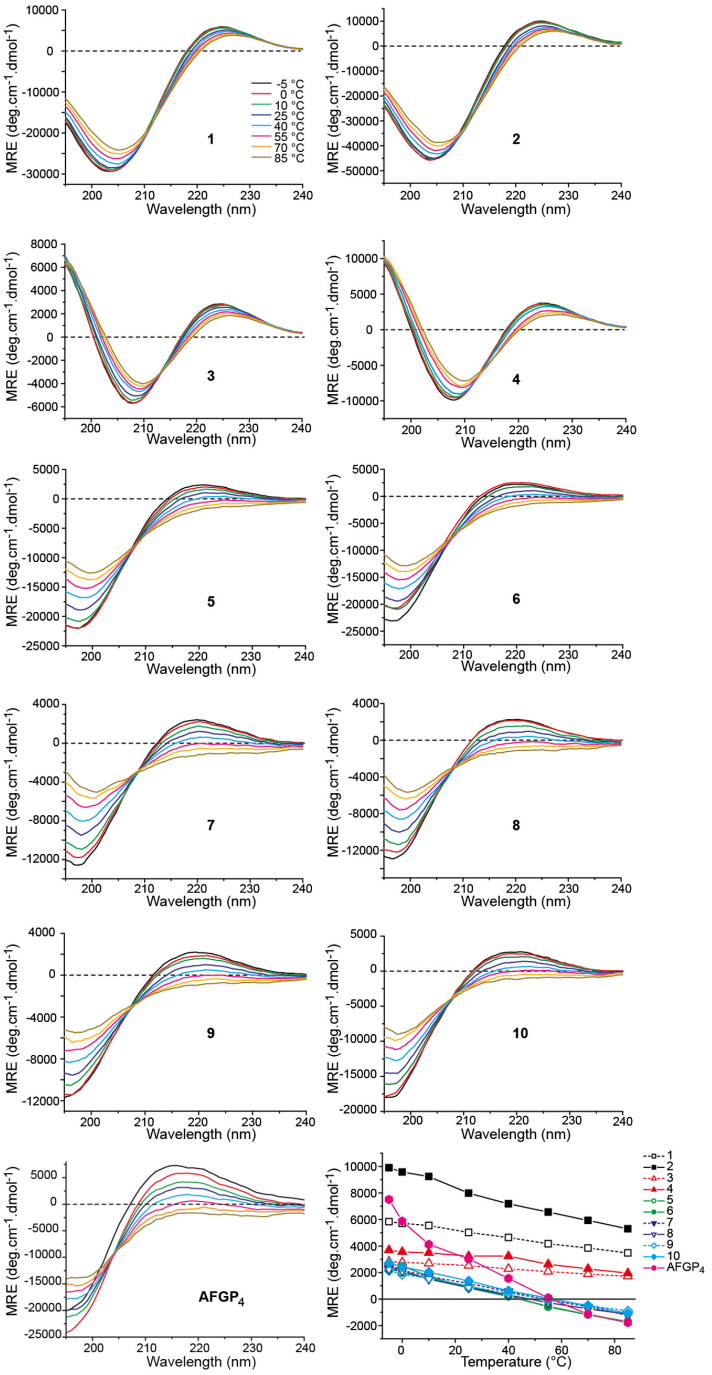

Figure 4. Temperature dependence of secondary structure. Circular dichroism (CD) spectra of peptides **1**–**10** and synthetic AGFP$_4$ in water at variable temperature (−5 °C to 85 °C). The temperature legend in the CD spectrum for **1** applies to all spectra. Data for synthetic AGFP$_4$ were reported previously.[22] Bottom right panel shows the loss of PPII structure with increasing temperature. Here the CD data for **1**–**10** and synthetic AFGP$_4$ at −5 °C at a single wavelength (from the wavelength maxima near 220 nm) are plotted against temperature. Concentrations of (glyco)peptides are the same as those reported in Figure 3.

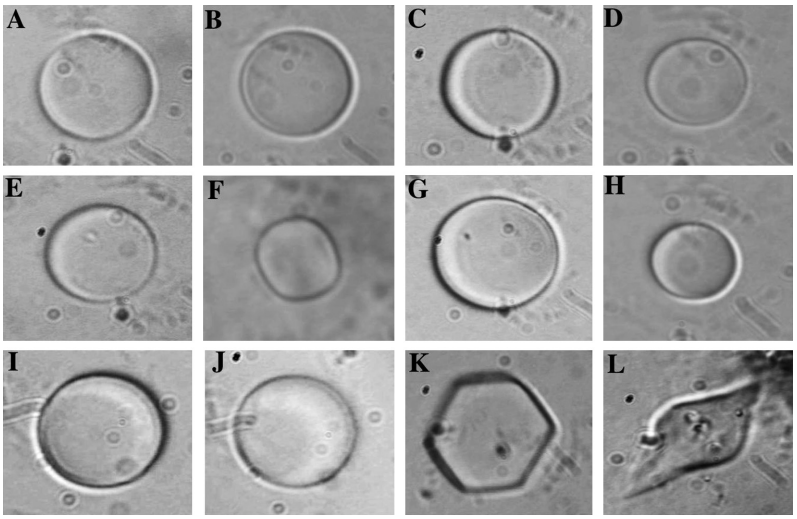

Figure 5. Ice crystal habit in the presence of: (A) **1**; (B) **2**; (C) **3**; (D) **4**; (E) **5**; (F) **6** (5 mg/mL); (G) **7**; (H) **8**; (I) **9**; (J) **10**; (K) synAFGP$_4$; (L) AFGP-8. All compounds were assayed in water at 10 mg/mL unless stated otherwise.

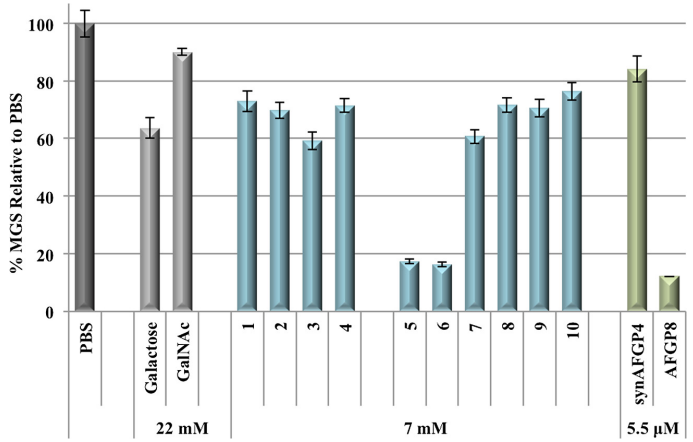

Figure 6. Ice recrystallization inhibition (IRI) activity of hydroxyproline derivatives **1**–**10** at 7 mM, synAFGP$_4$ and AFGP-8 at 5.5 μM, and D-galactose and *N*-acetyl-D-galactosamine (GalNAc) at 22 mM in PBS. The % MGS (mean grain size) relative to a PBS positive control is shown for all compounds.

ilar activity to unglycosylated **1** and **2**. However, when compared to a 22 mM solution of the monosaccharide GalNAc, conjugation to the Hyp backbone significantly improves activity.

Unglycosylated peptides **5** and **6** exhibited the most potent IRI activity in the series at a concentration of 7 mM. The activity of these compounds is comparable to that of AFGP-8, however AFGP-8 is active at the significantly lower concentration of 5.5 μM. Interestingly, while both **5** and **6** had similar IRI activities, only N-terminally acetylated **6** exhibited TH activity. Previous studies on AFGPs and synthetic *C*-linked AFGP analogues have reported that unglycosylated peptide backbones had significantly reduced IRI activity in comparison to the glycopeptides.[21,22,57] However, unglycosylated peptides of the AFGP sequence have also been shown to lack PPII structure.[21,22] In this current study, however, glycosylating the analogues containing (Ala-Hyp-Ala) tripeptide repeats was detrimental to activity. Both α-linked GalNAc containing glycopeptides **7** and **8**, and α-linked Gal-β-(1→3)-GalNAc containing glycopeptide **9** and **10** exhibited only moderate IRI activity at 7 mM (60–78% MGS relative to PBS). Our combined structure activity data for the (Ala-Hyp-Ala)$_4$ (glyco)peptides **5**–**10** and synthetic AFGPs reported previously[22] suggests that either incorporation of Hyp or glycosylation of Thr is sufficient to induce PPII structure while providing an γ-methylene or methyl group in the right orientation and spacing for antifreeze activity. In contrast, incorporation of a glycosylated Hyp modification, whilst sufficient for inducing PPII structure, dramatically reduces antifreeze activity, perhaps by modulating the properties of the ice-binding surface of the molecules.

3. Conclusions

In summary, we have successfully designed and synthesized a library of peptides and glycopeptides (**1**–**10**) containing contiguous Hyp residues or repeating Ala-Hyp-Ala motifs for the development of novel PPII helical structures with antifreeze activity. Suitably protected glycosyl-Hyp residues were synthesized and incorporated into the target glycopeptides **3**, **4** and **7**–**10** by Fmoc-strategy SPPS, while peptides **1**, **2**, **5** and **6** were synthesized by Fmoc-SPPS from commercially available amino acids. The secondary structures of **1**–**10** were evaluated via far-UV CD experiments. These studies showed that each of the (glyco)peptides possessed significant PPII helical structure in solution. Contiguous Hyp-containing peptides possessed the most thermally stable PPII helical structures, however, the incorporation of carbohydrate moieties to this structure did not further enhance this stability. The vast majority of the (glyco)peptides failed to show any TH activity or dynamic ice crystal shaping capabilities, suggesting that these compounds are not interacting with the ice lattice. However, N-acetylated peptide **6** did possess a TH gap and was capable of inducing a change in ice crystal habit. Most analogues exhibited moderate IRI activities at 7 mM concentrations. However, peptides **5** and **6**, containing an unglycosylated Ala-Hyp-Ala repeat exhibited potent IRI activity. These now serve as lead structures for further analogue studies, and are particularly attractive owing to their ease of synthesis compared to native AFGPs. However, a more detailed understanding of why differences in TH and IRI activity come about through such small structural changes will be important for the design of new generations of AFGP analogues with potent antifreeze activity and will be the focus of future work in our laboratories.

4. Experimental

4.1. Materials and methods

^{1}H, ^{13}C NMR and DEPT-135 spectra were recorded at 300 K using a Bruker Avance DRX500 spectrometer. Chemical shifts are reported in parts per million (ppm) and are referenced to solvent residual signals: $CDCl_3$ (δ 7.26 [^{1}H]) and (δ 77.16 [^{13}C]), CD_3OD (δ 3.31 [^{1}H]) and (δ 49.00 [^{13}C]). ^{1}H NMR data is reported as chemical shift (δ_H), multiplicity (s = singlet, d = doublet, t = triplet, q = quartet, dd = doublet of doublets, ddd = doublet of doublet of doublets), relative integral, coupling constant (*J* Hz) and assignment where possible.

Low-resolution mass spectra were recorded on a Shimadzu 2020 mass spectrometer (ESI) operating in positive mode. High resolution ESI-TOF mass spectra were measured on a Bruker–Daltonics Apex Ultra 7.0T Fourier transform mass spectrometer (FTICR). Infrared (IR) absorption spectra were recorded on either a Bruker ALPHA Spectrometer with Attenuated Total Reflection (ATR) capability (for neat spectra), or a Bruker TENSOR spectrometer with a Diffuse Reflectance (DRIFTS) capability (for KBr matrix), both using OPUS 6.5 software. Optical rotations were recorded on a Perkin–Elmer 341 polarimeter at 589 nm (sodium D line) with a cell path length of 0.2 dm, and the concentrations are reported in g/100 mL.

Analytical reverse-phase HPLC was performed on a Waters 2695 separations module with a 2996 DAD detector. Peptides were analyzed using a Waters Sunfire 5 μm, 2.1 × 150 mm column (C-18) at a flow rate of 0.2 mL min^{-1} using a mobile phase of 0.1% TFA in water (Solvent A) and 0.1% TFA in acetonitrile (Solvent B) with gradients as specified. Results were analyzed with Waters Empower 2 Pro software.

Preparative reverse-phase HPLC was performed using a Waters 600 Multisolvent Delivery System and pump with Waters 486 Tunable absorbance detector operating at 214 nm. Peptides were purified on a Waters Sunfire 5 μm, 19 × 150 mm (C-18) preparative column operating at a flow rate of 7 mL min^{-1} using a mobile phase of 0.1% TFA in water (Solvent A) and 0.1% TFA in acetonitrile (Solvent B).

Analytical thin layer chromatography (TLC) was performed on commercially prepared silica plates (Merck Kieselgel 60 0.25 mm F254). Flash column chromatography was performed using 230–400 mesh Kieselgel 60 silica eluting with analytical grade solvents as described. Ratios of solvents used for column chromatography are expressed in v/v as specified. Compounds were visualized by UV light at 254 nm and/or using 5% H_2SO_4 in ethanol charring solution.

Commercial materials were used as received unless otherwise noted. Reagents that were not commercially available were synthesized following literature procedures as referenced. Dichloromethane was distilled from calcium hydride. Anhydrous methanol, diethyl ether and *N*,*N*-dimethylformamide (DMF) were purchased from Sigma Aldrich. Reactions were carried out under an atmosphere of nitrogen or argon unless otherwise stated.

4.2. Solid-phase peptide synthesis—general procedures

4.2.1. Preloading 2-chloro-trityl chloride resin

2-Chloro-trityl chloride resin (1.22 mmol/g loading) was swollen in dry DCM for 30 min then washed with DCM (5 × 3 mL) and DMF (5 × 3 mL). A solution of Fmoc-Ala-OH or Fmoc-Hyp(O*t*Bu)-OH (4.0 equiv) and *i*Pr_2NEt (8.0 equiv) in 1:1 v/v DMF:DCM (final concentration 0.05 M) was added and the resin shaken at rt for 16 h. The resin was washed with DMF (5 × 3 mL) and DCM (5 × 3 mL). The resin was treated with a solution of DCM/CH_3OH/*i*Pr_2NEt (17:2:1 v/v/v, 3 mL) for 1 h and washed with DMF (5 × 3 mL), DCM (5 × 3 mL), and DMF (5 × 3 mL). The resin was subsequently submitted to iterative peptide assembly (Fmoc-SPPS).

4.2.2. General iterative peptide assembly (Fmoc-SPPS)

Deprotection: The resin was treated with 10 vol % piperidine/DMF (3 mL, 2 × 3 min) and washed with DMF (5 × 3 mL), DCM (5 × 3 mL) and DMF (5 × 3 mL).

General amino acid coupling: A preactivated solution of Fmoc-protected amino acid (4 equiv), PyBOP (4 equiv) and NMM (8 equiv) in DMF (final concentration 0.1 M) was added to the resin. After 1 h, the resin was washed with DMF (5 × 3 mL), DCM (5 × 3 mL) and DMF (5 × 3 mL).

Glycosylamino acid coupling: A solution of glycosylamino acid **11** or **12** (1.2 equiv), HATU (1.2 equiv) and *i*Pr_2NEt (2.4 equiv) in DMF (final concentration 0.1 M) was added to the resin (1.0 equiv) and shaken. After 20 h, the resin was washed with DMF (5 × 3 mL), DCM (5 × 3 mL), and DMF (5 × 3 mL).

Capping: Following coupling of an Fmoc-AA-OH or glycosylamino acid **11** or **12**, the resin was treated with acetic anhydride/pyridine (1:9 v/v, 3 mL) and shaken for 3 min. The resin was washed with DMF (5 × 3 mL), DCM (5 × 3 mL) and DMF (5 × 3 mL).

On resin O-deacetylation: A freshly prepared 5 vol % solution of hydrazine hydrate in DMF (3 mL) was added to the resin. The peptide was shaken at rt for 16 h and washed with DMF (10 × 3 mL), DCM (10 × 3 mL), and DMF (10 × 3 mL). A small portion of resin was cleaved using mixture of TFA, triisopropylsilane and water (90:5:5 v/v/v) and analyzed via LC–MS to ensure complete removal of the acetate groups. In the case of unreacted starting material, the deacetylation procedure was repeated once.

Cleavage: After washing thoroughly with DCM (7 × 3 mL), the resin was suspended in a mixture of TFA, triisopropylsilane and water (90:5:5 v/v/v), to a final concentration of 0.1 M. The suspension was shaken for 2 h and then filtered. The resin was washed with TFA (3 × 2 mL), and the washes combined with the filtrate.

Work-up: The combined filtrates were concentrated under a stream of nitrogen. The residue was precipitated from cold diethyl ether (2 mL) and the resulting white solid isolated by centrifugation. The precipitate was dissolved in water containing 0.1% TFA, filtered and purified by preparative HPLC, using gradient as specified.

4.3. Synthesis of glycosylamino acids 11 and 12

4.3.1. *O*-(2-Acetamido-3,4,6-tri-*O*-acetyl-2-deoxy-α-D-galactopyranosyl)-*N*-[(9*H*-fluoren-9-yl)-methoxycarbonyl]-(4*R*)-L-hydroxyproline *tert*-butyl ester (19)

Azide **18** (200 mg, 0.28 mmol) was dissolved in Ac_2O/AcOH/THF (100:17:100 v/v/v, 4.34 mL). The mixture was cooled to 0 °C before the addition of zinc nanopowder (270 mg, 4.13 mmol). The reaction mixture was stirred for 18 h at rt and then filtered through celite with additional THF. The filtrate was evaporated to dryness under reduced pressure and the remaining Ac_2O and AcOH was azeotroped with toluene. The resulting anomeric mixture was resolved by silica gel chromatography (eluent: EtOAc:MeOH:Petroleum spirit 9:1:10 v/v/v), affording the pure alpha isomer **19** as a white foam (136 mg, 66%), mp: 87–88 °C. $[\alpha]_D^{25}$ +55° (*c* 0.30, $CHCl_3$); IR (film) ν_{max}: 2957, 2925, 1743 (C═O), 1707 (C═O), 1682 (C═O), 1452, 1423, 1369, 1224, 1153, 1127, 1077, 1044 cm^{-1}; ^1H NMR (500 MHz, CD_3OD, reported as a ca. 1:1 mixture of rotational isomers): δ 7.82–7.79 (m, 2H, ArH), 7.68–7.67 (m, 0.5H, ArH), 7.65–7.60 (m, 1.5H, ArH), 7.42–7.39 (m, 2H, ArH), 7.34–7.31 (m, 2H, ArH), 5.44 (dd, 1H, $J_{3,4}$ = 3.1 Hz, $J_{4,5}$ = 6.5 Hz, H4), 5.11 (dd, 0.5H, $J_{2,3}$ = 11.9 Hz, 0.5H3), 5.09 (dd, 1H, $J_{2,3}$ = 11.9 Hz, 0.5H3), 5.03 (d, 0.5H, $J_{1,2}$ = 3.7 Hz, 0.5H1), 5.01 (d, 0.5H, $J_{1,2}$ = 3.7 Hz, 0.5H1), 4.51–4.48 (m, 0.5H, 0.5FmocCH_{2a}), 4.46–4.36 (m, 3H, 0.5FmocCH_{2a}, 0.5FmocCH_{2b}, H2, Hγ), 4.36–4.32 (m, 1H, Hα), 4.29–4.25 (m, 1.5H, 0.5FmocCH_{2b}, H5), 4.25–4.22 (m, 0.5H, 0.5FmocCH), 4.17–4.15 (m, 0.5H, 0.5FmocCH), 4.13–4.07 (m, 2H, H6$_a$, H6$_b$), 3.74–3.70 (m, 0.5H, 0.5Hδ$_a$), 3.62–3.60 (m, 1H, Hδ$_b$), 3.55 (dd, 0.5H, $J_{\gamma,\delta a}$ = 4.3 Hz, $J_{\delta a,\delta b}$ = 11.9 Hz, 0.5Hδ$_a$), 2.62–2.56 (m, 0.5H, 0.5Hβ$_a$), 2.55–2.49 (m, 0.5H, 0.5Hβ$_a$), 2.14 (m, 4H, Hβ$_b$, CH_3CO), 2.05 (s, 1.5H, 0.5CH_3CO), 2.03 (s, 1.5H, 0.5CH_3CO), 1.95 (s, 3H, CH_3CO), 1.89 (s, 1.5H, 0.5CH_3CO), 1.88 (s, 1.5H, 0.5CH_3CO), 1.45 (s, 4.5H, 0.5^{t}Bu), 1.41 (s, 4.5H, 0.5^{t}Bu) ppm. ^{13}C NMR (125 MHz, CD3OD, reported as a ca. 1:1 mixture of rotational isomers): δ 173.2, 173.1, 172.1, 172.1, 172.1, 172.1, 171.9, 171.9, 156.5, 156.4, 145.4, 145.2, 145.1, 144.8, 142.6, 142.6, 142.5, 128.9, 128.9, 128.3, 128.3, 128.2, 126.3, 126.1, 126.1, 121.1, 121.0, 121.0, 121.0, 98.7, 98.1, 83.2, 83.0, 77.9, 77.7, 69.4, 69.3, 68.8, 68.8, 68.7, 68.7, 68.5, 68.4, 63.5, 63.4, 60.3, 59.7, 53.4, 52.6, 48.9, 48.6, 48.3, 38.1, 37.2, 28.3, 28.2, 22.5, 22.5, 20.8, 20.7, 20.6, 20.5, 20.4 ppm. HRMS (ESI+) *m*/*z* calcd for $C_{38}H_{46}N_2O_{13}Na$ $(M+Na)^+$ 761.2892, found 761.2885.

4.3.2. *O*-(2-Acetamido-3,4,6-tri-*O*-acetyl-2-deoxy-α-D-galactopyranosyl)-*N*-[(9*H*-fluoren-9-yl)-methoxycarbonyl]-(4*R*)-L-hydroxyproline (11)

Ester **19** (81 mg, 0.11 mmol) was dissolved in TFA:H_2O (19:1 v/v, 10 mL), and the solution stirred at rt for 30 min. The solvent was removed under reduced pressure and the residual water was azeotroped with toluene. The residue was purified by silica gel chromatography (eluent: 0 → 10% MeOH in $CHCl_3$ v/v), affording 11 as an off-white solid (71 mg, 95%), mp: 127–130 °C. $[\alpha]_D^{25}$ +43.3° (*c* 0.30, $CHCl_3$); IR (KBr) ν_{max}: 1748 (C═O), 1714 (C═O), 1452, 1427, 1372, 1235, 1134, 1054, 762, 742 cm^{-1}; ^1H NMR (500 MHz, CD_3OD, reported as a ca. 1:1 mixture of rotational isomers): δ 7.78 (dd, 2H, *J* = 11.6, 7.8 Hz, ArH), 7.64–7.60 (m, 2H, ArH), 7.40–7.36 (m, 2H, ArH), 7.33–7.29 (m, 2H, ArH), 5.44–5.42 (m, 1H, H4), 5.12 (dd, 0.5H, $J_{3,4}$ = 3.1 Hz, $J_{2,3}$ = 11.7 Hz, 0.5H3), 5.09 (dd, 0.5H, $J_{3,4}$ = 3.1 Hz, $J_{2,3}$ = 11.7 Hz, 0.5H3), 5.03 (d, 0.5H, $J_{1,2}$ = 3.7 Hz, 0.5H1), 5.01 (d, 0.5H, $J_{1,2}$ = 3.7 Hz, 0.5H1), 4.48–4.38 (m, 4H, Hα, FmocCH_{2a}, H2, Hγ), 4.33–4.22 (m, 2.5H, FmocCH_{2b}, H5, 0.5FmocCH), 4.17 (dd, 0.5H, *J* = 6.6, 6.6 Hz, 0.5FmocCH), 4.13–4.07 (m, 2H, H6$_a$, H6$_b$), 3.73–3.69 (m, 0.5H, 0.5Hδ$_a$), 3.65 (dd, 0.5H, $J_{\gamma,\delta b}$ = 4.4 Hz, $J_{\delta a,\delta b}$ = 11.7 Hz, 0.5Hδ$_b$), 3.64–3.61 (m, 0.5H, 0.5Hδ$_a$), 3.59 (dd, 0.5H, $J_{\gamma,\delta b}$ = 4.4 Hz, $J_{\delta a,\delta b}$ = 11.7 Hz, 0.5Hδ$_b$), 2.65–2.59 (m, 0.5H, 0.5Hβ$_a$), 2.57–2.51 (m, 0.5H, 0.5Hβ$_a$), 2.24–2.16 (m, 1H, Hβ$_b$), 2.14 (s, 1.5H, 0.5CH_3CO), 2.13 (s, 1.5H, 0.5CH_3CO), 2.03 (s, 1.5H, 0.5CH_3CO), 2.02 (s, 1.5H, 0.5CH_3CO), 1.95 (s, 3H, CH_3CO), 1.91 (s, 1.5H, 0.5CH_3CO), 1.89 (s, 1.5H, 0.5CH_3CO) ppm; ^{13}C NMR (125 MHz, CD_3OD, reported as a ca. 1:1 mixture of rotational isomers): 173.6, 173.5, 172.3, 172.2, 172.1, 172.1, 171.9, 156.6, 156.5, 145.3, 145.2, 145.1, 145.0, 142.6, 142.4, 128.9, 128.8, 128.2, 126.1, 126.1, 121.0, 121.0, 121.0, 120.9, 98.2, 77.9, 77.7, 69.4, 69.3, 69.0, 68.8, 68.8, 68.5, 68.5, 63.7, 63.6, 59.4, 59.0, 53.2, 52.5, 48.9, 48.8, 48.4, 48.3, 38.2, 37.2, 22.5, 22.5, 20.7, 20.6, 20.5 ppm. HRMS (ESI+) *m*/*z* calcd for $C_{34}H_{38}N_2O_{13}Na$ $(M+Na)^+$ 705.2266, found 705.2260.

4.3.3. *O*-(2-Azido-4*O*,6*O*-benzylidene-2-deoxy-α-D-galactopyranosyl)-*N*-[(9*H*-fluoren-9-yl)-methoxycarbonyl]-(4*R*)-L-hydroxyproline *tert*-butyl ester (20)

To a solution of triacetate **18** (4.57 g, 6.32 mmol) in dry MeOH (150 mL) was added NaOMe (0.5 M in MeOH, ~885 μL, 0.44 mmol) to obtain a pH of 8–8.5. The pH level was maintained through occasional addition of NaOMe (0.5 M in MeOH) over 5 h, after which time the reaction mixture was neutralized with amberlite® IR-120H ion-exchange resin, filtered and evaporated to dryness under reduced pressure. The residue was dissolved in dry DMF (100 mL), and treated with benzaldehyde dimethylacetal (4.72 mL, 31.4 mmol) and *p*-TsOH (53 mg, 0.31 mmol). The reaction mixture was stirred at 50 °C and 120 mbar on a rotary evaporator for 16 h, before neutralizing with triethylamine. The mixture was concentrated at 50 °C under reduced pressure and the concentrate taken up in EtOAc (150 mL), washed with water (6 × 100 mL), followed by brine (100 mL), and concentrated under reduced pressure. The resulting anomeric mixture was resolved by silica gel chromatography (eluent: EtOAc:Petroleum spirit 1:2 v/v), affording **20** as a white foam (2.64 g, 61% over two steps), mp: 94–97 °C. $[\alpha]_D^{25}$ +75 ° (*c* 0.30, $CHCl_3$); IR (film) ν_{max}: 2107 (N_3), 1738 (C═O), 1702 (C═O), 1451, 1421, 1367, 1346, 1247, 1221, 1152, 1134, 1097, 1080, 1039, 1023, 996, 910 cm^{-1}; ^1H NMR (500 MHz, $CDCl_3$, reported as a ca. 1:1 mixture of rotational isomers) δ 7.76 (dd, 2H, *J* = 6.7, 6.7 Hz, ArH), 7.67 (d, 0.5H, *J* = 7.5 Hz), 7.63–7.59 (m, 1.5H, ArH), 7.50–7.48 (m, 2H, ArH), 7.42–7.38 (m, 5H, ArH), 7.34–7.31 (m, 2H, ArH), 5.59 (s, 1H, benzylideneCH), 5.11 (d, 0.5H, $J_{1,2}$ = 3.4 Hz, 0.5H1), 5.08 (d, 0.5H, $J_{1,2}$ = 3.4 Hz, 0.5H1), 4.49–4.44 (m, 1.5H, Hγ, 0.5Hα), 4.43–4.34 (m, 2.5H, 0.5Hα, FmocCH_{2a}, FmocCH_{2b}), 4.32–4.27 (m, 2.5H, H4, H6$_a$, 0.5Fmoc CH), 4.20–4.14 (m, 1.5H, 0.5FmocCH, H3), 4.12–4.10 (m, 1H, H6$_b$), 3.89–3.87 (m, 0.5H, 0.5Hδ$_a$), 3.78–3.71 (m, 2.5H, 0.5Hδ$_a$, Hδ$_b$, H5), 3.55 (dd, 0.5H, $J_{2,3}$ = 10.7 Hz, 0.5H2), 3.50 (dd, 0.5H, $J_{2,3}$ = 10.7 Hz, 0.5H2), 2.50–2.41 (m, 2H, Hβ$_a$, OH), 2.23–2.20 (m, 0.5H, 0.5Hβ$_b$), 2.18–2.14 (m, 0.5H, 0.5Hβ$_b$), 1.47 (s, 4.5H, 0.5^{t}Bu), 1.43 (s, 4.5H, 0.5^{t}Bu) ppm; ^{13}C NMR (125 MHz, $CDCl_3$, reported as a ca. 1:1 mixture of rotational isomers) δ 171.7, 171.5, 154.9, 154.7, 144.3, 144.1, 144.0, 143.9, 141.5, 141.4, 141.4, 141.4, 137.3, 137.3, 129.6, 128.5, 127.8, 127.2, 127.2, 127.2, 126.3, 125.6, 125.3, 125.3, 125.2, 120.1, 120.0, 101.5, 101.5, 98.8, 98.1, 82.1, 82.0, 75.6, 75.5, 75.0, 69.3, 68.1, 67.8, 67.2, 67.0, 63.7, 63.7, 60.4, 60.1, 59.0, 58.8, 52.0, 47.4, 47.3, 37.7, 36.5, 28.1 ppm; HRMS (ESI+) *m*/*z* calcd for $C_{37}H_{40}N_4O_9Na$ $(M+Na)^+$ 707.2688, found 707.2680.

4.3.4. *O*-[*O*-(2′,3′,4′,6′-Tetra-*O*-acetyl-β-D-galactopyranosyl)-[1′→3]-(2-azido-4*O*,6*O*-benzylidene-2-deoxy-α-D-galactopyranosyl)]-*N*-[(9*H*-fluoren-9-yl)-methoxycarbonyl]-(4*R*)-L-hydroxyproline *tert*-butyl ester (22)

Acceptor **20** (970 mg, 1.42 mmol), 2,3,4,6-tetra-*O*-acetyl-α-D-galactopyranosyl trichloroacetimidate **21** (1.05 g, 2.13 mmol) and activated 4 Å MS (400 mg) were combined in dry 1,2-dichloroethane (14 mL), and the resulting suspension stirred for 30 min at rt before cooling to −20 °C. TMSOTf (27 μL, 0.15 mmol) was added dropwise and the reaction mixture was stirred at −20 °C for 1 h. The reaction mixture was quenched with triethylamine and filtered through celite. The filtrate was concentrated under reduced pressure and then purified by silica gel chromatography (eluent: EtOAc:Petroleum spirit 2:3 → 1:1 v/v), affording disaccharide **22** as a white foam (908 mg, 63%), mp: 117–120 °C. $[\alpha]_D^{25}$ −70.0° (*c* 0.3, $CHCl_3$); IR (film) ν_{max} 2109 (N_3), 1745 (C=O), 1707 (C=O), 1420, 1367, 1218, 1146, 1128, 1075, 1043 cm^{-1}; ^1H NMR (500 MHz, $CDCl_3$, reported as a ca. 1:1 mixture of rotational isomers): δ 7.79–7.75 (m, 2H ArH), 7.69–7.67 (m, 0.5H, ArH), 7.63–7.58 (m, 1.5H, ArH), 7.54–7.51 (m, 2H, ArH), 7.43–7.29 (m, 7H, ArH), 5.56 (s, 1H, benzylideneCH), 5.40–5.38 (m, 1H, H4′), 5.28 (dd, 0.5H, $J_{1',2'}$ = 7.8 Hz, $J_{2',3'}$ = 10.2 Hz, 0.5H2′), 5.26 (dd, 0.5H, $J_{1',2'}$ = 7.8 Hz, $J_{2',3'}$ = 10.2 Hz, 0.5H2′), 5.12 (d, 0.5H, $J_{1,2}$ = 3.5 Hz, 0.5H1), 5.11 (d, 0.5H, $J_{1,2}$ = 3.5 Hz, 0.5H1), 5.00 (dd, 0.5H, $J_{3',4'}$ = 3.4 Hz, 0.5H3′), 4.98 (dd, 0.5H, $J_{3',4'}$ = 3.4 Hz, 0.5H3′), 4.73 (d, 0.5H, H1′), 4.72 (d, 0.5H, H1′), 4.51–4.47 (m, 1.5H, Hγ, 0.5Hα), 4.43–4.37 (m, 3H, 0.5Hα, $FmocCH_{2a}$, $0.5FmocCH_{2b}$, H4), 4.36–4.30 (m, 0.5H, $0.5FmocCH_{2b}$), 4.30–4.26 (m, 1.5H, H6a, 0.5FmocCH), 4.23–4.03 (m, 4.5H, 0.5FmocCH, H3, H6′$_a$, H6′$_b$, H6$_b$), 3.94–3.73 (m, 4H, H5′, H2, Hδ$_a$, Hδ$_b$), 3.72 (m, 1H, H5), 2.56–2.50 (m, 0.5H, 0.5Hβ$_a$), 2.49–2.43 (m, 0.5H, 0.5Hβ$_a$), 2.28–2.20 (m, 0.5H, 0.5Hβ$_b$), 2.18–2.12 (m, 3.5H, 0.5Hβb, CH_3CO), 2.04 (s, 1.5H, $0.5CH_3CO$), 2.03 (s, 1.5H, $0.5CH_3CO$), 2.02 (s, 1.5H, $0.5CH_3CO$), 1.98 (s, 1.5H, $0.5CH_3CO$), 1.97 (s, 1.5H, $0.5CH_3CO$), 1.96 (s, 1.5H, $0.5CH_3CO$), 1.47 (s, 4.5H, 0.5^{t}Bu), 1.44 (s, 4.5H, 0.5^{t}Bu) ppm; ^{13}C NMR (125 MHz, $CDCl_3$, reported as a ca. 1:1 mixture of rotational isomers) δ 171.6, 171.4, 170.4, 170.3, 170.2, 169.5, 154.9, 154.7, 144.2, 144.0, 143.8, 141.4, 141.4, 141.3, 137.6, 137.6, 129.1, 128.3, 127.9, 127.2, 127.2, 127.2, 127.1, 126.2, 125.5, 125.3, 125.2, 125.2, 120.1, 120.1, 120.1, 102.7, 100.8, 100.8, 98.8, 98.2, 82.2, 82.0, 77.2, 75.9, 75.8, 75.8, 75.7, 75.4, 71.1, 70.9, 70.9, 69.2, 68.7, 68.7, 68.1, 67.9, 67.0, 67.0, 64.0, 63.9, 61.4, 61.4, 59.0, 58.8, 58.5, 58.4, 52.1, 47.4, 47.3, 37.6, 36.6, 28.1, 20.8, 20.8, 20.7, 20.6 ppm; HRMS (ESI+) *m*/*z* calcd for $C_{51}H_{58}N_4O_{18}Na$ (M+Na)$^+$ 1037.3638, found 1037.3627.

4.3.5. *O*-[*O*-(2′,3′,4′,6′-Tetra-*O*-acetyl-β-D-galactopyranosyl)-[1′→3]-(4,6-di-*O*-acetyl-2-azido-2-deoxy-α-D-galactopyranosyl)]-*N*-[(9*H*-fluoren-9-yl)-methoxycarbonyl]-(4*R*)-L-hydroxyproline *tert*-butyl ester (23)

Benzylidine acetal **22** (738 mg, 0.73 mmol) was dissolved in AcOH/H_2O (4:1 v/v, 20 mL) and stirred for 20 h at 50 °C. The solution was evaporated to dryness under reduced pressure and the remaining solvent azeotroped with toluene. The residue was resuspended in Ac_2O/Pyr (1:9 v/v, 20 mL) with a catalytic quantity of DMAP, and the mixture stirred for 18 h at room temperature. The solvent was removed under reduced pressure and the remaining solvent azeotroped with toluene. The residue was purified by silica gel chromatography (eluent: EtOAc:Petroleum spirit 1:1 v/v), affording **23** as a white foam (600 mg, 81% over 2 steps), mp: 98–101 °C. $[\alpha]_D^{25}$ +52.5° (*c* 0.2, $CHCl_3$); IR (film) ν_{max} 2110 (N_3), 1744 (C=O), 1708 (C=O), 1452, 1420, 1368, 1219, 1150, 1125, 1050 cm^{-1}; ^1H NMR (500 MHz, $CDCl_3$, reported as a ca. 1:1 mixture of rotational isomers) δ 7.77–7.75 (m, 2H, ArH), 7.68–7.66 (m, 0.5H, ArH), 7.62–7.57 (m, 1.5H, ArH), 7.41–7.38 (m, 2H, ArH), 7.33–7.29 (m, 2H, ArH), 5.47–5.45 (m, 1H, H4), 5.36–5.33 (m, 1H, H4′), 5.16 (dd, 0.5H, $J_{1',2'}$ = 7.8 Hz, $J_{2',3'}$ = 5.1 Hz, 0.5H2′), 5.14 (dd, 0.5H, $J_{1',2'}$ = 7.8 Hz, $J_{2',3'}$ = 5.1 Hz, 0.5H2′), 5.04 (d, 0.5H, $J_{1,2}$ = 3.7 Hz, 0.5H1), 5.03 (d, 0.5H, $J_{1,2}$ = 3.7 Hz, 0.5H1), 4.98 (dd, 0.5H, $J_{3',4'}$ = 3.6 Hz, 0.5H3′), 4.96 (dd, 0.5H, $J_{3',4'}$ = 3.6 Hz, 0.5H3′), 4.66 (d, 0.5H, 0.5H1′), 4.64 (d, 0.5H, 0.5H1′), 4.48 (t, 0.5H, $J_{\alpha,\beta}$ = 7.6 Hz, 0.5Hα), 4.46–4.42 (m, 1H, Hγ), 4.41–3.70 (m, 2H, 0.5Hα, $FmocCH_{2a}$, $0.5FmocCH_{2b}$), 4.35–4.30 (m, 0.5H, $0.5FmocCH_{2b}$), 4.27 (t, 0.5H, *J* = 7.2, 0.5Fmoc CH), 4.19–3.99 (m, 6.5H, H6$_a$, H6$_b$, H6′$_a$, H6′$_b$, H3, H5, 0.5FmocCH), 3.91–3.81 (m, 1.5H, H5′, 0.5Hδ$_a$), 3.77–3.76 (m, 1H, Hδ$_b$), 3.72 (dd, 0.5H, *J* = 4.5, 12.0, 0.5Hδ$_a$), 3.61 (dd, 0.5H, $J_{2,3}$ = 10.7 Hz, 0.5H2), 3.56 (dd, 0.5H, $J_{2,3}$ = 10.7 Hz, 0.5H2), 2.57–2.46 (m, 1H, Hβ$_a$), 2.25–2.12 (m, 7H, Hβ$_b$, $2CH_3CO$), 2.08 (s, 1.5H, $0.5CH_3CO$), 2.08 (s, 1.5H, $0.5CH_3CO$), 2.05 (s, 1.5H, $0.5CH_3CO$), 2.04 (s, 1.5H, $0.5CH_3CO$), 2.02 (s, 1.5H, $0.5CH_3CO$), 1.99 (s, 1.5H, $0.5CH_3CO$), 1.97 (s, 1.5H, $0.5CH_3CO$), 1.96 (s, 1.5H, $0.5CH_3CO$), 1.46 (s, 4.5H, 0.5^{t}Bu), 1.43 (s, 4.5H, 0.5^{t}Bu) ppm; ^{13}C NMR (125 MHz, $CDCl_3$, reported as a ca. 1:1 mixture of rotational isomers) δ 171.5, 170.6, 170.5, 170.5, 170.4, 170.3, 170.2, 169.8, 169.7, 169.6, 154.8, 154.6, 144.2, 144.0, 144.0, 143.8, 141.4, 141.4, 141.3, 127.9, 127.9, 127.2, 127.2, 125.5, 125.3, 125.2, 125.2, 120.1, 120.1, 101.7, 98.3, 97.7, 82.2, 82.1, 77.6, 75.7, 74.6, 74.5, 70.9, 70.9, 69.5, 69.4, 68.9, 68.8, 68.4, 68.2, 68.1, 67.8, 66.9, 66.8, 63.0, 62.9, 61.1, 61.0, 59.2, 59.1, 58.9, 58.6, 52.1, 52.1, 47.4, 47.3, 37.4, 36.3, 28.1, 28.1, 20.9, 20.8, 20.8, 20.8, 20.7, 20.6 ppm; HRMS (ESI+) *m*/*z* calcd for $C_{48}H_{58}N_4O_{20}Na$ (M+Na)$^+$ 1033.3537, found 1033.3524.

4.3.6. *O*-[*O*-(2′,3′,4′,6′-Tetra-*O*-acetyl-β-D-galactopyranosyl)-[1′→3]-(2-acetamido-4,6-di-*O*-acetyl-2-deoxy-α-D-galactopyranosyl)]-*N*-[(9*H*-fluoren-9-yl)-methoxycarbonyl]-(4*R*)-L-hydroxyproline *tert*-butyl ester (24)

Azide **23** (550 mg, 0.54 mmol) was dissolved in Ac_2O/AcOH/THF (100:17:100, v/v/v, 4.34 mL). The mixture was cooled to 0 °C before the addition of zinc nanopowder (270 mg, 4.13 mmol). The reaction mixture was stirred for 18 h at rt and then filtered through celite with additional THF. The filtrate was evaporated to dryness under reduced pressure and the remaining solvent azeotroped with toluene. The residue was purified by silica gel chromatography (eluent: EtOAc:MeOH:Petroleum spirit 9:1:10 v/v/v), affording **24** as a white foam (514 mg, 92%), mp: 114–117 °C.

$[\alpha]_D^{25}$ +16.7° (*c* 0.30, $CHCl_3$); IR (film) ν_{max} 1743 (C=O), 1705 (C=O), 1682 (C=O), 1423, 1368, 1218, 1152, 1125, 1046 cm^{-1}; ^1H NMR (500 MHz, CD_3OD, reported as a ca. 1:1 mixture of rotational isomers) δ 7.89–7.80 (m, 2H, ArH), 7.69–7.60 (m, 2H, ArH), 7.42–7.39 (m, 2H, ArH), 7.33–7.31 (m, 2H, ArH), 5.42 (m, 1H, H4), 5.34 (m, 1H, H4′), 5.04–4.97 (m, 2H, H2′, H3′), 4.93 (d, 0.5H, $J_{1,2}$ = 3.7 Hz, 0.5H1), 4.90 (d, 0.5H, $J_{1,2}$ = 3.7 Hz, 0.5H1), 4.75 (d, 1H, $J_{1',2'}$ = 7.4 Hz, H1′), 4.52–4.30 (m, 4.5H, $FmocCH_{2a}$, $0.5FmocCH_{2b}$, Hα, Hγ, H2), 4.25–4.09 (m, 5.5H, $0.5FmocCH_{2b}$, FmocCH, H5, H6′$_a$, H6′$_b$, H6$_a$), 4.02–3.96 (m, 3H, H6$_b$, H5′, H3), 3.75–3.73 (m, 0.5H, 0.5Hδ$_a$), 3.65–3.57 (m, 1.5H, 0.5Hδ$_a$, Hδ$_b$), 2.64–2.58 (m, 0.5H, 0.5Hβ$_a$), 2.53–2.49 (m, 0.5H, 0.5Hβ$_a$), 2.18–2.11 (m, 7H, Hβ$_b$, $2CH_3CO$), 2.06 (s, 3H, CH_3CO), 2.01 (s, 1.5H, $0.5CH_3CO$), 2.01 (s, 1.5H, $0.5CH_3CO$), 1.99 (s, 1.5H, $0.5CH_3CO$), 1.98 (s, 1.5H, $0.5CH_3CO$), 1.93–1.92 (m, 6H, $2CH_3CO$), 1.44 (s, 4.5H, 0.5^{t}Bu), 1.42 (s, 4.5H, 0.5^{t}Bu) ppm; ^{13}C NMR (125 MHz, CD_3OD, reported as a ca. 1:1 mixture of rotational isomers) δ 173.1, 173.0, 172.3, 172.0, 172.0, 172.0, 171.5, 171.1, 156.5, 156.3, 145.4, 145.2, 145.1, 144.7, 142.6, 142.6, 142.5, 129.0, 128.9, 128.3, 126.3, 126.1, 126.1, 121.1, 102.4, 102.3, 99.3, 98.7, 83.3, 83.0, 78.2, 78.0, 74.3, 74.2, 72.1, 71.8, 71.3, 71.2, 70.1, 70.1, 69.2, 68.9, 68.8, 68.6, 64.3, 62.4, 60.4, 59.8, 53.6, 52.8, 50.4, 50.3, 48.5, 48.3, 38.2, 37.3, 28.3, 22.9, 22.8, 21.0, 21.0, 20.8, 20.8, 20.7, 20.7, 20.5, 20.5, 20.5 ppm; HRMS (ESI+) *m*/*z* calcd for $C_{50}H_{63}N_2O_{21}$ (M+H)$^+$ 1027.3918, found 1027.3917.

4.3.7. *O*-[*O*-(2′,3′,4′,6′-Tetra-*O*-acetyl-β-D-galactopyranosyl)-[1′→3]-(2-acetamido-4,6-di-*O*-acetyl-2-deoxy-α-D-galactopyranosyl)]-*N*-[(9*H*-fluoren-9-yl)-methoxycarbonyl]-(4*R*)-L-hydroxyproline (12)

Ester **24** (514 mg, 0.5 mmol) was dissolved in TFA:H_2O (19:1 v/v, 10 mL), and the solution stirred at rt for 30 min. The solvent was removed under reduced pressure and any remaining TFA was azeotroped with toluene. The residue was purified by silica gel chromatography (eluent: 0 → 10% MeOH in $CHCl_3$ v/v), affording **12** as an off-white solid (425 mg, 88%), mp: 135–138 °C.

$[\alpha]_D^{25}$ +45.0° (*c* 0.30, $CHCl_3$); IR (KBr) ν_{max} 1749 (C=O), 1715 (C=O), 1427, 1371, 1229, 1058, 762, 743 cm^{-1}; ^1H NMR (500 MHz, CD_3OD, reported as a ca. 1:1 mixture of rotational isomers) δ 7.85–7.78 (m, 2H, ArH), 7.66–7.62 (m, 2H, ArH), 7.43–7.38 (m, 2H, ArH), 7.34–7.30 (m, 2H, ArH), 5.42 (m, 1H, H4), 5.35 (m, 1H, H4′), 5.06–4.97 (m, 2H, H2′, H3′), 4.94 (d, 0.5H, $J_{1,2}$ = 3.60 Hz, 0.5H1), 4.91 (d, 0.5H, $J_{1,2}$ = 3.60 Hz, 0.5H1), 4.76 (d, 0.5H, $J_{1',2'}$ = 7.7 Hz, 0.5H1′), 4.74 (d, 0.5H, $J_{1',2'}$ = 7.7 Hz, 0.5H1′), 4.50–4.39 (m, 4H, FmocCH$_{2a}$, Hγ, Hα, H2), 4.29–4.09 (m, 6H, FmocCH$_{2b}$, H5, FmocCH, H6$_a$, 0.5H6$_b$, H6′$_a$, 0.5H6′$_b$), 4.01–3.97 (m, 3H, 0.5H6$_b$, 0.5H6′$_b$, H3, H5′), 3.76–3.73 (m 0.5H, 0.5Hδ$_a$), 3.68–3.62 (m 1.5H, 0.5Hδ$_a$, Hδ$_b$), 2.68–2.64 (m, 0.5H, 0.5Hβ$_a$), 2.58–2.53 (m, 0.5H, 0.5Hβ$_a$), 2.25–2.17 (m, 1H, Hβ$_b$), 2.13–2.12 (m, 6H, 2CH_3CO), 2.06 (s, 3H, CH_3CO), 2.02 (s, 1.5H, 0.5CH_3CO), 2.00 (s, 1.5H, 0.5CH_3CO), 2.00 (s, 1.5H, 0.5CH_3CO), 1.98 (s, 1.5H, 0.5CH_3CO), 1.95 (s, 1.5H, 0.5CH_3CO), 1.93 (s, 4.5H, 1.5CH_3CO) ppm; ^{13}C NMR (125 MHz, CD_3OD, reported as a ca. 1:1 mixture of rotational isomers) δ 173.1, 173.0, 172.5, 172.4, 172.0, 172.0, 172.0, 171.5, 171.1, 156.6, 156.5, 145.3, 145.2, 145.1, 145.0, 142.6, 142.5, 128.9, 128.3, 128.2, 126.2, 126.1, 126.1, 126.1, 121.0, 102.3, 102.3, 99.4, 98.7, 78.3, 77.9, 74.4, 74.3, 72.1, 71.8, 71.3, 71.2, 70.1, 69.2, 69.1, 68.9, 68.6, 64.5, 64.4, 62.4, 62.4, 59.5, 59.1, 53.5, 52.6, 50.3, 50.2, 48.4, 48.3, 38.3, 37.3, 22.9, 22.8, 20.8, 20.8, 20.7, 20.7, 20.7, 20.5, 20.5 ppm; HRMS (ESI+) *m*/*z* calcd for $C_{46}H_{54}N_2O_{21}$-Na $(M+Na)^+$ 993.3111, found 993.3096.

4.4. Synthesis of (glyco)peptides 1–10

Peptides **1**–**10** were prepared according to the general procedures outlined in Section 4.2 on a 100 μmol (**1**, **2**, **5** and **6**), 50 μmol (**7** and **8**) or 25 μmol (**3**, **4**, **9** and **10**) scale. Yields reported are based on original resin loading and after lyophilization.

Peptide ***1***: Yield: 64 mg, 47%; Preparative HPLC: 0–15% B over 40 min, 0.1% TFA; Analytical HPLC: R_t 22.3 min (0–5% B over 40 min, 0.1% TFA, λ = 214 nm); ESI^+ (*m*/*z*): 1376.2 $[M+H]^+$, 688.6 $[M+2H]^{2+}$.

Peptide ***2***: Yield: 105 mg, 74%; Preparative HPLC: 0–15% B over 40 min, 0.1% TFA; Analytical HPLC: R_t 18.3 min (0%B for 1 min, 0–15% B over 40 min, 0.1% TFA, λ = 214 nm); ESI^+ (*m*/*z*): 709.7 $[M+2H]^{2+}$, 720.5 $[M+H+Na]^{2+}$, 728.5 $[M+H+K]^{2+}$.

Glycopeptide ***3***: Yield: 13 mg, 14%; Preparative HPLC: 0–10% B over 60 min, 0.1% TFA; Analytical HPLC: R_t 14.2 min (0% B for 1 min, 0–15% B over 40 min, 0.1% TFA, λ = 214 nm). ESI^+ (*m*/*z*): 1271.8 $[M+3H]^{3+}$, 954.3 $[M+4H]^{4+}$, 959.9 $[M+3H+Na]^{4+}$, 963.7 $[M+3H+K]^{4+}$, 965.2 $[M+2H+2Na]^{4+}$, 969.3 $[M+2H+Na+K]^{4+}$.

Glycopeptide ***4***: Yield: 19 mg, 20%; Preparative HPLC: to 10% B over 60 min, 0.1% TFA; Analytical HPLC: R_t 16.4 min (0% B for 1 min, 0–15% B over 40 min, 0.1% TFA, λ = 214 nm); ESI^+ (*m*/*z*): 1286.0 $[M+3H]^{3+}$, 1293.5 $[M+2H+Na]^{3+}$, 1298.5 $[M+2H+K]^{3+}$, 964.8 $[M+4H]^{4+}$, 970.2 $[M+3H+Na]^{4+}$, 974.2 $[M+3H+K]^{4+}$.

Peptide ***5***: Yield: 54 mg, 52%; Preparative HPLC: 0–15% B over 40 min, 0.1% TFA; Analytical HPLC: R_t 23.8 min (0%B for 1 min, 0–15% B over 40 min, 0.1% TFA, λ = 214 nm); ESI^+ (*m*/*z*): 1039.6 $[M+H]^+$, 1077.6 $[M+K]^+$, 520.5 $[M+2H]^{2+}$.

Peptide ***6***: Yield: 74 mg, 68%; Preparative HPLC: 0–15% B over 40 min, 0.1% TFA; Analytical HPLC: R_t 27.9 min (0% B for 1 min, 0–15% B over 40 min, 0.1% TFA, λ = 214 nm); ESI^+ (*m*/*z*) 1103.5 $[M+Na]^+$, 1119.5 $[M+K]^+$.

Glycopeptide ***7***: Yield: 16 mg, 17%; Preparative HPLC: 0–15% B over 45 min, 0.1% TFA; Analytical HPLC: R_t 26.3 min (0% B for 1 min, 0–15% B over 40 min, 0.1% TFA, λ = 214 nm); ESI^+ (*m*/*z*): 926.8 $[M+2H]^{2+}$, 937.9 $[M+Na+H]^{2+}$, 945.8 $[M+K+H]^{2+}$, 948.8 $[M+2Na]^{2+}$, 956.7 $[M+K+Na]^{2+}$, 618.3 $[M+3H]^{3+}$, 625.8 $[M+2H+Na]^{3+}$, 631.0 $[M+2H+K]^{3+}$.

Glycopeptide ***8***: Yield: 25 mg, 26%; Preparative HPLC: 0–17% B over 40 min, 0.1% TFA; Analytical HPLC: R_t 23.6 min (0% B for 1 min, 0–25% B over 40 min, 0.1% TFA, λ = 214 nm); ESI^+ (*m*/*z*): 947.9 $[M+2H]^{2+}$, 958.9 $[M+H+Na]^{2+}$, 966.9 $[M+H+K]^{2+}$, 969.9 $[M+2Na]^{2+}$, 977.9 $[M+K+Na]^{2+}$, 632.3 $[M+3H]^{3+}$, 639.8 $[M+2H+Na]^{3+}$, 645.0 $[M+2H+K]^{3+}$, 652.4 $[M+Na+K+H]^{3+}$.

Glycopeptide ***9***: Yield: 13 mg, 21%; Preparative HPLC: 0–15% B over 45 min; Analytical HPLC: R_t 26.9 min (0–15% B over 40 min, 0.1% TFA, λ = 214 nm); ESI^+: 1251.0 $[M+2H]^{2+}$, 1262.1 $[M+H+Na]^{2+}$, 1269.8 $[M+K+H]^{2+}$, 1273.3 $[M+2Na]^{2+}$, 1280.9 $[M+Na+K]^{2+}$. HRMS (ESI+) *m*/*z* calcd for $[C_{100}H_{164}N_{16}O_{57}]/2$ $(M+2H)^{2+}$ 1251.0223, found 1251.0203.

Glycopeptide ***10***: Yield: 12 mg, 20%; Preparative HPLC: 0–20% B over 40 min; Analytical HPLC: R_t 22.6 min (0% B for 1 min, 0–25% B over 40 min, 0.1% TFA, λ = 214 nm); ESI^+: 1282.8 $[M+H+Na]^{2+}$, 1291.1 $[M+H+K]^{2+}$, 1294.1 $[M+2Na]^{2+}$, 848.5 $[M+3H]^{3+}$, 855.9 $[M+2H+Na]^{3+}$, 863.2 $[M+2Na+H]^{3+}$, 870.3 $[M+3Na]^{3+}$, 655.8 $[M+2H+2K]^{4+}$. HRMS (ESI+) *m*/*z* calcd for $[C_{102}H_{164}N_{16}O_{58}Na_2]/2$ $(M+2Na)^{2+}$ 1294.0095, found 1294.0099.

4.5. Circular dichroism (CD)

Far-UV CD spectra were recorded in 1-mm cells on a Jasco J-815 Spectropolarimeter equipped with a 6-position thermostatted Peltier MPTC-490S cell holder cooled by a Multitemp III waterbath (Pharmacia Biotech). Samples at the indicated concentrations (0.05–0.6 mg/mL) were dissolved in water and incubated at −5, 0, 10, 25, 40, 55, 70, 85 °C, as measured in the cell using a Digisense Thermometer (Exetech) equipped with a wire probe thermocouple. Data were collected in continuous scanning mode from 240–195 nm in 0.5-nm steps with a 1-nm bandwidth and 1-s digital integration time. Reported spectra are the average of 3 scans with buffer baseline correction and smoothing (5-point adjacent-averaging), and are normalized with respect to concentration and residue length. Selected samples were subjected to thermal denaturation (−5 to 85 °C), by heating at a rate of 1 °C/min and monitoring the CD signal at a single wavelength (220 nm).

4.6. Thermal hysteresis (TH) assay

Nanoliter osmometry was performed using a Clifton nanoliter osmometer (Clifton Technical Physics, Hartford, NY).[50] All measurements were performed in a phosphate buffered saline (PBS) solution. Ice crystal morphology was observed through a Leitz compound microscope equipped with an Olympus 20× (infinity-corrected) objective, a Leitz Periplan 32× photo eyepiece, and a Hitachi KPM2U CCD camera connected to a Toshiba MV13K1 TV/VCR system. Still images were captured directly using a Nikon CoolPix digital camera.

4.7. Ice recrystallization inhibition (IRI) assay

Sample analysis for IRI activity was performed using the 'splat-cooling' method as previously described.[54] In this method, the analyte was dissolved in PBS solution and a 10 μL droplet of this solution was dropped from a micropipette through a two meter high plastic tube (10 cm in diameter) onto a block of polished aluminum pre-cooled to approximately −80 °C. The droplet froze instantly on

the polished aluminum block and was approximately 1 cm in diameter and 20 μm thick. This wafer was then carefully removed from the surface of the block and transferred to a cryostage held at −6.4 °C for annealing. After a period of 30 min, the wafer was photographed between crossed polarizing filters using a digital camera (Nikon CoolPix 5000) fitted to the microscope. A total of three images were taken from each wafer. During flash freezing, ice crystals spontaneously nucleated from the supercooled solution. These initial crystals were relatively homogeneous in size and quite small. During the annealing cycle, recrystallization occurred, resulting in a dramatic increase in ice crystal size. A quantitative measure of the difference in recrystallization inhibition of two compounds is the difference in the ice crystal size distribution. Image analysis of the ice wafers was performed using a novel domain recognition software (DRS) program.[55] This processing employed the Microsoft Windows Graphical User Interface to allow a user to visually demarcate and store the vertices of ice domains in a digital micrograph. The data was then used to calculate the domain areas. All data was plotted and analyzed using Microsoft Excel. The mean grain (or ice crystal) size (MGS) of the sample was compared to the MGS of the control PBS solution for that same day of testing. IRI activity is reported as the percentage of the MGS (% MGS) relative to the PBS control, and the % MGS for each sample was plotted along with its standard error of the mean. Small percentages represent a small MGS, which is indicative of more potent IRI activity.

Acknowledgments

The authors would like to acknowledge the Henry Bertie and Mabel Gritton Scholarship (G.S.), the Australian Postgraduate Award (APA) (S.J.) schemes for Ph.D. funding, the Canadian Blood Services for a GFP award (C.J.C.) and the National Health and Medical Research Council for fellowship funding (J.M.M.). We would also like to thank Dr. Ian Luck and Dr. Nick Proschogo for technical support with NMR spectroscopy and mass spectrometry, respectively.

Supplementary data

Supplementary data associated with this article can be found, in the online version, at http://dx.doi.org/10.1016/j.bmc.2013.02.025.

References and notes

1. Devries, A. L. *Annu. Rev. Physiol.* **1983**, *45*, 245.
2. Yeh, Y.; Feeney, R. E. *Chem. Rev.* **1996**, *96*, 601.
3. Fletcher, G. L.; Hew, C. L.; Davies, P. L. *Annu. Rev. Physiol.* **2001**, *63*, 359.
4. Harding, M. M.; Anderberg, P. I.; Haymet, A. D. J. *Eur. J. Biochem.* **2003**, *270*, 1381.
5. Garner, J.; Harding, M. M. *ChemBioChem* **2010**, *11*, 2489.
6. Peltier, R.; Brimble, M. A.; Wojnar, J. M.; Williams, D. E.; Evans, C. W.; DeVries, A. L. *Chem. Sci.* **2010**, *1*, 538.
7. DeVries, A. L.; Wohlschlag, D. E. *Science* **1969**, *163*, 1073.
8. Raymond, J. A.; Devries, A. L. *Proc. Natl. Acad. Sci. U.S.A.* **1977**, *74*, 2589.
9. Knight, C. A.; Cheng, C. C.; Devries, A. L. *Biophys. J.* **1991**, *59*, 409.
10. Knight, C. A.; Driggers, E.; Devries, A. L. *Biophys. J.* **1993**, *64*, 252.
11. Knight, C. A.; Devries, A. L. *J. Cryst. Growth* **1994**, *143*, 301.
12. Wilson, P. W. *Cryo-Lett.* **1993**, *14*, 31.
13. DeVries, A. L.; Komatsu, S. K.; Feeney, R. E. *J. Biol. Chem.* **1970**, 245.
14. Lin, Y.; Devries, A. L.; Duman, J. G. *Biochem. Biophys. Res. Commun.* **1972**, *46*, 87.
15. Morris, H. R.; Thompson, M. R.; Osuga, D. T.; Ahmed, A. I.; Chan, S. M.; Vandenheede, J. R.; Feeney, R. E. *J. Biol. Chem.* **1978**, *253*, 5155.
16. Wohrmann, A. P. A. *Mar. Ecol.-Prog. Ser.* **1996**, *130*, 47.
17. Lane, A. N.; Hays, L. M.; Feeney, R. E.; Crowe, L. M.; Crowe, J. H. *Protein Sci.* **1998**, *7*, 1555.
18. Lane, A. N.; Hays, L. M.; Tsvetkova, N.; Feeney, R. E.; Crowe, L. M.; Crowe, J. H. *Biophys. J.* **2000**, *78*, 3195.
19. Bouvet, V. R.; Lorello, G.; Ben, R. N. *Biomacromolecules* **2006**, *7*, 565.
20. Bush, C. A.; Feeney, R. E. *Int. J. Pept. Protein Res.* **2009**, *28*, 386.
21. Tachibana, Y.; Fletcher, G. L.; Fujitani, N.; Tsuda, S.; Monde, K.; Nishimura, S. I. *Angew. Chem., Int. Ed.* **2004**, *43*, 856.
22. Wilkinson, B. L.; Stone, R. S.; Capicciotti, C. J.; Thaysen-Andersen, M.; Matthews, J. M.; Packer, N. H.; Ben, R. N.; Payne, R. J. *Angew. Chem., Int. Ed.* **2012**, *51*, 3606.
23. Crowe, J. H.; Tablin, F.; Tsvetkova, N.; Oliver, A. E.; Walker, N. J.; Crowe, L. M. *Cryobiology* **1999**, *38*, 180.
24. Tablin, F.; Oliver, A.; Walker, A. N. J.; Crowe, L. M.; Crowe, J. H. *J. Cell. Physiol.* **1996**, *168*, 305.
25. Wang, J.-H. *Cryobiology* **2000**, *41*, 1.
26. Palasz, A.-T.; Mapletoft, R. J. *Biotechnol. Adv.* **1996**, *14*, 127.
27. Fletcher, G. L.; Goddard, S. V.; Lu, Y. L. *Chemtech* **1999**, *29*, 17.
28. Tachibana, Y.; Matsubara, N.; Nakajima, F.; Tsuda, T.; Tsuda, S.; Monde, K.; Nishimura, S. I. *Tetrahedron* **2002**, *58*, 10213.
29. Heggemann, C.; Budke, C.; Schomburg, B.; Majer, Z.; Wissbrock, M.; Koop, T.; Sewald, N. *Amino Acids* **2010**, *38*, 213.
30. Nagel, L.; Budke, C.; Erdmann, R. S.; Dreyer, A.; Wennemers, H.; Koop, T.; Sewald, N. *Chem.-Eur. J.* **2012**, *18*, 12783.
31. Nagel, L.; Plattner, C.; Budke, C.; Majer, Z.; DeVries, A. L.; Berkemeier, T.; Koop, T.; Sewald, N. *Amino Acids* **2011**, *41*, 719.
32. Nagel, L.; Budke, C.; Dreyer, A.; Koop, T.; Sewald, N. *Beilstein J. Org. Chem.* **2012**, *8*, 1657.
33. Wojnar, J. M.; Evans, C. W.; DeVries, A. L.; Brimble, M. A. *Aust. J. Chem.* **2011**, *64*, 723.
34. Liu, S. H.; Ben, R. N. *Org. Lett.* **2005**, *7*, 2385.
35. Eniade, A.; Ben, R. N. *Biomacromolecules* **2001**, *2*, 557.
36. Hachisu, M.; Hinou, H.; Takamichi, M.; Tsuda, S.; Koshidaa, S.; Nishimura, S. I. *Chem. Commun.* **2009**, 1641.
37. Garner, J.; Jolliffe, K. A.; Harding, M. M.; Payne, R. J. *Chem. Commun.* **2009**, 6925.
38. Gibson, M. I.; Barker, C. A.; Spain, S. G.; Albertin, L.; Cameron, N. R. *Biomacromolecules* **2009**, *10*, 328.
39. Gibson, M. I. *Polym. Chem.* **2010**, *1*, 1141.
40. Miller, N.; Williams, G. M.; Brimble, M. A. *Org. Lett.* **2009**, *11*, 2409.
41. Tam, R. Y.; Rowley, C. N.; Petrov, I.; Zhang, T. Y.; Afagh, N. A.; Woo, T. K.; Ben, R. N. *J. Am. Chem. Soc.* **2009**, *131*, 15745.
42. Peltier, R.; Evans, C. W.; DeVries, A. L.; Brimble, M. A.; Dingley, A. J.; Williams, D. E. *Cryst. Growth Des.* **2010**, *10*, 5066.
43. Plattner, C.; Nagel, L.; Budke, C.; Koop, T.; Sewald, N. *Amino Acids* **2009**, *37*, 41.
44. Capicciotti, C. J.; Trant, J. F.; Leclere, M.; Ben, R. N. *Bioconjugate Chem.* **2011**, *22*, 605.
45. Balcerzak, A. K.; Ferreira, S. S.; Trant, J. F.; Ben, R. N. *Bioorg. Med. Chem. Lett.* **2012**, *22*, 1719.
46. Owens, N. W.; Stetefeld, J.; Lattova, E.; Schweizer, F. *J. Am. Chem. Soc.* **2010**, *132*, 5036.
47. Wang, S. Y.; Damodaran, S. *J. Agric. Food Chem.* **2009**, *57*, 5501.
48. Kim, J. S.; Damodaran, S.; Yethiraj, A. *J. Phys. Chem. A* **2009**, *113*, 4403.
49. Komatsu, S. K.; Devries, A. L.; Feeney, R. E. *J. Biol. Chem.* **1970**, *245*, 2909.
50. Chakrabartty, A.; Hew, C. L. *Eur. J. Biochem.* **1991**, *202*, 1057.
51. Goddard-Borger, E. D.; Stick, R. V. *Org. Lett.* **2007**, *9*, 3797.
52. Makowska, J.; Rodziewicz-Motowido, S.; Bagizska, K.; Vila, J. A.; Liwo, A.; Chmurzyski, L.; Scheraga, H. A. *Proc. Natl. Acad. Sci. U.S.A.* **2006**, *103*, 1744.
53. Rucker, A. L.; Creamer, T. P. *Protein Sci.* **2002**, *11*, 980.
54. Knight, C. A.; Hallett, J.; Devries, A. L. *Cryobiology* **1988**, *25*, 55.
55. Jackman, J.; Noestheden, M.; Moffat, D.; Pezacki, J. P.; Findlay, S.; Ben, R. N. *Biochem. Biophys. Res. Commun.* **2007**, *354*, 340.
56. Inada, T.; Lu, S. S. *Cryst. Growth Des.* **2003**, *3*, 747.
57. Eniade, A.; Purushotham, M.; Ben, R. N.; Wang, J. B.; Horwath, K. *Cell Biochem. Biophys.* **2003**, *38*, 115.

3.3.3 Results and Discussion of Antifreeze Activity of Peptides and Glycopeptide AFGP Analogues with PPII Solution Structure

The synthesis of the HyP AFGP derivatives was completed by collaborators in the laboratory of Dr. Richard J. Payne in the School of Chemistry at the University of Sydney. It began with the preparation of a suitable protected glycosyl-hydroxyproline analogue, containing either an α-GalNAc moiety or a β-Gal-(1,3)-α-GalNAc moiety (Schemes 1 and 2).[49] The (glyco)peptides were then prepared by Fmoc-SPPS using 2-chlorotrityl-chloride resin as described in Schemes 3 and 4. Acidic hydrolysis of the *tert*-butyl protecting groups or deacetylation with hydrazine followed by cleavage from the resin produced HyP derivatives **1**-**10**.

HyP derivatives **1**-**10** were all assessed for TH activity and DIS capabilities utilizing nanoliter osmometry[33] and IRI activity utilizing a "splat-cooling" assay.[34,35] The majority of the HyP derivatives did not exhibit TH activity or the ability to induce ice crystal shaping (Figure 5, A-J, reproduced below along with the structures of the HyP derivatives). This suggests these compounds are not interacting with the ice lattice.[49] The exception was the unglycosylated, N-terminally acetylated HyP derivative **6** which consisted of the tripeptide repeat of (Ala-HyP-Ala)$_4$. This compound induced oval ice crystal shapes rather than circular or disk-like shapes, and it exhibited a small but measureable TH gap of 0.05 ± 0.01 °C at a concentration of 5 mg/mL (Figure 5F). This compound could not be assessed at higher concentrations for TH activity due to solubility problems. These results were surprising as synAFGP$_4$, which is of analogous length to the HyP containing peptide and is more similar in structure to native AFGPs, had no measurable TH gap and induced hexagonal ice crystal shapes (Figure 5K; also see section 3.2).[31] Furthermore, glycosylation of the polypeptide (Ala-Thr-Ala)$_n$ backbone[19,31] and glycosylation of isolated native AFGPs is crucial for TH activity,[2] yet unglycosylated HyP derivative **6** was TH active. Glycosylation with both α-GalNAc (**8**) and β-Gal-(1,3)-α-GalNAc (**10**) diminished TH activity. Interestingly, the absence of the terminal N-acetyl group (**5**) also resulted in a loss of TH activity and ice shaping capability (Figure 5E).[49]

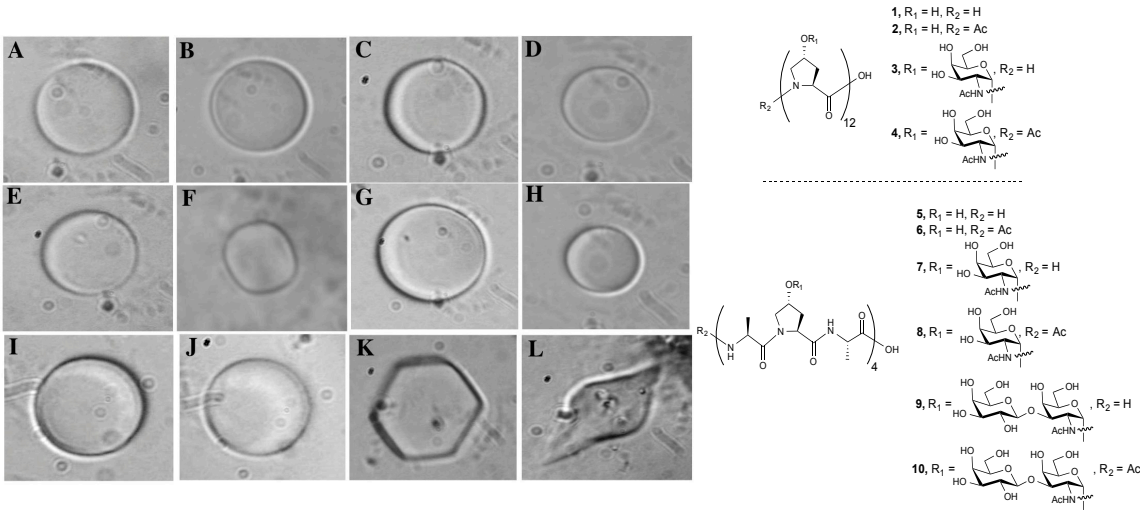

Figure 5. Ice crystal habit in the presence of: (A) **1**; (B) **2**; (C) **3**; (D) **4**; (E) **5**; (F) **6** (5 mg/mL); (G) **7**; (H) **8**; (I) **9**; (J) **10**; (K) synAFGP4; (L) AFGP-8. All compounds were assayed in water at 10 mg/mL unless stated otherwise.

The IRI activity of the HyP derivatives is presented in Figure 6 (reproduced below). The majority of the (glyco)peptides showed a weak to moderate ability to inhibit ice recrystallization at a concentration of 7 mM, resulting in a MGS between 60% and 75% of that of the PBS positive control. The contiguous HyP derivatives **1**-**4** were less IRI active than previously reported HyP_{44} at 7 mM,[48] suggesting that the IRI activity of HyP polymers may be dependent upon (glyco)peptide length, a result similar to that observed with polyvinyl alcohol (PVA)[48,50] and synAFGPs.[31] The presence or absence of an acetylated N-terminal residue did not have an effect on IRI activity. Furthermore, incorporating α-GalNAc residues to the contiguous HyP backbone did not improve the IRI activity with glycopeptides **3**-**4** exhibiting similar activity to unglycosylated **1**-**2**. However, compared with a 22 mM solution of the monosaccharide GalNAc, conjugation to the HyP backbone significantly improved activity (Figure 6).

Unglycosylated peptides **5** and **6** with the tripeptide repeat $(Ala\text{-}HyP\text{-}Ala)_4$ exhibited the most potent IRI activity in the series at a concentration of 7 mM (Figure 6). The activity of these compounds is comparable to that of AFGP-8, however AFGP-8 is active at the significantly lower concentration of 5.5 μM. Interestingly, only N-terminally acetylated **6** exhibited TH activity. Previous studies on AFGPs and synthetic *C*-linked AFGP analogues have reported that unglycosylated peptide backbones had significantly reduced IRI activity in comparison to the glycopeptides.[19,31,51] However, glycosylating the (Ala-Hyp-Ala) analogues was detrimental for activity with both carbohydrate residues introduced in this study (compounds **7**-**10**).

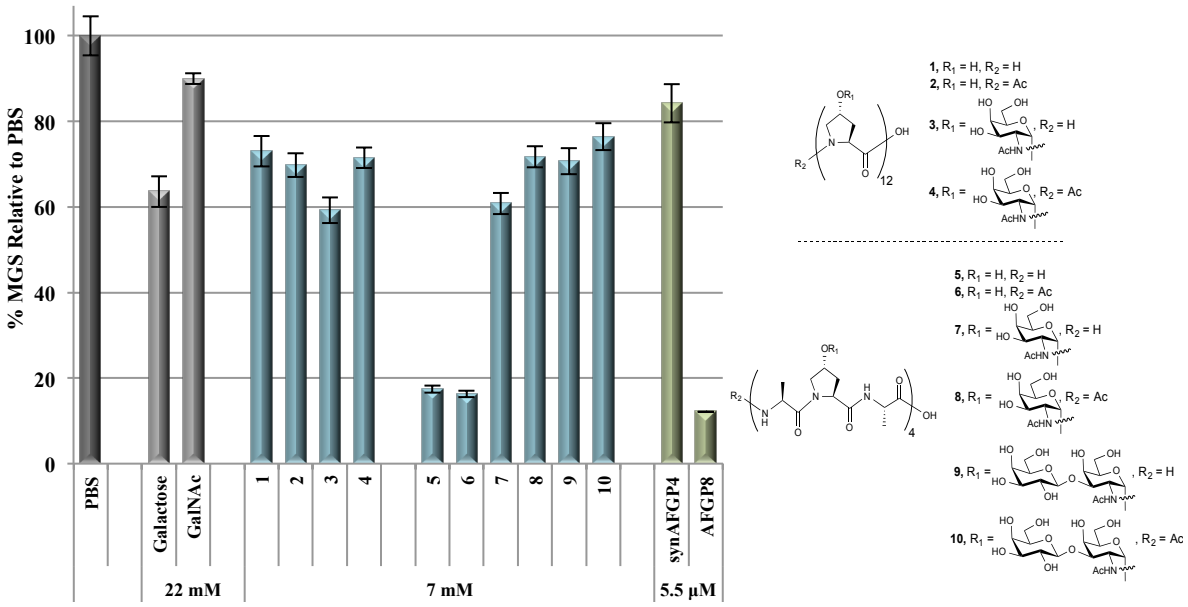

Figure 6. Ice recrystallization inhibition (IRI) activity of hydroxyproline derivatives **1–10** at 7 mM, synAFGP$_4$ and AFGP-8 at 5.5 μM, and D-galactose and N-acetyl-D-galactosamine (GalNAc) at 22 mM in PBS. The % MGS (mean grain size) relative to a PBS positive control is shown for all compounds.

Similar to the synAFGPs (section 3.2), all of the HyP derivatives (**1**-**10**) were suggested to adopt a PPII helical structure in solution (Figures 3 and 4, reproduced below) as determined by far-UV CD spectroscopy (CD spectroscopy studies were conducted by Dr. Richard J. Payne's laboratory at the University of Sydney).[49] The CD spectra of all HyP (glyco)peptides showed a strong negative minimum below 210 nm and a weak positive maximum between wavelengths of 215 and 230 nm. The most defined PPII helical structure was observed from the contiguous unglycosylated HyP derivatives **1**-**2** (Figure 3). Glycosylation with α-GalNAc (**3**-**4**) resulted in additional positive signals at wavelengths below 200 nm, however significant PPII character was still observed in these spectra. The temperature dependence (between -5 and 85 °C) of the secondary structures was also assessed for the HyP (glyco)peptides. While at high temperatures the contiguous HyP derivatives **1**-**4** maintained strong PPII character, (Ala-HyP-Ala)$_4$ derivatives **5**-**10** lost PPII structure in favour of random coil as temperatures were increased (Figure 4, see article in section 3.3.2)

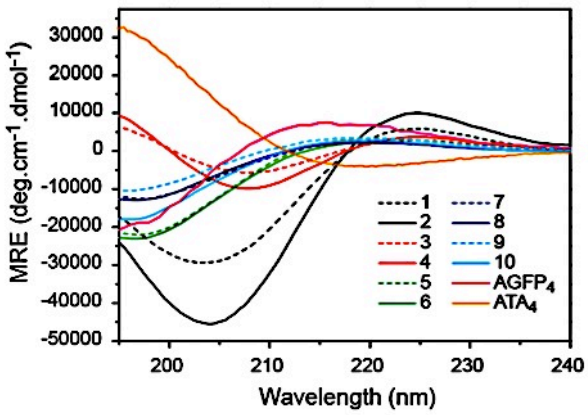

Figure 3. Circular dichroism (CD) spectra of peptides **1**–**10**, synthetic $AGFP_4$ and ATA_4 in water at -5 °C. Concentrations for each peptide were: **2**: 0.05 mg/mL; **1**, **5**, **6**, synthetic $AFGP_4$ and ATA_4: 0.1 mg/mL; **7**, **8**, and **10**: 0.2 mg/mL; **4**, and **9**: 0.4 mg/mL; **3**: 0.6 mg/mL. Data for $AGFP_4$ and ATA_4 have been reported previously.[31]

The results from this study with HyP AFGP derivatives and the synAFGP derivatives described above (section 3.2) suggest that glycosylation of the peptide backbone $(Ala\text{-}Thr\text{-}Ala)_4$ with β-Gal-(1,3)-α-GalNAc ($synAFGP_4$) is sufficient to induce PPII structure.[31] Incorporation of a HyP residue in place of the Thr residue ($(Ala\text{-}HyP\text{-}Ala)_4$, **5**-**6**) will also induce PPII structure, whereas the unglycosylated $(ATA)_4$ does not adopt this solution structure.[49] However, only N-terminally acetylated $(Ala\text{-}HyP\text{-}Ala)_4$ derivative **6** exhibited both TH and IRI activities, while **5** exhibited only IRI activity and $synAFGP_4$ was inactive for both activities (section 3.2). This suggests that specifically a PPII helical structure is not a prerequisite for TH or IRI activity. This hypothesis is further validated by the lack of activity observed for all other HyP derivatives, including the contiguous HyP (glyco)proteins (**1**-**2**) that exhibit strong PPII characteristics.

N-terminally acetylated $(Ala\text{-}HyP\text{-}Ala)_4$ derivative **6** produced a small TH gap of 0.05 °C, indicating that this compound was able to bind to ice. The N-terminal amine $(Ala\text{-}HyP\text{-}Ala)_4$ derivative **5** did not exhibit TH activity or the ability to induce ice crystal shaping, yet both **5** and **6** exhibited identical potent IRI activity (Figure 6). This could suggest that the ice binding ability of **6** may not be significantly contributing to the ability of this compound to inhibit ice recrystallization. The small structural variation of removing the N-terminal acetyl group in **6** diminished the TH activity and ice binding capabilities of this peptide, yet the potent IRI activity was retained. Further studies are required to elucidate the mechanism by which these compounds are exhibiting potent IRI activity. However, it is evident that for these HyP derivatives an unglycosylated hydroxyproline residue is required for potent activity, as well as the presence of alanine residues within the polypeptide backbone. The $(Ala\text{-}HyP\text{-}Ala)_4$ derivative **5** represents a

novel lead peptide that can exhibit potent IRI activity but not TH activity and will facilitate the design of other peptide derivatives with "custom-tailored" antifreeze activity for applications in cryopreservation.

3.3.4 Summary and Conclusions for the IRI Activity of HyP AFGP Analogues

Hydroxyproline containing AFGP analogues were assessed for their ability to inhibit ice recrystallization to determine the influence of PPII solution structure on IRI activity. It is evident from the results of this study that specifically the ability to adopt a PPII solution structure is not a prerequisite for a compound to exhibit IRI activity. All of the contiguous HyP peptides and the derivatives consisting of $(Ala\text{-}HyP\text{-}Ala)_n$ repeating motifs adopted a PPII helical structure in solution however, only unglycosylated $(Ala\text{-}HyP\text{-}Ala)_n$ derivatives **5** and **6** were potently IRI active. All other HyP containing derivatives exhibited moderate to weak IRI activity. While unglycosylated, N-terminally acetylated derivative **6** did induce a small TH gap and ice crystal shaping, it is unlikely that the ice binding ability of this compound is the only contributing factor for its potent IRI activity. This is because the unacetylated derivative **5** also exhibited similar potent IRI activity as **6**, yet this compound did not induce a TH gap or ice shaping capabilities.

The results from this study have identified a novel "custom-tailored" antifreeze analogue that has potent IRI activity but does not exhibit TH activity. This is the unglycosylated $(Ala\text{-}HyP\text{-}Ala)_n$ derivative **5** that bears an N-terminal amine. This compound exhibited similar IRI activity to native AFGP-8, but at a higher concentration of 7 mM (AFGP-8 had similar activity at 5.5 μM). Interestingly, glycosylation of this peptide is detrimental for this potent activity as derivatives **7** and **9** with an α-GalNAc (**8**) or β-Gal-(1,3)-α-GalNAc residues were significantly less IRI active. This was surprising as glycosylation was required for the potent activity of AFGPs and synthetic *C*-linked AFGP analogues.[19,31,51] The Ala residues of **5** were crucial for its potent activity as replacing them with HyP residues was also detrimental for IRI activity as the contiguous HyP derivatives (**1**-**4**) were IRI inactive. Collectively, the IRI results have identified structural features for IRI activity that were previously unknown. In particular, they have demonstrated that small unglycosylated peptides may also inhibit ice recrystallization, and these are attractive novel candidates for ice recrystallization inhibitors owing to their ease of synthesis compared to AFGPs or glycopeptides.

3.4 IRI and TH Activity of *C*-Linked Triazole AFGP Analogues

3.4.1 C-Linked Triazole AFGP Analogues

Our laboratory previously reported that *C*-linked AFGP analogue OGG-Gal (**1**, figure 3.5) possessed "custom-tailored" antifreeze activity. This derivative had equipotent IRI activity as native AFGP-8, but it did not exhibit TH activity, suggesting the compound was not binding to ice and that its mechanism of action differed from AFGPs.[22] While the exact mechanism by which it is exhibiting IRI activity is currently not known, structure-function studies have revealed key structural features of **1** that are crucial for its potent activity (see section 3.1 and figure 3.2). A highly hydrated monosaccharide moiety and six atoms in the side chain connecting the carbohydrate residue to the polypeptide backbone are beneficial for IRI activity.[22,24] Additionally, it has been demonstrated that replacement of the amide bond in the side chain connecting the galactosyl residue to the peptide backbone with a triazole-linkage is detrimental for activity.[25]

To futher investigate the potent IRI activity of **1**, derivatives **8b**, and **10**-**11** (figure 3.5) were prepared and assessed for both TH and IRI activity. These derivatives were synthesized in Dr. Rob M. J. Liskamp's laboratory at the Utrecht Institute for Pharmaceutical Sciences at Utrecht University. The synthesis of these compounds and their antifreeze specific acitvities were recently submitted in a manuscript to *ChemBioChem* in November 2013, and this article is provided in section 3.4.2. The antifreeze results are provided in section 3.4.3 with reproduced figures to complement the discussion. All compounds and figure numbers are in accordance with those in the manuscript. Derivatives **8b**, **10** and **11** all contained the same galactosyl-ornithine unit as OGG-Gal (**1**), and **11** is structurally very similar to **1** except it does not contain the terminal glycine unit and the C-terminal carboxylic acid was replaced with a primary amide. Compounds **10**-**11** have the peptide bond of the third glycine unit in the tripeptide repeat (Orn-Gly-Gly) replaced with a triazole linkage. Results from this study will facilitate an understanding of how OGG-Gal (**1**) is exhibiting potent IRI activity and elucidate the importance of the polypeptide backbone for this activity.

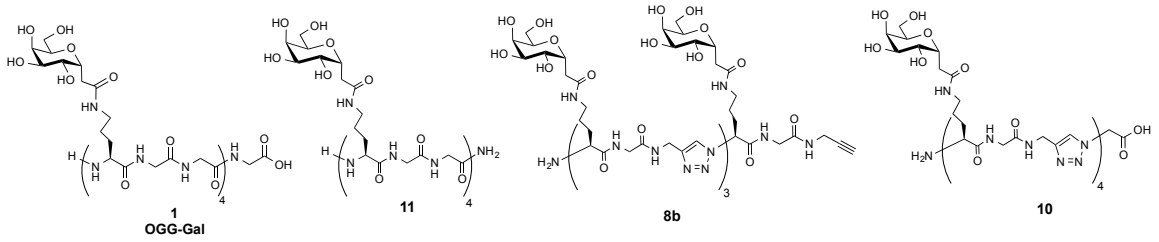

Figure 3.5 Structures of *C*-linked triazole-containing derivatives of OGG-Gal (**1**).

3.4.2 Article: "Synthesis and Evaluation of Linear CuAAC-Oligomerized Antifreeze Neo-Glycopeptides"

DOI: 10.1002/cbic.200((will be filled in by the editorial staff))

Synthesis and evaluation of linear CuAAC-oligomerized antifreeze neo-glycopeptides

Steffen van der Wal[a], Chantelle J. Capicciotti[b], Stamatia Rontogianni[a], Robert N. Ben[b], Rob M. J. Liskamp*[a]

Antifreeze glycoproteins (AFGPs) are important naturally occurring biological antifreezes that lower the freezing point of a solution, thereby preventing uncontrolled ice growth. These compounds also inhibit ice recrystallization. Described in this paper is a synthetic antifreeze glycopeptide-based polymer synthesized from an azide/alkyne glycopeptide building block by partial reduction of the azide and subsequent copper catalyzed azide alkyne cycloaddition (CuAAC) polymerization to obtain linear oligomers. To compare activity with native AFGPs, the linear dodecapeptide (oligomer with four repeating units) was synthesized and isolated which had a comparable length to AFGP-8, the lowest molecular mass glycoprotein AFGP found in nature. In terms of ice recrystallization inhibition (IRI) activity, the triazole based oligomers displayed only modest IRI activity compared with AFGP-8 and a previously described carbon-linked AFGP analogue. CD spectroscopy showed that the triazole-based tetramer possessed similar secondary structure to the related amide based carbon-linked AFGP tetramer based on AFGP-8, suggesting folding of the AFGP analogue in solution is not the only structural requirement for IRI activity.

Introduction

Antifreeze glycoproteins (AFGPs) are naturally occurring antifreeze compounds found in several deep sea teleost fish. These proteins play an important role in the survival of these organisms living in sub-zero temperatures.[1] In contrast to antifreeze proteins (AFPs) that show a relative diversity in their structures[2], the structure of AFGPs is relatively conserved. A key feature of these proteins is that they are mostly composed of repeating tripeptide units (figure 1).[3][4]

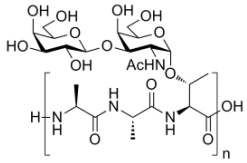

Figure 1. General structure of AFGPs with repeating structure H-(Ala-Ala-Thr(β-D-Gal-(1,3)α-D-GalNAc))$_n$-OH

The tripeptide repeat consists of two L-alanine residues and one L-threonine which is glycosylated with β-Gal-(1,3)α-GalNAc. AFGPs occur in different lengths and are named based on their size or molecular mass. The shortest fragments, named AFGP-8, consists of 4 tripeptide repeats, while the longest fraction, AFGP-1, contains approximately 50 repeats.[3]

AFGPs exhibit two distinct "antifreeze" properties. One is a lowering of the freezing point by the antifreeze compound, while the melting point remains unchanged. The difference between melting and freezing points is known as thermal hysteresis (TH).[5] This effect can lower the freezing point of a biological fluid enough to allow for survival in Arctic environments. The other "antifreeze" effect of the AFGPs is the ability to inhibit ice recrystallization. Specifically, this is the ability to prevent the enthalpically driven process of large ice crystals growing larger at the expense of small ice crystals.[6][7] Large ice crystals are highly damaging to cells and tissues, and as such the prevention of the formation of these large crystals is a good strategy in the cryopreservation of biological materials (cells, tissues etc.).[8]

It is thought that the interaction of the sugar hydroxyl moieties with the water/ice interface is responsible for its antifreeze properties of AFGPs. However, model AFGPs have recently been investigated, showing that the most active compound in terms of IRI activity showed a distinct folding, thereby creating a hydrophobic pocket that may be responsible for its specific water ice interface interactions. [9]

The use of antifreeze glycoproteins and their analogues for cryopreservation applications has been limited by the low availability of these compounds from natural sources. Consequently, effort has been undertaken to obtain these compounds synthetically. The total synthesis of natural AFGP has been described in the literature,[10][11][12] and while elegant, it is not

[a]

[b]

a viable large scale synthesis of antifreeze compounds on a cost-effective basis. Therefore, previous work has sought to simplify the structure of native AFGP-8 while maintaining the antifreeze activity, in particular the ability to inhibit ice recrystallization. To date, the best examples of this are the carbon-linked antifreeze glycoprotein analogues[13] (C-AFGPs), e.g. OGG-Gal analogue **1** shown in figure 2). Interestingly, these studies have demonstrated that glycopeptides containing the monosaccharide galactose are very effective ice recrystallization inhibitors,[14] despite the fact it is less structurally complex than the disaccharide moiety found in native AFGPs.

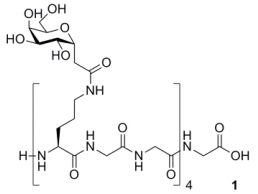

Figure 2. Structure of the galactose based Ornithine-Gly-Gly AFGP **1** by Ben *et al.*[13][15][8]

One of the most easily accessible structures was found to be a galactose derived carboxylic acid conjugated *via* the side chain of an ornithine instead of a threonine residue (**1**, figure 2).[15] Furthermore, it was found that replacing the two alanine residues in the natural AFGP by glycine did not result in a loss of IRI activity.

This compound, which is already more synthetically accessible than natural AFGP, was chosen as a starting point for creating a glycopeptide monomer that can be polymerized into longer compounds that resemble natural AFGPs and synthetic C-linked AFGPs. The idea of treating the tripeptide repeat as monomer has been explored before, using peptide coupling reagents as polymerization agents.[16] To simplify the polymerization and increase compatibility with more functional groups, the orthogonal CuAAC reaction was employed in our approach. (Figure 3) The triazole ring is a bioisostere of an amide bond, and the replacement should not interfere much with the overall shape of the molecule.[17][18] Previously, the strategy of incorporating azide and alkyne termini was used successfully in the synthesis of (biodegradable) peptide based polymers as well as the synthesis of Aβ peptide-based oligomers[19][20][21][22]

Figure 3. Left: The proposed structure of the glycopeptide monomer. Right:

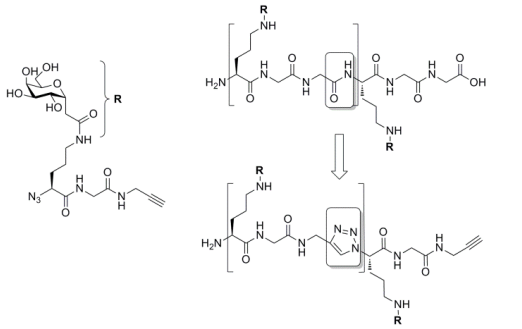

Comparison between the published AFGP mimic by Ben *et. al.* (top) and the resulting polymer obtained from the proposed monomer.

It has been found that this method may generate a significant amount of cyclic molecules due to intramolecular cycloaddition.[19][20][22] Although cyclic glycoproteins have been synthesized before and are a potentially interesting class of compounds[23], for direct comparison naturally occurring antifreeze glycoproteins, it was decided to focus on smaller linear oligomers to better compare the IRI activity of the CuAAC oligomerized antifreeze glycoproteins to native antifreeze glycoproteins. While the CuAAC approach has been utilized previously to link carbohydrate moieties to polypeptide backbones of various AFGP analogues, this is the first instance where it has been used to replace the amide bonds in the polypeptide backbone of an AFGP (analogue).[24][25][26]

One of the key steps in generating linear oligomers is blocking one of the reactive azide or alkyne endgroups of a (growing) oligomer chain (see figure 4). In the case of azide/alkyne monomers this can be accomplished either by having a fraction of the monomers protected on the alkyne, for example by the TIPS protecting group, or by reduction of a fraction of the azide to the amine. Both are potentially feasible strategies, but in the end the latter was the method of choice, as reduction of an azides to an amine can be performed with phosphine reducing agents that are compatible with CuAAC click

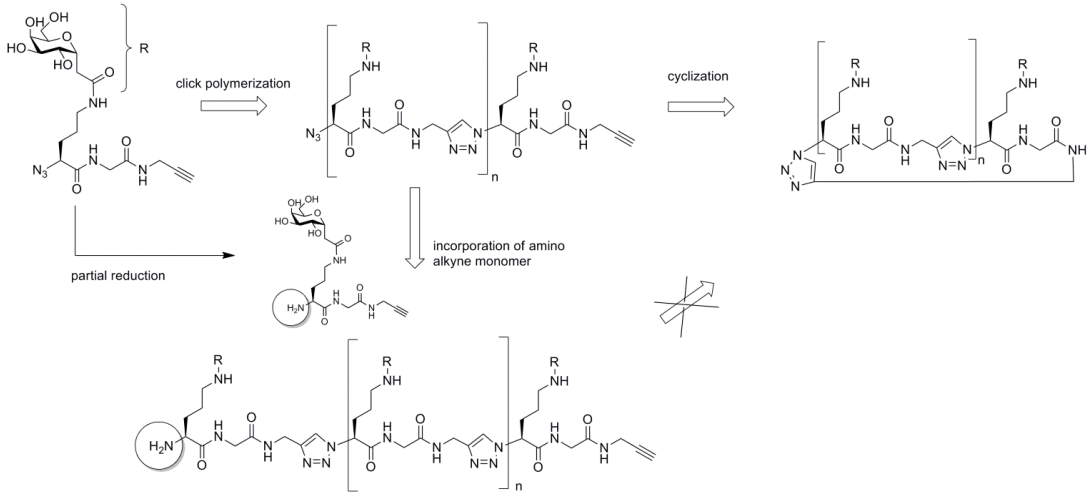

Figure 4. Schematic overview of obtaining AFGPs by linear polymerization of an azido-alkyne monomer using CuAAC

chemistry.[27] Since some of the starting azide/alkyne monomer can be converted into amino/alkyne monomer in the same pot by addition of a certain amount of phosphine, the two discrete starting monomers do not need to be synthesized separately, which is very advantageous.

The main aim of this research was to evaluate the design of the resulting oligomers by investigating whether the triazole moiety does not reduce IRI activity and whether the amide bonds in the polypeptide backbone of these analogues are not an essential structural feature for IRI activity. Therefore a synthetic oligomer with a similar length as natural AFGP-8 was synthesized.[28] This was accomplished by tuning the amount of phosphine to monomer ratio to 3:1. The resulting distribution of linear oligomers can then, when the hydroxyl groups of the carbohydrate are protected, be separated by HPLC. Separation was possible because every oligomer has one positive charge and a hydrophobic sugar moiety; the physical properties of short oligomers are likely to be more dominated by the positive charge whereas longer oligomers become more apolar due to the amount of hydrophobic moieties per molecule. The oligomers were deprotected and the isolated tetramer was compared with the previously described C-AFGP **1** (shown in figure 2) by evaluation of TH and IRI activity and determination of the secondary structure by CD spectroscopy.

Results and Discussion

Synthesis of azido-alkyne glycopeptide monomer

The azido/alkyne tripeptide backbone **4a** required for the synthesis of the glycopeptide monomer was synthesized from two building blocks (scheme 1). First, commercially available Boc-sidechain protected ornithine was transformed by diazotransfer into the corresponding α-azido compound **2** using imidazolium sulfonyl azide, in a slightly modified procedure[29]. Compound **2** was purified by crystallization as the dicyclohexylamine salt from diethyl ether in excellent yield.

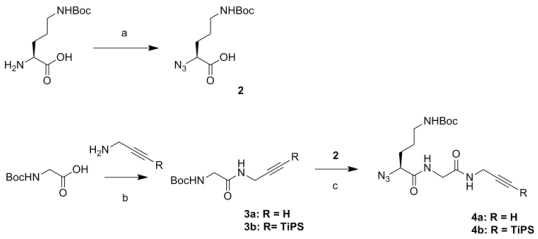

Scheme 1. a) imidazole-1-sulfonyl-azide hydrochloride, $CuSO_4$, MeOH, H_2O, 98%; b) BOP, DiPEA, CH_2Cl_2, 82%[a], 99%[b]; c) 1. TFA, CH_2Cl_2, 2. **2**, BOP, DiPEA, CH_2Cl_2, 55%[a], 75%[b]

Next, commercially available Boc-glycine was coupled to propargylamine using the BOP reagent. The resulting dipeptide **3a** could be purified by crystallization in good yield (82%). Precursor **4a** was assembled from these two building blocks by removal of the Boc protecting group of **3a** followed by BOP coupling with **2** and was obtained in an acceptable yield (55%). Solid compound **4a** could be stored at 4 ºC for 2 weeks without any significant auto-polymerization, but prolonged storage or at room temperature led to the formation of a mixture of oligomeric impurities. For smaller scale reactions this stability of compound **4a** was satisfactory, however, it was insufficient for synthesizing larger quantities. Thus, the triisopropylsilyl (TIPS) protected alkyne **4b** was also synthesized. The TIPS protecting group is one of the more stable silyl protecting groups and is tolerant to treatment with trifluoroacetic acid.[30]

Synthesis of TIPS protected azido/alkyne tripeptide **4b** was similar to the synthesis of the unprotected peptide **4a**, but uses TIPS protected propargylamine instead of propargylamine.[31] Since the intermediate **3b** and final product **4b** were oils, purification was carried out using silica chromatography. The resulting protected azide/alkyne tripeptide could be stored for months at room temperature without significant oligomerization or degradation. In view of its increased stability as compared with precursor **4a**, **4b** was chosen as starting material for the glycopeptide monomer **5a.**

Glycosylated TIPS-protected monomer **5b** was synthesized by Boc-deprotection of **4b** using TFA, followed by a coupling with the N-hydroxysuccinimide ester of the galactosylic acid **6** to obtain compound **5b** in good yield. (scheme 2)

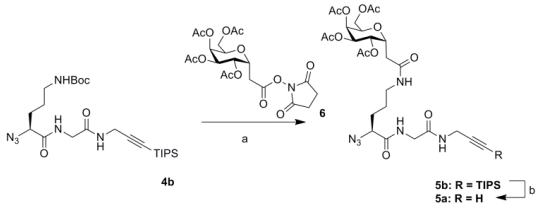

Scheme 2. a) 1. TFA/ CH_2Cl_2, 2. **5**, DiPEA, CH_2Cl_2 84% b) TBAF, phenol, THF, 90%

Deprotection of the TIPS-alkyne **5b** was first attempted with tetrabutylammonium fluoride trihydrate (TBAF) in THF. Equimolar or slightly higher amounts of TBAF gave sluggish reactions. To prevent deacetylation of the sugar moiety when an larger excess of TBAF was used, acetic acid was added to reduce the basic conditions of the reaction[32][33]. Unfortunately, even when 5 equivalents of TBAF and acetic acid were used, the reaction was still sluggish, so presumably acetic acid was too strong an acid, thereby reducing the nucleophilicity of F^- considerably. To our delight, when instead an equimolar amount of the weaker acid phenol was added to TBAF, complete deprotection to **5a** was observed in a relatively short time (1-3 hours) without any detectable deacetylation of the carbohydrate moiety.

Linear CuAAC oligomerization of the azido-alkyne monomer

The linear oligomerization of monomer **5a** consists of two steps in a one-pot procedure (scheme 3). In the first step, a trisubstituted phosphine is added to a solution of the azido/alkyne monomer to reduce a fraction of the azides to amines. Next, to the resulting mixture of this amino/alkyne and azido/alkyne, copper(I) is introduced to start polymerization. By performing this reaction at high concentration, intermolecular cycloaddition may outcompete intramolecular cyclization, which would otherwise result in cyclic peptides. Initially triphenylphosphine was chosen as the phosphine to reduce a fraction of the azides of **5a** due to its widespread use in the Staudinger Reaction.[34] Although the initial stage of the reduction of the azide to the phosphorus-aza-ylide was rapid, hydrolysis of the ylide to the amine was sluggish (data not shown).

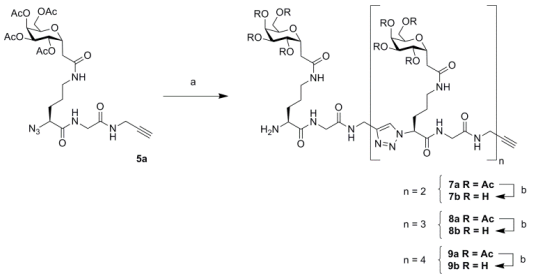

Scheme 3. a) 1. TCEP (0.25 eq), DiPEA, DMF/H_2O, 2. $CuSO_4.5H_2O$, sodium ascorbate, H_2O/DMF, b) NaOMe in MeOH

Instead, a more reactive and less sterically hindered phosphine, tris(2-carboxyethyl)phosphine hydrochloride (TCEP) was chosen, which has also the advantage that its aza-ylide should be more prone to hydrolysis due to the more polar nature of the phosphorus substituents. Indeed, it was observed that upon addition of TCEP, nitrogen gas evolved immediately, and after 2 hours at room temperature, both the reaction and hydrolysis of the ylide, appeared to be complete as was shown by HPLC and ESI-MS analysis.

This reaction mixture was used directly for the CuAAC polymerization: copper(II)sulfate was added followed by the reducing agent sodium ascorbate. It was allowed to polymerize for two hours at room temperature, after which the reaction mixture was diluted and acidified. HPLC analysis showed a distinct distribution of peaks with little of the starting materials present (figure 5, top).

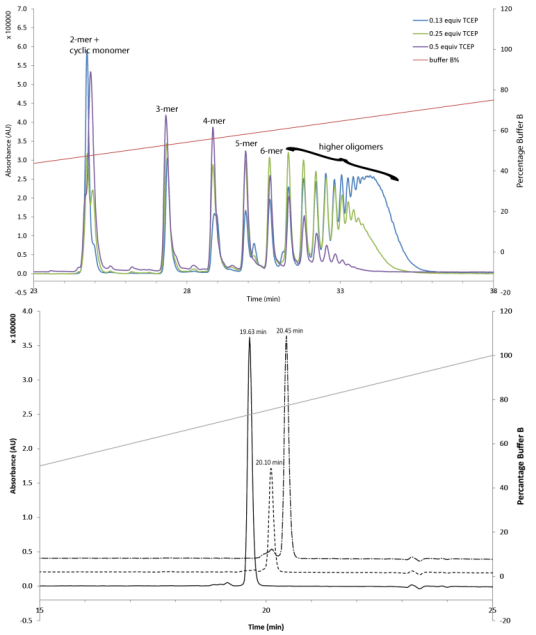

Figure 5. Top: HPLC trace of the crude polymeric mixtures of **5a** with three different TCEP amounts, using a 48 minute gradient. Bottom: HPLC traces of the purified 0.25 equiv. TCEP polymerization with **7a** (continuous), **8a** (dotted) and **9a** (semi continuous) on a 20 minute gradient, offset on the Y-axis.

As expected, the smaller linear oligomers are more polar and eluted first and the higher molecular weight oligomers eluted later. The degree of polymerization could be directed by adding different amounts of TCEP. Small amounts of mono-acetyl deprotected species were observed eluting slightly before the major peaks. Cyclic peptides however, aside from a small amount cyclic dimer, were not observed as major compounds. Separation of the main oligomer peaks of **5a** (**7a**, **8a** and **9a**) by preparative HPLC proved feasible and yielded these smaller oligomers (three to five tripeptide repeats) in good purity (figure 5 bottom). The identity of these compounds was confirmed by MALDI-TOF. Small amounts of impurities eluting slightly earlier than the oligomers could be attributed by MS to acetyl hydrolysis during the purification and subsequent lyophilisation. The higher oligomers (>7 tripeptide units) were collected together as a mixed oligomeric fraction.

Removal of the acetyl groups was performed with sodium methoxide in methanol, which caused precipitation of the deprotected oligomers. Water was later added to solubilize the suspension and cation exchange resin was used to neutralize the reaction mixture. After filtration of the resin and lyophilization, the oligomers **7b**, **8b** and **9b** were obtained in sufficient amounts for testing of antifreeze activity.

C-terminal variation of the synthetic AFGPs

The synthesized triazole-linked oligomers have a C-terminal alkyne moiety, compared to a C-terminal acid functionality of the natural AFGP-8 and earlier described OGG-Gal **1** (figures 1 and 2 respectively). Although oligomers **7b** – **9b** possess a free N-terminal amine, the C-terminus is an alkyne, whereas both the natural and earlier developed AFGPs are zwitterions by having in addition to the amine also a C-terminal carboxylic acid. Therefore the role of the zwitterionic nature of the AFGP on the structure of these triazole-linked oligomers was also studied. Thus, purified tetramer **8a**, containing a C-terminal alkyne was coupled to ethyl azidoacetate by CuAAC, which after deprotection yielded the structural triazole analogue of OGG-Gal, **10** (Scheme 4).

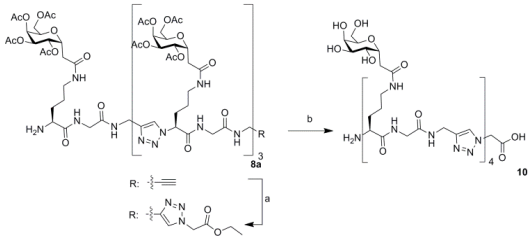

Scheme 4. a) ethyl azidoacetate, $CuSO_4.5H_2O$, sodium ascorbate, H_2O/THF, b) NaOMe in MeOH

Similarly, a C-terminal variation of OGG-Gal **1** was synthesized wherein the C-terminal glycine with a free carboxylic acid moiety was omitted, and a carboxamide moiety was introduced, leading to **11,** which corresponds to the structure of the triazole alkyne tetramer **8b**. This was accomplished by solid phase synthesis on a Rink-linker instead of the preloaded glycine-Wang resin as was used for the synthesis of OGG-Gal **1**. The resulting four compounds, that is the C-terminal acids **1** and **10** and noncharged C-terminal amides **8b** and **11** of both the peptidic and triazole tetramers of the synthetic AFGP are depicted in scheme 5.

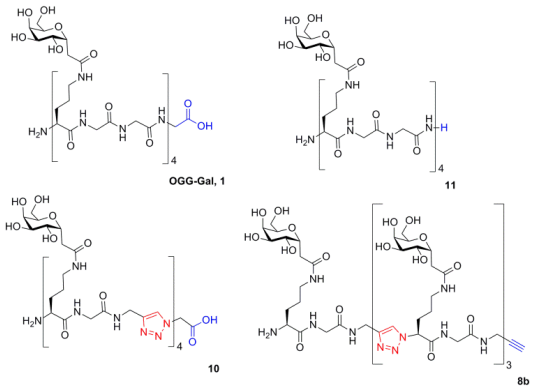

Scheme 5: Top left; Reference compound OGG-Gal (**1**), Top right, carboxamide terminated version of reference compound OGG-Gal (**11**), Bottom left, triazole linked mimic of reference OGG-Gal (**10**), bottom right, tetramer **8b**, which is a triazole linked mimic of compound **11**.

Evaluation of the antifreeze activity of the oligomers

All glycopeptides were assessed for thermal hysteresis (TH) activity using nanoliter osmometry[35] and ice recrystallization inhibition (IRI) activity using a "splat cooling" assay as was described earlier.[36][37] No TH activity or dynamic ice shaping capabilities were observed for these oligomers, as the water froze in circular form (center of the images), indicating that similarly to the reference compound OGG-Gal **1** these compounds are not interacting with the ice lattice (figure 6). [15]

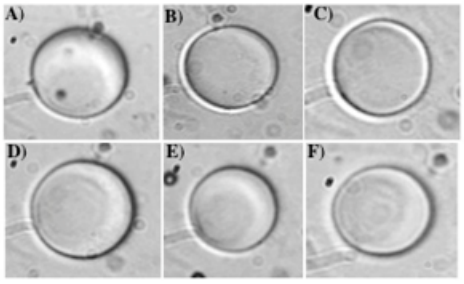

Figure 6: Ice crystal habit in the presence of: A) triazole tetramer, C-terminal alkyne **8b**; B) triazole tetramer, C-terminal acid **10** C) Peptide tetramer, C-terminal carboxamide **11**; D) triazole trimer, C-terminal alkyne **7b**; E) triazole pentamer C-terminal alkyne **9b**; F) triazole polymeric fraction (n = 6-17). All compounds were assayed in water at 10 mg/mL.

The IRI activity of the glycopeptides in scheme 5 is shown in figure 7. The triazole containing oligomer **8b** was only moderately IRI active at 5.5 mM, and was substantially less active than the related C-AFGP OGG-Gal **1**, even at a 1000-fold higher concentration. OGG-Gal **1** exhibits equipotent IRI activity to native AFGP-8 at a significantly lower concentration of 5.5 μM. These results indicate that the replacement of the peptide bonds with triazole linkages and loss of the C-terminal negative charge in the polypeptide backbone of OGG-gal **1** is detrimental and greatly reduces the potent IRI activity of this C-AFGP analogue. From the data presented in figure 7, it is also clear that the C-terminus also plays an dominant role in the IRI activity. Compound **11**, which contains a C-terminal carboxamide and is slightly shorter than the C-terminus of compound OGG-Gal **1**, displayed a similar reduction in IRI activity to the triazole with an alkyne terminus **8b**. Therefore we investigated compound **10**, which is a better mimic of reference compound **1**, since it also contains the C-terminal glycine-like moiety. Unfortunately, this modification did not restore the IRI activity back to a similar level as compound **1**, and it still displayed a similar reduced IRI activity as compound **8b**, suggesting that the presence of the triazole rings in AFGP-mimics **8b** and **10** is responsible for the majority of IRI activity loss

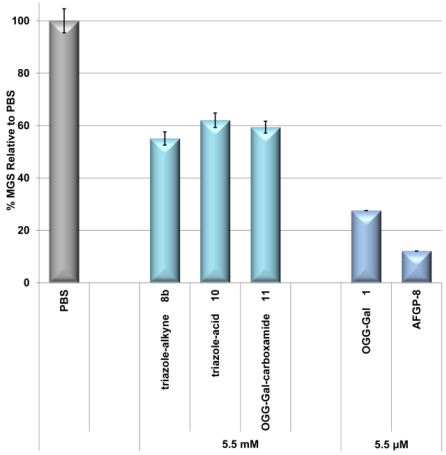

Figure 7: Ice recrystallization inhibition (IRI) activity of oligomers **8b**, **10**, and **11** at 5.5 mM, and OGG-Gal **1** and AFGP-8 at 5.5 μM in PBS. The % MGS (mean grain size) relative to a PBS positive control is shown for all compounds.

CD spectroscopy

To investigate whether this loss of IRI activity was caused by a change in the conformation of the backbone of the triazole containing AFGP, CD spectroscopy was performed. In view of the environment in which these peptides are normally active, measurements were performed in water at 4 ºC.[11] Interestingly, in spite of the differences in IRI activity, the CD spectra of the four AFGP mimics **8a**, **10, 11** and **1** were very similar (figure 8).

Strikingly, the peptide OGG-Gal **1** and the amidated mimic **11** showed a nearly identical CD spectrum, even though these compounds differed by 3 orders of magnitude in IRI activity. Similarly, the difference in CD spectrum between the two triazole linked AFGPs **8b** and **10** is small. From this, it can be concluded that the negative charge on the C-terminus does not influence the secondary structure of the peptide to a large degree.

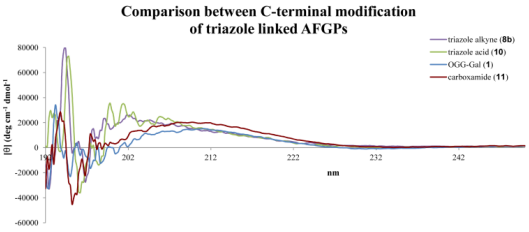

Figure 8: far-UV CD spectrogram comparisons: compound **1** (blue) and **11** (red), compound **10** (green) and **8b** (purple).

This is in contrast to the observed effect of the C-terminus on the IRI activity, especially in the case of the mimics **1** and **11**. On the whole, the conformational effect of the triazole on the structure of the AFGPs seemed limited; nevertheless a shift of the maximum [θ] was observed from 212 nm in the case of mimics **1** and **11** to 202 nm in the case of **8b** and **10**. Although different conformational organization of these peptides on the ice interface upon freezing cannot be excluded, the largest structural difference when substituting amide bonds by triazole moieties is the loss of a hydrogen bond donor per substituted amide bond. Potentially this loss leads to a different degree of hydration and/ or different interactions of the backbone with the carbohydrate part of antifreeze glycopeptide.

Conclusion

The synthesis of the simplified azide/alkyne glycopeptide building block described here was found to be efficient and simple. The use of the TIPS protecting group allowed long term storage and its removal was very facile.

The oligomerization approach with the *in situ* generation of a small amount of a terminating monomer worked quite conveniently and separation of the individual length oligomers by HPLC was feasible. While such separation might not be necessary or even ultimately desirable for use as antifreeze, for the purpose of this study the focus was a comparison with natural AFGP-8 and earlier made analogues.

Comparison of **8b** with natural AFGP-8, or the previously published OGG-Gal **1**, showed modest IRI activity for the C-terminal alkyne triazole analogue **8b**. Interestingly, the C-terminus plays a dominant role in the IRI activity of C-AFGPs, and removal of the C-terminal acid in reference compound OGG-Gal **1**, caused a 1000 fold reduction in IRI activity, similar as observed in the alkyne-triazole compound **8b**. Introduction of a C-terminal charge on the triazole analogue **8b** to give structure **10**, unfortunately did not restore activity. The secondary structure of mimics **8b** and **10** did not differ significantly from the parent AFGPs **1** and **11** as assayed with CD spectroscopy, suggesting that it does not play the crucial role, which was earlier suggested.[38]

Experimental Section

General: All reactions were carried out at ambient temperatures unless stated otherwise. Solvents used in these synthesis procedures were supplied by BioSolve BV, (Valkenswaard, The Netherlands) and stored over molecular sieves (CH_2Cl_2 and THF on 4Å and MeCN on 3Å). Routine analysis of reaction progression and product identity was checked by thin layer chromatography (TLC) on Merck precoated silicagel $60F_{254}$ glass plates. Spots were visualized by UV light and stained by ninhydrin or sulphuric acid charring for (protected) amine- and carbohydrate moieties respectively. Column chromatography was performed using Silicycle Siliflash P60 (40-63 µm) silicagel obtained from Screening Devices (Amersfoort, The Netherlands)

^{1}H NMR spectra, ^{13}C and Attached proton test (APT) spectra were recorded on a Varian Gemini 300 spectrometer at 300 MHz and 75 MHz respectively. High pressure liquid chromatography was performed analytically on a Shimadzu automated HPLC system with a dual wavelength detector at 220 and 254 nm operating at a flow-rate of 1 ml/min. An Alltech Alltima C8 column (100 Å, 5 µm, 250 x 4.6 mm) column was used together with acetonitrile TFA buffers for elution (buffer A: 5:95 MeCN:H_2O v/v + 0.1% TFA and buffer B: 95:5 MeCN:H_2O v/v + 0.1% TFA) in a 20- or 48 minute gradient. Preparative HPLC was performed on an Applied Biosystems system using identical buffers and an Alltech Alltima C8 column (100 Å, 10 µm, 250 x 22 mm) and a gradient of 100 minutes. Electron spray mass spectrometry was performed on a Shimadzu LCMS-QP8000 single quadrupole spectrometer operating in positive mode. MALDI-TOF analysis was performed on a Kratos Axima CFR spectrometer using α-cyano-4-hydroxycinnamic acid as matrix.

(S)-2-azido-5-((tert-butoxycarbonyl)amino)pentanoic acid (2)
To a solution of H-Orn(Boc)-OH (4.73 g, 20 mmol) in MeOH (100 ml), copper sulfate solution (42 mg, 0.2 mmol) in water (100 ml) was added, followed by K_2CO_3 (6.14 g, 44 mmol). Subsequently solid imidazole-1-sulfonyl-azide hydrochloride[29] (5.13 g, 24 mmol) was added and the reaction mixture was stirred for 4 hours. The reaction mixture was concentrated to about 100 ml, acidified with 1 M $KHSO_4$ and extracted with EtOAc. The organic layer was washed with saturated sodium chloride and dried with Na_2SO_4. After filtration and concentration *in vacuo*, the residual oil was dissolved in Et_2O and dicyclohexylamine (4 ml, 20 mmol) was added drop-wise while stirring. After cooling at -20 ºC overnight the white precipitate was collected by filtration and dried *in vacuo* to obtain the dicyclohexylamine salt of (S)-2-azido-5-((tert-butoxycarbonyl)amino) pentanoic acid (8.28 g, 18.8 mmol, 94%) as a fine white powder.
The free acid for subsequent reactions and analysis was obtained by suspending the salt in EtOAc in an extraction funnel and washing with 1 M $KHSO_4$. After drying the organic layer with saturated NaCl and Na_2SO_4 the free acid was obtained as an oil in near quantitative yield.

^{1}H NMR ($CDCl_3$): δ = 10.40 (bs, 1H, COOH), 6.46 + 4.72 (two bs. 1H, NH), 3.93 (bs, 1H, α-CH), 3.15 (bs, 2H, δ-CH_2), 1.89-1.77 (m, 2H, β-CH_2), 1.63 (m, 2H, γ-CH_2), 1.44 (s, 9H, Boc-CH_3)
^{1}H NMR (CD_3OD): δ = 3.98 (m, 1H, α-CH), 3.07 (t, *J*= 6.6 Hz, 2H, δ-CH_2), 1.91-1.68 (m, 2H, β-CH_2), 1.59 (m, 2H, γ-CH_2), 1.43 (s, 9H, Boc-CH_3)
^{13}C NMR (CD_3OD) δ = 172.4, 157.1, 78.5, 61.5, 39.2, 28.3, 27.4, 25.9

((N-tert-butoxycarbonyl)glycyl)-propargylamine (3a)
Propargylamine hydrochloride (4.25 g, 40 mmol) and Boc-Gly-OH (6.90 g, 40 mmol) were dissolved in CH_2Cl_2 (250 ml). The stirred mixture was cooled on ice, and diisopropylethylamine (DiPEA, 21 ml, 120 mmol) was added, followed by BOP (17.60 g, 40 mmol). After stirring for 2h at room temperature, the mixture was concentrated, redissolved in EtOAc and subsequently washed with 1 M $KHSO_4$, 5% $NaHCO_3$ and saturated NaCl. After drying with Na_2SO_4, the product was crystallized from CH_2Cl_2/ hexanes to yield colourless crystals of ((N-tert-butoxycarbonyl)glycyl)-propargylamine (6.6 g, 31 mmol, 79% overall yield).
^{1}H NMR ($CDCl_3$): δ = 6.46 (bs, 1H, amide-NH), 5.16 (bs, 1H, Boc-NH), 4.06 (dd, J_1=2.5 Hz, J_2=5.3 Hz, 2H, CH_2-propargyl), 3.81 (d, *J*=5.8 Hz, 2H, glycine-CH_2), 2.23 (t, *J*=2.5 Hz, 1H, alkyne-H), 1.45 (s, 9H, Boc-CH_3)
^{13}C NMR ($CDCl_3$): δ = 169.3, 156.1, 80.4, 79.2, 71.6, 44.3, 29.0, 28.3

Triisopropylsilyl-((N-tert-butoxycarbonyl)glycyl)-propargylamine (3b)
3-Triisopropylsilyl-propargylamine[31] (5.0 g, 23 mmol), Boc-Gly-OH (3.83 g, 21.9 mmol) and DiPEA (11.6 ml, 21.9 mmol) were dissolved in CH_2Cl_2 (200 ml) and cooled on ice. While stirring, BOP (9.68 g, 21.9 mmol) was added. After 3 hours at room temperature the reaction mixture was concentrated *in vacuo* and redissolved in EtOAc. This was washed with 1 M $KHSO_4$, 5% $NaHCO_3$ and saturated NaCl. After drying with Na_2SO_4 and concentration *in vacuo*, Triisopropylsilyl-((N-tert-butoxycarbonyl)glycyl)-propargylamine was obtained as a yellowish oil that solidified upon standing (8.61 gram, 23 mmol, 99%)
^{1}H NMR ($CDCl_3$): δ = 6.19 (bs, 1H, amide-NH), 5.08 (m, 1H, Boc-NH), 4.11 (m, 2H, CH_2-propargyl), 3.80 (d, *J*=5.9 Hz, 2H, glycine-CH_2), 1.46 (s, 9H Boc-CH_3), 1.06 (s, 21H, TIPS)
^{13}C NMR ($CDCl_3$): δ = 169.0, 156.2, 102.4, 84.8, 80.3, 44.3, 30.2, 28.3, 18.5, 11.1

(S)-2-azido-5-((tert-butoxycarbonyl)amino)pentanoyl-glycyl-propargylamine (4a)

The Boc-group in **3a** (2.0 g, 9.4 mmol) was removed by 1:1 TFA/ CH_2Cl_2 for 2 hours. After concentration *in vacuo* the oil was redissolved in CH_2Cl_2 (100 ml) and **2** (4.2 g as the dicyclohexylamine salt of **2**, workup as stated at **2**, 9.4 mmol), BOP (4.2 g, 9.4 mmol) and DiPEA (5.2 ml, 30 mmol) were added. After 2 hours the reaction mixture was concentrated *in vacuo*, redissolved in EtOAc, washed with 1M $KHSO_4$, 5% $NaHCO_3$ and brine. After drying of the organic layer over Na_2SO_4 and filtration the product was crystallized from EtOAc/ hexanes and obtained as a white solid (1.8g, 5.1 mmol, 55%).

^{1}H NMR ($CDCl_3$): δ = 7.27 (s, 1H, NH) 6.70 (s, 1H, NH), 4.73 (s, 1H, Boc-NH), 4.06 (m, 3H, propargyl-CH_2 + Orn-α-CH), 3.96 (d, 2H, gly-CH_2 *J*=4.7 Hz), 3.15 (m, 2H, Orn-δ-CH_2), 2.26 (s, 1H, alkyne-H), 1.89 (m, 2H, Orn-β-CH_2), 1.62 (m, 2H, Orn-γ-CH_2), 1.44 (s, 9H, Boc-CH_3)

^{13}C NMR ($CDCl_3$): δ = 170.5, 168.4, 156.2, 79.32, 79.26, 71.6, 62.8, 42.9, 39.7, 29.11, 29.08, 28.4, 25.9

Triisopropylsilyl-((S)-2-azido-5-((tert-butoxycarbonyl)-amino)pentanoyl-glycyl)-propargylamine (4b)

This procedure was analogous to the preparation of **4a**, using the following amounts: **3b** (4.0 g, 10.8 mmol), and **2** (4.8 g as the dicyclohexylamine salt of **2**, workup as stated at **2**, 10.8 mmol), BOP (4.8 g, 10.8 mmol) and DiPEA (5.7 ml, 32.4 mmol).

Purification by column chromatography instead of crystallization was performed using 10% acetone in CH_2Cl_2 to obtain **4b** as a colourless oil (4.1 g, 8.1 mmol, 75%)

^{1}H NMR ($CDCl_3$): δ = 7.21 (s, 1H, NH), 6.29 (s, 1H, NH), 4.70 (s, 1H, Boc-NH), 4.11 (m, 2H, propargyl-CH_2), 4.03 (m, 1H, Orn-α-CH), 3.93 (d, 2H, glycine-CH_2, *J*=5.3 Hz), 3.15 (m, 2H, Orn-δ-CH_2), 1.89 (m, 2H, Orn-β-CH_2), 1.63 (m, 2H, Orn-γ-CH_2), 1.42 (s, 9H, Boc-CH_3), 1.04 (s, 21H, TIPS)

^{13}C NMR ($CDCl_3$): δ = 170.3, 167.7, 156.2, 102.1, 85.1, 79.4, 63.0, 43.0, 39.5, 30.4, 29.2, 28.4, 26.0, 18.5, 11.1

Tetraacetylated carboxymethyl galactoside-OSu ester (6)

Carboxymethyl tetraacetyl galactoside[39][13] (1.0 g, 2.5 mmol) and N-hydroxysuccinimide (0.3 g, 2.7 mmol) were dissolved in dry CH_2Cl_2 (50 ml) and cooled on ice. DCC (0.6 g, 2.7 mmol) was subsequently added and the reaction mixture was stirred for 16 hours at room temperature. Precipitated DCU was removed by filtration and after concentration *in vacuo* to near dryness more precipitation occurred. After another filtration step the product was crystallized from CH_2Cl_2/ *i*PrOH to yield **6** as white fluffy needles (1.0 g, 2 mmol, 82%)

^{1}H NMR ($CDCl_3$): δ = 5.44 (bs, 1H, 4-H), 5.37 (m, 1H, 2-H), 5.20 (m, 1H, 3-H), 4.79 (dt, 1H 1-H, J_1=J_2=6.3 Hz,), 4.30-4.10 (m, 3H, 5-H+6-CH_2), 3.00 (m, 2H, 1-CH_2), 2.84 (s, 4H, 2xCH_2-Osu), 2.13 (s, 3H, acetyl-CH_3), 2.08 (s, 3H, acetyl-CH_3), 2.043 (s, 3H, acetyl-CH_3), 2.037 (s, 3H, acetyl-CH_3)

^{13}C NMR ($CDCl_3$): δ = 170.5, 170.0, 169.8, 169.6, 168.7, 165.6, 69.5, 68.6, 67.9, 67.2, 67.0, 60.9, 30.4, 25.5, 20.6

Triisopropylsilyl-((S)-2-azido-5-((peracetyl-1-carboxymethyl galactopyranoside)-amino)pentanoyl-glycyl)-propargylamine (5b)

4b (280 mg, 0.55 mmol) was Boc-deprotected in 1:1 TFA/ CH_2Cl_2 for two hours. After concentration *in vacuo* the oil was redissolved in CH_2Cl_2 (20 ml) and DiPEA (0.26 ml, 1.5 mmol) and **6** (195 mg, 0.5 mmol) were added. The reaction mixture was allowed to stir for 2 hours after which it was concentrated *in vacuo* and redissolved in EtOAc and subsequently washed with 1 M $KHSO_4$, 5% $NaHCO_3$ and saturated NaCl. The organic layer was dried with Na_2SO_4 and after evaporation crude **5b** was obtained.

Column chromatography using 4% MeOH in CH_2Cl_2 afforded **5b** as a colourless oil. (327 mg, 0.42 mmol, 84%)

^{1}H NMR ($CDCl_3$): δ = 7.37 (t, 1H, NH, *J*=5.1 Hz), 6.65 (m, 2x1H, NH), 5.41 (bs, 1H 4-H sugar), 5.28 (m, 1H, 2-sugar), 5.18 (m, 1H, 3-sugar), 4.70 (m, 1H, 1-H sugar), 4.3-4.1 (m, 5H, sugar 5-H, sugar-6-CH_2, propargyl-CH_2), 4.06 (m, 1H, Orn-α-CH), 3.96 (m, 2H, glycine-CH_2), 3.30 (m, 2H, Orn-δ-CH_2), 2.69-2.42 (m, 2H, 1-CH_2 sugar), 2.13 (s, 3H, acetyl-CH_3), 2.08 (s, 3H, acetyl-CH_3), 2.06 (s, 3H, acetyl-CH_3), 2.05 (s, 3H, acetyl-CH_3), 1.88 (m, 2H, Orn-β-CH_2), 1.66 (m, 2H, Orn-γ-CH_2), 1.06 (s, 21H, TIPS)

^{13}C NMR ($CDCl_3$): δ = 170.6, 170.2, 170.0, 169.9, 169.7, 169.6, 167.8, 102.2, 84.9, 69.2, 69.0, 67.9, 67.8, 67.0, 62.9, 61.2, 42.7, 38.5, 34.3, 30.4, 29.1, 25.3, 20.7, 18.5, 11.0

((S)-2-azido-5-((peracetyl-1-carboxymethyl galactopyranoside)-amino)pentanoyl-glycyl)-propargylamine (5a)

5b (160 mg, 0.2 mmol) was dissolved in anhydrous THF (25 ml). Phenol (96 mg, 1.0 mmol) and TBAF.$3H_2O$ (323 mg, 1.0 mmol) were added and the reaction mixture was stirred for 2h. The reaction mixture was diluted with EtOAc and washed with H_2O. After drying the organic layer with Na_2SO_4 and concentration *in vacuo*, the compound was purified through a small plug of silica using 4% MeOH in CH_2Cl_2 to yield **5a** as a white foam (113 mg, 0.18 mmol, 90%)

^{1}H NMR ($CDCl_3$): δ =7.35 (bt, 1H, NH, *J*=~5 Hz), 6.87 (bt, 1H, NH, *J*=~5 Hz), 6.62 (bt, 1H, NH, *J*=~5 Hz), 5.42 (bs, 1H, 4-H sugar), 5.27 (m, 1H, 2-H sugar), 5.19 (m, 1H 3-H sugar), 4.70 (m, 1H, 1-H sugar), 4.3-4.0 (m, 6H, sugar 5-H, sugar-6-CH_2, propargyl-CH_2, Orn-α-CH), 3.97 (d, 2H, glycine-CH_2, *J*=5.1 Hz), 3.31 (m, 2H, Orn-δ-CH_2), 2.7-2.4 (m, 2H, 1-CH_2 sugar), 2.29 (s, 1H, alkyne-CH), 2.13 (s, 3H, acetyl-CH_3), 2.08 (s, 3H, acetyl-CH_3), 2.06 (s,2x3H, acetyl-CH_3), 1.91 (m, 2H, Orn-β-CH_2), 1.66 (m, 2H, Orn-γ-CH_2)

^{13}C NMR ($CDCl_3$): δ = 170.7, 170.3, 170.01, 169.96, 169.8, 169.7, 168.2, 79.2, 71.8, 69.3, 69.0, 67.9, 67.8, 67.0, 62.8, 61.2, 42.8, 38.5, 34.3, 29.2, 29.1, 25.1, 20.7, 20.6,

Conditions for copper click mediated oligomerization

Azido/alkyne-monomer **5a** (100 mg, 160 µmol) was dissolved in a DiPEA/DMF solution (400 µl, 300 mM) in a 1.5 ml plastic reaction tube. A freshly prepared aqueous solution of TCEP (200 mM, 200 µl), was added to the monomer and shaken for 2 hours after which nitrogen evolution had ceased. Polymerization was then initiated by adding an aqueous copper sulfate solution (240 mM, 100 µl) followed by a freshly prepared aqueous sodium ascorbate solution (720 mM, 100 µl), added while vortexing. After 2 h the reaction mixture was diluted with acetonitrile/ water (1:2 v/v, 0.1% TFA added) and preparative HPLC was performed to separate oligomers by size. After lyophilisation the oligomers **7a**, **8a** and **9a** were obtained as white fluffy solids.

MALDI-TOF:

Trimer 7a (6 mg), calculated *M* for $C_{78}H_{110}N_{16}O_{36}$ 1846.7, found $[M+H]^+$ 1848.4, $[M+Na]^+$ 1870.5, $[M+K]^+$ 1886.7, [*M*-acetyl+Na]$^+$ 1828.3.

Tetramer 8a (5.5 mg), calculated *M* for $C_{104}H_{146}N_{22}O_{48}$ 2471.0, found $[M+Na]^+$ 2494.4, $[M+K]^+$ 2510.4 [*M*-acetyl+Na]$^+$ 2452.4.

Pentamer 9a (4 mg), calculated *M* for $C_{130}H_{182}N_{28}O_{60}$ 3095.2, found $[M+Na]^+$ 3118.0, $[M+K]^+$ 3133.9, [*M*-acetyl+Na]$^+$ 3075.9.

Higher oligomers (>7mer, 30 mg), found [8mer+Na]$^+$ 4990.8, [9mer+Na]$^+$ 5615.8, [10mer+Na]$^+$ 6239.2, higher oligomers did not ionize well enough to be distinguishable from the baseline noise.

Synthesis of reference compound OGG-Gal (1) and the C-terminal carboxamide analog 11

Fmoc-Orn(Boc)-OSu (5.0 g, 9.1 mmol) (this N-hydroxysuccinimide ester of the commercially available protected amino acid was synthesized using the methodology described for compound **6** with 88% yield) was dissolved in THF (150 ml). To this solution, a solution of H-Gly-Gly-OH (1.3 g, 10 mmol) and $NaHCO_3$ (1.68 g, 20 mmol) in water (30 ml) were added. The reaction mixture was stirred for 16 hours, after which the THF was mostly removed *in vacuo* and the mixture was diluted with EtOAc. Washing with 1M $KHSO_4$ and drying gave the crude Fmoc-Orn(Boc)-Gly-Gly-OH, which was further purified by crystallization from CH_2Cl_2/hexanes to give a white solid (4.6 gram, 8.1 mmol) which was used directly for the next reaction.

Removal of the Boc-group from the ornithine residue (3.0 gram, 5.3 mmol) was performed with 1:1 TFA/CH_2Cl_2 for 2 hours after which the reaction mixture was concentrated *in vacuo* and coevaporated with toluene to remove residual TFA. The residue was suspended in THF/H_2O (1:1 v/v, 100 ml) and the pH was adjusted to 8.5 with DiPEA.

Carbohydrate derivative **6** (2.3 g, 4.8 mmol), dissolved in THF was added and the pH was kept at 8 for 3 hours. The now homogeneous reaction mixture was acidified with 1M $KHSO_4$ and extracted with EtOAc. The combined organic layers were dried on Na_2SO_4, concentrated *in vacuo*, and the residue was recrystallized from CH_2Cl_2 (with a few drops of MeOH) by addition of Et_2O. Fmoc-Orn(carboxymethyl-Gal)-Gly-Gly-OH was obtained as a white powder (2.8 gram, 3.3 mmol, 61% over the combined three steps). ^{1}H-NMR was comparable to previously published characterization.[13]
Solid phase chemistry was performed as previously described on a preloaded Fmoc-Gly-wang resin (to obtain compound **1**) or Fmoc-Rink resin (to obtain compound **11**) to yield the tetramer, [13] which after deprotection (see below) was purified by preparative HPLC, using 0.1% TFA in water as buffer A to give retention and subsequently lyophilized to yield compound **1** and **11** as white fluffy solids.

CuAAC coupling of ethyl azidoacetate
Tetramer **8a** (6.5 mg, 2.5 µmol) and ethyl azidoacetate (1 mg, 7.5 µmol, 3 equiv.) were dissolved in THF (400 µl). To this solution copper(II)sulfate pentahydrate (0.2 mg, 0.8 µmol, 0.33 equiv. in 100 µl water) was added followed by sodium ascorbate (1 mg, 5 µmol 2 equiv. in 100 µl water). The reaction mixture was stirred for 6 hours, diluted with EtOAc, and washed with $Na_2S_2O_3$ solution. The resulting crude glycopeptide was deacetylated (see below) and purified with preparative HPLC using 0.1% TFA in water as buffer A.

Typical Procedure for deacetylation
Acetylated glycopeptide oligomer was dissolved in dry MeOH (500 µl/ 5 mg oligomer) and a catalytic amount of fresly prepared sodium methoxide was added. After 3 hours of reaction time water (500 µl/ 5 mg oligomer) was added to solubilize the formed precipitate and incubated for another 30 minutes. Dowex marathon C ion exchange resin (acid form and washed beforehand with methanol) was added to neutralize the reaction mixture. The mixture was filtered and lyophilized to afford the deacetylated oligomers in 2.5-4 mg amounts and the polymer in ~20 mg. Residual salts could be removed by reversed-phase solid phase extraction, washing with water and eluting the compound with gradual increments of MeCN up to 10% v/v MeCN in water.

ESI-MS after purification:
Deprotected triazole based tetramer (8b): calculated *M* for $C_{72}H_{114}N_{22}O_{32}$ 1798.80, found $[M+2H]^{2+}$ 900.75
Deprotected triazole based tetramer-acid (10): Calculated *M* for $C_{74}H_{117}N_{25}O_{34}$ 1899.82, found $[M+2H]^{2+}$ 950.65
Deprotected OGG-Gal (1): calculated *M* for $C_{70}H_{117}N_{17}O_{38}$ 1803.8, found $[M+2H]^{2+}$ 902.70
Deprotected carboxamide OGG-Gal (11): calculated *M* for $C_{68}H_{115}N_{17}O_{36}$ 1745.77, found $[M+2H]^{2+}$ 873.70

CD spectroscopy
CD spectra were recorded on a JASCO J-815 spectrometer using a 1 cm cuvet in a Peltier type cell holder operating at 4 °C. A 260-190 nm window was scanned at 50 nm/min with a data pitch of 0.2 nm. 10 accumulations of these measurements were recorded for each spectrum. The AFGP concentration used was 50 µM in milli-Q water and water blanks were subtracted.

Thermal Hysteresis (TH) assay
Nanoliter osmometry was performed using a Clifton nanoliter osmometer (Clifton Technical Physics, Hartford, NY).[35] All measurements were performed in a phosphate buffered saline (PBS) solution. Ice crystal morphology was observed through a Leitz compound microscope equipped with an Olympus 20× (infinity-corrected) objective, a Leitz Periplan 32× photo eyepiece, and a Hitachi KPM2U CCD camera connected to a Toshiba MV13K1 TV/VCR system. Still images were captured directly using a Nikon CoolPix digital camera.

Ice Recrystallization Inhibition (IRI) assay
Sample analysis for IRI activity was performed using the "splat cooling" method as previously described[37] In this method, the analyte was dissolved in a phosphate buffered saline (PBS) solution and a 10 µL droplet of this solution was dropped from a micropipette through a two meter high plastic tube (10 cm in diameter) onto a block of polished aluminum precooled to approximately -80 °C. The droplet froze instantly on the polished aluminum block and was approximately 1 cm in diameter and 20 µm thick. This wafer was then carefully removed from the surface of the block and transferred to a cryostage held at -6.4 °C for annealing. After a period of 30 min, the wafer was photographed between crossed polarizing filters using a digital camera (Nikon CoolPix 5000) fitted to the microscope. A total of three images were taken from each wafer. During flash freezing, ice crystals spontaneously nucleated from the supercooled solution. These initial crystals were relatively homogeneous in size and quite small. During the annealing cycle, recrystallization occurred, resulting in a dramatic increase in ice crystal size. A quantitative measure of the difference in recrystallization inhibition of two compounds is the difference in the ice crystal size distribution. Image analysis of the ice wafers was performed using a novel domain recognition software (DRS) program.[36] This processing employed the Microsoft Windows Graphical User Interface to allow a user to visually demarcate and store the vertices of ice domains in a digital micrograph. The data was then used to calculate the domain areas. All data was plotted and analyzed using Microsoft Excel. The mean grain (or ice crystal) size (MGS) of the sample was compared to the MGS of the control PBS solution for that same day of testing. IRI activity is reported as the percentage of the MGS (% MGS) relative to the PBS control, and the % MGS for each sample was plotted along with its standard error of the mean. Small percentages represent a small MGS, which is indicative of more potent IRI activity.

Acknowledgements

We gratefully acknowledge Britta Ramakers (Radboud University Nijmegen, The Netherlands) for assistance with CD measurements, carried out in the Bio-organic chemistry group of prof. J.C.M. van Hest. We also gratefully acknowledge Dr. Johan Kemmink (Medicinal Chemistry, Universiteit Utrecht) for his assistance with NMR measurements. C.J.C. acknowledges Canadian Blood Services (CBS) for a Graduate Fellowship Award.

Keywords: antifreeze ·glycopeptide · click chemistry · polymerization· CuAAC

[1] A. L. DeVries, D. E. Wohlschlag, *Science* **1969**, *163*, 1073–1075.
[2] S. Venketesh, C. Dayananda, *Crit. Rev. Biotechnol.* **2008**, *28*, 57–82.
[3] A. L. DeVries, S. K. Komatsu, R. E. Feeney, *J. Biol. Chem.* **1970**, *245*, 2901–2908.
[4] A. L. DeVries, J. Vandenheede, R. E. Feeney, *J. Biol. Chem.* **1971**, *246*, 305-308
[5] J. A. Raymond, A. L. DeVries, *Proc. Natl. Acad. Sci. U. S. A.* **1977**, *74*, 2589–2593
[6] C. Knight, J. Duman, *Cryobiology* **1986**, *262*, 256–262.
[7] C. J. Capicciotti, M. Doshi, R. N. Ben, in *Recent Developments in the Study of Recrystallization* (Ed.: P. Wilson), **2013**, ISBN: 978-953-51-0962-4, pp. 177–224.
[8] M. Leclère, B. K. Kwok, L. K. Wu, D. S. Allan, R. N. Ben, *Bioconjug. Chem.* **2011**, *22*, 1804–1810.
[9] R. Y. Tam, C. N. Rowley, I. Petrov, T. Zhang, N. A Afagh, T. K. Woo, R. N. Ben, *J. Am. Chem. Soc.* **2009**, *131*, 15745–15753.
[10] B. L. Wilkinson, R. S. Stone, C. J. Capicciotti, M. Thaysen-Andersen, J. M. Matthews, N. H. Packer, R. N. Ben, R. J. Payne, *Angew. Chem. Int. Ed. Engl.* **2012**, *51*, 3606–3610.
[11] Y. Tachibana, G. L. Fletcher, N. Fujitani, S. Tsuda, K. Monde, S-I. Nishimura, *Angew. Chem. Int. Ed. Engl.* **2004**, *43*, 856–862.
[12] R. Izumi, T. Matsushita, N. Fujitani, K. Naruchi, H. Shimizu, S. Tsuda, H. Hinou, S.-I. Nishimura, *Chem. Eur. J.* **2013**, *19*, 3913–3920.
[13] R. Ben, A. Eniade, L. Hauer, *Org. Lett.* **1999**, 1759–1762.
[14] A. K. Balcerzak, S. S. Ferreira, J. F. Trant, R. N. Ben, *Bioorg. Med. Chem. Lett.* **2012**, *22*, 1719–1721.

[15] P. Czechura, R. Y. Tam, E. Dimitrijevic, A. V Murphy, R. N. Ben, *J. Am. Chem. Soc.* **2008**, *130*, 2928–2929.
[16] T. Tsuda, S. Nishimura, *Chem. Commun.* **1996**, *2*, 2779-2780.
[17] T. Pirali, F. Pagliai, C. Mercurio, R. Boggio, P. L. Canonico, G. Sorba, G. C. Tron, A. a Genazzani, *J. Comb. Chem.* **2008**, *10*, 624–627.
[18] B. H. M. Kuijpers, S. Groothuys, A. C. Soede, P. Laverman, O. C. Boerman, F. L. van Delft, F. P. J. T. Rutjes, *Bioconjug. Chem.* **2007**, *18*, 1847–1854.
[19] M. Van Dijk, K. Mustafa, A. C. Dechesne, C. F. Van Nostrum, W. E. Hennink, D. T. S. Rijkers, R. M. J. Liskamp, *Biomacromolecules* **2007**, *8*, 327–330.
[20] M. van Dijk, M. L. Nollet, P. Weijers, A. C. Dechesne, C. F. van Nostrum, W. E. Hennink, D. T. S. Rijkers, R. M. J. Liskamp, *Biomacromolecules* **2008**, *9*, 2834–2843.
[21] M. van Dijk, C. F. van Nostrum, W. E. Hennink, D. T. S. Rijkers, R. M. J. Liskamp, *Biomacromolecules* **2010**, *11*, 1608–1614.
[22] R. C. Elgersma, M. van Dijk, A. C. Dechesne, C. F. van Nostrum, W. E. Hennink, D. T. S. Rijkers, R. M. J. Liskamp, *Org. Biomol. Chem.* **2009**, *7*, 4517–4525.
[23] M. Hachisu, H. Hinou, M. Takamichi, S. Tsuda, S. Koshida, S-I. Nishimura, *Chem. Commun.* **2009**, 1641–1643.
[24] C. J. Capicciotti, J. F. Trant, M. Leclère, R. N. Ben, *Bioconjug. Chem.* **2011**, *22*, 605–616.
[25] A. Norgren, C. Budke, Z. Majer, C. Heggemann, T. Koop, N. Sewald, *Synthesis.* **2009**, *2009*, 488–494.
[26] N. Miller, G. M. Williams, M. a Brimble, *Org. Lett.* **2009**, *11*, 2409–2412.
[27] M. Meldal, C. W. Tornøe, *Chem. Rev.* **2008**, *108*, 2952–3015.
[28] V. R. Bouvet, G. R. Lorello, R. N. Ben, *Biomacromolecules* **2006**, *7*, 565–571.
[29] E. D. Goddard-Borger, R. V Stick, *Org. Lett.* **2007**, *9*, 3797–3800.
[30] C. Ruecker, *Chem. Rev.* **1995**, *95*, 1009–1064.
[31] I. E. Valverde, A. F. Delmas, V. Aucagne, *Tetrahedron* **2009**, *65*, 7597–7602.
[32] C. M. Hayward, D. Yohannes, S. J. Danishefsky *J. Am. Chem. Soc.* **1993**, *115*, 9345–9346
[33] A. B. Smith III, S. S-Y. Chen, F. C. Nelson J. M. Reichert, B. A. Salvatore *J. Am. Chem. Soc.* **1997**, *119*, 10935–10946.
[34] E. F. V. Scriven, K. Turnbull, *Chem. Rev.* **1988**, *88, 297-368*.
[35] A. Chakrabartty, C. L. Hew, *Eur. J. Biochem.* **1991**, *202*, 1057–1063.
[36] J. Jackman, M. Noestheden, D. Moffat, J. P. Pezacki, S. Findlay, R. N. Ben, *Biochem. Biophys. Res. Commun.* **2007**, *354*, 340–344.
[37] C. A. Knight, J. Hallett, A. L. DeVries, *Cryobiology* **1988**, *25*, 55–60.
[38] L. Corcilius, G. Santhakumar, R. S. Stone, C. J. Capicciotti, S. Joseph, J. M. Matthews, R. N. Ben, R. J. Payne, *Bioorg. Med. Chem.* **2013**, *21*, 3569–3581.
[39] A. Giannis, K. Sandhoff, *Tetrahedron Lett.* **1985**, *26*, 1479–1482.

Received: ((will be filled in by the editorial staff))
Published online: ((will be filled in by the editorial staff))

3.4.3 Results and Discussion of Antifreeze Activity of Triazole-Containing OGG-Gal Derivatives

Glycopeptide derivatives **8b, 10** and **11** were assessed for TH activity using nanoliter osmometry[33] and IRI activity using a "splat-cooling" assay.[34,35] None of these derivatives exhibited TH activity or dynamic ice shaping capabilities, indicating these compounds were not interacting with the ice lattice (Figure 6A-C). The IRI activity of glycopeptides **8b, 10** and **11** at a concentration of 5.5 mM in PBS is presented in figure 7. At this concentration, these derivatives exhibited moderate activity that was ~60 % MGS relative to the PBS positive control. All of these derivatives were significantly less active than OGG-Gal (**1**) and native AFGP-8, both of which are highly active at a significantly lower concentration of 5.5 μM (figure 7).[22]

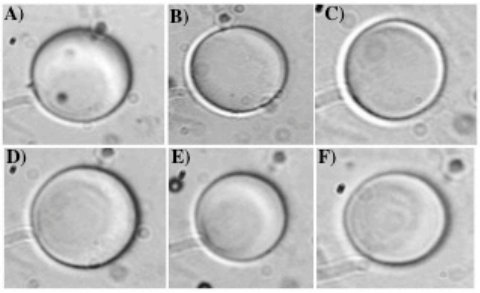

Figure 6 Ice crystal habit in the presence of: A) Triazole tetramer **8b**; B) **10** C) **11**; D) Triazole trimer (n=2); E) Triazole pentamer (n=4); F) Triazole polymer (n = 6-17). All compounds were assayed in water at 10 mg/mL

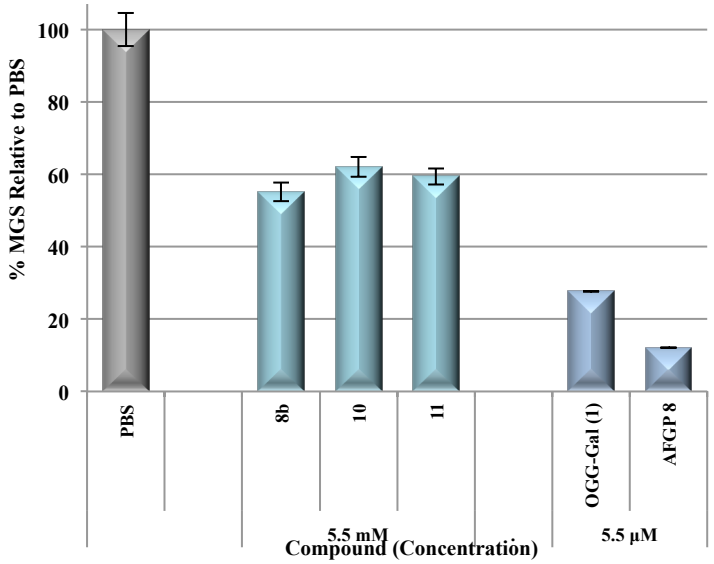

Figure 7 Ice recrystallization inhibition (IRI) activity of oligomers **8b, 10** and **11** at 5.5 mM, and OGG-Gal (**1**) and AFGP-8 at 5.5 μM in PBS. The % MGS (mean grain size) relative to a PBS positive control is shown for all compounds.

The IRI results from this study highlight additional structural features that are important for the potent activity of **1**. Removal of the C-terminal glycine residue and the presence of a terminal primary amide on this end of the glycopeptide were detrimental for activity as **11** was significantly less active than **1** at a much higher concentration. Incorporation of triazole-linkages within the tripeptide repeat also diminished activity as **10**-**11** were also IRI inactive. This supports the hypothesis that incorporating triazole rings into AFGP derivatives is detrimental for activity, which has been observed by our laboratory and others.[25,52,53] Analysis of the solution structure of **8b**, **10** and **11** using CD spectroscopy did not suggest that these glycopeptides are adopting a different structure than OGG-Gal (**1**) in solution (figure 8, in article). Consequently, it is currently not known why these modifications drastically reduce the potent IRI activity of OGG-Gal. However it is evident both the glycine units within the polypeptide backbone and the terminal glycine with C-terminal carboxylic acid are crucial for the ability of **1** to function as a potent IRI. This is in addition to the other structural features of **1** that are important for its exhibited activity, the presence of a highly hydrated monosaccharide moiety, as well as the amide bond and six atoms in the side chain connecting the carbohydrate residue to the polypeptide backbone (summarized in figure 3.6).

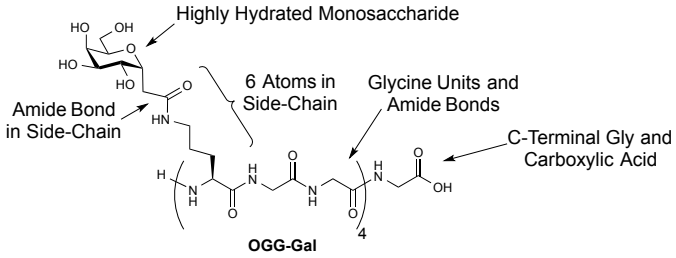

Figure 3.6 Structural features crucial for the potent activity of OGG-Gal.

3.5 Overall Summary and Conclusions for the IRI Activity of Peptide and Glycopeptide AFGP Analogues

A variety of synthetic AFGPs (synAFGPs) and AFGP analogues were prepared and assessed for both types of antifreeze specific activities, TH and IRI activity. The results from the synAFGPs consisting of an $(Ala\text{-}Thr\text{-}Ala)_n$ tripeptide repeat highlight the importance of glycopeptide size/length for both TH and IRI activity (section 3.2).[31] The results from this study have also indicated that minor variations in the amino acid sequence of AFGPs can have detrimental effects for both TH and IRI as native AFGP-8 with four repeats of $(Ala\text{-}Ala\text{-}Thr)_n$ exhibits both activities, whereas synAFGPs with four repeats of $(Ala\text{-}Thr\text{-}Ala)_n$ were inactive for both activities at equimolar concentration. While the synAFGPs were found to adopt a PPII helical structure in solution, this secondary structure is not a prerequisite for IRI or TH as HyP

AFGP derivatives that also adopt this structure failed to exhibit either activity (section 3.3).[49] While the TH activity of AFGPs has been extensively studied in the literature, these studies are the first reports that have examined the structural features that are important for the IRI activity of these biological antifreezes. Collectively, they indicate that even minor structure variations can have drastic effects on the potent IRI activity of AFGPs resulting in IRI inactive (glyco)peptides.

In addition to derivatives of AFGPs, we also examined the importance of the polypeptide backbone of one of our laboratory's most potently IRI active analogue, OGG-Gal. These derivatives of OGG-Gal contained triazole-linkages in place of peptide bonds in the tripeptide repeat. All of these derivatives were significantly less active than OGG-Gal at a much higher concentration, indicating that a triazole ring is not a suitable isostere of amide bonds within the backbone of this glycopeptide for IRI activity. This is not surprising as previous studies have demonstrated that modifications to other moieties of OGG-Gal, such as the carbohydrate residue or the side-chain connecting the carbohydrate residue to the peptide backbone, are also detrimental for the potent activity of this compound.[22,24,25]

The majority of the (glyco)peptide AFGP analogues examined were found to be inactive for both TH and IRI activity (sections 3.3 and 3.4). However, two peptides did emerge as novel compounds that possessed the property of interest to our laboratory, "custom-tailored" antifreeze activity (potent IRI without TH activity). These were HyP containing unglycosylated dodecapeptides with the tripeptide repeat $(Ala\text{-}HyP\text{-}Ala)_4$ (section 3.3).[49] These derivatives were potently IRI active at 7 mM, and are thus novel lead peptide structures for the development of ice recrystallization inhibitors for use cryopreservation applications. While further studies are required to determine the mechanism by which these peptides exhibit IRI, results from this work have demonstrated that glycosylation of the hydroxyproline residue with α-GalNAc or β-Gal-(1,3)-α-GalNAc is detrimental and abolishes activity. This result has identified structural features for IRI activity that were previously unknown and have demonstrated that small unglycosylated peptides may also inhibit ice recrystallization. These compounds are attractive novel candidates for ice recrystallization inhibitors owing to their ease of synthesis compared to AFGPs or glycopeptides.

3.6 References

1. DeVries, A.L. *Science*. **1971**, *172*, 1152-1155.
2. Komatsu, S.K.; DeVries, A.L.; Feeney, R.E. *J. Biol. Chem*. **1970**, *245*, 2909-2913.
3. DeVries, A.L.; Vandenheede, J.; Feeney, R.E. *J. Biol. Chem*. **1971**, *246*, 305-308.
4. Feeney, R.E.; Burcham, T.S.; Yeh, Y. *Annu. Rev. Biophys. Biophys. Chem*. **1986**, *15*, 59-78.
5. Harding, M.M.; Anderberg, P.I.; Haymet, A.D.J. *Eur. J. Biochem*. **2003**, *270*, 1381-1392.

6. Bouvet, V.; Ben, R.N. *Cell Biochem. Biophys.* **2003**, *39*, 133-144.

7. Garner, J.; Harding, M.M. *ChemBioChem.* **2010**, *11*, 2489-2498.

8. Peltier, R.; Brimble, M.A.; Wojnar, J.M.; Williams, D.E.; Evans, C.W.; DeVries, A.L. *Chem. Sci.* **2010**, *1*, 538-551.

9. Gibson, M.I. *Polym. Chem.* **2010**, *1*, 1141-1152.

10. Franks, F.; Morris, E.R. *Biochim. Biophys. Acta.* **1978**, *540*, 346-356.

11. Bush, C.A.; Feeney, R.E.; Osuga, D.T.; Ralapati, S.; Yeh, Y.I.N. *Int. J. Pept. Protein Res.* **1981**, *17*, 125-129.

12. Ahmed, A.I.; Feeney, R.E.; Osuga, D.T.; Yeh, Y. *J. Biol. Chem.* **1975**, *250*, 3344-3347.

13. Berman, E.; Allerhand, A.; DeVries, A.L. *J. Biol. Chem.* **1980**, *255*, 4407-4410.

14. Lane, A.N.; Hays, L.M.; Crowe, L.M.; Crowe, J.H.; Feeney, R.E. *Protein Sci.* **1998**, *7*, 1555-1563.

15. Tsvetkova, N.M.; Phillips, B.L.; Krishnan, V.V.; Feeney, R.E.; Fink, W.H.; Crowe, J.H.; Risbud, S.H.; Tablin, F.; Yeh, Y. *Biophys. J.* **2002**, *82*, 464-473.

16. Bush, C.A.; Feeney, R.E. *Int. J. Pept. Protein Res.* **1986**, *28*, 386-397.

17. Bush, C.A.; Ralapati, S.; Matson, G.M.; Yamasaki, R.B.; Osuga, D.T.; Yeh, Y.; Feeney, R.E. *Arch. Biochem. Biophys.* **1984**, *232*, 624-631.

18. Rao, B.N.N.; Bush, C.A. *Biopolymers.* **1987**, *26*, 1227-1244.

19. Tachibana, Y.; Fletcher, G.L.; Fujitani, N.; Tsuda, S.; Monde, K.; Nishimura, S.-I. *Angew. Chem. Int. Ed.* **2004**, *43*, 856-862.

20. Heggemann, C.; Budke, C.; Schomburg, B.; Majer, Z.; Wißbrock, M.; Koop, T.; Sewald, N. *Amino Acids.* **2010**, *38*, 213-222.

21. Liu, S.; Ben, R.N. *Org. Lett.* **2005**, *7*, 2385-2388.

22. Czechura, P.; Tam, R.Y.; Dimitrijevic, E.; Murphy, A.V.; Ben, R.N. *J. Am. Chem. Soc.* **2008**, *130*, 2928-2929.

23. Leclère, M.; Kwok, B.K.; Wu, L.K.; Allan, D.S.; Ben, R.N. *Bioconjugate Chem.* **2011**, *22*, 1804-1810.

24. Tam, R.Y.; Rowley, C.N.; Petrov, I.; Zhang, T.; Afagh, N.A.; Woo, T.K.; Ben, R.N. *J. Am. Chem. Soc.* **2009**, *131*, 15745-15753.

25. Capicciotti, C.J.; Trant, J.F.; Leclère, M.; Ben, R.N. *Bioconjugate Chem.* **2011**, *22*, 605-616.

26. Pegg, D.E. *Cryobiology.* **1992**, *29*, 774.

27. Rubinsky, B.; DeVries, A.L. *Cryobiology.* **1989**, *26*, 580.

28. Mugano, J.A.; Wang, T.; Layne, J.R., Jr.,; DeVries, A.L.; Lee, R.E. *Cryobiology.* **1995**, 556-557.

29. Larese, A.; Acker, J.; Muldrew, K.; Yang, H.Y.; McGann, L. *Cryo-letters.* **1996**, *17*, 172-182.

30. Wang, J.H.; Bian, H.W.; Huang, C.N.; Ge, J.G. *Acta Biol. Exp.* **1999**, *32*, 271-276.

31. Wilkinson, B.L.; Stone, R.S.; Capicciotti, C.J.; Thaysen-Andersen, M.; Matthews, J.M.; Packer, N.H.; Ben, R.N.; Payne, R.J. *Angew. Chem. Int. Ed.* **2012**, *51*, 3606-3610.

32. Hew, C.L.; Slaughter, D.; Fletcher, G.L.; Joshi, S.B. *Can. J. Zool.* **1981**, *59*, 2186-2192.

33. Chakrabartty, A.; Hew, C.L. *Eur. J. Biochem.* **1991**, *202*, 1057-1063.

34. Knight, C.A.; Hallett, J.; DeVries, A.L. *Cryobiology*. **1988**, *25*, 55-60.

35. Jackman, J.; Noestheden, M.; Moffat, D.; Pezacki, J.P.; Findlay, S.; Ben, R.N. *Biochem. Biophys. Res. Commun*. **2007**, *354*, 340-344.

36. Tachibana, Y.; Matsubara, N.; Nakajima, F.; Tsuda, T.; Tsuda, S.; Monde, K.; Nishimura, S.-I. *Tetrahedron*. **2002**, *58*, 10213-10224.

37. Izumi, R.; Matsushita, T.; Fujitani, N.; Naruchi, K.; Shimizu, H.; Tsuda, S.; Hinou, H.; Nishimura, S.-I. *Chem. Eur. J*. **2013**, *19*, 3913-3920.

38. Mulvihill, D.M.; Geoghegan, K.F.; Yeh, Y.; DeRemer, K.; Osuga, D.T.; Ward, F.C.; Feeney, R.E. *J. Biol. Chem*. **1980**, *255*, 659-662.

39. Osuga, D.T.; Ward, F.C.; Yeh, Y.; Feeney, R.E. *J. Biol. Chem*. **1978**, *253*, 6669-72.

40. Knight, C.A.; Driggers, E.; DeVries, A.L. *Biophys. J*. **1993**, *64*, 252-259.

41. Ma, K.; Kan, L.-s.; Wang, K. *Biochemistry*. **2001**, *40*, 3427-3438.

42. Rucker, A.L.; Creamer, T.P. *Protein Sci*. **2002**, *11*, 980-985.

43. Lane, A.N.; Hays, L.M.; Tsvetkova, N.; Feeney, R.E.; Crowe, L.M.; Crowe, J.H. *Biophys. J*. **2000**, *78*, 3195-3207.

44. Owens, N.W.; Stetefeld, J.; Lattová, E.; Schweizer, F. *J. Am. Chem. Soc*. **2010**, *132*, 5036-5042.

45. Bouvet, V.R.; Lorello, G.R.; Ben, R.N. *Biomacromolecules*. **2006**, *7*, 565-571.

46. Wilson, P.W. *Cryoletters*. **1993**, *14*, 31-36.

47. DeLuca, C.I.; Comley, R.; Davies, P.L. *Biophys. J*. **1998**, *74*, 1502-1508.

48. Gibson, M.I.; Barker, C.A.; Spain, S.G.; Albertin, L.; Cameron, N.R. *Biomacromolecules*. **2009**, *10*, 328-333.

49. Corcilius, L.; Santhakumar, G.; Stone, R.S.; Capicciotti, C.J.; Joseph, S.; Matthews, J.M.; Ben, R.N.; Payne, R.J. *Biorg. Med. Chem*. **2013**, *21*, 3569-3581.

50. Inada, T.; Lu, S.-S. *Cryst. Growth Des*. **2003**, *3*, 747-752.

51. Eniade, A.; Purushotham, M.; Ben, R.N.; Wang, J.B.; Horwath, K. *Cell Biochem. Biophys*. **2003**, *38*, 115-124.

52. Miller, N.; Williams, G.M.; Brimble, M.A. *Org. Lett*. **2009**, *11*, 2409-2412.

53. Norgren, A.S.; Budke, C.; Majer, Z.; Heggemann, C.; Koop, T.; Sewald, N. *Synthesis*. **2009**, *2009*, 488-494.

Chapter 4: Modulating Antifreeze Activity and the Effect Upon Post-Thaw Cell Viability

4.1 Introduction

Antifreeze proteins (AFPs) and glycoproteins (AFGPs) are found in many different organisms such as fish, insects and plants that inhabit subzero environments.[1-6] The ultimate purpose of these BAs is to protect these organisms against cryo-injury and death.[7] As described in detail in section 1.2.1, AFPs are structurally diverse and consist of four different subtypes, AFP I-IV.[8,9] AFGPs have a homogeneous structure consisting of a tripeptide repeat of $(Ala\text{-}Ala\text{-}Thr)_n$, in which the secondary hydroxyl group of threonine is glycosylated with the disaccharide β-D-galactosyl-(1-3)-α-*N*-acetyl-D-galactosamine (also refer to chapter 3).[1]

Regardless of the large variation in structure, all BAs exhibit two types of antifreeze activity. The first is thermal hysteresis (TH) activity, which is defined as the selective depression of the freezing point relative to the melting point, resulting in a thermal hysteretic gap.[10] The size of this gap is dependent upon the type of BA. AFGPs and types I, II and III AFPs exhibit moderate TH activity with TH gaps of 1-2 °C at millimolar concentrations.[10,11] Hyperactive AFPs typically have TH activities of 4-6 °C at sub-millimolar concentrations.[12-15] The mechanism of TH has been extensively studied and TH activity is attributed to an irreversible adsorption of the BA to the surface of an ice crystal. This irreversible binding results in a localized freezing point depression through the Kelvin effect (see section 1.2.3 for a more detailed discussion).[16-19] For AFPs, adsorption occurs with an ice-binding face (IBF) that is hydrophobic, relatively flat and has a discrete complementarity with the planes of ice to which it binds (see section 1.2.4 for a more detailed discussion).[8,20-23]

It is well established that biological antifreezes (BAs) are also excellent inhibitors of ice recrystallization. Ice recrystallization is a significant contributing factor to cell death during cryopreservation (discussed in greater detail in section 1.4 and chapter 8), and thus potent IRI activity is a highly desirable property for a cryoprotectant.[24-31] Biological antifreezes have been examined as potential additives for various cellular preservation methods including cryopreservation, vitrification and hypothermic storage. The results of these studies suggest that the mechanisms of cryoprotection with BAs are complex and that while BAs can be beneficial additives and can inhibit ice growth and recrystallization, they also can also be detrimental due to their ability to bind to ice and they can also exhibit cytotoxic effects and facilitate the nucleation of ice. The cryoprotective ability of BAs is dependent upon many variables including storage protocol, dose, type of BA, and the presence of a CPA such as DMSO.[32] This is discussed in

greater detail in section 1.4.4. While there are reports of the successful use of BAs as cryoprotectants, they often fail to protect mammalian cells from cryoinjury at temperatures outside of the TH gap. BAs change the habit of single ice crystals when they bind, resulting in very characteristic shapes (sections 1.2.2-1.2.3). At temperatures outside of the TH gap, such as those associated with the cryopreservation of biological materials (cells, tissues etc.), this change in ice crystal habit due to the irreversible binding of the BA to ice may actually facilitate cellular damage during cryopreservation.[33-38] Thus, the rational design of potent inhibitors of ice recrystallization that do not possess TH activity is of great importance.[39-43]

Despite the tremendous number of structure function studies elucidating the mechanism by which AFPs and AFGPs exhibit TH activity,[8,20,22,23,44-47] the mechanism by which these compounds inhibit ice recrystallization is considerably less understood. IRI activity is often overlooked and not assessed in reports of AFPs and AFGPs, which is unfortunate as BAs are the most potent ice recrystallization inhibitors identified to date. Furthermore, the cryoprotective ability of BAs is often associated with their TH activity and ice binding capabilities, and their potent IRI activity is often not discussed or correlated to cryopreservation results. The relationship between TH and IRI has been debated throughout the literature. It has been suggested that these activities were closely correlated and that IRI activity originated from the ability of BAs to interact and/or bind with the ice lattice.[48-50] Recently, the IBFs of AFPs were claimed to be responsible for both activities (TH and IRI).[51] However, in plant AFPs little or no correlation between TH and IRI activity has been observed since they typically exhibit very potent IRI activity, but a low degree of TH activity.[52,53] Furthermore, hyperactive AFPs exhibiting elevated TH activity often do not exhibit superior IRI activity.[51] In addition, our laboratory has demonstrated that *C*-linked AFGP analogues (chapter 3) and several carbohydrate-based small molecules (chapters 6 and 7) have "custom-tailored" antifreeze activity.[54-58] These molecules are potent inhibitors of ice recrystallization but do not exhibit TH activity and in many cases do not exhibit dynamic ice shaping which is characteristic of interactions with the ice lattice. While our *C*-AFGPs have very different structures than native AFGPs, these results validate the hypothesis that the two types of antifreeze activity can be decoupled.

As very few studies have emerged examining the relationship between TH and IRI activity, this chapter will focus on investigating the correlation between these activities using naturally occurring BAs. For this study, we chose several different classes of BAs including: AFGP-8 from *Gadus ogac* (rock cod);[59] Type I AFP from *Pseudopleuronectes americanus* (winter flounder);[60] Type III AFP from *Macrozoarces americanus* (ocean pout);[60] wild-type (WT) and mutant plant AFPs from *Lolium perenne* (*Lp*AFP).[52,53,61] The *Lp*AFP and a number of single point protein

mutants have previously been recombinantly expressed and well characterized for their structure, solution conformation and TH activity.[51-53,61-64] TH and IRI activity for these BAs were quantified to identify if whether a correlation exists between these two types of antifreeze activities within various classes of BAs to support the hypothesis that potent IRI activity can be decoupled from TH activity. Furthermore, we examine the ability of these BAs and mutants to cryopreserve human HepG2 cells and correlate post-thaw viabilities and recoveries to TH and IRI activity, as well as single ice crystal morphology and ice growth progressions. Thus, this chapter will describe the following:

1. The *Lp*AFPs (WT and mutants) were recombinantly expressed in *E. coli*. Consequently, prior to assessing the antifreeze specific activity or cryopreservation ability of these proteins, their solution structure was explored using CD spectroscopy. These results are discussed in section 4.2.
2. The TH and IRI activities were quantified using nanolitre osmometry and a "splat-cooling" assay, respectively. These results are provided in sections 4.3 and 4.4. A discussion on the correlation between these types of antifreeze-specific activities (TH and IRI) is provided in section 4.5. This section highlights how each activity can be modulated independently and is dependent upon the type of BA rather than ice binding capabilities.
3. The cryopreservation potential of these BAs with a HepG2 cell line was also explored. These results are discussed in section 4.6. While many of these BAs were detrimental to cell survival during cryopreservation, the ice crystal habit and growth progression in the presence of the BAs was found to have a significant impact on the cryopreservation ability of the BA or BA mutant. This is discussed in greater detail in section 4.7.

4.2 Conformational Analysis of *Lp*AFPs

The WT (*Lp*AFP) and five single point mutants were recombinantly expressed in *Escherichia coli* as described previously.[51-53,61-64] This was done in collaboration with Dr. Christopher Boddy in the Department of Chemistry at the University of Ottawa. Prior to assessing the IRI, TH and cryopreservation ability of these proteins, their solution conformation was confirmed by CD analysis of the purified recombinant *Lp*AFPs to evaluate the impact of each mutation on the overall protein fold. High resolution structural work has shown that *Lp*AFP consists of a beta-roll with a flat beta-sheet 'a'-side opposite the beta-sheet 'b'-side which contains a bulge due to a single amino acid insertion in three of the beta-sheet strands.[64] The structure of this protein is shown in figure 4.1A, which was prepared in collaboration with James Davey in Dr. Roberto

Chica's laboratory in the Department of Chemistry at the University of Ottawa. In this current study, two mutants had threonine residues on the 'a'-side (the IBF) mutated to larger tyrosine residues (T51Y and T67Y).[61] Similarly, an asparagine on the 'b'-side was mutated to tyrosine (N72Y) and two residues on either edge of the parallel beta-sheets that form the beta-roll were each mutated to tyrosine (T62Y and S55Y) (shown in figure 4.1A). The CD spectra of all five mutants showed nearly identical features to the spectra of the WT *Lp*AFP (Figure 4.1B). All CD spectra displayed a maximum at 200 nm and a minimum at 220 nm, consistent with a beta-sheet fold. The mean molar ellipticity of the CD spectra for the T67Y *Lp*AFP is decreased relative to the magnitude of the other *Lp*AFPs assessed. While this could suggest that this protein is partially denaturing, this seems unlikely since the TH data for the T67Y *Lp*AFP mutant (figure 4.2, section 4.3) is identical to that previously reported for this mutant.[61] Moreover, this mutant has previously been demonstrated to have an identical CD spectrum to the WT *Lp*AFP.[61] A plausible explanation for the decrease in magnitude for the CD spectrum of the T67Y *Lp*AFP mutant could be that the concentration assessed for these experiments was less than the other *Lp*AFPs. Regardless, these results are consistent with previous conformational analyses of *Lp*AFPs and suggest that the expressed proteins were properly folded.[61,63]

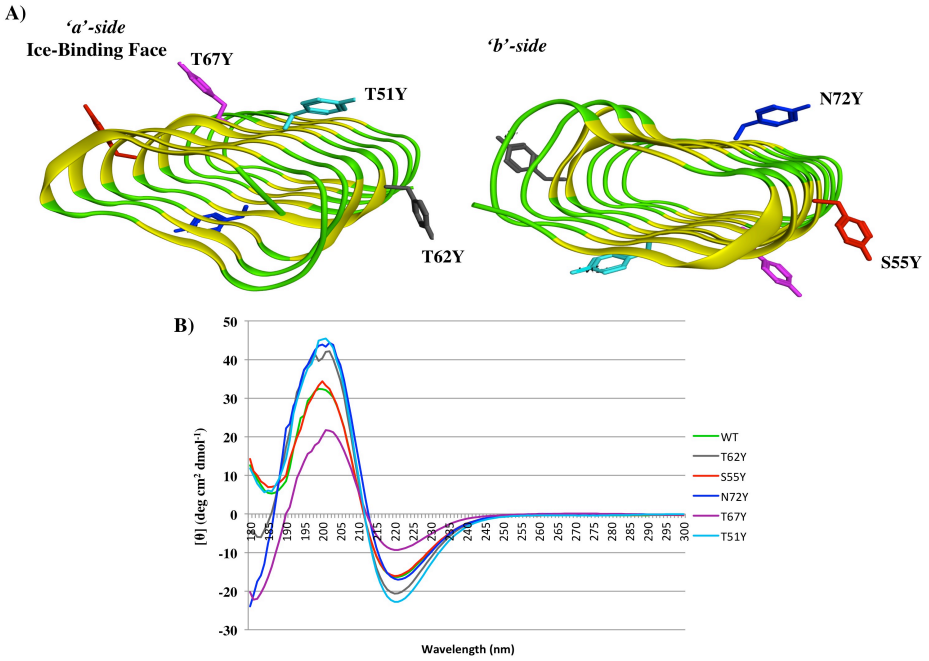

Figure 4.1 Structure and CD spectra of WT and mutant *Lp*AFPs. **(A)** Structure of *Lp*AFP showing the IBF 'a'-side and the 'b'-side. *Lp*AFP structure was obtained from monomer A of Protein Data Bank entry 3ult,[64] and was minimized to remove steric clashes from the tyrosine side chains using an Amber99 force field with a distance-dependent dielectric constant. The side chains of the steric mutations to tyrosine are illustrated by stick representations. **(B)** CD spectra of WT and mutant *Lp*AFPs. All spectra were acquired at 0 °C and a protein concentration of 24 μM in phosphate buffer. Baseline corrections were made against each sample using phosphate buffer as a blank.

4.3 Thermal Hysteresis (TH) Activity of the Biological Antifreezes

The TH activity of AFGP-8, Type I and Type III AFPs, and the *Lp*AFP and mutant *Lp*AFPs is presented in figure 4.2. At 5 mg/mL Type I AFP, Type III AFP and *Lp*AFP (WT) all exhibited significant TH gaps. The values of the TH gaps for the Type I AFP (~0.46°C) and Type III AFP (~0.36°C) were obtained from Fletcher *et al*. in reference 60.[60] The WT *Lp*AFP resulted in a gap that was similar to the Type III AFP at ~0.32°C. In contrast, AFGP-8 has a much smaller TH gap at 5 mg/mL (~0.08°C), consistent with the fact that the lowest molecular weight fraction of AFGPs are generally less active than many of the other BAs.[10,11]

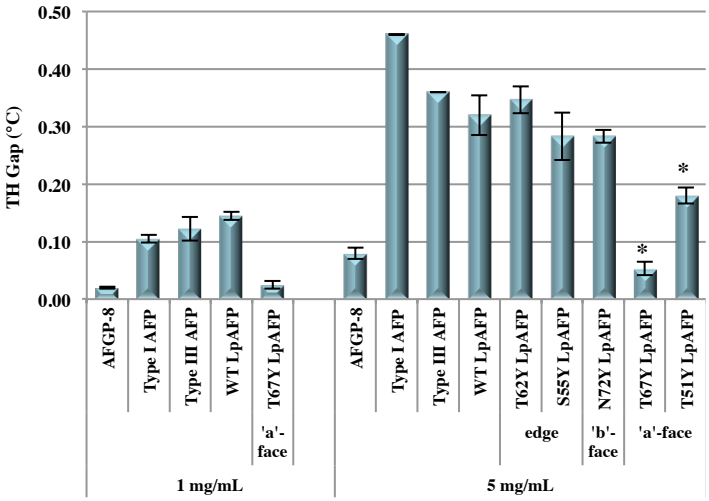

Figure 4.2 TH activity of the BAs assayed at 1 mg/mL in water or 5 mg/mL in PBS. TH values for Type I and Type III AFPs at 5 mg/mL were obtained from reference 60.[60] Asterisks indicate significant difference as determined by the unpaired student's T-test ($p < 0.05$) of the *Lp*AFP mutants relative to the WT *Lp*AFP control.

The TH activity of the WT and mutant *Lp*AFPs are consistent with that previously reported at 5 mg/mL.[61] However, the WT *Lp*AFP had a gap that was slightly lower than what has previously been reported in a Tris-HCl/NaCl/EDTA buffer.[61] In PBS the TH gap of WT *Lp*AFP at 5 mg/mL was 0.32°C (figure 4.2), whereas it was reported to be ~0.49 °C in the Tris buffer.[61] It has also been reported that in pure water the TH gap of *Lp*AFP is 0.1 °C and in 30% sucrose solution is 0.45 °C, both at 5 mg/mL.[53] TH activity is enhanced by low molecular weight solutes and salt solutions.[65-67] Thus, it appears that for the *Lp*AFP a PBS solution does not enhance TH activity to the same extent that a sucrose solution or a Tris-HCl/NaCl/EDTA buffer solution enhances TH activity. The mutants of *Lp*AFPs exhibited varying degrees of TH activity depending upon where the mutation occurred. Mutations to the "edge" of the protein (T62Y and S55Y) had no effect on the TH gap (figure 4.2). Similarly, mutations to the "b-face" (non-ice binding face) also had no effect upon the TH gap. However, mutations to the "a-face" (T67Y and T51Y) resulted in a

decrease in TH activity. This change in activity is due to the fact that the "a-face" of the protein is the IBF, and as previously described, mutations on the IBF can change the surface-surface complementarity between the AFP and ice, resulting in reduced activity.[61]

The TH gaps of AFGP-8, T67Y, WT *Lp*AFP, Type I AFP and Type III AFP were also determined at 1 mg/mL (figure 4.2), the same concentration at which the cryopreservation assays were performed (section 4.5). At 1 mg/mL, TH activity was markedly decreased for all proteins. Interestingly, at this concentration, the gaps for WT *Lp*AFP, Type I AFP and Type III AFP were all similar (0.1°C-0.15°C), whereas at 5 mg/mL the Type I AFP was significantly more TH active than all other proteins. The TH gaps of AFGP-8 and T67Y *Lp*AFP were virtually non-existent at 1 mg/mL and were less than 0.02°C. The TH activity for all proteins assayed at 1 mg/mL are consistent with values previously reported in the literature.[60,61,68]

4.4 Ice Recrystallization Inhibition Activity of the Biological Antifreezes

The IRI activity of the Type I and Type III AFPs have previously not been quantified, whereas AFGP-8 was previously assessed for IRI activity by our laboratory at 5.5 μM and 55 nM.[55] While the WT and a few different *Lp*AFP mutants have been assessed for IRI,[51] this was done utilizing a capillary method assay.[69] This assay may not be the best choice to assess ice recrystallization as ice growth may be driven by the release of strain on the snap-frozen samples in the capillaries and/or as a result of new ice nucleation in the sample.[51] Consequently, this ice restructuring inhibition activity (as defined by Davies and co-workers) may not be the same measurement of ice recrystallization inhibition measured by the standard "splat-cooling" assay.[51] Thus, IRI activity was assessed using the traditional "splat-cooling" assay where recrystallization can be easily distinguished as it is easy to follow the change in size of individual ice grains.[48,50] Activity was then quantified using a novel domain recognition software program, which has been shown to be an accurate measure of IRI activity, and individual samples can be easily quantified and compared providing information on small and subtle changes in activity within a series of analogues.[70]

The IRI activity of the BAs is presented in figure 4.3. All of the BAs were assessed for activity at 55 nM in PBS as at higher concentrations many of the proteins produced ice crystals sizes that were too small to be accurately measured. However, AFGP-8 and the T67Y and T51Y *Lp*AFP mutants could be accurately assessed for IRI at 5.5 μM. The Type I and Type III AFPs could also be assessed at 550 nM. At 5.5 μM, AFGP-8, T67Y *Lp*AFP and T51Y *Lp*AFP exhibited very potent IRI activity, and all resulted in ice crystal sizes that were less than 12% of the PBS control. A ten-fold dilution in concentration (550 nM) drastically reduced activity to 45-50%

MGS for AFGP-8 and T67Y *Lp*AFP. Interestingly, the T51Y *Lp*AFP mutant retained potent activity (10% MGS relative to PBS) at 550 nM despite the decrease in concentration (figure 4.3). Both the Type I and Type III AFPs were also potent inhibitors of ice recrystallization at 550 nM.

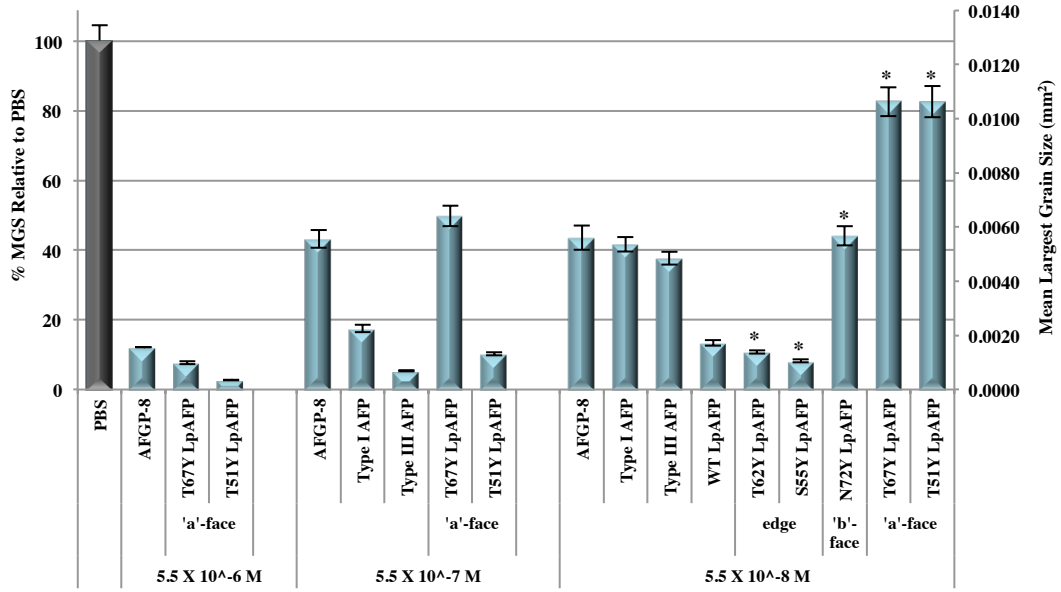

Figure 4.3 IRI activity of BAs assayed at concentrations ranging from 5.5 μM to 55 nM in PBS. The % MGS (mean grain size) of ice crystals has been quantified and plotted relative to the PBS positive control. Asterisks indicate significant difference as determined by the unpaired student's T-test ($p < 0.05$) of the *Lp*AFP mutants relative to the WT *Lp*AFP control.

Differences between the different BAs are most evident at 55 nM. At 55 nM the IRI activity of AFGP-8 as well as Type I and Type III AFP is approximately 40% that of PBS (figure 4.3). In contrast, WT *Lp*AFP and the two *Lp*AFP mutants possessing mutations on the "edge" of the protein were very potent inhibitors of ice recrystallization with mean grain sizes of approximately 10% that of PBS. All of the mutants, irrespective of the location of the mutation, had a statistically significant difference in IRI activity in comparison to WT *Lp*AFP. Both mutations on the edge of *Lp*AFP (T62Y and S55Y, structures shown in Figure 4.1A) had a statistically significant increase in IRI activity (smaller ice crystal sizes) in comparison to the WT. The 'b'-side N72Y mutant had IRI activity that was significantly decreased (larger ice crystal sizes) in comparison to the WT. Additionally, both 'a'-side *Lp*AFP mutants (T67Y and T51Y) had significantly decreased IRI activity in comparison to the WT, and were essentially inactive at this concentration.

4.5 Investigating the Relationship between TH and IRI Activity

A comparison of the TH (figure 4.2) and IRI results (figure 4.3) for all of the BAs assessed in this study is provided in table 4.1. It is evident from these results that TH and IRI activity are both

modulated independently, especially within the different classes of BAs. At both 1 and 5 mg/mL, AFGP-8 exhibited the lowest degree of TH activity (TH gap of 0.02 and 0.08°C, respectively) compared with the Type I AFP, Type III AFP and the WT *Lp*AFP. However, AFGP-8 exhibits similar IRI activity as the Type I and Type III AFPs at 55 nM (~40% MGS). The WT *Lp*AFP exhibits TH activity that is similar to the Type III AFP at 5 mg/mL (0.32-0.36°C), and the Type I AFP is the most TH active at this concentration with a gap of 0.46°C. However, at 55 nM the WT *Lp*AFP is the most IRI active (13% MGS), while the Type I and III AFPs are only moderately IRI active (~40% MGS). At the higher concentration of 550 nM, the IRI activity of the Type I and III AFPs increases, with the Type III being more active than the Type I. In contrast, at the higher concentration at which TH was assessed, the Type I was significantly more TH active. The ice crystal sizes of the WT *Lp*AFP at 550 nM were too small to be accurately measured, indicating that at the higher concentration this protein was still more IRI active that the Type I and Type III, despite their TH activities being similar.

Table 4.1 Summary of quantified TH activity (°C) and IRI activity (% MGS relative to PBS) for the BAs assessed in this study.

Protein	Approx. MW	TH Activity		IRI Activity	
		1 mg/mL	5 mg/mL	55 nM	550 nM
AFGP-8	2400	0.02°C ± 0.002	0.08°C ± 0.01	43.5% ± 3.4	43.2% ± 2.5
Type I AFP	3300	0.15°C ± 0.007	0.46°C	41.7% ± 2.1	17.5% ± 1.0
Type III AFP	6000	0.12°C ± 0.02	0.36°C	37.7% ± 1.8	5.4% ± 0.2
WT LpAFP	13500	0.15°C ± 0.007	0.32°C ± 0.03	13.4% ± 0.8	N/A
T62Y LpAFP (edge)	13500	N/A	0.35°C ± 0.02	10.8% ± 0.5	N/A
S55Y LpAFP (edge)	13500	N/A	0.28°C ± 0.04	8.2% ± 0.4	N/A
N72Y LpAFP ('b-face')	13500	N/A	0.28°C ± 0.01	44.0% ± 2.7	N/A
T67Y LpAFP ('a-face')	13500	0.03°C ± 0.007	0.05°C ± 0.01	82.6% ± 4.2	49.8% ± 2.9
T51Y LpAFP ('a-face')	13500	N/A	0.18°C ± 0.01	82.6% ± 4.4	10.2% ± 0.4

TH activity is typically assessed in w/v concentrations, whereas IRI activity is typically assessed in molar concentrations.[51,55,60,61,70] For the BAs assessed in this study there is a large difference in their molecular masses (provided in table 4.1). The most potent IRI active BA at 55 nM was *Lp*AFP. A 55 nM solution of *Lp*AFP corresponds to 0.74 μg/mL, which is approximately double the w/v concentration of the Type III AFP (0.33 μg/mL) and approximately five times that of the Type I and AFGP-8 (~0.15 μg/mL) at equimolar concentration. However, a 55 nM solution of *Lp*AFP (0.74 μg/mL) has a lower w/v concentration than a 550 nM solution of the Type I AFP (1.8 μg/mL) or AFGP-8 (1.3 μg/mL). A 55 nM solution of the WT *Lp*AFP results in more potent IRI activity (13%) than the 550 nM solutions of both AFGP-8 and Type I AFP (43% and 18%,

respectively). Thus, it appears that the exhibited activities are attributed to the type of BA rather than differences in either w/v or molar concentrations. This is further validated when comparing the TH results. A 5 mg/mL solution of the WT *Lp*AFP corresponds to 0.37 mM. This is half the molar concentration of a 5 mg/mL solution of the Type I AFP (0.85 mM), yet both BAs exhibit similar TH activities. Moreover, a 5 mg/mL solution of AFGP-8 is six times the molar concentration of the WT *LpAFP* (2.1 mM compared with 0.37 mM). However, AFGP-8 exhibits significantly less TH activity than *Lp*AFP, suggesting this activity is dependent upon the type of BA.

Collectively, these results highlight how TH and IRI activity are modulated independently and are dependent upon the type of BA, as the magnitude of TH activity was not always reflected with a similar magnitude of IRI activity. The Type I AFP was the most TH active BA assessed, however it exhibited similar IRI activity at 55 nM as the least TH active BA, AFGP-8. Furthermore, the *Lp*AFP was the most potently IRI active class of BA assessed, yet it did not exhibit the greatest TH activity. A similar observation was also seen with the mutant *Lp*AFPs where TH and IRI activity were modulated independently, however this is within a single class of AFP rather than through a comparison of various different classes.

Prior studies have demonstrated that mutation of the threonine residues to bulky tyrosine residues on the 'a'-face of the *Lp*AFP (structure shown in figure 4.1A) resulted in a dramatic decrease in TH activity in comparison to the WT. This was attributed to a change in surface-surface complementarity between the AFP and ice as the 'a'-side of *Lp*AFP was the IBF.[61] Mutants on the 'b'-face or on either edge of the *Lp*AFP (structure shown in figure 4.1A) had TH activities similar to the WT *Lp*AFP, suggesting that these faces were not involved in ice binding. Data collected in the present study are in agreement with this conclusion (figure 4.2, table 4.1). *Lp*AFP mutants with mutations on the 'b'-side (N72Y) or on the edge of the *Lp*AFP (T62Y and S55Y) had TH activities that were statistically indistinguishable from the WT. The *Lp*AFPs with mutations on the 'a'-side (T67Y and T51Y) had TH activities that were significantly decreased in comparison to the WT. When comparing the two 'a'-side mutants, T67Y and T51Y had a statistically significant difference in TH activity.

It has been well documented from previous studies that TH activity is the result of an adsorption of a specific IBF of an AFP to the surface of ice.[22,23,47] However, the effect these mutations had on IRI activity was not assessed. If the structure of the IBF is also important or relevant for IRI activity, it is reasonable to expect that changes in TH activity by mutations of well-characterized AFPs would be closely reflected in IRI activity. In this study however, it can be seen that this is not the case. Mutations on either edge of *Lp*AFP (T62Y and S55Y), which

resulted in the same TH activity as the WT (Figure 4.2), resulted in a small, but significant increase in IRI activity as compared to WT *Lp*AFP (figure 4.3, table 4.1) (p<0.005, unpaired student's T-test). In fact, the S55Y mutant resulted in ice crystal sizes that were 60% the size of the WT control. Furthermore, the mutation on the 'b'-side of *Lp*AFP (N72Y), which also resulted in the same TH activity as the WT (figure 4.2, table 4.1), had significantly decreased IRI activity in comparison to the WT. The IRI activity of the WT was decreased from 13% MGS to 44% MGS (relative to the PBS control) with the N72Y mutation.

It is evident that the 'a'-side (the IBF) of *Lp*AFP is essential for TH activity.[61] This face is also important for the IRI activity of *Lp*AFP as disrupting it with site-specific mutations (T67Y and T51Y) resulted in a significant reduction in activity at 55 nM (figure 4.3, table 4.1). However, a comparison of TH and IRI activities of the mutations on the 'a'-side of *Lp*AFP suggests that other contributing factors on this face of the protein are also influential on IRI activity. The T67Y mutation decreased the TH activity of the WT by 83% (from 0.32°C for the WT to 0.05°C for T67Y), while the T51Y mutation decreased the TH activity of the WT by 44% (from 0.32°C for the WT to 0.18°C for T61Y) (table 4.1). However, both mutations resulted in an 84% decrease in the IRI activity of the WT (from 13% MGS for the WT to 83% MGS). Thus, while both 'a'-side mutations (T67Y and T51Y) had statistically different TH activities from each other, they both exhibited identical IRI activities.

The results obtained with the mutant *Lp*AFPs were surprising and further indicated that TH and IRI activity can be modulated independently even within an individual class of BA. At 55 nM the magnitude that each IBF mutation decreased TH activity was not reflected in IRI activity. Interestingly, when the concentration was increased to either 550 nM or 5.5 μM, the more potently TH active IBF mutant (T51Y) was also the more potently IRI active mutant (table 4.1). However, *Lp*AFP mutants with mutations not on the IBF (T62Y, S55Y and N72Y) had no effect on the TH activity but a large effect on the IRI activity of this protein. The mutations on the edge of *Lp*AFP (T62Y and S55Y) increased IRI activity (relative to WT) while the 'b'-side mutant (N72Y) decreased activity, yet all mutations exhibited similar TH activity. Collectively, these results suggest that other factors in addition to ice binding contribute to the IRI activity of this class of protein. It is interesting to also note that the T67Y *Lp*AFP and AFGP-8 exhibit similar TH profiles at 1 and 5 mg/mL (figure 4.2, table 4.1). Furthermore, at 5.5 μM and 550 nM the IRI activity of these two BAs was also very similar (figure 4.3). Upon decreasing the concentration to 55 nM a difference in IRI activity is observed, with AFGP-8 being almost twice as active as T67Y *Lp*AFP (44% MGS compared with 83% MGS, respectively, table 4.1). Thus, despite the weak TH activity exhibited by both of these BAs, at the lowest concentration assessed in this

study the BA AFGP-8 is still a moderate inhibitor of ice recrystallization, whereas the BA T67Y *Lp*AFP is only a weak inhibitor. This again highlights how one type of antifreeze activity can be modulated independently of the other depending upon the BA.

4.6 Cryopreservation Ability of BAs

Given that cellular damage due to ice recrystallization is directly responsible for the majority of cell death observed during cryopreservation,[24-31,71,72] we sought to explore the ability of the BAs in this study to act as cryoprotectants. Previous work by our laboratory has demonstrated that *C*-AFGPs with "custom-tailored" antifreeze activity (see section 1.3.1 and chapter 3) can function as effective cryoprotectants for a human embryonic liver cell line.[73] The post-thaw cell viabilities using 1-1.5 mg/mL of the *C*-AFGPs was comparable to that obtained with a 2.5% DMSO solution and were double the post-thaw cell viability of the negative control (only cell medium). These *C*-AFGPs exhibited potent IRI activity but did not exhibit TH activity.[54,55] Thus, there was particular interest in examining the cryoprotective ability of the BAs in this study that were potent ice recrystallization inhibitors but possessed a low degree of TH activity, such as the T67Y *Lp*AFP (figures 4.2 and 4.3). AFGP-8 exhibited a similar antifreeze activity profile as T67Y *Lp*AFP, however AFGP-8 has previously been demonstrated to be detrimental to cell survival in cryopreservation experiments.[34,36,74,75] To the best of our knowledge, the cryopreservation ability of the *Lp*AFPs has not been explored.

We examined the ability of all BAs in this study to protect a human liver cell line (HepG2) during cryopreservation. The BAs were assessed in the cryopreservation experiments at a concentration of 1 mg/mL as high concentrations of BAs have been shown to be detrimental to cell survival during cryopreservation.[37,38,76] Furthermore, our laboratory's beneficial *C*-AFGP cryo-additive was most effective at 1 mg/mL.[73] Our laboratory has also demonstrated that the addition of low concentrations of DMSO (1-2%) to carbohydrate containing cryoprotective solutions can increase post-thaw cell viabilities compared with the DMSO control on its own and the carbohydrate solution on its own.[77] Consequently, different amounts of DMSO (0, 2, 5 and 10% DMSO) were added to the cryopreservation media with the BAs. Cultured HepG2 cells were cryopreserved as described previously with cooling 1°C/min to -80°C, followed by storage in liquid nitrogen at -196°C.[77] Samples were thawed using fast-thaw conditions at 37°C and post-thaw HepG2 cell viability and viable apoptotic cells (% apoptosis) were quantified utilizing flow cytometry.[77-80]

There are a number of striking differences when examining the data of HepG2 cells cryopreserved with different amounts of DMSO in the presence of the BAs or BA mutants

(figures 4.4-4.5). Firstly, when HepG2 cells are cryopreserved in the absence of DMSO, almost all BAs failed to enhance cell survival as post-thaw cell viabilities were between 5-10% irrespective of the BA used or BA mutant (figure 4.4A). In addition, of the small percentage of viable cells, 30-60% of these are apoptotic and thus are already in the stage of programmed cell death. The only BA that resulted in increased viability and decreased apoptosis in the cryo-solutions absent of DMSO was the Type I AFP. Only 13% of the viable cells were apoptotic when the Type I AFP was used, however viability was still very low at only 14%.

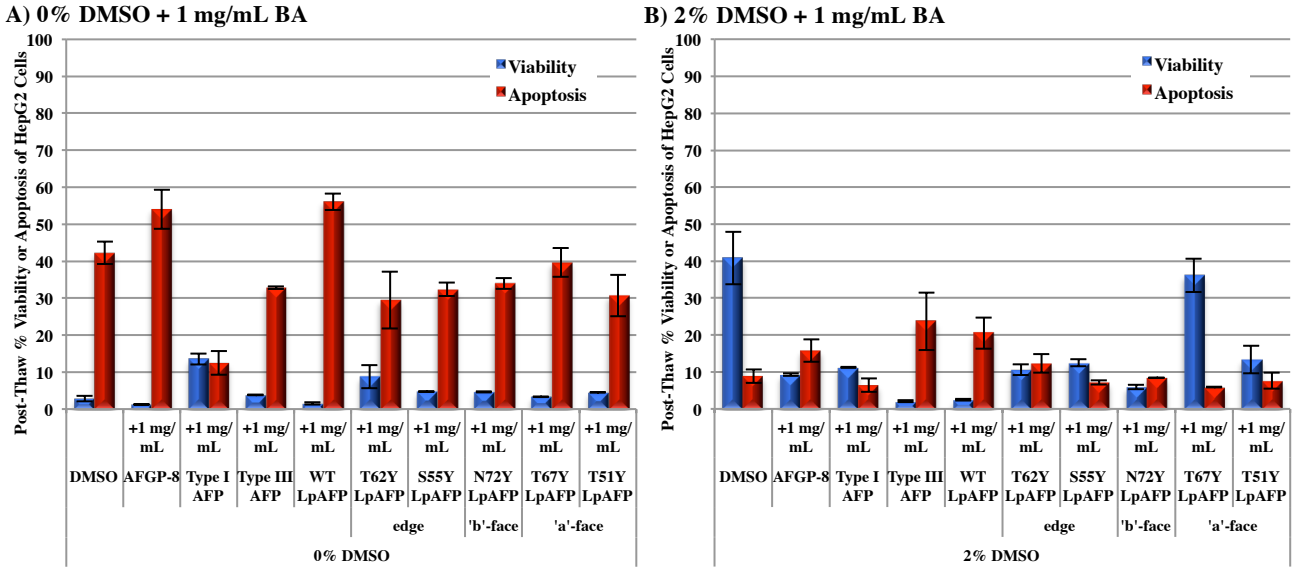

Figure 4.4 Percent post-thaw cell viability and apoptosis of HepG2 cells cryopreserved with 1 mg/mL BA in **A)** 0% DMSO (cell medium only) or **B)** 2% DMSO containing cryoprotectant solutions. Samples were thawed under fast-thaw conditions (37°C).

When 2% DMSO was added to the samples almost all BAs were detrimental to cell survival (figure 4.4B). A 2% DMSO solution alone resulted in 40% HepG2 cell viability post-thaw. However, the addition of 1 mg/mL of the BAs drastically decreased this viability to 10% or less, suggesting that these proteins are exacerbating cellular damage during the cryopreservation process. The exception was the T67Y *Lp*AFP mutant, whose addition to 2% DMSO did not facilitate additional cellular damage during cryopreservation as post-thaw viabilities with this protein were comparable to that of the 2% DMSO control (36% compare with 40%, figure 4.4B). This is interesting as this particular *Lp*AFP mutant exhibited potent IRI activity with dramatically reduced TH activity. At the highest concentration T67Y *Lp*AFP was assessed for IRI (5.5 μM), this protein was a potent inhibitor of ice recrystallization resulting in 8% MGS relative to PBS (figure 4.3). Thus, at 1 mg/mL, which corresponds to a molar concentration of 74 μM, this

protein would still retain potent IRI. However, at 1 mg/mL T67Y *Lp*AFP possessed only a small TH gap of 0.03°C (figure 4.2).

Cryopreservation using the various BAs in the presence of 5% DMSO resulted in very good cell viabilities (70-85%) with very few apoptotic cells (figure 4.5A) for almost all BA assessed. Thus, the detrimental effect of adding the BAs to a 2% DMSO solution for cryo-preservation appears to be negated when the BAs are added to a 5% DMSO solution. The exception was the Type I and Type III AFPs, which had significantly reduced cell viabilities of only 35 and 10%, respectively (figure 4.5A). Cryopreservation results using 10% DMSO (figure 4.5B) closely resemble those with 5% DMSO; however, cell viabilities in the presence of Type I and Type III AFPs increased to 70 and 50%, respectively.

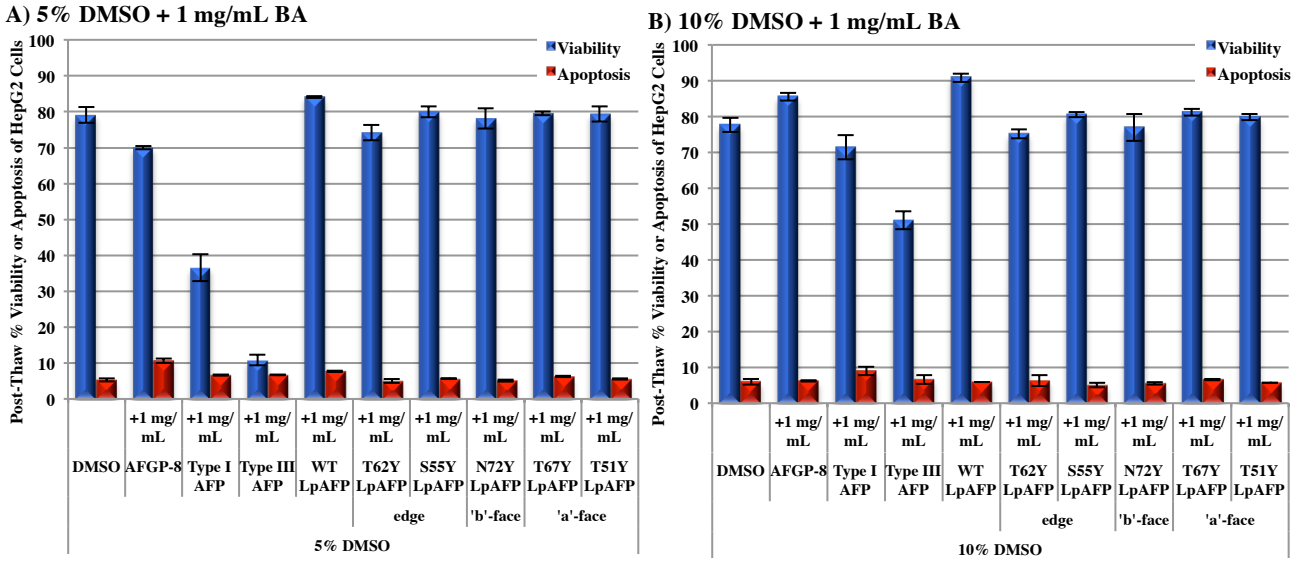

Figure 4.5 Percent post-thaw cell viability and apoptosis of HepG2 cells cryopreserved with 1 mg/mL BA in **A)** 5% DMSO or **B)** 10% DMSO containing cryoprotectant solutions. Samples were thawed under fast-thaw conditions (37°C).

Overall, these results indicate that with low DMSO concentrations (2%) the addition of the BAs is detrimental for cell survival during cryopreservation. In most instances, increasing the amount of DMSO to 5% appears to overcome any negative effects of the BAs. However, Type I and Type III AFPs proved once again to be the exception to this observation. Increasing the amount of DMSO to 10% can negate the damaging effect of these proteins and increase cell viability. However, the Type III AFP appears to cause the most cellular damage during the cryopreservation of HepG2 cells as its addition to even 10% DMSO significantly decreased viability from 80% (for 10% DMSO alone) to 50% (figure 4.5B).

4.7 The Relationship between Ice Crystal Growth Progression and Cryopreservation Ability

The cryopreservation results (section 4.6) indicated that, with the exception of the T67Y *Lp*AFP, when 2% DMSO was used in the cryo-solution, the addition of the BAs facilitate cellular damage resulting in negligible cell viabilities (figure 4.4B). Much of this damage was overcome upon increasing DMSO concentrations, except for the Type I and Type III AFPs (figure 4.5A-B). It was initially hypothesized that the increase in DMSO concentration was eliciting an adverse effect on the BAs and was potentially denaturing the proteins making them inactive. To ensure that this was not occurring, the TH activity of some of the BAs was assessed at 1 mg/mL in DMSO solutions and compared to TH activity in water (figure 4.6). In all instances, TH gaps in DMSO (both 2 and 5%) were similar to those in water, indicating that the addition of DMSO was not denaturing the BAs and decreasing their antifreeze properties or rendering them inactive.

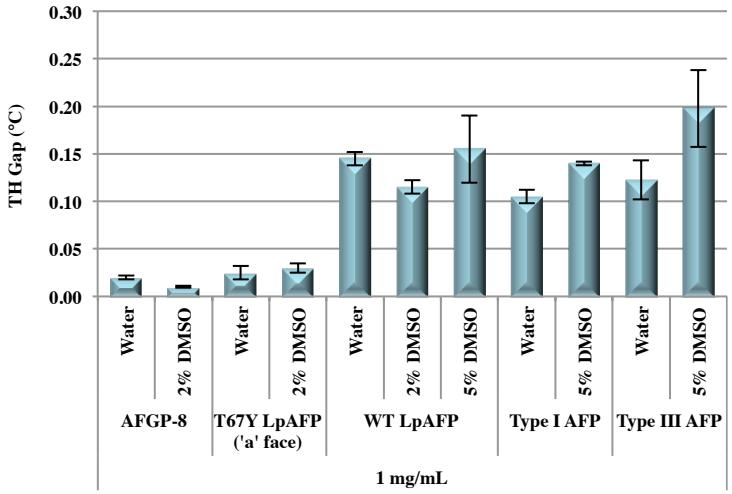

Figure 4.6 TH activity of the BAs assayed at 1 mg/mL in water or 2% or 5% DMSO solutions.

BAs possess the ability to bind to the surface of an ice crystal in an irreversible manner. This leads to a shaping of the ice crystal (dynamic ice shaping, DIS) and ultimately a localized freezing point depression and thermal hysteresis.[16-19,81] The DIS has been shown to be very destructive to cells and tissues at temperatures outside of the TH gap such as those associated with cryopreservation.[33-38] The ice crystal habits of the different BAs are shown in figure 4.7. In addition, the ice crystal habits of these BAs in the presence of DMSO are also presented. As expected, AFGP-8 at 1 mg/mL exhibits typical hexagonal bipyramidal structure where the basal plane has been "flattened" (figure 4.7A).[82,83] This crystal habit is the same in the presence of a 2% DMSO solution (figure 4.7B). Type I and Type III AFPs exhibit the expected hexagonal bipyramidal structure (figure 4.7G and I) that "spiculate" at temperatures below the freezing point of the TH gap,[83] resulting in increase cellular damage. Again, the ice crystal habits for both the

Type I and Type III AFPs were the same in DMSO (figure 4.7H and J). The ice crystal habits in the presence of the WT *Lp*AFP exhibit similar hexagonal bipyramidal structure as AFGP-8 and the Type I and Type III AFPs both in DMSO, water and PBS (figure 4.7E, F and K, respectively). This structure is identical to that described previously for the *Lp*AFP.[83] In addition, the ice crystal habits in the presence of the T67Y and T51Y *Lp*AFP mutants are also hexagonal bipyramidal in structure where the tips have been truncated (figure 4.7 C-D and L), similar to that observed with AFGP-8.[82,83] However, with these particular *Lp*AFP mutants the width of the basal plane is considerably larger than that observed with the other BAs such that the crystal resemble "barrel-like" shapes.

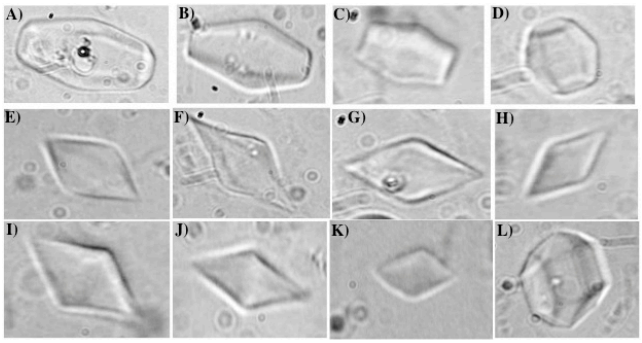

Figure 4.7 Ice crystal habits in the presence of: **A)** 1 mg/mL AFGP-8 in water; **B)** 1 mg/mL AFGP-8 in 2% DMSO; **C)** 1 mg/mL T67Y *Lp*AFP in water; **D)** 1 mg/mL T67Y *Lp*AFP in 2% DMSO; **E)** 1 mg/mL WT *Lp*AFP in water; **F)** 1 mg/mL WT *Lp*AFP in 2% DMSO; **G)** 1 mg/mL Type I AFP in water; **H)** 1 mg/mL Type I AFP in 5% DMSO; **I)** 1 mg/mL Type III AFP in water; **J)** 1 mg/mL Type III AFP in 5% DMSO; **K)** 5 mg/mL WT *Lp*AFP PBS; **L)** 5 mg/mL T51Y *Lp*AFP PBS.

At the concentrations assessed in the cryopreservation experiments (1 mg/mL), all of the BAs exhibited potent IRI activity and, although small for AFGP-8 and T67Y *Lp*AFP, a TH gap (figure 4.6). They also all induced hexagonal bipyramidal ice crystal structures with some BAs inducing "pointed" tips and others "truncated" tips (figure 4.7). However, all BAs except for T67Y *Lp*AFP were detrimental to cell survival when added to a 2% DMSO cryo-solution (figure 4.4B). This was surprising as the T67Y *Lp*AFP exhibited similar antifreeze activity (Both TH and IRI) and ice crystal shapes as AFGP-8; however, AFGP-8 resulted in negligible post-thaw cell viabilities. In addition, when present in a 5% DMSO solution, this negative effect from the BAs is overcome. Again, the exception to this is with the Type I and Type III AFPs (figure 4.5A). While the BAs assessed in this study have similar ice crystal structures, they have distinctly difference burst growth patterns when temperatures are lowered below the freezing point of the TH gap. As such, we hypothesize that the difference in cryopreservation ability of the BAs may be attributed to differences in ice crystal growth patterns and not only initial ice crystal habit as previously proposed.[33-38]

The Type I and Type III AFPs at 1 mg/mL in both water and DMSO resulted in rapid burst growth of the single ice crystal that was initiated from the tips of the hexagonal bipyramid (the c-axis) when the temperature was lowered beyond the freezing point. This is the characteristic spicular ice growth that results from many fish AFPs and high concentrations of AFGPs.[10,60,68,83,84] These were the only two BAs in this study that exhibited this spiculated ice growth at 1 mg/mL, and these proteins were the most detrimental during cryopreservation even in 10% DMSO solutions. Thus, this validates previous hypotheses that cellular damage during cryopreservation can be exacerbated by a change in ice crystal morphology and growth that is induced in the presence of BAs when the resulting ice crystal shapes and growth patterns are spiculated.[33,34]

Figure 4.8 shows the ice crystal growth patterns as a function of time for AFGP-8, T67Y *Lp*AFP and WT *Lp*AFP at 1 and 5 mg/mL. In all instances, the single ice crystals are formed as flattened hexagonal bipyramidal structures. Over time within the TH gap, the tips of the ice crystals in the presence of the WT *Lp*AFP begin to form and become pointed (figure 4.8C and F), particularly as the temperatures approach the freezing point.[83] The ice growth progressions (in both water and water/DMSO) are very different in the presence of T67Y *Lp*AFP, AFGP8 and WT *Lp*AFP. As seen in figure 4.8B and E, ice crystals in the presence of T67Y *Lp*AFP grow outward along the a-axes as a large "plate" or "disc". In the presence of AFGP-8, growth occurs as large "column-like" ice crystals, with ice growth occurring predominately along the c-axis or basal plane and slow growth along the a-axis (figure 4.8A and D). Single ice crystals in the presence of WT *Lp*AFP grow in a manner similar to those grown in the presence of T67Y *Lp*AFP, where ice growth occurs mostly in the direction of the a-axis (figure 4.8C and F). However, slow growth along the c-axis is also observed resulting in column-like crystals similar to those observed in the presence of AFGP-8.[83] The overall burst ice growth occurs at a much slower rate with the T67Y *Lp*AFP than with the WT *Lp*AFP and AFGP-8, and burst growth or violent ice crystal expansion is not observed with T67Y mutant. In comparison, the TH activity of the T67Y *Lp*AFP and AFGP-8 are both extremely small (~0.02°C) and they are both potent inhibitors of ice recrystallization. However, the ice crystal growth patterns between T67Y *Lp*AFP and AFGP-8 are quite different, and T67Y *Lp*AFP did not exhibit rapid burst growth. Thus, we suggest that while IRI activity is important for cryoprotective abilities, both the ice crystal habit and the dynamic manner in which the ice crystal grows at temperatures outside the TH gap also play key roles in the cryoprotective function of a BA or a BA analogue.

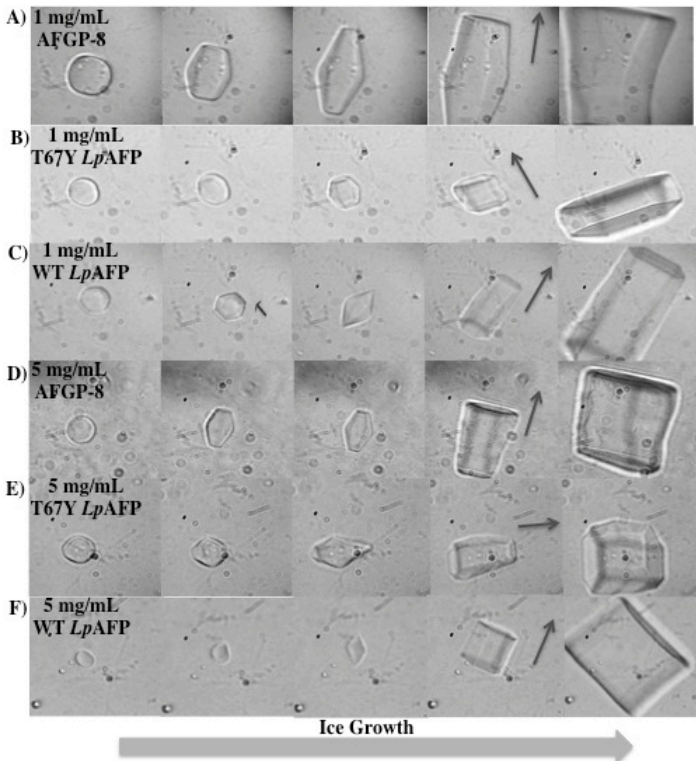

Figure 4.8 Ice crystal growth patterns beginning at T_m (frame 1) to temperatures within (frames 2, 3) the TH gap and burst growth below T_f (frames 4, 5) outside the TH gap. **(A)** 1 mg/mL AFGP-8 in 2% DMSO; **B)** 1 mg/mL T67Y *Lp*AFP in 2% DMSO; **C)** 1 mg/mL WT *Lp*AFP in water; **D)** 5 mg/mL AFGP-8 in water; **E)** 5 mg/mL T67Y *Lp*AFP in PBS; **F)** 5 mg/mL WT *Lp*AFP in PBS. The arrow indicates the direction of the *c*-axis. Time lapse between images 1-5 in A-E is 40 s, 1 min, 7 min, 2 min, 1.5 min and 8 min, respectively.

Ice crystal growth habit has been shown to influence freeze concentration inhibition in frozen food products,[82] and the results presented in this chapter demonstrate that this may also be the case for the cryopreservation of cells, tissues and other biological materials. Of course, this may not be the only contributing factor and potential cytotoxic effects of these proteins cannot be overlooked or ignored.[32] Overall, the results from this study demonstrate that in general these BAs facilitate cellular damage during cryopreservation, suggesting that the ability of these proteins to bind to ice and alter ice crystal shape is detrimental for a cryoprotectant. However, this is also dependent upon the ice crystal structure and the manner in which the crystal grows in the presence of the BA. This was demonstrated by the T67Y *Lp*AFP, which did not have an adverse effect upon the freezing of HepG2 cells in a 2% DMSO solution. Consequently, the most effective cryoprotectants are still hypothesized to be rationally designed ice recrystallization inhibitors that do not interact with the ice surface resulting in changes in ice crystal habit that lead to cellular damage during the freezing event.

4.8 Summary and Conclusions for the TH, IRI, Ice Crystal Growth Habits and Cryopreservation Ability of Various Classes of Biological Antifreezes

With the use of naturally occurring biological antifreezes and single-point BA mutants the relationship between the two types of antifreeze activities, TH and IRI, was examined. The results of this study further validate previous reports that hypothesized TH and IRI activity were not tightly correlated. This was achieved both by a comparison of the two activities between difference classes of BA, as well as within a single class of AFP and its mutants (the *Lp*AFP). The results from this study highlight how TH and IRI activity can be modulated independently and are dependent upon the type of BA. Within different classes of BAs, more potent TH activity did not always result in the more potent ice recrystallization inhibitor. AFGP-8 has weak TH activity, whereas Type I and Type III AFPs have significantly larger TH gaps. However, the IRI activity of these proteins is relatively similar over a range of concentrations. Moreover, the WT *Lp*AFP has similar TH activity as the Type I and Type III AFPs, yet it is significantly more IRI active at low concentrations. Within the *Lp*AFP class of BAs, mutant *Lp*AFPs with mutations not on the IBF (N72Y, T62Y and S55Y) resulted in similar TH activity as the WT. However, the IRI activity of these mutants differed from that of the WT, with the edge mutants (T62Y and S55Y) increasing IRI activity and the 'b'-side mutant (N72Y) drastically decreasing activity. Furthermore, both mutations on the IBF of *Lp*AFP (T67Y and T51Y) differed in the extent they reduced the TH activity of the WT, yet they both exhibited a similar reduction in IRI activity. While it is evident that the IBF of *Lp*AFP is important for IRI activity, the results of this study indicate that other faces on this protein that do not influence TH activity are influential on its IRI activity, and have highlighted how changes in TH activity do not influence IRI activity in the same manner.

Finally, in this study we have also demonstrated that in general these BAs are not effective cryoprotectants and that, as described previously, can be detrimental and decrease cell survival post cryopreservation with HepG2 cells. However, protein-ice interactions leading to changes in ice crystal habit as well as changes in ice growth progressions can have a significant impact upon post-thaw recoveries. Overall, the BA that resulted in the least amount of cellular damage during cryopreservation was the T67Y *Lp*AFP mutant. This protein had distinctly different ice growth habits and progressions, which may attribute to it not being as damaging to cells during cryopreservation as the other BAs assessed. As such, this protein may be a potential candidate as a cryoprotectant upon further optimization of cryopreservation protocols and cytotoxicity assessments since the T67Y *Lp*AFP exhibited potent IRI activity but very low TH activity.

4.9 Experimental Section for Chapter 4

AFGP-8 from *Gadus ogac* (rock cod) was obtained from A/F Protein Inc. (Waltham, MA). Type I AFP from *Pseudopleuronectes americanus* (winter flounder) and Type III AFP from *Macrozoarces americanus* (ocean pout) were generously donated from Professor Garth Fletcher (Memorial University). The pET 24a+ vector with His-tagged WT and mutant *Lp*AFPs was kindly provided by Prof. Peter L. Davies (Queens University, Canada).

Recombinant Expression and Purification of LpAFPs:

The pET 24a+ vector with His-tagged WT and mutant *Lp*AFPs was kindly provided by Prof. Peter L. Davies (Queen's University, Canada). The His-tagged *Lp*AFP expression vectors were confirmed by DNA sequencing (OHRI, Ottawa, ON, Canada). Recombinant *Lp*AFPs were expressed in *E. coli* BL21(DE3) as described previously.[56,61,63] Briefly, 750 mL of LB media containing 50 μg/mL of kanamycin was inoculated with 0.5 % (*v*/*v*) of a dense overnight culture of *E. coli* BL21(DE3), transformed with either wild-type or mutant *Lp*AFP expression vectors, and incubated at 37 °C until an $OD_{600\,nm}$ of ~0.6 was reached. Incubation was continued at 24°C until the $OD_{600\,nm}$ reached ~1.0 at which time protein expression was induced by the addition of IPTG to a final concentration of 0.2 mM. Cultures were then incubated an additional 18 h at 24 °C. The cells were harvested by centrifugation at 4000g at 4 °C, and resuspended in 50 mL of lysis buffer (50 mM Tris-HCl and 100 mM NaCl). The resuspended cells were lysed by boiling for 8 min and allowed to cool to 4 °C on ice. The lysate was clarified by centrifugation at 15000g and 4 °C for 1 h, and the resulting supernatant was purified by nickel affinity chromatography. The supernatant was incubated with Ni-NTA superflow (QIAGEN) for 1 h at 4°C, then loaded to the column and the flow-through was collected. After washing the column with wash buffer (100 mM Tris and 300 mM NaCl), the protein was eluted with wash buffer supplemented with a gradient of imidazole concentrations (20 mM, then 2 × 100 mM, then 3 × 250 mM). Fractions containing *Lp*AFPs were collected and concentrated by centrifugation with an Amicon Ultra-15 Filter Device (5000 MWCO, Millipore) and buffer exchanged by washing five times with water (5 × 15 mL). The final purified protein solution was concentrated to a final volume of 1 mL. Purity was analyzed using SDS-PAGE and pure *Lp*AFPs were lyophilized and stored as a white powder at -78 °C.

Circular Dichroism (CD) and Solution Conformation:

CD spectra of the *Lp*AFPs were obtained using a Jasco Model *J*-810 automatic recorder spectropolarimeter. All measurements were performed in a quartz cell of 0.1 cm path lengths.

Spectra were obtained with a 1.0 nm bandwidth, a time constant of 0.5 s and a scan speed of 50 nm/min. All the spectra were recorded between 180 nm and 300 nm. All CD experiments were performed with a protein concentration of 24 μM in a phosphate buffer at pH 7.5 with the temperature maintained at 0 °C. A minimum of five scans were averaged and baseline corrections were made against each sample using phosphate buffer as a blank. Data obtained from CD spectroscopy was converted into molar ellipticity (deg cm^2 $dmol^{-1}$) and the curves were compared to previously reported CD spectra of the *Lp*AFP.[61,63]

Ice Recrystallization Inhibition (IRI) Assay:

Sample analysis for IRI activity was performed using the "splat cooling" method as previously described.[48] In this method, the analyte was dissolved in a phosphate buffered saline (PBS) solution and a 10 μL droplet of this solution was dropped from a micropipette through a two meter high plastic tube (10 cm in diameter) onto a block of polished aluminum precooled to approximately -80 °C. The droplet froze instantly on the polished aluminum block and was approximately 1 cm in diameter and 20 μm thick. This wafer was then carefully removed from the surface of the block and transferred to a cryostage held at -6.4 °C for annealing. After a period of 30 min, the wafer was photographed between crossed polarizing filters using a digital camera (Nikon CoolPix 5000) fitted to the microscope. A total of three images were taken from each wafer. During flash freezing, ice crystals spontaneously nucleated from the supercooled solution. These initial crystals were relatively homogeneous in size and quite small. During the annealing cycle, recrystallization occurred, resulting in a dramatic increase in ice crystal size. A quantitative measure of the difference in recrystallization inhibition of two compounds is the difference in the ice crystal size distribution. Image analysis of the ice wafers was performed using a novel domain recognition software (DRS) program.[70] This processing employed the Microsoft Windows Graphical User Interface to allow a user to visually demarcate and store the vertices of ice domains in a digital micrograph. The data were then used to calculate the domain areas. All data was plotted and analyzed using Microsoft Excel. The mean grain (or ice crystal) size (MGS) of the sample was compared to the MGS of the control PBS solution for that same day of testing. IRI activity is reported as the percentage of the MGS (% MGS) relative to the PBS control, and the % MGS for each sample were plotted along with its standard error of the mean. Small percentages represent a small MGS, which is indicative of more potent IRI activity. Unpaired student's T-tests were performed to a 95% confidence level.

Thermal Hysteresis (TH) Assay:

Nanolitre osmometry was performed using a Clifton nanolitre osmometer (Clifton Technical Physics, Hartford, NY).[85] All measurements were performed in a phosphate buffered saline (PBS) solution. Ice crystal morphology was observed through a Leitz compound microscope equipped with an Olympus 20× (infinity-corrected) objective, a Leitz Periplan 32× photo eyepiece, and a Hitachi KPM2U CCD camera connected to a Toshiba MV13K1 TV/VCR system. Still images were captured directly using a Nikon CoolPix digital camera. Unpaired student's T-tests were performed to a 95% confidence level.

HepG2 Cell culture:

HepG2 (human liver hepatocellular carcinoma cells, ATCC, HB-8065) were cultured in Eagle's minimum essential media (MEM) supplemented with 10% FBS (fetal bovine serum), 1% non- essential amino acids, 1 mM sodium pyruvate and 1% penicillin–streptomycin in 75cm^2 Corning® flasks.[77] Cells were incubated in a 37°C incubator supplied with 5% CO_2. Passages 5–18 were used in this study. No evidence of overgrowth or morphological changes consistent with apoptosis was observed. All cells were removed from the plates using 3 mL Accutase solution for use in experiments.

HepG2 Cryopreservation and Thawing:

HepG2 cells were cultured and detached as described above.[77] Cells were diluted with culture media and counted using a hemocytometer. Aliquots containing 1×10^6 cells were added to 1.5 mL Eppendorf tubes and cells were pelleted by centrifugation for 10 min at 580×g. The supernatant was removed and the cells were resuspended in 100 μL MEM supplemented with the desired (glyco)peptide and/or DMSO cryo-additives. Cell suspensions were transferred to 2 mL cryogenic vials and placed in a "Mr. Frosty" freezing container. The container was placed in a –80°C freezer for 16 h to provide a cooling rate of 1°C/min. Samples were then stored in the vapor phase of liquid nitrogen (–196°C) for a minimum of 24 hours. Following storage, samples were rapidly thawed in a 37°C water bath with gentle agitation for flow cytometry analysis.

Post-Thaw HepG2 Flow Cytometry:

After cryopreservation and thawing, cell suspensions were diluted with 400 μL of 1X Annexin V binding buffer and 100 μL were transferred to polypropylene flow cytometry tubes. 5 μL of 7-AAD and 4 μL of Annexin V-PE were added and samples were vortexed and incubated for 15 min in the dark.[77] Following incubation, 10 μL of CountBright counting beads were added and

samples were diluted to 500 μL with 1X Annexin V binding buffer. Flow cytometry analysis on 100,000 cells was carried out on a Beckman Coulter FC500 flow cytometer. Annexin V-PE was measured with 575nm optical filter (FL-2), while 7-AAD was measured with 675 nm optical filter (FL-4). Viability was determined by the total number of 7-AAD$^-$ cells detected. Apoptosis was determined by the number of 7-AAD$^-$ cells that were Annexin V$^+$. Cell recoveries were calculated from total cells counted and the sample volume analyzed, determined from the number of counting beads detected and the concentration of beads in the analyzed solution. Counting beads were measured with 610 nm optical filter (FL3). Time between thawing and analysis by flow cytometry was less than 1 h. All samples were tested in duplicate.

4.10 References

1. DeVries, A.L.; Komatsu, S.K.; Feeney, R.E. *J. Biol. Chem.* **1970**, *245*, 2901-2908.

2. DeVries, A.L. *Science*. **1971**, *172*, 1152-1155.

3. Scholander, P.F.; Maggert, J.E. *Cryobiology*. **1971**, *8*, 371-374.

4. Feeney, R.E.; Burcham, T.S.; Yeh, Y. *Annu. Rev. Biophys. Biophys. Chem.* **1986**, *15*, 59-78.

5. Yeh, Y.; Feeney, R.E. *Chem. Rev.* **1996**, *96*, 601-618.

6. Harding, M.M.; Anderberg, P.I.; Haymet, A.D.J. *Eur. J. Biochem.* **2003**, *270*, 1381-1392.

7. DeVries, A.L.; Wohlschlag, D.E. *Science*. **1969**, *163*, 1073-1075.

8. Davies, P.L.; Baardsnes, J.; Kuiper, M.J.; Walker, V.K. *Philos. Trans. R. Soc. London, Ser. B.* **2002**, *357*, 927-935.

9. Jia, Z.; Davies, P.L. *Trends Biochem. Sci.* **2002**, *27*, 101-106.

10. Fletcher, G.L.; Hew, C.L.; Davies, P.L. *Annu. Rev. Physiol.* **2001**, *63*, 359-390.

11. Davies, P.L.; Hew, C.L. *FASEB J.* **1990**, *4*, 2460-2468.

12. Duman, J.G.; Li, N.; Verleye, D.; Goetz, F.W.; Wu, D.W.; Andorfer, C.A.; Benjamin, T.; Parmelee, D.C. *J. Comp. Physiol. B.* **1998**, *168*, 225-232.

13. Graham, L.A.; Liou, Y.-C.; Walker, V.K.; Davies, P.L. *Nature*. **1997**, *388*, 727-728.

14. Marshall, C.B.; Fletcher, G.L.; Davies, P.L. *Nature*. **2004**, *429*, 153-153.

15. Gilbert, J.A.; Davies, P.L.; Laybourn-Parry, J. *FEMS Microbiol. Lett.* **2005**, *245*, 67-72.

16. Raymond, J.A.; DeVries, A.L. *Proc. Natl. Acad. Sci. U.S.A.* **1977**, *74*, 2589-2593.

17. Wilson, P.W. *Cryoletters*. **1993**, *14*, 31-36.

18. Knight, C.A.; Cheng, C.C.; DeVries, A.L. *Biophys. J.* **1991**, *59*, 409-418.

19. Knight, C.A.; Driggers, E.; DeVries, A.L. *Biophys. J.* **1993**, *64*, 252-259.

20. Doxey, A.C.; Yaish, M.W.; Griffith, M.; McConkey, B.J. *Nat. Biotechnol.* **2006**, *24*, 852-855.

21. Baardsnes, J.; Davies, P.L. *Biochim. Biophys. Acta: Proteins Proteom.* **2002**, *1601*, 49-54.

22. Baardsnes, J.; Kondejewski, L.H.; Hodges, R.S.; Chao, H.; Kay, C.; Davies, P.L. *FEBS Lett.* **1999**, *463*, 87-91.

23. Marshall, C.B.; Daley, M.E.; Graham, L.A.; Sykes, B.D.; Davies, P.L. *FEBS Lett*. **2002**, *529*, 261-267.

24. Mazur, P.C. *Science*. **1970**, *168*, 939-949.

25. Mazur, P. *Am. J. Physiol. - Cell Physiol*. **1984**, *247*, C125-C142.

26. Fowler, A.; Toner, M. *Ann. N.Y. Acad. Sci*. **2005**, *1066*, 119-135.

27. Toner, M.; Caravalho, E.G.; Karel, M. *J. Appl. Phys*. **1990**, *67*, 1582-1593.

28. Muldrew, K.; McGann, L.E. *Biophys. J*. **1990**, *57*, 525-532.

29. Mazur, P. *Cell Biophys*. **1990**, *17*, 53-92.

30. Fowler, A.; Toner, M. *Ann. N.Y. Acad. Sci*. **1998**, *858*, 245-252.

31. Farrant, J.; Molyneux, P.; Hasted, J.B.; Peares, P.; Echlin, P. *Philos. Trans. R. Soc. London, Ser. B*. **1977**, *278*, 191-205.

32. Wang, J.H. *Cryobiology*. **2000**, *41*, 1-9.

33. Mugano, J.A.; Wang, T.; Layne, J.R., Jr.,; DeVries, A.L.; Lee, R.E. *Cryobiology*. **1995**, 556-557.

34. Rubinsky, B.; DeVries, A.L. *Cryobiology*. **1989**, *26*, 580.

35. Wang, T.; Zhu, Q.; Yang, X.; Layne, J.R.J.; DeVries, A.L. *Cryobiology*. **1994**, *31*, 185-192.

36. Rubinsky, B.; Arav, A.; DeVries, A.L. *Cryobiology*. **1992**, *29*, 69-79.

37. Carpenter, J.F.; Hansen, T.N. *Proc. Natl. Acad. Sci. U.S.A*. **1992**, *89*, 8953-8957.

38. Chao, H.; Davies, P.L.; Carpenter, J.F. *J. Exp. Biol*. **1996**, *199*, 2071-2076.

39. Garner, J.; Harding, M.M. *ChemBioChem*. **2010**, *11*, 2489-2498.

40. Peltier, R.; Brimble, M.A.; Wojnar, J.M.; Williams, D.E.; Evans, C.W.; DeVries, A.L. *Chem. Sci*. **2010**, *1*, 538-551.

41. Gibson, M.I.; Barker, C.A.; Spain, S.G.; Albertin, L.; Cameron, N.R. *Biomacromolecules*. **2009**, *10*, 328-333.

42. Gibson, M.I. *Polym. Chem*. **2010**, *1*, 1141-1152.

43. Capicciotti, C.J.; Doshi, M.; Ben, R.N. Ice Recrystallization Inhibitors: From Biological Antifreezes to Small Molecules. In: P. Wilson, editor. Recent Developments in the Study of Recrystallization ed.). New York: InTech; 2013. p 177-224.

44. Chao, H.; Houston, M.E.; Hodges, R.S.; Kay, C.M.; Sykes, B.D.; Loewen, M.C.; Davies, P.L.; Sönnichsen, F.D. *Biochemistry*. **1997**, *36*, 14652-14660.

45. Haymet, A.D.J.; Ward, L.G.; Harding, M.M.; Knight, C.A. *FEBS Lett*. **1998**, *430*, 301-306.

46. Zhang, W.; Laursen, R.A. *J. Biol. Chem*. **1998**, *273*, 34806-34812.

47. DeLuca, C.I.; Davies, P.L.; Ye, Q.; Jia, Z. *J. Mol. Biol*. **1998**, *275*, 515-525.

48. Knight, C.A.; Hallett, J.; DeVries, A.L. *Cryobiology*. **1988**, *25*, 55-60.

49. Hall, D.G.; Lips, A. *Langmuir*. **1999**, *15*, 1905-1912.

50. Knight, C.A.; Wen, D.; Laursen, R.A. *Cryobiology*. **1995**, *32*, 23-34.

51. Yu, S.O.; Brown, A.; Middleton, A.J.; Tomczak, M.M.; Walker, V.K.; Davies, P.L. *Cryobiology*. **2010**, *61*, 327-334.

52. Sidebottom, C.; Buckley, S.; Pudney, P.; Twigg, S.; Jarman, C.; Holt, C.; Telford, J.; McArthur, A.; Worrall, D.; Hubbard, R.; Lillford, P. *Nature*. **2000**, *406*, 256.

53. Pudney, P.D.A.; Buckley, S.L.; Sidebottom, C.M.; Twigg, S.N.; Sevilla, M.-P.; Holt, C.B.; Roper, D.; Telford, J.H.; McArthur, A.J.; Lillford, P.J. *Arch. Biochem. Biophys*. **2003**, *410*, 238-245.

54. Liu, S.; Ben, R.N. *Org. Lett*. **2005**, *7*, 2385-2388.

55. Czechura, P.; Tam, R.Y.; Dimitrijevic, E.; Murphy, A.V.; Ben, R.N. *J. Am. Chem. Soc*. **2008**, *130*, 2928-2929.

56. Capicciotti, C.J.; Leclère, M.; Perras, F.A.; Bryce, D.L.; Paulin, H.; Harden, J.; Liu, Y.; Ben, R.N. *Chem. Sci*. **2012**, *3*, 1408-1416.

57. Balcerzak, A.K.; Febbraro, M.; Ben, R.N. *RSC Adv*. **2013**, *3*, 3232-3236.

58. Trant, J.F.; Biggs, R.A.; Capicciotti, C.J.; Ben, R.N. *RSC Adv*. **2013**, *3*, 26005-26009.

59. Bouvet, V.R.; Lorello, G.R.; Ben, R.N. *Biomacromolecules*. **2006**, *7*, 565-571.

60. Kao, M.H.; Fletcher, G.L.; Wang, N.C.; Hew, C.L. *Can. J. Zool*. **1986**, *64*, 578-582.

61. Middleton, A.J.; Brown, A.M.; Davies, P.L.; Walker, V.K. *FEBS Lett*. **2009**, *583*, 815-819.

62. Kumble, K.D.; Demmer, J.; Fish, S.; Hall, C.; Corrales, S.; DeAth, A.; Elton, C.; Prestidge, R.; Luxmanan, S.; Marshall, C.J.; Wharton, D.A. *Cryobiology*. **2008**, *57*, 263-268.

63. Lauersen, K.J.; Brown, A.; Middleton, A.; Davies, P.L.; Walker, V.K. *Cryobiology*. **2011**, *62*, 194-201.

64. Middleton, A.J.; Marshall, C.B.; Faucher, F.; Bar-Dolev, M.; Braslavsky, I.; Campbell, R.L.; Walker, V.K.; Davies, P.L. *J. Mol. Biol*. **2012**, *416*, 713-724.

65. Evans, R.P.; Hobbs, R.S.; Goddard, S.V.; Fletcher, G.L. *Comp. Biochem. Physiol. A: Mol. Integr. Physiol*. **2007**, *148*, 556-561.

66. Kristiansen, E.; Pedersen, S.A.; Zachariassen, K.E. *Cryobiology*. **2008**, *57*, 122-129.

67. Li, N.; Andorfer, C.A.; Duman, J.G. *J. Exp. Biol*. **1998**, *201*, 2243-2251.

68. Tachibana, Y.; Fletcher, G.L.; Fujitani, N.; Tsuda, S.; Monde, K.; Nishimura, S.-I. *Angew. Chem. Int. Ed*. **2004**, *43*, 856-862.

69. Tomczak, M.M.; Marshall, C.B.; Gilbert, J.A.; Davies, P.L. *Biochem. Biophys. Res. Commun*. **2003**, *311*, 1041-1046.

70. Jackman, J.; Noestheden, M.; Moffat, D.; Pezacki, J.P.; Findlay, S.; Ben, R.N. *Biochem. Biophys. Res. Commun*. **2007**, *354*, 340-344.

71. Mazur, P. Life in the Frozen State - Principles of Cryobiology (Boca Baton, FL: CRC Press; 2004.

72. Acker, J.P.; McGann, L.E. *Cell Transplant*. **2002**, *11*, 563-571.

73. Leclère, M.; Kwok, B.K.; Wu, L.K.; Allan, D.S.; Ben, R.N. *Bioconjugate Chem*. **2011**, *22*, 1804-1810.

74. Rubinsky, B.; Arav, A.; Mattioli, M.; DeVries, A.L. *Biochem. Biophys. Res. Commun*. **1990**, *173*, 1369-1374.

75. Rubinsky, B.; Arav, A.; DeVries, A.L. *Cryo-letters*. **1991**, *12*, 93-106.

76. Wang, J.H.; Bian, H.W.; Huang, C.N.; Ge, J.G. *Acta Biol. Exp*. **1999**, *32*, 271-276.

77. Chaytor, J.L.; Tokarew, J.M.; Wu, L.K.; Leclère, M.; Tam, R.Y.; Capicciotti, C.J.; Guolla, L.; von Moos, E.; Findlay, C.S.; Allan, D.S.; Ben, R.N. *Glycobiology*. **2012**, *22*, 123-133.

78. Koopman, G.; Reutelingsperger, C.; Kuijten, G.; Keehnen, R.; Pals, S.; van Oers, M. *Blood*. **1994**, *84*, 1415-1420.

79. Vermes, I.; Haanen, C.; Steffens-Nakken, H.; Reutellingsperger, C. *J. Immunol. Methods*. **1995**, *184*, 39-51.

80. Latt, S.A. *Can. J. Genet. Cytol*. **1977**, *19*, 603-623.

81. Knight, C.A.; DeVries, A.L. *J. Cryst. Growth*. **1994**, *143*, 301-310.

82. Yamanouchi, T.; Xiao, N.; Hanada, Y.; Kamijima, T.; Sakashita, M.; Nishimiya, Y.; Miura, A.; Kondo, H.; Tsuda, S. *Low Temp. Sci*. **2013**, *71*, 91-96.

83. Bar-Dolev, M.; Celik, Y.; Wettlaufer, J.S.; Davies, P.L.; Braslavsky, I. *J. Roy. Soc. Interface*. **2012**, *9*, 3249-3259.

84. Wilkinson, B.L.; Stone, R.S.; Capicciotti, C.J.; Thaysen-Andersen, M.; Matthews, J.M.; Packer, N.H.; Ben, R.N.; Payne, R.J. *Angew. Chem. Int. Ed*. **2012**, *51*, 3606-3610.

85. Chakrabartty, A.; Hew, C.L. *Eur. J. Biochem*. **1991**, *202*, 1057-1063.

Chapter 5: Small Carbohydrate-Based Molecules as Ice Recrystallization Inhibitors – Simple Mono- and Disaccharides and Complex Oligosaccharides

5.1 Introduction

Compounds described in the literature that are potent ice recrystallization inhibitors have been large peptides or glycopeptides that are biological antifreezes (BAs),[1-12] analogues of BAs,[4,7,13-15] or high molecular weight polymers such as polyvinyl alcohol (PVA) (see section 1.3, or Chapters 3 and 4).[2,16-20] Despite advances in the synthesis of complex peptides and glycopeptides, their synthesis remains complex, time consuming and costly. Thus, interest has arisen in designing small molecule ice recrystallization inhibitors. These are attractive alternatives to peptides and glycopeptides as they can be efficiently synthesized and thus are amenable to large-scale preparation for the many medical, commercial and industrial applications of IRIs. Another advantage of small molecules is less likelihood of immunogenic responses and non-specific toxic effects that can be observed with peptides and glycopeptides in biological systems.

Our laboratory has reported that simple carbohydrates, both mono- and disaccharides, can exhibit moderate IRI activity (section 1.3.3).[21] It was hypothesized that the ability of simple mono- and disaccharides to inhibit ice recrystallization was related to their compatibility with bulk-water, which is ultimately correlated to the hydration of the carbohydrate.[21] Highly hydrated carbohydrates, such as D-galactose or meliobiose, have a poor "fit" and are less compatible with the three-dimensional hydrogen-bonded network of bulk-water.[22-24] These carbohydrates cause bulk-water to disrupt or disorder to make the sugar fit into this hydrogen bond network. For ice recrystallization to occur, bulk-water molecules transfer from a highly ordered ice lattice to a semi-ordered quasi-liquid layer (QLL), then subsequently from the QLL to a growing ice crystal (see section 1.1 for more detailed discussion).[25,26] The carbohydrates are likely concentrated at the bulk-water-QLL interface.[21] Those that are more highly hydrated cause a greater disturbance and disorder bulk-water, thus increasing the energy associated with transferring water molecules to a more ordered QLL or ice lattice, resulting in ice recrystallization inhibition (Figure 5.1). Less hydrated carbohydrates, such as D-talose or sucrose, fit well into bulk-water and cause less of a disturbance to the pre-ordering of bulk-water, thus inhibition of ice recrystallization was not observed.

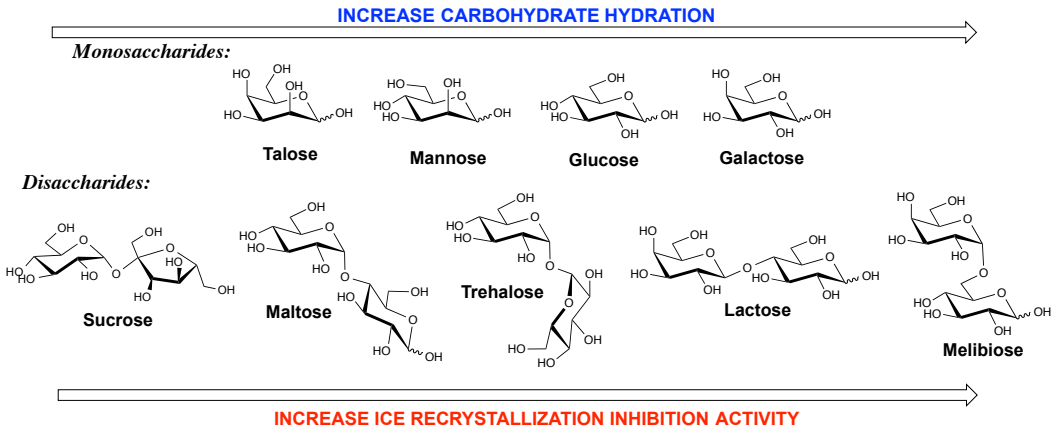

Figure 5.1 An illustration of the correlation between carbohydrate hydration and IRI activity.

The hydration layer or hydration shell of a carbohydrate is defined as the number of tightly bound water molecules that surround the carbohydrate in aqueous solution. Key parameters that dictate hydration characteristics include partial molar volumes, isentropic partial molar compressibilities and hydration numbers.[22-24,27-31] The isentropic partial molar compressibility and partial molar volume values of the carbohydrates quantify their "compatibility" with the three-dimensional hydrogen-bond network of bulk-water as they are related to the size or volume the carbohydrate occupies upon hydration by water.[22-24] Hydration numbers predict the number of water molecules that are hydrogen-bonded to the carbohydrate. These parameters are related to the relative orientation of the hydroxyl groups on carbohydrate ring. In particular, the C2 and C4 hydroxyl groups were highly influential on hydration characteristics, and thus IRI activity.[21] For instance, D-talose has axial C2 and C4 hydroxyl groups and was the least hydrated monosaccharide assessed. It is also the most compatible monosaccharide with the three-dimension hydrogen-bonded network of bulk-water and thus disrupts this network the least and was the least IRI active monosaccharide. D-galactose has an equatorial C2 hydroxyl group and an axial C4 hydroxyl. This monosaccharide is more hydrated than other monosaccharides and thus has a poorer fit within bulk water. This results in a disordering of the hydrogen-bonded network of bulk-water, and thus a more effective inhibitor of ice recrystallization.

While disaccharides have approximately twice the hydration number of monosaccharides,[23] they were not twice as IRI active.[21] This was attributed to a difference in total steric volume between mono- and disaccharides. By representing the hydration of the substrate as a function of it size or volume occupied in solution, this can indicate the degree of hydration per molar volume of carbohydrate. This is referred to as the hydration index (HI) of the carbohydrate (hydration number divided by partial molar volume). The HI is useful for justifying why highly hydrated

monosaccharides exhibited similar IRI activity as highly hydrate disaccharides, despite hydration numbers of monosaccharides being half that of disaccharides (see section 1.3.3 for a more detailed discussion).

This discovery that carbohydrates can effectively inhibit ice recrystallization was the first report of its kind. Subsequent to this, carbohydrate derivatives such as *C*-allylated, *O*-allylated and *O*-methylated glycosides have also been explored as ice recrystallization inhibitors. However, all of these derivatives exhibited only moderate IRI activity and potently IRI active small molecules have not been identified.[21,32,33] To facilitate the design of potent small molecule ice recrystallization inhibitors, we sought to explore key motifs on carbohydrates in addition to the configuration of the C2- and C4-positions that were important for IRI activity. This included modifying and/or removing hydroxyl groups, in particular at the C6 position, to determine their influence on activity. Furthermore, we sought to examine how the addition of functional groups at the anomeric position altered IRI activity, with the overall goal to identify potently IRI active small molecules. Thus, this chapter will describe the following:

1. Considering carbohydrate hydration and IRI activity are affected by the configuration of the hydroxyl groups at the C2 and C4 positions, we sought to explore how other hydroxyl groups on carbohydrates affect activity. The importance of the C6 hydroxyl group and anomeric position (C1) for the IRI activity of simple monosaccharides and monosaccharide derivatives was explored. This included modifying these positions with various functional groups to examine their influence on activity compared to the parent monosaccharides. The results from these studies are discussed in sections 5.2.
2. Various di-, tri- and oligosaccharides and their derivatives were examined as ice recrystallization inhibitors. This would determine if a cooperative effect due to an increase in the number of carbohydrate residues could increase IRI activity. The results from these studies are discussed in section 5.3.

5.2 Elucidating Key Structural Features Necessary for IRI Activity in Simple Monosaccharides and Monosaccharide Derivatives

5.2.1 Monosaccharides and Derivatives with Modifications to the C6 and C1 Positions

It has been demonstrated that the hydration characteristics of simple monosaccharides is largely dictated by substituents at the C2 and C4 positions.[23] In addition, our laboratory has demonstrated that the IRI activity of these simple monosaccharides is influenced by the relative configuration of the hydroxyl groups at these positions.[21] To investigate the importance of other positions on monosaccharides for IRI activity, derivatives were prepared in which the C6 and C1

hydroxyl groups were modified with various functional groups. The monosaccharides that were the focus of this study were D-galactose and D-glucose as these were the two most IRI active monosaccharides.

We chose to modify the C6 position as previous work with AFGPs demonstrated that oxidation of both C6 hydroxyl groups on the native disaccharide resulted in a complete loss in TH activity.[34] This demonstrated the importance of these primary hydroxyl groups for TH activity; however, IRI activity was not assessed and thus it is unknown whether this position is important for this activity. Furthermore, Simons *et al*. have proposed that the strength of intramolecular hydrogen bond networks in the pyranose ring govern the hydration of carbohydrates and that the C6-OH group is an important position for the addition of water molecules to this network.[35-39] Using ultraviolet and infrared spectroscopy experiments along with density functional theory calculations the preferred conformation of phenyl-substituted glycosides and their hydrated complexes in the gas phase were determined.[35,36] It was proposed that water molecules are incorporated into the weakest intramolecular hydrogen bond within the intramolecular hydrogen bond network. This strengthens the hydrogen bond network and also results in a significant change in the preferred conformation of the carbohydrate. The first water molecules inserted into the intramolecular hydrogen bond networks of β-phenyl-D-galactopyranoside and β-phenyl-D-glucopyranoside occurred at the C6-OH. For galactose, water inserted between the C6-OH and the endocyclic ring oxygen, whereas it inserted between the C4-OH and C6-OH for glucose (figure 5.2).[35] Collectively these results suggest that the C6 position is influential for carbohydrate hydration and conformation, and thus may also be influential on IRI activity.

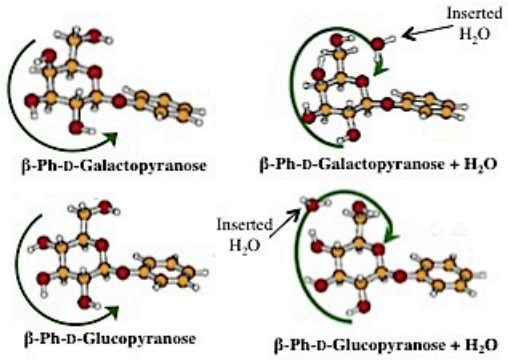

Figure 5.2 Lowest energy conformers calculated for β-phenyl-D-galactopyranoside and β-phenyl-D-glucopyranoside and their singly hydrated states determines by Simons *et al*.[35] The position of inserted water molecules is indicated for both carbohydrates. Green arrows indicate the direction of the intramolecular hydrogen bond network.

To examine the importance of the C6-OH group for the inhibition of ice recrystallization, several galactose and glucose derivatives possessing different functionality at C6 were prepared

and assessed for IRI activity (figure 5.3). This included commercially available monosaccharides, such as fucose, arabinose and xylose, which do not possess the C6 hydroxyl group (fucose) or the hydroxymethyl group (arabinose and xylose). We also examined the IRI activity of the commercially available 1,6-anhydrosugars for both galactose and glucose (**1** and **7**, respectively) and the C6-carboxylic acid derivatives galacturonic acid (**4**) and glucuronic acid (**5**). The anhydrosugars were interesting structures as not only was the C6 position modified, but the fused ring system forces a $^{1}C_{4}$ chair conformation of the pyranose, as opposed to the typical $^{4}C_{1}$ conformation of most pyranoses. Galactose derivatives **2**-**6** were also prepared, in which the C6-OH group was substituted with a methyl group (**2** and methylene-derivative **3**) or extended the hexopyranose by an extra carbon to the heptopyranose (6-deoxy derivative **5** and heptose **6**). The 6-deoxy-hetpoglucopyranose derivative **9** was also prepared to compare to galactose derivative **5**. Finally, we also assessed the IRI activity of inositols **10**-**12** (generously provided by Dr. Mark Nitz from the department of Chemistry at the University of Toronto) to examine the influence of the endocylic ring oxygen as well as the C6-OH.

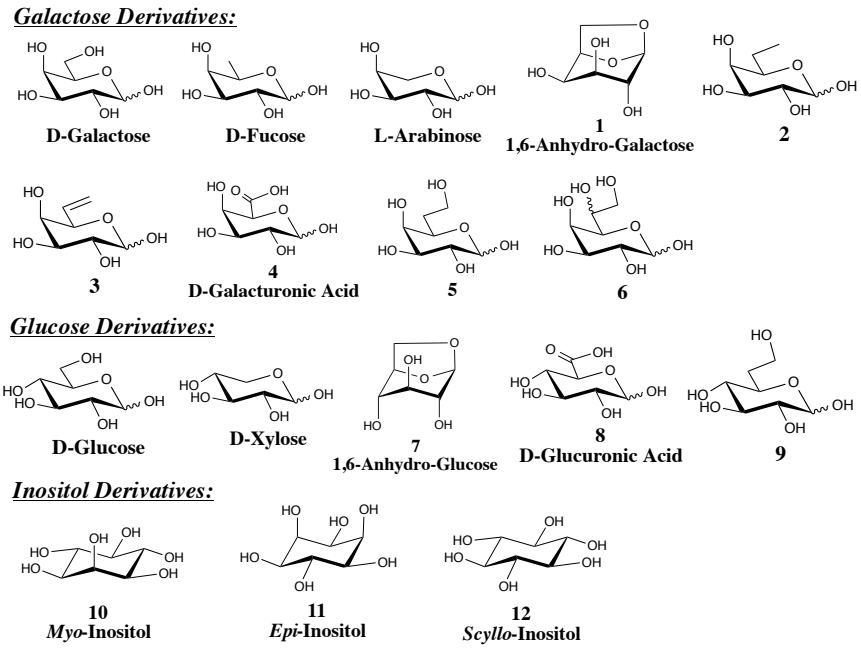

Figure 5.3 Structures of C6-modified monosaccharides, anhydrosugars and inositols assessed for IRI activity.

The preparation of the galactose derivatives **2**, **3**, **5** and **6** all begin with the common alkene intermediate **14**. This intermediate is prepared from D-galactose by protection of the 1,2 and 3,4 *cis*-hydroxyl groups as isopropylidene ketals, followed by Dess-Martin oxidation of the primary C6-hydroxyl group with Dess-Martin periodinane (DMP) and olefination using the Wittig

reaction with methyltriphenylphosphonium bromide (scheme 5.1a). Alkene derivative **3** was prepared from **14** by acidic hydrolysis of the isopropylidene ketals, and hydrogenation of **3** afforded galactose derivative **2** (scheme 5.1a). The 6-deoxyheptogalactopyranose (**5**) was prepared from **14** by hydroboration-oxidation to install the C7-OH group (**15**), followed by acid catalyzed hydrolysis of the isopropylidenes to afford compound **5** (scheme 5b).

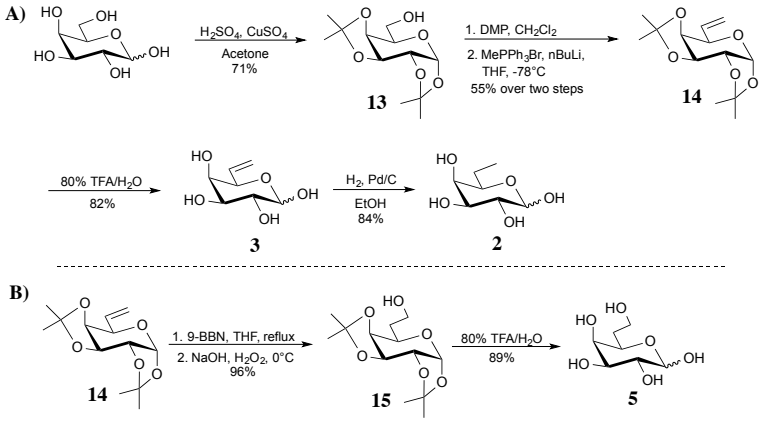

Scheme 5.1 Synthesis of galactose derivatives **2**, **3** and **5** from the common galactose intermediate **14**.

The heptogalactose **6** was prepared by dihydroxylation of the alkene on **14** to install the C6 and C7 hydroxyl groups (scheme 5.2). Depending upon the dihydroxylation conditions used, different diastereomeric ratios of **16a** (S-isomer at C6) and **16b** (R-isomer at C6) were obtained (table 5.1). Dihydroxylation using potassium osmate resulted in a 1:3.5 ratio of **16a**:**16b** (entry b).[40,41] The formation of **16b** is favoured over **16a** presumably due to steric hinderance from the axial C4 hydroxyl group, favouring the R-isomer at C6 rather than the S-isomer. Sharpless asymmetric dihydroxylation (AD) using AD-mix α increased the diastereomeric ratio of **16a**:**16b** to 1:6 (entry a).[42] Formation of the S-isomer at C6 (**16a**) could be favoured using Sharpless asymmetric dihydroxilation with AD-mix β to provide a ratio of **16a**:**16b** of 2:1 (entry c). The ratio of products **16a** and **16b** was determined by integration of the anomeric protons and each diastereomer was assigned based on previously published NMR spectra for these compounds.[41,43] Owing to the difficulty in separating **16a** and **16b** by standard flash chromatography, even with the addition of bulky hydroxyl protecting groups, such as silyl ether TBDMS (*t*-butyl-dimethylsilyl ether), the mixtures were deprotected by acidic hydrolysis of the isopropylidenes (scheme 5.2). Thus, different mixed ratios of products **6a** and **6b** were assessed for IRI activity.

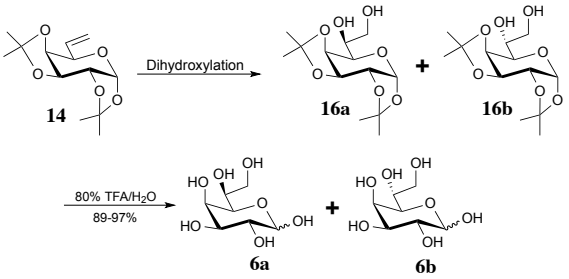

Scheme 5.2 Synthesis of heptogalactose derivatives **6a** and **6b** by asymmetric dihydroxylations of **14**

Table 5.1 Asymmetric dihydroxylation conditions to afford **16a** and **16b**.

Entry	Dihydroxylation Reaction Condition	Ratio **16a**:**16b**	Yield
a	AD-mix α 1:1 ^{t}BuOH/H_2O	1:6	72%
b	K_2OsO_4, NMO Acetone/H_2O	1:3.5	31%
c	AD-mix β 1:1 ^{t}BuOH/H_2O	2:1	70%

The synthesis of the 6-deoxyheptoglucose derivative **9** (scheme 5.3) began with β-D-glucosepentaacetate, which was glycosidated at the anomeric position with a *para*-methoxyphenyl group (compound **17**). Zemplén deacetylation followed by selective protection of the primary C6 hydroxyl group with TBDMS and benzylation of the C2, C3 and C4 hydroxyl groups afforded orthogonally protected glucose **19**. Removal of the TBDMS group with tetrabutylammonium fluoride (TBAF) furnished the primary C6 hydroxyl group (**20**) that was subjected to Dess-Martin oxidation with DMP and Wittig olefination to yield alkene intermediate **21**. Hydroboration-oxidation with 9-BBN was then utilized to install the C7 hydroxyl group of **22**. Removal of the C1 *para*-methoxyphenyl protecting group was achieved using ceric ammonium nitrate (CAN), followed by removal of the benzyl protecting groups by hydrogenation to provide product **9**.

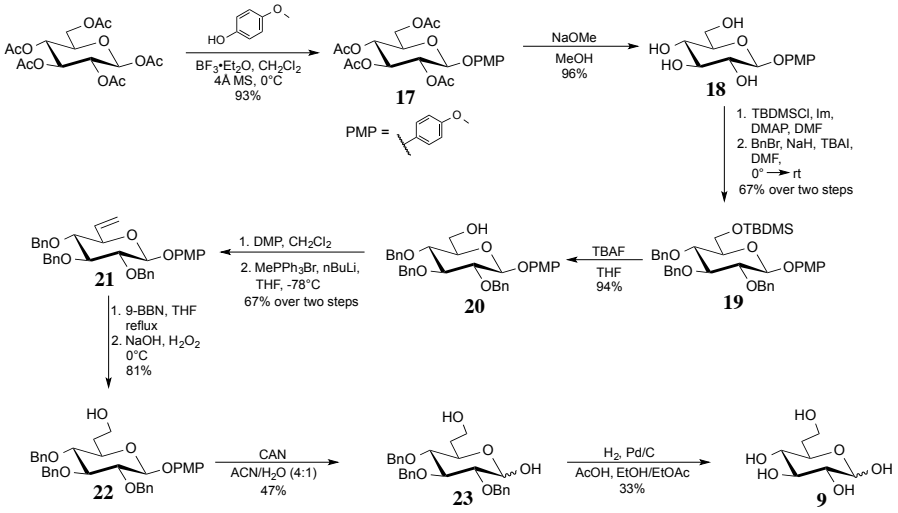

Scheme 5.3 Synthesis of 6-deoxyheptoglucopyranose derivative **9**.

In addition to the influence of the C6 position, we also sought to further explore the influence of the C1 position on the IRI activity of monosaccharides. Previously, our laboratory reported that

α-*carbon*-linked allyl glycosides (α-*C*-allyl glycosides) of galactose, glucose and mannose (**24**-**26**) exhibited similar IRI activity as the parent free-reducing sugars.[21] However, the β-*C*-allyl glycosides (**27**-**28**) had reduced IRI activity, suggesting that anomeric substituents and their relative configuration can impact IRI activity. To further investigate this, the IRI activity of simple C1 methylated galactosides, glucosides and mannosides, both α- and β-linked (**29**-**33**), were assessed to determine the influence of this position (figure 5.4). Methylated glycosides were selected as they are commercially available and have measured hydration parameters including hydration numbers and partial molar volumes.[23] Thus, the influence of carbohydrate hydration could also be further explored.

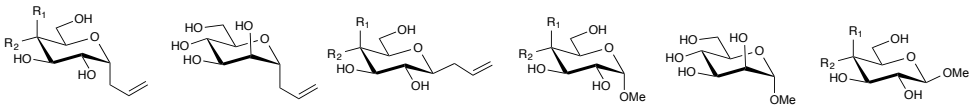

Figure 5.4 Structures of α- and β-linked *C*-allyl and *O*-methyl galactosides, glucosides and mannosides.

5.2.2 IRI Activity of C6-Modified Galactosides and Glucosides

The IRI activity of the C6-modified galactosides and glucosides is presented in figure 5.5. It is evident from this data that modifications to the C6 hydroxyl group of galactose are detrimental for activity, as all galactoside derivatives assessed had significantly reduced activity. Removal of the C6 hydroxyl and the hydroxymethyl group (D-fucose and L-arabinose, respectively) decreased the IRI activity of D-galactose from 64% MGS to 85-90% MGS. Linking the C6-OH to the C1 position also drastically reduced activity as evidenced by the fact that anhydrosugar **1** did not inhibit ice recrystallization. This suggests that fused ring system and the flip from a $^4C_1$ to $^1C_4$ chair conformation is unfavorable for activity. Alternatively, it could also indicate that a free hydroxyl group at C6 and a reducing sugar (C1 OH) is important. A more thorough examination is necessary. However, oxidizing the primary C6-OH (**4**), replacing it with a methyl (**2**) or introducing an alkene at C6-C7 (**3**) all reduced activity to approximately 85% MGS. This suggests that in anhydrosugar **1** the change to $^1C_4$ conformation may be the reason for the observed loss in IRI activity. Interestingly, reintroducing a hydroxyl group either at the C7 position (**5**) or at both the C6 and C7 position (diols **6a** and **6b**) did not restore IRI activity as these derivatives all resulted in approximately 80% MGS.

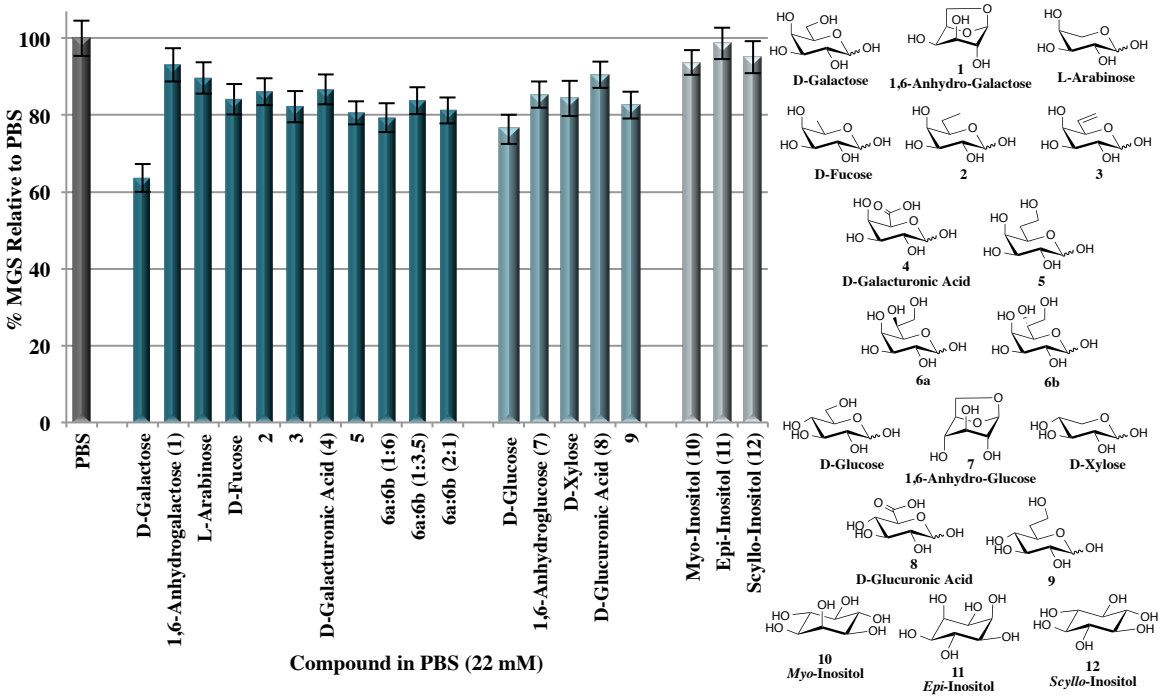

Figure 5.5 IRI activity of anhydrosugars **1** and **7**, C6-modified galactose and glucose derivatives **2-6** and **8-9** and inositols **10-12** at 22 mM in PBS. The % MGS (mean grain size) relative to a PBS positive control is shown for all compounds.

Similar results were also obtained when the C6 hydroxyl group of glucose was modified. Removing the hydroxymethyl group (D-xylose), oxidizing the C6-OH to the carboxylic acid (**8**), or introducing a one-carbon extension at the C6 position (heptose derivative **9**) all reduced IRI activity relative to D-glucose (figure 5.5). The glucose anhydrosugar (**7**) also exhibited decreased activity compared to D-glucose, and exhibited similar IRI activity as the galactose anhydrosugar **1**. Furthermore, all of the inositols assessed (myo-, epi- and scyllo-inositol, **10**-**12**) failed to inhibit ice recrystallization and had ice crystal sizes that were similar to the PBS control. This highlights the importance of both the C6-hydroxymethyl group and the endocyclic ring oxygen.

Collectively, these results underscore the importance of the C6 position for IRI activity because modification to this position resulted in a significant decrease in activity, especially for the galactose derivatives. Interestingly, all derivatives that were modified at this position, whether on galactose or glucose, inhibited ice recrystallization to similar extent with activity ranging from 83-93% (figure 5.5). The galactose and glucose hexopyranoses have hydration numbers of 8.7 and 8.4, respectively.[23] Arabinose and xylose, which are pentose analogues of galactose and glucose, have hydration numbers of 7.6 and 6.8, respectively. This decrease in hydration is attributed to the absence of the hydroxymethyl group.[23] Unfortunately, hydration parameters of the other C6-modified carbohydrate derivatives assessed in this study are not reported in the

literature. However, all of these derivatives had reduced IRI activity. These data suggests that in addition to the C2 and C4 position, both carbohydrate hydration and IRI activity are influenced by the C6 position of monosaccharides.

5.2.3 IRI Activity of C1-Modified Monosaccharides

As described earlier, carbohydrate hydration is largely dictated by the configuration of C2 and C4 positions of monosaccharides.[23] However, our laboratory reported that β-linked *C*-allyl glycosides were less IRI active than α-linked *C*-allyl glycosides, suggesting that substituents at the C1 position and the configuration of this position may also play a role in hydration and therefore IRI activity.[21] To further investigate this, a number of monosaccharides with known hydration parameters were assessed and correlated to IRI activity. In addition, *O*-methylated galactosides (previously tested by Jennifer Chaytor),[44] glucosides and mannosides both α- and β-linked at the C1-position (**29**-**33**), and 3-*O*-methyl-glucopyranoside (**34**), all with calculated hydration parameters were also assessed for IRI activity. These results are shown in figure 5.6.

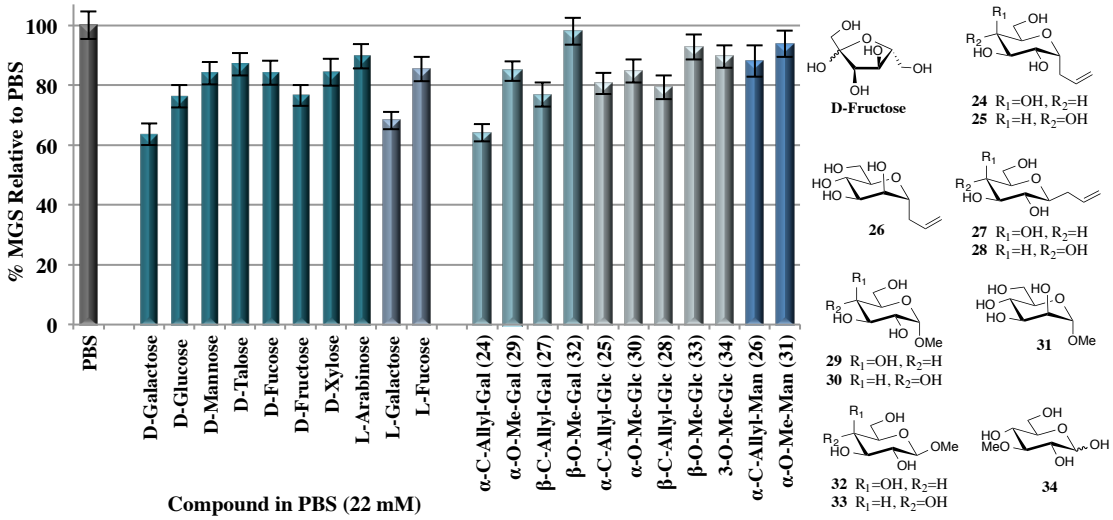

Figure 5.6 IRI activity of monosaccharides and derivatives *C*-allylated at the C1 position (**24**-**28**) or *O*-methylated at the C1 (**29**-**33**) or C3 (**34**) position at 22 mM in PBS. The % MGS (mean grain size) relative to a PBS positive control is shown for all compounds.

All monosaccharides as reducing sugars had reduced IRI activity compared to the most active monosaccharide D-galactose (figure 5.6). The ketofuranose D-fructose exhibited similar activity as the aldopyranose D-glucose, and as described previously, the pyranose-based aldo-pentoses D-xylose and L-arabinose were less IRI active than the parent monosaccharides D-glucose and D-galactose, respectively. Arabinose was assessed as the L-sugar, however the hydration parameters of all monosaccharides assessed by Galema and Høiland were D-sugars.[23] To determine if D- or L-

configuration affected IRI activity L-galactose and L-fucose were assessed for their ability to inhibit ice recrystallization. Both L-sugars had identical IRI activities to the corresponding D-sugars (p>0.3, two-tailed student's T-test), indicating that the enantiomers of the monosaccharides would also likely have similar hydration characteristics.

With the exception of the α-linked glucosides (*C*-Allyl-Glc **25** and *O*-Me-Glc **30**) all *O*-methylated glycosides exhibited less IRI activity than the *C*-allylated glycosides (figure 5.6). They were also significantly less active than the corresponding parent monosaccharides D-galactose, D-glucose or D-mannose. This was surprising as the methylated glycosides were more hydrated than the free-reducing monosaccharides. For instance, α- and β-*O*-Me-Gal (**29** and **32**) have hydration numbers of 9.4, whereas D-galactose has a hydration number of 8.7.[23] Furthermore, β-*O*-Me-Glc (**33**) has a higher hydration number (8.8) than D-glucose (8.4), while 3-*O*-Me-Glc (**34**) has a lower hydration number (8.1) than D-glucose. However, both **33** and **34** had similar IRI activity that was markedly decreased from D-glucose (figure 5.6). *O*-Methylation also significantly increases the partial molar volumes of the monosaccharide derivatives.[23] The IRI activity of carbohydrates was previously demonstrated to be influenced by hydration as a function of carbohydrate size/volume in solution (hydration index, section 5.1 and 1.3.3).[21] Thus, the activities of the monosaccharides assessed in this study were compared to the hydration index (HI, hydration number divided by partial molar volume) of the carbohydrates to determine their correlation (figure 5.7).

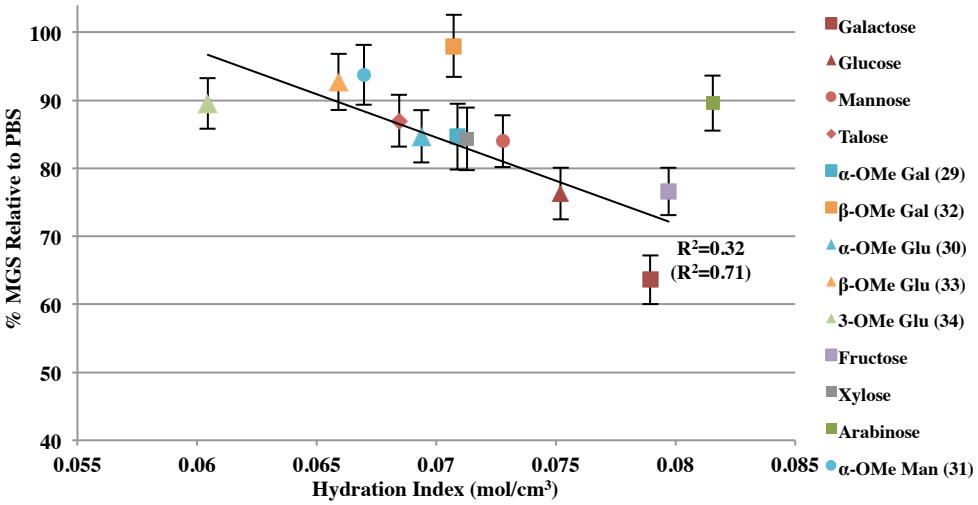

Figure 5.7 IRI activity of monosaccharides and *O*-methylated monosaccharides **29**-**34** correlated to their respective hydration indices (hydration number/partial molar volume) (mol/cm^3).[21,23] The R^2 (coefficient of determination) for the linear correlation of all monosaccharides was 0.32 and 0.71 when L-Arabinose and **32** were excluded from the linear series (indicated in parentheses).

As is evident from figure 5.7, there is a weak linear correlation between the hydration index of all of the monosaccharides assessed in this study and IRI activity (R^2= 0.32). Based on their hydration indices, both β-*O*-Me-Gal (**32**) and L-arabinose would be predicted to be significantly more IRI active than their actual measured activity. The activity of β-*O*-Me-Gal (**32**) would be similar to that exhibited by α-*O*-Me-Gal (**29**), whereas the activity of L-arabinose should be better than D-galactose. An exclusion of these two outliers results in a stronger linear correlation between hydration index and IRI (R^2= 0.71), similar to what our laboratory has reported previously with mono- and disaccharides.[21] Carbohydrate hydration is ultimately related to the ability of the sugar to disrupt or disorder bulk-water for it to "fit" into water's three-dimensional hydrogen bond network. Thus, overall this data still suggests that highly hydrated monosaccharides that have a poor fit and disorder bulk-water to a greater extent will have greater IRI activity. However, as this trend was not maintained for all monosaccharides with known hydration parameters, other factors in addition to hydration are also contributing to a molecule's ability to inhibit ice recrystallization. Hydration characteristics of monosaccharides are largely dictated by the C2 and C4 hydroxyl groups.[23] However, as described in section 5.2.2, the C6 position is highly influential on the IRI activity of monosaccharides. Thus, while hydration indices indicate that D-galactose and L-arabinose should have the same IRI activity, a plausible explanation for L-arabinose being a worse inhibitor could be the absence of the C6-hydroxymethyl group. Further studies are still required to determine the mechanism by which these carbohydrates are exhibiting ice recrystallization and the influence of other factors such as hydrogen-bond donation/acceptance ability of the hydroxyl groups and hydrophobic interactions of monosaccharide derivatives (discussed in more detail in chapter 6).

5.3 Di-, Tri- and Oligosaccharides as Ice Recrystallization Inhibitors

5.3.1 Methylated and Reducing Di-, Tri- and Oligosaccharide Derivatives

The most IRI active disaccharide assessed for IRI activity by our laboratory was melibiose (section 5.1 and 1.3.3).[21] This disaccharide is an α-D-galactosyl-(1-6)-D-glucopyranose (figure 5.8) and it is also the most highly hydrated disaccharide assessed by Galema and Høiland.[23] Melibiose contains a highly hydrated D-galactose moiety, and interestingly both melibiose and D-galactose exhibited identical IRI activities (64% MGS relative to the PBS control).[21] However, it also contains a less hydrated D-glucose moiety. In an effort to design more potently IRI active compounds, we sought to investigate if replacing the D-glucose unit with a D-galactose unit could increase the activity of melibiose. Thus, the disaccharide α-D-galactosyl-(1-6)-D-galactopyranose (**35**, figure 5.8) was prepared and assessed for its ability to inhibit ice recrystallization.

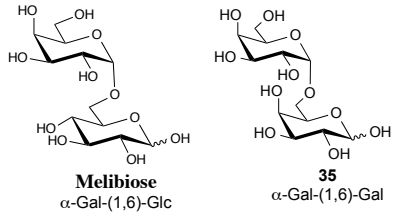

Figure 5.8 Structures of melibiose and disaccharide **35**.

Disaccharide **35** was prepared by glycosylation of galactosyl acceptor **13** (synthesis described in scheme 5.1a, section 5.2.1) with bromo-galactosyl donor **38**, which was prepared from methyl-α-D-galactopyranoside by benzylation, to afford intermediate **36**, followed removal of the anomeric methyl group by acidic hydrolysis to yield free-reducing galactoside **37** (scheme 5.4). Conversion of the anomeric hydroxyl to bromine was achieved using oxalyl bromide and catalytic DMF to give donor **38**. Glycosylation of **38** with galactosyl acceptor **13** in the presence of silver triflate afforded orthogonally protected disaccharide **39.** The β-anomer was favored over the α-anomer (α/β ratio of 1:1.7) with these glycosylation conditions despite the use of ether as solvent, which typically favours the formation of the α-anomer. The desired α-linked disaccharide was separated from the β-product by flash chromatography. Removal of the benzyl groups by hydrogenation followed by acidic hydrolysis of the isopropylidene ketals provided the desired α-Gal-(1,6)-Gal disaccharide **35**.

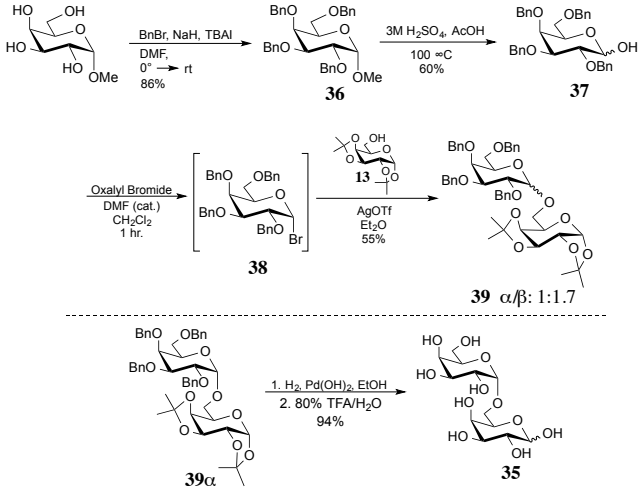

Scheme 5.4 Synthesis of α-linked disaccharide **35** from galactosyl donor **38** and acceptor **14**.

In addition to a derivative of melibiose, there was also interest in investigating β-(1,3)-linked di- and trisaccharide derivatives for IRI activity. This linkage is found in the native disaccharide β-D-galactosyl-(1-3)-α-*N*-acetyl-D-galactosamine (β-Gal-(1,3)-GalNAc) of potently IRI active AFGPs.[4,5,7,45-47] Balcerzak *et al*. in our laboratory demonstrated that an *O*-allylated derivative of

the native disaccharide with a β-(1,3)-glycosidic bond (**40**, figure 5.9) exhibits moderate IRI that is similar to melibiose.[33] Furthermore, it was demonstrated that replacing the C2-acetylated amine of this derivative with a C2 hydroxyl (**41**, figure 5.9) retained activity indicating that the C2-NAc group was not required for IRI activity. Both of these *O*-allylated disaccharides (**40** and **41**) were significantly more IRI active than the parent *O*-allylated monosaccharide **42** (figure 5.9). This suggested that glycosylation with highly hydrated monosaccharides may increase the IRI activity of weakly active carbohydrates. We therefore sought to explore disaccharides containing β-(1,3)-linkages to the IRI inactive monosaccharides β-*O*-Me-Gal (disaccharide **43**) or α-*O*-Me-Man (disaccharide **45**) to determine if the additional monosaccharide units could increase activity. Furthermore, trisaccharide derivatives **44** and **46** (figure 5.9) with β-(1,3)- and β-(1,6)-linkages were also assessed for their ability to inhibit ice recrystallization to determine if a cooperative effect with increasing monosaccharide units further increased and was beneficial for IRI activity.

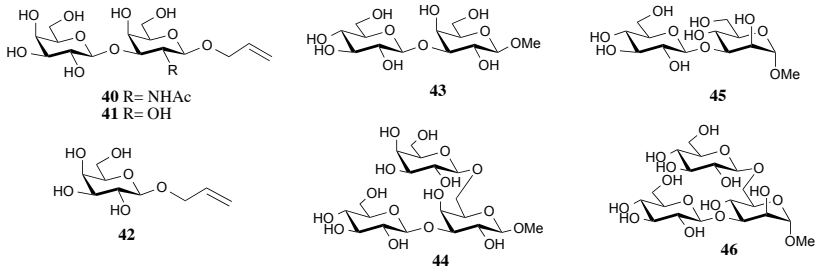

Figure 5.9 Structures of di- and trisaccharide derivatives containing β-(1,3)- and β-(1,6)-glycosidic bonds.

The di- and trisaccharide derivatives **43**-**46** were provided by Dr. Mark Taylor's laboratory in the Department of Chemistry at the University of Toronto. They were prepared by glycosylation conditions using regioselective activation of the equatorial hydroxyl group of *cis*-1,2-diols on glycosyl acceptors utilizing a diphenylborinic acid catalyst (**47**).[48-53] An example of this synthesis is provided in scheme 5.5. The *cis*-1,2-diol is activated by complexation with the organoboron catalyst to form a tetrahedral borinate intermediate.[49,50,53] Upon activation of the halogenated glycosyl donor, selective glycosylation with the more nucleophilic boron-bound oxygen occurs.[49] This is the equatorial O3 for galactose and mannose acceptors orthogonally protected at the primary C6 hydroxyl to form a β-1,3-linked disaccharide (for example, **48**). Subsequently, glycosylation can selectively occur at the C6-position upon desilylation and borinic acid catalyst-controlled glycosylation to form branched trisaccharides on both galactose and mannose cores (for example, **49**).[49,50] Deacetylation of the protected di- and trisaccharide intermediates then provided the desired products **43**-**46** to assess for IRI activity.

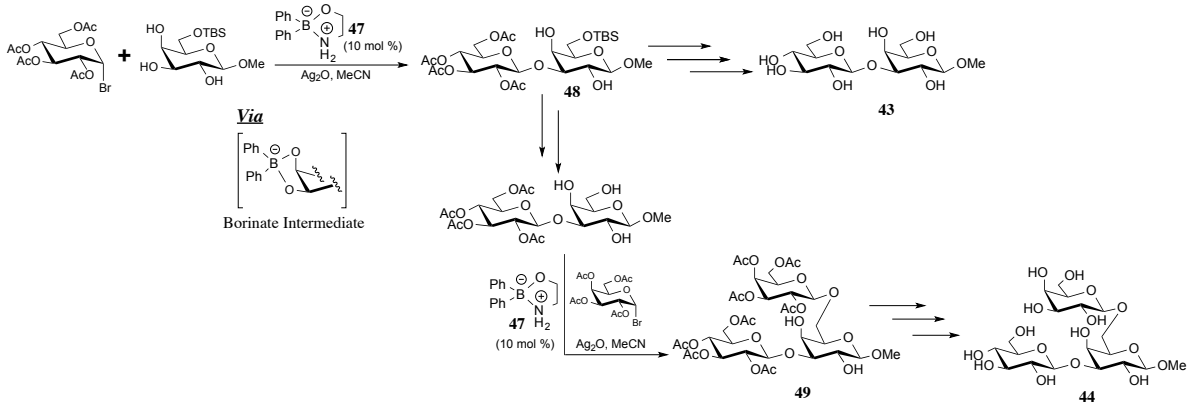

Scheme 5.5 General synthetic scheme for the preparation of β-1,3-linked disaccharides and β-1,3-/β-1,6-linked trisaccharides by Taylor *et al*.[49,50,53]

Finally, we also sought to explore various complex oligosaccharides for their ability to inhibit ice recrystallization. Although the hydration parameters for mono- and disaccharides have been reported in the literature,[22-24] those for oligosaccharides containing greater than two monosaccharide units have not been recorded. Hydration numbers are larger for disaccharides compared with monosaccharides.[23] Partial molar volumes are also significantly greater for disaccharides. However, the volume these disaccharides occupy in solution is dependent upon the type of glycosidic linkage (α or β) as well as the configuration of the carbons bearing the disaccharide hydroxyl groups.[23,54-57] Additionally, it has been proposed that cooperative inter-ring hydrogen-bonds in disaccharides create stronger intramolecular hydrogen bond networks compared to monosaccharides.[35,38,58,59] These inter-ring hydrogen-bond networks are also suggested to be dependent up the conformation of the disaccharide in solution, the glycosidic linkage and hydroxyl group positioning.[35,38,54-59] As such, we sought to investigate the ability of both linear and branched human milk oligosaccharides (**50**-**56**, figure 5.10) to inhibit ice recrystallization. The human milk oligosaccharides were generously provided by professor Hans H. Baer and contain a lactose-based core that is glycosylated with mono- and disaccharides including fucose and *N*-acetyl-lactosamine. Investigation of the IRI activity of oligosaccharides was pursued to determine if cooperative effects by increasing the number of monosaccharide units can increase activity resulting in more potently IRI active analogues.

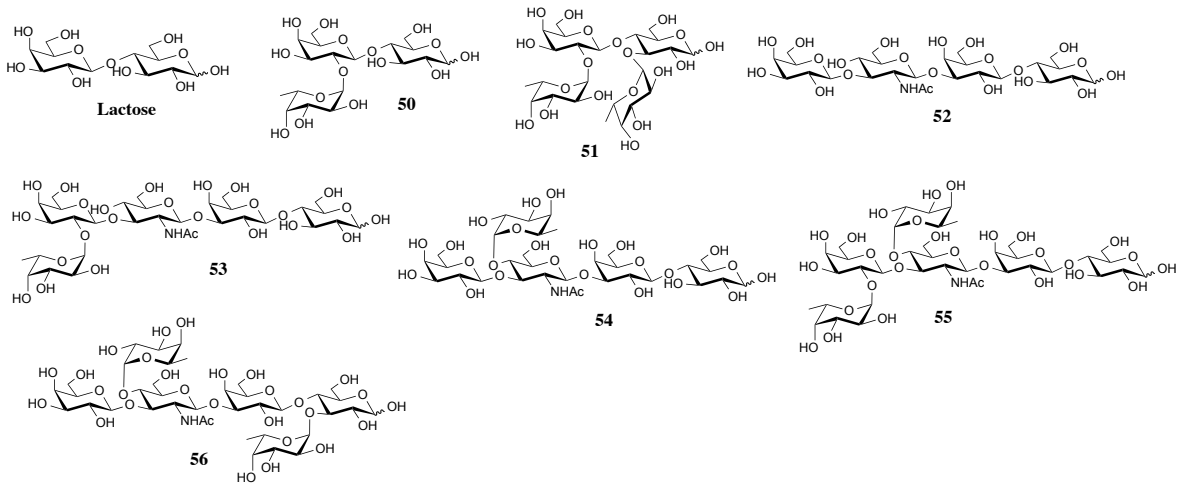

Figure 5.10 Structures of lactose and human milk oligosaccharides **50-56**.

5.3.2 IRI Activity of Di-, Tri- and Oligosaccharide Derivatives

The IRI activity of α-Gal-(1,6)-Gal (**35**) and methylated di- and trisaccharides **43**-**46** is presented in figure 5.11. Disaccharide **35** is an analogue of melibiose in which the less hydrated D-glucose moiety has been replaced with a more hydrated D-galactose moiety. Both melibiose and **35** exhibited identical IRI activity, and both had activity that was identical to the monosaccharide D-galactose (64% MGS relative to PBS). This suggests that the IRI activity of these 1,6-linked disaccharides may be dominated by the galactosyl-donor residue, and that the glycoside α-linked to this moiety has little effect on IRI activity. Interestingly, lactose is also a galactose-containing disaccharide where the galactosyl unit is β-linked to the C4 position of glucose. Lactose is less IRI active than melibiose with 72% MGS relative to PBS (figure 5.12). This may also indicate that the configuration of the glycosidic bond is also influential for the IRI activity of galactose-based disaccharides, a similar effect seen with *C*-allylated and *O*-methylated glycosides. However, further studies are required to determine the influence of anomeric configuration for the IRI activity of 1,6-linked disaccharides. Regardless, these results indicate that replacing the less hydrated glucose moiety of melibiose with a more hydrated galactose was not beneficial for activity and did not result in a more potently IRI active analogue suggesting that a cooperative effect for IRI is not occurring.

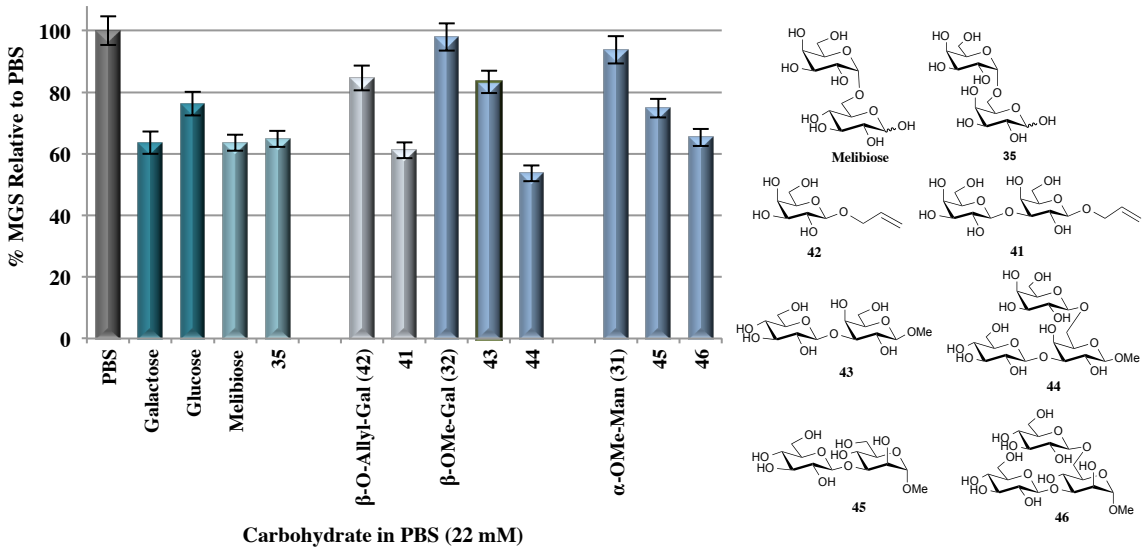

Figure 5.11 IRI activity of di- and trisaccharide derivatives **35** and **41**-**46** at 22 mM in PBS. The % MGS (mean grain size) relative to a PBS positive control is shown for all compounds.

As described earlier, glycosylation of a galactose unit to the weakly IRI active β-*O*-Allyl-Gal (**42**) significantly increased IRI activity (disaccharide **41**, figure 5.11).[33] The same trend was also observed for the β-*O*-Me-Gal and α-*O*-Me-Man containing di- and trisaccharides (**43**-**46**), where the addition of monosaccharide units increased activity. The installment of a glucose residue β-linked to the O3 of β-*O*-Me-Gal increased activity from 98% for the monosaccharide **32**, to 83% for the disaccharide **43** (figure 5.11). Similarly, the addition of a glucose residue β-linked to the O3 of α-*O*-Me-Man increased activity to 75% (for disaccharide **45**) from 94% (for monosaccharide **31**). Furthermore, both trisaccharide derivatives with glycosyl units β-linked at the O6 of the β-*O*-Me-Gal or the α-*O*-Me-Man residues (**44** and **46**) were more IRI active than their corresponding parent disaccharides (**43** and **45**, respectively). Thus, the addition of carbohydrate residues to weakly IRI active monosaccharide derivatives appears to be beneficial and increases the IRI activity of these analogues. Interestingly, the *O*-allylated and *O*-methylated disaccharides **41**, **43** and **45** all contain a β-1,3-glycosidic linkage similar to that found in the disaccharide of potently IRI active AFGPs. While these disaccharides are not conjugated to a peptide backbone, all exhibited only moderate to weak IRI activity that was similar to simple monosaccharides. This suggests that this glycosidic linkage may not be crucial for the IRI activity of small carbohydrate-based molecules.

Trisaccharide **44** is glycosylated at the C6 position with a β-galactosyl unit, whereas trisaccharide **46** is glycosylated at the same position with a β-glucosyl unit. Trisaccharide **44** resulted in 54% MGS (increased from 83% for disaccharide **43**) and **46** resulted in 65% MGS

(increased from 75% MGS for disaccharide **45**) (figure 5.11). Thus, the conjugation of a more highly hydrated galactose moiety resulted in a greater increase in IRI activity than a less hydrated glucose moiety. Another contributing factor to this difference in IRI activity may also be attributed to the core monosaccharide unit of the trisaccharides. Carbohydrate **44** is branched off of a core galactose moiety whereas **46** is branched off a core mannose moiety. It is suggested that cooperative inter-ring hydrogen-bond networks are influenced by the configuration of the carbons bearing hydroxyl groups.[35,38,54-59] Unfortunately, the relative strengths of the hydrogen bond networks of the di- and trisaccharides assessed in this study are not currently known. However, it is reasonable to suggest that the difference in relative orientation of the hydroxyl groups on these carbohydrates may also contribute to the difference in their exhibited IRI activity. Further studies are still required to determine the influence of glycosylation of monosaccharide moieties with different hydration characteristic to these core monosaccharide units on IRI activity. Preliminarily, this data suggests that glycosylation with a more hydrated galactose is more beneficial resulting in analogues with a higher degree of IRI activity.

To further investigate if increasing the number of monosaccharide units within an oligosaccharide resulted in more potent IRI activity, human milk oligosaccharides (**50**-**56**) were assessed for their ability to inhibit ice recrystallization (figure 5.12). These are linear and branched lactose-based oligosaccharides ranging from three to six monosaccharide residues. Both trisaccharide **50** and branched tetrasaccharide **51** had similar activity to lactose, indicating that the additional fucose units did not increase the ability to inhibit ice recrystallization. Oligosaccharides **52**-**56** were only slightly more IRI active than lactose and **50**-**51**, with the most potent analogue being branched hexasaccharide **56** (53% MGS relative to PBS). This hexasaccharide also had similar activity as *O*-methylated trisaccharide **44** (figure 5.11). These results highlight how increasing the number of monosaccharide residues in an oligosaccharide does not always result in more potent IRI activity. This may be attributed to the fact that these oligosaccharides contain fucose units, which are significantly less hydrated than both galactose and glucose. However, even glycosylation with additional galactose residues (oligosaccharides **52**-**54**) did not increase activity (figure 5.12). This result was surprising and was different from that obtained when galactose or glucose residues were glycosylated to disaccharides **43** and **45**, which increased activity (figure 5.11). It is currently not known how these oligosaccharides are inhibiting ice recrystallization or what structural features of these molecules are necessary for this activity. While increasing the number and type of monosaccharide units on oligosaccharides can effect the hydration of these carbohydrates, it is evident that simply increasing the number of residues on oligosaccharides does not result in potently active analogues. Furthermore, this

demonstrates that complex oligosaccharides are not an ideal class of compounds for effective ice recrystallization inhibitors.

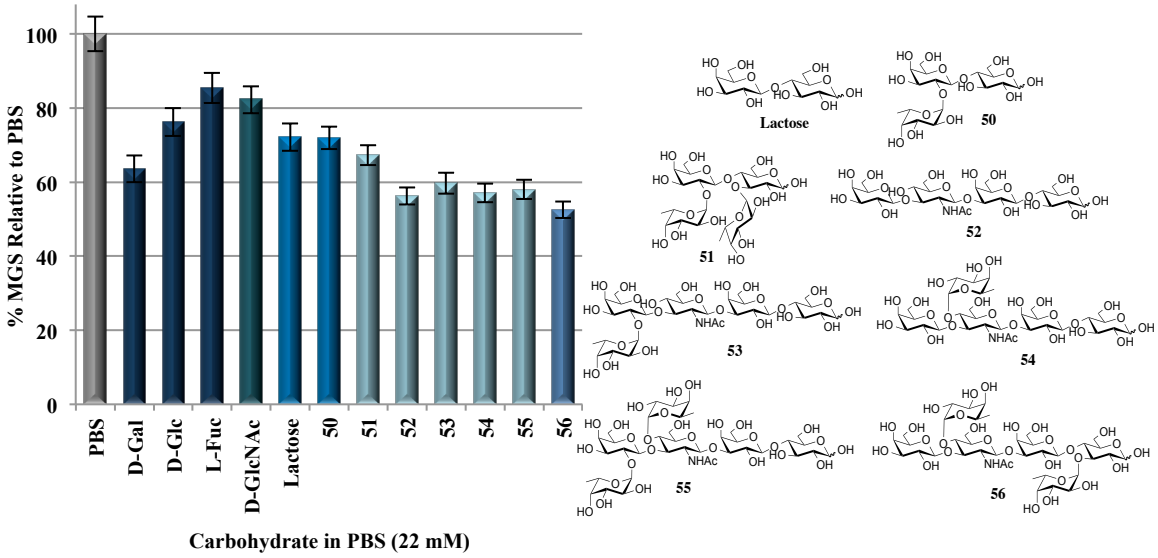

Figure 5.12 IRI activity of human milk oligosaccharides **50-56** at 22 mM in PBS. The % MGS (mean grain size) relative to a PBS positive control is shown for all compounds.

5.4 Summary and Conclusions for the IRI Activity of Simple Mono- and Disaccharides and Complex Oligosaccharides

From the IRI activity exhibited by simple mono- and disaccharides and their derivatives, a number of important structural features for IRI have been determined. It is evident that the C6 hydroxyl group of monosaccharides is influential for activity as all modifications to this position on both galactose and glucose resulted in less IRI active derivatives (section 5.2.2). Substituents at the C1 position and the configuration of this position are also important for IRI activity, and different substituents influence activity in different manners. α-*C*-allylated glycosides do not alter IRI activity compared to the parent free reducing sugars, whereas β-*C*-allylated and α/β-*O*-methylated glycosides exhibit reduced activity (section 5.2.2). Although it was found that the hydration characteristics (hydration numbers, partial molar volumes and hydration index) of monosaccharides and their derivatives is a very useful parameter for predicting IRI activity, not all monosaccharides fit well into this trend. In particular, β-*O*-Me-Gal and L-arabinose were significantly less IRI active than their calculated hydration indices predicted. This suggests that other contributing factors may influence the ability of a compound to inhibit ice recrystallization. Carbohydrate hydration did typically correlated to IRI activity indicating that the ability of a monosaccharide to disrupt or disorder the structure of bulk-water plays a key role in the inhibition of ice recrystallization.

The results from the di-, tri- and oligosaccharides assessed in this study indicate that increasing the number of monosaccharide residues does not necessarily result in more potent IRI activity. In some instances, glycosylation with more highly hydrated monosaccharide units was beneficial and increased activity (section 5.2.4). However, in other instances no effect was observed even when complex hexasaccharide derivatives were assessed. All of the carbohydrate derivatives (mono-, di- and oligosaccharides) assessed in this section exhibited only moderate activity. Many of these derivatives were as active as the simple monosaccharide D-galactose (64% MGS), with only a select few di- or trisaccharides being slightly more active with 54% MGS. Thus, overall these data suggests that these classes of compounds are not ideal as ice recrystallization inhibitors, because none of these carbohydrates had potent IRI activity. Regardless, this data does reveal structural features previously unknown that are important for the exhibited moderate IRI activity of carbohydrates.

5.5 Experimental Procedures and Compound Characterizations for Chapter 5

Ice Recrystallization Inhibition (IRI) Assay:

Sample analysis for IRI activity was performed using the "splat cooling" method as previously described.[1] In this method, the analyte was dissolved in phosphate buffered saline (PBS) solution and a 10 μL droplet of this solution was dropped from a micropipette through a two metre high plastic tube (10 cm in diameter) onto a block of polished aluminum precooled to approximately -80 °C. The droplet froze instantly on the polished aluminum block and was approximately 1 cm in diameter and 20 μm thick. This wafer was then carefully removed from the surface of the block and transferred to a cryostage held at -6.4 °C for annealing. After a period of 30 min, the wafer was photographed between crossed polarizing filters using a digital camera (Nikon CoolPix 5000) fitted to the microscope. A total of three images were taken from each wafer. During flash freezing, ice crystals spontaneously nucleated from the supercooled solution. These initial crystals were relatively homogeneous in size and quite small. During the annealing cycle, recrystallization occurred, resulting in a dramatic increase in ice crystal size. A quantitative measure of the difference in recrystallization inhibition of two compounds X and Y is the difference in the dynamics of the ice crystal size distribution. Image analysis of the ice wafers was performed using a novel domain recognition software (DRS) program.[60] This processing employed the Microsoft Windows Graphical User Interface to allow a user to visually demarcate and store the vertices of ice domains in a digital micrograph. The data were then used to calculate the domain areas. All data were plotted and analyzed using Microsoft Excel. The mean grain (or

ice crystal) size (MGS) of the sample was compared to the MGS of the control PBS solution for that same day of testing. IRI activity is reported as the percentage of the MGS (% MGS) relative to the PBS control, and the % MGS for each sample was plotted along with its standard error of the mean. Small percentages represent a small MGS (small ice crystals), which is indicative of high IRI activity.

General Experimental:

All anhydrous reactions were performed in flame-dried glassware under a positive pressure of dry argon. Air or moisture-sensitive reagents and anhydrous solvents were transferred with oven-dried syringes or cannulae. All flash chromatography was performed with E. Merck silica gel 60 (230-400 mesh). All solution phase reactions were monitored using analytical thin layer chromatography (TLC) with 0.2 mm pre-coated silica gel aluminum plates 60 F254 (E. Merck). Components were visualized by illumination with a short-wavelength (254 nm) ultra-violet light and/or staining (ceric ammonium molybdate, potassium permanganate, or phosphomolybdate stain solution). All solvents used for anhydrous reactions were distilled. Tetrahydrofuran (THF) and diethyl ether (Et_2O) were distilled from sodium/benzophenone under nitrogen. Dichloromethane (DCM) was distilled from calcium hydride. *N,N*-dimethylformamide (DMF) was stored over activated 4-Å molecular sieves under argon. ^1H (400 or 500 MHz) and ^{13}C NMR (100 or 125 MHz) spectra were recorded at ambient temperature on a Bruker Avance 400, Bruker Avance 500, or Varian Inova 500 spectrometer. Deuterated chloroform ($CDCl_3$) or water (D_2O) were used as NMR solvents, unless otherwise stated. Chemical shifts are reported in ppm using the solvent residual peak as an internal standard. Splitting patterns are designated as follows: s, singlet; d, doublet; t, triplet; q, quartet; quint, quintet; m, multiplet and br, broad. Low resolution mass spectrometry (LRMS) was performed on a Micromass Quatro-LC Electrospray spectrometer with a pump rate of 20 μL/min using electrospray ionization (ESI).

NMR spectra for novel compounds and final compounds assessed for IRI activity are provided. Compounds **1**, **4**, **7**, **8**, and **29**-**33** are commercially available carbohydrates. Inositols **10**-**12** were generously provided by Dr. Mark Nitz. *C*-Allylated derivatives **24**-**28** were previously reported by our laboratory.[21] *O*-Allylated derivatives were prepared as previously described by Anna Balcerzak.[33] Di- and trisaccharides **43**-**46** were generously provided by Dr. Mark Taylor.[49,50] Oligosaccharides **50**-**56** were generously provided by Dr. Hans Baer.

1,2:3,4-Di-*O*-iso-propylidene-α-D-Galactopyranose (13)

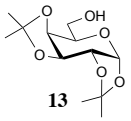
13

To a suspension of D-galactopyranose (2.0 g, 11 mmol) and anhydrous $CuSO_4$ (4.0 g, 50 mmol) in acetone (50 mL), concentrated H_2SO_4 (250 μL) was added. The mixture was stirred at room temperature for 40 h, filtered and washed with acetone. The filtrate was treated with saturated $NaHCO_3$ and then evaporated to a syrup. Purification of the crude syrup by column chromatography (3:2 hexanes/ethyl acetate) afforded **13** as a colourless syrup (2.02 g, 71%). Characterization data is consistent with those previously reported.[61] ^{1}H NMR (400 MHz, $CDCl_3$): δ 5.55 (d, *J* = 5.0 Hz, 1H), 4.59 (dd, *J* = 7.9, 2.4 Hz, 1H), 4.31 (dd, *J* = 5.0, 2.4 Hz, 1H), 4.25 (dd, *J* = 7.9, 1.6 Hz, 1H), 3.86-3.80 (m, 2H), 3.75-3.70 (m, 2H), 1.51 (s, 3H), 1.44 (s, 3H), 1.32 (s, 6H). ^{13}C NMR (100 MHz, $CDCl_3$): δ 109.4, 108.7, 96.3, 71.6, 70.7, 70.5, 68.1, 62.3, 26.0, 25.9, 24.9, 24.3. LRMS (ESI): *m/z* calcd. for $C_{12}H_{20}NaO_6$ $[M+Na]^+$ 283.3; found, 283.2.

6,7-Dideoxy-1,2:3,4-di-*O*-iso-propylidene-α-D-*galacto*-hept-6-enopyranose (14)

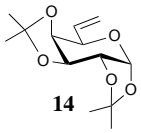
14

To a stirred suspension of **13** (250 mg, 0.96 mmol) in CH_2Cl_2 (5 mL) Dess-Martin periodinane (420 mg, 0.99 mmol) was added, and the reaction mixture was stirred at room temperature for 3 h. The reaction mixture was quenched with a 1:1 mixture of 1 M sodium thiosulfate/sat. $NaHCO_3$ until both organic and aqueous layers were clear. The solution was extracted with CH_2Cl_2, washed with saturated $NaHCO_3$, dried over $MgSO_4$ and concentrated. The crude aldehyde was then dissolved three times with toluene and the volatiles were evaporated to remove residual water as an azeotrope, prior to use in the subsequent reaction without further purification.

To a flame dried flask under argon, methyltriphenylphosphonium bromide (470 mg, 1.32 mmol) was dissolved in dry THF and cooled to -78°C. A 2.55 M solution of *n*-butyllithium (nBuLi) in THF (530 μL, 1.3 mmol) was added dropwise to this mixture which was stirred for 30 min at -78°C. The concentration of nBuLi was determined by titration with diphenylacetic acid (DPA) as described previously.[62] After stirring for 30 min at -78°C the reaction mixture was warmed slowly to 0°C and stirred for 1 h, and a solution of the crude aldehyde in dry THF (5 mL) was transferred dropwise to this solution at 0°C. The reaction was stirred overnight, slowly warming to room temperature over 2 h, quenched with saturated ammonium chloride, and extracted with hexanes. The mixture was subsequently washed with ammonium chloride, $NaHCO_3$, water and brine, then dried over $MgSO_4$ and concentrated. Column chromatography (19:1 hexanes/ethyl acetate) afforded **14** as a colourless syrup (141 mg, 57%). Characterization data is consistent with that previously reported.[63] ^{1}H NMR (400 MHz, $CDCl_3$): δ 5.93 (ddd, *J* =

17.3, 10.6, 6.0 Hz, 1H), 5.58 (d, *J* = 5.0 Hz, 1H), 5.37 (dt, *J* = 17.4, 1.5 Hz, 1H), 5.28 (dt, *J* = 10.6, 1.4 Hz, 1H), 4.62 (dd, *J* = 7.9, 2.4 Hz, 1H), 4.30 (ddd, *J* = 9.7, 5.5, 1.9 Hz, 2H), 4.22 (dd, *J* = 7.9, 2.0 Hz, 1H), 1.54 (s, 3H), 1.47 (s, 3H), 1.34 (s, 6H). ^{13}C NMR (101 MHz, $CDCl_3$): δ 133.9, 117.4, 109.2, 108.4, 96.4, 73.4, 70.8, 70.4, 69.0, 26.1, 25.9, 24.9, 24.3. LRMS (ESI): *m/z* calcd. for $C_{13}H_{20}NaO_5$ $[M+Na]^+$ 279.3; found, 279.2.

6,7-Dideoxy-D-*galacto*-hept-6-enopyranose (3)

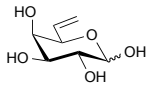

3

A solution of **14** (212 mg, 0.83 mmol) in 80% trifluoroacetic acid (5 mL) in water was stirred at room temperature for 1 h. The solvent was then evaporated and the crude product was dissolved three times with toluene and the volatiles were evaporated to remove residual water as an azeotrope**.** Column chromatography (4:1:1:1 EtOAc/ACN/MeOH/H_2O) afforded **3** as a white solid (120 mg, 82%). Characterization data is consistent with that previously reported.[64] ^{1}H NMR (400 MHz, D_2O): δ 5.91 (ddd, *J* = 17.4, 10.8, 5.7 Hz, 2H), 5.40-5.25 (m, 4H), 4.59 (d, *J* = 7.9 Hz, 1H, H1 β-anomer), 4.55 (d, *J* = 5.1 Hz, 1H, H1 α-anomer), 4.19 (dd, *J* = 5.7, 1.3 Hz, 1H), 3.94-3.87 (m, 4H), 3.79 (dd, *J* = 10.2, 3.9 Hz, 1H), 3.67 (dd, *J* = 9.9, 3.5 Hz, 1H), 3.47 (dd, *J* = 10.0, 7.9 Hz, 1H). ^{13}C NMR (101 MHz, MeOD): δ 136.9, 136.3, 117.1, 116.8, 98.7 (C1 β-anomer), 94.2 (C1 α-anomer), 77.1, 75.1, 73.7, 73.6, 73.0, 72.4, 71.3, 70.2. LRMS (ESI): *m/z* calcd. for $C_7H_{12}NaO_5$ $[M+Na]^+$ 199.2; found, 199.2.

6,7-Dideoxy-D-*galacto*-heptopyranose (2)

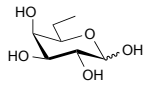

2

To a solution of **3** (45 mg, 0.26 mmol) in ethanol (5 mL) Pd/C (5 mol %) was added and the reaction mixture was purged three times with H_2. The mixture was stirred under H_2 atmosphere overnight, filtered over Celite® and the volatiles were evaporated to afford **2** as a white powder (38 mg, 84%). ^{1}H NMR (400 MHz, D_2O): δ 5.19 (d, *J* = 3.8 Hz, 1H, H1 α-anomer), 4.52 (d, *J* = 7.9 Hz, 1H, H1 β-anomer), 3.89-3.79 (m, 4H), 3.76 (d, *J* = 3.8 Hz, 1H), 3.59 (dd, *J* = 9.9, 3.5 Hz, 1H), 3.50 (t, *J* = 7.0 Hz, 1H), 3.44 (dd, *J* = 10.0, 7.9 Hz, 1H), 1.64-1.54 (m, 4H), 0.93-0.88 (m, 6H). ^{13}C NMR (101 MHz, D_2O): δ 96.3 (C1 β-anomer), 92.1 (C1 α-anomer), 76.3, 73.1, 71.9, 71.7, 70.1, 69.6, 69.4, 68.4, 22.9, 22.9, 9.3. LRMS (ESI): *m/z* calcd. for $C_7H_{14}NaO_5$ $[M+Na]^+$ 201.2; found, 201.2.

6-Deoxy-1,2:3,4-di-*O*-iso-propylidene-α-D-g*alacto*-heptopyranose (15)

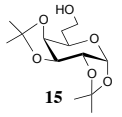

15

To a solution of **14** (150 mg, 0.59 mmol) in dry THF (10 mL) a solution of 9-BBN (6 mL of 0.5 M solution in THF, 3 mmol) was added. The resulting solution was heated

under reflux for 5 h., then cooled to room temperature, and then to 0°C and treated slowly with 10% NaOH (5 mL), followed by 35% H_2O_2 (5 mL). The resulting biphasic reaction mixture was stirred for 30 min and diluted with CH_2Cl_2. The aqueous layer was extracted with CH_2Cl_2 and combined organic layers were washed with 10% sodium metabisulfite, water, brine, then dried over $MgSO_4$, filtered and concentrated. Column chromatography (7:3 hexanes/ethyl acetate) afforded **15** as a colourless syrup (158 mg, 98%). Characterization data is consistent with those previously reported.[65,66] ^{1}H NMR (400 MHz, $CDCl_3$): δ 5.52 (d, *J* = 5.1 Hz, 1H), 4.60 (dd, *J* = 7.9, 2.4 Hz, 1H), 4.31 (dd, *J* = 5.1, 2.4 Hz, 1H), 4.14 (dd, *J* = 7.9, 1.8 Hz, 1H), 4.00 (ddd, *J* = 9.6, 3.8, 1.8 Hz, 1H), 3.83-3.74 (m, 2H), 2.01-1.95 (m, 1H), 1.75 (dddd, *J* = 14.5, 7.5, 4.9, 3.9 Hz, 1H), 1.53 (s, 3H), 1.46 (s, 3H), 1.35 (s, 3H), 1.33 (s, 3H). LRMS (ESI): *m/z* calcd. for $C_{13}H_{22}NaO_6$ $[M+Na]^+$ 297.3; found, 297.2.

6-Deoxy-D-*galacto*-heptopyranose (5)

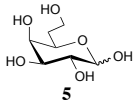

5

A solution of **15** (158 mg, 0.58 mmol) in 80% trifluoroacetic acid (5 mL) in water was stirred at room temperature for 1 h. Volatiles were evaporated and the crude product was dissolved three times with toluene and the volatiles were evaporated to remove residual water as an azeotrope**.** Column chromatography (4:1:1:1 EtOAc/ACN/MeOH/H_2O) afforded **5** as a white solid (99 mg, 89%). Characterization data is consistent with that previously reported.[65,66] ^{1}H NMR (400 MHz, D_2O): δ 5.20 (d, *J* = 3.7 Hz, 1H, H1 α-anomer), 4.54 (d, *J* = 7.9 Hz, 1H, H1 β-anomer), 4.14 (dd, *J* = 8.7, 5.2 Hz, 1H), 3.85 (dt, *J* = 8.4, 2.9 Hz, 1H), 3.79-3.62 (m, 9H), 3.45 (dd, *J* = 10.0, 7.9 Hz, 1H), 1.95-1.74 (m, 4H). ^{13}C NMR (126 MHz, D_2O): δ 96.3, 92.1, 72.9, 71.7, 71.4, 71.0, 70.5, 69.2, 68.2, 67.0, 58.2, 58.0, 32.5. LRMS (ESI): *m/z* calcd. for $C_7H_{14}NaO_6$ $[M+Na]^+$ 217.2; found, 217.1.

1,2:3,4-di-*O*-iso-propylidene- L/D-*glycero*-α-D-*galacto*-heptopyranose (16a and 16b)

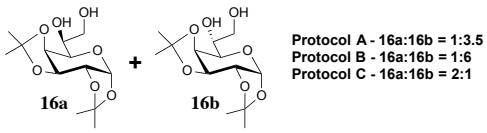

Protocol A: To a stirred solution of **14** (50 mg, 0.20 mmol) and *N*-methylmorpholine *N*-oxide (NMO) in an 8:1 acetone/water solution (2 mL) at 0°C was added potassium osmate (3 mg, 0.01 mmol), warmed slowly to room temperature and stirred for 6 h. The mixture was then diluted with ethyl acetate and water, extracted, and the organic phase was stirred with saturated sodium bisulfite for 1 h. The organic layer was then separated, washed with brine until the layer was

clear, dried over $MgSO_4$ and concentrated. Column chromatography (3:2 hexanes/ethyl acetate) afforded a mitxture of **16a** and **16b** (1:3.5) as a colourless syrup (17 mg, 31%).

Protocol B: Sharpless asymmetric dihydroxylation was conducted with AD-mix α as described previously.[42] To a stirred solution of AD-mix α (574 mg) in a 1:1 ^{t}BuOH/water solution (4 mL) at 0°C was added **14** (105 mg, 0.41 mmol). The reaction was slowly warmed to room temperature and stirred overnight. The reaction mixture was then cooled to 0°C. Sodium sulfite (574 mg) was added to the mixture, which was stirred for 30 min. The mixture was extracted with ethyl acetate and the organic phase was dried over $MgSO_4$ and concentrated. Column chromatography over a gradient (7:3 then 3:7 hexanes/ethyl acetate) afforded a mixture of **16a** and **16b** (1:6) as a colourless syrup (86 mg, 72%).

Protocol C: Sharpless asymmetric dihydroxylation was conducted similar to "protocol B" with AD-mix β, as described previously.[42] Column chromatography over a gradient (7:3 then 3:7 hexanes/ethyl acetate) afforded a mixture of **16a** and **16b** (2:1) as a colourless syrup (60 mg, 70%).

Characterization data from products **16a and 16b** obtained from all protocols were consistent with that previously reported.[43,67] ^{1}H NMR (400 MHz, $CDCl_3$): δ 5.59 (d, *J* = 5.0 Hz, 1H, H1-**16a**), 5.52 (d, *J* = 5.0 Hz, 1H, H1-**16b**), 4.63 (ddd, *J* = 9.4, 8.0, 2.4 Hz, 2H), 4.45 (dd, *J* = 8.0, 1.9 Hz, 1H), 4.34 (qd, *J* = 4.5, 2.3 Hz, 3H), 3.97 (dt, *J* = 6.0, 4.4 Hz, 1H), 3.87 (dd, *J* = 6.0, 1.7 Hz, 2H), 3.82-3.73 (m, 5H), 1.52 (s, 6H), 1.47 (s, 6H), 1.34 (s, 12H). ^{13}C NMR (101 MHz, $CDCl_3$): δ 109.6, 109.4, 108.9, 108.8, 96.4 (C1-**16a**), 96.3 (C1-**16b**), 71.7, 71.2, 70.9, 70.9, 70.7, 70.6, 70.6, 70.4, 67.4, 67.4, 64.0, 62.4, 26.0, 26.0, 26.0, 25.9, 25.0, 24.4, 24.2. LRMS (ESI): *m/z* calcd. for $C_{13}H_{22}NaO_7$ $[M+Na]^+$ 313.3; found, 313.2.

L/D-*Glycero*-D-*galacto*-heptopyranose (6a + 6b)

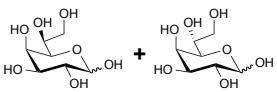

6a **6b**

A solution of the **16a/16b** mixture (57 mg, 0.20 mmol) in 80% trifluoroacetic acid (5 mL) in water was stirred at room temperature for 1 h. The solvent was then evaporated and the crude product was dissolved three times with toluene and the volatiles were evaporated to remove residual water as an azeotrope. Column chromatography (4:1:1:1 EtOAc/ACN/MeOH/H_2O) afforded the **6a/6b** mixture as white solid (40 mg, 97%). ^{1}H NMR (400 MHz, D_2O): δ 5.26 (d, *J* = 2.6 Hz, 1H, H1 α-anomer), 5.21 (d, *J* = 3.5 Hz, 1H, H1 α-anomer), 4.54 (d, *J* = 7.9, 1H, H1 β-anomer), 4.54 (d, *J* = 7.9, 1H, H1 β-anomer), 4.12 (dd, *J* = 2.9, 0.7 Hz, 1H), 4.06 (dd, *J* = 3.3, 0.8 Hz, 1H), 3.98-3.96 (m, 2H), 3.93-3.75 (m, 10H), 3.72 (t, *J* = 3.3 Hz, 2H), 3.67-3.56 (m, 8H), 3.52-3.45 (m, 4H). ^{13}C

NMR (101 MHz, D_2O): δ 96.6, 96.5, 75.0, 73.5, 73.0, 72.9, 71.8, 71.8, 71.18, 71.0, 70.1, 69.7, 69.4, 69.2, 69.1, 68.7, 68.3, 68.2, 67.7, 62.8, 61.9, 61.8. LRMS (ESI): *m/z* calcd. for $C_7H_{14}NaO_7$ $[M+Na]^+$ 233.1; found, 233.0.

***para*-Methoxyphenyl-2,3,4-tri-*O*-benzyl-6-*O*-*tert*-butyldimethylsilyl-β-D-glucopyranoside (19)**

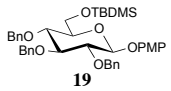

19

To a mixture of **18** (6.71 g, 23.4 mmol) (β-PMP-Glc, preparation and characterization described in chapter 7) in dry DMF (50 mL) under argon *tert*-butyldimethylsilyl chloride (4.24 g, 28.1 mmol), 4-dimethylaminopyridine (286 mg, 2.34 mmol) and imidazole (3.51 g, 51.5 mmol) were added. The reaction mixture was stirred overnight, then evaporated to a syrup that was dissolved in ethyl acetate and washed with 10% HCl, saturated $NaHCO_3$, water and brine, dried over $MgSO_4$ and concentrated. The crude silylated product was dissolved in 10 mL of dry DMF and added dropwise over 30 min to a mixture of 66% sodium hydride (2.46 g, 61.8 mmol), benzyl bromide (10 mL, 84.2 mmol) and tetrabutylammonium iodide (692 mg, 1.87 mmol) stirring at 0°C under argon. The reaction mixture was slowly warmed to room temperature and stirred overnight. The reaction was quenched with brine, then diluted with ethyl acetate and extracted. The aqueous layer was washed twice with ethyl acetate, and the combined organic extracts were dried over $MgSO_4$ and concentrated. Column chromatography (9:1 hexanes/ethyl acetate) afforded **19** as a white solid (10.4 g, 83%). ^{1}H NMR (300 MHz, $CDCl_3$): δ 7.39-7.30 (m, 15H), 7.07-7.02 (m, 2H), 6.85-6.79 (m, 2H), 5.06 (d, *J* = 10.9 Hz, 1H), 4.94 (d, *J* = 10.8 Hz, 1H), 4.89-4.81 (m, 4H), 4.68 (d, *J* = 10.9 Hz, 1H), 3.88 (dd, *J* = 11.3, 1.8 Hz, 1H), 3.80-3.74 (m, 1H), 3.78 (s, 3H) 3.72-3.62 (m, 3H), 3.39 (ddd, *J* = 9.3, 4.9, 1.8 Hz, 1H), 0.90 (s, 9H), 0.05 (d, *J* = 9.5 Hz, 6H). ^{13}C NMR (76 MHz, $CDCl_3$): δ 151.6, 138.5, 138.4, 138.2, 128.4, 128.4, 128.1, 128.0, 128.0, 127.8, 127.7, 127.7, 118.7, 114.5, 103.0, 84.7, 82.3, 77.5, 76.1, 75.9, 75.0, 62.3, 55.6, 25.9, 18.3, -5.1, -5.4. LRMS (ESI): *m/z* calcd. for $C_{40}H_{54}NO_7Si$ $[M+NH_4]^+$ 688.4; found, 688.3.

***para*-Methoxyphenyl-2,3,4-tri-*O*-Benzyl-β-D-glucopyranoside (20)**

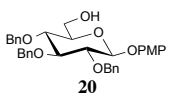

20

To a solution of **19** (10.4 g, 15.5 mmol) in dry THF under argon tetrabutylammonium fluoride (8.1 g, 30.9 mmol) was added. The reaction mixture was stirred overnight at room temperature, diluted with ethyl acetate and extracted. The organic phase was washed with brine, dried over $MgSO_4$, and concentrated. Recrystallization with hot chloroform and hexanes afforded **20** as a white solid (8.1 g, 94%). Characterization data is consistent with that previously reported.[68] ^{1}H NMR (300 MHz, $CDCl_3$): δ

7.35-7.28 (m, 15H), 7.00-6.96 (m, 2H), 6.86-6.82 (m, 2H), 5.03 (d, *J* = 10.9 Hz, 1H), 4.97-4.95 (m, 2H), 4.90-4.80 (m, 3H), 4.66 (d, *J* = 10.9 Hz, 1H), 3.89 (ddd, *J* = 12.0, 6.1, 2.6 Hz, 1H), 3.77 (s, 3H), 3.75-3.62 (m, 4H), 3.47 (ddd, *J* = 9.6, 4.5, 2.6 Hz, 1H), 1.87 (t, *J* = 6.9, 1H). ^{13}C NMR (101 MHz, $CDCl_3$): δ 155.4, 151.2, 138.4, 138.1, 137.9, 128.5, 128.4, 128.2, 128.1, 128.0, 127.9, 127.8, 127.7, 118.1, 114.7, 102.5, 84.4, 82.1, 75.7, 75.3, 75.1, 75.1, 62.0, 55.6. LRMS (ESI): *m/z* calcd. for $C_{34}H_{40}NO_7$ $[M+NH_4]^+$ 574.8; found, 574.2.

***para*-Methoxyphenyl-6,7-dideoxy-2,3,4-tri-*O*-benzyl-β-D-*gluco*-hept-6-enopyranose (21)**

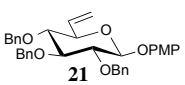

21

To a stirred suspension of **20** (1.6 g, 2.87 mmol) in CH_2Cl_2 (15 mL) was added Dess-Martin periodinane (1.46 g, 3.45 mmol) and the reaction mixture was stirred at room temperature for 3 h. The reaction mixture was quenched with a 1:1 mixture of 1 M sodium thiosulfate/sat. $NaHCO_3$ until both organic and aqueous layers were clear. The solution was extracted with CH_2Cl_2, washed with saturated $NaHCO_3$, dried over $MgSO_4$ and concentrated. The crude aldehyde dissolved three times with toluene and the volatiles were evaporated to remove residual water as an azeotrope and used in the subsequent reaction without further purification.

To a flame dried flask under argon, methyltriphenylphosphonium bromide (1.54 g, 4.31 mmol) was dissolved in dry THF (50 mL) and cooled to -78°C. A 2.55 M solution of *n*-butyllithium (nBuLi) in THF (1.67 mL, 4.31 mmol) was added dropwise to this mixture and stirred for 30 min at -78°C. The concentration of *n*BuLi was determined by titration with diphenylacetic acid (DPA) as described previously.[62] After stirring for 30 min at -78°C the reaction mixture was warmed slowly to 0°C and stirred for 1 h, and a solution of the crude aldehyde in dry THF (10 mL) was transferred dropwise to this solution at 0°C. The reaction was stirred overnight, slowly warming to room temperature, and then was quenched with saturated ammonium chloride, extracted with hexanes. The mixture was subsequently washed with ammonium chloride, $NaHCO_3$, water and brine, then dried over $MgSO_4$ and concentrated. Column chromatography (19:1 hexanes/ethyl acetate) afforded **21** as a white solid (1.03 g, 65%). ^{1}H NMR (400 MHz, C_6D_6): δ 7.42-7.35 (m, 4H), 7.28-7.26 (m, 2H), 7.20-7.08 (m, 11H), 6.72-6.68 (m, 2H), 5.99 (ddd, *J* = 17.3, 10.7, 5.3 Hz, 1H), 5.50 (dt, *J* = 17.2, 1.6 Hz, 1H), 5.14 (d, *J* = 11.4 Hz, 1H), 5.12-5.08 (m, 1H), 5.00 (d, *J* = 11.4 Hz, 1H), 4.92 (d, *J* = 7.7 Hz, 1H), 4.86 (d, *J* = 11.4 Hz, 2H), 4.74 (d, *J* = 11.3 Hz, 1H), 4.50 (d, *J* = 11.2 Hz, 1H), 3.82 (dd, *J* = 9.1, 7.8 Hz, 1H), 3.68 (t, *J* = 9.0 Hz, 2H), 3.33 (t, *J* = 9.3 Hz, 1H), 3.28 (s, 3H). ^{13}C NMR (76 MHz, C_6D_6): δ 156.0, 152.2, 139.5, 139.3, 139.0, 135.1, 128.6, 128.5, 128.5, 128.0, 127.8, 119.1, 117.1, 115.0,

103.5, 84.6, 82.6, 82.5, 75.6, 75.6, 75.1, 75.1, 55.2. LRMS (ESI): *m/z* calcd. for $C_{35}H_{36}NaO_6$ $[M+Na]^+$ 575.7; found, 575.5.

para-Methoxyphenyl-6-deoxy-2,3,4-tri-_O_-benzyl-β-D-_gluco_-heptopyranose (22)

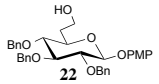

22

To a solution of **21** (267 mg, 0.48 mmol) in dry THF (10 mL), a solution of 9-BBN (4.8 mL of 0.5 M solution in THF, 2.4 mmol) was added. The resulting solution was heated under reflux for 5 h., cooled to room temperature, and then to 0°C and treated slowly with 10% NaOH (5 mL), followed by 35% H_2O_2 (5 mL). The resulting biphasic reaction mixture was stirred for 30 min then diluted with CH_2Cl_2. The aqueous layer was then extracted with CH_2Cl_2 and combined organic layers were washed with 10% sodium metabisulfite, water, brine, then dried over $MgSO_4$, filtered and concentrated. Column chromatography (7:3 hexanes/ethyl acetate) afforded **22** as a white solid (223 mg, 81%). ^{1}H NMR (300 MHz, C_6D_6): δ 7.41-7.34 (m, 4H), 7.27-7.18 (m, 4H), 7.14-7.04 (m, 6H), 6.79-6.73 (m, 2H), 5.13 (d, *J* = 11.3 Hz, 1H), 5.03 (d, *J* = 11.4 Hz, 1H), 4.85 (td, *J* = 10.7, 7.4 Hz, 4H), 4.46 (d, *J* = 11.4 Hz, 1H), 3.80 (dd, *J* = 9.1, 7.8 Hz, 1H), 3.64 (dt, *J* = 15.4, 7.3 Hz, 2H), 3.56-3.48 (m, 1H), 3.45-3.38 (m, 1H), 3.28 (dt, *J* = 5.7, 3.6 Hz, 1H), 3.29 (s, 3H) 1.96 (dddd, *J* = 13.9, 8.2, 5.4, 2.5 Hz, 1H), 1.62-1.51 (m, 1H), 1.22 (dd, *J* = 6.2, 4.3 Hz, 1H). ^{13}C NMR (76 MHz, C_6D_6): δ 156.0, 151.9, 139.5, 139.2, 139.1, 128.6, 128.6, 128.1, 127.9, 127.9, 118.7, 115.1, 103.0, 84.9, 82.6, 81.8, 75.6, 75.1, 75.0, 73.6, 59.8, 55.2, 36.7, 34.7. LRMS (ESI): *m/z* calcd. for $C_{35}H_{34}NO_7$ $[M+NH_4]^+$ 588.8; found, 588.2.

6-deoxy-2,3,4-tri-_O_-benzyl-β-D-_Gluco_-heptopyranose (23)

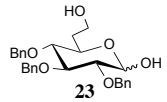

23

To a solution of **22** (50 mg, 0.088 mmol) in 4:1 ACN/water (2 mL) cooled to 0°C, ceric ammonium nitrate (120 mg, 0.22 mmol) was added. The reaction was warmed slowly to room temperature and stirred overnight. The mixture was then was diluted with CH_2Cl_2, extracted and the organic layer was washed with saturated $NaHCO_3$, water, brine, dried over $MgSO_4$ and concentrated. Column chromatography (2:3 hexanes/ethyl acetate) afforded **23** as a white solid (19 mg, 47%). ^{1}H NMR (300 MHz, $CDCl_3$): δ 7.37-7.27 (m, 30H), 5.14 (d, *J* = 3.6 Hz, 1H), 4.93 (m, 4H), 4.83 (d, *J* = 10.9 Hz, 1H), 4.79-4.68 (m, 4H), 4.62 (d, *J* = 11.0 Hz, 2H), 4.09 (td, *J* = 9.7, 2.8 Hz, 1H), 3.96 (t, *J* = 9.2 Hz, 1H), 3.78-3.71 (m, 4H), 3.65 (t, *J* = 9.1 Hz, 1H), 3.56-3.51 (m, 2H), 3.40-3.30 (m, 1H), 3.25 (t, *J* = 9.4 Hz, 1H), 2.07 (ddt, *J* = 12.9, 4.8, 4.0 Hz, 2H), 1.73-1.59 (m, 2H), 1.32-1.29 (m, 1H), 0.94-0.84 (m, 1H). ^{13}C NMR (101 MHz, $CDCl_3$): δ 138.5, 138.4, 138.3, 138.0, 137.9, 137.8, 128.5, 128.5, 128.4, 128.4, 128.4, 128.1, 128.0, 128.0,

127.9, 127.9, 127.8, 127.7, 127.7, 97.5, 97.5, 90.9, 90.9, 84.5, 83.2, 83.2, 81.5, 81.5, 81.5, 81.5, 81.4, 81.3, 80.2, 80.1, 75.7, 75.7, 75.2, 74.8, 74.5, 73.2, 70.1, 60.8, 60.7, 33.7, 33.6. LRMS (ESI): *m/z* calcd. for $C_{28}H_{36}NO_6$ $[M+NH_4]^+$ 482.6; found, 482.5.

6-deoxy-D-*gluco*-heptopyranose (9)

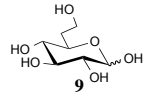

9

To a solution of **23** (35 mg, 0.075 mmol) in a 1:7:2 acetic acid/EtOH/EtOAc mixture (5 mL) was added Pd/C (5 mol %) and the reaction mixture was purged three times with H_2. The mixture was stirred under H_2 atmosphere overnight, filtered over Celite and the solvent was evaporated. Column chromatography (4:1:1:1 EtOAc/ACN/MeOH/H_2O) afforded **9** as a white powder (8 mg, 33%)**.** Characterization data is consistent with that previously reported.[66] ^{1}H NMR (400 MHz, D_2O): δ 5.17 (d, *J* = 3.8 Hz, 1H, H1 α-anomer), 4.60 (d, *J* = 7.9 Hz, 1H, H1 β-anomer), 3.87 (td, *J* = 9.8, 2.7 Hz, 1H), 3.78-3.63 (m, 6H), 3.52 (dd, *J* = 9.8, 3.8 Hz, 1H), 3.49-3.41 (m, 2H), 3.25-3.19 (m, 3H), 2.12-2.04 (m, 2H), 1.69-1.60 (m, 2H). ^{13}C NMR (101 MHz, D_2O): δ 97.0, 92.9, 73.6, 72.5, 71.7, 71.0, 70.0, 69.2, 68.2, 67.0, 58.9, 58.2, 33.3. LRMS (ESI): *m/z* calcd. for $C_7H_{14}NaO_6$ $[M+Na]^+$ 217.2; found, 217.1.

Methyl-2,3,4,6-tetra-*O*-benzyl-α-D-galactopyranoside (36)

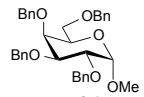

36

To stirred solution of methyl-α-D-galactopyranose (5 g, 25.7 mmol) in dry DMF under argon at 0°C, 66% sodium hydride (5.3 g, 134 mmol) was added portion wise over 30 min. The mixture was stirred for 30 min a 0°C and benzyl bromide (18.3 mL, 154 mmol) was added, followed by tetrabutylammonium iodide (960 mg, 2.6 mmol). The reaction mixture was slowly warmed to room temperature and stirred overnight. The reaction was quenched with brine, then diluted with ethyl acetate and extracted. The aqueous layer was washed twice with ethyl acetate, and the combined organic extracts were dried over $MgSO_4$ and concentrated. Column chromatography (17:3 hexanes/ethyl acetate) afforded **36** as a colourless syrup (12.3 g, 86%). Characterization data is consistent with that previously reported.[69] ^{1}H NMR (300 MHz, $CDCl_3$): δ 7.38-7.22 (m, 20H), 4.93 (d, *J* = 11.5 Hz, 1H), 4.82 (dd, *J* = 11.9, 5.0 Hz, 2H), 4.73-4.65 (m, 3H), 4.56 (d, *J* = 11.5 Hz, 1H), 4.46 (d, *J* = 11.8 Hz, 1H), 4.38 (d, *J* = 11.8 Hz, 1H), 4.02 (dd, *J* = 10.4, 3.1 Hz, 1H), 3.94-3.86 (m, 3H), 3.51 (d, *J* = 6.4 Hz, 2H), 3.35 (s, 3H). ^{13}C NMR (76 MHz, $CDCl_3$): δ 138.8, 138.5, 138.3, 137.8, 128.1, 128.0, 128.0, 128.0, 127.9, 127.7, 127.7, 127.6, 127.6, 127.5, 98.4, 79.3, 76.4, 75.1, 74.7, 73.5, 73.5, 73.3, 69.2, 69.1, 55.7. LRMS (ESI): *m/z* calcd. for $C_{35}H_{42}NO_6$ $[M+NH_4]^+$ 572.8; found, 572.5.

2,3,4,6-tetra-*O*-benzyl-D-galactopyranoside (37)

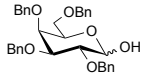

37

A solution of **36** (2.75 g, 4.96 mmol) in 0.5 M H_2SO_4 in acetic acid (95 mL) was heated gently at reflux for 2 h. Following this, the mixture was cooled to room temperature, diluted with water and extracted with ethyl acetate. The organic layer was washed with water, brine, then dried over $MgSO_4$ and concentrated. Column chromatography (1:3 hexanes/ethyl acetate) afforded **37** as a colourless syrup (1.6 g, 60%). Characterization data is consistent with that previously reported.[70] ^{1}H NMR (400 MHz, $CDCl_3$): δ 7.40-7.27 (m, 40H), 5.28 (d, *J* = 3.6 Hz, 1H, H1 α-anomer), 4.93 (dt, *J* = 11.1, 5.4 Hz, 2H), 4.85-4.70 (m, 8H), 4.59 (dd, *J* = 11.5, 7.8 Hz, 2H), 4.48 (d, *J* = 11.9 Hz, 2H), 4.41 (d, *J* = 11.9 Hz, 2H), 4.18-4.15 (m, 1H), 4.04 (dd, *J* = 9.9, 3.6 Hz, 1H), 3.97-3.96 (m, 1H), 3.93-3.88 (m, 2H), 3.77 (dd, *J* = 9.6, 7.5 Hz, 1H), 3.61-3.47 (m, 4H). ^{13}C NMR (101 MHz, $CDCl_3$): δ 138.6, 138.5, 138.5, 138.3, 138.2, 137.9, 137.7, 128.4, 128.3, 128.2, 128.2, 128.2, 128.2, 128.0, 128.0, 127.9, 127.8, 127.8, 127.7, 127.6, 127.6, 127.6, 127.5, 127.5, 97.8, 91.9, 82.2, 80.7, 78.7, 77.2, 76.6, 75.1, 74.7, 74.6, 73.6, 73.6, 73.5, 73.0, 72.9, 69.5, 68.9, 68. 9. LRMS (ESI): *m/z* calcd. for $C_{34}H_{36}NaO_6$ $[M+Na]^+$ 563.7; found, 563.6.

6-*O*-(2,3,4,6-tetra-*O*-benzyl-α-D-galactopyranosyl)-1,2:3,4-di-*O*-isopropylidene-α-D-galactopyranoside (39α)

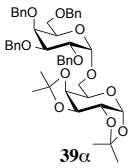

39α

Compound **37** was brominated as described previously.[71] To a solution of **37** (300 mg, 0.56 mmol) in dry CH_2Cl_2 (5 mL) and dry DMF (1 μL) under argon, oxalyl bromide (73 μL, 0.78 mmol) was added. The reaction mixture was stirred for 1 h, quenched with saturated $NaHCO_3$ and extracted with CH_2Cl_2. The organic phase was washed with saturated $NaHCO_3$, water, brine, dried over $MgSO_4$ and concentrated. The crude glycosyl bromide was dissolved three times with toluene and the volatiles were evaporated to remove residual water as an azeotrope and then dissolved in a 1:1 mixture of dry CH_2Cl_2/ether (3 mL) and added dropwise to a mixture of **13** (157 mg, 0.61 mmol) and silver triflate (155 mg, 0.61 mmol) stirring in dry CH_2Cl_2/ether (1:1, 5 mL) with 4Å molecular sieves under argon. The reaction mixture was stirred overnight, the diluted with CH_2Cl_2, washed with brine, dried over $MgSO_4$ and concentrated. Column chromatography (4:1 hexanes/ethyl acetate) afforded a mixture of **39α/β** (1:1.7) as a white solid (237 mg, 55%). Further purification by column chromatography (20:20:1 CH_2Cl_2/pet. Ether/acetone) afforded pure **39α** (37 mg, 9%). Characterization data is consistent with that previously reported.[72] ^{1}H NMR (500 MHz, $CDCl_3$): δ 7.38-7.27 (m, 20H), 5.51 (d, *J* = 5.0 Hz, 1H), 5.00 (d, *J* = 3.7 Hz, 1H), 4.93 (d, *J* = 11.5 Hz, 1H), 4.83 (d, *J* = 11.6 Hz, 1H), 4.75-4.72 (m, 3H), 4.59-4.56 (m, 2H), 4.47 (d, *J* = 11.8 Hz, 1H), 4.41 (d, *J* = 11.8 Hz, 1H),

4.32-4.29 (m, 2H), 4.06-4.00 (m, 4H), 3.95 (dd, *J* = 10.1, 2.8 Hz, 1H), 3.78 (dd, *J* = 10.5, 6.4 Hz, 1H), 3.73 (dd, *J* = 10.5, 7.1 Hz, 1H), 3.56 (dd, *J* = 9.2, 7.6 Hz, 1H), 3.51 (dd, *J* = 9.2, 5.7 Hz, 1H), 1.52 (s, 3H), 1.43 (s, 3H), 1.32 (s, 3H), 1.30 (s, 3H). ^{13}C NMR (126 MHz, $CDCl_3$): δ 138.9, 138.7, 138.0, 128.4, 128.3, 128.2, 128.2, 127.8, 127.7, 127.6, 127.5, 127.4, 127.4, 127.4, 109.2, 108.5, 97.5, 96.3, 79.0, 76.4, 73.4, 73.0, 72.7, 70.9, 70.6, 70.6, 69.1, 68.7, 66.3, 65.8, 26.1, 26.0, 24.9, 24.6. LRMS (ESI): *m/z* calcd. for $C_{46}H_{54}KO_{11}$ $[M+K]^+$ 822.0; found, 821.3.

6-*O*-(α-D-galactopyranosyl)-D-galactopyranoside (35)

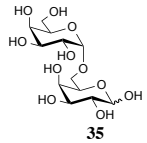

35

To a solution of **39α** (37 mg, 0.047 mmol) in a 1:1 EtOH/EtOAc mixture (5 mL), Pd/C (5 mol %) was added and the reaction mixture was purged three times with H_2. The mixture was stirred under H_2 atmosphere overnight, filtered over Celite® and the solvent was evaporated. The product was then dissolved in in 80% trifluoroacetic acid (5 mL) in water was stirred at room temperature for 1 h. The solvent was then evaporated and the crude product was dissolved three times with toluene and the volatiles were evaporated to remove residual water as an azeotrope. Purification by reversed-phase C18-SPE (solid phase extraction) cartridge over a gradient (water, then 20% ACN in water, then 50% ACN in water) afforded **35** (15 mg, 93%) as a white solid. ^{1}H NMR (500 MHz, D_2O): δ 5.24 (d, *J* = 3.5 Hz, 1H), 4.96 (d, *J* = 3.4 Hz, 2H), 4.57 (d, *J* = 7.8 Hz, 1H), 4.25 (t, *J* = 6.2 Hz, 1H), 4.01-3.96 (m, 5H), 3.88-3.79 (m, 8H), 3.73-3.62 (m, 7H), 3.49-3.45 (m, 1H). ^{13}C NMR (126 MHz, D_2O): δ 98.4, 96.4, 92.3, 72.9, 72.6, 71.8, 70.9, 70.9, 69.3, 69.2, 69.1, 69.0, 68.7, 68.4, 68.2, 68.2, 68.2, 66.7, 66.5, 61.1, 61.1. LRMS (ESI): *m/z* calcd. for $C_{12}H_{22}KO_{11}$ $[M+K]^+$ 381.4; found, 381.4.

5.6 References

1. Knight, C.A.; Hallett, J.; DeVries, A.L. *Cryobiology*. **1988**, *25*, 55-60.

2. Knight, C.A.; Wen, D.; Laursen, R.A. *Cryobiology*. **1995**, *32*, 23-34.

3. Knight, C.A.; DeVries, A.L.; Oolman, L.D. *Nature*. **1984**, *308*, 295-296.

4. Garner, J.; Harding, M.M. *ChemBioChem*. **2010**, *11*, 2489-2498.

5. Harding, M.M.; Anderberg, P.I.; Haymet, A.D.J. *Eur. J. Biochem*. **2003**, *270*, 1381-1392.

6. Harding, M.M.; Ward, L.G.; Haymet, A.D.J. *Eur. J. Biochem*. **1999**, *264*, 653-665.

7. Peltier, R.; Brimble, M.A.; Wojnar, J.M.; Williams, D.E.; Evans, C.W.; DeVries, A.L. *Chem. Sci*. **2010**, *1*, 538-551.

8. Davies, P.L.; Baardsnes, J.; Kuiper, M.J.; Walker, V.K. *Philos. Trans. R. Soc. London, Ser. B*. **2002**, *357*, 927-935.

9. Davies, P.L.; Hew, C.L. *FASEB J*. **1990**, *4*, 2460-2468.

10. Jia, Z.; Davies, P.L. *Trends Biochem. Sci.* **2002**, *27*, 101-106.

11. Yu, S.O.; Brown, A.; Middleton, A.J.; Tomczak, M.M.; Walker, V.K.; Davies, P.L. *Cryobiology*. **2010**, *61*, 327-334.

12. Pudney, P.D.A.; Buckley, S.L.; Sidebottom, C.M.; Twigg, S.N.; Sevilla, M.-P.; Holt, C.B.; Roper, D.; Telford, J.H.; McArthur, A.J.; Lillford, P.J. *Arch. Biochem. Biophys.* **2003**, *410*, 238-245.

13. Eniade, A.; Purushotham, M.; Ben, R.N.; Wang, J.B.; Horwath, K. *Cell Biochem. Biophys.* **2003**, *38*, 115-124.

14. Czechura, P.; Tam, R.Y.; Dimitrijevic, E.; Murphy, A.V.; Ben, R.N. *J. Am. Chem. Soc.* **2008**, *130*, 2928-2929.

15. Liu, S.; Ben, R.N. *Org. Lett.* **2005**, *7*, 2385-2388.

16. Inada, T.; Lu, S.-S. *Cryst. Growth Des.* **2003**, *3*, 747-752.

17. Inada, T.; Lu, S.-S. *Chem. Phys. Lett.* **2004**, *394*, 361-365.

18. Budke, C.; Koop, T. *ChemPhysChem*. **2006**, *7*, 2601-2606.

19. Gibson, M.I. *Polym. Chem.* **2010**, *1*, 1141-1152.

20. Gibson, M.I.; Barker, C.A.; Spain, S.G.; Albertin, L.; Cameron, N.R. *Biomacromolecules*. **2009**, *10*, 328-333.

21. Tam, R.Y.; Ferreira, S.S.; Czechura, P.; Chaytor, J.L.; Ben, R.N. *J. Am. Chem. Soc.* **2008**, *130*, 17494-17501.

22. Galema, S.A.; Engberts, J.B.F.N.; Hoeiland, H.; Foerland, G.M. *J. Phys. Chem.* **1993**, *97*, 6885-6889.

23. Galema, S.A.; Høiland, H. *J. Phys. Chem.* **1991**, *95*, 5321-5326.

24. Galema, S.A.; Howard, E.; Engberts, J.B.F.N.; Grigera, J.R. *Carbohydr. Res.* **1994**, *265*, 215-225.

25. Bilgram, J.H. *Prog. Cryst. Growth Charact. Mater.* **1993**, *26*, 99-119.

26. Halter, P.U.; Bilgram, J.H.; Känzig, W. *J. Chem. Phys.* **1988**, *89*, 2622-2629.

27. Stokes, R.H.; Robinson, R.A. *J. Phys. Chem.* **1966**, *70*, 2126-2131.

28. Suggett, A.; Ablett, S.; Lillford, P.J. *J. Solution Chem.* **1976**, *5*, 17-31.

29. Tait, M.J.; Suggett, A.; Franks, F.; Ablett, S.; Quickenden, P.A. *J. Solution Chem.* **1972**, *1*, 131-151.

30. Uedaira, H.; Uedaira, H. *J. Solution Chem.* **1985**, *14*, 27-34.

31. Walkinshaw, M.D. *J. Chem. Soc. Perkin Trans. 2*. **1987**, 1903-1906.

32. Chaytor, J.L.; Ben, R.N. *Bioorg. Med. Chem. Lett.* **2010**, *20*, 5251-5254.

33. Balcerzak, A.K.; Ferreira, S.S.; Trant, J.F.; Ben, R.N. *Bioorg. Med. Chem. Lett.* **2012**, *22*, 1719-1721.

34. DeVries, A.L.; Komatsu, S.K.; Feeney, R.E. *J. Biol. Chem.* **1970**, *245*, 2901-2908.

35. Çarçabal, P.; Jockusch, R.A.; Hünig, I.; Snoek, L.C.; Kroemer, R.T.; Davis, B.G.; Gamblin, D.P.; Compagnon, I.; Oomens, J.; Simons, J.P. *J. Am. Chem. Soc.* **2005**, *127*, 11414-11425.

36. Cocinero, E.J.; Stanca-Kaposta, E.C.; Scanlan, E.M.; Gamblin, D.P.; Davis, B.G.; Simons, J.P. *Chem. Eur. J.* **2008**, *14*, 8947-8955.

37. Hunig, I.; Painter, A.J.; Jockusch, R.A.; Carcabal, P.; Marzluff, E.M.; Snoek, L.C.; Gamblin, D.P.; Davis, B.G.; Simons, J.P. *Phys. Chem. Chem. Phys.* **2005**, *7*, 2474-2480.

38. Simons, J.P.; Jockusch, R.A.; ÇarÇabal, P.; Hünig, I.; Kroemer, R.T.; Macleod, N.A.; Snoek, L.C. *Int. Rev. Phys. Chem.* **2005**, *24*, 489-531.

39. Simons, J.P.; Davis, B.G.; Cocinero, E.J.; Gamblin, D.P.; Stanca-Kaposta, E.C. *Tetrahedron: Asymmetry*. **2009**, *20*, 718-722.

40. Dong, L.; Roosenberg, J.M.; Miller, M.J. *J. Am. Chem. Soc.* **2002**, *124*, 15001-15005.

41. Brimacombe, J.S.; Kabir, A.K.M.S. *Carbohydr. Res.* **1986**, *150*, 35-51.

42. Kolb, H.C.; VanNieuwenhze, M.S.; Sharpless, K.B. *Chem. Rev.* **1994**, *94*, 2483-2547.

43. Khare, N.K.; Sood, R.K.; Aspinall, G.O. *Can. J. Chem.* **1994**, *72*, 237-246.

44. Chaytor, J.L., *Examining the Role of Carbohydrate Hydration and Structure in Preventing Ice Recrystallization*, 2010, Ph. D. Dissertation, Department of Chemistry, University of Ottawa.

45. DeVries, A.L.; Vandenheede, J.; Feeney, R.E. *J. Biol. Chem.* **1971**, *246*, 305-308.

46. Feeney, R.E.; Burcham, T.S.; Yeh, Y. *Annu. Rev. Biophys. Biophys. Chem.* **1986**, *15*, 59-78.

47. Bouvet, V.; Ben, R.N. *Cell Biochem. Biophys.* **2003**, *39*, 133-144.

48. Chan, L.; Taylor, M.S. *Org. Lett.* **2011**, *13*, 3090-3093.

49. Gouliaras, C.; Lee, D.; Chan, L.; Taylor, M.S. *J. Am. Chem. Soc.* **2011**, *133*, 13926-13929.

50. Lee, D.; Taylor, M.S. *Synthesis*. **2012**, *44*, 3421-3431.

51. Lee, D.; Taylor, M.S. *J. Am. Chem. Soc.* **2011**, *133*, 3724-3727.

52. Lee, D.; Williamson, C.L.; Chan, L.; Taylor, M.S. *J. Am. Chem. Soc.* **2012**, *134*, 8260-8267.

53. McClary, C.A.; Taylor, M.S. *Carbohydr. Res.* **2013**, *381*, 112-122.

54. Heyden, M.; Bründermann, E.; Heugen, U.; Niehues, G.; Leitner, D.M.; Havenith, M. *J. Am. Chem. Soc.* **2008**, *130*, 5773-5779.

55. Campen, R.K.; Vila Verde, A.; Kubicki, J.D. *J. Phys. Chem. B*. **2007**, *111*, 13775-13785.

56. Lerbret, A.; Bordat, P.; Affouard, F.; Guinet, Y.; Hédoux, A.; Paccou, L.; Prévost, D.; Descamps, M. *Carbohydr. Res.* **2005**, *340*, 881-887.

57. Choi, Y.; Cho, K.W.; Jeong, K.; Jung, S. *Carbohydr. Res.* **2006**, *341*, 1020-1028.

58. Çarçabal, P.; Hünig, I.; Gamblin, D.P.; Liu, B.; Jockusch, R.A.; Kroemer, R.T.; Snoek, L.C.; Fairbanks, A.J.; Davis, B.G.; Simons, J.P. *J. Am. Chem. Soc.* **2006**, *128*, 1976-1981.

59. Cocinero, E.J.; Gamblin, D.P.; Davis, B.G.; Simons, J.P. *J. Am. Chem. Soc.* **2009**, *131*, 11117-11123.

60. Jackman, J.; Noestheden, M.; Moffat, D.; Pezacki, J.P.; Findlay, S.; Ben, R.N. *Biochem. Biophys. Res. Commun.* **2007**, *354*, 340-344.

61. Yang, J.; Fu, X.; Jia, Q.; Shen, J.; Biggins, J.B.; Jiang, J.; Zhao, J.; Schmidt, J.J.; Wang, P.G.; Thorson, J.S. *Org. Lett.* **2003**, *5*, 2223-2226.

62. Juaristi, E.; Martinez-Richa, A.; Garcia-Rivera, A.; Cruz-Sanchez, J.S. *J. Org. Chem.* **1983**, *48*, 2603-2606.

63. Ali, M.H.; Collins, P.M.; Overend, W.G. *Carbohydr. Res.* **1990**, *205*, 428-434.

64. Dolhem, F.; Lièvre, C.; Demailly, G. *J. Org. Chem.* **2004**, *69*, 3400-3407.

65. Kuberan, B.; Sikkander, S.A.; Tomiyama, H.; Linhardt, R.J. *Angew. Chem. Int. Ed.* **2003**, *42*, 2073-2075.

66. Shashkov, A.S.; Pakulski, Z.; Grzeszczyk, B.; Zamojski, A. *Carbohydr. Res.* **2001**, *330*, 289-294.

67. Kim, M.; Grzeszczyk, B.; Zamojski, A. *Tetrahedron*. **2000**, *56*, 9319-9337.

68. Ishiwata, A.; Munemura, Y.; Ito, Y. *Eur. J. Org. Chem.* **2008**, *2008*, 4250-4263.

69. Fletcher, S.; Jorgensen, M.R.; Miller, A.D. *Org. Lett.* **2004**, *6*, 4245-4248.

70. Xie, J.; Molina, A.; Czernecki, S. *J. Carbohydr. Chem.* **1999**, *18*, 481-498.

71. Grayson, E.J.; Ward, S.J.; Hall, A.L.; Rendle, P.M.; Gamblin, D.P.; Batsanov, A.S.; Davis, B.G. *J. Org. Chem.* **2005**, *70*, 9740-9754.

72. Lafont, D.; Carrière, F.; Ferrato, F.; Boullanger, P. *Carbohydr. Res.* **2006**, *341*, 695-704.

5.7 NMR Spectra of Compounds in Chapter 5

3

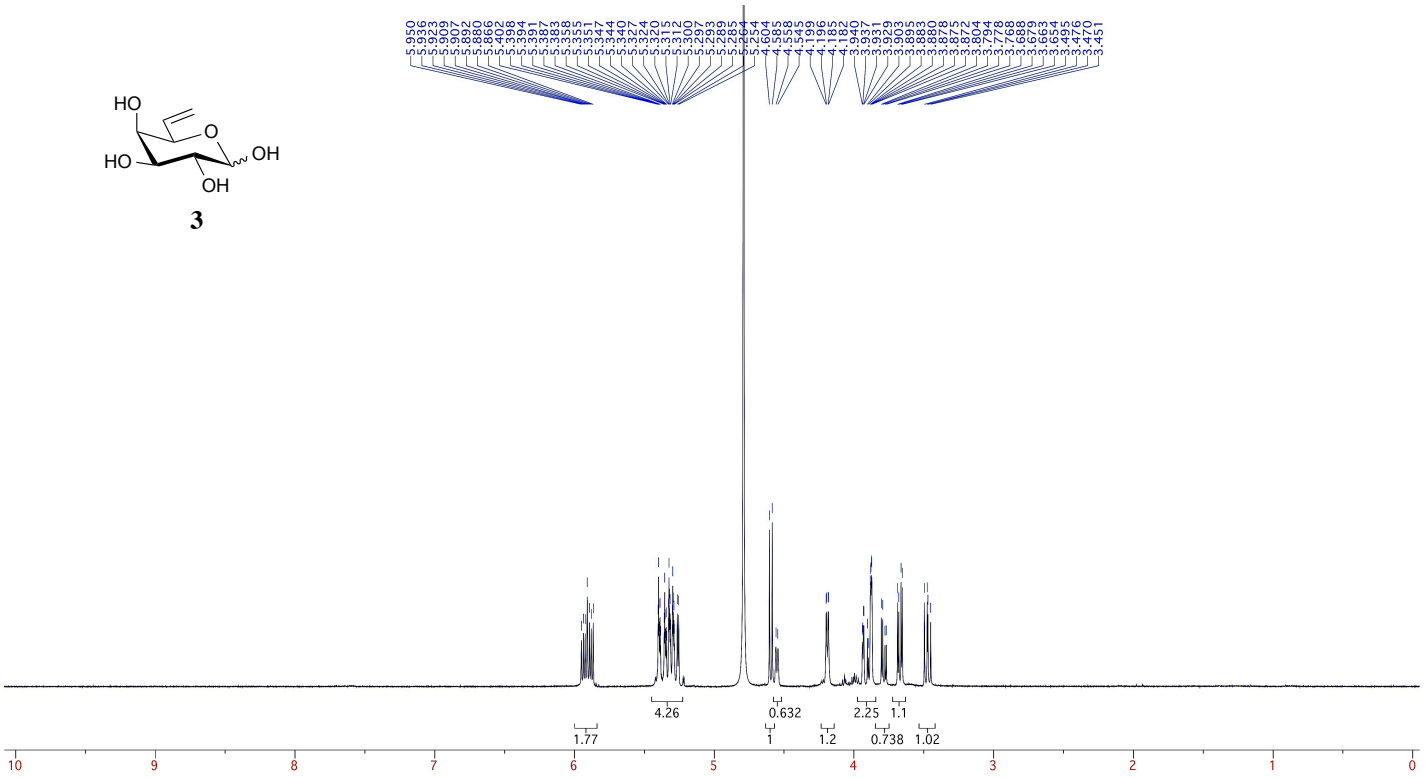

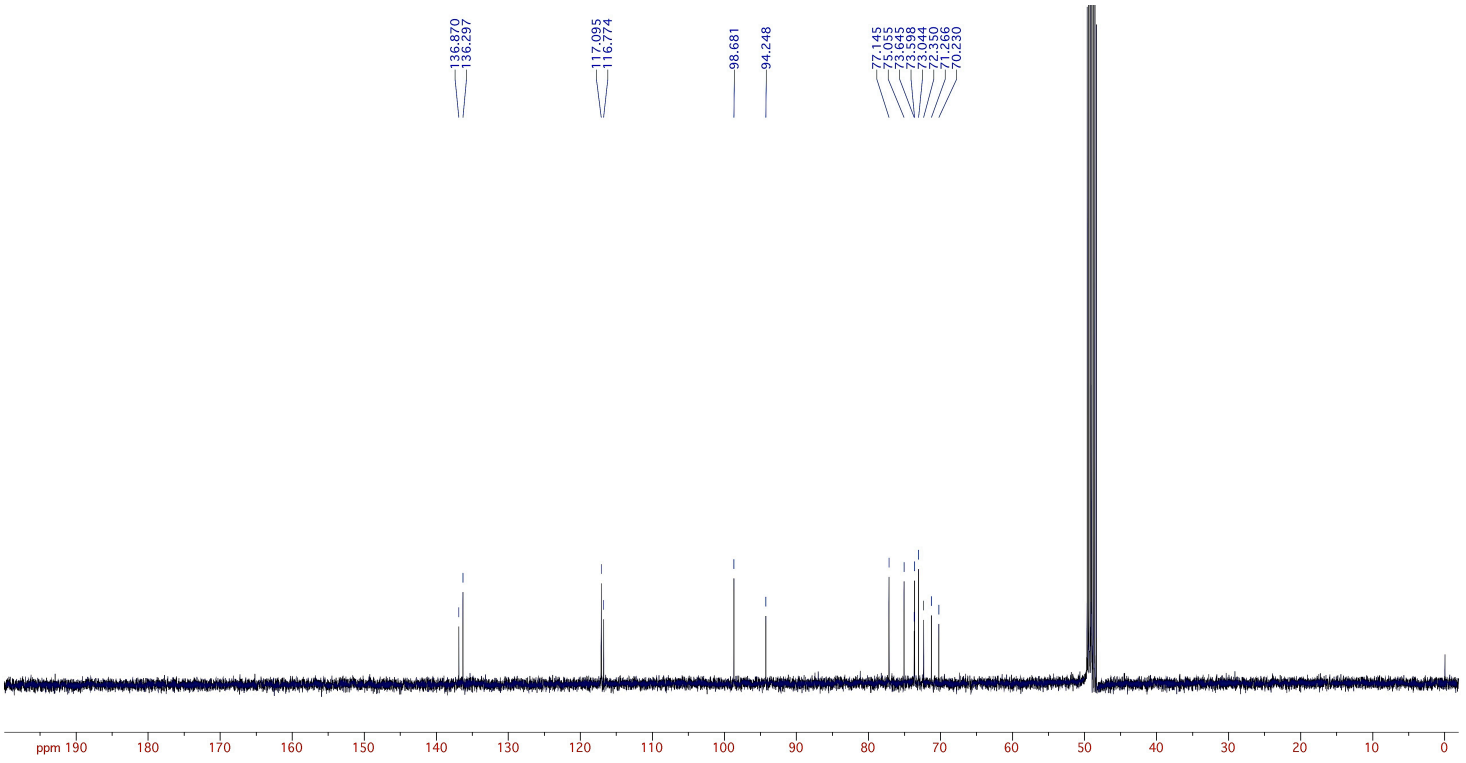

HO
O
OH
HO
OH

2

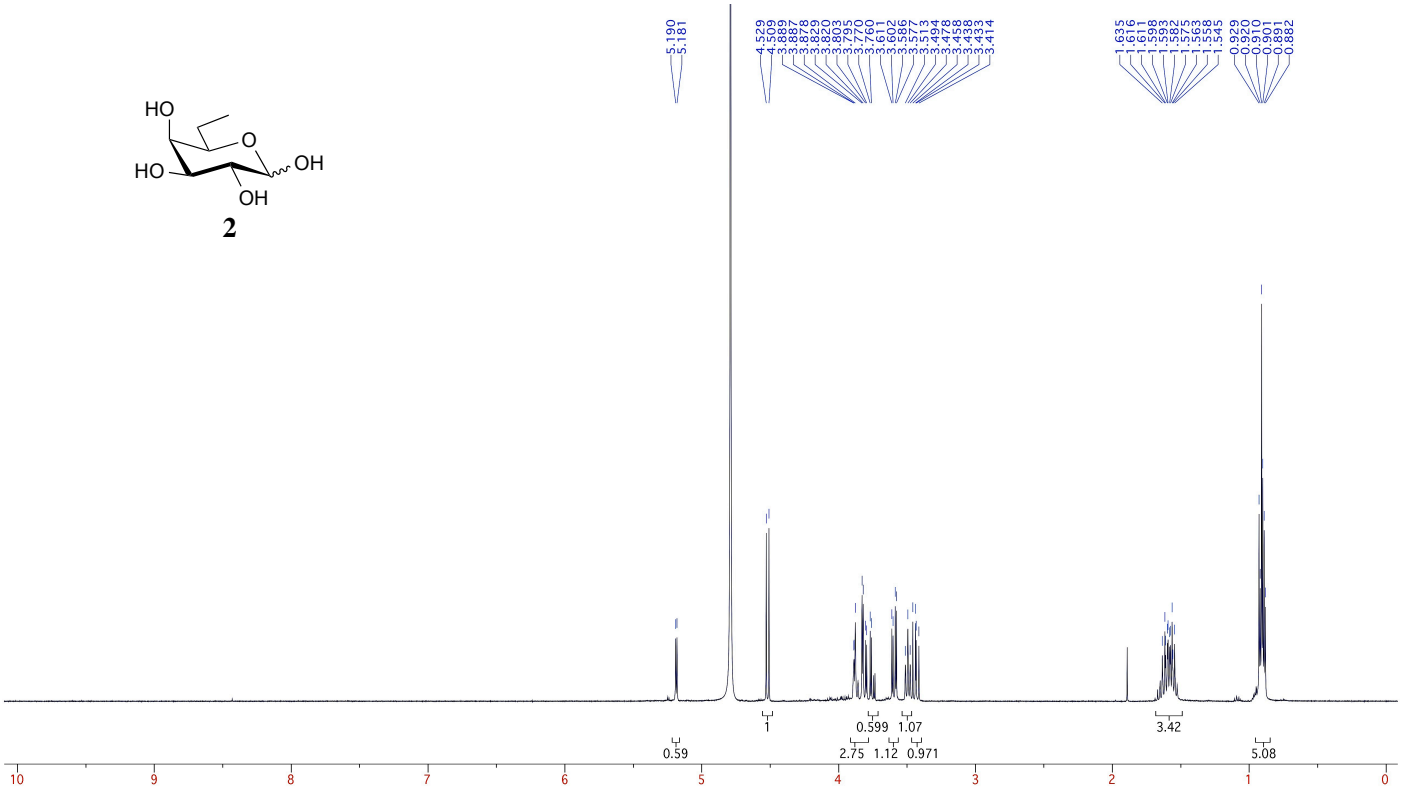
5.190
5.181
4.529
4.509
4.489
3.887
3.878
3.829
3.820
3.803
3.795
3.770
3.760
3.601
3.586
3.577
3.513
3.494
3.478
3.458
3.438
3.433
3.414
1.635
1.616
1.611
1.598
1.593
1.582
1.572
1.563
1.558
1.545
0.929
0.920
0.911
0.901
0.891
0.882
1
0.599
1.07
3.42
0.59
2.75
1.12
0.971
5.08
10
9
8
7
6
5
4
3
2
1
0

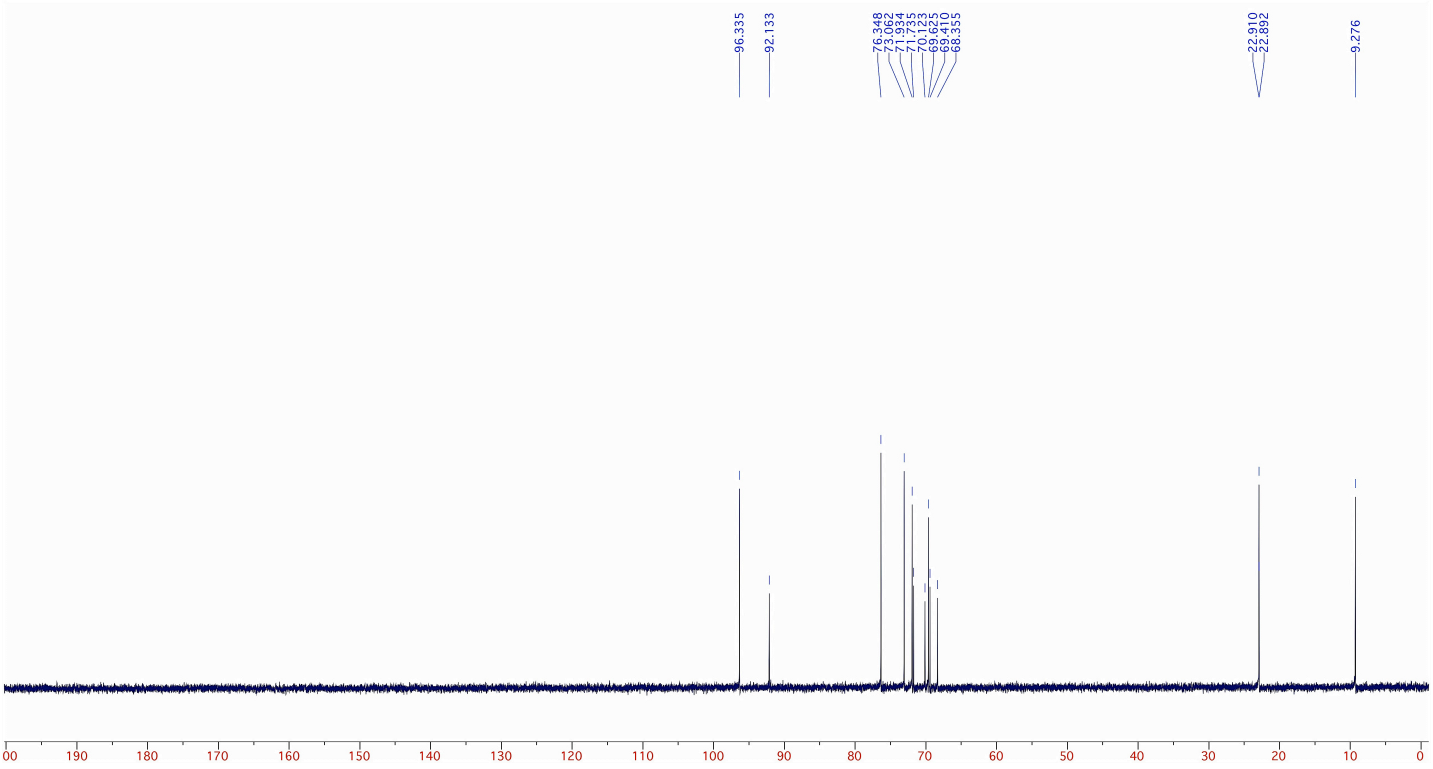
96.335
92.133
76.348
73.062
71.934
71.735
71.523
69.623
69.410
68.355
22.910
22.892
9.276
00
190
180
170
160
150
140
130
120
110
100
90
80
70
60
50
40
30
20
10
0

HO
HO
O
OH
HO
OH

5

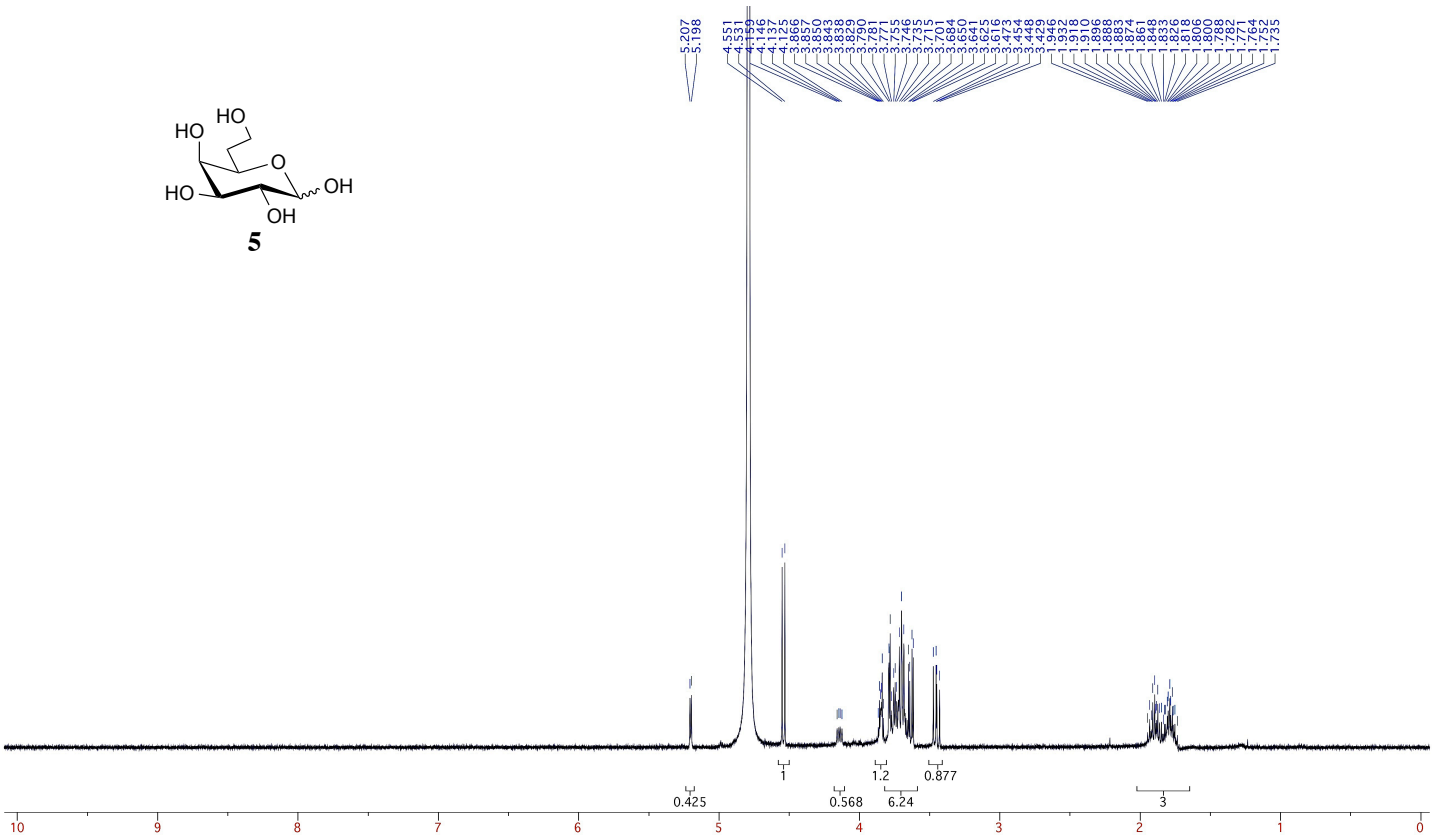
5.207
5.198
4.551
4.531
4.159
4.146
4.137
4.125
3.865
3.857
3.850
3.843
3.839
3.830
3.790
3.781
3.771
3.755
3.746
3.735
3.715
3.701
3.684
3.650
3.641
3.625
3.616
3.573
3.454
3.448
3.429
1.946
1.938
1.918
1.910
1.896
1.888
1.883
1.874
1.861
1.848
1.833
1.826
1.818
1.806
1.800
1.788
1.781
1.771
1.764
1.752
1.735
1
1.2
0.877
0.425
0.568
6.24
3
10
9
8
7
6
5
4
3
2
1
0

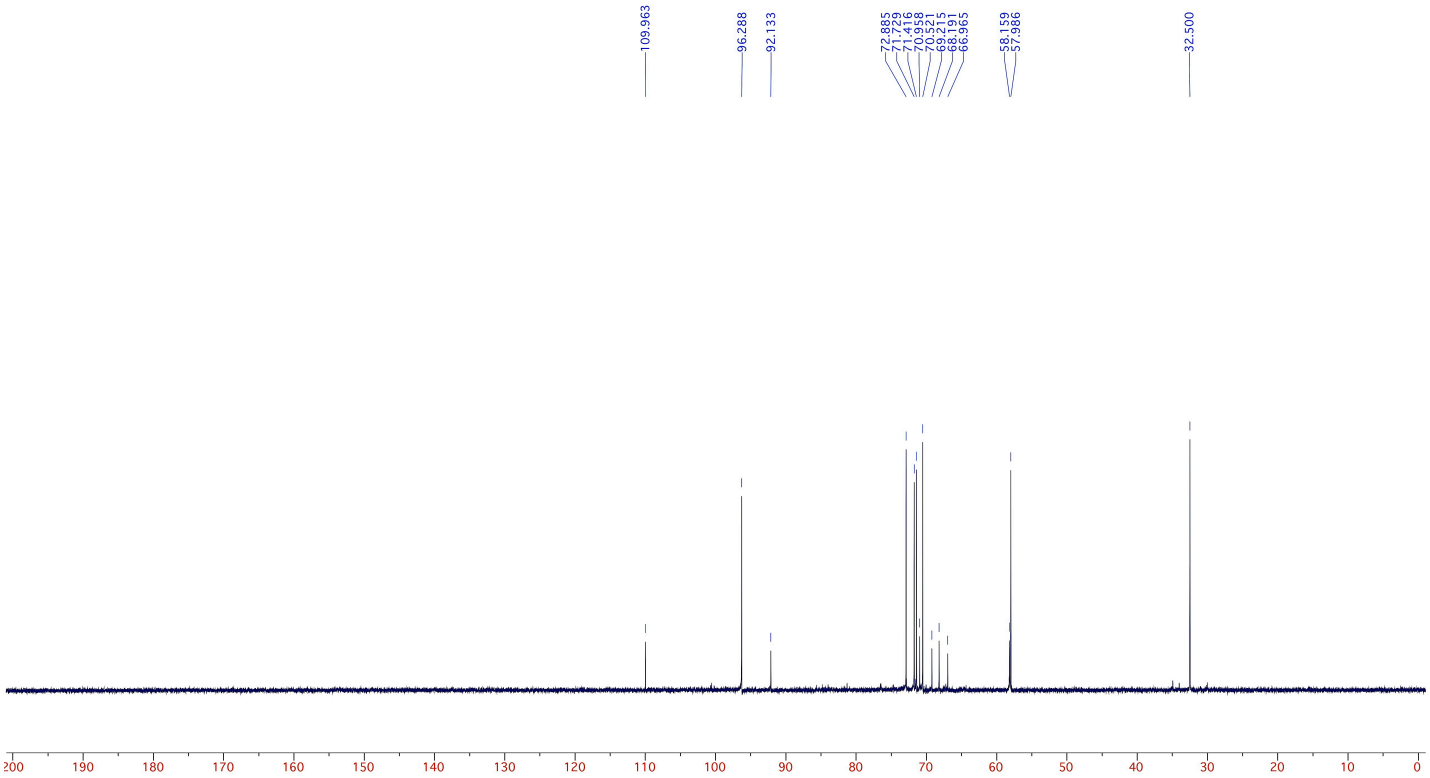
109.963
96.288
92.133
72.885
72.379
71.416
71.178
70.958
70.521
69.215
68.911
66.965
58.159
57.986
32.500
200
190
180
170
160
150
140
130
120
110
100
90
80
70
60
50
40
30
20
10
0

6a + **6b**

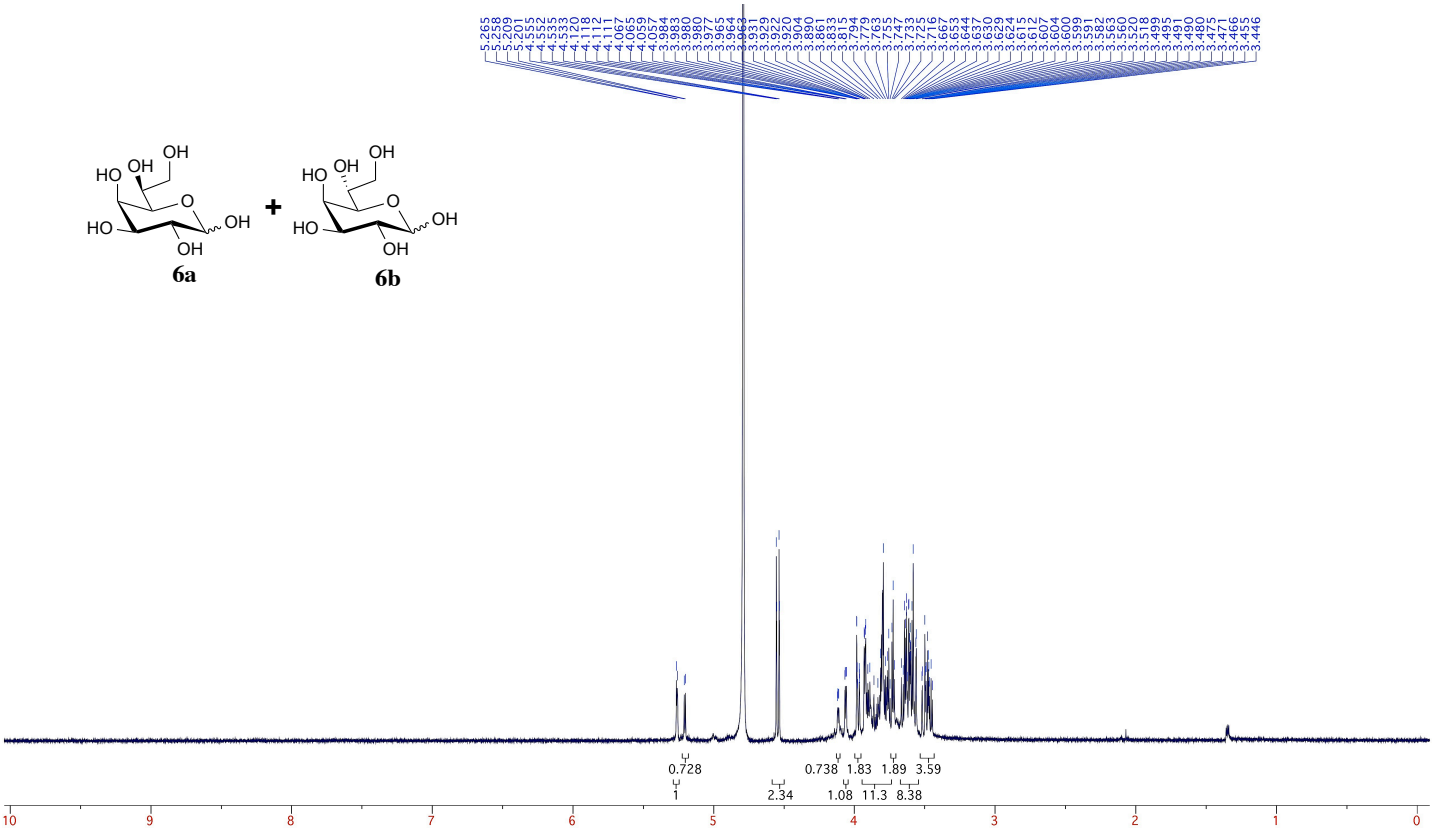

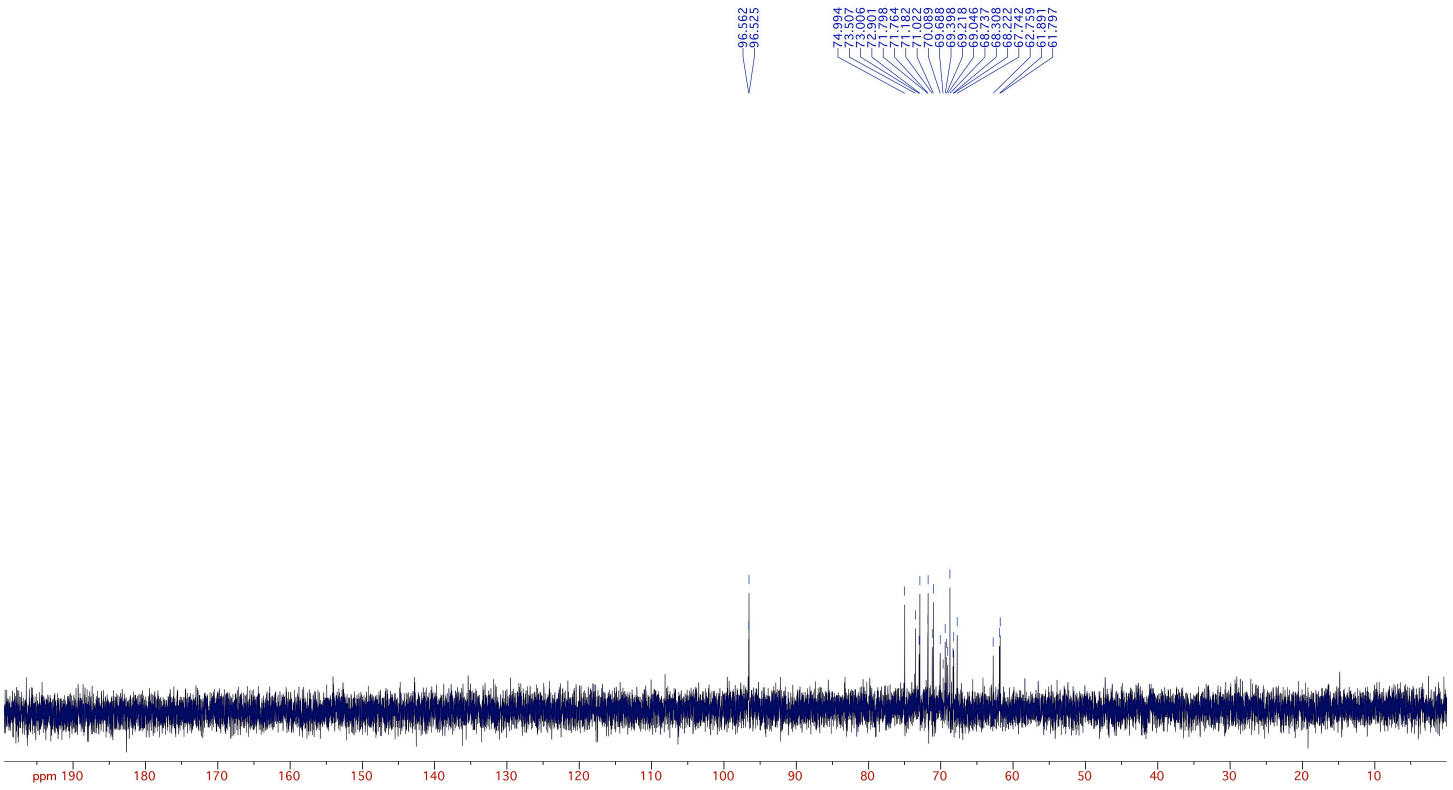

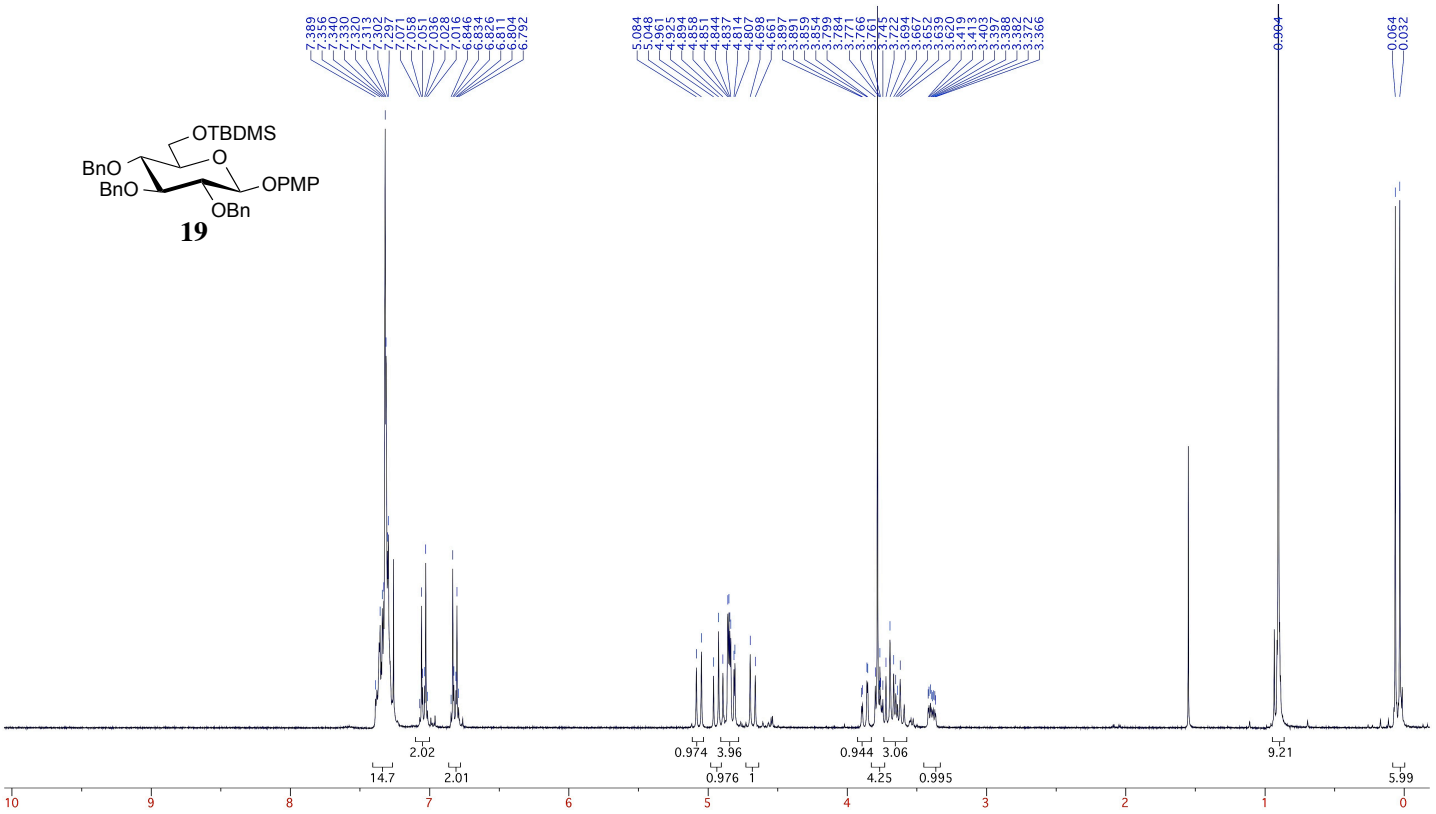
OTBDMS
O
BnO
BnO
OPMP
OBn
19

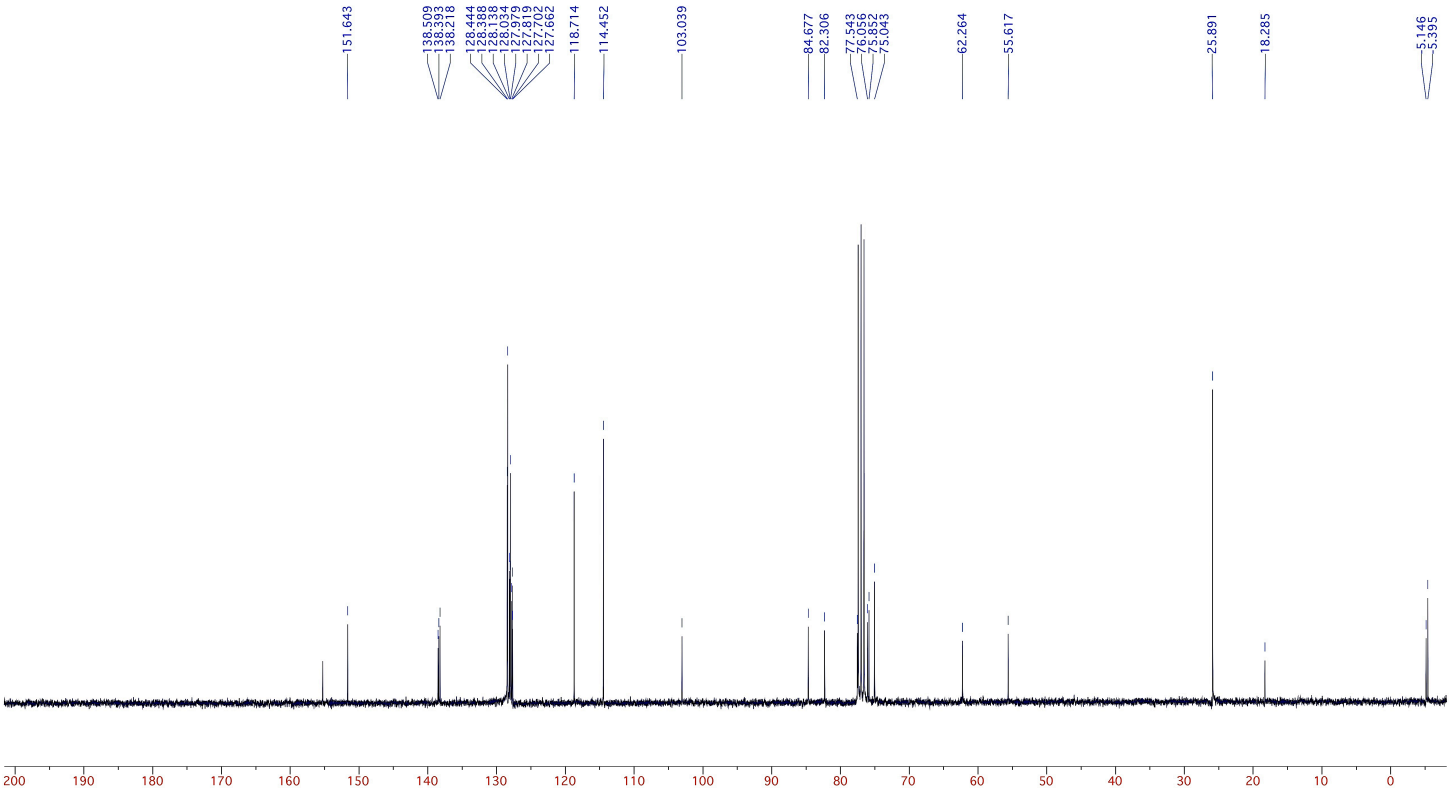

20

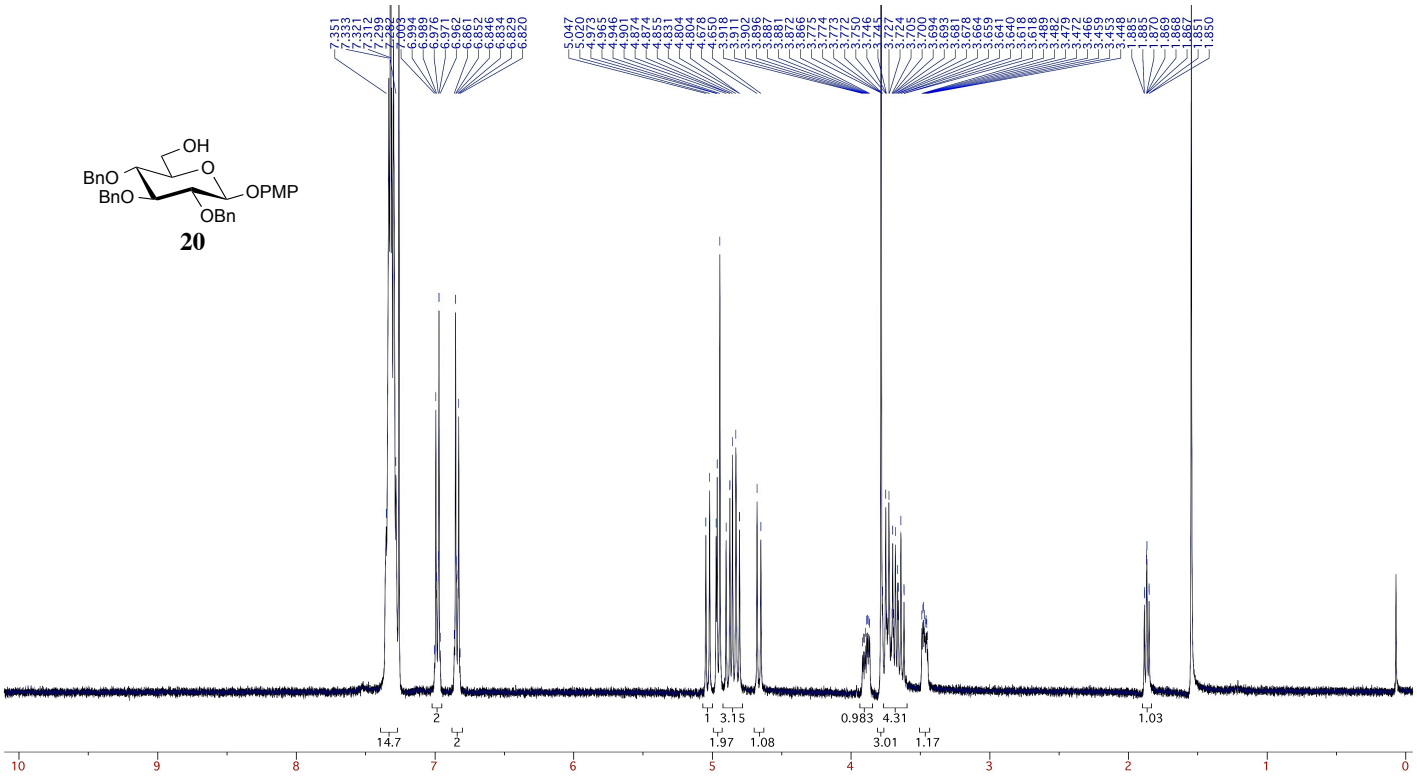

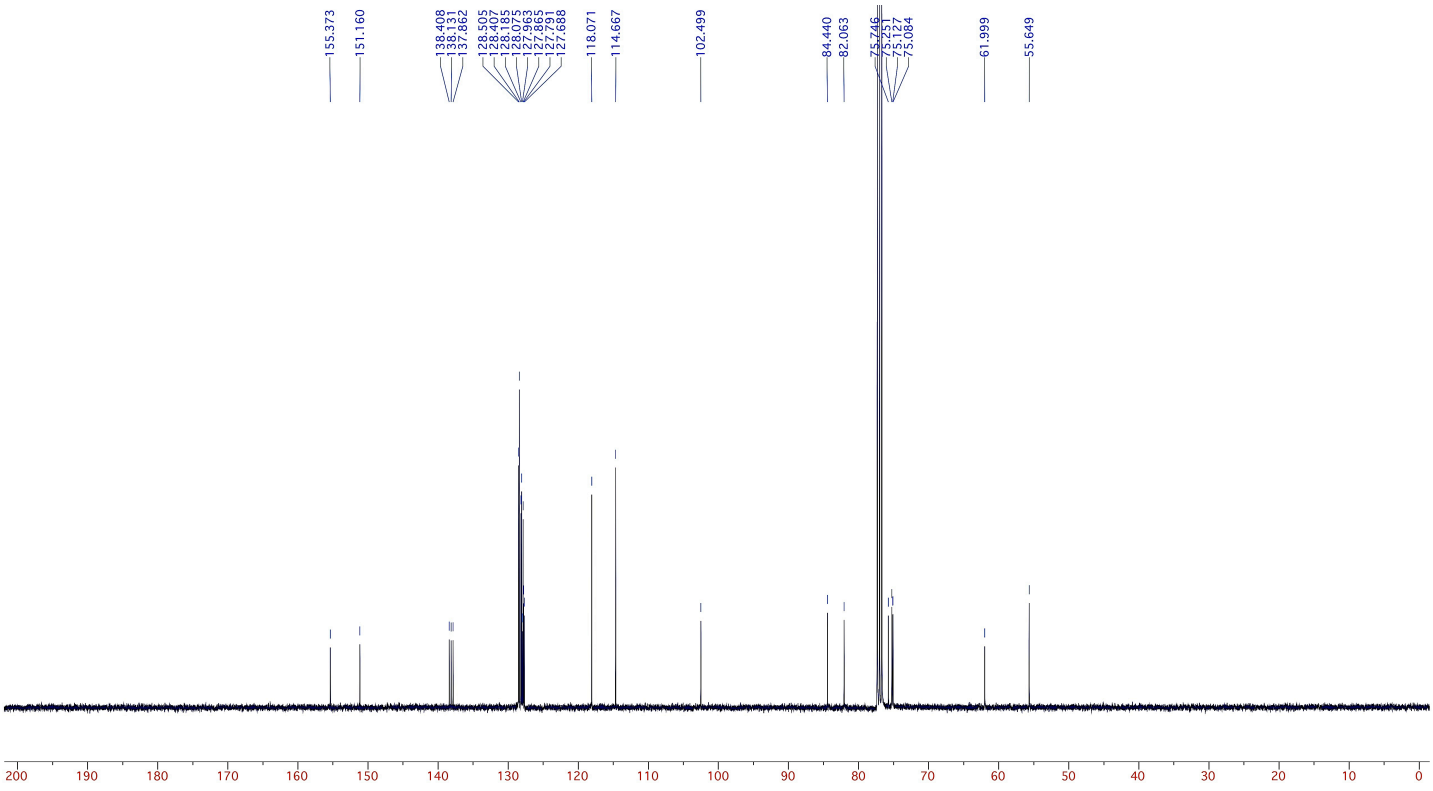

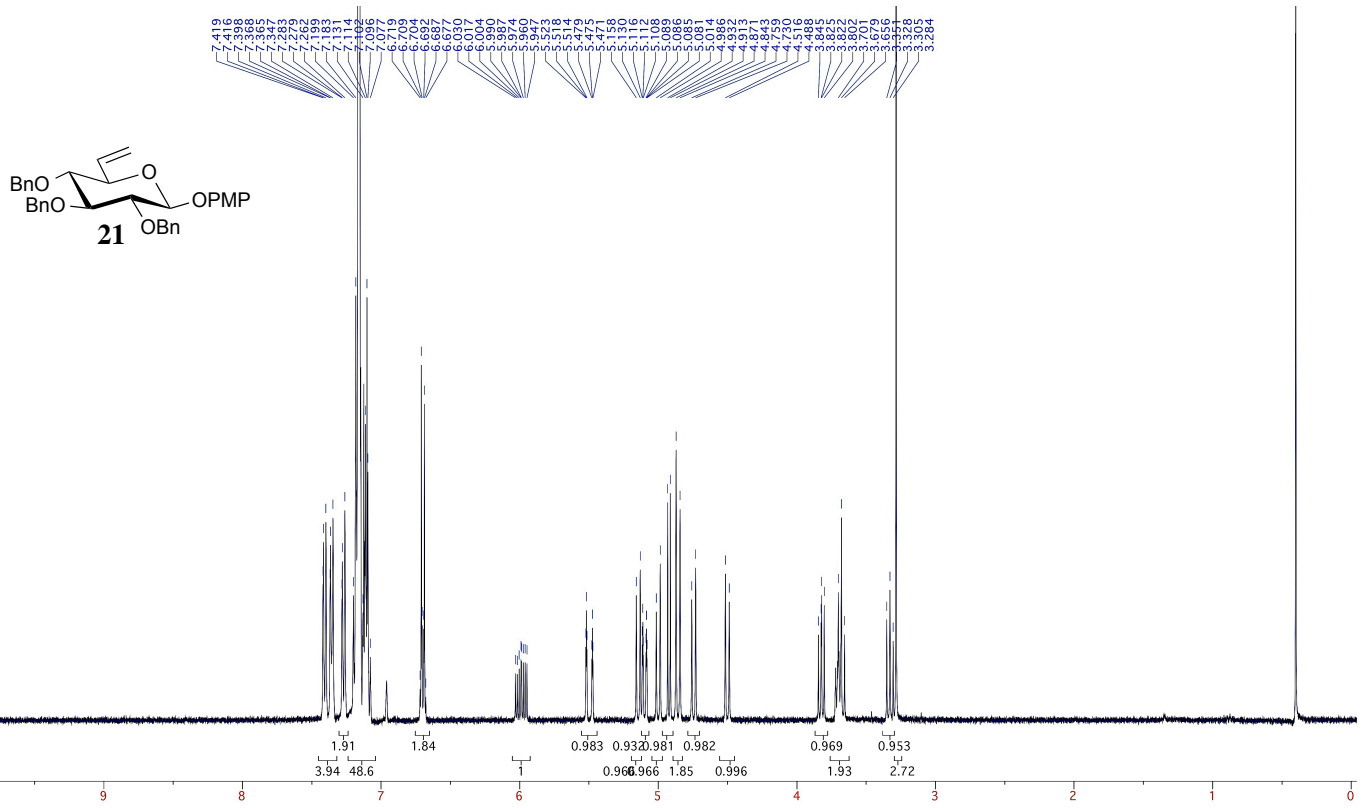
BnO
BnO
O
OPMP
OBn
21

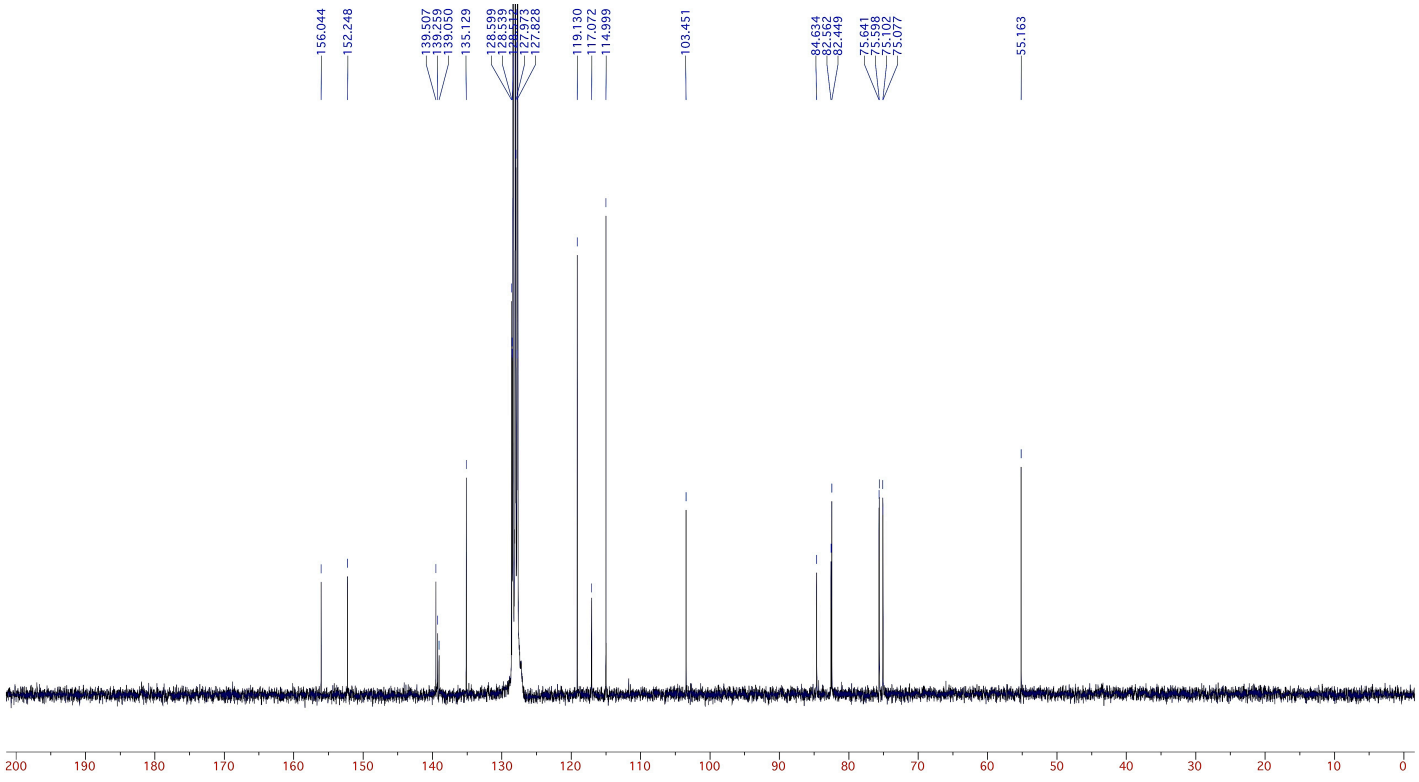

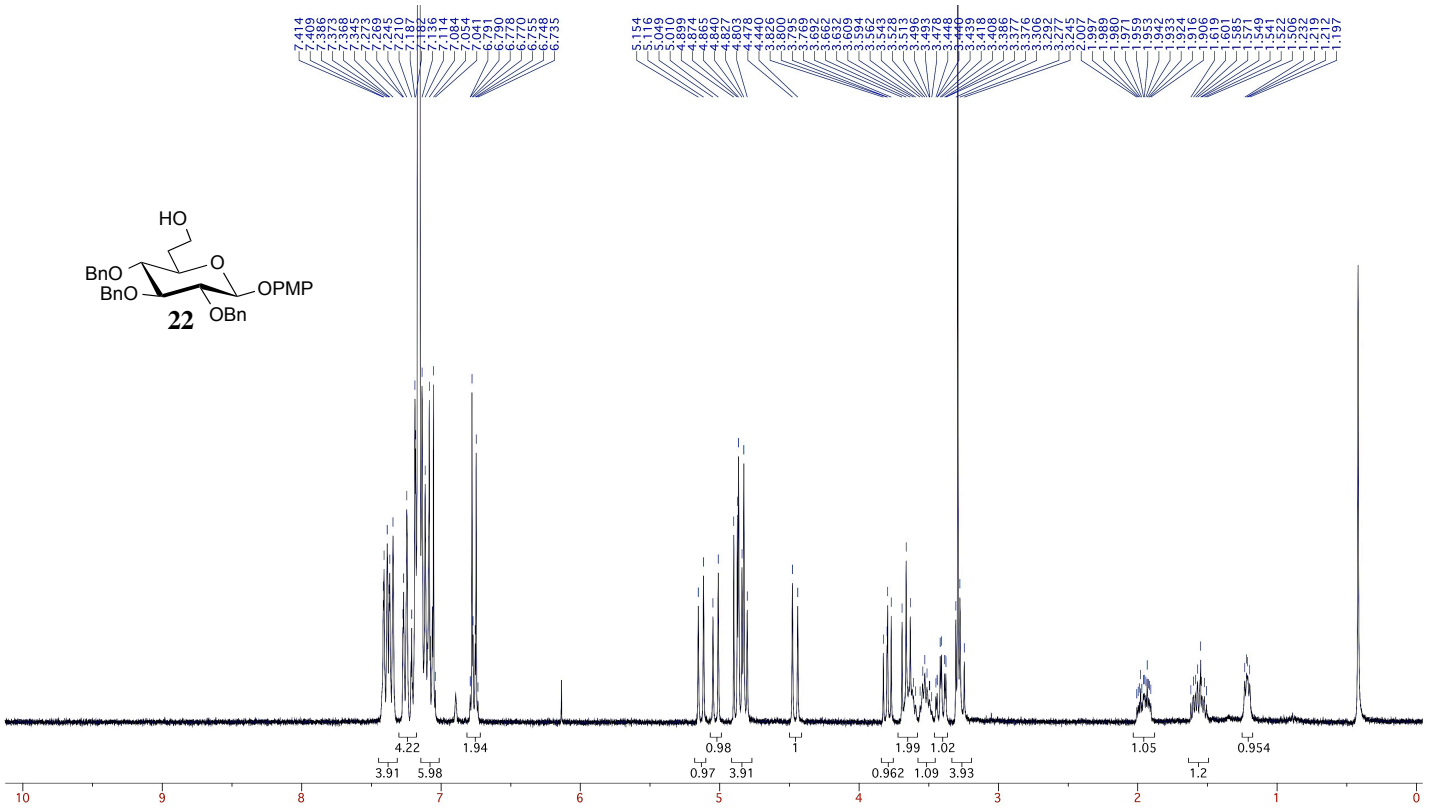
HO
O
BnO
BnO
OPMP
OBn
22

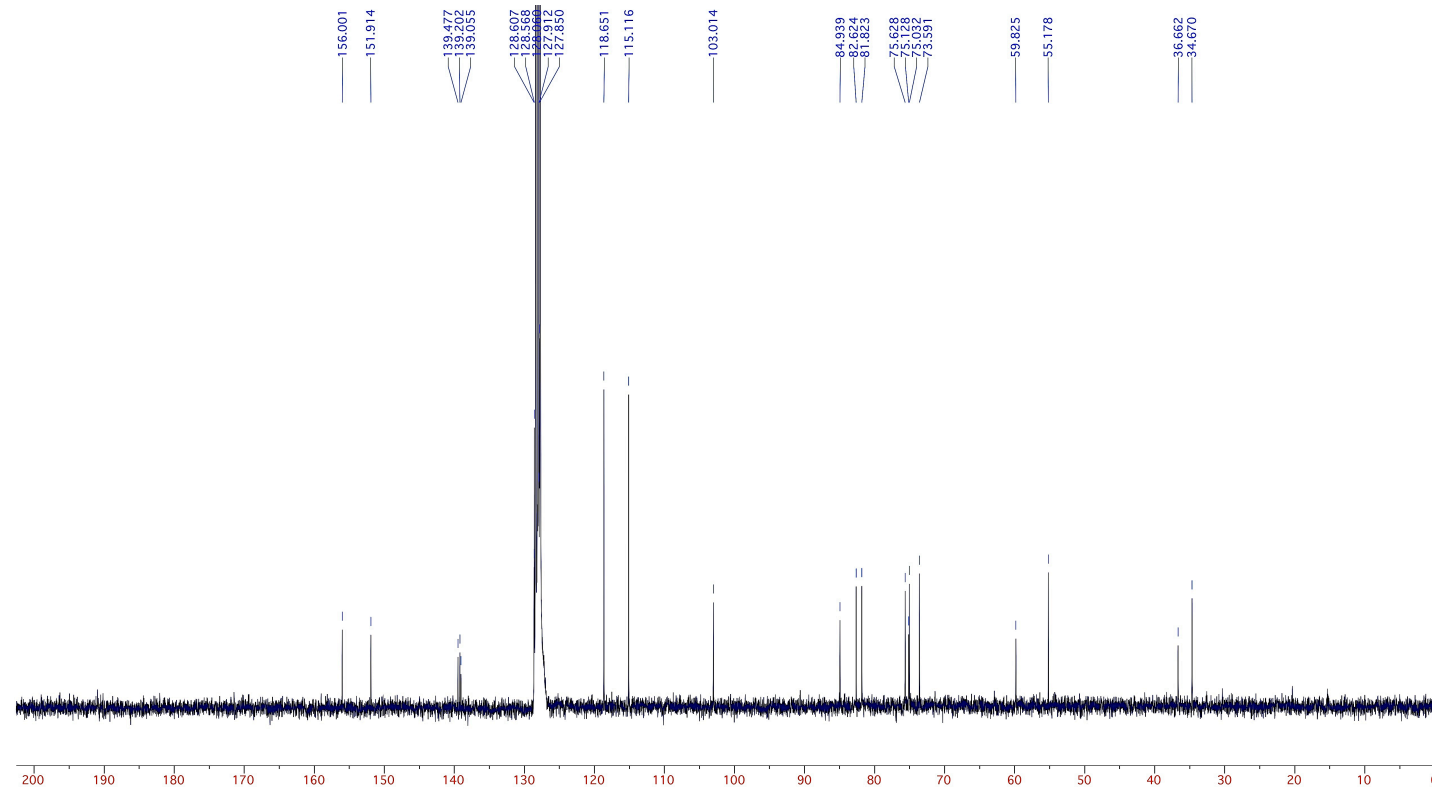

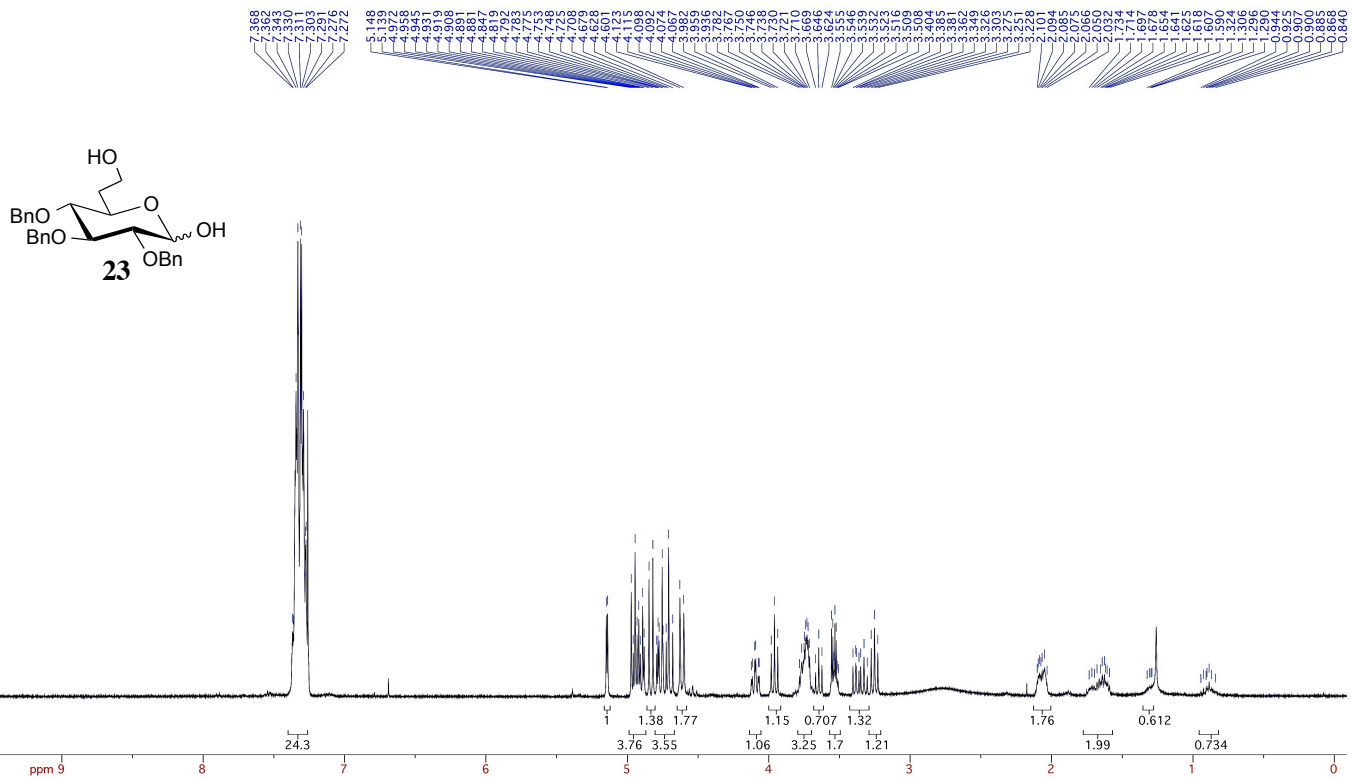
HO
BnO
BnO
O
OH
OBn
23
ppm 9
8
7
6
5
4
3
2
1
0

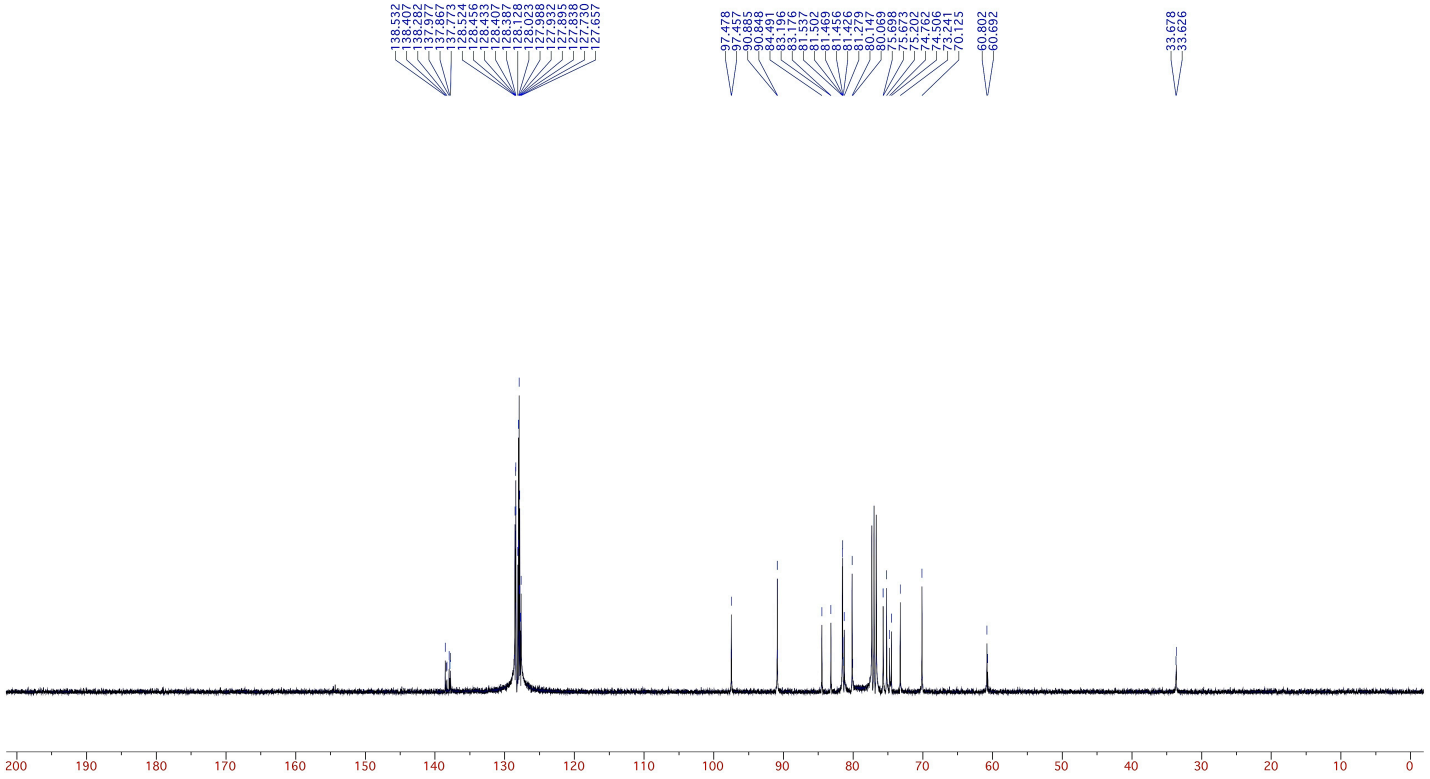
200
190
180
170
160
150
140
130
120
110
100
90
80
70
60
50
40
30
20
10
0

HO
HO
HO
O
OH
OH

9

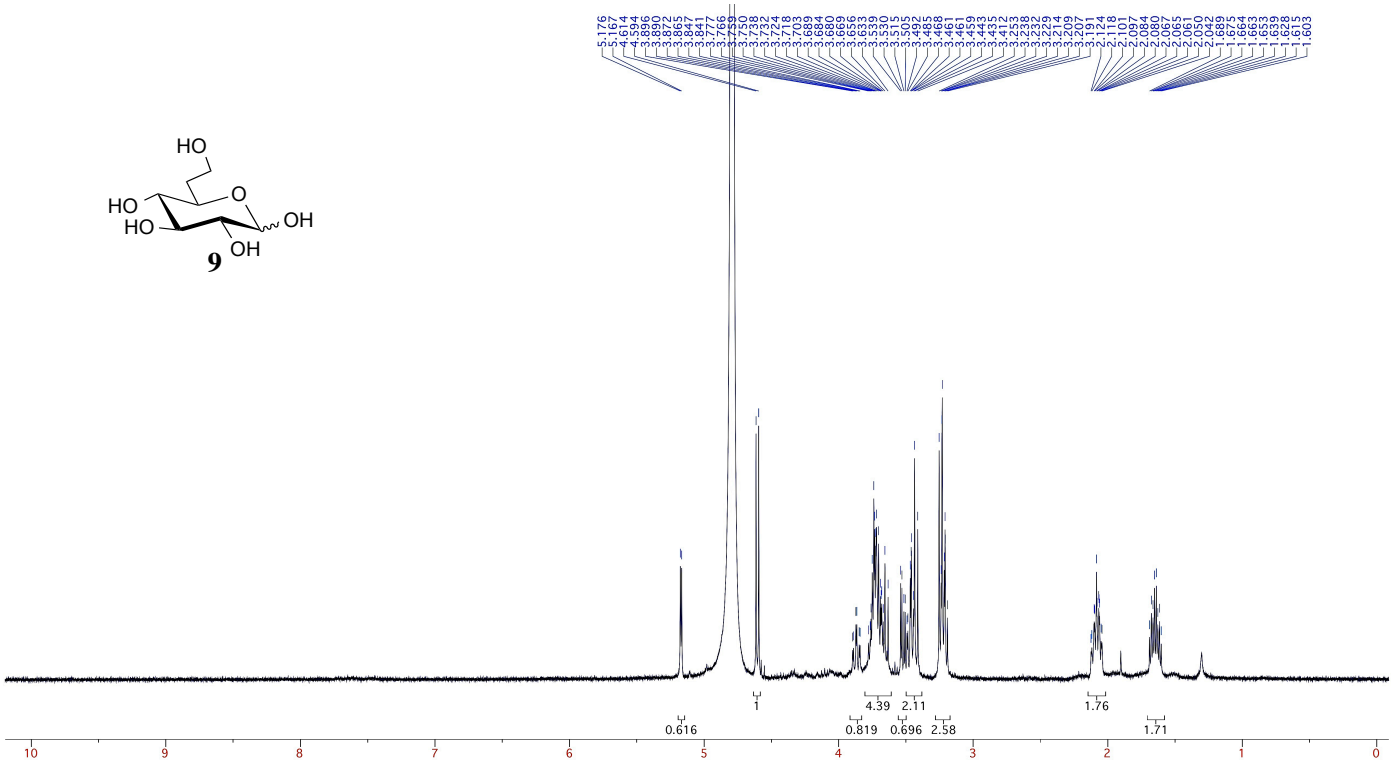
5.176
5.167
4.614
4.594
3.896
3.890
3.872
3.865
3.847
3.841
3.777
3.768
3.750
3.738
3.732
3.724
3.718
3.703
3.689
3.684
3.680
3.669
3.656
3.533
3.519
3.330
3.315
3.305
3.492
3.485
3.468
3.461
3.459
3.443
3.435
3.412
3.353
3.238
3.232
3.229
3.214
3.209
3.207
3.191
2.124
2.118
2.101
2.097
2.084
2.080
2.067
2.065
2.061
2.050
2.042
1.689
1.675
1.664
1.663
1.653
1.639
1.628
1.615
1.613
1.603
1
4.39
2.11
1.76
0.616
0.819
0.696
2.58
1.71
10
9
8
7
6
5
4
3
2
1
0

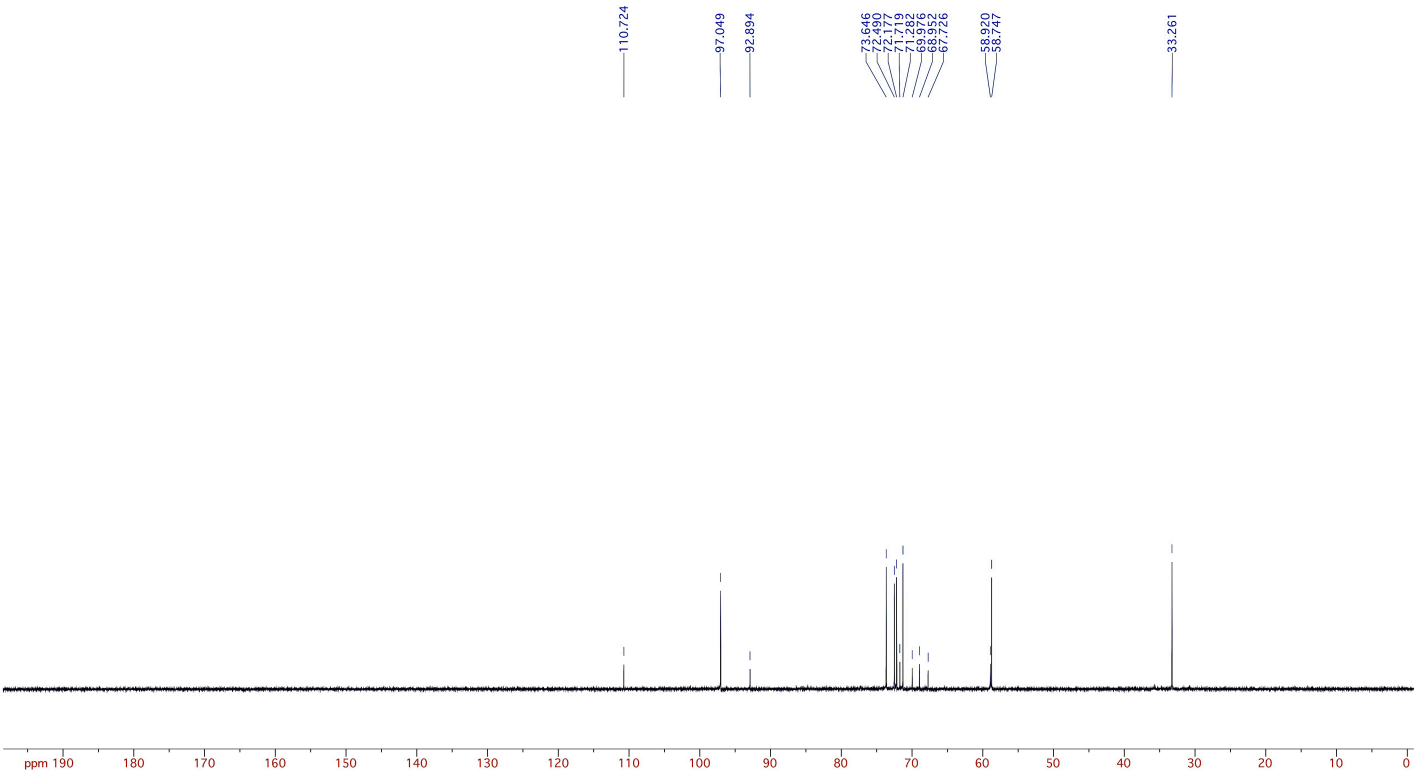
110.724
97.049
92.894
73.646
72.490
72.177
71.719
71.282
69.976
68.952
67.726
58.920
58.747
33.261
ppm 190
180
170
160
150
140
130
120
110
100
90
80
70
60
50
40
30
20
10
0

39α

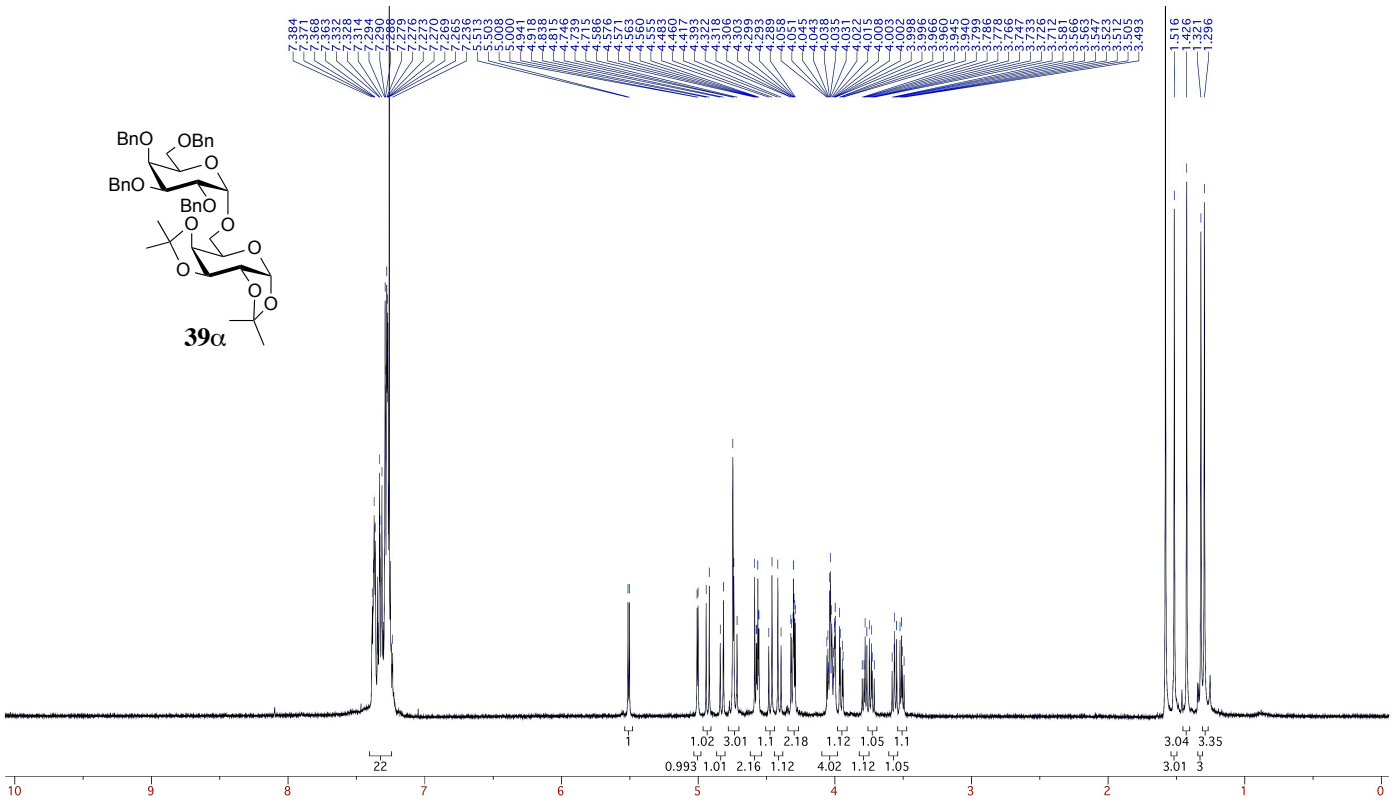

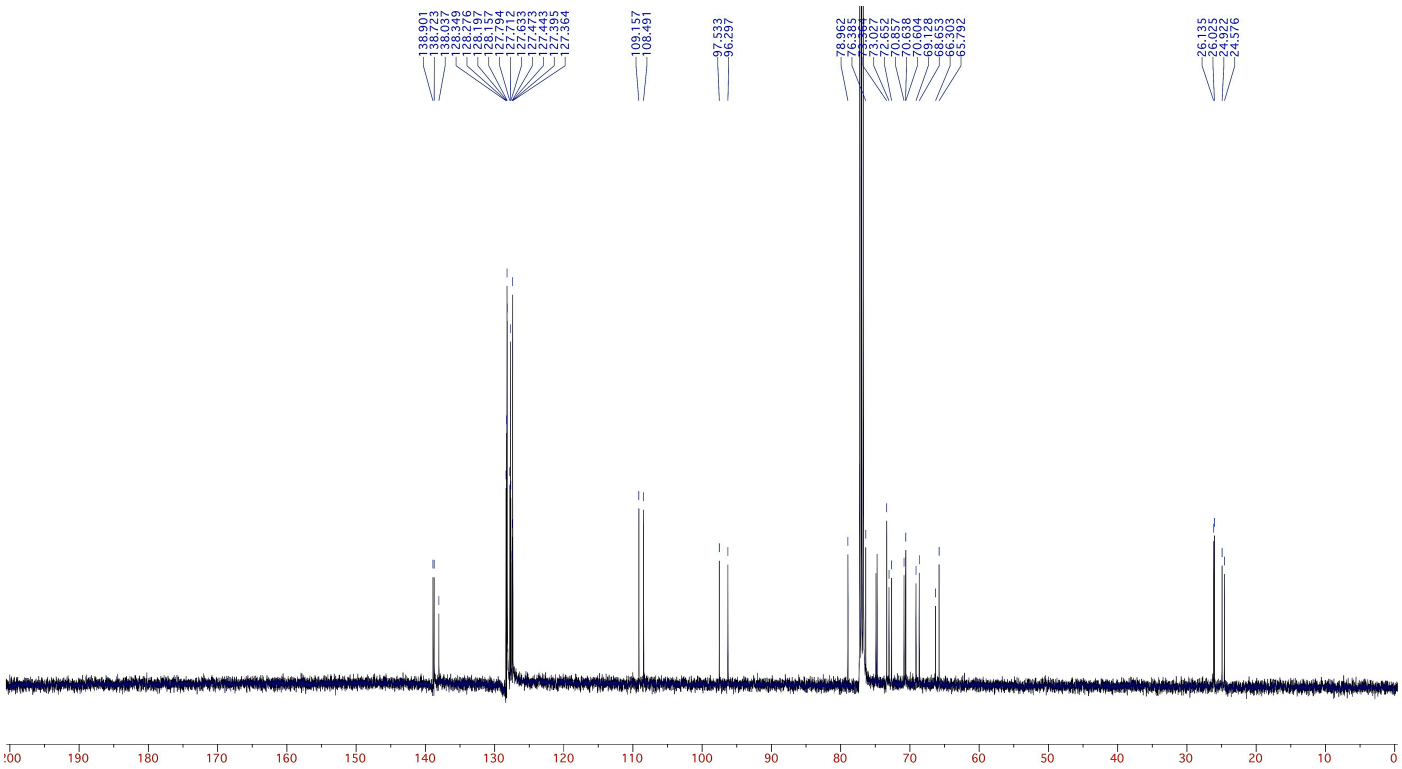

HO
OH
O
HO
HO
HO
O
O
HO
OH
OH

35

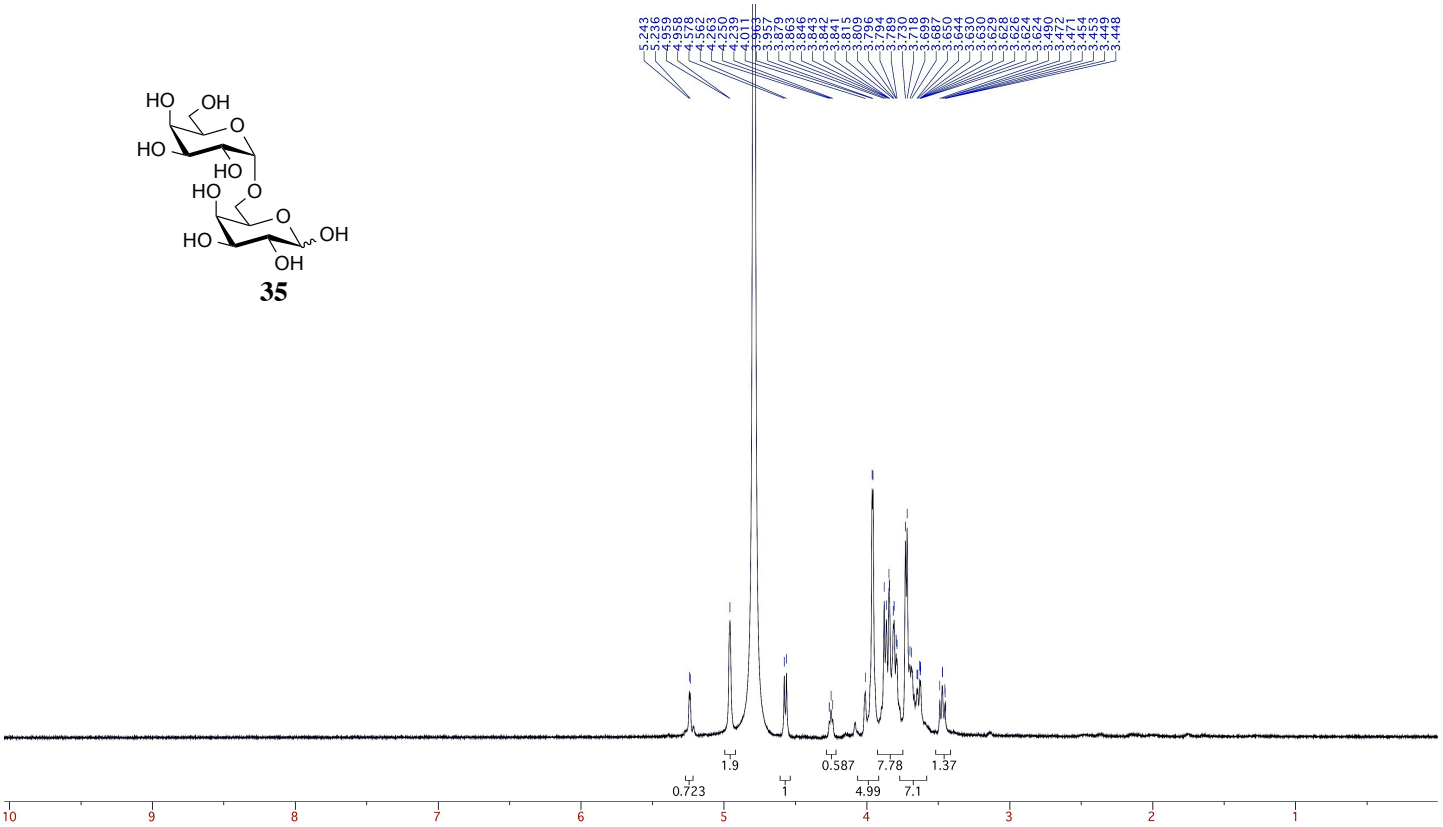
5.243
5.236
4.559
4.558
4.578
4.562
4.563
4.250
4.239
4.011
3.963
3.957
3.879
3.863
3.846
3.843
3.842
3.841
3.815
3.809
3.796
3.794
3.789
3.730
3.718
3.699
3.657
3.650
3.644
3.630
3.630
3.628
3.628
3.626
3.624
3.624
3.490
3.472
3.471
3.454
3.453
3.449
3.448
1.9
0.587
7.78
1.37
0.723
1
4.99
7.1
10
9
8
7
6
5
4
3
2
1

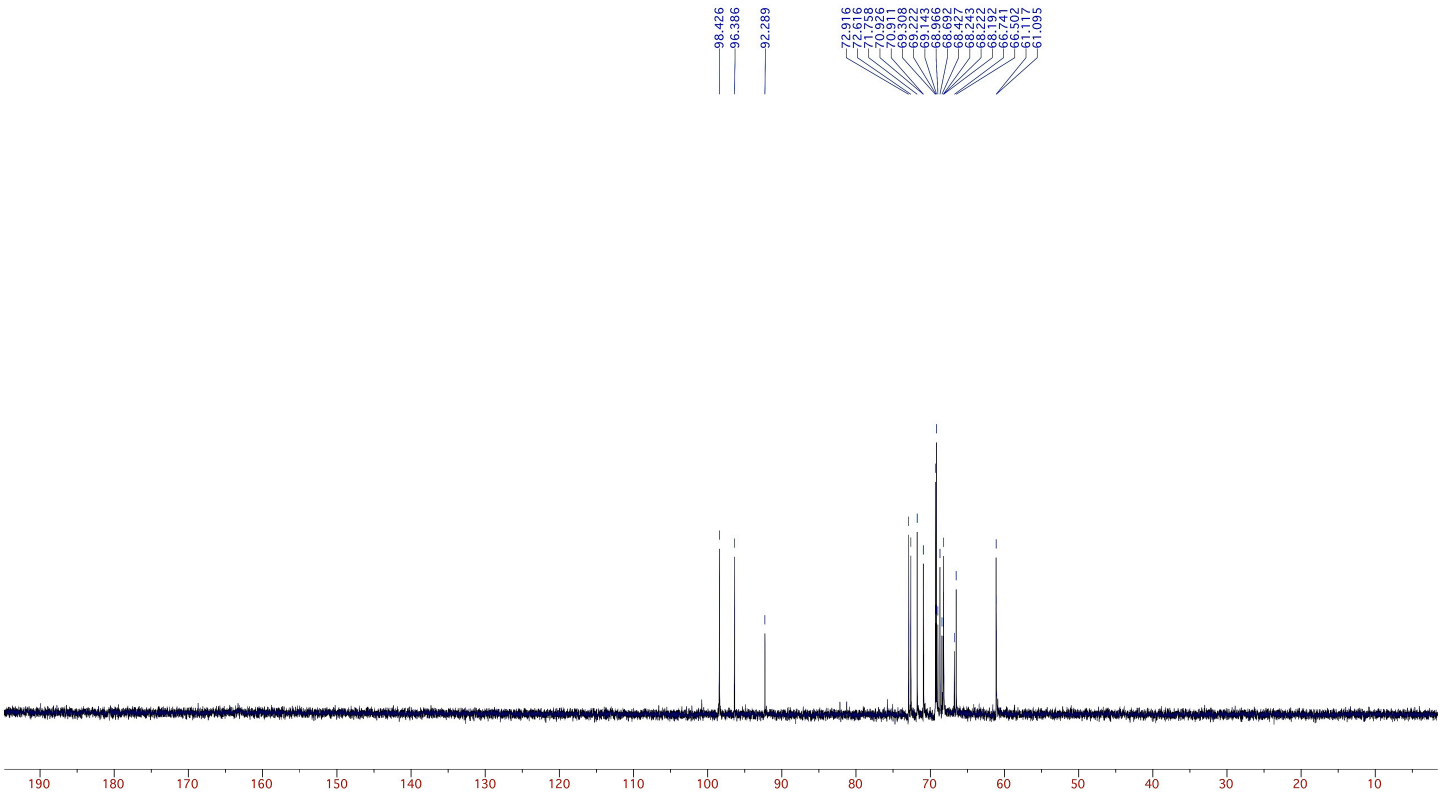
98.426
96.386
92.289
72.916
72.616
71.758
71.036
70.911
69.308
69.222
69.143
68.866
68.692
68.427
68.243
68.222
68.199
66.741
66.502
61.117
61.095
190
180
170
160
150
140
130
120
110
100
90
80
70
60
50
40
30
20
10

Chapter 6: Small Carbohydrate-Based Molecules as Ice Recrystallization Inhibitors – Carbohydrate-Based Surfactants and Hydrogelators

6.1 Introduction

The IRI activity exhibited by simple mono- and disaccharides was attributed to their ability to disrupt or disorder the structure of bulk-water.[1] The greater the disruption on the three-dimensional hydrogen-bond network of water due to a poorer "fit" into this network resulted in more IRI active carbohydrates. These carbohydrates exhibited relatively weak to moderate IRI activity compared with potent IRI derivatives, such as large peptides, glycopeptides and high molecular weight polymers.[2-21]

In an effort to design potently IRI active small molecules, interest arose in investigating carbohydrate-based molecules that were known to alter and/or sequester the structure of bulk-water for IRI activity. Such compounds included surfactants, organogelators and hydrogelators. These are amphiphilic molecules with a hydrophilic head and a hydrophobic tail that are able to self-assemble in water (or other solvents) to form micelles or hydrogels (figure 6.1).[22,23] Micelles are formed from surfactants where above the critical micelle concentration (CMC) in aqueous solution aggregates assemble with the hydrophobic tails sequestering in the center of the micelle allowing the hydrophilic head groups to interact with the solvent molecules. Above the CMC, micelles can convert to disk-like micelles and then cylindrical micelle fibres such as rods.[22] These fibres generally precipitate, however if they are formed with molecules that are hydrogelators they can become entangled and trap water molecules due to surface tension. This forms hydrogels, where the complete volume of solvent is immobilized within the fibers and the gel can support its own weight without collapsing (figure 6.1).[22,23]

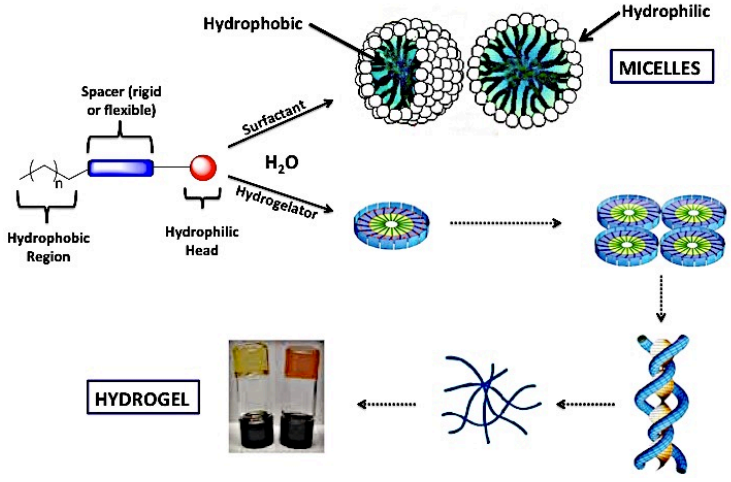

Figure 6.1 Illustration of the formation of micelles and hydrogels in aqueous solution with surfactants and hydrogelators.[22]

The IRI activity of the carbohydrate-based surfactants and hydrogelators was reported in an article published in *Chemical Science* in 2012. This article is provided in section 6.2. It describes the discovery of the first reported potently IRI active small molecules, the surfactant *n*-octyl-β-D-galactopyranoside (**4**) and the hydrogelator *N*-octyl-D-gluconamide (**5**) (figure 6.2).[24] The results described in section 6.3 are from this article, the synthesis of the molecules are described in section 6.3.1 and a summary and discussion of the IRI results are found in section 6.3.2. Ice binding studies are discussed in section 6.3.3 and rheology studies to examine the relationship between hydrogel formation and structure and IRI activity are described in section 6.3.4. All figures, schemes and compound numbers will be as indicated in the article and are reproduced with the same numbering schemes in sections 6.3 to complement the discussions. Compounds numbers from these syntheses are as reported in the supplementary information. Subsequent to this article, derivatives of the potently IRI active surfactant **4** and hydrogelator **5** were prepared to further investigate important structural features for their activity (structures described and shown in section 6.3.1). Compound numbers for these derivatives begin at **17** and any additional figures will be numbered continuing from figure 6.3.

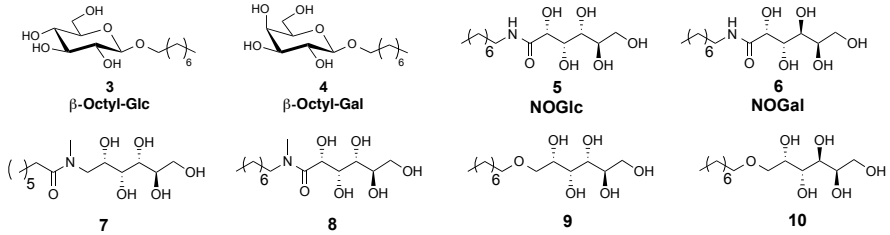

Figure 6.2 Structures of carbohydrate-based surfactants n-octyl-β-D-gluco- and galactopyranoside **3** and **4** and hydrogelators *N*-octyl-D-glucon- and galactonamide **5** and **6** assessed for IRI activity in the article in section 6.2. Surfactant **4** and hydrogelator **6** were the first reported small molecule ice recrystallization inhibitors.[24]

6.2 Article: "Potent Ice Recrystallization Inhibition by Low Molecular Weight Carbohydrate-Based Surfactants and Hydrogelators"

Chemical Science

www.rsc.org/chemicalscience

Volume 3 | Number 5 | May 2012 | Pages 1345–1716

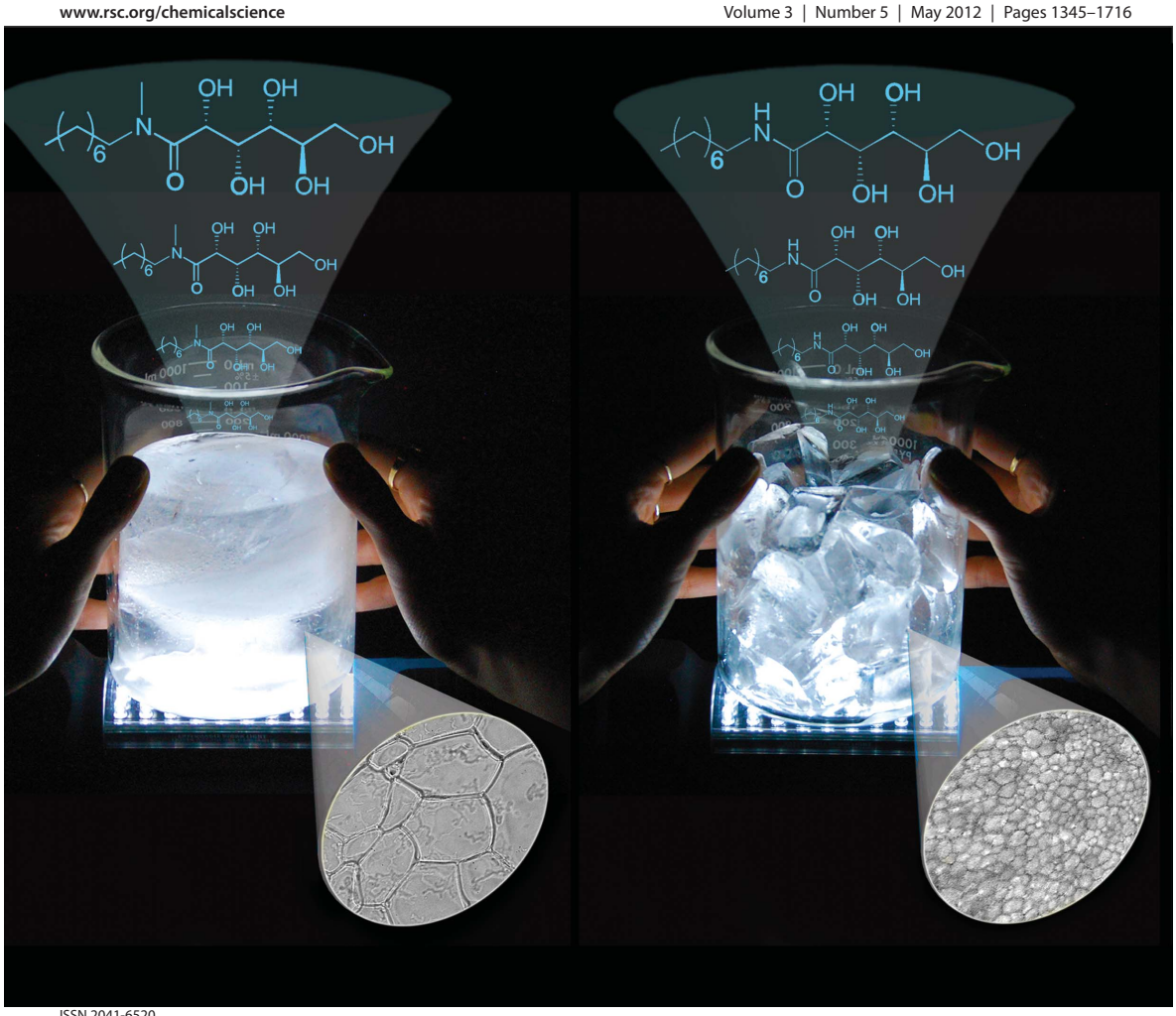

ISSN 2041-6520

RSC Publishing

EDGE ARTICLE

R. N. Ben *et al.*

Potent inhibition of ice recrystallization by low molecular weight carbohydrate-based surfactants and hydrogelators

Chemical Science

Dynamic Article Links

Cite this: *Chem. Sci.*, 2012, **3**, 1408

www.rsc.org/chemicalscience

EDGE ARTICLE

Potent inhibition of ice recrystallization by low molecular weight carbohydrate-based surfactants and hydrogelators†

Chantelle J. Capicciotti,[a] Mathieu Leclère,[a] Frédéric A. Perras,[a] David L. Bryce,[a] Hilary Paulin,[b] James Harden,[b] Yun Liu[c] and Robert N. Ben*[a]

Received 5th November 2011, Accepted 2nd February 2012
DOI: 10.1039/c2sc00885h

Ice recrystallization inhibition (IRI) activity is a very desirable property for an effective cryoprotectant. This property was first observed in biological antifreezes (BAs), which cannot be utilized in cryopreservation due to their ability to bind to ice. To date, potent IRI active compounds have been limited to BAs or synthetic *C*-linked AFGP analogues (**1** and **2**), all of which are large peptide-based molecules. This paper describes the first example of low molecular weight carbohydrate-based derivatives that exhibit potent IRI activity. Non-ionic surfactant *n*-octyl-β-D-galactopyranoside (**4**) exhibited potent IRI activity at a concentration of 22 mM, whereas hydrogelator *N*-octyl-D-gluconamide (**5**) exhibited potent IRI activity at a low concentration of 0.5 mM. Thermal hysteresis measurements and solid-state NMR experiments indicated that these derivatives are not exhibiting IRI activity by binding to ice. For non-ionic surfactant derivatives (**3** and **4**), we demonstrated that carbohydrate hydration is important for IRI activity and that the formation of micelles in solution is not a prerequisite for IRI activity. Furthermore, using solid-state NMR and rheology we demonstrated that the ability of hydrogelators **5** and **6** to form a hydrogel is not relevant to IRI activity. Structure–function studies indicated that the amide bond in **5** is an essential structural feature required for potent IRI activity.

Introduction

Biological antifreezes (BAs) are a very interesting class of molecules comprised of antifreeze proteins (AFPs) and antifreeze glycoproteins (AFGPs).[1,2] The "antifreeze" properties of these biomolecules protect organisms inhabiting sub-zero environments from cryo-injury and death. This unique ability was first recognized in the late 1960's and has attracted great interest due to potential applications in cryopreservation. However, attempts to utilize BAs as cryoprotectants have been met with limited success.[3,4] This is largely because BAs exhibit thermal hysteresis (TH) activity, meaning they have the ability to selectively depress the freezing point of a solution below that of the melting point.[5] The thermal hysteresis (TH) activity associated with these compounds is a result of irreversible binding of BAs to the surface of ice,[6] exacerbating cellular damage at cryopreservation temperatures.[7,8] This is unfortunate as BAs are also potent inhibitors of ice recrystallization. The ability to inhibit ice recrystallization is a very desirable property for a cryoprotectant[8–10] and compounds with potent ice recrystallization inhibition (IRI) activity have tremendous potential for applications in medicine and industry.

During the last decade, the rational design of novel compounds based on BAs has featured prominently in the literature.[11,12] However, only a few of these molecules have the ability to inhibit ice recrystallization, limiting compounds with potent IRI activity to BAs (native AFPs and AFGPs), synthetic analogues of AFGPs,[11,13,14] polyvinyl alcohol (PVA) and other high molecular weight polymers.[12,15,16] Our laboratory has demonstrated that *C*-linked AFGP analogues (**1** and **2**, Fig. 1) possess "custom-tailored" antifreeze activity. They are potent

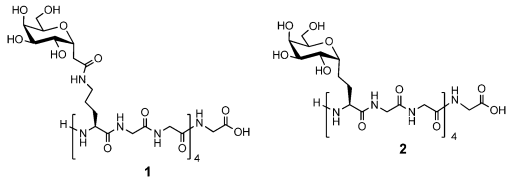

Fig. 1 The structures of previously prepared *C*-linked AFGP analogues.

This journal is © The Royal Society of Chemistry 2012

inhibitors of ice recrystallization but do not exhibit thermal hysteresis activity.[13,14] The cryoprotective ability of *C*-linked analogues **1** and **2** has been assessed and while **1** was not as effective as the commonly used 10% dimethyl sulfoxide (DMSO) cryoprotective solution, it was found to be as effective as a 2.5% solution of DMSO for the cryopreservation of human embryonic liver cells.[17] We have also demonstrated that simple mono- and disaccharides are moderate inhibitors of ice recrystallization.[18,19] Using these simple carbohydrates, we have demonstrated that inhibition of ice recrystallization during cryopreservation with human embryonic liver cell lines[20] and human umbilical cord blood[21] leads to increased cell viability after thawing. While these simple carbohydrates classify as small molecules, they are not potent inhibitors of ice recrystallization. Consequently, small molecules exhibiting potent IRI activity are very attractive, but efforts to design such molecules have been impeded because the structural attributes necessary to inhibit ice recrystallization remain unknown.

A number of articles and reviews have been published describing large peptide-based molecules related to BAs that exhibit IRI activity.[11,12,15] To date, there have been no reports of small molecule ice recrystallization inhibitors. We have postulated that the moderate IRI activity observed with simple carbohydrates was based upon their ability to alter the structure of bulk water, which is ultimately related to the degree of carbohydrate hydration.[18,22,23] Thus, in an effort to identify potent small molecule inhibitors of ice recrystallization, we sought to investigate the ability of various small molecules that alter the structure of bulk water and/or sequester bulk water to inhibit ice recrystallization. Such compounds include surfactants, organogelators and hydrogelators. In this paper, we systematically assess the ability of representative low molecular weight carbohydrate-based compounds in these classes to inhibit ice recrystallization and demonstrate that some of these compounds are potent ice recrystallization inhibitors.

Results and discussion

Assessment of IRI activity of carbohydrate-based non-ionic surfactants

n-Octyl-β-D-glycosides (**3** and **4**, Fig. 2) are well-known non-ionic surfactants. These surfactants have been extensively studied for many applications, including crystallization and solubilisation of membrane proteins, as well as lipid-based drug delivery systems.[24,25] However, one application which has yet to be explored for these surfactants is the ability to inhibit ice recrystallization. Thus, both carbohydrate-based non-ionic surfactants **3** and **4** were synthesized (supplementary information†) and their IRI activity was assessed using a "splat cooling" assay.[26] In this assay, the area of ice crystals are measured after a 30 min annealing time at −6.4 °C and compared to a positive control for ice recrystallization, resulting in a quantitative measurement of the mean ice grain size.[27] For a positive control, a phosphate buffered saline (PBS) solution was utilized. All samples are normalized to the PBS positive control.

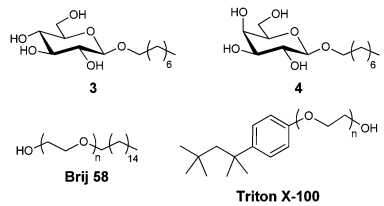

Fig. 2 The structures of non-ionic surfactants *n*-octyl-β-D-glucopyranoside (**3**), *n*-octyl-β-D-galactopyranoside (**4**), Brij 58 (average M_n = 1124, $n = 20$)[29] and Triton X-100 (average $M_n = 625$, $n = 9$–10).[30]

The IRI activity of carbohydrate-based non-ionic surfactants **3** and **4** is shown in Fig. 3. The IRI activity of **3** (β-Octyl Glc) at 22 mM was statistically similar[28] to that of D-glucose (Fig. 3). This result is consistent with what has previously been reported by our laboratory, where the nature of the substituent at the C1 position had little influence upon IRI activity (relative to the parent carbohydrate) at concentrations of 22 mM.[18] Even at a concentration of 44 mM, the IRI activity of **3** is still identical to that of 22 mM D-glucose. Interestingly, the IRI activity of its diastereomer **4** (β-Octyl Gal) at 11, 22 and 44 mM was, in all cases, significantly better than 22 mM D-galactose.

A 22 mM solution of **3** is expected to form micelles in solution, as its critical micelle concentration (CMC) in water is 18–22 mM.[25,31] However, the CMC of **4** in water is 30 mM.[31,32] While these values are reported in water and not PBS, it has been documented that the CMCs of non-ionic surfactants are only slightly lower in salt solutions.[33,35] Thus, it would be expected that the CMC values for **3** and **4** would be slightly decreased in PBS. The fact that **3** is expected to form micelles at concentrations of 22 mM and higher, but it does not exhibit potent IRI activity even at 44 mM suggests that micelle formation may be unrelated to IRI activity. Similarly, a 22 mM solution of **4** is below its CMC value of 30 mM, but a 22 mM solution of **4** is a very potent inhibitor of ice recrystallization. It seems reasonable to conclude that if IRI activity were dependent on the ability to form micelles, then any compound with the capacity to form micelles should inhibit ice recrystallization at concentrations above its CMC. However, this is not what we observed for non-ionic carbohydrate-based surfactants **3** and **4**. To further explore this hypothesis, the IRI activity of several other common surfactants was examined. Sodium dodecyl sulphate (SDS) is an anionic surfactant with a CMC in PBS of 5 mM.[34] The IRI activity of SDS was assessed at concentrations at, above and below this value (5, 10 and 0.5 mM, respectively) and these results are presented in Fig. 3. At all three concentrations, SDS exhibited no IRI activity, again suggesting that the formation of micelles in solution is not correlated to IRI activity. However, SDS is an anionic surfactant and might not be regarded as an accurate comparison to non-ionic surfactants **3** and **4**. Consequently, the IRI activity of Brij 58 and Triton X-100 (Fig. 2), non-ionic surfactants which are structurally unrelated to the carbohydrate-based surfactants, were also examined. The CMC values of Brij 58 and Triton X-100 in water are 0.08 mM[29,33] and 0.24 mM, respectively,[30,33] and their IRI was assessed at concentrations well above their CMC values (Fig. 3). At 10 mM, both Brij 58 and Triton X-100 exhibited weak to moderate IRI activity, while at 5 mM (a concentration still well above their CMC values) they were only weakly IRI active. This suggests that the moderate IRI activity observed at 10 mM for these

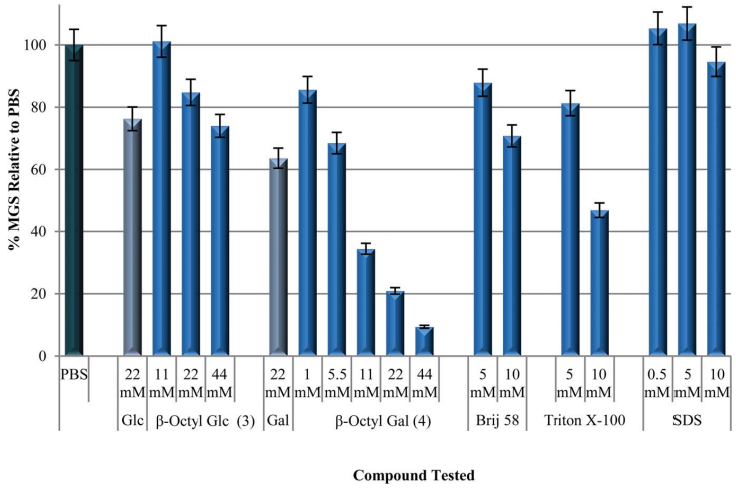

Fig. 3 IRI activity of non-ionic surfactants **3** (CMC = 18–22 mM),[25,31] **4** (CMC = 30 mM),[31,32] Brij 58 (average M_n = 1124, n = 20, CMC = 0.08 mM),[29,33] Triton X-100 (average M_n = 625, n = 9–10, CMC = 0.24 mM)[30,33] and anionic surfactant SDS (CMC = 5 mM).[34] All compounds are represented as a % MGS (mean grain size) of ice crystals relative to the PBS positive control.

non-ionic surfactants is likely a result of increased concentration and not micelle formation. While these non-ionic surfactants do exhibit some IRI activity above their respective CMC values, an 11 mM solution of **4** is more IRI active and this concentration is below the CMC of **4**. These results provide further evidence that the potent IRI activity of non-ionic surfactant **4** at 22 mM is unrelated to micelle formation.

Our laboratory has previously correlated IRI activity to hydration index (HI). The hydration index is a function of the hydration number of a carbohydrate divided by the apparent molar volume and provides an indication of the degree of hydration in a substrate as a function of size or volume.[18] This metric has proven useful to rationalize the fact that highly hydrated disaccharides, such as melibiose (hydration number 15.5),[22] exhibit the same IRI activity as highly hydrated monosaccharides, such as D-galactose (hydration number 8.7),[22] at concentrations of 22 mM or lower. However, at much higher concentrations (*e.g.* 220 mM) hydration numbers, not hydration indices, are better predictors of IRI activity.[20] The work described above was the first to correlate IRI activity to hydration of a carbohydrate and suggested that IRI activity may be predicted provided that the hydration of a substrate (hydration index, molar compressibility values, *etc.*) has been previously quantified. In this current work, the non-ionic carbohydrate-based surfactants were assessed for IRI activity at concentrations of 44 mM or lower. Thus, the hydration of these derivatives may be correlated to their IRI activity by use of their hydration indices. The molar isentropic compressibility of **3** and, subsequently, hydration numbers and apparent molar volumes have been reported in the literature.[36] The hydration number of **3** is 16,[36] which is twice that reported for D-glucose (8.4).[22] However, the apparent molar volume of **3** is approximately twice that of D-glucose,[36] resulting in a hydration index that is nearly identical to that calculated for D-glucose.[18] Thus, the similar IRI activity observed for **3** and D-glucose at 22 mM is not surprising as their hydration indices are very similar. This is the first instance where hydration index has predicted the IRI activity of a molecule other than a simple reducing mono- or disaccharide. The fact that **3** (derived from D-glucose) is less active than **4** (derived from D-galactose) correlates with previously published IRI data of simple monosaccharides[18] and *C*-linked AFGP analogues.[13] Despite the presence of an alkyl chain at the C1 position, the highly hydrated D-galactopyranose ring of **4** results in increased IRI activity. Unfortunately, the hydration number and apparent molar volume of **4** have not been reported in the literature and thus calculation of a hydration index is not possible. However, the increased hydration associated with a D-galactopyranose residue[22] and the potent IRI activity associated with **4** would suggest that its hydration numbers are much greater than those of **3**. Thus, it seems that surfactants derived from pyranose derivatives possessing a highly hydrated head group will be more potent inhibitors of ice recrystallization. The role of the octyl chain at C1 and its effect upon hydration is currently being investigated and other carbohydrate derivatives of **3** and **4** are being synthesized in an effort to further study the correlation between hydration of the pyranose ring and IRI activity.

Assessment of IRI activity of carbohydrate-based hydrogelators

N-Octyl-D-aldonamides (**5** and **6**, Fig. 4) are another class of low molecular weight carbohydrate-based compounds known to self-assemble in water.[37–40] These compounds are prone to aggregation and formation of fibres and hydrogels. Small organic molecules that are capable of gelling aqueous solvents have generated intense interest due to the many possible applications, which include controlled drug delivery, enzyme inhibition assays and biocompatible scaffolds for tissue repair and tissue engineering.[41] High molecular weight hydrogel systems (*e.g.* gelatin, alginate, fibrinogen) have been investigated in cryopreservation to form scaffolds for cells, however, the addition of

This journal is © The Royal Society of Chemistry 2012

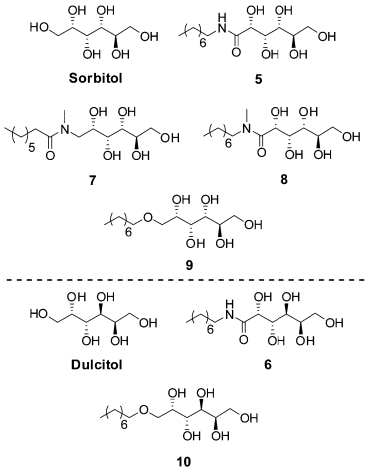

Fig. 4 The structures of D-sorbitol, D-dulcitol, low molecular weight hydrogelator derivatives *N*-octyl-D-gluconamide (NOGlc, **5**) and *N*-octyl-D-galactonamide (NOGal, **6**), *N*-methylated derivatives **7** and **8**, and ether-linked derivatives **9** and **10**.

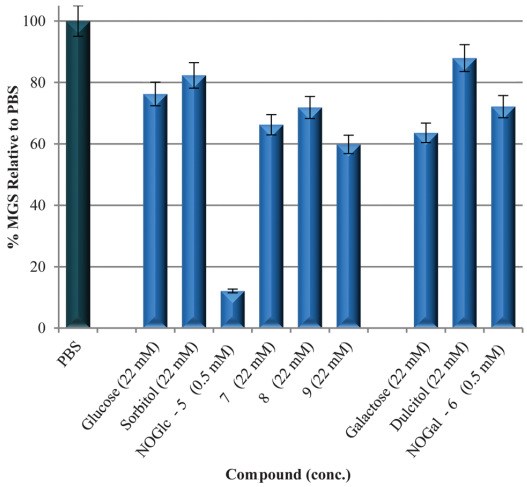

Fig. 5 IRI activity of D-sorbitol, D-dulcitol, low molecular weight hydrogelator derivatives **5** (NOGlc) and **6** (NOGal), *N*-methylated derivatives **7** and **8**, and ether-linked derivative **9**. All compounds are represented as a % MGS (mean grain size) of ice crystals relative to the PBS positive control.

a cryoprotectant like DMSO is still required for cells to survive the freezing and thawing process.[42] To date, the use of low molecular weight hydrogelators as cryoprotectants or as ice recrystallization inhibitors has yet to be explored. Consequently, we synthesized several low molecular weight carbohydrate-based hydrogelators and assessed their ability to inhibit ice recrystallization.

The carbohydrate moiety of the *N*-octyl-D-aldonamides is in the open-chain alditol form. Therefore, prior to assessing the IRI activity of these hydrogelators, we assessed the activity of D-sorbitol and D-dulcitol (structures shown in Fig. 4), the open-chain and reduced form of D-glucose and D-galactose, respectively (Fig. 5). The importance of the pyranose ring for IRI activity is evident as both of these alditols had decreased activity relative to their pyranose forms. While hydration numbers for the pyranose forms of D-galactose and D-glucose have previously been reported,[22] the hydration numbers for the alditols (D-dulcitol and D-sorbitol) are not known. However, it is known that the hydration of a monosaccharide is mostly dependent on the relative stereochemistry of the C2 and C4 hydroxyl groups of the pyranose ring.[22,43] There is a significant decrease in IRI activity for D-dulcitol in comparison to D-galactose and the IRI activity of both alditols (D-dulcitol and D-sorbitol) are statistically similar.[28] This result suggests that removal of the rigid pyranose ring of a monosaccharide directly influences hydration and results in a loss of IRI activity.

The IRI activity of low molecular weight carbohydrate-based hydrogelators **5** and **6** is shown in Fig. 5. Due to the poor solubilities associated with these compounds in water and PBS,[38–40] they could only be assessed for IRI activity at 0.5 mM. Surprisingly, *N*-octyl-D-gluconamide (NOGlc, **5**) exhibited potent IRI activity at 0.5 mM, while its diastereomer, *N*-octyl-D-galactonamide (NOGal, **6**) exhibited only moderate IRI activity. In fact, the activity of **6** at 0.5 mM was statistically similar[28] to the activity of D-galactose at 22 mM. These results are unprecedented and, to the best of our knowledge, this is the first example where a D-glucose derivative was a more potent inhibitor of ice recrystallization than a D-galactose derivative. From the previous section, the moderate IRI activity observed for carbohydrate-based surfactant **3** at 22 mM was correlated to carbohydrate hydration by its hydration index and the potent activity of **4** at 22 mM was hypothesized to result from the presence of a highly hydrated D-galactopyranose ring. However, hydration characteristics for the *N*-octyl-D-aldonamides (**5** and **6**) and their alditol carbohydrate residues (D-dulcitol or D-sorbitol) are not known, and so the influence of hydration on the potent IRI activity of **5** cannot be elucidated at this time. Nevertheless, *N*-octyl-D-gluconamide (**5**) is the first example of a small molecule having potent IRI activity at a significantly lower concentration than 22 mM. Interestingly, much like non-ionic D-galactose-based surfactant **4**, D-glucose-based hydrogelator **5** is capable of forming micelles in solution and has a CMC of 10 mM in water.[37] A 0.5 mM solution of **5** is well below the reported CMC value, yet **5** exhibits unusually potent IRI activity at this concentration. Also, similar to **4**, the IRI activity of **5** is concentration dependent. A 0.25 mM solution of **5** exhibited moderate IRI activity and a 0.1 mM solution of **5** exhibited weak IRI activity (supplementary information, Fig. S1†). This provides additional evidence that the formation of micelles is not a prerequisite for potent IRI activity.

Compound **5** is capable of forming a hydrogel at 1% w/v in water,[37,38] which corresponds to a concentration of 33 mM. The fact that **5** exhibits potent IRI activity at 0.5 mM (below its gelation concentration) implies that this activity is not related to the formation of a hydrogel. Compound **6** also forms a hydrogel at a concentration of 0.5% w/v (16 mM),[38,39] but **6** is significantly less IRI active than **5**. These results indicate that IRI activity is not dependent on formation of a hydrogel. In order to further

investigate the structural features responsible for the potent IRI activity of **5**, D-glucose derivatives **7–9** (Fig. 4) were synthesized (supplementary information†) and their IRI activity was assessed.

It has previously been reported that the amide bond in **5** was important for hydrogel formation[37,38] and that *N*-methylated derivative **7** lacked that ability to form hydrogels.[37] This was attributed to the hydrogen-bond donating ability of the amide linkage. In order to assess whether the amide bond of **5** played a similar role in IRI activity, the *N*-methylated derivative **7** was synthesized and its IRI activity was assessed (Fig. 5). The results suggest that the proton on the nitrogen of the amide bond is an important structural feature for the IRI activity of **5**, as **7** had significantly reduced activity at a much higher concentration (22 mM). The orientation of the amide bond in **7** is actually "reversed" relative to **5** and thus **8**, the direct *N*-methylated derivative of **5**, was synthesized (supplementary information†) and assessed for IRI activity. Compound **8** exhibited similar IRI activity to **7** at 22 mM, further validating the importance of the proton on the amide bond in **5** for potent IRI activity. Replacement of the amide bond in D-glucose derivative **5** with an ether linkage (**9**) resulted in a dramatic decrease in IRI activity. Ether-linked derivative **9** exhibited IRI activity similar to **7** and **8** at 22 mM. Collectively, these results indicate that the amide bond of **5** is crucial for potent IRI activity.

Interestingly, **9**, the open-chain alditol derivative of non-ionic D-glucose-based surfactant **3** (Fig. 2), was a better inhibitor of ice recrystallization than **3** at 22 mM (Fig. 3 and 5). This was surprising, as the IRI activity of the alditols D-sorbitol and D-dulcitol (Fig. 5) was decreased in comparison to the corresponding pyranose forms of the sugars (D-glucose and D-galactose, respectively). As non-ionic D-galactose surfactant **4** (Fig. 2) exhibited potent IRI activity at 22 mM (Fig. 3), we synthesized **10** (supplementary information†), the open-chain alditol derivative of **4**, to further examine the influence of the alditol moiety on IRI activity. Unfortunately, even at 11 mM, **10** was insoluble in PBS, and thus its IRI activity could not be assessed at similar concentrations which **4** and **9** were assessed.

Assessment of interactions with the ice lattice

Our laboratory has previously demonstrated that *C*-linked AFGP analogues **1** and **2** exhibited potent IRI activity but did not possess TH activity.[13,14] This suggested that the mechanism of action for these potent inhibitors of ice recrystallization is different from native AF(G)Ps as no direct interaction with the ice lattice was observed. As both D-galactose derivative **4** (at 22 mM) and D-glucose derivative **5** (at 0.5 mM) are novel potent low molecular weight inhibitors of ice recrystallization, we investigated whether they were interacting directly with the ice lattice. Thus, carbohydrate derivatives **3–6** were examined for TH activity using nanolitre osmometry.[44] Briefly, in this assay a single droplet of the sample in water is suspended in the centre of an oil-filled well in a sample holder plate. The sample is then rapidly frozen using a thermoelectrically controlled microscope stage, then the temperature is raised and the sample melted until only a single ice crystal remains. Once a single ice crystal is obtained, its growth and behaviour upon increasing/decreasing the temperature can be viewed under a microscope.

Our previously synthesized *C*-linked AFGP analogues and carbohydrate derivatives were assessed for TH activity at 10 mg mL^{-1}.[13,14,18] Derivatives **3–6** could not be assessed for TH activity at this concentration due to their amphiphilic nature. During the process of melting the frozen sample to obtain a single ice crystal, the droplet dissolved in the oil resulting in one phase. Thus, derivatives **3** and **4** were assayed at a concentration of 1 mg mL^{-1}, and derivatives **5** and **6** were assayed at a concentration of 0.01 mg mL^{-1}. None of these derivatives (**3–6**) exhibited TH activity or dynamic ice shaping at these concentrations (Fig. 6(a–d)). The absence of dynamic ice shaping indicated there was no interaction with the ice lattice.

Many AF(G)Ps have measureable TH gaps at concentrations as low as 0.5 mg mL^{-1}.[2b,2c,45] However, only hyperactive AFPs have been reported to have measureable TH activity at concentrations of 0.01–0.05 mg mL^{-1}.[46] Therefore, native AFGP-8 was assayed at a concentration of 0.01 mg mL^{-1} for dynamic ice shaping and TH activity. While no measureable TH gap was obtained for AFGP-8 at 0.01 mg mL^{-1}, dynamic ice shaping was observed (Fig. 6(e)). This indicated that even at a low concentration of 0.01 mg mL^{-1} evidence of an interaction with the ice lattice can still be observed, even in the absence of a measurable TH gap. The fact that **5** and **6** do not exhibit this activity suggests that these compounds are not interacting with the ice lattice. However, as derivatives **5** and **6** could not be tested for TH activity at a concentration higher than 0.01 mg mL^{-1}, we investigated if interactions with the ice lattice could be further examined by another method. Consequently, we attempted to ascertain whether such interactions could be observed using solid-state NMR.

Solid-state NMR has been utilized to observe the interaction of a type III AFP with ice.[47] In this study, one of the findings was that the ^2H spin–lattice relaxation rate (R_1) of frozen D_2O in the presence of the AFP was much faster in comparison to the ^2H R_1 of frozen D_2O on its own. It was also found that the R_1 of frozen D_2O in the presence of ubiquitin was similar to that of frozen D_2O on its own. The faster relaxation in the presence of the AFP was hypothesized to be a direct result of the AFP binding to ice, as the R_1 of frozen D_2O in the presence of the negative control, ubiquitin, was similar to that of D_2O on its own and ubiquitin does not interact with the ice lattice.

Prior to measuring the ^2H R_1 of frozen D_2O in the presence of derivatives **3–6**, we measured the R_1 of pure D_2O at −25 °C, as well as the R_1 of frozen D_2O in the presence of three positive

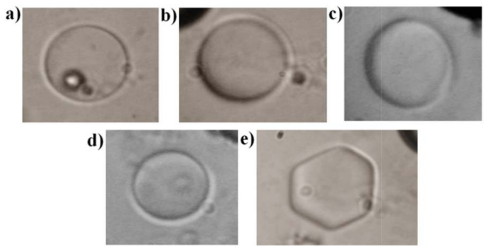

Fig. 6 Ice crystal habits in the presence of (a) **3** (1 mg mL^{-1}), (b) **4** (1 mg mL^{-1}), (c) **5** (0.01 mg mL^{-1}), (d) **6** (0.01 mg mL^{-1}) and (e) AFGP-8 (0.01 mg mL^{-1}) in water.

This journal is © The Royal Society of Chemistry 2012

controls and one negative control for ice binding. The saturation recovery curves for these measurements are shown in Fig. 7(a). Two of the positive controls chosen were a type I AFP (winter flounder, *Pseudopleuronectes americanus*) and a type III AFP (ocean pout, *Macrozoarces americanus*).[48] As can been seen from Fig. 7(a), the R_1 of frozen D_2O with both type I and type III AFP is much faster than the R_1 of frozen D_2O on its own. The third positive control used was the wild-type AFP of a perennial ryegrass, *Lolium perenne* (WT *Lp*AFP).[49,50] This AFP was chosen as it can be recombinantly expressed in *Escherichia coli* (*E. coli*). In addition, a mutant of this AFP (T67Y *Lp*AFP) could be utilized as a negative control for ice binding, as it has previously been demonstrated that substitution to a bulky tyrosine residue disrupted the discrete complementarity between the ice-binding face of the AFP and ice, resulting in minimal TH activity.[50] Thus, WT *Lp*AFP and T67Y *Lp*AFP were recombinantly expressed in *E. coli* (supplementary information†) and the R_1 of frozen D_2O in their presence was measured (Fig. 7(a)). The R_1 of frozen D_2O with T67Y *Lp*AFP was similar to that of frozen D_2O on its own. In contrast, a significantly faster ^2H relaxation rate was observed in the presence of all three positive controls, which are known to bind to ice.

Next we recorded the saturation recovery curves of frozen D_2O in the presence of derivatives **3–6**, as well as D-glucose and D-galactose. All of these molecules are significantly smaller than the AFP positive controls. Therefore, to account for the drastic difference in molecular weights, the concentration at which each carbohydrate derivative was measured was corrected to a total overall proton concentration of 1234 mM – the overall protein proton concentration used for the type III AFP in the original study.[47] As shown in Fig. 7b, in the presence of D-galactose derivative **4**, the R_1 of frozen D_2O was similar to that of D_2O on its own, suggesting it is not interacting with the ice lattice. Similar results were also obtained for D-galactose, D-glucose and D-glucose derivative **3** (supplementary information, Fig. S2(a–c)†), where the R_1 of frozen D_2O in the presence of these compounds was similar to the R_1 of frozen D_2O on its own. These results further validated the previous TH results and suggest that the potent IRI activity of **4** at 22 mM is not due to an interaction with the ice lattice.

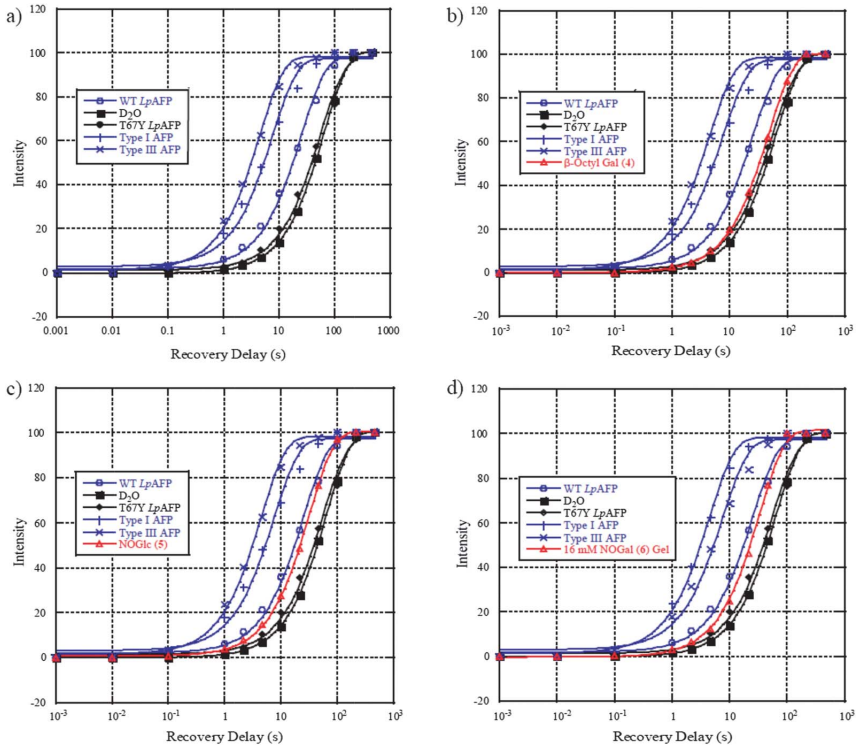

Fig. 7 Saturation recovery curves of frozen D_2O with AFPs or carbohydrate derivatives. The concentration of all carbohydrate derivatives was corrected to a total overall proton concentration of 1234 mM, unless stated otherwise. The ^2H relaxation rate for frozen D_2O was $R_1 = 0.0154 \pm 0.0002\ s^{-1}$. (a) Three positive controls for ice binding: Type I AFP ($R_1 = 0.13 \pm 0.01\ s^{-1}$), Type III AFP ($R_1 = 0.22 \pm 0.01\ s^{-1}$), WT *Lp*AFP ($R_1 = 0.039 \pm 0.002\ s^{-1}$); one negative control for ice binding: T67Y *Lp*AFP ($R_1 = 0.018 \pm 0.001\ s^{-1}$). (b) AFP controls and derivative **4** ($R_1 = 0.0209 \pm 0.0002\ s^{-1}$). The concentration at which **4** was measured was 44 mM. (c) AFP controls and frozen hydrogel of derivative **5** ($R_1 = 0.0310 \pm 0.0005\ s^{-1}$). The concentration at which **5** was measured was 42 mM. (d) AFP controls and frozen hydrogel of derivative **6** ($R_1 = 0.030 \pm 0.001\ s^{-1}$). The concentration at which **6** was measured was 16 mM, which corresponds to a total overall proton concentration of 479 mM.

The saturation recovery curve of frozen D_2O with D-glucose derivative **5** is shown in Fig. 7(c). Surprisingly, the R_1 of frozen D_2O in the presence of **5** was faster than that of frozen D_2O on its own. However, since the TH measurements of **5** indicated no dynamic ice shaping, it seemed unlikely that the faster R_1 was due to an interaction with the ice lattice. As the concentration of the low molecular weight carbohydrate derivatives were corrected to a total overall proton concentration of 1234 mM, this corresponded to a 42 mM concentration of **5** in solution. At 42 mM, **5** forms a hydrogel, and so consequently the NMR measurements were conducted on a frozen hydrogel. The formation of a gel is inevitably going to be accompanied by a decrease in correlation time due to an increased mobility of the water molecules in the solid-state.[51,52] This is expected to cause an increase in R_1, which was seen experimentally. Therefore, we believe that the faster R_1 observed for frozen D_2O with **5** is due to increased molecular motion during these measurements caused by gelation. This hypothesis was further supported by the saturation recovery curve of frozen D_2O with D-galactose derivative **6** (Fig. 7(d)). Due to solubility problems, the highest concentration at which **6** could be measured was its gelation concentration of 0.5% w/v,[38,39] which corresponds to a concentration of 16 mM. A similar effect to what was seen with **5** (Fig. 7(c)) was observed with **6** where the R_1 of D_2O in the frozen hydrogel of **6** was faster than the R_1 of frozen D_2O on its own (Fig. 7(d)). However, a 16 mM solution of **6** has a total overall proton concentration of only 479 mM and at a similar protein proton concentration with the WT *Lp*AFP, the measured R_1 value is similar to frozen D_2O on its own (supplementary information, Fig. S2(d)†). As expected, the effect of ice binding on R_1 is concentration dependant.[47] Thus, as at the lower total proton concentration a faster R_1 was observed for the frozen hydrogel of **6**; these results suggest that the faster relaxation rates of frozen D_2O observed with **5** and **6** are likely due to an effect of gelation.

Interestingly, the R_1 values of frozen D_2O in both of the hydrogels (**5** and **6**) are similar (Fig. 7(c–d)) despite their dramatic difference in IRI activity. This result further validates the hypothesis that simply the ability to form a hydrogel does not necessarily result in potent IRI activity. Regardless of concentration, both **5** and **6** were studied as frozen hydrogels in the solid-state NMR experiments and both had the same relative increase in the relaxation rate of frozen D_2O. However, only D-glucose derivative **5** had potent IRI activity (Fig. 5).

Characterization of hydrogels

While the ability of the D-glucose derivative **5** and the D-galactose derivative **6** to self-assemble into hydrogel phases has previously been reported,[37–40] the characterization of these hydrogels has not been discussed in the literature. Therefore, we sought to study the hydrogel phases of derivatives **5** and **6** using microscopy and rheology to determine their microstructural and mechanical properties, with the aim to examine any relationships between the material properties and IRI activity in these systems. We first observed the morphologies of hydrogels formed with **5** and **6** in water and PBS using scanning transmission electron microscopy (STEM). Images of these gels are shown in Fig. 8. The fibres in the hydrogel of **5** in water consist of a lattice-like network of helices with well-defined junctions serving as crosslinks (Fig. 8(a)). In contrast, the fibres in the hydrogel of **6** in water consist of a less organized entangled, fibrous phase of ribbons (Fig. 8b). These results are consistent with what has previously been reported for these compounds.[37–40] The morphology of these hydrogels is very similar in PBS, the solvent used in the IRI assay, as shown in Fig. 8(c) (for **5**) and Fig. 8(d) (for **6**).

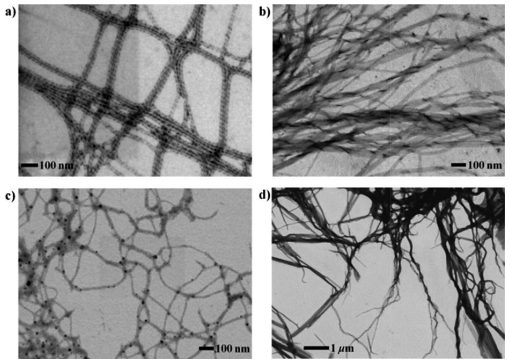

Fig. 8 STEM images of the hydrogels of (a) 1% w/v NOGlc (**5**) in water (33 mM), (b) 0.5% w/v NOGal (**6**) in water (16 mM), (c) 1% w/v NOGlc (**5**) in PBS (33 mM), (d) 0.5% w/v NOGal (**6**) in PBS (16 mM). All hydrogels were negatively stained using 1% phosphotungstic acid.

The hydrogel phases of **5** and **6** have different mechanical properties. Hydrogels of **5** are relatively stable solid phases with viscoelastic properties reminiscent of chemically cross-linked polymer gels. Plots of the storage and loss moduli, $G'(\omega)$ and $G''(\omega)$ respectively, as a function of the frequency (ω) of the applied oscillatory strain are shown in Fig. 9 for several concentrations of **5** in water and PBS. For all but the lowest concentration of **5** in water (1% w/v), these hydrogels behave as viscoelastic solids with frequency-independent $G'(\omega)$ and $G''(\omega)$, and a large ratio, $G'(\omega)/G''(\omega)$, indicating relatively weak dissipative behaviour. At the lowest concentration of **5** in water

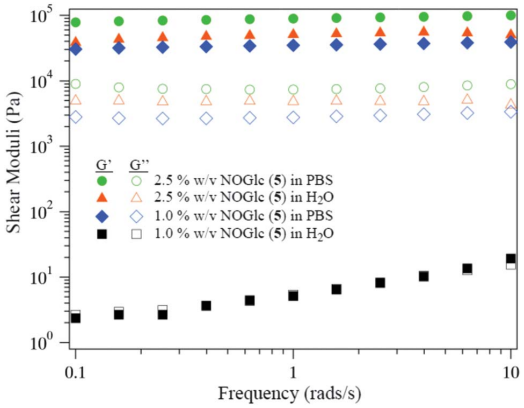

Fig. 9 Dynamic shear moduli of the hydrogels of NOGlc (**5**) in water and PBS as a function of angular frequency ω. $G'(\omega)$ represents the storage (elastic) modulus while $G''(\omega)$ is the loss (viscous) modulus.

This journal is © The Royal Society of Chemistry 2012

(1% w/v), $G'(\omega)$ and $G''(\omega)$ are comparable in magnitude and increase with ω, indicating the onset of gelation at this concentration. The moduli of the hydrogel phases of **5** are dependent on concentration and strongly increase with higher concentrations of NOGlc (**5**). Additionally, they are strongly dependent on the solvent, with superior hydrogel properties in PBS. In contrast, solutions of NOGal (**6**) form fragile, solid phases in both water and PBS. Modest mechanical agitation of these phases results in a fluidization of the hydrogel into a viscous slurry. Thus, we were unable to obtain reliable rheological data for **6**.

The results of the STEM and rheological studies indicate that NOGlc (**5**) forms a much stronger and more stable hydrogel than NOGal (**6**). Interestingly, derivative **5** is also significantly more IRI active than derivative **6**. However, as previously discussed, **5** and **6** were assessed for IRI activity at 0.5 mM, a concentration well below both of their gelation concentrations (33 mM for **5** and 16 mM for **6**). It therefore seems unlikely that gelation strength is related to IRI activity, as simply the ability to form a hydrogel does not necessarily result in IRI activity. There is a drastic difference in the solubilities of **5** and **6** in hot water: NOGlc is soluble to 50% w/v (1630 mM), whereas NOGal is significantly less soluble, being saturated at 0.5% w/v (16 mM).[38–40] Consequently, we believe that the difference in the strengths of the hydrogels of **5** and **6** is a result of the significant difference in solubilities of these derivatives. The insolubility of **6** could result in the hydrogel being more prone to collapsing and fluidization and could account for its more fragile hydrogel phase. However, it is interesting that the IRI activity for hydrogelators **5** and **6** follows the trend for solubility and hydrogel strength.

Conclusions

In summary, we have discovered D-galactose derivative **4** and D-glucose derivative **5**, which are novel potent low molecular weight carbohydrate-based ice recrystallization inhibitors. The non-ionic surfactant *n*-octyl-β-D-galactopyranoside (**4**) exhibited potent IRI activity at a concentration of 22 mM, whereas the low molecular weight carbohydrate-based hydrogelator *N*-octyl-D-gluconamide (**5**) exhibited potent IRI activity at a low concentration of 0.5 mM. The exact mechanism by which these compounds are exhibiting IRI activity is not known. Our laboratory has previously proposed that the mechanism by which simple carbohydrates exhibit moderate IRI activity is based upon their ability to disrupt and/or disorder the structure of bulk water, which is ultimately related to the hydration of the carbohydrate.[18] While the hydration of non-ionic surfactant **3** has previously been quantified[36] and its IRI activity could be predicted by its hydration index, the hydration characteristics for derivatives **4–6** are not known. Consequently, further studies will be required to elucidate whether **5** is inhibiting ice recrystallization by a similar mechanism. However, we have demonstrated that for non-ionic surfactant **4**, the presence of a highly hydrated D-galactopyranose ring results in significantly more potent IRI activity than D-glucose derivative **3** and that the formation of micelles in solution does not appear to be a prerequisite for the IRI activity of these molecules. We have also demonstrated that even though D-glucose derivative **5** is a hydrogelator, the ability to form a hydrogel does not necessarily result in potent IRI activity, as D-galactose derivative **6** also forms hydrogels and was significantly less IRI active than **5**. Furthermore, the amide bond in **5** is an essential structural feature required for potent IRI activity.

Thermal hysteresis measurements and solid-state NMR experiments indicated that **3–6** were not interacting with the ice lattice, suggesting that binding to ice is not a prerequisite for the potent IRI activity exhibited by these small molecules. This is consistent with our previous hypothesis for the mechanism of action of ice recrystallization inhibitors.[13,18] The solid-state NMR results further validated that the ability to form a hydrogel is not correlated to the potent IRI activity of **5**. However, the fact that **5** is both a potent inhibitor of ice recrystallization and forms a strong hydrogel makes this compound a promising biomaterial for encapsulation of therapeutic cells in a cryoprotecting environment. Further investigation of the structural features necessary for the potent IRI activity of **5**, as well as cytotoxicity profiles and cryoprotective ability will be reported in due course.

Acknowledgements

The authors acknowledge the Natural Sciences and Engineering Research Council of Canada (NSERC), Canadian Blood Services (CBS) and Canadian Foundation for Innovation (CFI) for financial support. The views expressed herein do not necessarily represent the view of the federal government. We would like to thank Peter L. Davies (Queens University, Canada) for providing the *Lp*AFP plasmids and Christopher N. Boddy (University of Ottawa, Canada) for assistance with recombinant protein expression. C. J. C. thanks CBS for a GFP award.

Notes and references

1 (*a*) A. L. DeVries and D. E. Wohlschlag, *Science*, 1969, **163**, 1073; (*b*) A. L. DeVries, S. K. Komatsu and R. E. Feeney, *J. Biol. Chem.*, 1970, **245**, 2901; (*c*) A. L. DeVries, *Science*, 1971, **172**, 1152; (*d*) P. F. Scholander and J. E. Maggert, *Cryobiology*, 1971, **8**, 371.
2 (*a*) R. E. Feeney and T. S. Burcham, *Annu. Rev. Biophys. Biophys. Chem.*, 1986, **15**, 59; (*b*) Y. Yeh and R. E. Feeney, *Chem. Rev.*, 1996, **96**, 601; (*c*) G. L. Fletcher, C. L. Hew and P. L. Davies, *Annu. Rev. Physiol.*, 2001, **63**, 359; (*d*) M. M. Harding, P. I. Anderberg and A. D. J. Haymet, *Eur. J. Biochem.*, 2003, **270**, 1381.
3 T. Wang, Q. Zhu, X. Yang, J. R. J. Layne and A. L. DeVries, *Cryobiology*, 1994, **31**, 185.
4 B. Rubinsky, A. Arav and A. L. DeVries, *Cryobiology*, 1992, **29**, 69.
5 (*a*) J. A. Raymond and A. L. DeVries, *Proc. Natl. Acad. Sci. U. S. A.*, 1977, **74**, 2589; (*b*) C. A. Knight and A. L. DeVries, *J. Cryst. Growth*, 1994, **143**, 301; (*c*) P. W. Wilson, *Cryoletters*, 1993, **14**, 31.
6 (*a*) C. A. Knight, C. C. Cheng and A. L. DeVries, *Biophys. J.*, 1991, **59**, 409; (*b*) C. A. Knight, E. Driggers and A. L. DeVries, *Biophys. J.*, 1993, **64**, 252.
7 J. F. Carpenter and T. N. Hansen, *Proc. Natl. Acad. Sci. U. S. A.*, 1992, **89**, 8953.
8 H. Chao, P. L. Davies and J. F. Carpenter, *J. Exp. Biol.*, 1996, **199**, 2071.
9 (*a*) P. C. Mazur, *Science*, 1970, **168**, 939; (*b*) P. Mazur, *Am. J. Physiol.-Cell Ph.*, 1984, **247**, C125.
10 A. Fowler and M. Toner, *Ann. N. Y. Acad. Sci.*, 2006, **1066**, 119.
11 For recent reviews, see: (*a*) J. Garner and M. M. Harding, *ChemBioChem*, 2010, **11**, 2489; (*b*) R. Peltier, M. A. Brimble, J. M. Wojnar, D. E. Williams, C. W. Evans and A. L. DeVries, *Chem. Sci.*, 2010, **1**, 538.
12 M. I. Gibson, C. A. Barker, S. G. Spain, L. Albertin and N. R. Cameron, *Biomacromolecules*, 2009, **10**, 328.

13 P. Czechura, R. Y. Tam, E. Dimitrijevic, A. V. Murphy and R. N. Ben, *J. Am. Chem. Soc.*, 2008, **130**, 2928.
14 S. Liu and R. N. Ben, *Org. Lett.*, 2005, **7**, 2385.
15 M. I. Gibson, *Polym. Chem.*, 2010, **1**, 1141.
16 T. Inada and S.-S. Lu, *Cryst. Growth Des.*, 2003, **3**, 747.
17 M. Leclère, B. K. Kwok, L. K. Wu, D. S. Allan and R. N. Ben, *Bioconjugate Chem.*, 2011, **22**, 1804.
18 R. Y. Tam, S. S. Ferreira, P. Czechura, J. L. Chaytor and R. N. Ben, *J. Am. Chem. Soc.*, 2008, **130**, 17494.
19 J. L. Chaytor and R. N. Ben, *Bioorg. Med. Chem. Lett.*, 2010, **20**, 5251.
20 J. L. Chaytor, J. M. Tokarew, L. K. Wu, M. Leclère, R. Y. Tam, C. J. Capicciotti, L. Guolla, E. von Moos, C. S. Findlay, D. S. Allan and R. N. Ben, *Glycobiology*, 2012, **22**, 123.
21 L. K. Wu, J. M. Tokarew, J. L. Chaytor, E. von Moos, Y. Li, C. Palii, R. N. Ben and D. S. Allan, *Carbohydr. Res.*, 2011, **346**, 86.
22 S. A. Galema and H. Hoeiland, *J. Phys. Chem.*, 1991, **95**, 5321.
23 (*a*) S. A. Galema, J. B. F. N. Engberts, H. Hoeiland and G. M. Foerland, *J. Phys. Chem.*, 1993, **97**, 6885; (*b*) S. A. Galema, E. Howard, J. B. F. N. Engberts and J. R. Grigera, *Carbohydr. Res.*, 1994, **265**, 215.
24 (*a*) E. Lorente, A. Rodríguez, E. Aicart and E. Junquera, *Colloid Polym. Sci.*, 2007, **285**, 1321; (*b*) P. Harvie, F. M. P. Wong and M. B. Bally, *Biophys. J.*, 1998, **75**, 1040; (*c*) H. Michel and D. Oesterhelt, *Proc. Natl. Acad. Sci. U. S. A.*, 1980, **77**, 1283.
25 B. Lorber, J. B. Bishop and L. J. DeLucas, *Biochim. Biophys. Acta, Biomembr.*, 1990, **1023**, 254.
26 C. A. Knight, J. Hallett and A. L. DeVries, *Cryobiology*, 1988, **25**, 55.
27 J. Jackman, M. Noestheden, D. Moffat, J. P. Pezacki, S. Findlay and R. N. Ben, *Biochem. Biophys. Res. Commun.*, 2007, **354**, 340.
28 Statistically significant differences are defined as $p < 0.05$ based on a two-sample unequal variance Student's T-test.
29 Brij 58 values provided by supplier (Sigma-Aldrich).
30 Triton X-100 values provided by supplier (Sigma-Aldrich). Critical micelle concentration (CMC) range: 0.2–0.9 mM.
31 T. T. Chong, R. Hashim and R. A. Bryce, *J. Phys. Chem. B*, 2006, **110**, 4978.
32 J. Haller and U. Kaatze, *J. Phys. Chem. B*, 2009, **113**, 12283.
33 A. Helenius and K. Simons, *Biochim. Biophys. Acta, Rev. Biomembr.*, 1975, **415**, 29.
34 A. P. Romani, A. E. d. H. Machado, N. Hioka, D. Severino, M. S. Baptista, L. Codognoto, M. R. Rodrigues and H. P. M. de Oliveira, *J. Fluoresc.*, 2009, **19**, 327.
35 A. Ray and G. Némethy, *J. Am. Chem. Soc.*, 1971, **93**, 6787.
36 O. Pastor, E. Junquera and E. Aicart, *Langmuir*, 1998, **14**, 2950.
37 B. Pfannemüller and W. Welte, *Chem. Phys. Lipids*, 1985, **37**, 227.
38 J. H. Fuhrhop, P. Schnieder, E. Boekema and W. Helfrich, *J. Am. Chem. Soc.*, 1988, **110**, 2861.
39 J. H. Fuhrhop and C. Boettcher, *J. Am. Chem. Soc.*, 1990, **112**, 1768.
40 J. H. Fuhrhop, S. Svenson, C. Boettcher, E. Roessler and H. M. Vieth, *J. Am. Chem. Soc.*, 1990, **112**, 4307.
41 For recent reviews, see: (*a*) L. A. Estroff and A. D. Hamilton, *Chem. Rev.*, 2004, **104**, 1201; (*b*) M. de Loos, B. L. Feringa and J. H. van Esch, *Eur. J. Org. Chem.*, 2005, **2005**, 3615.
42 (*a*) S. Sui, X. Wang, P. Liu, Y. Yan and R. Zhang, *J. Bioact. Compat. Polym.*, 2009, **24**, 473; (*b*) X. H. Wang and H. R. Xu, *Cryobiology*, 2010, **61**, 345; (*c*) X. H. Wang, K. S. Paloheimo, H. R. Xu and C. Liu, *J. Bioact. Compat. Polym.*, 2010, **25**, 634; (*d*) R. Malpique, F. Ehrhart, A. Katsen-Globa, H. Zimmermann and P. M. Alves, *Tissue Eng., Part C*, 2009, **15**, 373.
43 J. L. Dashnau, K. A. Sharp and J. M. Vanderkooi, *J. Phys. Chem. B*, 2005, **109**, 24152.
44 A. Chakrabartty and C. L. Hew, *Eur. J. Biochem.*, 1991, **202**, 1057.
45 (*a*) V. R. Bouvet, G. R. Lorello and R. N. Ben, *Biomacromolecules*, 2006, **7**, 565; (*b*) J. Baardsnes and P. L. Davies, *Biochim. Biophys. Acta, Proteins Proteomics*, 2002, **1601**, 49; (*c*) A. D. J. Haymet, L. G. Ward and M. M. Harding, *J. Am. Chem. Soc.*, 1999, **121**, 941.
46 (*a*) L. A. Graham, Y.-C. Liou, V. K. Walker and P. L. Davies, *Nature*, 1997, **388**, 727; (*b*) C. B. Marshall, G. L. Fletcher and P. L. Davies, *Nature*, 2004, **429**, 153; (*c*) J. A. Gilbert, P. L. Davies and J. Laybourn-Parry, *FEMS Microbiol. Lett.*, 2005, **245**, 67.
47 A. B. Siemer, K.-Y. Huang and A. E. McDermott, *Proc. Natl. Acad. Sci. U. S. A.*, 2010, **107**, 17580.
48 M. H. Kao, G. L. Fletcher, N. C. Wang and C. L. Hew, *Can. J. Zool.*, 1986, **64**, 578.
49 (*a*) C. Sidebottom, S. Buckley, P. Pudney, S. Twigg, C. Jarman, C. Holt, J. Telford, A. McArthur, D. Worrall, R. Hubbard and P. Lillford, *Nature*, 2000, **406**, 256; (*b*) P. D. A. Pudney, S. L. Buckley, C. M. Sidebottom, S. N. Twigg, M.-P. Sevilla, C. B. Holt, D. Roper, J. H. Telford, A. J. McArthur and P. J. Lillford, *Arch. Biochem. Biophys.*, 2003, **410**, 238; (*c*) K. D. Kumble, J. Demmer, S. Fish, C. Hall, S. Corrales, A. DeAth, C. Elton, R. Prestidge, S. Luxmanan, C. J. Marshall and D. A. Wharton, *Cryobiology*, 2008, **57**, 263.
50 A. J. Middleton, A. M. Brown, P. L. Davies and V. K. Walker, *FEBS Lett.*, 2009, **583**, 815.
51 H. W. Spiess, *J. Chem. Phys.*, 1980, **72**, 6755.
52 D. A. Torchia and A. Szabo, *J. Magn. Reson.*, 1982, **49**, 107.

This journal is © The Royal Society of Chemistry 2012

6.3 Carbohydrate Based-Surfactants and Hydrogelators as Potent Ice Recrystallization Inhibitors

6.3.1 Synthesis of Carbohydrate-Based Surfactant and Hydrogelator Derivatives

The carbohydrate-based surfactants and hydrogelators assessed for their ability to inhibit ice recrystallization were the *n*-octyl-β-glycosides and the *N*-octyl-aldonamides, respectively.[24] The structures of these compounds are shown in Figs. 2 and 4 in the article provided in section 6.2 and these are reproduced below. The *n*-octyl-β-glycosides are pyranose-based non-ionic surfactants containing either a glucose (**3**) or galactose (**4**) hydrophilic head group (Fig. 2). In addition, commercially available Brij 58 and Triton X-100,[25] which are non-ionic surfactants structurally unrelated to **3** and **4**, were also assessed to determine the influence of CMCs and the ability to form micelles in solution on IRI activity.

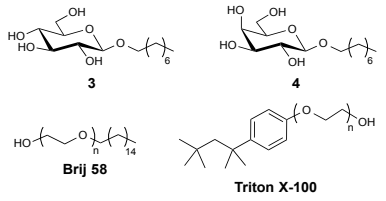

Fig. 2 The structures of non-ionic surfactants *n*-octyl-β-D-glucopyranoside (**3**), *n*-octyl-β-D-galactopyranoside (**4**), Brij58 (average M_n = 1124, n=20) and Triton X-100 (average M_n = 625, n= 9-10).

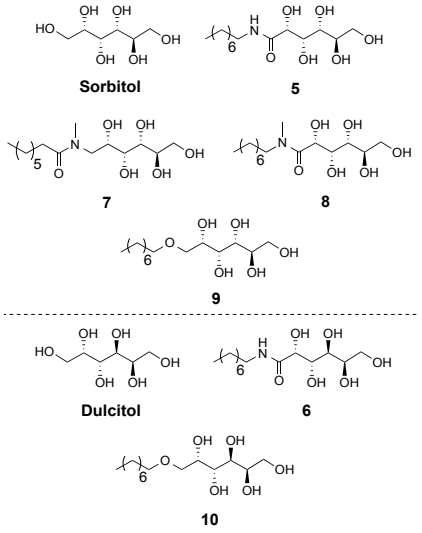

Fig. 4 The structures of D-sorbitol, D-dulcitol, low molecular weight hydrogelator derivatives *N*-octyl-D-gluconamide (NOGlc, **5**) and *N*-octyl-D-galactonamide (NOGal, **6**), *N*-methylated derivatives **7** and **8**, and ether-linked derivatives **9** and **10**.

The *N*-octyl-aldonamides are low molecular weight compounds that are known to self-assemble in water to form hydrogels.[26-29] The compounds assessed in this study were *N*-octyl-D-gluconamide (NOGlc, **5**) and *N*-octyl-D-galactonamide (NOGal, **6**) (Fig. 4). These are open-chain alditol-based derivatives containing a D-sorbitol or D-dulcitol carbohydrate hydrophilic head group, which are the open-chain alditol forms of D-glucose and D-galactose, respectively. In addition, derivatives of hydrogelators **5** and **6** were prepared and assessed for their ability to inhibit ice recrystallization to elucidate structural features that were important for IRI activity. This included *N*-methylated NOGlc derivatives **7** and **8** and ether-linked derivatives of NOGlc

and NOGal, **9** and **10**. *N*-methylated derivative **7** was chosen as it was previously reported that the hydrogen-bond donating ability of the amide bond in **5** was important for hydrogel formation as *N*-methylated derivative **7** lacked that ability to form hydrogels.[26,28] By assessing the IRI activity of **7**, this would also deduce the importance of the amide bond hydrogen-bond donation ability for the potent activity of **5**. As the orientation of the amide bond in **7** is actually "reversed" relative to **5**, the direct *N*-methylated derivative **8** was also assessed for IRI activity to ensure the directionality of the amide-linkage did not affect activity. Finally, ether-linked derivatives **9** and **10** were assessed for IRI activity to provide information on the importance of the amide bond for IRI, as this linkage is important for the hydrogelation ability of **5** and **6**.[26,28]

The carbohydrate-based non-ionic surfactants **3** and **4** were prepared from pentaacetylated glucose or galactose (**11a** or **11b**) as indicated in scheme 6.1. Lewis-acid catalyzed activation of the β-linked anomeric acetate with boron trifluoride diethyl etherate (BF_3•OEt_2) allowed for glycosidation with *n*-octanol providing exclusively the β-linked *n*-octyl-glycosides **12a** (glucoside) and **12b** (galactoside) due to achimeric assistance from the C2-*O*-acetyl group. Zemplén deacetylation of **12a** and **12b** afforded the desired non-ionic surfactants *n*-octyl-β-D-glucopyranose (**3**) and *n*-octyl-β-D-galactopyranose (**4**).

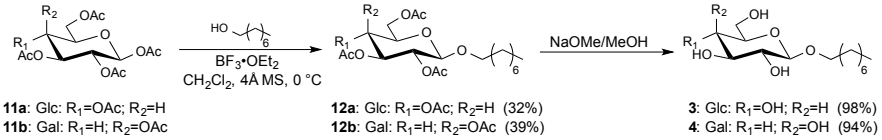

Scheme 6.1 Synthesis of carbohydrate-based non-ionic surfactants **3** and **4**.

The hydrogelator NOGlc (**5**) was prepared as described previously.[26-28,30,31] Nucleophilic addition of *n*-octylamine to D-gluconolactone opened the pyranose ring to afford the alditol derivative NOGlc (**5**, scheme 6.2A). NOGal (**6**) was prepared from calcium galactonate, which the carboxylate was chlorinated with thionyl chloride ($SOCl_2$) then reacted with *n*-octylamine to give **6** (scheme 6.2B). The synthesis of the two methylated derivatives of NOGlc (compounds **7** and **8**) is described in scheme 6.3. Compound **7** was prepared by the formation of the mixed anhydride of octanoic acid followed by conjugation to *N*-methyl-D-glucamine to furnish the methylate derivative containing an amide bond that is reversed in comparison to NOGlc (scheme 6.2A). The direct *N*-methylated derivative **8** was prepared similar to NOGlc with *N*-methyl-octylamine being utilized instead of *n*-octylamine (scheme 6.3B).

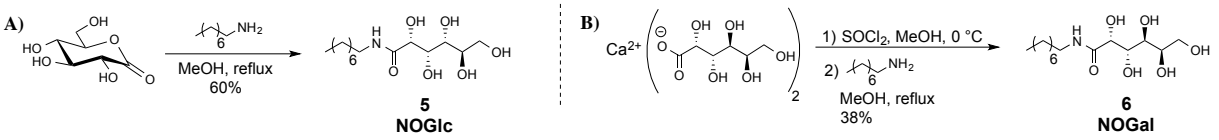

Scheme 6.2 Preparation of carbohydrate-based hydrogelators **5** and **6**. A) Synthesis of NOGlc (**5**); B) Synthesis of NOGal (**6**).

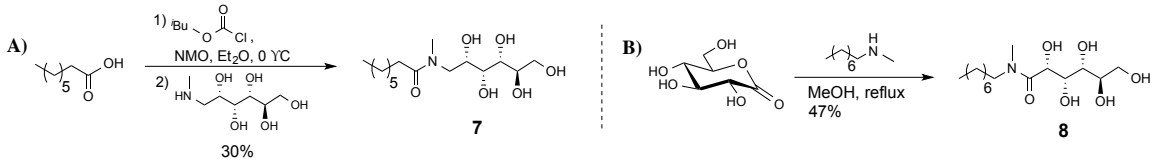

Scheme 6.3 Synthesis of *N*-methylated derivatives **7** (A) and **8** (B) of NOGlc.

Both ether-linked derivatives **9** and **10** were prepared from the corresponding benzylated free-reducing D-glucose or D-galactose derivatives **13a** and **13b**, respectively (scheme 6.4). Free-reducing carbohydrates exist in equilibrium in the α- and β-pyranose ring conformations and in trace amounts of the open-chain aldehyde (<1% depending on the carbohydrate). This aldehyde can be selectively reduced with lithium aluminum hydride to trap and selectively produce the open-chain reduced alditols of D-glucose or D-galactose, **14a** and **14b**. Orthogonal protecting group manipulation by silylating the primary C1-OH with TBDMS, followed by benzylation of the C5 position and subsequent desilylation with TBAF afforded derivatives **15a** and **15b** containing a free C1-OH to attach the desired octyl hydrocarbon chain. This was achieved through an S_N2 reaction with iodooctane yielding intermediates **16a** and **16b**. Removal of the benzyl protecting groups by hydrogenation then afforded ether-linked derivatives **9** and **10**.

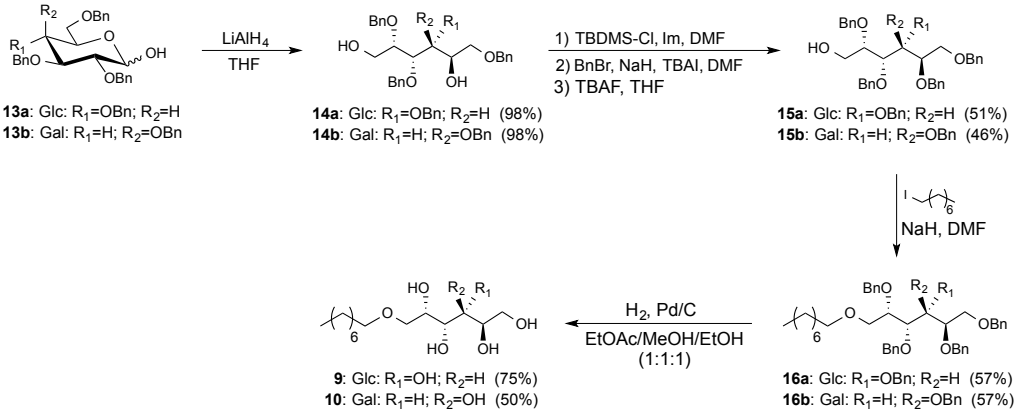

Scheme 6.4 Synthesis of ether-linked derivatives **9** and **10**.

In addition to the compounds described in the article in section 6.2, derivatives of the potently IRI active β-Octyl-Gal (**4**) and NOGlc (**5**) have been prepared to elucidate key structural features

for their potent activity (figure 6.3). Compound **17** was prepared as a derivative of β-Octyl-Gal (**4**) to assess the importance of the hydrophobic octyl-chain for IRI activity. This derivative has a more hydrophilic polyethylene glycol (PEG) tail that contains the same number of atoms (eight) as the octyl tail of **4**. Derivative **17** was prepared in a similar manner to **4** by Lewis acid catalyzed glycosidation of galactose pentaacetate with the appropriate PEG-alcohol acceptor to yield intermediate **22**, followed by Zemplén deacetylation to afford **17** (scheme 6.5A).

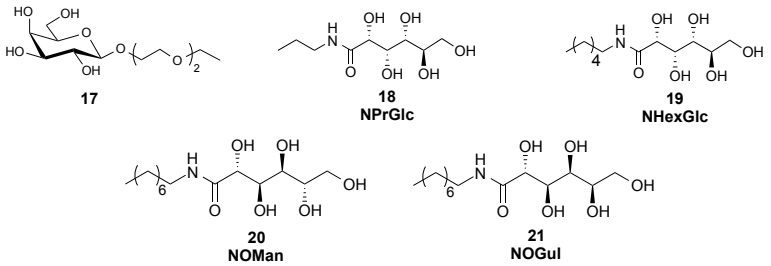

Figure 6.3 Structures of β-Octyl-Gal derivative **17** and NOGlc derivatives **18-21**.

Derivatives of NOGlc that were also prepared included *N*-propyl-D-gluconamide (NPrGlc, **18**) and *N*-hexyl-D-gluconamide (NHexGlc, **19**). These compounds were used to assess the importance of hydrocarbon tail length for the potent activity of NOGlc (**5**). Both NPrGlc and NHexGlc have shorter hydrocarbon chain lengths of three and six carbons, respectively. They were prepared in a similar manner to NOGlc by reacting D-gluconolactone with the appropriate *n*-propyl or *n*-hexyl amine (scheme 6.5B). Additionally, *N*-octyl-L-mannonamide (NOMan, **20**) and *N*-octyl-D-gulonamide (NOGul, **21**) were assessed for IRI activity to determine the influence of relative hydroxyl group orientation on the carbohydrate head group. This would provide further structure-function information on the carbohydrate residue in addition to glucose and galactose derivatives **5** and **6**. Both NOMan and NOGul were prepared similarly to NOGlc by reacting *n*-octylamine with the appropriate γ-lactone (1,4-lactone) of L-mannose or D-gulose (scheme 6.5C).

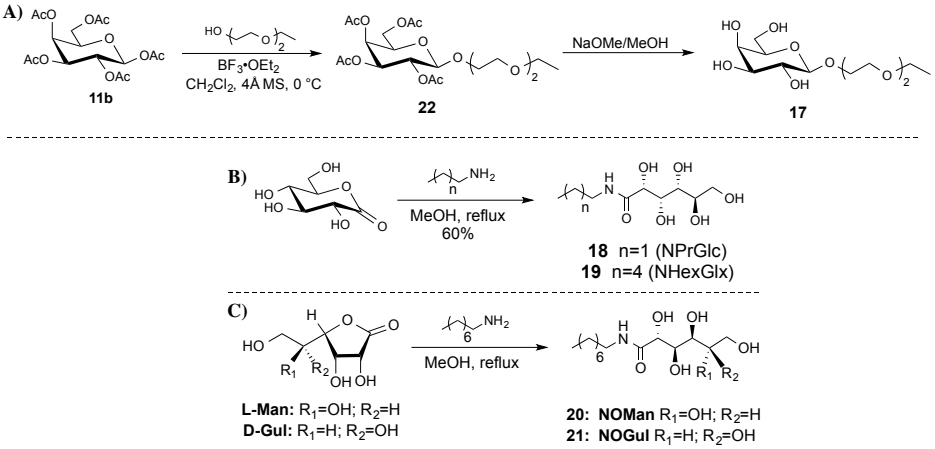

Scheme 6.5 Preparation of β-Octyl-Gal and NOGlc derivatives assessed for IRI activity. A) Synthesis of β-Octyl-Gal derivative **17**; B) Synthesis of NOGlc derivatives NPrGlc (**18**) and NHexGlc (**19**) with decreased hydrocarbon chain lengths; C) Synthesis of NOGlc derivatives NOMan (**20**) and NOGul (**21**) with various carbohydrate head-groups.

6.3.2 IRI Activity of Carbohydrate-Based Surfactants

The IRI activity of the non-ionic surfactants β-octyl-Glc (**3**) and β-octyl-Gal (**4**) was presented in Fig. 3 in the article provided in section 6.2 and this figure is reproduced below. The activity of **3** (β-octyl Glc) at 22 mM was statistically similar ($p > 0.1$, two-tailed Student's T-test) to that of D-glucose.[24] Even at a concentration of 44 mM, the IRI activity of **3** was still identical to that of 22 mM D-glucose ($p > 0.6$, two-tailed Student's T-test). Interestingly, the IRI activity of β-octyl-Gal (**4**) at 11, 22 and 44 mM was, in all cases, significantly better than 22 mM D-galactose. This derivative was potently IRI active even at 11 mM (34% MGS relative to PBS), a concentration that is half of which all previously reported simple pyranose-based monosaccharides were only moderately IRI active (see chapter 5).[1,32,33] At a concentration of 5.5 mM, β-octyl-Gal (**4**) was as active as a 22 mM D-galactose solution.

β-Octyl-Glc (**3**) and β-octyl-Gal are non-ionic surfactants and both have calculated CMC values. The CMC of **3** in water is 18 – 22 mM,[34,35] whereas the CMC of **4** in water is 30 mM.[35,36] Thus, while **3** is expected to form micelles in solution at 22 mM, the concentration that IRI activity is typically assessed, **4** is not.[24] The CMC values are reported in water and not PBS. However, it has been documented that the CMCs of non-ionic surfactants are only slightly lower in salt solutions, therefore it is likely that these values would only be slightly decreased in PBS.[25,37] The fact that **3** is expected to form micelles at concentrations of 22 mM and higher, but it does not exhibit potent IRI activity even at 44 mM suggests that micelle formation may be unrelated to IRI activity. Similarly, both a 22 and 11 mM solution of **4** is below its CMC value of 30 mM, but a 22 mM solution of **4** is a very potent inhibitor of ice recrystallization.

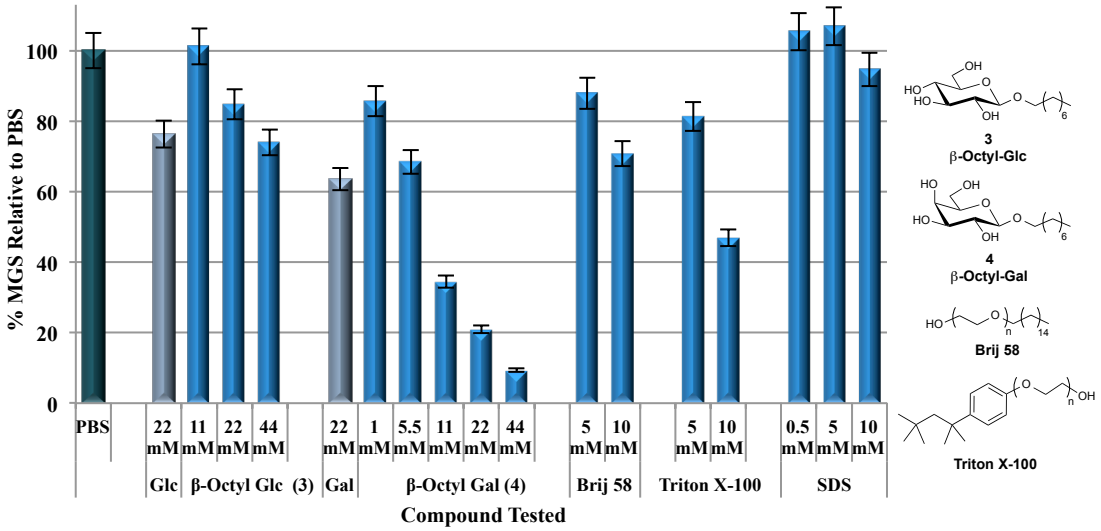

Fig. 3 IRI activity of non-ionic surfactants **3** (CMC = 18 – 22 mM),[34,35] **4** (CMC = 30 mM),[35,36] Brij 58 (average M_n = 1124, n = 20, CMC = 0.08 mM),[25] Triton X-100 (average M_n = 625, n = 9 – 10, CMC = 0.24 mM)[25,38] and anionic surfactant SDS (CMC = 5 mM).[39,40] All compounds are represented as a % MGS (mean grain size) of ice crystals relative to the PBS positive control.

To further investigate if the formation of micelles in solution had an impact on the inhibition of ice recrystallization, several other common surfactants with known CMC values were examined for IRI activity.[24] The anionic surfactant sodium dodecyl sulphate (SDS) has a CMC in PBS of 5 mM.[39] The IRI activity of SDS was assessed at concentrations at, above and below this value (5, 10 and 0.5 mM respectively) (Fig 3). At all three concentrations, SDS exhibited no IRI activity, again suggesting that the formation of micelles in solution is not correlated to IRI activity. The activity of non-ionic surfactants Brij 58 and Triton X-100 were also examined. These are structurally unrelated to the carbohydrate-based non-ionic surfactants β-Octyl-Glc (**3**) and β-Octyl-Gal (**4**). Similar to PBS, these non-ionic surfactants were assessed for IRI at concentrations well above their CMCs (0.08 mM for Brij 58 and 0.24 mM for Triton X-100).[25,38,40] At 10 mM, both Brij 58 and Triton X-100 exhibited weak to moderate IRI activity, while at 5 mM (a concentration still well above their CMC values) they were only weakly IRI active (Fig. 3). This suggests that the moderate IRI activity observed at 10 mM for these non-ionic surfactants is a result of increased concentration and not micelle formation. Similar results have also been observed for cationic quaternary ammonium salts from studies in our laboratory conducted by Anna Balcerzak. The potent IRI activity exhibited by some of these cationic surfactants was found to be concentration dependent and unrelated to micelle formation.[41] Collectively, these results provide further evidence that the potent IRI activity of non-ionic surfactant **4** at 22 mM is likely independent of its ability to form micelles.

As described in section 5.2 our laboratory has previously correlated IRI activity to hydration index (HI – hydration number divided by partial molar volume), which is the degree of hydration of a carbohydrate as a function of size or volume.[1] The molar isentropic compressibility of β-Octyl-Glc (**3**) and subsequently, hydration numbers and apparent molar volumes have been reported in the literature.[42] The hydration number of **3** is 16,[42] which is nearly twice as large as that reported for D-glucose (8.4).[43] However, the apparent molar volume of **3** is approximately twice that of D-glucose[42] resulting in a hydration index that is nearly identical to that calculated for D-glucose.[1] Thus, the similar IRI activity observed for **3** and D-glucose at 22 mM is not surprising as their hydration indices are very similar (Fig. 3).

Unfortunately, the hydration number and apparent molar volume of **4** have not been reported in the literature and thus calculation of a hydration index is not possible. However, the fact that D-glucose derivative **3** is less active than D-galactose derivative **4** correlates well with previously published IRI data of *C*-linked AFGP analogues and simple monosaccharides.[1,15] Thus, it seems that the hydration of the hydrophilic carbohydrate head-group influences IRI activity and that surfactants derived from more highly hydrated pyranose rings will be more potent inhibitors of ice recrystallization. To further investigate if other structural features of **4** may be important for its potent activity, we explored the influence of the hydrophobic octyl tail of this surfactant. Thus, derivative **17** was assessed for IRI activity, and these results are presented in figure 6.4.

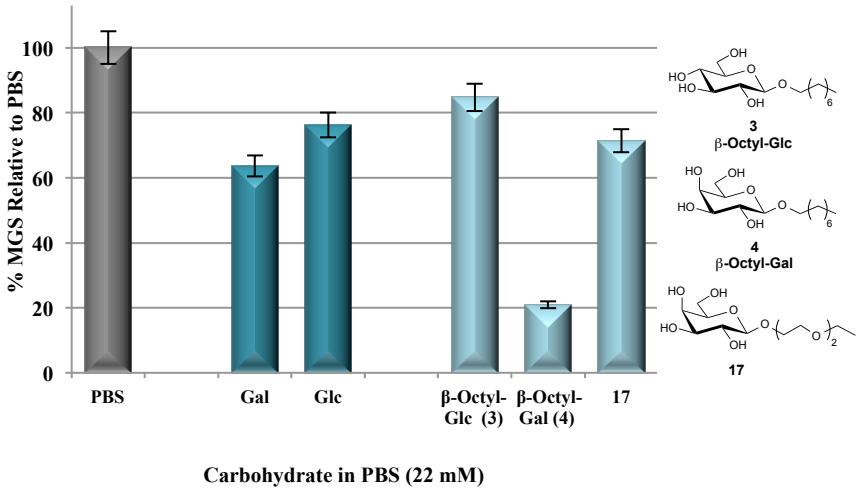

Figure 6.4 IRI activity of carbohydrate-based non-ionic surfactants **3** and **4** and β-Octyl-Gal derivative **17** at 22 mM in PBS. All compounds are represented as a % MGS (mean grain size) of ice crystals relative to the PBS positive control.

Derivative **17** contains an eight-atom PEG tail on a D-galactose head-group that is more hydrophilic than the octyl hydrocarbon tail of **4** due to the incorporation of oxygen atoms. This derivative was significantly less IRI active than **4** with a % MGS of 71% (compared with 21% for

4). In fact, **17** was less active than D-galactose and exhibited similar activity to D-glucose. This suggests that the hydrophobicity of hydrocarbon tail of **4** is crucial for its potent activity. The importance of hydrophobic moieties for the inhibition of ice recrystallization has also been demonstrated with lysine-based derivatives and truncated *C*-AFGP derivatives (general structures shown in figure 6.5).[41,44] Similar to **4**, all of the derivatives that exhibited potent IRI activity possessed long alkyl chains attached to specific moieties of these molecules. However, D-glucose derivative **3**, which also contains a long hydrophobic alkyl tail, did not have the ability to inhibit ice recrystallization (Fig. 3 and figure 6.4).[24] Thus, it is evident that with the non-ionic carbohydrate-based surfactants the combination of a hydrophobic tail along with a highly hydrated head-group is important for IRI activity. While the exact mechanism by which these compounds are exhibiting IRI activity is unknown, the importance of hydrophobicity and the relative orientation of the hydroxyl groups on the carbohydrate residue are further discussed in this section with the hydrogelators **5** and **6**.

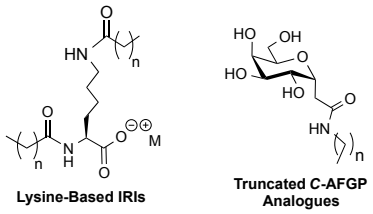

Figure 6.5 Structures of potently IRI active lysine-based derivatives and truncated *C*-AFGP analogues that contain hydrophobic alkyl tails.

6.3.3 IRI Activity of Carbohydrate-Based Hydrogelators

The IRI activity of the carbohydrate-based hydrogelators **5** and **6** was presented in Fig. 5 in the article provided in section 6.2 and this data is reproduced below.[24] These compounds could only be assessed for activity at 0.5 mM due to their poor solubility in water and PBS.[28-29] At 0.5 mM the glucose derivative NOGlc (**5**) exhibited potent IRI activity, while the galactose derivative NOGal (**6**) exhibited only moderate IRI activity. This was surprising as all previous studies with carbohydrate derivatives reported compounds with weak to moderate activity at 22 mM, making NOGlc (**5**) the first reported example of a small molecule potent ice recrystallization inhibitor at a significantly lower concentration than 22 mM.[24] The carbohydrate moieties of **5** and **6** are in the open-chain alditol form. Both D-sorbitol and D-dulcitol were only weak inhibitors of ice recrystallization at 22 mM, highlighting the importance of the pyranose ring for IRI activity as both of these alditols had decreased activity relative to the pyranose forms (Fig.5). Similar to β-Octyl-Gal (**4**) where the conjugation of a long hydrophobic alkyl chain to a galactopyranose residue increased activity (Fig. 3), the conjugation of an alkyl chain *via* an amide-linkage to the

alditol moieties also increased activity. However, in contrast to the carbohydrate-based surfactants, this drastic increase resulted into potent activity for a glucose-based derivative and not a galactose-based derivative. This was unprecedented and was the first example where a D-glucose derivative was a more potent inhibitor of ice recrystallization than a D-galactose derivative.

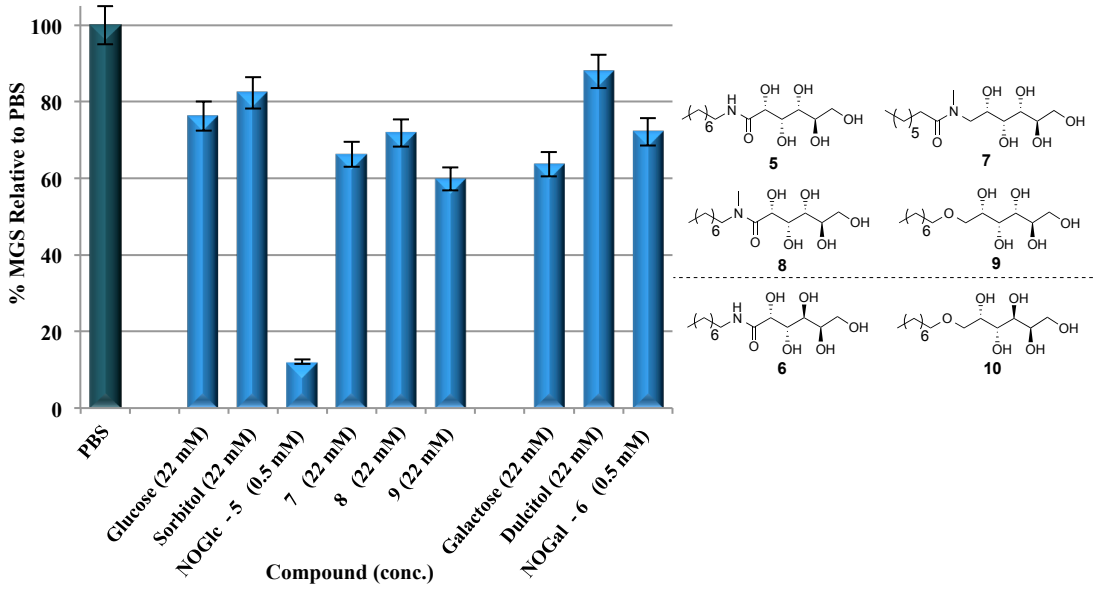

Fig. 5 IRI activity of D-sorbitol, D-dulcitol, low molecular weight hydrogelator derivatives **5** (NOGlc) and **6** (NOGal), *N*-methylated derivatives **7** and **8**, and ether-linked derivative **9**. All compounds are represented as a % MGS (mean grain size) of ice crystals relative to the PBS positive control.

Compounds **5** and **6** are capable of forming a hydrogel at 1% and 0.5% w/v in water, which corresponds to a concentration of 33 mM and 16 mM, respectively.[27-29] The fact that **5** exhibits potent IRI activity at 0.5 mM (well below its gelation concentration) implies that this activity is not related to the formation of a hydrogel.[24] Moreover, since **6** also forms a hydrogels, but is significantly less IRI active than **5**, this indicates that IRI activity is not dependent on formation of a hydrogel. This has also been observed with lysine-based derivatives that were capable of forming gels (general structure shown in figure 6.5), further demonstrating that gelation ability is not a prerequisite for potent activity.[33]

To investigate the structural features responsible for the potent IRI activity of **5** at 0.5 mM, derivatives **7**-**9** were assessed for their ability to inhibit ice recrystallization (Fig. 5). All of these derivatives exhibited significantly reduced activity compared with **5** and were only moderately active at a much higher concentration of 22 mM.[24] It has previously been reported that the amide bond in **5** was important for hydrogel formation[26,28] and that *N*-methylated derivative **7** lacked that ability to form hydrogels.[26] This was attributed to the hydrogen-bond donating ability of the

amide linkage. Thus, the decreased activity of **7** suggests that the proton on the nitrogen of the amide bond is also an important structural feature for the potent activity of **5**. This is further validated with **8**, which is the direct *N*-methylated derivative of **5**. Compound **8** exhibited similar IRI activity to **7** at 22 mM further validating the importance of the hydrogen-bond donating ability in the amide bond of **5** for potent IRI activity. This result also suggests that the "reversed" directionality of the amide-bond in **7** did not influence activity as both **7** and **8** had statistically similar % MGS relative to PBS (~70% MGS, $p > 0.2$, two-tailed Student's T-test).

Replacement of the amide bond in **5** with an ether linkage (**9**) resulted in a dramatic decrease in IRI activity (Fig. 5).[24] Ether-linked derivative **9** exhibited IRI activity similar to **7** and **8** at 22 mM. Collectively, these results indicate that the amide bond of **5** is crucial for its potent IRI activity. Interestingly **9**, the open-chain alditol derivative of non-ionic pyranose-based surfactant β-Octyl-Glc (**3**), was a better inhibitor of ice recrystallization than **3** at 22 mM (Figs. 3 and 5). At 22 mM β-Octyl-Glc (**3**) resulted in 85% MGS relative to PBS (Fig. 3) whereas **9** resulted in 60% MGS relative to PBS (Fig. 5). This was surprising as the IRI activity of the alditols D-sorbitol and D-dulcitol (Fig. 5) was decreased in comparison to the corresponding pyranose forms of the sugars (D-glucose and D-galactose, respectively). As non-ionic D-galactopyranose-based surfactant β-Octyl-Gal (**4**) exhibited potent IRI activity at 22 mM (Fig. 3), galactose-based ether linked derivative **10** (Fig. 5), the open-chain alditol derivative of **4**, was prepared to further examine the influence of the alditol moiety on IRI activity. Unfortunately, even at 11 mM, **10** was insoluble in PBS, and thus its IRI activity could not be assessed at similar concentrations which **4** and **9** were assessed.

The hydration characteristics for the *N*-octyl-D-aldonamides (**5** and **6**) and their alditol carbohydrate residues (D-dulcitol or D-sorbitol) have presently not been calculated and so the relation of hydration to the potent IRI activity of **5** cannot be elucidated at this time. However, it is known that much like non-ionic D-galactose-based surfactant **4**, hydrogelator NOGlc (**5**) is capable of forming micelles in solution and has a CMC of 10 mM in water.[26] A 0.5 mM solution of **5** is well below the reported CMC value, yet **5** exhibits unusually potent IRI activity at this concentration. Also, similar to **4**, the IRI activity of **5** is concentration dependent.[24] A 0.25 mM solution of **5** exhibited moderate IRI activity and a 0.1 mM solution of **5** exhibited weak IRI activity (figure 6.6). This provides additional evidence that the formation of micelles is not a prerequisite for potent IRI activity.

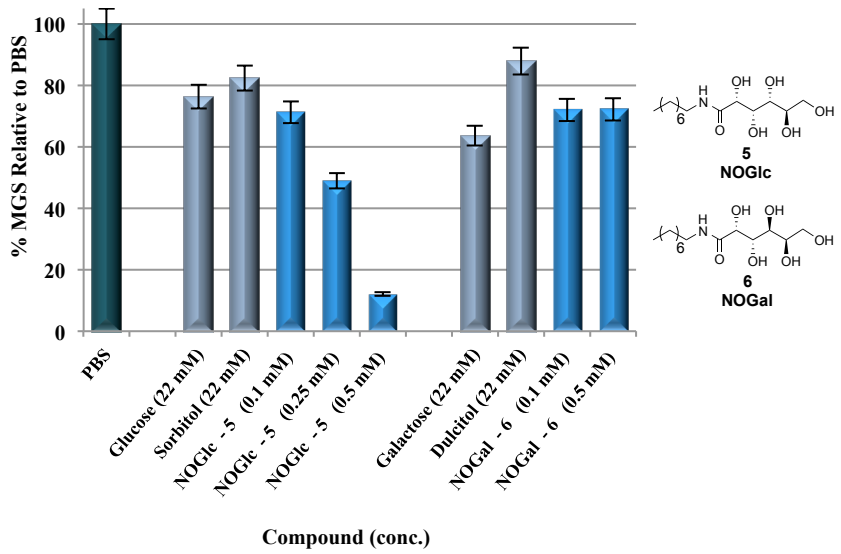

Figure 6.6 Concentration dependence of the IRI activity of NOGlc (**5**). All compounds are represented as a % MGS (mean grain size) of ice crystals relative to the PBS positive control.

Thus far, it has been described for the carbohydrate-based hydrogelators that NOGlc (**5**) is a potent inhibitor of ice recrystallization at the low concentration of 0.5 mM. The amide bond in **5** is crucial for this potent activity as its methylation or replacement with an ether-linkage abolishes activity. Interestingly, hydrogelator NOGal (**6**) only exhibited moderate IRI activity and it differs from **5** only by the configuration of the hydroxyl group at the C4 position. This suggests the carbohydrate head group is also highly influential on IRI activity. To further investigate the importance of this group, other monosaccharide units were utilized as the head-groups, including L-mannose and D-gulose for derivatives NOMan (**20**) and NOGul (**21**), respectively. Additionally, similar to lysine-based derivatives,[41] the presence of long alkyl chains and the hydrophobicity of the hydrocarbon tail of β-Octyl-Gal (**4**) was determined to be important for IRI activity (figure 6.4). Thus, derivatives of NOGlc (**5**) with shorter alkyl hydrocarbon tails (NHexGlc (**19**) and NPrGlc (**18**)) were assessed for IRI to determine the importance of hydrophobicity for the potent activity of **5**. The results from these studies are presented in figure 6.7.

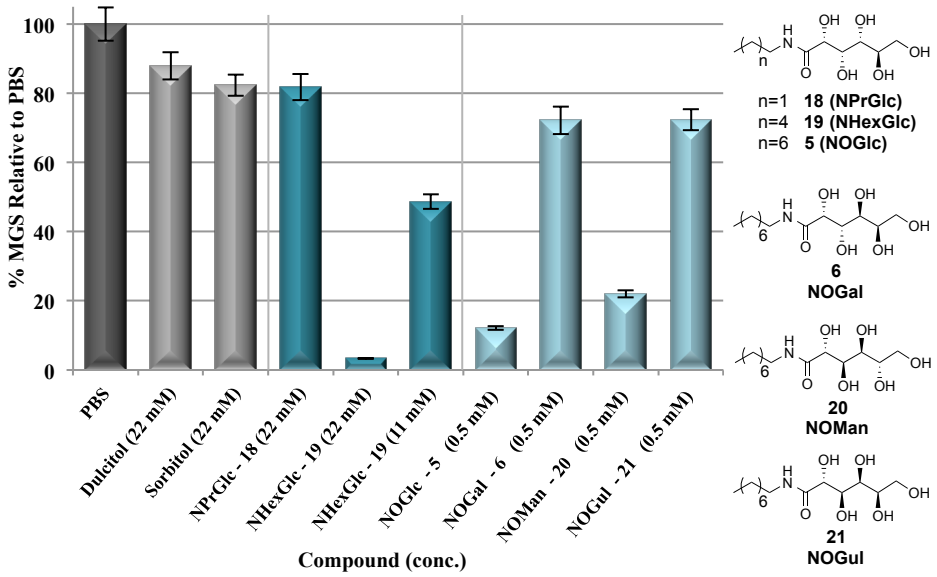

Figure 6.7 IRI activity of NOGlc derivatives NPrGlc (**18**), NHexGlc (**19**) and octyl-chain derivatives NOMan (**20**) and NOGul (**21**) at indicated concentrations in PBS. All compounds are represented as a % MGS (mean grain size) of ice crystals relative to the PBS positive control.

It is evident from figure 6.7 that the IRI activity of the *N*-alkyl-D-gluconamides is dependent upon the length of the hydrocarbon chain conjugated to the carbohydrate moiety. Propyl derivative NPrGlc (**18**) exhibited weak activity at 22 mM (82% MGS), and when the alkyl chain length was increased to six carbons in length as in hexyl derivative NHexGlc (**19**), activity significantly increased to 3% MGS relative to the PBS control. While at 22 mM NHexGlc (**19**) exhibited very potent IRI activity, at 11 mM this activity was drastically reduced resulting in only 50% MGS relative to the PBS control. By increasing the hydrocarbon chain length to eight carbons as in octyl derivative NOGlc (**5**), potent activity at a much lower concentration of 0.5 mM is observed. These results suggest that there is a balance between hydrophilicity (from the carbohydrate moiety) and hydrophobicity (from the longer alkyl chains) for potent IRI activity. Increasing the hydrophobicity and length of the hydrocarbon chain can enhance the ability of the compound to inhibit ice recrystallization, and these results are similar to what has been observed with lysine-based derivatives and truncated *C*-AFGP analogues possessing long hydrocarbon tails.[41,44] While for NOGlc the longer alkyl chain resulted in potent activity at the low concentration which it was soluble, it has been found for truncated *C*-AFGP analogues (figure 6.5) that the increase in chain length does not always result in potent activity at low concentrations. Thus, a balance between hydrophilic and hydrophobic groups is required as solubility in aqueous solutions drastically decreases with increasing hydrocarbon chain lengths.[24,27-29,41,44]

The octyl-chain derivatives possessing different monosaccharide units for the carbohydrate head groups are also presented in figure 6.7. All derivatives were assessed at 0.5 mM to compare to potently IRI active NOGlc (**5**). Interestingly, both NOGal (**6**) and NOGul (**21**) were significantly less IRI active than **5** (72% MGS for both **6** and **21** versus 12% for **5**). However, NOMan (**20**), while less active than **5**, still exhibited potent IRI activity at 0.5 mM (22% MGS). NOGal (**6**) differs from NOGlc (**5**) by the configuration of the C4-OH group, and NOGul (**21**) differs from **5** at both the C3- and C4-OH groups (numbering shown in figure 6.8). Both of these derivatives had reduced activity from **5**, suggesting the stereochemical orientation of these hydroxyl groups may influence IRI. However, NOMan (**20**) (derived from L-mannose) differed from NOGlc (**5**) at all hydroxyl group positions except for C2, yet **20** was still potently IRI active. Furthermore, NOGul (**21**) only differs from **20** by the C5-OH, but **21** is IRI inactive. These results preliminarily indicate that for the open-chain aldonamide carbohydrate derivatives there is not a defined stereochemical orientation that is required on the head group for potent activity. It also suggests that unlike pyranose-based derivatives, specific hydroxyl group positions may not be more influential than others for IRI.

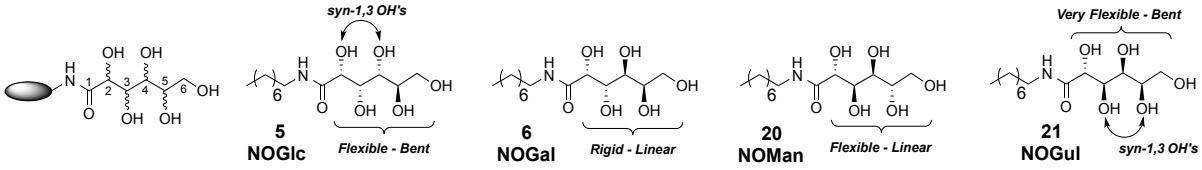

Figure 6.8 Numbering sequence of carbons on the carbohydrate head group of the *N*-octyl-aldonamides, identification of *syn*-1,3-hydroxyl groups and the conformation and flexibility of the carbohydrate head groups.

It has been demonstrated that the configuration of the carbons bearing hydroxyl groups on the carbohydrate moiety is highly influential on the conformation these aldonamides adopt in solution.[27-29,31] This was also suggested to influence the solubility of these compounds and the hydration of the head groups. Both NOGul (**21**) and NOGlc (**5**) have *syn*-1,3-hydroxyl groups that cause steric interactions within the head groups resulting in a disturbance in linear conformation observed with all *trans*-1,3-hydroxyl groups (shown in figure 6.8). This results in a flexible bent conformation of the carbohydrate head group and is suggested to enhance the hydration of these head groups and to be the reason for why NOGul (**21**) and NOGlc (**5**) were the most soluble in boiling water (100% and 50% w/v, respectively).[29] However, the bent conformation, flexible head group, or increased head group hydration and compound solubility did not correlate with more potent IRI activity as NOGul (**21**) was one of the least active derivatives. Moreover, both NOGal (**6**) and NOMan (**20**) do not contain *syn*-1,3-hydroxyl groups

and adopt a linear conformation for their head groups (figure 6.8) and are drastically less soluble in hot water (3% w/v for NOMan and <0.5% w/v for NOGal).[27,29,31] However similar to NOGlc (**5**), NOMan (**20**) was highly IRI active (figure 6.7). Thus, it appears that the flexibility of the head group or the presence/absence of *syn*-1,3-hydroxyl groups does not correlate with the IRI activity of these derivatives. Further studies are still required to definitively understand the role of head group conformation on IRI activity and unfortunately the exact mechanism by which these compounds inhibit ice recrystallization is currently not understood. However, it is clear that similar to what has been observed for pyranose-based derivatives, the orientation of the hydroxyl groups on the alditol carbohydrate head group can be highly influential on the IRI activity of these derivatives.

6.3.4 Assessment of Ice Lattice Interactions

Having identified the novel potently IRI active small molecules β-Octyl-Gal (**4**) and NOGlc (**5**), we sought to determine if these derivatives exhibit this potent activity by binding to or interacting with the ice lattice. With the exception of PVA,[18,19] the ability to bind to ice and exhibit thermal hysteresis (TH) activity is property that is unique to biological antifreezes (see section 1.2).[45-49] As described previously, this property is detrimental for a cryoprotectant and can exacerbate cellular damage during cryopreservation (see section 1.4.4 and Chapter 4).[50-54] Our laboratory has previously reported that *C*-AFGPs can exhibit "custom-tailored" antifreeze activity, meaning they are potently IRI active but do not possess TH activity or ice-shaping capabilities, suggesting they are not interacting with the ice lattice (section 1.3.1 and Chapter 3).[15,16] Thus, to ensure that the novel potently IRI active small molecules were exhibiting custom-tailored activity and were not binding to ice, carbohydrate derivatives **3**-**6** were examined for TH activity using nanolitre osmometry.[55] These results of the ice crystal habits in the presence of these compounds were presented in Fig. 6 in the article provided in section 6.2 and this figure is reproduced below.[24]

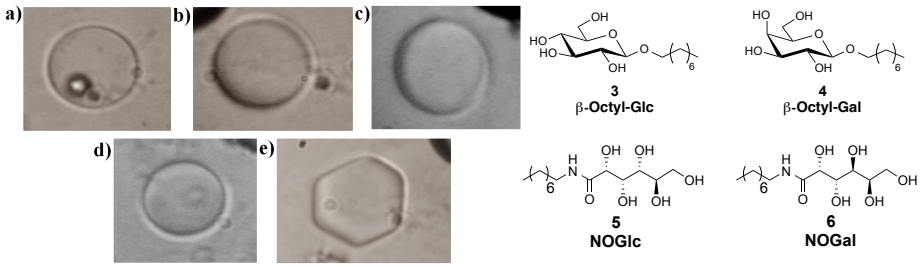

Fig. 6 Ice crystal habits in the presence of (a) **3** (1 mg/mL), (b) **4** (1 mg/mL), (c) **5** (0.01 mg/mL), (d) **6** (0.01 mg/mL) and (e) AFGP-8 (0.01 mg/mL) in water.

Our laboratory typically assesses all compounds for TH activity at a weight/volume concentration of 5-10 mg/mL (see Chapters 3 and 4).[56-57,58] Derivatives **3**–**6** could not be assessed for TH activity at these concentrations due to their amphiphilic nature.[24] In the nanolitre osmometry assay a single droplet of the sample in water is suspended in the center of an oil-filled well.[55] The sample is then rapidly frozen using a thermoelectrically controlled microscope stage, and the temperature is raised to melt the sample until only a single ice crystal remains. Once a single ice crystal is obtained, its growth and behavior upon increasing/decreasing the temperature can be viewed under a microscope. However, during the process of melting the frozen samples of **3**-**6** to obtain a single ice crystal, the droplet dissolved in the oil resulting in one phase. Thus, derivatives **3** and **4** could only be assayed at a concentration of 1 mg/mL, and derivatives **5** and **6** could only be assayed at a concentration of 0.01 mg/mL. None of these derivatives (**3**–**6**) exhibited TH activity or dynamic ice shaping at these concentrations (Fig. 6a-d), indicating they were not interacting with the ice lattice.

Many AF(G)Ps have measurable TH gaps at concentrations as low as 0.5 mg/mL.[59-63] Thus the lack of ice shaping and TH activity observed for **3** and **4** at 1 mg/mL suggests these compounds are not able to bind to ice.[24] Only hyperactive AFPs have been reported to have measurable TH activity at concentrations of 0.01 - 0.05 mg/mL.[64-66] Native AFGP-8 was assayed at a concentration of 0.01 mg/mL for dynamic ice shaping (DIS) and TH activity. While no measurable TH gap was obtained for AFGP-8 at 0.01 mg/mL, DIS was observed (Fig. 6e). This indicated that even at a low concentration of 0.01 mg/mL and in the absence of a measurable TH gap, evidence of an interaction with the ice lattice can still be observed. Thus, as **5** and **6** did not exhibit DIS capabilities, this suggests that these compounds are not interacting with the ice lattice. However, we sought to further demonstrate that these compounds were not interacting with the ice lattice using solid-state NMR to definitively prove these novel small molecule IRIs had "custom-tailored" antifreeze activity.

In 2010, a study utilizing solid-state NMR to observe the interaction of a type III AFP with ice was reported.[67] It was determined that the ^{2}H spin-lattice relaxation rate (R_1) of frozen D_2O in the presence of the AFP was much faster in comparison to the ^{2}H R_1 of frozen D_2O on its own. No change in the R_1 of frozen D_2O in the presence of ubiquitin (a small protein that does not bind to ice) was reported, suggesting that the faster relaxation rate in the presence of the AFP was a direct result of the AFP binding to ice. In our 2012 *Chemical Science* article (section 6.2), deriving from our collaboration with Fréderic Perras and Dr. David Bryce in the Department of Chemistry at the University of Ottawa, we further demonstrated that the R_1 of frozen D_2O is much faster in the presence of various other different AFPs than the R_1 of frozen D_2O on its own.[24]

The saturation recovery curves for these measurements are shown in Fig. 7a (reproduced below). The three positive controls for ice binding used were a type I AFP (winter flounder, *Pseudopleuronectes americanus*),[68] a type III AFP (ocean pout, *Macrozoarces americanus*)[68] and the wild-type AFP of the perennial ryegrass *Lolium perenne* (WT *Lp*AFP).[69-71,72] A full characterization of the antifreeze activity of these proteins is described in chapter 4. As can been seen from Fig. 7a, the R_1 of frozen D_2O with all three positive controls was much faster than the R_1 of frozen D_2O on its own. This is attributed to the ice binding capabilities of these proteins and that they exhibit strong TH activity (chapter 4).[24,67] As a negative control, a mutant of an AFP (T67Y *Lp*AFP) was used as opposed to ubiquitin. T67Y *Lp*AFP was used as the substitution of this threonine residue on the ice-binding face (IBF) to a bulky tyrosine residue disrupted the discrete complementarity between the IBF of the AFP and ice, resulting in minimal TH activity (see chapter 4 for antifreeze activity and recombinant expression in *E. coli*).[72] The R_1 of frozen D_2O in the presence of T67Y *Lp*AFP was similar to that of frozen D_2O on its own (Fig. 7a).[24]

The saturation recovery curves of frozen D_2O in the presence of derivatives **5** and **6** are presented in Figs 7c-d.[24] These molecules are significantly smaller than the AFP positive controls, therefore to account for the drastic difference in molecular weights, the concentration which each carbohydrate derivative was measured was corrected to a total overall proton concentration of 1234 mM. This was the overall protein proton concentration used for the Type III AFP in the original 2010 study.[67] The saturation recovery curve of frozen D_2O with NOGlc (**5**) is shown in Fig. 7c. Surprisingly, the R_1 of frozen D_2O in the presence of **5** was faster than that of frozen D_2O on its own. A similar effect was also observed with NOGal (**6**) where the R_1 of D_2O in the presence of **6** was faster than the R_1 of frozen D_2O on its own (Fig. 7d). However, since the TH measurements of **5** and **6** indicated no dynamic ice shaping, it seemed unlikely this was due to an interaction with the ice lattice.

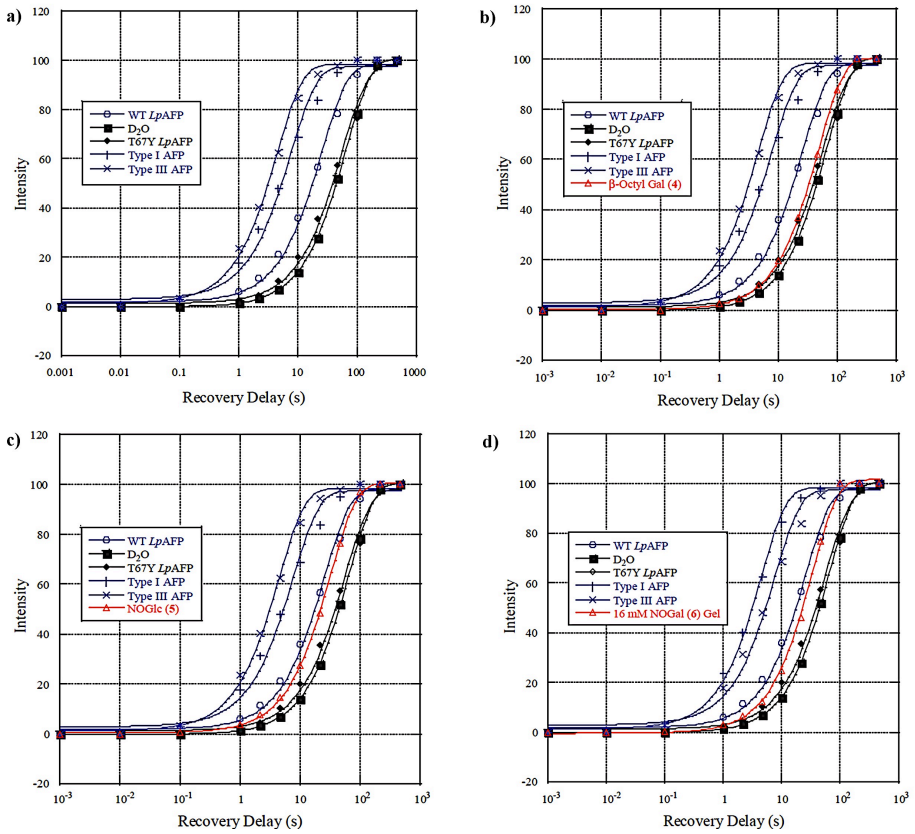

Fig. 7 Saturation recovery curves of frozen D_2O with AFPs or carbohydrate derivatives. The concentration of all carbohydrate derivatives was corrected to a total overall proton concentration of 1234 mM, unless stated otherwise. The ^2H relaxation rate for frozen D_2O was $R_1 = 0.0154 \pm 0.0002$ s^{-1}. (a) Three positive controls for ice binding: Type I AFP ($R_1 = 0.13 \pm 0.01$ s^{-1}), Type III AFP ($R_1 = 0.22 \pm 0.01$ s^{-1}), WT *Lp*AFP ($R_1 = 0.039 \pm 0.002$ s^{-1}); one negative control for ice binding: T67Y *Lp*AFP ($R_1 = 0.018 \pm 0.001$ s^{-1}). (b) AFP controls and derivative **4** ($R_1 = 0.0209 \pm 0.0002$ s^{-1}). The concentration at which **4** was measured was 44 mM. (c) AFP controls and frozen hydrogel of derivative **5** ($R_1 = 0.0310 \pm 0.0005$ s^{-1}). The concentration at which **5** was measured was 42 mM. (d) AFP controls and frozen hydrogel of derivative **6** ($R_1 = 0.030 \pm 0.001$ s^{-1}). The concentration at which **6** was measured was 16 mM, which corresponds to a total overall proton concentration of 479 mM.

Since the concentration of the low molecular weight carbohydrate derivatives were corrected to a total overall proton concentration of 1234 mM, this corresponded to a 42 mM concentration of **5** in solution, at which **5** forms a hydrogel. Due to solubility problems, the highest concentration at which **6** could be measured was its gelation concentration of 0.5% w/v,[28,27] which corresponds to a concentration of 16 mM. Consequently, solid-state NMR measurements were conducted on the frozen hydrogels of **5** and **6**. As described in the article provided in section 6.2, the formation of a gel is inevitably accompanied by a decrease in correlation time due to an increased mobility of the water molecules in the solid-state.[73,74] This is expected to cause an increase in R_1, which was observed experimentally. Therefore, it is likely the faster R_1 observed for frozen D_2O with **5** is due to increased molecular motion during these measurements caused by

gelation. This hypothesis was further supported by the saturation recovery curve of frozen D_2O with NOGal (**6**) (Fig. 7d). A 16 mM solution of **6** has a total overall proton concentration of only 479 mM and at a similar protein proton concentration with the WT *Lp*AFP, the measured R_1 value is similar to frozen D_2O on its own.[24] As expected, the effect of ice binding on R_1 is concentration dependent.[67] Thus, as at the lower total proton concentration a faster R_1 was observed for the frozen hydrogel of **6**, these results suggest that the faster relaxation rates of frozen D_2O observed with **5** and **6** are likely due to an effect of gelation.

Interestingly, the R_1 values of frozen D_2O in both of the hydrogels (**5** and **6**) were similar (Fig. 7c-d), further supporting the hypothesis that the faster relaxation times are due to a gelation effect. However, both **5** and **6** have dramatic differences in their exhibited IRI activity. This result further validates the hypothesis that simply the ability to form a hydrogel does not necessarily result in potent IRI activity. Regardless of concentration, both **5** and **6** were studied as frozen hydrogels in the solid-state NMR experiments, and both had the same relative increase in the relaxation rate of frozen D_2O. However, only NOGlc (**5**) had potent IRI activity (Fig. 5). To further study the relationship between the hydrogelation properties of these molecules and their ability to inhibit ice recrystallization, we also characterized their microstructural and mechanical properties using microscopy and rheology to examine any correlations with IRI activity.[24]

6.3.5 Characterization of Hydrogels and the Relationship with IRI Activity

The morphologies of hydrogels formed with **5** and **6** in water and PBS were observed using scanning transmission electron microscopy (STEM) in collaboration with Dr. Yun Liu at the Centre for Catalysis Research and Innovation at the University of Ottawa.[24] Images of these gels were shown in Fig. 8 of the article in section 6.2 and are reproduced below. The fibres in the hydrogel of NOGlc (**5**) in water and PBS consist of a lattice-like network of right-handed helices with well-defined junctions serving as crosslinks (Figs. 8a and c). In contrast, the fibres in the hydrogel of NOGal (**6**) in water and PBS consist of a less organized entangled, fibrous phase of ribbons (Fib. 8b and d). Additionally, the fibres in the hydrogel of NOMan (**20**) in water consist of multi-layered cylinders or rods with no defined turns or helices within the fibrous networks (figure 6.9). NOGul (**21**), which was also assessed for IRI activity, did not form hydrogels in aqueous solution. These results are consistent with what has previously been reported for these compounds.[26-29]

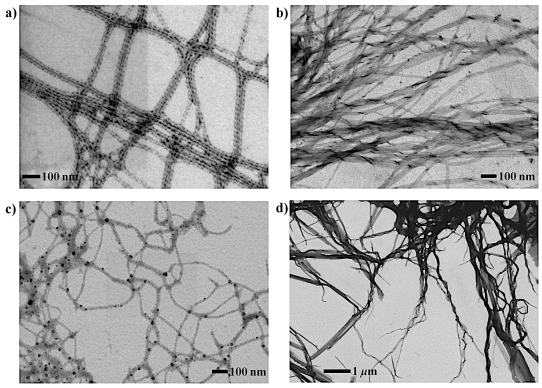

Fig. 8 STEM images of the hydrogels of (a) 1% w/v NOGlc (**5**) in water (33 mM), (b) 0.5% w/v NOGal (**6**) in water (16 mM), (c) 1% w/v NOGlc (**5**) in PBS (33 mM), (d) 0.5% w/v NOGal (**6**) in PBS (16 mM). All hydrogels were negatively stained using 1% phosphotungstic acid.

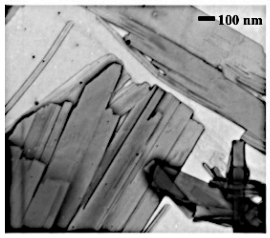

Figure 6.9 STEM image of the hydrogel of 1% w/v NOMan (**20**) in water (33 mM) negatively stained using 1% phosphotungstic acid.

The hydrogel phases of **5** and **6** had different mechanical properties as determined by studying the rheology of these compounds. This was done in collaboration with Dr. James Harden in the Department of Physics at the University of Ottawa. Fig. 9 (reproduced below) represents a plot of the storage and loss moduli, G'(ω) and G''(ω) respectively, as a function of the frequency (ω) of the applied oscillatory strain for several concentrations of **5** in water and PBS. Solutions of NOGal (**6**) formed fragile, solid gel phases in both water and PBS and modest agitation of these gels resulted in fluidization. Thus, reliable rheological data for **6** was unable to be obtained. However, hydrogels of NOGlc (**5**) were relatively stable solid gel phases with relatively weak dissipative behaviour.[24] The strength of the hydrogel phases of **5** were concentration dependent and increased with higher concentrations of NOGlc (**5**). Additionally, they were also strongly dependent on the solvent, with superior hydrogel properties being observed in PBS.[24]

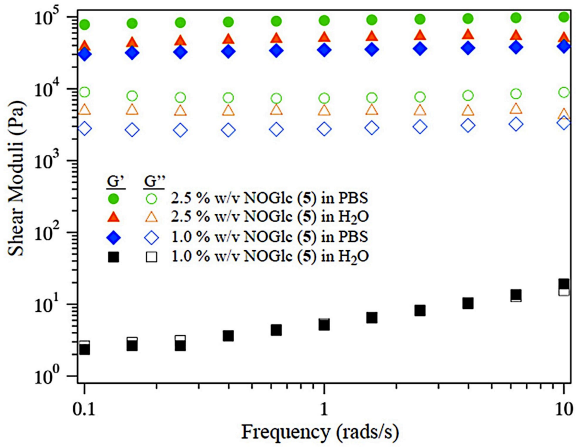

Fig. 9 Dynamic shear moduli of the hydrogels of NOGlc (**5**) in water and PBS as a function of angular frequency ω. G'(ω) represents the storage (elastic) modulus while G"(ω) is the loss (viscous) modulus.

Collectively, the STEM and rheological studies results indicate that NOGlc (**5**) forms a much stronger and more stable hydrogel than NOGal (**6**). Interestingly, derivative **5** is also significantly more IRI active than derivative **6**. However, as previously discussed, **5** and **6** were assessed for IRI activity at 0.5 mM, a concentration well below both of their gelation concentrations (33 mM for **5** and 16 mM for **6**). It therefore seems unlikely that gelation strength is related to IRI activity, as simply the ability to form a hydrogel does not necessarily result in IRI activity. As described in section 6.3.3, there is a drastic difference in the solubilities of **5** and **6** in hot water, with NOGal (**6**) being significantly less soluble than NOGlc (**5**).[27-29] The difference in the strengths of the hydrogels of **5** and **6** may be a result of the significant difference in solubilities of these derivatives. However, NOGul (**21**) has a higher solubility than NOGlc (**5**) but NOGul does not form hydrogels and precipitates when cooled.[27-29] The rheological properties of NOMan (**20**) have currently not been examined, thus the relationship between hydrogel strength and solubility is unclear. Regardless, as described in section 6.3.3, the solubility of the aldonamides along with their ability to form hydrogels in solution appears to be unrelated to the potent IRI activity of both NOGlc (**5**) and NOMan (**20**).

6.4 Summary and Conclusions for the IRI Activity of Carbohydrate-Based Surfactants and Hydrogelators

It was originally hypothesized that the ability of carbohydrate derivatives to alter the structure of bulk-water could result in the discovery of small molecules with the ability to inhibit ice recrystallization. As such, carbohydrate-based non-ionic surfactants and hydrogelators, which were known to alter and/or sequester bulk-water and to self-assemble in solution, were explored as ice recrystallization inhibitors. Of these compounds, three novel small molecules have been identified that exhibit potent IRI activity. One of these compounds was the non-ionic surfactant β-Octyl-Gal (**4**), and the other two were hydrogelators NOGlc (**5**) and NOMan (**20**). While β-Octyl-Gal was potently IRI active at 22 mM, both NOGlc (**5**) and NOMan (**20**) were potently IRI active at a much lower concentration of 0.5 mM. NOGlc (**5**) was the most highly IRI active compound discovered and, owing to it being active at a low concentration, is currently the first and most potent small molecule ice recrystallization inhibitor reported to date.[24] This represents a tremendous advancement in the field of ice recrystallization inhibitors, as prior to this all known ice recrystallization inhibitors were large peptides, glycopeptides or polymers.

It is evident that key structural features of these derivatives are important for their potent activity. For the pyranose-based surfactant β-octyl-Gal (**4**) the presence of a highly hydrated galactose head-group was highly beneficial for activity, whereas a less hydrated glucose head-group was detrimental as β-octyl-Glc (**3**) was weakly IRI active (section 6.3.2). Additionally, a

hydrophobic alkyl tail was also required, and altering this tail to be more hydrophilic was detrimental. This is in agreement with other amphiphilic molecules that have been assessed for IRI by our laboratory and highlights the importance of hydrophobic moieties for IRI activity.[24,41,44] The dependence of hydrophobicity and hydrocarbon chain length was also demonstrated with NOGlc (**5**) as reducing the length of the octyl tail reduced activity, further validating this hypothesis (section 6.3.3).

It was also determined that for NOGlc (**5**) the amide bond connecting the hydrocarbon tail to the carbohydrate head-group was crucial for its potent activity. Replacing it with an ether-linkage or methylating the nitrogen abolished IRI activity. The reduced activity of the *N*-methylated derivatives also indicated that the hydrogen-bond donating ability of this amide bond is also important for the ability of **5** to inhibit ice recrystallization. Additionally, the relative orientation of the hydroxyl groups on the carbohydrate moiety was highly influential. While NOMan derivative **20** retained potent IRI activity, both NOGal (**6**) and NOGul (**21**) were inactive at equimolar concentration (section 6.3.3).

Potently IRI active β-Octyl-Gal (**4**), NOGlc (**5**) and NOMan (**20**) were all capable of forming micelles and/or hydrogels in solution. However, it was ultimately determined that neither the ability to form micelles nor the ability to form a hydrogel were prerequisites for the ability of these compounds to inhibit ice recrystallization. Unfortunately, the exact mechanism by which these derivatives are exhibiting potent activity is currently not known. However, from TH measurements and solid-state NMR experiments we have demonstrated that these novel small molecule IRIs are not acting by bind to ice or interacting with the ice lattice (section 6.3.4). Thus, these small molecules possess the "custom-tailored" antifreeze activity that is a highly desirable property for a cryoprotectant. As such, these compounds are interesting ideal candidates for use as novel cryoprotectants and have been explored in various cryopreservation applications as described in Chapter 8. They also serve as a basis for the rational design of other small molecule ice recrystallization inhibitors and have facilitated the discovery of additional carbohydrate-based and non-carbohydrate-based derivatives that exhibit potent IRI activity (discussed in Chapter 7).

6.5 Experimental Procedures and Compound Characterizations for Chapter 6

Thermal Hysteresis (TH) Assay:

Nanolitre osmometry was performed using a Clifton nanolitre osmometer (Clifton Technical Physics, Hartford, NY), as described by Chakrabartty and Hew.[55] All of the measurements were performed in doubly distilled water. Ice crystal morphology was observed through a Leitz compound microscope equipped with an Olympus 20× (infinity-corrected) objective, a Leitz Periplan 32X photo eyepiece, and a Hitachi KPM2U CCD camera connected to a Toshiba MV13K1 TV/VCR system. Still images were captured directly using a Nikon CoolPix digital camera.

Ice Recrystallization Inhibition (IRI) Assay:

Sample analysis for IRI activity was performed using the "splat cooling" method as previously described.[2] In this method, the analyte was dissolved in phosphate buffered saline (PBS) solution and a 10 μL droplet of this solution was dropped from a micropipette through a two meter high plastic tube (10 cm in diameter) onto a block of polished aluminum precooled to approximately -80 °C. The droplet froze instantly on the polished aluminum block and was approximately 1 cm in diameter and 20 μm thick. This wafer was then carefully removed from the surface of the block and transferred to a cryostage held at -6.4 °C for annealing. After a period of 30 min, the wafer was photographed between crossed polarizing filters using a digital camera (Nikon CoolPix 5000) fitted to the microscope. A total of three images were taken from each wafer. During flash freezing, ice crystals spontaneously nucleated from the supercooled solution. These initial crystals were relatively homogeneous in size and quite small. During the annealing cycle, recrystallization occurred, resulting in a dramatic increase in ice crystal size. A quantitative measure of the difference in recrystallization inhibition of two compounds X and Y is the difference in the dynamics of the ice crystal size distribution. Image analysis of the ice wafers was performed using a novel domain recognition software (DRS) program.[75] This processing employed the Microsoft Windows Graphical User Interface to allow a user to visually demarcate and store the vertices of ice domains in a digital micrograph. The data was then used to calculate the domain areas. All data was plotted and analyzed using Microsoft Excel. The mean grain (or ice crystal) size (MGS) of the sample was compared to the MGS of the control PBS solution for that same day of testing. IRI activity is reported as the percentage of the MGS (% MGS) relative to the PBS control, and the % MGS for each sample was plotted along with its standard error of

the mean. Small percentages represent a small MGS (small ice crystals), which is indicative of high IRI activity.

Recombinant Expression and Purification of LpAFP:

WT and T67Y *Lp*AFP were recombinantly expressed in *E. coli* BL21 DE3 as described previously (also see chapter 4).[72] The gene sequences for His-tagged WT and T67Y *Lp*AFP in a pET 24a+ vector were verified by DNA sequencing (OHRI, Ottawa, ON, Canada). After transformation, WT or T67Y *Lp*AFP cultures were grown in 750 mL of LB media containing 50 μg/mL of kanamycin at 37 °C until an $OD_{600\,nm}$ of ~0.6 was reached. Growth was continued at 24 °C until the $OD_{600\,nm}$ reached ~1.0 before protein expression was induced by the addition of IPTG to a final concentration of 0.2 mM. After overnight growth at 24 °C, the cells were harvested by centrifugation at 4 °C and resuspended in 50 mL of lysis buffer (50 mM Tris-HCl and 100 mM NaCl). The resuspended cells were lysed by boiling for 8 min and allowed to cool to 4 °C on ice. The lysate was clarified by centrifugation at 8000 RPM for 1 h at 4 °C and the resulting supernatant was purified by nickel affinity chromatography. The supernatant was incubated with Ni-NTA superflow (QIAGEN) for 1 h at 4 °C, then loaded to the column and the flow-through was collected. After washing the column with elution buffer (100 mM Tris and 300 mM NaCl), the protein was eluted with elution buffer and an imidazole gradient (20 mM, then 2 X 100 mM, then 3 X 250 mM). Fractions containing WT or T67Y *Lp*AFP were collected and purified by centrifugation with an Amicon Ultra-15 Filter Device (Millipore) by washing five times with H_2O (15 mL). The protein solution was then concentrated to a final volume of 1 mL. Purity was analyzed using SDS-PAGE. Pure WT or T67Y *Lp*AFP were then lyophilized and stored as a white powder at -78 °C. WT or T67Y *Lp*AFP were dissolved in D_2O to the desired concentration for the solid-state NMR measurements. Prior to measuring the saturation recovery curves of frozen D_2O with these proteins, TH activity was measured in D_2O and TH values for both WT *Lp*AFP and T67Y *Lp*AFP were consistent with what has previously been reported.[72]

Solid State NMR Spectroscopy:

All experiments were conducted at a magnetic field of 9.39 T ($\nu_0(^2H)$ = 61.422 MHz) and a temperature of -25 °C using a Bruker 7 mm double resonance wideline probe. The D_2O solutions were pipetted into a Bruker 7 mm o.d. rotors and frozen prior to use. ^2H spin-lattice relaxation times (R_1) were measured using a saturation recovery sequence. The signal was detected using a quadrupolar echo sequence (90° - τ - 90° - τ - acquire) and was saturated, prior to a recovery

delay, with the use of fifty 45° saturation pulses. The 90° pulse length was of 3.88 μs and the echo delay (τ) was set to 30 μs.[67]

Rheology:

Dynamical shear stress measurements were performed on Physica MCR 301 (Anton Paar, Graz, Austria) rheometer using a 25mm diameter plate-plate geometry with a 1mm gap. Plate surfaces were roughened to minimize hydrogel slip and pre-heated to 80 °C. The analyte was dissolved in either de-ionied water or phosphate buffered saline (PBS) solution heated to 95 °C to achieve a homogeneous fluid solution. After loading between rheometer plates, the solutions were cooled to 37 ºC at a rate of 10 ºC/min and the resulting gel phase was allowed to equilibrate for an additional 5 min at 37 ºC before measurements commenced. Dynamic oscillation mode was used to measure the storage and loss components of the dynamic shear modulus of the hydrogels at a shear strain amplitude of 0.25% from 0.1 to 10 rads/s. All tests were made in a controlled humidity and temperature cell at 37 ºC and saturated vapor conditions.

Scanning Transmission Electron Microscopy (STEM):

Negatively stained gel solutions for the electron microscopy study were prepared by adding 1% phosphotungstic acid to the hydrogel solutions at their desired concentrations (1% w/v for NOGlc (**5**) and 0.5% w/v for NOGal (**6**)). Carbon film coated grids were dipped into the stained gel solutions, which were heated in a water bath until solutions became clear. The dipped grids were subsequently dried at room temperature. Bright field scanning transmission electron micrographs were obtained using a JEOL JSM-7500F field emission scanning electron microscope, operating under transmission electron imaging mode.

General Experimental:

All anhydrous reactions were performed in flame-dried glassware under a positive pressure of dry argon. Air or moisture-sensitive reagents and anhydrous solvents were transferred with oven-dried syringes or cannulae. All flash chromatography was performed with E. Merck silica gel 60 (230-400 mesh). All solution phase reactions were monitored using analytical thin layer chromatography (TLC) with 0.2 mm pre-coated silica gel aluminum plates 60 F254 (E. Merck). Components were visualized by illumination with a short-wavelength (254 nm) ultra-violet light and/or staining (ceric ammonium molybdate, potassium permanganate, or phosphomolybdate stain solution). All solvents used for anhydrous reactions were distilled. Tetrahydrofuran (THF) and diethyl ether (Et_2O) were distilled from sodium/benzophenone under nitrogen.

Dichloromethane (DCM) was distilled from calcium hydride. *N*,*N*-dimethylformamide (DMF) was stored over activated 4Å molecular sieves under argon. ^{1}H (400 or 500 MHz) and ^{13}C NMR (100 or 125 MHz) spectra were recorded at ambient temperature on a Bruker Avance 400, Bruker Avance 500, or Varian Inova 500 spectrometer. Deuterated chloroform ($CDCl_3$) or water (D_2O) were used as NMR solvents, unless otherwise stated. Chemical shifts are reported in ppm using the solvent residual peak as an internal standard. Splitting patterns are designated as follows: s, singlet; d, doublet; t, triplet; q, quartet; quint, quintet; m, multiplet and br, broad. Low resolution mass spectrometry (LRMS) was performed on a Micromass Quatro-LC Electrospray spectrometer with a pump rate of 20 μL/min using electrospray ionization (ESI).

NMR spectra for novel compounds and final compounds assessed for IRI activity are provided.

_n_-Octyl-2,3,4,6-tetra-_O_-acetyl-β-D-glucopyranoside (12a)

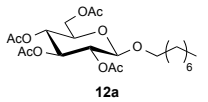

12a

To a mixture of 1,2,3,4,6-Penta-*O*-acetyl-β-D-glucopyranose (**11a**, 275 mg, 0.70 mmol), 1-octanol (215 μL, 1.36 mmol) and 4 Å MS in anhydrous CH_2Cl_2 (6 mL) stirring at 0 °C under Ar, boron trifluoride diethyl etherate (160 μL, 1.27 mmol) was slowly added**.** The reaction mixture was stirred overnight, then diluted with CH_2Cl_2 and quenched with sodium bicarbonate. The solution was filtered through Celite®, then extracted with CH_2Cl_2. The organic layer was washed with sodium bicarbonate, water, saturated brine, then dried over $MgSO_4$ and concentrated. Column chromatography (7:3 hexanes/EtOAc) afforded **12a** as a white powder (103 mg, 32%). Characterization data is consistent with that previously reported in the literature.[76,77] ^{1}H NMR (400 MHz, $CDCl_3$): δ 5.20 (t, *J* = 9.5 Hz, 1H), 5.09 (t, *J* = 9.7 Hz, 1H), 4.98 (dd, *J* = 9.6, 8.0 Hz, 1H), 4.49 (d, *J* = 8.0 Hz, 1H), 4.26 (dd, *J* = 12.3, 4.7 Hz, 1H), 4.13 (dd, *J* = 12.3, 2.5 Hz, 1H), 3.87 (dt, *J* = 9.6, 6.4 Hz, 1H), 3.67 (ddd, *J* = 10.0, 4.7, 2.5 Hz, 1H), 3.47 (dt, *J* = 9.6, 6.8 Hz, 1H), 2.09 (s, 3H), 2.04 (s, 3H), 2.02 (s, 3H), 2.01 (s, 3H), 1.64-1.48 (m, 2H), 1.34-1.21 (m, 10H), 0.88 (t, *J* = 6.9 Hz, 3H). ^{13}C NMR (100 MHz, $CDCl_3$): δ 170.7, 170.3, 169.4, 169.3, 100.8, 72.9, 71.7, 71.4, 70.3, 68.5, 62.0, 31.8, 29.4, 29.3, 29.2, 25.8, 22.6, 20.7, 20.6, 20.6, 20.6, 14.1. LRMS (ESI): *m*/*z* calcd. for $C_{22}H_{40}NO_{10}$ $[M+NH_4]^+$ 478.5; found, 478.4.

_n_-Octyl-β-D-glucopyranoside (3)

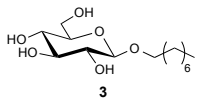

3

Compound **12a** (103 mg, 0.22 mmol) was dissolved in a solution of sodium methoxide in methanol (5 mL) and stirred for one hour at room temperature. The solution was then neutralized with Amberlite® IR-120 (H^+) ion-exchange resin, filtered and concentrated. The

product was purified by column chromatography (9:1 CH_2Cl_2/MeOH) to afford **3** as a white powder (64 mg, 98%). ^{1}H NMR (400 MHz, D_2O): δ 4.44 (d, *J* = 8.0 Hz, 1H), 3.95-3.87 (m, 2H), 3.75-3.62 (m, 2H), 3.50-3.33 (m, 3H), 3.24 (dd, *J* = 9.24, 8.03 Hz, 1H), 1.62 (quint, *J* =7.1 Hz, 2H), 1.38-1.24 (m, 10H), 0.86 (t, *J* = 7.0 Hz, 3H). ^{13}C NMR (100 MHz, D_2O): δ 102.1, 75.8, 75.7, 73.0, 70.6, 69.5, 60.7, 31.1, 28.7, 28.5, 28.4, 25.1, 22.0, 13.4. LRMS (ESI): *m/z* calcd. for $C_{14}H_{28}NaO_6$ $[M+Na]^+$ 315.4; found, 315.3.

***n*-Octyl-2,3,4,6-tetra-*O*-acetyl-β-D-galactopyranoside (12b)**

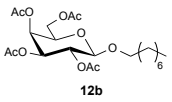

12b

To a mixture of 1,2,3,4,6-Penta-*O*-acetyl-β-D-galactopyranose (**11b**, 500 mg, 1.28 mmol), 1-octanol (280 μL, 1.79 mmol) and 4 Å MS in anhydrous CH_2Cl_2 (10 mL) stirring at 0 °C under Ar, boron trifluoride diethyl etherate (210 μL, 1.66 mmol) was slowly added**.** The reaction mixture was stirred overnight, then diluted with CH_2Cl_2 and quenched with sodium bicarbonate. The solution was filtered through Celite®, then extracted with CH_2Cl_2. The organic layer was washed with sodium bicarbonate, water, saturated brine, then dried over $MgSO_4$ and concentrated. Column chromatography (7:3 hexanes/EtOAc) afforded **12b** as a white powder (228 mg, 39%)**.** Characterization data is consistent with that previously reported in the literature.[76,78] ^{1}H NMR (400 MHz, $CDCl_3$): δ 5.38 (dd, *J* = 3.4, 0.9 Hz, 1H), 5.20 (dd, *J* = 10.5, 7.9 Hz, 1H), 5.01 (dd, *J* = 10.5, 3.4 Hz, 1H), 4.45 (d, *J* = 8.0 Hz, 1H), 4.23-4.08 (m, 2H), 3.93-3.84 (m, 2H), 3.47 (dt, *J* = 9.6, 6.9 Hz, 1H), 2.15 (s, 3H), 2.05 (s, 3H), 2.05 (s, 3H), 1.98 (s, 3H), 1.62-1.53 (m, 2H), 1.34-1.22 (m, 10H), 0.88 (t, *J* = 6.9 Hz, 3H). ^{13}C NMR (100 MHz, $CDCl_3$): δ 170.4, 170.3, 170.2, 169.4, 101.4, 71.0, 70.6, 70.3, 68.9, 67.1, 61.3, 31.8, 29.4, 29.3, 29.2, 25.8, 22.6, 20.7, 20.7, 20.7, 20.6, 14.1. LRMS (ESI): *m/z* calcd. for $C_{22}H_{36}KO_{10}$ $[M+K]^+$ 499.6; found, 499.4.

***n*-Octyl-β-D-galactopyranoside (4)**

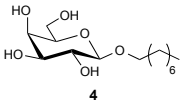

4

Compound **12b** (183 mg, 0.40 mmol) was dissolved in a solution of sodium methoxide in methanol (5 mL) and stirred for one hour at room temperature. The solution was then neutralized with Amberlite® IR-120 (H^+) ion-exchange resin, filtered and concentrated. The product was purified by column chromatography (9:1 CH_2Cl_2/MeOH) to afford 4 as a white powder (109 mg, 94%). ^{1}H NMR (400 MHz, D_2O): δ 4.38 (d, *J* = 7.9 Hz, 1H), 3.95-3.89 (m, 2H), 3.81-3.72 (m, 2H), 3.70-3.61 (m, 3H), 3.49 (dd, *J* = 9.9, 7.9 Hz, 1H), 1.62 (quint, *J* =7.0 Hz, 2H), 1.39-1.24 (m, 10H), 0.86 (t, *J* = 7.0 Hz, 3H). ^{13}C NMR (100 MHz, D_2O): δ 102.7, 75.0, 72.7, 70.7, 70.6, 68.5, 60.8, 31.0, 28.7, 28.4, 28.3, 25.0, 21.9, 13.3. LRMS (ESI): *m/z* calcd. for $C_{14}H_{28}NaO_6$ $[M+Na]^+$ 315.4; found, 315.3.

***N*-Octyl-D-gluconamide (5)**

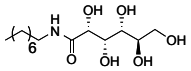

5

To a solution of D-gluconic acid-δ-lactone (1.4 g, 7.86 mmol) in MeOH (30 mL), *n*-octylamine (1.3 mL, 7.86 mmol) was added. The mixture was heated to reflux for 1 hour then cooled in an ice bath. The precipitate was filtered off and washed with cold MeOH to afford **5** as a white powder (1.45 g, 60%). Characterization data is consistent with that previously reported in the literature.[30,31] ^{1}H NMR (500 MHz, DMSO-d_6): δ 7.59, (t, J = 6.0 Hz, 1H), 5.34 (d, J = 5.1 Hz, 1H), 4.53 (t, J = 4.8 Hz, 1H), 4.47 (d, J = 5.1 Hz, 1H), 4.39 (d, J = 7.2 Hz, 1H), 4.33 (d, J = 5.8 Hz, 1H), 3.97 (dd, J = 4.9, 3.8 Hz, 1H), 3.89 (ddd, J = 7.2, 3.7, 2.2 Hz, 1H), 3.57 (m, 1H), 3.46 (m, 2H), 3.37 (m, 1H), 3.06 (m, 2H), 1.40 (quint, J = 6.6 Hz, 2H), 1.31-1.18 (m, 10H), 0.86 (t, J = 6.7 Hz, 3H). ^{13}C NMR (125 MHz, DMSO-d_6): δ 172.2, 73.6, 72.4, 71.5, 70.1, 63.4, 38.3, 31.3, 29.2, 28.8, 28.7, 26.4, 22.1, 14.0. LRMS (ESI): *m/z* calcd. for $C_{14}H_{30}NO_6$ $[M+H]^+$ 308.2; found 308.3.

***N*-Octyl-D-galactonamide (6)**

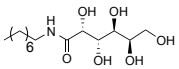

6

A solution of calcium galactonate (200 mg, 0.46 mmol) in methanol (2 mL) was cooled to 0 °C and $SOCl_2$ (70 **μ**L, 0.93 mmol) was added dropwise. The solution was slowly warmed to room temperature and was stirred overnight. The mixture was then evaporated and dried *in vacuo* to give 200 mg of a white powder. This powder was then dissolved in methanol (2 mL) and *n*-octylamine (230 **μ**L, 1.44 mmol) was added. The mixture was refluxed for 2 hours then cooled in an ice bath. The precipitate was filtered off and washed with cold methanol to afford **6** as a white powder (112 mg, 38%). Characterization data is consistent with that previously reported in the literature.[30,31] ^{1}H NMR (500 MHz, DMSO-d_6): δ 7.53, (t, J = 6.0 Hz, 1H), 5.07 (d, J = 7.2 Hz, 1H), 4.44 (t, J = 5.6 Hz, 1H), 4.28 (d, J = 8.1 Hz, 1H), 4.17 (d, J = 6.6 Hz, 1H), 4.12 (d, J = 7.5 Hz, 1H), 4.08 (d, J = 8.1 Hz, 1H), 3.78 (t, J = 8.7 Hz, 1H), 3.69 (q, J = 5.6 Hz, 1H), 3.45-3.37 (m, 3H), 3.07 (m, 2H), 1.40 (m, 2H), 1.31-1.18 (m, 10H), 0.86 (t, J = 6.6 Hz, 3H). ^{13}C NMR (125 MHz, DMSO-d_6): δ 173.3, 70.9, 70.7, 69.8, 69.1, 63.2, 38.3, 31.3, 29.3, 28.8, 28.7, 26.4, 22.1, 14.0. LRMS (ESI): *m/z* calcd. for $C_{14}H_{30}NaNO_6$ $[M+Na]^+$ 330.2; found 330.2.

***N*-Octanoyl-*N*-methyl-D-glucamine (7)**

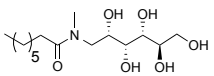

7

A solution of octanoic acid (0.89 mL, 5.63 mmol) in Et_2O (10 mL) was cooled to 0 ºC and isobutyl chloroformate (0.74 mL, 5.63 mmol) was added. After stirring for 5 min at 0 ºC, *N*-methylmorpholine (0.68 mL, 5.63 mmol) was added dropwise and the mixture was

stirred for 10 min. The precipitate was removed by filtration trough Celite® and the filter cake washed with 10 mL of Et_2O. The solution of the crude mixed anhydride in Et_2O was then added by cannula to a cooled solution (0 ºC) of *N*-methyl-D-glucamine (500 mg, 2.56 mmol) in MeOH (10 mL). The mixture was warmed to room temperature, stirred for 1 hour and concentrated *in vacuo*. Recrystallization in MeOH afforded 7 (250 mg, 30%) as a white powder. ^{1}H NMR (500 MHz, DMSO-d_6, present as a 1.3:1 mixture of rotamers): δ 4.87 (d, *J* = 5.2 Hz, 1H, major), 4.72 (d, *J* = 5.1 Hz, 1H, minor), 4.51 (d, *J* = 5.4 Hz, 1H, major), 4.47 (d, *J* = 5.5 Hz, 1H, minor), 4.41-4.26 (m, *3*H), 3.74 (m, 1H), 3.56 (m, 2H), 3.52-3.35 (m, 4H), 3.29 (dd, *J* = 14.4, 3.7 Hz, 1H, major), 3.21 (dd, *J* = 13.2, 8.1 Hz, 1H, minor), 2.99 (s, 3H, minor), 2.80 (s, 3H, major), 2.34 (m, 2H, major), 2.26 (t, *J* = 7.4 Hz, 2H, minor), 1.46 (m, 2H), 1.24 (m, 8H), 0.86 (t, *J* = 6.7 Hz, 3H). ^{13}C NMR (125 MHz, DMSO-d_6, present as a mixture of rotamers): δ (major) 172.4, 71.5, 71.5, 70.8, 69.9, 63.3, 51.9, 33.5, 32.2, 31.2, 28.9, 28.7, 24.9, 22.1, 14.0; δ (minor) 172.6, 72.5, 71.4, 71.3, 69.3, 63.3, 50.8, 36.7, 32.7, 31.2, 28.8, 28.7, 24.9, 22.1, 14.0. HRMS (ESI): *m/z* calcd. for $C_{15}H_{32}NO_6$ $[M+H]^+$ 322.223; found 322.285.

N-Methyl-N-octyl-D-gluconamide (8)

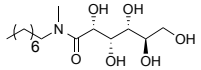

8

To a solution of D-gluconic acid-δ-lactone (950 mg, 5.3 mmol) in MeOH (20 mL) was added *N*-methyl-*N*-octylamine (760 mg, 5.3 mmol). The mixture was stirred under reflux for 1 hour. The clear solution was cooled to room temperature and filtered successively through Dowex-1X8 resin (OH^-) followed by Amberlite IR-120 (H^+). The solvent was evaporated and the residue was dried *in vacuo* to afford **8** as a waxy solid (800 mg, 47%). ^{1}H NMR (500 MHz, DMSO-d_6, present as a 1.1:1 mixture of rotamers): δ 4.77 (d, *J* = 7.2 Hz, 1H, minor), 4.71 (d, *J* = 7.1 Hz, 1H, major), 4.50-4.25 (m, 5H), 3.82 (m, 1H), 3.57 (m, 1H), 3.47 (m, 1H), 3.42-3.20 (m, 4H), 2.99 (s, 3H, major), 2.80 (s, 3H, minor), 1.52 (quint, *J* = 6.7 Hz, 2H, minor), 1.43 (quint, *J* = 6.7 Hz, 2H, major), 1.25 (m, 10H), 0.86 (t, *J* = 6.7 Hz, 3H). ^{13}C NMR (125 MHz, DMSO-d_6, present as a mixture of rotamers): δ (major) 171.5, 71.6, 71.5, 70.4, 69.5, 63.4, 47.2, 34.4, 31.2, 28.8, 28.7, 26.4, 26.2, 22.1, 14.0; δ (minor) 171.6, 71.7, 71.1, 70.9, 69.2, 63.4, 48.5, 33.1, 31.2, 28.8, 28.7, 26.4, 26.2, 22.1, 14.0. HRMS (ESI): *m/z* calcd. for $C_{15}H_{31}NaNO_6$ $[M+Na]^+$ 322.223; found 322.260.

2,3,4,6-tetra-O-benzyl-D-glucitol (14a)

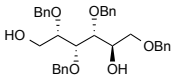

14a

To a stirred solution of 2,3,4,6-tetra-*O*-benzyl-D-glucopyranoside[79] (**13a**, 200 mg, 0.37 mmol) in THF was added $LiAlH_4$ (56 mg, 1.5 mmol). After stirring overnight at

room temperature, the mixture was cooled to 0 °C and the excess of $LiAlH_4$ was carefully quenched with a few drops of water. The mixture was diluted with Et_2O and the organic phase was washed successively with 1% HCl, water and brine. The organic layer was dried over $MgSO_4$ and evaporated. Column chromatography (7:3 Pet. Ether/EtOAc) afforded **14a** (200 mg, quant.) as a viscous oil. ^{1}H NMR (400 MHz, $CDCl_3$): δ 7.39-7.18 (m, 20H), 4.70 (d, *J* = 11.7 Hz, 1H), 4.66 (d, *J* = 11.7 Hz, 1H), 4.65 (d, *J* = 11.7 Hz, 1H), 4.62 (d, *J* = 11.7 Hz, 1H), 4.58 (d, *J* = 11.2 Hz, 1H), 4.54 (d, *J* = 11.7 Hz, 1H), 4.53 (d, *J* = 11.2 Hz, 1H), 4.50 (d, *J* = 11.7 Hz, 1H), 4.02 (m, 1H), 3.88 (m, 1H), 3.77 (m, 2H), 3.72 (dd, J = 11.8, 4.5 Hz, 1H), 3.63 (m, 2H), 3.55 (dd, *J* = 11.7, 4.5 Hz, 1H), 2.27 (br, 2H). ^{13}C NMR (100 MHz, $CDCl_3$): δ 138.1, 137.9, 137.8, 137.8, 128.5, 128.4, 128.4, 128.4, 128.1, 128.0, 127.9, 127.9, 127.8, 127.8, 79.4, 79.1, 77.3, 74.5, 73.4, 73.2, 73.1, 71.1, 70.7, 61.8. LRMS (ESI) *m/z* calcd. for $C_{34}H_{42}NO_6$ $[M+NH_4]^+$ 560.3; found 560.3.

2,3,4,5,6-penta-*O*-benzyl-D-glucitol (15a)

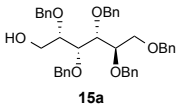

15a

To a solution of **14a** (200 mg, 0.37 mmol) in DMF (2 mL) was added imidazole (60 mg, 0.89 mmol) and TBDMS-Cl (66 mg, 0.44 mmol), successively. After stirring overnight, the reaction mixture was diluted with Et_2O and washed with 1M $KHSO_4$, water and brine. The solvent was evaporated and crude material dried under high vacuum for several hours. The resulting alcohol was re-dissolved in DMF (5 mL) and NaH (18 mg, 0.44 mmol) was added. The mixture was stirred for 30 min and then benzyl bromide (66 μL, 0.55 mmol) and TBAI (14 mg, 0.04 mmol) were added. After stirring overnight, the mixture was diluted with water and organic phase was extracted with Et_2O. The organic layer was washed with water and brine, dried over $MgSO_4$ and the solvent evaporated. This crude material was re-dissolved in THF (2 mL) and TBAF (400 μL, 0.4 mmol) were added and the reaction stirred for 2 hours at room temperature. The mixture was diluted with Et_2O and the organic layer was washed with water and brine, and the solvent was evaporated. Column chromatography (4:1 Pet. Ether/EtOAc) afforded **15a** (120 mg, 51%) as a colorless oil. ^{1}H NMR (500 MHz, $CDCl_3$): δ 7.33-7.19 (m, 25H), 4.74 (d, *J* = 11.4 Hz, 1H), 4.66 (d, *J* = 11.6 Hz, 1H), 4.63 (d, *J* = 12.0 Hz, 2H), 4.61 (d, *J* = 11.4 Hz, 1H), 4.57 (s, 2H), 4.50 (d, *J* = 11.9 Hz, 1H), 4.47 (d, *J* = 11.9 Hz, 1H), 4.43 (d, *J* = 11.6 Hz, 1H), 3.95 (t, *J* = 4.7 Hz, 1H), 3.86 (ddd, *J* = 8.3, 4.8, 3.5 Hz, 2H), 3.83 (dd, *J* = 5.4, 4.8 Hz, 1H), 3.70 (dd, *J* = 11.3, 6.0 Hz, 1H), 3.67 (m, 2H), 3.49 (q, *J* = 6.9 Hz, 1H). ^{13}C NMR ($CDCl_3$, 125 MHz): δ 138.6, 138.4, 138.3, 138.2, 138.2, 128.4, 128.3, 128.3, 128.3, 128.2, 128.1, 127.9, 127.7, 127.7, 127.6, 127.5, 127.4, 79.3, 79.3, 78.9, 78.6, 74.7, 73.8, 73.3, 72.7, 71.9, 69.6, 61.8. LRMS (ESI) *m/z* calcd. for $C_{41}H_{48}NO_6$ $[M+NH_4]^+$ 650.4; found 650.5.

2,3,4,5,6-penta-*O*-benzyl-1-*O*-octyl-D-glucitol (16a)

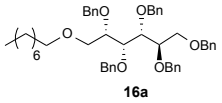

16a

To a solution of **15a** (95 mg, 0.15 mmol) in DMF (2 mL) was added NaH (12 mg, 0.30 mmol). The solution was stirred for 30 min then 1-iodooctane (54 μL, 0.30 mmol) was added and the mixture was stirred overnight. The following day, NaH (6 mg, 0.15 mmol) and 1-iodooctane (27 μL, 0.15 mmol) were added and the mixture was stirred for an additional 24 hours. The reaction mixture was then carefully quenched with water and extracted with Et_2O. The organic layer was washed with water and brine, dried over $MgSO_4$ and the solvent evaporated. Column chromatography (20:1 Pet. Ether/EtOAc) afforded **16a** (64 mg, 57%) as a viscous oil. ^{1}H NMR (400 MHz, $CDCl_3$): δ 7.32-7-20 (m, 25H), 4.72 (d, *J* = 11.9 Hz, 1H), 4.70 (d, *J* = 11.9 Hz, 1H), 4.62 (d, *J* = 11.9 Hz, 1H), 4.60 (s, 2H), 4.59 (d, *J* = 11.9 Hz, 1H), 4.59 (d, *J* = 11.9 Hz, 1H), 4.57 (d, *J* = 11.9 Hz, 1H), 4.42 (s, 2H), 3.96 (m, 3H), 3.89 (dd, *J* = 9.3, 4.7 Hz, 1H), 3.67 (dd, *J* = 10.0, 5.5 Hz, 1H) 3.64 (dd, *J* = 10.0, 4.7 Hz, 1H) 3.61 (dd, *J* = 10.1, 5.6 Hz, 1H) 3.57 (dd, *J* = 10.1, 4.7 Hz, 1H), 3.30 (t, *J* = 6.7 Hz, 2H), 1.50 (quint, *J* = 6.7 Hz, 2H), 1.32-1.20 (m, 10H), 0.87 (t, *J* = 7.0 Hz, 3H). ^{13}C NMR (100 MHz, $CDCl_3$): δ 138.9, 138.9, 138.8, 138.7, 138.2, 128.3, 128.2, 128.2, 127.8, 127.7, 127.7, 127.6, 127.5, 127.4, 127.3, 78.9, 78. 9, 78.4, 78.3, 73.7, 73.7, 73.2, 72.8, 72.6, 71.5, 71.0, 70.5, 31.8, 29.7, 29.5, 29.3, 26.2, 22.6, 14.1. LRMS (ESI) *m/z* calcd. for $C_{49}H_{64}NO_6$ $[M+NH_4]^+$ 762.5; found 762.6.

1-*O*-octyl-D-glucitol (9)

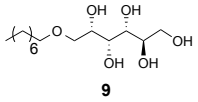

9

A solution **16a** (60 mg, 0.13 mmol) in 3 mL of 1:1:1 mixture of EtOAc/EtOH/MeOH and 5% Pd/C (33 mg, 0.013 mmol) was stirred for 6 hours under an atmosphere of H_2. The flask was purged with N_2 and the catalyst removed by filtration through Celite®. The solvents were removed *in vacuo* and the solid was carefully washed with EtOAc to afford **9** (17 mg, 75%) as a white solid. ^{1}H NMR (500 MHz, D_2O): δ 3.90 (dt, *J* = 10.2, 6.1 Hz, 1H), 3.80-3.77 (m, 2H), 3.74-3.71 (m, 1H), 3.62-3.58 (m, 3H), 3.55-3.47 (m, 3H), 1.54 (quint, *J* = 6.7 Hz, 2H), 1.30-1.23 (m, 10H), 0.82 (t, *J* = 6.7 Hz, 3H). ^{13}C NMR (125 MHz, D_2O): δ 72.0, 71.8, 71.7, 71.6, 71.4, 70.0, 63.2, 31.7, 29.3, 29.2, 29.1, 25.9, 22.5, 13.8. LRMS (ESI) *m/z* calcd. for $C_{14}H_{30}NaO_6$ $[M+Na]^+$ 317.2; found 317.2.

2,3,4,6-tetra-*O*-benzyl-D-galactitol (14b)

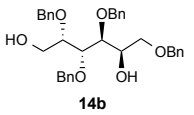

14b

This compound was prepared from 2,3,4,6-tetra-*O*-benzyl-D-galactopyranoside[80] (**13b**, 500 mg, 0.93 mmol) following the same procedure as described for the preparation of **13a**. Column chromatography (7:3 Pet. Ether/EtOAc) afforded **14b** (500 mg, quant.) as a viscous oil. ^{1}H NMR (400 MHz, $CDCl_3$): δ 7.35-7.20 (m, 20H), 4.74 (d, *J* = 11.2 Hz, 1H), 4.67 (d, *J* = 11.2 Hz, 1H), 4.66 (d, *J* = 11.6 Hz, 1H), 4.63 (d, *J* = 11.2 Hz, 1H), 4.58 (d, *J* = 11.6 Hz, 1H), 4.48 (d, *J* = 11.2 Hz, 1H), 4.46 (d, *J* = 11.8 Hz, 1H), 4.41 (d, *J* = 11.8 Hz, 1H), 4.04 (m, 1H), 3.88 (m, 2H), 3.79 (dd, J = 12.8, 5.8 Hz, 1H), 3.71 (m, 2H), 3.54 (dd, J = 9.3, 5.8 Hz, 1H), 3.49 (dd, *J* = 9.3, 6.7 Hz, 1H), 2.60 (br s, 2H). ^{13}C NMR (100 MHz, $CDCl_3$): δ 137.9, 137.9, 137.9, 137.8, 128.5, 128.4, 128.4, 128.4, 128.1, 127.9, 127.9, 127.8, 127.7, 80.1, 79.04, 77.4, 74.3, 73.8, 73.3, 72.3, 70.8, 69.8, 60.9. LRMS (ESI) *m/z* calcd. for $C_{34}H_{42}NO_6$ $[M+NH_4]^+$ 560.3; found 560.4.

2,3,4,5,6-penta-*O*-benzyl-D-galactitol (15b)

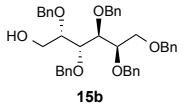

15b

This compound was prepared from **14b** (300 mg, 0.55 mmol) following the same procedure as described for the preparation of **15a**. Column chromatography (4:1 Pet. Ether/EtOAc) afforded **15b** (160 mg, 46%) as a colorless oil. ^{1}H NMR (400 MHz, $CDCl_3$): δ 7.33-7.20 (m, 25H), 4.70 (d, *J* = 11.7 Hz, 1H), 4.69 (s, 2H), 4.61 (d, *J* = 11.7 Hz, 2H), 4.57 (d, *J* = 11.7 Hz, 1H), 4.56 (d, *J* = 11.7 Hz, 1H), 4.52 (d, *J* = 11.7 Hz, 1H), 4.46 (d, *J* = 12.0 Hz, 1H), 4.40 (d, *J* = 12.0 Hz, 1H), 4.03 (dd, *J* = 6.0, 4.2 Hz, 1H), 3.96 (dt, *J* = 5.9, 4.2 Hz, 1H) 3.83 (dd, *J* = 5.3, 4.2 Hz, 1H), 3.77-3.71 (m, 3H), 3.66 (dd, *J* = 10.3, 4.5 Hz, 1H), 3.63 (dd, *J* = 10.3, 4.1 Hz, 1H), 1.59 (br s, 1H). ^{13}C NMR (100 MHz, $CDCl_3$): δ 138.7, 138.4, 138.3, 138.3, 138.1, 128.3, 128.3, 128.3, 128.3, 128.2, 127.9, 127.9, 127.8, 127. 8, 127.7, 127.6, 127.6, 127.5, 127.4, 79.8, 79.4, 79.3, 78.8, 74.6, 73.3, 73.3, 73.0, 72.2, 70.1, 61.1. LRMS (ESI) *m/z* calcd. for $C_{41}H_{48}NO_6$ $[M+NH_4]^+$ 650.4; found 650.4.

2,3,4,5,6-penta-*O*-benzyl-1-*O*-octyl-D-galactitol (16b)

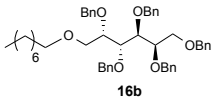

16b

This compound was prepared from **15b** (120 mg, 0.19 mmol) following the same procedure as described for the preparation of **16a**. Column chromatography (20:1 Pet. Ether/EtOAc) afforded **16b** (80 mg, 57%) as a viscous oil. ^{1}H NMR (500 MHz, $CDCl_3$): δ 7.32-7.19 (m, 25H), 4.74 (d, *J* = 11.8 Hz, 1H), 4.70 (d, *J* = 11.8 Hz, 1H), 4.67 (d, *J* = 11.8 Hz, 1H), 4.63 (s, 2H), 4.59 (d, *J* = 11.8 Hz, 1H) 4.55 (d, *J* = 11.8 Hz, 1H) 4.51 (d, *J* = 11.8 Hz, 1H) 4.47 (d, *J* = 11.8 Hz, 1H) 4.44 (d, *J* = 11.8 Hz, 1H), 4.01 (t, *J* = 4.2 Hz, 1H),

3.87-3.77 (m, 4H), 3.71 (m, 1H), 3.52 (dd, *J* = 10.1, 3.1 Hz, 1H), 3.45 (dd, *J* = 10.1, 4.8 Hz, 1H), 3.26 (dt, *J* = 6.7, 2.0 Hz, 2H), 1.48 (quint, *J* = 6.7 Hz, 2H), 1.32-1.17 (m, 10H), 0.87 (t, *J* = 6.7 Hz, 3H). ^{13}C NMR (100 MHz, $CDCl_3$): δ 138.8, 138.8, 138.7, 138.7, 138.4, 128.3, 128.2, 128.2, 128.2, 128.0, 127.9, 127.6, 127.4, 127.4, 127.4, 127.4, 127.3, 79.3, 79.3, 79.2, 78.6, 74.7, 74.1, 73.2, 72.8, 71.9, 71.4, 71.1, 70.0, 31.8, 29.7, 29.4, 29.3, 26.2, 22.7, 14.1. LRMS (ESI) *m/z* calcd. for $C_{49}H_{61}O_6$ $[M+H]^+$ 745.5; found 745.6.

1-*O*-octyl-D-galactitol (10)

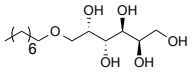

10

This compound was prepared from **16b** (60 mg, 0.081 mmol) following the same procedure as described for the preparation of **9**. Compound **10** (12 mg, 50%) was obtained as a white solid. ^{1}H NMR (500 MHz, CD_3OD): δ 4.63 (s, 2H), 4.04 (dd, *J* = 6.6, 5.8 Hz, 1H), 3.92 (dd, *J* = 6.6, 5.8 Hz, 1H), 3.64 (m, 4H), 3.57 (dd, *J* = 9.6, 5.8 Hz, 1H), 3.53 (dd, *J* = 9.6, 6.7 Hz, 1H), 3.49 (t, *J* = 6.6 Hz, 2H), 1.58 (quint, *J* = 6.7 Hz, 2H), 1.41-1.25 (m, 10H), 0.90 (t, *J* = 6.7 Hz, 3H). ^{13}C NMR (125 MHz, Pyridine-d_5): δ 75.3, 73.2, 73.0, 73.0, 72.8, 70.9, 66.5, 33.2, 31.4, 30.9, 30.7, 27.7, 24.1, 15.5. LRMS (ESI) *m/z* calcd. for $C_{14}H_{30}NaO_6$ $[M+Na]^+$ 317.2; found 317.3.

***n*-3,6-dioxaoctyl-2,3,4,6-tetra-*O*-acetyl-β-D-galactopyranoside (22)**

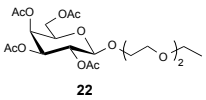

22

To a mixture of 1,2,3,4,6-Penta-*O*-acetyl-β-D-galactopyranose (500 mg, 1.28 mmol), 3,6-dioxaoctanol (240 μL, 1.79 mmol) and 4 Å MS in anhydrous CH_2Cl_2 (10 mL) stirring at 0 °C under Ar, was slowly added boron trifluoride diethyl etherate (805 μL, 6.4 mmol). The reaction mixture was stirred overnight, then diluted with CH_2Cl_2 and quenched with sodium bicarbonate. The solution was filtered through Celite®, then extracted with CH_2Cl_2. The organic layer was washed with sodium bicarbonate, water, saturated brine, then dried over $MgSO_4$ and concentrated. Column chromatography (3:2 hexanes/EtOAc) afforded **22** as a clear syrup (275 mg, 59%). Characterization data is consistent with that previously reported in the literature.[81,82] ^{1}H NMR (400 MHz, $CDCl_3$): δ 5.38 (dd, *J* = 3.4, 1.0 Hz, 1H), 5.21 (dd, *J* = 10.5, 8.0 Hz, 1H), 5.01 (dd, *J* = 10.5, 3.4 Hz, 1H), 4.57 (d, *J* = 8.0 Hz, 1H), 4.15 (qd, *J* = 9.1, 6.8 Hz, 2H), 3.99-3.89 (m, 2H), 3.76 (ddd, *J* = 11.1, 7.1, 4.0 Hz, 1H), 3.67-3.61 (m, 4H), 3.58-3.50 (m, 4H), 2.15 (s, 3H), 2.06 (s, 3H), 2.05 (s, 3H), 1.98 (s, 3H), 1.21 (t, *J* = 7.0 Hz, 3H). ^{13}C NMR (101 MHz, $CDCl_3$): δ 170.7, 170.6, 170.2, 169.7, 101.4, 71.3, 70.6, 70.3, 69.5, 69.4, 69.4, 69.2, 68.9, 67.1, 61.5, 21.2, 21.0, 20.7, 20.6, 12.1. LRMS (ESI): *m/z* calcd. for $C_{20}H_{36}NO_{12}$ $[M+NH_4]^+$ 482.6; found, 482.1.

***n*-3,6-dioxaoctyl-β-D-galactopyranoside (17)**

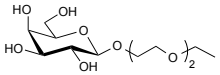
17

Compound **22** (181 mg, 0.39 mmol) was dissolved in a solution of sodium methoxide in methanol (5 mL) and stirred for one hour at room temperature. The solution was then neutralized with Amberlite® IR-120 (H^+) ion-exchange resin, filtered and concentrated. The product was purified by column chromatography (9:1 CH_2Cl_2/MeOH) to afford **17** as a white powder (113 mg, 98%). ^{1}H NMR (400 MHz, D_2O): δ 4.42 (d, *J* = 7.8 Hz, 1H), 4.07 (dt, *J* = 11.5, 4.3 Hz, 1H), 3.92-3.91 (m, 1H), 3.86-3.57 (m, 13H), 3.53 (dd, *J* = 9.9, 7.9 Hz, 1H), 1.19 (t, *J* = 7.1 Hz, 3H). ^{13}C NMR (101 MHz, D_2O): δ 102.8, 75.2, 72.7, 70.8, 69.7, 69.6, 68.9, 68.6, 66.6, 61.0, 14.0. LRMS (ESI): *m/z* calcd. for $C_{12}H_{24}NaO_8$ $[M+Na]^+$ 319.3; found, 319.1.

***N*-Propyl-D-gluconamide (18)**

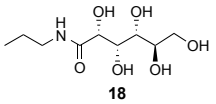
18

To a solution of D-gluconic acid-δ-lactone (500 mg, 2.81 mmol) in MeOH (15 mL) was added *n*-propylamine (230 μL, 2.81 mmol). The mixture was refluxed for 1 hour then cooled in an ice bath. The precipitate was filtered off and washed with cold MeOH to afford **18** as a white powder (158 mg, 24%). ^{1}H NMR (300 MHz, DMSO-d_6): δ 7.61 (t, *J* = 5.9 Hz, 1H), 5.36 (d, *J* = 5.1 Hz, 1H), 4.54 (d, *J* = 5.0 Hz, 1H), 4.47 (d, *J* = 5.5 Hz, 1H), 4.40 (d, *J* = 7.2 Hz, 1H), 4.33 (t, *J* = 5.7 Hz, 1H), 3.97 (t, *J* = 4.4 Hz, 1H), 3.91-3.87 (m, 1H), 3.59-3.54 (m, 1H), 3.49-3.43 (m, 2H), 3.40-3.37 (m, 1H), 3.04 (qd, *J* = 6.5, 3.1 Hz, 2H), 1.48-1.36 (m, 2H), 0.82 (t, *J* = 7.4 Hz, 3H). ^{13}C NMR (76 MHz, DMSO-d_6): δ 172.3, 73.7, 72.4, 71.5, 70.1, 63.4, 40.0, 22.4, 11.4 LRMS (ESI): *m/z* calcd. for $C_9H_{20}NO_6$ $[M+H]^+$ 238.3; found 238.2.

***N*-Hexyl-D-gluconamide (19)**

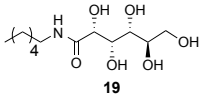
19

To a solution of D-gluconic acid-δ-lactone (1.4 g, 7.86 mmol) in MeOH (30 mL) was added *n*-hexylamine (1.03 mL, 7.86 mmol). The mixture was refluxed for 1 hour then cooled in an ice bath. The precipitate was filtered off and washed with cold MeOH to afford **19** as a white powder (945 g, 43%). ^{1}H NMR (300 MHz, DMSO-d_6): δ 7.60 (t, *J* = 5.9 Hz, 1H), 5.35 (d, *J* = 5.0 Hz, 1H), 4.55-4.53 (m, 1H), 4.48-4.46 (m, 1H), 4.39 (d, *J* = 7.2 Hz, 1H), 4.34 (t, *J* = 5.4 Hz, 1H), 3.96 (t, *J* = 4.2 Hz, 1H), 3.90-3.88 (m, 1H), 3.59-3.55 (m, 1H), 3.46-3.43 (m, 2H), 3.37 (t, *J* = 0.4 Hz, 1H), 3.12-3.02 (m, 2H), 1.42-1.38 (m, 2H), 1.25 (d, *J* = 10.3 Hz, 6H), 0.86 (t, *J* = 6.7 Hz, 3H). ^{13}C NMR (76 MHz, DMSO-d_6): δ 172.2, 73.7, 72.4,

71.5, 70.1, 63.4, 38.3, 31.1, 29.2, 26.1, 22.1, 14.0. LRMS (ESI): *m/z* calcd. for $C_{12}H_{26}NO_6$ $[M+H]^+$ 280.3; found 280.2.

N-Octyl-L-Mannonamide (20)

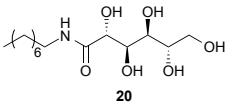

20

To a solution of L-mannonic acid-γ-lactone (1.4 g, 7.86 mmol) in MeOH (30 mL) was added *n*-octylamine (1.3 mL, 7.86 mmol). The mixture was refluxed for 1 hour then cooled in an ice bath. The precipitate was filtered off and washed with cold MeOH to afford **20** as a white powder (1.25 g, 52%). Characterization data is consistent with that previously reported in the literature.[30,31] ^{1}H NMR (300 MHz, DMSO-d_6): δ 7.88 (t, J = 5.8 Hz, 1H), 5.47 (d, J = 6.3 Hz, 1H), 4.47 (dt, J = 9.2, 4.9 Hz, 3H), 4.29 (t, J = 5.7 Hz, 1H), 3.87 (t, J = 6.7 Hz, 1H), 3.77 (t, J = 6.4 Hz, 1H), 3.62-3.57 (m, 1H), 3.49-3.45 (m, 2H), 3.39 (dd, J = 7.9, 4.4 Hz, 1H), 3.10-3.04 (m, 2H), 1.43-1.38 (m, 2H), 1.30-1.24 (m, 11H), 0.86 (t, J = 6.7 Hz, 3H). ^{13}C NMR (76 MHz, DMSO-d_6): δ 173.6, 71.9, 70.9, 70.5, 70.3, 63.8, 38.3, 31.3, 29.1, 28.78, 28.71, 26.4, 22.1, 14.0. LRMS (ESI): *m/z* calcd. for $C_{14}H_{30}NO_6$ $[M+H]^+$ 308.2; found 308.4.

N-Octyl-D-Gulonamide (21)

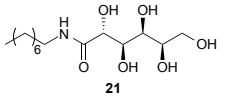

21

To a solution of D-gulonic acid-γ-lactone (736 mg, 4.13 mmol) in MeOH (20 mL) was added *n*-octylamine (683 μL, 4.13 mmol). The mixture was refluxed for 1 hour then cooled in an ice bath. The precipitate was filtered off and washed with cold MeOH to afford **21** as a white powder (697 mg, 55%). ^{1}H NMR (300 MHz, DMSO-d_6): δ 7.82 (t, J = 5.9 Hz, 1H), 5.44 (d, J = 6.5 Hz, 1H), 4.66 (d, J = 4.7 Hz, 1H), 4.48 (d, J = 4.6 Hz, 1H), 4.43 (t, J = 5.6 Hz, 1H), 4.36 (d, J = 5.9 Hz, 1H), 3.90 (t, J = 6.4 Hz, 1H), 3.62 (t, J = 5.0 Hz, 2H), 3.54 (t, J = 5.1 Hz, 1H), 3.43 (q, J = 5.4 Hz, 1H), 3.35 (t, J = 8.2 Hz, 1H), 3.09-3.03 (m, 2H), 1.42-1.38 (m, 2H), 1.28-1.20 (m, 10H), 0.86 (t, J = 6.7 Hz, 3H). ^{13}C NMR (76 MHz, DMSO-d_6): δ 173.6, 73.8, 73.3, 72.4, 70.0, 63.0, 38.8, 31.7, 29.5, 29.2, 29.2, 26.8, 22.6, 14.5. LRMS (ESI): *m/z* calcd. for $C_{14}H_{30}NO_6$ $[M+H]^+$ 308.2; found 308.3.

6.6 References

1. Tam, R.Y.; Ferreira, S.S.; Czechura, P.; Chaytor, J.L.; Ben, R.N. *J. Am. Chem. Soc.* **2008**, *130*, 17494-17501.

2. Knight, C.A.; Hallett, J.; DeVries, A.L. *Cryobiology*. **1988**, *25*, 55-60.

3. Knight, C.A.; Wen, D.; Laursen, R.A. *Cryobiology*. **1995**, *32*, 23-34.

4. Knight, C.A.; DeVries, A.L.; Oolman, L.D. *Nature*. **1984**, *308*, 295-296.

5. Garner, J.; Harding, M.M. *ChemBioChem*. **2010**, *11*, 2489-2498.

6. Harding, M.M.; Anderberg, P.I.; Haymet, A.D.J. *Eur. J. Biochem.* **2003**, *270*, 1381-1392.

7. Harding, M.M.; Ward, L.G.; Haymet, A.D.J. *Eur. J. Biochem.* **1999**, *264*, 653-665.

8. Peltier, R.; Brimble, M.A.; Wojnar, J.M.; Williams, D.E.; Evans, C.W.; DeVries, A.L. *Chem. Sci.* **2010**, *1*, 538-551.

9. Davies, P.L.; Baardsnes, J.; Kuiper, M.J.; Walker, V.K. *Philos. Trans. R. Soc. London, Ser. B.* **2002**, *357*, 927-935.

10. Davies, P.L.; Hew, C.L. *FASEB J.* **1990**, *4*, 2460-2468.

11. Jia, Z.; Davies, P.L. *Trends Biochem. Sci.* **2002**, *27*, 101-106.

12. Yu, S.O.; Brown, A.; Middleton, A.J.; Tomczak, M.M.; Walker, V.K.; Davies, P.L. *Cryobiology.* **2010**, *61*, 327-334.

13. Pudney, P.D.A.; Buckley, S.L.; Sidebottom, C.M.; Twigg, S.N.; Sevilla, M.-P.; Holt, C.B.; Roper, D.; Telford, J.H.; McArthur, A.J.; Lillford, P.J. *Arch. Biochem. Biophys.* **2003**, *410*, 238-245.

14. Eniade, A.; Purushotham, M.; Ben, R.N.; Wang, J.B.; Horwath, K. *Cell Biochem. Biophys.* **2003**, *38*, 115-124.

15. Czechura, P.; Tam, R.Y.; Dimitrijevic, E.; Murphy, A.V.; Ben, R.N. *J. Am. Chem. Soc.* **2008**, *130*, 2928-2929.

16. Liu, S.; Ben, R.N. *Org. Lett.* **2005**, *7*, 2385-2388.

17. Inada, T.; Lu, S.-S. *Cryst. Growth Des.* **2003**, *3*, 747-752.

18. Inada, T.; Lu, S.-S. *Chem. Phys. Lett.* **2004**, *394*, 361-365.

19. Budke, C.; Koop, T. *ChemPhysChem.* **2006**, *7*, 2601-2606.

20. Gibson, M.I. *Polym. Chem.* **2010**, *1*, 1141-1152.

21. Gibson, M.I.; Barker, C.A.; Spain, S.G.; Albertin, L.; Cameron, N.R. *Biomacromolecules.* **2009**, *10*, 328-333.

22. Estroff, L.A.; Hamilton, A.D. *Chem. Rev.* **2004**, *104*, 1201-1218.

23. de Loos, M.; Feringa, B.L.; van Esch, J.H. *Eur. J. Org. Chem.* **2005**, *2005*, 3615-3631.

24. Capicciotti, C.J.; Leclère, M.; Perras, F.A.; Bryce, D.L.; Paulin, H.; Harden, J.; Liu, Y.; Ben, R.N. *Chem. Sci.* **2012**, *3*, 1408-1416.

25. Helenius, A.; Simons, K. *Biochim. Biophys. Acta, Rev. Biomembr.* **1975**, *415*, 29-79.

26. Pfannemüller, B.; Welte, W. *Chem. Phys. Lipids.* **1985**, *37*, 227-240.

27. Fuhrhop, J.H.; Boettcher, C. *J. Am. Chem. Soc.* **1990**, *112*, 1768-1776.

28. Fuhrhop, J.H.; Schnieder, P.; Boekema, E.; Helfrich, W. *J. Am. Chem. Soc.* **1988**, *110*, 2861-2867.

29. Fuhrhop, J.H.; Svenson, S.; Boettcher, C.; Roessler, E.; Vieth, H.M. *J. Am. Chem. Soc.* **1990**, *112*, 4307-4312.

30. Svenson, S.; Kirste, B.; Fuhrhop, J.-H. *J. Am. Chem. Soc.* **1994**, *116*, 11969-11975.

31. Svenson, S.; Schafer, A.; Fuhrhop, J.-H. *J. Chem. Soc. Perkin Trans. 2.* **1994**, 1023-1028.

32. Chaytor, J.L.; Ben, R.N. *Bioorg. Med. Chem. Lett.* **2010**, *20*, 5251-5254.

33. Balcerzak, A.K.; Ferreira, S.S.; Trant, J.F.; Ben, R.N. *Bioorg. Med. Chem. Lett.* **2012**, *22*, 1719-1721.

34. Lorber, B.; Bishop, J.B.; DeLucas, L.J. *Biochim. Biophys. Acta*. **1990**, *1023*, 254-265.

35. Chong, T.T.; Hashim, R.; Bryce, R.A. *J. Phys. Chem. B*. **2006**, *110*, 4978-4984.

36. Haller, J.; Kaatze, U. *J. Phys. Chem. B*. **2009**, *113*, 12283-12292.

37. Ray, A.; Némethy, G. *J. Am. Chem. Soc*. **1971**, *93*, 6787-6793.

38. *Brij 58 CMC values provided by supplier (Sigma-Aldrich).*

39. Romani, A.P.; Machado, A.d.H.; Hioka, N.; Severino, D.; Baptista, M.S.; Codognoto, L.; Rodrigues, M.R.; de Oliveira, H.P.M. *J. Fluoresc*. **2009**, *19*, 327-332.

40. *Triton X-100 values provided by supplier (Sigma-Aldrich). Critical micelle concentration (CMC) range: 0.2 - 0.9 mM.*

41. Balcerzak, A.K.; Febbraro, M.; Ben, R.N. *RSC Adv*. **2013**, *3*, 3232-3236.

42. Pastor, O.; Junquera, E.; Aicart, E. *Langmuir*. **1998**, *14*, 2950-2957.

43. Galema, S.A.; Høiland, H. *J. Phys. Chem*. **1991**, *95*, 5321-5326.

44. Trant, J.F.; Biggs, R.A.; Capicciotti, C.J.; Ben, R.N. *RSC Adv*. **2013**, *3*, 26005-26009.

45. Knight, C.A.; Cheng, C.C.; DeVries, A.L. *Biophys. J*. **1991**, *59*, 409-418.

46. Knight, C.A.; Driggers, E.; DeVries, A.L. *Biophys. J*. **1993**, *64*, 252-259.

47. Raymond, J.A.; DeVries, A.L. *Proc. Natl. Acad. Sci. U.S.A*. **1977**, *74*, 2589-2593.

48. Knight, C.A.; DeVries, A.L. *J. Cryst. Growth*. **1994**, *143*, 301-310.

49. Wilson, P.W. *Cryoletters*. **1993**, *14*, 31-36.

50. Pegg, D.E. *Cryobiology*. **1992**, *29*, 774.

51. Rubinsky, B.; DeVries, A.L. *Cryobiology*. **1989**, *26*, 580.

52. Mugano, J.A.; Wang, T.; Layne, J.R., Jr.,; DeVries, A.L.; Lee, R.E. *Cryobiology*. **1995**, 556-557.

53. Larese, A.; Acker, J.; Muldrew, K.; Yang, H.Y.; McGann, L. *Cryo-letters*. **1996**, *17*, 172-182.

54. Wang, J.H.; Bian, H.W.; Huang, C.N.; Ge, J.G. *Acta Biol. Exp*. **1999**, *32*, 271-276.

55. Chakrabartty, A.; Hew, C.L. *Eur. J. Biochem*. **1991**, *202*, 1057-1063.

56. Czechura, P.; Tam, R.Y.; Dimitrijevic, E.; Murphy, A.V.; Ben, R.N. *J. Am. Chem. Soc*. **2008**, *130*, 2928-2929.

57. Liu, S.; Ben, R.N. *Org. Lett*. **2005**, *7*, 2385-2388.

58. Tam, R.Y.; Ferreira, S.S.; Czechura, P.; Chaytor, J.L.; Ben, R.N. *J. Am. Chem. Soc*. **2008**, *130*, 17494-17501.

59. Bouvet, V.R.; Lorello, G.R.; Ben, R.N. *Biomacromolecules*. **2006**, *7*, 565-571.

60. Fletcher, G.L.; Hew, C.L.; Davies, P.L. *Annu. Rev. Physiol*. **2001**, *63*, 359-390.

61. Baardsnes, J.; Davies, P.L. *Biochim. Biophys. Acta*. **2002**, *1601*, 49-54.

62. Haymet, A.D.J.; Ward, L.G.; Harding, M.M. *J. Am. Chem. Soc*. **1999**, *121*, 941-948.

63. Yeh, Y.; Feeney, R.E. *Chem. Rev*. **1996**, *96*, 601-618.

64. Graham, L.A.; Liou, Y.-C.; Walker, V.K.; Davies, P.L. *Nature*. **1997**, *388*, 727-728.

65. Marshall, C.B.; Fletcher, G.L.; Davies, P.L. *Nature*. **2004**, *429*, 153-153.

66. Gilbert, J.A.; Davies, P.L.; Laybourn-Parry, J. *FEMS Microbiol. Lett*. **2005**, *245*, 67-72.

67. Siemer, A.B.; Huang, K.-Y.; McDermott, A.E. *Proc. Natl. Acad. Sci. U.S.A.* **2010**, *107*, 17580-17585.

68. Kao, M.H.; Fletcher, G.L.; Wang, N.C.; Hew, C.L. *Can. J. Zool.* **1986**, *64*, 578-582.

69. Sidebottom, C.; Buckley, S.; Pudney, P.; Twigg, S.; Jarman, C.; Holt, C.; Telford, J.; McArthur, A.; Worrall, D.; Hubbard, R.; Lillford, P. *Nature*. **2000**, *406*, 256.

70. Pudney, P.D.A.; Buckley, S.L.; Sidebottom, C.M.; Twigg, S.N.; Sevilla, M.-P.; Holt, C.B.; Roper, D.; Telford, J.H.; McArthur, A.J.; Lillford, P.J. *Arch. Biochem. Biophys.* **2003**, *410*, 238-245.

71. Kumble, K.D.; Demmer, J.; Fish, S.; Hall, C.; Corrales, S.; DeAth, A.; Elton, C.; Prestidge, R.; Luxmanan, S.; Marshall, C.J.; Wharton, D.A. *Cryobiology*. **2008**, *57*, 263-268.

72. Middleton, A.J.; Brown, A.M.; Davies, P.L.; Walker, V.K. *FEBS Lett.* **2009**, *583*, 815-819.

73. Spiess, H. *J. Chem. Phys.* **1980**, *72*, 6755.

74. Torchia, D.A.; Szabo, A. *J. Magn. Reson.* **1982**, *49*, 107-121.

75. Jackman, J.; Noestheden, M.; Moffat, D.; Pezacki, J.P.; Findlay, S.; Ben, R.N. *Biochem. Biophys. Res. Commun.* **2007**, *354*, 340-344.

76. Tsui, D.S.K.; Gorin, P.A.J. *Carbohydr. Res.* **1985**, *144*, 137-147.

77. Akita, H.; Kawahara, E.; Kato, K. *Tetrahedron: Asymmetry*. **2004**, *15*, 1623-1629.

78. Li, X.-B.; Ogawa, M.; Monden, T.; Maeda, T.; Yamashita, E.; Naka, M.; Matsuda, M.; Hinou, H.; Nishimura, S.-I. *Angew. Chem. Int. Ed.* **2006**, *45*, 5652-5655.

79. Dasgupta, S.; Nitz, M. *J. Org. Chem.* **2011**, *76*, 1918-1921.

80. Adinolfi, M.; Barone, G.; Iadonisi, A.; Mangoni, L. *Tetrahedron Lett.* **1998**, *39*, 2021-2024.

81. Otman, O.; Boullanger, P.; Lafont, D.; Hamaide, T. *Macromol. Chem. Phys.* **2008**, *209*, 2410-2422.

82. Chevolot, Y.; Bouillon, C.; Vidal, S.; Morvan, F.; Meyer, A.; Cloarec, J.-P.; Jochum, A.; Praly, J.-P.; Vasseur, J.-J.; Souteyrand, E. *Angew. Chem. Int. Ed.* **2007**, *46*, 2398-2402.

6.7 NMR Spectra of Compounds in Chapter 6

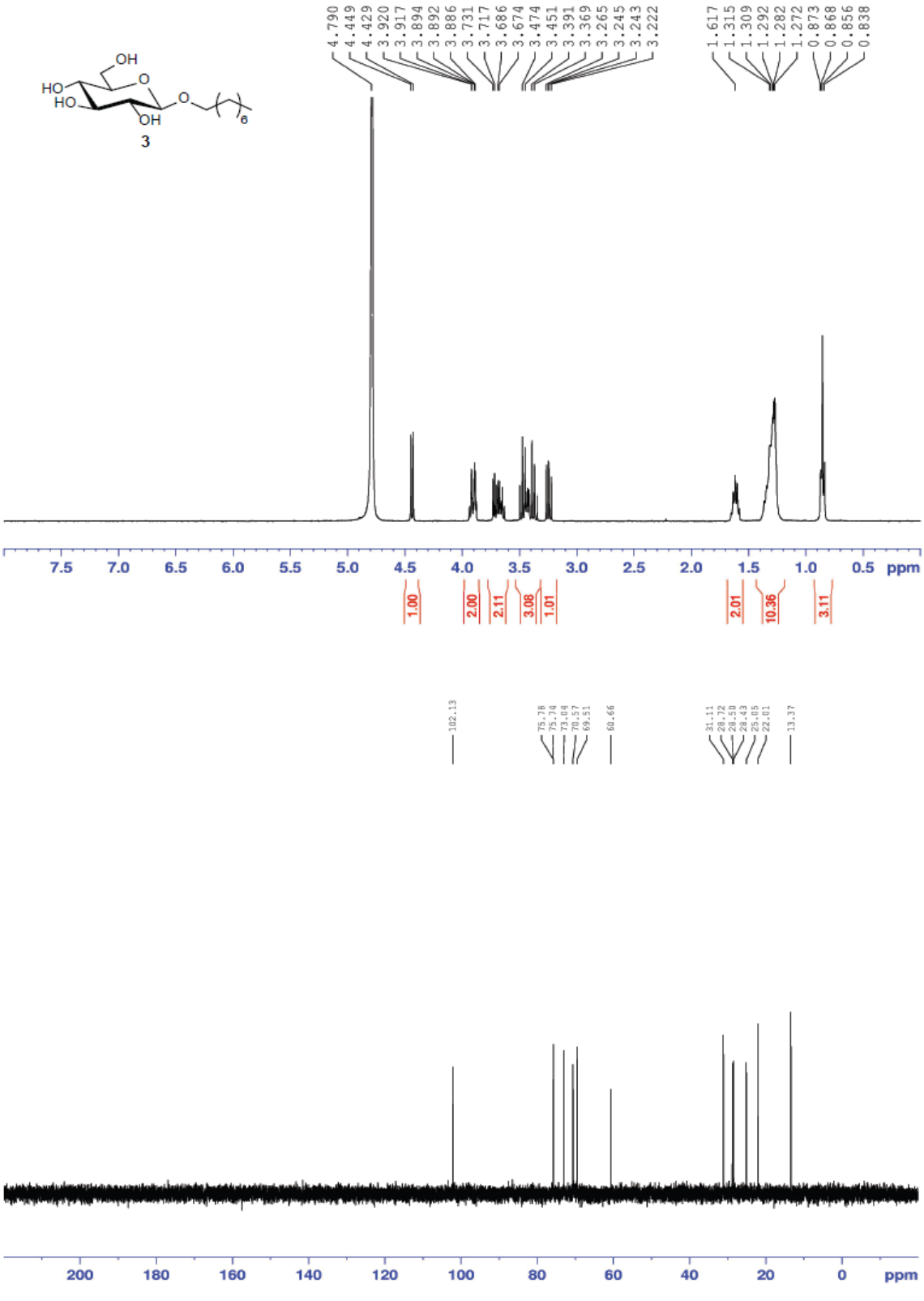

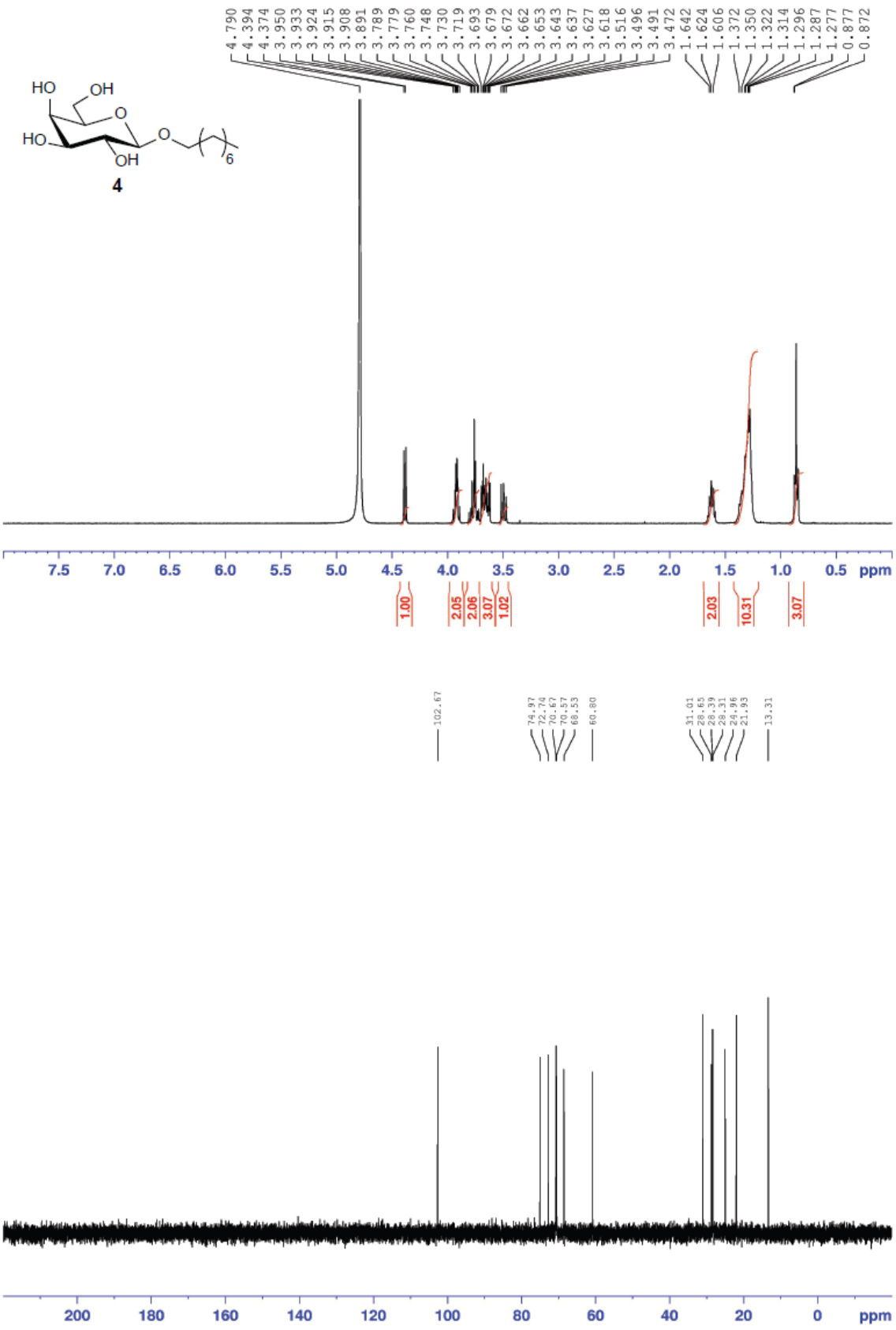
4.790
4.394
4.374
3.950
3.933
3.924
3.915
3.908
3.891
3.789
3.779
3.760
3.748
3.730
3.719
3.693
3.679
3.672
3.662
3.653
3.643
3.637
3.627
3.618
3.516
3.496
3.491
3.472
1.642
1.624
1.606
1.372
1.350
1.322
1.314
1.296
1.287
1.277
0.877
0.872
HO
OH
O
HO
O
OH
6
4
7.5 7.0 6.5 6.0 5.5 5.0 4.5 4.0 3.5 3.0 2.5 2.0 1.5 1.0 0.5 ppm
1.00
2.05
2.06
3.07
1.02
2.03
10.31
3.07
102.67
74.97
72.74
70.67
70.57
68.53
60.80
31.01
28.65
28.39
28.31
24.96
21.93
13.31
200 180 160 140 120 100 80 60 40 20 0 ppm

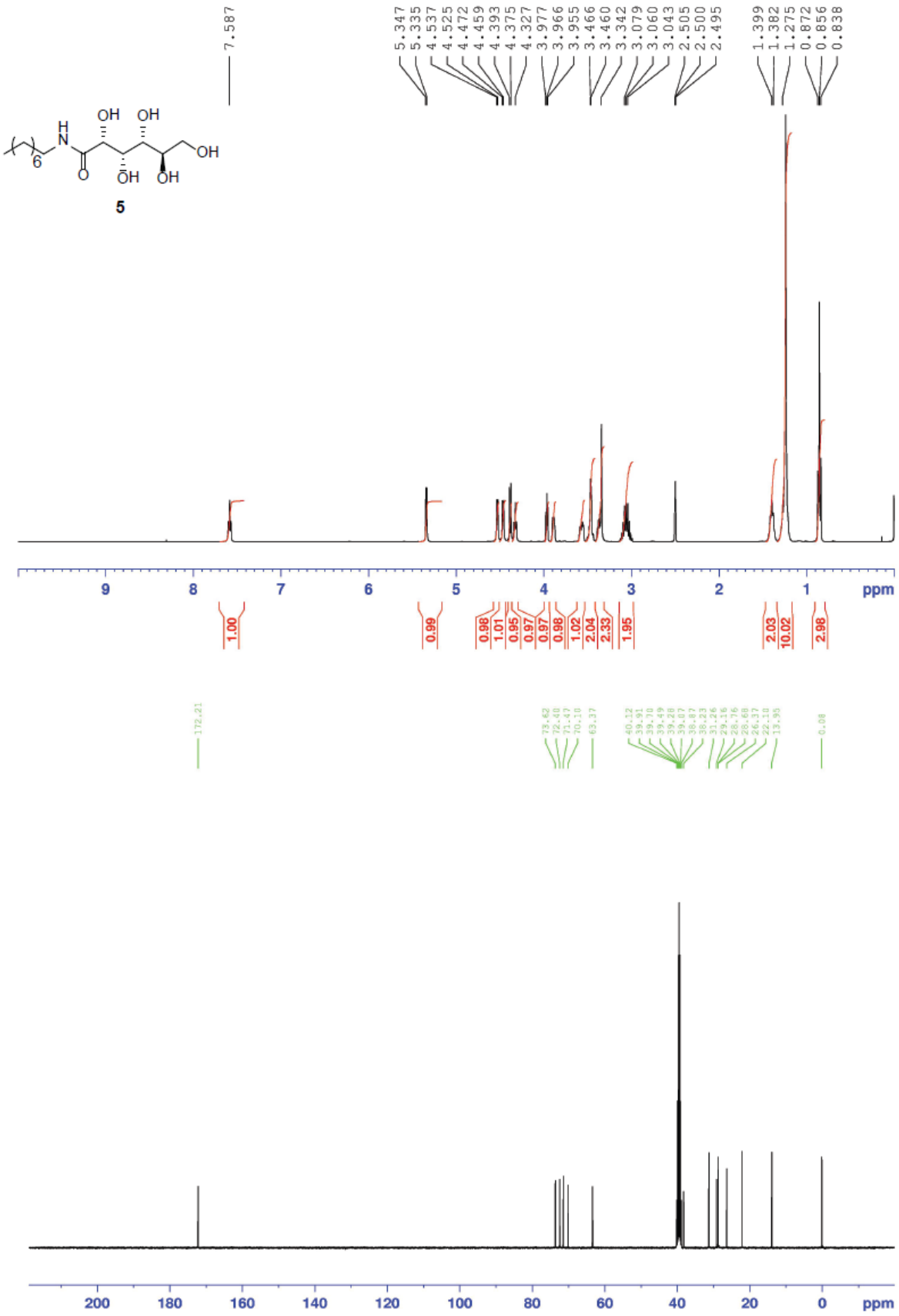
7.587
5.347
5.335
4.537
4.525
4.472
4.459
4.393
4.375
4.327
3.977
3.966
3.955
3.466
3.460
3.342
3.079
3.060
3.043
2.505
2.500
2.495
1.399
1.382
1.275
0.872
0.856
0.838
OH
OH
OH
OH
OH
H
N
O
6
5
9
8
7
6
5
4
3
2
1
ppm
1.00
0.99
0.98
1.01
0.95
0.97
0.97
0.98
1.02
2.04
2.33
1.95
2.03
10.02
2.98
172.21
73.62
72.40
71.47
70.10
63.37
40.12
39.91
39.70
39.49
39.28
39.07
38.87
38.23
31.26
29.16
28.76
28.60
26.37
22.10
13.95
0.08
200
180
160
140
120
100
80
60
40
20
0
ppm

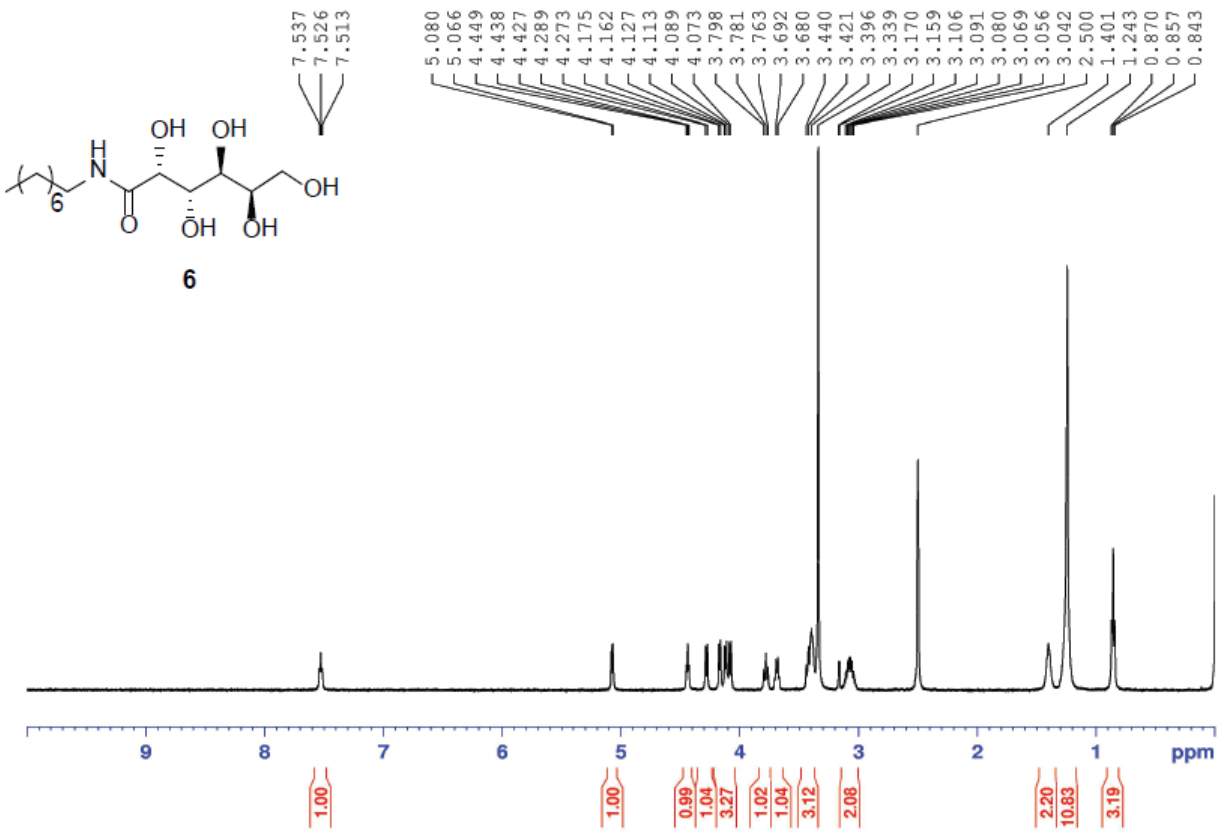
7.537
7.526
7.513
5.080
5.066
4.449
4.438
4.427
4.289
4.273
4.175
4.162
4.127
4.113
4.089
4.073
3.798
3.781
3.763
3.692
3.680
3.440
3.421
3.396
3.339
3.170
3.159
3.106
3.091
3.080
3.069
3.056
3.042
2.500
1.401
1.243
0.870
0.857
0.843
OH
OH
H
N
6
O
OH
OH
OH
9
8
7
6
5
4
3
2
1
ppm
1.00
1.00
0.99
1.04
3.27
1.02
1.04
3.12
2.08
2.20
10.83
3.19

6

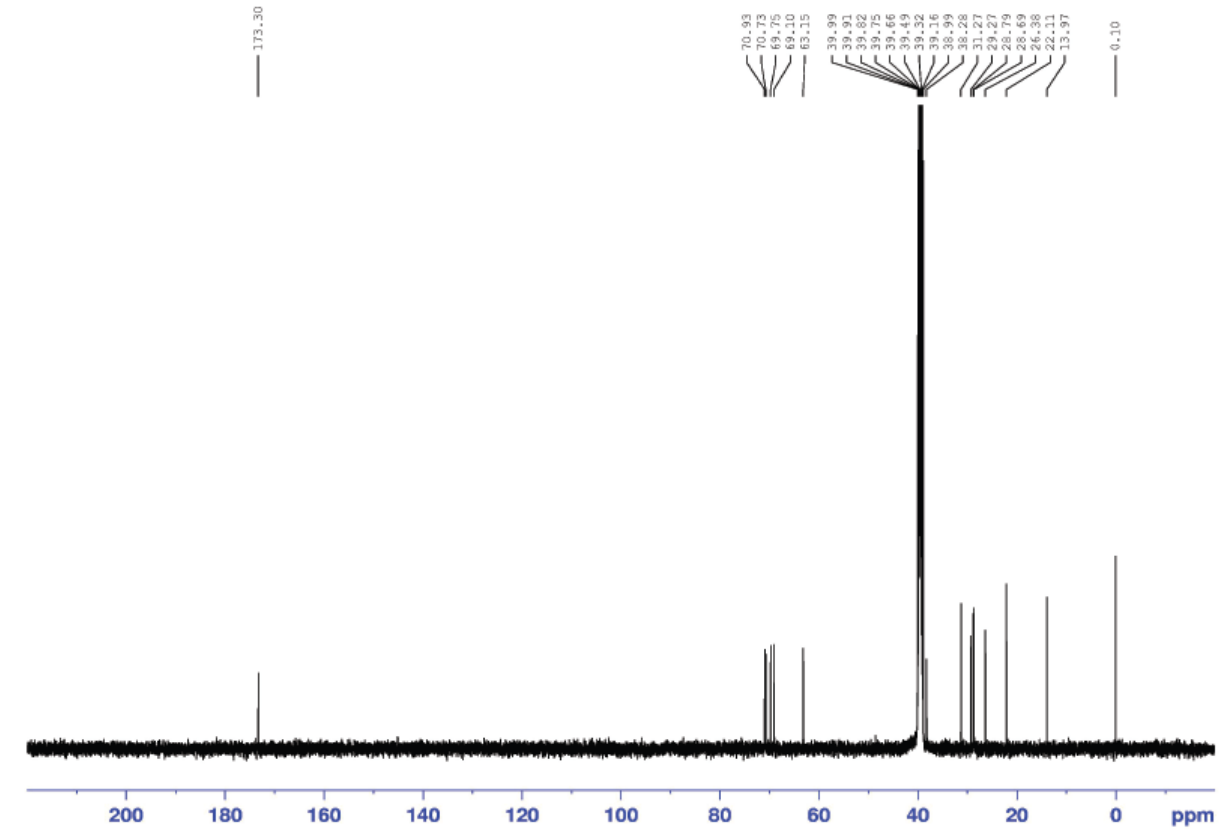
173.30
70.93
70.73
69.75
69.10
63.15
39.99
39.91
39.82
39.75
39.66
39.49
39.32
39.16
38.99
38.28
31.27
29.27
28.79
28.69
26.38
22.11
13.97
0.10
200
180
160
140
120
100
80
60
40
20
0
ppm

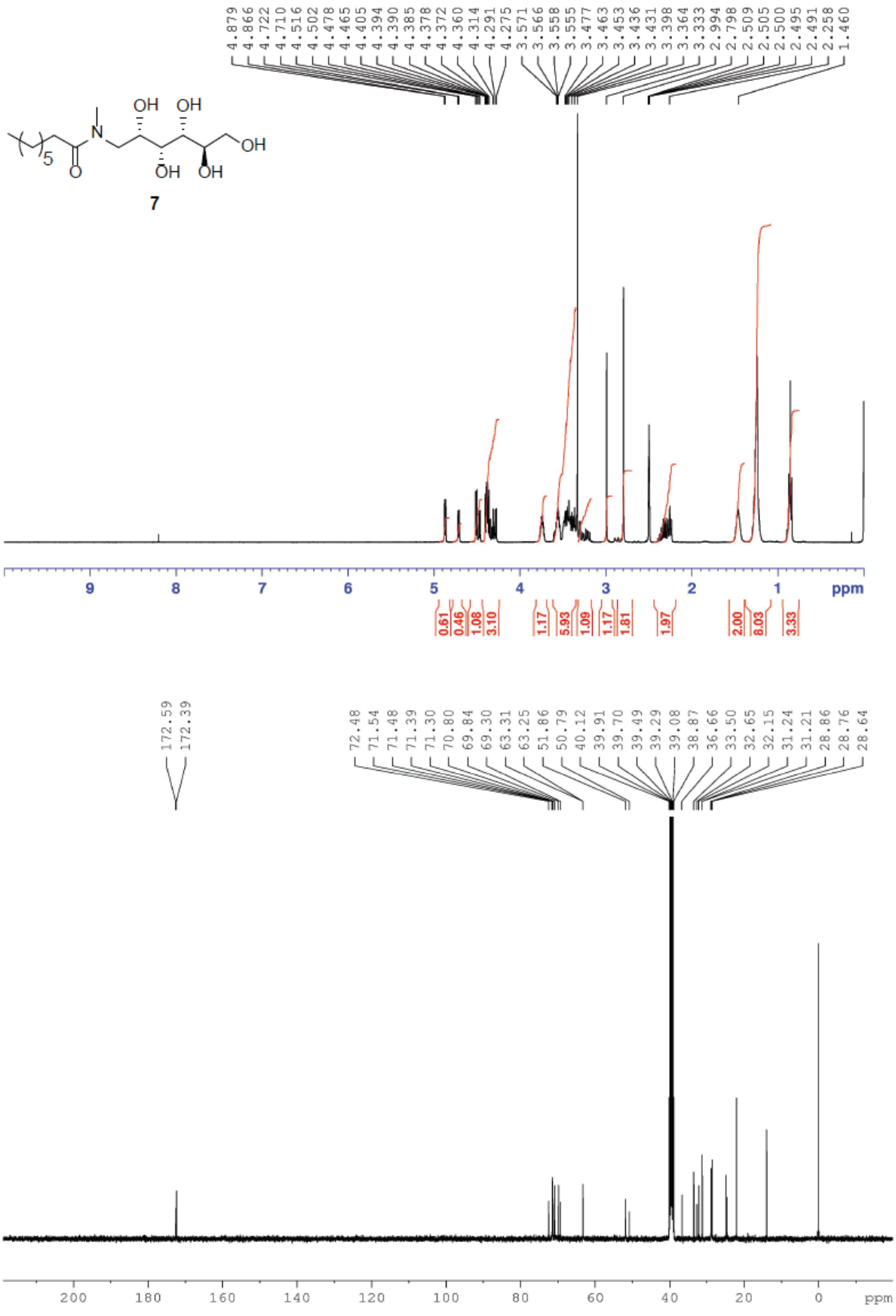
4.879
4.866
4.722
4.710
4.516
4.502
4.478
4.465
4.405
4.394
4.390
4.385
4.378
4.372
4.360
4.314
4.291
4.275
3.571
3.566
3.558
3.555
3.477
3.463
3.453
3.436
3.431
3.398
3.364
3.333
2.994
2.798
2.509
2.505
2.500
2.495
2.491
2.258
1.460
OH
OH
N
OH
OH
OH
O
5
7
9
8
7
6
5
4
3
2
1
ppm
0.61
0.46
1.08
3.10
1.17
5.93
1.09
1.17
1.81
1.97
2.00
8.03
3.33
172.59
172.39
72.48
71.54
71.48
71.39
71.30
70.80
69.84
69.30
63.31
63.25
51.86
50.79
40.12
39.91
39.70
39.49
39.29
39.08
38.87
36.66
33.50
32.65
32.15
31.24
31.21
28.86
28.76
28.64
200
180
160
140
120
100
80
60
40
20
0
ppm

OH
OH
N
6
O
OH
OH
OH

8

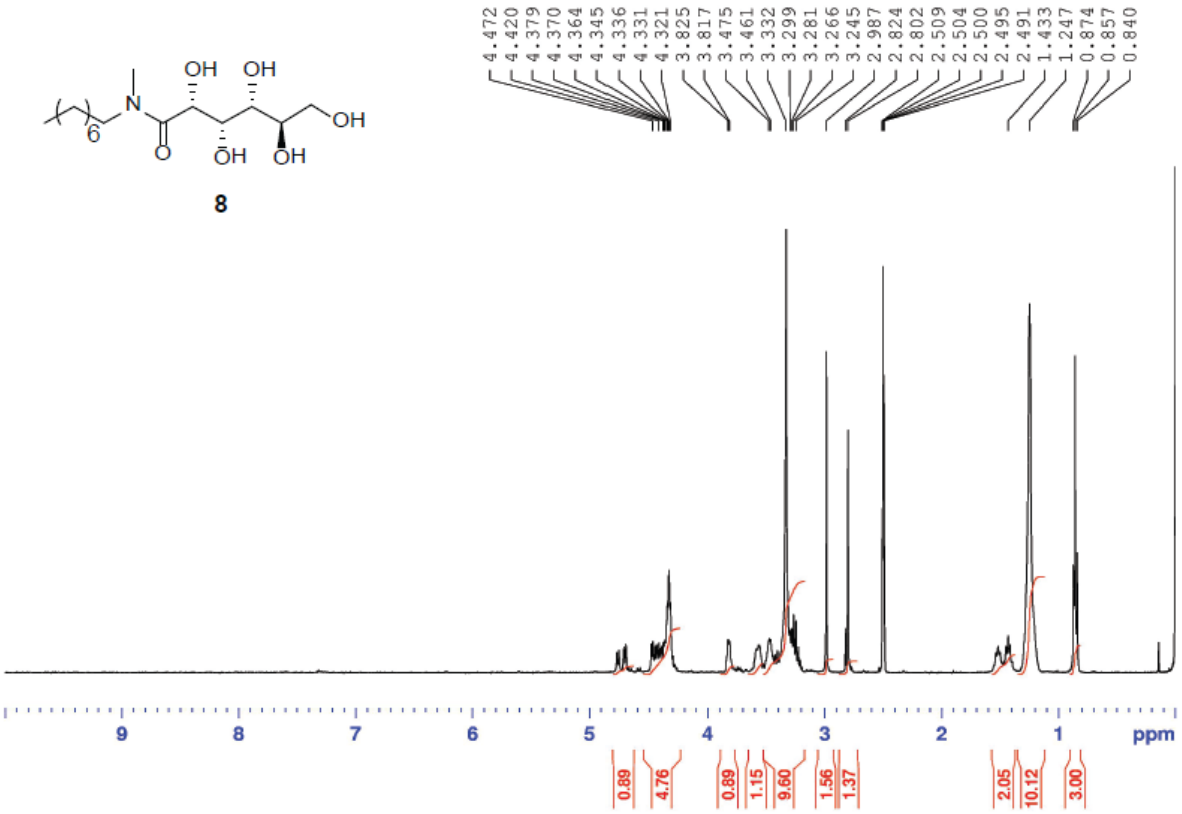
4.472
4.420
4.379
4.370
4.364
4.345
4.336
4.331
4.321
3.825
3.817
3.475
3.461
3.332
3.299
3.281
3.266
3.245
2.987
2.824
2.802
2.509
2.504
2.500
2.495
2.491
1.433
1.247
0.874
0.857
0.840
9
8
7
6
5
4
3
2
1
ppm
0.89
4.76
0.89
1.15
9.60
1.56
1.37
2.05
10.12
3.00

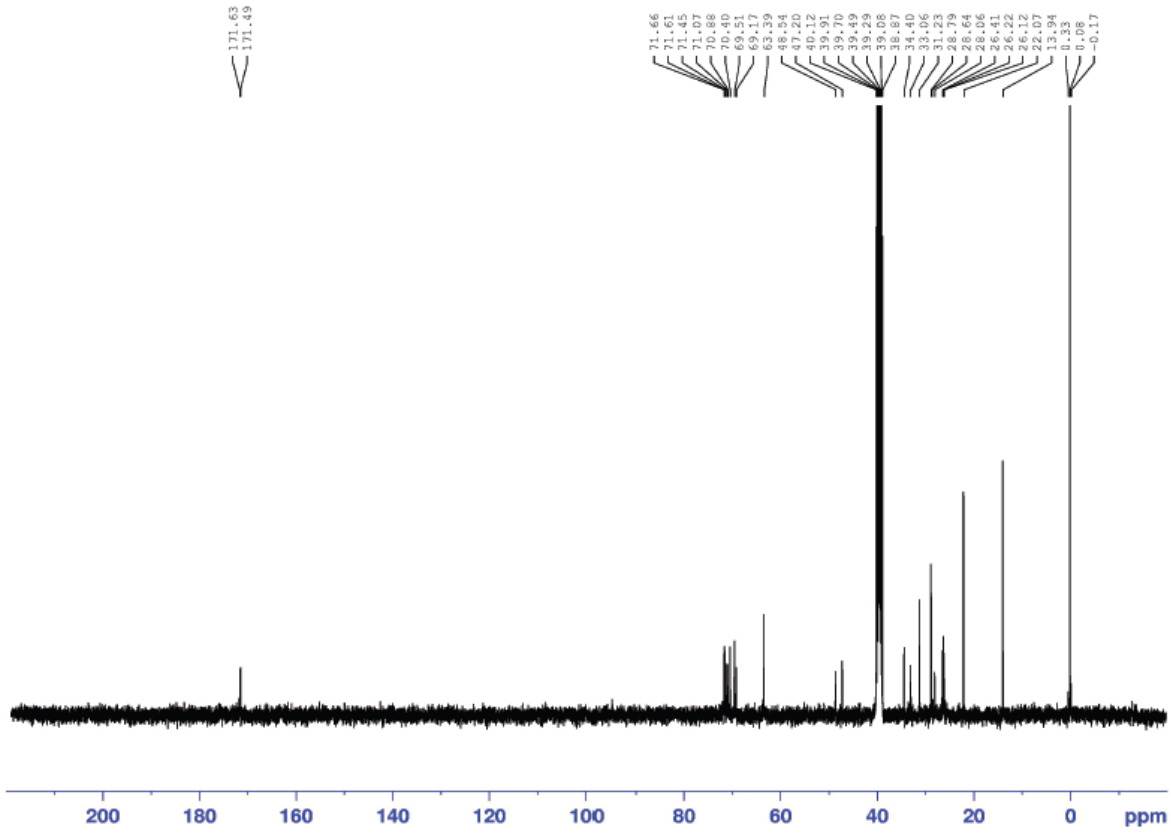
171.63
171.49
71.66
71.61
71.45
71.07
70.88
70.40
69.51
69.17
63.39
48.54
47.20
40.12
39.91
39.70
39.49
39.29
39.08
38.87
34.40
33.06
31.23
28.79
28.64
28.06
26.41
26.21
26.12
22.07
13.94
0.33
0.08
-0.17
200
180
160
140
120
100
80
60
40
20
0
ppm

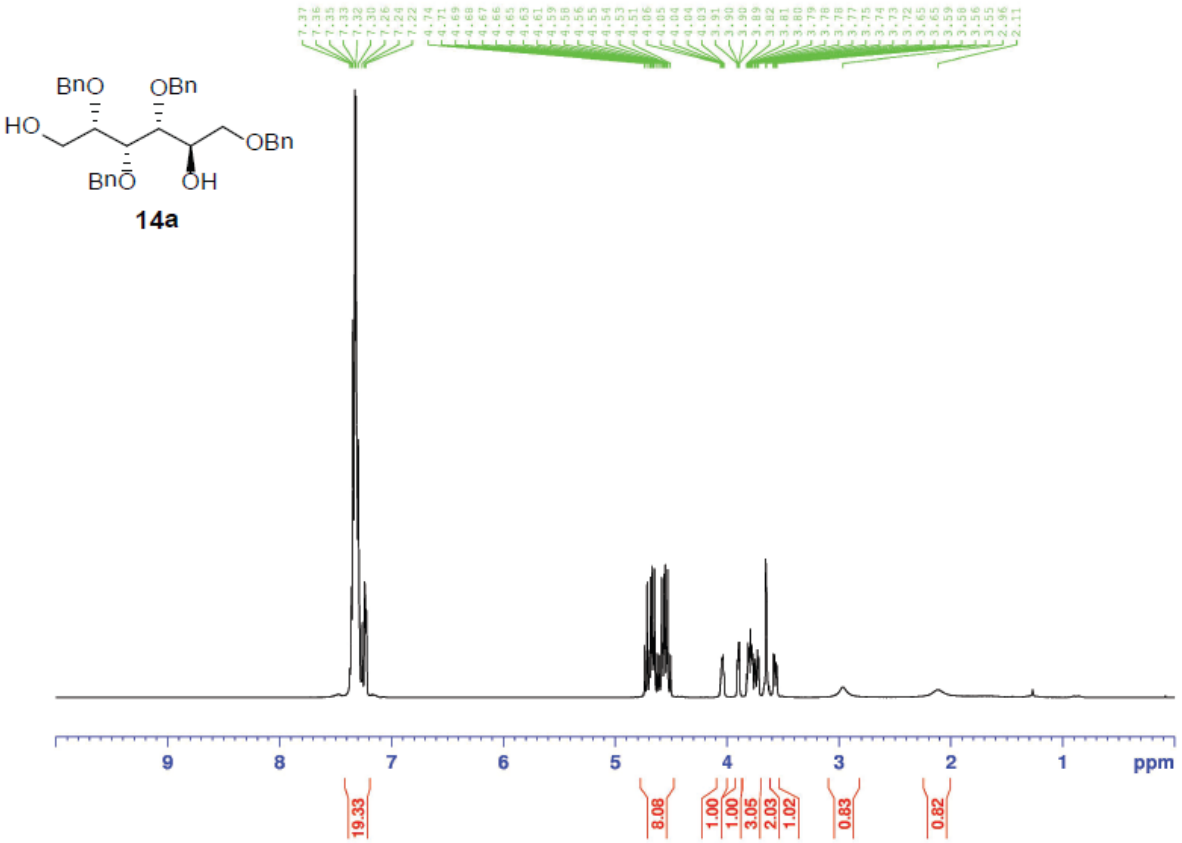
BnO
OBn
HO
OBn
BnO
OH
14a
ppm
19.33
8.08
1.00
1.00
3.05
2.03
1.02
0.83
0.82

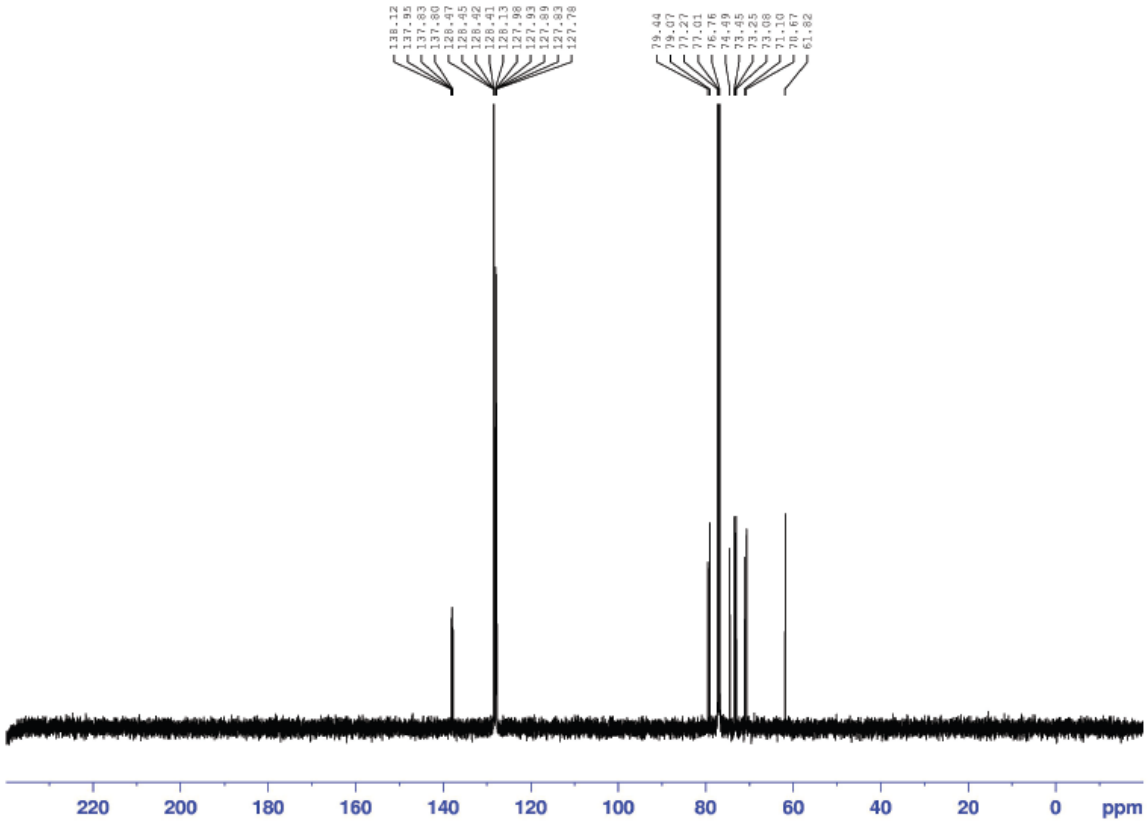
ppm

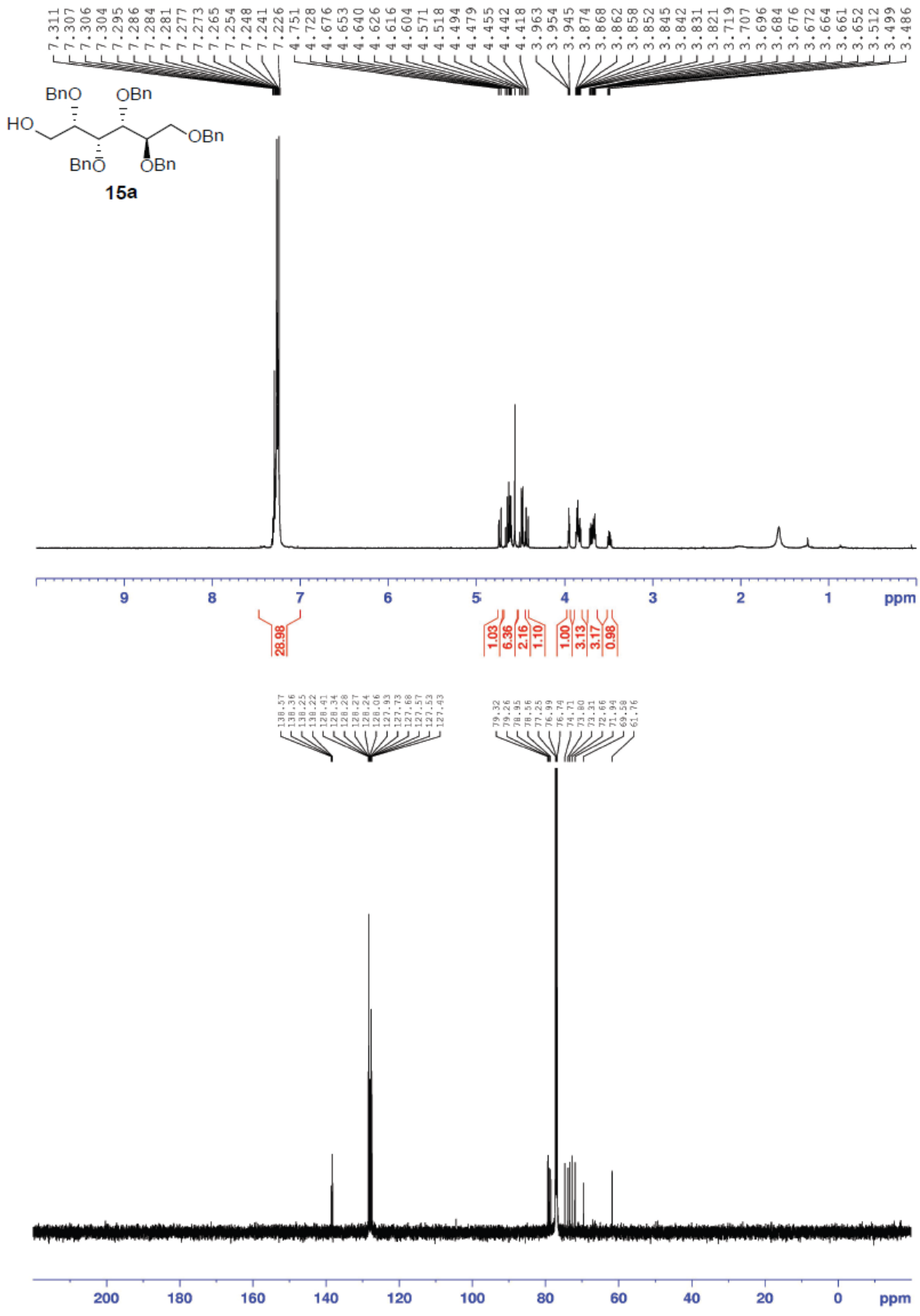
7.311
7.307
7.306
7.304
7.295
7.286
7.284
7.281
7.277
7.273
7.265
7.254
7.248
7.241
7.226
4.751
4.728
4.676
4.653
4.640
4.626
4.616
4.604
4.571
4.518
4.494
4.479
4.455
4.442
4.418
3.963
3.954
3.945
3.874
3.868
3.862
3.858
3.852
3.845
3.842
3.831
3.821
3.719
3.707
3.696
3.684
3.676
3.672
3.664
3.661
3.652
3.512
3.499
3.486
BnO
OBn
HO
OBn
BnO
OBn
15a
9
8
7
6
5
4
3
2
1
ppm
28.98
1.03
6.36
2.16
1.10
1.00
3.13
3.17
0.98
138.57
138.36
138.25
138.22
128.41
128.34
128.28
128.27
128.24
128.06
127.93
127.73
127.68
127.57
127.53
127.43
79.32
79.26
78.95
78.55
77.25
76.99
76.74
76.71
73.80
73.71
72.66
72.04
69.58
61.76
200
180
160
140
120
100
80
60
40
20
0
ppm

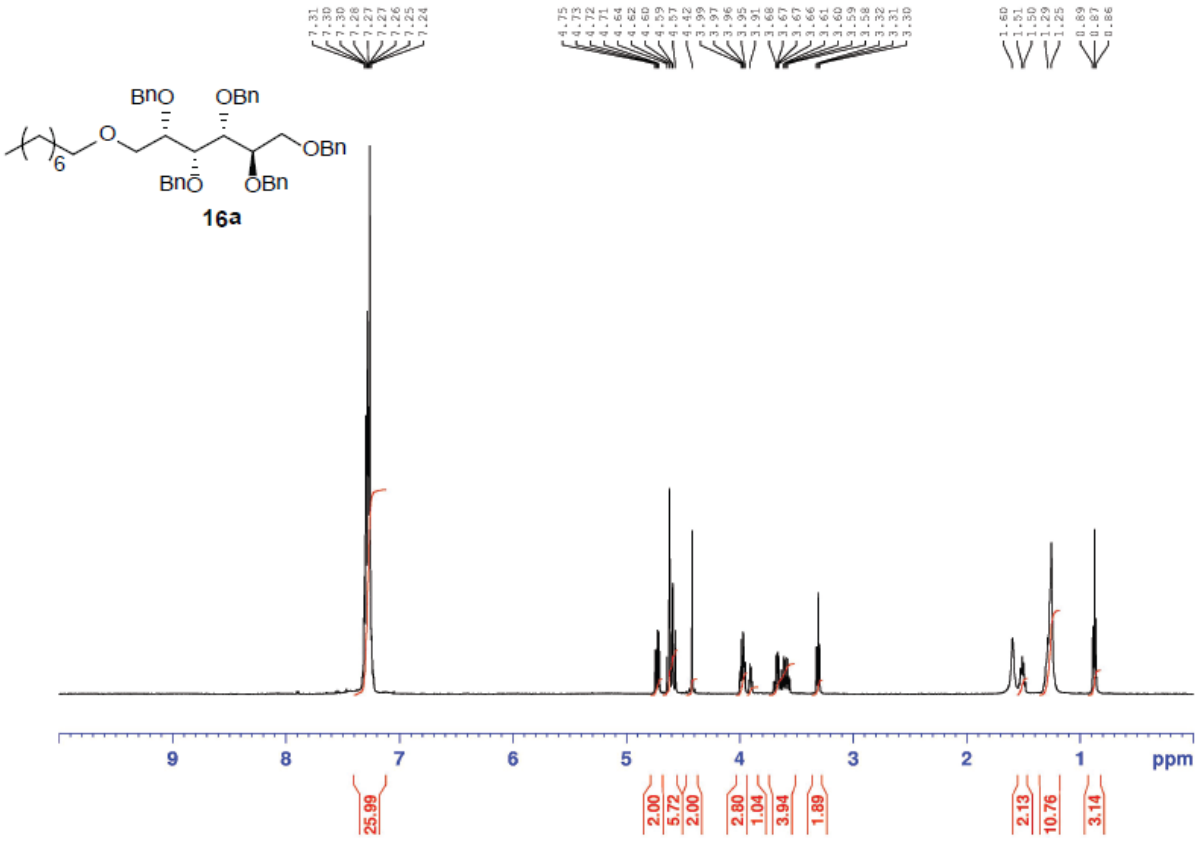
BnO
OBn
OBn
BnO
OBn
6
16a
ppm
25.99
2.00
5.72
2.00
2.80
1.04
3.94
1.89
2.13
10.76
3.14

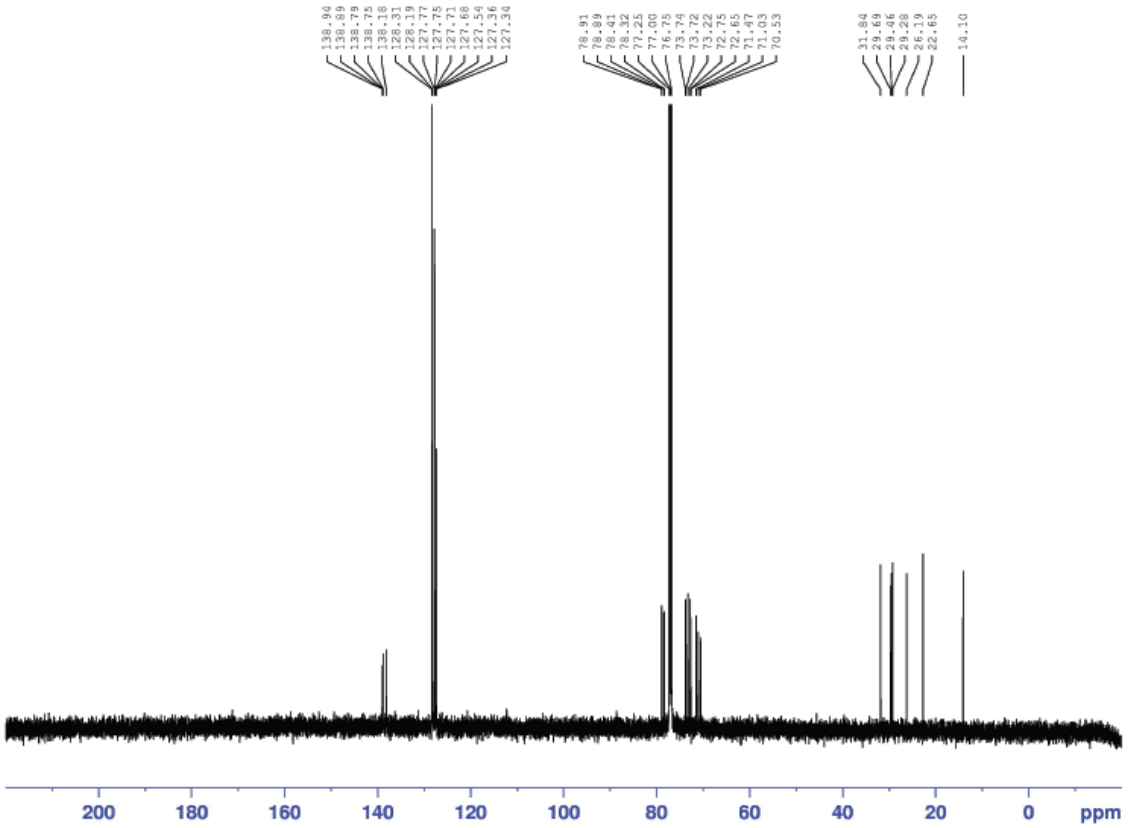
ppm

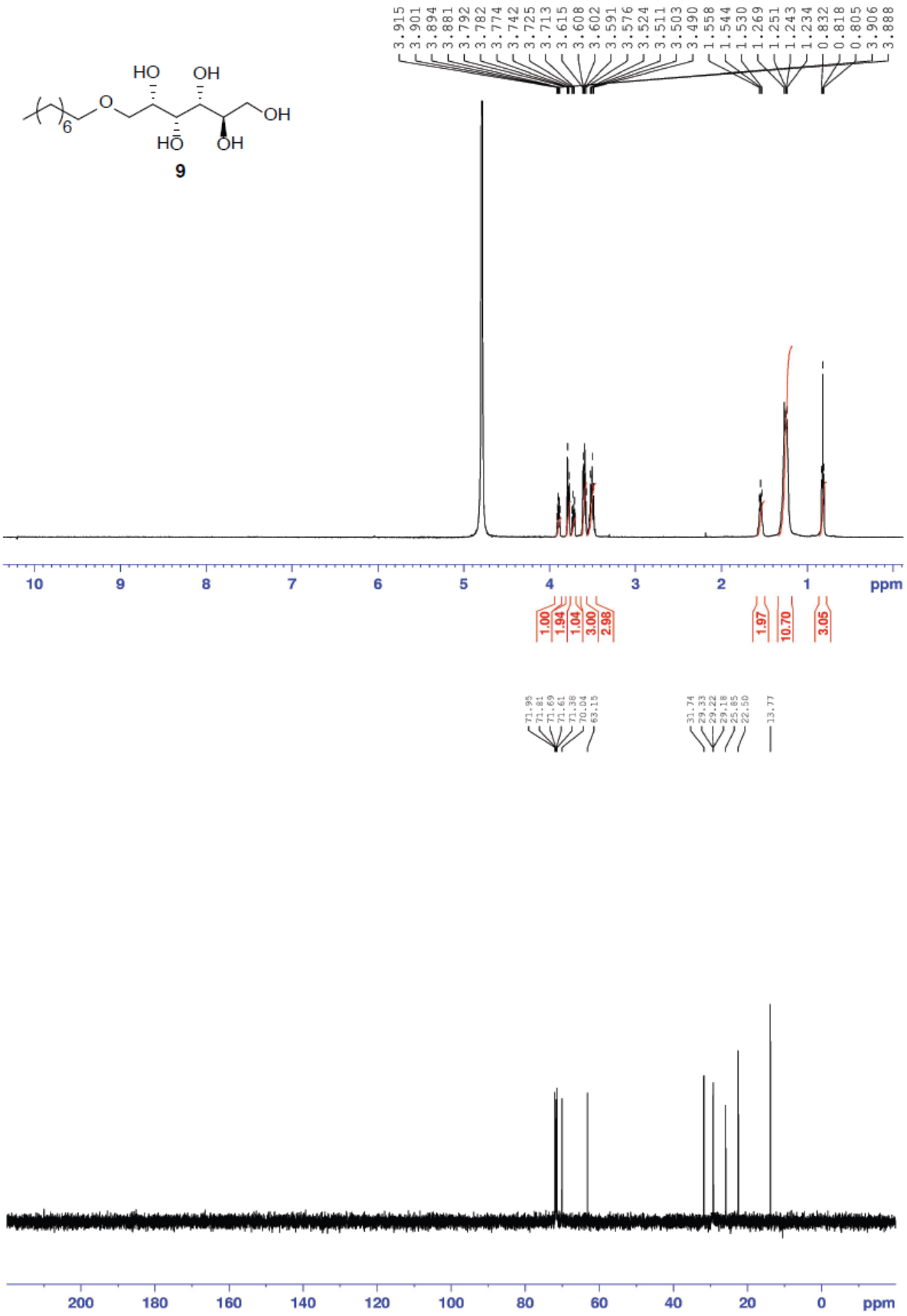
HO
OH
O
OH
HO
OH
6
9
3.915
3.901
3.894
3.881
3.792
3.782
3.774
3.742
3.725
3.713
3.615
3.608
3.602
3.591
3.576
3.524
3.511
3.503
3.490
1.558
1.544
1.530
1.269
1.251
1.243
1.234
0.832
0.818
0.805
3.906
3.888
10
9
8
7
6
5
4
3
2
1
ppm
1.00
1.94
1.04
3.00
2.98
1.97
10.70
3.05
71.95
71.81
71.69
71.61
71.38
70.04
63.15
31.74
29.33
29.22
29.18
25.85
22.50
13.77
200
180
160
140
120
100
80
60
40
20
0
ppm

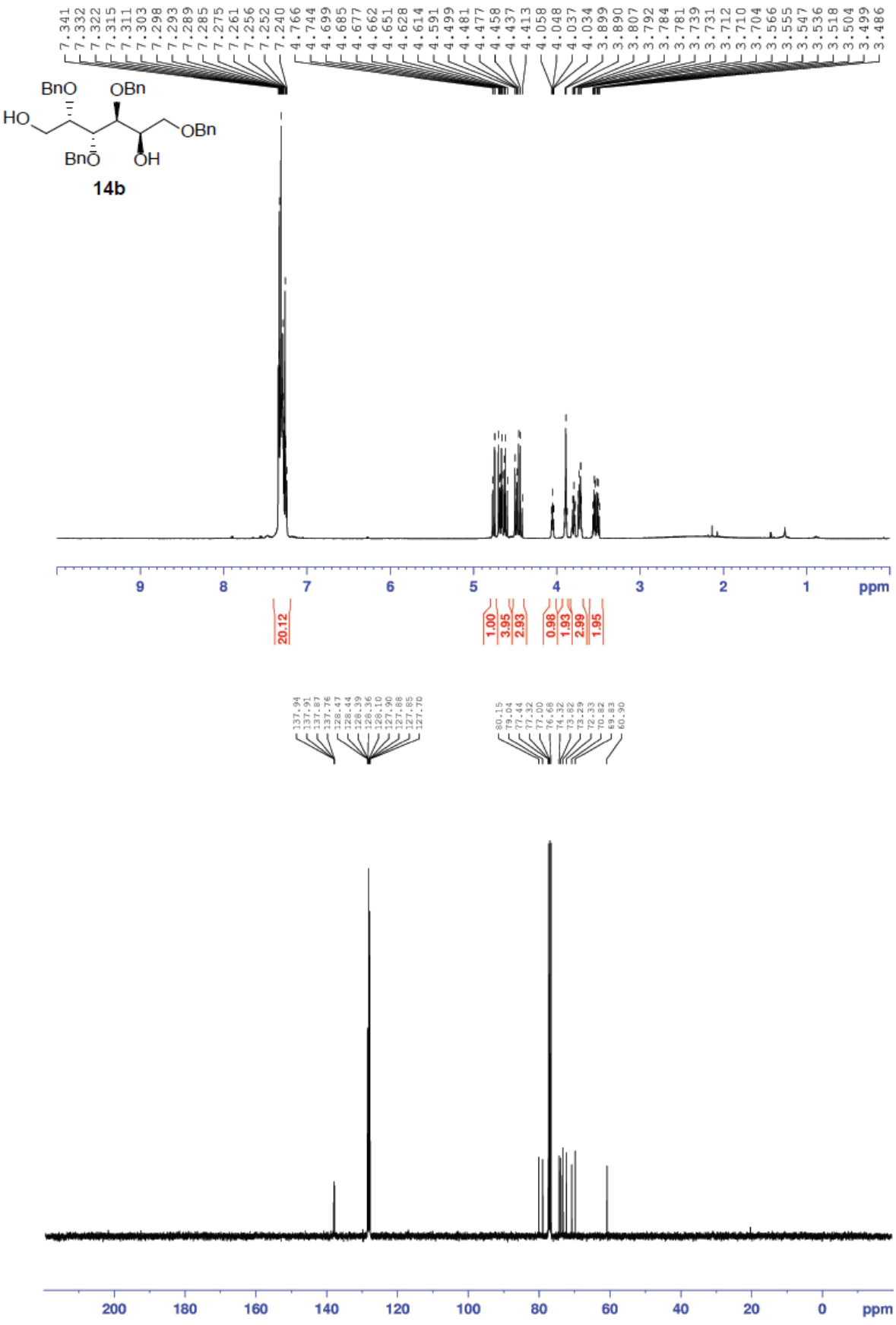
7.341
7.332
7.322
7.315
7.311
7.303
7.298
7.293
7.289
7.285
7.275
7.261
7.256
7.252
7.240
4.766
4.744
4.699
4.685
4.677
4.662
4.651
4.628
4.614
4.591
4.499
4.481
4.477
4.458
4.437
4.413
4.058
4.048
4.037
4.034
3.899
3.890
3.807
3.792
3.784
3.781
3.739
3.731
3.712
3.710
3.704
3.566
3.555
3.547
3.536
3.518
3.504
3.499
3.486
BnO
OBn
HO
OBn
BnO
OH
14b
9
8
7
6
5
4
3
2
1
ppm
20.12
1.00
3.95
2.93
0.98
1.93
2.99
1.95
137.94
137.91
137.87
137.76
128.47
128.44
128.39
128.36
128.10
127.90
127.88
127.85
127.70
80.15
79.04
77.44
77.32
77.00
76.60
74.32
73.82
73.29
72.33
70.82
69.83
60.90
200
180
160
140
120
100
80
60
40
20
0
ppm

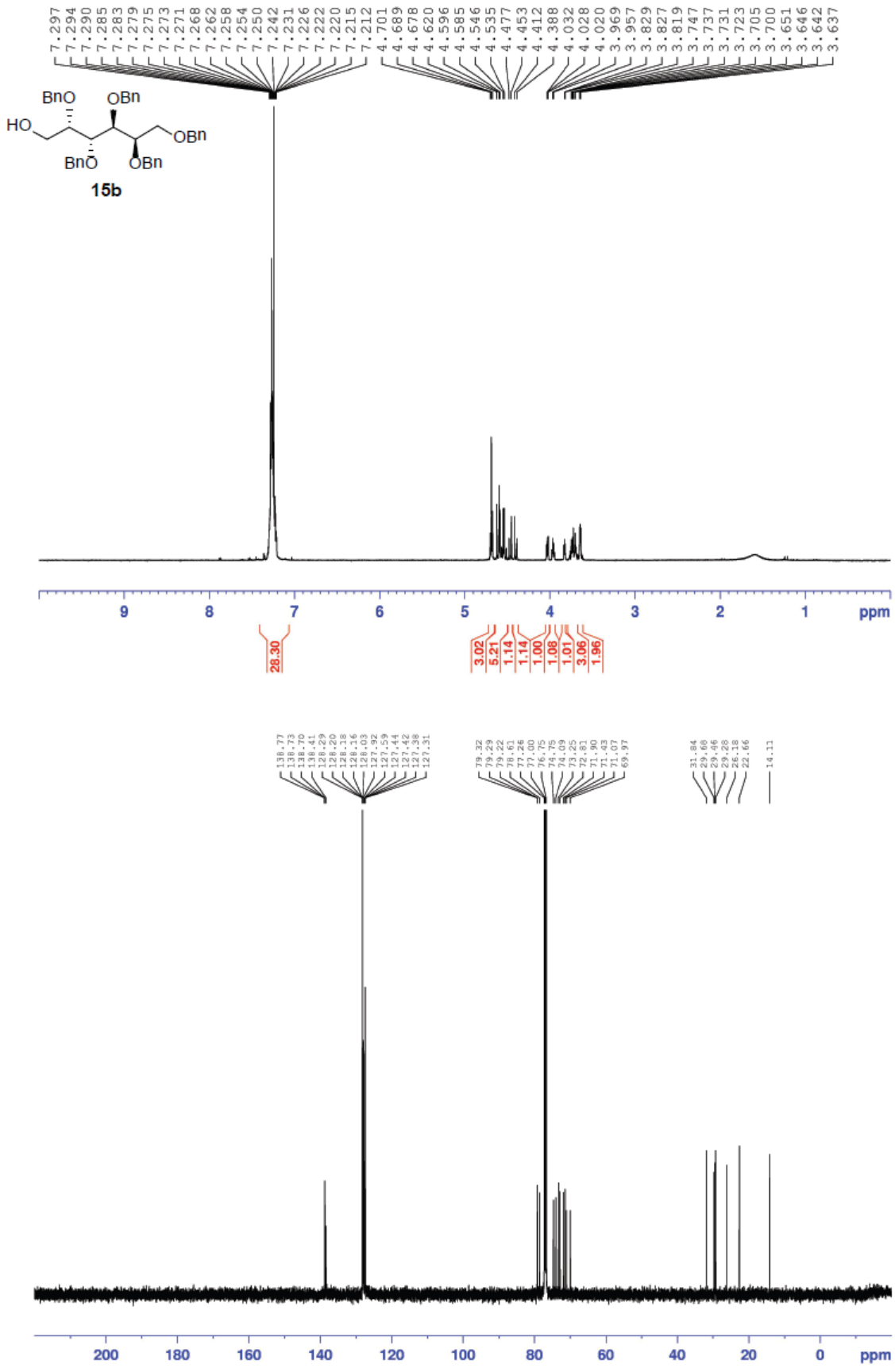
7.297
7.294
7.290
7.285
7.283
7.279
7.275
7.273
7.271
7.268
7.262
7.258
7.254
7.250
7.242
7.231
7.226
7.222
7.220
7.215
7.212
4.701
4.689
4.678
4.620
4.596
4.585
4.546
4.535
4.477
4.453
4.412
4.388
4.032
4.028
4.020
3.969
3.957
3.829
3.827
3.819
3.747
3.737
3.731
3.723
3.705
3.700
3.651
3.646
3.642
3.637
BnO
OBn
HO
OBn
BnO
OBn
15b
9
8
7
6
5
4
3
2
1
ppm
28.30
3.02
5.21
1.14
1.14
1.00
1.08
1.01
3.06
1.96
138.77
138.73
138.70
138.41
128.29
128.20
128.18
128.16
128.03
127.92
127.59
127.44
127.42
127.38
127.31
79.32
79.29
79.22
78.61
77.26
77.00
76.75
74.09
73.25
72.81
71.90
71.43
71.07
69.97
31.84
29.68
29.46
29.28
26.18
22.66
14.11
200
180
160
140
120
100
80
60
40
20
0
ppm

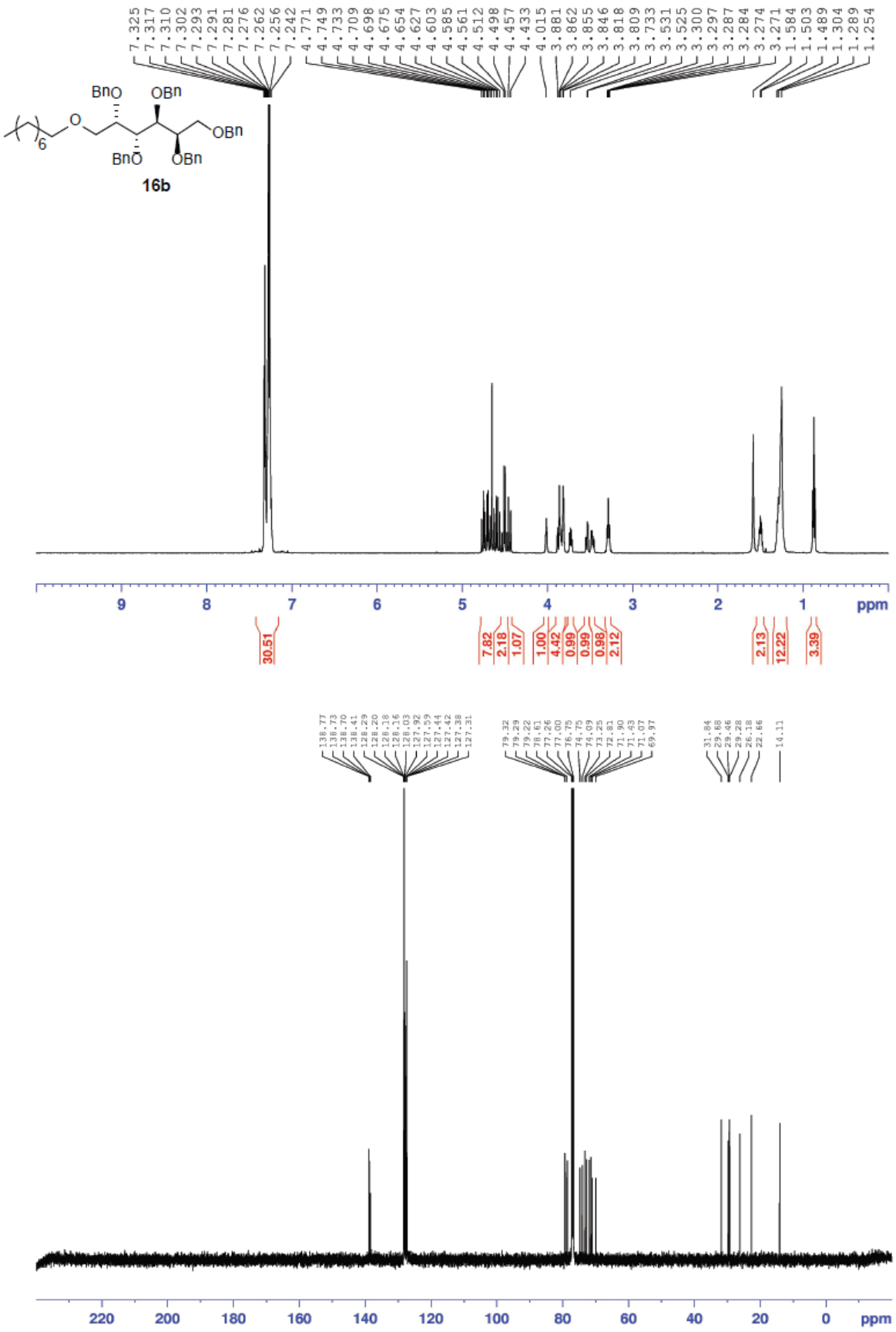
7.325
7.317
7.310
7.302
7.293
7.291
7.281
7.276
7.262
7.256
7.242
4.771
4.749
4.733
4.709
4.698
4.675
4.654
4.627
4.603
4.585
4.561
4.512
4.498
4.457
4.433
4.015
3.881
3.862
3.855
3.846
3.818
3.809
3.733
3.531
3.525
3.300
3.297
3.287
3.284
3.274
3.271
1.584
1.503
1.489
1.304
1.289
1.254
BnO
OBn
OBn
BnO
OBn
O
6
16b
9
8
7
6
5
4
3
2
1
ppm
30.51
7.82
2.18
1.07
1.00
4.42
0.99
0.99
0.98
2.12
2.13
12.22
3.39
138.77
138.73
138.70
138.41
128.29
128.20
128.18
128.16
128.03
127.92
127.59
127.44
127.42
127.38
127.31
79.32
79.29
79.22
78.61
77.26
77.00
76.75
74.75
74.09
73.25
72.81
71.90
71.43
71.07
69.97
31.84
29.68
29.46
29.28
26.18
22.66
14.11
220
200
180
160
140
120
100
80
60
40
20
0
ppm

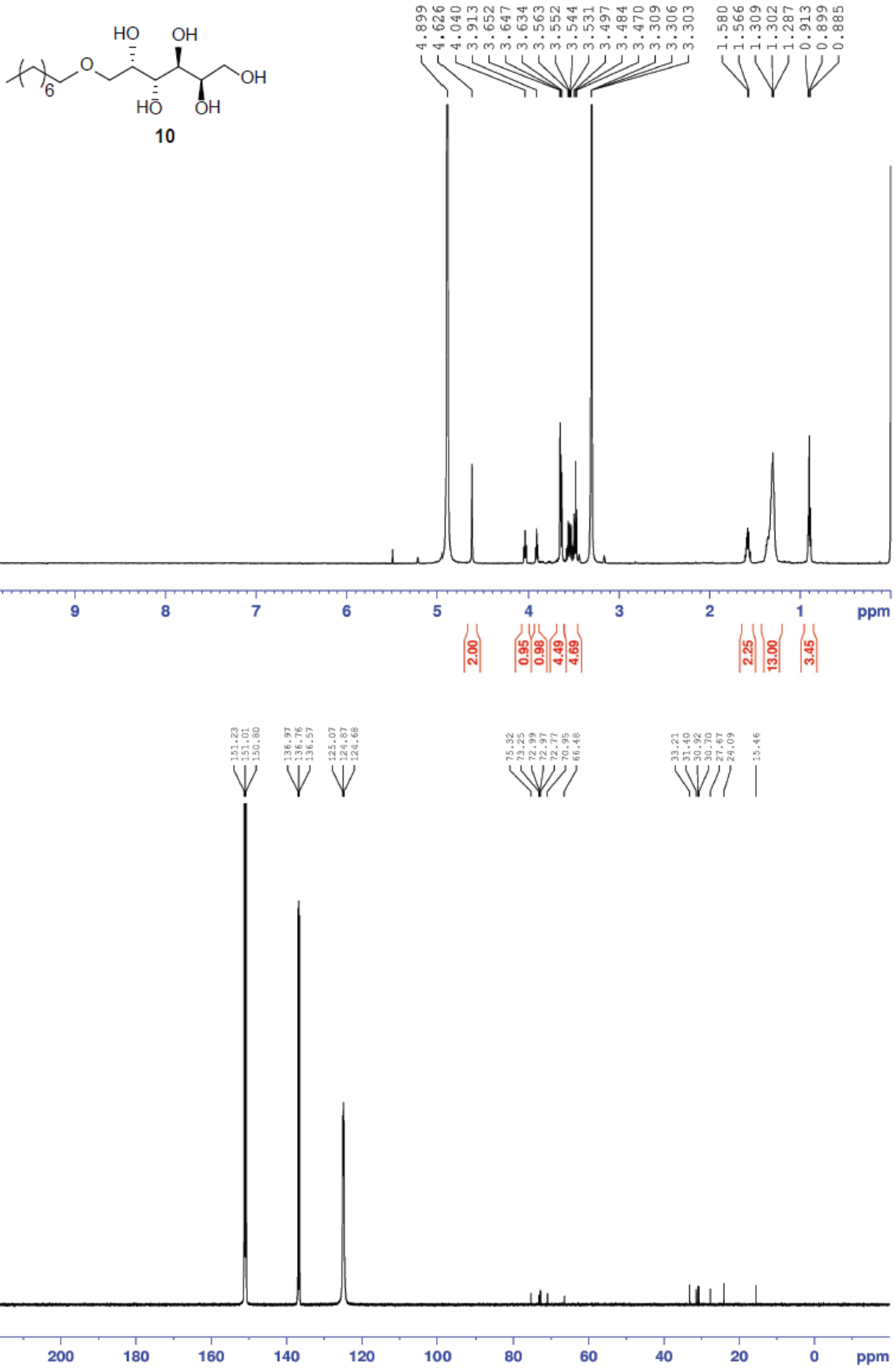
HO
OH
O
6
OH
HO
OH
10
4.899
4.626
4.040
3.913
3.652
3.647
3.634
3.563
3.552
3.544
3.531
3.497
3.484
3.470
3.309
3.306
3.303
1.580
1.566
1.309
1.302
1.287
0.913
0.899
0.885
9
8
7
6
5
4
3
2
1
ppm
2.00
0.95
0.98
4.49
4.69
2.25
13.00
3.45
151.23
151.01
150.80
136.97
136.76
136.57
125.07
124.87
124.68
75.32
73.25
72.99
72.97
72.77
70.95
66.48
33.21
31.40
30.92
30.70
27.67
24.09
15.46
200
180
160
140
120
100
80
60
40
20
0
ppm

17

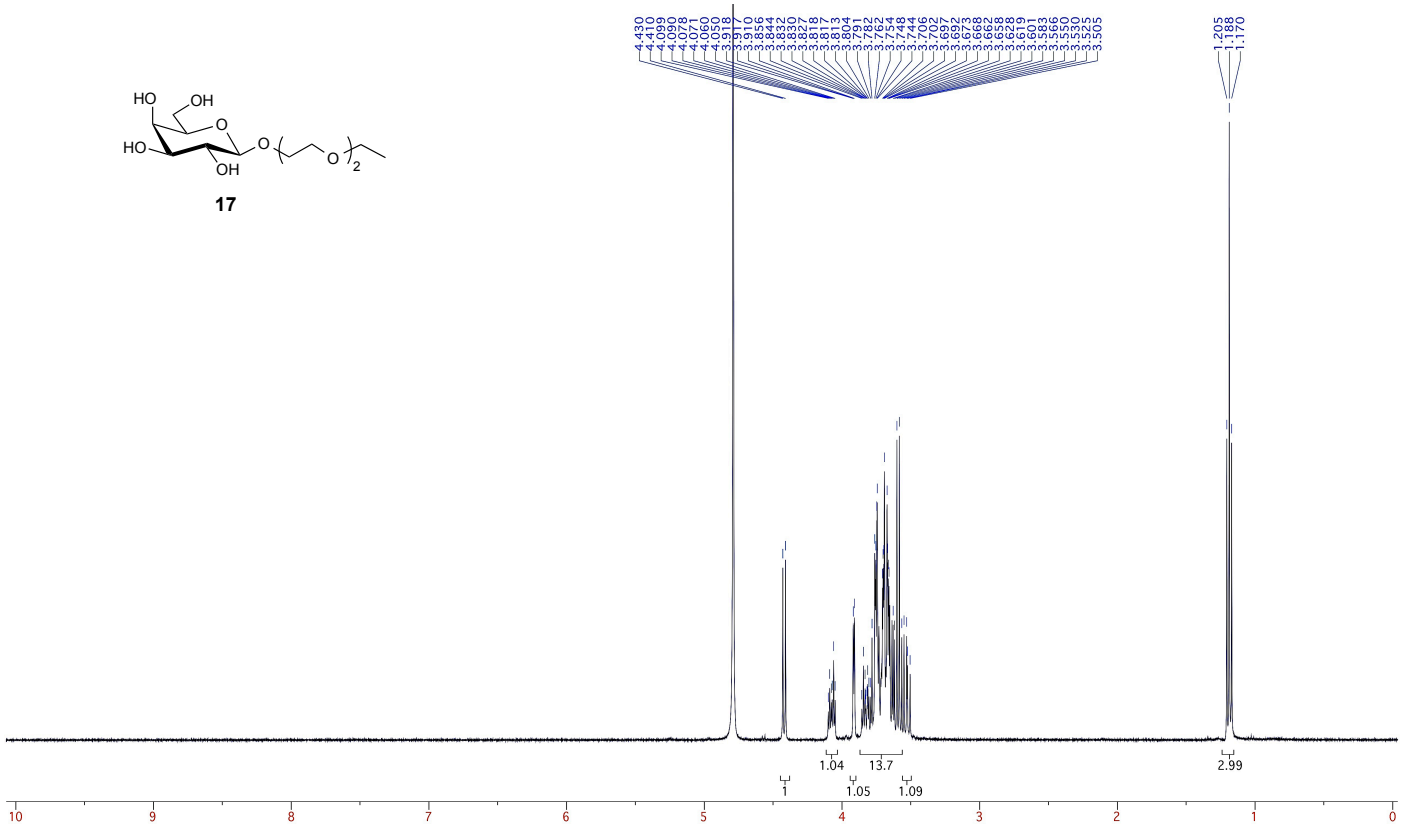
4.430
4.410
4.099
4.090
4.078
4.071
4.060
4.050
4.018
3.917
3.910
3.856
3.844
3.832
3.830
3.827
3.818
3.817
3.813
3.804
3.791
3.782
3.762
3.754
3.748
3.744
3.706
3.702
3.697
3.692
3.673
3.668
3.662
3.658
3.628
3.619
3.601
3.583
3.566
3.550
3.530
3.525
3.505
1.205
1.188
1.170
1.04
13.7
2.99
1
1.05
1.09
10
9
8
7
6
5
4
3
2
1
0

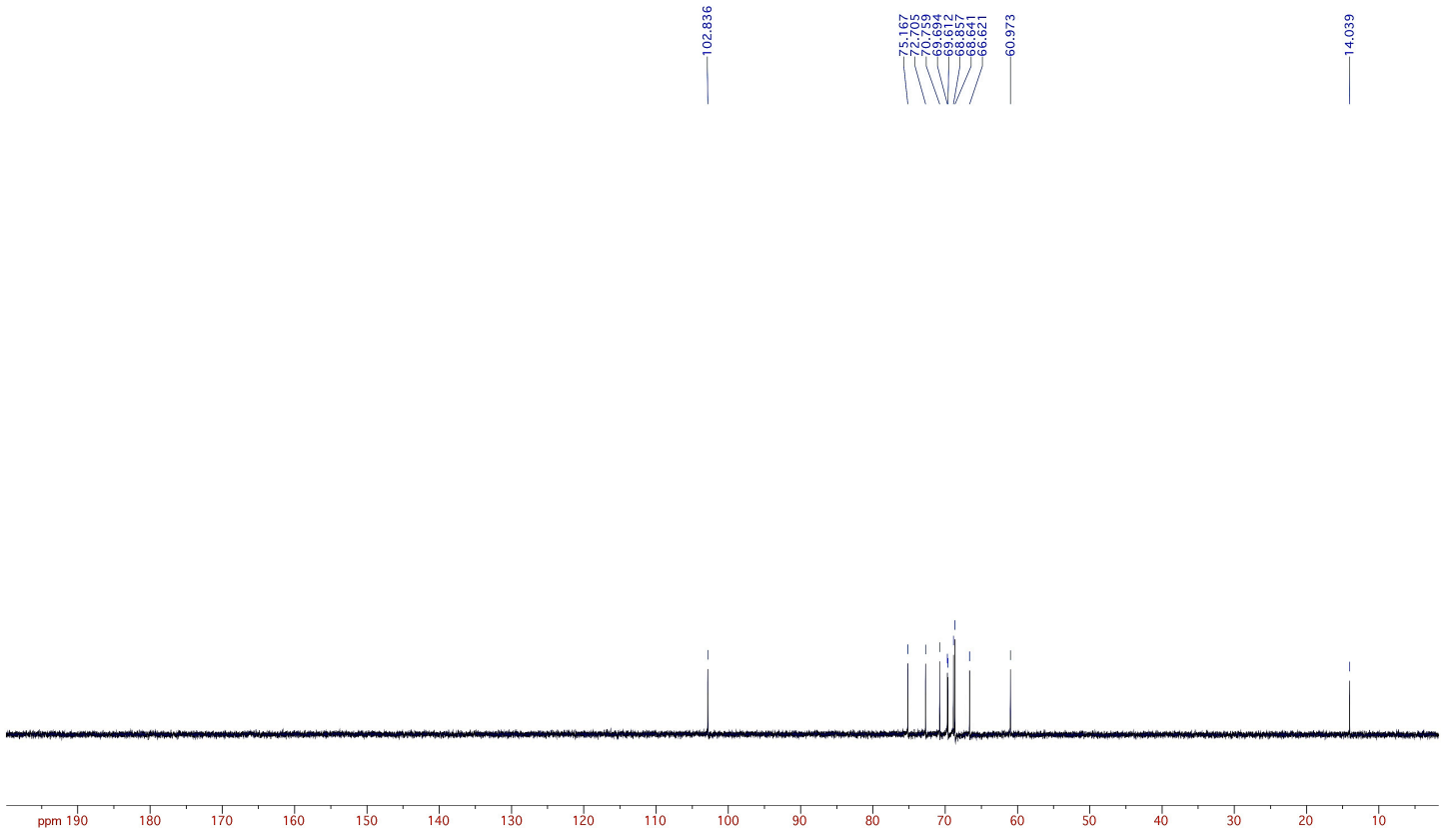
102.836
75.167
72.705
70.759
70.694
69.617
68.857
68.641
66.621
60.973
14.039
ppm 190
180
170
160
150
140
130
120
110
100
90
80
70
60
50
40
30
20
10

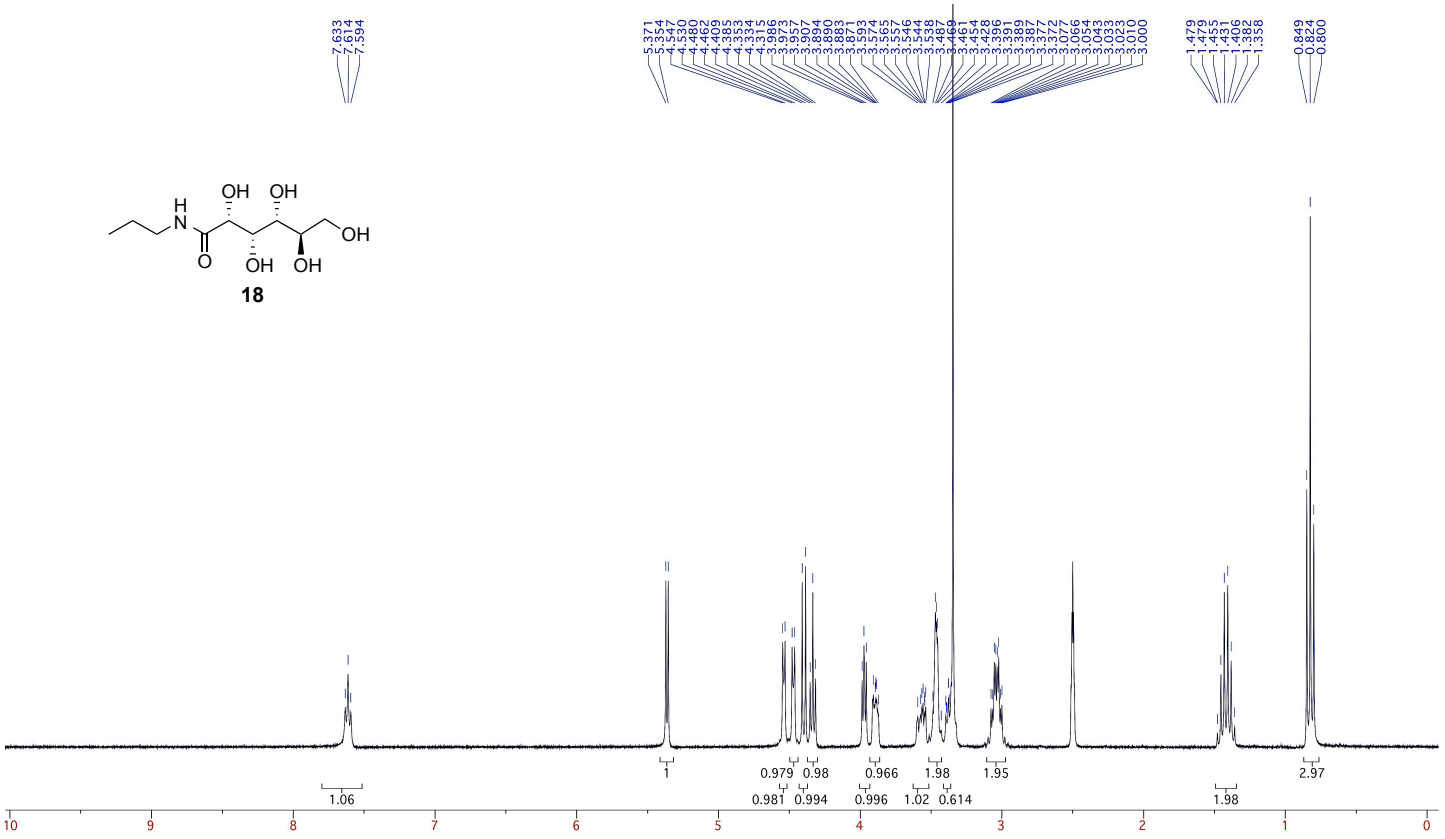
7.633
7.614
7.594
5.371
5.354
4.547
4.530
4.480
4.462
4.400
4.385
4.353
4.334
4.315
4.286
3.973
3.957
3.907
3.894
3.890
3.883
3.871
3.593
3.574
3.557
3.546
3.544
3.538
3.469
3.461
3.454
3.428
3.426
3.391
3.389
3.387
3.377
3.372
3.077
3.066
3.054
3.043
3.023
3.010
3.000
1.479
1.479
1.455
1.431
1.406
1.382
1.358
0.849
0.824
0.800
1
0.979
0.98
0.966
1.98
1.95
2.97
1.06
0.981
0.994
0.996
1.02
0.614
1.98
10
9
8
7
6
5
4
3
2
1
0

H
N
O
OH
OH
OH
OH
OH

18

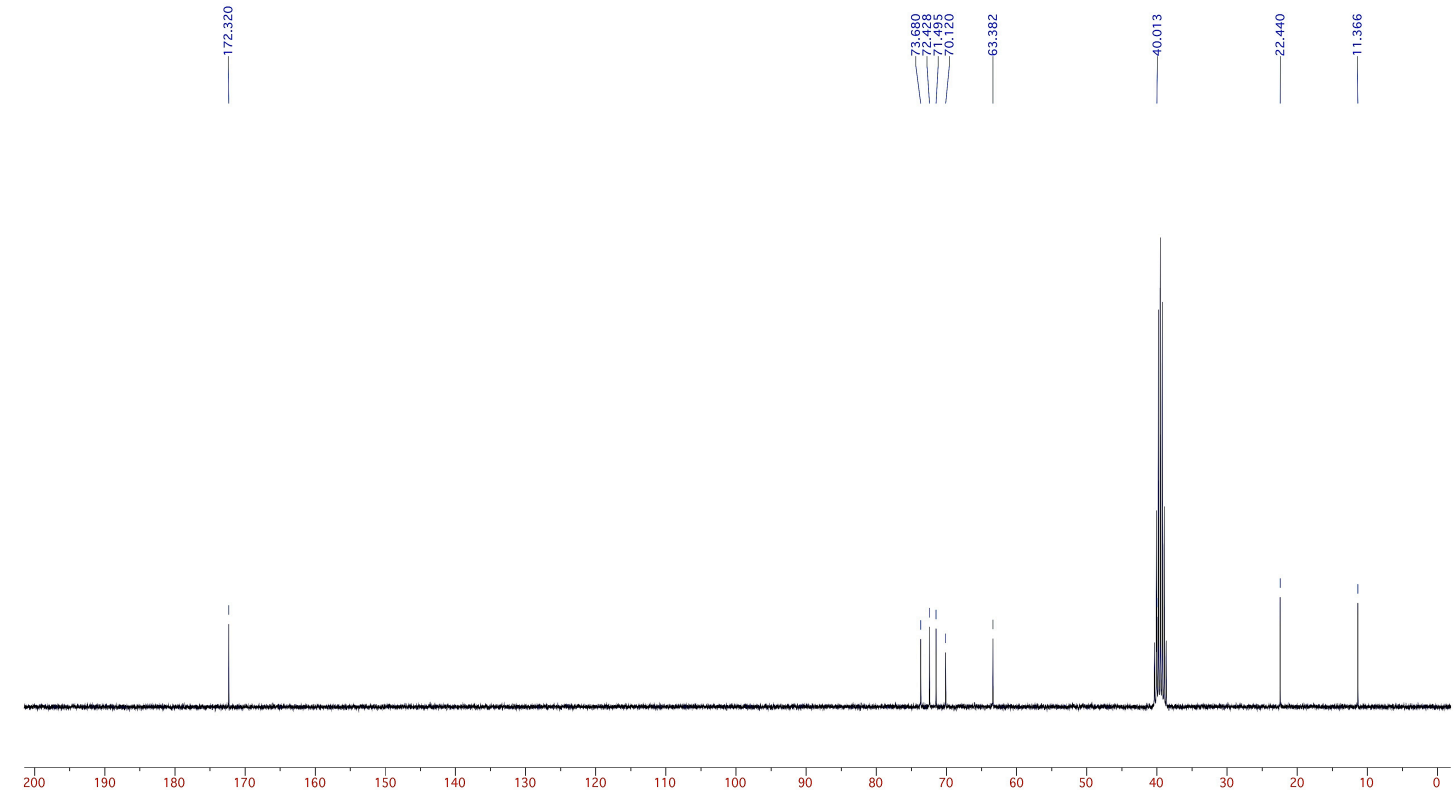
172.320
73.680
73.428
71.495
70.120
63.382
40.013
22.440
11.366
200
190
180
170
160
150
140
130
120
110
100
90
80
70
60
50
40
30
20
10
0

H
N
OH
OH
OH
OH
OH
4
O

19

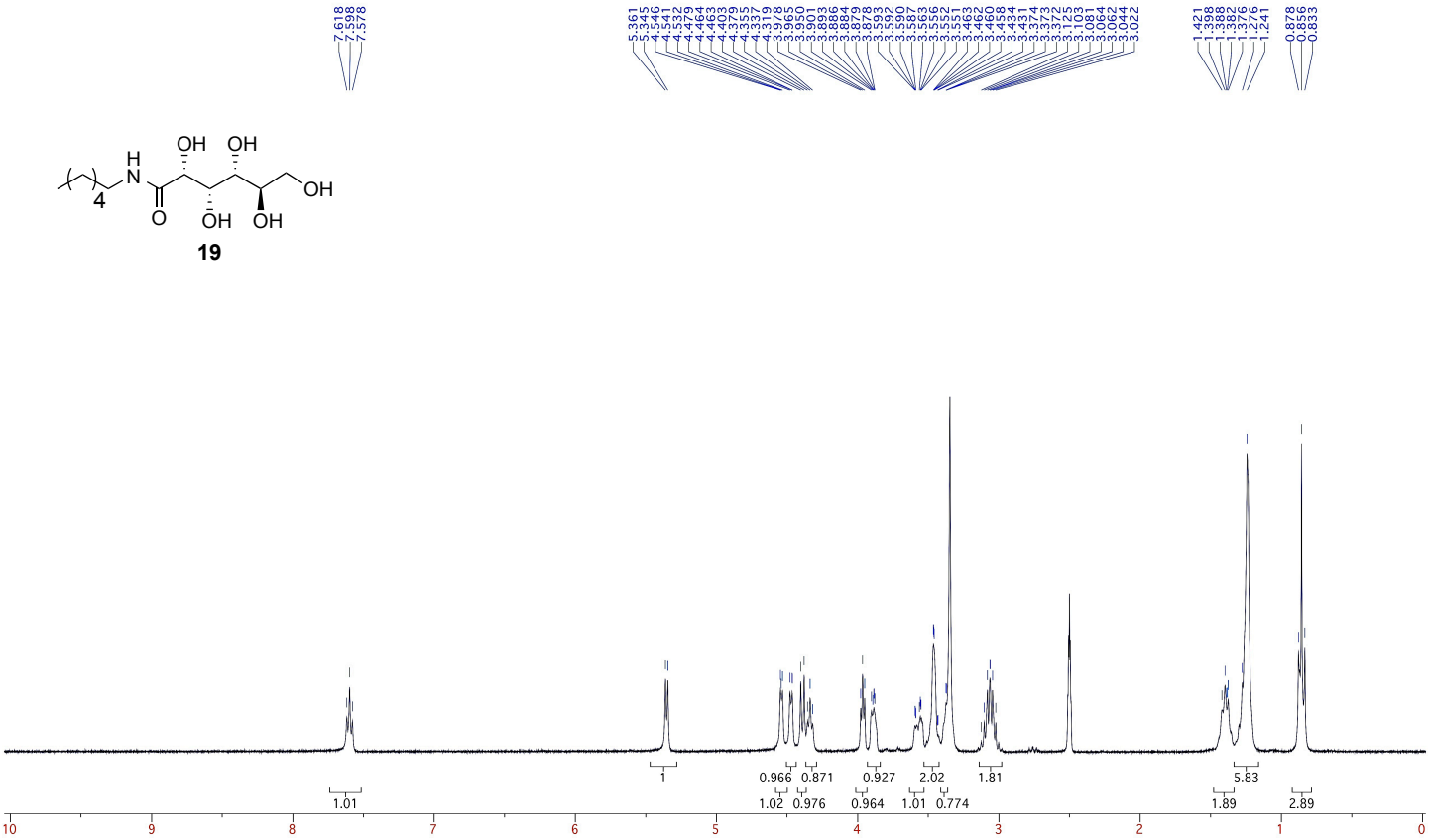
7.618
7.598
7.578
5.361
5.345
5.346
4.541
4.532
4.479
4.464
4.463
4.403
4.379
4.355
4.337
4.318
3.978
3.965
3.950
3.901
3.883
3.886
3.884
3.879
3.878
3.593
3.590
3.587
3.563
3.556
3.552
3.551
3.463
3.462
3.460
3.458
3.434
3.431
3.374
3.373
3.372
3.125
3.103
3.081
3.064
3.062
3.044
3.022
1.421
1.398
1.388
1.382
1.376
1.241
1.241
0.878
0.856
0.833
1.01
1
0.966
0.871
0.927
2.02
1.81
5.83
1.02
0.976
0.964
1.01
0.774
1.89
2.89
10
9
8
7
6
5
4
3
2
1
0

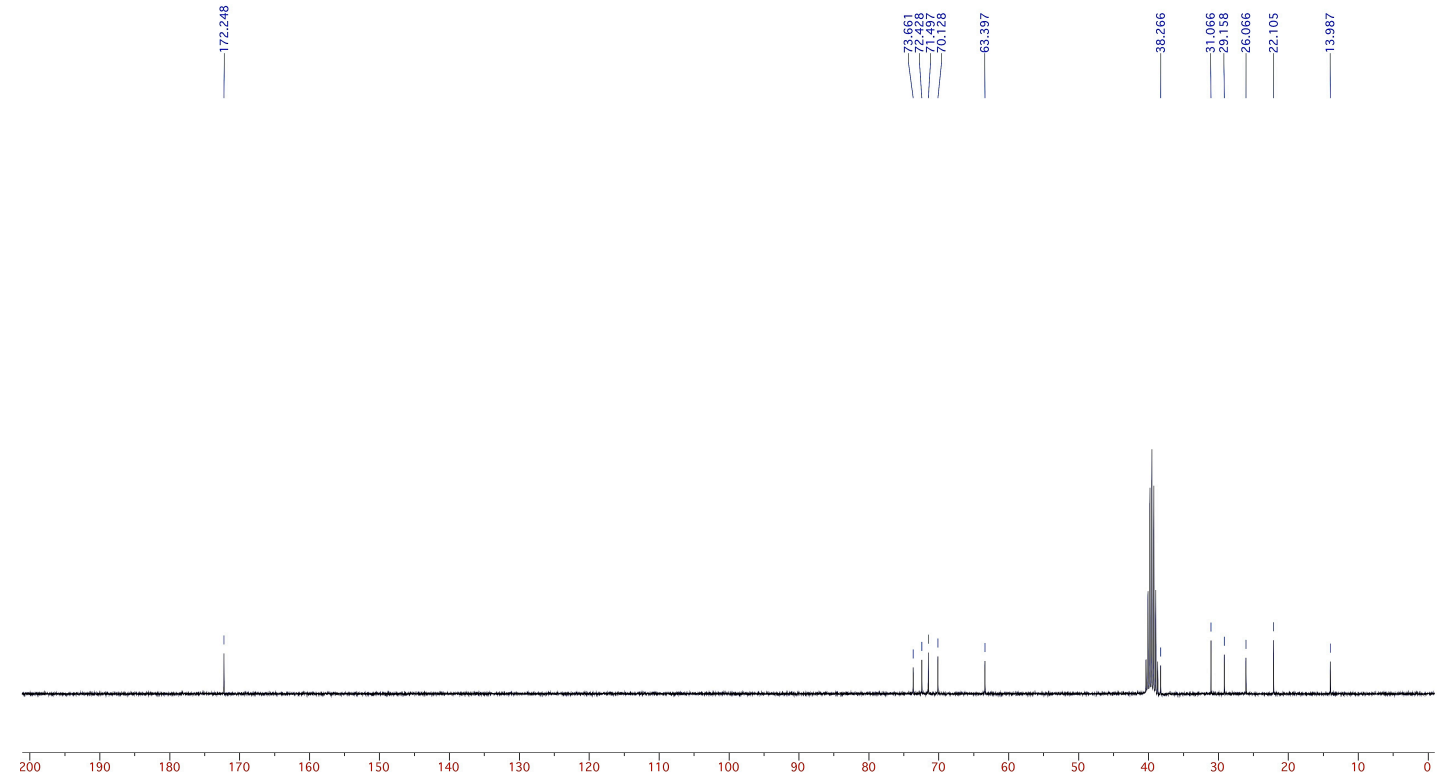
172.248
73.661
72.428
71.497
70.128
63.397
38.266
31.066
29.158
26.066
22.105
13.987
200
190
180
170
160
150
140
130
120
110
100
90
80
70
60
50
40
30
20
10
0

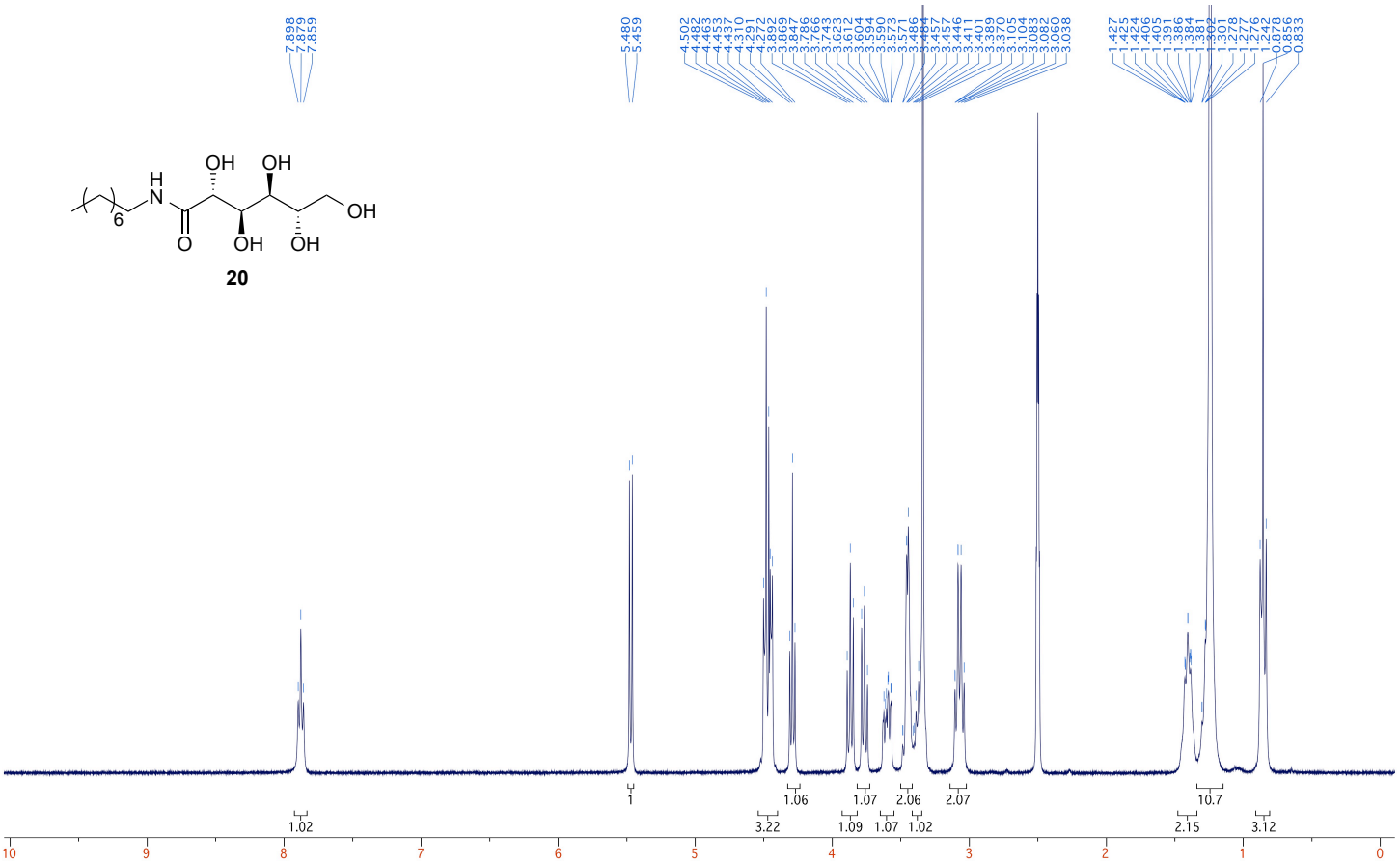
7.898
7.879
7.859
5.480
5.459
4.502
4.482
4.463
4.453
4.437
4.310
4.291
4.271
3.892
3.869
3.847
3.786
3.743
3.623
3.612
3.604
3.590
3.573
3.571
3.486
3.457
3.446
3.411
3.401
3.389
3.370
3.105
3.104
3.083
3.060
3.038
1.427
1.425
1.424
1.406
1.405
1.391
1.386
1.384
1.381
1.302
1.278
1.277
1.276
1.242
1.238
0.856
0.833
1
1.06
1.07
2.06
2.07
10.7
1.02
3.22
1.09
1.07
1.02
2.15
3.12
10
9
8
7
6
5
4
3
2
1
0

OH
OH
H
N
6
OH
O
OH
OH

20

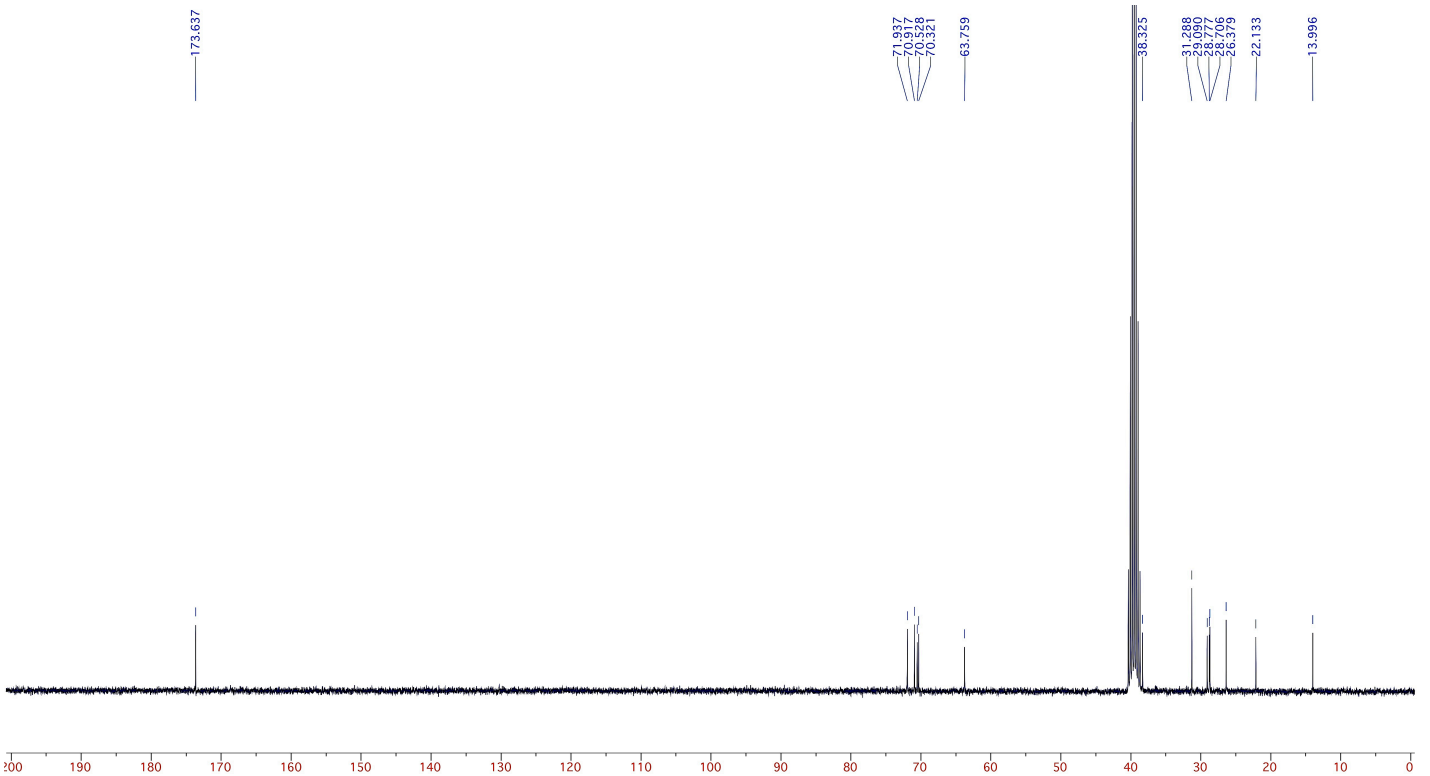
173.637
71.937
71.317
70.528
70.321
63.759
38.325
31.288
29.090
28.777
28.706
26.379
22.133
13.996
200
190
180
170
160
150
140
130
120
110
100
90
80
70
60
50
40
30
20
10
0

OH
OH
H
N
6
OH
O
OH
OH

21

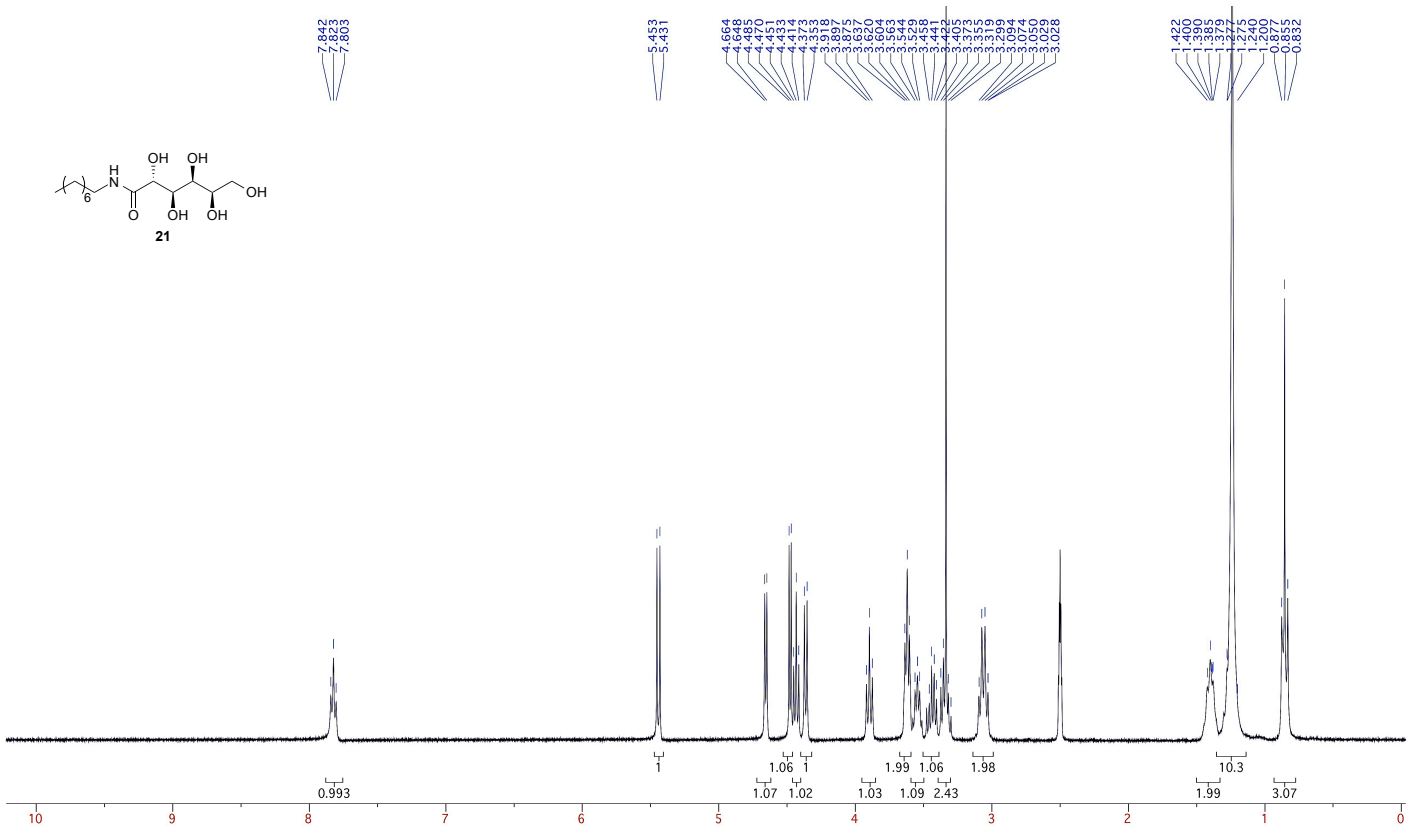
7.842
7.823
7.803
5.453
5.431
4.664
4.648
4.485
4.470
4.451
4.433
4.414
4.373
4.353
4.318
3.897
3.875
3.637
3.620
3.604
3.563
3.544
3.529
3.518
3.441
3.422
3.405
3.373
3.355
3.319
3.299
3.094
3.074
3.050
3.029
3.028
1.422
1.400
1.390
1.385
1.379
1.275
1.240
1.200
0.857
0.855
0.832
1
1.06
1
1.99
1.06
1.98
10.3
0.993
1.07
1.02
1.03
1.09
2.43
1.99
3.07
10
9
8
7
6
5
4
3
2
1
0

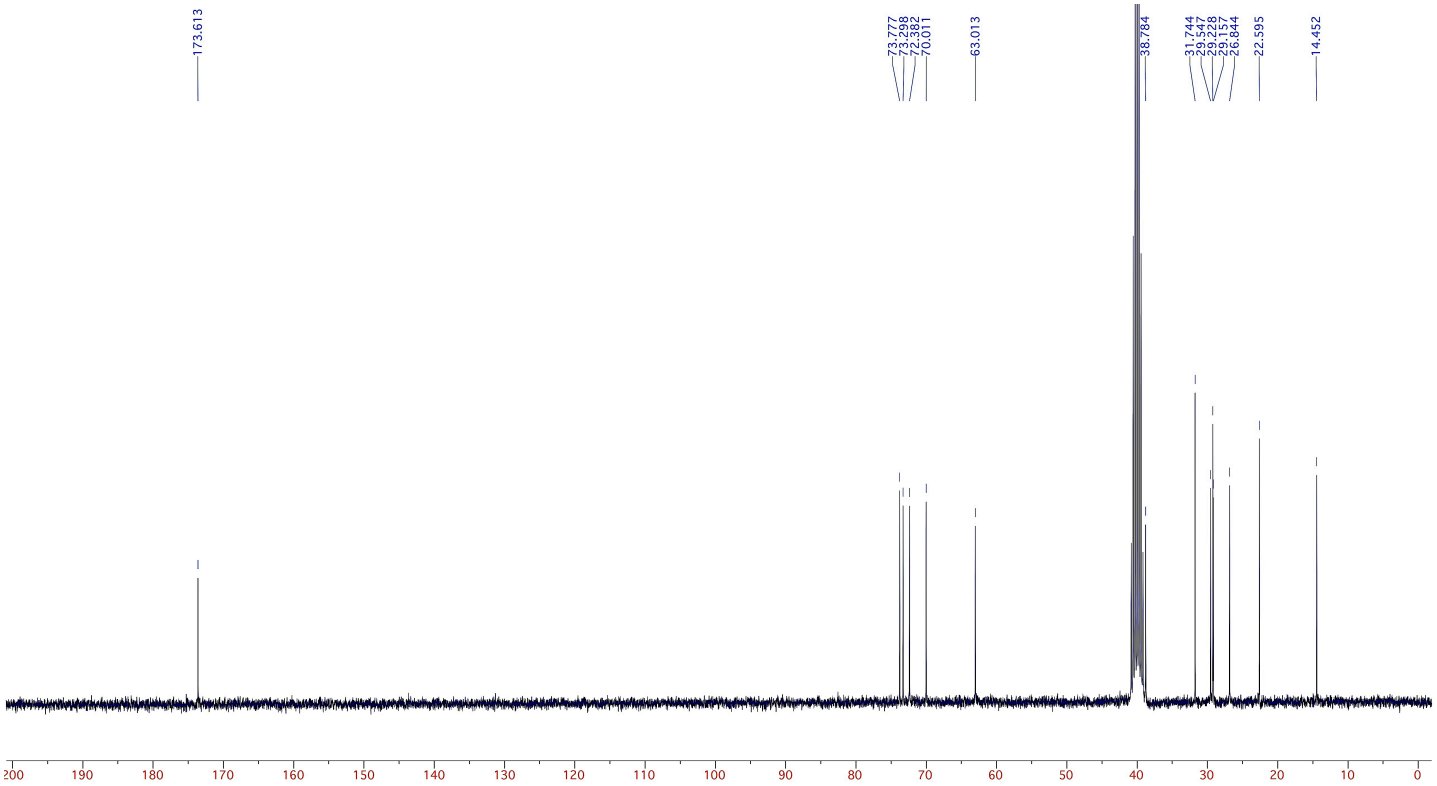
173.613
73.777
73.298
72.382
70.011
63.013
38.784
31.744
29.547
29.228
29.157
26.844
22.595
14.452
200
190
180
170
160
150
140
130
120
110
100
90
80
70
60
50
40
30
20
10
0

Chapter 7: Small Carbohydrate-Based Molecules as Ice Recrystallization Inhibitors – Phenolic-Glycosides

7.1 Introduction

Prior to the work described in Chapter 6, all reported small molecules were only moderate inhibitors of ice recrystallization.[1-4] This was hypothesized to be attributed to their ability to disrupt or disorder the structure of bulk-water.[1,3] The best way in which to validate this hypothesis would be to assess the IRI activity of molecules that are known to disrupt or disorder bulk water. Thus, we assessed the IRI activity of several small molecules that are known to disrupt, alter and/or sequester the structure of bulk-water by self-assembling in solution. In 2012 our laboratory reported the first examples of potent small molecule ice recrystallization inhibitors that were carbohydrate-based surfactants and hydrogelators (section 6.2).[5] The most potent analogues discovered in each class were the pyranose-based surfactant β-octyl-Gal and the aldonamide-based hydrogelator NOGlc (figure 7.1). β-Octyl-Gal exhibited potent IRI activity at 22 mM (21% MGS relative to PBS) whereas NOGlc was highly IRI active at a significantly lower concentration of 0.5 mM (12% MGS relative to PBS).[5]

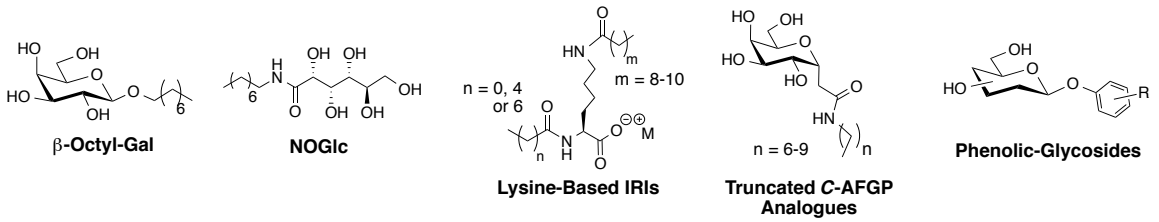

Figure 7.1 Structures of small molecule potent ice recrystallization inhibitors and the general structure of phenolic-glycosides.

The carbohydrate-based surfactants and hydrogelators are amphiphilic molecules. Structure-function studies on these derivatives indicated that the presence of hydrophobic moieties was essential for potent IRI activity (section 6.2). This has also been demonstrated by our laboratory with lysine-based derivatives and truncated analogues of one of our laboratory's most potent *C*-AFGP, OGG-Gal.[6,7] The addition of long alkyl chains greater than nine carbons in length to the ε-amino group of lysine derivatives resulted in potent IRI activity (figure 7.1).[6] Derivatives with alkyl chains shorter than nine carbons in length at this position were significantly less active. Furthermore, truncated analogues of *C*-AFGP OGG-Gal were also potent IRIs when alkyl chains greater than seven carbons in length were conjugated to the amide bond of the *C*-linked galatosyl moiety (figure 7.1).[7] Analogues with alkyl chains six carbons or less were only weak to moderately IRI active.

Thus far, all of the small molecules that have exhibited potent IRI activity are amphiphilic molecules containing long alkyl chains.[5-7] However, these molecules possess surfactant-like characteristics, which can be detrimental to cells and can solubilize cell membranes.[8-14] We therefore sought to explore if other hydrophobic moieties on carbohydrates would also result in potently IRI active small molecules. As such, we chose to employ an aryl ring as a hydrophobic moiety and various phenolic-glycosides were explored to identify a second class of small molecule potent IRIs (general structure shown in figure 7.1). Some of these phenolic-glycosides were utilized to study the concentration and time dependence of ice recrystallization inhibition providing valuable information on how these molecules are inhibiting this process.[15] Thus, the goals and objectives of this chapter are as follows:

1. The potently IRI active non-ionic surfactant β-octyl-Gal contains a β-*O*-linked alkyl chain glycosidated to the C1 position of the carbohydrate. Thus, we sought to prepare phenolic-glycosides β-*O*-linked to the anomeric position and assess their ability to inhibit ice recrystallization (general structure shown in figure 7.1). These phenolic-glycosides contained various substituents at the ortho-, meta- and para-positions of the aromatic ring. These phenols were also glycosidated to various mono- and di- and trisaccharide moieties to investigate the influence of the carbohydrate head-group. Finally, the configuration of the glycosyl bond conjugating the phenol to the carbohydrate residue was also varied to elucidate the importance of a β- or α-linked aglycone on activity. The results from these studies are discussed in section 7.2.
2. We also sought to explore the dependence of concentration and time on the inhibition of ice recrystallization with various compounds that exhibit different degrees of IRI activity. This would provide information on the "end-points" of IRI, as well as indicate if there is a linear dependence of IRI on concentration to provide more details towards understanding the mechanism by which carbohydrate derivatives are exhibiting IRI activity. These results are presented in section 7.3.

7.2 Phenolic-Glycosides as Ice Recrystallization Inhibitors

7.2.1 Structures and Synthesis of Para-Substituted Phenolic Glycosides

The first phenolic-glycosides investigated for IRI activity contained a β-linked *para*-methoxyphenyl (PMP) moiety. These were β-PMP-glycosides of D-galactose, D-glucose, D-mannose, D-xylose and L-arabinose, the structures of which are shown in figure 7.2. β-PMP-Gal (**1**), β-PMP-Glc (**2**) and β-PMP-Xyl (**4**) were prepared by Lewis acid-catalyzed (BF_3OEt_2) glycosidation of the appropriate pentaacetylated monosaccharide with *para*-methoxyphenol, as

described previously (scheme 7.1).[16,17] Only the β-linked PMP-glycoside was observed for all three glycosidations (**1a** for galactose, **2a** for glucose and **4a** for xylose) due to anchimeric assistance from the C2-*O*-acetyl group. Zemplén deacetylation then afforded the desired phenolic-glycosides β-PMP-Gal (**1**), β-PMP-Glc (**2**) or β-PMP-xyl (**4**). β-PMP-arab (**5**) is commercially available and was generously provided by Dr. Mark Taylor from the Department of Chemistry at the University of Toronto.

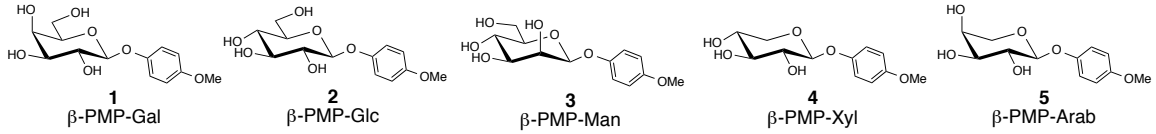

Figure 7.2 Structures of phenolic-glycosides β-PMP-Gal (**1**), β-PMP-Glc (**2**), β-PMP-Man (**3**), β-PMP-Xyl (**4**) and β-PMP-Arab (**5**).

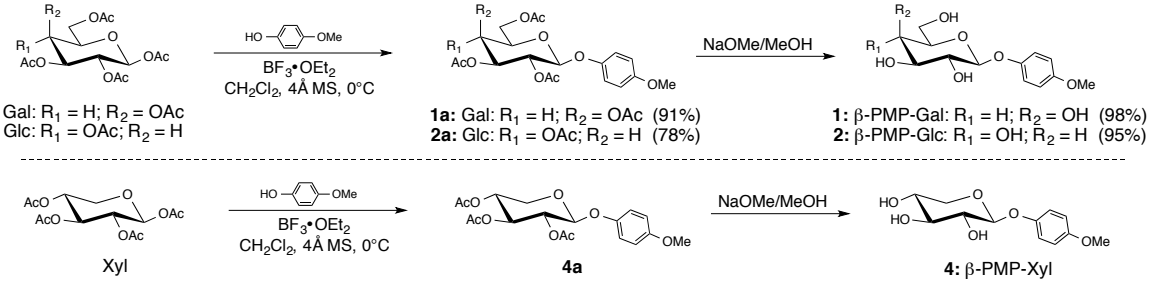

Scheme 7.1 Synthesis of β-PMP-Gal (**1**), β-PMP-Glc (**2**) and β-PMP-Xyl (**4**).

β-linkages on galactose or glucose (*trans*-1,2 (eq,eq) relationship between the C1 and C2 substituents) are relatively easy to obtain synthetically due to the possibility of neighbouring group participation from the C2 substituent. In contrast, α-linkages on galactose or glucose (*cis*-1,2-ax,eq) are more difficult to produce, and the most difficult linkages to obtain in carbohydrate chemistry are β-linkage on mannose (*cis*-1,2-eq,ax). There are only a few methods that effectively create the β-glycosidic linkage on mannose, one of which is the Crich β-mannosylation method that employs the use of glycosyl triflates to form the β-linkage with high selectivity.[18-20] Thus, this method was utilized to prepare the β-PMP-Man derivative (**3**) and this is described in scheme 7.2.

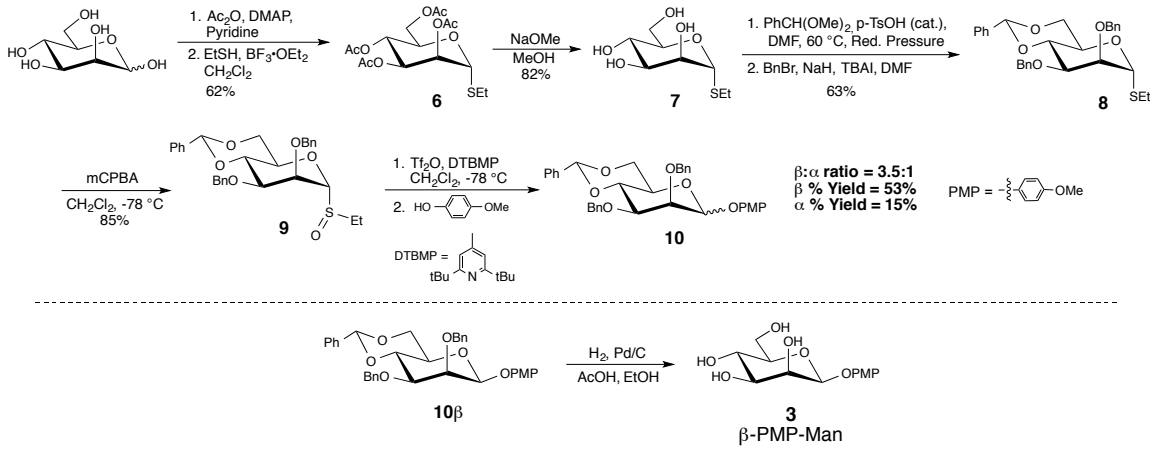

Scheme 7.2 Synthesis of β-PMP-Man (**3**) using Crich's method for the preparation of β-mannose linkages using glycosyl triflates.

Prior to glycosidation with *para*-methoxyphenol, preparation of the sulfoxide derivative **9** was required (scheme 7.2). This was achieved from D-mannose, which was acetylated and glycosidated with ethanethiol to provide thioethyl mannose intermediate **6**.[21] Zemplén deacetylation yielded intermediate **7**, which was then subjected to selective 4,6-benzylidene acetal formation followed by benzylation of the C2 and C3 hydroxyl groups, to afford orthogonally protected derivative **8**.[22] The benzylidene acetal was required to form a rigid trans-fused ring system, which favoured formation of the β-linked product in the glycosidation step.[19,23] Thio-derivative **8** was then oxidized to sulfoxide **9** using mCPBA, which was the glycosyl donor employed to form the β-mannoside. The protected β-PMP-mannoside **10** was prepared by activating the mannosyl sulfoxide **9** with triflic anhydride, which forms *in situ* selectively the α-mannosyl triflate.[18,23,24] *para*-methoxyphenol was then added to the triflate and the β-PMP-mannoside of **10** was favoured over the α-PMP-mannoside by 3.5:1 (scheme 7.2). This glycosidation is hypothesized to proceed through a contact ion pair or solvent-separated ion pair of the triflate anion with the α-face of the mannosyl oxacarbenium ion, effectively shielding that face against nucleophilic attack from the alcohol, favouring the β-linked product.[23,24] The desired β-PMP-mannoside **10β** could be separated from the α-product by column chromatography, and hydrogenation under acidic conditions hydrolyzed the benzylidene acetal and removed the benzyl protecting groups to afford the desired β-PMP-Man (**3**).

In addition to *para*-methoxy substituted phenolic-glycosides, the effect of the substituent at the *para*-position of the aryl ring had on IRI activity was further explored. Thus, β-linked phenolic-glycosides of both galactose and glucose were prepared in which the *para*-methoxy substituent on the aglycone was substituted with various atoms or functional groups. This included both electron donating and electron withdrawing groups such as methyl, amino, nitro

and carboxylate groups, as well as halogens. The structures of these derivatives are provided in figure 7.3 (glucopyranose derivatives **11**-**23** and galactopyranose derivatives **24**-**36**). Similar to β-PMP-Gal (**1**) and β-PMP-Glc (**2**), they were prepared by Lewis acid catalyzed glycosidation with the appropriate pentaacetylated sugar and appropriate phenol to provide intermediates **11a**-**36a**,[16,17] then Zemplén deacetylation provided the desired phenolic-glycoside. A general synthetic procedure for this is outlined in scheme 7.3. A Master's student in our laboratory, Matt Alteen, prepared phenolic-glycosides **15**, **18**, **20**, **28**, and **31**-**33**. A former doctoral student, John Trant, prepared phenolic-galactosides **26**, **29**-**30** and **34**-**35** with assistance from an undergraduate student at that time, Malay Doshi.[25] All remaining *para*-substituted phenolic-glycosides were prepared with assistance from an undergraduate student, Ross Mancini.

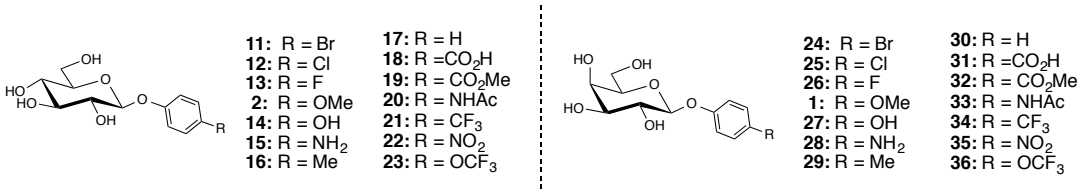

Figure 7.3 Structures of various *para*-substituted phenolic-glucosides (**11**-**23**) and galactosides (**24**-**36**).

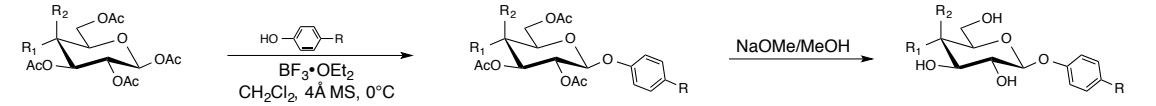

Scheme 7.3 A general synthetic scheme for the preparation of phenolic glycosides by Lewis acid catalyzed glycosidation.

7.2.2 IRI Activity of Para-Substituted Phenolic Glycosides

The IRI activity of phenolic-glycosides of D-galactose, D-glucose, D-mannose, D-xylose and L-arabinose containing a β-linked *para*-methoxyphenyl moiety is presented in figure 7.4. The D-galactose derivative β-PMP-Gal (**1**) and D-mannose derivative β-PMP-Man (**3**) both exhibited weak IRI activity that was similar to that exhibited by D-mannose (78% MGS relative to PBS). The D-xylose derivative β-PMP-Xyl (**4**) and the L-arabinose derivative β-PMP-Arab (**5**) both exhibited moderate activity and were more potent than β-PMP-Gal (**1**) and β-PMP-Man (**3**). Furthermore, the D-glucose derivative β-PMP-Glc (**2**) exhibited potent IRI activity with a 23% MGS relative to the PBS control. β-PMP-Glc (**2**) was significantly more active than all other PMP-containing monosaccharides assessed. In fact, β-PMP-Glc (**3**) exhibited potent activity that was very similar to the previously reported non-ionic surfactant β-Octyl-Gal (figure 7.1) at equimolar concentration (Chapter 6).[5]

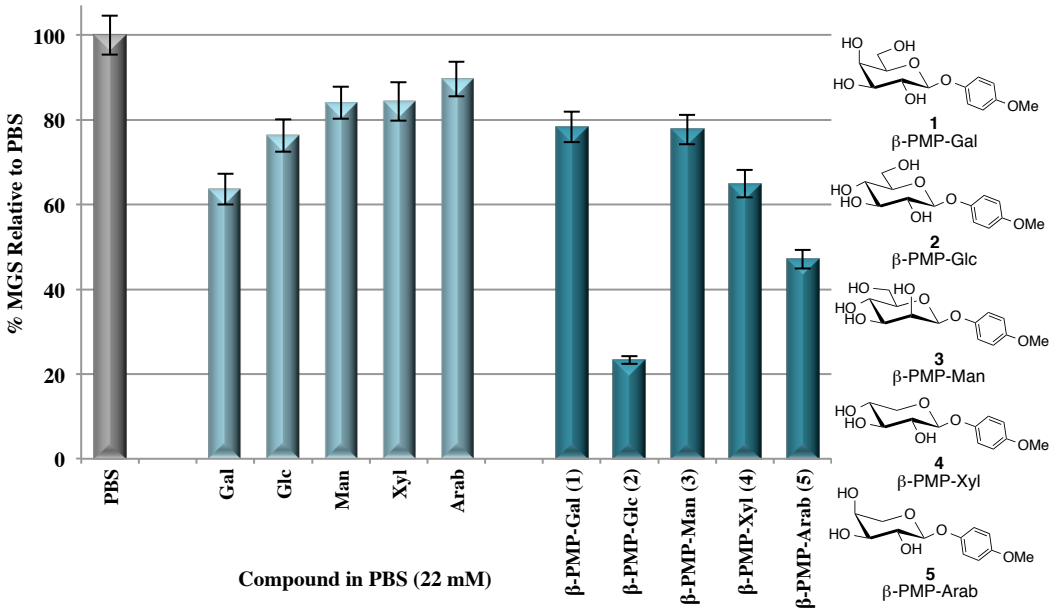

Figure 7.4 IRI activity of β-PMP-linked monosaccharides **1**-**5** at 22 mM in PBS. The % MGS (mean grain size) relative to a PBS positive control is shown for all compounds.

Our laboratory has previously correlated IRI activity to carbohydrate hydration and reported that highly hydrated monosaccharides, such as D-galactose,[26] were more IRI active than less hydrated monosaccharides such as D-glucose and D-mannose (section 1.3.3 and chapter 5).[1] Furthermore, carbohydrate-derivatives and glycoconjugates containing a more highly hydrated galactose moiety were also more active than those with glucose moieties.[1,5,27] For example, the non-ionic pyranose-based surfactant possessing a highly hydrated D-galactose head group (β-octyl-Gal, figure 7.1) was significantly more IRI active than the surfactant possessing the less hydrated D-glucose head group (β-octyl-Glc) (see chapter 6).[5] The result of the glucose derivative β-PMP-Glc (**2**) being a potent inhibitor of ice recrystallization (figure 7.4), whereas galactose derivative β-PMP-Gal (**1**) was only weakly IRI active, was surprising and unprecedented. It is the first example where a pyranose-based derivative possessing a D-glucose moiety has been significantly more active than one containing a D-galactose moiety. Furthermore, it was also surprising that both β-PMP-Gal (**1**) and β-PMP-Man (**3**) exhibited identical IRI activities despite the difference in hydration between these two pyranose residues.[1,26,27]

Interestingly, both β-PMP-Xyl (**4**) and β-PMP-Arab (**5**) were also more IRI active than β-PMP-Gal (**1**) (figure 7.4). This was also surprising as xylose and arabinose have hydration values that are lower than that of mannose,[26] and these monosaccharides were poor IRIs (figure 7.4 and chapter 5, section 5.2.2). β-PMP-Xyl (**4**) was significantly less active than β-PMP-Glc (**2**) (65% MGS for **4** and 23% MGS for **2**), suggesting the C6-OH group of β-PMP-Glc (**2**) is important for its potent activity. This is in agreement with the results discussed in chapter 5, section 5.2.2

where it was hypothesized that this position influences carbohydrate hydration,[28-30] and thus IRI activity. In contrast, β-PMP-Arab (**5**) exhibited more potent activity than β-PMP-Gal (**1**) with a 47% MGS (for **5**) compared with 78% MGS (for **1**). Removing the hydroxymethyl group of β-PMP-Gal (**1**) almost doubled the IRI activity of this derivative (β-PMP-Arab (**5**)). A plausible explanation for these results is that the hydration characteristics of **1**-**5** may be very different than the parent monosaccharides due to the presence of the PMP moiety. Unfortunately, hydration numbers or molar compressibilities of *para*-methoxyphenol or its effect on the hydration characteristics of the monosaccharide units of **1**-**5** are not known. However, our results clearly demonstrate that incorporating the PMP moiety increases the ability of the monosaccharide to inhibit ice recrystallization, and can be very beneficial resulting in potent activity for glucose derivative β-PMP-Glc (**2**).

To investigate the anomalous potent IRI activity of β-PMP-Glc (**2**) we chose to first investigate the influence of the PMP group. Towards this end, β-linked phenolic-glucosides were prepared in which the *para*-methoxy substituent on the aglycone was substituted was various atoms or functional groups (derivatives **11**-**23**, structures provided in figure 7.5). The IRI activity of these phenolic-glucosides is shown in figure 7.5. Additionally, the *para*-methoxy substituent of β-PMP-Gal (**1**) was also substituted with similar atoms or functional groups as the glucose derivatives to examine their effect on the weak IRI activity of **1** (derivatives **24**-**36**). The IRI results of the phenolic-galactosides are shown in figure 7.6.

Many of the *para*-substituted phenolic-glucosides exhibited moderate to weak IRI activity ranging from 50-89% MGS relative to the PBS control (figure 7.5), indicating that the *para*-methoxy substituent is desirable for potent activity. The exceptions were when the methoxy substituent was replaced with a halogen (Br, Cl or F, **11**-**13**) or a trifluoromethyl group (CF_3, **21**). The *para*-fluoro and *para*-methoxy derivative exhibited identical activities (23% MGS), while the *para*-chloro was more active (14% MGS) and the *para*-bromo derivative exhibited the most potent IRI activity (8% MGS). The *para*-trifluoromethyl derivative was less active than β-PMP-Glc with a %MGS of 33%. It is evident that the methyl of the methoxy substituent is crucial for the potent activity of β-PMP-Glc as *para*-hydroxyl derivative **14** had drastically decreased activity (figure 7.5). In addition, the oxygen atom between the aryl ring and the methyl group is also important as *para*-methyl derivative **16** exhibited similar reduced activity as **14**. Interestingly, replacing the hydrogens of the methoxy group with fluorines as in *para*-trifluoromethoxy derivative **23** was also detrimental for the potent activity of **2**. In contrast, replacing the hydrogens of the *para*-methyl (derivative **16**) with fluorines (*para*-trifluoromethyl derivative **21**) was beneficial and increased the activity of the *para*-methyl derivative. Finally, it

appears that the IRI activity of these phenolic-glucosides is not influenced by electronics since the methoxy (OMe), hydroxyl (OH) and amino (NH_2) groups are all electron donating (**2**, **14** and **15**), yet **2** was potently active while **15** was the least active derivative assessed. Moreover, both nitro (NO_2) and trifluoromethyl (CF_3) are strong electron withdrawing groups; however, CF_3 containing derivative **21** was potently active while NO_2 containing derivative **22** was only moderately IRI active. The relationship between IRI and electronic effects is discussed in more detail later in this section.

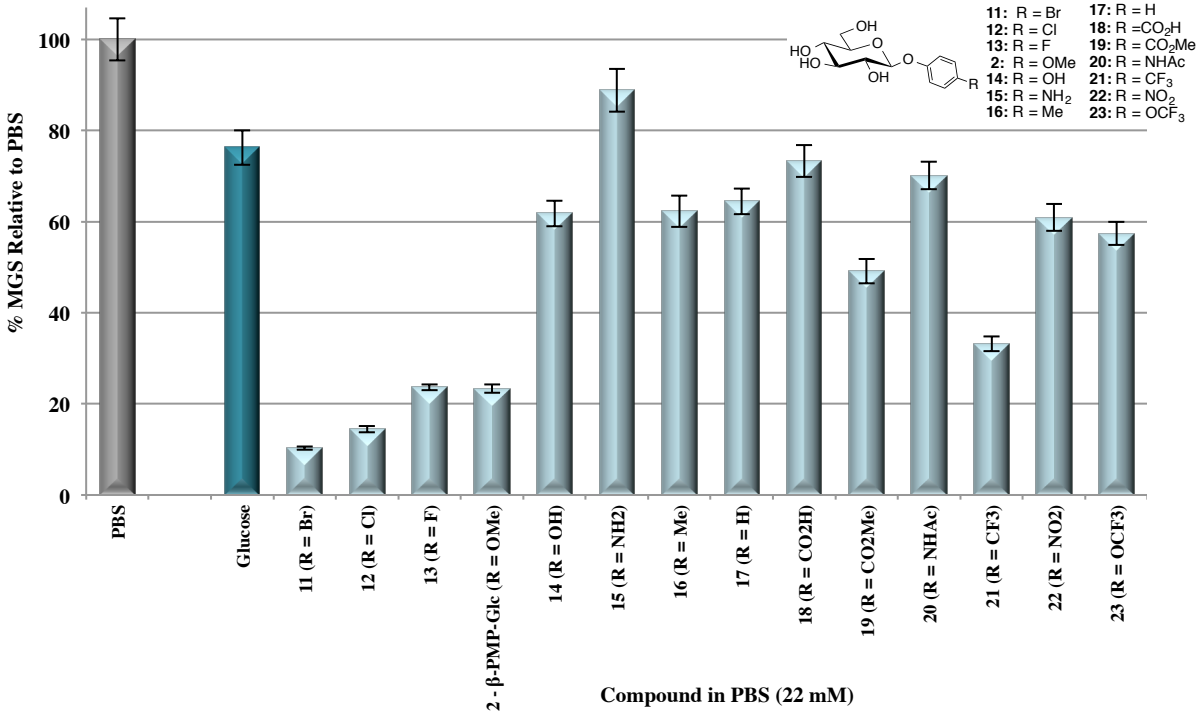

Figure 7.5 IRI activity of para-substituted phenolic-glucosides **2** and **11**-**23** at 22 mM in PBS. The % MGS (mean grain size) relative to a PBS positive control is shown for all compounds.

The *para*-substituted phenolic-galactosides **24**-**36** (figure 7.6) result in a very different IRI profile than that of the *para*-substituted phenolic-glucosides. Most of the phenolic-galactosides resulted in ~80% MGS relative to the PBS control (figure 7.6), whereas only one phenolic-glucoside resulted in 80% MGS (derivative **15**, figure 7.5). Phenolic-glucosides with halogen substituents were all potently IRI active (**11**-**13**, figure 7.5). While phenolic-galactosides with bromo- and chloro- substituents were potently active (**24**-**25**), the *para*-fluoro derivative **26** exhibited weak activity (figure 7.6). Interestingly, the *para*-CO_2Me galactoside derivative **32** resulted in high IRI activity (30% MGS), but in contrast the glucoside derivative **19** resulted in moderate IRI activity (50% MGS). The only phenolic-galactosides assessed in this study that were more IRI active than the corresponding glucose derivatives were **28**, **32** and **35** with a *para*-substituted NH_2, CO_2Me or NO_2 group (compared with **15**, **19** and **22**, respectively).

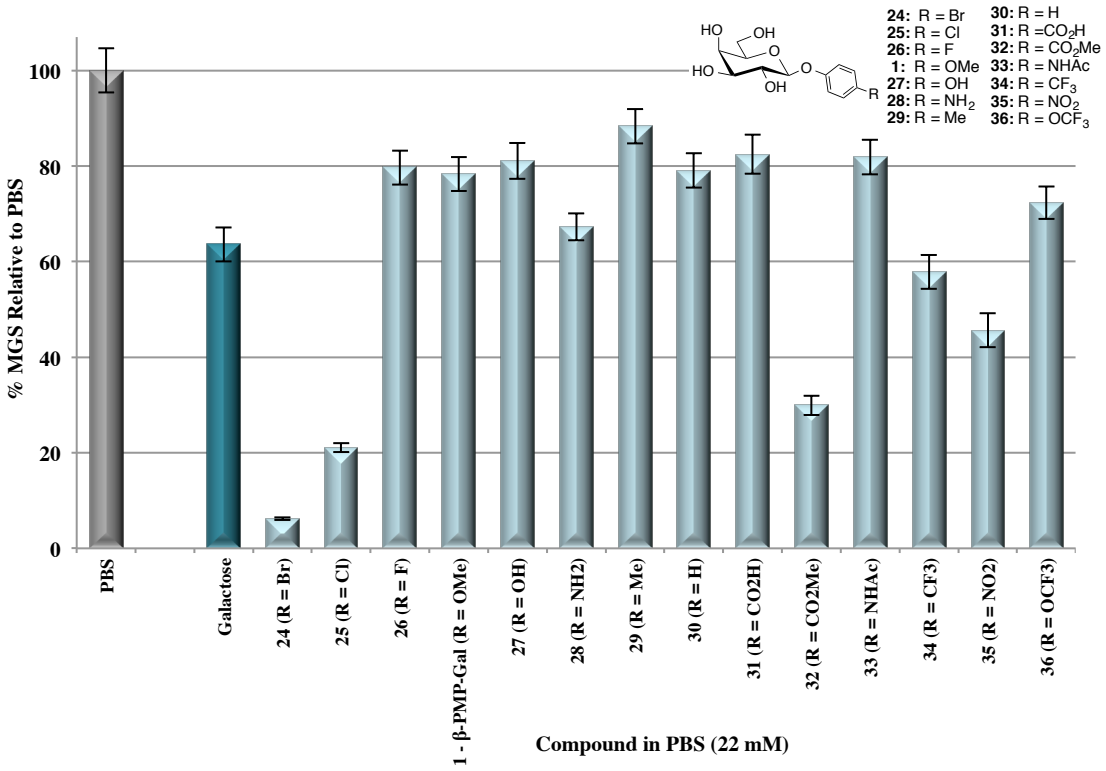

Figure 7.6 IRI activity of para-substituted phenolic-galactosides **1** and **24**-**36** at 22 mM in PBS. The % MGS (mean grain size) relative to a PBS positive control is shown for all compounds.

Overall, the results of the *para*-substituted phenolic-glycosides indicate that the IRI activity of these derivatives is sensitive to the substituent at this position. The activity of the glucosides is strongly influenced by modifications to this position, and in general the phenolic-glucosides are more IRI active than the phenolic-galactosides. While a few galactose derivatives were potent inhibitors of ice recrystallization, the phenolic-glucosides are more suited as a novel class of potent small molecule IRIs as five of these derivatives were potently active. Two of the most active phenolic glucosides discovered from this study were β-PMP-Glc (**2**) and β-pBrPh-Glc (**11**) (figure 7.5).

As described previously, the *para*-substituent on the phenolic-glycosides were varied to be either electron donating or electron withdrawing groups. Preliminarily, the IRI results of the *para*-substituted phenolic-glycosides indicated that the ability of these compounds to inhibit ice recrystallization was unrelated to the electronics of the aryl ring (figures 7.5 and 7.6). To definitively support this observation, a Hammett plot was constructed to elucidate the relationship between IRI activity and its sensitivity to changes in electronic effects of the *para*-substituent (figure 7.7). The Hammett equation is a linear free energy relationship that relates changes in reaction rates or equilibrium constants to changes in electronics of substituents and their electron donating/withdrawing ability.[31-35] The Hammett equation is defined in equation 7.1, where K_R is

the equilibrium constant (or reaction rate, k) for a given reaction with substituent R, K_0 is the reference equilibrium constant (or reaction rate, k_0) where R is a hydrogen, σ is the substituent constant and ρ is the reaction constant.[31,32,34] The substituent constant σ is dependent only on the electronics of the substituent.[32,34,36] This constant is an empirical electronic substituent parameter that was derived from the K_a's of substituted benzoic acids by defining the reaction constant ρ as 1. The ionization of benzoic acid and substituted benzoic acids results in anionic carboxylate that can be stabilized by electron withdrawing substituents. *Para*-substituted electron withdrawing substituents thus have a positive σ^{para} value as they stabilize this negatively charged species resulting in an increased acidity of the substituted benzoic acid. *Para*-substituted electron donating substituents destabilize the carboxylate anion increasing the acidity of the substituted benzoic acid and thus have a negative σ^{para} value.

$$\log (K_R/K_0) = \sigma\rho$$

Equation 7.1 Hammett Equation.

With defined σ values the Hammett equation can be utilized to determine how sensitive a reaction is to electronic effects of substituents by measuring reaction rates (k) or equilibrium constants (K) of unsubstituted and substituted derivatives. The sensitivity of a particular reaction to electron effects is determined by the reaction constant ρ. The reaction constant ρ is equivalent to the slope of the Hammett plot, which is a plot of $\log(K_R/K_0)$ *versus* σ^R values of each substituent R (*meta*- or *para*-substituent).[32-35] If ρ (the slope) is greater than 1 ($\rho>1$) the reaction is more sensitive to the electronics of the substituents than the ionization of benzoic acid. Thus, electron withdrawing groups stabilize a negative charge increasing the reaction rate or equilibrium constant with these substituents present. If $\rho<0$ the reaction is favoured by electron donating substituents that stabilize a positive charge. When ρ is greater than 0 but less than 1 there is a weaker relation to electron withdrawing substituents and the reaction is less sensitive to these electronic effects than the ionization of benzoic acid. When $\rho=0$ and the Hammett plot does not have a linear correlation this indicates there is no relation between the electronic effects of the substituent and the reaction rate or equilibrium constant.

Ice recrystallization is a thermodynamically driven Ostwald ripening process that leads to an overall increase in mean ice crystal size and a decrease in the number of ice crystals (and also total surface area) with an overall constant volume (section 1.1.2).[15,37,38] The IRI assay utilized by our laboratory does not calculate or quantify ice recrystallization rate (or rate constant) that is necessary for a Hammett plot. However, an approximation of this rate constant can be made based on the % MGS at the time point where ice crystal size is measured (30 minutes for all samples) as this is a dynamic parameter of the Oswald ripening process and the rate is

proportional to this size.[15,37] Thus, a Hammett plot comparing the ratio of %MGS for the *para*-substituted phenolic-glycosides to the unsubstituted phenyl-glycosides was constructed using the respective σ^{para} values[32,34] for each substitution to determine the relationship between IRI and aryl ring substituent electronics. These results are presented in figure 7.7A for the *para*-substituted phenolic-glucosides and 7.7B for the *para*-substituted phenolic-galactosides.

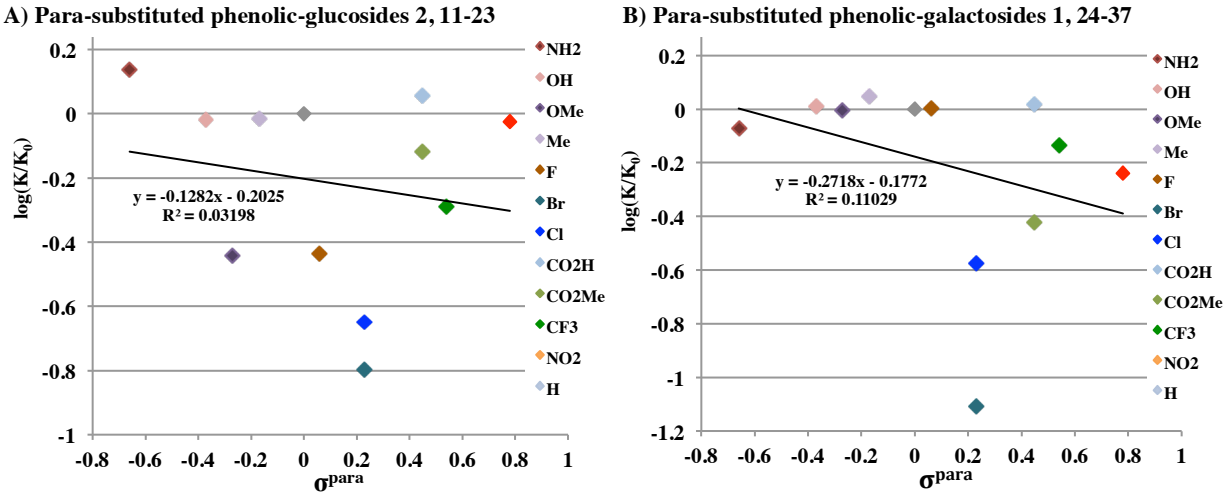

Figure 7.7 Hammett plots of the relationship between %MGS and the electronic effect of the *para*-substituent for phenolic-glucosides (A) and phenolic galactosides (B). The $\log(K/K_0)$ for each derivative is plotted against σ^{para} values for each *para*-substituent, where K represents the %MGS of the para-substituted phenolic-glycoside after 30 min annealing time and K_0 represents the %MGS of the unsubstituted phenyl-glycoside after the 30 min annealing time.

As is evident from the Hammett plots for the phenolic-glucosides (figure 7.7A) and galactosides (figure 7.7B) there is not a linear correlation between IRI and electronic effects of the *para*-substituents. The linear correlation coefficients for both plots were $R = 0.032$ for the phenolic-glucosides and $R = 0.11$ for the phenolic-galactosides. Thus, we can conclude that the *para*-substituents of these phenolic-glycosides are not acting to stabilize a negative or positive charge by inductive effects during the ice recrystallization process. Other contributing factors unrelated to the electronics of the aryl aglycone must therefore be contributing to the potent IRI activity of the phenolic-glucosides **2**, **11**-**13**, and **21** (R = *para*-OMe, Br, Cl, F and CF_3) and phenolic-galactosides **24**-**25** (R = *para*-Br and Cl) (figures 7.5 and 7.6). While it is presently not known why this class of compound exhibits potent IRI activity, it is remarkable that simply changing a single atom or functional group at the *para*-position of the phenolic ring can have such a significant impact on the ability of the glycoside to inhibit ice recrystallization. Furthermore, it is also very interesting that altering the configuration of the C4 position such that the C4-OH group is axial (for the galactosides) rather than equatorial (for the glucosides)

adversely affects IRI activity resulting, in most instances, in inactive derivatives for the galactosides while the glucosides were potently active.

Since a few of the phenolic-glycosides were identified to be novel potent small molecule ice recrystallization inhibitors, we sought to explore whether the phenolic glycosides were binding to ice in a manner similar to naturally occurring biological antifreezes. Two of the most IRI active phenolic-glucosides β-PMP-Glc (**2**) and β-pBrPh-Glc (**11**) were assessed for interactions with the ice lattice and TH activity using nanolitre osmometry.[39] The ice crystal habits in the presence of either **2** or **11** are presented in figure 7.8A and B, respectively. Neither of these derivatives exhibited TH activity or dynamic ice shaping capabilities indicating there was no interaction with the ice lattice. This is consistent with the lack of TH activity reported previously for the potently IRI active carbohydrate-based and lysine-based surfactants and hydrogelators,[5,6] and the custom-tailored *C*-AFGPs previously published by our laboratory.[27,40] Thus, these phenolic-glycosides that are potent IRIs are novel small molecules that exhibit "custom-tailored" antifreeze activity and may be ideally suited for applications in cryopreservation to mitigate cellular damage cause by ice recrystallization (discussed further in chapter 8).

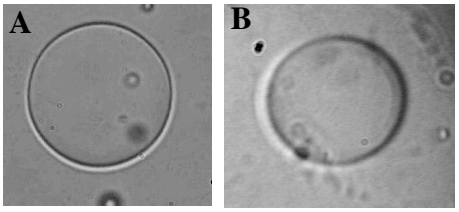

Figure 7.8 Ice crystal habits in the presence of A) 10 mg/mL β-PMP-Glc **(2)** and B) 10 mg/mL β-pBrPh-Glc (**11**) in water.

7.2.3 Regioisomers of β-PMP-Glc, Modifications to the Glycosidic Linkage and Derivatives of β-PMP-Glc

As described in section 7.2.2, β-PMP-Glc (**2**) was found to be a potent inhibitor of ice recrystallization, whereas β-PMP-Gal (**1**) and β-PMP-Man (**3**) were only weakly IRI active. This was unprecedented as it was the first instance where a pyranose-based D-glucose derivative exhibited potent activity and was significantly more active than a pyranose-based D-galactose derivative. Further exploration on the affect of the *para*-substituent on IRI activity indicated that only a few functional groups were beneficial at this position and resulted in potent activity. To investigate other structural features of β-PMP-Glc that are important for its potent activity, various derivatives with structural modifications to parent β-PMP-Glc structure were prepared and assessed for IRI activity. Regioisomers of β-PMP-Glc in which the methoxy substituent on the aryl ring was in the *meta*- or *ortho*-position were prepared and assessed for IRI to determine if simply the presence of a methoxy group on the aryl ring is sufficient for potent activity (**37**-**38**,

figure 7.9). *Meta*-substituted hydroxyl (**39**) and methyl (**40**) phenyl-glucosides were also assessed for their ability to inhibit ice recrystallization and compared to *para*-derivatives **14** and **16** to determine if regiochemistry influences the IRI of these derivatives in a similar manner as the methoxy derivatives. Additionally, PMP-Glc derivatives where glycosidic linkage was modified were prepared, including α-linked derivatives (**41**-**46**), *N*- and *S*-linked derivatives (**47** and **48**), and a *para*-methoxybenzyl derivative (**49**). Finally, the influence of the C6-OH group was examined for its importance for the potent activity of β-PMP-Glc by assessing the IRI of derivatives **50** and **51**. The C6 position was investigated for its influence on activity as this hydroxyl group had previously been demonstrated to be influential for the IRI activity of simple monosaccharides, and modifying it significantly decreased activity (Chapter 5, section 5.2.2). The PMP group was also conjugated to this position to determine if its attachment to other hydroxyl groups on the glucose ring also resulted in potent activity (derivative **52**).

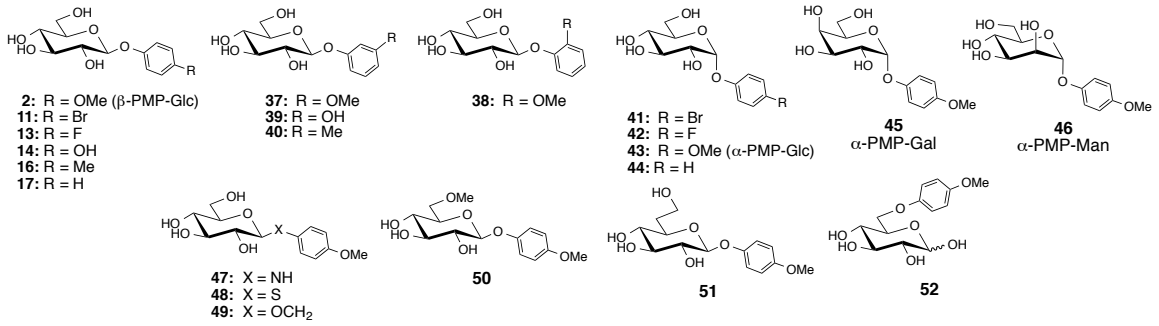

Figure 7.9 Structures of β-PMP-Glc monosaccharide derivatives **37-52** assessed for IRI activity.

The *meta*-substituted glucosides **37** and **40** were prepared with assistance from an undergraduate student, Ross Mancini, utilizing a similar synthetic procedure as β-PMP-Glc (**2**) (scheme 7.1) by Lewis acid catalyzed glycosidation with penta-*O*-acetyl-β-D-glucopyranose to provide intermediates **37a** and **40a**.[16,17] Zemplén deacetylation then provided the desired phenolic-glycoside **37** and **40** (scheme 7.4). The *meta*-hydroxyphenyl derivative **39** (prepared by Ross Mancini) was obtained as a byproduct from a disaccharide synthesis and is described in scheme 7.13C in section 7.2.5. The *ortho*-methoxyphenyl-glucoside **38** was prepared by a former Masters student Matt Alteen.

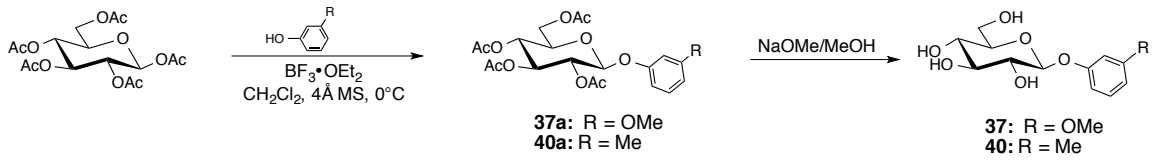

Scheme 7.4 Preparation of meta-substituted phenolic glycosides **37** and **40**.

The α-PMP-Glc derivative **43** was initially prepared utilizing Lemieux's halide ion catalyzed glycosylation chemistry, which employs the use of an armed brominated glycosyl donor such as

56 (scheme 7.5).[41-43] This synthesis began with the preparation of the benzylated free-reducing glucoside **55**, which was prepared from D-glucose. An orthogonal *N*,*O*-dimethylhydroxylamine protecting group was first installed at the C1 position to give intermediate **53**.[44,45] This intermediate was then benzylated to afford **54**, and the anomeric protecting group was removed with NCS (*N*-chlorosuccinimide) to provide **55**.[44] The benzylated free-reducing glucoside **55** was then brominated using oxalyl bromide ($(COBr)_2$) and catalytic DMF to afford donor **56** (scheme 7.5).[46,47] Glycosidation of this donor using halide ion catalyzed glycosylation conditions with tetra-ethylammonium bromide (Et_4NBr) and *para*-methoxyphenol, in the presence of the base DIPEA, resulted in the α-PMP-Glc **57α** product being favoured over the β-linked product (α/β ratio of 11:1). This reaction proceeds via *in situ* anomerization of the α-glycosyl bromide **56α** to form the less stable β-glycosyl bromide **56β** (scheme 7.5).[43] The β-glycosyl bromide does not possess a stabilizing anomeric effect with the electronegative bromine at the C1 position and thus can flip from a $^4C_1$ chair conformation to a $^{1,4}B$ boat conformation, in which there is an anomeric effect. This is the reactive intermediate that the nucleophilic alcohol reacts with to displace the β-bromide to form the α-linked glycosidated product (scheme 7.5). The mixture of *O*-benzylated PMP-glucosides **57α** and **57β** was not separated at this stage and the *O*-benzyl groups were removed by hydrogenation in the presence of palladium hydroxide. Recrystallization of the deprotected product decreased the quantity of the β-product in the mixture resulting in a 13:1 ratio of α-PMP-Glc (**43**) to β-PMP-Glc (**2**).

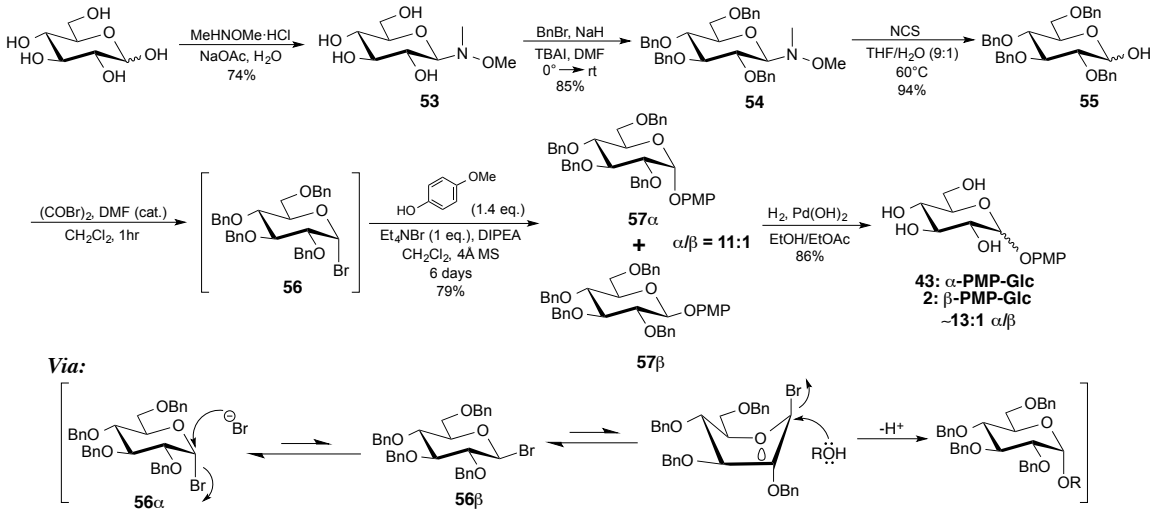

Scheme 7.5 Preparation of α-PMP-Glc (**43**) using Lemieux's halide ion catalyzed glycosidation conditions and the proposed in situ anomerization mechanism to form the α-glycosidated product.

In contrast to smaller-scale preparations of β-PMP-Glc (**2**) (<1 g, scheme 7.1) where the β-product was selectively formed, it was observed during the large-scale preparation of **2** (5-15 g) for cryopreservation work (see Chapter 8) that traces of the α-PMP-Glc product was also

obtained. Furthermore, refluxing the reaction mixture in the presence of 4-5 equivalents of *para*-methoxyphenol further increased the amount of the α-PMP-Glc formed, and after refluxing for 2 days a diastereomeric ratio of 1:1.6 α- to β-PMP-Glc was obtained, with an overall good yield for the mixture (**60**, scheme 7.6). The ratio of α- and β-anomers was calculated based on ^{1}H NMR analysis by integration of the anomeric H-1's of each product. The α- and β-linked PMP products could be easily separated to provide the pure **60α** to assess for IRI activity upon deprotection of the *O*-acetyl groups affording the α-PMP-Glc **43**. Formation of the α-linked glycoside under these reaction conditions likely occurs via an *in situ* anomerization type mechanism, similar to that described above (scheme 7.5).[43] The β-linked glycoside is formed first and in high selectivity initially due to neighboring group participation with the C2-*O*-acetyl group. However, under refluxing conditions with excess of the *para*-methoxyphenol, nucleophilic attack of the alcohol on the bottom face of the pyranose ring to displace the β-*para*-methoxyphenol would form the more thermodynamically stable α-linked glycoside.

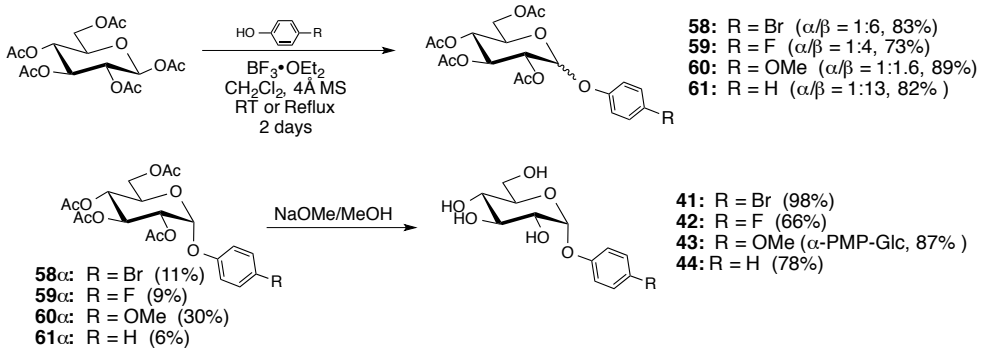

Scheme 7.6 Preparation of α-linked phenolic-glucosides **41**-**44**.

While the overall isolated yield of the protected α-product was low, this method was still a beneficial synthetic route to α-linked phenolic glycosides to assess for IRI as only small quantities are required for the assay and they could be obtained in one step from a commercially available starting material. In contrast, many other synthetic routes to α-linked glycosides utilize the benzylated glucose derivative **55**, which is typically prepared in 3 steps (scheme 7.5). Furthermore, these methods still result in mixtures of α- and β-linked products (scheme 7.5 and scheme 7.12 in section 7.2.5). The β-linked *para*-substituted phenolic glycosides **2** (β-PMP-Glc), **11** (β-pBrPh-Glc), **13** (β-pFPh-Glc) and **17** (β-Ph-Glc) (figure 7.9) were prepared on large-scale for cryopreservation experiments (Chapter 8). Thus, Lewis acid catalyzed glycosidation reactions were refluxed for 2 days to also form sufficient quantities of the α-linked products (**58α**-**61α**) to isolate, deprotect (**41**-**44**) and assess for IRI activity (scheme 7.6). Additionally, α-PMP-Gal (**45**) was prepared using this synthetic strategy (scheme 7.7A) as β-PMP-Gal (**1**) was also examined for its cryopreservation potential (chapter 8). These reactions were carried out by undergraduate

student, Jessica Poisson, who prepared **1**, **11**, **13** and **17** for cryopreservation experiments and isolated **58α**-**62α** (schemes 7.6 and 7.7A). The α-PMP-Man derivative **46** was also prepared utilizing Lewis acid catalyzed glycosidation chemistry from penta-*O*-acetyl-α-D-mannopyranose however, this reaction selectively forms the α-linked glycoside due to the anomeric effect and anchimeric assistance from the C2-*O*-acetyl group (scheme 7.7B).

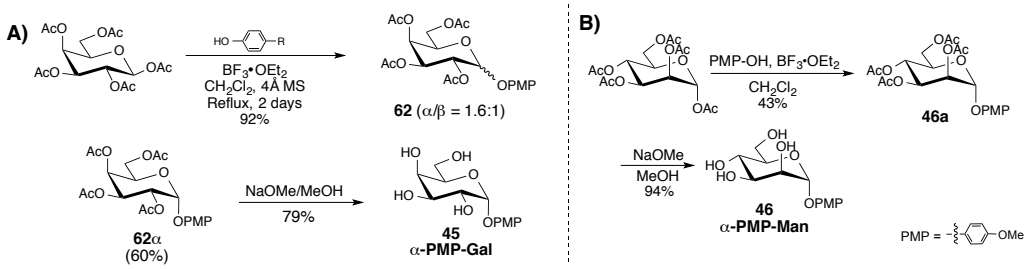

Scheme 7.7 Preparation of A) α-PMP-Gal (**45**) and B) α-PMP-Man (**46**).

In addition to exploring the importance of the configuration of the glycosidic bond on IRI activity, we also sought to explore the importance of the oxygen linking the glucose residue to the aromatic ring for the potent activity of β-PMP-Glc (**2**). Thus, the *O*-glycosidic linkage was replaced with an *N*- or *S*-glycosidic linkage (**47** and **48**, respectively). In addition, *para*-methoxybenzyl-glucopyranoside **49** (β-PMB-Glc) was also prepared to determine if the oxygen-linker needs to be directly attached to the *para*-substituted aryl ring for potent activity. The *N*-linked derivative **47** was prepared by condensation of *para*-anisidine with D-glucose in refluxing ethanol (scheme 7.8A).[48,49] The *S*-linked derivative **48** was prepared by Lewis acid catalyzed (BF_3OEt_2) glycosidation of penta-*O*-acetyl-β-D-glucopyranose with *para*-methoxythiophenol (**48a**), followed by deprotection of the *O*-acetyl protecting groups (scheme 7.8B). β-PMB-Glc (**49**) was prepared from a brominated glucosyl donor[27] and *para*-methoxybenzyl alcohol by activation with silver carbonate to afford intermediate **49a** (scheme 7.8C). Zemplén deacetylation of this intermediate then afforded the desired glycoside **49**.

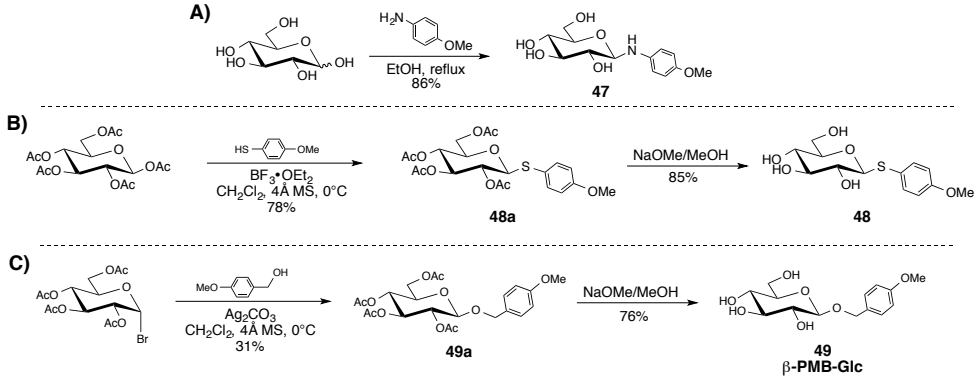

Scheme 7.8 Modifications to *O*-linked β-PMP-Glc. A) Preparation of *N*-linked derivative **47**. B) Preparation of *S*-linked derivative **48**. C) Preparation of β-PMB-Glc (**49**).

We also sought to explore the importance of the C6 hydroxyl for the potent IRI activity exhibited by β-PMP-Glc (**2**). The C6 position was chosen as this hydroxyl group had previously been demonstrated to be influential for the IRI activity of simple monosaccharides, and modifying this position significantly decreased activity (Chapter 5, section 5.2.2). Consequently, β-linked PMP derivatives **50** and **51** were prepared. Derivative **50** contains a methylated C6 hydroxyl to examine the influence of a hydrogen-bond donor at this position as the configuration of the intramolecular hydrogen bonded networks is believed to be controlled by this hydroxyl group (see section 5.2.1 for more discussion).[28,29] This derivative was prepared by methylation of a deprotected C6-OH group on a tri-*O*-benzylated β-PMP-Glc derivative (compound **20** from chapter 5, section 5.2.1, scheme 5.3) with methyl iodide (scheme 7.9A). Hydrogenolysis removed the benzyl protecting groups to afford the C6-*O*-Me-β-PMP-Glc derivative **50**. Derivative **51** contains a one-carbon extension at the C6-OH group and is a β-PMP-linked 6-deoxy-gluco-heptose. It was prepared from an *O*-benzylated precursor that was described in section 5.2.1 (compound **22** in chapter 5, section 5.2.1, scheme 5.3) by hydrogenolysis to remove the benzyl protecting groups (scheme 7.9B).

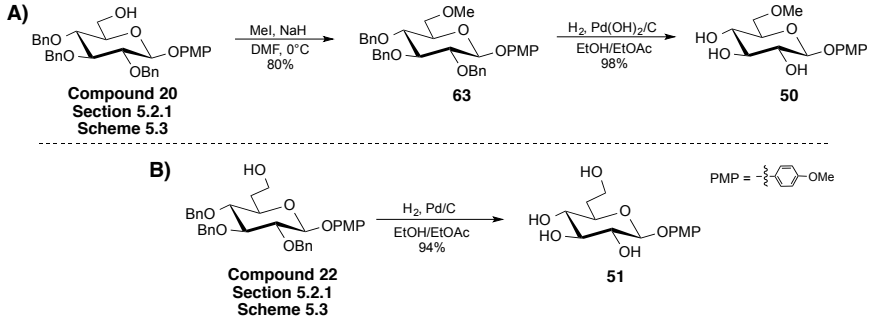

Scheme 7.9 Preparation of C6-modified β-PMP-Glc derivatives. A) Synthesis of C6-*O*-methylated β-PMP-Glc **50**. B) Synthesis of β-PMP-Glc heptose derivative **51**.

Finally, we sought to investigate if conjugating the PMP group to other hydroxyl groups on the glucose moiety would also result in potent IRI activity. Thus, C6-*O*-PMP-Glc derivative **52** was prepared and assessed for IRI activity as the C6-position is not a stereocentre and it is the easiest position to access synthetically. This derivative was prepared in seven steps from methyl-α-D-glucopyranoside (scheme 7.10). Selective formation of the 4,6-benzylidene acetal (**64**) was achieved using benzaldehyde dimethyl acetal and catalytic camphorsulfonic acid,[50,51] and benzylation then provided intermediate **65**. Next, the benzylidene acetal was subjected to a regioselective reductive ring opening to provide 4-*O*-benzylated product **66** with a free C6-OH group. While there are many conditions that can be employed for this transformation,[52-55] the conditions utilized here for the regioselective reductive opening of the benzylidene acetal were borane-THF with TMSOTf (scheme 7.10).[56] The C6-OH was then tosylated (**67**),[57] and this tosyl

group was displaced with *para*-methoxyphenol to provide the protected C6-*O*-PMP derivative **68** (scheme 7.10). Acidic hydrolysis of the anomeric methoxy group, followed by removal of the benzyl protecting groups by hydrogenation afforded the desired C6-*O*-PMP-Glc derivative **52**.

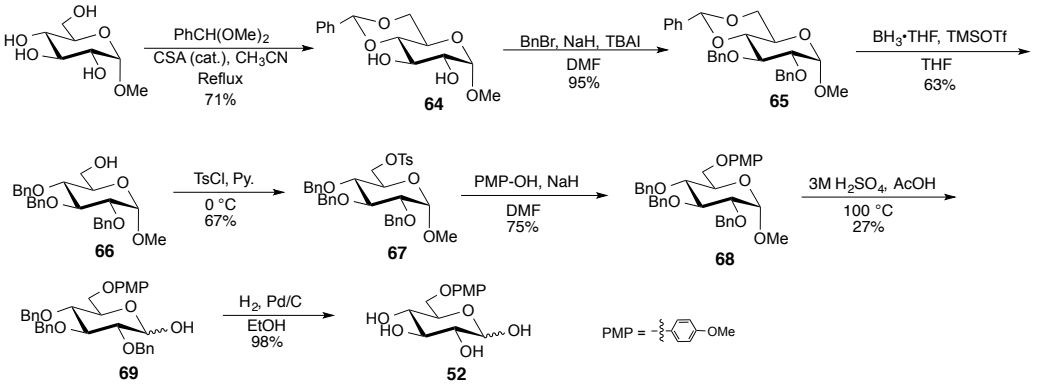

Scheme 7.10 Synthesis of C6-*O*-PMP-Glc derivative **52**.

7.2.4 IRI Activity of β-PMP-Glc Derivatives

The IRI activity of the *meta*- and *ortho*- substituted methoxyphenyl-glucosides **37** and **38** is presented in figure 7.10. These regioisomers of β-PMP-Glc (**2**) were moderate to weakly IRI active, and both were significantly less active than *para*-substituted derivative **2**. This highlights the importance of having the methoxy substituent at the *para*-position on the aryl ring for the potent IRI activity of **2**. Interestingly, the *meta*-substituted hydroxy derivative **39** also exhibited reduced activity compared with *para*-substituted derivative **14**. This result was similar to *meta*-substituted methoxy derivative **37 s**uggesting that even for moderately active derivatives such as **14**, altering the regiochemistry of the substituent on the aryl ring can be detrimental for activity. However, this trend was not maintained for all substitutions of the phenolic aglycone as *meta*-methyl glucoside derivative **40** had identical activity to *para*-methyl derivative **16**, suggesting that IRI activity is also sensitive to the substituent at the *meta*-position. It is interesting to note that of the *para*-substituted glucoside derivatives the presence of a *para*-methoxy substituent resulted in the most potent IRI activity for this series of compounds presented in figure 7.10 (β-PMP-Glc, **2**). However, of the meta-substituted derivatives a methyl substituent resulted in the most potent analogue assessed in this series (compound **40**). However, none of these *meta*- or *ortho*-substituted derivatives exhibited potent IRI activity and all were significantly less active than β-PMP-Glc (**2**).

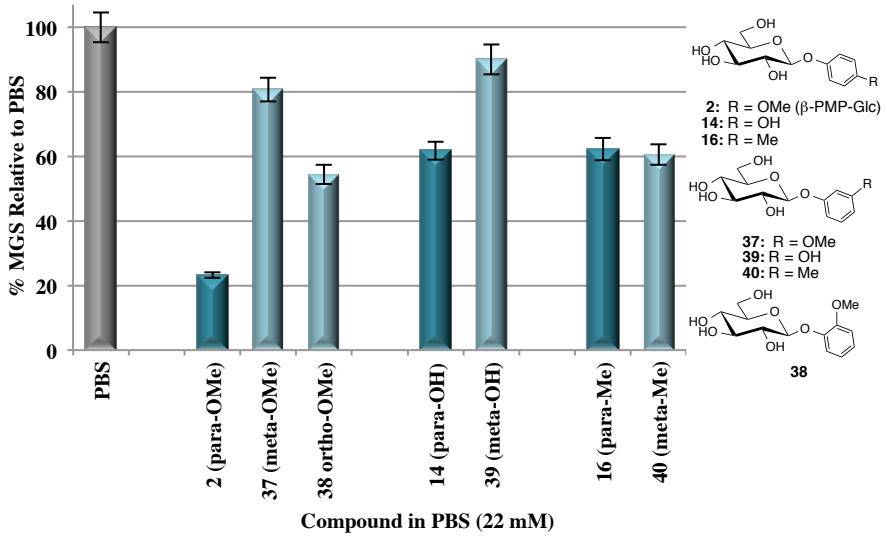

Figure 7.10 IRI activity of *para*-, *meta*- and *ortho*-substituted phenolic-glucosides **2**, **14**, **16** and **37**-**40** at 22 mM in PBS. The % MGS (mean grain size) relative to a PBS positive control is shown for all compounds.

In addition to the regiochemistry of the substituent on the aryl ring, another modification explored for its impact on IRI activity was the stereochemistry of the glycosidic linkage. α-Linked derivatives of PMP-Gal, -Glc and –Man (**43**, **45**-**46**) were thus explored for their ability to inhibit ice recrystallization to compare to the activity of the β-PMP derivatives **1**-**3**. Furthermore, α-linked derivatives of potently IRI active *para*-substituted phenolic-glucosides bearing a bromo- or fluoro-substituent were also explored (**41**-**42**), along with the α-linked derivative of the moderately active Ph-Glc (**44**). These results are presented in figure 7.11.

Both α-PMP-Gal (**45**) and α-PMP-Man (**46**) exhibited a similar ability to inhibit ice recrystallization as the β-linked derivatives β-PMP-Gal (**1**) and β-PMP-Man (**3**) (figure 7.11). This suggests that altering the anomeric configuration of these compounds is not detrimental for activity, but it also does not increase activity as **45** and **46** were weakly IRI active with a MGS 75% of the PBS control. In contrast, modifying the glycosidic linkage to an α- rather than β-linkage for PMP-Glc was detrimental to activity. IRI activity was decreased from the potent activity of β-PMP-Glc (**2**) (23% MGS) to 63% MGS for α-PMP-Glc (**43**). Furthermore, both α-pBrPh-Glc (**41**) and α-pFPh-Glc (**42**) exhibited significantly reduced activity (75-81% MGS) compared to potently IRI active β-pBrPh-Glc (**11**) and β-pFPh-Glc (**13**) (figure 7.11). These results indicate that for the potently IRI active phenolic-glucosides **2**, **11** and **13**, a β-glycosidic linkage is essential for activity. Interestingly, regardless of carbohydrate moiety (Gal, Glc, or Man) or the substituent at the *para*-position of the phenolic aglycone (Br, F, OMe or H), all α-linked phenolic-glycosides exhibited similar moderate IRI activity that ranged from 63-80% MGS relative to the PBS control. Thus, it appears that the IRI activity of the α-linked phenolic-

glycosides is not as sensitive to carbohydrate head-group modifications or aryl-substituent modifications as the β-linked phenolic glycosides.

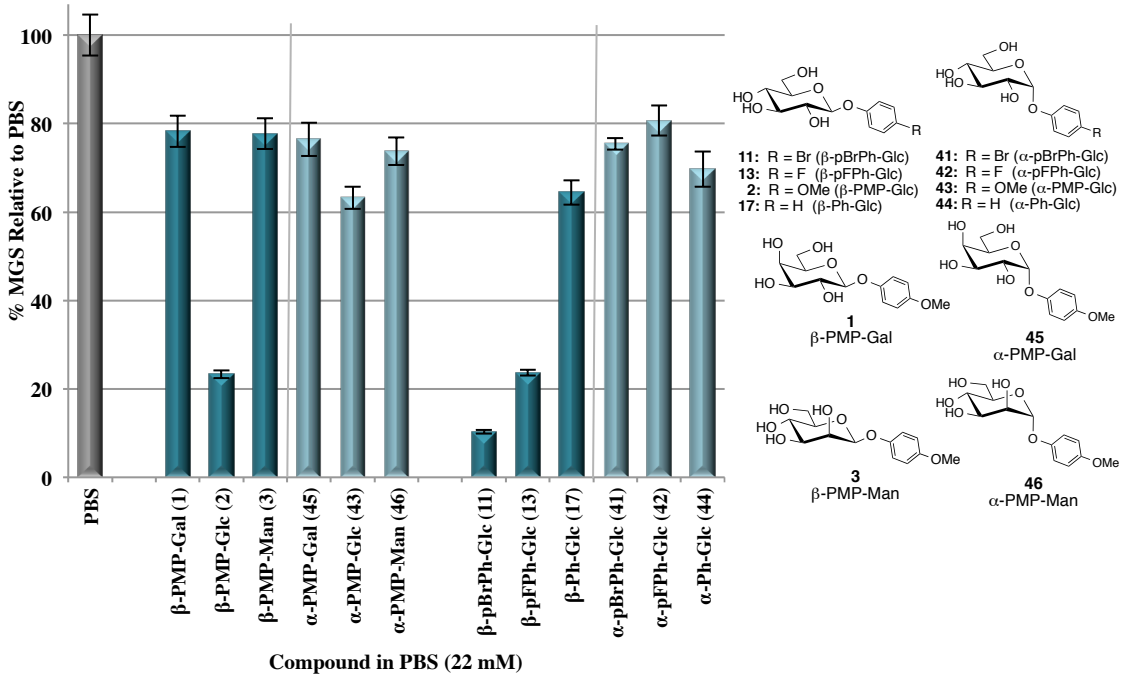

Figure 7.11 IRI activity of α-linked phenolic-glycosides **41**-**46** at 22 mM in PBS. The % MGS (mean grain size) relative to a PBS positive control is shown for all compounds.

Having established the necessity of a β-linkage for the potent activity of β-PMP-Glc (**2**), interest then arose in exploring the importance of an oxygen-linked glycosidic bond. Thus, the *O*-linked PMP moiety was replaced with an *N*-linked PMP (NH, amino group, **47**) and an *S*-linked PMP (thio group, **48**). In addition, β-linked *para*-methoxybenzyl derivative **49** (β-PMB-Glc) possessing a methylene spacer between the *O*-glycosidic bond and the aryl ring was also assessed for its ability to inhibit ice recrystallization. The IRI results for derivatives **47**-**49** in comparison to β-PMP-Glc (**2**) are presented in figure 7.12. It is evident that modifying the *O*-glycosidic linkage is detrimental for the potent activity of **2** because **47**-**49** had drastically decreased IRI activity. Interestingly, the *S*-linked derivative **48** resulted in the greatest decrease in activity compared with β-PMP-Glc despite sulfur containing two free lone pairs and being in a similar column in the periodic table as oxygen. However, it is plausible that the increased carbon-sulfur bond lengths combined with poor orbital overlap making sulfur a poor donor for the *exo*-anomeric effect may alter the preferred conformation of the *S*-linked phenolic-glucoside, thus affecting its ability to inhibit ice recrystallization.[58-62] The β-PMB-Glc derivative **49** resulted in 69% MGS relative to the PBS control, which is markedly decreased from the 23% MGS obtained with β-PMP-Glc

(figure 7.12). This indicates that, in addition to an oxygen atom linking the carbohydrate moiety to the aryl ring, a direct connection of the aryl ring to this C1 oxygen is crucial for potent activity.

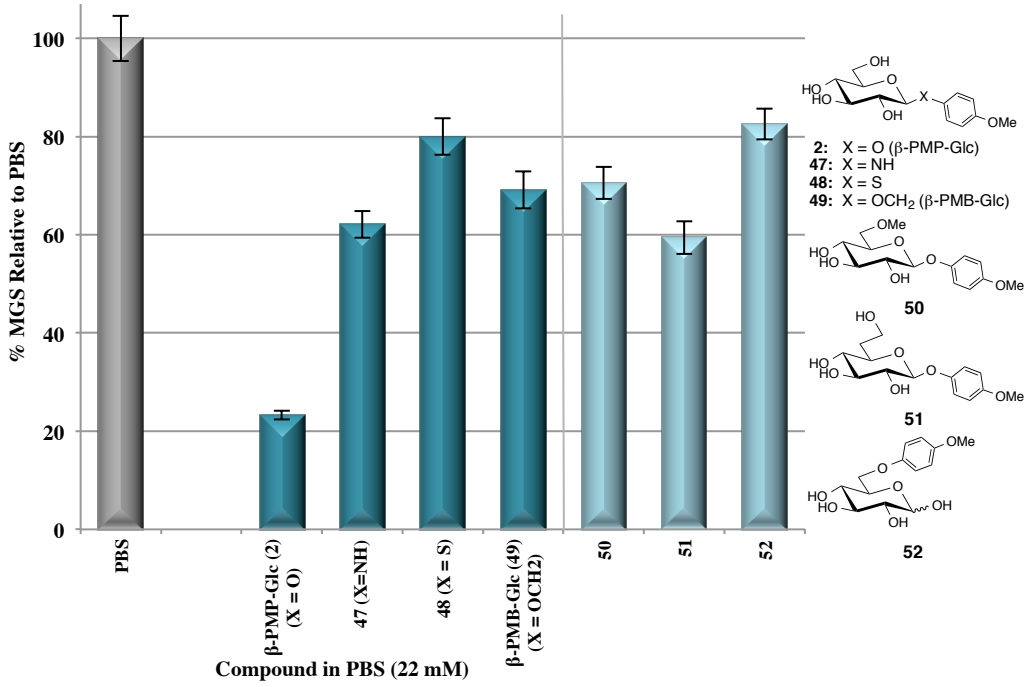

Figure 7.12 IRI activity of *N*- and *S*-linked β-PMP-Glc derivatives **47** and **48**, β-PMB-Glc (**49**), C6-modified β-PMP-Glc derivatives **50** and **51** and C6-O-PMP-Glc (**52**) at 22 mM in PBS. The % MGS (mean grain size) relative to a PBS positive control is shown for all compounds.

The final modifications conducted on the monosaccharide derivative β-PMP-Glc (**2**) to elucidate key structural features that are important for its potent IRI activity were done to the C6-position on the glucose residue. As described in chapter 5, the C6 position of both galactose and glucose is highly influential for their exhibited activity, and modifying this position significantly decreased the moderate activity of these simple monosaccharides (section 5.2.2). Furthermore, β-PMP-Xyl (**4**) was significantly less active than β-PMP-Glc (**2**) (65% MGS for **4** and 23% MGS for **2**), suggesting the C6-OH group of β-PMP-Glc (**2**) is important for its potent activity (figure 7.4, section 7.2.2). This hypothesis is further validated with the IRI results obtained from derivatives **50** and **51** (figure 7.12). Both the C6-OMe β-PMP-Glc derivative **50** and the 6-deoxy-β-PMP-glucoheptose derivative **51** that possesses a one-carbon extension at the C6 position were less active than β-PMP-Glc with 60-70% MGS relative to the PBS control. In addition, conjugating the PMP moiety to the C6 position (6-*O*-PMP-glucoside **52**) resulted in only weak IRI activity indicating that the PMP group must be conjugated to the C1 position of the glucose residue. In fact, C6-*O*-PMP derivative **52** was less IRI active than D-glucose alone (83% MGS for **52**, 77% MGS for D-glucose).

Collectively, the results described in this section with derivatives of IRI active β-PMP-Glc (**2**) indicate that essentially all structural variations and modifications to β-PMP-Glc are highly detrimental for activity. The activity of this compound is sensitive to changes in the relative orientation of hydroxyl groups on the carbohydrate ring, glycosidic-linkage modifications, and changes in aryl group substituents and their position on the aryl ring. The only modification to β-PMP-Glc that is tolerated and retains or increases the activity of this compound is replacing the *para*-methoxy substituent with either a halogen (Br, Cl or F) or a trifluoromethyl group (CF_3). While the exact mechanism by which this compound is exhibiting potent IRI activity is currently not known, it is evident that this activity is specific to β-PMP-Glc (**2**) (and the four *para*-substituted derivatives with Br, Cl, F or CF_3, **11**-**13** and **21**, respectively), making these compounds a very unique class of small molecule potent ice recrystallization inhibitors.

7.2.5 β-linked PMP Containing Di- and Trisaccharide Derivatives

In addition to monosaccharide derivatives containing the PMP moiety, we also sought to explore if the addition of this group to di- and trisaccharides could increase IRI activity. The structures of these di- and trisaccharides are presented in figure 7.13. There was particular interest in investigating the IRI activity of disaccharides in which the PMP moiety was conjugated to a glucose motif, as the monosaccharide β-PMP-Glc (**2**) was highly IRI active (section 7.2.2). Thus, β-linked PMP melibiose derivative **70** and β-linked PMP lactose derivative **73** were prepared and assessed for their ability to inhibit ice recrystallization. In addition, **71** and **72**, which are derivatives of PMP-melibiose, were also prepared to explore the influence of the glycosyl donor moiety at the C6 position and the configuration of the glycosidic-bond on IRI activity.

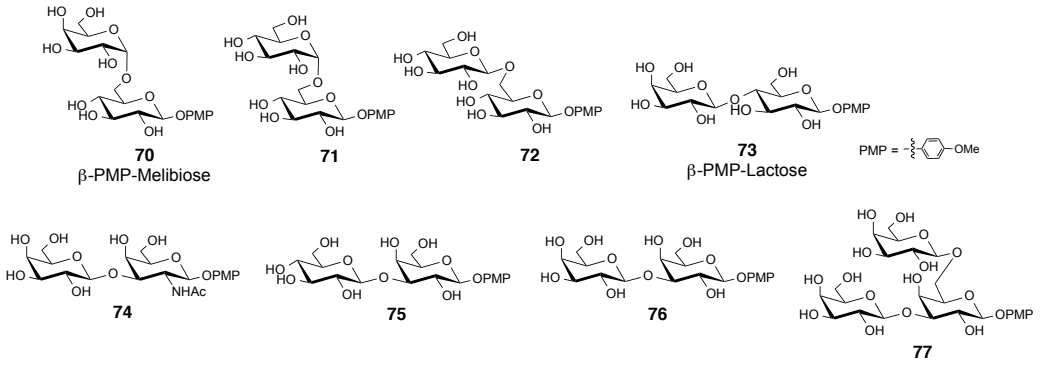

Figure 7.13 Structures of β-linked PMP-containing di- and trisaccharide derivatives **70**-**77**.

There was also interest in investigating the IRI activity of PMP-containing β-(1,3)-linked di- and trisaccharide derivatives (**74**-**77**, figure 7.13). With the exception of **74**, these are structurally similar to the *O*-methylated di- and trisaccharides that were assessed for activity in section 5.3

(chapter 5). The PMP-linked di- and trisaccharides **75**-**77** contain a core β-PMP-Gal moiety and β-PMP-Gal was only weakly IRI active (section 7.2.2). Thus, **75**-**77** were of interest to determine whether additional monosaccharide units would increase the IRI activity of this monosaccharide derivative. Compound **74** is a PMP-linked derivative of the native disaccharide found in potently IRI active AFGPs, β-D-galactosyl-(1-3)-α-*N*-acetyl-D-galactosamine (β-Gal-(1,3)-GalNAc).[63-68] As an *O*-allylated derivative of β-Gal-(1,3)-GalNAc was found to only be moderately IRI active,[4] we sought to explore if the PMP moiety could increase the IRI activity of this disaccharide unit.

Both β-PMP-melibiose and β-PMP-lactose were prepared from melibiose or lactose, respectively (scheme 7.11A-B). Acetylation was achieved with acetic anhydride and sodium acetate, which favoured the formation of the β-OAc at the C1-position.[69] The β-OAc anomer of melibiose was isolated by recrystallization (**78**, scheme 7.11A), whereas the acetylated lactose was used in the glycosidation reactions as a mixture of the two α/β-anomers (**80**, scheme 7.11B). Lewis acid catalyzed glycosidation conditions then afforded the β-linked PMP-disaccharides (**79** for melibiose and **81** for lactose) that were deprotected to provide **70** and **73**. The β-PMP disaccharide derivative of β-Gal-(1,3)-GalNAc (**74**) was prepared from the appropriate acetylated intermediate **74a** (previously prepared by former doctoral student Pawel Czechura)[70] by Zemplén deacetylation (scheme 7.11C).

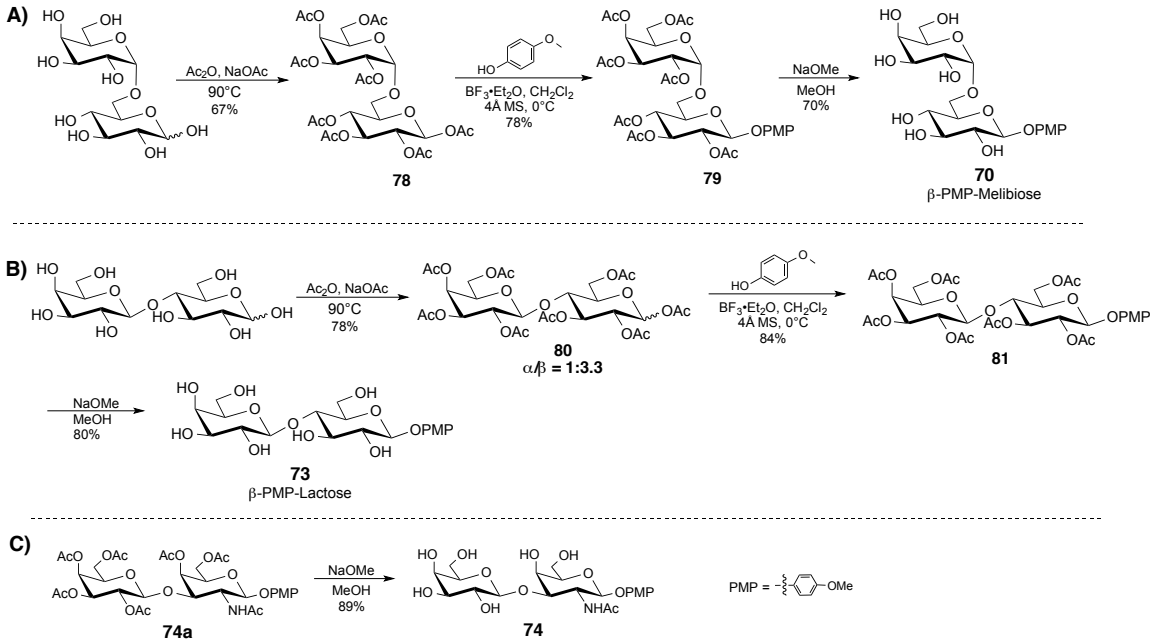

Scheme 7.11 Preparation of A) β-PMP-melibiose (**70**), B) β-PMP-lactose (**73**) and C) β-PMP containing β-Gal-(1,3)-GalNAc (**74**).

Disaccharides **71** and **72** were prepared from glycosyl donor **56** (see scheme 7.5 in section 7.2.3)[46,47] using Lemieux's halide ion catalyzed glycosylation conditions (scheme 7.12).[41-43] The

conditions employed were similar to those described in scheme 7.5 in section 7.2.3 however, a protected β-PMP-glucosyl acceptor was utilized in the coupling. The acceptor that was used in the glycosylation conditions was described previously in chapter 5 (compound **20**, scheme 5.3, section 5.2.1). Under these glycosylation conditions, formation of the α-linked disaccharide was favoured over the β-linked disaccharide, with a diastereomeric ratio of 6:1 (scheme 7.12). The α- and β- disaccharide products could be separated using flash chromatography, and the isolated **82α** or **82β** was deprotected by hydrogenation to provide disaccharides **71** and **72**, respectively (scheme 7.12).

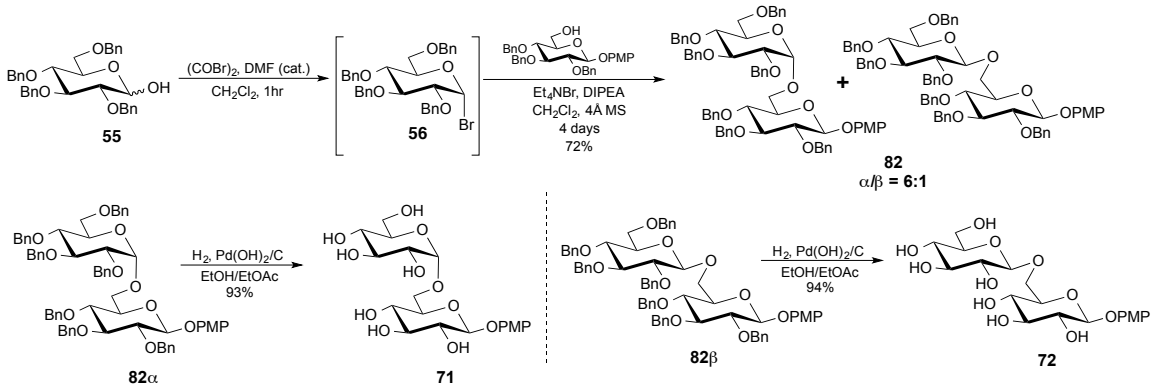

Scheme 7.12 Preparation of β-PMP disaccharides **71** and **72** utilizing Lemieux's halide ion catalyzed glycosylation conditions.

The di- and trisaccharide derivatives **74**-**76** were provided by collaborators in Dr. Mark S. Taylor's laboratory in the Department of Chemistry at the University of Toronto. These compounds were prepared in a similar manner as the methylated di- and trisaccharides described in chapter 5, section 5.3.1. Professor Taylor's synthetic approach involved regioselective activation of an equatorial hydroxyl group of *cis*-1,2-diols on glycosyl acceptors utilizing a diphenylborinic acid catalyst to react with the appropriate galactose or glucose glycosyl donors.[71-76] This method was described in more detail in section 5.3.1 and scheme 5.5 in chapter 5.

The final set of disaccharide derivatives in the phenolic-glycoside class that were assessed for IRI activity were **83**-**86** (figure 7.14). These disaccharides consisted of two monosaccharide units (glucose or galactose) that were connected through a dihydroxybenzene moiety either in a *para*- or *meta*-relationship. Disaccharides **83**-**86** were prepared and assessed for IRI activity by undergraduate student Ross Mancini. *Para*-linked **83** and **84** and *meta*-linked **86** were synthesized by Lewis acid-catalyzed glycosidation with the appropriate glucose or galactose pentaacetylated sugar with hydroquinone (for **83a**-**84a**) or resorcinol (for **86a**) (scheme 7.13A and C).[16] The acetylated disaccharides were then deacetylated to provide the desired products **83**, **84** and **86** to assess for their ability to inhibit ice recrystallization. While these glycosidations

were successful in producing the desired disaccharides, they also produced the mono-glycosylated products **14a**, **27a** or **39a** that could also be deprotected and assessed for IRI activity (see section 7.2.2 for **14a** and **27a** and section 7.2.4 for **39a**). Moreover, glucose derivative **14a** was also utilized to produce the disaccharide **85a** that contains both a glucose and galactose residue in a *para*-substituted relationship on the aryl ring, which was de-acetylated to provide disaccharide **85** (scheme 7.13B).

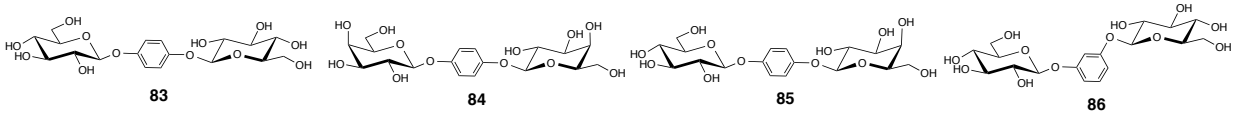

Figure 7.14 Structures of dihydroxybenzene-linked disaccharides **83-86.**

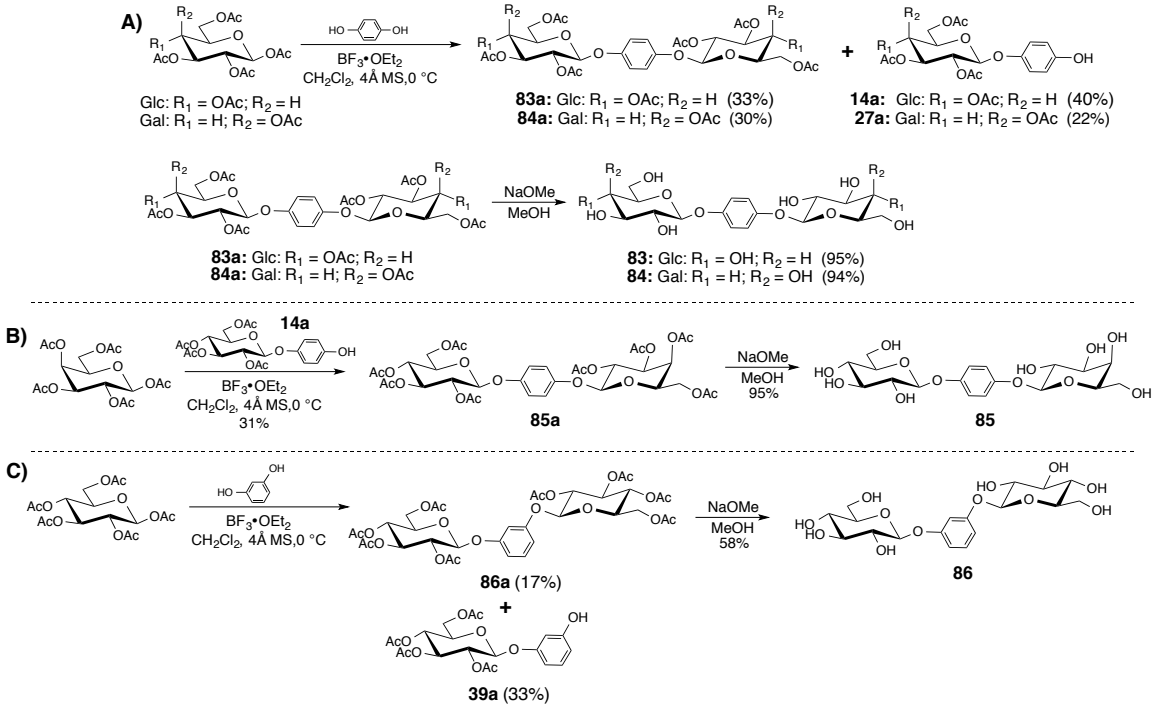

Scheme 7.13 Synthesis of dihydroxybenzene-linked disaccharides **83-86**. A) Preparation of *para*-substituted glucose-based disaccharide **83** and galactose-based disaccharide **84**. B) Preparation of *para*-substituted disaccharide **85** from intermediate **14a**. C) Preparation of *meta*-substituted glucose-based disaccharide **86**.

7.2.6 IRI Activity of β-PMP-Di- and Trisaccharide Derivatives

As described in section 7.2.5 the β-linked PMP moiety was conjugated to various di- and trisaccharides to explore if this group could increase the moderate activity of these carbohydrates. Di- and trisaccharides in which the PMP moiety was conjugated to a reducing glucose or galactose residue were thus assessed for their ability to inhibit ice recrystallization, and these results are shown in figure 7.15. β-PMP-melibiose (**70**) contains an α-galactosyl moiety glycosylated at the C6 position of a β-PMP-Glc residue and this compound was only moderately

IRI active with a MGS 66% of the PBS control. Similarly, PMP-containing disaccharide **71**, which is a derivative of β-PMP-melibiose where a glucosyl moiety has replaced the galactosyl moiety α-linked to the C6 position of β-PMP-Glc, also exhibited moderate IRI activity identical to that of β-PMP-melibiose (**70**). Modifying the α-(1,6)-glycosidic linkage of **71** to a β-(1,6)-linkage between the two glucose residues had no effect on activity as **72** had identical IRI activity as both **70** and **71**. These PMP-containing disaccharides (**70**-**72**) exhibited IRI activity that was similar to melibiose alone, indicating that the addition of the PMP moiety was not able to increase the activity of this disaccharide. In comparison to the "parent" monosaccharide β-PMP-Glc (**2**), all three of these disaccharides (**70**-**72**) resulted in a significant decrease in activity (figure 7.15). The glycosylation of additional carbohydrate residues at the C6 position was detrimental for the potent activity of **2** suggesting that a cooperative effect with increasing monosaccharide residues does not increase IRI activity. This result is consistent with the results presented in chapter 5 with the methylated and reducing di-, tri- and oligosaccharide derivatives (section 5.3).

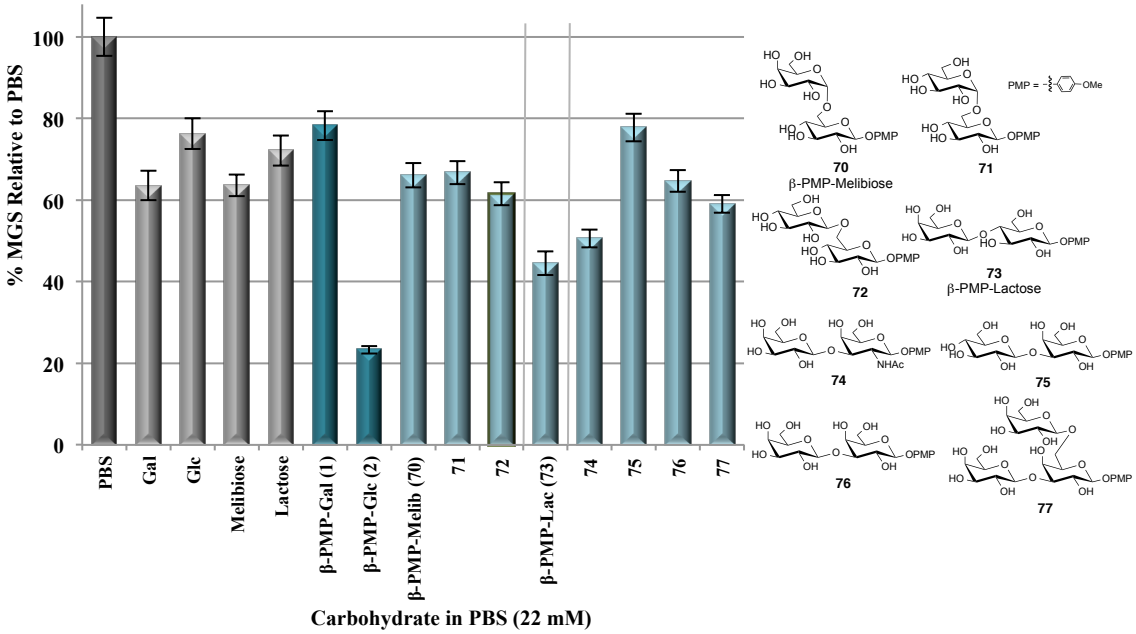

Figure 7.15 IRI activity of β-PMP-linked di- and trisaccharides **70**-**77** at 22 mM in PBS. The % MGS (mean grain size) relative to a PBS positive control is shown for all compounds.

Interestingly, all of the β-PMP-Glc containing disaccharides (**70**-**72**) where the glycosidic bond was at the C6 position of the β-PMP-Glc residue exhibited identical IRI activity (~65% MGS) as the C6-modified PMP-Glc derivatives **50** and **51** (section 7.2.4) and β-PMP-Xyl (**4**) (section 7.2.2). This validates the hypothesis that the C6 position of β-PMP-Glc (**2**) is crucial for its potent activity and an unmodified hydroxyl group at this position is required. However, the C4-position appears to be less influential than the C6 position based on the IRI results of β-PMP-

lactose (**73**) (figure 7.15). While glycosylating the C4 position with a galactosyl moiety (β-PMP-Lac derivative **73**) did reduce activity compared to β-PMP-Glc, this decrease was less drastic than that observed with the C6-glycosylated disaccharides **70**-**72**. β-PMP-lac (**73**) resulted in 45% MGS size relative to the PBS control, whereas **70**-**72** resulted in 65% MGS.

In addition to disaccharides containing a β-PMP-Glc residue as the core, there was also interest in exploring di- and trisaccharide derivatives containing a β-PMP-Gal moiety to determine if cooperative effects from increasing monosaccharide units could increase the weak IRI activity of β-PMP-Gal (**1**). Towards this end, disaccharides **74**-**76** and trisaccharide **77** possessing core β-PMP-Gal residues were assessed for their ability to inhibit ice recrystallization. These results are also described in figure 7.15. Glycosylating the C3 position of β-PMP-Gal with a glucose residue did not increase activity as **75** resulted in identical MGS as β-PMP-Gal (**1**) (78% MGS). However, glycosylating the same position with a more hydrated galactose residue was beneficial and activity increased to 65% MGS for disaccharide **76**. Glycosylation of **76** with an additional galactose unit at the C6 position of the β-PMP-Gal core failed to further increase activity and trisaccharide derivative **77** was as IRI active as disaccharide **76** (60% MGS). Interestingly, replacing the C2-OH group of the β-PMP-Gal core of disaccharide **76** with a C2-acetamido group (disaccharide **74**) was favourable and resulted in an increase from 65% MGS for **76** to 50% for **74**. This was surprising as previous results from our laboratory indicated that the C2-acetamido group did not influence the IRI activity of *O*-allylated disaccharide derivatives of **74** and **76** where the PMP moiety was substituted with an *O*-allyl group (section 5.2.5).[4] Unfortunately, none of the di- and trisaccharide derivatives exhibited potent IRI activity similar to β-PMP-Glc (**2**), indicating that these PMP-containing carbohydrates are not suitable as IRIs.

A second class of disaccharides assessed for their ability to inhibit ice recrystallization were the dihydroxybenzene-linked disaccharides **83**-**86**. These derivatives contained a *para*- or *meta*-substituted phenolic-glucoside or galactoside in which the *para*- or *meta*-substituent was a second β-linked galactose or glucose residue. The structure and IRI activity of these disaccharides (**83**-**86**) is presented in figure 7.16. Interestingly, the *para*-substituted disaccharide **83** that contains two β-linked glucose units glycosidated to the dihydroxybenzene resulted IRI activity that was slightly decreased from β-PMP-Glc (**2**). Thus, it appears that replacing the *para*-methoxy substituent with another glucose residue can retain the potent activity of this phenolic-glycoside. The *para*-substituted disaccharide **84** containing two galactose units resulted in an identical %MGS as the monosaccharide β-PMP-Gal (**1**), indicating that the additional galactose unit at the *para*-position had no effect on IRI (figure 7.16). However, substituting the *para*-methoxy substituent of β-PMP-Gal with a glucose residue (disaccharide **85**) increased activity relative to

84 and **1** (58% for **85** compared with 78% for **84** and **1**). Relative to the di-glucose containing disaccharide **83** and β-PMP-Glc (**2**), the activity of disaccharide **85** possessing both a galactose and glucose moiety *para*-substituted on the dihydroxybenzene was significantly reduced. These results were surprising as this is the first instance where the addition of a less hydrated glucose unit to disaccharide derivatives increased IRI activity, whereas the addition of a more hydrated galactose unit was detrimental for activity. Finally, the *meta*-substituted dihydroxybenzene disaccharide **86** possessing two glucose units was less IRI active than *para*-substituted disaccharide **84**. This result is in agreement with the IRI activity of the previously described *meta*-methoxy PMP-Glc derivative **37** (section 7.2.4) and further highlights the importance of regiochemistry for the potent activity of these novel phenolic-glucoside ice recrystallization inhibitors.

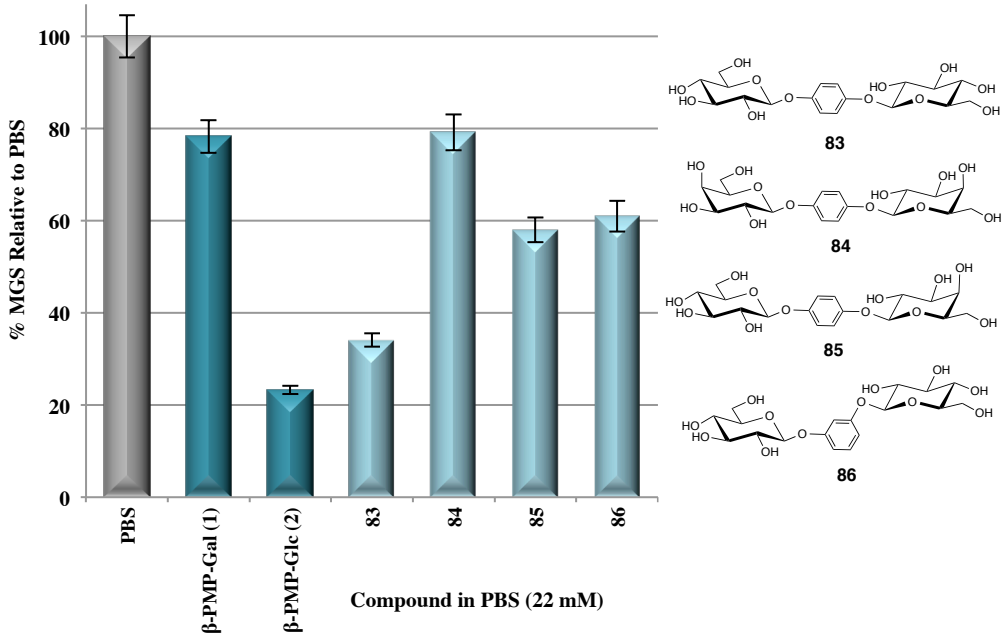

Figure 7.16 IRI activity of dihydroxybenzene-linked disaccharides **83**-**86** at 22 mM in PBS. The % MGS (mean grain size) relative to a PBS positive control is shown for all compounds.

7.3 Quantifying the Relative Rates of Different IRI Active Small Molecules

As described in section 1.1.2, ice recrystallization is a thermodynamically driven Ostwald ripening process that results in an overall reduction in energy of the ice crystal-QLL (Quasi-liquid layer) interface by large ice crystals growing larger at the expense of small crystals.[15,37,38] This process leads to an overall reduction in the number of ice crystals with an increase in mean ice crystal size with an overall constant volume. The rate of ice recrystallization is dependent upon temperature and is most prevalent at temperatures slightly below 0°C.[3,15,37,38,77] It is also dependent

upon the presence of an inhibitor, as well as the type and concentration of inhibitor utilized to calculate the rate.[15,38,77-81]

Many reports have approximated the kinetics of ice recrystallization in the presence of an inhibitor using Lifshitz Slyozov Wagner (LSW) theory of Ostwald ripening.[15,37,38,77,79,80,82,83] LSW theory suggests that at constant temperature the increase in mean ice crystal radius (r) should follow equation 7.2 where r_0 is the initial mean radius when time (t) equals zero and k_d is the observed rate constant of recrystallization. The recrystallization rate (k_d) can be obtained by this relationship by the slope of r^3 (cubed mean radius) *versus* time. The mechanism by which LSW theory of Ostwald ripening approximates recrystallization is diffusional growth. Diffusional growth is the diffusion of water molecules from smaller to larger ice crystals through an intermediate liquid layer, such as the QLL. However, this liquid layer must occupy most of the volume of the sample as ice crystals cannot be in direct contact, resulting in a small total ice volume fraction and a large total liquid volume fraction during the recrystallization process.[15,37,77] A sucrose-based IRI assay can approximate ice recrystallization kinetics using LSW theory as it results in a large volume of liquid in between ice crystals due to the high concentrations of sucrose (30-45% w/v) that are typically used for the analyte solvent and positive control for ice recrystallization.[15,37,77,84,85] Unfortunately, the IRI assay utilized by our laboratory employs PBS as the solvent for analytes and not a sucrose solution, and thus LSW theory cannot be used to determine the kinetics of ice recrystallization. Our assay results in a large ice crystal volume with a small total liquid volume and crystals are in close proximity to each other. This results in calculated r^3 and ice crystal diameters exceeding the thickness and total volume of the sample in the IRI assay, and underestimates the total volume of the QLL.[37] Thus, it is not an accurate approximation for ice recrystallization kinetics using the PBS assay. While Ostwald ripening of polycrystalline ice at high ice volume fractions is hypothesized to occur by accretion, this is also not an accurate model of ice recrystallization as it suggests that two ice crystals directly coalesce to form a single larger ice crystal.[15] As described in section 1.1.2, ice recrystallization occurs by bulk-water molecules transferring to the QLL, then subsequently from the QLL to the growing ice lattice.[1,86,87]

$$r^3(t) = r_0^3 + k_d t$$

Equation 7.2 Rate of recrystallization based on LSW theory

While at the present time there is not an appropriate model for the kinetics of ice recrystallization with large ice crystal volume and small total liquid volume as observed with the PBS IRI assay utilized by our laboratory, we sought to explore the dependence of ice crystal size as a function of time and concentration of inhibitor. Towards this end, the mean ice crystal area observed with the PBS positive control was measured over a range of time increments from 0 min

(initial transfer from -80 °C to the annealing temperature) to 120 min at constant annealing temperature of -6.4°C. Additionally, these measurements were repeated with two different inhibitors of ice recrystallization, one with moderate activity at 22 mM and the other with potent activity at 22 mM. The moderate inhibitor utilized for this study was D-galactose and the potent inhibitor was β-PMP-Glc (**2**). Finally, the effect of inhibitor concentration was also examined using these time-dependent IRI studies. The profiles of mean ice crystal area *versus* time for galactose solutions of 22, 55, 110 and 220 mM and β-PMP-Glc solutions of 5.5, 11 and 22 mM were determined. The profiles for PBS and various concentrations of galactose are shown in figure 7.17A and figure 7.17B shows the profiles for PBS and β-PMP-Glc (**2**).

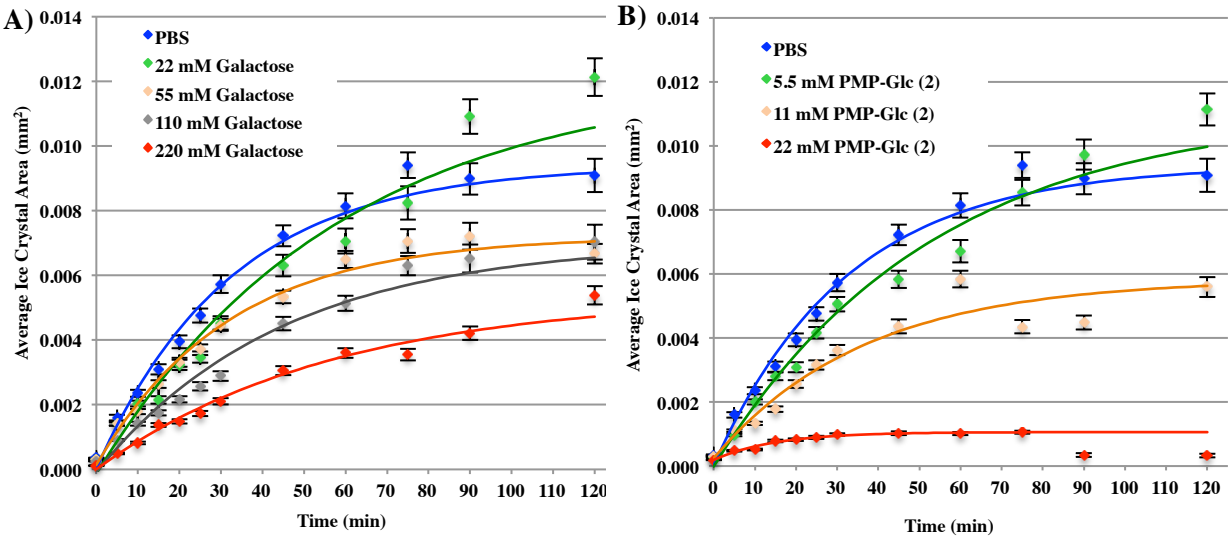

Figure 7.17 Relationship between time and mean ice crystal area (in mm^2) for ice recrystallization in the presence of A) galactose at 22, 55, 110 and 220 mM in PBS and B) β-PMP-Glc (**2**) at 5.5, 11 and 22 mM in PBS.

The results of the PBS curve indicate that past the 30 min annealing time employed in our labortory's IRI assay the mean ice crystal area continues to increase (figure 7.17A and B). It appears that ice crystal size for the PBS solution initially increases in an exponential type manner, and that the size of the crystals start to remain constant at a large area around 75 min. Interestingly, a 22 mM galactose solution at 30 min results in a mean ice crystal size that is 64% that of the mean PBS ice crystal size.[1] However, extending the recrystallization time past 30 min results in ice crystal sizes that are similar to that of the PBS control (figure 7.17A). In fact, the ice crystal size of a 22 mM galactose solution at 120 min is larger than that of PBS. This was surprising and suggested that the end-points of recrystallization are different for various solutions with or without inhibitors. This hypothesis is further validated when observing the profiles of the different concentrations of the galactose ice recrystallization inhibitor (figure 7.17A). All concentrations resulted in an exponential type curve with the observed mean ice crystal size

becoming consistent over time at approximately 75 minutes. However, the final ice crystal size or end point at 120 min varied depending upon the concentration of the galactose solution. At 120 min, a 22 mM galactose solution had ice crystals sizes greater than the PBS control, whereas 55 mM and 110 mM galactose solutions had a final ice crystal size that was approximately 66% of the PBS control. Interestingly, at 30 min both 22 and 55 mM galactose solutions resulted in identical ice crystal sizes (64% of the PBS control), whereas 110 mM has smaller ice crystal sizes that were half that of the PBS control. A 220 mM solution of galactose resulted in ice crystal sizes that were 33% of the PBS control at 30 min, however at 120 min the ice crystal sizes were half that of PBS. Thus, not only is IRI activity dependent upon the concentration of the inibitor, but end-points of recrystallization and ice crystal size can vary drastically depending on annealing time.

Similar results were observed for the inhibitor β-PMP-Glc (figure 7.17B). A 5.5 mM solution of β-PMP-Glc had a time-dependent IRI profile that was similar to that of PBS, indicating that at this concentration inhibition of ice recrystallization is not occuring. Increasing the concentration to 11 mM resulted in significantly smaller ice crystal sizes over all time points. Ice crystal sizes of the 11 mM β-PMP-Glc solution remained constant at approximately 45 min and were half the size of the PBS control and 5.5 mM β-PMP-Glc up to 120 min. The most interesting curve is that of the 22 mM β-PMP-Glc (figure 7.17B). Ice crystal sizes with this solution remain consistently very small beginning at an early time point (10-15 min) and past this time they do not appear to grow larger. Thus, the end-point of recrystallization in the presence of β-PMP-Glc at 22 mM is achieved at a very early stage in the recrystallization process and this potent inhibitor prevents further growth of ice crystal up to 120 min.

The results from this study provide insight into the mechanism of action of these ice recrystallization inhibitors. It appears that moderate inhibitors of ice recrystallization such as a 22 mM galactose solution, act similarly to "reversible" inhibitors. While initially (up to 30 min) inibition of ice recrystallization is occuring resulting in smaller ice crystals sizes than the PBS control, over time this inhibition is lost and ice crystal sizes are similar to the PBS control. Increasing the concentration of the galactose inhibitor can abolish this loss in inhibition activity over time, as is evident with the 55, 110 and 220 mM solutions resulting is signficantly small ice crystal sizes at 120 min compared with the PBS control (figure 7.17B). The higher concentrations of galactose and the β-PMP-Glc inhibitor at at 11 and 22 mM however appear to act more as "irreversible" inhibitors. In particular, this is observed with a 22 mM β-PMP-Glc solution where the initial potent inhibition of ice recrystallization observed at an early stage in the recrystallization process, and is maintained throughout the entire time period of 120 min (figure

7.17B). Thus, overall these results highlight how at constant temperature, ice recrystallization inhibition occurs *via* different methods depending upon the type of inhibitor used and its concentration, and the total time alotted for ice recrystallization before quantifying ice crystal size. However, further studies are still required to determine recrystallization rate constants in the presence of these inhibitors and inhibition constants to elucidate the type of inhibition occuring during the process of recrystallization using a method that accurately approximates the mechanism of ice recrystallization.

7.4 Summary and Conclusions for the IRI Activity of Phenolic-Glycosides

Overall this chapter has described the discovery of an anomalous potent small molecule inhibitor of ice recrystallization β-PMP-Glc (**2**). This derivative is the first glucopyranose-based derivative exhibiting potent IRI activity while the analogous galactopyranose-based derivative was IRI inactive. Extensive structure-function studies on β-PMP-Glc (**2**) indicated that essentially all structural variations and modifications to β-PMP-Glc are highly detrimental for activity (sections 7.2.2 and 7.2.4). Changes in the relative orientation of hydroxyl groups on the carbohydrate residue, glycosidic-linkage modifications, and changes in aryl group substituents and their position all resulted in a drastic decrease in IRI activity. The only modification to β-PMP-Glc that was tolerated and retained or increased the activity of this compound was replacing the *para*-methoxy substituent with select functional groups or atoms. Halogens (Br, Cl or F, derivatives **11**-**13**) or a trifluoromethyl group (CF_3, derivative **21**) at the *para*-position of the phenolic-glucoside resulted in potently IRI active carbohydrate derivatives. Furthermore, it was determined that similar to simple monosaccharides (chapter 5), the C6 hydroxyl group of β-PMP-Glc is crucial for its potent activity and all modifications to this position reduced activity (section 7.2.4). Moreover, while conjugating the PMP moiety to a glucose residue resulted in potent activity, this appears to be unique to glucose as all other PMP-containing mono-, di- and trisaccharide derivatives were only moderately to weakly IRI active (sections 7.2.2 and 7.2.6).

Insights into the mechanism of ice recrystallization inhibition from time- and concentration-dependent measurements of ice crystal sizes highlight how recrystallization end-points vary depending upon the type of inhibitor (section 7.3). In the case of the inhibitor β-PMP-Glc at 22 mM, potent inhibition occurs at a very early stage in the recrystallization process and this is maintained throughout longer time periods resulting in very small ice crystal sizes even after 120 min. Unfortunately, the exact mechanism by which this compound is exhibiting potent IRI activity is currently not known. However, the structure-function studies described above have elucidated key structural requirements for these molecules that are necessary for potent activity.

Furthermore, it is known that both β-PMP-Glc (**2**) and β-pBrPh-Glc (**11**) are not acting by binding to ice or interacting with the ice lattice (section 7.2.2). Thus, these novel potent small molecule ice recrystallization inhibitors are ideal candidates for use in cryopreservation, as they do not possess the undesirable thermal hysteresis antifreeze activity. As such, these phenolic-glycosides have been examined for their potential in cryopreservation experiments utilizing various different cell types to elucidate if these novel IRIs are also effective cryoprotectants (described in Chapter 8).

7.5 Experimental Procedures and Compound Characterizations for Chapter 7

Ice Recrystallization Inhibition (IRI) Assay:

Sample analysis for IRI activity was performed using the "splat cooling" method as previously described.[88] In this method, the analyte was dissolved in phosphate buffered saline (PBS) solution and a 10 μL droplet of this solution was dropped from a micropipette through a two meter high plastic tube (10 cm in diameter) onto a block of polished aluminum precooled to approximately -80 °C. The droplet froze instantly on the polished aluminum block and was approximately 1 cm in diameter and 20 μm thick. This wafer was then carefully removed from the surface of the block and transferred to a cryostage held at -6.4 °C for annealing. After a period of 30 min, the wafer was photographed between crossed polarizing filters using a digital camera (Nikon CoolPix 5000) fitted to the microscope. A total of three images were taken from each wafer. During flash freezing, ice crystals spontaneously nucleated from the supercooled solution. These initial crystals were relatively homogeneous in size and quite small. During the annealing cycle, recrystallization occurred, resulting in a dramatic increase in ice crystal size. A quantitative measure of the difference in recrystallization inhibition of two compounds X and Y is the difference in the dynamics of the ice crystal size distribution. Image analysis of the ice wafers was performed using a novel domain recognition software (DRS) program.[89] This processing employed the Microsoft Windows Graphical User Interface to allow a user to visually demarcate and store the vertices of ice domains in a digital micrograph. The data was then used to calculate the domain areas. All data was plotted and analyzed using Microsoft Excel. The mean grain (or ice crystal) size (MGS) of the sample was compared to the MGS of the control PBS solution for that same day of testing. IRI activity is reported as the percentage of the MGS (% MGS) relative to the PBS control, and the % MGS for each sample was plotted along with its standard error of the mean. Small percentages represent a small MGS (small ice crystals), which is indicative of high IRI activity.

Thermal Hysteresis (TH) Assay:

Nanolitre osmometry was performed using a Clifton nanoliter osmometer (Clifton Technical Physics, Hartford, NY), as described by Chakrabartty and Hew.[39] All of the measurements were performed in doubly distilled water. Ice crystal morphology was observed through a Leitz compound microscope equipped with an Olympus 20× (infinity-corrected) objective, a Leitz Periplan 32X photo eyepiece, and a Hitachi KPM2U CCD camera connected to a Toshiba MV13K1 TV/VCR system. Still images were captured directly using a Nikon CoolPix digital camera.

General Experimental:

All anhydrous reactions were performed in flame-dried glassware under a positive pressure of dry argon. Air or moisture-sensitive reagents and anhydrous solvents were transferred with oven-dried syringes or cannulae. All flash chromatography was performed with E. Merck silica gel 60 (230-400 mesh). All solution phase reactions were monitored using analytical thin layer chromatography (TLC) with 0.2 mm pre-coated silica gel aluminum plates 60 F254 (E. Merck). Components were visualized by illumination with a short-wavelength (254 nm) ultra-violet light and/or staining (ceric ammonium molybdate, potassium permanganate, or phosphomolybdate stain solution). All solvents used for anhydrous reactions were distilled. Tetrahydrofuran (THF) and diethyl ether (Et_2O) were distilled from sodium/benzophenone under nitrogen. Dichloromethane (DCM) was distilled from calcium hydride. *N,N*-dimethylformamide (DMF) was stored over activated 4Å molecular sieves under argon. ^1H (400 or 500 MHz) and ^{13}C NMR (100 or 125 MHz) spectra were recorded at ambient temperature on a Bruker Avance 400, Bruker Avance 500, or Varian Inova 500 spectrometer. Deuterated chloroform ($CDCl_3$) or water (D_2O) were used as NMR solvents, unless otherwise stated. Chemical shifts are reported in ppm using the solvent residual peak as an internal standard. Splitting patterns are designated as follows: s, singlet; d, doublet; t, triplet; q, quartet; quint, quintet; m, multiplet and br, broad. Low resolution mass spectrometry (LRMS) was performed on a Micromass Quatro-LC Electrospray spectrometer with a pump rate of 20 μL/min using electrospray ionization (ESI).

NMR spectra for novel compounds and final compounds assessed for IRI activity are provided. β-linked *para*-methoxyphenyl derivatives **5** and **75**-**77** were generously provided by Dr. Mark Taylor.[49,50] Compounds **15**, **18**, **20**, **28**, **31**-**33** and **38** were prepared by a former Master's student in our laboratory, Mathew Alteen. Compound **26**, **29**-**30** and **34**-**35** were prepared by a former

doctoral student, John Trant, with assistance from an undergraduate student at the time, Malay Doshi.[25] Disaccharide **74a** was prepared by a former doctoral student Pawel Czechura.[70]

4-Methoxyphenyl-2,3,4,6-tetra-O-acetyl-β-D-galactopyranoside (1a)

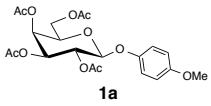

1a

To a mixture of 1,2,3,4,6-penta-*O*-acetyl-β-D-galactopyranose (5.0 g, 12.8 mmol), 4-methoxyphenol (2.22 g, 17.9 mmol) and 4 Å MS in anhydrous CH_2Cl_2 (50 mL) stirring at 0 °C under Ar, was slowly added boron trifluoride diethyl etherate (2.09 mL, 16.6 mmol)**.** The reaction mixture was stirred overnight, then diluted with CH_2Cl_2 and quenched with sodium bicarbonate. The solution was filtered through Celite®, then extracted with CH_2Cl_2. The organic layer was washed with sodium bicarbonate, water, saturated brine, then dried over $MgSO_4$ and concentrated. Column chromatography (3:1 hexanes/ethyl acetate) afforded **1a** as a white powder (5.3 g, 91%). Characterization data is consistent with that previously reported.[17] ^{1}H NMR (500 MHz, $CDCl_3$): δ 6.97-6.94 (m, 2H), 6.84-6.80 (m, 2H), 5.47-5.44 (m, 2H), 5.09 (dd, *J* = 10.4, 3.4 Hz, 1H), 4.92 (d, *J* = 8.0 Hz, 1H), 4.23 (dd, *J* = 11.3, 6.8 Hz, 1H), 4.16 (dd, *J* = 11.3, 6.5 Hz, 1H), 4.02-3.99 (m, 1H), 3.78 (s, 3H), 2.18 (s, 3H), 2.09 (s, 3H), 2.06 (s, 3H), 2.01 (s, 3H). ^{13}C NMR (100 MHz, $CDCl_3$): δ 170.3, 170.0, 169.4, 169.3, 155.8, 150.9, 118.7, 114.5, 100.7, 72.4, 71.3, 70.2, 66.3, 61.4, 55.5, 20.7, 20.6, 20.6, 20.5. LRMS (ESI): *m/z* calcd. for $C_{21}H_{30}NO_{11}$ $[M+NH_4]^+$ 472.5; found, 472.3.

4-Methoxyphenyl-β-D-galactopyranoside (1)

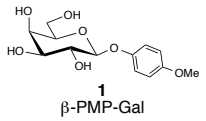

1
β-PMP-Gal

Compound **1a** (5.3 g, 11.6 mmol) was dissolved in a solution of sodium methoxide in methanol (25 mL) and stirred for one hour at room temperature. The solution was then neutralized with Amberlite® IR-120 (H^+) ion-exchange resin and filtered. The filtrate was concentrated and the product was lyophilized to yield **1** as a white powder (3.3 g, 98%). Characterization data is consistent with that previously reported.[17] ^{1}H NMR (400 MHz, CD_3OD): δ 7.08-7.04 (m, 2H), 6.85-6.81 (m, 2H), 4.72 (d, *J* = 7.7 Hz, 1H), 3.89 (dd, *J* = 3.4, 0.8 Hz, 1H), 3.78-3.74 (m, 3H), 3.74 (s, 3H), 3.63 (ddd, *J* = 6.7, 5.5, 1.1 Hz, 1H), 3.55 (dd, *J* = 9.7, 3.4 Hz, 1H). ^{13}C NMR (101 MHz, D_2O): δ 154.6, 151.0, 118.1, 115.0, 101.7, 75.4, 72.6, 70.6, 68.5, 60.7, 55.8. LRMS (ESI): *m/z* calcd. for $C_{13}H_{18}NaO_7$ $[M+Na]^+$ 309.3; found, 309.3.

4-Methoxyphenyl-2,3,4,6-tetra-O-acetyl-β-D-glucopyranoside (2a)

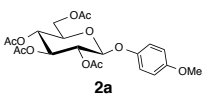

2a

To a mixture of 1,2,3,4,6-penta-*O*-acetyl-β-D-glucopyranose (15 g, 38.4 mmol), 4-methoxyphenol (6.7 g, 53.8 mmol) and 4 Å MS in anhydrous CH_2Cl_2 (100 mL) stirring at 0 °C under Ar, was slowly added boron trifluoride diethyl etherate

(9.64 mL, 76.8 mmol). The reaction mixture was stirred overnight, then diluted with CH_2Cl_2 and quenched with sodium bicarbonate. The solution was filtered through Celite®, then extracted with CH_2Cl_2. The organic layer was washed with sodium bicarbonate, water, saturated brine, then dried over $MgSO_4$ and concentrated. Column chromatography (6:4 hexanes/ethyl acetate) afforded **2a** as a white powder (13.6 g, 78%). Characterization data is consistent with that previously reported.[16] ^{1}H NMR (300 MHz, $CDCl_3$): δ 6.97-6.92 (m, 2H), 6.84-6.78 (m, 2H), 5.31-5.20 (m, 2H), 5.16 (t, *J* = 9.6 Hz, 1H), 4.95 (d, *J* = 7.6 Hz, 1H), 4.29 (dd, *J* = 12.3, 5.2 Hz, 1H), 4.18 (dd, *J* = 12.3, 2.5 Hz, 1H), 3.83-3.79 (m, 1H), 3.77 (s, 3H), 2.08 (s, 3H), 2.07 (s, 3H), 2.04 (s, 3H) 2.03 (s, 3H). ^{13}C NMR (75 MHz, $CDCl_3$): δ 170.6, 170.3, 169.4, 169.3, 155.8, 150.9, 118.7, 114.5, 100.3, 72.7, 71.9, 71.2, 68.3, 61.9, 55.6, 20.7, 20.7, 20.6, 20.6. LRMS (ESI): *m/z* calcd. for $C_{21}H_{30}NO_{11}$ $[M+NH_4]^+$ 472.5; found, 472.2; *m/z* calcd. for $C_{21}H_{26}NaO_{11}$ $[M+Na]^+$ 477.4; found, 477.1.

4-Methoxyphenyl-β-D-glucopyranoside (2)

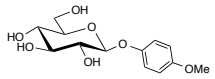

2
β-PMP-Glc

Compound **2a** (6.75 g, 14.9 mmol) was dissolved in a solution of sodium methoxide in methanol (25 mL) and stirred for one hour at room temperature. The solution was then neutralized with Amberlite® IR-120 (H^+) ion-exchange resin, filtered and concentrated. The filtrate was concentrated and the product was lyophilized to yield **2** as a white powder (4.1 g, 95%). ^{1}H NMR (400 MHz, D_2O): δ 7.14-7.10 (m, 2H), 7.01-6.96 (m, 2H), 5.01 (d, *J* = 7.6 Hz, 1H), 3.92 (dd, *J* = 12.4, 2.2 Hz, 1H), 3.81 (s, 3H), 3.75 (dd, *J* = 12.4, 5.7 Hz, 1H), 3.62-3.54 (m, 3H), 3.48 (dd, *J* = 9.6, 9.2 Hz, 1H). ^{13}C NMR (101 MHz, D_2O): δ 154.7, 150.9, 118.2, 115.0, 101.2, 76.1, 75.5, 72.9, 69.4, 60.5, 55.8. LRMS (ESI): *m/z* calcd. for $C_{13}H_{18}NaO_7$ $[M+Na]^+$ 309.3; found, 309.3.

4-Methoxyphenyl-2,3,4-tri-O-acetyl-β-D-xylopyranoside (4a)

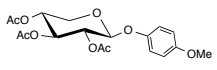

4a

Compound **4a** was prepared in a similar manner as **2a** from 1,2,3,4-penta-*O*-acetyl-β-D-xylopyranose (340 mg, 1.07 mmol), 4-methoxyphenol (186 mg, 1.5 mmol) with boron trifluoride diethyl etherate (402 μL, 3.2 mmol). Column chromatography (7:3 hexanes/ethyl acetate) afforded **4a** as a white powder (228 mg, 60%). Characterization data is consistent with that previously reported.[90] ^{1}H NMR (500 MHz, $CDCl_3$): δ 6.94 (d, *J* = 9.1 Hz, 2H), 6.82 (d, *J* = 9.1 Hz, 2H), 5.22 (t, *J* = 8.1 Hz, 1H), 5.15 (dd, *J* = 8.2, 6.4 Hz, 1H), 5.03-4.99 (m, 2H), 4.20 (dd, *J* = 12.0, 4.8 Hz, 1H), 3.77 (s, 3H), 3.47 (dd, *J* = 12.0, 8.1 Hz, 1H), 2.09 (s, 3H), 2.07 (s, 3H), 2.07 (s, 3H). ^{13}C NMR (126 MHz, $CDCl_3$): δ 167.0, 169.8,

169.4, 155.6, 150.6, 118.5, 114.6, 99.8, 71.0, 70.4, 68.6, 61.9, 55.6, 20.7, 20.7. LRMS (ESI): *m/z* calcd. for $C_{18}H_{22}NaO_9$ $[M+Na]^+$ 405.4; found, 405.3.

4-Methoxyphenyl-β-D-xylopyranoside (4)

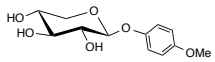

4: β-PMP-Xyl

Compound **4a** (74 mg, 0.19 mmol) was dissolved in a solution of sodium methoxide in methanol (5 mL) and stirred for one hour at room temperature. The solution was then neutralized with Amberlite® IR-120 (H^+) ion-exchange resin, filtered and concentrated. The filtrate was concentrated and the product was lyophilized to yield **4** as a white powder (44 mg, 89%). Characterization data is consistent with that previously reported.[91] ^{1}H NMR (500 MHz, D_2O): δ 7.12-7.09 (m, 2H), 7.00-6.97 (m, 2H), 4.97 (d, *J* = 7.5 Hz, 1H), 4.00 (dd, *J* = 11.6, 5.5 Hz, 1H), 3.82 (s, 3H), 3.72-3.68 (m, 1H), 3.56-3.50 (m, 2H), 3.43 (dd, *J* = 11.5, 10.6 Hz, 1H). ^{13}C NMR (126 MHz, D_2O): δ 154.8, 150.6, 118.3, 115.0, 101.8, 75.5, 72.8, 69.0, 65.1, 55.7. LRMS (ESI): *m/z* calcd. for $C_{12}H_{16}NaO_6$ $[M+Na]^+$ 279.2; found, 279.4.

Ethyl 2,3,4,6-tetra-O-acetyl-1-thio-α-D-mannopyranoside (6)

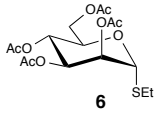

6

To a solution of D-mannose (2.0 g, 11.1 mmol) in dry pyridine (45 mL) was added acetic anhydride (26 mL) and the reaction mixture was stirred at 0 °C for 1 hour. A catalytic amount of 4-dimethylaminopyridine was added and the mixture was stirred at room temperature overnight. Ethanol was added and the solvent was evaporated under *in vacuo* and the residue was diluted in ethyl acetate, washed with sodium bicarbonate, water and brine. The mixture was dried with $MgSO_4$, filtered and concentrated. The crude product was then added to a solution of ethanethiol (1.23 mL, 16. 6 mmol) and 4 Å MS in anhydrous CH_2Cl_2 (30 mL) stirring at 0 °C under Ar and boron trifluoride diethyl etherate (4.2 mL, 33.3 mmol) was added dropwise. The reaction mixture was stirred overnight, then diluted with CH_2Cl_2 and quenched with sodium bicarbonate. The solution was filtered through Celite®, then extracted with CH_2Cl_2. The organic layer was washed with sodium bicarbonate, water, saturated brine, then dried over $MgSO_4$ and concentrated. Column chromatography (7:3 hexanes/ethyl acetate) afforded **6** as a syrup (2.7 g, 62%). Characterization data is consistent with that previously reported.[21] ^{1}H NMR (300 MHz, $CDCl_3$): δ 5.34 (dd, *J* = 3.2, 1.6 Hz, 1H), 5.31-5.27 (m, 3H), 4.40 (td, *J* = 7.1, 2.5 Hz, 1H), 4.32 (dd, *J* = 12.1, 5.3 Hz, 1H), 4.10 (dd, *J* = 12.1, 2.2 Hz, 1H), 2.71-2.57 (m, 2H), 2.17 (s, 3H), 2.10 (s, 3H), 2.05 (s, 3H), 1.99 (s, 3H), 1.31 (t, *J* = 7.4 Hz, 3H). ^{13}C NMR (75 MHz, $CDCl_3$): δ 170.6, 170.0, 169.8, 169.7, 82.2, 71.1, 69.5, 68.9, 66.3, 62.4, 25.4, 20.9, 20.7, 20.7, 20.6, 14.7. LRMS (ESI): *m/z* calcd. for $C_{16}H_{24}NaO_9S$ $[M+Na]^+$ 415.4; found, 415.2.

Ethyl 1-thio-α-D-mannopyranoside (7)

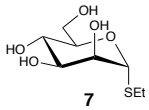

7

Compound **6** (2.7 g, 6.9 mmol) was dissolved in a solution of sodium methoxide in methanol (10 mL) and stirred for one hour at room temperature. The solution was neutralized with Amberlite® IR-120 (H^+) ion-exchange resin, filtered and concentrated to yield **7** as a solid (1.5 g, 95%). Characterization data is consistent with that previously reported.[92] ^{1}H NMR (300 MHz, $CDCl_3$): δ 5.31 (d, *J* = 1.5 Hz, 1H), 4.03 (dd, *J* = 3.3, 1.6 Hz, 1H), 4.01-3.96 (m, 1H), 3.87 (dd, *J* = 12.3, 2.3 Hz, 1H), 3.79-3.72 (m, 2H), 3.65 (t, *J* = 9.7 Hz, 1H), 2.75-2.57 (m, 2H), 1.26 (t, *J* = 7.4 Hz, 3H). ^{13}C NMR (75 MHz, $CDCl_3$): δ 84.2, 73.0, 71.8, 71.0, 67.1, 60.8, 24.7, 14.0. LRMS (ESI): *m/z* calcd. for $C_8H_{15}O_5S$ $[M-H]^-$ 223.3; found, 223.0.

Ethyl 4,6-O-benzylidene-2,3-O-benzyl-1-thio-α-D-mannopyranoside (8)

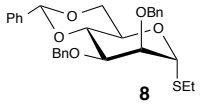

8

To a solution of **7** (375 mg, 1.67 mmol) in DMF (3 mL) were added benzaldehyde dimethyl acetal (251 μL, 1.67 mmol) and catalytic *p*-toluenesulfonic acid. The solution was stirred under reduced pressure at 60 °C for 3 hours then cooled to room temperature and triethylamine (50 μL) was added. The mixture was then evaporated and crystallized from CH_2Cl_2/pet. ether to afford 360 mg (69%) of the crude product that was used without further purification. The crude product (166 mg, 0.53 mmol) was dissolved in DMF (5 mL) and to this solution was added NaH (85 mg, 2.12 mmol) and the mixture was stirred for 10 mins. Benzyl bromide (189 μL, 1.59 mmol) was added, followed by a catalytic amount of tetrabutylammonium iodide and the reaction mixture was stirred overnight. The mixture was quenched the following day with brine and diluted with ethyl acetate. The organic layer was washed with brine, then dried over $MgSO_4$ and concentrated. Purification by column chromatography (19:1 hexanes/ethyl acetate) yielded **8** (221 mg, 91%, 63% overall) as a syrup. Characterization data is consistent with that previously reported.[22] ^{1}H NMR (300 MHz, $CDCl_3$): δ 7.53-7.50 (m, 2H), 7.39-7.28 (m, 13H), 5.65 (s, 1H), 5.31 (d, *J* = 0.8 Hz, 1H), 4.82-4.71 (m, 3H), 4.63 (d, *J* = 12.2 Hz, 1H), 4.32-4.16 (m, 3H), 3.94-3.87 (m, 3H), 2.68-2.48 (m, 2H), 1.24 (t, *J* = 7.4 Hz, 3H). ^{13}C NMR (76 MHz, $CDCl_3$): δ 138.4, 137.9, 137.6, 128.8, 128.4, 128.3, 128.2, 128.1, 127.8, 127.6, 127.5, 126.1, 101.4, 83.5, 79.2, 78.1, 76.4, 73.1, 73.0, 68.6, 64.6, 25.3, 14.9. LRMS (ESI): *m/z* calcd. for $C_{29}H_{33}O_5S$ $[M+H]^+$ 493.6; found, 493.2.

Ethyl 4,6-O-benzylidene-2,3-O-Benzyl-1-thio-α-D-mannopyranoside S-Oxide (9)

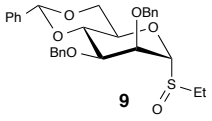

9

To a stirred solution of **8** (89 mg, 0.181 mmol) in dry dichloromethane (3 mL) at -78 °C was added 70% *meta*-chloroperbenzoic acid (41 mg, 0.181 mmol). The reaction mixture was stirred at -78 °C for 4 hours then warmed to -20 °C and quenched with a saturated sodium carbonate solution. The organic layer was washed with Na_2CO_3, water and brine, then dried over MgSO4 and concentrated. Purification by column chromatography (2:1 Hex/EtOAc) yielded **9** (78 mg, 85%).[18] ^{1}H NMR (300 MHz, $CDCl_3$): δ 7.47-7.25 (m, 15H), 5.61 (s, 1H), 4.85-4.77 (m, 2H), 4.71-4.64 (m, 2H), 4.59 (d, *J* = 1.4 Hz, 1H), 4.49 (dd, *J* = 3.4, 1.4 Hz, 1H), 4.32 (dd, *J* = 10.0, 9.0 Hz, 1H), 4.18 (dd, *J* = 9.8, 4.2 Hz, 1H), 4.10 (dd, *J* = 10.1, 3.4 Hz, 1H), 3.81-3.67 (m, 2H), 2.93-2.83 (m, 1H), 2.68-2.56 (m, 1H), 1.33 (t, *J* = 7.5 Hz, 3H). ^{13}C NMR (76 MHz, $CDCl_3$): δ 138.7, 137.4, 137.2, 128.6, 128.3, 128.3, 128.0, 127.9, 127.8, 127.6, 127.5, 125.6, 101.9, 92.2, 78.2, 77.1, 76.4, 73.1, 73.0, 68.3, 64.6, 45.4, 6.9. LRMS (ESI): *m/z* calcd. for $C_{29}H_{32}KO_6S$ $[M+K]^+$ 547.7; found, 547.1.

4'-Methoxyphenyl-4,6-O-benzylidene-2,3-O-benzyl-β-D-mannopyranoside (10β)

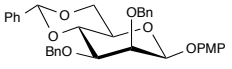

10β

Glycosidation conditions to form the β-linked mannopyranoside were as described by Crich et al.[19,20] To a stirred solution of sulfoxide **9** (17.6 mg, 0.035 mmol) and 2,6-di-*tert*-butyl-4-methylpyridine (14.2 mg, 0.069 mmol) in dry dichloromethane (1 mL) cooled to –78 °C under argon was added trifluoromethanesulfonic anhydride (6.4 μL, 0.038 mmol). After stirring for 2-5 minutes a solution of 4-methoxyphenol (4.7 mg, 0.038 mmol) in dry dichloromethane (1 mL) was added dropwise. The reaction mixture was stirred at -78 °C for 2 hours then warmed to 0 °C over 2 hours and maintained at 0 °C for 30 minutes before quenching with saturated sodium bicarbonate, washing with brine, drying over $MgSO_4$ and concentrating. Purification by column chromatography over a gradient (19:1 hexanes/ethyl acetate to 8:2 hexanes/ethyl acetate) gave a 3.5:1 β:α mixture and yielded pure β-anomer (as determined by ^{1}H NMR analysis and $J_{1,2}$ values[93]) (10.1 mg, 53%) and pure α-anomer (2.9 mg, 15%). Characterization data for **10 β-anomer**: ^{1}H-NMR (500 MHz; $CDCl_3$): δ 7.55-7.50 (m, 4H), 7.40-7.28 (m, 11H), 6.95-6.93 (m, 2H), 6.83-6.81 (m, 2H), 5.65 (s, 1H), 5.08 (d, *J* = 12.3 Hz, 1H), 5.01 (d, *J* = 12.2 Hz, 1H), 4.96 (d, *J* = 0.6 Hz, 1H), 4.75 (d, *J* = 12.5 Hz, 1H), 4.65 (d, *J* = 12.4 Hz, 1H), 4.34 (dt, *J* = 10.4, 5.2 Hz, 1H), 4.29 (d, *J* = 9.7 Hz, 1H), 4.11 (d, *J* = 3.0 Hz, 1H), 3.98 (t, *J* = 10.3 Hz, 1H), 3.77 (s, 3H), 3.68 (dd, *J* = 9.9, 3.1 Hz, 1H), 3.46-3.41 (m, 1H). ^{13}C NMR (126 MHz; $CDCl_3$): δ 155.3, 151.0, 138.2, 138.2, 137.5, 128.9, 128.7, 128.3, 128.2, 128.2,

127.7, 127.6, 127.6, 126.0, 117.9, 114.5, 101.5, 100.8, 78.5, 77.8, 76.0, 75.0, 72.6, 68.6, 67.6, 55.6. LRMS (ESI): *m/z* calcd. for $C_{34}H_{34}KO_7$ $[M+K]^+$ 593.7; found, 593.3.

4-Methoxyphenyl-β-D-mannopyranoside (3)

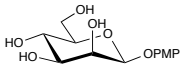

3
β-PMP-Man

A solution **10β** (8.6 mg, 0.016 mmol) in 4 mL of a 3:1 mixture of EtOH/AcOH and 5% Pd/C was stirred for 16 hours under an atmosphere of H_2. The flask was purged with air, the catalyst was removed by filtration through Celite® and the solvents were removed *in vacuo*. Purification by C-18 solid-phase extraction cartridge over a gradient (water to 9:1 water/ACN to 8:2 water/ACN to 1:1 water/ACN) afforded **3** (3.3 mg, 74%) as a white solid. ^{1}H NMR (500 MHz, D_2O): δ 7.11 (d, *J* = 9.1 Hz, 2H), 7.00 (d, *J* = 9.1 Hz, 2H), 5.28 (s, 1H), 4.20 (d, *J* = 2.9 Hz, 1H), 3.94 (dd, *J* = 12.3, 2.2 Hz, 1H), 3.82 (s, 3H), 3.79-3.74 (m, 2H), 3.68 (t, *J* = 9.7 Hz, 1H), 3.51 (ddd, *J* = 9.3, 6.5, 2.5 Hz, 1H). ^{13}C NMR (126 MHz, D_2O): δ 154.4, 150.5, 117.7, 114.9, 98.3, 76.2, 72.7, 70.5, 66.5, 60.8, 55.7. LRMS (ESI): *m/z* calcd. for $C_{13}H_{17}O_7$ $[M-H]^-$ 285.3; found, 285.1.

4-Bromophenyl-2,3,4,6-tetra-O-acetyl-β-D-glucopyranoside (11a)

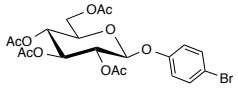

11a

Compound **11a** was prepared in a similar manner as **2a** from 1,2,3,4,6-penta-*O*-acetyl-β-D-glucopyranose (1.5 g, 3.84 mmol), 4-bromophenol (798 mg, 4.61 mmol) with boron trifluoride diethyl etherate (723 μL, 5.76 mmol). Column chromatography (4:1 hexanes/ethyl acetate) afforded **11a** as a white powder (1.33 g, 69%). Characterization data is consistent with that previously reported.[94] ^{1}H NMR (400 MHz, $CDCl_3$): δ 7.42-7.39 (m, 2H), 6.90-6.86 (m, 2H), 5.31-5.23 (m, 2H), 5.16 (t, *J* = 9.6 Hz, 1H), 5.03 (d, *J* = 7.6 Hz, 1H), 4.28 (dd, *J* = 12.3, 5.4 Hz, 1H), 4.16 (dd, *J* = 12.3, 2.4 Hz, 1H), 3.84 (ddd, *J* = 10.0, 5.4, 2.5 Hz, 1H), 2.08 (s, 3H), 2.06 (s, 3H), 2.05 (s, 3H), 2.03 (s, 3H). ^{13}C NMR (101 MHz, $CDCl_3$): δ 170.5, 170.2, 169.4, 155.8, 132.5, 118.8, 115.9, 99.1, 72.6, 72.1, 71.1, 68.2, 61.9, 20.8, 20.8, 20.7, 20.6. LRMS (ESI): *m/z* calcd. for $C_{20}H_{27}BrNO_{10}$ $[M+NH_4]^+$ 520.2; found, 520.0.

4-Bromophenyl-β-D-glucopyranoside (11)

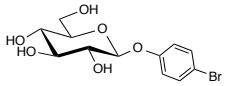

11

Compound **11a** (200 mg, 0.40 mmol) was dissolved in a solution of sodium methoxide in methanol (5 mL) and stirred for one hour at room temperature. The solution was then neutralized with Amberlite® IR-120 (H^+) ion-exchange resin, filtered and concentrated. The filtrate was concentrated and the product was lyophilized to yield **11** as a white powder (123 mg, 92%). ^{1}H NMR (400 MHz, D_2O): δ 7.54-7.50 (m, 2H), 7.07-7.03 (m, 2H), 5.09

(d, *J* = 7.5 Hz, 1H), 3.92 (dd, *J* = 12.5, 2.3 Hz, 1H), 3.74 (dd, *J* = 12.5, 5.7 Hz, 1H), 3.64-3.53 (m, 3H), 3.49 (dd, *J* = 9.7, 8.9 Hz, 1H). ^{13}C NMR (101 MHz, D_2O): δ 155.7, 132.6, 118.5, 115.0, 100.2, 76.1, 75.5, 72.9, 69.4, 60.5. LRMS (ESI): *m/z* calcd. for $C_{12}H_{15}BrNaO_6$ $[M+Na]^+$ 357.0; found, 357.0.

4-Chlorophenyl-2,3,4,6-tetra-O-acetyl-β-D-glucopyranoside (12a)

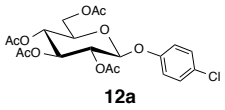

12a

Compound **12a** was prepared in a similar manner as **2a** from 1,2,3,4,6-penta-*O*-acetyl-β-D-glucopyranose (500 mg, 1.28 mmol), 4-chlorophenol (230 mg, 1.79 mmol) with boron trifluoride diethyl etherate (803 μL, 6.4 mmol). Column chromatography (3:2 hexanes/ethyl acetate) afforded **12a** as a white powder (234 mg, 40%). Characterization data is consistent with that previously reported.[95] ^{1}H NMR (400 MHz, $CDCl_3$): δ 7.27-7.23 (m, 4H), 6.95-6.91 (m, 2H), 5.31-5.23 (m, 2H), 5.16 (t, *J* = 9.6 Hz, 1H), 5.03 (d, *J* = 7.6 Hz, 1H), 4.28 (dd, *J* = 12.3, 5.4 Hz, 1H), 4.18-4.15 (m, 1H), 3.84 (ddd, *J* = 9.9, 5.3, 2.4 Hz, 1H), 2.08 (s, 3H), 2.06 (s, 3H), 2.05 (s, 3H), 2.04 (s, 3H). ^{13}C NMR (101 MHz, $CDCl_3$): δ 170.5, 170.2, 169.3, 169.2, 155.3, 129.5, 128.5, 118.4, 99.2, 72.6, 72.1, 71.1, 68.2, 61.9, 20.7, 20.6, 20.6, 20.6. LRMS (ESI): *m/z* calcd. for $C_{20}H_{27}ClNO_{10}$ $[M+NH_4]^+$ 476.9; found, 476.3.

4-Chlorophenyl-β-D-glucopyranoside (12)

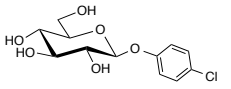

12

Compound **12a** (150 mg, 0.33 mmol) was dissolved in a solution of sodium methoxide in methanol (5 mL) and stirred for one hour at room temperature. The solution was then neutralized with Amberlite® IR-120 (H^+) ion-exchange resin, filtered and concentrated. The filtrate was concentrated and the product was lyophilized to yield **12** as a white powder (92 mg, 97%). ^{1}H NMR (400 MHz, D_2O): δ 7.39-7.35 (m, 2H), 7.12-7.08 (m, 2H), 5.09 (d, *J* = 7.5 Hz, 1H), 3.92 (dd, *J* = 12.5, 2.2 Hz, 1H), 3.74 (dd, *J* = 12.4, 5.7 Hz, 1H), 3.64-3.53 (m, 3H), 3.49 (t, *J* = 9.3 Hz, 1H). ^{13}C NMR (101 MHz, D_2O): δ 155.2, 129.6, 127.5, 118.0, 100.3, 76.1, 75.5, 72.9, 69.4, 60.5. LRMS (ESI): *m/z* calcd. for $C_{12}H_{15}ClNaO_6$ $[M+Na]^+$ 313.7; found, 313.1.

4-Fluorophenyl-2,3,4,6-tetra-O-acetyl-β-D-glucopyranoside (13a)

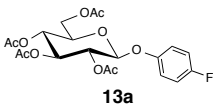

13a

Compound **13a** was prepared in a similar manner as **2a** from 1,2,3,4,6-penta-*O*-acetyl-β-D-glucopyranose (500 mg, 1.28 mmol), 4-fluorophenol (200 mg, 1.58 mmol) with boron trifluoride diethyl etherate (803 μL, 6.4 mmol). Column chromatography (3:2 hexanes/ethyl acetate) afforded **13a** as a white powder (416 mg, 77%).

Characterization data is consistent with that previously reported.[96] ^{1}H NMR (400 MHz, $CDCl_3$): δ 7.10-7.08 (m, 2H), 6.91-6.88 (m, 2H), 5.30-5.25 (m, 2H), 5.16 (t, *J* = 9.7 Hz, 1H), 5.03-5.01 (m, 1H), 4.29 (dd, *J* = 12.2, 5.2 Hz, 1H), 4.17 (dd, *J* = 12.2, 2.5 Hz, 1H), 3.83 (ddd, *J* = 10.0, 5.3, 2.5 Hz, 1H), 2.08 (s, 3H), 2.06 (s, 3H), 2.04 (s, 3H), 2.03 (s, 3H). ^{13}C NMR (101 MHz, $CDCl_3$): δ 170.5, 170.2, 169.4, 169.2, 160.0, 157.6, 152.9, 152.9, 118.8, 118.7, 116.1, 115.9, 99.8, 72.6, 72.1, 71.2, 68.2, 61.9, 20.7, 20.6, 20.6, 20.6. LRMS (ESI): *m/z* calcd for $C_{20}H_{27}FNO_{10}$ $[M+NH_4]^+$ 460.5; found, 460.2.

4-Fluorophenyl-β-D-glucopyranoside (13)

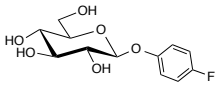

13

Compound **13a** (198 mg, 0.45 mmol) was dissolved in a solution of sodium methoxide in methanol (5 mL) and stirred for one hour at room temperature. The solution was then neutralized with Amberlite® IR-120 (H^+) ion-exchange resin, filtered and concentrated. The filtrate was concentrated and the product was lyophilized to yield **13** as a white powder (120 mg, 98%). ^{1}H NMR (400 MHz, D_2O): δ 7.15-7.09 (m, 4H), 5.06 (d, *J* = 7.5 Hz, 1H), 3.93 (dd, *J* = 12.4, 2.3 Hz, 1H), 3.75 (dd, *J* = 12.4, 5.6 Hz, 1H), 3.63-3.53 (m, 3H), 3.52-3.47 (m, 1H). ^{13}C NMR (101 MHz, D_2O): δ 152.7, 118.2, 118.2, 116.2, 116.0, 100.9, 76.1, 75.5, 72.9, 69.4, 60.5. LRMS (ESI): *m/z* calcd. for $C_{12}H_{15}FNaO_6$ $[M+Na]^+$ 297.2; found, 297.1.

4-Hydroxyphenyl-2,3,4,6-tetra-O-acetyl-β-D-glucopyranoside (14a) and 1,4-Bis-(2,3,4,6- tetra-O-acetyl-β-D-glucopyranosyl)benzene (83a)

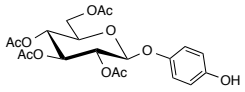

14a

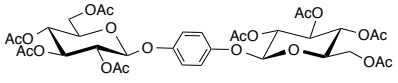

83a

Compounds **14a** and **83a** were prepared in a similar manner as **2a** from 1,2,3,4,6-penta-*O*-acetyl-β-D-glucopyranose (1 g, 2.56 mmol), hydroquinone (211 mg, 1.92 mmol) with boron trifluoride diethyl etherate (482 μL, 3.84 mmol). Column chromatography (7:3 hexanes/ethyl acetate) afforded both **14a**[97] (339 mg, 40%) and **83a**[16] (491 mg, 33%) as white powders.

Characterization data for **14a**:[97]

^{1}H NMR (400 MHz, $CDCl_3$): δ 6.90-6.86 (m, 2H), 6.77-6.72 (m, 2H), 5.30-5.20 (m, 2H), 5.16 (t, *J* = 9.5 Hz, 2H), 4.93 (d, *J* = 7.6 Hz, 1H), 4.28 (dd, *J* = 12.3, 5.1 Hz, 1H), 4.16 (dd, *J* = 12.3, 2.5 Hz, 1H), 3.79 (ddd, *J* = 9.9, 5.1, 2.5 Hz, 1H), 2.09 (d, *J* = 1.5 Hz, 3H), 2.07-2.05 (m, 5H), 2.02 (s, 3H). ^{13}C NMR (101 MHz, $CDCl_3$): δ 170.7, 170.3, 169.5, 169.4, 151.8, 150.8, 118.9, 116.0,

100.3, 72.7, 71.9, 71.2, 68.3, 61.9, 20.7, 20.7, 20.6, 20.6. LRMS (ESI): *m/z* calcd. for $C_{20}H_{24}NaO_{11}$ $[M+Na]^+$ 463.4; found, 463.2.

Characterization data for **83a**:[16]

^{1}H NMR (400 MHz, $CDCl_3$): δ 6.92 (s, 4H), 5.30-5.21 (m, 4H), 5.16 (t, *J* = 9.6 Hz, 2H), 4.98 (d, *J* = 7.6 Hz, 2H), 4.28 (dd, *J* = 12.3, 5.1 Hz, 2H), 4.16 (dd, *J* = 12.3, 2.5 Hz, 2H), 3.81 (ddd, *J* = 9.9, 5.1, 2.5 Hz, 2H), 2.07 (s, 6H), 2.06 (s, 6H), 2.04 (s, 7H), 2.03 (s, 6H). ^{13}C NMR (101 MHz, $CDCl_3$): δ 170.5, 170.2, 169.3, 169.2, 152.8, 118.4, 99.8, 72.6, 72.0, 71.1, 68.2, 61.8, 20.7, 20.6, 20.6, 20.6. LRMS (ESI): *m/z* calcd. for $C_{34}H_{42}KO_{20}$ $[M+K]^+$ 809.9; found, 809.2.

4-Hydroxyphenyl-β-D-glucopyranoside (14)

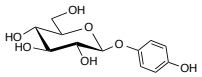

14

Compound **14a** (200 mg, 0.45 mmol) was dissolved in a solution of sodium methoxide in methanol (5 mL) and stirred for one hour at room temperature. The solution was then neutralized with Amberlite® IR-120 (H^+) ion-exchange resin, filtered and concentrated. The filtrate was concentrated and the product was lyophilized to yield **14** as a white powder (122 mg, 98%). ^{1}H NMR (400 MHz, D_2O): δ 7.07-7.03 (m, 2H), 6.89-6.85 (m, 2H), 4.99 (d, *J* = 7.6 Hz, 1H), 3.92 (dd, *J* = 12.4, 2.2 Hz, 1H), 3.75 (dd, *J* = 12.5, 5.6 Hz, 1H), 3.61-3.52 (m, 3H), 3.48 (dd, *J* = 9.7, 8.9 Hz, 1H). ^{13}C NMR (101 MHz, D_2O): δ 151.2, 150.4, 118.4, 116.2, 101.3, 76.0, 75.5, 73.0, 69.4, 60.5. LRMS (ESI): *m/z* calcd. for $C_{12}H_{16}NaO_7$ $[M+Na]^+$ 295.3; found, 295.2.

4-Methylphenyl-2,3,4,6-tetra-O-acetyl-β-D-glucopyranoside (16a)

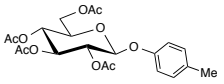

16a

Compound **16a** was prepared in a similar manner as **2a** from 1,2,3,4,6-penta-*O*-acetyl-β-D-glucopyranose (500 mg, 1.28 mmol), 4-methylphenol (190 mg, 1.79 mmol) with boron trifluoride diethyl etherate (800 μL, 6.40 mmol)**.** Column chromatography (7:3 hexanes/EtOAc) afforded **16a** as a white powder (205 mg, 37%). Characterization data is consistent with that previously reported in the literature.[98] ^{1}H NMR (400 MHz, $CDCl_3$): δ 7.09 (d, *J* = 8.2 Hz, 2H), 6.89 (d, *J* = 8.6 Hz, 2H), 5.31-5.23 (m, 2H), 5.16 (t, *J* = 9.6 Hz, 1H), 5.02 (d, *J* = 7.7 Hz, 1H), 4.29 (dd, *J* = 12.2, 5.3 Hz, 1H), 4.16 (dd, *J* = 12.3, 2.3 Hz, 1H), 3.85-3.81 (m, 1H), 2.30 (s, 3H), 2.08 (s, 3H), 2.06 (s, 3H), 2.05 (s, 3H), 2.03 (s, 3H). ^{13}C NMR (101 MHz, $CDCl_3$): δ 170.6, 170.3, 169.4, 169.3, 154.8, 132.9, 130.0, 117.0, 99.6, 72.8,

72.0, 71.2, 68.3, 62.0, 20.7, 20.7, 20.6, 20.6, 20.6. LRMS (ESI): *m/z* calcd. for $C_{21}H_{30}NO_{10}$ $[M+NH_4]^+$ 456.4; found, 456.1.

4-Methylphenyl-β-D-glucopyranoside (16)

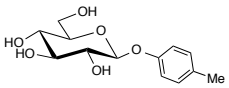

16

Compound **16a** (124 mg, 0.28 mmol) was dissolved in a solution of sodium methoxide in methanol (5 mL) and stirred for one hour at room temperature. The solution was then neutralized with Amberlite® IR-120 (H^+) ion-exchange resin, filtered and concentrated. The product was purified by recrystallization in hot ethyl acetate to afford **16** as a white powder (68 mg, 89%). Characterization data is consistent with that previously reported in the literature.[98] ^{1}H NMR (400 MHz, D_2O): δ 7.24-7.22 (m, 2H), 7.06-7.04 (m, 2H), 5.08 (d, *J* = 7.6 Hz, 1H), 3.92 (dd, *J* = 12.4, 2.3 Hz, 1H), 3.75 (dd, *J* = 12.4, 5.7 Hz, 1H), 3.63-3.53 (m, 3H), 3.49 (dd, *J* = 10.0, 8.6 Hz, 1H), 2.30 (s, 3H). ^{13}C NMR (101 MHz, D_2O): δ 154.4, 133.3, 130.2, 116.6, 100.5, 76.1, 75.6, 73.0, 69.5, 60.6, 19.6. LRMS (ESI): *m/z* calcd. for $C_{13}H_{18}NaO_6$ $[M+Na]^+$ 293.2; found, 293.1.

Phenyl-2,3,4,6-tetra-O-acetyl-β-D-glucopyranoside (17a)

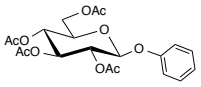

17a

Compound **17a** was prepared in a similar manner as **2a** from 1,2,3,4,6-penta-*O*-acetyl-β-D-glucopyranose (500 mg, 1.28 mmol), phenol (169 mg, 1.79 mmol) with boron trifluoride diethyl etherate (209 μL, 1.66 mmol)**.** Column chromatography (7:3 hexanes/EtOAc) afforded **17a** as a white powder (420 mg, 77%). Characterization data is consistent with that previously reported in the literature.[99] ^{1}H NMR (400 MHz, $CDCl_3$): δ 7.30 (dd, *J* = 8.7, 7.4 Hz, 2H), 7.08 (dd, *J* = 7.8, 7.0 Hz, 1H), 6.99 (dt, *J* = 7.8, 1.0 Hz, 2H), 5.33-5.25 (m, 2H), 5.17 (t, *J* = 9.7 Hz, 1H), 5.09 (d, *J* = 7.8 Hz, 1H), 4.29 (dd, *J* = 12.3, 5.4 Hz, 1H), 4.17 (dd, *J* = 12.3, 2.5 Hz, 1H), 3.86 (ddd, *J* = 10.0, 5.3, 2.5 Hz, 1H), 2.09 (s, 3H), 2.06 (s, 3H), 2.05 (s, 3H), 2.04 (s, 3H).^{13}C NMR (75 MHz, $CDCl_3$): δ 170.6, 170.2, 169.4, 169.3, 156.8, 129.6, 123.4, 117.0, 99.1, 72.7, 72.0, 71.2, 68.3, 61.9, 20.7, 20.6, 20.6. LRMS (ESI): *m/z* calcd. for $C_{20}H_{23}O_{10}$ $[M-H]^-$ 423.4; found, 423.3.

Phenyl-β-D-glucopyranoside (17)

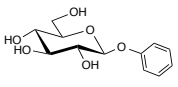

17

Compound **17a** (400 mg, 0.94 mmol) was dissolved in a solution of sodium methoxide in methanol (5 mL) and stirred for one hour at room temperature. The solution was then neutralized with Amberlite® IR-120 (H^+) ion-exchange resin, filtered and concentrated. The filtrate was concentrated and the product was lyophilized to yield **17** as a white powder (229 mg, 95%). ^{1}H NMR (400 MHz, D_2O): δ 7.41-7.37 (m, 2H), 7.16-7.13 (m, 3H), 5.13

(d, *J* = 7.5 Hz, 1H), 3.94-3.90 (m, 1H), 3.74 (dd, *J* = 12.5, 5.7 Hz, 1H), 3.64-3.54 (m, 3H), 3.48 (dd, *J* = 9.8, 8.9 Hz, 1H). ^{13}C NMR (101 MHz, D_2O): δ 156.5, 129.9, 123.3, 116.5, 100.1, 76.1, 75.5, 72.9, 69.4, 60.5. LRMS (ESI): *m/z* calcd. for $C_{12}H_{15}O_6$ $[M-H]^-$ 255.3; found, 255.1.

4-(Methoxycarbonyl)phenyl-2,3,4,6-tetra-O-acetyl-β-D-glucopyranoside (19a)

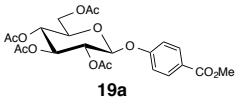

19a

Compound **19a** was prepared in a similar manner as **2a** from 1,2,3,4,6-penta-*O*-acetyl-β-D-glucopyranose (500 mg, 1.28 mmol), 4-(methoxycarbonyl)phenol (234 mg, 1.53 mmol) with boron trifluoride diethyl etherate (209 μL, 1.66 mmol)**.** Column chromatography (3:2 hexanes/EtOAc) afforded **19a** as a white powder (258 mg, 77%). Characterization data is consistent with that previously reported in the literature.[16] ^{1}H NMR (400 MHz, $CDCl_3$): δ 8.02-7.99 (m, 2H), 7.03-6.99 (m, 2H), 5.35-5.28 (m, 2H), 5.20-5.15 (m, 2H), 4.29 (dd, *J* = 12.3, 5.5 Hz, 1H), 4.18 (dd, *J* = 12.3, 2.4 Hz, 1H), 3.92 (m, 1H), 3.90 (s, 3H), 2.08 (d, *J* = 5.8 Hz, 3H), 2.05 (s, 6H), 2.05 (d, *J* = 5.6 Hz, 3H). ^{13}C NMR (101 MHz, $CDCl_3$): δ 170.5, 170.2, 169.4, 169.2, 166.4, 160.1, 131.6, 116.1, 98.2, 72.6, 72.2, 71.0, 68.2, 61.9, 52.0, 20.7, 20.7, 20.6, 20.6. LRMS (ESI): *m/z* calcd. for $C_{22}H_{26}NaO_{12}$ $[M+Na]^+$ 505.4; found, 505.3.

4-(Methoxycarbonyl)phenyl-β-D-glucopyranoside (19)

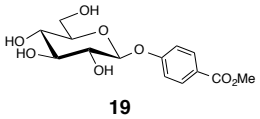

19

Compound **19a** (150 mg, 0.31 mmol) was dissolved in a solution of sodium methoxide in methanol (5 mL) and stirred for one hour at room temperature. The solution was then neutralized with Amberlite® IR-120 (H^+) ion-exchange resin, filtered and concentrated. The filtrate was concentrated and the product was lyophilized to yield **19** as a white powder (87 mg, 89%). ^{1}H NMR (400 MHz, D_2O): δ 8.01 (d, *J* = 8.8 Hz, 2H), 7.18 (d, *J* = 8.9 Hz, 2H), 5.23 (d, *J* = 7.0 Hz, 1H), 3.95-3.92 (m, 1H), 3.90 (s, 3H), 3.75 (dd, *J* = 12.4, 5.6 Hz, 1H), 3.69-3.65 (m, 1H), 3.62-3.58 (m, 2H), 3.50 (t, *J* = 9.3 Hz, 1H). ^{13}C NMR (101 MHz, D_2O): δ 169.6, 161.2, 132.4, 124.7, 116.8, 100.1, 76.9, 76.1, 73.5, 70.0, 61.1, 53.2. LRMS (ESI): *m/z* calcd. for $C_{14}H_{18}NaO_8$ $[M+Na]^+$ 337.3; found, 337.2.

4-Trifluoromethylphenyl-2,3,4,6-tetra-O-acetyl-β-D-glucopyranoside (21a)

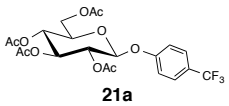

21a

Compound **21a** was prepared in a similar manner as **2a** from 1,2,3,4,6-penta-*O*-acetyl-β-D-glucopyranose (500 mg, 1.28 mmol), 4-trifluoromethylphenol (290 mg, 1.79 mmol) with boron trifluoride diethyl etherate (1.6 mL, 12.8 mmol)**.** Column chromatography (3:2 hexanes/EtOAc) afforded **21a** as a white powder (189 mg, 30%). ^{1}H NMR

(400 MHz, $CDCl_3$): δ 7.57 (d, *J* = 8.5 Hz, 2H), 7.07 (d, *J* = 8.4 Hz, 2H), 5.34-5.27 (m, 2H), 5.20-5.14 (m, 2H), 4.29 (dd, *J* = 12.3, 5.4 Hz, 1H), 4.18 (dd, *J* = 12.3, 2.4 Hz, 1H), 3.92-3.87 (m, 1H), 2.07 (s, 3H), 2.06 (s, 3H), 2.06 (s, 3H), 2.04 (s, 3H). ^{13}C NMR (101 MHz, $CDCl_3$): δ 170.5, 170.2, 169.4, 169.2, 127.1, 127.0, 127.0, 127.0, 116.7, 98.4, 72.5, 72.2, 71.0, 68.1, 61.9, 20.7, 20.6, 20.6. LRMS (ESI): *m/z* calcd. for $C_{21}H_{23}F_3NaO_{10}$ $[M+Na]^+$ 515.4; found, 515.2.

4-Trifluoromethylphenyl-β-D-glucopyranoside (21)

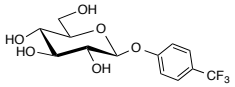

21

Compound **21a** (117 mg, 0.24 mmol) was dissolved in a solution of sodium methoxide in methanol (5 mL) and stirred for one hour at room temperature. The solution was then neutralized with Amberlite® IR-120 (H^+) ion-exchange resin, filtered and concentrated. The filtrate was concentrated and the product was lyophilized to yield **21** as a white powder (74 mg, 96%). ^1H NMR (400 MHz, D_2O): δ 7.70 (d, *J* = 8.7 Hz, 2H), 7.24 (d, *J* = 8.5 Hz, 2H), 5.21 (d, *J* = 7.6 Hz, 1H), 3.93 (dd, *J* = 12.4, 2.2 Hz, 1H), 3.75 (dd, *J* = 12.4, 5.7 Hz, 1H), 3.69-3.65 (m, 1H), 3.62-3.60 (m, 2H), 3.50 (t, *J* = 9.4 Hz, 1H). ^{13}C NMR (101 MHz, D_2O): δ 159.0, 127.3, 127.2, 127.2, 127.2, 116.5, 99.6, 76.2, 75.5, 72.8, 69.4, 60.5. LRMS (ESI): *m/z* calcd. for $C_{13}H_{15}F_3NaO_6$ $[M+Na]^+$ 347.2; found, 347.1.

4-Nitrophenyl-2,3,4,6-tetra-O-acetyl-β-D-glucopyranoside (22a)

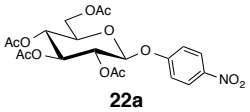

22a

Compound **22a** was prepared in a similar manner as **2a** from 1,2,3,4,6-penta-*O*-acetyl-β-D-glucopyranose (420 mg, 1.08 mmol), 4-nitrophenol (210 mg, 1.51 mmol) with boron trifluoride diethyl etherate (180 μL, 1.40 mmol)**.** Column chromatography (8:2 hexanes/EtOAc) afforded **22a** as a white powder (347 mg, 68%). Characterization data is consistent with that previously reported in the literature.[99] ^1H NMR (500 MHz, $CDCl_3$): δ 8.23-8.20 (m, 2H), 7.09-7.06 (m, 2H), 5.16-5.11 (m, 3H), 5.09 (d, *J* = 3.7 Hz, 1H), 4.28 (dd, *J* = 12.3, 5.2 Hz, 1H), 4.18 (dd, *J* = 12.3, 2.3 Hz, 1H), 3.86-3.82 (m, 1H), 2.07 (s, 3H), 2.06 (s, 3H), 2.03 (s, 3H), 2.02 (s, 3H). ^{13}C NMR (101 MHz, $CDCl_3$): δ 170.7, 170.2, 169.7, 169.3, 160.8, 140.9, 124.7, 115.5, 98.1, 74.7, 73.9, 71.2, 68.1, 61.9, 20.9, 20.7, 20.6, 20.5. LRMS (ESI): *m/z* calcd. for $C_{20}H_{22}NO_{12}$ $[M-H]^-$ 468.4; found, 468.2.

4-Nitrophenyl -β-D-glucopyranoside (22)

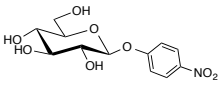

22

Compound **22a** (250 mg, 0.53 mmol) was dissolved in a solution of sodium methoxide in methanol (4 mL) and stirred for one hour at room temperature. The solution was then neutralized with Amberlite® IR-120 (H^+) ion-exchange resin, filtered and

concentrated. The product was purified by column chromatography (4:1:1:1 EtOAc/ACN/H_2O/MeOH) to afford **22** as a white powder (128 mg, 80%). ^{1}H NMR (400 MHz, D_2O): δ 8.28-8.24 (m, 2H), 7.26-7.22 (m, 2H), 5.27 (d, *J* = 7.7 Hz, 1H), 3.93 (dd, *J* = 12.3, 2.1 Hz, 1H), 3.75 (dd, *J* = 12.3, 5.7 Hz, 1H), 3.71-3.67 (m, 1H), 3.63-3.61 (m, 2H), 3.51 (t, *J* = 9.4 Hz, 1H). ^{13}C NMR (101 MHz, D_2O): δ 161.7, 142.6, 126.1, 116.4, 99.4, 76.3, 75.4, 72.7, 69.3, 60.4. LRMS (ESI): *m/z* calcd. for $C_{12}H_{14}NO_8$ $[M-H]^-$ 300.3; found, 300.5. LRMS (ESI): *m/z* calcd. for $C_{24}H_{28}N_2O_{16}$ $[M-H]^-$ Dimer 601.5; found, 601.0.

4-Trifluoromethoxyphenyl-2,3,4,6-tetra-O-acetyl-β-D-glucopyranoside (23a)

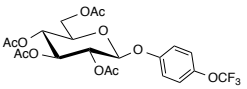

23a

Compound **23a** was prepared in a similar manner as **2a** from 1,2,3,4,6-penta-*O*-acetyl-β-D-glucopyranose (250 mg, 0.64 mmol), 4-trifluoromethoxyphenol (116 μL, 0.90 mmol) with boron trifluoride diethyl etherate (161 μL, 1.28 mmol)**.** Column chromatography (4:1 hexanes/EtOAc) afforded **23a** as a white powder (291 mg, 89%). ^{1}H NMR (300 MHz, $CDCl_3$): δ 7.15 (d, *J* = 8.9 Hz, 2H), 7.00 (d, *J* = 9.0 Hz, 2H), 5.33-5.23 (m, 2H), 5.16 (t, *J* = 9.5 Hz, 1H), 5.06 (d, *J* = 7.3 Hz, 1H), 4.28 (dd, *J* = 12.3, 5.3 Hz, 1H), 4.16 (dd, *J* = 12.3, 2.3 Hz, 1H), 3.88-3.82 (m, 1H), 2.07 (s, 6H), 2.05 (s, 3H), 2.03 (s, 3H). ^{13}C NMR (76 MHz, $CDCl_3$): δ 170.5, 170.2, 169.4, 169.2, 155.1, 144.6, 122.5, 118.1, 99.1, 72.6, 72.1, 71.1, 68.1, 61.8, 20.6, 20.6, 20.6. LRMS (ESI): *m/z* calcd. for $C_{21}H_{22}F_3NaO_{11}$ $[M-H]^-$ 507.4; found, 507.2.

4-Trifluoromethoxyphenyl-β-D-glucopyranoside (23)

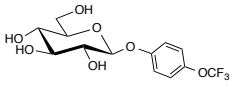

23

Compound **23a** (180 mg, 0.35 mmol) was dissolved in a solution of sodium methoxide in methanol (5 mL) and stirred for one hour at room temperature. The solution was then neutralized with Amberlite® IR-120 (H^+) ion-exchange resin, filtered and concentrated. The filtrate was concentrated and the product was lyophilized to yield **23** as a white powder (110 mg, 91%). ^{1}H NMR (500 MHz, D_2O): δ 7.30 (d, *J* = 9.1 Hz, 2H), 7.17-7.15 (m, 2H), 5.09 (d, *J* = 7.3 Hz, 1H), 3.91 (dd, *J* = 12.5, 2.1 Hz, 1H), 3.73 (t, *J* = 9.0 Hz, 1H), 3.62-3.55 (m, 3H), 3.48 (d, *J* = 9.2 Hz, 1H). ^{13}C NMR (126 MHz, D_2O): δ 155.0, 144.1, 122.6, 119.2, 117.6, 100.3, 76.1, 75.4, 72.8, 69.3, 60.4. LRMS (ESI): *m/z* calcd. for $C_{13}H_{14}F_3NaO_7$ $[M-H]^-$ 339.2; found, 339.1.

4-Bromophenyl-2,3,4,6-tetra-O-acetyl-β-D-galactopyranoside (24a)

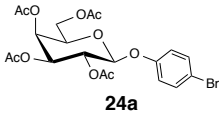

24a

Compound **24a** was prepared in a similar manner as **1a** from 1,2,3,4,6-penta-*O*-acetyl-β-D-galactopyranose (500 mg, 1.28 mmol), 4-bromophenol (266 mg, 1.54 mmol) with boron trifluoride diethyl etherate (209 μL, 1.66 mmol). Column chromatography (3:2 hexanes/ethyl acetate) afforded **24a** as a white powder (406 g, 63%). Characterization data is consistent with that previously reported.[94] ^{1}H NMR (400 MHz, $CDCl_3$): δ 7.41-7.37 (m, 2H), 6.90-6.86 (m, 2H), 5.49-5.44 (m, 2H), 5.10 (dd, *J* = 10.4, 3.4 Hz, 1H), 4.99 (d, *J* = 7.9 Hz, 1H), 4.21 (dd, *J* = 11.3, 7.1 Hz, 1H), 4.15 (dd, *J* = 11.3, 6.2 Hz, 1H), 4.06-4.03 (m, 1H), 2.18 (s, 3H), 2.06 (s, 3H), 2.05 (s, 3H), 2.01 (s, 3H). ^{13}C NMR (101 MHz, $CDCl_3$): δ 170.3, 170.2, 170.0, 169.3, 155.9, 132.4, 118.7, 115.8, 99.6, 71.1, 70.7, 68.5, 66.8, 61.3, 20.7, 20.6, 20.6. LRMS (ESI): *m/z* calcd. for $C_{20}H_{27}BrNO_{10}$ $[M+NH_4]^+$ 521.4; found, 522.2.

4-Bromophenyl-β-D-galactopyranoside (24)

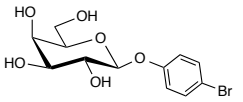

24

Compound **24a** (300 mg, 0.60 mmol) was dissolved in a solution of sodium methoxide in methanol (5 mL) and stirred for one hour at room temperature. The solution was then neutralized with Amberlite® IR-120 (H^+) ion-exchange resin, filtered and concentrated. The filtrate was concentrated and the product was lyophilized to yield **24** as a white powder (159 mg, 80%). ^{1}H NMR (400 MHz, D_2O): δ 7.54-7.50 (m, 2H), 7.08-7.04 (m, 2H), 5.03 (d, *J* = 7.3 Hz, 1H), 3.99 (d, *J* = 2.8 Hz, 1H), 3.88-3.84 (m, 1H), 3.82-3.73 (m, 4H). ^{13}C NMR (101 MHz, D_2O): δ 155.9, 132.5, 118.4, 114.8, 100.7, 75.4, 72.5, 70.5, 68.4, 60.7. LRMS (ESI): *m/z* calcd. for $C_{12}H_{15}BrNaO_6$ $[M+Na]^+$ 357.0; found, 357.2.

4-Chlorophenyl-2,3,4,6-tetra-O-acetyl-β-D-galactopyranoside (25a)

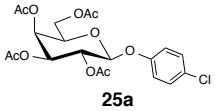

25a

Compound **25a** was prepared in a similar manner as **1a** from 1,2,3,4,6-penta-*O*-acetyl-β-D-galactopyranose (500 mg, 1.28 mmol), 4-chlorophenol (197 mg, 1.54 mmol) with boron trifluoride diethyl etherate (209 μL, 1.66 mmol). Column chromatography (3:2 hexanes/ethyl acetate) afforded **25a** as a white powder (294 mg, 50%). Characterization data is consistent with that previously reported.[95] ^{1}H NMR (400 MHz, $CDCl_3$): δ 7.27-7.23 (m, 2H), 6.96-6.92 (m, 2H), 5.49-5.44 (m, 2H), 5.10 (dd, *J* = 10.4, 3.4 Hz, 1H), 4.99 (d, *J* = 7.9 Hz, 1H), 4.22 (dd, *J* = 11.3, 7.0 Hz, 1H), 4.15 (dd, *J* = 11.3, 6.2 Hz, 1H), 4.06-4.03 (m, 1H), 2.18 (s, 3H), 2.07 (s, 3H), 2.05 (s, 3H), 2.01 (s, 3H). ^{13}C NMR (101 MHz, $CDCl_3$): δ 170.3, 170.2, 170.1, 169.3, 155.4, 129.5, 128.4, 118.3, 99.7, 71.1, 70.7, 68.5, 66.8, 61.3, 20.7, 20.6, 20.6. LRMS (ESI): *m/z* calcd. for $C_{20}H_{27}ClNO_{10}$ $[M+NH_4]^+$ 476.9; found, 476.3.

4-Chlorophenyl-β-D-galactopyranoside (25)

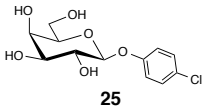

25

Compound **25a** (250 mg, 0.55 mmol) was dissolved in a solution of sodium methoxide in methanol (5 mL) and stirred for one hour at room temperature. The solution was then neutralized with Amberlite® IR-120 (H^+) ion-exchange resin, filtered and concentrated. The filtrate was concentrated and the product was lyophilized to yield **25** as a white powder (146 mg, 92%). ^{1}H NMR (400 MHz, D_2O): δ 7.39-7.35 (m, 2H), 7.13-7.09 (m, 2H), 5.03 (d, *J* = 7.2 Hz, 1H), 3.99 (dd, *J* = 3.1, 0.8 Hz, 1H), 3.86 (t, *J* = 6.5 Hz, 1H), 3.82-3.74 (m, 4H). ^{13}C NMR (101 MHz, D_2O): δ 156.1, 130.2, 128.1, 118.7, 101.5, 76.1, 73.2, 71.2, 69.1, 61.4. LRMS (ESI): *m/z* calcd. for $C_{12}H_{15}ClNaO_6$ $[M+Na]^+$ 313.7; found, 313.2.

4-Hydroxyphenyl-2,3,4,6-tetra-O-acetyl-β-D-galactopyranoside (27a) and 1,4-Bis-(2,3,4,6-tetra-O-acetyl-β-D-galactopyranosyl)benzene (84a)

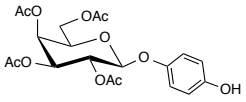

27a

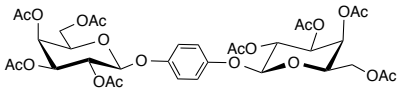

84a

Compounds **27a** and **84a** were prepared in a similar manner as **1a** from 1,2,3,4,6-penta-*O*-acetyl-β-D-galactopyranose (1 g, 2.56 mmol), hydroquinone (211 mg, 1.92 mmol) with boron trifluoride diethyl etherate (482 μL, 3.84 mmol). Column chromatography (7:3 hexanes/ethyl acetate) afforded both **27a**[97] (185 mg, 22%) and **84a**[16] (451 mg, 30%) as white powders.

Characterization data for **27a**:[97]

^{1}H NMR (400 MHz, $CDCl_3$): δ 6.92-6.88 (m, 2H), 6.77-6.73 (m, 2H), 5.47-5.43 (m, 2H), 5.08 (dd, *J* = 10.5, 3.4 Hz, 1H), 4.90 (d, *J* = 8.0 Hz, 1H), 4.24 (dd, *J* = 11.3, 6.9 Hz, 1H), 4.17-4.11 (m, 1H), 4.00 (td, *J* = 6.7, 1.0 Hz, 1H), 2.18 (s, 3H), 2.09 (s, 3H), 2.05 (s, 3H), 2.01 (s, 3H). ^{13}C NMR (101 MHz, $CDCl_3$): δ 170.4, 170.3, 170.2, 169.5, 151.7, 151.0, 118.8, 116.0, 100.8, 70.9, 70.9, 68.8, 66.9, 61.3, 20.8, 20.7, 20.6. LRMS (ESI): *m/z* calcd. for $C_{20}H_{24}NaO_{11}$ $[M+Na]^+$ 463.4; found, 463.3.

Characterization data for **84a**:[16]

^{1}H NMR (400 MHz, $CDCl_3$): δ 6.94 (s, 4H), 5.48-5.44 (m, 4H), 5.11-5.07 (m, 2H), 4.95 (d, *J* = 7.9 Hz, 2H), 4.25-4.20 (m, 2H), 4.17-4.12 (m, 2H), 4.03-4.00 (m, 2H), 2.18 (s, 6H), 2.07 (s, 6H), 2.05 (s, 6H), 2.01 (s, 6H). ^{13}C NMR (101 MHz, $CDCl_3$): δ 170.3, 170.2, 170.1, 169.3, 152.9,

118.3, 100.4, 71.0, 70.8, 68.6, 66.8, 61.2, 20.7, 20.7, 20.6. LRMS (ESI): *m/z* calcd. for $C_{34}H_{46}NO_{20}$ $[M+NH_4]^+$ 788.8; found, 788.6.

4-Hydroxyphenyl-β-D-galactopyranoside (27)

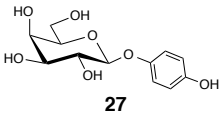

27

Compound **27a** (95 mg, 0.22 mmol) was dissolved in a solution of sodium methoxide in methanol (5 mL) and stirred for one hour at room temperature. The solution was then neutralized with Amberlite® IR-120 (H^+) ion-exchange resin, filtered and concentrated. The filtrate was concentrated and the product was lyophilized to yield **27** as a white powder (41 mg, 70%). ^{1}H NMR (400 MHz, D_2O): δ 7.07-7.02 (m, 2H), 6.88-6.83 (m, 2H), 4.91 (d, *J* = 7.6 Hz, 1H), 3.97 (d, *J* = 2.6 Hz, 1H), 3.82-3.71 (m, 5H). ^{13}C NMR (101 MHz, D_2O): δ 151.1, 150.6, 118.3, 116.2, 101.9, 75.3, 72.6, 70.6, 68.5, 60.7. LRMS (ESI): *m/z* calcd. for $C_{12}H_{16}NaO_7$ $[M+Na]^+$ 295.3; found, 295.2.

4-Trifluoromethoxyphenyl-2,3,4,6-tetra-O-acetyl-β-D-galactopyranoside (36a)

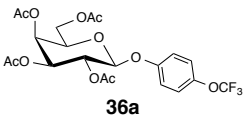

36a

Compound **36a** was prepared in a similar manner as **1a** from 1,2,3,4,6-penta-*O*-acetyl-β-D-galactopyranose (154 mg, 0.40 mmol), 4-trifluoromethoxyphenol **(**61 μL, 0.47 mmol) with boron trifluoride diethyl etherate (69 μL, 0.55 mmol). Column chromatography (4:1 hexanes/EtOAc) afforded **36a** as a white powder (125 mg, 89%). ^{1}H NMR (300 MHz, $CDCl_3$): δ 7.15 (d, *J* = 9.1 Hz, 2H), 7.03-6.98 (m, 2H), 5.48-5.45 (m, 2H), 5.10 (dd, *J* = 10.4, 3.4 Hz, 1H), 5.01 (d, *J* = 7.9 Hz, 1H), 4.26-4.12 (m, 2H), 4.05 (td, *J* = 6.6, 1.0 Hz, 1H), 2.18 (s, 3H), 2.07 (s, 3H), 2.05 (s, 3H), 2.01 (s, 3H). ^{13}C NMR (76 MHz, $CDCl_3$): δ 170.3, 170.2, 170.1, 169.3, 155.2, 144.6, 122.4, 122.1, 118.7, 118.0, 99.7, 77.2, 71.1, 70.7, 68.5, 66.8, 61.3, 20.7, 20.6, 20.5. LRMS (ESI): *m/z* calcd. for $C_{21}H_{22}F_3NaO_{11}$ $[M-H]^-$ 507.4; found, 507.2.

4-Trifluoromethoxyphenyl-β-D-galactopyranoside (36)

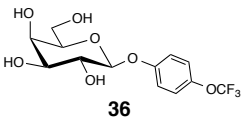

36

Compound **36a** (125 mg, 0.25 mmol) was dissolved in a solution of sodium methoxide in methanol (5 mL) and stirred for one hour at room temperature. The solution was then neutralized with Amberlite® IR-120 (H^+) ion-exchange resin, filtered and concentrated. The filtrate was concentrated and the product was lyophilized to yield **36** as a white powder (77 mg, 92%). ^{1}H NMR (500 MHz, D_2O): δ 7.35-7.33 (m, 2H), 7.21 (d, *J* = 9.2 Hz, 2H), 5.07 (d, *J* = 7.5 Hz, 1H), 4.02 (d, *J* = 3.2 Hz, 1H), 3.89 (t, *J* = 6.2 Hz, 1H),

3.85-3.77 (m, 4H). ^{13}C NMR (126 MHz, D_2O): δ 155.2, 122.6, 117.6, 116.1, 100.9, 75.4, 72.4, 70.4, 68.4, 60.6. LRMS (ESI): *m/z* calcd. for $C_{13}H_{14}F_3NaO_7$ $[M-H]^-$ 339.2; found, 339.1.

3-Methoxyphenyl-2,3,4,6-tetra-O-acetyl-β-D-glucopyranoside (37a)

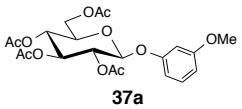

37a

Compound **37a** was prepared in a similar manner as **2a** from 1,2,3,4,6-penta-*O*-acetyl-β-D-glucopyranose (500 mg, 1.28 mmol), 3-methoxyphenol (222 mg, 1.79 mmol) with boron trifluoride diethyl etherate (803 μL, 6.4 mmol)**.** Column chromatography (3:2 hexanes/EtOAc) afforded **37a** as a white powder (162 mg, 28%). ^{1}H NMR (400 MHz, $CDCl_3$): δ 7.21-7.17 (m, 1H), 6.64-6.56 (m, 3H), 5.32-5.24 (m, 2H), 5.16 (t, *J* = 9.7 Hz, 1H), 5.08 (d, *J* = 7.7 Hz, 1H), 4.28 (dd, *J* = 12.3, 5.5 Hz, 1H), 4.17 (dd, *J* = 12.2, 2.4 Hz, 1H), 3.86 (ddd, *J* = 10.0, 5.5, 2.5 Hz, 1H), 3.78 (s, 3H), 2.08 (s, 3H), 2.06 (s, 3H), 2.05 (s, 3H), 2.03 (s, 3H). ^{13}C NMR (101 MHz, $CDCl_3$): δ 170.6, 170.2, 169.4, 169.3, 160.8, 158.0, 130.0, 108.9, 108.6, 103.6, 99.0, 72.7, 72.0, 71.1, 68.3, 62.0, 55.4, 30.9, 20.6, 20.6, 20.6. LRMS (ESI): *m/z* calcd. for $C_{21}H_{30}NO_{11}$ $[M+NH_4]^+$ 475.5; found, 472.1.

3-Methoxyphenyl-β-D-glucopyranoside (37)

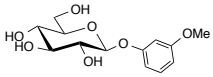

37

Compound **37a** (162 mg, 0.33 mmol) was dissolved in a solution of sodium methoxide in methanol (5 mL) and stirred for one hour at room temperature. The solution was then neutralized with Amberlite® IR-120 (H^+) ion-exchange resin, filtered and concentrated. The filtrate was concentrated and the product was lyophilized to yield **37** as a white powder (90 mg, 95%). ^{1}H NMR (400 MHz, D_2O): δ 7.34-7.30 (m, 1H), 6.78-6.75 (m, 3H), 5.12 (d, *J* = 7.2 Hz, 1H), 3.93 (dd, *J* = 12.1, 1.2 Hz, 1H), 3.82 (s, 3H), 3.76-3.72 (m, 1H), 3.65-3.54 (m, 3H), 3.51-3.46 (m, 1H). ^{13}C NMR (101 MHz, D_2O): δ 160.1, 157.7, 130.6, 109.0, 108.9, 102.9, 100.1, 76.2, 75.5, 72.9, 69.5, 60.6, 55.5. LRMS (ESI): *m/z* calcd. for $C_{13}H_{22}NO_7$ $[M+NH_4]^+$ 304.4; found, 304.1.

3-Hydroxyphenyl-2,3,4,6-tetra-O-acetyl-β-D-glucopyranoside (39a) and 1,3-Bis-(2,3,4,6- tetra-O-acetyl-β-D-glucopyranosyl)benzene (86a)

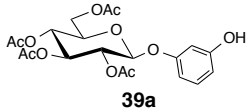

39a

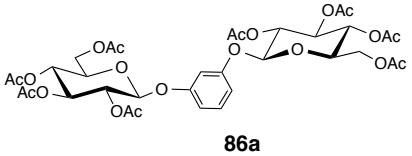

86a

Compounds **39a** and **86a** were prepared in a similar manner as **2a** from 1,2,3,4,6-penta-*O*-acetyl-β-D-glucopyranose (1 g, 2.56 mmol), resorcinol (170 mg, 1.54 mmol) with boron trifluoride

diethyl etherate (804 μL, 6.4 mmol). Column chromatography (3:2 hexanes/ethyl acetate) afforded both **39a**[97] (221 mg, 33%) and **86a**[16] (200 mg, 17%) as white powders.

Characterization data for **39a**:[97]

^{1}H NMR (400 MHz, $CDCl_3$): δ 7.10 (t, *J* = 8.2 Hz, 1H), 6.55-6.51 (m, 3H), 5.25 (qd, *J* = 11.2, 9.4 Hz, 2H), 5.14 (t, *J* = 9.4 Hz, 1H), 5.05 (d, *J* = 7.5 Hz, 1H), 4.27 (dd, *J* = 12.3, 5.3 Hz, 1H), 4.16 (dd, *J* = 12.3, 2.3 Hz, 1H), 3.84 (ddd, *J* = 9.9, 5.2, 2.4 Hz, 1H), 2.07 (s, 3H), 2.04 (s, 3H), 2.03 (s, 3H), 2.02 (s, 3H). ^{13}C NMR (101 MHz, $CDCl_3$): δ 171.0, 170.4, 169.5, 157.9, 157.1, 130.1, 110.4, 108.7, 104.6, 98.9, 72.7, 71.9, 71.2, 68.3, 61.9, 20.6, 20.6, 20.52. LRMS (ESI): *m/z* calcd. for $C_{20}H_{24}NaO_{11}$ $[M+Na]^+$ 463.4; found, 463.1.

Characterization data for **86a**:[16]

^{1}H NMR (400 MHz, $CDCl_3$): δ 7.20 (t, *J* = 8.3 Hz, 1H), 6.69 (dd, *J* = 8.3, 2.3 Hz, 2H), 6.61 (d, *J* = 2.2 Hz, 1H), 5.26 (dq, *J* = 16.9, 8.6 Hz, 4H), 5.17-5.09 (m, 4H), 4.27 (dd, *J* = 12.3, 5.4 Hz, 2H), 4.15 (dd, *J* = 12.3, 2.4 Hz, 2H), 3.86 (ddd, *J* = 10.0, 5.4, 2.5 Hz, 2H), 2.07 (s, 6H), 2.05 (s, 6H), 2.04 (s, 6H), 2.03 (s, 6H). ^{13}C NMR (101 MHz, $CDCl_3$): δ 170.6, 170.2, 169.4, 169.2, 157.7, 130.1, 111.1, 106.4, 98.6, 72.7, 72.0, 71.1, 68.3, 61.9, 20.6, 20.6, 20.6, 20.6. LRMS (ESI): *m/z* calcd. for $C_{34}H_{42}NaO_{20}$ $[M+Na]^+$ 793.7; found, 793.1.

3-Hydroxyphenyl-β-D-glucopyranoside (39)

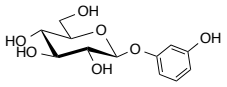

39

Compound **39a** (88 mg, 0.20 mmol) was dissolved in a solution of sodium methoxide in methanol (5 mL) and stirred for one hour at room temperature. The solution was then neutralized with Amberlite® IR-120 (H^+) ion-exchange resin, filtered and concentrated. The filtrate was concentrated and the product was lyophilized to yield **39** as a white powder (54 mg, 98%). ^{1}H NMR (400 MHz, D_2O): δ 7.25 (t, *J* = 8.5 Hz, 1H), 6.70 (ddd, *J* = 8.3, 2.2, 0.9 Hz, 1H), 6.65 (dquintet, *J* = 4.8, 1.6 Hz, 2H), 5.10 (d, *J* = 7.6 Hz, 1H), 3.93 (dd, *J* = 12.4, 2.2 Hz, 1H), 3.75 (dd, *J* = 12.4, 5.7 Hz, 1H), 3.65-3.52 (m, 3H), 3.48 (dd, *J* = 9.7, 8.9 Hz, 1H). ^{13}C NMR (101 MHz, D_2O): δ 158.5, 157.6, 131.4, 111.0, 109.0, 104.7, 100.7, 76.8, 76.2, 73.6, 70.1, 61.2. LRMS (ESI): *m/z* calcd. for $C_{12}H_{16}O_7$ $[M+Na]^+$ 295.2; found, 295.1.

3-Methylphenyl-2,3,4,6-tetra-O-acetyl-β-D-glucopyranoside (40a)

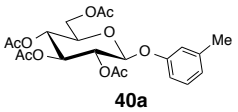

40a

Compound **40a** was prepared in a similar manner as **2a** from 1,2,3,4,6-penta-*O*-acetyl-β-D-glucopyranose (500 mg, 1.28 mmol), 3-methylphenol

(190 mg, 1.79 mmol) with boron trifluoride diethyl etherate (1.61 mL, 12.8 mmol)**.** Column chromatography (7:3 hexanes/EtOAc) afforded **40a** as a white powder (226 mg, 40%). Characterization data is consistent with that previously reported in the literature.[95] ^{1}H NMR (400 MHz, $CDCl_3$): δ 7.17 (t, *J* = 7.8 Hz, 1H), 6.90-6.88 (m, 1H), 6.81-6.77 (m, 2H), 5.32-5.24 (m, 2H), 5.16 (t, *J* = 9.6 Hz, 1H), 5.07 (d, *J* = 7.7 Hz, 1H), 4.28 (dd, *J* = 12.3, 5.5 Hz, 1H), 4.17 (dd, *J* = 12.3, 2.4 Hz, 1H), 3.86 (ddd, *J* = 10.0, 5.5, 2.5 Hz, 1H), 2.33 (s, 3H), 2.08 (s, 3H), 2.06 (s, 3H), 2.05 (s, 3H), 2.03 (s, 3H). ^{13}C NMR (101 MHz, $CDCl_3$): δ 170.6, 170.2, 169.4, 169.3, 156.9, 139.7, 129.3, 124.1, 117.7, 113.7, 99.1, 72.7, 72.0, 71.2, 68.4, 62.0, 21.5, 20.7, 20.6, 20.6. LRMS (ESI): *m/z* calcd. for $C_{21}H_{30}NO_{10}$ $[M+NH_4]^+$ 456.5; found, 456.2.

3-Methylphenyl-β-D-glucopyranoside (40)

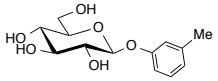

40

Compound **40a** (142 mg, 0.33 mmol) was dissolved in a solution of sodium methoxide in methanol (5 mL) and stirred for one hour at room temperature. The solution was then neutralized with Amberlite® IR-120 (H^+) ion-exchange resin, filtered and concentrated. The filtrate was concentrated and the product was lyophilized to yield **40** as a white powder (79 mg, 89%). ^{1}H NMR (400 MHz, D_2O): δ 7.29 (t, *J* = 7.9 Hz, 1H), 7.01-6.94 (m, 3H), 5.12 (d, *J* = 7.6 Hz, 1H), 3.93 (dd, *J* = 12.4, 2.2 Hz, 1H), 3.75 (dd, *J* = 12.7, 5.8 Hz, 1H), 3.65-3.54 (m, 3H), 3.49 (dd, *J* = 9.7, 9.1 Hz, 1H), 2.34 (s, 2H). ^{13}C NMR (101 MHz, D_2O): δ 156.6, 140.6, 129.7, 124.0, 117.1, 113.4, 100.1, 76.1, 75.6, 72.9, 69.5, 60.6, 20.5. LRMS (ESI): *m/z* calcd. for $C_{13}H_{18}NaO_6$ $[M+Na]^+$ 293.3; found, 293.1.

4-Bromophenyl-2,3,4,6-tetra-O-acetyl-α-D-glucopyranoside (58α)

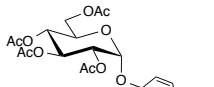

58α

Compound **58α** was prepared in a similar manner as **2a** from 1,2,3,4,6-penta-*O*-acetyl-β-D-glucopyranose (8 g, 20.5 mmol), 4-bromophenol (4.25 mg, 24.6 mmol) with boron trifluoride diethyl etherate (3.86 mL, 30.8 mmol)**.** The reaction mixture was refluxed for 2 days, and following quenching, washing and concentration the crude mixture showed a 1:6 ratio of α:β-linked products. Column chromatography (4:1 hexanes/EtOAc) afforded **58α** as a white powder (1.14 g, 11%). Characterization data is consistent with that previously reported in the literature.[100] ^{1}H NMR (300 MHz, $CDCl_3$): δ 7.39 (d, *J* = 9.0 Hz, 2H), 6.96 (d, *J* = 9.0 Hz, 2H), 5.69-5.62 (m, 2H), 5.13 (t, *J* = 9.8 Hz, 1H), 5.01 (dd, *J* = 10.3, 3.6 Hz, 1H), 4.22 (dd, *J* = 12.1, 4.6 Hz, 1H), 4.09-4.01 (m, 2H), 2.05 (s, 3H), 2.04 (s, 3H), 2.03 (s, 3H), 2.02 (s, 3H). ^{13}C NMR (76 MHz, $CDCl_3$): δ 170.5, 170.2, 169.3, 169.2, 155.3, 129.5, 128.5,

118.4, 94.6, 72.6, 72.1, 71.1, 68.2, 61.9, 20.7, 20.6, 20.6, 20.6. LRMS (ESI): *m/z* calcd. for $C_{20}H_{27}BrNO_{10}$ $[M+NH_4]^+$ 521.4; found, 522.2.

4-Bromophenyl-α-D-glucopyranoside (41)

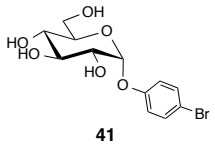

41

Compound **58α** (25 mg, 0.050 mmol) was dissolved in a solution of sodium methoxide in methanol (2 mL) and stirred for one hour at room temperature. The solution was then neutralized with Amberlite® IR-120 (H^+) ion-exchange resin, filtered and concentrated. The filtrate was concentrated and the product was lyophilized to yield **41** as a white powder (17 mg, 98%). ^{1}H NMR (300 MHz, D_2O): δ 7.51 (d, *J* = 9.0 Hz, 2H), 7.09 (d, *J* = 9.1 Hz, 2H), 5.61 (d, *J* = 3.8 Hz, 1H), 3.90 (t, *J* = 9.4 Hz, 1H), 3.77-3.69 (m, 4H), 3.50 (t, *J* = 9.5 Hz, 1H). ^{13}C NMR (76 MHz, D_2O): δ 151.5, 128.4, 114.3, 110.8, 96.0, 71.9, 71.3, 68.7, 65.2, 56.3. LRMS (ESI): *m/z* calcd. for $C_{12}H_{15}BrNaO_6$ $[M+Na]^+$ 357.0; found, 357.2.

4-Fluorophenyl-2,3,4,6-tetra-O-acetyl-α-D-glucopyranoside (59α)

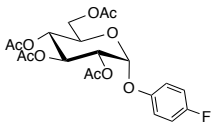

59α

Compound **59α** was prepared in a similar manner as **2a** from 1,2,3,4,6-penta-*O*-acetyl-β-D-glucopyranose (10 mg, 25.6 mmol), 4-fluorophenol (3.45 g, 30.8 mmol) with boron trifluoride diethyl etherate (4.5 mL, 35.8 mmol). The reaction mixture was refluxed for 2 days, and following quenching, washing and concentration the crude mixture showed a 1:4 ratio of α:β-linked products. Column chromatography (4:1 hexanes/EtOAc) afforded **59α** as a white powder (1.02 g, 9%). ^{1}H NMR (300 MHz, $CDCl_3$): δ 7.03-6.99 (m, 4H), 5.71-5.64 (m, 2H), 5.14 (t, *J* = 9.7 Hz, 1H), 5.02 (dd, *J* = 10.3, 3.7 Hz, 1H), 4.24 (dd, *J* = 11.9, 4.4 Hz, 1H), 4.15-4.04 (m, 2H), 2.07 (s, 3H), 2.05 (s, 3H), 2.04 (s, 3H), 2.04 (s, 3H). ^{13}C NMR (76 MHz, $CDCl_3$): δ 170.5, 170.1, 169.6, 160.2, 157.0, 152.2, 152.1, 118.0, 117.9, 116.3, 116.0, 94.8, 70.4, 69.9, 68.3, 68.0, 61.6, 20.7, 20.6, 20.6. LRMS (ESI): *m/z* calcd for $C_{20}H_{27}FNO_{10}$ $[M+NH_4]^+$ 460.5; found, 460.4.

4-Fluorophenyl-α-D-glucopyranoside (42)

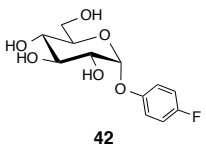

42

Compound **59α** (15 mg, 0.033 mmol) was dissolved in a solution of sodium methoxide in methanol (2 mL) and stirred for one hour at room temperature. The solution was then neutralized with Amberlite® IR-120 (H^+) ion-exchange resin, filtered and concentrated. The filtrate was concentrated and the product was lyophilized to yield **42** as a white powder (6 mg, 66%). ^{1}H NMR (300 MHz, D_2O): δ 7.18-7.07 (m, 4H), 5.55 (d, *J* = 3.7 Hz, 1H), 3.90 (t, *J* = 9.5 Hz, 1H), 3.82-3.69 (m, 5H), 3.50 (t, *J* = 9.4

Hz, 1H). ^{13}C NMR (76 MHz, D_2O): δ 148.9, 118.2, 118.2, 116.2, 114.4, 97.1, 75.5, 72.9, 72.3, 69.4, 60.5. LRMS (ESI): *m/z* calcd. for $C_{12}H_{15}FNaO_6$ $[M+Na]^+$ 297.2; found, 297.3.

4-Methoxyphenyl-2,3,4,6-tetra-O-acetyl-α-D-glucopyranoside (60α)

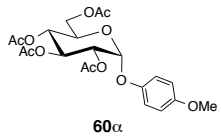

60α

Compound **60α** was prepared in a similar manner as **2a** from 1,2,3,4,6-penta-*O*-acetyl-β-D-glucopyranose (4 g, 10.3 mmol), 4-methoxyphenol (1.78 g, 14.4 mmol) with boron trifluoride diethyl etherate (2.6 mL, 20.5 mmol)**.** The reaction mixture was refluxed for 2 days, and following quenching, washing and concentration the crude mixture showed a 1:1.6 ratio of α:β-linked products. Column chromatography (4:1 hexanes/EtOAc) afforded **60α** as a white powder (1.43 g, 30%). Characterization data is consistent with that previously reported in the literature.[101] ^{1}H NMR (300 MHz, $CDCl_3$): δ 7.02-6.97 (m, 2H), 6.84-6.79 (m, 2H), 5.68 (dd, *J* = 10.0, 9.7 Hz, 1H), 5.61 (d, *J* = 3.6 Hz, 1H), 5.13 (dd, *J* = 10.1, 9.4 Hz, 1H), 5.00 (dd, *J* = 10.3, 3.7 Hz, 1H), 4.24 (dd, *J* = 12.1, 4.5 Hz, 1H), 4.15 (ddd, *J* = 10.2, 4.5, 2.0 Hz, 1H), 4.06 (dd, *J* = 12.1, 2.2 Hz, 1H), 3.76 (s, 3H), 2.06 (s, 3H), 2.05 (s, 3H), 2.04 (s, 3H), 2.03 (s, 3H). ^{13}C NMR (101 MHz, $CDCl_3$): δ 170.6, 170.3, 169.4, 169.3, 158.7, 151.5, 118.7, 115.3, 96.2, 72.2, 71.4, 71.2, 68.3, 61.9, 55.8, 20.7, 20.7, 20.6, 20.6. LRMS (ESI): *m/z* calcd. for $C_{21}H_{30}NO_{11}$ $[M+NH_4]^+$ 472.5; found, 472.3.

4-Methoxyphenyl-2,3,4,6-tetra-O-acetyl-α-D-glucopyranoside (43)

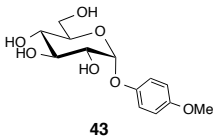

43

Compound **60α** (1.43 g, 3.15 mmol) was dissolved in a solution of sodium methoxide in methanol (15 mL) and stirred for one hour at room temperature. The solution was then neutralized with Amberlite® IR-120 (H^+) ion-exchange resin, filtered and concentrated. The filtrate was concentrated and the product was lyophilized to yield **43** as a white powder (780 mg, 87%). ^{1}H NMR (300 MHz, D_2O): δ 7.17-7.12 (m, 2H), 7.02-6.96 (m, 2H), 5.52 (d, *J* = 3.7 Hz, 1H), 3.90 (t, *J* = 9.4 Hz, 1H), 3.84-3.76 (m, 3H), 3.81 (s, 3H), 3.70 (dd, *J* = 9.8, 3.8 Hz, 1H), 3.51 (t, *J* = 9.5 Hz, 1H). ^{13}C NMR (126 MHz, D_2O): δ 154.5, 150.2, 118.8, 114.9, 98.0, 72.9, 72.3, 71.0, 69.2, 60.1, 55.6. LRMS (ESI): *m/z* calcd. for $C_{13}H_{17}O_7$ $[M-H]^-$ 285.3; found, 285.1.

Phenyl-2,3,4,6-tetra-O-acetyl-α-D-glucopyranoside (61α)

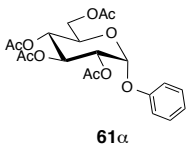

61α

Compound **61α** was prepared in a similar manner as **2a** from 1,2,3,4,6-penta-*O*-acetyl-β-D-glucopyranose **(**7.5 g, 19.2 mmol), phenol (2.2 g, 23.1 mmol) with boron trifluoride diethyl etherate (4.8 mL, 38.4 mmol). The reaction

mixture was refluxed for 2 days, and following quenching, washing and concentration the crude mixture showed a 1:13 ratio of α:β-linked products. Column chromatography (4:1 hexanes/EtOAc) afforded **61α** as a white powder (486 mg, 6%). ^{1}H NMR (300 MHz, $CDCl_3$): δ 7.31 (dd, *J* = 8.9, 7.2 Hz, 2H), 7.10-7.04 (m, 3H), 5.75-5.68 (m, 2H), 5.16 (dd, *J* = 10.2, 9.4 Hz, 1H), 5.04 (dd, *J* = 10.2, 3.7 Hz, 1H), 4.25 (dd, *J* = 12.1, 4.5 Hz, 1H), 4.16-4.11 (m, 1H), 4.06 (dd, *J* = 12.2, 2.2 Hz, 1H), 2.06 (s, 3H), 2.06 (s, 3H), 2.04 (s, 3H), 2.04 (s, 3H). ^{13}C NMR (76 MHz, $CDCl_3$): δ 170.5, 170.1, 169.6, 156.0, 129.6, 123.0, 116.5, 94.2, 70.4, 70.1, 68.3, 67.9, 61.6, 20.7, 20.6, 20.6. LRMS (ESI): *m/z* calcd. for $C_{20}H_{23}O_{10}$ $[M-H]^-$ 423.4; found, 423.3.

Phenyl-α-D-glucopyranoside (44)

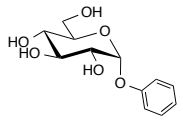

44

Compound **61α** (26 mg, 0.06 mmol) was dissolved in a solution of sodium methoxide in methanol (2 mL) and stirred for one hour at room temperature. The solution was then neutralized with Amberlite® IR-120 (H^+) ion-exchange resin, filtered and concentrated. The filtrate was concentrated and the product was lyophilized to yield **44** as a white powder (12 mg, 78%). ^{1}H NMR (300 MHz, D_2O): δ 7.41 (dd, *J* = 8.8, 7.3 Hz, 2H), 7.21-7.12 (m, 3H), 5.65 (d, *J* = 3.7 Hz, 1H), 3.94 (t, *J* = 9.5 Hz, 1H), 3.81-3.71 (m, 4H), 3.52 (t, *J* = 9.3 Hz, 1H). ^{13}C NMR (76 MHz, D_2O): δ 155.9, 129.9, 123.1, 117.2, 97.0, 73.0, 72.4, 71.1, 69.3, 60.2. LRMS (ESI): *m/z* calcd. for $C_{12}H_{15}O_6$ $[M-H]^-$ 255.3; found, 255.2.

4-Methoxyphenyl-2,3,4,6-tetra-O-acetyl-α-D-galactopyranoside (62α)

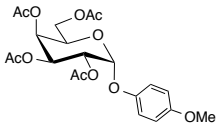

62α

Compound **62α** was prepared in a similar manner as **1a** from 1,2,3,4,6-penta-*O*-acetyl-β-D-galactopyranose (2 g, 5.12 mmol), 4-methoxyphenol (1.91 g, 15.4 mmol) with boron trifluoride diethyl etherate (2.6 mL, 20.5 mmol)**.** The reaction mixture was refluxed for 2 days, and following quenching, washing and concentration the crude mixture showed a 1.6:1 ratio of α:β-linked products. Column chromatography (4:1 hexanes/EtOAc) afforded **62α** as a white powder (1.4 g, 60%). Characterization data is consistent with that previously reported in the literature.[101] ^{1}H NMR (300 MHz, $CDCl_3$): δ 7.00-6.96 (m, 2H), 6.85-6.81 (m, 2H), 5.65 (d, *J* = 3.7 Hz, 1H), 5.58-5.51 (m, 2H), 5.26 (dd, *J* = 10.4, 3.6 Hz, 1H), 4.39 (t, *J* = 6.7 Hz, 1H), 4.10 (t, *J* = 6.6 Hz, 2H), 3.77 (s, 3H), 2.16 (s, 3H), 2.08 (s, 3H), 2.02 (s, 3H), 1.97 (s, 3H). ^{13}C NMR (101 MHz, $CDCl_3$): δ 170.5, 170.5, 170.3, 170.2, 155.6, 150.4, 118.2, 114.8, 95.9, 68.1, 68.0, 67.7, 67.1, 61.7, 55.8, 20.9, 20.8, 20.8, 20.8. LRMS (ESI): *m/z* calcd. for $C_{21}H_{30}NO_{11}$ $[M+NH_4]^+$ 472.5; found, 472.0.

4-Methoxyphenyl-α-D-galactopyranoside (45)

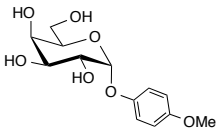

45

Compound **62α** (1.4 g, 3.15 mmol) was dissolved in a solution of sodium methoxide in methanol (15 mL) and stirred for one hour at room temperature. The solution was then neutralized with Amberlite® IR-120 (H^+) ion-exchange resin, filtered and concentrated. The filtrate was concentrated and the product was lyophilized to yield **45 as a white powder (600 mg, 67%).** ^{1}H NMR (300 MHz, D_2O): δ 7.17-7.12 (m, 2H), 7.01-6.97 (m, 2H), 5.53 (d, *J* = 3.8 Hz, 1H), 4.12 (t, *J* = 6.2 Hz, 1H), 4.08-4.03 (m, 2H), 3.99-3.94 (m, 1H), 3.81 (s, 3H), 3.72-3.70 (m, 2H). ^{13}C NMR (76 MHz, D_2O): δ 154.6, 150.4, 119.1, 115.0, 98.5, 71.6, 69.4, 69.1, 68.1, 61.0, 55.7. LRMS (ESI): *m/z* calcd. for $C_{13}H_{17}O_7$ $[M-H]^-$ 285.3; found, 285.1.

4-Methoxyphenyl-2,3,4,6-Tetra-O-Acetyl-α-D-Mannopyranoside (46a)

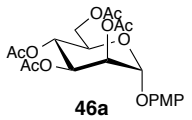

46a

Compound **46a** was prepared in a similar manner as **2a** from 1,2,3,4,6-penta-*O*-acetyl-α-D-mannopyranose (250 mg, 0.64 mmol), 4-methoxyphenol (95 mg, 0.77 mmol) with boron trifluoride diethyl etherate (113 μL, 0.9 mmol)**.** Column chromatography (3:2 hexanes/EtOAc) afforded **46a** as a white powder (124 mg, 43%). Characterization data is consistent with that previously reported.[102] ^{1}H NMR (500 MHz, $CDCl_3$): δ 7.03-7.00 (m, 2H), 6.84-6.80 (m, 2H), 5.54 (dd, *J* = 10.0, 3.5 Hz, 1H), 5.43 (dd, *J* = 3.5, 1.8 Hz, 1H), 5.41 (d, *J* = 1.8 Hz, 1H), 5.35 (t, *J* = 10.1 Hz, 1H), 4.28 (dd, *J* = 12.2, 5.3 Hz, 1H), 4.13 (ddd, *J* = 10.1, 5.3, 2.2 Hz, 1H), 4.08 (dd, *J* = 12.1, 2.3 Hz, 1H), 3.77 (s, 3H), 2.19 (s, 3H), 2.05 (s, 3H), 2.05 (s, 3H), 2.03 (s, 3H). ^{13}C NMR (126 MHz, $CDCl_3$): δ 170.6, 170.0, 169.9, 169.8, 155.4, 149.6, 117.7, 114.6, 96.6, 69.5, 69.0, 68.9, 66.0, 62.2, 55.6, 20.9, 20.7, 20.7. LRMS (ESI): *m/z* calcd. for $C_{21}H_{30}NO_{11}$ $[M+NH_4]^+$ 472.5; found, 472.4.

4-Methoxyphenyl-α-D-Mannopyranoside (46)

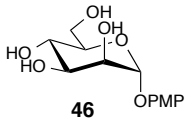

46

Compound **46a** (103 mg, 3.15 mmol) was dissolved in a solution of sodium methoxide in methanol (5 mL) and stirred for one hour at room temperature. The solution was then neutralized with Amberlite® IR-120 (H^+) ion-exchange resin, filtered and concentrated. The filtrate was concentrated and the product was lyophilized to yield **46** as a white powder (61 mg, 94%). ^{1}H NMR (500 MHz, D_2O): δ 7.13-7.09 (m, 2H), 6.98-6.94 (m, 2H), 5.47 (d, *J* = 1.8 Hz, 1H), 4.14 (dd, *J* = 3.4, 1.8 Hz, 1H), 4.00 (dd, *J* = 8.9, 3.4 Hz, 1H), 3.78-3.74 (m, 1H), 3.78 (s, 3H), 3.75-3.69 (m, 3H). ^{13}C NMR (76 MHz, D_2O): δ 154.5,

149.5, 118.7, 114.9, 99.2, 73.3, 70.3, 69.9, 66.5, 60.6, 55.7. LRMS (ESI): *m/z* calcd. for $C_{13}H_{17}O_7$ $[M-H]^-$ 285.3; found, 285.2.

N-(4-Methoxyphenyl)-1-β-D-glucopyranoside (47)

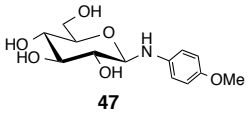

47

To a solution of D-glucose (50 mg, 0.28 mmol) in ethanol (2 mL) was added *para*-anisidine. The solution was refluxed for 1 h, cooled to room temperature, then 0°C to precipitate the product. The product was filtered and lyophilized to yield **47** as a white powder (68 mg, 86%). ^{1}H NMR (500 MHz, D_2O): δ 6.81-6.79 (m, 2H), 6.76-6.73 (m, 2H), 4.55 (d, *J* = 8.8 Hz, 1H), 3.74 (dd, *J* = 12.4, 2.3 Hz, 1H), 3.66 (s, 3H), 3.57 (dd, *J* = 12.4, 5.7 Hz, 1H), 3.45 (t, *J* = 9.1 Hz, 1H), 3.40 (ddd, *J* = 9.8, 5.7, 2.3 Hz, 1H), 3.32-3.26 (m, 2H). ^{13}C NMR (126 MHz, D_2O): δ 152.4, 139.7, 115.9, 115.2, 85.7, 76.8, 76.4, 72.7, 69.7, 60.7, 55.8. LRMS (ESI): *m/z* calcd. for $C_{13}H_{19}NO_6$ $[M+K]^+$ 324.3; found, 324.2.

4-Methoxyphenyl-2,3,4,6-tetra-O-acetyl-1-thio-β-D-glucopyranoside (48a)

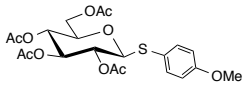

48a

Compound **48a** was prepared in a similar manner as **2a** from 1,2,3,4,6-penta-*O*-acetyl-β-D-glucopyranose (200 mg, 0.51 mmol), 4-methoxythiophenol (76 μL, 0.62 mmol) with boron trifluoride diethyl etherate (97 μL, 0.77 mmol)**.** Column chromatography (7:3 hexanes/EtOAc) afforded **48a** as a white powder (188 mg, 78%). Characterization data is consistent with that previously reported in the literature.[103] ^{1}H NMR (500 MHz, $CDCl_3$): δ 7.46-7.43 (m, 2H), 6.86-6.83 (m, 2H), 5.20 (t, *J* = 9.3 Hz, 1H), 5.00 (t, *J* = 9.8 Hz, 1H), 4.89 (dd, *J* = 10.0, 9.3 Hz, 1H), 4.55 (d, *J* = 10.0 Hz, 1H), 4.20-4.18 (m, 2H), 3.82 (s, 3H), 3.69-3.66 (m, 1H), 2.11 (s, 3H), 2.08 (s, 3H), 2.01 (s, 3H), 1.98 (s, 3H). ^{13}C NMR (126 MHz, $CDCl_3$): δ 170.6, 170.2, 169.4, 169.3, 136.6, 120.8, 114.4, 85.7, 75.7, 74.0, 69.8, 68.1, 62.0, 55.3, 20.2, 20.8, 20.8. LRMS (ESI): *m/z* calcd. for $C_{21}H_{27}O_{10}S$ $[M+H]^+$ 471.5; found, 471.3.

4-Methoxyphenyl-1-thio-β-D-glucopyranoside (48)

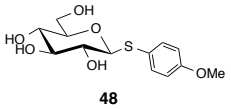

48

Compound **48a** (108 mg, 0.23 mmol) was dissolved in a solution of sodium methoxide in methanol (5 mL) and stirred for one hour at room temperature. The solution was then neutralized with Amberlite® IR-120 (H^+) ion-exchange resin, filtered and concentrated. The filtrate was concentrated and the product was lyophilized to yield **48** as a white powder (59 mg, 85%). ^{1}H NMR (500 MHz, D_2O): δ 7.54 (dd, *J* = 8.9, 0.6 Hz, 2H), 6.99 (dd, *J* = 9.0, 0.6 Hz, 2H), 4.60 (d, *J* = 9.8 Hz, 2H), 3.87-3.84 (m, 1H), 3.83 (dd, *J* = 10.6, 1.2 Hz, 3H),

3.70-3.66 (m, 1H), 3.47 (td, *J* = 9.0, 0.6 Hz, 1H), 3.42-3.38 (m, 1H), 3.35-3.31 (m, 1H), 3.23 (td, *J* = 9.4, 0.6 Hz, 1H). ^{13}C NMR (126 MHz, D_2O): δ 159.4, 135.1, 122.0, 114.7, 87.7, 79.8, 77.1, 71.5, 69.3, 60.7, 55.4. LRMS (ESI): *m/z* calcd. for $C_{13}H_{17}O_6S$ $[M-H]^-$ 302.3; found, 302.0.

4-Methoxybenzyl-2,3,4,6-tetra-O-acetyl-β-D-glucopyranoside (49a)

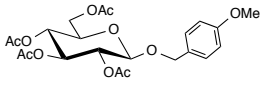

49a

To a mixture of 4-methoxybenzyl alcohol (109 mg, 0.79 mmol), Ag_2CO_3 (250 mg, 0.91 mmol) and 4 Å MS in anhydrous CH_2Cl_2 (3 mL) stirring in the dark under Ar was added bromo-2,3,4,6-tetra-*O*-acetyl-β-D-glucopyranose[27] (250 mg, 0.61 mmol) in anhydrous CH_2Cl_2 (2 mL) dropwise over 20 minutes**.** The reaction mixture was diluted with CH_2Cl_2 and filtered through Celite®, then washed with sodium bicarbonate, water, saturated brine, then dried over $MgSO_4$ and concentrated. Column chromatography over a gradient (8:2 hexanes/EtOAc to 3:2 hexanes/EtOAc) afforded **49a** as a white powder (88 mg, 31%). ^{1}H NMR (400 MHz, $CDCl_3$): δ 7.22-7.19 (m, 2H), 6.89-6.85 (m, 2H), 5.18-5.07 (m, 2H), 5.03 (dd, *J* = 9.5, 8.0 Hz, 1H), 4.82 (d, *J* = 11.9 Hz, 1H), 4.56 (d, *J* = 11.9 Hz, 1H), 4.51 (d, *J* = 7.9 Hz, 1H), 4.27 (dd, *J* = 12.3, 4.7 Hz, 1H), 4.17 (dd, *J* = 12.3, 2.4 Hz, 1H), 3.81 (s, 3H), 3.66 (ddd, *J* = 9.7, 4.7, 2.5 Hz, 1H), 2.11 (s, 3H), 2.01 (s, 3H), 1.99 (s, 3H), 1.99 (s, 3H). ^{13}C NMR (101 MHz, $CDCl_3$): δ 170.7, 170.3, 169.4, 169.3, 159.5, 129.5, 128.5, 113.9, 98.8, 72.8, 71.8, 71.3, 70.4, 68.4, 62.0, 55.3, 20.8, 20.7, 20.6, 20.6. LRMS (ESI): *m/z* calcd. for $C_{22}H_{32}NO_{11}$ $[M+NH_4]^+$ 486.5; found, 486.1.

4-Methoxybenzyl-β-D-glucopyranoside (49)

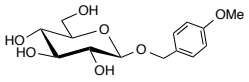

49
β-PMB-Glc

Compound **49a** (70 mg, 0.15 mmol) was dissolved in a solution of sodium methoxide in methanol (3 mL) and stirred for one hour at room temperature. The solution was then neutralized with Amberlite® IR-120 (H^+) ion-exchange resin, filtered and concentrated. The product was purified by recrystallization in hot ethyl acetate to afford **49** as a white powder (34 mg, 76%). ^{1}H NMR (400 MHz, D_2O): δ 7.44-7.41 (m, 2H), 7.05-7.01 (m, 2H), 4.88 (d, *J* = 11.3 Hz, 1H), 4.70 (d, *J* = 11.4 Hz, 1H), 4.50 (d, *J* = 8.0 Hz, 1H), 3.92 (dd, *J* = 12.3, 2.0 Hz, 1H), 3.85 (s, 3H), 3.73 (dd, *J* = 12.3, 5.7 Hz, 1H), 3.47-3.38 (m, 3H), 3.28 (dd, *J* = 9.0, 8.1 Hz, 1H). ^{13}C NMR (101 MHz, D_2O): δ 158.9, 130.6, 129.1, 114.1, 100.9, 75.92, 75.82, 73.1, 71.1, 69.7, 60.8, 55.4. LRMS (ESI): *m/z* calcd. for $C_{14}H_{24}NO_7$ $[M+NH_4]^+$ 318.3; found, 318.2.

***para*-Methoxyphenyl-6-*O*-methyl-2,3,4-tri-*O*-benzyl-β-D-glucopyranoside (63)**

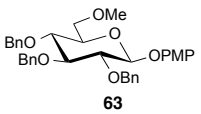

63

To a stirred solution of 66% sodium hydride (21 mg, 0.54 mmol) in dry DMF under argon at 0°C was added *para*-methoxyphenyl-2,3,4-tri-*O*-Benzyl-β-D-glucopyranoside (250 mg, 0.45mmol) (compound **20**, chapter 5). The mixture was stirred at 0°C for 20 min and methyl iodide (31 μL, 0.49 mmol) was added and the reaction mixture was stirred overnight. The reaction was quenched with brine, diluted with ethyl acetate and the organic layer was washed with saturated sodium thiosulfate, water, brine, then dried over $MgSO_4$ and concentrated. Column chromatography (4:1 hexanes/EtOAc) afforded **63** as a white powder (206 mg, 80%). ^{1}H NMR (300 MHz, $CDCl_3$): δ 7.36-7.29 (m, 15H), 7.06-7.00 (m, 2H), 6.87-6.82 (m, 2H), 5.06 (d, *J* = 10.9 Hz, 1H), 4.96 (d, *J* = 11.0 Hz, 1H), 4.91-4.81 (m, 4H), 4.65 (d, *J* = 10.9 Hz, 1H), 3.79 (s, 3H), 3.72-3.60 (m, 5H), 3.54-3.50 (m, 1H), 3.39 (s, 3H). ^{13}C NMR (76 MHz, $CDCl_3$): δ 155.2, 151.5, 138.5, 138.2, 138.1, 128.4, 128.4, 128.2, 128.0, 127.8, 127.7, 127.6, 118.3, 114.5, 102.8, 84.5, 82.0, 75.7, 75.08, 75.02, 74.8, 71.1, 59.4, 55.6. LRMS (ESI): *m/z* calcd. for $C_{35}H_{38}NaO_7$ $[M+Na]^+$ 593.7; found, 593.4.

***para*-Methoxyphenyl-6-*O*-methyl-β-D-glucopyranoside (50)**

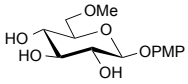

50

To a solution of **63** (142 mg, 0.25 mmol) in ethanol (4 mL) was added palladium hydroxide (5 mol %) and the reaction mixture was purged three times with H_2. The mixture was stirred under H_2 atmosphere overnight, filtered over Celite® and the solvent was evaporated to afforded **50** as a white powder (74 mg, 98%)**.** ^{1}H NMR (500 MHz, D_2O): δ 7.10-7.07 (m, 2H), 6.97-6.94 (m, 2H), 4.98 (d, *J* = 7.6 Hz, 1H), 3.79 (s, 3H), 3.78-3.75 (m, 1H), 3.68-3.62 (m, 2H), 3.59-3.50 (m, 2H), 3.47 (t, *J* = 9.2 Hz, 1H), 3.37 (s, 3H). ^{13}C NMR (126 MHz, D_2O): δ 154.6, 150.8, 118.0, 114.9, 101.1, 75.4, 74.6, 72.8, 70.8, 69.5, 58.5, 55.7. LRMS (ESI): *m/z* calcd. for $C_{14}H_{20}NaO_7$ $[M+Na]^+$ 323.3; found, 323.1.

***para*-Methoxyphenyl-6-deoxy-β-D-*gluco*-heptopyranose (51)**

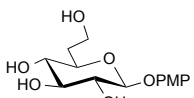

51

To a solution of *para*-Methoxyphenyl-6-deoxy-2,3,4-tri-*O*-Benzyl-β-D-*Gluco*-heptopyranose (209 mg, 0.37 mmol) (compound **22**, chapter 5) in ethanol (4 mL) was added Pd/C (5 mol %) and the reaction mixture was purged three times with H_2 under closed atmosphere. The mixture was stirred under H_2 atmosphere overnight, filtered over Celite and the solvent was evaporated to afforded **51** as a white powder (103 mg, 94%)**.** ^{1}H NMR (300 MHz, D_2O): δ 7.09-7.03 (m, 2H), 6.99-6.94 (m, 2H), 4.97 (d, *J* = 7.7 Hz, 1H), 3.79 (s, 3H), 3.74-3.63 (m, 2H), 3.60-3.50 (m, 3H), 3.31 (t, *J* = 9.3 Hz, 1H), 2.19-2.08 (m,

1H), 1.72-1.60 (m, 1H). ^{13}C NMR (76 MHz, D_2O): δ 154.6, 150.7, 117.9, 115.0, 100.8, 75.4, 73.3, 73.1, 72.6, 57.8, 55.7, 33.3. LRMS (ESI): *m/z* calcd. for $C_{14}H_{20}NaO_7$ $[M+Na]^+$ 323.3; found, 323.2.

Methyl-2,3,4-tri-*O*-Benzyl-6-*O*-(4-methylbenzenesulfonyl)-α-D-glucopyranoside (67)

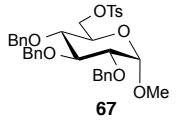

67

To a solution of methyl-2,3,4-tri-*O*-benzyl-α-D-glucopyranoside (122 mg, 0.26 mmol) (**66**, prepared as described previously)[56] and pyridine (47 μL, 0.58 mmol) in dry CH_2Cl_2 stirring at 0°C under argon was added TsCl (86 mg, 0.45 mmol). The reaction mixture was stirred overnight, then diluted with CH_2Cl_2. The organic layer was washed with water, brine, then dried over $MgSO_4$ and concentrated. Column chromatography (19:1 toluene/EtOAc) afforded **67** as a white powder (143 mg, 88%). Characterization data is consistent with that previously reported.[57] ^{1}H NMR (500 MHz, $CDCl_3$): δ 7.77 (d, *J* = 8.3 Hz, 2H), 7.36-7.28 (m, 15H), 7.15 (dt, *J* = 4.8, 2.3 Hz, 2H), 4.98 (d, *J* = 10.9 Hz, 1H), 4.80 (td, *J* = 14.6, 8.3 Hz, 3H), 4.64 (d, *J* = 12.1 Hz, 1H), 4.53 (d, *J* = 3.5 Hz, 1H), 4.44 (d, *J* = 10.7 Hz, 1H), 4.20 (qd, *J* = 9.8, 3.2 Hz, 2H), 3.96 (t, *J* = 9.3 Hz, 1H), 3.76 (ddd, *J* = 10.1, 3.9, 2.1 Hz, 1H), 3.49-3.43 (m, 2H), 3.32 (s, 3H), 2.40 (s, 3H). ^{13}C NMR (126 MHz, $CDCl_3$): δ 144.8, 138.5, 137.9, 137.7, 132.8, 129.8, 128.5, 128.4, 128.1, 128.0, 127.9, 127.9, 127.9, 127.8, 127.6, 98.0, 81.8, 79.6, 76.8, 75.7, 74.9, 73.4, 68.5, 68.4, 55.3, 21.6. LRMS (ESI): *m/z* calcd. for $C_{35}H_{38}NaO_8S[M+Na]^+$ 657.7; found, 657.5.

Methyl-2,3,4-tri-*O*-benzyl-6-*O*-(4-methoxyphenyl)-α-D-glucopyranoside (68)

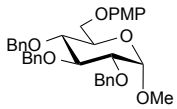

68

To a stirred solution of 66% sodium hydride (9 mg, 0.23 mmol) in dry DMF under argon was added *para*-methoxyphenol (26 mg, 0.21mmol). The mixture was stirred for 20 min and **67** (65 mg, 0.11 mmol) was added and the reaction mixture was stirred overnight. The reaction was quenched with brine, diluted with ethyl acetate and the organic layer was washed with saturated sodium thiosulfate, water, brine, then dried over $MgSO_4$ and concentrated. Column chromatography (9:1 pet. ether/EtOAc) afforded **68** as a white powder (45 mg, 75%). ^{1}H NMR (500 MHz, $CDCl_3$): δ 7.39-7.18 (m, 15H), 6.85-6.80 (m, 4H), 5.02 (d, *J* = 10.8 Hz, 1H), 4.86 (dt, *J* = 15.5, 10.6 Hz, 3H), 4.70 (d, *J* = 12.1 Hz, 1H), 4.66 (d, *J* = 3.5 Hz, 1H), 4.53 (d, *J* = 10.9 Hz, 1H), 4.12-4.03 (m, 3H), 3.91 (dt, *J* = 10.0, 2.8 Hz, 1H), 3.77 (s, 3H), 3.75 (t, *J* = 7.7 Hz, 1H), 3.62 (dd, *J* = 9.6, 3.6 Hz, 1H), 3.40 (s, 3H). ^{13}C NMR (126 MHz, $CDCl_3$): δ 153.9, 152.7, 138.7, 138.1, 138.0, 128.4, 128.4, 128.1, 128.0, 127.9, 127.7, 127.6, 115.5, 114.5,

98.2, 82.1, 79.8, 77.4, 75.8, 75.2, 73.4, 69.3, 67.1, 55.6, 55.2. LRMS (ESI): *m/z* calcd. for $C_{35}H_{38}NaO_7$ $[M+K]^+$ 609.7; found, 609.5.

2,3,4-tri-*O*-benzyl-6-*O*-(4-methoxyphenyl)-D-glucopyranoside (69)

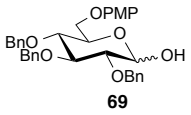

69

A solution of **68** (45 g, 0.08 mmol) in 0.5 M H_2SO_4 in acetic acid (1.2 mL) was refluxed gently for 2 h. Following this, the mixture was cooled to room temperature, diluted with water and extracted with ethyl acetate. The organic layer was extract with water, brine, then dried over $MgSO_4$ and concentrated**.** Column chromatography (4:1 hexanes/ethyl acetate) afforded **69** as a white solid (12 mg, 27%). ^{1}H NMR (500 MHz, $CDCl_3$): δ 7.36-7.28 (m, 20H), 7.24 (d, *J* = 1.5 Hz, 5H), 7.18-7.16 (m, 5H), 6.84-6.79 (m, 8H), 5.26 (d, *J* = 3.6 Hz, 1H), 4.97 (d, *J* = 10.9 Hz, 3H), 4.89-4.85 (m, 4H), 4.80 (d, *J* = 11.8 Hz, 2H), 4.71 (d, *J* = 11.7 Hz, 1H), 4.55 (t, *J* = 10.3 Hz, 1H), 4.18 (dt, *J* = 10.0, 2.8 Hz, 1H), 4.09 (d, *J* = 2.9 Hz, 2H), 4.02 (t, *J* = 9.3 Hz, 2H), 3.79-3.75 (m, 9H), 3.64 (dd, *J* = 9.4, 3.6 Hz, 2H), 3.47-3.43 (m, 1H). ^{13}C NMR (126 MHz, $CDCl_3$): δ 154.0, 152.75, 152.69, 138.57, 138.42, 138.24, 137.97, 137.81, 137.74, 128.54, 128.46, 128.41, 128.40, 128.15, 128.12, 128.07, 128.04, 128.02, 127.93, 127.87, 127.77, 127.67, 97.6, 91.4, 84.5, 83.1, 81.7, 80.0, 77.46, 77.39, 75.76, 75.72, 75.21, 75.14, 74.8, 74.0, 73.4, 69.8, 67.6, 67.2, 55.7. LRMS (ESI): *m/z* calcd. for $C_{34}H_{36}NaO_7$ $[M+Na]^+$ 579.6; found, 579.4.

6-*O*-(4-methoxyphenyl)-D-glucopyranoside (52)

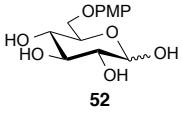

52

To a solution of **69** (8 mg, 0.15mmol) in ethanol (2 mL) was added Pd/C (5 mol %) and the reaction mixture was purged three times with H_2. The mixture was stirred under H_2 atmosphere overnight, filtered over Celite® and the solvent was evaporated to afforded **52** as a white powder (4 mg, 98%)**.** ^{1}H NMR (500 MHz, D_2O): δ 7.02-6.96 (m, 8H), 5.24 (d, *J* = 3.8 Hz, 1H), 4.67 (dd, *J* = 8.0, 0.6 Hz, 1H), 4.31-4.29 (m, 1H), 4.24 (dd, *J* = 10.9, 2.0 Hz, 1H), 4.17 (ddd, *J* = 18.6, 11.1, 5.4 Hz, 2H), 4.10-4.07 (m, 1H), 3.79 (d, *J* = 19.4 Hz, 6H), 3.73 (t, *J* = 9.6 Hz, 2H), 3.60-3.55 (m, 3H), 3.52-3.49 (m, 1H), 3.28 (dd, *J* = 9.0, 8.1 Hz, 1H). ^{13}C NMR (126 MHz, D_2O): δ 153.6, 153.5, 152.4, 152.3, 116.3, 116.3, 115.1, 96.0, 92.1, 75.6, 74.1, 74.0, 72.7, 71.4, 69.7, 69.5, 69.5, 68.0, 67.8, 55.8. LRMS (ESI): *m/z* calcd. for $C_{13}H_{18}KO_7$ $[M+K]^+$ 325.3; found, 325.1.

4-Methoxyphenyl-6-*O*-(2,3,4,6-tetra-*O*-acetyl-α-D-galactopyranosyl)-2,3,4-tri-*O*-acetyl-β-D-glucopyranoside (79)

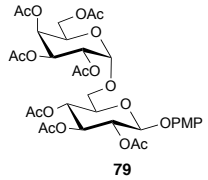

79

Compound **79** was prepared in a similar manner as **2a** from 6-*O*-(2,3,4,6-tetra-*O*-acetyl-α-D-galactopyranosyl)-1,2,3,4-tetra-*O*-acetyl-β-D-glucopyranoside[69] (175 mg, 0.26 mmol), 4-methoxyphenol (45 mg, 0.36 mmol) with boron trifluoride diethyl etherate (42 μL, 0.34 mmol)**.** Column chromatography (1:1 hexanes/EtOAc) afforded **79** as a white powder (150 mg, 78%). ^{1}H NMR (400 MHz, $CDCl_3$): δ 6.93-6.87 (m, 4H), 5.35-5.23 (m, 3H), 5.17 (dd, *J* = 9.7, 7.9 Hz, 1H), 5.10-5.00 (m, 4H), 4.15-4.12 (m, 1H), 3.89-3.88 (m, 2H), 3.84-3.74 (m, 5H), 3.54-3.51 (m, 1H), 2.09 (s, 5H), 2.05 (s, 6H), 2.01 (s, 3H), 1.98 (s, 3H), 1.94 (s, 3H). ^{13}C NMR (101 MHz, $CDCl_3$): δ 170.5, 170.3, 170.2, 170.2, 169.8, 169.4, 169.4, 155.7, 150.4, 117.7, 114.7, 98.9, 96.0, 77.2, 72.7, 71.2, 68.8, 68.1, 67.3, 66.4, 66.3, 61.5, 55.6, 20.8, 20.6, 20.7, 20.6, 20.6. LRMS (ESI): *m/z* calcd. for $C_{33}H_{44}NO_{19}$ $[M+NH_4]^+$ 761.7; found, 761.2.

4-Methoxyphenyl-6-*O*-(α-D-galactopyranosyl)-β-D-glucopyranoside (70)

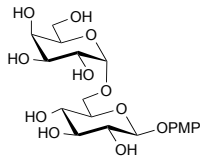

70
β-PMP-Melibiose

Compound **79** (66 mg, 0.089 mmol) was dissolved in a solution of sodium methoxide in methanol (2 mL) and stirred for one hour at room temperature. The solution was then neutralized with Amberlite® IR-120 (H^+) ion-exchange resin, filtered and concentrated. The filtrate was concentrated and the product was lyophilized to yield **70** as a white powder (28 mg, 70%). ^{1}H NMR (500 MHz, D_2O): δ 7.11 (dd, *J* = 9.2, 1.1 Hz, 2H), 6.99 (dd, *J* = 9.2, 1.1 Hz, 2H), 5.12 (d, *J* = 7.7 Hz, 1H), 4.95 (s, 1H), 3.89-3.86 (m, 1H), 3.82 (s, 3H), 3.79-3.74 (m, 6H), 3.66-3.50 (m, 6H). ^{13}C NMR (126 MHz, D_2O): δ 154.5, 150.3, 117.7, 114.9, 100.0, 97.5, 75.7, 74.5, 72.9, 70.6, 69.6, 69.3, 69.1, 68.2, 65.4, 61.0, 55.8. LRMS (ESI): *m/z* calcd. for $C_{19}H_{27}O_{12}$ $[M-H]^-$ 447.4; found, 447.2.

4-Methoxyphenyl-4-*O*-(2,3,4,6-tetra-*O*-acetyl-β-D-galactopyranosyl)-2,3,6-tri-*O*-acetyl-β-D-glucopyranoside (81)

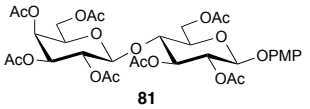

81

Compound **81** was prepared in a similar manner as **2a** from 4-*O*-(2,3,4,6-tetra-*O*-acetyl-β-D-galactopyranosyl)-1,2,3,6-tetra-*O*-acetyl-β-D-glucopyranoside[69] (500 mg, 0.74 mmol), 4-methoxyphenol (128 mg, 1.03 mmol) with boron trifluoride diethyl etherate (460 μL, 3.68 mmol)**.** Column chromatography (1:1 hexanes/EtOAc) afforded **81** as a white powder (461 mg, 84%). ^{1}H NMR (500 MHz, $CDCl_3$): δ 6.94-6.90 (m, 2H), 6.82-6.79 (m, 2H), 5.35 (dd, *J* = 3.4, 0.9 Hz, 1H), 5.26 (t, *J* = 9.1 Hz, 1H), 5.16-5.10 (m, 2H),

4.96 (dd, *J* = 10.4, 3.4 Hz, 1H), 4.92 (d, *J* = 7.8 Hz, 1H), 4.51-4.49 (m, 2H), 4.16-4.12 (m, 2H), 4.08 (dd, *J* = 11.1, 7.4 Hz, 1H), 3.90-3.86 (m, 2H), 3.77 (s, 3H), 3.72 (ddd, *J* = 9.9, 5.6, 2.1 Hz, 1H), 2.16 (s, 3H), 2.10 (s, 3H), 2.07 (s, 6H), 2.07 (s, 3H), 2.05 (s, 3H), 1.97 (s, 3H). ^{13}C NMR (126 MHz, $CDCl_3$): δ 170.37, 170.32, 170.15, 170.08, 169.77, 169.63, 169.1, 155.7, 150.8, 118.6, 114.5, 101.1, 99.9, 76.2, 72.78, 72.68, 71.5, 70.9, 70.7, 69.0, 66.5, 61.9, 60.8, 55.6, 20.83, 20.73, 20.67, 20.65, 20.54. LRMS (ESI): *m/z* calcd. for $C_{33}H_{44}NO_{19}$ $[M+NH_4]^+$ 761.7; found, 761.5.

4-Methoxyphenyl-4-*O*-(β-D-galactopyranosyl)-β-D-glucopyranoside (73)

Compound **81** (171 mg, 0.23 mmol) was dissolved in a solution of sodium methoxide in methanol (2 mL) and stirred for one hour at room temperature. The solution was then neutralized with Amberlite® IR-120 (H^+) ion-exchange resin, filtered and concentrated. The filtrate was concentrated and the product was lyophilized to yield **73** as a white powder (83 mg, 80%). ^{1}H NMR (500 MHz, D_2O): δ 6.95-6.93 (m, 2H), 6.82-6.80 (m, 2H), 4.87 (d, *J* = 7.9 Hz, 1H), 4.30 (d, *J* = 7.8 Hz, 1H), 3.82-3.79 (m, 1H), 3.75 (d, *J* = 3.4 Hz, 1H), 3.67 (d, *J* = 4.3 Hz, 1H), 3.63 (s, 3H), 3.61-3.55 (m, 6H), 3.49 (dd, *J* = 10.0, 3.4 Hz, 1H), 3.42-3.36 (m, 3H). ^{13}C NMR (126 MHz, D_2O): δ 154.6, 150.7, 118.1, 114.9, 102.8, 100.9, 77.9, 75.3, 74.8, 74.1, 72.55, 72.39, 70.8, 68.4, 60.9, 59.7, 55.7. LRMS (ESI): *m/z* calcd. for $C_{19}H_{28}NaO_{12}$ $[M+NaH]^+$ 471.4; found, 471.0.

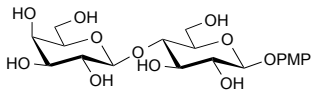

73
β-PMP-Lactose

4-Methoxyphenyl-6-*O*-(2,3,4,6-tetra-*O*-benzyl-D-glucopyranosyl)-2:3,4-tri-*O*-benzyl-β-D-glucopyranoside (82α and 82β)

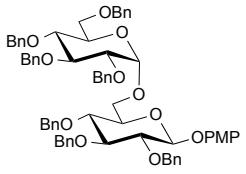

82α

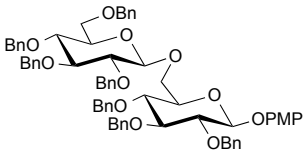

82β

Compound **55**[44] (273mg, 0.51 mmol) was brominated as described previously (see chapter 5, compound **39α**).[46] The crude glycosyl bromide **56** was dissolved three times with toluene and volatiles were removed as an azeotrope with water, then dissolved dry CH_2Cl_2 (1 mL) and added dropwise to a mixture of *para*-methoxyphenyl-2,3,4-tri-*O*-Benzyl-β-D-glucopyranoside (compound **20**, chapter 5) (140 mg, 0.25 mmol), tetraethylammonium bromide (106 mg, 0.51 mmol) and DIPEA (88 μL, 0.51 mmol) stirring in dry CH_2Cl_2 (5 mL) with 4Å molecular sieves under argon. The reaction mixture was stirred for 4 days, then diluted with CH_2Cl_2, washed with brine, dried over $MgSO_4$ and concentrated. Column chromatography over a gradient (9:1 then 7:3

hexanes/ethyl acetate) afforded a mixture of **82α/β** (6:1) as a white solid (195 mg, 72%). Further purification with flash chromatography (50:50:1 CH_2Cl_2/hexanes/acetone) afforded pure **82α** (154 mg, 57%) and pure **82β** (18 mg, 7%).

Characterization data for 82α:

^{1}H NMR (500 MHz, $CDCl_3$): δ 7.39-7.22 (m, 30H), 7.10 (dd, *J* = 6.5, 2.8 Hz, 2H), 7.04-7.03 (m, 2H), 6.79-6.77 (m, 2H), 5.00-4.95 (m, 3H), 4.93-4.90 (m, 2H), 4.85-4.77 (m, 5H), 4.73 (dd, *J* = 11.5, 6.4 Hz, 2H), 4.66 (d, *J* = 11.1 Hz, 1H), 4.59 (d, *J* = 12.1 Hz, 1H), 4.45 (dd, *J* = 18.9, 11.6 Hz, 2H), 3.97 (t, *J* = 9.3 Hz, 1H), 3.85-3.82 (m, 2H), 3.77 (dd, *J* = 11.4, 1.4 Hz, 1H), 3.71-3.63 (m, 4H), 3.61-3.54 (m, 7H). ^{13}C NMR (126 MHz, $CDCl_3$): δ 155.4, 151.4, 138.8, 138.5, 138.5, 138.4, 138.3, 138.1, 137.9, 128.4, 128.4, 128.3, 128.3, 128.2, 128.2, 127.9, 127.9, 127.8, 127.8, 127.8, 127.7, 127.6, 127.5, 119.0, 114.6, 103.1, 97.3, 82.1, 81.8, 80.0, 77.6, 75.7, 75.1, 75.0, 74.9, 74.7, 73.3, 72.5, 70.1, 68.4, 66.0, 55.4. LRMS (ESI): *m/z* calcd. for $C_{68}H_{70}KO_{12}$ $[M+K]^+$ 1118.3; found, 1118.5.

Characterization data for 82β:

^{1}H NMR (500 MHz, $CDCl_3$): δ 7.36-7.28 (m, 30H), 7.02-6.99 (m, 2H), 6.68-6.67 (m, 2H), 5.05 (d, *J* = 10.9 Hz, 1H), 4.97-4.91 (m, 4H), 4.81 (ddd, *J* = 11.0, 7.1, 4.0 Hz, 5H), 4.67 (d, *J* = 11.0 Hz, 1H), 4.60-4.58 (m, 2H), 4.53-4.44 (m, 4H), 4.18 (d, *J* = 9.3 Hz, 1H), 3.76-3.68 (m, 7H), 3.60 (s, 4H), 3.56 (m, 1H), 3.47 (dd, *J* = 9.8, 7.0 Hz, 1H). ^{13}C NMR (126 MHz, $CDCl_3$): δ 156.2, 150.7, 138.8, 138.5, 138.5, 138.4, 138.3, 138.1, 137.9, 128.4, 128.4, 128.3, 128.3, 128.2, 128.2, 127.9, 127.9, 127.8, 127.8, 127.8, 127.7, 127.6, 127.5, 118.2, 114.8, 103.1, 99.8, 82.1, 81.2, 80.4, 77.6, 75.7, 75.1, 75.0, 74.9, 74.7, 73.9, 72.5, 71.1, 67.4, 66.0, 56.4. LRMS (ESI): *m/z* calcd. for $C_{68}H_{70}NaO_{12}$ $[M+K]^+$ 1102.3; found, 1102.0.

4-Methoxyphenyl-6-*O*-(α-D-glucopyranosyl)-β-D-glucopyranoside (71)

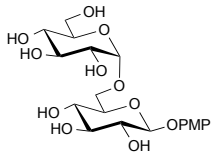

71

To a solution of **82α** (117 mg, 0.11 mmol) in ethanol (4 mL) was added palladium hydroxide (5 mol %) and the reaction mixture was purged three times with H_2. The mixture was stirred under H_2 atmosphere overnight, filtered over Celite ® and the solvent was evaporated to afforded **71** as a white powder (45 mg, 93%)**.** ^{1}H NMR (500 MHz, D_2O): δ 7.14-7.10 (m, 2H), 7.00-6.97 (m, 2H), 5.06 (d, *J* = 7.4 Hz, 1H), 4.93 (d, *J* = 3.7 Hz, 1H), 3.95 (dd, *J* = 11.4, 5.4 Hz, 1H), 3.81 (s, 3H), 3.78 (dd, *J* = 6.2, 2.2 Hz, 2H), 3.75-3.62 (m, 4H), 3.60-3.53 (m, 4H), 3.41 (t, *J* = 9.4 Hz, 1H). ^{13}C NMR (126 MHz,

D_2O): δ 154.6, 150.7, 117.9, 115.0, 100.8, 97.8, 75.7, 74.4, 73.05, 72.89, 71.7, 71.4, 69.31, 69.28, 65.6, 60.3, 55.8. LRMS (ESI): *m/z* calcd. for $C_{19}H_{28}NaO_{12}$ $[M+Na]^+$ 471.4; found, 471.2.

4-Methoxyphenyl-6-*O*-(β-D-glucopyranosyl)-β-D-glucopyranoside (72)

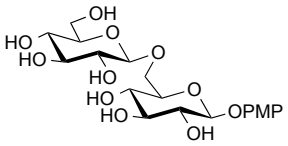

72

To a solution of **82β** (117 mg, 0.11 mmol) in ethanol (4 mL) was added palladium hydroxide (5 mol %) and the reaction mixture was purged three times with H_2. The mixture was stirred under H_2 atmosphere overnight, filtered over Celite® and the solvent was evaporated to afforded **72** as a white powder (45 mg, 93%)**.** ^{1}H NMR (500 MHz, D_2O): δ 7.15-7.11 (m, 2H), 7.01-6.98 (m, 2H), 5.06 (d, *J* = 7.9 Hz, 1H), 4.47 (d, *J* = 7.9 Hz, 1H), 4.19 (dd, *J* = 12.0, 1.7 Hz, 1H), 3.91-3.86 (m, 2H), 3.82 (s, 3H), 3.79-3.77 (m, 1H), 3.68 (dd, *J* = 12.4, 5.9 Hz, 1H), 3.60-3.52 (m, 3H), 3.44-3.26 (m, 4H). ^{13}C NMR (126 MHz, D_2O): δ 154.7, 150.7, 118.2, 115.0, 102.4, 100.9, 75.8, 75.59, 75.42, 75.33, 73.05, 72.86, 69.6, 69.3, 68.1, 60.6, 55.8. LRMS (ESI): *m/z* calcd. for $C_{19}H_{28}NaO_{12}$ $[M+Na]^+$ 471.4; found, 471.0.

1,4-Bis-(β-D-glucopyranosyl)benzene (83)

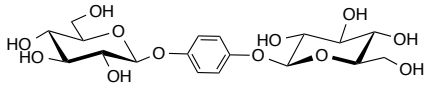

83

Compound **83a** (300 mg, 0.4 mmol) was dissolved in a solution of sodium methoxide in methanol (5 mL) and stirred for one hour at room temperature. The solution was then neutralized with Amberlite® IR-120 (H^+) ion-exchange resin, filtered and concentrated. The filtrate was concentrated and the product was lyophilized to yield **83** as a white powder (160 mg, 95%). ^{1}H NMR (400 MHz, D_2O): δ 7.11 (s, 4H), 5.04 (d, *J* = 7.5 Hz, 2H), 3.91 (dd, *J* = 12.4, 2.2 Hz, 2H), 3.74 (dd, *J* = 12.5, 5.7 Hz, 2H), 3.61-3.45 (m, 8H). ^{13}C NMR (101 MHz, D_2O): δ 152.3, 118.0, 100.8, 76.1, 75.5, 72.9, 69.4, 60.5. LRMS (ESI): *m/z* calcd. for $C_{18}H_{26}NaO_{12}$ $[M+Na]^+$ 457.4; found, 457.2.

1,4-Bis-(β-D-galactopyranosyl)benzene (84)

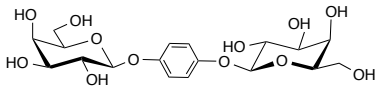

84

Compound **84a** (100 mg, 0.13 mmol) was dissolved in a solution of sodium methoxide in methanol (5 mL) and stirred for one hour at room temperature. The solution was then neutralized with Amberlite® IR-120 (H^+) ion-exchange resin, filtered and concentrated. The filtrate was concentrated and the product was lyophilized to yield **84** as a white powder (53 mg, 94%). ^{1}H NMR (400 MHz, D_2O): δ 7.11 (s, 4H), 4.98 (d, *J* = 7.0 Hz, 2H), 3.98 (d, *J* = 2.8 Hz, 2H), 3.85-

3.72 (m, 11H). ^{13}C NMR (101 MHz, D_2O): δ 152.4, 117.9, 101.4, 75.4, 72.5, 70.6, 68.5, 60.7. LRMS (ESI): *m/z* calcd. for $C_{18}H_{26}NaO_{12}$ $[M+Na]^+$ 457.4; found, 457.3.

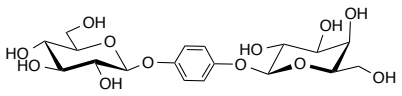

85

1-O-(β-D-glucopyranosyl)-4-O-(β-D-galactopyranosyl)-benzene (85)

Compound **85a** (10 mg, 0.013 mmol) was dissolved in a solution of sodium methoxide in methanol (5 mL) and stirred for one hour at room temperature. The solution was then neutralized with Amberlite® IR-120 (H^+) ion-exchange resin, filtered and concentrated. The filtrate was concentrated and the product was lyophilized to yield **85** as a white powder (5 mg, 94%). ^{1}H NMR (400 MHz, D_2O): δ 7.14-7.12 (m, 4H), 5.05 (d, *J* = 7.5 Hz, 1H), 4.99 (d, *J* = 7.2 Hz, 1H), 3.99 (dd, *J* = 3.0, 0.7 Hz, 1H), 3.92 (dd, *J* = 12.4, 2.2 Hz, 1H), 3.84-3.81 (m, 1H), 3.79-3.72 (m, 6H), 3.62-3.46 (m, 6H). ^{13}C NMR (101 MHz, D_2O): δ 152.5, 152.3, 152.2, 118.0, 117.9, 101.4, 100.9, 76.1, 75.6, 75.4, 72.9, 72.6, 70.6, 69.4, 68.5, 60.8, 60.5. LRMS (ESI): *m/z* calcd. for $C_{18}H_{26}NaO_{12}$ $[M+Na]^+$ 457.4; found, 457.0.

1,3-Bis-(β-D-glucopyranosyl)benzene (86)

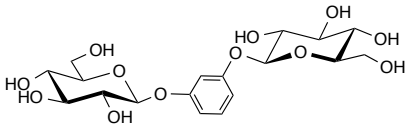

86

Compound **86a** (85 mg, 0.11 mmol) was dissolved in a solution of sodium methoxide in methanol (5 mL) and stirred for one hour at room temperature. The solution was then neutralized with Amberlite® IR-120 (H^+) ion-exchange resin, filtered and concentrated. The filtrate was concentrated and the product was lyophilized to yield 86 as a white powder (28 mg, 58%). ^{1}H NMR (400 MHz, D_2O 7.36-7.32 (m, 1H), 6.93-6.86 (m, 3H), 5.12 (d, *J* = 7.3 Hz, 2H), 3.93 (m, 2H), 3.74 (dd, *J* = 12.4, 6.0 Hz, 3H), 3.67-3.45 (m, 9H). ^{13}C NMR (101 MHz, D_2O): δ 157.6, 130.7, 111.1, 105.0, 100.0, 76.2, 75.6, 72.9, 69.5, 60.6. LRMS (ESI): *m/z* calcd. for $C_{18}H_{30}NO_{12}$ $[M+NH_4]^+$ 452.5; found, 452.2.

7.6 References

1. Tam, R.Y.; Ferreira, S.S.; Czechura, P.; Chaytor, J.L.; Ben, R.N. *J. Am. Chem. Soc.* **2008**, *130*, 17494-17501.

2. Chaytor, J.L.; Ben, R.N. *Bioorg. Med. Chem. Lett.* **2010**, *20*, 5251-5254.

3. Chaytor, J.L.; Tokarew, J.M.; Wu, L.K.; Leclère, M.; Tam, R.Y.; Capicciotti, C.J.; Guolla, L.; von Moos, E.; Findlay, C.S.; Allan, D.S.; Ben, R.N. *Glycobiology*. **2012**, *22*, 123-133.

4. Balcerzak, A.K.; Ferreira, S.S.; Trant, J.F.; Ben, R.N. *Bioorg. Med. Chem. Lett.* **2012**, *22*, 1719-1721.

5. Capicciotti, C.J.; Leclère, M.; Perras, F.A.; Bryce, D.L.; Paulin, H.; Harden, J.; Liu, Y.; Ben, R.N. *Chem. Sci.* **2012**, *3*, 1408-1416.

6. Balcerzak, A.K.; Febbraro, M.; Ben, R.N. *RSC Adv.* **2013**, *3*, 3232-3236.

7. Trant, J.F.; Biggs, R.A.; Capicciotti, C.J.; Ben, R.N. *RSC Adv.* **2013**, *3*, 26005-26009.

8. de Almeida, M.V.; Le Hyaric, M. *Mini-Rev. Org. Chem.* **2005**, *2*, 283-297.

9. Lorber, B.; Bishop, J.B.; DeLucas, L.J. *Biochim. Biophys. Acta.* **1990**, *1023*, 254-265.

10. Michel, H.; Oesterhelt, D. *Proc. Natl. Acad. Sci. U.S.A.* **1980**, *77*, 1283-1285.

11. Harvie, P.; Wong, F.M.P.; Bally, M.B. *Biophys. J.* **1998**, *75*, 1040-1051.

12. Hildreth, J.E. *Biochem. J.* **1982**, *207*, 363-366.

13. Baron, C.; Thompson, T.E. *Biochim. Biophys. Acta.* **1975**, *382*, 276-285.

14. Plusquellec, D.; Chevalier, G.; Talibart, R.; Wróblewski, H. *Anal. Biochem.* **1989**, *179*, 145-153.

15. Budke, C.; Heggemann, C.; Koch, M.; Sewald, N.; Koop, T. *J. Phys. Chem. B.* **2009**, *113*, 2865-2873.

16. Smits, E.; Engberts, J.B.F.N.; Kellogg, R.M.; van Doren, H.A. *J. Chem. Soc., Perkin Trans. 1.* **1996**, 2873-2877.

17. McGill, N.W.; Williams, S.J. *J. Org. Chem.* **2009**, *74*, 9388-9398.

18. Crich, D.; Sun, S. *Tetrahedron.* **1998**, *54*, 8321-8348.

19. Crich, D.; Sun, S. *J. Org. Chem.* **1997**, *62*, 1198-1199.

20. Crich, D.; Sun, S. *J. Org. Chem.* **1996**, *61*, 4506-4507.

21. Mukhopadhyay, B.; Kartha, K.P.R.; Russell, D.A.; Field, R.A. *J. Org. Chem.* **2004**, *69*, 7758-7760.

22. Garegg, P.J.; Kvarnström, I.; Niklasson, A.; Niklasson, G.; Svensson, S.C.T. *J. Carbohydr. Chem.* **1993**, *12*, 933-953.

23. Crich, D.; Chandrasekera, N.S. *Angew. Chem. Int. Ed.* **2004**, *43*, 5386-5389.

24. Crich, D.; Sun, S. *J. Am. Chem. Soc.* **1997**, *119*, 11217-11223.

25. Trant, J.F., *Importance of the Structural Components of C-linked Glycopeptides to Specific-Antifreeze Activity: From Glycopeptides to Small Molecule Inhibitors of Ice Recrystallization*, 2012, Ph. D. Dissertation, Department of Chemistry, University of Ottawa.

26. Galema, S.A.; Høiland, H. *J. Phys. Chem.* **1991**, *95*, 5321-5326.

27. Czechura, P.; Tam, R.Y.; Dimitrijevic, E.; Murphy, A.V.; Ben, R.N. *J. Am. Chem. Soc.* **2008**, *130*, 2928-2929.

28. Çarçabal, P.; Jockusch, R.A.; Hünig, I.; Snoek, L.C.; Kroemer, R.T.; Davis, B.G.; Gamblin, D.P.; Compagnon, I.; Oomens, J.; Simons, J.P. *J. Am. Chem. Soc.* **2005**, *127*, 11414-11425.

29. Cocinero, E.J.; Stanca-Kaposta, E.C.; Scanlan, E.M.; Gamblin, D.P.; Davis, B.G.; Simons, J.P. *Chem. Eur. J.* **2008**, *14*, 8947-8955.

30. Hunig, I.; Painter, A.J.; Jockusch, R.A.; Carcabal, P.; Marzluff, E.M.; Snoek, L.C.; Gamblin, D.P.; Davis, B.G.; Simons, J.P. *Phys. Chem. Chem. Phys.* **2005**, *7*, 2474-2480.

31. Hammett, L.P. *Chem. Rev.* **1935**, *17*, 125-136.

32. Hammett, L.P. *J. Am. Chem. Soc.* **1937**, *59*, 96-103.

33. Hansch, C.; Leo, A.; Taft, R.W. *Chem. Rev.* **1991**, *91*, 165-195.

34. Lowry, T.H.; Richardson, K.S. Mechanism and theory in organic chemistry (Harper & Row New York; 1981.

35. Jaffé, H.H. *Chem. Rev.* **1953**, *53*, 191-261.

36. Hansch, C.; Leo, A.; Unger, S.H.; Kim, K.H.; Nikaitani, D.; Lien, E.J. *J. Med. Chem.* **1973**, *16*, 1207-1216.

37. Sutton, R.L.; Lips, A.; Piccirillo, G.; Sztehlo, A. *J. Food Sci.* **1996**, *61*, 741-745.

38. Hagiwara, T.; Hartel, R.; Matsukawa, S. *Food Biophys.* **2006**, *1*, 74-82.

39. Chakrabartty, A.; Hew, C.L. *Eur. J. Biochem.* **1991**, *202*, 1057-1063.

40. Tam, R.Y.; Rowley, C.N.; Petrov, I.; Zhang, T.; Afagh, N.A.; Woo, T.K.; Ben, R.N. *J. Am. Chem. Soc.* **2009**, *131*, 15745-15753.

41. Lemieux, R.U.; Driguez, H. *J. Am. Chem. Soc.* **1975**, *97*, 4063-4069.

42. Lemieux, R.U.; Driguez, H. *J. Am. Chem. Soc.* **1975**, *97*, 4069-4075.

43. Lemieux, R.U.; Hendriks, K.B.; Stick, R.V.; James, K. *J. Am. Chem. Soc.* **1975**, *97*, 4056-4062.

44. Dasgupta, S.; Nitz, M. *J. Org. Chem.* **2011**, *76*, 1918-1921.

45. Peri, F.; Dumy, P.; Mutter, M. *Tetrahedron.* **1998**, *54*, 12269-12278.

46. Grayson, E.J.; Ward, S.J.; Hall, A.L.; Rendle, P.M.; Gamblin, D.P.; Batsanov, A.S.; Davis, B.G. *J. Org. Chem.* **2005**, *70*, 9740-9754.

47. Blom, P.; Ruttens, B.; Van Hoof, S.; Hubrecht, I.; Van der Eycken, J.; Sas, B.; Van hemel, J.; Vandenkerckhove, J. *J. Org. Chem.* **2005**, *70*, 10109-10112.

48. Kulakov, I.V.; Il'in, A.I.; Kabyl, Z.A.; Gazaliev, A.M. *Russ. Chem. Bull.* **2008**, *57*, 2443-2445.

49. Whistler, R.L.; Wolfrom, M.L.; BeMiller, J.N. Methods in carbohydrate chemistry - Volume 2. (New York; London: Academic Press; 1963.

50. Demchenko, A.V.; Pornsuriyasak, P.; De Meo, C. *J. Chem. Educ.* **2006**, *83*, 782.

51. Matwiejuk, M.; Thiem, J. *Chem. Commun.* **2011**, *47*, 8379-8381.

52. Ohlin, M.; Johnsson, R.; Ellervik, U. *Carbohydr. Res.* **2011**, *346*, 1358-1370.

53. Daragics, K.; Szabó, P.; Fügedi, P. *Carbohydr. Res.* **2011**, *346*, 1633-1637.

54. Johnsson, R.; Cukalevski, R.; Dragén, F.; Ivanisevic, D.; Johansson, I.; Petersson, L.; Wettergren, E.E.; Yam, K.B.; Yang, B.; Ellervik, U. *Carbohydr. Res.* **2008**, *343*, 2997-3000.

55. Johnsson, R.; Olsson, D.; Ellervik, U. *J. Org. Chem.* **2008**, *73*, 5226-5232.

56. Daragics, K.; Fügedi, P. *Tetrahedron Lett.* **2009**, *50*, 2914-2916.

57. Xu, W.; Springfield, S.A.; Koh, J.T. *Carbohydr. Res.* **2000**, *325*, 169-176.

58. Horton, D.; Hutson, D.H. Developments in the Chemistry of Thio Sugars. In: L.W. Melville and R.S. Tipson, editor. Advances in Carbohydrate Chemistry ed.). Academic Press; 1963. p 123-199.

59. Tvaroska, I.; Mazeau, K.; Blanc-Muesser, M.; Lavaitte, S.; Driguez, H.; Taravel, F.R. *Carbohydr. Res.* **1992**, *229*, 225-231.

60. Vishveshwara, S.; Rao, V.S.R. *Carbohydr. Res.* **1982**, *104*, 21-32.

61. Alabugin, I.V.; Zeidan, T.A. *J. Am. Chem. Soc.* **2002**, *124*, 3175-3185.

62. Alabugin, I.V.; Manoharan, M.; Zeidan, T.A. *J. Am. Chem. Soc.* **2003**, *125*, 14014-14031.

63. DeVries, A.L.; Vandenheede, J.; Feeney, R.E. *J. Biol. Chem.* **1971**, *246*, 305-308.

64. Feeney, R.E.; Burcham, T.S.; Yeh, Y. *Annu. Rev. Biophys. Biophys. Chem.* **1986**, *15*, 59-78.

65. Harding, M.M.; Anderberg, P.I.; Haymet, A.D.J. *Eur. J. Biochem.* **2003**, *270*, 1381-1392.

66. Bouvet, V.; Ben, R.N. *Cell Biochem. Biophys.* **2003**, *39*, 133-144.

67. Garner, J.; Harding, M.M. *ChemBioChem.* **2010**, *11*, 2489-2498.

68. Peltier, R.; Brimble, M.A.; Wojnar, J.M.; Williams, D.E.; Evans, C.W.; DeVries, A.L. *Chem. Sci.* **2010**, *1*, 538-551.

69. Damkaci, F.; DeShong, P. *J. Am. Chem. Soc.* **2003**, *125*, 4408-4409.

70. Czechura, P., *Elucidating the Relationship Between Hydration and Ice Recrystallization Inhibition with C-Linked Antifreeze Glycoproteins*, 2009, Ph. D. Dissertation, Department of Chemistry, University of Ottawa.

71. Chan, L.; Taylor, M.S. *Org. Lett.* **2011**, *13*, 3090-3093.

72. Gouliaras, C.; Lee, D.; Chan, L.; Taylor, M.S. *J. Am. Chem. Soc.* **2011**, *133*, 13926-13929.

73. Lee, D.; Taylor, M.S. *Synthesis.* **2012**, *44*, 3421-3431.

74. Lee, D.; Taylor, M.S. *J. Am. Chem. Soc.* **2011**, *133*, 3724-3727.

75. Lee, D.; Williamson, C.L.; Chan, L.; Taylor, M.S. *J. Am. Chem. Soc.* **2012**, *134*, 8260-8267.

76. McClary, C.A.; Taylor, M.S. *Carbohydr. Res.* **2013**, *381*, 112-122.

77. Hagiwara, T.; Sakiyama, T.; Watanabe, H. *Food Biophys.* **2009**, *4*, 340-346.

78. Heggemann, C.; Budke, C.; Schomburg, B.; Majer, Z.; Wißbrock, M.; Koop, T.; Sewald, N. *Amino Acids.* **2010**, *38*, 213-222.

79. Nagel, L.; Plattner, C.; Budke, C.; Majer, Z.; Devries, A.L.; Berkemeier, T.; Koop, T.; Sewald, N. *Amino Acids.* **2011**, *41*, 719-732.

80. Nagel, L.; Budke, C.; Erdmann, R.S.; Dreyer, A.; Wennemers, H.; Koop, T.; Sewald, N. *Chem. Eur. J.* **2012**, *18*, 12783-12793.

81. Peltier, R.; Evans, C.W.; DeVries, A.L.; Brimble, M.A.; Dingley, A.J.; Williams, D.E. *Cryst. Growth Des.* **2010**, *10*, 5066-5077.

82. Lifshitz, I.M.; Slyozov, V.V. *J. Phys. Chem. Solids.* **1961**, *19*, 35-50.

83. Wagner, C. *Z. Elektrochem.* **1961**, *65*, 581-591.

84. Pudney, P.D.A.; Buckley, S.L.; Sidebottom, C.M.; Twigg, S.N.; Sevilla, M.-P.; Holt, C.B.; Roper, D.; Telford, J.H.; McArthur, A.J.; Lillford, P.J. *Arch. Biochem. Biophys.* **2003**, *410*, 238-245.

85. Smallwood, M.; Worrall, D.; Byass, L.; Elias, L.; Ashford, D.; Doucet, C.J.; Holt, C.; Telford, J.; Lillford, P.; Bowles, D.J. *Biochem. J.* **1999**, *340*, 385-391.

86. Bilgram, J.H. *Prog. Cryst. Growth Charact. Mater.* **1993**, *26*, 99-119.

87. Halter, P.U.; Bilgram, J.H.; Känzig, W. *J. Chem. Phys.* **1988**, *89*, 2622-2629.

88. Knight, C.A.; Hallett, J.; DeVries, A.L. *Cryobiology.* **1988**, *25*, 55-60.

89. Jackman, J.; Noestheden, M.; Moffat, D.; Pezacki, J.P.; Findlay, S.; Ben, R.N. *Biochem. Biophys. Res. Commun.* **2007**, *354*, 340-344.

90. Dasgupta, S.; Rajput, V.K.; Roy, B.; Mukhopadhyay, B. *J. Carbohydr. Chem.* **2007**, *26*, 91-106.

91. Lopez, R.; Fernandez-Mayoralas, A. *J. Org. Chem.* **1994**, *59*, 737-745.

92. Saksena, R.; Zhang, J.; Kováč, P. *J. Carbohydr. Chem.* **2002**, *21*, 453-470.

93. Bubb, W.A. *Conc. Magn. Reson. A.* **2003**, *19A*, 1-19.

94. Schwizer, D.; Gäthje, H.; Kelm, S.; Porro, M.; Schwardt, O.; Ernst, B. *Biorg. Med. Chem.* **2006**, *14*, 4944-4957.

95. Li, Y.; Mo, H.; Lian, G.; Yu, B. *Carbohydr. Res.* **2012**, *363*, 14-22.

96. Aich, U.; Loganathan, D. *Carbohydr. Res.* **2006**, *341*, 19-28.

97. Li, Z.-J.; Cai, L.-N.; Cai, M.-S. *Synth. Commun.* **1992**, *22*, 2121-2124.

98. Desai, R.N.; Blackwell, L.F. *Synlett.* **2003**, *2003*, 1981-1984.

99. Hansen, T.N.; Smith, K.M.; Brockbank, K.G.M. *Transplant. Proc.* **1993**, *25*, 3182-3184.

100. Clerici, F.; Gelmi, M.L.; Mottadelli, S. *J. Chem. Soc., Perkin Trans. 1.* **1994**, 985-988.

101. Alberti, A.; Della Bona, M.A.; Macciantelli, D.; Pelizzoni, F.; Sello, G.; Torri, G.; Vismara, E. *Tetrahedron.* **1996**, *52*, 10241-10248.

102. Balthaser, B.R.; McDonald, F.E. *Org. Lett.* **2009**, *11*, 4850-4853.

103. Santra, A.; Sau, A.; Misra, A.K. *J. Carbohydr. Chem.* **2011**, *30*, 85-93.

7.7 NMR Spectra of Compounds in Chapter 7

1

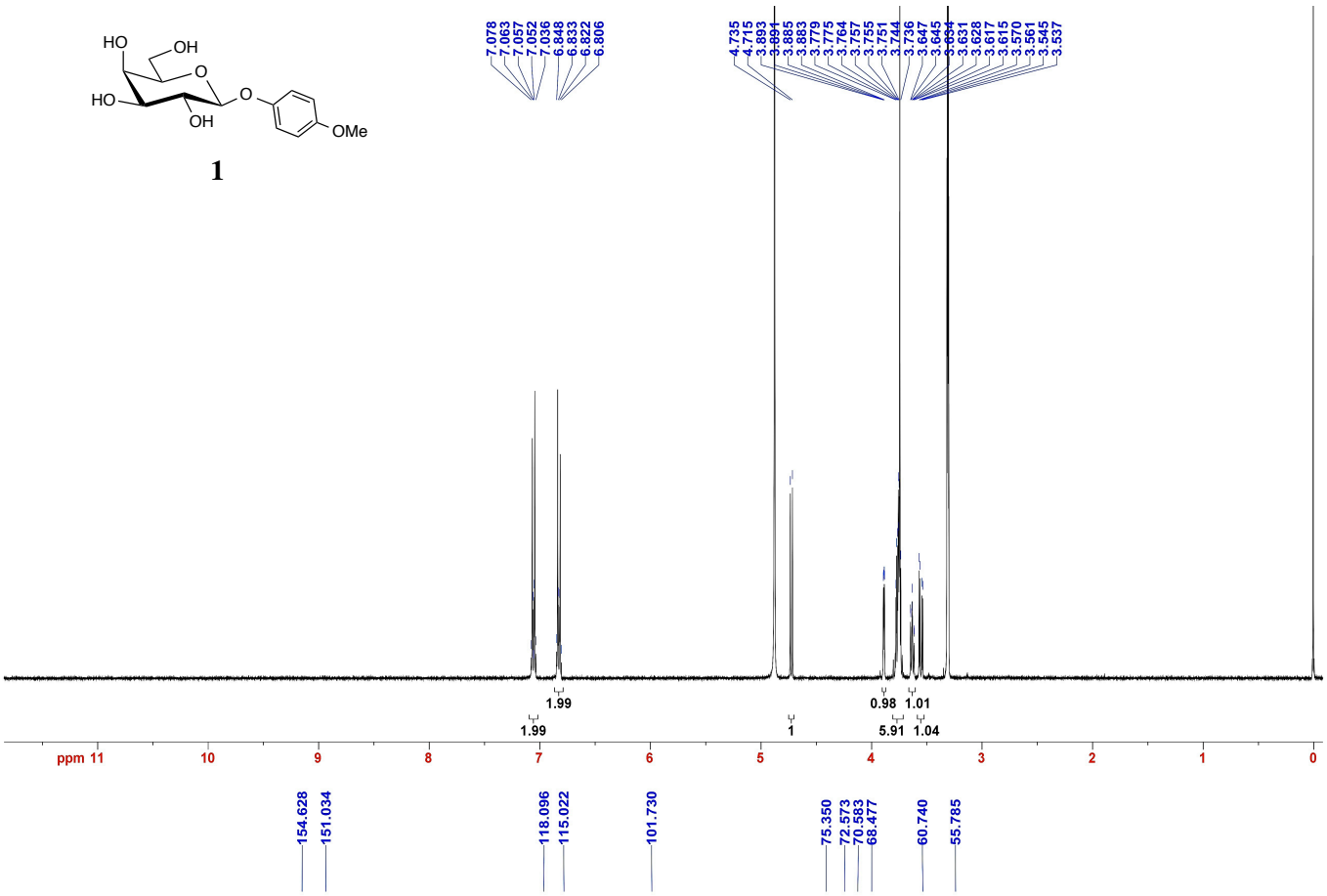

OH
HO
HO
OH
O
O
OMe

2

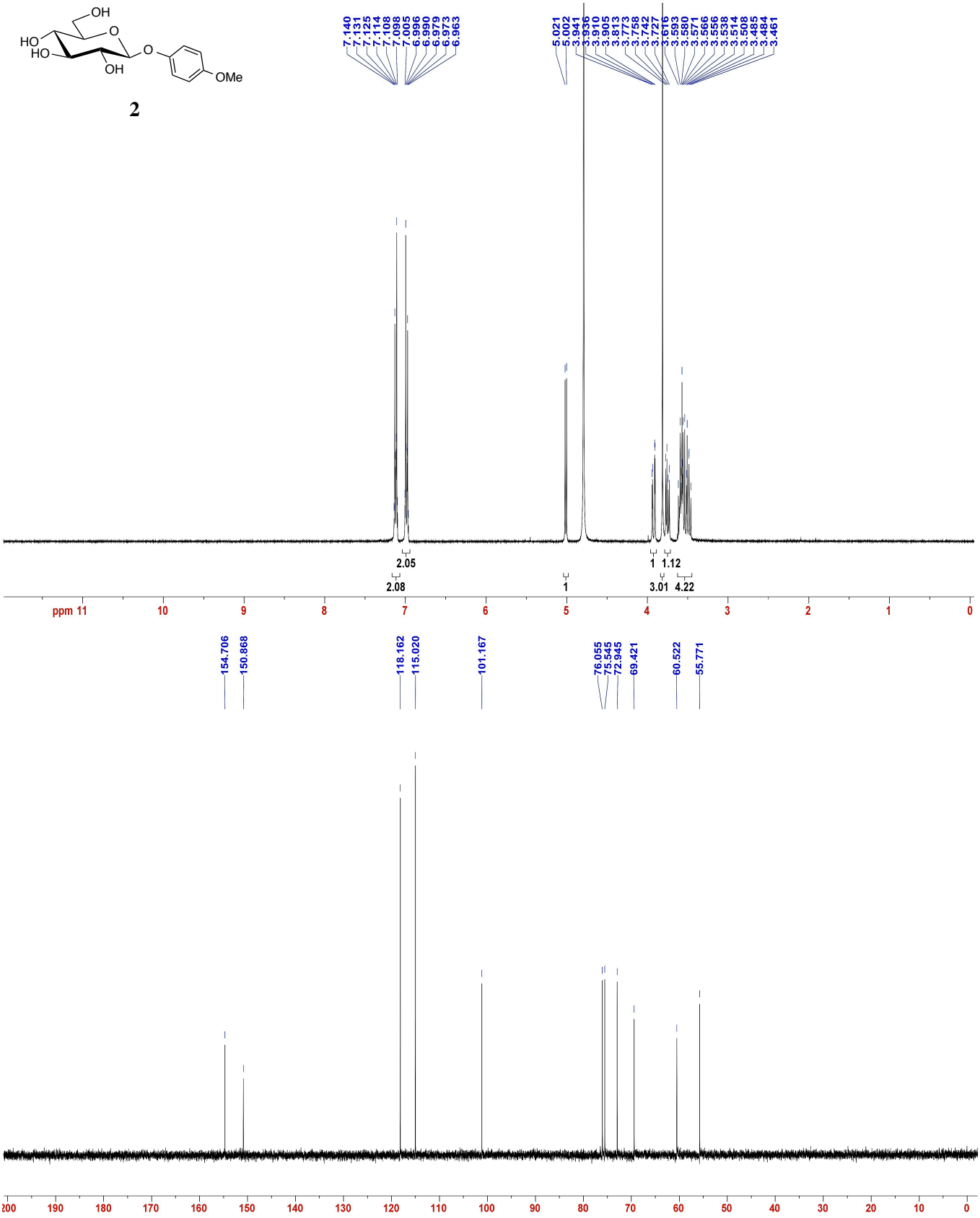
7.140
7.131
7.125
7.114
7.108
7.085
6.996
6.990
6.979
6.973
6.963
5.021
5.002
3.941
3.936
3.910
3.905
3.813
3.773
3.758
3.742
3.727
3.616
3.593
3.580
3.571
3.566
3.556
3.538
3.514
3.508
3.485
3.484
3.461
2.05
2.08
1
1
1.12
3.01
4.22
ppm 11
10
9
8
7
6
5
4
3
2
1
0
154.706
150.868
118.162
115.020
101.167
76.055
75.545
72.945
69.421
60.522
55.771
200
190
180
170
160
150
140
130
120
110
100
90
80
70
60
50
40
30
20
10
0

HO
HO
OH
O
O
OMe

4: β-PMP-Xyl

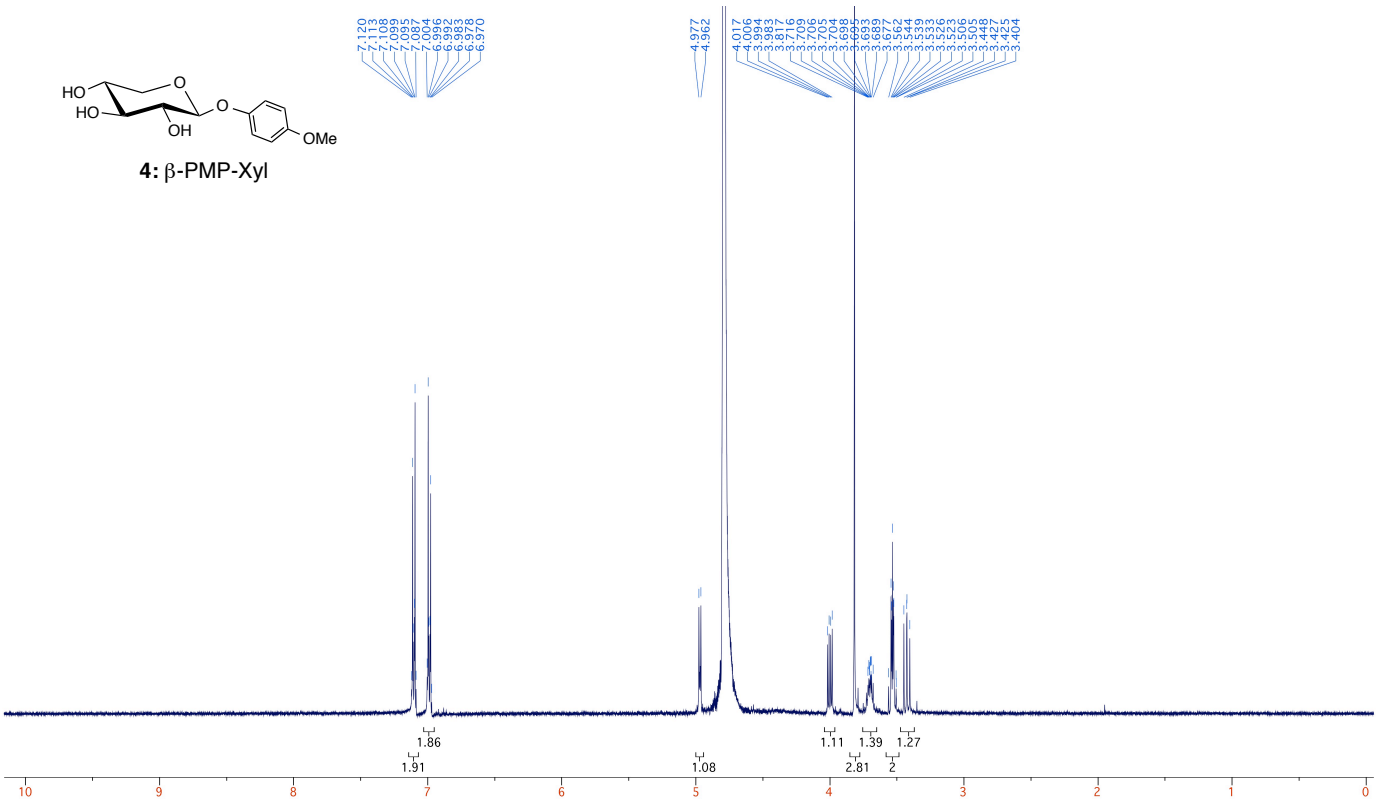
7.120
7.113
7.108
7.099
7.095
7.087
7.004
6.992
6.983
6.978
6.970
4.977
4.962
4.017
4.006
3.994
3.983
3.817
3.716
3.709
3.706
3.705
3.704
3.698
3.693
3.689
3.677
3.672
3.544
3.539
3.533
3.526
3.523
3.506
3.505
3.448
3.427
3.425
3.404
1.86
1.91
1.08
1.11
1.39
1.27
2.81
2
10
9
8
7
6
5
4
3
2
1
0

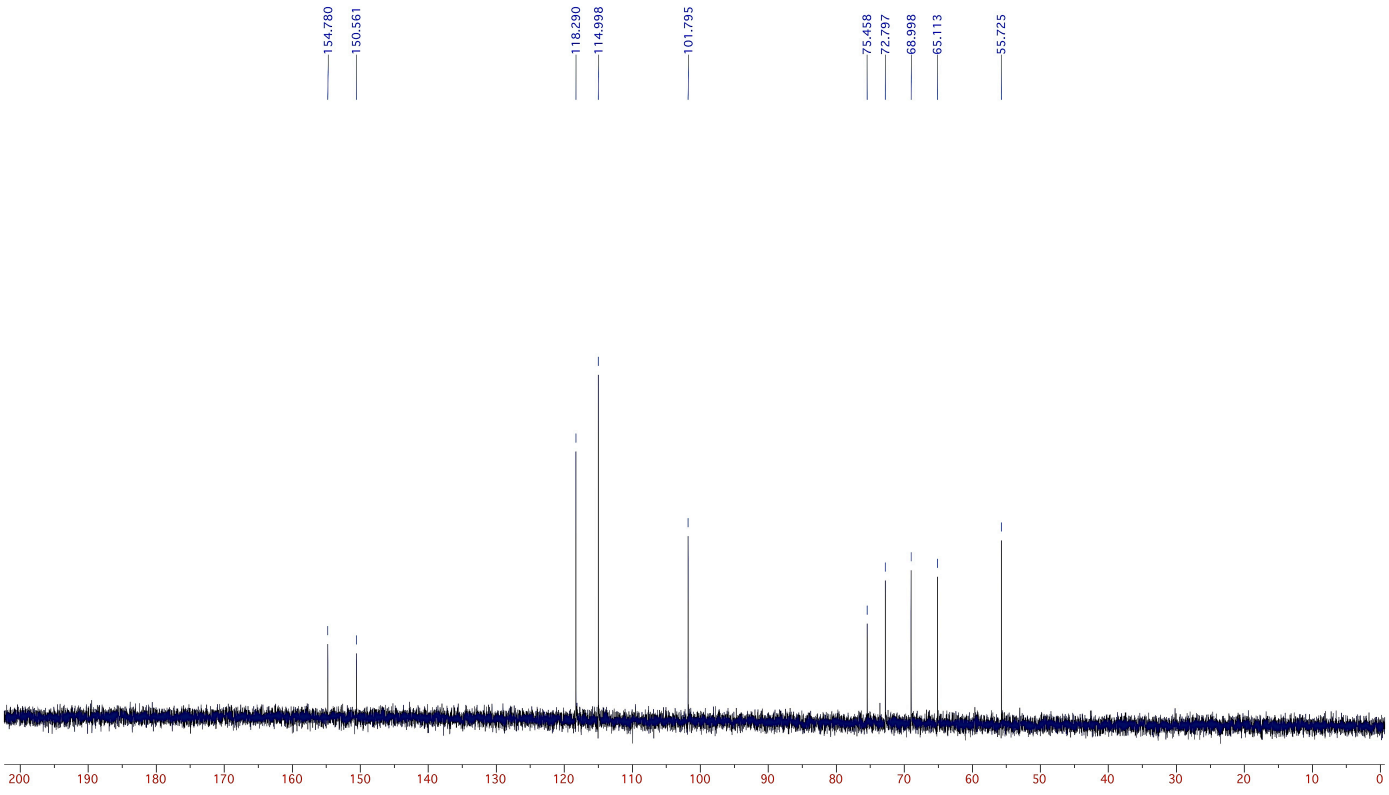
154.780
150.561
118.290
114.998
101.795
75.458
72.797
68.998
65.113
55.725
200
190
180
170
160
150
140
130
120
110
100
90
80
70
60
50
40
30
20
10
0

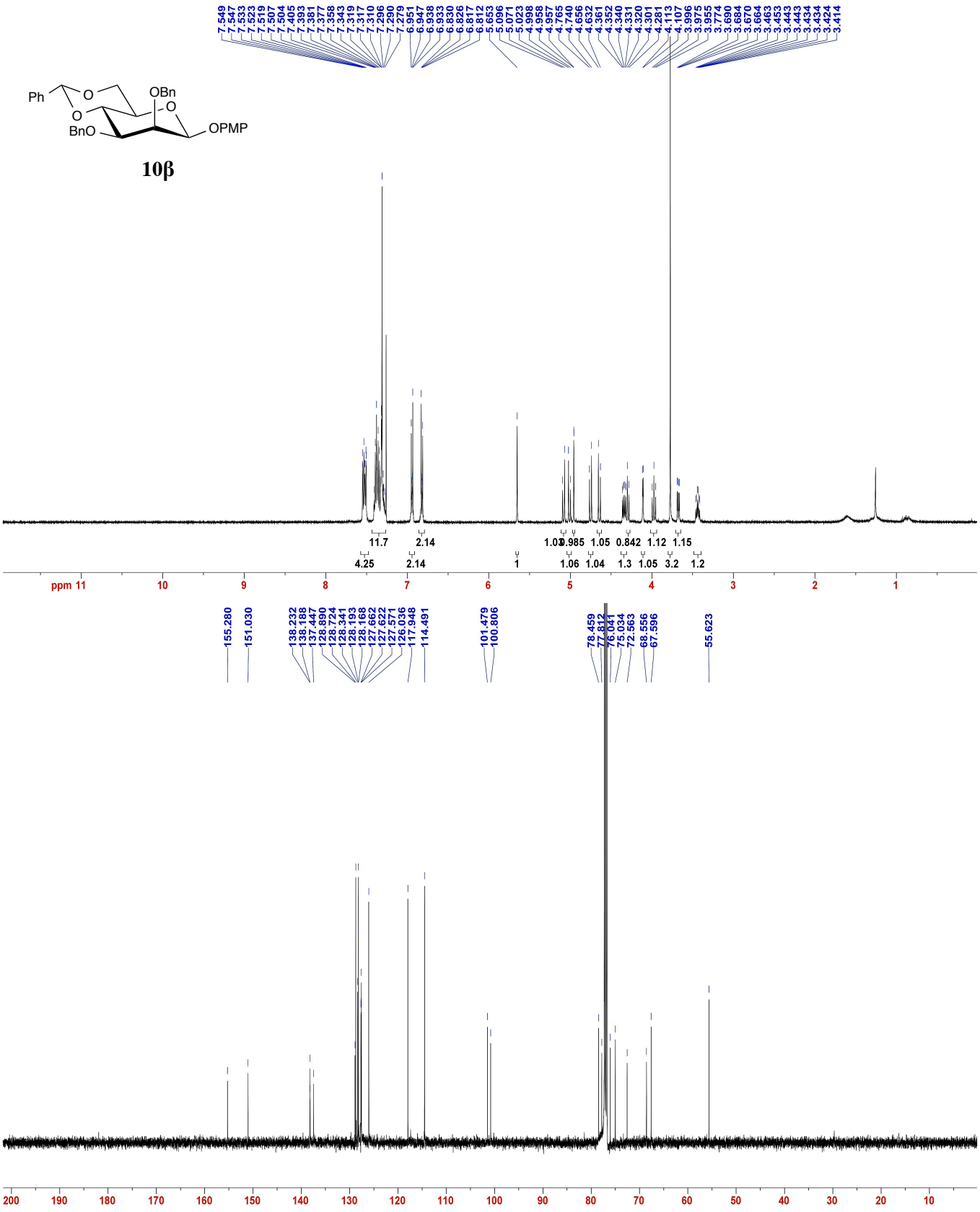
Ph
O
OBn
O
O
BnO
OPMP
10β
7.549 7.547 7.533 7.523 7.519 7.507 7.504 7.405 7.393 7.381 7.377 7.358 7.343 7.319 7.317 7.310 7.296 7.290 7.279 6.951 6.947 6.938 6.933 6.830 6.826 6.817 6.812 5.653 5.096 5.071 5.023 4.998 4.958 4.957 4.765 4.740 4.656 4.632 4.361 4.352 4.340 4.331 4.320 4.301 4.281 4.113 4.107 3.996 3.975 3.955 3.774 3.690 3.684 3.670 3.664 3.463 3.453 3.443 3.443 3.434 3.434 3.424 3.414
11.7 2.14 1.03 0.985 1.05 0.842 1.12 1.15
4.25 2.14 1 1.06 1.04 1.3 1.05 3.2 1.2
ppm 11 10 9 8 7 6 5 4 3 2 1
155.280 151.030 138.232 138.188 137.447 128.890 128.724 128.341 128.193 128.168 127.662 127.622 127.571 126.036 117.948 114.491 101.479 100.806 78.459 77.812 76.041 75.034 72.563 68.556 67.596 55.623
200 190 180 170 160 150 140 130 120 110 100 90 80 70 60 50 40 30 20 10

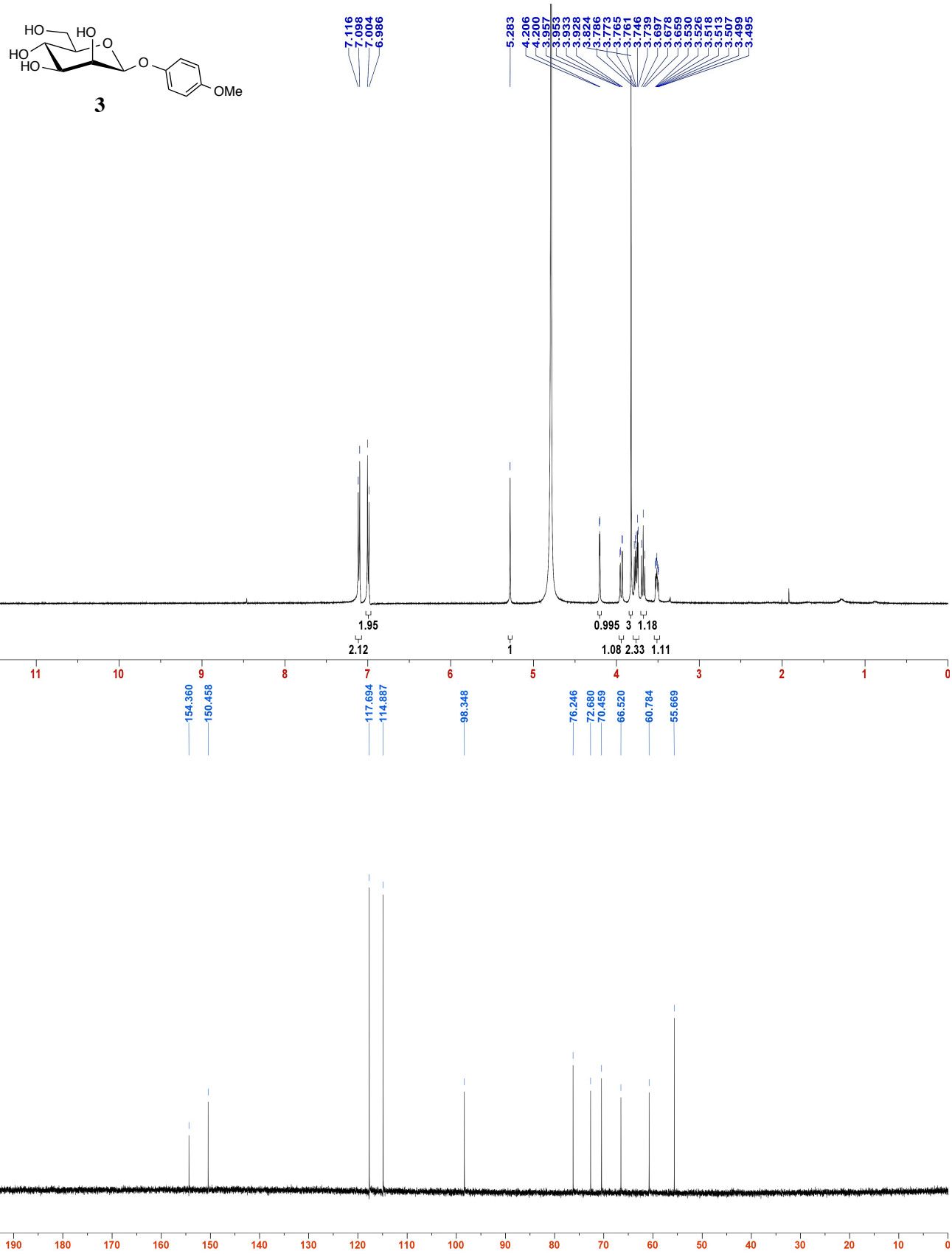
HO
HO
HO
HO
O
O
OMe
3
7.116
7.098
7.004
6.986
5.283
4.206
4.200
3.957
3.953
3.933
3.928
3.824
3.786
3.773
3.765
3.761
3.746
3.739
3.697
3.678
3.659
3.530
3.526
3.518
3.513
3.507
3.499
3.495
1.95
2.12
1
0.995
3
1.18
1.08
2.33
1.11
154.360
150.458
117.694
114.887
98.348
76.246
72.680
70.459
66.520
60.784
55.669

OH
HO
HO
OH
O
O
Br

11

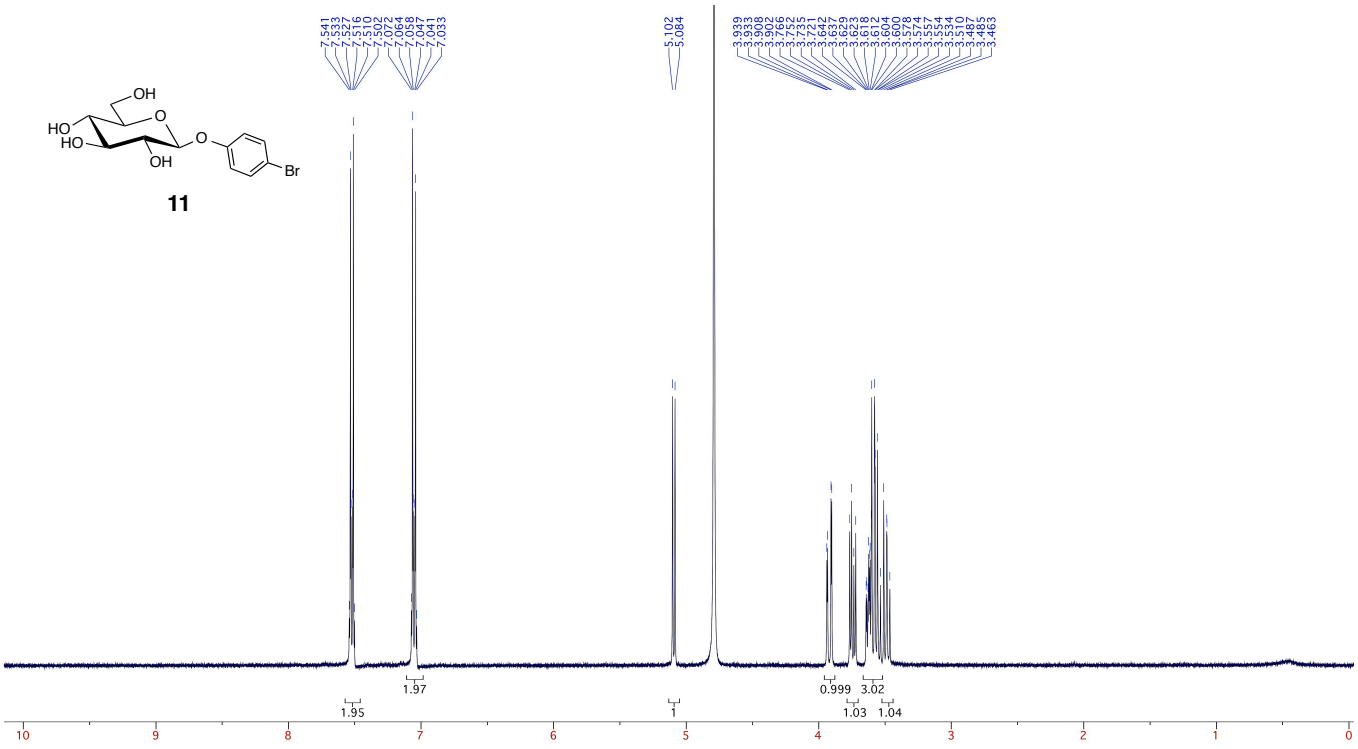
7.541
7.533
7.527
7.516
7.510
7.502
7.072
7.064
7.049
7.047
7.041
7.033
5.102
5.084
3.939
3.933
3.908
3.902
3.766
3.752
3.725
3.721
3.642
3.637
3.623
3.619
3.618
3.612
3.604
3.600
3.578
3.574
3.557
3.554
3.534
3.510
3.487
3.485
3.463
1.95
1.97
1
0.999
1.03
3.02
1.04
10
9
8
7
6
5
4
3
2
1
0

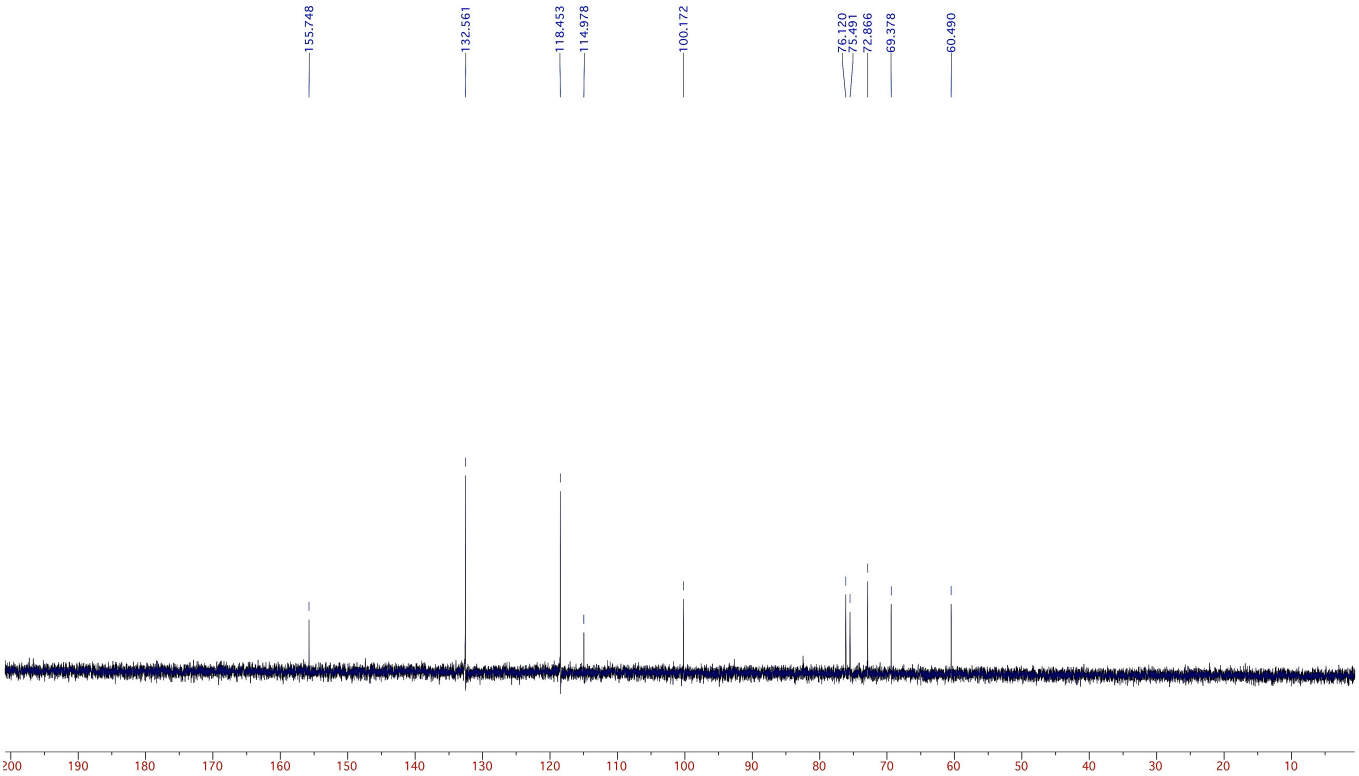
155.748
132.561
118.453
114.978
100.172
76.120
75.491
72.866
69.378
60.490
200
190
180
170
160
150
140
130
120
110
100
90
80
70
60
50
40
30
20
10

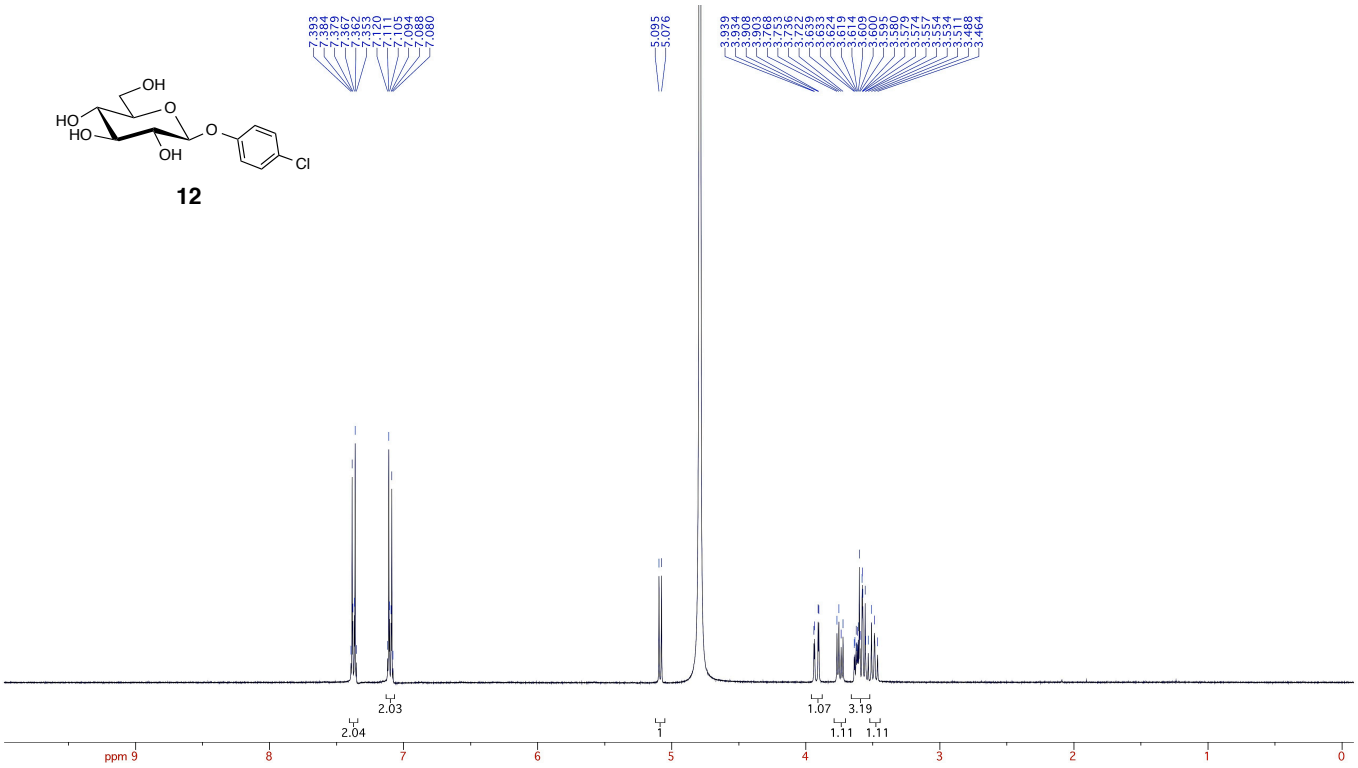
7.393
7.384
7.379
7.367
7.362
7.353
7.120
7.111
7.105
7.094
7.088
7.080
5.095
5.076
3.939
3.934
3.908
3.903
3.768
3.753
3.736
3.732
3.639
3.633
3.624
3.619
3.614
3.609
3.600
3.595
3.580
3.579
3.574
3.557
3.554
3.534
3.511
3.488
3.464
OH
HO
HO
OH
O
O
Cl
12
2.04
2.03
1
1.07
1.11
3.19
1.11
ppm 9
8
7
6
5
4
3
2
1
0

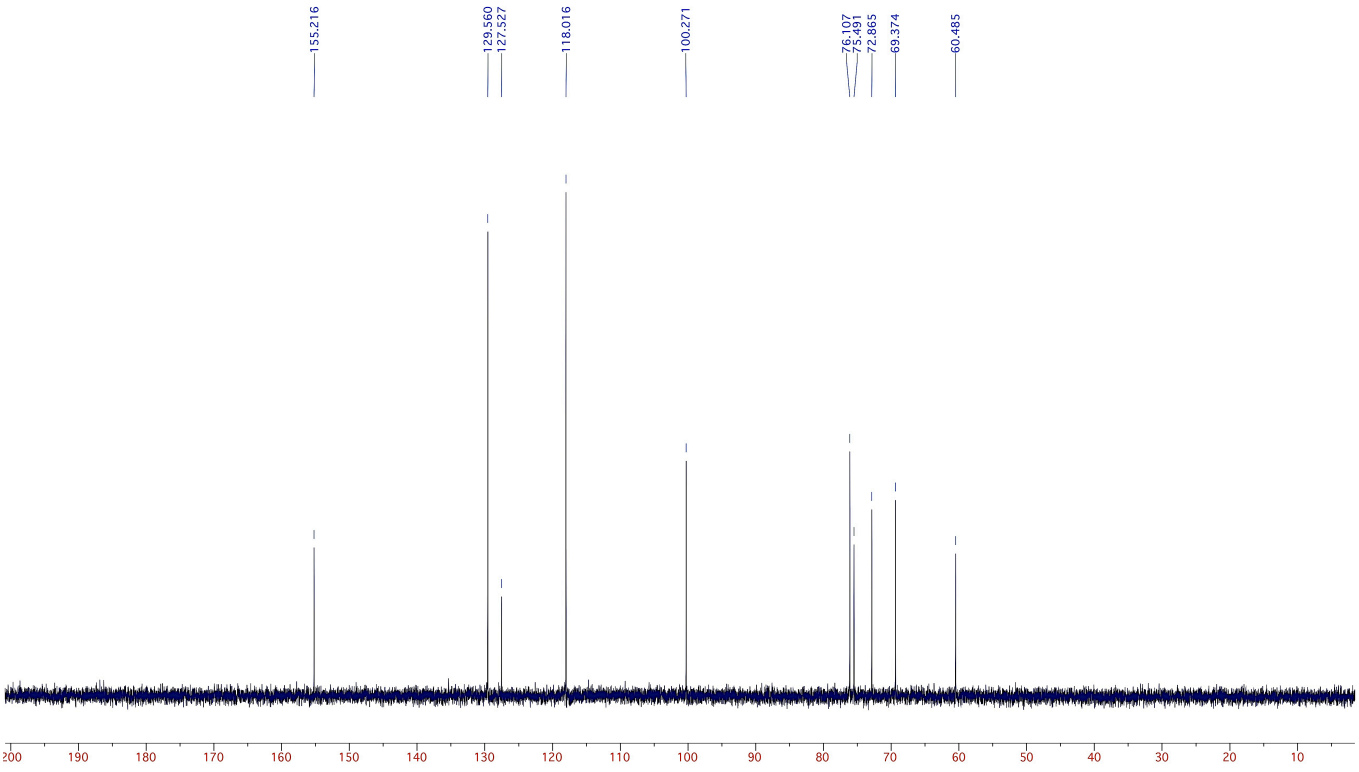
155.216
129.560
127.527
118.016
100.271
76.107
75.491
72.865
69.374
60.485
200
190
180
170
160
150
140
130
120
110
100
90
80
70
60
50
40
30
20
10

OH
HO
HO
OH
O
O
F

13

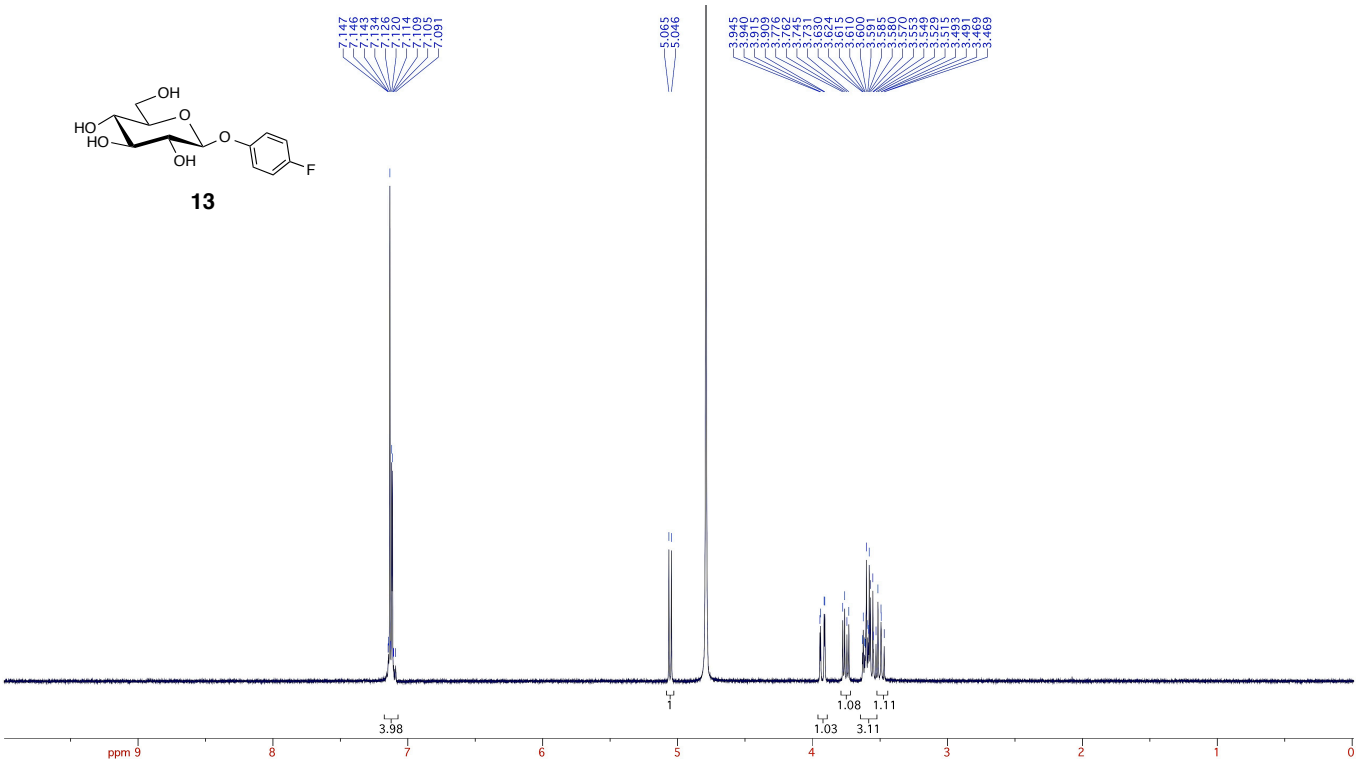
7.147
7.146
7.143
7.134
7.126
7.120
7.114
7.109
7.105
7.091
5.065
5.046
3.945
3.940
3.915
3.909
3.776
3.762
3.745
3.731
3.630
3.624
3.615
3.610
3.600
3.591
3.585
3.580
3.570
3.553
3.549
3.529
3.515
3.493
3.491
3.469
3.469
1
1.08
1.11
3.98
1.03
3.11
ppm 9
8
7
6
5
4
3
2
1
0

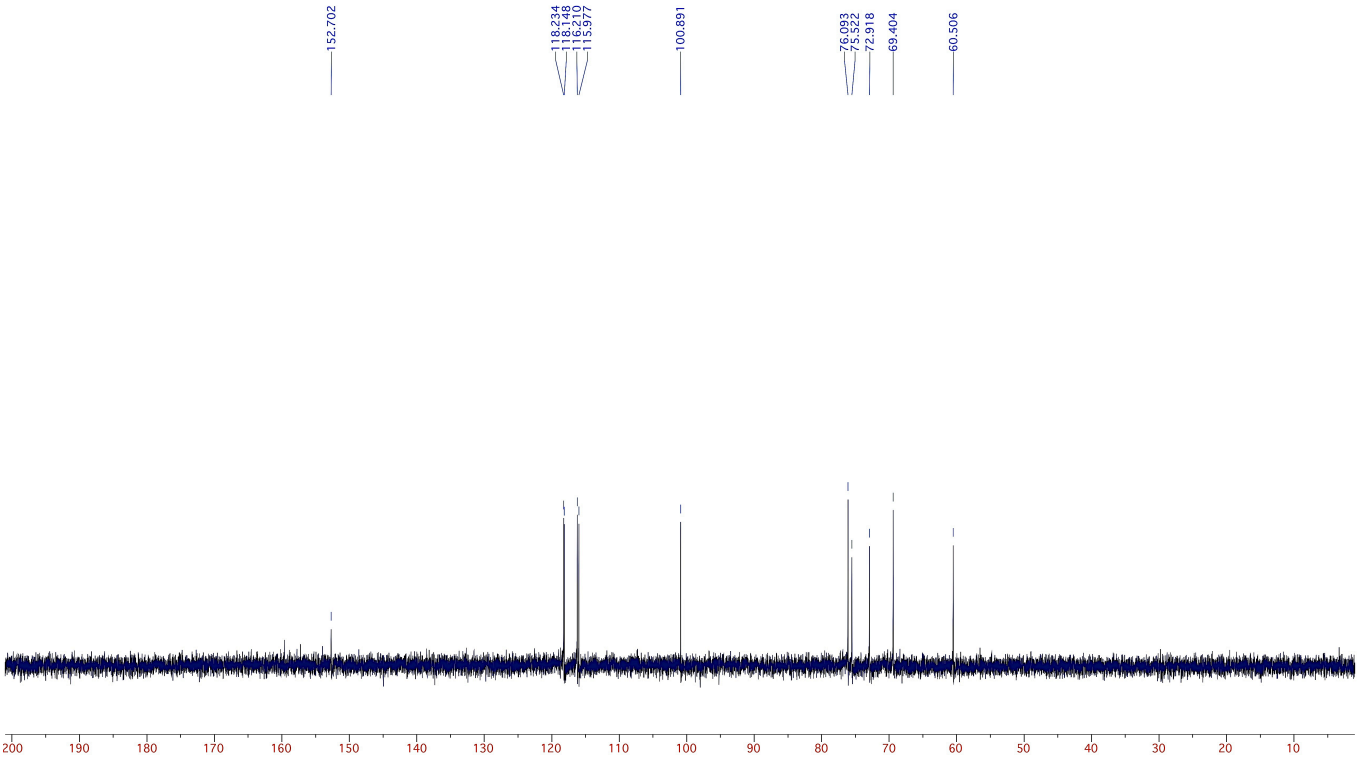
152.702
118.234
118.148
118.210
115.977
100.891
76.093
75.522
72.918
69.404
60.506
200
190
180
170
160
150
140
130
120
110
100
90
80
70
60
50
40
30
20
10

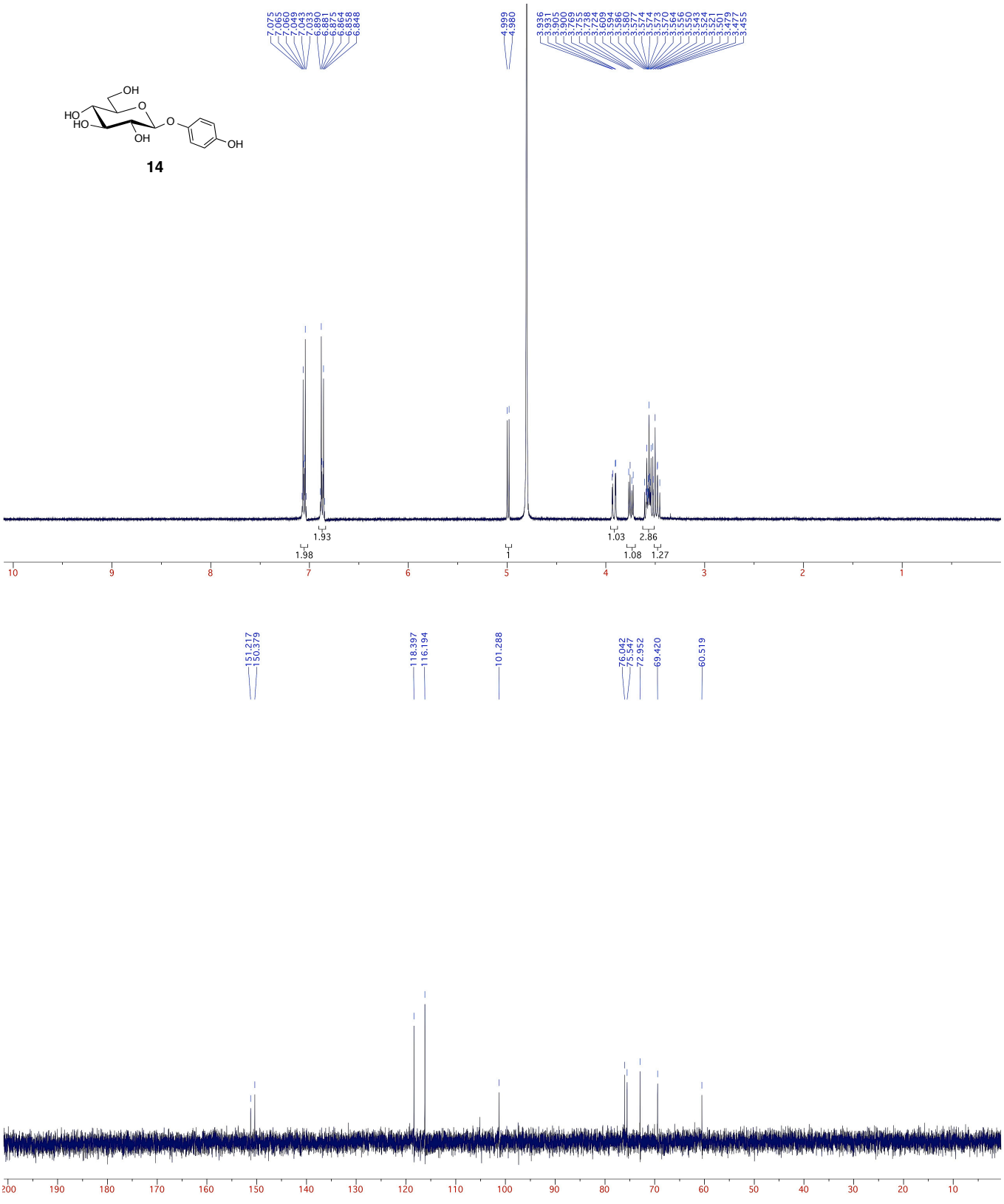
7.075
7.065
7.060
7.049
7.043
7.033
6.890
6.881
6.875
6.864
6.858
6.848
4.999
4.980
3.936
3.931
3.905
3.900
3.769
3.755
3.738
3.724
3.609
3.594
3.586
3.580
3.577
3.574
3.574
3.573
3.570
3.564
3.556
3.550
3.543
3.524
3.521
3.501
3.479
3.477
3.455
OH
HO
HO
OH
O
O
OH
14
1.98
1.93
1
1.03
1.08
2.86
1.27
151.217
150.379
118.397
116.194
101.288
76.042
75.547
72.952
69.420
60.519

OH
O
HO
HO
O
OH
Me

16

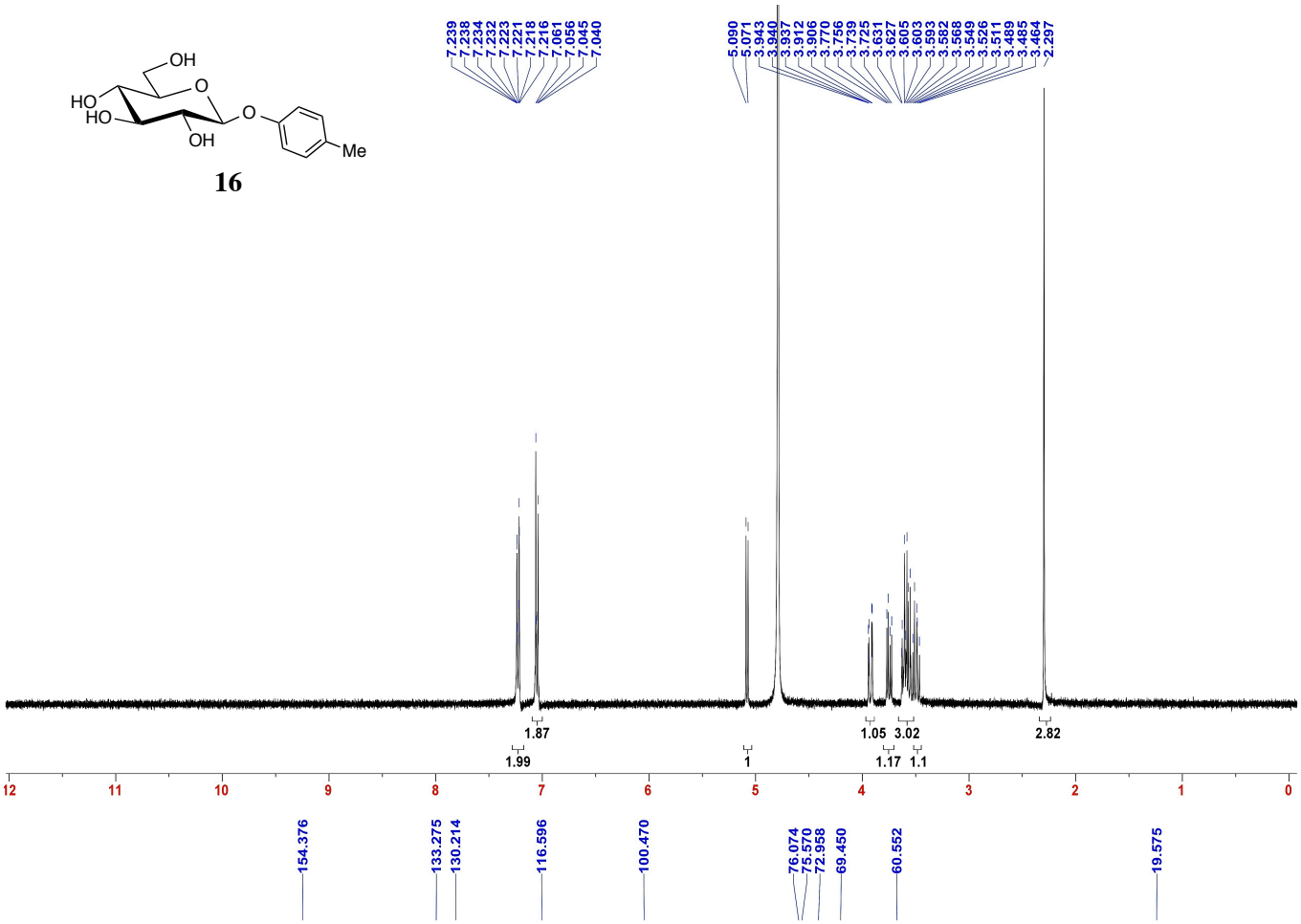
7.239
7.238
7.234
7.232
7.223
7.221
7.218
7.216
7.061
7.056
7.045
7.040
5.090
5.071
3.943
3.940
3.937
3.912
3.906
3.770
3.756
3.739
3.725
3.631
3.627
3.605
3.603
3.593
3.582
3.568
3.549
3.526
3.511
3.489
3.485
3.464
2.297
1.87
1.99
1
1.05
1.17
3.02
1.1
2.82
12
11
10
9
8
7
6
5
4
3
2
1
0

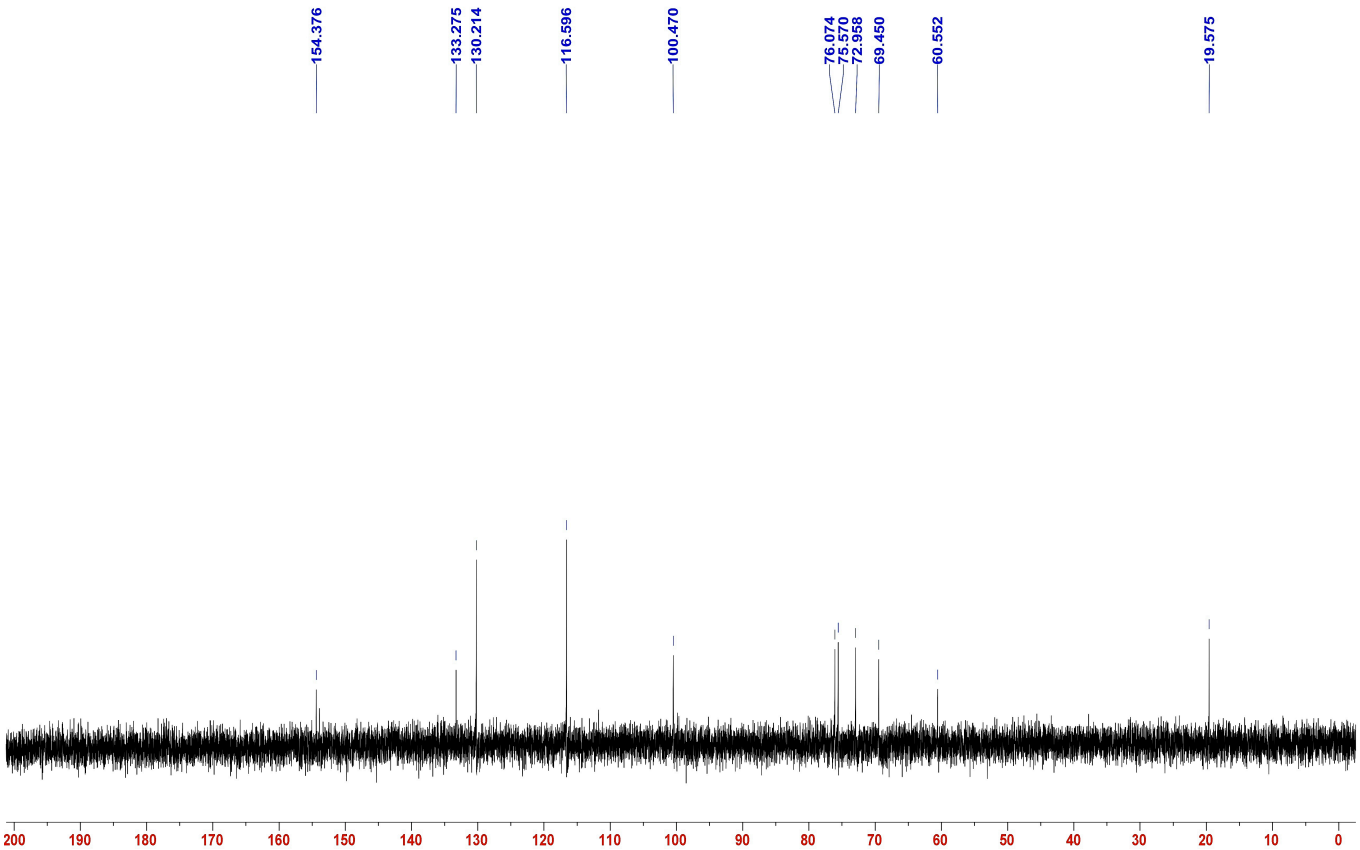
154.376
133.275
130.214
116.596
100.470
76.074
75.570
72.958
69.450
60.552
19.575
200
190
180
170
160
150
140
130
120
110
100
90
80
70
60
50
40
30
20
10
0

OH
HO
HO
OH
O
O

17

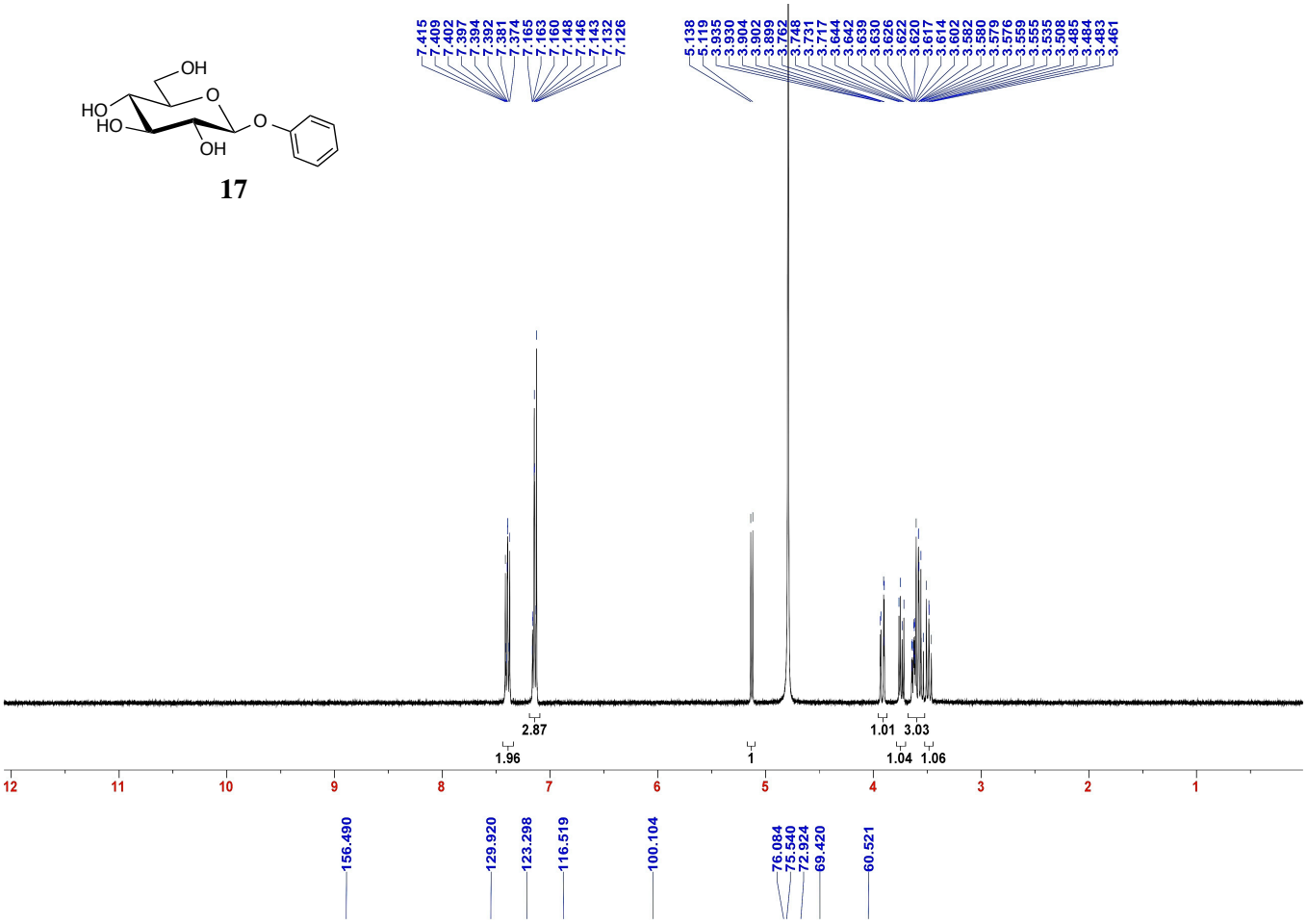
7.415
7.409
7.402
7.397
7.394
7.392
7.391
7.391
7.165
7.163
7.160
7.148
7.146
7.143
7.132
7.126
5.138
5.119
3.935
3.930
3.904
3.902
3.899
3.762
3.748
3.731
3.717
3.644
3.642
3.639
3.630
3.626
3.622
3.620
3.617
3.614
3.602
3.582
3.580
3.579
3.576
3.559
3.555
3.535
3.508
3.485
3.484
3.483
3.461
2.87
1.96
1
1.01
3.03
1.04
1.06
12
11
10
9
8
7
6
5
4
3
2
1
156.490
129.920
123.298
116.519
100.104
76.084
75.540
72.924
69.420
60.521

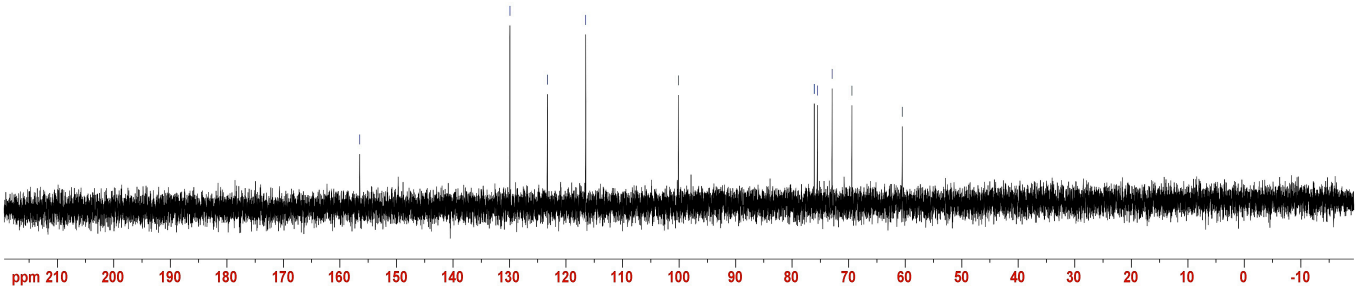
ppm 210
200
190
180
170
160
150
140
130
120
110
100
90
80
70
60
50
40
30
20
10
0
-10

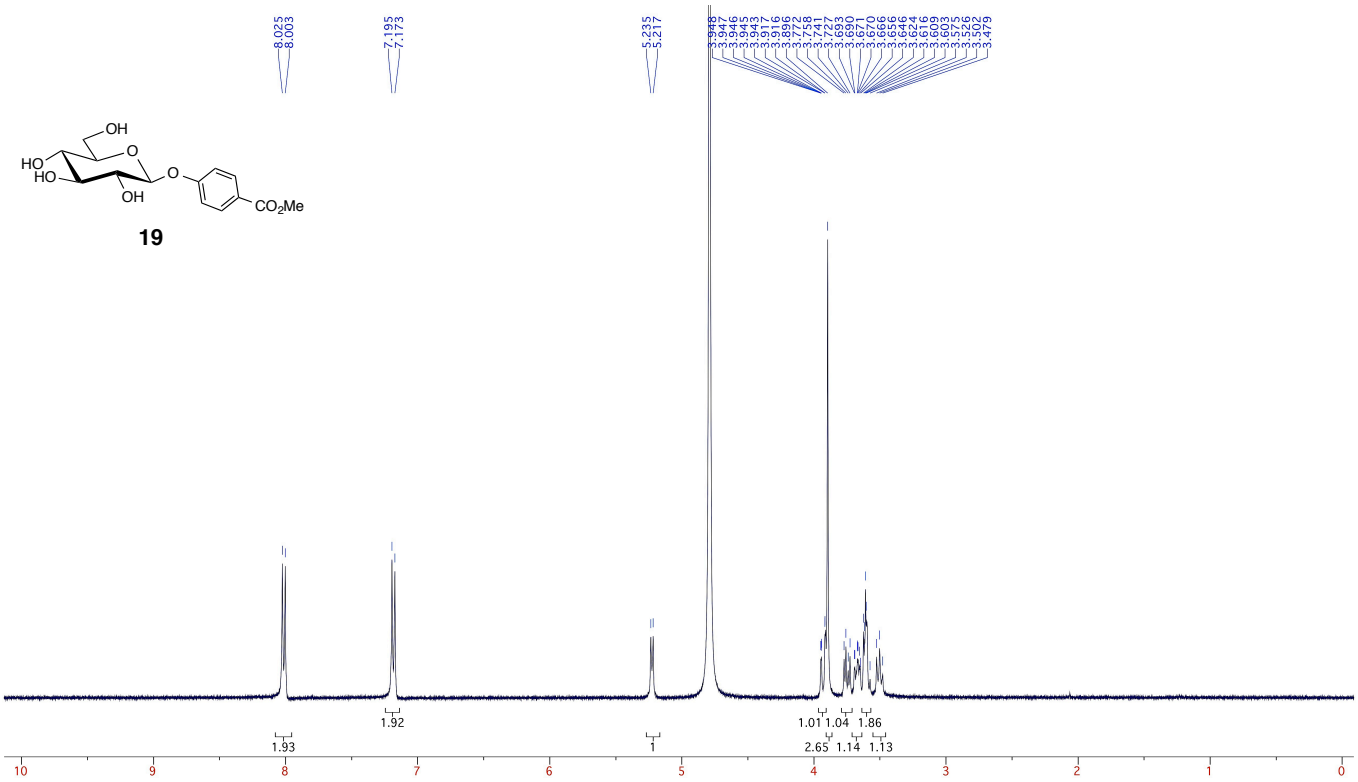
8.025
8.003
7.195
7.173
5.235
5.217
3.948
3.947
3.946
3.945
3.943
3.917
3.916
3.772
3.758
3.741
3.727
3.693
3.690
3.671
3.670
3.656
3.646
3.614
3.609
3.603
3.575
3.526
3.502
3.479
OH
HO
HO
OH
O
O
CO2Me
19
1.93
1.92
1
1.01
1.04
1.86
2.65
1.14
1.13
10
9
8
7
6
5
4
3
2
1
0

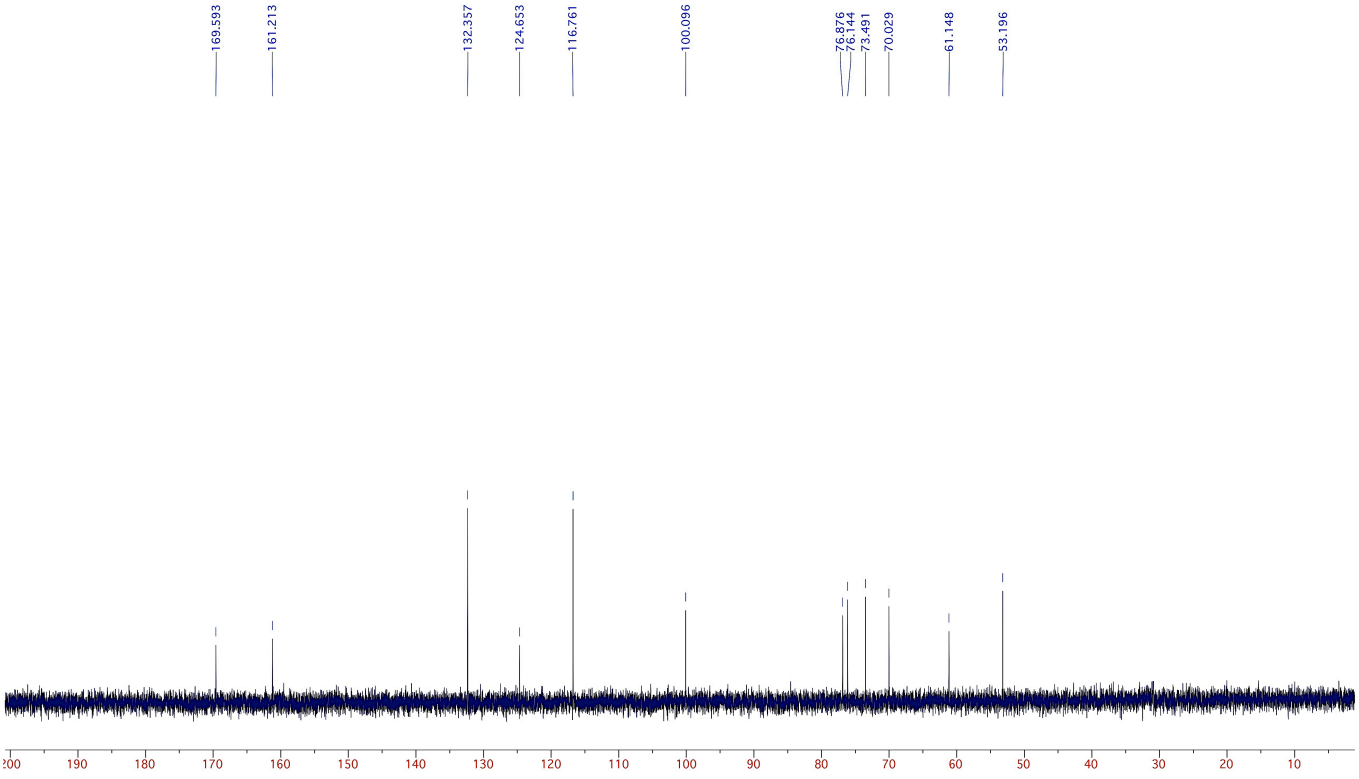
169.593
161.213
132.357
124.653
116.761
100.096
76.876
76.144
73.491
70.029
61.148
53.196
200
190
180
170
160
150
140
130
120
110
100
90
80
70
60
50
40
30
20
10

OAc
AcO
AcO
OAc
O
O
CF3

21a

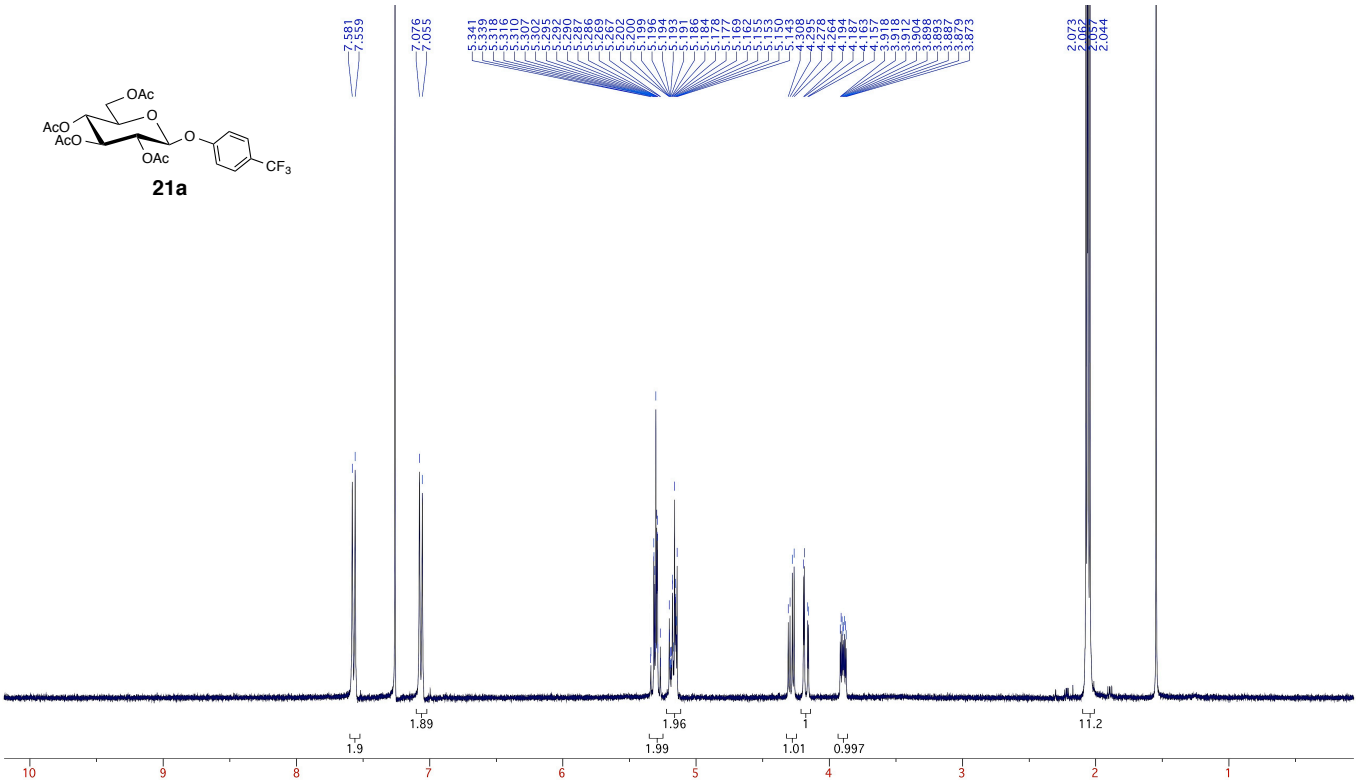
7.581
7.559
7.076
7.055
5.341
5.339
5.318
5.316
5.310
5.307
5.302
5.292
5.290
5.287
5.286
5.269
5.267
5.202
5.200
5.199
5.196
5.194
5.193
5.191
5.186
5.184
5.178
5.177
5.169
5.162
5.155
5.153
5.150
5.143
4.308
4.295
4.278
4.264
4.187
4.163
4.157
3.918
3.912
3.904
3.898
3.893
3.887
3.879
3.873
2.073
2.067
2.044
1.9
1.89
1.99
1.96
1.01
1
0.997
11.2
10
9
8
7
6
5
4
3
2
1

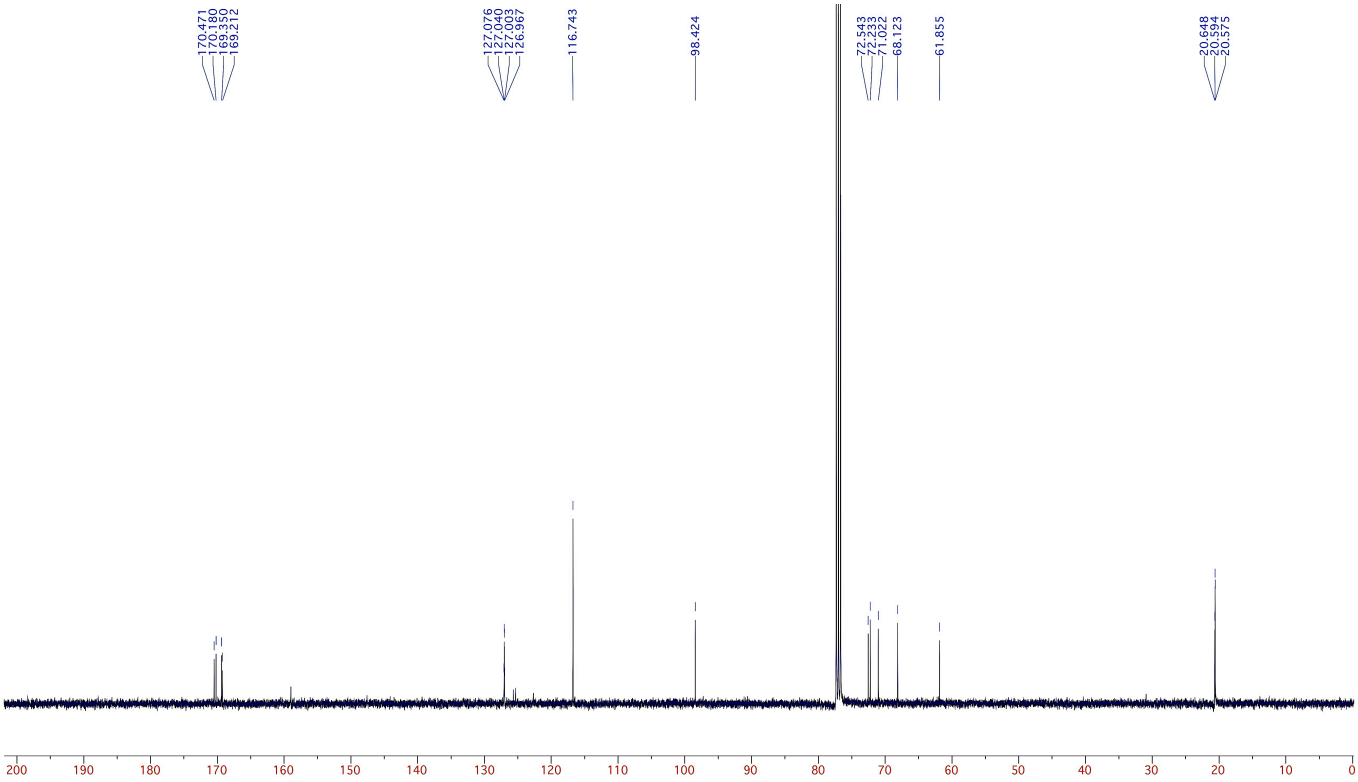
170.471
170.180
169.350
169.212
127.076
127.040
127.003
126.967
116.743
98.424
72.543
72.233
71.622
68.123
61.855
20.648
20.594
20.575
200
190
180
170
160
150
140
130
120
110
100
90
80
70
60
50
40
30
20
10
0

OH
HO
HO
OH
O
O
CF3

21

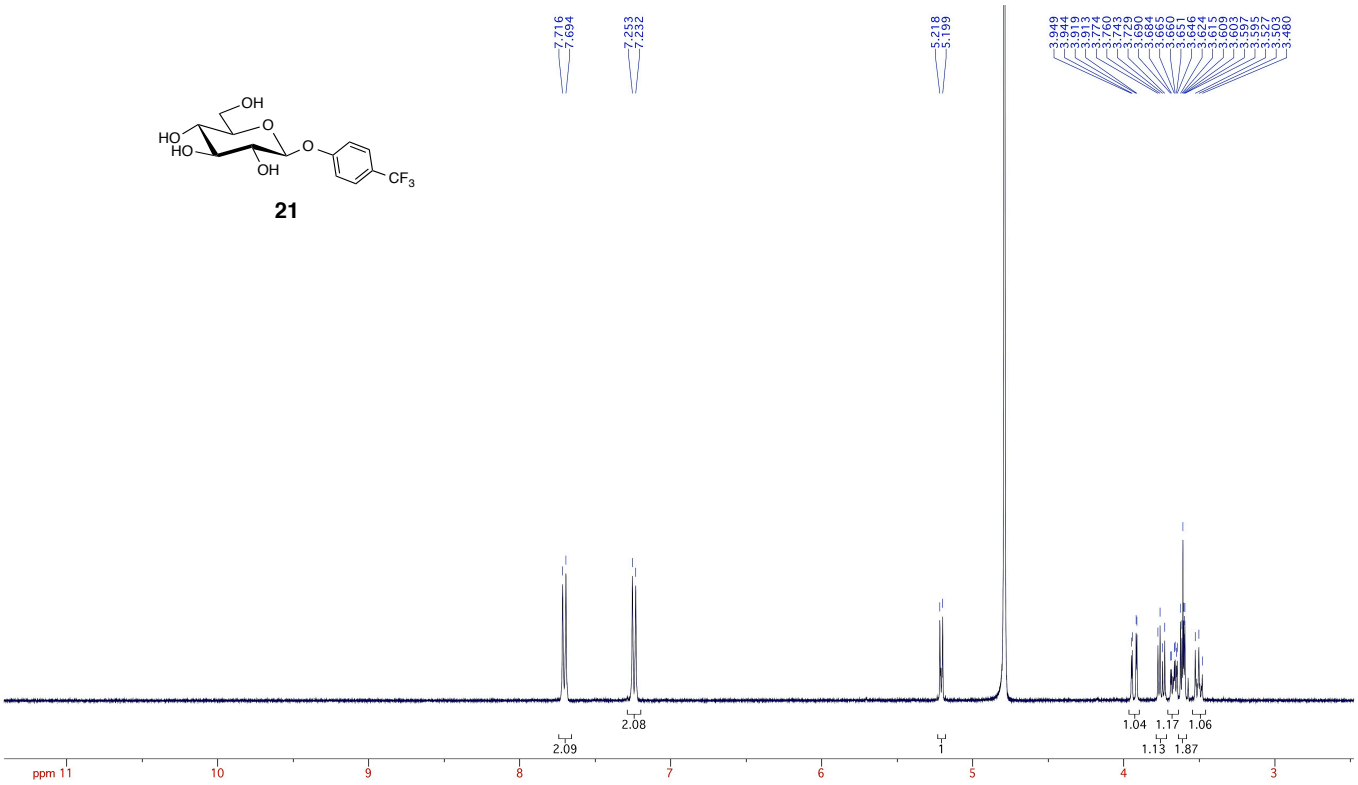
7.716
7.694
7.253
7.232
5.218
5.199
3.949
3.944
3.919
3.913
3.774
3.760
3.743
3.729
3.690
3.684
3.665
3.660
3.651
3.646
3.624
3.615
3.609
3.603
3.597
3.595
3.527
3.503
3.480
2.09
2.08
1
1.04
1.17
1.06
1.13
1.87
ppm 11
10
9
8
7
6
5
4
3

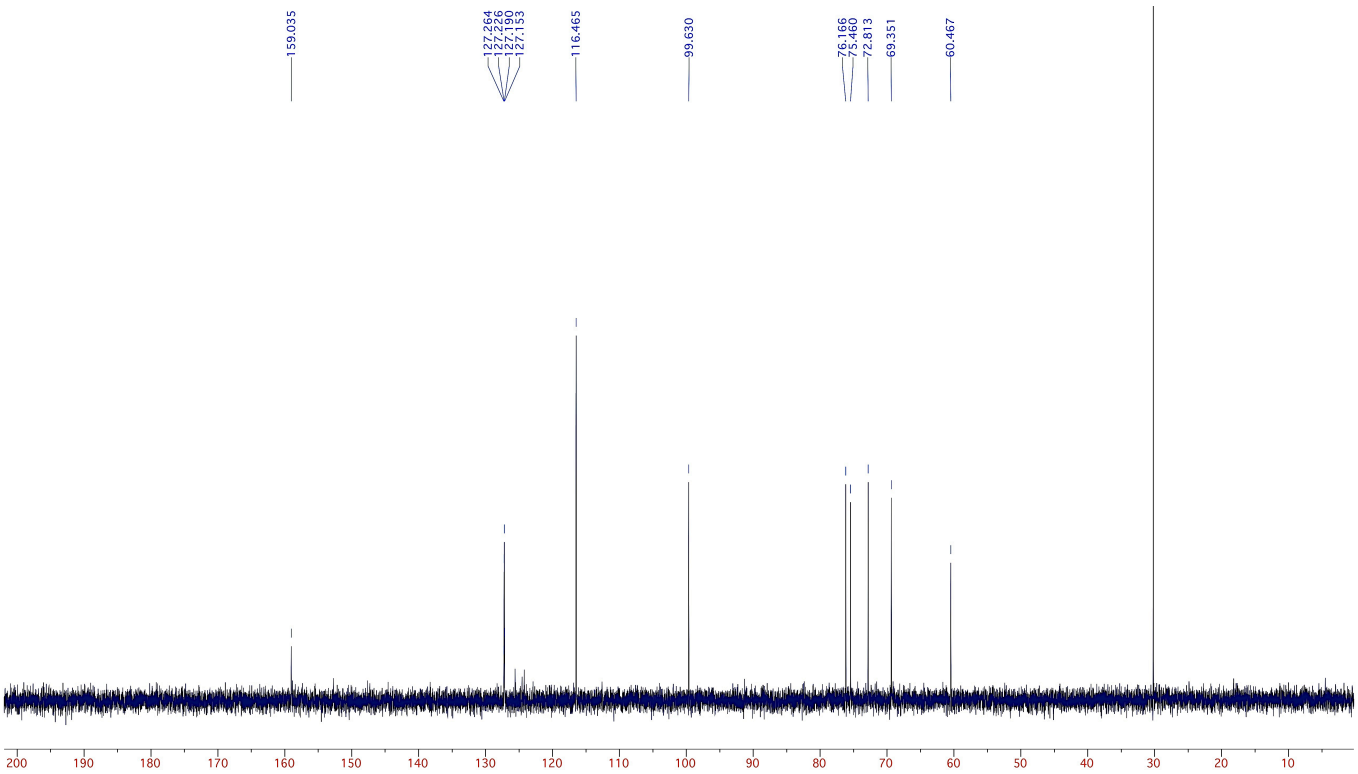
159.035
127.264
127.226
127.190
127.153
116.465
99.630
76.166
75.460
72.813
69.351
60.467
200
190
180
170
160
150
140
130
120
110
100
90
80
70
60
50
40
30
20
10

OH
O
HO
HO
O
OH
NO2

22

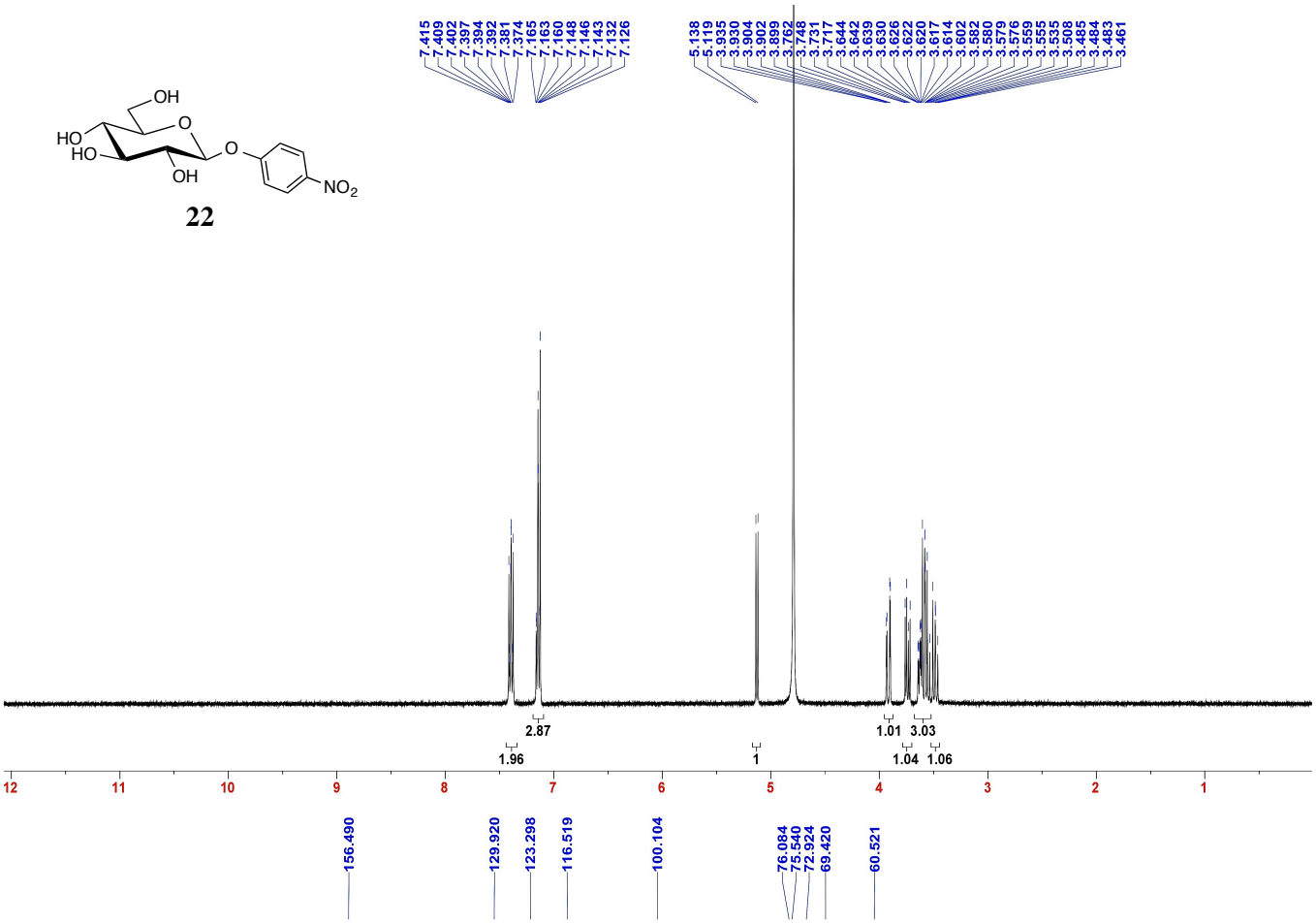
7.415
7.409
7.402
7.397
7.394
7.392
7.391
7.365
7.163
7.160
7.148
7.146
7.143
7.132
7.126
5.138
5.119
3.935
3.930
3.904
3.902
3.899
3.762
3.748
3.731
3.717
3.644
3.642
3.639
3.630
3.626
3.622
3.620
3.617
3.614
3.602
3.582
3.580
3.579
3.576
3.559
3.555
3.535
3.508
3.485
3.484
3.483
3.461
2.87
1.96
1
1.01
3.03
1.04
1.06
12
11
10
9
8
7
6
5
4
3
2
1
156.490
129.920
123.298
116.519
100.104
76.084
75.540
72.924
69.420
60.521

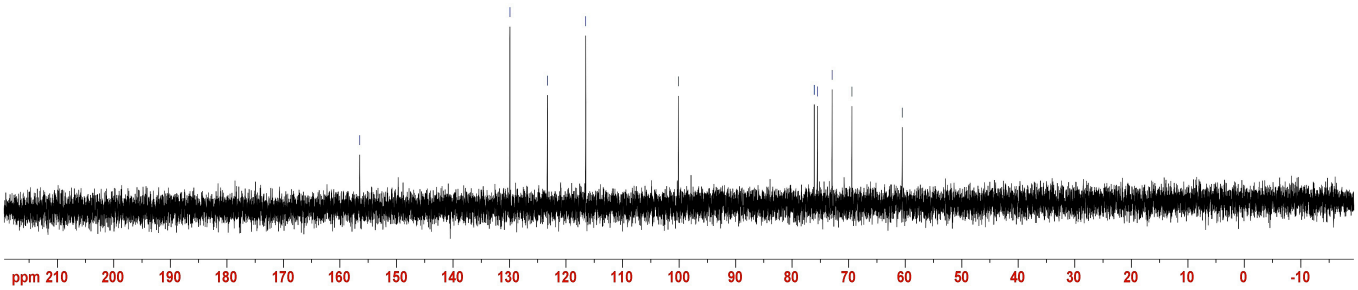
ppm 210
200
190
180
170
160
150
140
130
120
110
100
90
80
70
60
50
40
30
20
10
0
-10

OAc
AcO
AcO
OAc
O
O
OCF3

23a

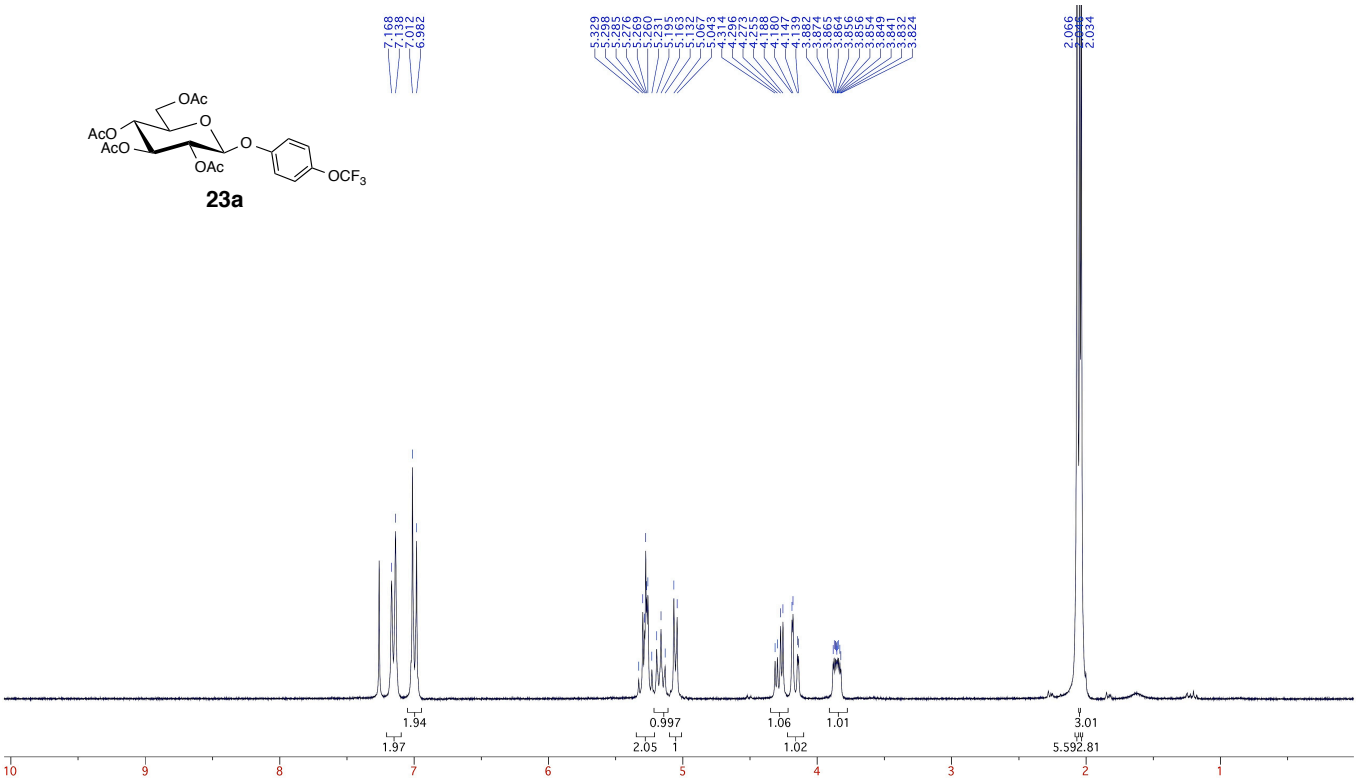
7.168
7.138
7.102
6.982
5.329
5.288
5.285
5.276
5.269
5.230
5.231
5.195
5.163
5.132
5.067
5.043
4.314
4.296
4.273
4.255
4.188
4.180
4.147
4.139
3.882
3.874
3.865
3.864
3.856
3.854
3.849
3.841
3.832
3.824
2.066
2.064
2.034
1.94
1.97
0.997
2.05
1
1.06
1.02
1.01
3.01
5.592.81

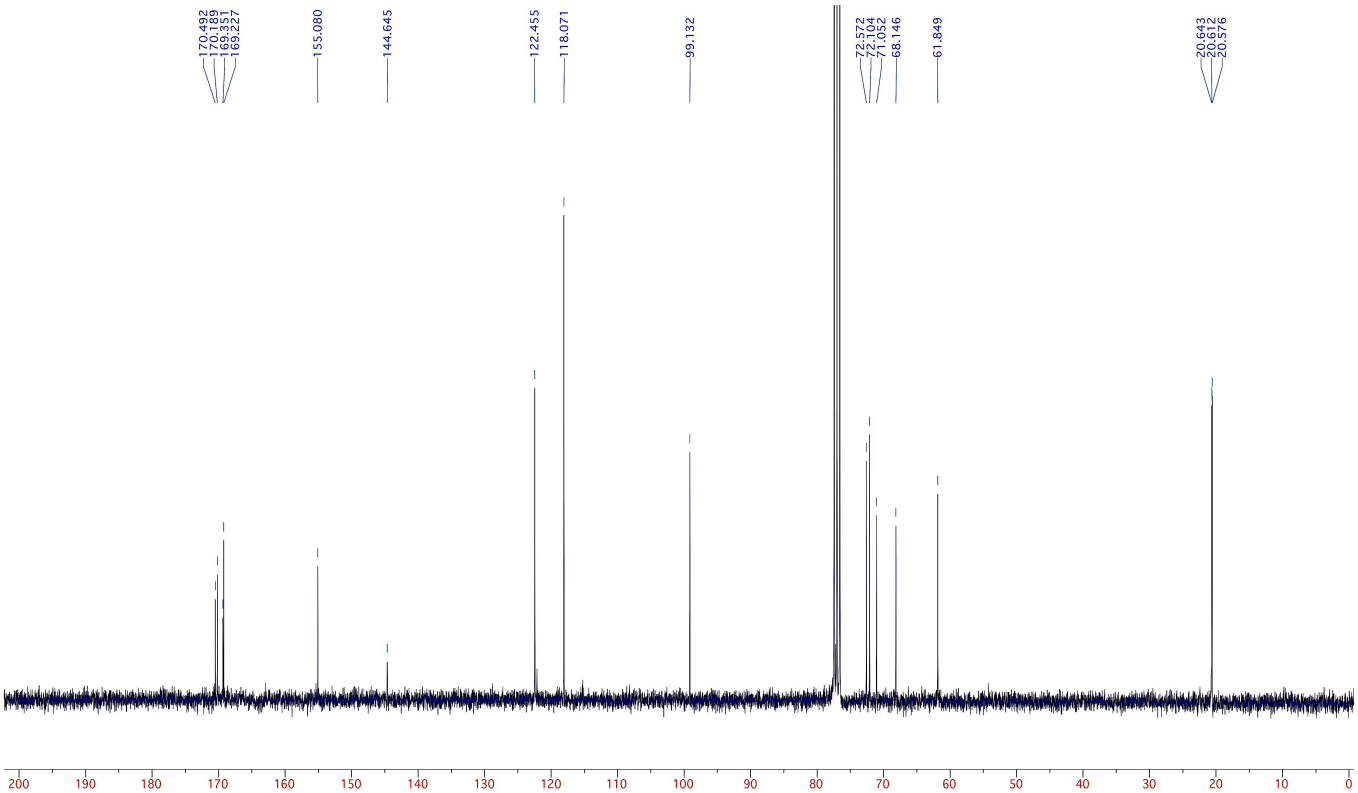
170.492
170.189
169.331
169.227
155.080
144.645
122.455
118.071
99.132
72.572
72.304
71.052
68.146
61.849
20.643
20.612
20.576

OH
O
HO
HO
O
OH
OCF3

23

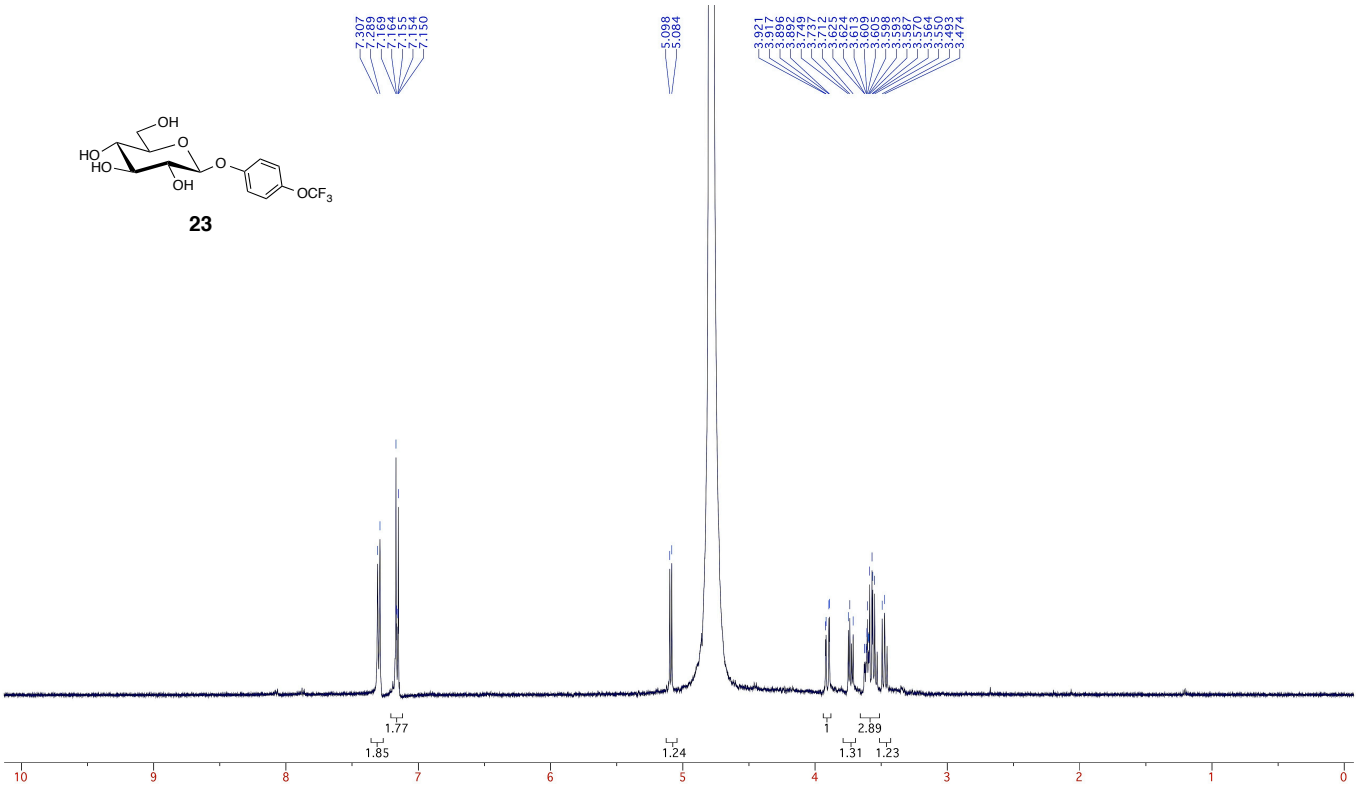
7.307
7.289
7.169
7.164
7.155
7.154
7.150
5.098
5.084
3.921
3.917
3.896
3.892
3.749
3.737
3.712
3.625
3.613
3.609
3.605
3.598
3.593
3.587
3.570
3.554
3.550
3.493
3.474
1.77
1.85
1.24
1
2.89
1.31
1.23
10
9
8
7
6
5
4
3
2
1
0

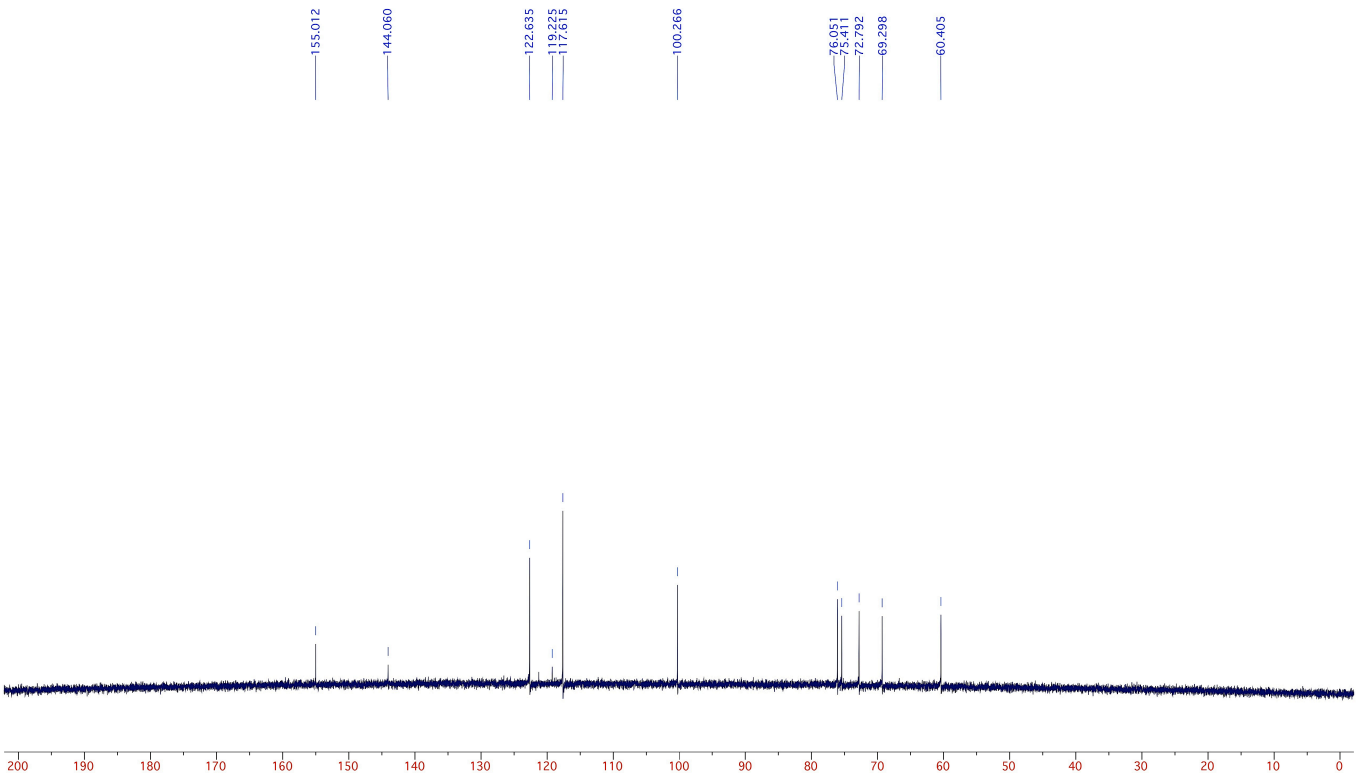
155.012
144.060
122.635
119.225
117.615
100.266
76.051
75.411
72.792
69.298
60.405
200
190
180
170
160
150
140
130
120
110
100
90
80
70
60
50
40
30
20
10
0

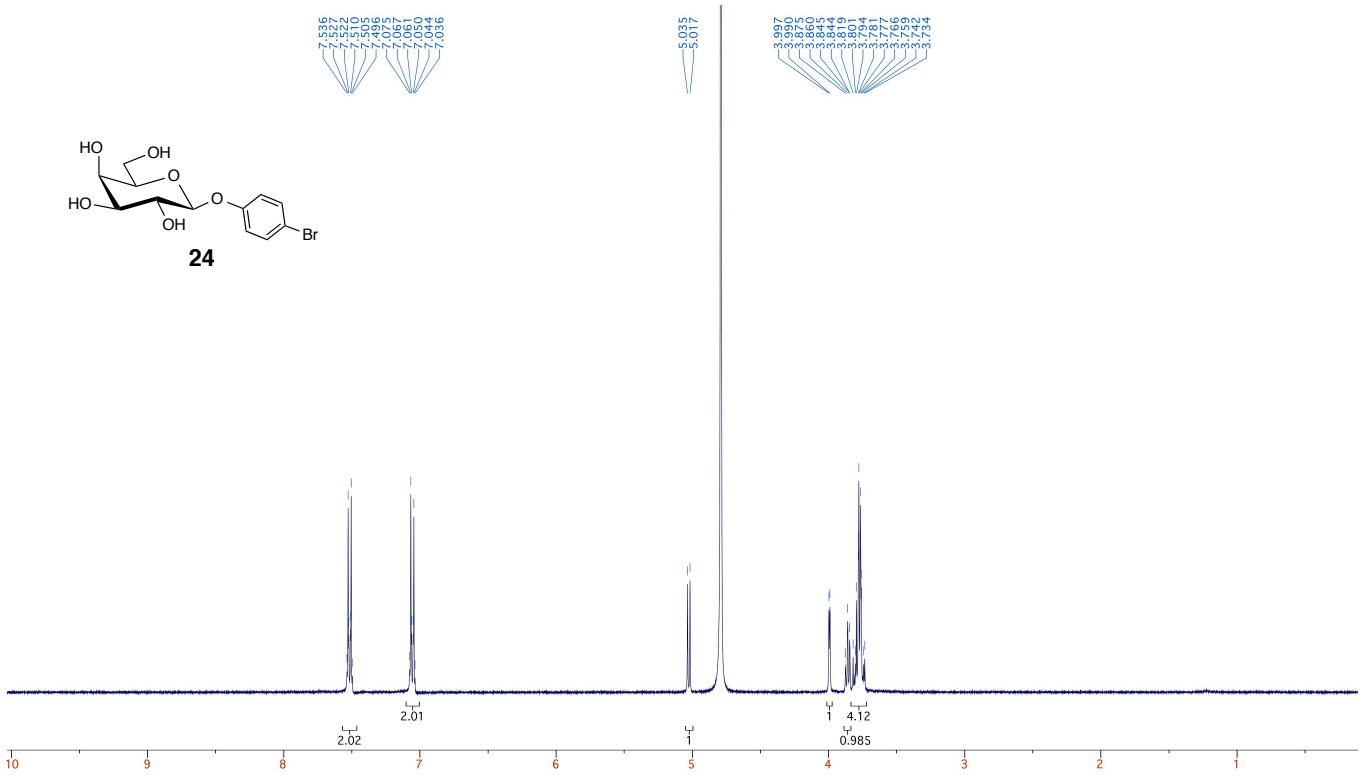
7.536
7.527
7.512
7.510
7.505
7.496
7.067
7.061
7.050
7.044
7.036
5.035
5.017
3.997
3.990
3.875
3.860
3.845
3.844
3.819
3.801
3.784
3.781
3.777
3.766
3.759
3.742
3.734
HO
OH
O
HO
O
OH
Br
24
2.02
2.01
1
1
4.12
0.985

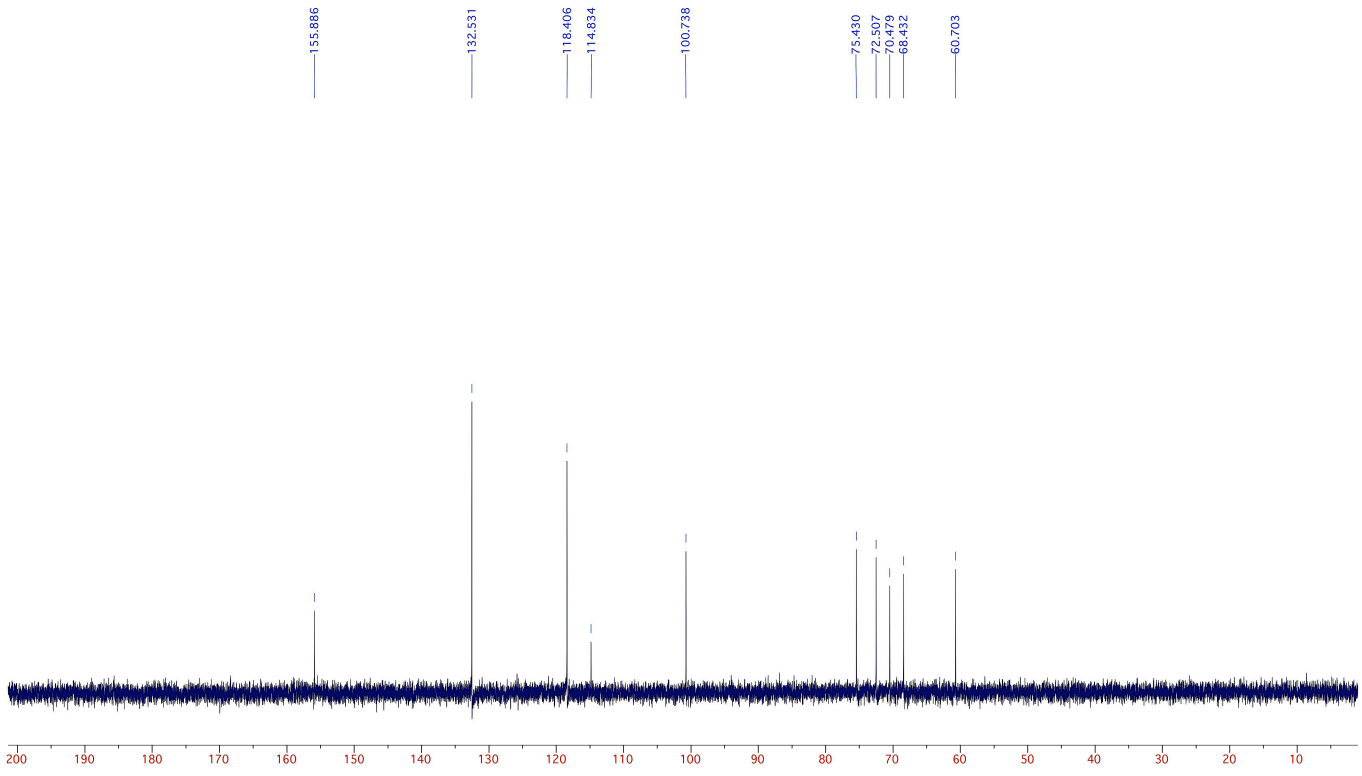
155.886
132.531
118.406
114.834
100.738
75.430
72.507
70.479
68.432
60.703

HO
OH
O
HO
O
OH
Cl

25

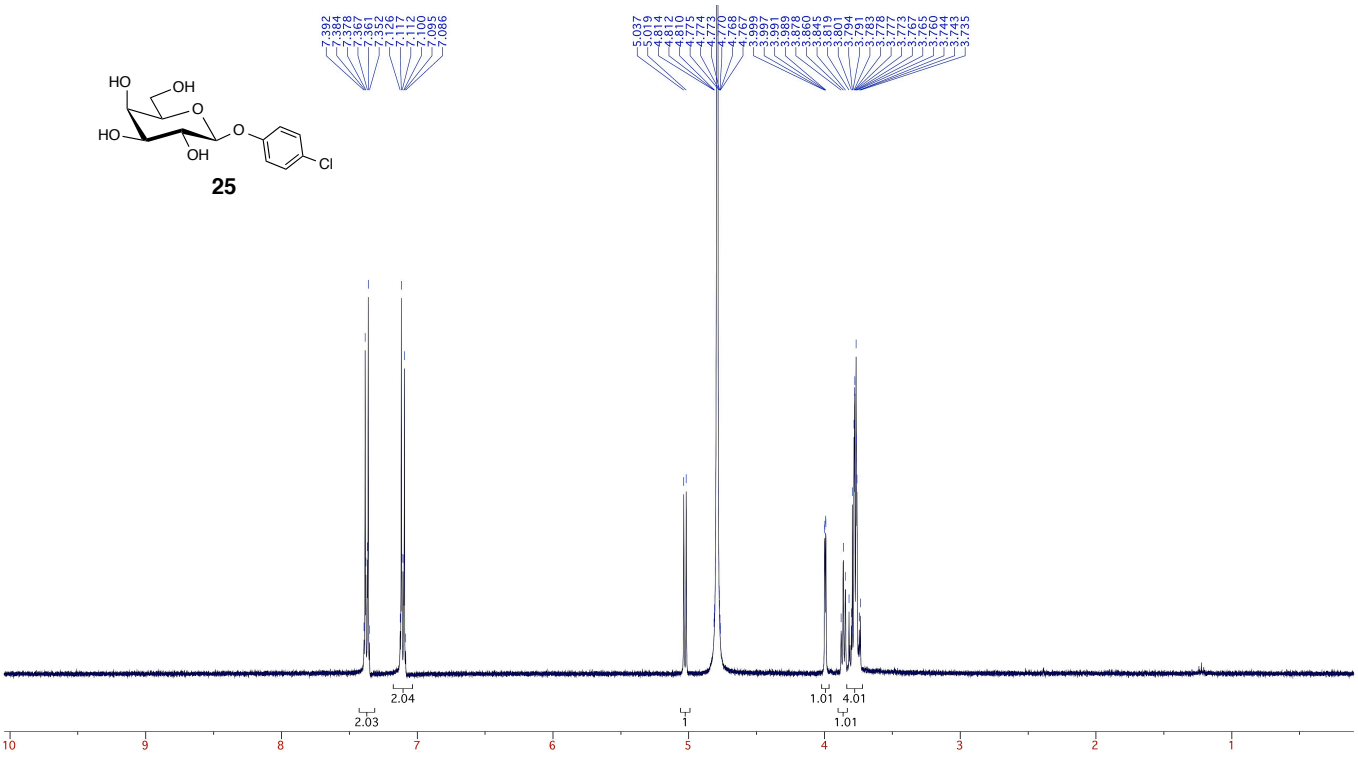
7.392
7.384
7.378
7.367
7.361
7.352
7.126
7.117
7.112
7.100
7.095
7.086
5.037
5.029
5.014
4.812
4.810
4.775
4.774
4.773
4.770
4.768
4.767
3.999
3.997
3.991
3.989
3.878
3.860
3.845
3.819
3.801
3.794
3.781
3.783
3.778
3.777
3.773
3.767
3.765
3.760
3.744
3.743
3.735
2.04
2.03
1
1.01
4.01
1.01

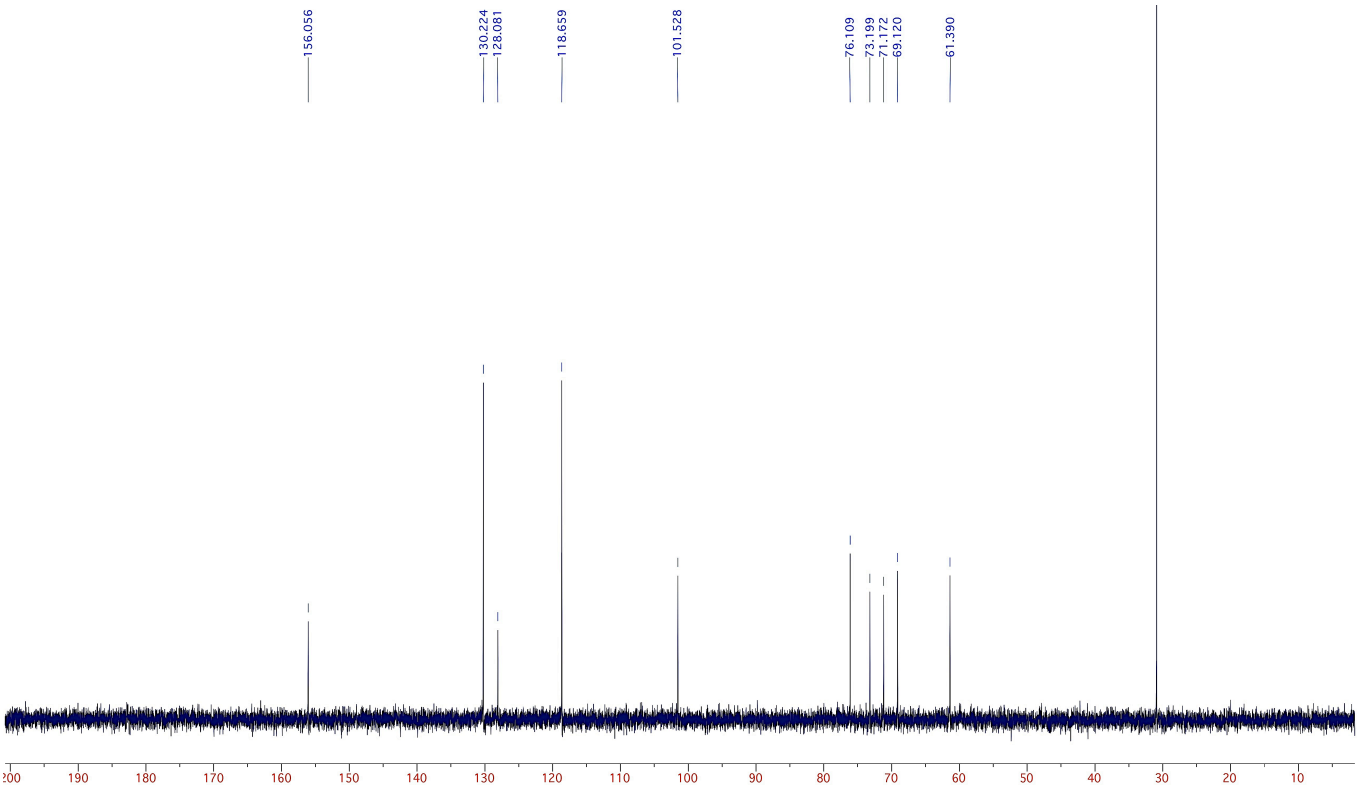
156.056
130.224
128.081
118.659
101.528
76.109
73.199
71.172
69.120
61.390

HO
OH
O
HO
O
OH
OH

27

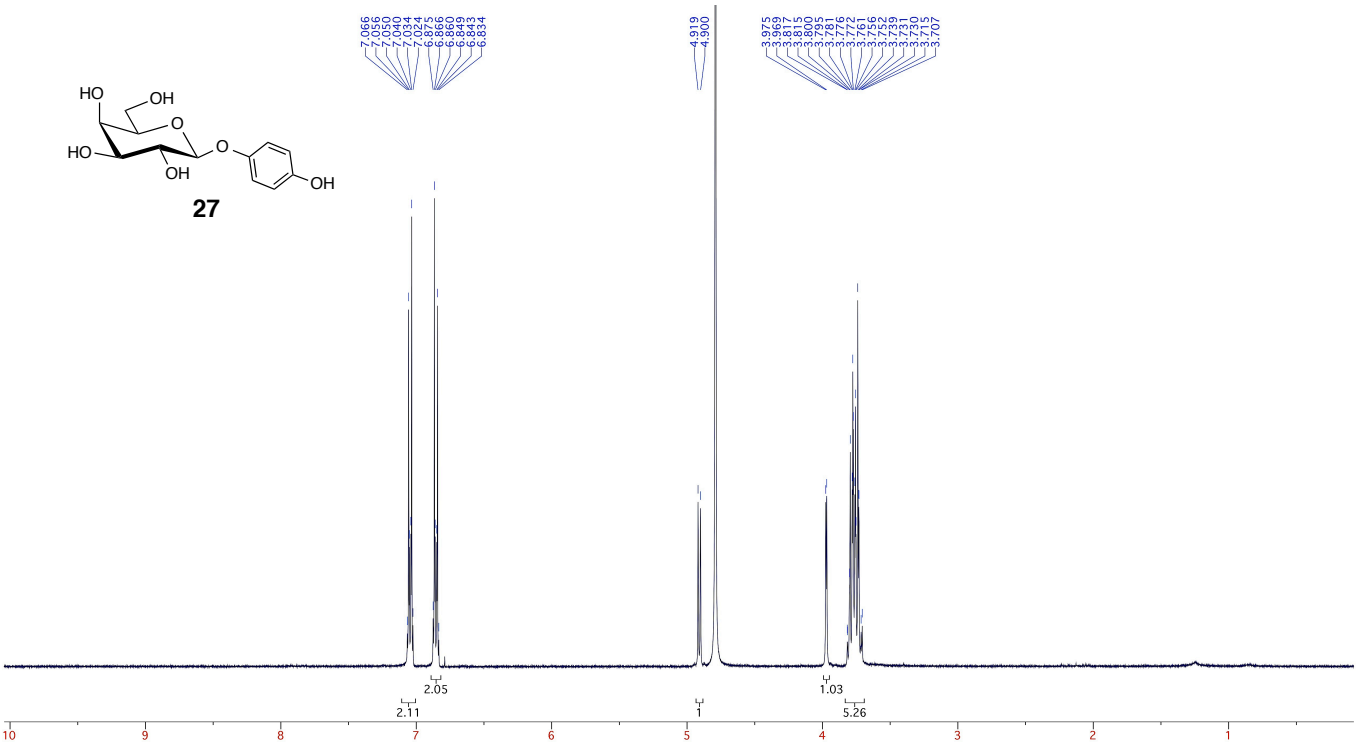
7.066
7.056
7.050
7.040
7.034
7.024
6.875
6.866
6.860
6.849
6.843
6.834
4.919
4.900
3.975
3.969
3.817
3.815
3.800
3.795
3.781
3.776
3.772
3.761
3.756
3.752
3.739
3.731
3.730
3.715
3.707
2.11
2.05
1
1.03
5.26
10
9
8
7
6
5
4
3
2
1

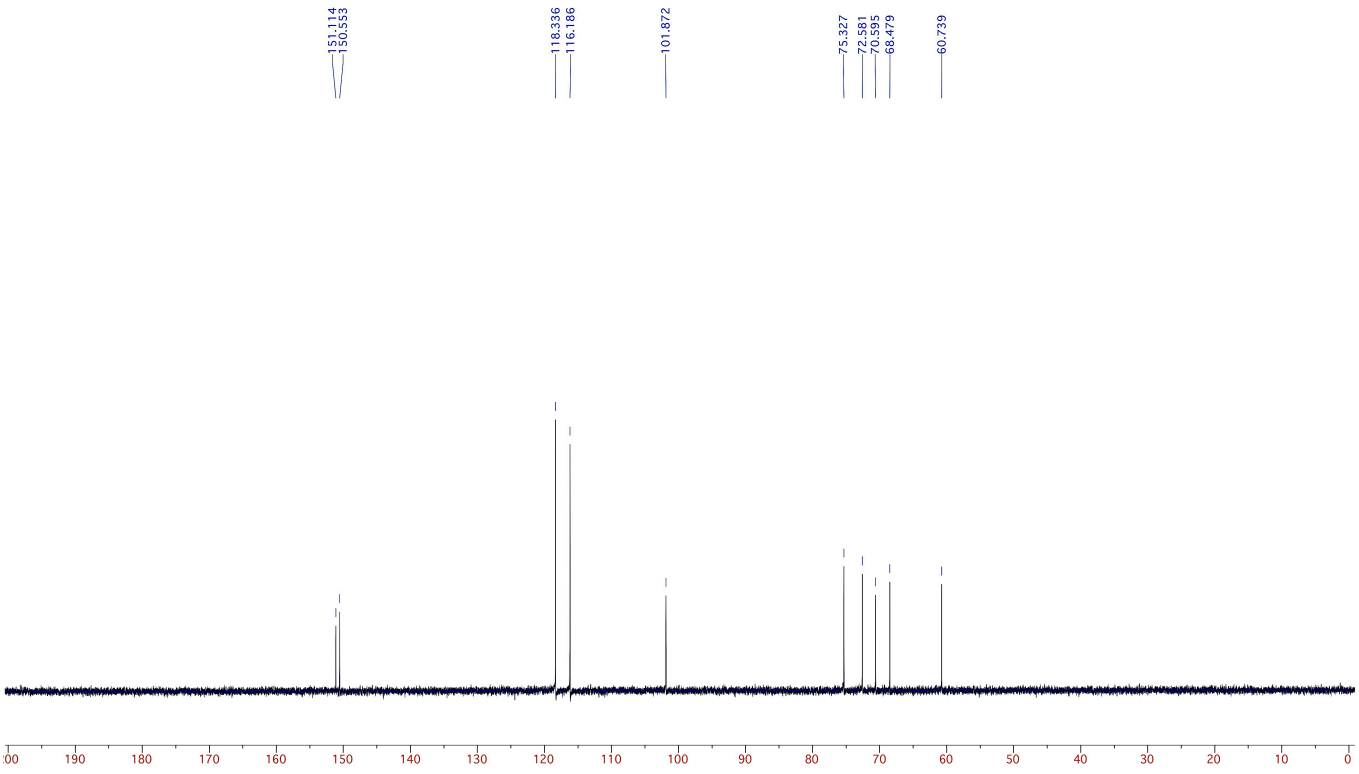
151.114
150.553
118.336
116.186
101.872
75.327
72.581
70.595
68.479
60.739
200
190
180
170
160
150
140
130
120
110
100
90
80
70
60
50
40
30
20
10
0

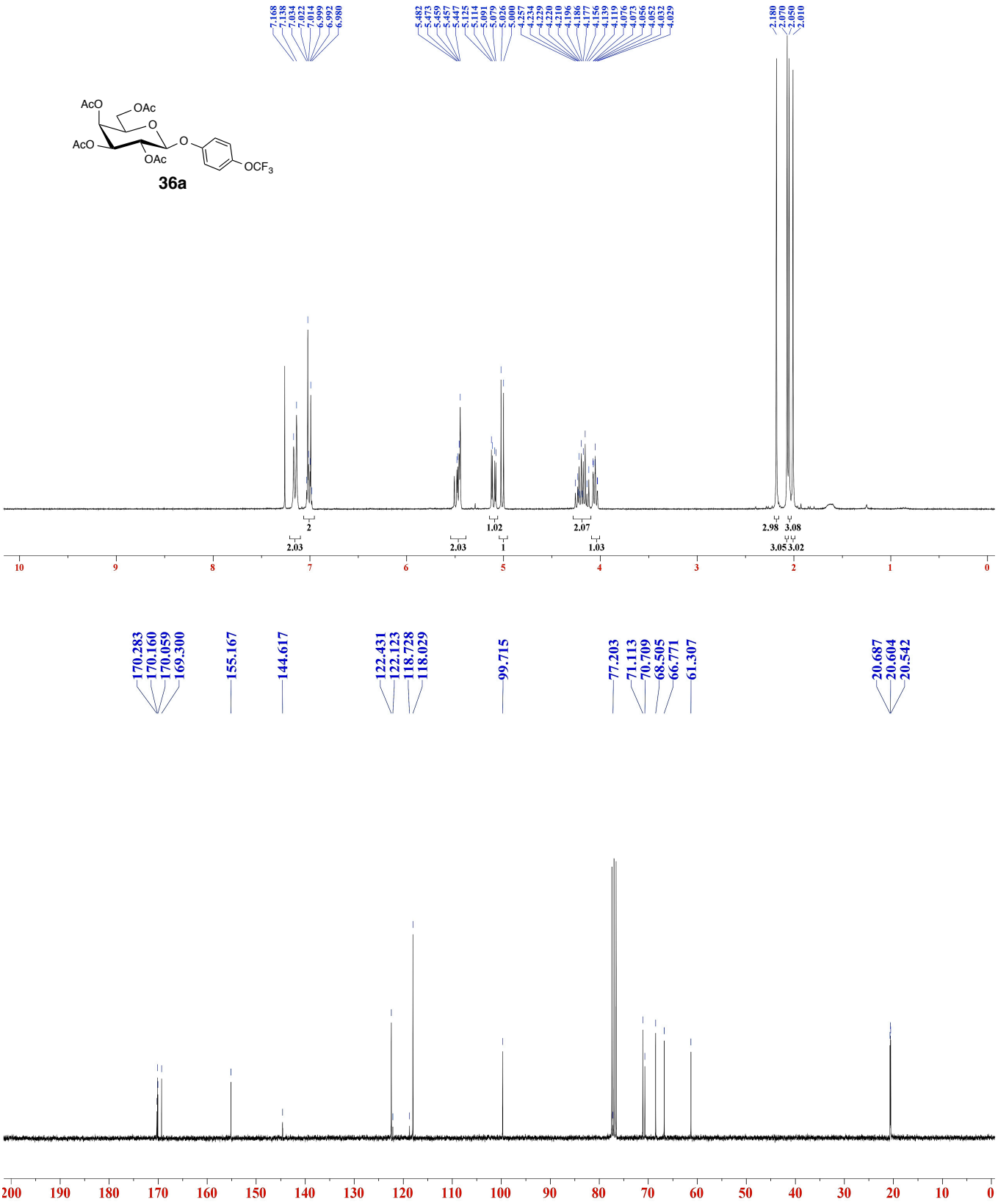
7.168
7.138
7.034
7.022
7.014
6.999
6.992
6.980
5.482
5.473
5.459
5.457
5.447
5.125
5.114
5.091
5.079
5.026
5.000
4.257
4.234
4.229
4.220
4.210
4.196
4.186
4.177
4.156
4.139
4.119
4.076
4.073
4.056
4.052
4.033
4.029
2.180
2.070
2.050
2.010
AcO
OAc
O
AcO
OAc
O
OCF3
36a
2
2.03
1.02
2.03
1
2.07
1.03
2.98
3.08
3.05
3.02
10
9
8
7
6
5
4
3
2
1
0
170.283
170.160
170.059
169.300
155.167
144.617
122.431
122.123
118.728
118.029
99.715
77.203
71.113
70.709
68.505
66.771
61.307
20.687
20.604
20.542
200
190
180
170
160
150
140
130
120
110
100
90
80
70
60
50
40
30
20
10
0

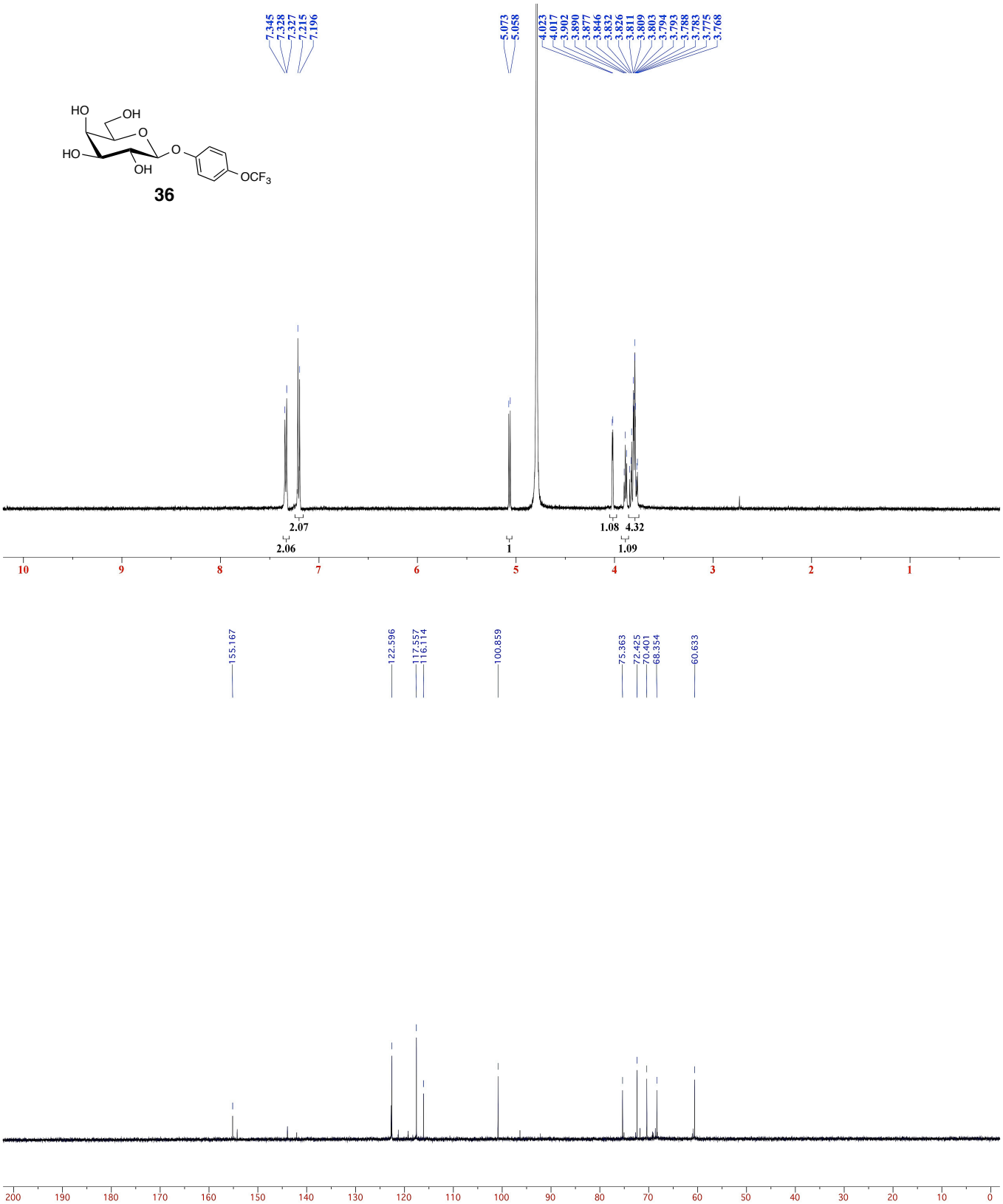
7.345
7.328
7.327
7.215
7.196
5.073
5.058
4.023
4.017
3.902
3.890
3.877
3.846
3.832
3.826
3.811
3.809
3.803
3.794
3.793
3.788
3.783
3.775
3.768
HO
OH
O
HO
O
OH
OCF3
36
2.07
2.06
1
1.08
4.32
1.09
10
9
8
7
6
5
4
3
2
1
155.167
122.596
117.557
116.114
100.859
75.363
72.425
70.401
68.354
60.633
200
190
180
170
160
150
140
130
120
110
100
90
80
70
60
50
40
30
20
10
0

OAc
O
AcO
AcO
O
OMe
OAc

37a

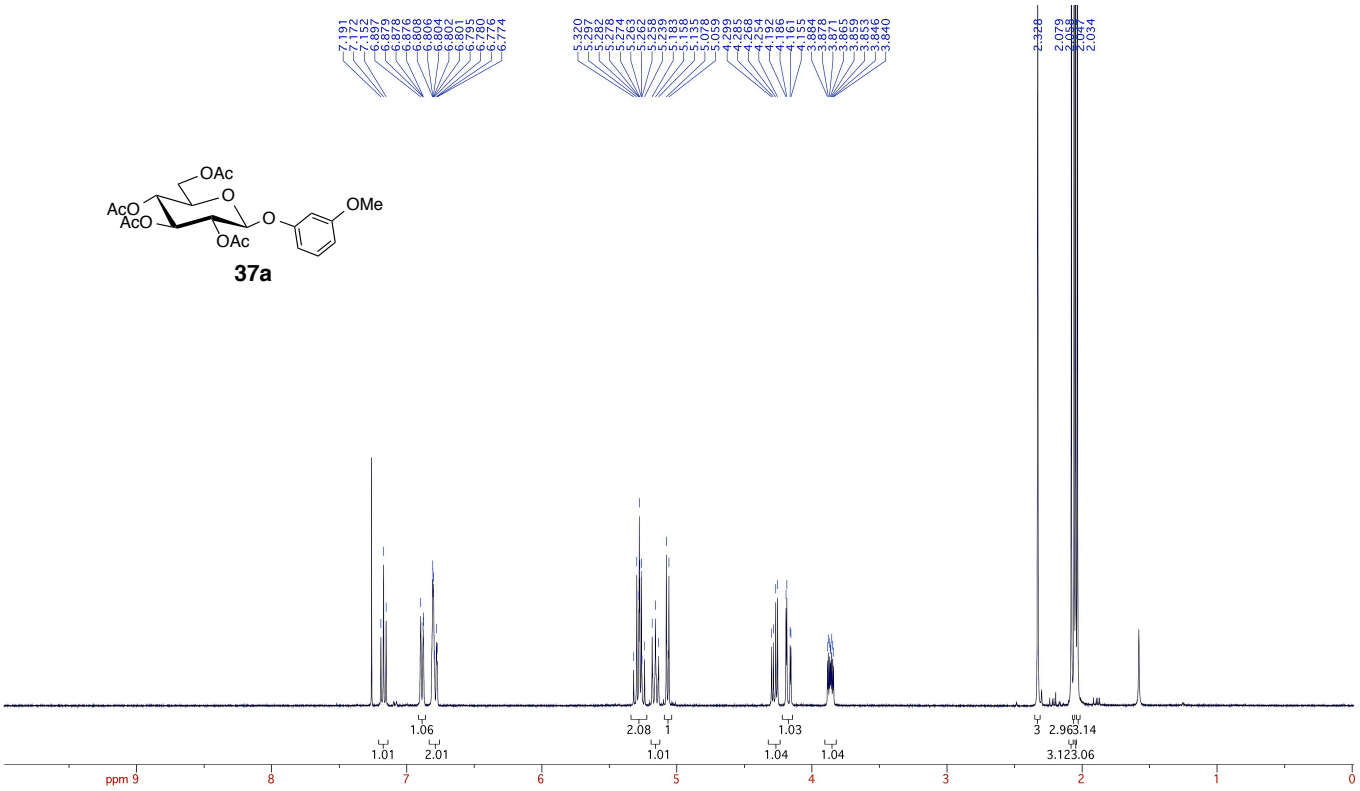
7.191
7.172
7.152
6.897
6.879
6.878
6.876
6.808
6.806
6.804
6.802
6.801
6.795
6.780
6.776
6.774
5.320
5.297
5.282
5.278
5.264
5.262
5.258
5.239
5.233
5.158
5.135
5.078
5.059
4.299
4.285
4.268
4.254
4.192
4.186
4.161
4.155
3.884
3.878
3.871
3.855
3.853
3.846
3.840
2.328
2.079
2.059
2.034
1.06
2.08
1
1.03
3
2.96
3.14
1.01
2.01
1.01
1.04
1.04
3.12
3.06
ppm 9
8
7
6
5
4
3
2
1
0

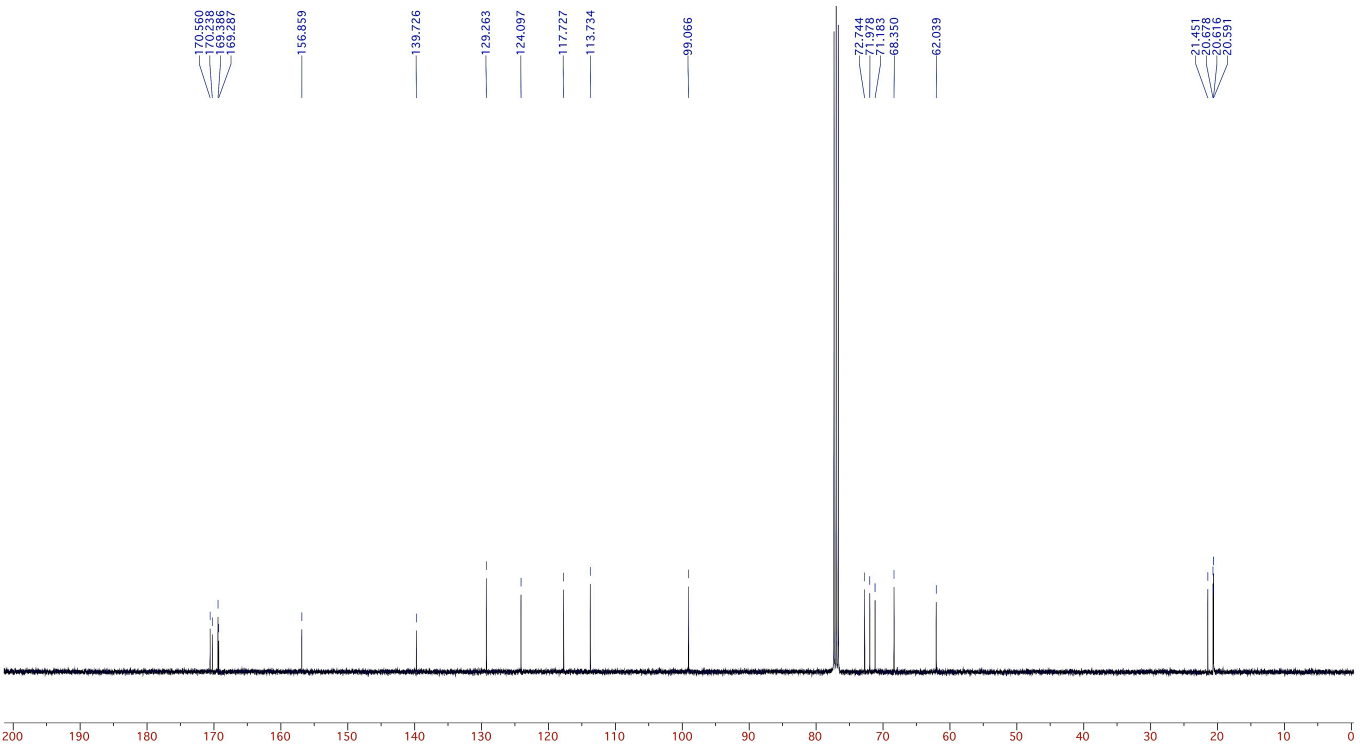
170.560
170.238
169.386
169.287
156.859
139.726
129.263
124.097
117.727
113.734
99.066
72.744
71.978
71.183
68.350
62.039
21.451
20.678
20.616
20.591
200
190
180
170
160
150
140
130
120
110
100
90
80
70
60
50
40
30
20
10
0

OH
O
HO
HO
O
OMe
OH

37

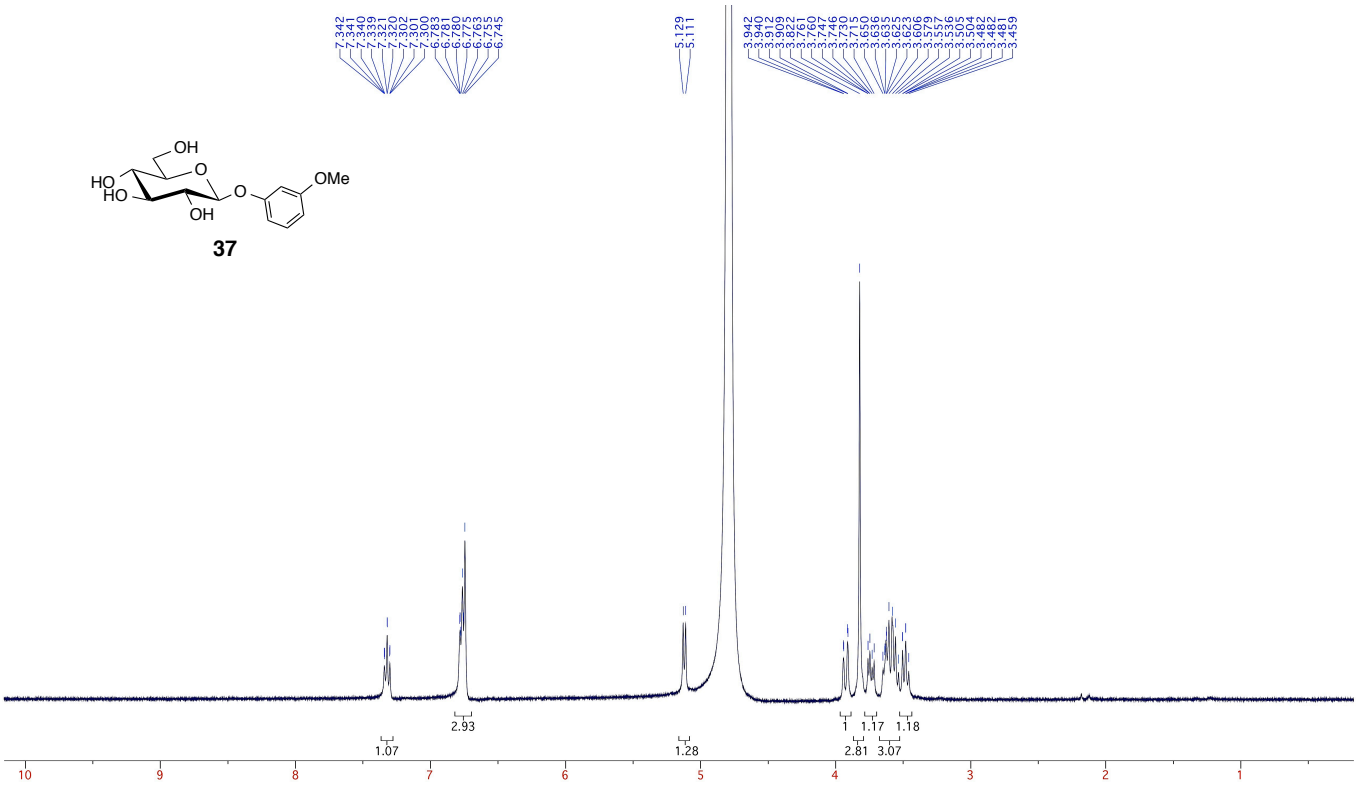
7.342
7.341
7.340
7.339
7.321
7.320
7.302
7.301
7.300
7.283
6.781
6.780
6.775
6.763
6.755
6.745
5.129
5.111
3.942
3.940
3.911
3.909
3.822
3.821
3.760
3.747
3.746
3.710
3.650
3.636
3.635
3.623
3.606
3.579
3.557
3.536
3.505
3.484
3.482
3.481
3.459
2.93
1.07
1.28
1
1.17
1.18
2.81
3.07
10
9
8
7
6
5
4
3
2
1

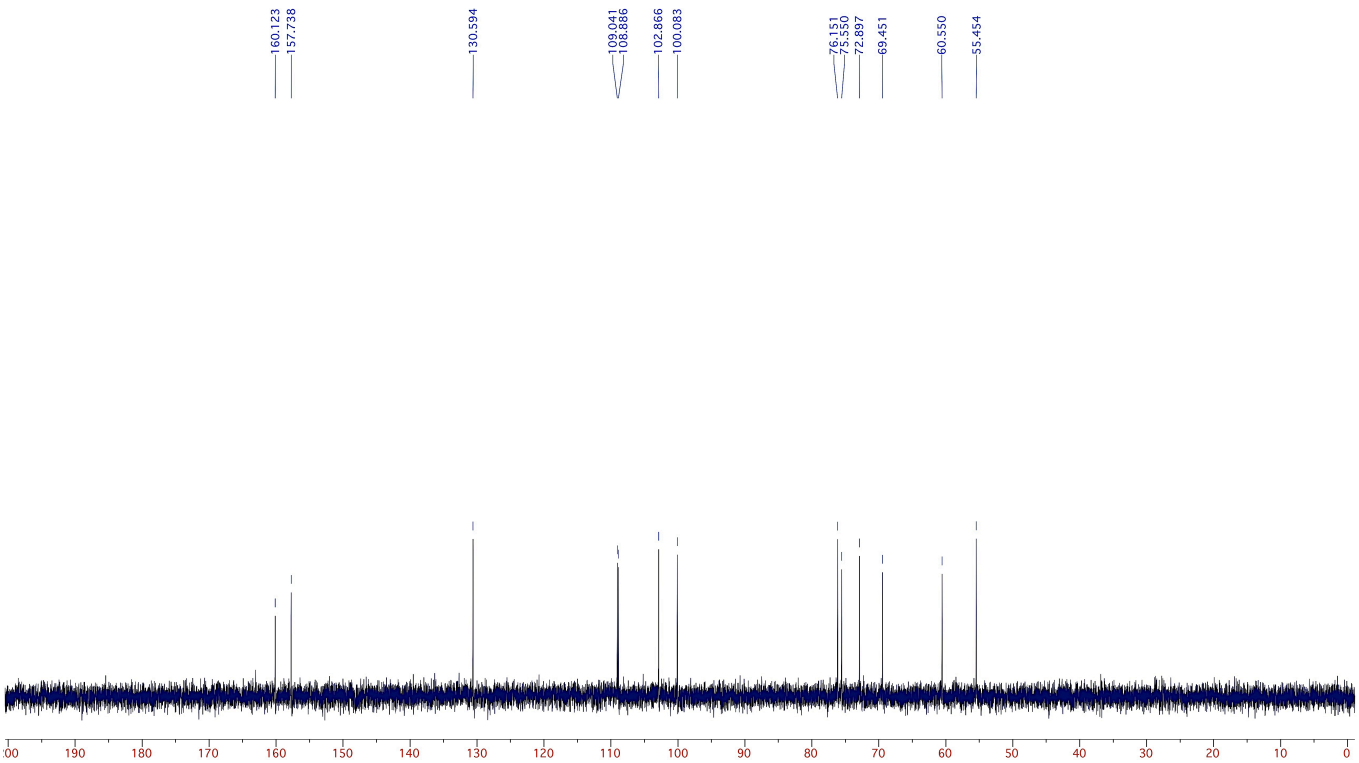
160.123
157.738
130.594
109.041
108.886
102.866
100.083
76.151
75.550
72.897
69.451
60.550
55.454
190
180
170
160
150
140
130
120
110
100
90
80
70
60
50
40
30
20
10
0

OH
O
HO
HO
O
OH
OH

39

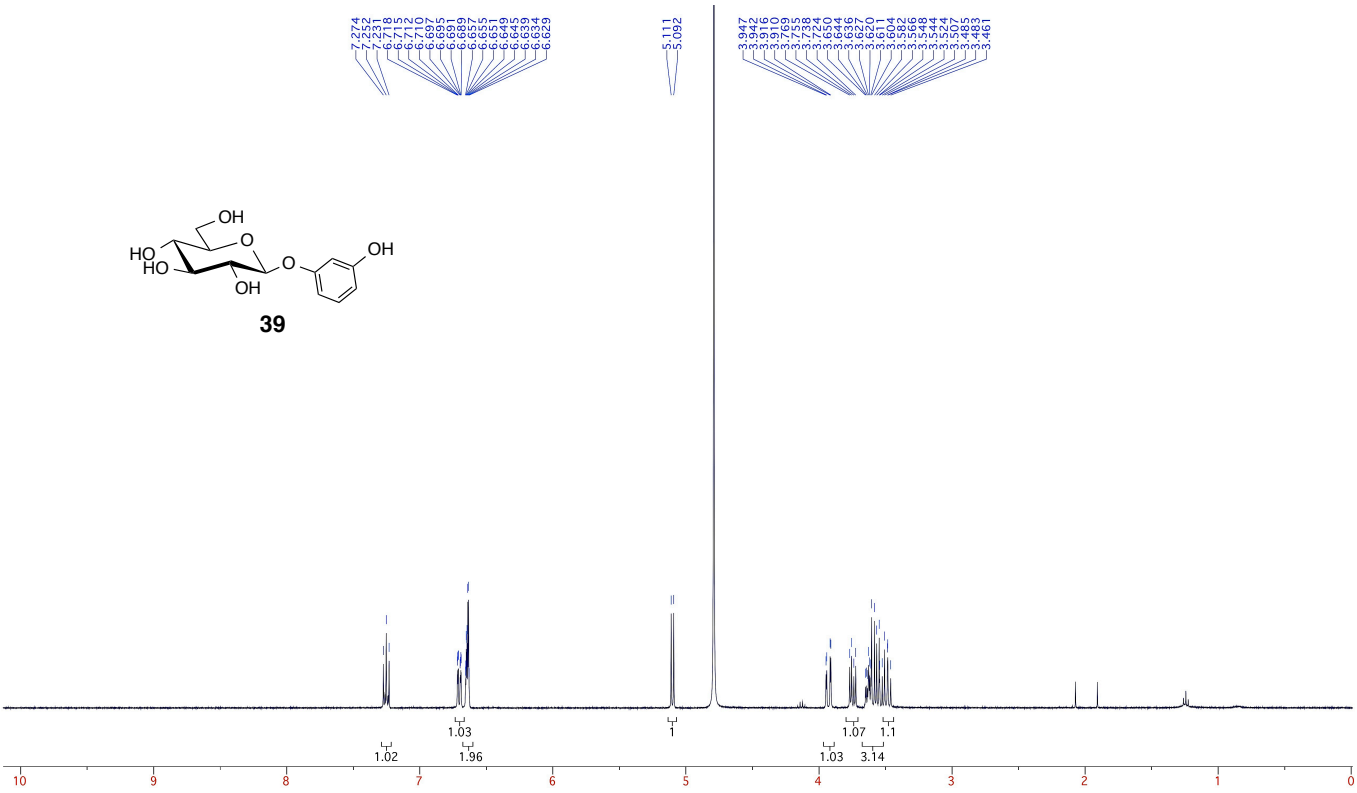
7.274
7.232
7.231
6.718
6.715
6.712
6.710
6.697
6.695
6.693
6.691
6.657
6.655
6.653
6.651
6.645
6.639
6.634
6.629
5.111
5.092
3.947
3.942
3.916
3.910
3.769
3.755
3.738
3.724
3.650
3.644
3.636
3.627
3.620
3.611
3.604
3.582
3.566
3.548
3.544
3.524
3.507
3.487
3.483
3.461
1.02
1.03
1.96
1
1.03
1.07
3.14
1.1
10
9
8
7
6
5
4
3
2
1
0

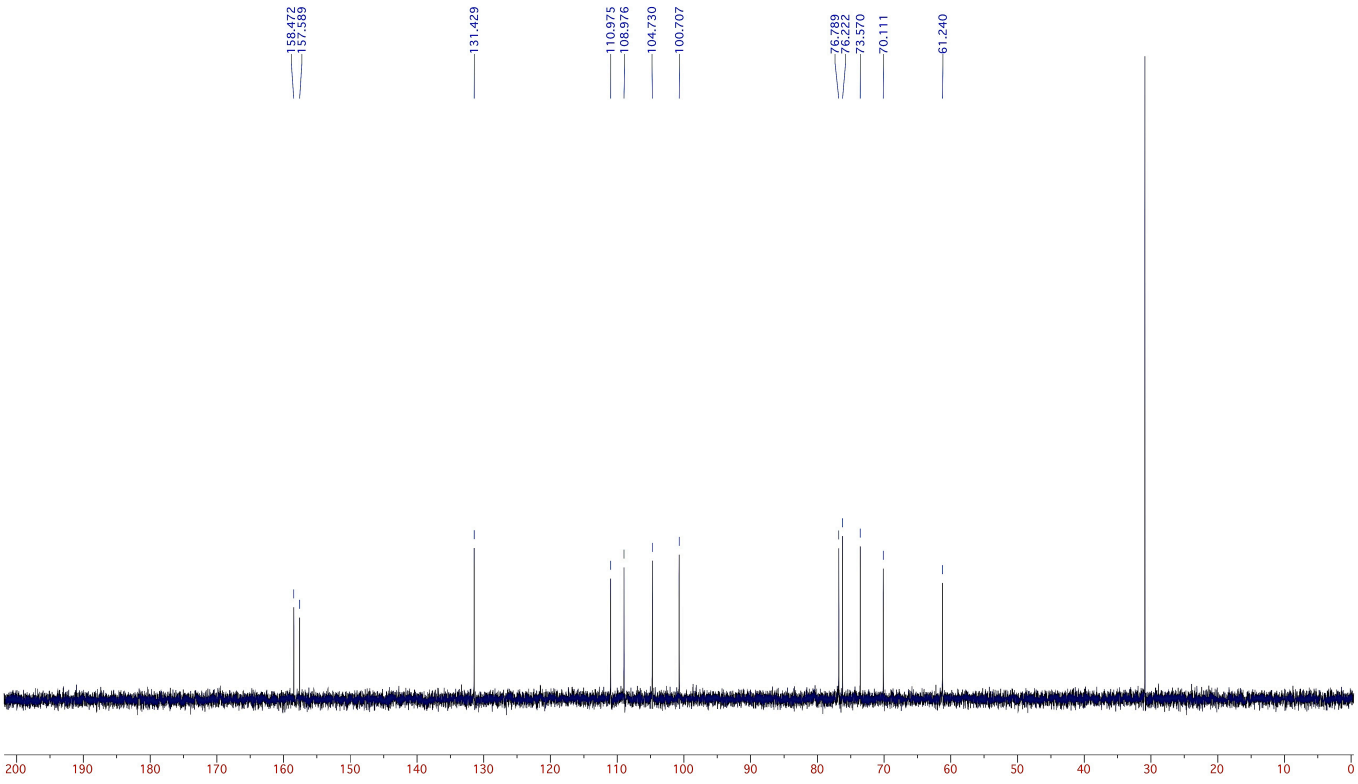
158.472
157.589
131.429
110.975
108.976
104.730
100.707
76.789
76.222
73.570
70.111
61.240
200
190
180
170
160
150
140
130
120
110
100
90
80
70
60
50
40
30
20
10
0

OH
HO
HO
O
O
Me
OH

40

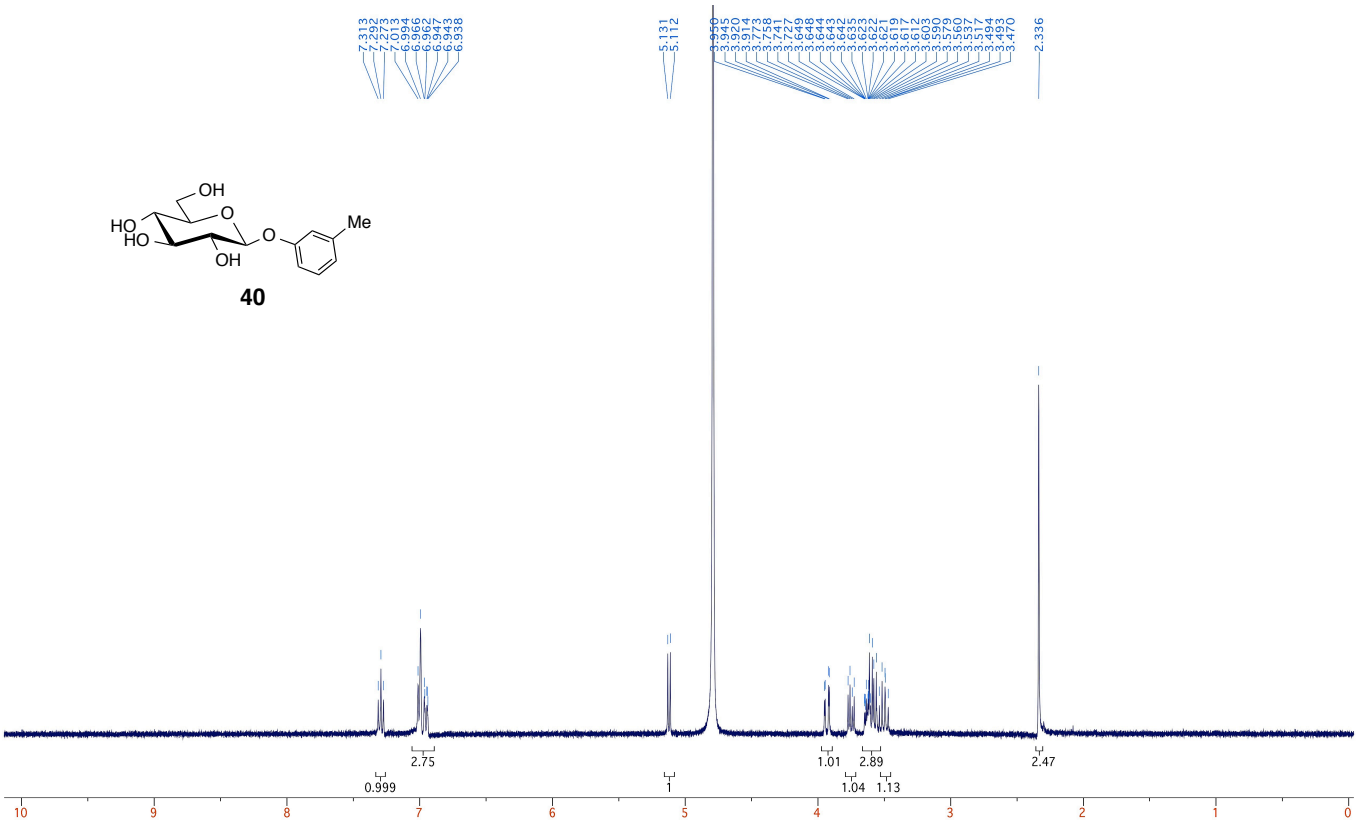
7.313
7.292
7.273
7.013
6.994
6.966
6.962
6.947
6.943
6.938
5.131
5.112
3.950
3.945
3.920
3.774
3.773
3.758
3.741
3.727
3.649
3.648
3.644
3.643
3.642
3.635
3.623
3.622
3.621
3.619
3.617
3.612
3.603
3.590
3.579
3.560
3.537
3.517
3.494
3.493
3.470
2.336
2.75
0.999
1
1.01
2.89
1.04
1.13
2.47
10
9
8
7
6
5
4
3
2
1
0

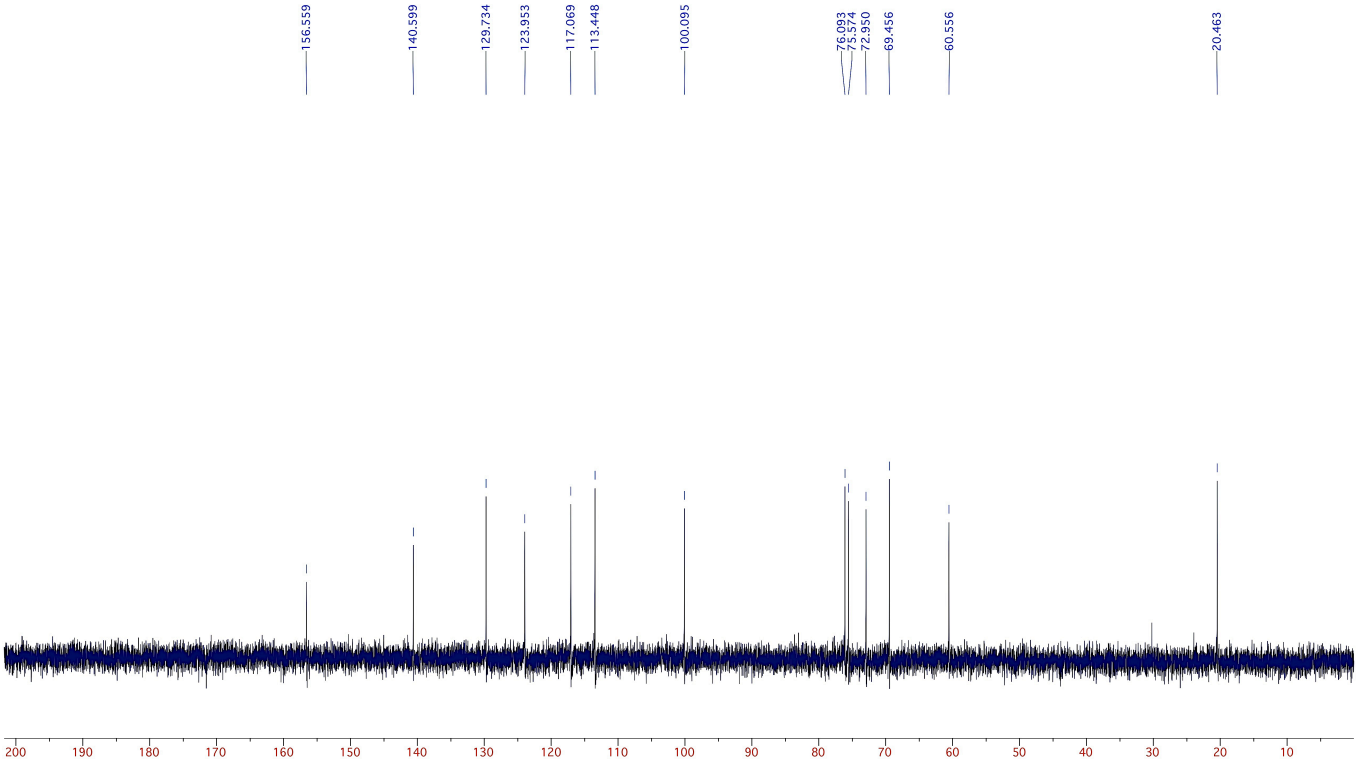
156.559
140.599
129.734
123.953
117.069
113.448
100.095
76.093
75.574
72.950
69.456
60.556
20.463
200
190
180
170
160
150
140
130
120
110
100
90
80
70
60
50
40
30
20
10

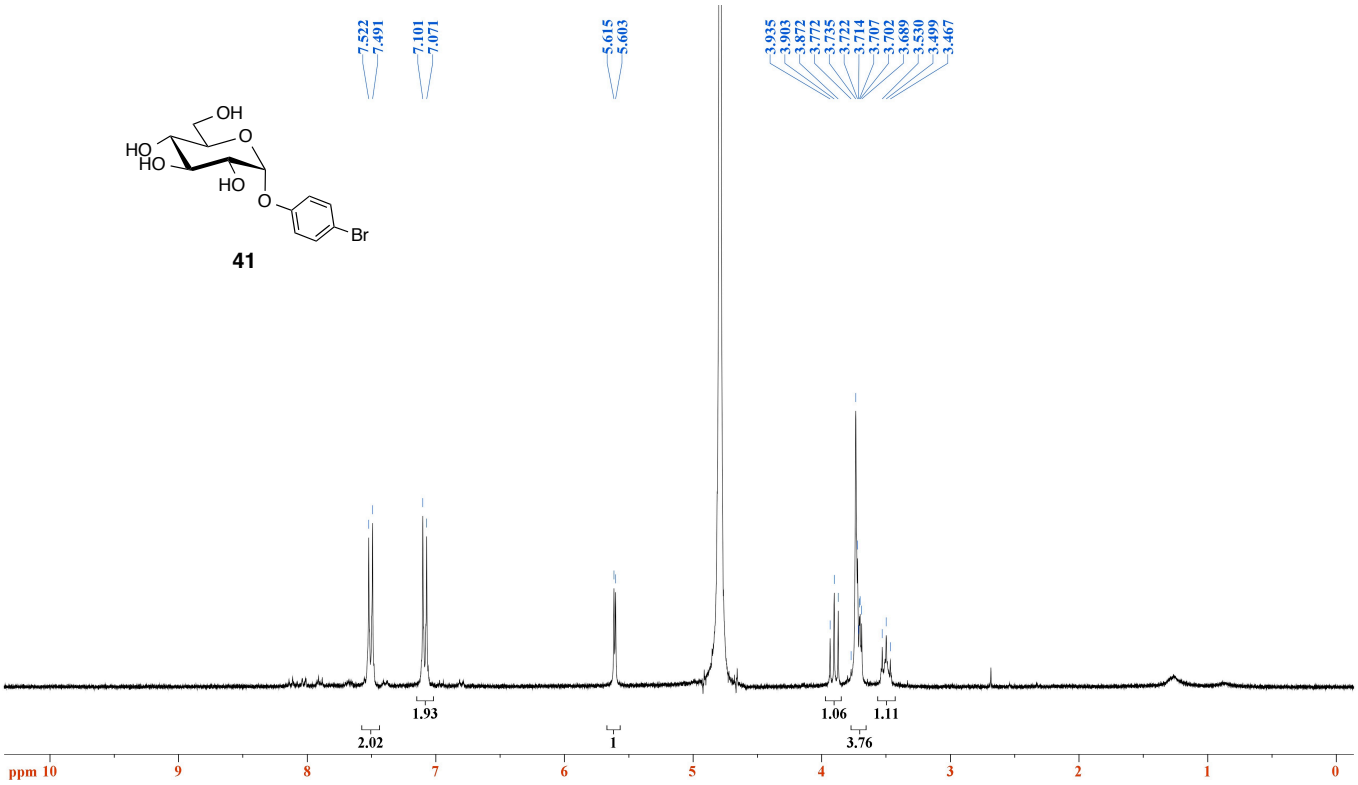
7.522
7.491
7.101
7.071
5.615
5.603
3.935
3.903
3.872
3.772
3.735
3.722
3.714
3.707
3.702
3.689
3.530
3.499
3.467
OH
O
HO
HO
HO
O
Br
41
1.93
1.06
1.11
2.02
1
3.76
ppm 10
9
8
7
6
5
4
3
2
1
0

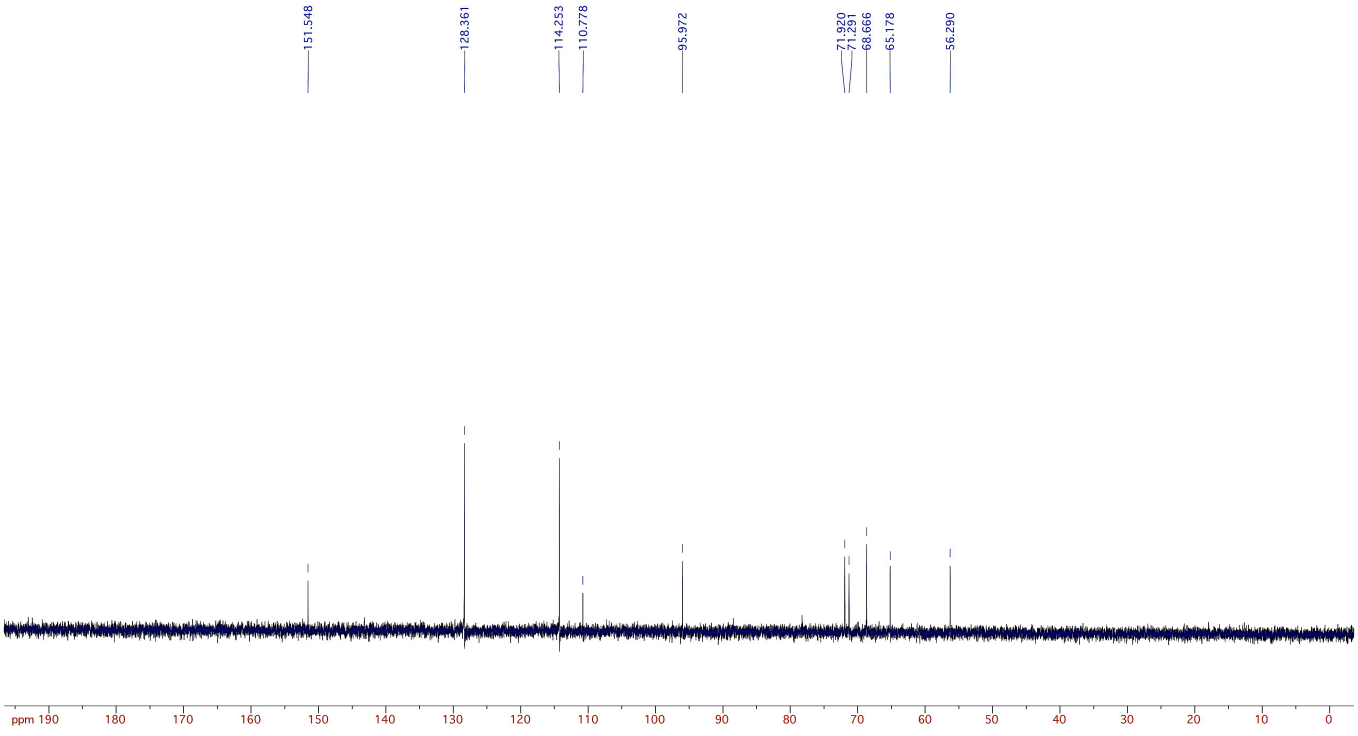
151.548
128.361
114.253
110.778
95.972
71.920
71.291
68.666
65.178
56.290
ppm 190
180
170
160
150
140
130
120
110
100
90
80
70
60
50
40
30
20
10
0

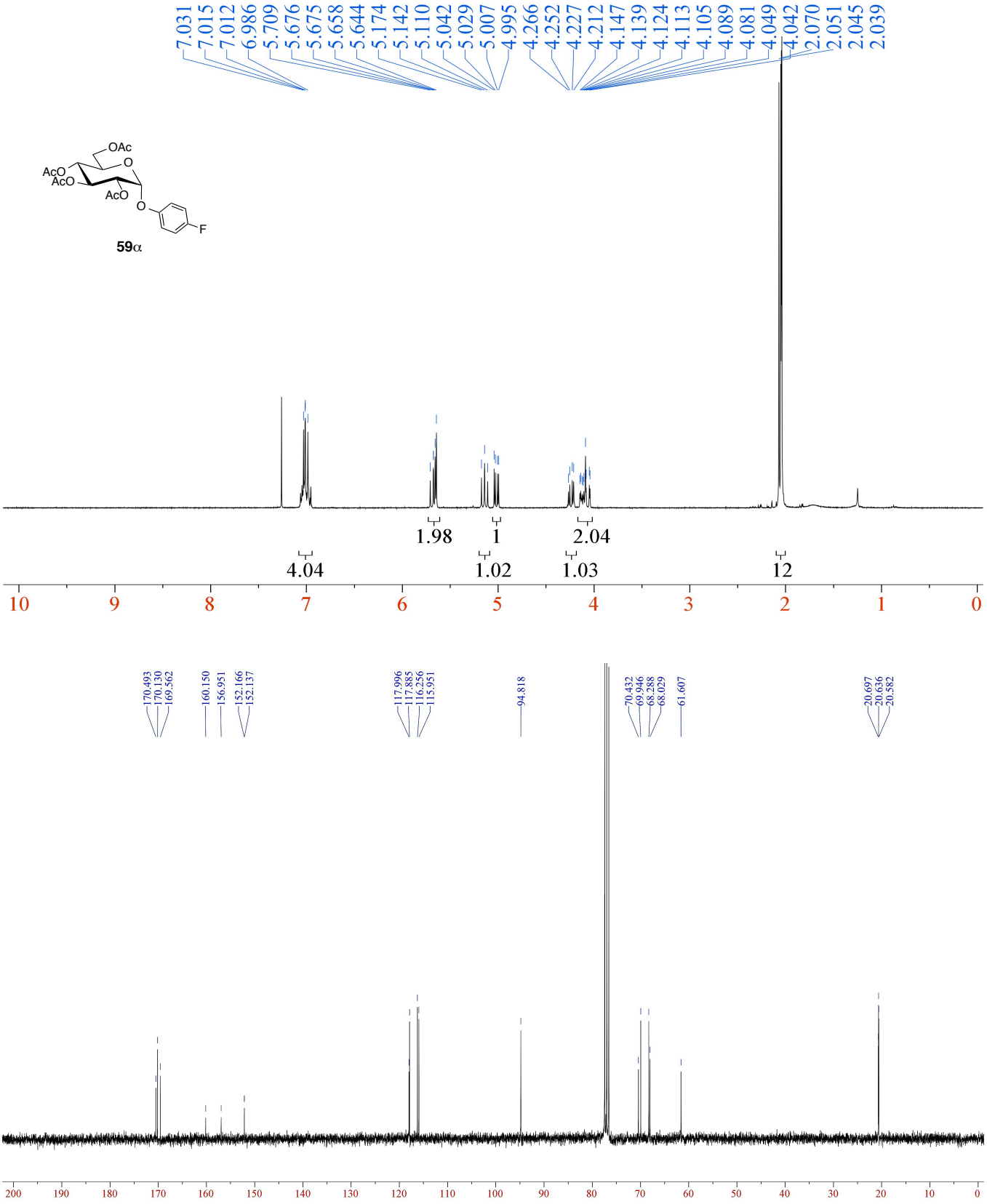
7.031
7.015
7.012
6.986
5.709
5.676
5.675
5.658
5.644
5.174
5.142
5.110
5.042
5.029
5.007
4.995
4.266
4.252
4.227
4.212
4.147
4.139
4.124
4.113
4.105
4.089
4.081
4.049
4.042
2.070
2.051
2.045
2.039
OAc
AcO
AcO
AcO
O
O
F
59α
1.98
1
2.04
4.04
1.02
1.03
12
10
9
8
7
6
5
4
3
2
1
0
170.493
170.130
169.562
160.150
156.951
152.166
152.137
117.996
117.885
116.256
115.951
94.818
70.432
69.946
68.288
68.029
61.607
20.697
20.636
20.582
200
190
180
170
160
150
140
130
120
110
100
90
80
70
60
50
40
30
20
10
0

OH
O
HO
HO
HO
O
F

42

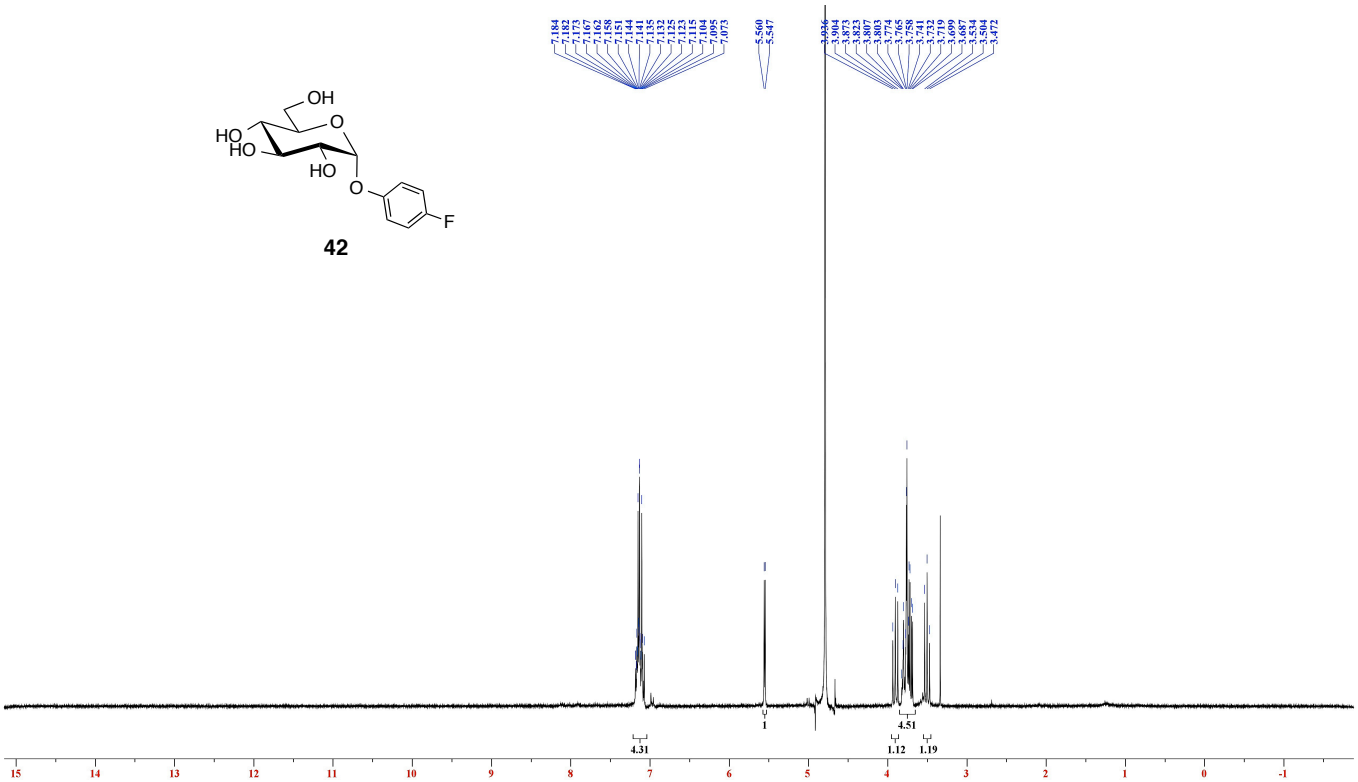
7.184
7.182
7.173
7.167
7.162
7.158
7.151
7.144
7.141
7.135
7.132
7.122
7.123
7.115
7.104
7.094
7.073
5.560
5.547
3.936
3.904
3.873
3.832
3.807
3.803
3.774
3.765
3.758
3.741
3.732
3.719
3.699
3.687
3.534
3.494
3.472
4.31
1
4.51
1.12
1.19
15
14
13
12
11
10
9
8
7
6
5
4
3
2
1
0
-1

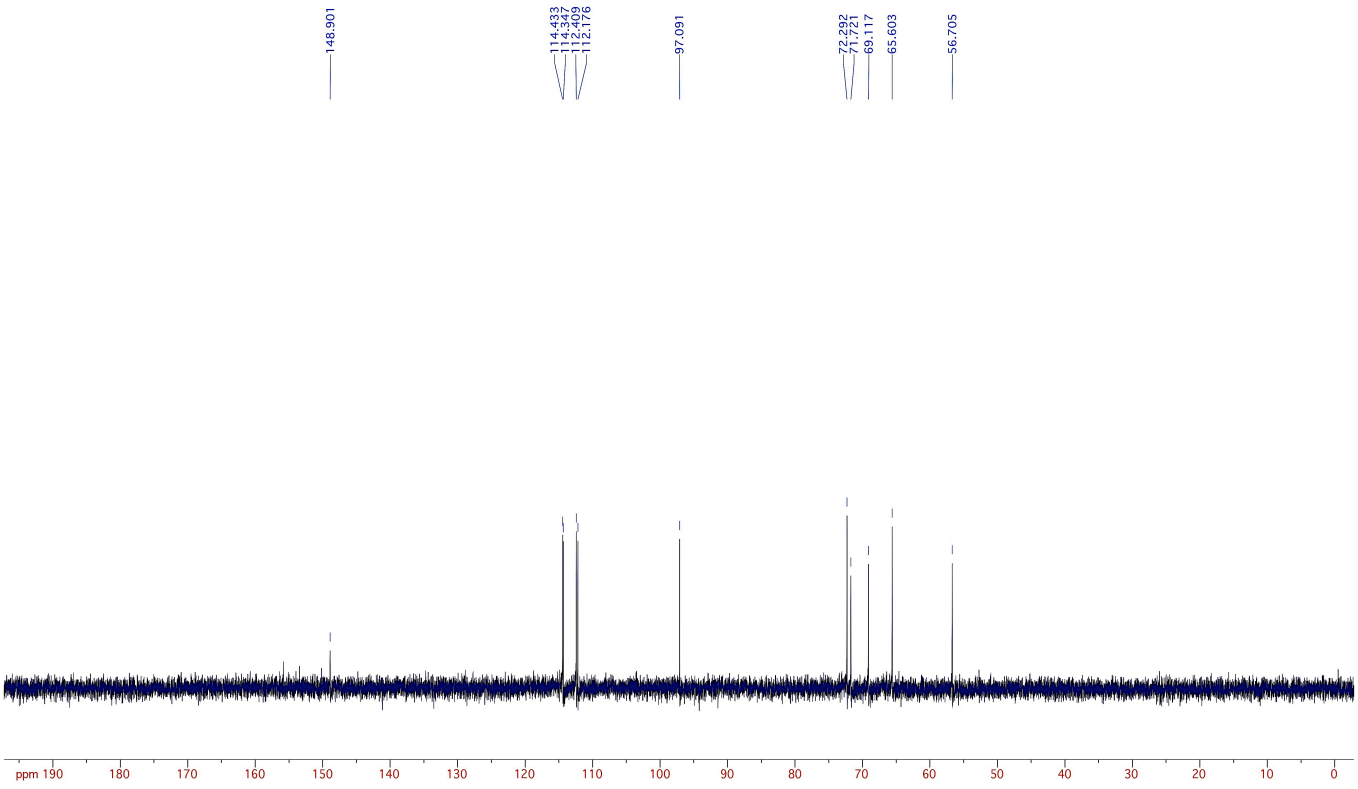
148.901
114.433
114.347
112.269
112.176
97.091
72.292
71.721
69.117
65.603
56.705
ppm 190
180
170
160
150
140
130
120
110
100
90
80
70
60
50
40
30
20
10
0

OH
HO
HO
HO
O
O
OMe

43

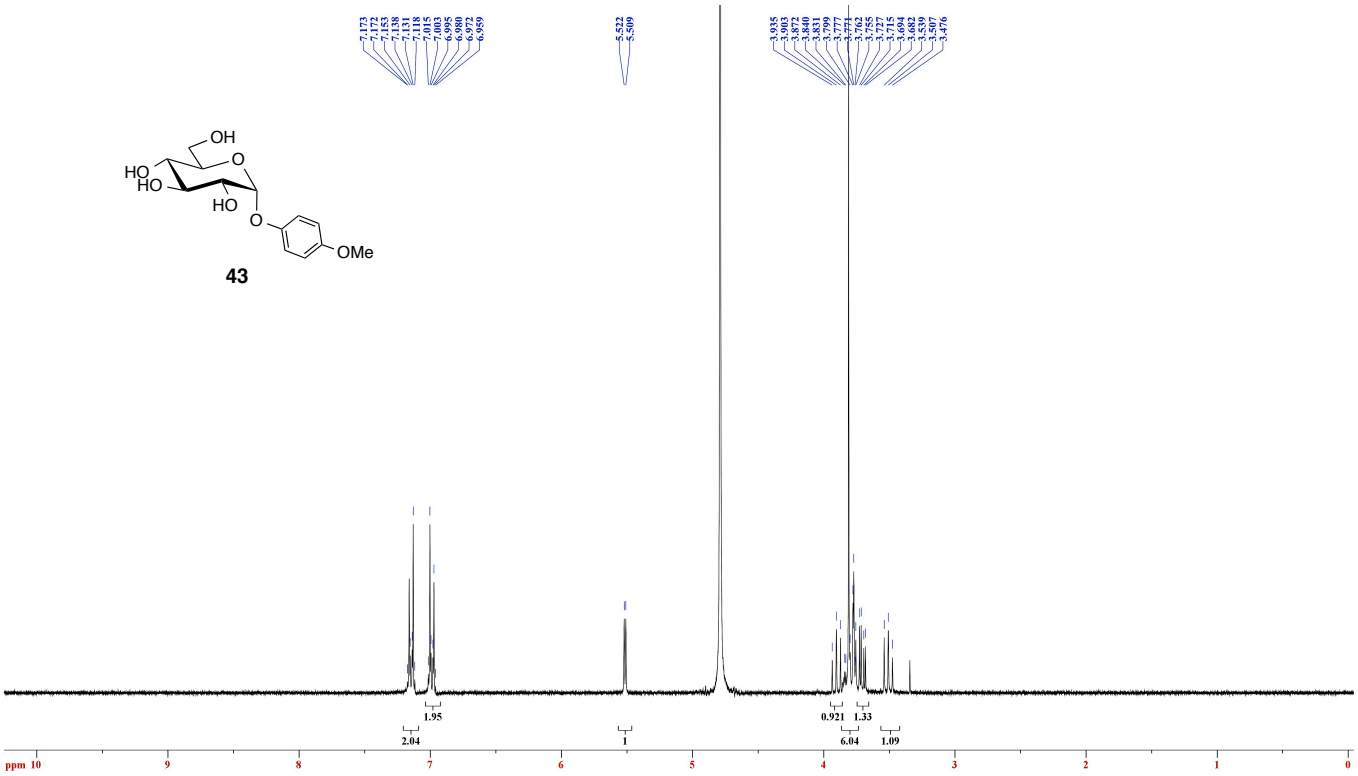
7.173
7.172
7.153
7.138
7.131
7.118
7.015
7.003
6.995
6.980
6.972
6.959
5.532
5.509
3.935
3.903
3.872
3.840
3.831
3.799
3.777
3.771
3.762
3.755
3.727
3.715
3.694
3.663
3.539
3.507
3.476
1.95
2.04
1
0.921
1.33
6.04
1.09
ppm 10
9
8
7
6
5
4
3
2
1
0

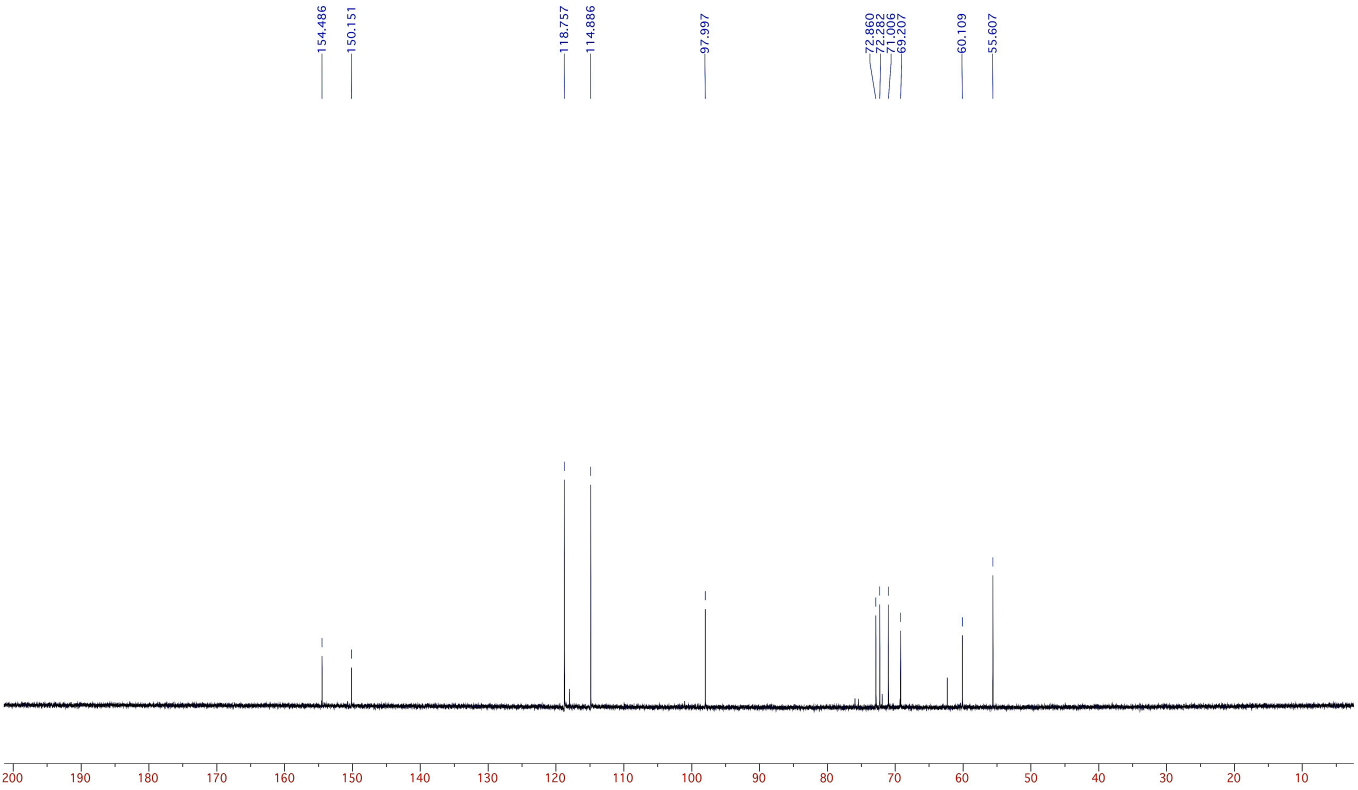
154.486
150.151
118.757
114.886
97.997
72.860
72.282
71.006
69.207
60.109
55.607
200
190
180
170
160
150
140
130
120
110
100
90
80
70
60
50
40
30
20
10

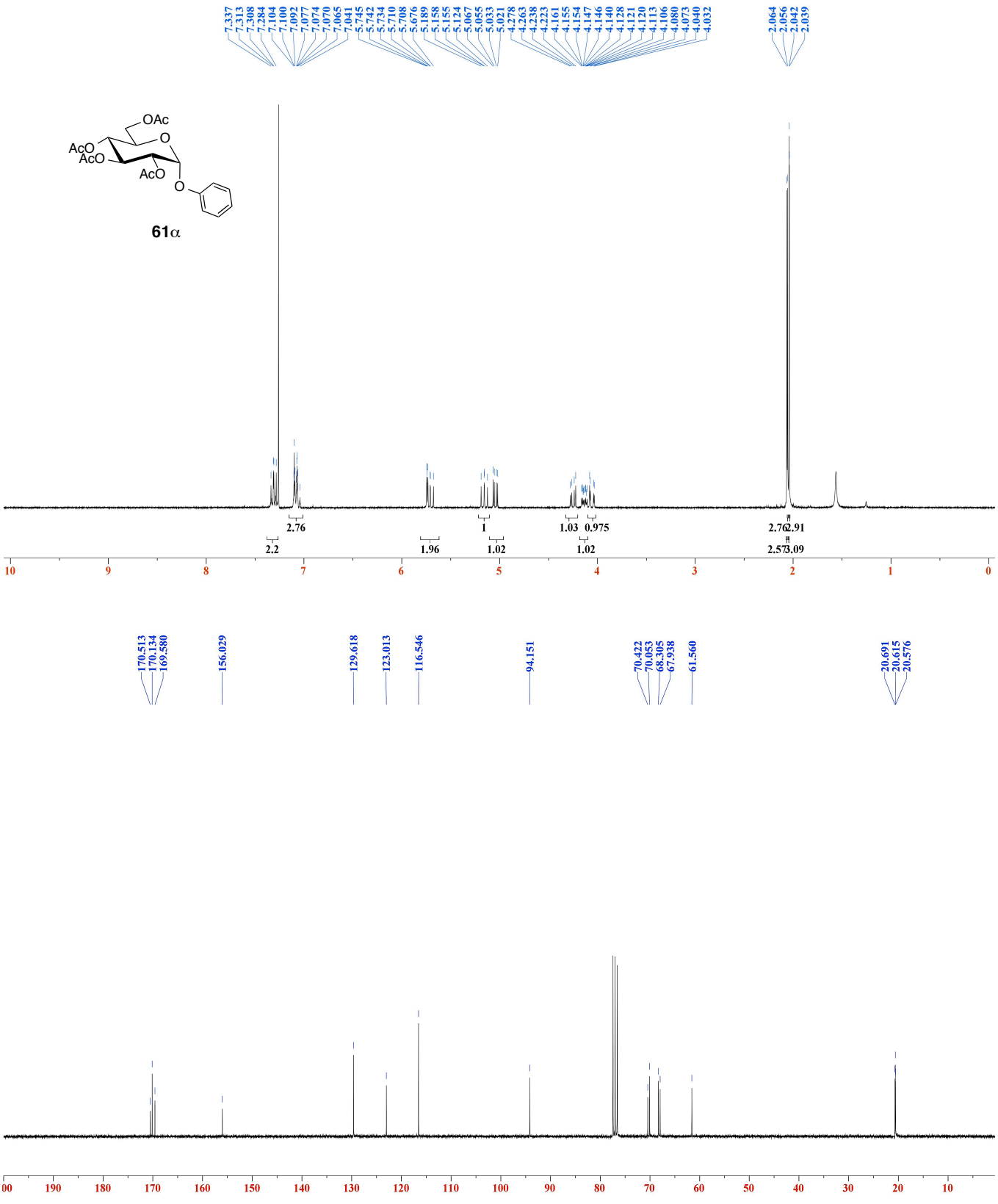
7.337
7.313
7.308
7.284
7.104
7.100
7.092
7.077
7.074
7.070
7.065
7.041
5.745
5.742
5.734
5.710
5.708
5.676
5.189
5.158
5.155
5.124
5.067
5.055
5.033
5.021
4.278
4.263
4.238
4.223
4.161
4.155
4.154
4.147
4.146
4.140
4.128
4.121
4.120
4.113
4.106
4.080
4.073
4.040
4.032
2.064
2.056
2.042
2.039
OAc
AcO
AcO
AcO
O
O
61α
2.76
1
1.03
0.975
2.2
1.96
1.02
1.02
2.76
2.91
2.57
3.09
10
9
8
7
6
5
4
3
2
1
0
170.513
170.134
169.580
156.029
129.618
123.013
116.546
94.151
70.422
70.053
68.305
67.938
61.560
20.691
20.615
20.576
00
190
180
170
160
150
140
130
120
110
100
90
80
70
60
50
40
30
20
10

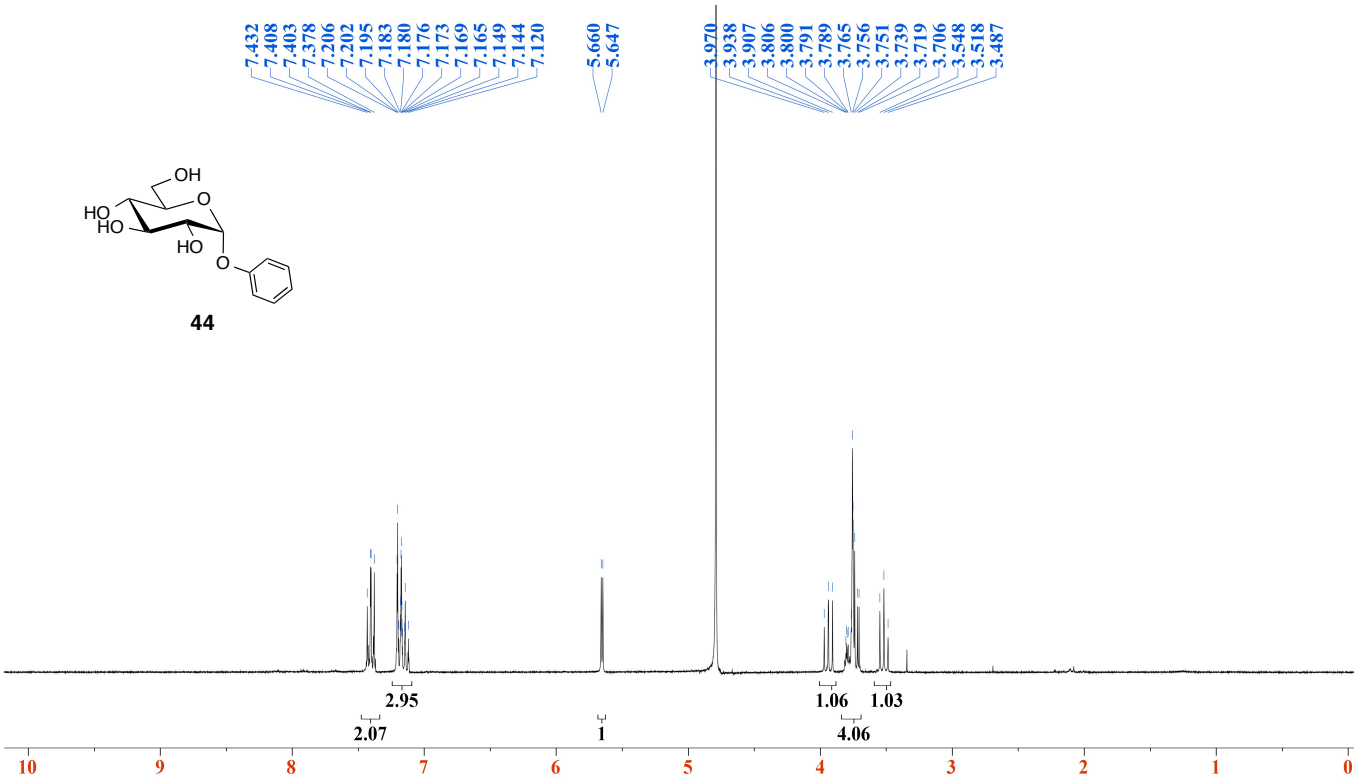
7.432
7.408
7.403
7.378
7.206
7.202
7.195
7.183
7.180
7.176
7.173
7.169
7.165
7.149
7.144
7.120
5.660
5.647
3.970
3.938
3.907
3.806
3.800
3.791
3.789
3.765
3.756
3.751
3.739
3.719
3.706
3.548
3.518
3.487
OH
O
HO
HO
HO
O
2.95
2.07
1
1.06
1.03
4.06
10
9
8
7
6
5
4
3
2
1
0

44

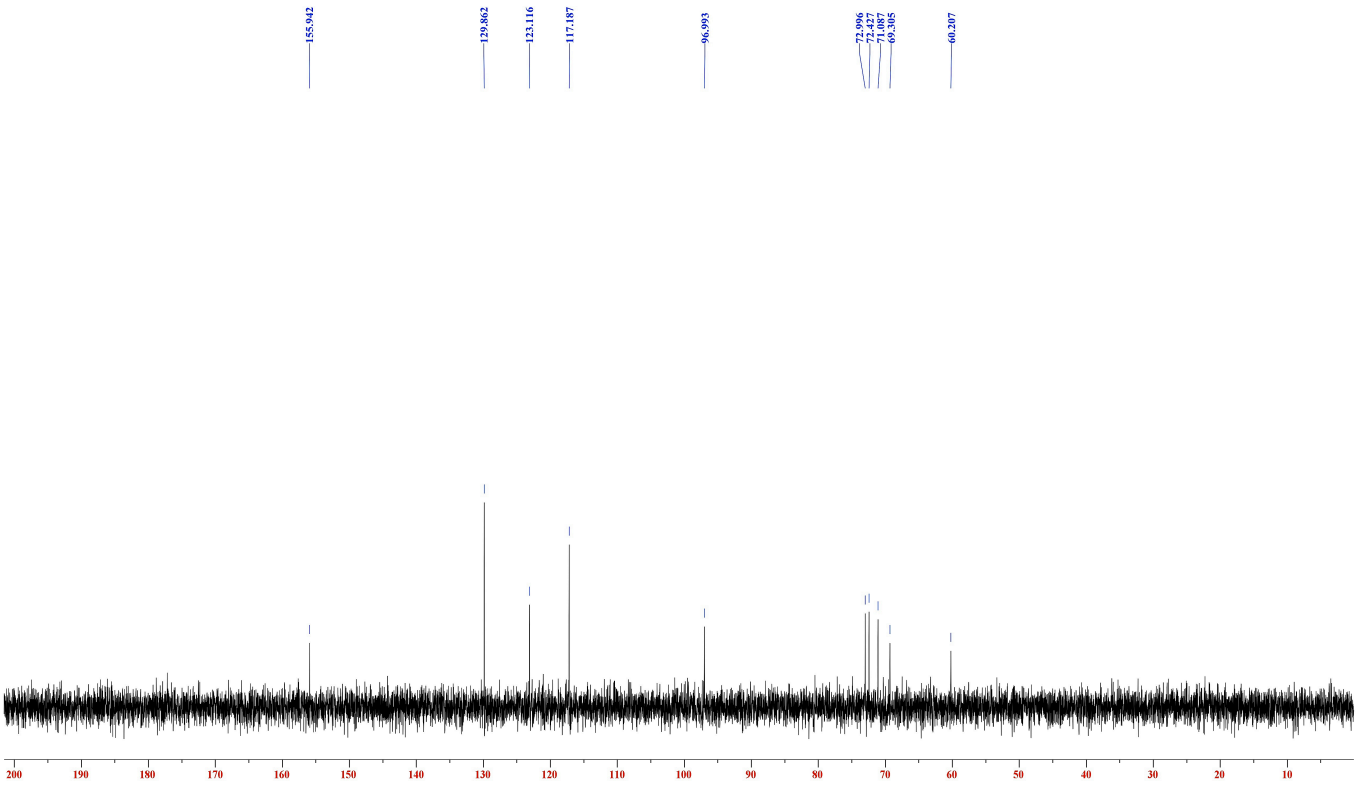
155.942
129.862
123.116
117.187
96.993
72.996
72.127
71.087
69.305
60.207
200
190
180
170
160
150
140
130
120
110
100
90
80
70
60
50
40
30
20
10

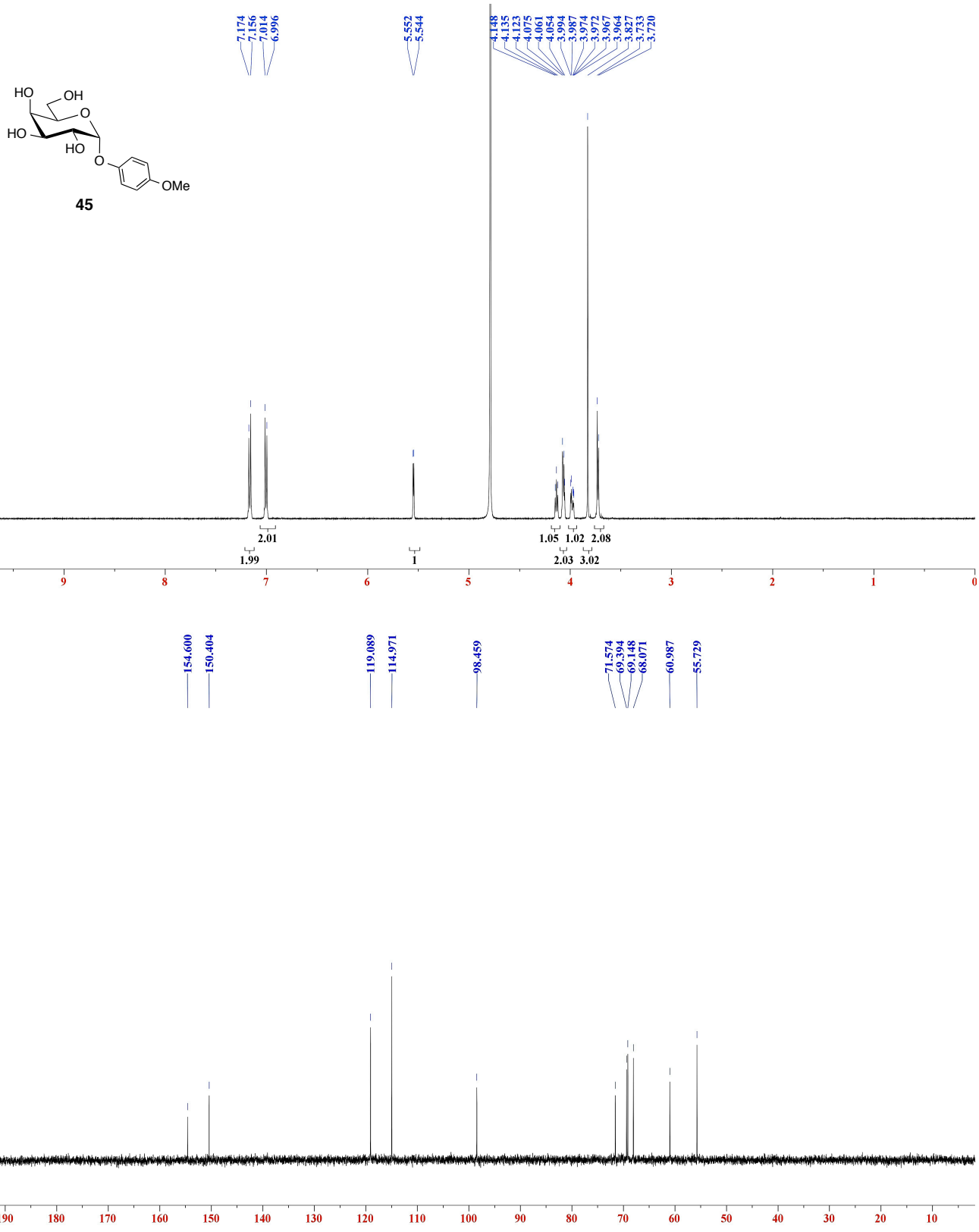
HO
OH
O
HO
HO
O
OMe
45
7.174
7.156
7.014
6.996
5.552
5.544
4.148
4.135
4.123
4.075
4.061
4.054
3.994
3.987
3.974
3.972
3.967
3.964
3.827
3.733
3.720
2.01
1.99
1
1.05
1.02
2.08
2.03
3.02
154.600
150.404
119.089
114.971
98.459
71.574
69.394
69.148
68.071
60.987
55.729

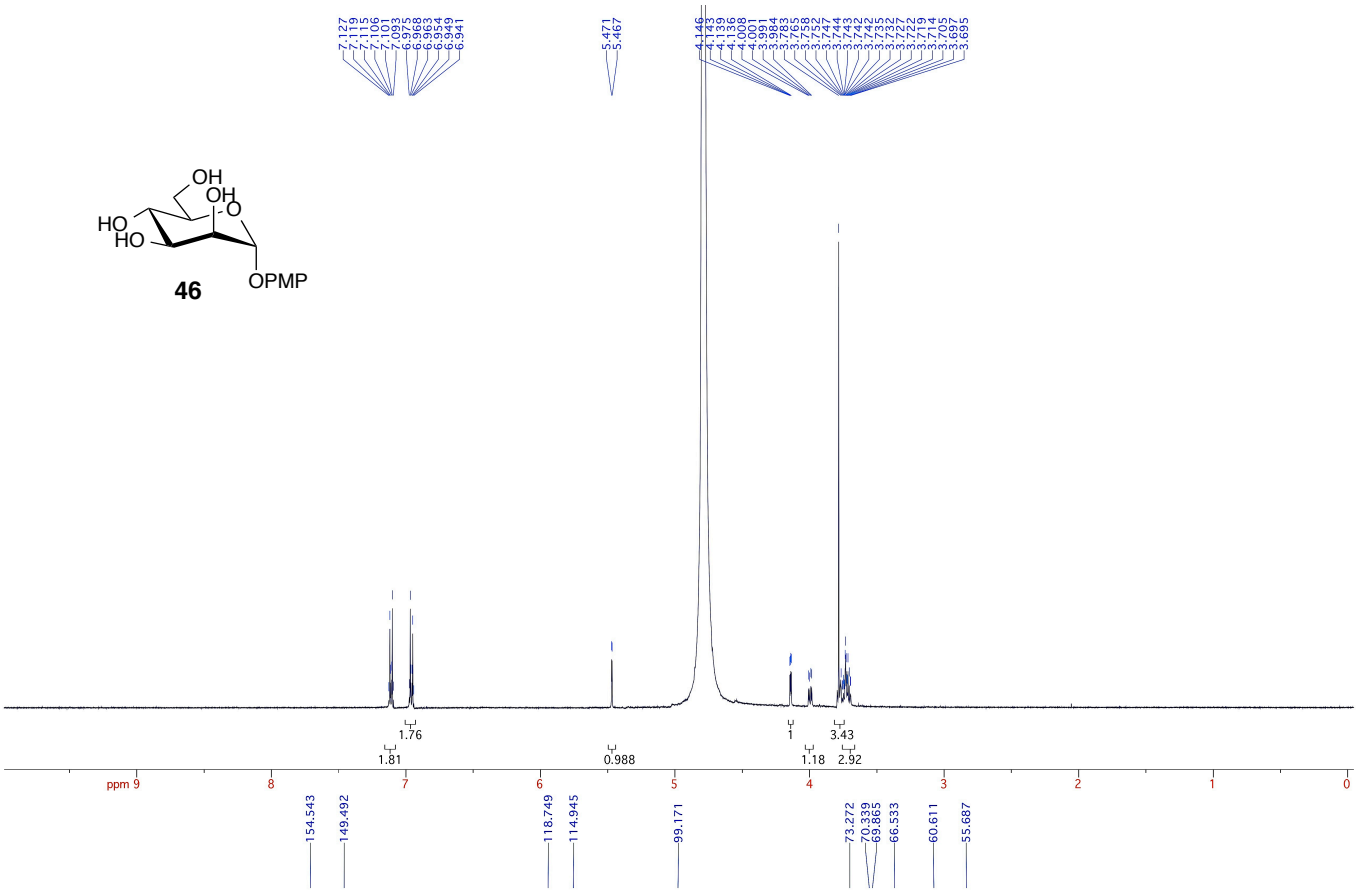
OH
OH
HO
HO
O
OPMP
46
7.127
7.119
7.115
7.106
7.101
7.093
6.968
6.963
6.954
6.949
6.941
5.471
5.467
4.146
4.143
4.139
4.136
4.008
4.001
3.991
3.984
3.783
3.765
3.758
3.747
3.744
3.743
3.742
3.735
3.732
3.727
3.722
3.719
3.714
3.705
3.697
3.695
1.81
1.76
0.988
1
1.18
3.43
2.92
ppm 9
8
7
6
5
4
3
2
1
0

154.543
149.492
118.749
114.945
99.171
73.272
70.339
69.865
66.533
60.611
55.687

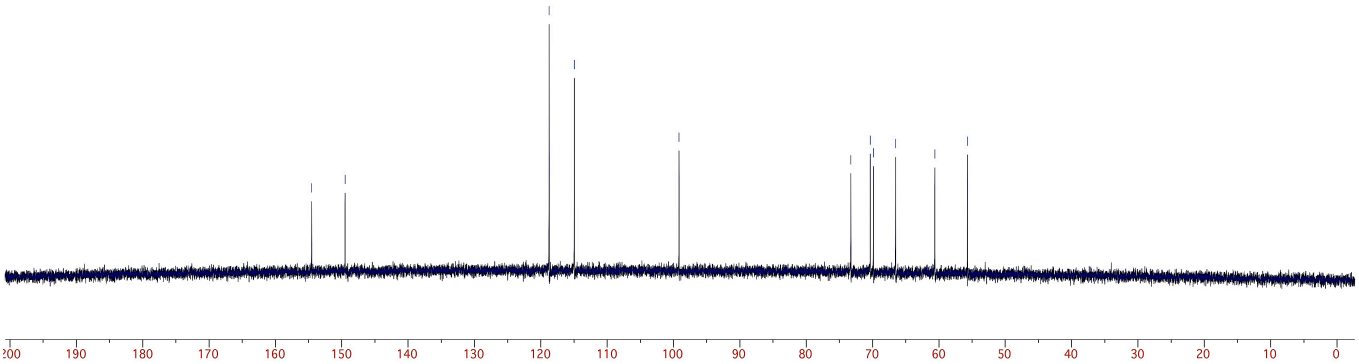
200
190
180
170
160
150
140
130
120
110
100
90
80
70
60
50
40
30
20
10
0

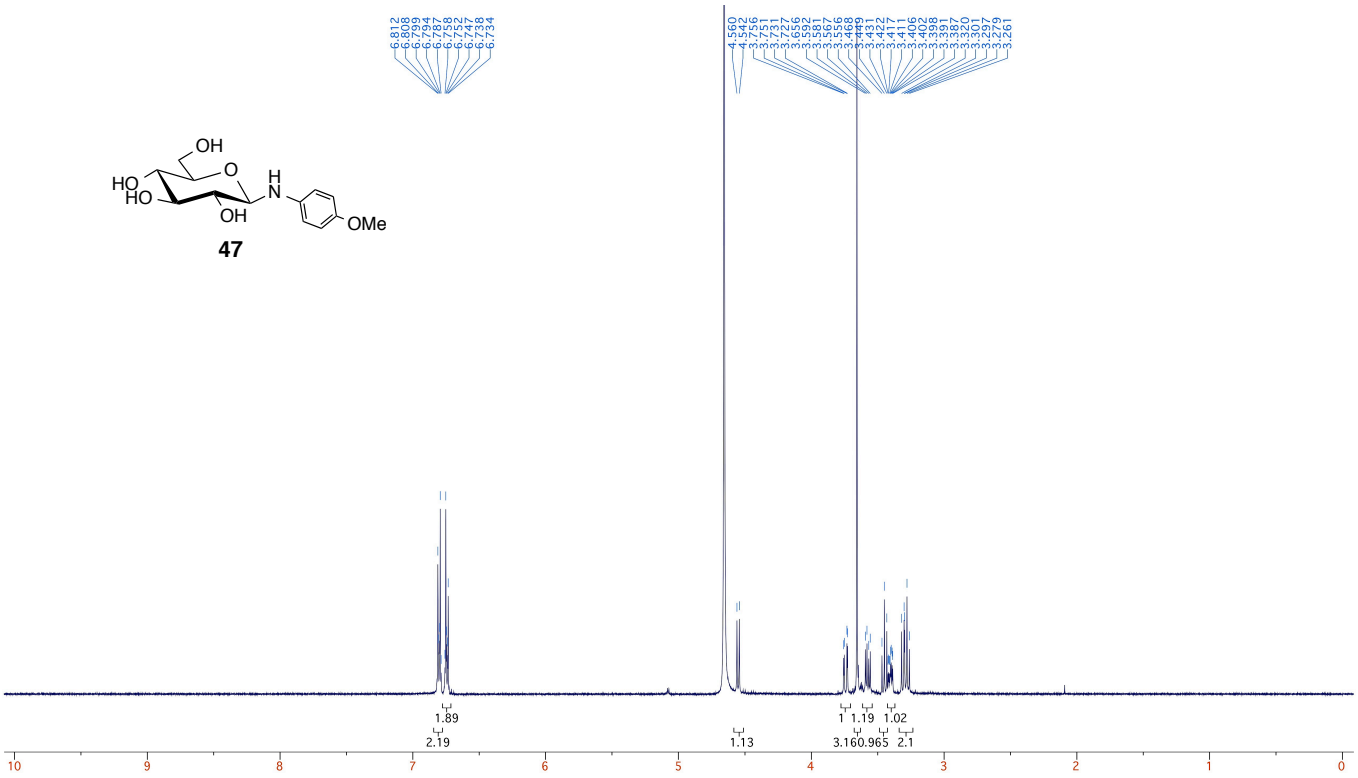
6.812
6.808
6.799
6.794
6.787
6.758
6.752
6.747
6.738
6.734
4.560
4.542
3.756
3.751
3.727
3.717
3.656
3.592
3.581
3.567
3.556
3.468
3.449
3.431
3.422
3.417
3.411
3.406
3.402
3.398
3.391
3.387
3.320
3.301
3.297
3.279
3.261
OH
HO
HO
O
OH
H
N
OMe
47
1.89
2.19
1.13
1
1.19
1.02
3.16
0.965
2.1
10
9
8
7
6
5
4
3
2
1
0

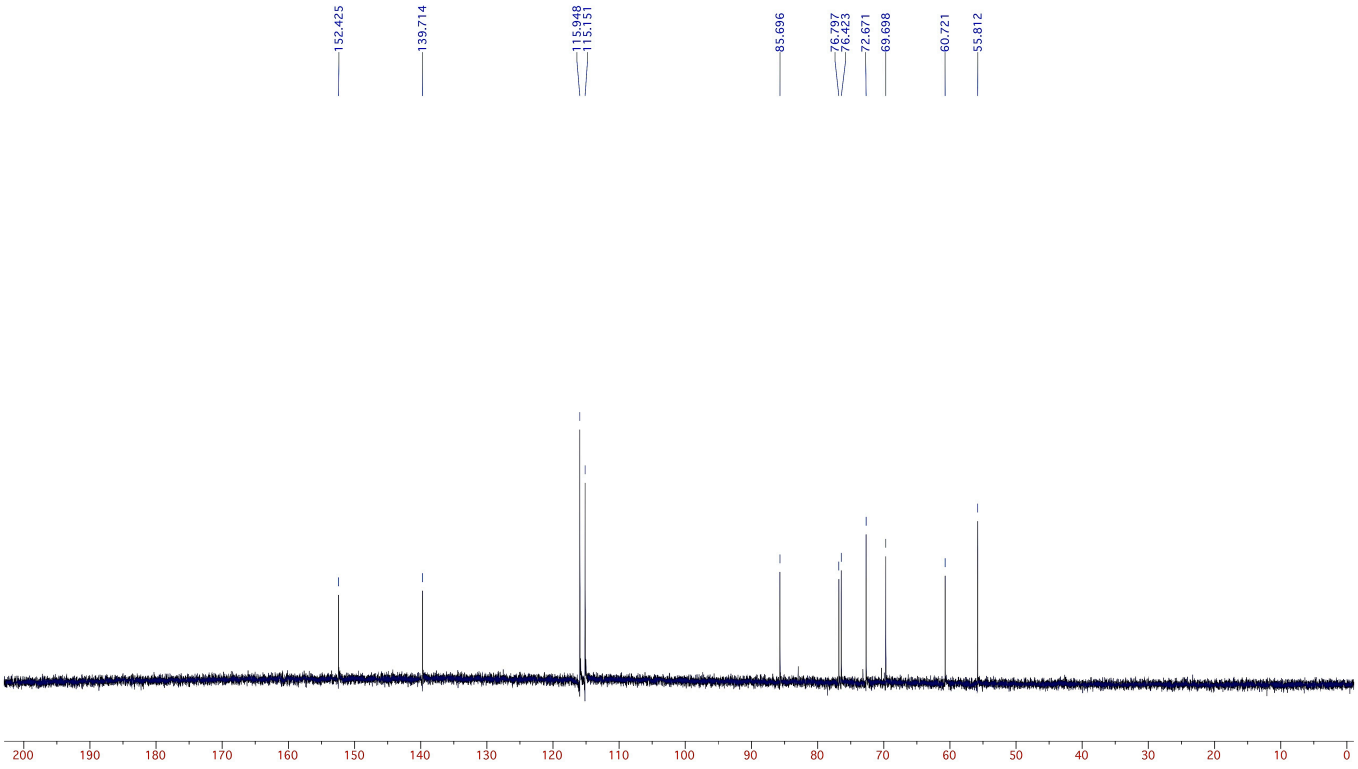
152.425
139.714
115.948
115.151
85.696
76.797
76.423
72.671
69.698
60.721
55.812
200
190
180
170
160
150
140
130
120
110
100
90
80
70
60
50
40
30
20
10
0

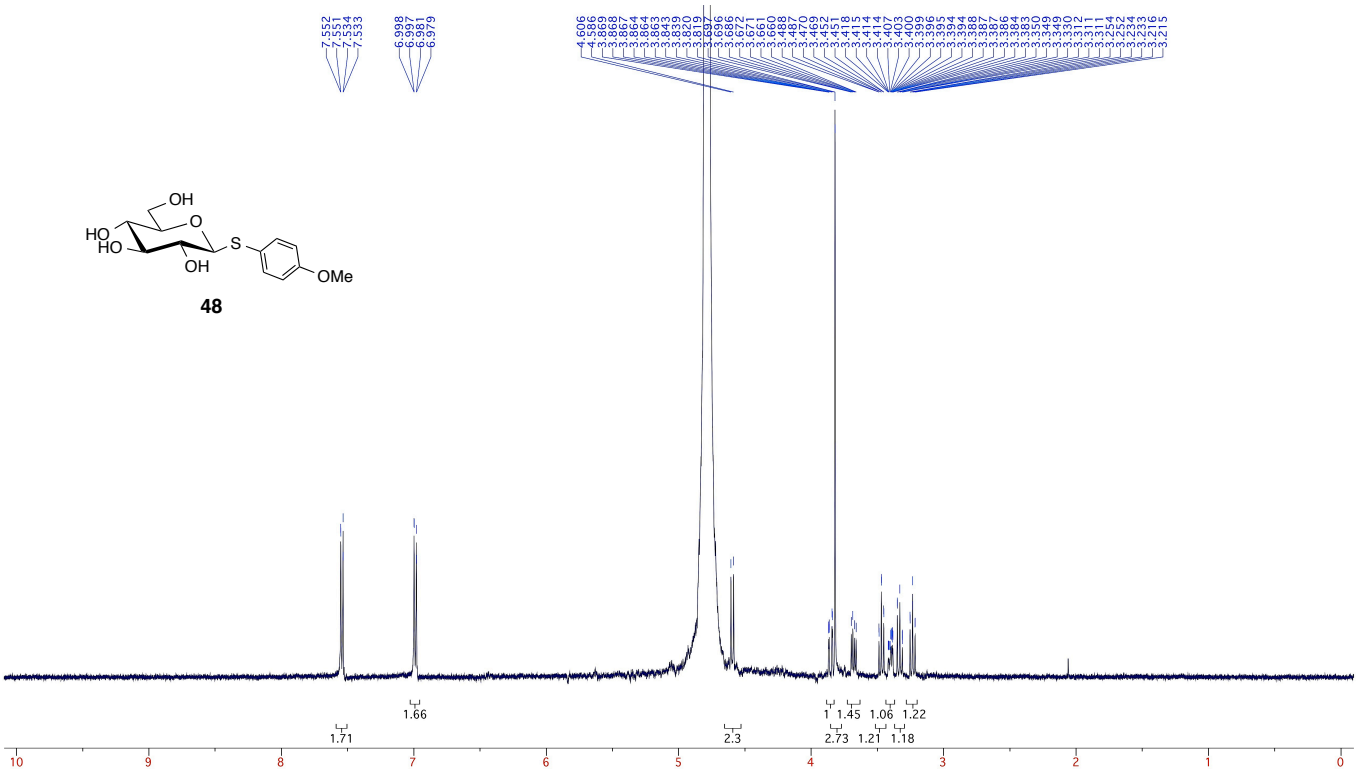
7.552
7.551
7.534
7.533
6.998
6.997
6.981
6.979
4.606
4.605
4.869
4.868
3.867
3.864
3.863
3.843
3.839
3.820
3.819
3.697
3.696
3.686
3.672
3.671
3.661
3.660
3.488
3.487
3.470
3.469
3.452
3.451
3.418
3.415
3.414
3.407
3.403
3.400
3.399
3.396
3.395
3.394
3.394
3.388
3.387
3.387
3.386
3.384
3.383
3.350
3.350
3.349
3.349
3.310
3.312
3.311
3.311
3.254
3.252
3.234
3.233
3.216
3.215
OH
O
HO
HO
OH
S
OMe
48
1.71
1.66
2.3
1
1.45
2.73
1.21
1.06
1.18
1.22
10
9
8
7
6
5
4
3
2
1
0

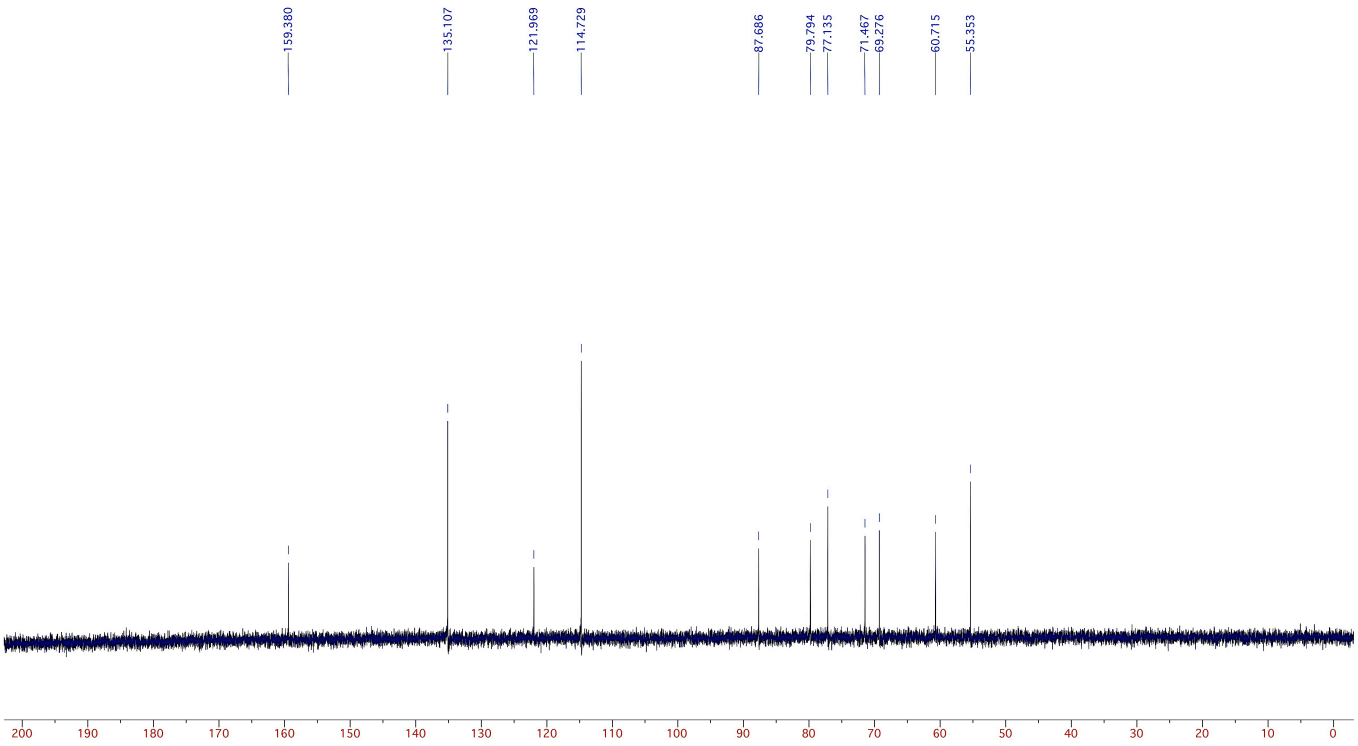
159.380
135.107
121.969
114.729
87.686
79.794
77.135
71.467
69.276
60.715
55.353
200
190
180
170
160
150
140
130
120
110
100
90
80
70
60
50
40
30
20
10
0

OAc
AcO
AcO
OAc
O
O
OMe

49a

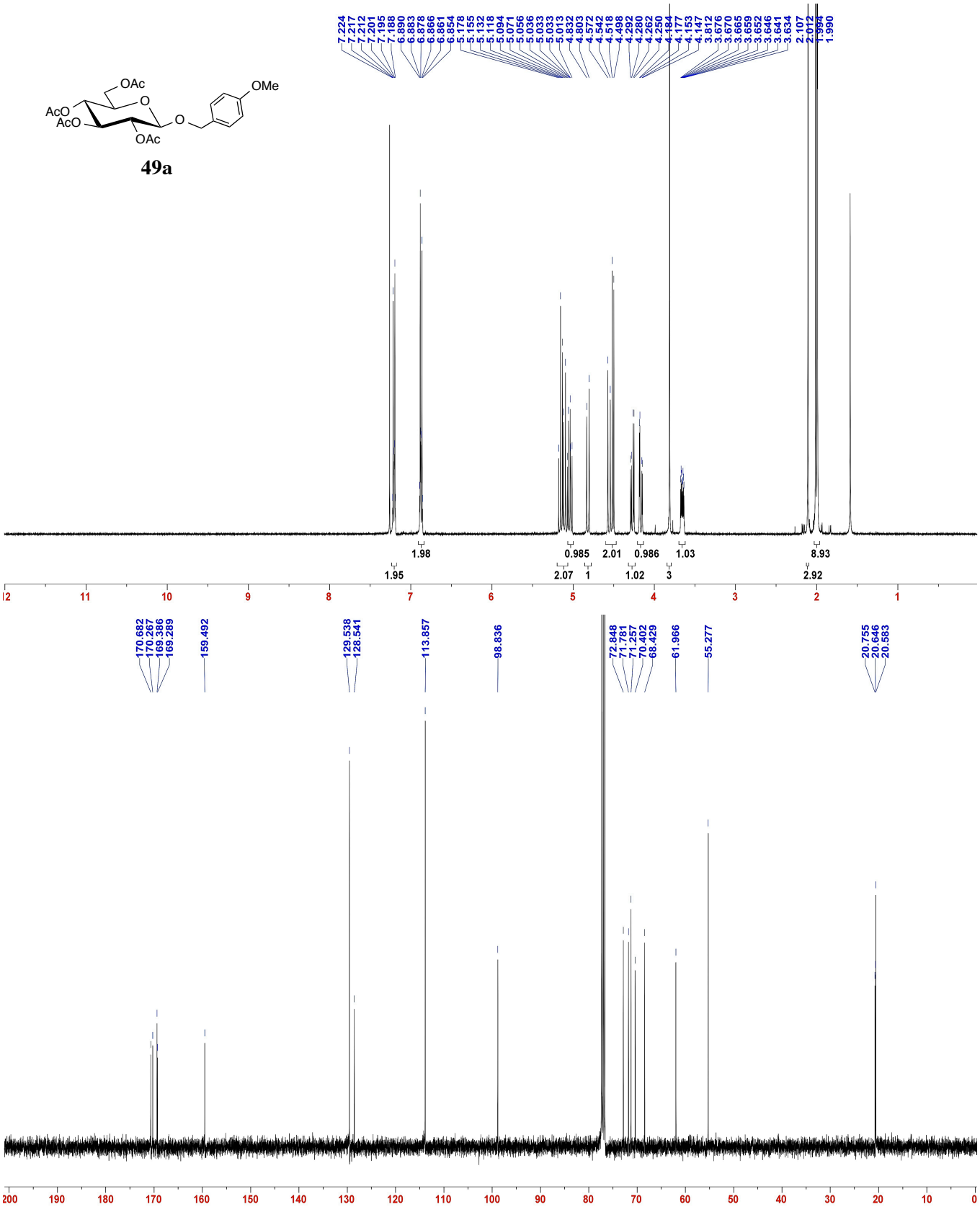
7.224
7.217
7.212
7.201
7.195
7.188
6.890
6.883
6.878
6.866
6.861
6.854
5.178
5.155
5.132
5.118
5.094
5.071
5.056
5.036
5.033
5.013
4.832
4.803
4.572
4.542
4.518
4.498
4.292
4.260
4.252
4.184
4.177
4.153
4.147
3.812
3.676
3.670
3.665
3.659
3.652
3.646
3.641
3.634
2.107
2.012
1.998
1.990
1.98
0.985
2.01
0.986
1.03
8.93
1.95
2.07
1
1.02
3
2.92
170.682
170.267
169.386
169.289
159.492
129.538
128.541
113.857
98.836
72.848
71.781
71.257
70.402
68.429
61.966
55.277
20.755
20.646
20.583

OH
O
HO
HO
O
OMe
OH

49

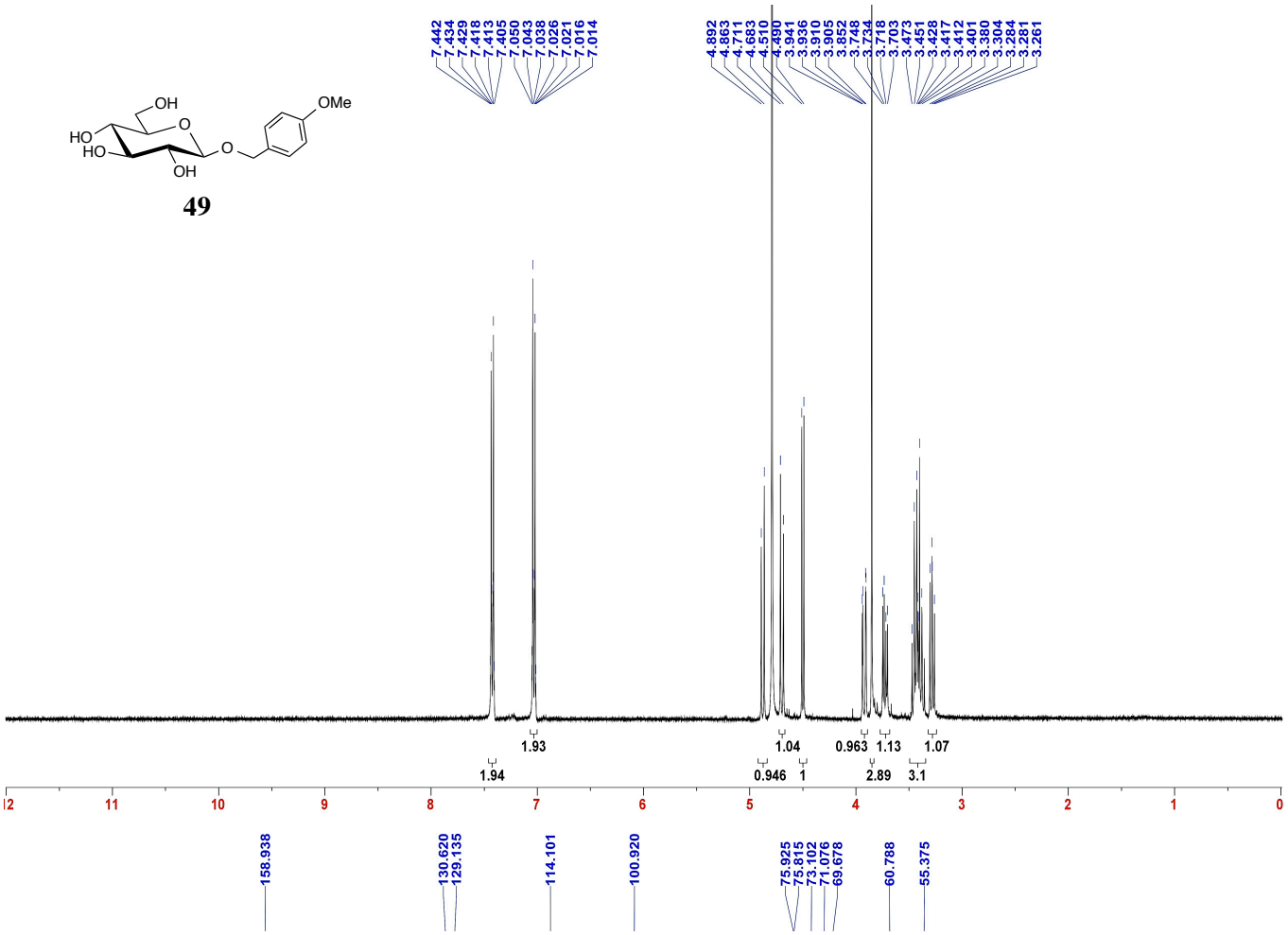
7.442
7.434
7.429
7.418
7.413
7.405
7.050
7.043
7.038
7.026
7.021
7.016
7.014
4.892
4.863
4.711
4.683
4.510
4.490
3.941
3.936
3.910
3.905
3.852
3.748
3.734
3.718
3.703
3.473
3.451
3.428
3.417
3.412
3.401
3.380
3.304
3.284
3.261
3.261
1.93
1.04
0.963
1.13
1.07
1.94
0.946
1
2.89
3.1
12
11
10
9
8
7
6
5
4
3
2
1
0

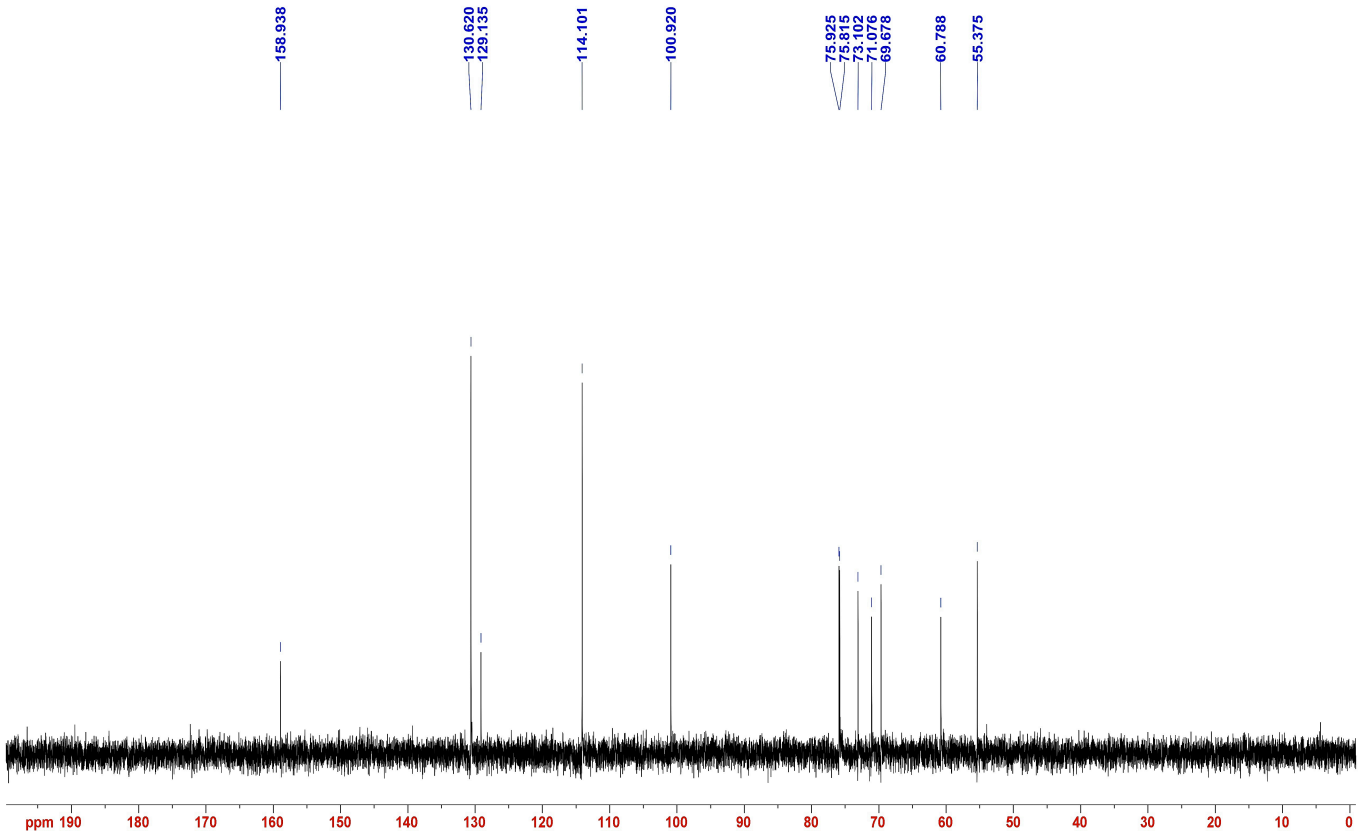
158.938
130.620
129.135
114.101
100.920
75.925
75.815
73.102
71.076
69.678
60.788
55.375
ppm 190
180
170
160
150
140
130
120
110
100
90
80
70
60
50
40
30
20
10
0

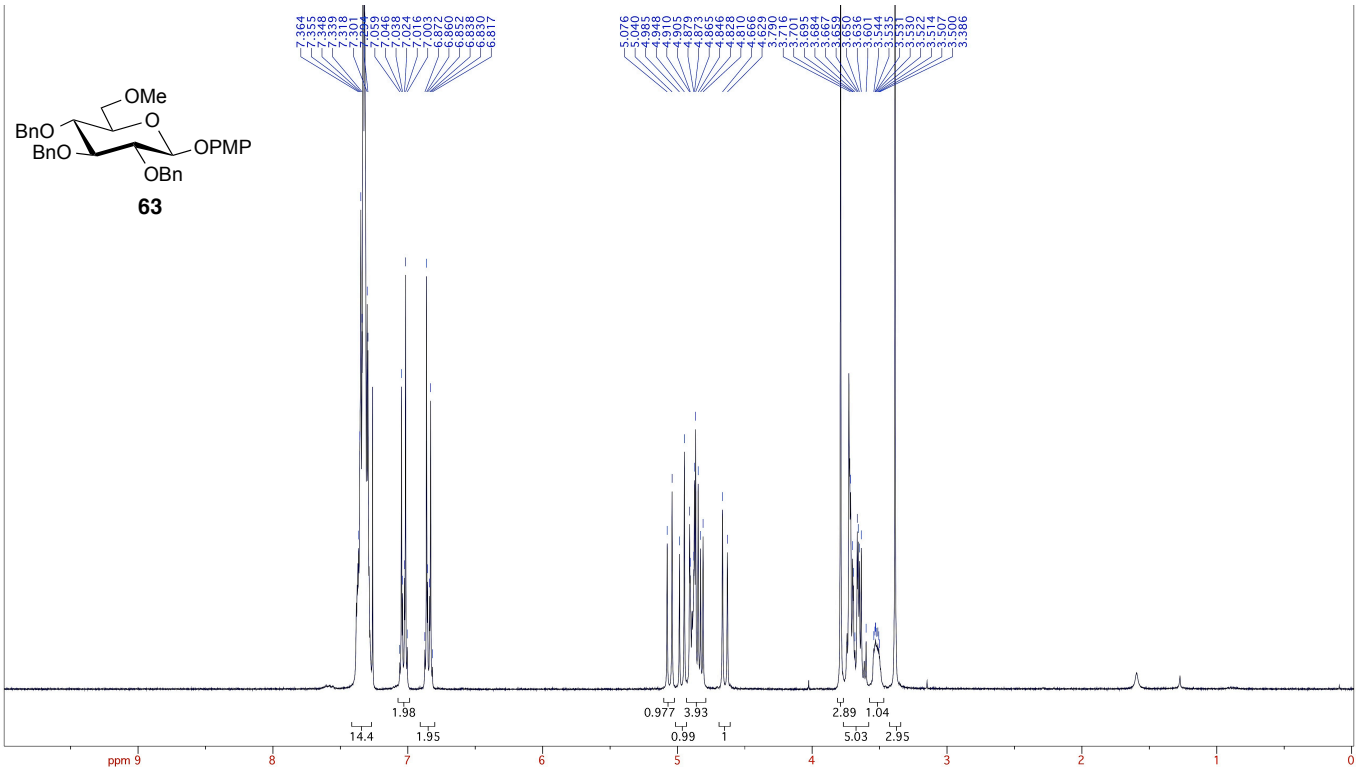
OMe
O
BnO
BnO
OPMP
OBn
63
7.364
7.357
7.348
7.339
7.318
7.301
7.294
7.059
7.046
7.028
7.024
7.016
7.003
6.872
6.867
6.852
6.838
6.830
6.817
5.076
5.040
5.035
4.948
4.910
4.905
4.879
4.873
4.865
4.846
4.828
4.810
4.666
4.629
4.590
3.716
3.701
3.695
3.684
3.667
3.659
3.650
3.636
3.601
3.544
3.535
3.531
3.530
3.522
3.514
3.507
3.500
3.386
1.98
0.977
3.93
2.89
1.04
14.4
1.95
0.99
1
5.03
2.95
ppm 9
8
7
6
5
4
3
2
1
0

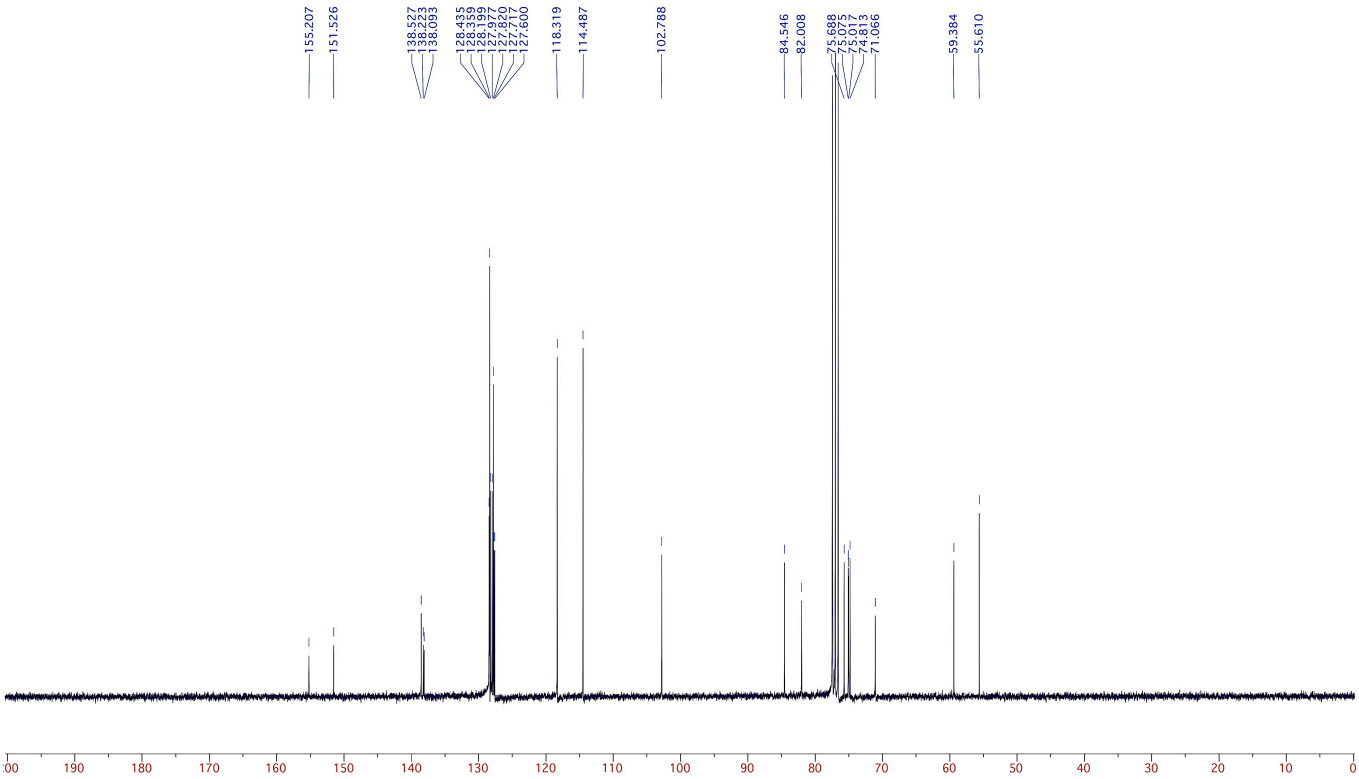
155.207
151.526
138.527
138.243
138.093
128.435
128.359
128.179
128.077
127.820
127.717
127.600
118.319
114.487
102.788
84.546
82.008
75.688
75.057
75.017
74.813
71.066
59.384
55.610
190
180
170
160
150
140
130
120
110
100
90
80
70
60
50
40
30
20
10
0

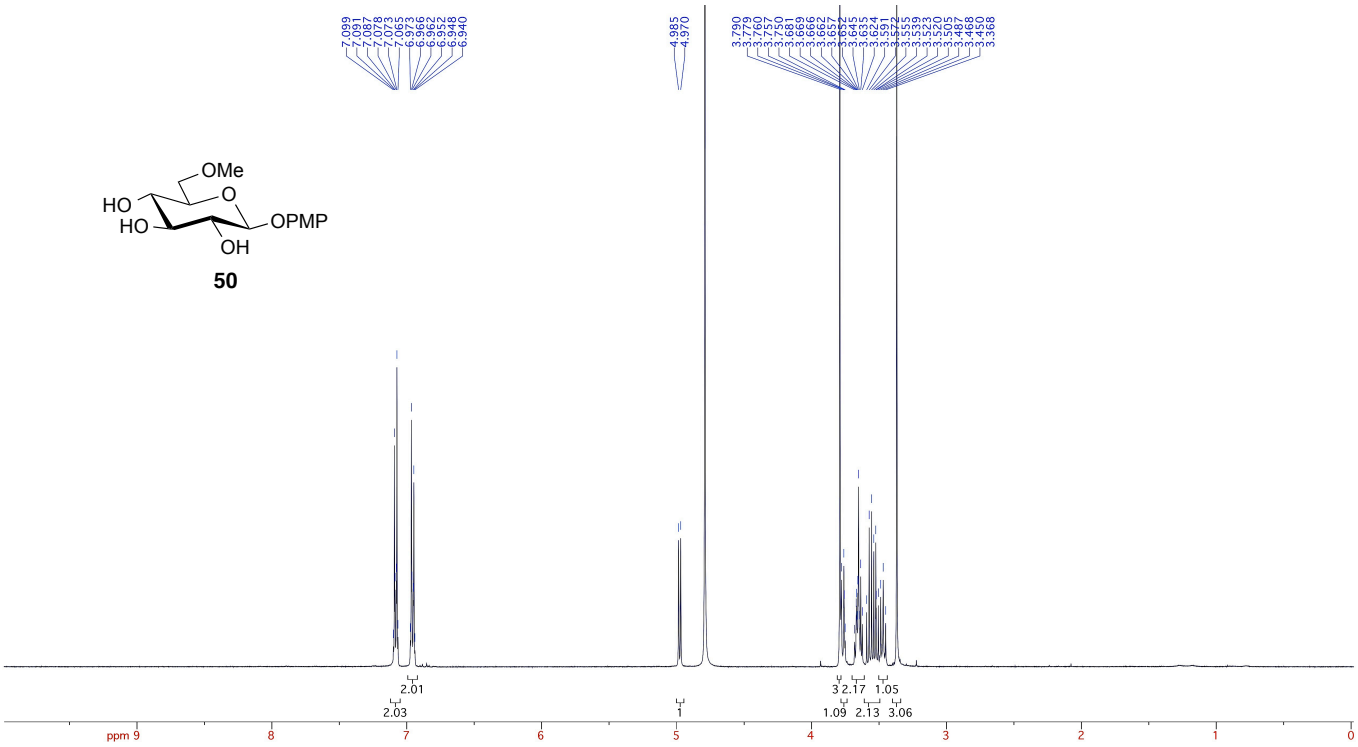
7.099
7.091
7.087
7.078
7.073
7.065
6.963
6.962
6.952
6.948
6.940
4.985
4.970
3.790
3.779
3.760
3.757
3.750
3.681
3.669
3.666
3.662
3.657
3.647
3.645
3.635
3.624
3.621
3.572
3.555
3.539
3.533
3.523
3.520
3.505
3.487
3.468
3.450
3.368
2.01
2.03
1
3
2.17
1.05
1.09
2.13
3.06
ppm 9
8
7
6
5
4
3
2
1
0

OMe
O
HO
HO
OPMP
OH

50

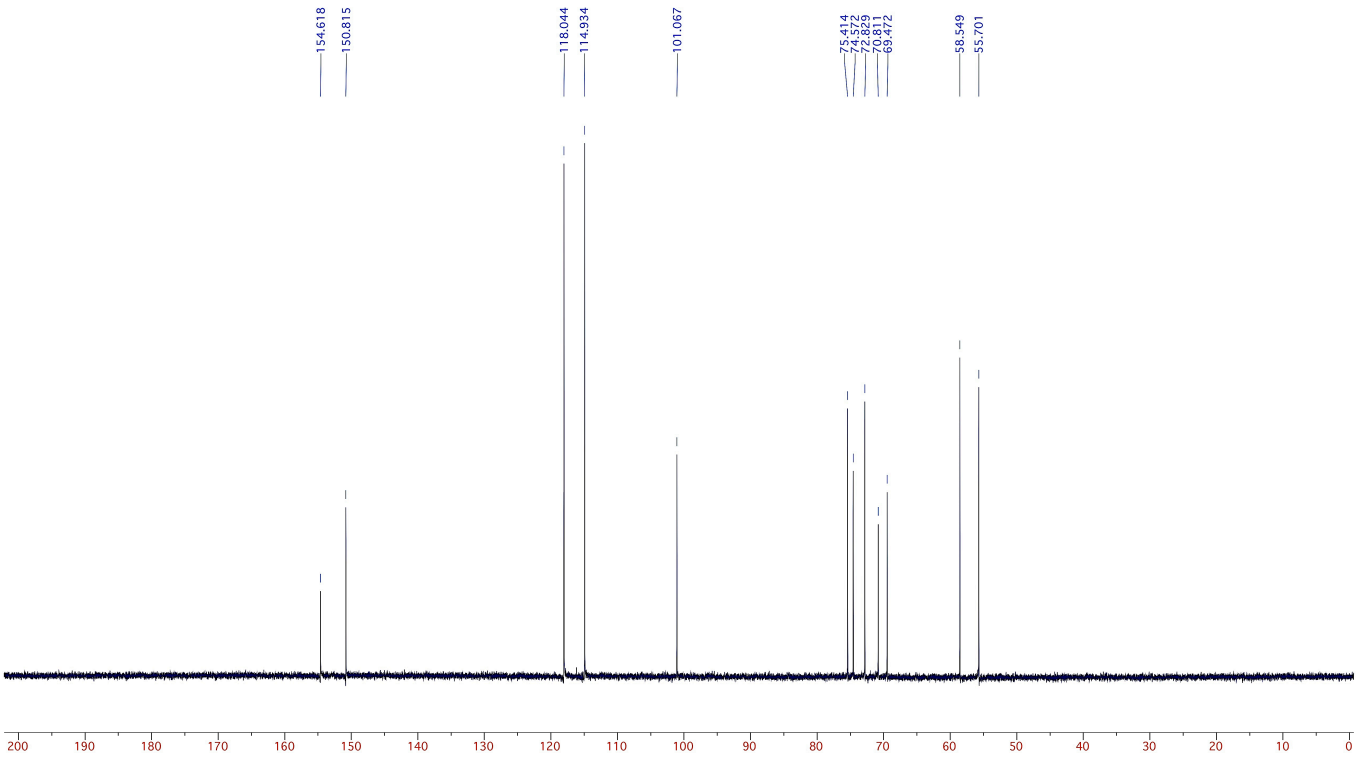
154.618
150.815
118.044
114.934
101.067
76.414
74.572
72.829
70.811
69.472
58.549
55.701
200
190
180
170
160
150
140
130
120
110
100
90
80
70
60
50
40
30
20
10
0

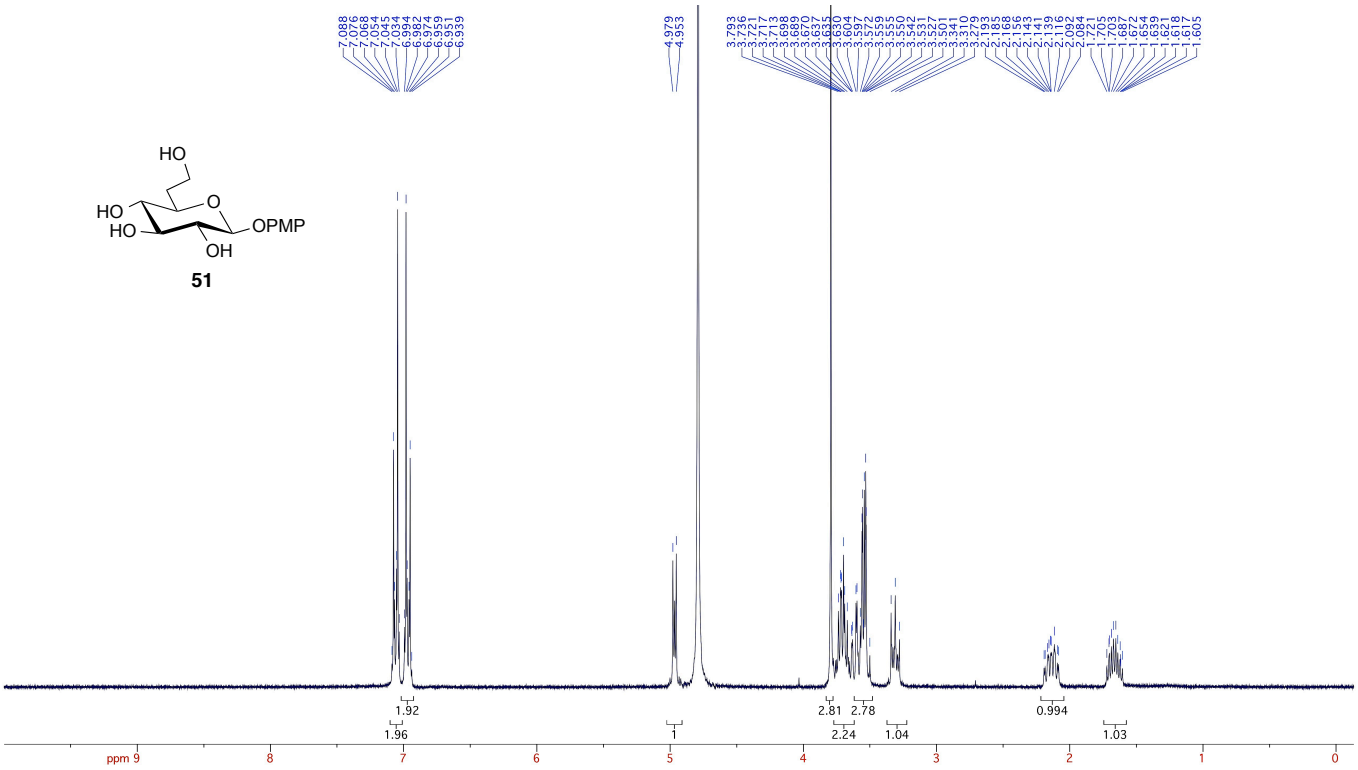
HO
HO
HO
O
OPMP
OH
51
7.088
7.076
7.068
7.054
7.045
7.034
6.982
6.974
6.959
6.951
6.939
4.979
4.953
3.793
3.736
3.721
3.717
3.713
3.698
3.689
3.670
3.637
3.630
3.604
3.597
3.572
3.559
3.555
3.550
3.542
3.531
3.527
3.501
3.341
3.310
3.279
2.193
2.185
2.168
2.156
2.143
2.141
2.139
2.116
2.092
2.084
1.721
1.705
1.703
1.687
1.672
1.654
1.639
1.627
1.618
1.617
1.605
1.92
1.96
1
2.81
2.78
2.24
1.04
0.994
1.03
ppm 9
8
7
6
5
4
3
2
1
0

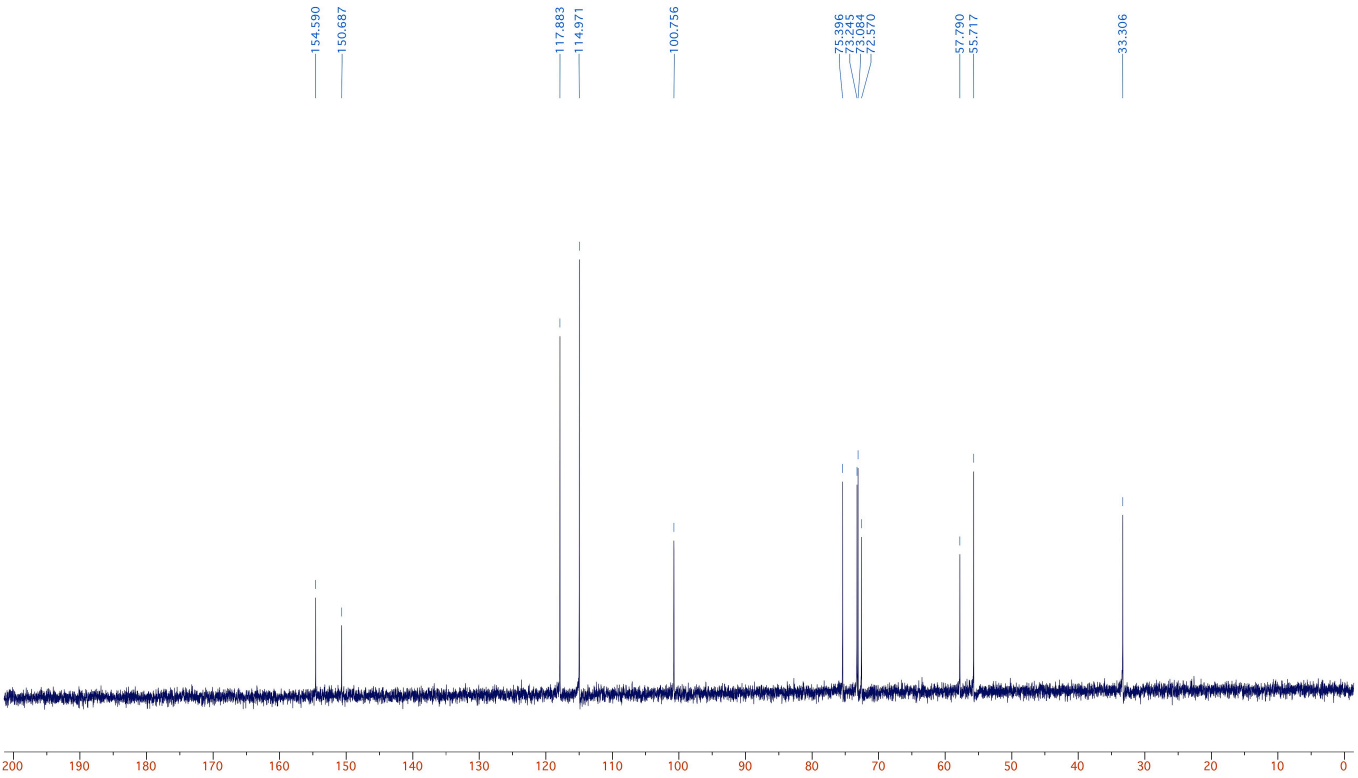
154.590
150.687
117.883
114.971
100.756
75.396
73.245
73.084
72.570
57.790
55.717
33.306
200
190
180
170
160
150
140
130
120
110
100
90
80
70
60
50
40
30
20
10
0

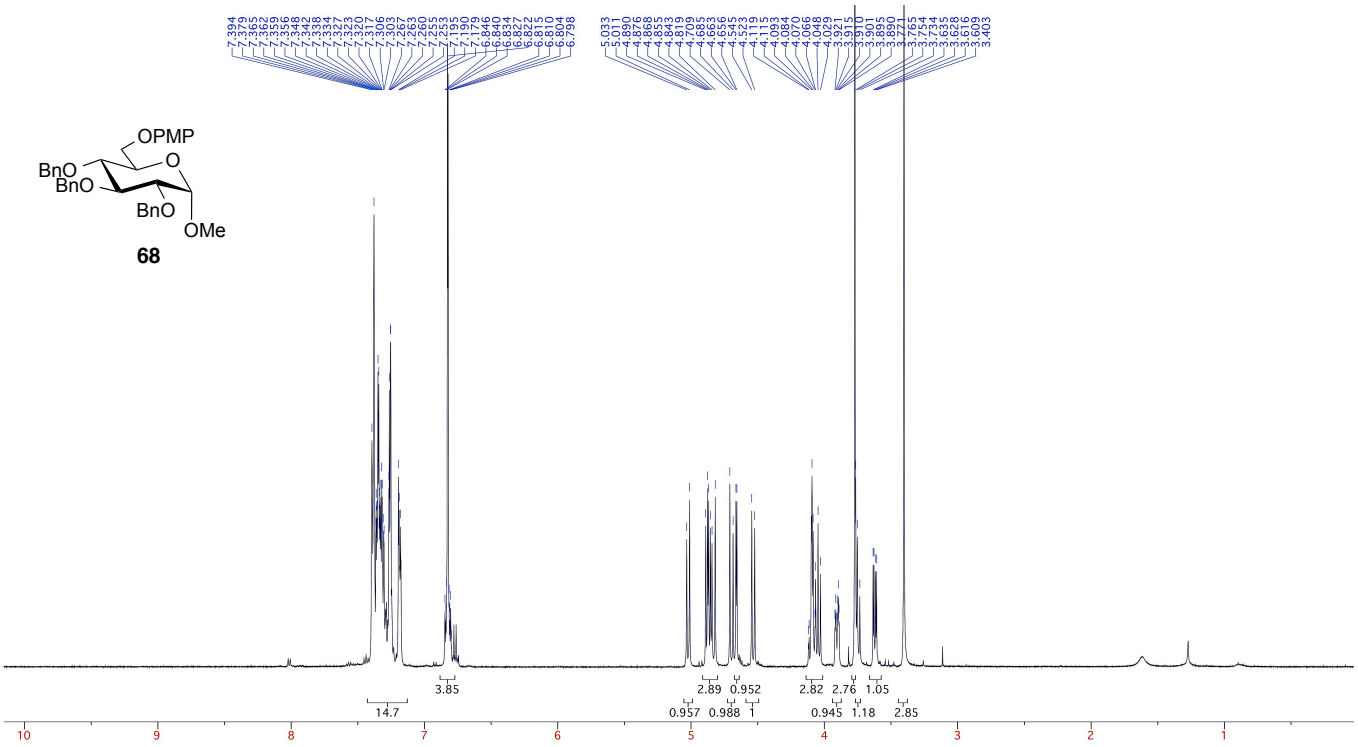
OPMP
BnO
BnO
BnO
OMe
68

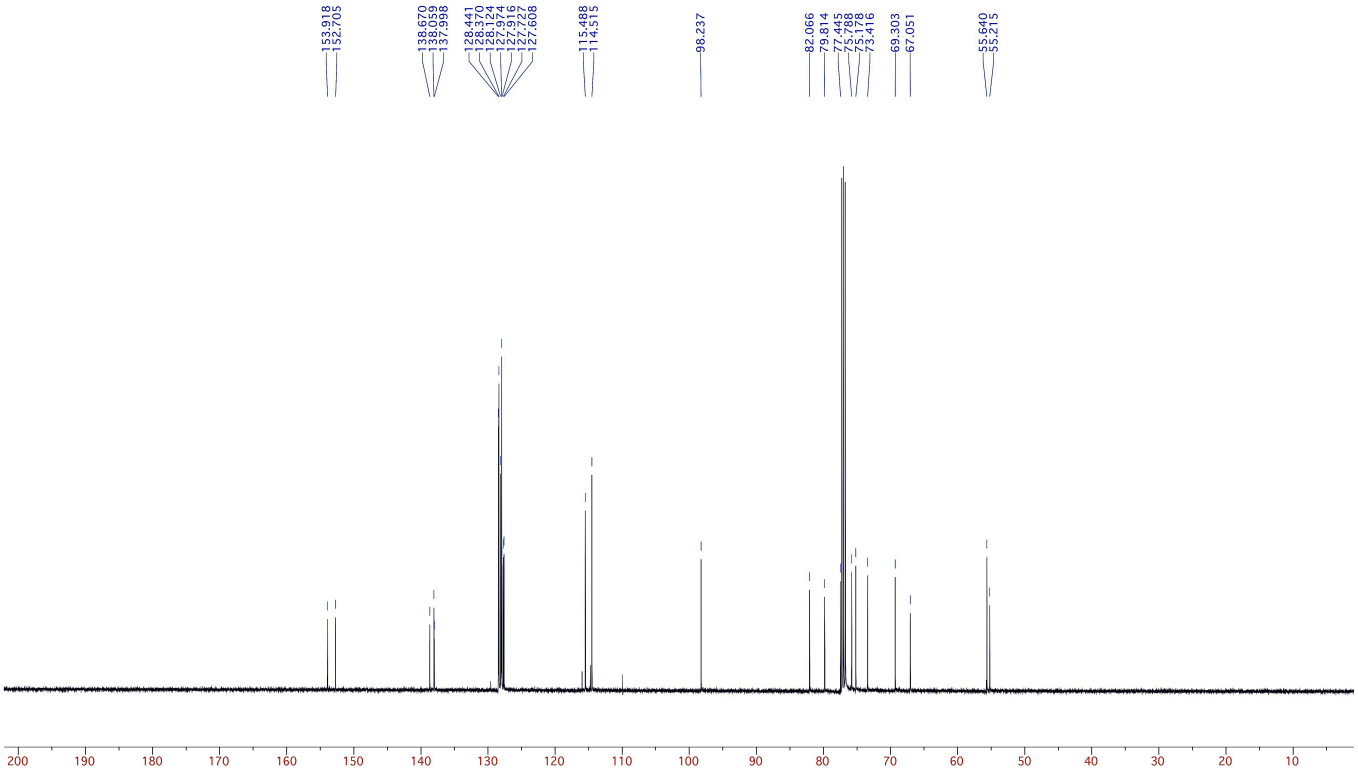

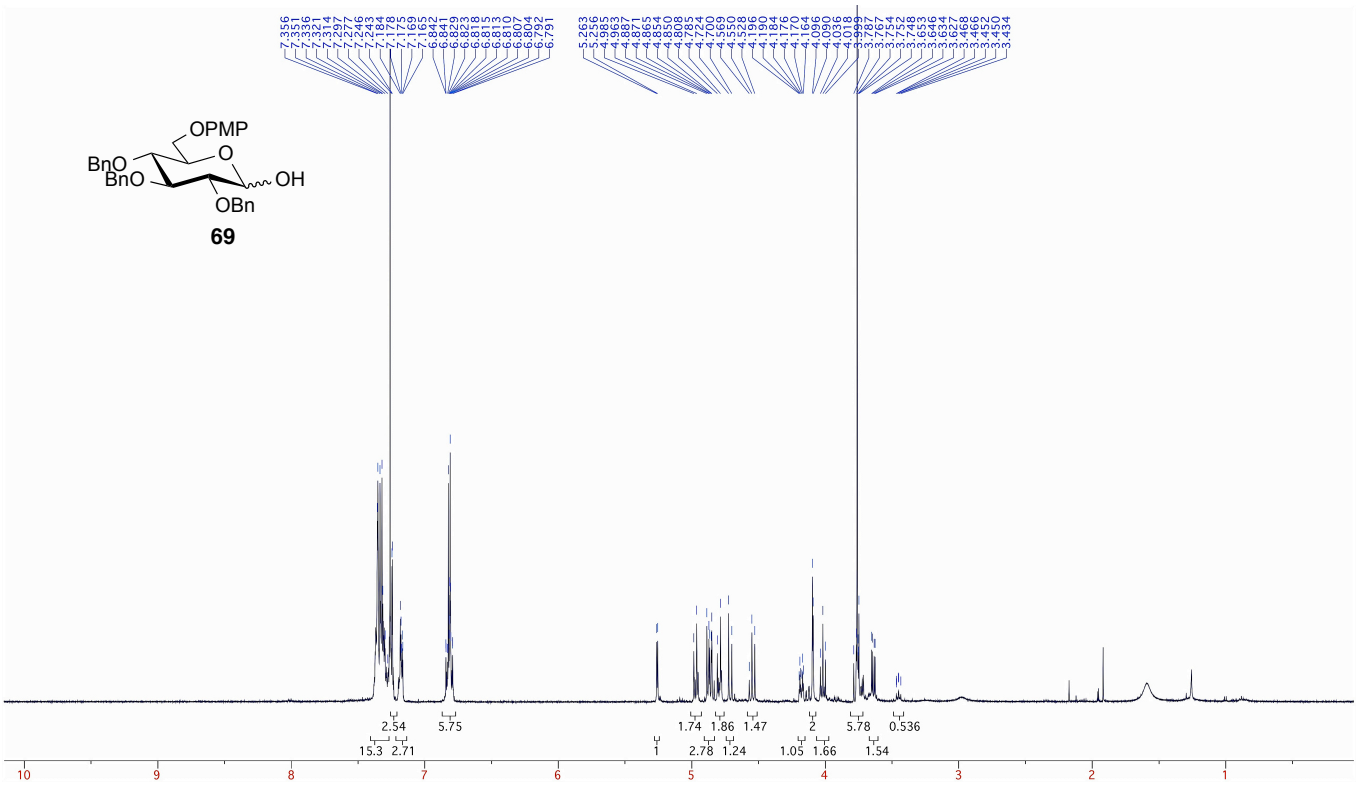
OPMP
O
BnO
BnO
OH
OBn
69

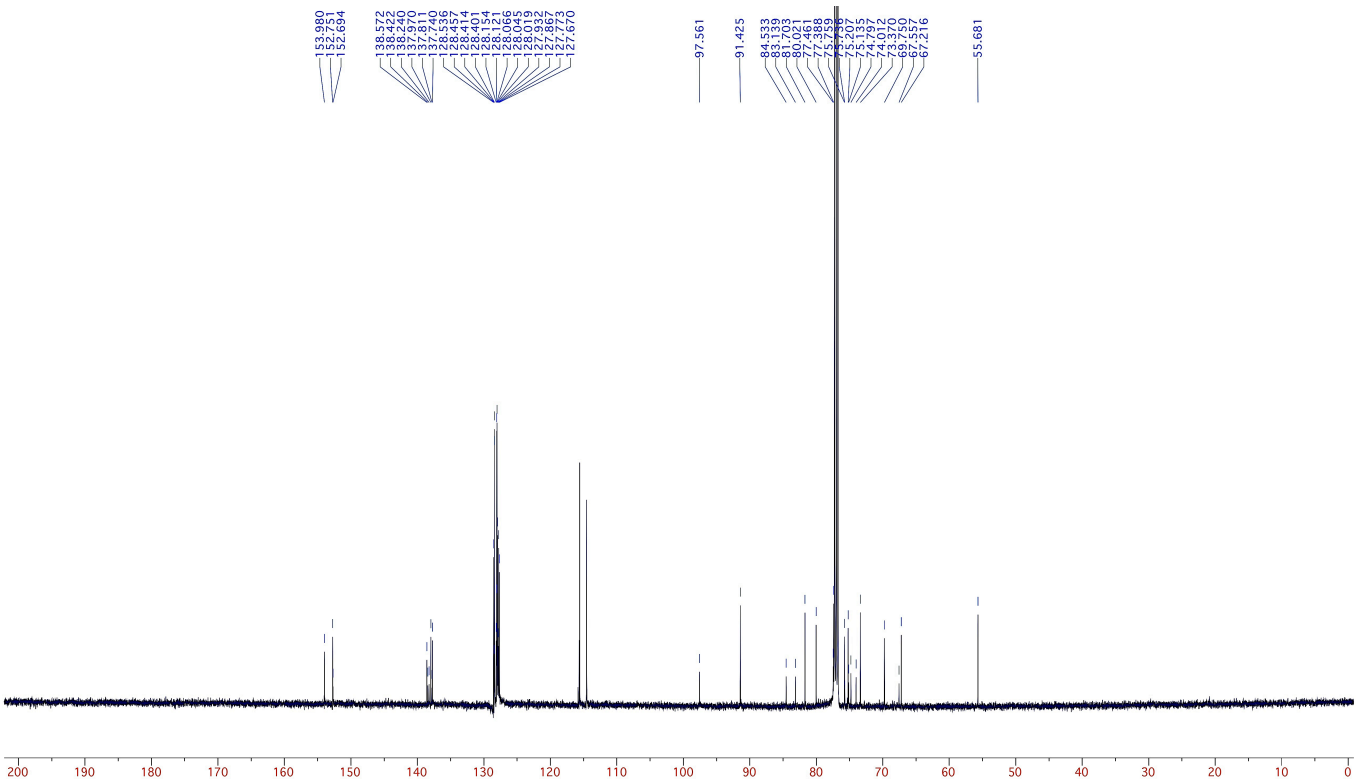

OPMP
O
HO
HO
OH
OH

52

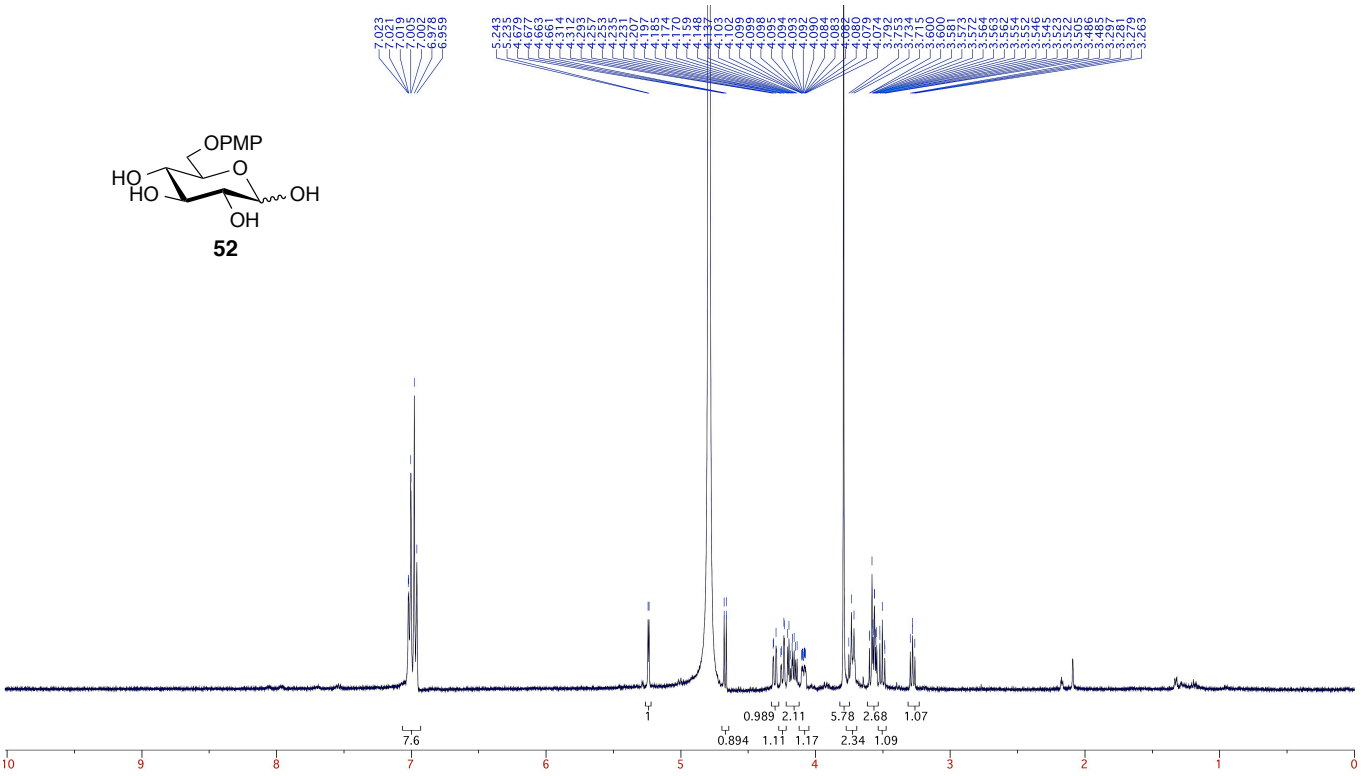
7.023
7.021
7.019
7.005
7.002
6.978
6.959
5.243
5.235
4.679
4.677
4.663
4.661
4.314
4.312
4.293
4.257
4.253
4.235
4.231
4.207
4.197
4.185
4.174
4.170
4.159
4.148
4.132
4.103
4.102
4.099
4.099
4.098
4.095
4.094
4.093
4.092
4.090
4.084
4.083
4.082
4.080
4.079
4.074
3.792
3.793
3.734
3.715
3.600
3.601
3.581
3.573
3.572
3.564
3.563
3.562
3.554
3.552
3.546
3.545
3.523
3.522
3.505
3.486
3.485
3.297
3.281
3.279
3.263
1
0.989
2.11
5.78
2.68
1.07
7.6
0.894
1.11
1.17
2.34
1.09
10
9
8
7
6
5
4
3
2
1
0

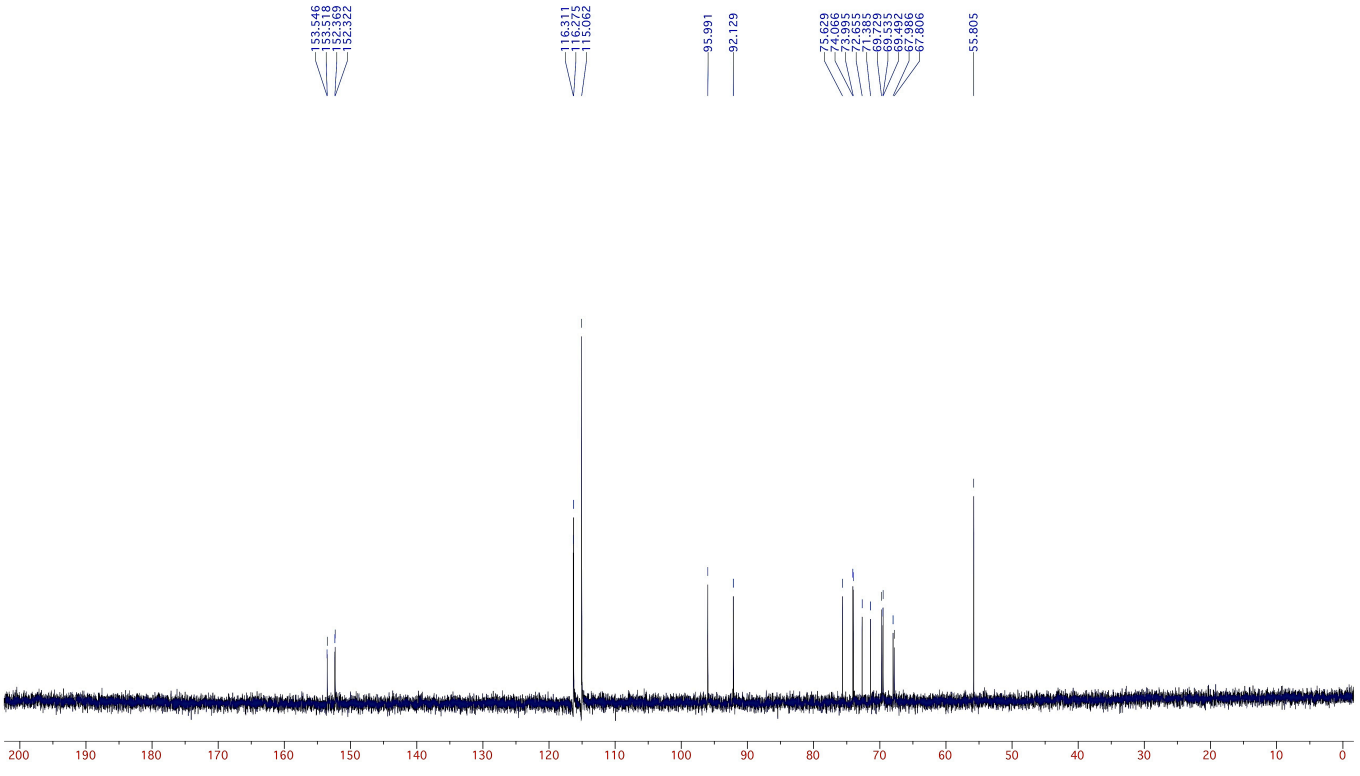
153.546
153.518
153.368
153.339
152.322
116.311
116.275
115.062
95.991
92.129
75.629
74.066
73.955
72.665
71.385
69.729
69.535
69.432
67.986
67.806
55.805
200
190
180
170
160
150
140
130
120
110
100
90
80
70
60
50
40
30
20
10
0

79

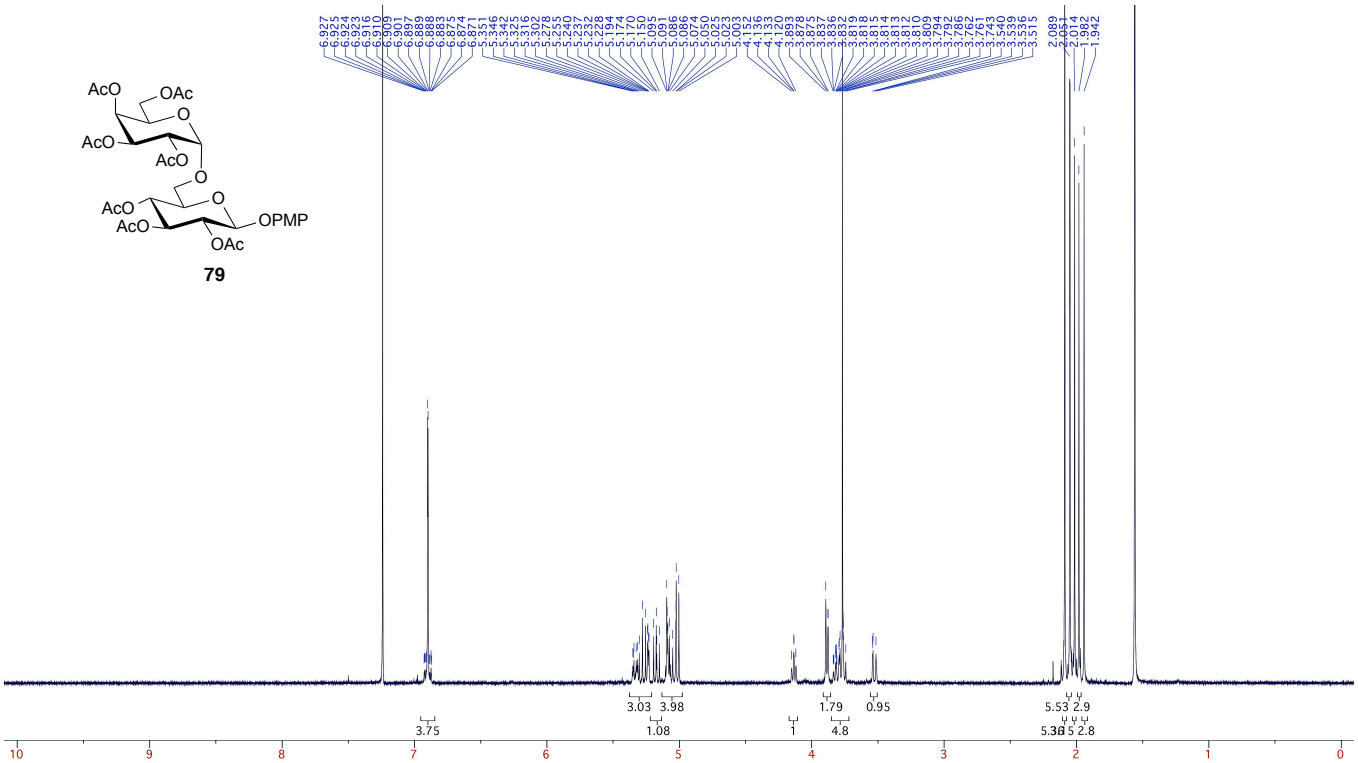

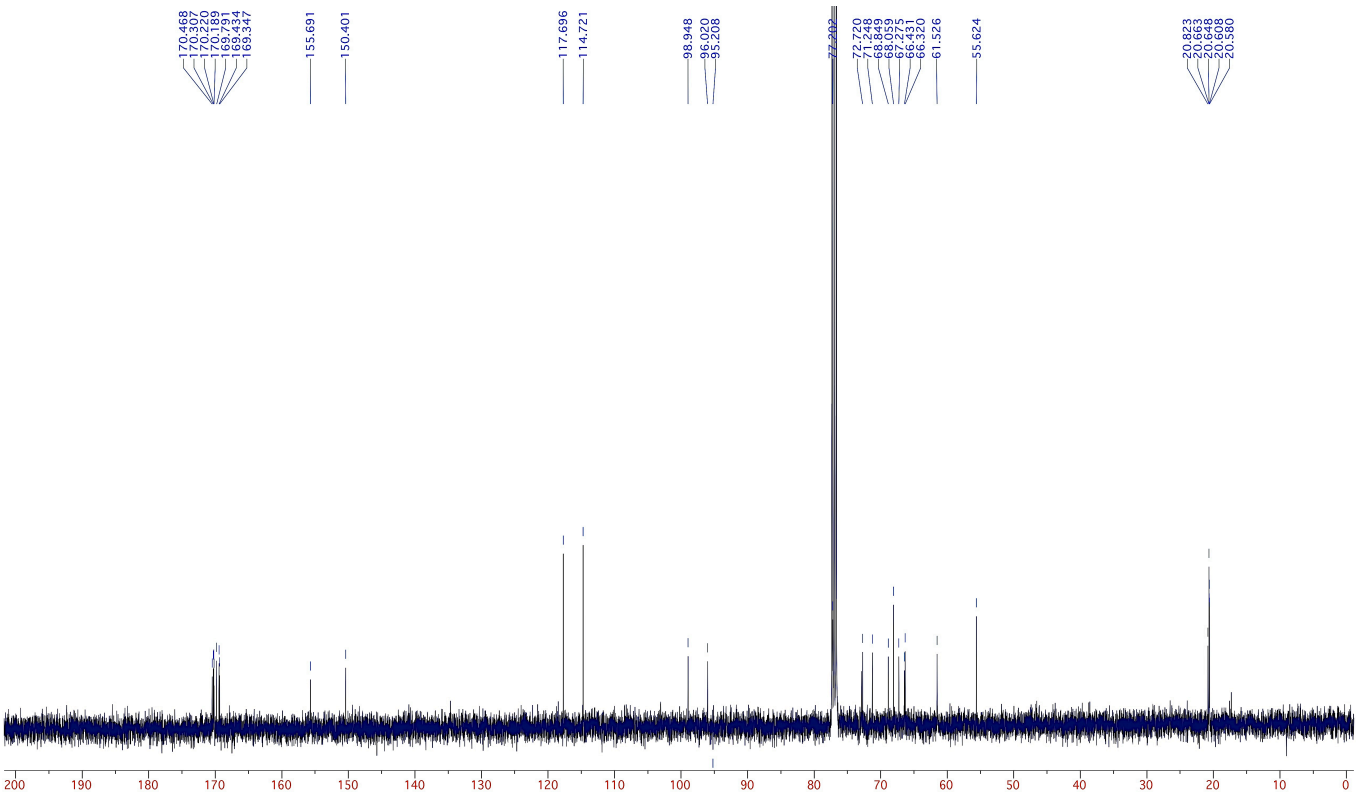

70

β-PMP-Melibiose

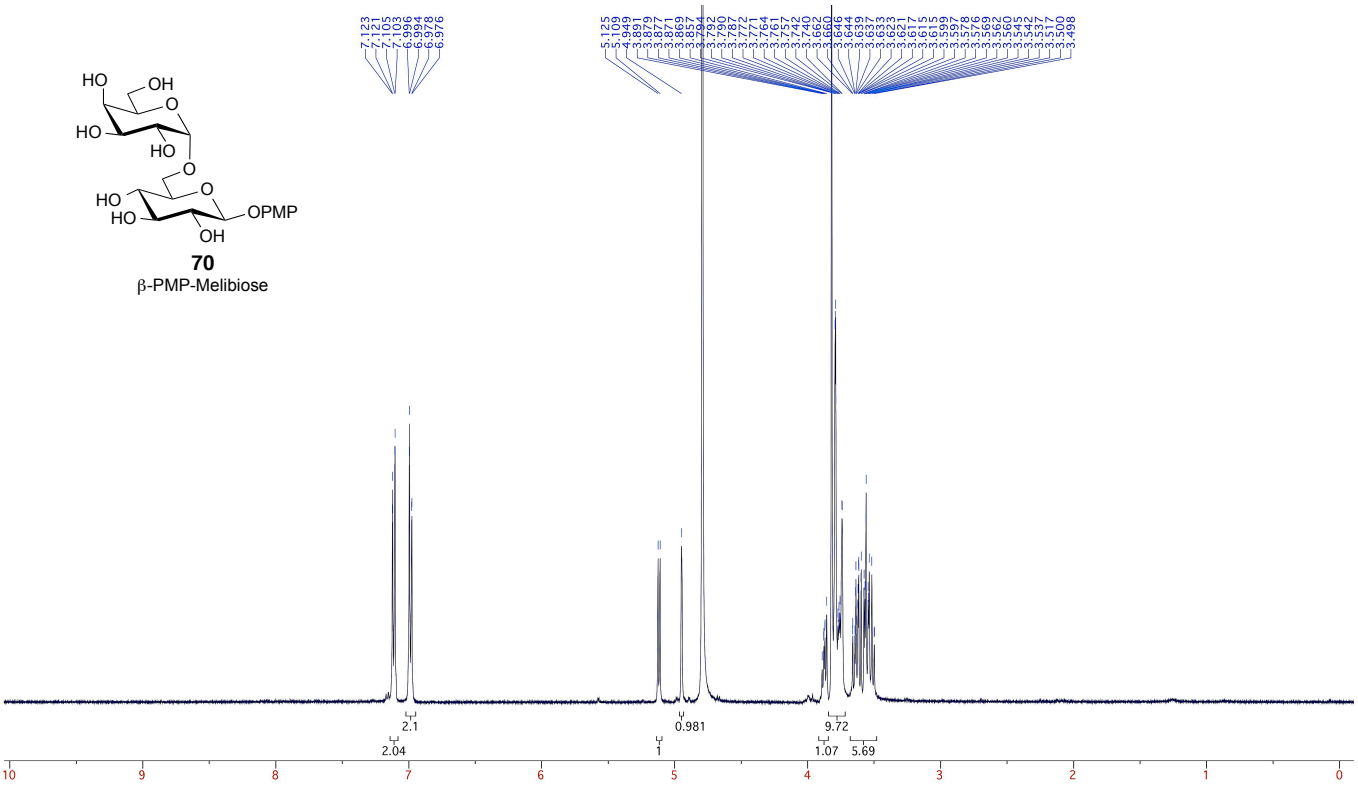

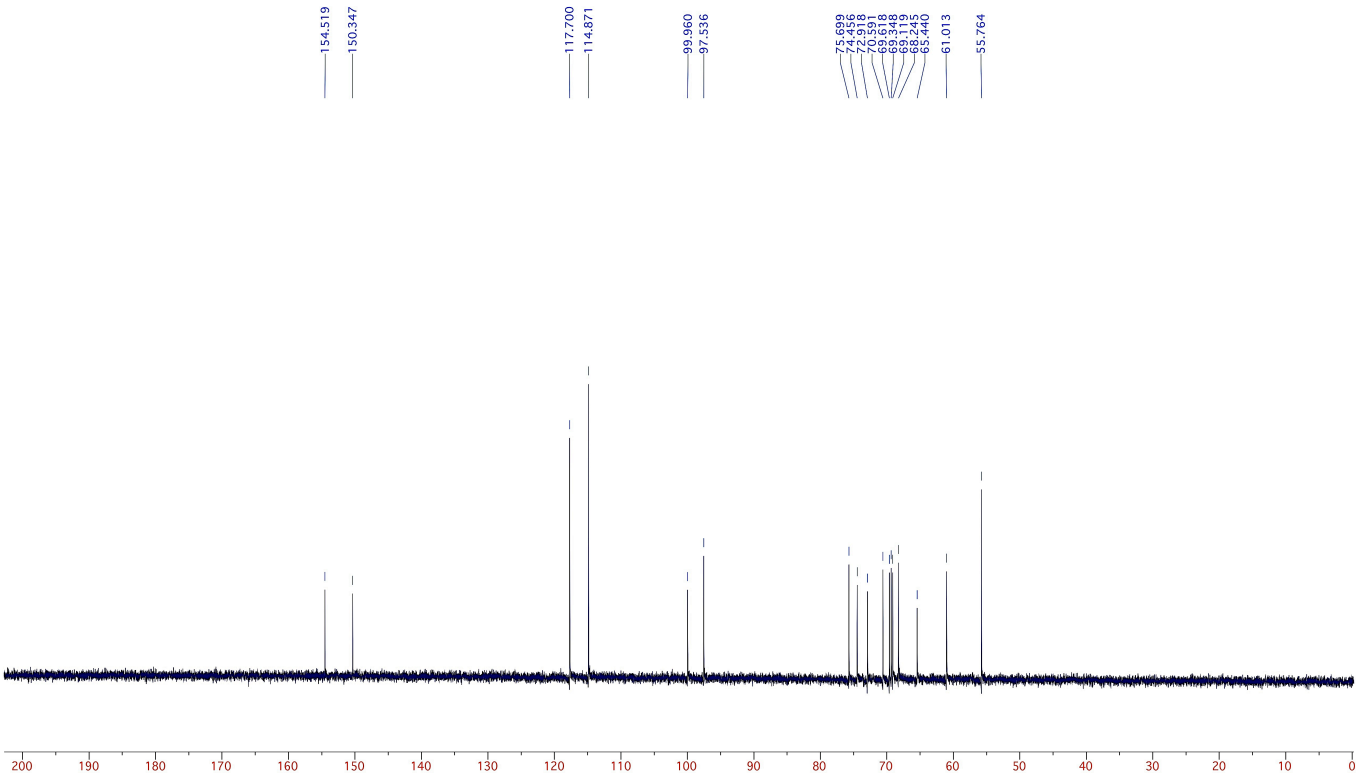

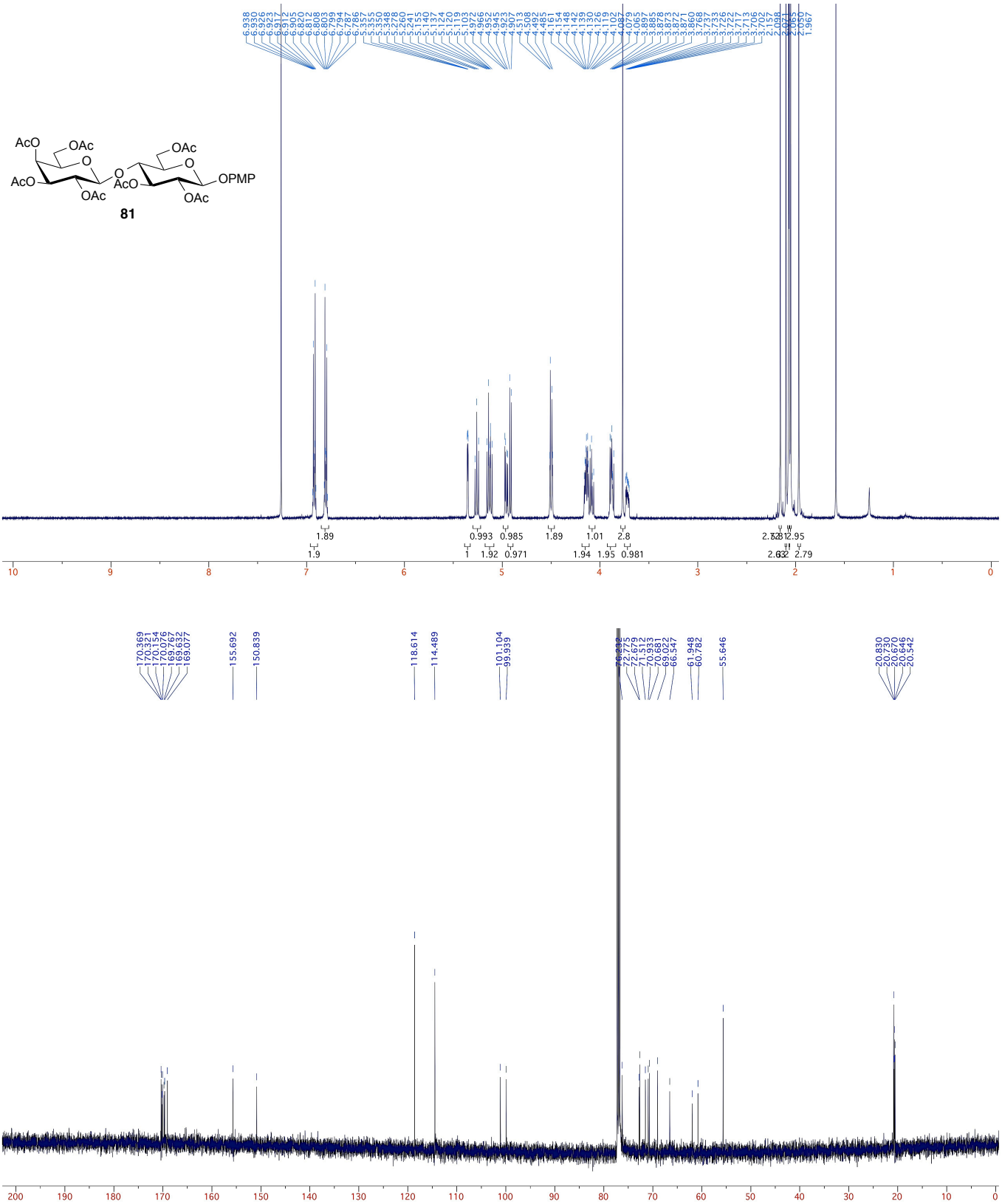
AcO
OAc
O
AcO
OAc
O
AcO
OAc
O
OPMP
OAc
OAc
81

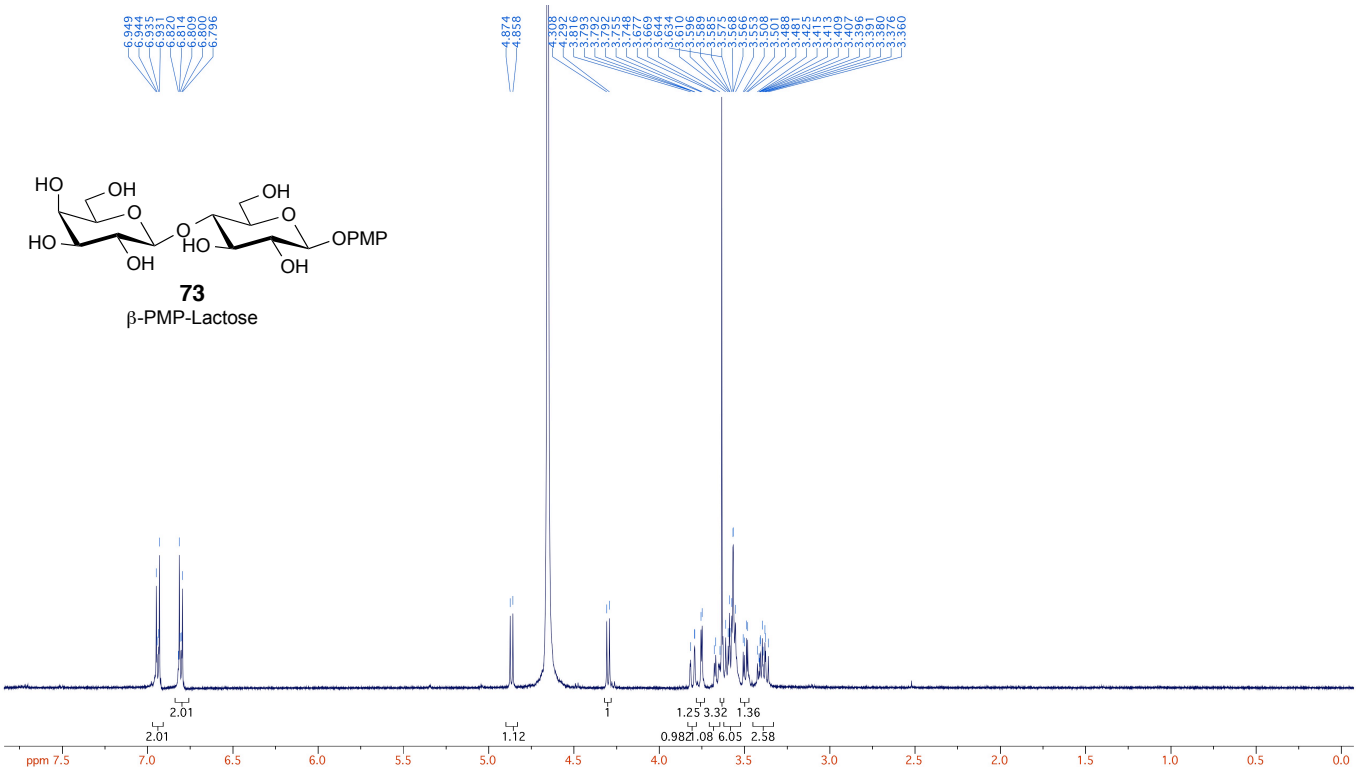
6.949
6.944
6.935
6.931
6.820
6.814
6.809
6.800
6.796
4.874
4.858
4.308
4.292
4.281
4.276
3.793
3.792
3.752
3.751
3.748
3.677
3.669
3.644
3.634
3.610
3.586
3.585
3.585
3.575
3.568
3.566
3.553
3.508
3.501
3.488
3.481
3.425
3.415
3.413
3.409
3.407
3.396
3.391
3.380
3.376
3.360
HO
OH
O
O
HO
OH
OH
O
HO
OPMP
OH
73
β-PMP-Lactose
2.01
2.01
1.12
1
1.25
3.32
1.36
0.982
1.08
6.05
2.58
ppm 7.5
7.0
6.5
6.0
5.5
5.0
4.5
4.0
3.5
3.0
2.5
2.0
1.5
1.0
0.5
0.0

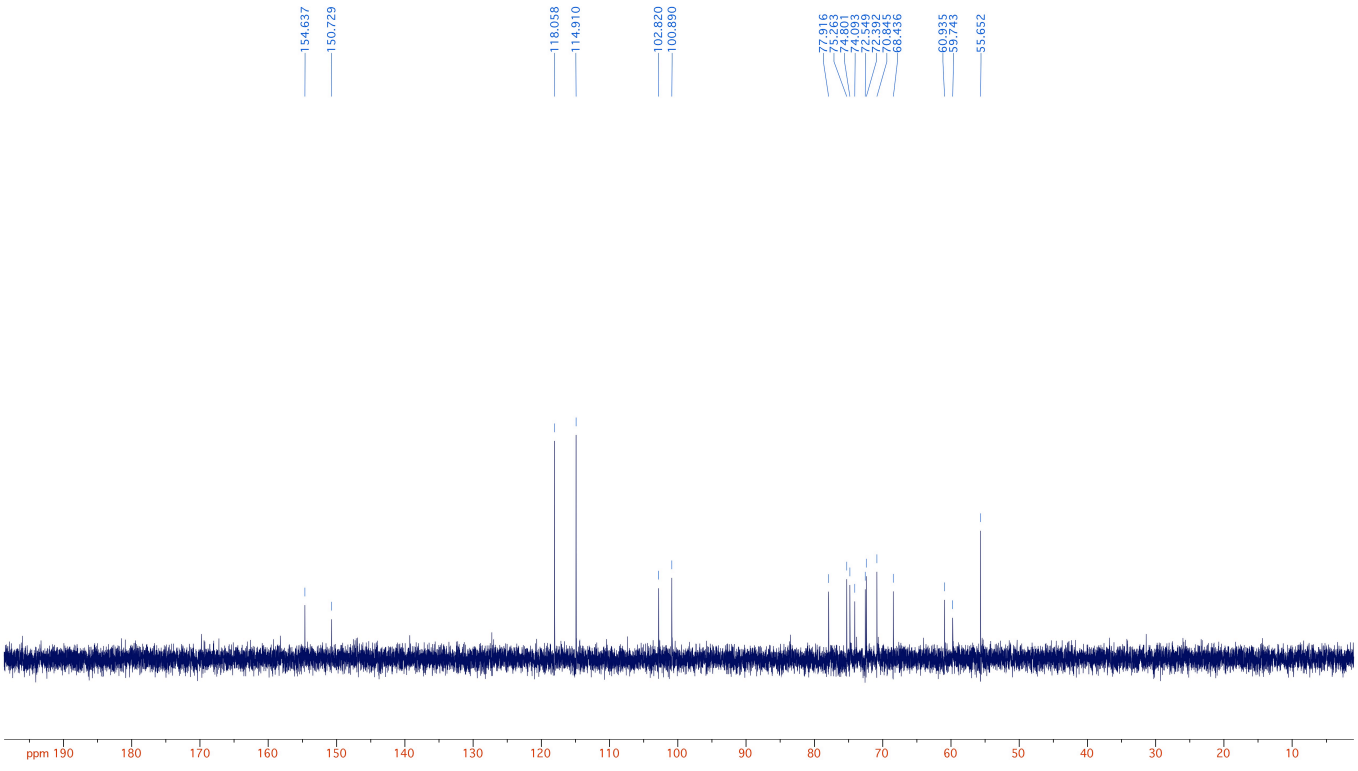
154.637
150.729
118.058
114.910
102.820
100.890
77.916
75.263
75.201
74.003
72.549
72.392
70.845
68.456
60.935
55.743
55.652
ppm 190
180
170
160
150
140
130
120
110
100
90
80
70
60
50
40
30
20
10

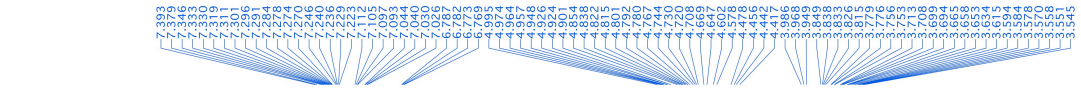

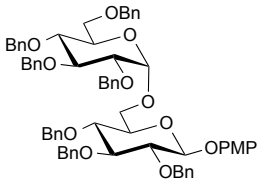
OBn
O
BnO
BnO
BnO
O
O
BnO
BnO
OPMP
OBn

82α

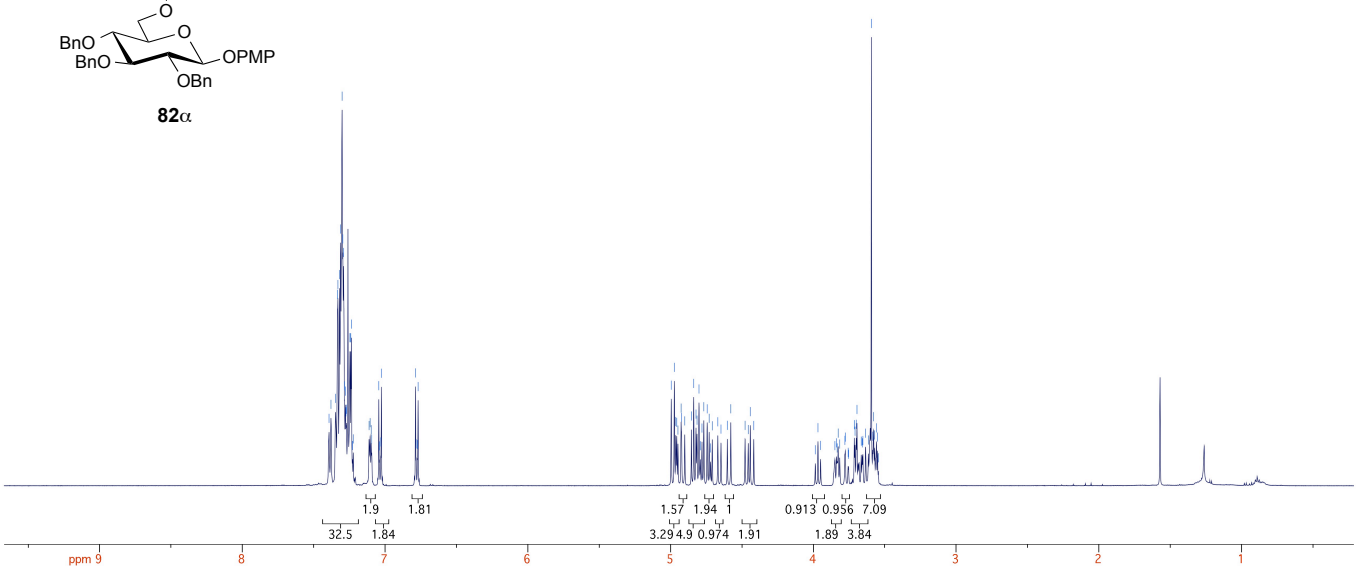
1.9
1.81
1.57
1.94
1
0.913
0.956
7.09
32.5
1.84
3.29
4.9
0.974
1.91
1.89
3.84
ppm 9
8
7
6
5
4
3
2
1

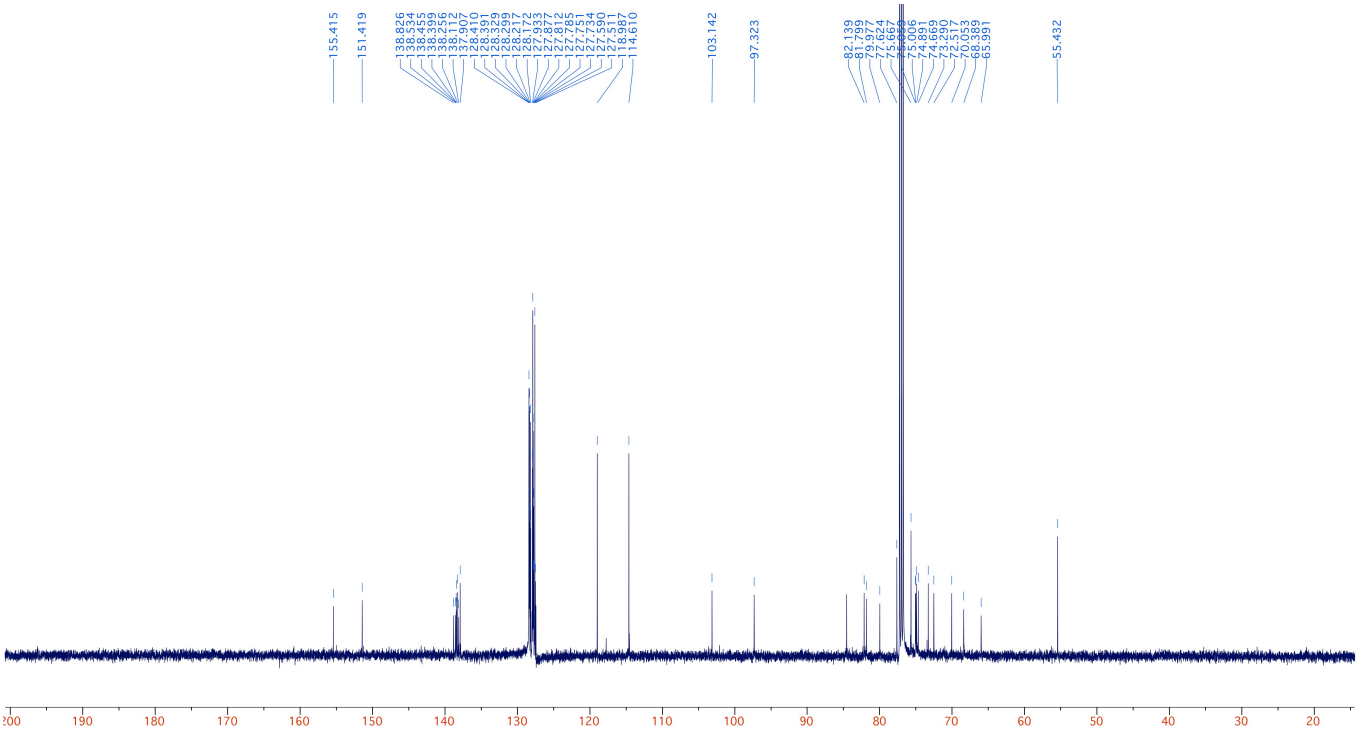
155.415
151.419
103.142
97.323
55.432
200
190
180
170
160
150
140
130
120
110
100
90
80
70
60
50
40
30
20

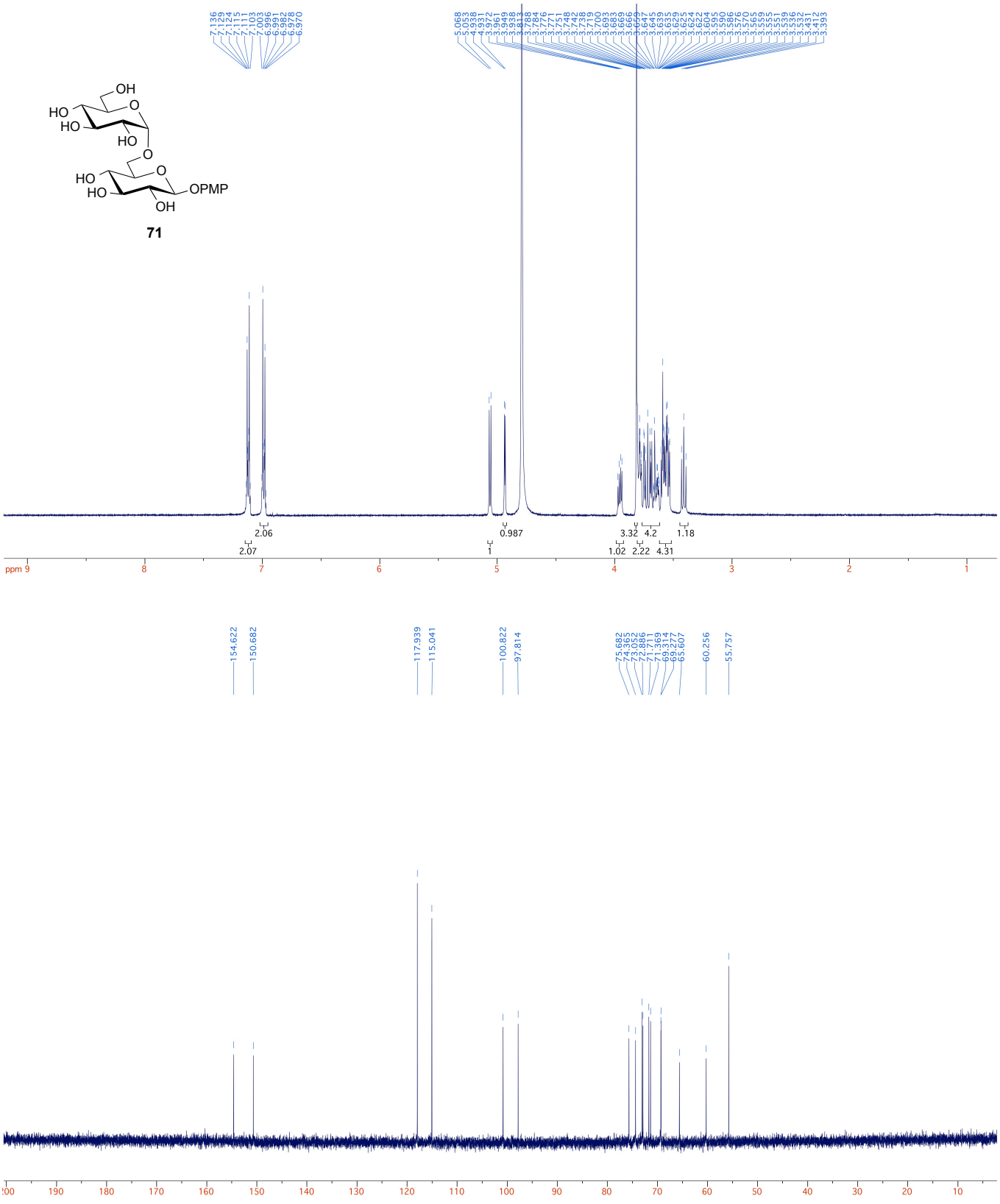
OH
HO
HO
HO
O
O
HO
HO
O
OPMP
OH
71
7.136
7.129
7.124
7.115
7.111
7.103
7.003
6.996
6.991
6.982
6.978
6.970
5.068
5.053
4.938
4.931
3.972
3.961
3.949
3.938
3.813
3.784
3.776
3.771
3.751
3.748
3.742
3.738
3.719
3.700
3.693
3.683
3.666
3.660
3.659
3.647
3.645
3.635
3.629
3.625
3.624
3.622
3.604
3.595
3.590
3.586
3.576
3.570
3.565
3.559
3.555
3.551
3.539
3.536
3.532
3.431
3.412
3.393
2.06
0.987
3.32
4.2
1.18
2.07
1
1.02
2.22
4.31
ppm 9
8
7
6
5
4
3
2
1
154.622
150.682
117.939
115.041
100.822
97.814
75.682
74.365
73.052
72.886
72.791
71.369
69.314
68.277
65.607
60.256
55.757
200
190
180
170
160
150
140
130
120
110
100
90
80
70
60
50
40
30
20
10

OH
HO
HO
O
O
HO
HO
HO
O
OPMP
OH

72

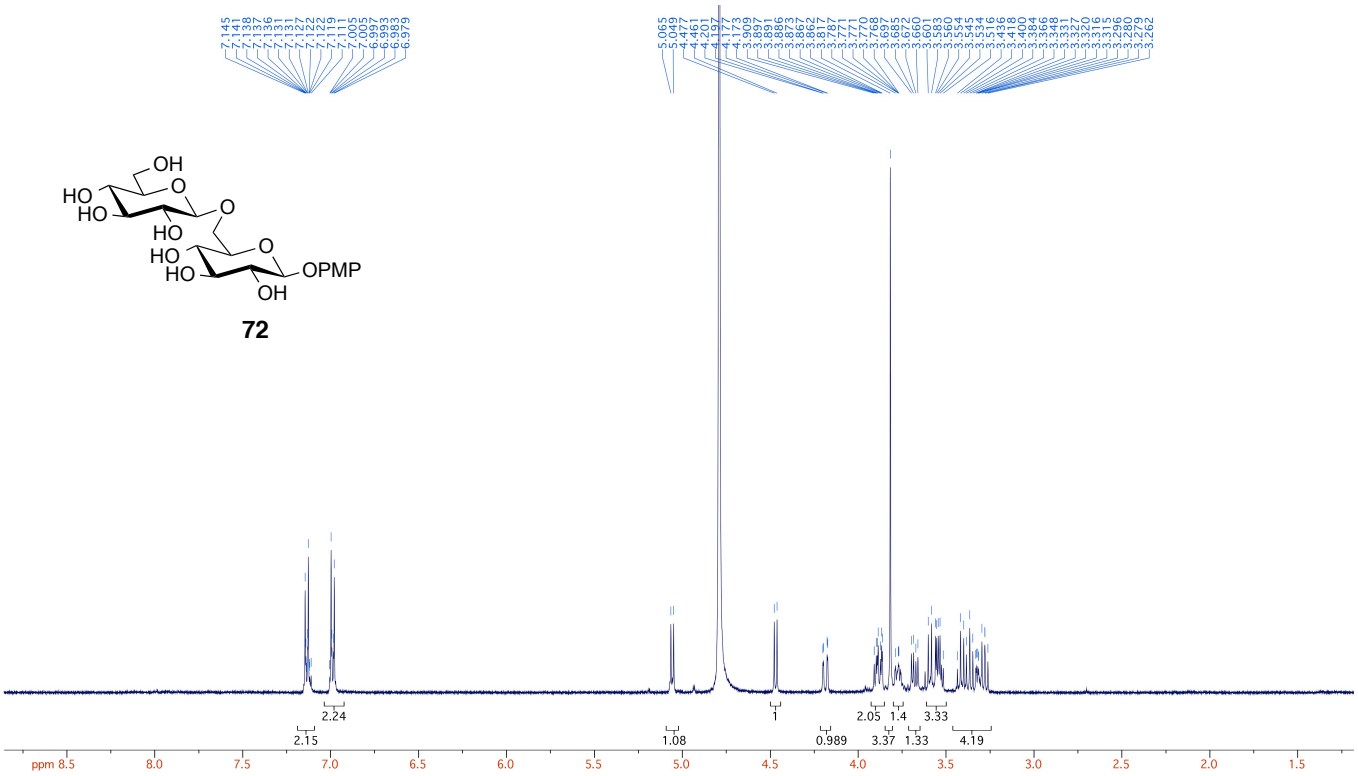
2.15
2.24
1.08
1
0.989
2.05
3.37
1.4
1.33
3.33
4.19
ppm 8.5
8.0
7.5
7.0
6.5
6.0
5.5
5.0
4.5
4.0
3.5
3.0
2.5
2.0
1.5

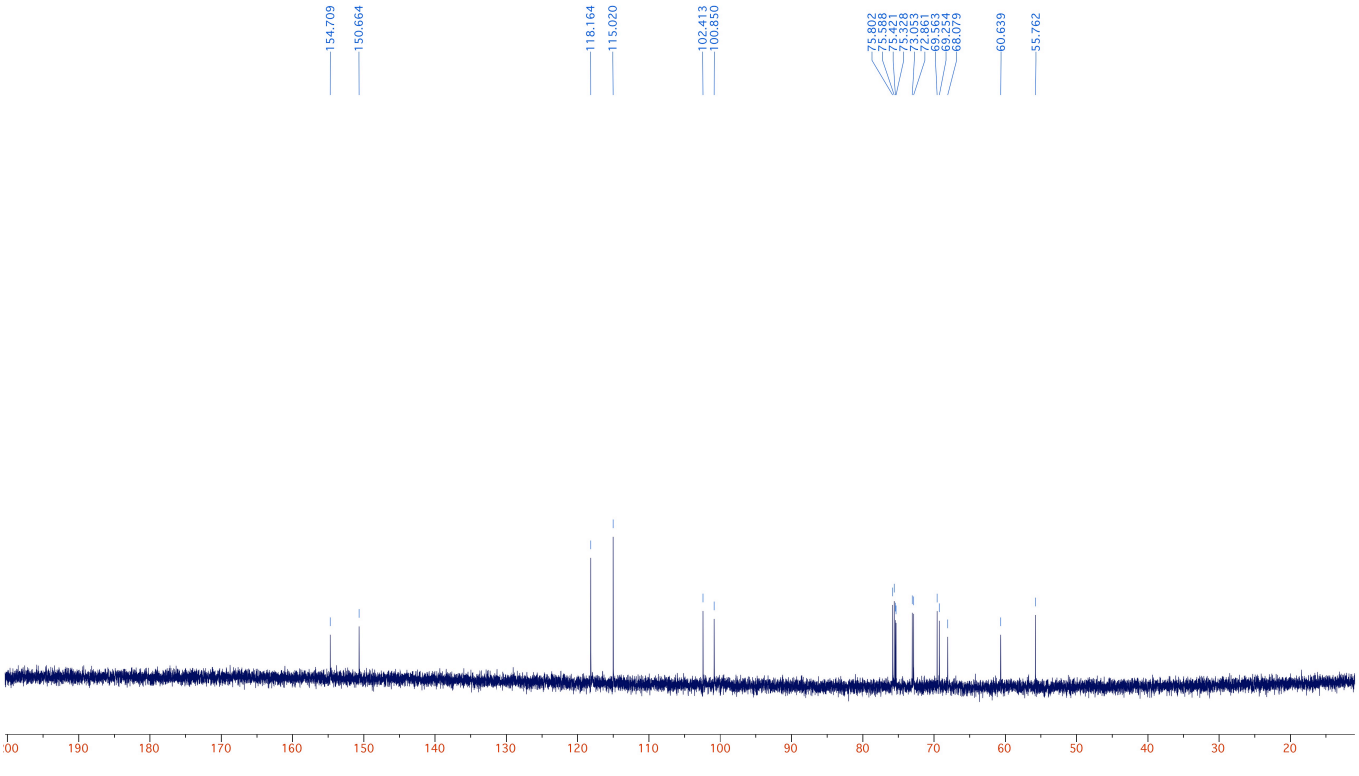
154.709
150.664
118.164
115.020
102.413
100.850
75.802
75.588
75.421
75.328
73.053
72.861
69.563
69.254
68.079
60.639
55.762
190
180
170
160
150
140
130
120
110
100
90
80
70
60
50
40
30
20

OH
HO
HO
OH
O
O
O
HO
OH
OH
O
OH

83

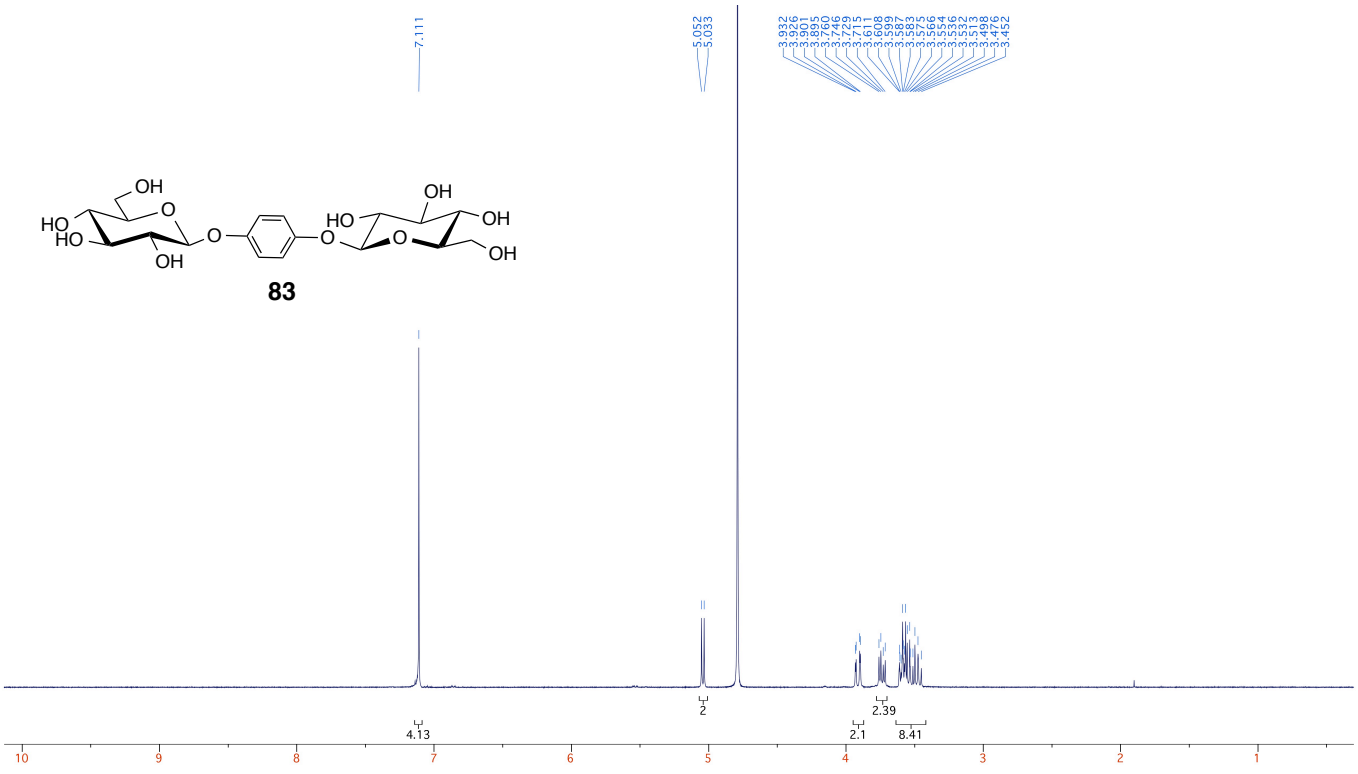
7.111
5.052
5.033
3.932
3.926
3.901
3.895
3.760
3.746
3.729
3.711
3.611
3.608
3.599
3.587
3.583
3.575
3.566
3.554
3.536
3.532
3.513
3.498
3.476
3.452
4.13
2
2.1
2.39
8.41
10
9
8
7
6
5
4
3
2
1

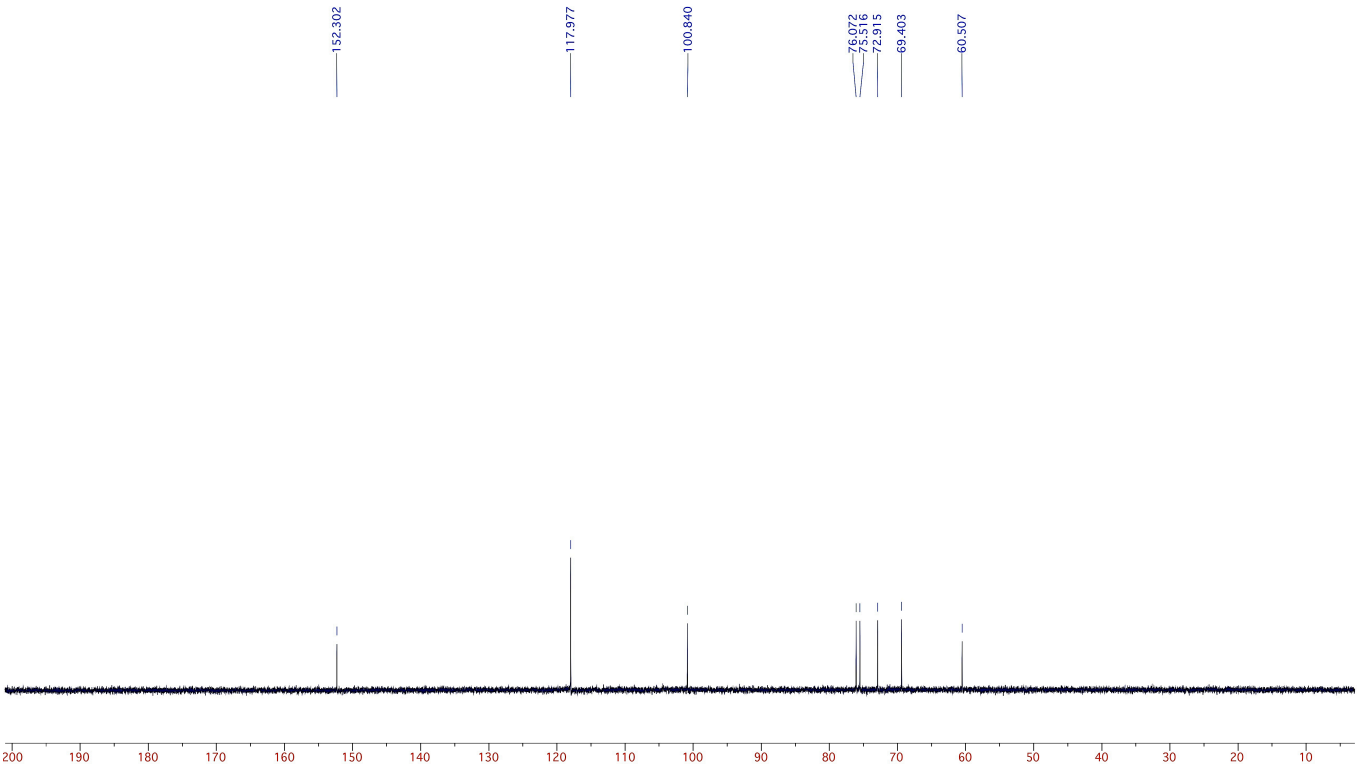
152.302
117.977
100.840
76.072
75.516
72.915
69.403
60.507
200
190
180
170
160
150
140
130
120
110
100
90
80
70
60
50
40
30
20
10

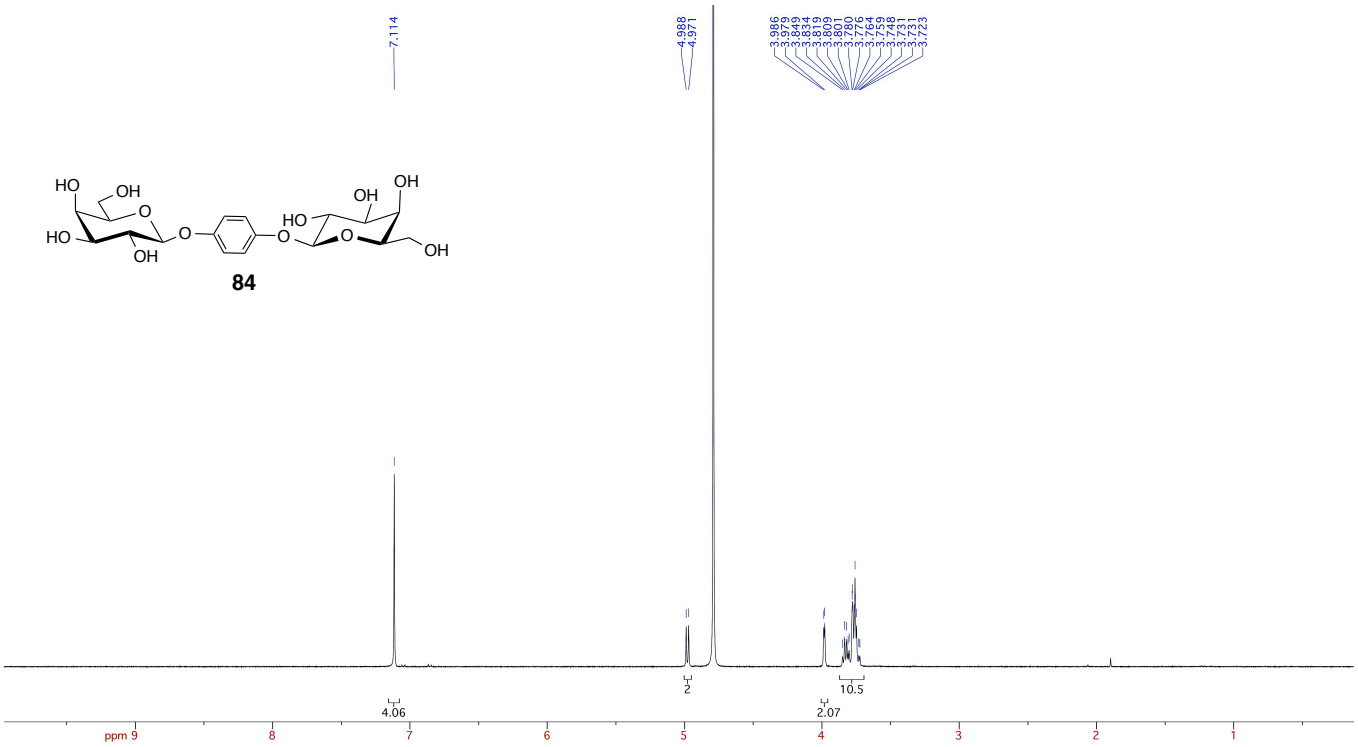
7.114
4.988
4.971
3.986
3.973
3.849
3.834
3.819
3.809
3.801
3.780
3.776
3.764
3.759
3.748
3.731
3.711
3.723
HO
OH
O
HO
OH
O
HO
OH
OH
O
OH
4.06
2
2.07
10.5
ppm 9
8
7
6
5
4
3
2
1

84

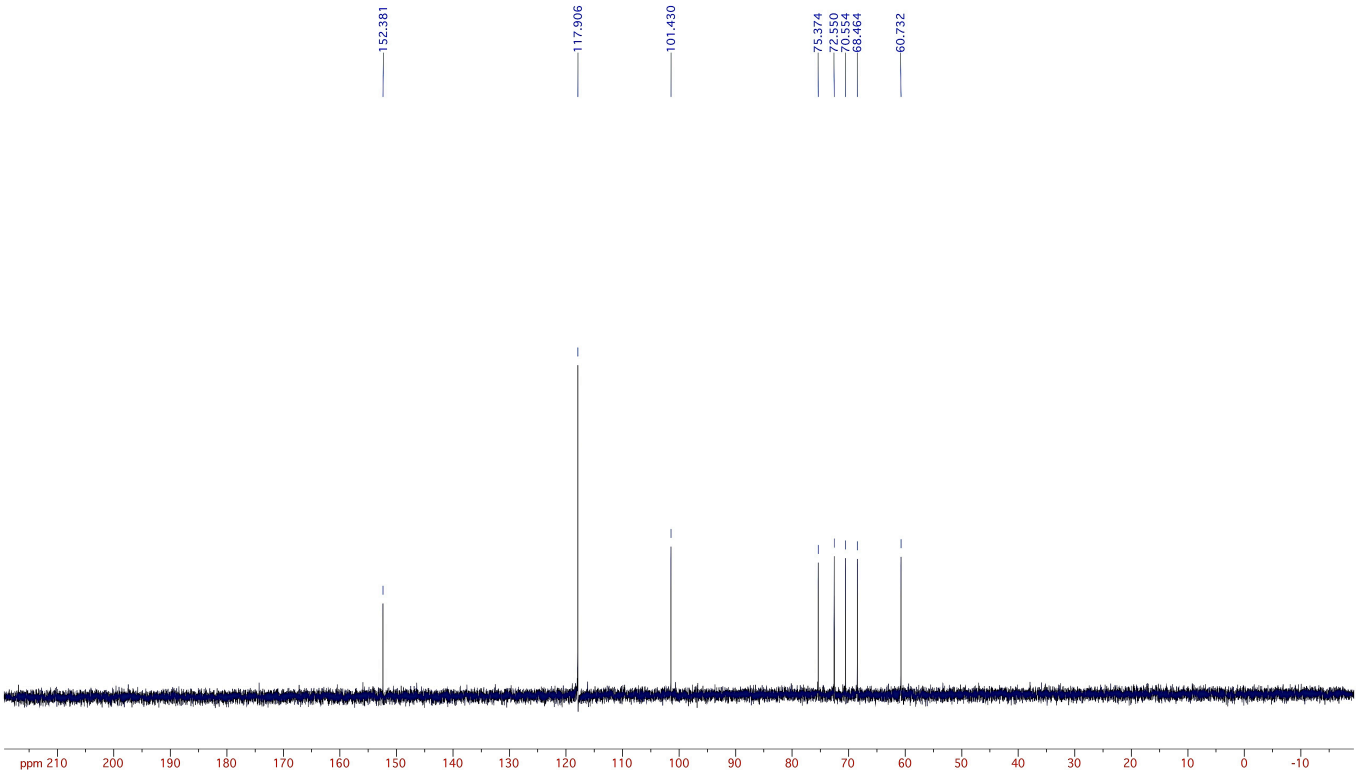
152.381
117.906
101.430
75.374
72.550
70.554
68.464
60.732
ppm 210
200
190
180
170
160
150
140
130
120
110
100
90
80
70
60
50
40
30
20
10
0
-10

85

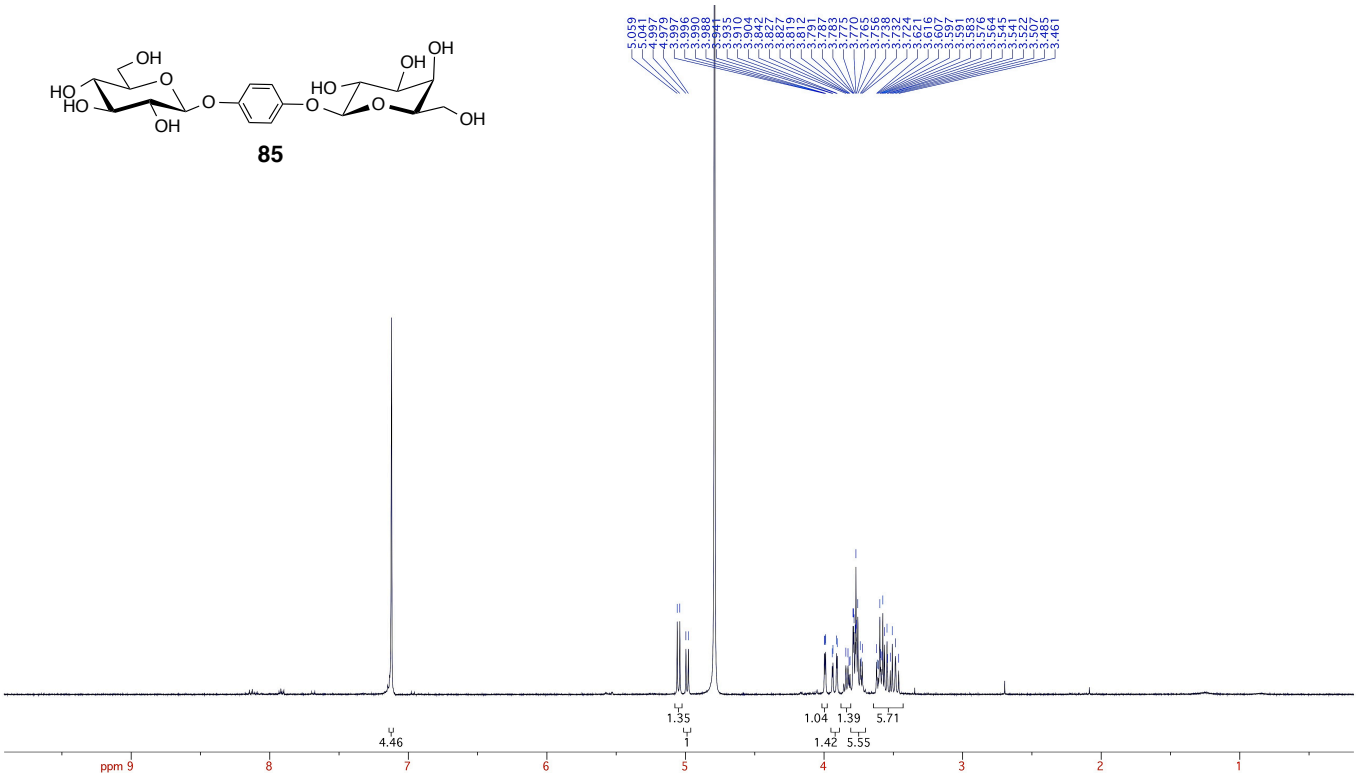
5.059
5.041
4.997
4.979
4.997
3.996
3.990
3.988
3.944
3.935
3.910
3.904
3.842
3.822
3.827
3.819
3.812
3.791
3.787
3.783
3.775
3.770
3.765
3.756
3.738
3.732
3.724
3.621
3.616
3.607
3.597
3.591
3.583
3.576
3.564
3.545
3.541
3.522
3.507
3.485
3.461
1.35
1.04
1.39
5.71
4.46
1
1.42
5.55
ppm 9
8
7
6
5
4
3
2
1

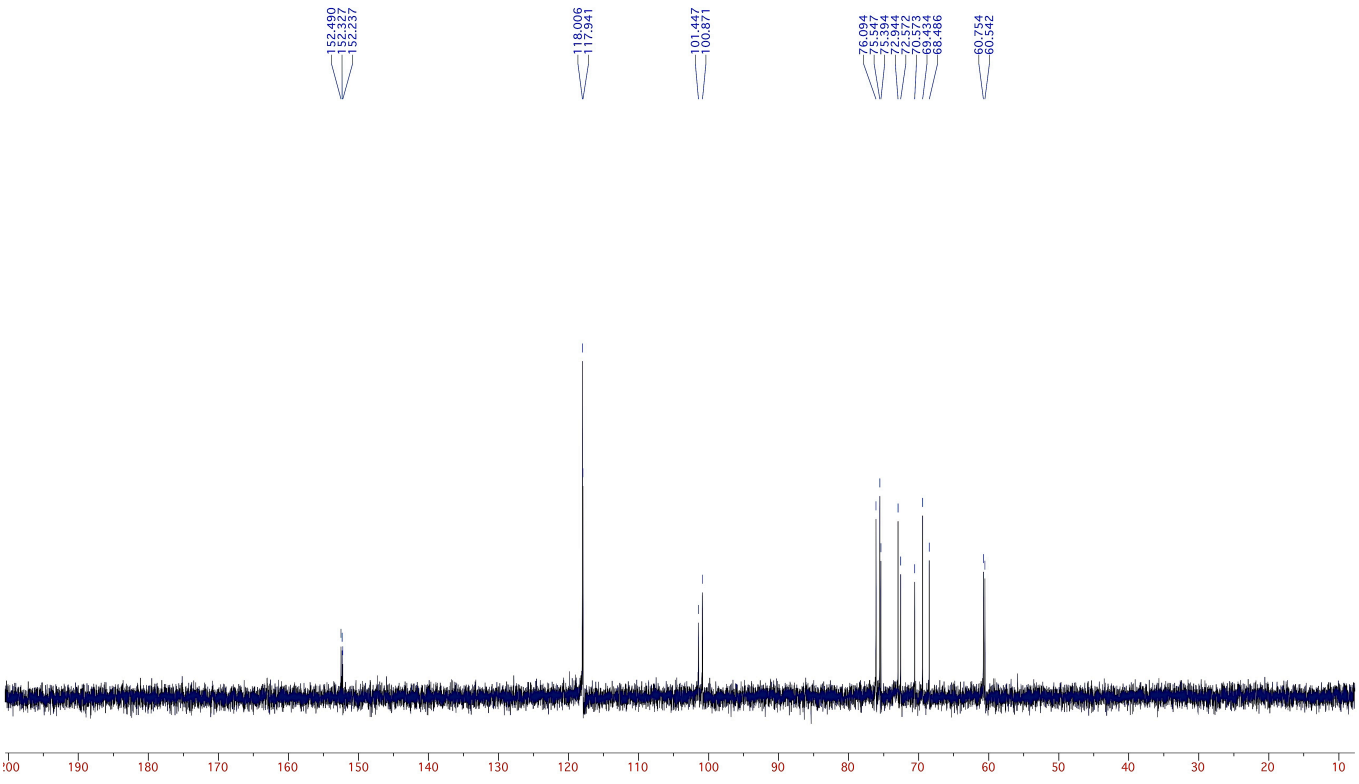
152.490
152.327
152.237
118.006
117.941
101.447
100.871
76.094
75.547
75.344
72.944
72.572
70.573
69.434
68.486
60.754
60.542
200
190
180
170
160
150
140
130
120
110
100
90
80
70
60
50
40
30
20
10

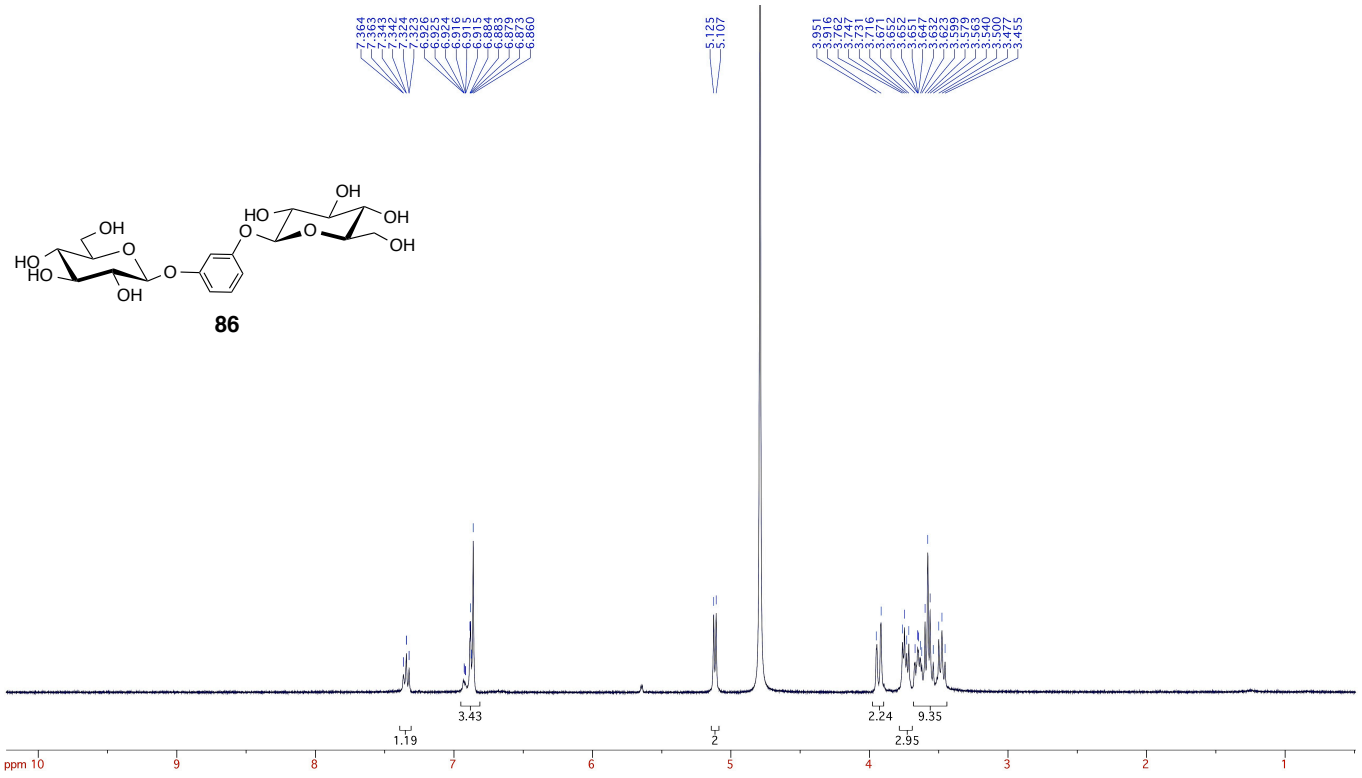
7.364
7.363
7.343
7.342
7.324
7.323
7.326
6.925
6.924
6.916
6.915
6.911
6.884
6.883
6.879
6.873
6.860
5.125
5.107
3.951
3.916
3.762
3.747
3.731
3.716
3.671
3.652
3.651
3.647
3.632
3.623
3.593
3.579
3.563
3.540
3.500
3.477
3.455
OH
HO
HO
O
O
OH
OH
HO
O
O
OH
OH
86
3.43
1.19
2
2.24
9.35
2.95
ppm 10
9
8
7
6
5
4
3
2
1

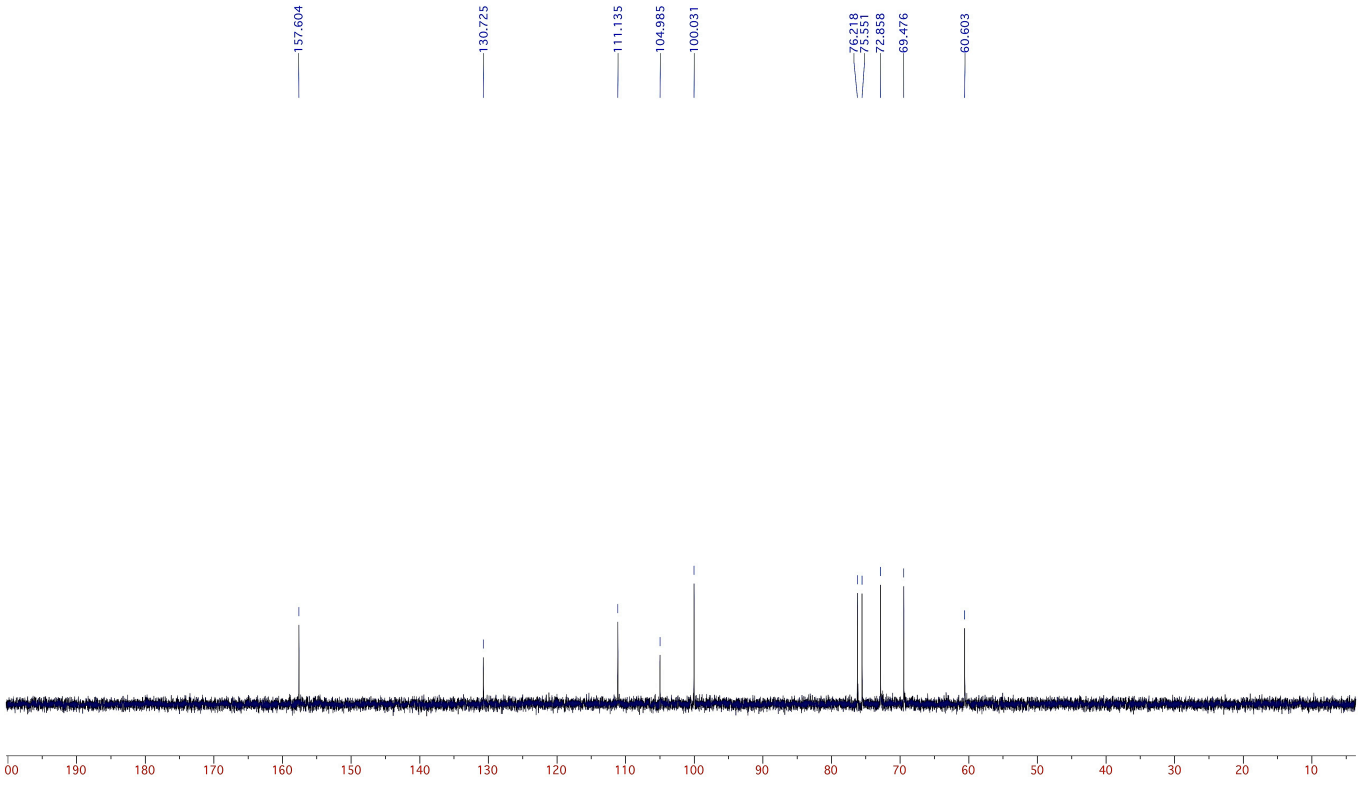
157.604
130.725
111.135
104.985
100.031
76.218
75.551
72.858
69.476
60.603
00
190
180
170
160
150
140
130
120
110
100
90
80
70
60
50
40
30
20
10

Chapter 8: Cryopreservation Ability of Novel IRI Active Carbohydrate-Based Small Molecules

8.1 Introduction

Cryopreservation is the process whereby cells and tissues are stored at subzero temperatures (typically -80 °C or -196 °C). It is very attractive for the long-term preservation of biological materials as at theses temperatures all biochemical processes are effectively stopped, and cells can be stored clinically for 10-20 years depending upon the cell type. However, cryopreservation is a highly complex process during which careful attention to sample volume, cooling rates and cryoprotectants are extremely important to ensure cells survive the process.[1-4] There are many diverse mechanisms of cryo-injury and cell death during cryopreservation (for a detailed discussion on the mechanism of cryo-injury see chapter 1, section 1.4).[5,6] However, it is widely accepted that the formation and recrystallization of both intra- and extracellular ice can be detrimental to cells during the freezing and thawing processes of cryopreservation.[7,8] This is eloquently summarized by Mazur's two-factor hypothesis on the major forms of freezing damage. This hypothesis states that that for every cell type there is an optimal cooling/warming rate depending upon the permeability of the cell membrane (see section 1.4.1 for detailed discussion).[9] This optimal cooling and/or warming rate avoids excessive dehydration of the cell and thus prevents exposing the cell to excessively high and toxic electrolyte concentrations.[7,10-17] Furthermore, this ideal cooling/warming rate also prevents intracellular ice formation (which is lethal) by sufficiently dehydrating the cell resulting in better post-thaw recoveries.[10,18-22]

Cryoprotectants are typically used to mitigate damage incurred during cryopreservation. There are two types of cryoprotectants that are commonly employed depending upon cooling rates, penetrating[23-32] and nonpenetrating cryoprotectants.[23,24,33-36] The protective mechanisms of these two classes of cryoprotectants are quite different and are described in detail in section 1.4.2. The two most commonly employed cryoprotective agents (CPAs) for all clinical cryopreservation protocols are the penetrating CPAs DMSO and glycerol. While these CPAs are very effective at increasing post-thaw cell viabilities, they exhibit significant cytotoxic effects, especially DMSO, which complicates the cryopreservation process as they often must be removed post-thaw (see section 1.4.3).[29-32,37-41] Thus, there is an urgent need for improvements in the cryopreservation protocols to significantly reduce or eliminate the use of DMSO or glycerol cryoprotectants.

As a significant contributing factor to cell-injury and death during cryopreservation is attributed to the formation and recrystallization of ice, interest has arose in employing ice recrystallization inhibitors as novel cryoprotectants. Biological antifreezes were the first

identified molecules capable of inhibiting ice recrystallization and thus were a logical starting point to examine the cryoprotecting abilities of potent IRIs. There are only a few reports describing the successful use of BAs as cryoprotectants to preserve biological material, as they often fail to protect mammalian cells from cryoinjury at temperatures outside of the TH gap and actually facilitate cellular damage during cryopreservation.[42-53] This is discussed in greater detail in section 1.4.4 and was also demonstrated by the results presented in chapter 4. The decrease in post-thaw cell viabilities has been attributed to the change in ice crystal morphology that is induced due to ice binding capabilities of BAs.[46,49] As such, it is hypothesized that compounds that exhibit "custom-tailored" antifreeze activity will be beneficial cryo-additives and will increase post-thaw cell viabilities. Such compounds possess the desirable property of potent IRI activity without the ability to bind to ice or exhibit ice shaping capabilities or TH activity.

Our laboratory has previously demonstrated that *C*-AFGPs exhibiting "custom-tailored" antifreeze activity can function as effective cryoprotectants for a human embryonic liver cell line.[54] The post-thaw cell viabilities using 1-1.5 mg/mL of the *C*-AFGPs was comparable to that obtained with a 2.5% DMSO solution and were double the post-thaw cell viability of the negative control (only cell medium). Furthermore, our laboratory has also reported that at high concentrations (220 or 500 mM) IRI active carbohydrates exhibiting minimal cytotoxicity significantly increased cell viabilities post-thaw.[55] These studies demonstrated that compounds acting as "custom-tailored" ice recrystallization inhibitors were beneficial additives for cryopreservation and could increase cell viabilities and recoveries post-thaw.

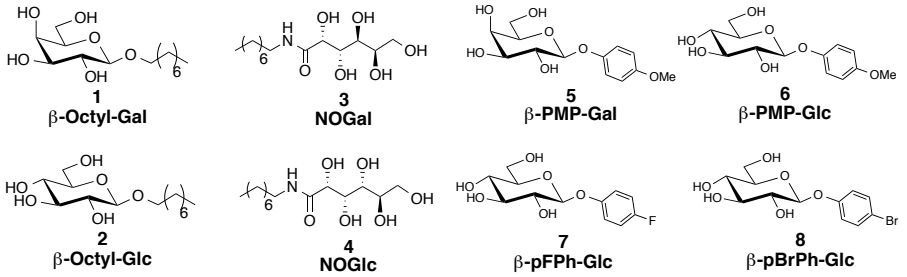

Figure 8.1 Structures of carbohydrate-based surfactants (**1**-**2**) and hydrogelators (**3**-**4**) examined for IRI activity in chapter 6, and phenolic-glycosides **5**-**8** examined for IRI activity in chapter 7. Derivatives **1** and **6**-**8** were potently IRI active at 22 mM, whereas derivative **4** was potently IRI active at 0.5 mM.

Chapters 6 and 7 describe the identification of a number of novel small molecule ice recrystallization inhibitors that are carbohydrate-based derivatives.[56] The structures of these derivatives are provided in figure 8.1. All of these potent IRIs were determined to exhibit "custom-tailored" antifreeze activity as nanoliter osmometry indicated these compounds did not possess TH activity nor did they exhibit ice shaping capabilities. As such, these small molecule IRIs have tremendous potential for use as novel cryoprotectants to improve upon

cryopreservation protocols by either significantly reducing or eliminating the use of DMSO or glycerol CPAs. Consequently, the cytotoxicity of these compounds and their effectiveness as cryo-additives for the cryopreservation of various different cell types was examined. The cell types explored were HepG2 cells (human liver hepatocellular carcinoma cells), hematopoietic progenitor (stem) cells (HSCs) obtained from human umbilical cord blood (UCB), and red blood cells (RBCs) obtained from human peripheral blood. A detailed discussion on the drawbacks of current clinical cryopreservation protocols for HSCs from UCB and RBCs from peripheral blood donations is provided in section 1.4.3 of chapter 1. This highlights the urgent need to improve upon the long-term storage protocols for these precious cell types, and in particular underscores the necessity for reducing or eliminating the use of DMSO CPA for UCB and glycerol CPA for RBCs. A brief summary is also provided in section 8.3 for UCB cryopreservation and 8.4 for RBC cryopreservation. The main focus of this chapter will be on the application of the novel small molecule IRIs described in chapters 6 and 7 (structures shown in figure 8.1) as cryo-additives to improve upon the cryopreservation protocols of blood and blood products. Thus, this chapter will describe the following:

1. Prior to utilizing the small molecule IRIs for the cryopreservation of UCB or RBCs, these derivatives were assessed for cytotoxic effects with an immortalized cell line (HepG2 cells) using an MTT assay. Additionally, the potently IRI active small molecules were initially assessed for their cryoprotective ability with HepG2 cells as a general preliminary screen for their effectiveness as cryo-additives with an immortal cell line prior to exploring their use for the cryopreservation of blood or blood products. These results are described in section 8.2.
2. The use of the novel small molecule IRIs for the cryopreservation of HSCs from UCB was also examined. Leukocyte concentrates (LCs) that contain HSCs from processed UCB units were cryopreserved utilizing the small molecule IRIs as cryoprotectants in combination with reduced concentrations of DMSO. Post-thaw cell viabilities and recoveries of HSCs and leukocytes were quantified to determine whether our small molecule IRIs could be effective cryo-additives for UCB cryopreservation. The results from this study are presented in section 8.3.
3. Finally, small molecule IRIs were employed as cryo-additives for the freezing of RBCs using reduced quantities of glycerol. Results from this work indicated that specific phenolic-glycosides were effective at reducing post-thaw hemolysis with significantly lower glycerol concentrations than what is used in a clinical setting. Deglycerolization experiments were then conducted post-freeze-thaw using the successful cryo-additives

for RBC freezing to determine if the novel additives in the presence of reduced glycerol could also improve deglycerolization procedures to allow for faster access to thawed deglycerolized RBC units. The results from these studies are discussed in section 8.4.

8.2 Cytotoxic Effects and Cryopreservation Ability of Carbohydrate-Based Small Molecule IRIs with HepG2 Cells

8.2.1 Assessing Cytotoxicity of the Carbohydrate-Based Small Molecule IRIs

The cytotoxicity exhibited by the novel small molecule carbohydrate-based IRIs was determined using a conventional MTT assay (3-(4,5-dimethylthiazol-2-yl)-2,5-diphenyl-tetrazolium bromide) on HepG2 cells.[55,57,58] This is a colorimetric assay that measures metabolic activity of living cells as a means of determining cell viability. MTT is a water-soluble yellow tetrazolium salt that can be converted to an insoluble purple formazan by mitochondrial and cytosolic dehydrogenase enzymes in metabolically active cells. Solubilization of the formazan using isopropanol allows for the absorbance of the dissolved formazan to be measured spectrophotometrically to quantify cell viability. Thus, an intense purple colour is representative of normal metabolically active cells.

The cytotoxicity of the IRI active carbohydrate based-surfactant β-octyl-Gal (**1**) and hydrogelator NOGlc (**4**) over a range of concentrations is shown in figure 8.2. For comparison, the cytotoxicity of DMSO is also provided. DMSO is typically used at a concentration of 10% (v/v) in cryopreservation protocols. As is evident in figure 8.2, DMSO is toxic both at 5% and 10% v/v concentrations, resulting in HepG2 cell viabilities less than 40%. This is consistent with previous reports documenting the high toxicity of this CPA.[37-41] At 1-2% DMSO is relatively non-cytotoxic, however at these concentrations DMSO is a poor cryoprotectant resulting in low post-thaw cell viabilities and recoveries (see sections 8.2.2 and section 8.3).

β-Octyl-Gal (**1**) and NOGlc (**4**) exhibited potent IRI activity at 22 mM and 0.5 mM, respectively (chapter 6).[56] Consequently, cytotoxicity was assessed at a range of concentrations above and below the concentration at which they were IRI active (figure 8.2). From the data presented in figure 8.2, it is evident that β-octyl-Gal (**1**) is highly cytotoxic even at low concentrations. A 1 mM solution of β-octyl-Gal (**1**) results in HepG2 cell viability of only 61%, and doubling this concentration significantly decreases viability to 38%. A 2 mM solution of β-octyl-Gal (**1**) results in similar viabilities as a 5 and 10% DMSO solution, and a further increase in the concentration of β-octyl-Gal (**1**) drastically increases these cytotoxic effects. This is not surprising as **1** is a non-ionic surfactant and compounds belonging to this class of molecules have been used as detergents to solubilize membranes to obtain membrane proteins (in particular β-

octyl-Glc (**2**), figure 8.1).[59-65] In contrast, NOGlc (**4**), which is also an amphiphilic surfactant-type molecule, was significantly less toxic than β-Octyl-Gal (**1**). At concentrations ranging from 0.1 mM to 1 mM NOGlc (**4**) was relatively non-cytotoxic resulting in HepG2 cell viabilities greater than 85% after incubation for 18 hours with the solution of **4** (figure 8.2). A 2 mM solution is moderately toxic resulting in 55% cell viability, whereas a 5 mM solution of NOGlc (**4**) is highly toxic with less than 4% of HepG2 cells surviving the incubation period. The cytotoxic results of NOGlc (**4**) were thus very promising as at the concentration it was highly IRI active (0.5 mM) it did not exhibit any cytotoxic effects. Moreover, its concentration could be quadrupled before any decrease in cell viability was observed.

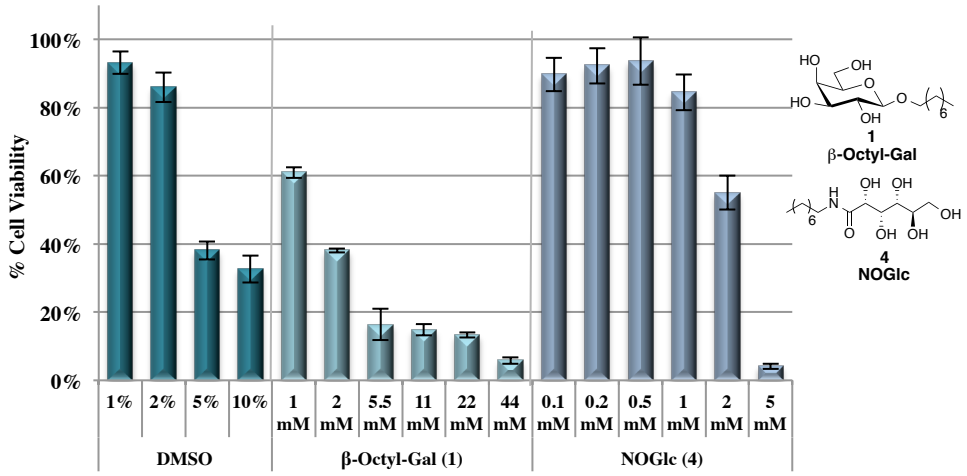

Figure 8.2 Percent cell viability of HepG2 cells treated with various concentrations of DMSO, β-Octyl-Gal (**1**) and NOGlc (**4**) following incubation for 18 h at 37°C as determined by MTT assay.

In addition to the carbohydrate-based surfactants and hydrogelators, potently IRI active phenolic-glycosides were also examined for cytotoxicity. The results of the phenolic-glycosides β-PMP-Glc (**6**), β-pFPh-Glc (**7**) and β-pBrPh-Glc (**8**), are presented in figure 8.3. Phenolic-glucosides **6**-**8** were IRI active at 22 mM, thus their cytotoxicity was assessed at concentrations ranging from 11-220 mM. Both β-PMP-Glc (**6**) and β-pFPh-Glc (**7**) were relatively non-cytotoxic at 11 and 22 mM, the concentration at which they were IRI active. At 44 and 55 mM both **6** and **7** were moderately toxic, resulting in HepG2 cell viabilities of ~60%. Increasing their concentration to 110 and 220 mM was detrimental and essentially no HepG2 cells survived the incubation time with these high concentrations of **6** and **7**. In contrast, β-pBrPh-Glc (**8**) had a significantly different cytotoxicity profile than **6** and **7**. At 11 mM β-pBrPh-Glc (**8**) was moderately cytotoxic, resulting in cell viability of 51%. However, at 22 mM or higher, β-pBrPh-Glc (**8**) was highly cytotoxic resulting in cell viabilities less than 1% (figure 8.3). This was surprising as **8** differs from **6** or **7** only by the substitution of one atom at the *para*-position on the

aryl ring. However, it is evident from these results that this single modification can drastically alter the tolerance and toxicity of these compounds with HepG2 cells.

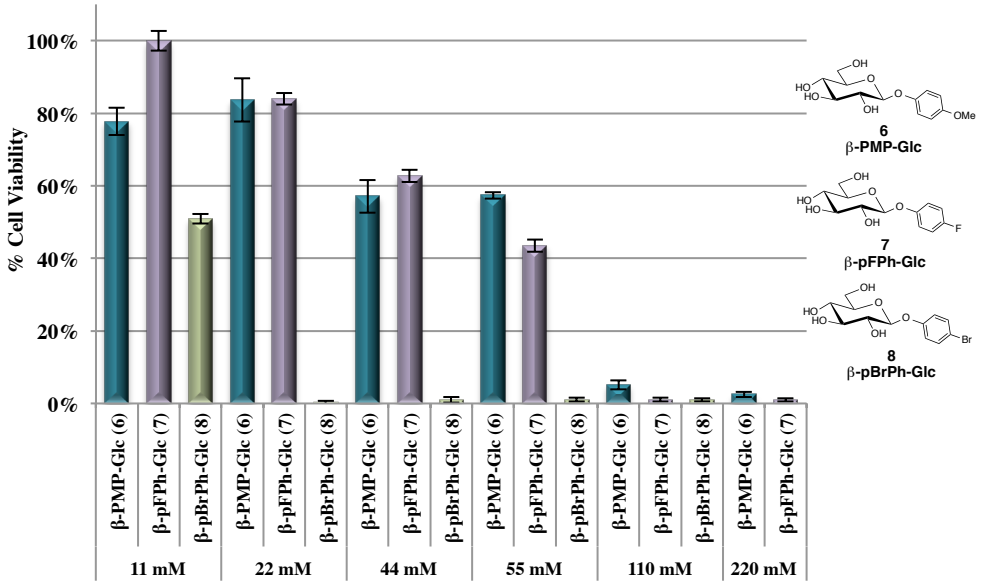

Figure 8.3 Percent cell viability of HepG2 cells treated with various concentrations of β-PMP-Glc (**6**), β-pFPh-Glc (**7**) and β-pBrPh-Glc (**8**) following incubation for 18 h at 37°C as determined by MTT assay.

8.2.2 Assessing Cryopreservation Ability of the Carbohydrate-Based Small Molecule IRIs with HepG2 Cells

In addition to assessing cytotoxic effects, some of the IRI active small carbohydrate-based molecules were also examined for their cryoprotective ability with HepG2 cells. Ideally, the best cryoprotectant would exhibit little or no cytotoxic effects and be a potent inhibitor of ice recrystallization. However, previous work by laboratory has suggested that in practice, a compromise between cytotoxicity and cryopreservation ability is observed with effective cryoprotectants (for instance, consider DMSO).[55] Simple carbohydrates were more effective cryoprotectants at concentrations approximately ten times greater than the concentration at which they are IRI active, despite the fact there was an increase in cytotoxicity observed at these higher concentrations. Our laboratory has also demonstrated that the addition of much less DMSO (only 1-2% versus 10%) to carbohydrate cryoprotective solutions can increase post-thaw cell viabilities compared with the DMSO control on its own and the carbohydrate solution on its own.[55] Consequently, cryoprotective solutions containing phenolic-glucosides **6**-**8** with no or 2% DMSO were utilized to cryopreserve HepG2 cells to assess if these novel IRI active small molecules were beneficial cryo-additives for HepG2 cryopreservation. In an effort to compromise

cytotoxicity and cryoprotective ability of the phenolic-glucosides, **6** and **7** were utilized in the cryopreservation assays at 55 and 110 mM and **8** was utilized at 22 and 55 mM.

The freezing protocol used in these experiments was cooling 1°C/min to -80°C, followed by storage in liquid nitrogen at -196°C. Samples were thawed under fast-thaw conditions at 37°C and post-thaw HepG2 % cell viability, % viable cells that were apoptotic (% apoptosis) and % HepG2 cell recovery was quantified utilizing flow cytometry.[55,66-68] Post-thaw cell viability was determined with the fluorescent marker 7-AAD (7-aminoactinomycin D), which intercalates in double-stranded DNA. Although 7-AAD does not readily pass through cell membranes, cells can be marked as 7-AAD-positive if their membranes have been compromised or damaged due to cryo-injury.[66,67] Apoptosis was determined with the marker Annexin V-PE (phycoerythrin). Annexin V is a protein that strongly binds to phosphotidylserine (PS), which is expressed on cell surfaces when apoptosis (programmed cell death) has been activated. Annexin V is conjugated to a fluorescent tag such as PE, such that viable cells that are activate for apoptosis can be identified as Annexin V-PE-positive (Annexin V-PE^{+}).[68] Cell recoveries were calculated by determining cell concentrations post-thaw using an internal standard with the cytometric analysis (CountBright Absolute Counting Beads) and compared to cell concentrations utilized originally in the cryo experiments. Post-thaw cell viabilities and apoptosis results for the phenolic-glucoside containing cryo-solutions are presented in figure 8.4 and post-thaw cell recoveries are presented in figure 8.5.

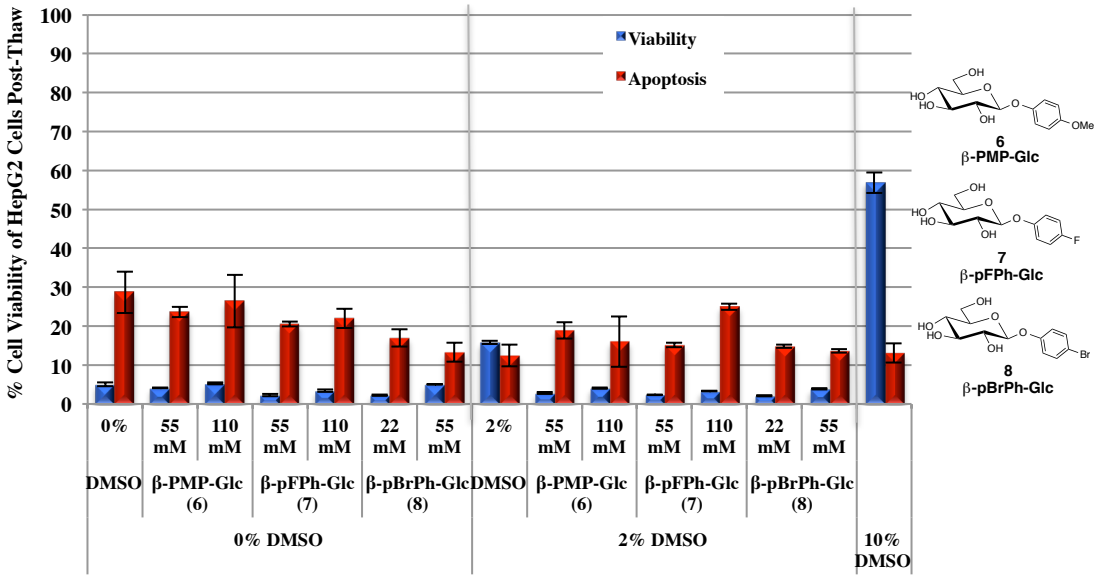

Figure 8.4 Percent post-thaw cell viability and apoptosis of HepG2 cells cryopreserved with various concentrations of β-PMP-Glc (**6**), β-pFPh-Glc (**7**) and β-pBrPh-Glc (**8**) in DMSO cryoprotectant solutions. Samples were thawed under fast-thaw conditions (37°C).

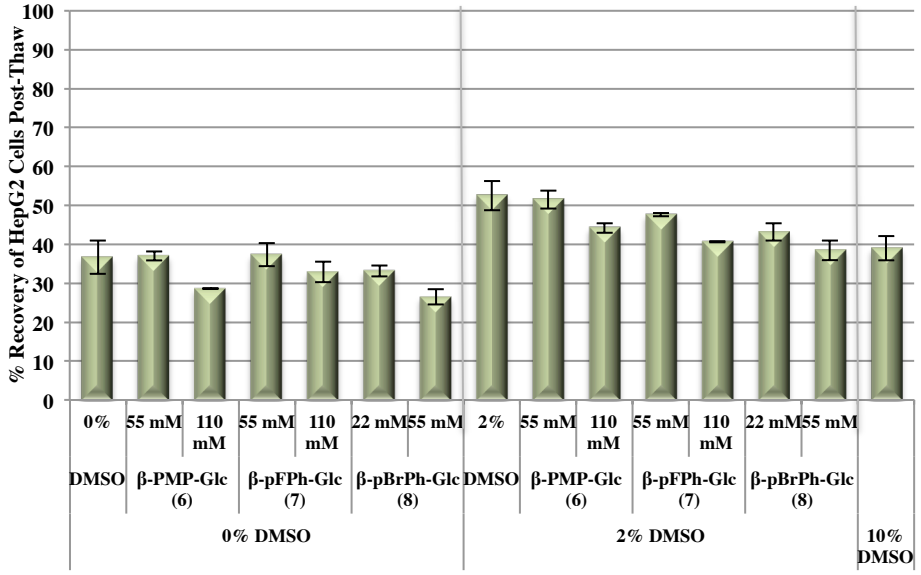

Figure 8.5 Percent post-thaw cell recoveries of HepG2 cells cryopreserved with various concentrations of β-PMP-Glc (**6**), β-pFPh-Glc (**7**) and β-pBrPh-Glc (**8**) in DMSO cryoprotectant solutions. Samples were thawed under fast-thaw conditions (37°C).

Unfortunately, none of the phenolic-glucosides assessed (**6**-**8**) were beneficial cryo-additives for HepG2 cells. The phenolic-glucosides alone in cryo-solution failed to increase post-thaw cell viabilities relative to the 0% DMSO control (cell medium only) (figure 8.4). Regardless of the concentration of the carbohydrate used, **6**-**8** all resulted in post-thaw cell viabilities of approximately 5%. Furthermore, using cryo-solutions containing only **6**, **7** or **8**, the percent of viable cells that were apoptotic ranged from 13-26%, which is similar to that observed with the 0% DMSO control. In contrast to what our laboratory has previously observed with simple carbohydrates,[55] the addition of 2% DMSO to the phenolic-glucoside cryo-solutions was not beneficial for the cryopreservation of HepG2 cells. In fact, cryopreservation with phenolic-glucosides **6**-**8** and 2% DMSO resulted in lower cell viabilities post-thaw than the 2% DMSO control alone (figure 8.4). 2% DMSO solutions containing **6**-**8** resulted in less than 5% viable HepG2 cells post-thaw whereas a 2% DMSO solution resulted in 16% viable HepG2 cells post-thaw. All post-thaw HepG2 cell recoveries were similar regardless whether DMSO was present or absent in the cryo-solution, and recoveries were similar to a 10% DMSO control, ranging from 30-50% HepG2 cell recovery (figure 8.5).

The cryopreservation results presented in this section indicate that β-PMP-Glc (**6**), β-pFPh-Glc (**7**) and β-pBrPh-Glc (**8**) are poor cryoprotectants for the cryopreservation of HepG2 cells. While this was initially disappointing, it is known that different cell types can be more or less susceptible to the damages associated with cryopreservation and can respond differently to cryoprotective solutions. As demonstrated previously by our laboratory, a 5% DMSO solution

results in greater than 80% viability when used to cryopreserve WRL-68 cells;[54,55] however, viability of HepG2 and HEK293 cells with 10% DMSO typically range from 50-60% (HepG2 viabilities with DMSO also present in figure 8.4).[55] 10% DMSO solutions also result in high post-thaw viabilities (90-98%) when utilized to cryopreserve HSCs from UCB and mesenchymal stem cells (MSCs).[69-73] Moreover, our laboratory has demonstrated that HepG2 cells and HEK293 cells respond differently and have drastically different post-thaw cell viabilities when carbohydrate solutions are employed as CPAs.[55] Thus, even though the phenolic-glucosides **6**-**8** explored in this study were poor cryoprotectants for HepG2 cells, this may not necessarily translate to poor cryopreservation ability with other cell types including those found in blood and blood products.

8.2.3 Summary and Conclusions for Cytotoxicity and Cryoprotective Ability of Small Molecule IRIs with HepG2 Cells

Many of the small molecule IRIs assessed for cytotoxic effects with HepG2 were determined to be relatively non-toxic at low concentrations. This includes carbohydrate-based hydrogelator NOGlc (**4**) (figure 8.2) and phenolic-glucosides β-PMP-Glc (**6**) and β-pFPh-Glc (**7**) (figure 8.3). In contrast, the potently IRI active carbohydrate-based surfactant β-octyl-Gal (**1**) was found to be highly toxic at 2 mM and potently IRI active phenolic-glucoside β-pBrPh-Glc (**8**) was found to be highly toxic at 22 mM. Cryopreservation experiments using the phenolic-glucosides **6**-**8** as cryo-additives indicated that these derivatives are poor cryoprotectants for HepG2 cells (figure 8.4). Moreover, the addition of these derivatives to a 2% DMSO solution was detrimental and decreased post-thaw cell viabilities relative to a 2% DMSO solution alone. However, as susceptibility to cryopreservation damage and the effectiveness of different cryo-solutions is dependent upon cell type, these derivatives may still prove to be effective cryo-additives for the cryopreservation of other cell types.

8.3 Cryopreservation Ability of Carbohydrate-Based Small Molecule IRIs with UCB

8.3.1 Introduction – Cryopreservation of HSCs from UCB

HSC transplants from UCB have been increasingly used for regenerative medicine therapies and to treat a number of different conditions including hematological cancers, hematological diseases, anemias and immunodeficiencies.[74,75] A main advantage of HSC transplantation from UCB over bone marrow is the reduced risk of severe acute graft versus host disease (GVHD).[76] The banking of UCB by cryopreservation has also ensured that units are rapidly available for transplantation when required.[77] Clinical protocols for UCB cryopreservation use 10% DMSO

cryoprotectant solution. While high HSC post-thaw viabilities are observed, a significant drawback with the use of DMSO is its significant toxicity not only to cells, but also to patients upon re-infusion of thawed HSCs (this is discussed in greater detail in section 1.4.3).[37-39] Furthermore, studies have indicated that increased incidents of apoptosis in DMSO cryopreserved HSCs can result in impaired engraftment capacity of these stem cells.[40,41] Thus, there is an urgent need for improvements in the cryopreservation protocols of UCB HSCs to significantly reduce or eliminate the use of DMSO cryoprotectant.

Efforts towards improving cryopreservation protocols of UCB include decreasing DMSO concentrations and altering freezing and thawing rates based upon the permeability of the HSCs to DMSO.[69,70,78-83] Combinations of reduced DMSO quantities with ethylene glycol, propylene glycol or the non-penetrating cryoprotectant hydroxyethylstarch (HES) have also been explored.[81,84-86] Furthermore, simple mono- and disaccharides, such as sucrose, trehalose, glucose and galactose, have been examined as potential UCB cryoprotectants. These studies have explored the use of these carbohydrates alone, or in combination with DMSO or DMSO/antioxidant mixtures with either catalase or ascorbic acid.[87-91] While many reports describe advantages with utilizing modified cryo-solutions or freezing protocols, a 10% DMSO cryoprotective solution still remains superior and the most effective for UCB cryopreservation.[38,83,92]

Having identified novel small molecule ice recrystallization inhibitors (chapters 6 and 7), interest arose in exploring if these molecules would be beneficial cryo-additives for the cryopreservation of UCB using decreased quantities of DMSO. Thus, this section will describe the results of using cryo-solutions containing galactose, sucrose, NOGlc (**4**) and β-PMP-Glc (**6**) with reduced DMSO concentrations for the cryopreservation of UCB. The results from these studies are discussed in section 8.3.2.

8.3.2 Effect of Small Molecule IRIs for the Cryopreservation of UCB

The cryopreservation experiments were conducted following protocols used clinically in the United States and Canada for the banking of UCB units. This work was completed with assistance from a fellow doctoral student Jennie Briard and post-doctoral research associate Dr. Mathieu Leclère. The procedure was based upon Rubinstein's method for UCB processing and cryopreservation that was described in 1995.[93] UCB units were processed to obtain volume reduced leukocyte concentrates (LCs) by sedimentation of RBCs by rouleaux formation (stacks of hemagglutinated RBCs) that is enhanced by a strong sedimentation agent such as pentastarch (Pentaspan) or HES.[72,93] A leukocyte rich buffy coat supernatant is then separated by

centrifugation and subsequently removed and centrifuged to pellet the leukocytes from plasma. Following removal of the supernatant, resuspension of the leukocytes in plasma provides the LC to be utilized for the cryopreservation experiments. The percentage of cells in the UCB unit and/or the processed LC that are HSCs or hematopoietic progenitor cells ranges from 0.1-1% of the total leukocytes present in the unit.[72,78,93,94]

The LCs containing HSCs were then cryopreserved using cryoprotectant solutions containing the small molecule IRIs without or in combination with DMSO. Standard clinical freezing rates were employed with cooling at a rate of 1°C/min to -80°C followed by storage in liquid nitrogen (-196°C).[72,93] Thawing was achieved using either fast-thaw conditions (37°C) or slow-thaw conditions (room temperature) to exacerbate cellular damage due to ice recrystallization to investigate if the IRI active molecules could prevent this damage.[91,95,96] Post-thaw HSC cell viability was determined by flow cytometry using ISHAGE guidelines (International Society of Hematotherapy and Graft Engineering).[97] All human leukocytes (mononuclear cells), including hematopoietic progenitor cells express the leukocyte common antigen (LCA) CD45 on their cell surfaces.[97-101] HSCs also express the CD34 antigen and this antigen is not present on mature leukocytes. Thus, fluorescently tagged antibodies for both CD45 and CD34 can be employed to identify the cell population within the leukocytes that are HSCs using a specific gating strategy with flow cytometry.[97,98,100] HSCs are identified as $CD45^+$ and $CD34^+$ cells, whereas remaining leukocytes (or total mononuclear cells) are $CD45^+$ but $CD34^-$. By also employing 7-AAD in the flow cytometric analysis, post-thaw cell viabilities of both of these cell types present in the LC can be quantified.

The first carbohydrates explored for their potential cryoprotective benefits with UCB were the simple mono- and disaccharide galactose and sucrose. While at 22 mM galactose and sucrose were moderate to weak ice recrystallization inhibitors (64% MGS for Gal, 83% MGS for Suc),[102] at 220 mM both exhibited potent IRI activity (38% MGS for Gal, 19% MGS for Suc).[55] At 220 mM these carbohydrates were also reported to be effective at cryopreserving human embryonic liver cells.[55] Consequently, they were explored as cryo-additives for UCB cryopreservation at 220 mM both with and without 2% DMSO added to the solution. The post-thaw viabilities of $CD34^+$ cells (HSCs) using these cryo-solutions is presented in figure 8.6, along with the viabilities of 5 and 10% DMSO cryo-solutions for comparison. Both fast- and slow-thaw conditions were utilized in these cryopreservation experiments to determine if the IRIs were capable of mitigating cellular damage due to ice recrystallization during slow thawing, thus resulting in increased cell viabilities.[91,95,96]

With fast-thaw conditions, both galactose as sucrose cryo-solutions increased the post-thaw viability of $CD34^+$ cells relative to the control with no DMSO (cryo-solution consisted of only plasma). The 0% DMSO control resulted in viabilities of only 15% and this was doubled when 220 mM of either galactose or sucrose was added to the cryo-solution (figure 8.6). When 2% DMSO was added to the cryo-solutions however, this increase in $CD34^+$ cell viability observed with the addition of either galactose or sucrose was not observed. All three cryo-solutions containing 2% DMSO resulted in similar viabilities of $CD34^+$ cells (35-40% viable $CD34^+$ cells post-thaw). Unfortunately, the post-thaw viabilities when cryo-solutions containing no or 2% DMSO were used were quite low and approximately half of that observed with either 5 or 10% DMSO. A 5% DMSO solution results in 75% viable $CD34^+$ cells post-thaw, whereas a 10 % DMSO solution results in 86% viable cells post-thaw.

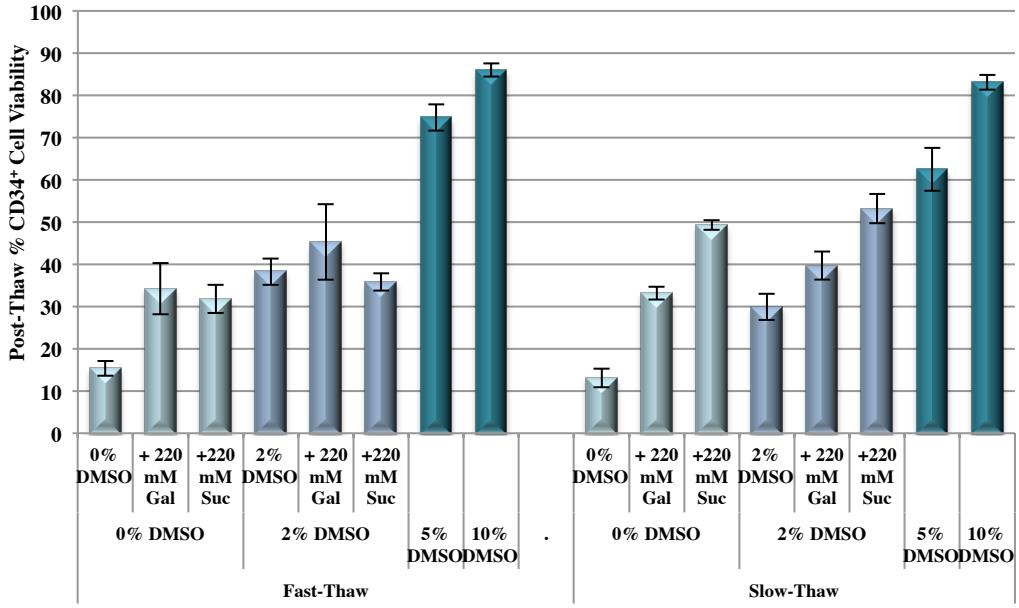

Figure 8.6 Post-thaw % cell viability of HSCs ($CD34^+$ cells) cryopreserved with 220 mM galactose (Gal) or 220 mM sucrose (Suc) in DMSO cryoprotectant solutions. Fast-thaw conditions involved thawing samples at 37°C. Slow-thaw conditions involved thawing samples at room temperature.

The most interesting results obtained with the galactose and sucrose cryo-solutions were under slow-thaw conditions. Thawing with slow-thaw conditions when DMSO was used as the cryoprotectant typically resulted in lower cell viabilities (figure 8.6). A 2% DMSO solution thawed under fast-thaw conditions resulted in 38% viable $CD34^+$ cells, while under slow-thaw conditions resulted in 30% viable $CD34^+$ cells. Similarly, the viability a 5% DMSO solution was decreased from 75% to 62% when slow-thaw conditions were employed. However, when 220 mM galactose was added to 0% or 2% DMSO solutions, this decrease in cell viability under slow-thaw conditions was no longer observed. A 220 mM galactose solution alone resulted in

34% viable $CD34^+$ under both fast- and slow-thaw conditions, and when 2% DMSO was added to the galactose solution viabilities were ~40% for both thawing conditions.

With fast-thaw conditions a 220 mM sucrose solution with or without 2% DMSO resulted in ~33% viable $CD34^+$. With slow-thaw conditions, viability was significantly increased to ~50% using the sucrose solutions with or without 2% DMSO (figure 8.6). In fact, 220 mM sucrose ± 2% DMSO resulted in post-thaw viabilities that were close to that of a 5% DMSO solution (62% viable $CD34^+$ cells) when slow-thaw conditions were employed. These results are highly significant as the 220 mM sucrose cryo-solution resulted in 50% viable hematopoietic progenitor cells in the absence of the toxic cryoprotectant DMSO. This is tremendous progress towards the optimization of UCB cryopreservation protocols where the reduction or elimination of the CPA DMSO is required. Further studies are still required to determine if the sucrose cryo-solution under slow-thaw conditions decreases the incidence of apoptosis with $CD34^+$ cells since this is correlated to the engraftment capacity of transplanted HSCs.[40,41,91] Furthermore, the proliferative capacity of these progenitors must be assessed utilizing a colony-forming unit assay to provide insight into the functional capacity of the cryopreserved HSCs.

Slow-thaw conditions subject cells to a high amount of ice recrystallization injury. It is evident that the ability of a compound to inhibit this process is beneficial for cryopreservation and can result in increased post-thaw cell viabilities. A 220 mM galactose solution is less IRI active than a 220 mM sucrose solution (38% MGS for Gal compared with 19% MGS for Suc).[55] When ice recrystallization injury was high (slow-thaw conditions), the more potent IRI (sucrose) resulted in higher post-thaw $CD34^+$ cell viability compared to the less potent IRI (galactose) (figure 8.6). When thawed under conditions with low ice recrystallization injury (fast-thaw conditions), the effect of the carbohydrate IRI was less apparent and both galactose and sucrose resulted in similar viabilities of $CD34^+$ cells. These results further support the hypothesis that the ability of a compound to inhibit ice recrystallization is a highly desirable property for a cryoprotectant and can result in increased post-thaw cell viabilities.

Following the encouraging results with galactose and sucrose, IRI active derivative NOGlc (**4**) was examined for its cryopreservation ability with UCB. NOGlc (**4**) exhibits potent IRI activity at 0.5 mM (chapter 6)[56] and was determined to be relatively non-toxic up to 2 mM (figure 8.2, section 8.2.1). Consequently, NOGlc was explored as a cryoprotectant with UCB at 0.5, 1 and 2 mM either with or without 2% DMSO. The post-thaw $CD34^+$ cell viability (fast-thaw conditions) using these cryo-solutions are presented in figure 8.7. It is evident that NOGlc (**4**) without or in combination with 2% DMSO is not a beneficial cryoprotectant for UCB. At a concentration of 0.5 mM in 0% or 2% DMSO, post-thaw $CD34^+$ viabilities were similar to the DMSO controls

(15% for 0% DMSO solutions ± 0.5 mM NOGlc, 35% for 2% DMSO solutions ± 0.5 mM NOGlc), indicating that this compound failed to provide any extra protection during cryopreservation. When the concentration of NOGlc was increased to 1 and 2 mM in the cryo-solutions, $CD34^+$ cell viability actually decreased relative to the 0 or 2% DMSO control. This suggests that the presence of NOGlc at these concentrations causes increased damage during the cryopreservation process. A plausible explanation for this is that at higher concentrations NOGlc does become more cytotoxic. This is consistent with the observation that 2 mM NOGlc resulted in only 60% viable HepG2 cells as determined by an MTT assay (figure 8.2, section 8.2.2). Regardless, the UCB cryopreservation results preliminarily indicate that NOGlc in not an ideal cryo-additive for the successful cryopreservation of HSCs ($CD34^+$ cells) in UCB.

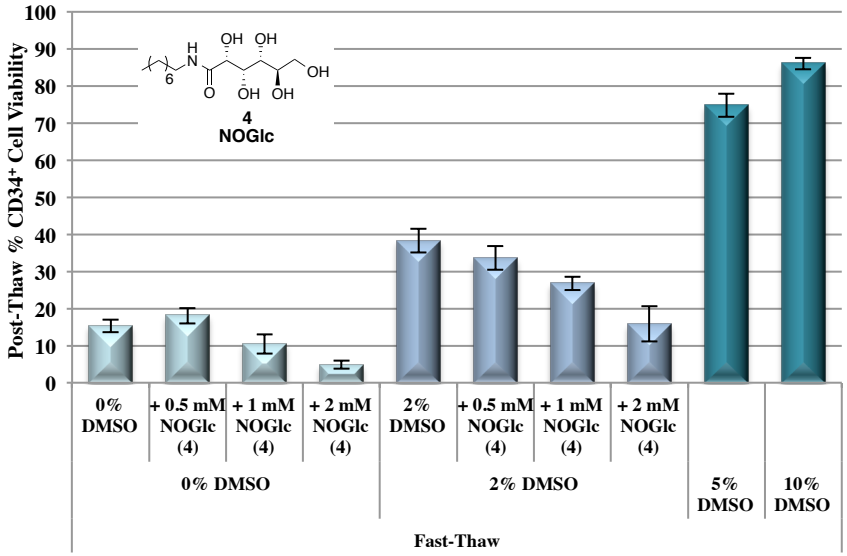

Figure 8.7 Post-thaw % cell viability of HSCs ($CD34^+$ cells) cryopreserved with 0.5, 1, and 2 mM NOGlc (**4**) in DMSO cryoprotectant solutions. Samples were thawed under fast-thaw (37°C).

IRI active phenolic-glucoside β-PMP-Glc (**6**) was also assessed for its cryopreservation potential with UCB. Similar to what was observed with the cryopreservation of HepG2 cells (figure 8.4, section 8.2.2), this compound was detrimental to UCB cryopreservation (figure 8.8). All post-thaw $CD34^+$ cell viabilities when this compound was present in the cryo-solution were less than 1%, irrespective of the thawing conditions (fast- or slow-thaw) or whether DMSO was added. The antioxidant catalase is often added to cryoprotectant solutions of sucrose or trehalose to increase viabilities of $CD34^+$ cells post-thaw. Catalase protects cells from oxidative damage to proteins, lipids and DNA by scavenging reactive oxygen species such as peroxides that can be formed during hypothermia and freezing in the cryopreservation process.[89,90] As such, we explored if the addition of catalase to the cryoprotectant solutions containing β-PMP-Glc (**6**) could increase post-thaw $CD34^+$ cell viability by protecting from additional oxidative stress that

may have been caused by glucose derivative **6**. Unfortunately, the addition of catalase to the β-PMP-Glc cryo-solutions had no effect, and post-thaw $CD34^+$ cell viabilities were still less than 1% (figure 8.8). It is currently not known why β-PMP-Glc (**6**) has such an adverse effect on both the cryopreservation of HepG2 cells and HSCs ($CD34^+$ cells). However, the results presented in this section and section 8.2.2 indicate that despite the potent IRI activity exhibited by the phenolic-glucosides (**6**-**8**), this class of compound are poor cryoprotectants for HepG2 and $CD34^+$ cells and actually exacerbate cellular damage resulting in less than 5% post-thaw viability.

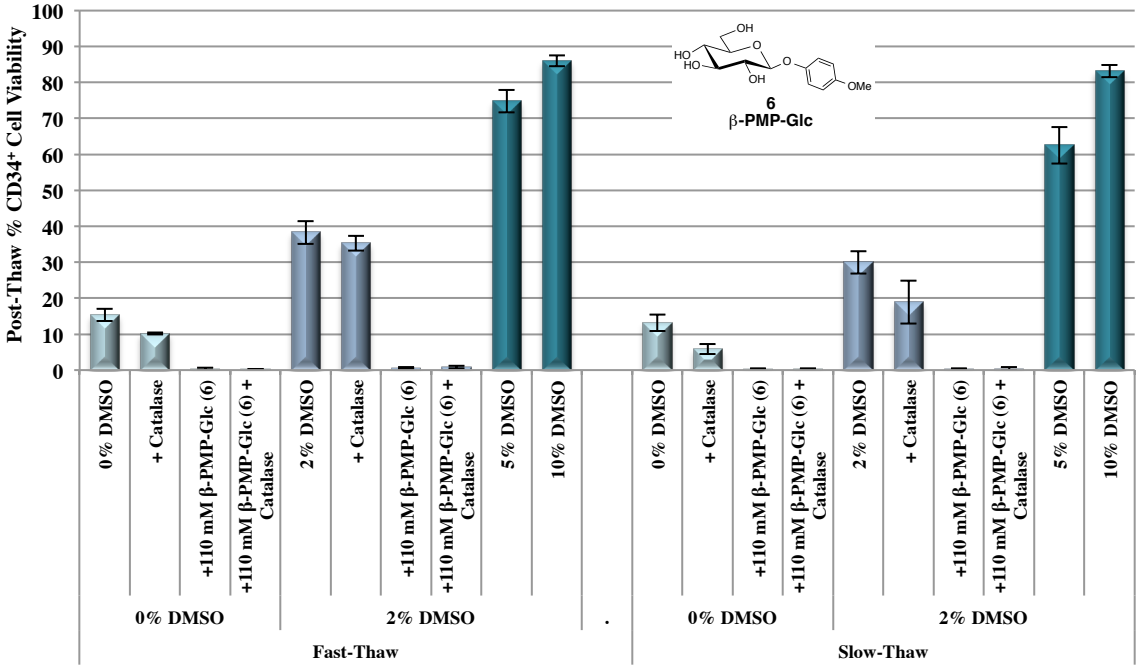

Figure 8.8 Post-thaw % cell viability of HSCs ($CD34^+$ cells) cryopreserved with 110 mM β-PMP-Glc (**6**) in DMSO cryoprotectant solutions with or without 100 μg/mL catalase. Fast-thaw conditions involved thawing samples at 37°C. Slow-thaw conditions involved thawing samples at room temperature.

8.3.3 Summary and Conclusions for UCB Cryopreservation with Small Molecule IRIs

IRI active small molecules NOGlc (**4**) (chapter 6) and β-PMP-Glc (**6**) (chapter 7) were assessed for their ability to cryopreserve HSCs ($CD34^+$ cells) from UCB. Unfortunately, both of these derivatives were unsuccessful for UCB cryopreservation and often resulted in reduced cell viabilities relative to the DMSO controls. Interestingly, the simple monosaccharide galactose and disaccharide sucrose were determined to be beneficial cryo-additives for UCB cryopreservation (figure 8.6). While $CD34^+$ cell viabilities were low, a 220 mM galactose or 220 mM sucrose cryo-solution doubled the viability of the negative control (no DMSO, only plasma) from 15% to 30-35%. The most surprising result was that of the 220 mM sucrose cryo-solution when slow-thaw conditions were employed. $CD34^+$ cell viabilities were close to that of a 5% DMSO control, with 50% viable $CD34^+$ cells post-thaw obtained with the sucrose solution and 62% viable $CD34^+$ cells

obtained with 5% DMSO. This is highly significant as moderate post-thaw cell viabilities were observed with cryopreservation conditions that completely eliminated the presence of the toxic cryoprotective agent DMSO. Further optimization and cryopreservation studies are still required such as quantifying apoptosis and assessing the proliferative capacity of the hematopoietic progenitor cells by a colony-forming unit (CFU) assay. Regardless, these results provide a rationale for further development of ice recrystallization inhibitors that could potentially be successful for the cryopreservation of precious HSCs obtained from UCB.

8.4 Cryopreservation Ability of Carbohydrate-Based Small Molecule IRIs with RBCs

8.4.1 Introduction – Cryopreservation of RBCs

The most commonly used blood product in blood banks is red blood cells (RBCs). Patients requiring RBC transfusions may use anywhere from 5-10 units for surgeries or cancer treatments, 2-8 units per week for bone marrow transplants and leukemia treatments, and up to 50 units for acute to severe blood loss (eg. car accident victims).[4] Thus, there is a very high demand for access to readily available and safe blood supplies. RBC donations from peripheral blood are typically hypothermically preserved for a maximum of 42 days. This storage time period is limiting and can result in shortages of blood supplies when high numbers of emergency blood transfusions are required.[103,104] This biopreservation method can also result in hypothermic storage lesions that reduce *in vivo* RBC survival and function.[4,105-110]

Cryopreservation of RBC units can extend storage time to 10 years. Despite this advantage, this preservation method is not routinely employed (see section 1.4.3 for detailed discussion).[4,111,112] One of the main reasons for this is that current cryopreservation protocols do not permit the direct transfusion of RBCs immediately after thawing due the use of the penetrating CPA glycerol. Deglycerolization is required post-thaw to reduce intracellular glycerol concentrations to less than 1% prior to transfusion to prevent post-transfusion intravascular hemolysis.[4,111,113-115] This deglycerolization process is complicated, time consuming and is damaging to RBCs resulting in up to a 20% loss of RBC volume. Deglycerolized units must also be transfused in a patient within 24 h.[116,117] However, while current cryopreservation methods are less than ideal for large-scale inventory management,[111] it remains the only technology that can readily deliver multiple units of pre-screened RBCs to patients with rare blood groups or complex alloimmunity, and for military applications where RBC units are required for casualty care in remote areas of the world.[105] Thus, improved cryopreservation methods using nontoxic cryoprotective additives and significantly reduced glycerol concentrations are urgently required.

In Canada and the United States clinical cryopreservation conditions follow high glycerol/slow freeze protocols. 40% v/v glycerol concentrations are utilized along with slow freezing at a rate of 1°C/min and storage at -80 °C to ensure high post-freeze-thaw-deglycerolized recoveries of RBCs after cryopreservation.[4,113] In Europe, clinical cryopreservation protocols typically follow the low glycerol/rapid freeze conditions where glycerol is utilized at 20% v/v and freezing is rapid (greater than 100 °C/min) in liquid nitrogen.[118] While this is an effective freezing method, there are significant drawbacks associated with the protocol that are discussed in more detail in section 1.4.3.[4,111,112] The rapid freezing conditions for the low glycerol method is a necessity to ensure high RBC recoveries post-freeze-thaw and deglycerolization, and slow freezing conditions are detrimental to the RBCs with low glycerol concentrations.[118] However, deglycerolization times with the low glycerol method are half that of the high glycerol method. Thus, there is tremendous interest in Canada and the United States to effectively reduce glycerol concentrations to reduce deglycerolization processing times, without significantly altering the freezing protocols that are currently used clinically.

Research on improving RBC cryopreservation has focused on a number of different aspects of the cryopreservation protocol. A major area has been on improving upon current deglycerolization procedures to allow for faster access to transfusion-ready RBC units post-thaw.[115,117,119-122] In addition, various storage solutions have been examined for their effectiveness for storing deglycerolized RBC units past 24 hours.[119,120,123] Alternative cryoprotectants have also been explored. This has included extracellular non-penetrating CPAs such as HES, PVP or dextran.[4,124-127] Simple carbohydrates and oligosaccharides have also been explored as RBC cryoprotectants, and an active area of research is the use of trehalose along with methods to internalize this non-penetrating disaccharide.[128-131] To date, the use of small molecule ice recrystallization inhibitors for RBC cryopreservation has yet to be explored.

The focus of this section will be on the use of the novel small molecule IRIs described in chapters 6 and 7 as beneficial cryo-additives for the freezing of RBCs. In particular, the phenolic-glucosides were able to effectively reduce post-thaw RBC hemolysis (increase % RBC integrity) in combination with decreased glycerol concentrations (10-15%) utilizing the standard clinical freezing protocol employed in Canada and the United States. This is described in an article that was recently submitted to *Organic and Biomolecular Chemistry* in November 2013. This article is provided in section 8.4.2 and it describes the discovery of β-PMP-Glc (**6**) at a concentration of 110 mM as an effective cryo-additive for the freezing of RBCs with 15% glycerol. These results are summarized in sections 8.4.3 and 8.4.4, along with reproduced figures from the article to complement the discussion. All figures from the article are numbered as they appear within the

manuscript, and any additional figures are numbered starting from figure 8.9. Compound numbers in this chapter are already consistent with the numbering from the article. Any additional compounds described in section 8.4.5 are numbered in sequential order beginning from **9**. In addition to the discovery of β-PMP-Glc (**6**) as a beneficial cryo-additive for RBC freezing, many other phenolic-glycosides were assessed for their cryoprotective ability. These results are discussed in section 8.4.5 and they describe the discovery of β-pBrPh-Glc (**8**) as a more effective cryo-additive at a significantly lower concentration than β-PMP-Glc (**6**). Finally, the RBC samples frozen in the novel cryo-additive solutions containing β-PMP-Glc (**6**) or β-pBrPh-Glc (**8**) we subjected to deglycerolization conditions to quantify final post-freeze-thaw and deglycerolized RBC recoveries. The deglycerolization studies are discussed in sections 8.4.6-8.4.11. All of the RBC cryopreservation studies were done in collaboration with the Research and Development Department of Canadian Blood Services (CBS) in Edmonton, Alberta with Dr. Jason Acker and his laboratory technicians Jayme Kurach, Tracey Turner and Adele Hansen. Thus, many of the protocols used for these are consistent with those employed in a clinical setting at the largest blood bank in Canada (CBS).

8.4.2 Article – "Small Molecule Inhibitors of Ice Recrystallization Enable Freezing of Human Red Blood Cells with Greatly Reduced Quantities of Glycerol"

Organic & Biomolecular Chemistry

RSCPublishing

PAPER

Small molecule inhibitors of ice recrystallization enable freezing of human red blood cells with greatly reduced quantities of glycerol†

Chantelle J. Capicciotti,[a] Jayme D. R. Kurach,[b] Tracey R. Turner,[b] Jason P. Acker[b] and Robert N. Ben*[a]

Cite this: DOI: 10.1039/x0xx00000x

Received ooth January 2012,
Accepted ooth January 2012

DOI: 10.1039/x0xx00000x

www.rsc.org/

Red blood cells (RBCs) are typically cryopreserved in a clinical setting using approximately 40% glycerol with slow cooling (1 °C/min) and storage in a mechanical freezer at -80 °C. This is known as the high glycerol/slow freeze cryopreservation method. To avoid intravascular hemolysis, deglycerolization must be performed prior to transfusion to decrease intracellular glycerol concentrations to less than 1%. This process is both time consuming and expensive, requiring specialized equipment. Small molecule ice recrystallization inhibitors such as β-PMP-Glc (**6**) have the ability to prevent ice recrystallization. The process of ice recrystallization is associated with decreased cell recoveries and function after cryopreservation. Conventional cryoprotectants such as glycerol and dimethyl sulfoxide (DMSO) do not inhibit ice recrystallization but protect cells during cryopreservation through different mechanisms. Our studies indicate that addition of 110 mM β-PMP-Glc (**6**) to a 15% glycerol solution increases post-thaw RBC integrity by 25-30% when slowly cooled to -40 or -50°C and then rapidly frozen and stored at -80 °C. The results from two-step interrupted freezing experiments indicate that β-PMP-Glc is conferring cryoprotection through a mechanism consistent with that of a cell penetrating cryoprotectant. Cryomicroscopy confirms that the structure of ice around frozen human RBCs in the presence of β-PMP-Glc is very different than that observed with glycerol alone. Collectively, these results suggest that small molecule inhibitors of ice recrystallization have an unrealized role as cryoprotectants for the preservation of cells.

Introduction

Red blood cell (RBC) transfusions are lifesaving by increasing RBC mass in patients with low oxygen-carrying capacity resulting from acute blood loss (traumatic/surgical haemorrhage), decreased RBC production in bone marrow (leukemias), or decreased RBC survival (hemolytic anemias).[1] Hypothermic preservation of RBCs has enabled blood banks to ensure a readily available and safe blood supply. However, this clinical biopreservation method is limited to a 42 day storage time period that can result in shortages of blood supplies when high numbers of emergency blood transfusions are required such as in the wake of a natural disaster.[2-4] While cryopreservation of RBC units can extend storage time to 10 years, it is currently limited to rare blood phenotypes, autologous RBC storage and military applications for blood and blood product storage.[1,5,6] One of the main reasons cryopreserved RBC units are not routinely used in transfusion medicine is that current cryopreservation protocols do not

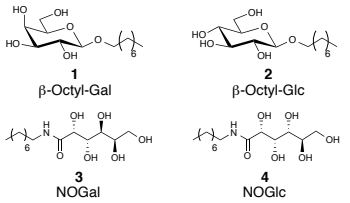

Fig. 1 Structures of the first low molecular weight carbohydrate-based ice recrystallization inhibitors. *n*-Octyl-β-D-galactopyranoside (β-Octyl-Gal, **1**) exhibited potent IRI activity at 22 mM and *N*-octyl-D-gluconamide (NOGlc, **4**) exhibited potent IRI activity at 0.5 mM.

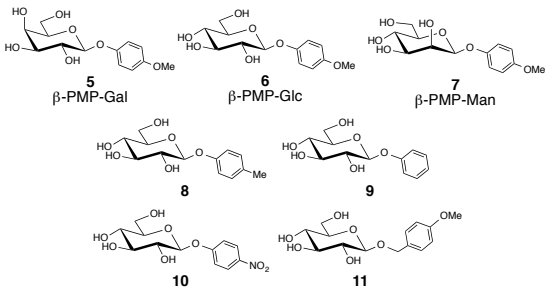

Fig. 2 Structures of phenolic-glycosides β-PMP-Gal (**5**), β-PMP-Glc, (**6**), β-PMP-Man (**7**), phenolic-glucopyranosides **8**-**10** and *para*-methoxybenzyl-β-D-glucopyranoside **11**.

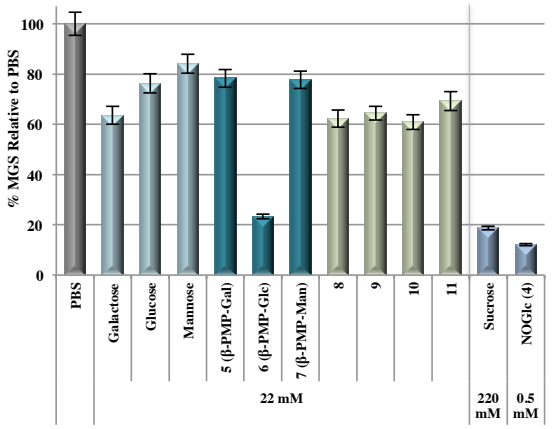

Fig. 3 IRI activity of phenolic-glycosides β-PMP-Gal (**5**), β-PMP-Glc (**6**), β-PMP-Man (**7**), phenolic-glucopyranosides **8**-**10** and *para*-methoxybenzyl-β-D-glucopyranoside **11**. All compounds are represented as a % MGS (mean grain size) of ice crystals relative to the PBS positive control.

permit the direct transfusion of RBCs immediately after thawing. In Canada and the United States, clinical RBC cryopreservation protocols utilize the high glycerol/slow freeze method. High concentrations of the permeating cryoprotectant glycerol (> 40% v/v) are used with slow cooling 1 °C/minute and storage at -80 °C in a mechanical freezer to ensure high recovery of RBCs.[1,7] However, complicated and time consuming post-thaw deglycerolization procedures are necessary to ensure glycerol concentrations are reduced to less than 1% prior to transfusion to prevent post-transfusion intravascular hemolysis.[5,7-9] More over, these units must be transfused within 24 hours imposing challenging logistics due to significant time and/or distance constraints on the transportation of cryopreserved RBCs.[10,11] While current cryopreservation methods are less than ideal for large-scale inventory management,[5] it remains the only technology that can readily deliver multiple units of pre-screened RBCs to patients with rare blood groups or complex alloimmunity, and for military applications where RBC units are required for casualty care in remote areas of the world.[12] Thus, improved cryopreservation methods using nontoxic cryoprotective additives are urgently required.

Ice recrystallization during the freezing and thawing of cryopreservation is a significant contributor to cellular damage and death.[13-15] As a consequence, there has been tremendous interest in designing compounds that inhibit ice recrystallization to function as novel cryoprotectants.[16-20] Our laboratory has recently reported the rational design and synthesis of glycoconjugates[21-23] and small molecules (Fig. 1)[24,25] that are potent inhibitors of ice recrystallization. We hypothesize that inhibiting ice recrystallization using these compounds will reduce cellular injury during cryopreservation and enhance the post-thaw recovery of cells with specialized cellular functions.[23,26] In this paper we describe a novel small molecule phenolic-glycoside (β-PMP-Glc, **6)** that is an effective inhibitor of ice recrystallization. This compound is also an effective cryo-additive capable of decreasing the amount of post-thaw hemolysis of human RBCs (increasing post-thaw RBC integrity) in the presence of reduced amounts of glycerol using rate-controlled slow cooling conditions. This result has tremendous potential for improving RBC cryopreservation protocols by reducing post-thaw deglycerolization processing times.

Results and discussion

Ice recrystallization inhibition (IRI) activity of phenolic-glycosides

Prior work by our laboratory has demonstrated that amphiphilic small molecule carbohydrate derivatives (Fig. 1) and lysine-based derivatives can be potent inhibitors of ice recrystallization.[24,25] In these examples, the hydrophobic portion was an alkyl chain of varying length. While these molecules exhibited potent IRI activity, they also possessed surfactant-like characteristics, which can be detrimental to cells and cell membranes. In the present study we chose to employ an aryl ring as a hydrophobic moiety instead of an alkyl chain. Consequently, phenolic-glycosides of D-galactose, D-glucose and D-mannose containing a β-linked *para*-methoxyphenyl (PMP) moiety (Fig. 2) were synthesized (supplementary information) and assessed for their ability to inhibit ice recrystallization. IRI activity was assessed using a splat-cooling assay[27] where the area of ice crystals were measured after annealing at -6.4 °C for 30 minutes using a domain recognition software, resulting in a quantitative measurement of the mean ice grain size.[28] IRI activity is represented as a ratio of the mean grain size (MGS) of the sample to a phosphate buffered saline (PBS) solution, a positive control for ice recrystallization. Thus, smaller MGS values indicate smaller ice crystal sizes and greater IRI activity.

The D-galactose derivative β-PMP-Gal (**5**) and D-mannose derivative β-PMP-Man (**7**) both exhibited weak IRI activity that was similar to that exhibited by D-mannose (Fig. 3). This preliminary data suggested that an aryl group may not be a suitable hydrophobic substitute for an alkyl chain because

This iournal is © The Roval Societv of Chemistrv 2012

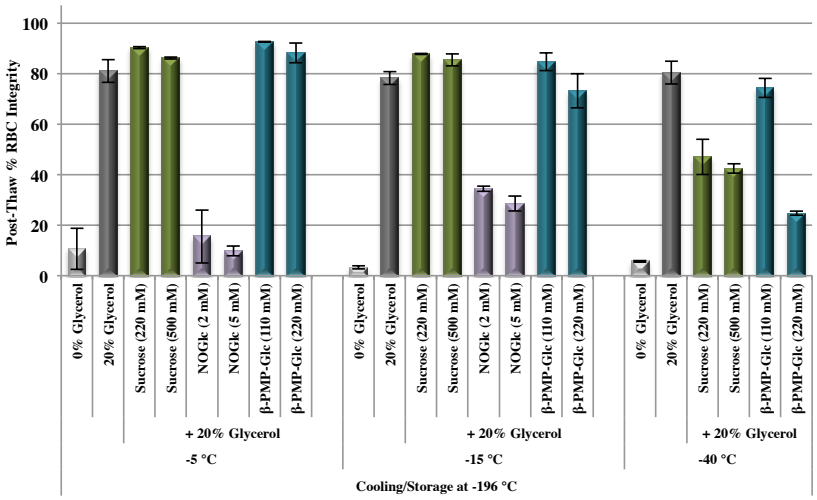

Fig. 4 The effect of novel IRI active small molecules NOGlc (**4**, Fig.1), β-PMP-Glc (**6**) and sucrose on post-thaw RBC integrities. RBC samples in indicated cryo-solutions were slow-cooled 1 °C/min to defined sub-zero temperatures and subsequently rapidly cooled and stored in liquid nitrogen (-196 °C) prior to thawing at 37 °C. % hemolysis was quantified post-thaw using Drabkin's assay to determine % RBC integrity (100 - % hemolysis).

β-Octyl-Gal (**1**, Fig. 1) was a potent inhibitor of ice recrystallization while β-PMP-Gal (**5**) was much less active at equimolar concentration.[24] However, the D-glucose derivative β-PMP-Glc (**6**) exhibited potent IRI activity and was significantly more active than β-PMP-Gal (**5**) and β-PMP-Man (**7**). In fact, β-PMP-Glc (**6**) exhibited potent activity very similar to the previously reported non-ionic surfactant β-Octyl-Gal (**1**) at equimolar concentration. β-PMP-Glc (**6**) also exhibited comparable IRI activity to a 220 mM solution of sucrose, which is commonly utilized in many cryopreservation solutions.[26]

Our laboratory has previously correlated IRI activity to carbohydrate hydration and reported that highly hydrated monosaccharides, such as D-galactose were more IRI active than less hydrated monosaccharides such as D-glucose and D-mannose.[29] For example, the non-ionic pyranose-based surfactant possessing a highly hydrated D-galactose head group (β-Octyl-Gal, **1**, Fig. 1) was significantly more IRI active than the surfactant possessing the less hydrated D-glucose head group (β-Octyl-Glc, **2**).[24] The fact that the D-glucopyranose derivative β-PMP-Glc (**6**) exhibited potent IRI activity and was significantly more IRI active than D-galactopyranose derivative β-PMP-Gal (**5**) (Fig. 3) is unprecedented and thus is the first example where a pyranose-based derivative possessing a D-glucose moiety has been significantly more active than one containing a D-galactose moiety. Furthermore, it was also surprising that both β-PMP-Gal (**5**) and β-PMP-Man (**7**) exhibited identical IRI activities despite the difference in hydration between these two pyranose residues.[22,29,30] A plausible explanation for these results is that the hydration characteristics of **5**-**7** are very different than the parent monosaccharides due to the presence of the PMP moiety. While hydration numbers or molar compressibilities of **5**-**7** are not known, we chose to investigate the influence of the PMP group on IRI activity. Towards this end, β-linked phenolic-glucosides were prepared in which the *para*-methoxy substituent on the aglycone was substituted with a methyl (**8**), hydrogen (**9**), or nitro group (**10**, structures shown in Fig. 2) and assessed for IRI activity (Fig. 3). All of these derivatives exhibited similar IRI activity and more importantly were significantly less active than β-PMP-Glc (**6**). In addition, the β-linked *para*-methoxybenzyl derivative (**11**) possessing a methylene spacer between the *O*-glycosidic bond and the aryl ring exhibited a similar decrease in activity. These preliminary results indicate that for these glucopyranoside derivatives, an electron rich aryl ring with direct connection to the C1 oxygen is essential for IRI activity. The degree to which this substituent affects the hydration characteristics of the molecule is currently not known.

Freezing of red blood cells (RBCs) with IRI active small molecules

The freezing of human RBCs was carried out using a two-step interrupted freezing protocol (see supplementary information) to assess the effectiveness of small molecule ice recrystallization inhibitors as cryo-additives.[31-33] In this protocol, RBCs suspended in the cryoprotectant solution were cooled to -5 °C where ice nucleation was induced. Samples were cooled at a rate of 1 °C/min to pre-defined sub-zero temperatures then rapidly cooled to -196 °C (plunged into liquid nitrogen) for storage prior to thawing. Samples were thawed under fast-thawing conditions in a 37 °C water bath and

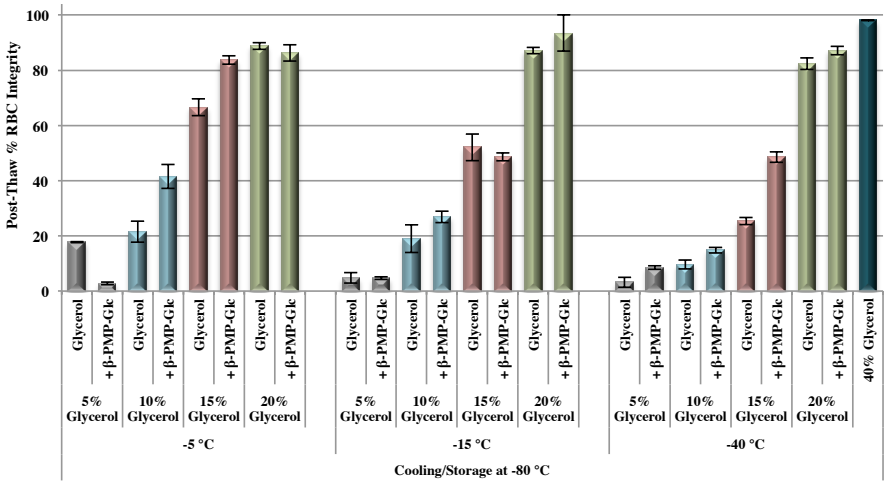

Fig. 5 The effect of β-PMP-Glc (**6**) on post-thaw RBC integrity (100 - % hemolysis) using reduced concentrations of glycerol. RBC samples in glycerol solutions with or without 110 mM β-PMP-Glc (**6**) were slow cooled 1 °C/min to defined sub-zero temperatures and subsequently rapidly cooled and stored at -80 °C prior to thawing at 37 °C.

post-thaw hematocrits were measured. Hemolysis was quantified utilizing Drabkin's assay.[34,35] The two-step interrupted freezing protocol provides valuable information with respect to the mechanisms of cryoinjury and more importantly can indicate how a cryoprotectant is functioning.[32] The percent of post-thaw RBC integrity (100 - % hemolysis) obtained after freezing and thawing is shown in Fig. 4.

Two different glucose-based IRI active small molecules, NOGlc (Fig. 1, **4**) and β-PMP-Glc (**6**), were assessed for their effectiveness as cryo-additives for the freezing human RBCs. Previous work conducted by our laboratory reported that simple carbohydrates were more effective cryoprotectants at concentrations approximately ten times greater than the concentration at which they are IRI active.[26] Thus, NOGlc (**4**), which is IRI active at 0.5 mM (Fig. 3),[24] was used in cryo-solutions at 2 mM or 5 mM concentrations while β-PMP-Glc (**6**) was used at 110 mM or 220 mM. Additionally, sucrose was examined as an additive for RBC freezing at 220 mM and 500 mM as it has previously been reported to have potent IRI activity and be effective at cryopreserving human embryonic liver cells.[26] The cryo-solutions used contained either 0% or 20% glycerol (low glycerol conditions) in addition to the novel IRI active small molecules and all results were compared to a 20% glycerol control.

From the data presented in Fig. 4 it is evident that sucrose and NOGlc (**4**) were not effective cryo-additives for RBCs as a decrease in post-thaw RBC integrity is observed with these solutions. NOGlc in a 20% glycerol solution resulted in significant post-thaw RBC hemolysis with only 34% (± 1.0) RBC integrity. The % post-thaw integrity for the 20% glycerol control was 80% (± 4.5). 220 mM and 500 mM solutions of sucrose in 20% glycerol resulted in post-thaw integrities identical to those obtained with the 20% glycerol controls when samples were rapidly cooled and stored in liquid nitrogen from -5 °C or -15 °C. However, integrities were reduced to 40-45% when slow-cooled to -40 °C prior to rapid cooling/storage at –196 °C. It is important to note that without the addition of glycerol to the cryoprotective solutions the compounds were not effective additives and had post-thaw RBC integrities identical to those obtained from a saline solution containing no glycerol (supplementary information Fig. S1).

Interestingly, a 110 mM solution containing the small molecule ice recrystallization inhibitor β-PMP-Glc (**6**) in 20% glycerol resulted in equal or slightly higher post-thaw RBC integrities than the 20% glycerol control upon cooling to -5 °C or -15 °C prior to rapid cooling/–196 °C storage. The post-thaw integrities when cooled to -5 °C were 93% (± 0.1) when the solution contained 110 mM β-PMP-Glc and 81% (± 4.5) for the 20% glycerol control. When cooled to -15 °C post-thaw integrities were 85% (± 3.5) when the solution contained 110 mM β-PMP-Glc and 78% (± 3.5) with only 20% glycerol. The 20% glycerol cryo-solutions with or without 110 mM β-PMP-Glc had identical post-thaw integrities when slowly cooled to -40 °C prior to rapid cooling/storage at –196 °C. However, post-thaw integrities were significantly decreased when 220 mM β-PMP-Glc was used (25% ± 0.9) with the same freezing conditions.

The results obtained with cryo-solutions containing 110 mM β-PMP-Glc (**6**) were very encouraging and suggested that this compound may be a beneficial additive for the cryopreservation of RBCs. This was the only instance where the post-thaw integrity of RBCs was similar to or better than

 This journal is © The Royal Society of Chemistry 2012

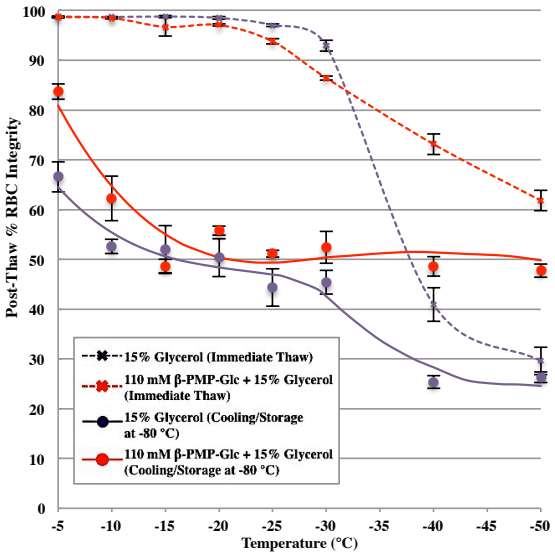

Fig. 6 The effect of 15% glycerol cryo-solutions with or without 110 mM β-PMP-Glc (**6**) on post-thaw RBC integrity (100 - % hemolysis). Samples were slow cooled 1 °C/min to defined sub-zero temperatures then either immediately thawed ("cooling" curves, dashed lines) or rapidly cooled and stored at -80 °C prior to thawing at 37 °C ("cooling/storage" curves, solid lines).

the 20% glycerol control. A 20% glycerol solution alone is a very effective cryoprotectant for RBCs and is used clinically in European countries with the low glycerol/rapid freeze (>100°C/min to -196 °C) method for RBC cryopreservation.[1,5,36,37] Fast freezing rates must be employed in this method to ensure adequate post-thaw and deglycerolization recoveries of the RBCs with the lower concentration of glycerol. However, in Canada and the United States, clinical cryopreservation protocols use 40% glycerol (high glycerol) so a slow rate-controlled freezing protocol (1 °C/min) is employed with storage in a freezer at -80 °C.[1,4,8,38] Consequently, the increase in post-thaw RBC recoveries observed with the 110 mM β-PMP-Glc solution using slow freezing conditions was very promising. Given the potential benefits to using reduced glycerol concentrations in the clinical setting (i.e. decreased post-thaw deglycerolization processing times), we investigated the ability of β-PMP-Glc to effectively freeze RBCs to -80°C utilizing reduced concentrations of glycerol.

Freezing of RBCs using β-PMP-Glc in the presence of reduced glycerol concentrations

Solutions containing 110 mM β-PMP-Glc with 5, 10, 15 or 20% (wt/vol) glycerol were used to freeze human RBCs with the interrupted freezing protocol described previously (also see supplementary information).[31-33] Samples were cooled at a rate of 1 °C/min to the indicated sub-zero temperature and then rapidly frozen to -80 °C. This cooling rate and -80 °C storage temperature was selected as these more closely reflect clinical RBC cryopreservation protocols utilized in Canada and the United States. The post-thaw RBC integrities with rate-controlled cooling to different sub-zero temperatures are shown in Fig. 5. A 20% glycerol solution either with or without 110 mM β-PMP-Glc resulted in post-thaw integrities were similar to those observed at -196 °C storage temperatures for all cooling conditions (refer to Fig. 4 for -196 °C storage temperatures). Low post-thaw RBC integrities were observed with 5% and 10% glycerol solutions indicating these concentrations of glycerol used in conjunction with a slow cooling rate are not effective for the freezing RBCs (Fig. 5). However, the addition of 110 mM β-PMP-Glc to the 10% glycerol solution increased post-thaw integrities from 21% ± 3.8 (for 10% glycerol) to 42% ± 4.3 when RBC samples were held at -5 °C and nucleated prior to rapid cooling/storage at -80 °C.

The advantage of adding 110 mM β-PMP-Glc to the glycerol solution is most evident with a 15% glycerol solution where upon cooling to -5 °C and rapid cooling to -80 °C, RBC integrity increased from 67% ± 3.8 (for 15% glycerol) to 84% ± 1.4 with β-PMP-Glc (Fig. 5). Interestingly, post-thaw integrities were identical when samples were cooled to -15 °C prior to rapid cooling to -80°C (approximately 50%). However, β-PMP-Glc doubled the post-thaw integrity of RBCs when slow-cooled to -40 °C prior to storage at -80 °C (49% ± 1.9 with β-PMP-Glc versus 25% ± 1.3 for 15% glycerol). This increase is significant as it has been previously demonstrated that storage at -80 °C with low glycerol concentrations (typically less than 40%) is detrimental and RBC recoveries are much lower than those observed at -196 °C.[36]

With these promising results, experiments were designed that would provide insight into whether β-PMP-Glc was protecting RBCs during the slow cooling stage and/or during the rapid cooling to -80 °C stage of the freezing process. To accomplish this, a two-step interrupted freezing protocol to sub-zero temperatures between -5 to -50 °C was utilized where samples were either thawed immediately from the defined sub-zero temperature (see "cooling" profiles in Fig. 6) or rapidly cooled and stored at -80 °C prior to thawing (see "cooling/storage" profiles in Fig. 6).[33]

The "cooling" profile (Fig. 6, dashed lines) for the 15% glycerol control is typical of that observed with a cell penetrating cryoprotectant where a progressive decrease in post-thaw RBC integrity is observed at lower sub-zero temperatures. Higher RBC post-thaw integrities are observed at temperatures above -30 °C (Fig. 6). This is presumably due to the colligative effects of glycerol and its ability to decrease the amount of ice present at any sub-zero temperature thus delaying and mitigating osmotic pressures that ultimately result in cellular damage.[33,39] The poorer post-thaw RBC integrities observed upon slow cooling to lower sub-zero temperatures (i.e. below -30 °C) are a result of cellular damage due to concentrating solutes, consistent with the two factor hypothesis of freezing injury.[39] However, when β-PMP-Glc (110 mM) is added to the 15% glycerol solution, we observe a progressive increase in RBC integrity at lower sub-zero cooling temperatures. For instance, at -40 °C, RBC integrity with the 15% glycerol solution is 41% ± 3.9 and this is increased to

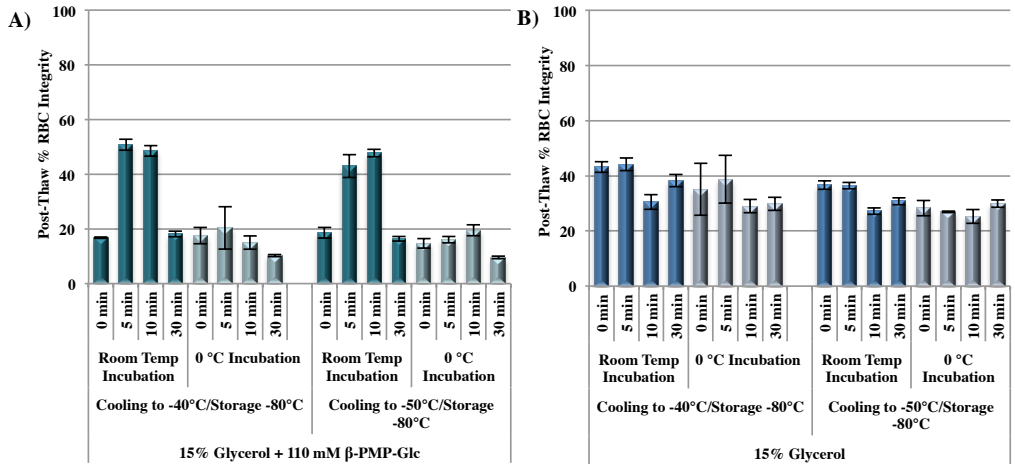

Fig. 7 The effect of pre-incubation of cryo-solutions on post-thaw RBC integrity. **A)** RBC samples were incubated for indicated time and at indicated temperature with a 110 mM β-PMP-Glc + 15% glycerol solution prior to freezing using an interrupted freezing protocol. **B)** RBC samples were incubated for indicated time and at indicated temperature with a 15% glycerol solution prior to freezing using an interrupted freezing protocol.

73% ± 3.9 with the addition of 110 mM β-PMP-Glc. Significantly better post-thaw RBC integrities were also obtained with β-PMP-Glc at -50 °C (62% ± 2.0) compared to the 15% glycerol solution (29% ± 2.8). The fact that the addition of β-PMP-Glc to the 15% glycerol freezing solution resulted in less hemolysis (increased integrities) under the slow-cooling/immediate thaw conditions is consistent with the profile of a cell penetrating cryoprotectant,[33] suggesting that β-PMP-Glc is being internalized in the RBCs. However, it is also plausible that a synergistic effect between the internalized glycerol and inhibition of ice recrystallization in the extracellular environment due to β-PMP-Glc may be occurring. Irrespective of the mechanism of action, these results clearly demonstrate that β-PMP-Glc provides additional protection during the slow-cooling phase of the freezing protocol when added to a 15% glycerol solution (low glycerol conditions).

When samples were rapidly cooled to -80 °C after slow cooling to sub-zero temperatures, different profiles were obtained (Fig. 6, solid lines). Freezing of RBCs using a 15% glycerol solution resulted in drastically decreased integrities. As the temperature to which the samples were slow-cooled was decreased, integrities also decreased averaging between 45-55% when cooled to temperatures between -10 °C and -30 °C prior to rapid cooling and storage at -80°C. When cooled to temperatures lower than -30 °C, RBC integrities further decreased to approximately 25%. The higher post-thaw integrities at temperatures above -30 °C can be attributed to the rapid cooling being initiated at higher sub-zero temperatures. This would create an overall faster cooling rate to the -80 °C storage temperature. These results are consistent with the need for a rapid cooling rate for the cryopreservation of RBCs when using lower concentrations of glycerol.[36,40,41] When 110 mM β-PMP-Glc is added to 15% glycerol, post-thaw RBC integrities are 5 - 15% better at all sub-zero cooling temperatures higher than -30 °C. Interestingly, β-PMP-Glc appears to have the greatest affect when freezing conditions involve slow cooling to -40 or -50 °C prior to rapid freezing to -80 °C. The post-thaw RBC integrities are approximately 50% when the solution contains β-PMP-Glc, which is double that of the 15% glycerol solution alone.

Collectively, the results from the interrupted freezing protocol experiments indicate that β-PMP-Glc (**6**) can significantly decrease post-thaw RBC hemolysis (increase integrities) when added to a 15% glycerol solution as it confers protection during the slow-cooling stage of the freezing protocol. Furthermore β-PMP-Glc is protecting during rapid cooling to -80 °C regardless of the initial sub-zero cooling temperature resulting in less hemolysis than the 15% glycerol control. The greatest benefit of this cryo-additive is observed with lower sub-zero cooling temperatures (-40 or -50 °C), which is significant as these freezing conditions mimic RBC clinical cryopreservation protocols that utilize slow freezing rates but high glycerol concentrations (i.e. 40% glycerol).

Pre-incubation studies and cryomicroscopy

The cryoprotective ability of glycerol is largely attributed to its ability to penetrate cells and it is well established that RBCs are highly permeable to glycerol.[42-44] Transport of glucose across human RBC membranes readily occurs through facilitated diffusion, a process that is mediated by glucose transporters (GLUTs) that are expressed in high levels on the surface of RBCs.[45,46] However, uptake of glucose and glucose derivatives is dependant upon hydroxyl group stereochemistry and the "shape" of the molecule.[47,48] Thus, glucose derivatives may not

 This journal is © The Royal Society of Chemistry 2012

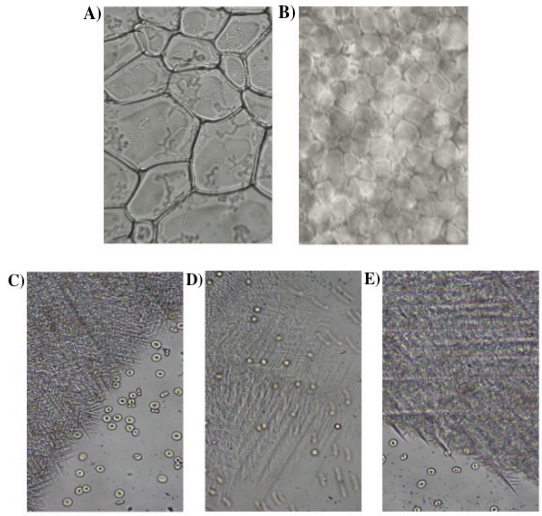

Fig. 9 Photographs illustrating the IRI activity of β-PMP-Glc (**6**) and the advancing ice-front during RBC freezing. **A-B)** Ice crystal grains from a frozen **(A)** PBS solution, or **(B)** 22 mM β-PMP-Glc solution in PBS annealed at -6.4 °C for 30 mins in a splat-cooling assay. **C-E)** Advancing ice fronts during RBC freezing in the presence of 110 mM β-PMP-Glc + 15% glycerol solution **(C)**, 110 mM β-PMP-Glc in dextrose/saline solution **(D)**, or 15% glycerol solution **(E)**.

be transported or the rate of transport may be considerably decreased depending on their structure. As the freezing data presented in the previous section suggest that β-PMP-Glc may be conferring protection against cryo-injury through a mechanism consistent with a cell penetrating cryoprotectant, we sought to explore if the observed increase in post-thaw integrities was the result of internalization of β-PMP-Glc. Towards this end, suspensions of RBCs in 15% glycerol containing 110 mM β-PMP-Glc cryoprotective solution were incubated for 0, 5, 10 and 30 min time periods at room temperature or 0°C as it has previously been demonstrated that the rate of sugar transport can be considerably slowed at 0°C.[49] After incubation, freezing of the samples was conducted using the two-step interrupted freezing protocol described previously with slow cooling to -40 °C or -50 °C followed by rapid cooling to -80 ^{o}C and storage prior to thawing. Post-thaw RBC integrities from these experiments are shown in Fig. 7.

From the data described in Fig. 7A it is evident that the optimal incubation times of RBCs with the 15% glycerol/β-PMP-Glc solution is 5 to 10 min at room temperature. Post-thaw integrities for these time periods were similar for both freezing conditions (approximately 50%). In contrast, suspension of RBCs with the 15% glycerol/β-PMP-Glc solution followed by immediate freezing yielded RBC integrities less than 20% at -40 and -50 ^{o}C. Interestingly, a similar decrease in post-thaw RBC integrity was also observed upon incubation for 30 min at room temperature prior to freezing. This was surprising and suggested a cytotoxic effect of β-PMP-Glc may be associated with long incubation times. However, less than 1% hemolysis (>99% RBC integrity) was observed upon incubation of RBCs with β-PMP-Glc for 60 min at room temperature without freezing (supplementary information, Fig. S2), indicating that hemolysis is not occurring during the pre-incubation stage of the protocol.

Incubation of RBCs at 0 °C in the 15% glycerol/β-PMP-Glc solution for 5 and 10 min prior to freezing also resulted in decreased post-thaw integrity (Fig. 7A). This drastic decrease at 0 °C was only observed when β-PMP-Glc was added to the freezing solution as a 15% glycerol solution containing no β-PMP-Glc resulted in similar post-thaw integrities independent of incubation time or temperature (approximately 20-35%, Fig. 7B). While the permeability of glycerol into cells is temperature dependent,[33] the rate at which glycerolization occurs in RBCs is fast even at 0 °C.[43] Thus, at the lower temperatures and shorter incubation times, the RBCs are likely glycerolized prior to freezing. Overall, this data is consistent with the hypothesis that the transport of β-PMP-Glc into RBCs is occurring and is important for its protective effect during freezing as slowing the rate of sugar transport at 0°C resulted in a decrease in post-thaw RBC integrity. However, further studies are required to determine the quantity and rate of its transport into RBCs.

As β-PMP-Glc is a potent inhibitor of ice recrystallization, it is expected to affect the structure of ice in a frozen sample, ultimately decreasing the overall size of individual ice crystals. This is anticipated to result in less mechanical damage to the cells and higher post-thaw integrity. Fig. 9A shows images of the ice crystals observed for the phosphate buffered saline (PBS) control used in the IRI assay. PBS is a positive control for ice recrystallization and the ice crystals have an average size of 20-40 μm. In contrast, Fig. 9B depicts ice crystals of a 22 mM β-PMP-Glc (**6**) solution in PBS. The magnification of Figs. 9A and B are identical and as expected, the average size of ice crystals in the presence of β-PMP-Glc is much smaller. Cryomicroscopy experiments have also confirmed that the structure of ice during the freezing process with RBCs is also different when β-PMP-Glc is utilized. In fact, depending on the cryoprotective solution used, the structure of ice in the frozen sample differs dramatically. Figs. 9C-E depict images of RBCs frozen on a Linkam cryostage and imaged using a Nikon 80i microscope. RBCs were frozen in the presence of a 110 mM β-PMP-Glc solution with (9C) and without 15% glycerol (9D). The image in Fig. 9E is of RBCs frozen using only a 15% glycerol solution. These images show the advancing ice-front (photographed during the freezing of the sample) in the different cryoprotective solutions. All three solutions resulted in a very different structure of ice during freezing. The most interesting images are those shown in Fig. 9C and 9E which are the 15% glycerol solution both with and without β-PMP-Glc where the ice structure in the presence of β-PMP-Glc is very different and we obtain significantly increased post-thaw RBC integrities. This is the first example where a novel small molecule ice recrystallization inhibitor as a beneficial cryo-additive is confirmed to influence ice structure in the presence of RBCs cells *in vitro*.

Conclusions

Typical clinical cryopreservation protocols for RBCs rely on using high amounts of glycerol (approximately 40%) combined with rate controlled freezing (1 °C/min) to storage at -80 °C. Following thawing, deglycerolization must be performed prior to transfusion and this process is labor-intensive, costly and time-consuming.

Small molecule ice recrystallization inhibitors such as β-PMP-Glc have potential applications in the cryopreservation of biological materials and represent a novel class of cryoprotectants. We have demonstrated that a 110 mM solution of β-PMP-Glc (**6**) is capable of increasing post-thaw RBC integrities when utilized in combination with 15% glycerol for the freezing of human RBCs. More importantly, we have demonstrated that it is possible to do this using slow cooling conditions to -80 °C with reduced glycerol concentrations (significantly less than 40%). In this instance, RBC integrities are double that observed with glycerol alone (50% with β-PMP-Glc versus 25% without). Analysis of the post-thaw RBC integrities using the two-step interrupted freezing protocol suggests that β-PMP-Glc (**6**) is internalized into the RBCs. Incubation of RBCs with the 110 mM β-PMP-Glc/15% glycerol solution for up to 60 min at room temperature did not result in hemolysis. However, incubation of β-PMP-Glc at 0 °C prior to freezing resulted in decreased RBC integrity post-thaw suggesting that β-PMP-Glc is functioning as a penetrating cryoprotecant. These results constitute the first reported example of a novel small molecule ice recrystallization inhibitor that is able to increase integrities of human RBCs using lower glycerol concentrations and slow-cooling freezing protocols to a temperature of -80 °C. The exact mechanism by which β-PMP-Glc is protecting human RBCs from cryoinjury is currently being investigated and will be reported in due course.

Acknowledgements

The authors acknowledge the Natural Sciences and Engineering Research Council of Canada (NSERC), Canadian Blood Services (CBS) and Canadian Foundation for Innovation (CFI) for financial support. The views expressed herein do not necessarily represent the view of the federal government. C. J. C. thanks CBS for a Graduate Fellowship Program (GFP) award.

Notes and references

1 K. L. Scott, J. Lecak and J. P. Acker, *Transfus. Med. Rev.*, 2005, **19**, 127.
2 T. Kanias and J. P. Acker, *FEBS J.*, 2010, **277**, 343.
3 G. Ramsey, *Transfusion*, 2008, **48**, 2053.
4 C. F. Högman, *Vox Sang.*, 1998, **74**, 177.
5 J. R. Hess, *Transfus. Med.*, 2004, **14**, 1.
6 J. R. Hess and T. G. Greenwalt, *Transfus. Med. Rev.*, 2002, **16**, 283.
7 *American Association of Blood Banks Technical Manual*, American Association of Blood Banks, Bethesda, MD, 2006.
8 H. T. Meryman and M. Hornblower, *Transfusion*, 1972, **12**, 145.
9 C. R. Valeri, G. Ragno, L. E. Pivacek, R. Srey, J. R. Hess, L. E. Lippert, F. Mettille, R. Fahie, E. M. O'Neill and I. O. Szymanski, *Transfusion*, 2001, **41**, 933.
10 C. C. M. Lelkens, F. Noorman, J. G. Koning, R. Truijens-de Lange, P. S. Stekkinger, J. C. Bakker, J. W. M. Lagerberg, A. Brand and A. J. Verhoeven, *Transfusion*, 2003, **43**, 157.
11 N. Bandarenko, J. Cancelas, E. L. Snyder, S. N. Hay, N. Rugg, T. Corda, A. D. Joines, J. F. Gormas, G. P. Pratt, R. Kowalsky, M. Rose, L. Rose, J. Foley and M. A. Popovsky, *Transfusion*, 2007, **47**, 680.
12 J. L. Holovati, J. L. Hannon, M. I. C. Gyongyossy-Issa and J. P. Acker, *Transfus. Med. Rev.*, 2009, **23**, 25.
13 P. C. Mazur, *Science*, 1970, **168**, 939.
14 P. Mazur, *Am. J. Physiol. - Cell Physiol.*, 1984, **247**, C125.
15 A. Fowler and M. Toner, *Ann. N.Y. Acad. Sci.*, 2005, **1066**, 119.
16 J. Garner and M. M. Harding, *ChemBioChem*, 2010, **11**, 2489.
17 R. Peltier, M. A. Brimble, J. M. Wojnar, D. E. Williams, C. W. Evans and A. L. DeVries, *Chem. Sci.*, 2010, **1**, 538.
18 M. I. Gibson, *Polym. Chem.*, 2010, **1**, 1141.
19 M. I. Gibson, C. A. Barker, S. G. Spain, L. Albertin and N. R. Cameron, *Biomacromolecules*, 2009, **10**, 328.
20 C. J. Capicciotti, M. Doshi and R. N. Ben, in *Recent Developments in the Study of Recrystallization*, ed. P. Wilson, InTech, New York, 2013, pp. 177-224.
21 S. Liu and R. N. Ben, *Org. Lett.*, 2005, **7**, 2385.
22 P. Czechura, R. Y. Tam, E. Dimitrijevic, A. V. Murphy and R. N. Ben, *J. Am. Chem. Soc.*, 2008, **130**, 2928.
23 M. Leclère, B. K. Kwok, L. K. Wu, D. S. Allan and R. N. Ben, *Bioconjugate Chem.*, 2011, **22**, 1804.
24 C. J. Capicciotti, M. Leclère, F. A. Perras, D. L. Bryce, H. Paulin, J. Harden, Y. Liu and R. N. Ben, *Chem. Sci.*, 2012, **3**, 1408.
25 A. K. Balcerzak, M. Febbraro and R. N. Ben, *RSC Adv.*, 2013, **3**, 3232.
26 J. L. Chaytor, J. M. Tokarew, L. K. Wu, M. Leclère, R. Y. Tam, C. J. Capicciotti, L. Guolla, E. von Moos, C. S. Findlay, D. S. Allan and R. N. Ben, *Glycobiology*, 2012, **22**, 123.
27 C. A. Knight, J. Hallett and A. L. DeVries, *Cryobiology*, 1988, **25**, 55.
28 J. Jackman, M. Noestheden, D. Moffat, J. P. Pezacki, S. Findlay and R. N. Ben, *Biochem. Biophys. Res. Commun.*, 2007, **354**, 340.
29 R. Y. Tam, S. S. Ferreira, P. Czechura, J. L. Chaytor and R. N. Ben, *J. Am. Chem. Soc.*, 2008, **130**, 17494.
30 S. A. Galema and H. Høiland, *J. Phys. Chem.*, 1991, **95**, 5321.
31 J. L. Holovati, M. I. C. Gyongyossy-Issa and J. P. Acker, *Cryobiology*, 2009, **58**, 75.
32 J. Farrant, C. A. Walter, H. Lee and L. E. McGann, *Cryobiology*, 1977, **14**, 273.
33 L. E. McGann, *Cryobiology*, 1978, **15**, 382.
34 D. L. Drabkin, *Am. J. Med. Sci.*, 1948, **215**, 110.
35 S. O. Sowemimo-Coker, *Transfus. Med. Rev.*, 2002, **16**, 46.
36 A. W. Rowe, E. Eyster and A. Kellner, *Cryobiology*, 1968, **5**, 119.
37 H. W. Krijnen, J. J. F. M. de Wit, A. C. J. Kuivenhoven, J. A. Loos and H. K. Prins, *Vox Sang.*, 1964, **9**, 559.
38 H. T. Meryman, *Transfus. Med. Rev.*, 1989, **3**, 121.

 This journal is © The Royal Society of Chemistry 2012

8.4.3 Freezing of RBCs using β-PMP-Glc in the Presence of Reduced Glycerol Concentrations

Sucrose, NOGlc (**4**) and β-PMP-Glc (**6**) were assessed for their cryoprotective ability with human RBCs.[132] These results were presented in Fig. 4 in the article provided in section 8.4.2, and this data is reproduced below. RBC freezing was carried out using a two-step interrupted freezing protocol.[23,128,133] In this protocol, RBCs suspended in the cryoprotectant solution were cooled to -5°C where ice nucleation was induced. Samples were then cooled at a rate of 1°C/min to pre-defined sub-zero temperatures then rapidly cooled and stored at -196 °C by plunging into liquid nitrogen. The two-step interrupted freezing protocol provides valuable information with respect to the mechanisms of cryoinjury and more importantly can indicate how a cryoprotectant is functioning (this is discussed in greater detail in section 8.4.4).[23,133] Samples were thawed under fast-thaw conditions at 37°C, and post-thaw hematocrits (Hct, packed RBC volume) were measured and hemolysis was quantified utilizing Drabkin's assay.[134,135] Drabkin's assay is the standard assay used to determine RBC hemolysis by comparing total and supernatant hemoglobin quantities. The ferrous ions (Fe^{2+}) of hemoglobin (Hgb) are oxidized to ferric ions (Fe^{3+}) to form methemoglobin (metHgb) that reacts with cyanide ions to produce cyanmethemoglobin. The amount of cyanmethemoglobin can be quantified spectrophotometrically to determine Hgb in the sample by comparison to known standards of Hgb.[34,35136] Percent hemolysis is calculated according to equation 8.1 using the Hct and the measured supernatant Hgb (Hgb_S) and the total Hgb in the RBC sample (Hgb_T). RBC freezing results are reported as the percent post-thaw RBC integrity (100 - % hemolysis), which indicates the quantity of RBCs that were not hemolyzed during the freezing and thawing process.

$$\% \text{ Hemolysis} = ((100\text{-Hct}) \times Hgb_S)/Hgb_T$$

Equation 8.1 % Hemolysis as determined by Drabkin's assay.

The cryo-solutions used for the initial assessment of the cryopreservation ability of the novel IRI active molecules with RBCs contained either 0% or 20% glycerol (low glycerol conditions) and all results were compared to a 20% glycerol control (Fig. 4). It is evident that sucrose and NOGlc (**4**) were not effective cryo-additives for RBCs as a decrease in post-thaw RBC integrity is observed with both of these solutions. NOGlc in a 20% glycerol solution resulted in significant hemolysis with a maximum of only 34% RBC integrity for all freezing conditions.[132] The % post-thaw integrity for the 20% glycerol control was ~80%. When samples were rapidly cooled and stored in liquid nitrogen from -5 °C or -15 °C, both solutions of sucrose (220 and 500 mM) in 20% glycerol resulted in post-thaw integrities identical to the 20% glycerol controls. However, integrities were reduced to 40-45% when slow-cooled to -40 °C prior to rapid cooling/storage at –196 °C. Without the addition of glycerol to the cryoprotective solutions the compounds were not

effective additives and had post-thaw RBC integrities identical to those obtained from a saline solution containing no glycerol (figure 8.9).

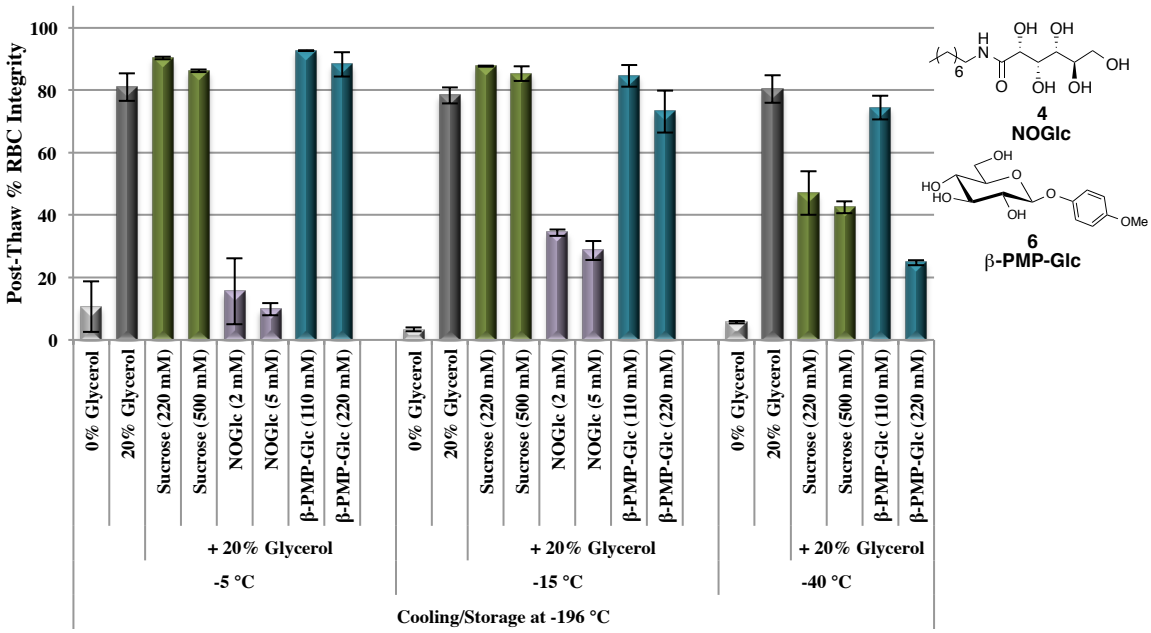

Fig. 4 The effect of novel IRI active small molecules NOGlc (**4**), β-PMP-Glc (**6**) and sucrose on post-thaw RBC integrities. RBC samples in indicated cryo-solutions were slow-cooled 1°C/min to defined sub-zero temperatures and subsequently rapidly cooled and stored in liquid nitrogen (-196°C) prior to thawing at 37 °C. % hemolysis was quantified post-thaw using Drabkin's assay to determine % RBC integrity (100 - % hemolysis).

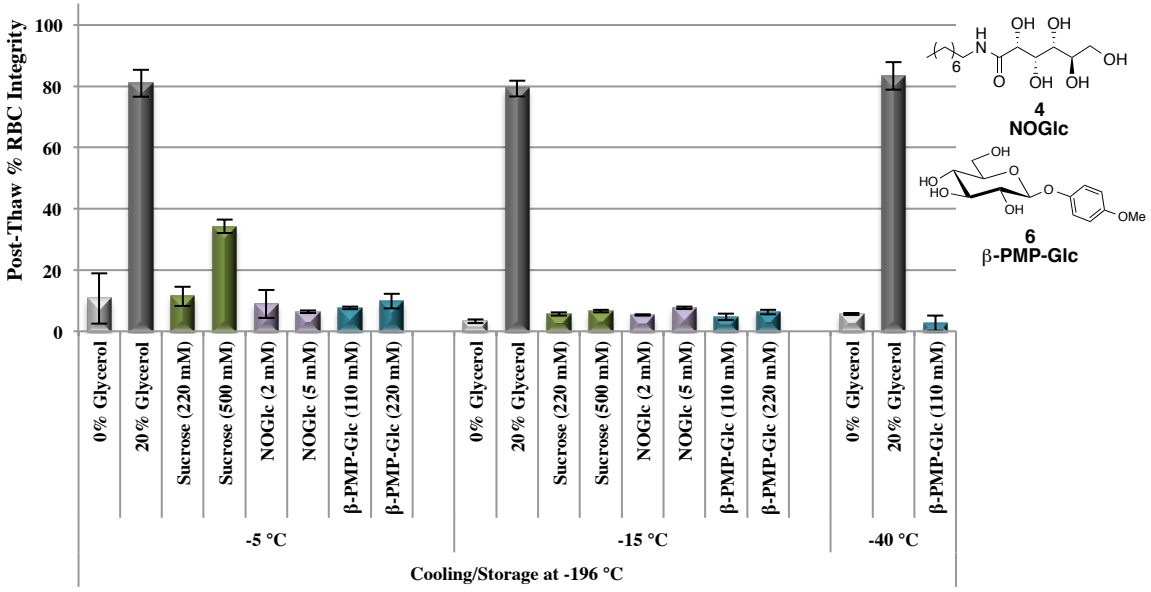

Figure 8.9 The effect of NOGlc (**4**), β-PMP-Glc (**6**) and sucrose on post-thaw RBC integrities. RBC samples suspended in indicated cryo-solutions in dextrose/saline buffer were slow-cooled 1 °C/min to defined subzero temperatures and subsequently rapidly cooled and stored in liquid nitrogen (-196 °C) prior to thawing at 37 °C. % hemolysis was quantified post-thaw using Drabkin's assay to determine % RBC integrity (100 - % hemolysis).

The most interesting results were those of the 110 mM β-PMP-Glc (**6**) in 20% glycerol. This cryo-solution resulted in equal or slightly higher post-thaw RBC integrities than the 20% glycerol control upon cooling to -5 °C or -15 °C prior to rapid cooling/–196 °C storage (Fig 4).[132] The post-thaw integrities when cooled to -5 °C were 93% when the solution contained 110 mM β-PMP-Glc and 81% for the 20% glycerol control. When cooled to -15 °C post-thaw integrities were 85% when the solution contained 110 mM β-PMP-Glc and 78% with only 20% glycerol. The 20% glycerol cryo-solutions with or without 110 mM β-PMP-Glc had identical post-thaw integrities when slowly cooled to -40 °C prior to rapid cooling/storage at –196 °C. A 220 mM solution of β-PMP-Glc in 20% glycerol was detrimental for RBC freezing as under the same freezing conditions (slow cooling to -40°C, storage -80 °C) post-thaw integrities were significantly decreased to 25%. Collectively, these results suggested that 110 mM β-PMP-Glc (**6**) might be a beneficial additive for the cryopreservation of RBCs. This was the only instance where the post-thaw integrity of RBCs was similar to or better than the 20% glycerol control. However, a 20% glycerol solution alone is a very effective cryoprotectant for RBCs and is used clinically in European countries with the low glycerol/rapid freeze method for RBC cryopreservation (see section 8.4.1 and section 1.4.3).[4,111,118,137] This made it difficult to definitively ascertain the effectiveness of β-PMP-Glc as a cryo-additive for RBC cryopreservation. Consequently, solutions containing 110 mM β-PMP-Glc (**6**) with 5, 10, 15 or 20% (wt/vol) glycerol were used to freeze human RBCs with the interrupted freezing protocol described previously.[23,128,133]

Samples were cooled at a rate of 1°C/min to the indicated sub-zero temperature and then rapidly frozen to -80°C. This cooling rate and -80°C storage temperature was selected as these more closely reflect clinical RBC cryopreservation protocols utilized in Canada and the United States. The post-thaw RBC integrities for these were presented in Fig. 5 of the article provided in section 8.4.2 and this figure is reproduced below. Low post-thaw RBC integrities were observed with 5% and 10% glycerol solutions indicating these concentrations of glycerol used in conjunction with a slow cooling rate are not effective for the freezing RBCs (Fig. 5).[132] However, the addition of 110 mM β-PMP-Glc to the 10% glycerol solution increased post-thaw integrities to 42% from 21% for 10% glycerol alone when RBC samples were held at -5°C and nucleated prior to rapid cooling/storage at -80°C. The advantage of adding 110 mM β-PMP-Glc to the glycerol solution is most evident with a 15% glycerol solution. The greatest increase in RBC integrities were observed with the cooling to -5°C/storage at -80°C freezing conditions and the cooling to -40°C/storage at -80°C freezing conditions (Fig. 5). When samples were rapidly cooled from -5°C to -80°C RBC integrity increased from 67% (for 15% glycerol) to 84% with β-PMP-Glc. Furthermore, when samples were slow-cooled to -40°C prior to -80°C storage, double post-

thaw RBC integrities were observed when β-PMP-Glc was present in the cryo-solution (49% with β-PMP-Glc *versus* 25% for 15% glycerol). This increase is significant as it has been previously demonstrated that storage at -80°C with low glycerol concentrations (typically less than 25%) is detrimental resulting in almost negligible RBC recoveries.[118]

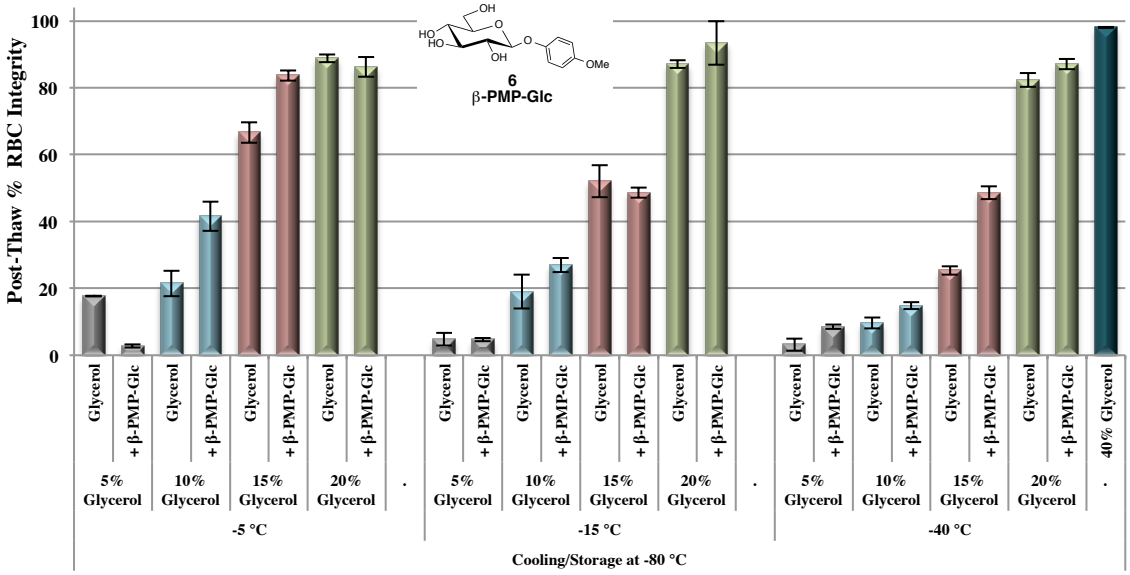

Fig. 5 The effect of β-PMP-Glc (**6**) on post-thaw RBC integrity (100 - % hemolysis) using reduced concentrations of glycerol. RBC samples in glycerol solutions with or without 110 mM β-PMP-Glc (6) were slow cooled 1 °C/min to defined sub-zero temperatures and subsequently rapidly cooled and stored at -80 °C prior to thawing at 37 °C.

8.4.4 Internalization and Cryomicroscopy Studies for the Freezing of RBCs in the Presence of β-PMP-Glc

We next sought to further exploit the interrupted freezing protocol to investigate the mechanism of action for the cryoprotective nature of β-PMP-Glc.[132] This would also provide information as to whether β-PMP-Glc was protecting RBCs during the slow cooling stage and/or during the rapid cooling to -80°C stage of the freezing process. To accomplish this, the two-step interrupted freezing protocol was repeated to sub-zero temperatures between -5 to -50°C and samples were either thawed immediately from the defined sub-zero temperature (see "cooling" profiles in Fig. 6) or rapidly cooled and stored at -80°C prior to thawing (see "cooling/storage" profiles in Fig. 6).[23] The results from this study were presented in Fig 6 in the article provided in section 8.4.2 and this data is reproduced below.

The "cooling" profile (Fig. 6, dashed lines) for 15% glycerol is typical of that observed with a cell penetrating cryoprotectant. A progressive decrease in post-thaw RBC integrity is observed as the temperature to which the samples were cooled was decreased, with higher post-thaw integrities observed at temperatures above -30°C and lower integrities observed upon slow

cooling to lower sub-zero temperatures (i.e. below -30°C).[23] The higher integrities obtained above -30°C are presumably due to the colligative effects of glycerol and its ability to decrease the amount of ice present at any sub-zero temperature thus delaying and mitigating osmotic pressures that ultimately result in cellular damage (for a detailed discussion on mechanisms of cryo-injury see section 1.4).[9,23] The lower RBC integrities below -30°C are likely attributed to cellular damage due to concentrating solutes, consistent with Mazur's two-factor hypothesis of freezing injury (see section 1.4 for a detailed discussion).[9]

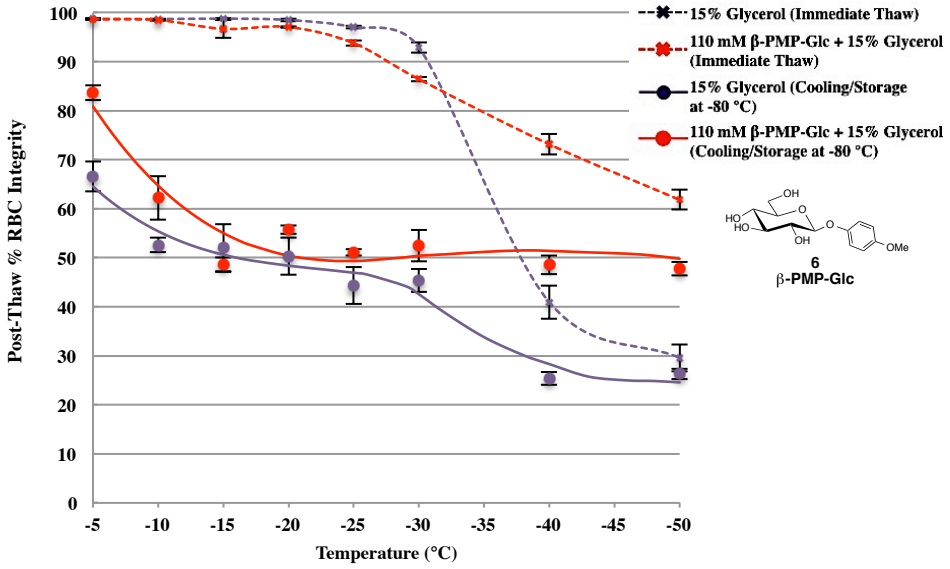

Fig. 6 The effect of 15% glycerol cryo-solutions with or without 110 mM β-PMP-Glc (**6**) on post-thaw RBC integrity (100 - % hemolysis). Samples were slow cooled 1 °C/min to defined sub-zero temperatures then either immediately thawed ("cooling" curves, dashed lines) or rapidly cooled and stored at -80 °C prior to thawing at 37 °C ("cooling/storage" curves, solid lines)

A similar "cooling" profile is also observed when 110 mM β-PMP-Glc (**6**) is added to the 15% glycerol solution. However, the addition of β-PMP-Glc results in a significant increase in RBC integrity at lower sub-zero cooling temperatures.[132] At -40°C, RBC integrity with 15% glycerol is 41% and this is increased to 73% with the addition of 110 mM β-PMP-Glc. A similar result was also obtained with β-PMP-Glc at -50 °C compared to the 15% glycerol solution (62% RBC integrity *versus* 29%). The fact that the addition of β-PMP-Glc to the 15% glycerol freezing solution resulted in increased integrities (reduced hemolysis) under the slow-cooling/immediate thaw conditions is consistent with the profile of a cell penetrating cryoprotectant.[23] This suggests that β-PMP-Glc is being internalized into the RBCs. A second plausible explanation for this reduced hemolysis is that a synergistic effect between the internalized glycerol and inhibition of ice recrystallization in the extracellular environment due to β-PMP-Glc may be occurring. Irrespective of the mechanism of action, these results clearly demonstrate that β-PMP-Glc

provides additional protection during the slow-cooling phase of the freezing protocol when added to a 15% glycerol solution.

Different profiles were obtained with the "cooling/storage" conditions of the RBC samples frozen in the same cryo-solutions (Fig. 6, solid lines).[132] For the 15% glycerol cryo-solution, as the temperature to which the samples were slow-cooled was decreased, integrities also decreased averaging between 45-55% when cooled to temperatures between -10°C and -30°C prior to rapid cooling and storage at -80°C. When cooled to temperatures lower than -30 °C, RBC integrities further decreased to approximately 25%. The higher post-thaw integrities at temperatures above -30°C is likely due to the rapid cooling being initiated at higher sub-zero temperatures. This would create an overall faster cooling rate to -80°C, and this is consistent with the need for a rapid cooling rate for the low glycerol/rapid freeze cryopreservation method of RBCs.[34,118,138] When 110 mM β-PMP-Glc is added to 15% glycerol, post-thaw RBC integrities are 5 - 15% better at all sub-zero cooling temperatures higher than -30 °C. Interestingly, β-PMP-Glc appears to have the greatest effect when freezing conditions involve slow cooling to -40 or -50 °C prior to rapid freezing. The post-thaw RBC integrities are approximately 50% when the solution contains β-PMP-Glc, which is double that of the 15% glycerol solution alone.

Collectively, the results from the interrupted freezing protocol experiments indicate that β-PMP-Glc (**6**) confers protection during the slow-cooling stage of the freezing protocol. Moreover, β-PMP-Glc is also protecting during rapid cooling to -80 °C regardless of the initial sub-zero cooling temperature resulting in less hemolysis than the 15% glycerol control. The greatest benefit of this cryo-additive is observed with lower sub-zero cooling temperatures (-40 or -50 ºC), which is significant as these freezing conditions mimic RBC clinical cryopreservation protocols that utilize slow freezing rates but high glycerol concentrations (i.e. 40% glycerol).

The best cryoprotectants routinely used are penetrating CPAs such as DMSO or glycerol. As described previously, the "cooling" profile obtained when 110 mM β-PMP-Glc was added to the 15% glycerol solution suggested that this compound might be conferring protection against cryo-injury through a mechanism consistent with a cell penetrating cryoprotectant. Thus, we sought to explore if the observed increase in post-thaw integrities was the result of internalization of β-PMP-Glc. Transport of glucose across human RBC membranes readily occurs through facilitated diffusion, a process that is mediated by glucose transporters (GLUTs) that are expressed in high levels on the surface of RBCs.[139,140] However, uptake of glucose and glucose derivatives is dependent upon hydroxyl group stereochemistry and the "shape" of the molecule.[141,142] Thus,

glucose derivatives may not be transported or the rate of transport may be considerably decreased depending on their structure.

It has previously been demonstrated that the rate of sugar transport can be considerably slowed at 0°C.[143] To elucidate whether the internalization of β-PMP-Glc was important for its cryo-protective ability, prior to freezing suspensions of RBCs in 15% glycerol containing 110 mM β-PMP-Glc cryoprotective solution were incubated for 0, 5, 10 and 30 min time periods at room temperature or 0°C.[132] After incubation, freezing was conducted using the two-step interrupted freezing protocol described previously with slow cooling to -40°C or -50°C followed by rapid cooling and storage at -80°C prior to thawing. The post-thaw RBC integrities resulting from these experiments were shown in Fig. 7 of the article provided in section 8.4.2 and this figure is reproduced below.

It is evident that the optimal incubation times prior to RBC freezing with the 15% glycerol/β-PMP-Glc solution is 5 to 10 min at room temperature (Fig. 7A).[132] Post-thaw integrities for these time periods were similar for both freezing conditions (approximately 50%). In contrast, immediate freezing or incubation for 30 min at room temp yielded RBC integrities less than 20%. This was surprising and suggested a cytotoxic effect of β-PMP-Glc may be associated with long incubation times. However, less than 1% hemolysis (>99% RBC integrity) was observed upon incubation of RBCs with β-PMP-Glc for 60 min at room temperature without freezing (figure 8.10), indicating that hemolysis is not occurring during the pre-incubation stage of the protocol.

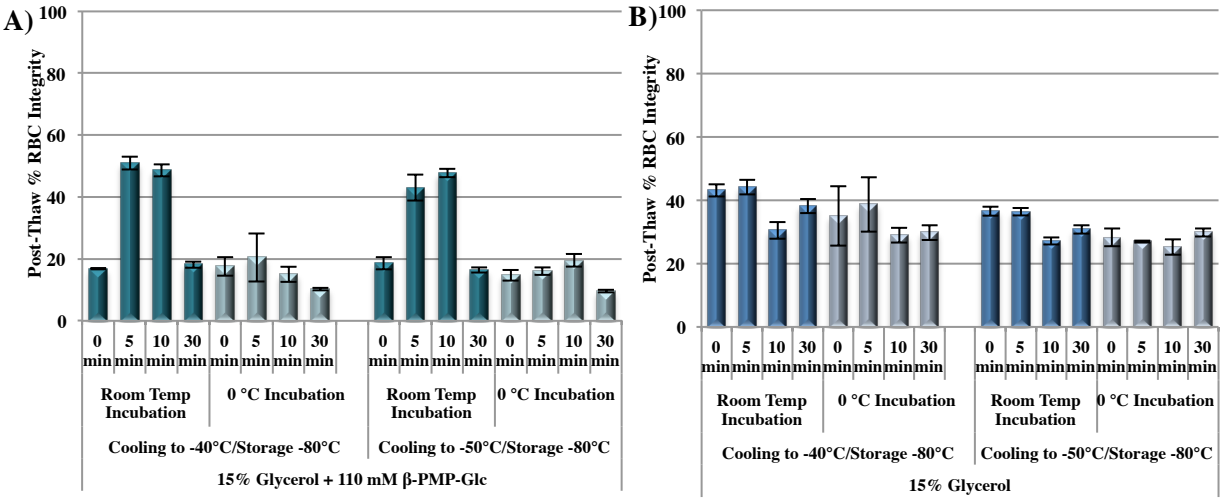

Fig. 7 The effect of pre-incubation of cryo-solutions on post-thaw RBC integrity. A) RBC samples were incubated for indicated time and at indicated temperature with a 110 mM β-PMP-Glc + 15% glycerol solution prior to freezing using an interrupted freezing protocol. B) RBC samples were incubated for indicated time and at indicated temperature with a 15% glycerol solution prior to freezing using an interrupted freezing protocol.

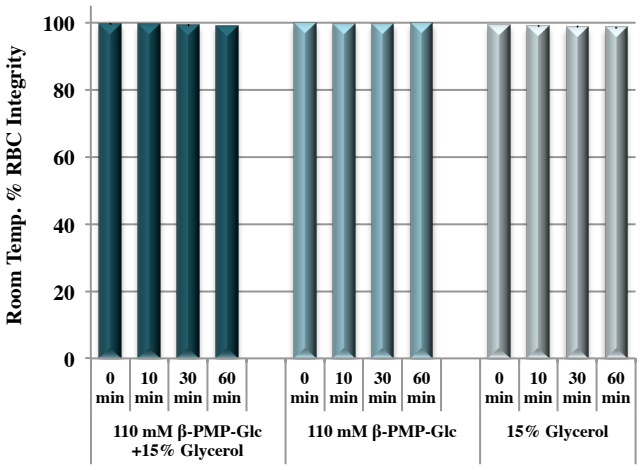

Figure 8.10 RBC integrities after room temperature incubation for indicated time period with cryo-solutions without freezing.

When incubation with the 15% glycerol/β-PMP-Glc solution was conducted at 0°C prior to freezing, at 5 and 10 min a drastic decrease in post-thaw integrity was observed (Fig. 7A). This was only observed at 0°C when β-PMP-Glc was added to the freezing solution, and a 15% glycerol solution alone resulted in similar post-thaw integrities independent of incubation time or temperature (approximately 20-35%, Fig. 7B). It is well established that RBCs are highly permeable to glycerol.[25,144,145] While this permeability is temperature dependent,[23] the rate at which glycerolization occurs in RBCs is fast even at 0 °C.[145] Thus, at the lower temperatures and shorter incubation times, the RBCs are likely glycerolized prior to freezing. Overall, this data is consistent with the hypothesis that the transport of β-PMP-Glc into RBCs is occurring and is important for its protective effect during freezing as slowing the rate of sugar transport at 0°C resulted in a decrease in post-thaw RBC integrity. However, further studies are required to determine the quantity and rate of its transport into RBCs.

The final RBC freezing experiment conducted with the effective cryo-additive β-PMP-Glc was cryomicroscopy to investigate the structure of ice during the freezing process with RBCs.[132] This was shown in Fig 9 in the article provided in section 8.4.2 and this is reproduced below. The cryo-solutions explored for these RBC freezing experiments were 110 mM β-PMP-Glc + 15% glycerol (Fig. 9C), 110 mM β-PMP-Glc in saline (Fig. 9D), and 15% glycerol alone (Fig 9E). Interestingly, depending on the cryoprotective solution used, the structure of ice in the frozen sample differed dramatically. These images in Fig 9 show the advancing ice-front (photographed during the freezing of the sample) in the different cryoprotective solutions. All three solutions resulted in a very different structure of ice during freezing. The most interesting images are those shown in Fig. 9C and 9E which are the 15% glycerol solution both with and without β-PMP-Glc

where the ice structure in the presence of β-PMP-Glc is very different and we obtain significantly increased post-thaw RBC integrities. While unfortunately at this time it is not known what effect this difference in ice structure has on post-thaw RBC integrities, this is the first example where a novel small molecule ice recrystallization inhibitor has been demonstrated to be a beneficial cryo-additive and is confirmed to influence ice structure in the presence of RBCs cells *in vitro*.

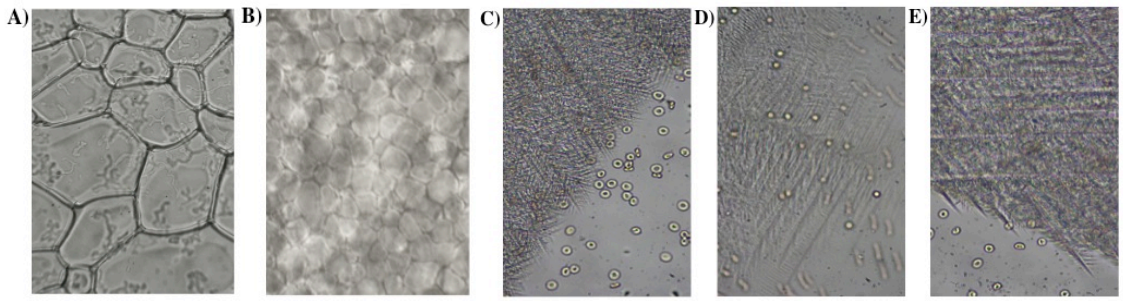

Fig. 9 Photographs illustrating the IRI activity of β-PMP-Glc (**6**) and the advancing ice-front during RBC freezing. A-B) Ice crystal grains from a frozen (A) PBS solution, or (B) 22 mM β-PMP-Glc solution in PBS annealed at -6.4 °C for 30 mins in a splat-cooling assay. C-E) Advancing ice fronts during RBC freezing in the presence of 110 mM β-PMP-Glc + 15% glycerol solution (C), 110 mM β-PMP-Glc in dextrose/saline solution (D), or 15% glycerol solution (E).

8.4.5 The Ability of Phenolic-Glycosides to Protect RBCs during Freezing with Reduced Glycerol Concentrations

Having established that the potently IRI active phenolic-glucoside β-PMP-Glc (**6**) was a beneficial cryo-additive for RBC freezing and that its addition to a 15% glycerol solution doubled post-thaw integrities relative to 15% glycerol alone using slow-cooling conditions, interest arose in exploring other IRI active phenolic-glycosides as cryo-additives for RBCs. Thus, β-Linked phenolic-glucosides **7**-**12** were assessed for their cryoprotective ability with RBCs, along with disaccharide **13**, α-PMP-Glc derivative **14**, glucose alone and *para*-methoxyphenol alone (structures shown in figure 8.11). These derivatives were presented in chapter 7, and their IRI activity ranged from high to moderate depending on the compound (% MGS for each compound is provided in figure 8.11). These studies will provide insight into the structural features of β-PMP-Glc that are required for its cryoprotective ability with RBCs to complement the extensive structure-function work completed for the potent IRI activity of β-PMP-Glc (chapter 7). In addition, as the phenolic-glucosides vary in terms of their degree of IRI activity, these studies will elucidate the importance of ice recrystallization inhibition for RBC cryopreservation.

Cryo-solutions containing 110 mM or 55 mM of the phenolic-glucoside, glucose or *para*-methoxyphenol in 15% glycerol were used for the RBC freezing experiments. RBC samples suspended in cryo-solution were subjected to the interrupted freezing protocol as described in sections 8.4.3 and 8.4.4 where after nucleation at -5°C samples were slow-cooled to -40°C or -

50°C then rapidly cooled and stored at -80°C.[23,128,132,133] Concentrations of 110 mM were chosen for a direct comparison to β-PMP-Glc as this compound was a beneficial cryo-additive for RBC freezing at this concentration. The exceptions were β-pBrPh-Glc (**8**) and β-pOCF$_3$Ph-Glc (**12**), which were insoluble at 110 mM and consequently assessed at 55 mM. Samples were thawed under fast-thaw conditions, and the post-thaw RBC integrities are presented in figure 8.11.

The two moieties that β-PMP-Glc (**6**) is comprised of are glucose and *para*-methoxyphenol. A 110 mM solution of glucose in 15% glycerol is not an effective cryo-solution for RBCs as post-thaw integrities were similar to or worse than the 15% glycerol control. When RBC samples in the glucose containing solution were slow-cooled to either -40°C or -50°C prior to -80°C storage integrities were 17% and 30%, respectively, whereas 15% glycerol post-thaw integrities were 27% for both freezing conditions (figure 8.11). A 110 mM solution of *para*-methoxyphenol in 15% glycerol resulted in similar post-thaw integrities as the 110 mM β-PMP-Glc/15% glycerol cryo-solution with both freezing conditions. However, it was observed that the RBC samples and supernatants post-thaw were brown/black in colour as opposed to the typically observed deep red colour. Spectrophotometric analysis indicated that 98% of the Hgb in the samples frozen with the *para*-methoxyphenol/glycerol solution was oxidized to metHgb. This is highly undesirable and alters the function of the RBCs since metHgb is not able to bind to or carry oxygen.[103] Thus, while β-PMP-Glc can effectively increase post-thaw RBC integrities, the two individual components of this molecule on their own are not beneficial cryo-additives for the freezing of RBCs.

When the *para*-methoxy substituent on β-PMP-Glc was replaced with a fluorine (β-pFPh-Glc, **7**) or a bromine (β-pBrPh-Glc, **8**), potent IRI activity was retained or increased (for **7** and **8** respectively, see Chapter 7 and figure 8.11). Both potently IRI active derivatives also resulted in similar integrities as β-PMP-Glc that were ~50% post-thaw for both freezing conditions employed (figure 8.11). The most surprising result was with the 55 mM β-pBrPh-Glc (**8**) in 15% glycerol solution. This cryo-solution resulted in 50% post-thaw RBC integrity (similar to β-PMP-Glc), but half the concentration of the phenolic-glycoside was utilized in the cryo-solution relative to β-PMP-Glc due to the solubility of the compound. When β-PMP-Glc was used at 55 mM post-thaw integrities were lower than that of the 15% glycerol control (figure 8.11). Thus, simply replacing the *para*-substituent on the phenolic-glucoside with a bromine atom can significantly increase IRI activity (8% MGS for **8** compared with 23% for β-PMP-Glc (**6**)) and also results in a better cryo-additive that can be utilized for RBC freezing with reduced glycerol concentrations (15% *versus* the clinically used 40%) and lower concentration of the carbohydrate

additive. A more detailed examination of the benefits of adding β-pBrPh-Glc (**8**) to the cryo-solution is discussed later in this section.

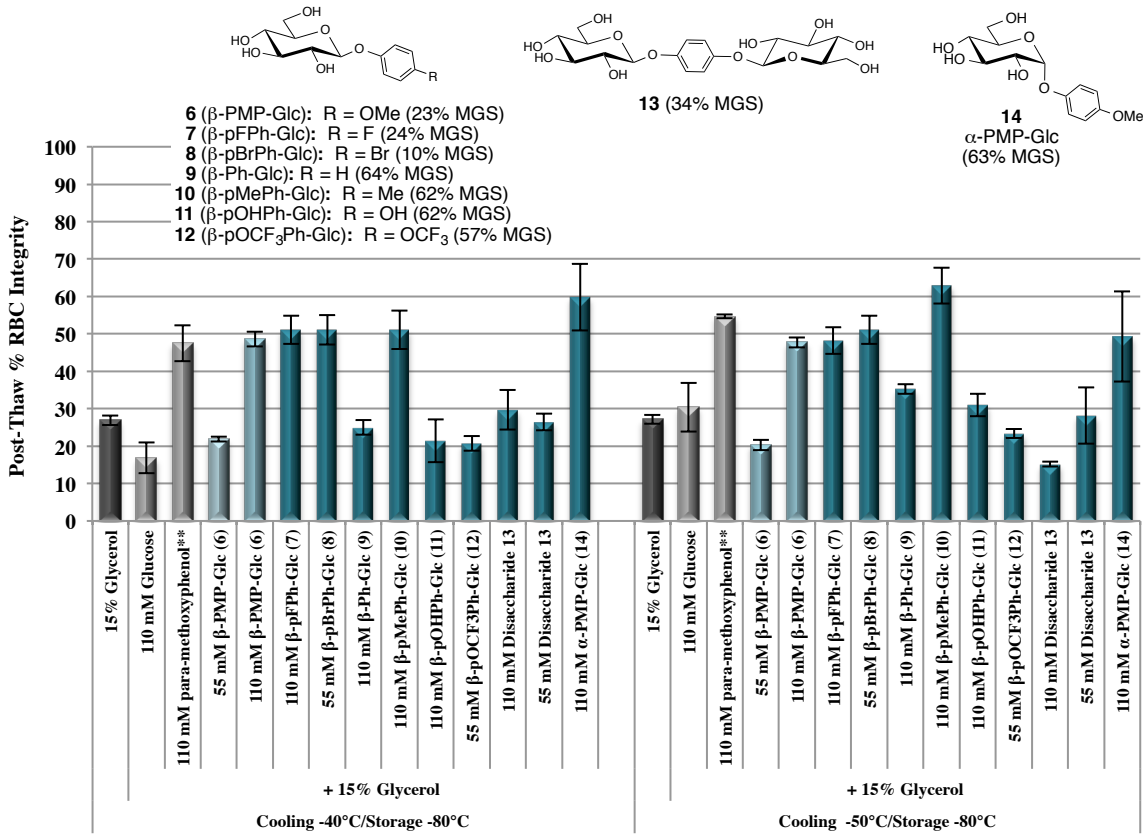

Figure 8.11 Post-thaw RBC integrities (100 - % hemolysis) of RBC samples frozen with 15% glycerol solutions containing novel phenolic-glycoside additives **7**-**14**. RBC samples in cryo-solutions were slow cooled 1 °C/min to defined sub-zero temperatures and subsequently rapidly cooled and stored at -80 °C prior to thawing at 37 °C. Double asterisks (**) indicates post-thaw Hgb was oxidized to 98% metHgb.

Many of the moderately IRI active phenolic-glucosides did not increase post-thaw integrities relative to the 15% glycerol control. This included β-Ph-Glc (**9**), β-pOHPh-Glc (**11**) and β-pOCF$_3$Ph-Glc (**8**), which all resulted in 20-30% post-thaw RBC integrity for both freezing conditions (figure 8.11). Interestingly, the moderately active β-pMePh-Glc (**10**) and α-PMP-Glc (**14**) at 110 mM in 15% glycerol had similar post-thaw integrity results as the potently IRI active derivatives **6**-**8**. Thus, the presence of a *para*-methyl group either directly connected to the aryl ring (β-pMePh-Glc (**10**)) or linked through an oxygen atom (β-PMP-Glc (**6**)) resulted in an effective cryo-additive. In addition, regardless of the glycosidic-linkage stereochemistry, a *para*-methoxy aglycone resulted in a decrease in post-thaw RBC hemolysis (increase in integrity) relative to the 15% glycerol control (both α- and β-PMP-Glc). A similar result was also obtained when β-PMP-Gal (**5**) was employed as a cryo-additive, as described later in this section (figure 8.12).

The disaccharide **13** contains two β-linked glucose residues conjugated to a *para*-substituted dihydroxybenzene linker. This derivative was potently IRI active, resulting in 34% MGS relative to the positive PBS control (section 7.2.6, chapter 7). This disaccharide at 110 mM in 15% glycerol failed to increase post-thaw RBC integrities, resulting in 15-30% RBC integrity depending on the freezing condition employed (figure 8.11). These results are similar to what was observed with the 15% glycerol control solution. It was initially hypothesized that this may be attributed to a toxic effect with the disaccharide as at equimolar concentration disaccharide **13** contains double the relative glucoside concentration as β-PMP-Glc (**6**). At 220 mM, β-PMP-Glc (**6**) was detrimental additive to a 20% glycerol solution, drastically reducing post-thaw integrities (Fig. 4, section 8.2.2 and 8.2.3).[132] However, even at 55 mM disaccharide **13** resulted in similar post-thaw integrities as the 15% glycerol control (~27%), indicating that despite its potent IRI activity, this compound is not a beneficial cryo-additive for the freezing of RBCs (figure 8.11).

The disaccharide trehalose is an α,α-(1,1)-glucose dimer, and this carbohydrate is not able to cross RBC membranes. For trehalose to be an effective CPA for RBCs however, it is required on both sides on of the cell membrane.[128] Results described in section 8.4.4 suggested that β-PMP-Glc is being internalized into RBCs and that this is important for increasing post-thaw RBC integrities. It is not currently known if disaccharide **13** is being internalized by RBCs. However, a plausible explanation for the poor RBC integrities observed with disaccharide **13** (the β-1,1-glucose dimer linked through a dihydroxybenzene) may be that, similar to trehalose, it cannot cross RBC membranes, but its internalization may be required for a cryoprotective effect to be observed. Consequently, further studies are still required to elucidate if internalization of disaccharide **13** is important for its cryoprotective ability, similar to treahose.

β-pBrPh-Gal (**15**) and α-PMP-Gal (**16**) were also explored as cryo-additives for the freezing of RBCs. Freezing and thawing was conducted as described previously using the interrupted freezing protocol,[23,128,132,133] and the post-thaw RBC integrities are presented in figure 8.12. In these studies, galactose was also examined as a control. As described earlier in this section, glucose (110 mM in 15% glycerol) did not increase post-thaw RBC integrities relative to the 15% glycerol control, however galactose (110 mM in 15% glycerol) increases integrities by approximately ~10%. The 110 mM Gal/15% glycerol cryo-solution resulted in 42% RBC integrity post-thaw for both freezing conditions employed (figure 8.12). This result is similar to what our laboratory has observed with various other cells lines including WRL-68 cells, HepG2 cells,[55] and HSCs ($CD34^+$ cells) from UCB (figure 8.6, section 8.3) where the addition of galactose as a CPA could significantly increase post-thaw cell viabilities. Interestingly, the galactose derivatives β-PMP-Gal (**5**), β-pBrPh-Gal (**15**) in the 15% glycerol solution resulted in

post-thaw RBC integrities that were higher than that observed with the glucose derivatives β-PMP-Glc (**6**), β-pBrPh-Glc (**8**). When slow-cooled to -50°C followed by -80°C storage, the galactose derivatives **5** and **15** resulted in ~62% post-thaw RBC integrity, whereas the glucose derivatives **6** and **8** resulted in ~50% RBC integrity. In contrast, the α-linked PMP-glucose derivative **14** resulted in higher post-thaw integrity than the corresponding galactose derivative **16**. When α-PMP-Glc (**14**) was added to the 15% glycerol solution post-thaw RBC integrity was ~50% RBC, whereas α-PMP-Gal (**16**) has no effect on RBC freezing and resulted in post-thaw integrities similar to the 15% glycerol control (~27%, figure 8.12).

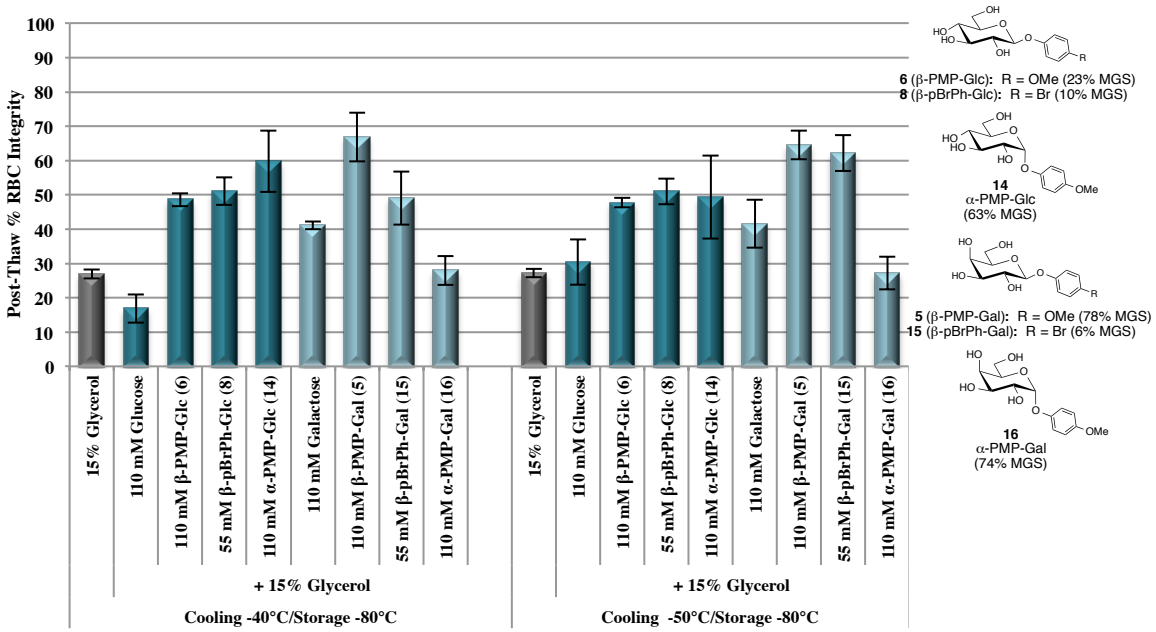

Figure 8.12 Post-thaw RBC integrities (100 - % hemolysis) of RBC samples frozen with 15% glycerol solutions containing phenolic-glycoside additives **5**-**6**, **8**, or **14**-**16**. RBC samples in cryo-solutions were slow cooled 1 °C/min to defined sub-zero temperatures and subsequently rapidly cooled and stored at -80 °C prior to thawing at 37 °C.

β-pBrPh-Glc derivative **8** is a promising novel phenolic-glucoside cryo-additive for RBC freezing. This compound in a 15% glycerol solution resulted in similar post-thaw RBC integrities as β-PMP-Glc (**6**) in 15% glycerol (~50%), but it is important to note that this result was obtained at half the concentration that β-PMP-Glc was effective at (55 mM). β-pBrPh-Glc is very similar in structure to β-PMP-Glc, however, this compounds has not been studied in our laboratory to the same extent as β-PMP-Glc. As such, we investigated β-pBrPh-Glc more closely in RBC freezing experiments with greatly reduced glycerol concentrations. Decreased quantities of glycerol are desirable for RBC cryopreservation as this can significantly decrease post-thaw deglycerolization times allowing for faster access to cryopreserved RBC units for transfusions.

RBC post-thaw integrities with varying concentrations of β-pBrPh-Glc (**8**) in 15% glycerol solutions after freezing using the interrupted freezing protocol are presented in figure 8.13.[23,128,132,133] From this data it is evident that a 55 mM solution of β-pBrPh-Glc was the least effective concentration for the freezing of RBCs. When slow-cooled to -40°C followed by storage at -80°C, 20 mM and 40-50 mM β-pBrPh-Glc in 15% glycerol resulted in post-thaw integrities of 60-65% (compared with 50% for 55 mM β-pBrPh-Glc). The most effective concentration range for this compound was 25-35 mM resulting in greater than 70% post-thaw integrities with the same freezing conditions. Similar results were also obtained with cooling to -50°C followed by storage at -80°C where the least effect concentration of β-pBrPh-Glc was 55 mM and the optimal concentration for this additive ranged from 25-45 mM, resulting in ~65% RBC integrity post-thaw. Thus, the concentration of the phenolic-glucoside β-pBrPh-Glc (**8**) could effectively be reduced resulting in higher post-thaw RBC integrities (less hemolysis).

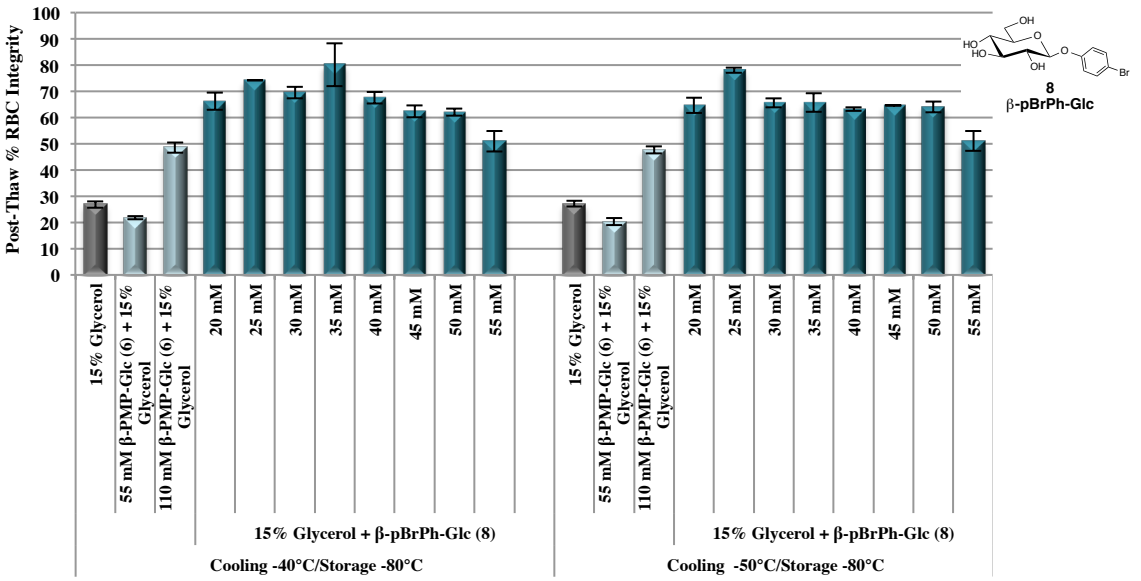

Figure 8.13 The effect of β-pBrPh-Glc (**8**) concentration in a 15% glycerol solution on post-thaw RBC integrity (100 - % hemolysis). RBC samples in glycerol solutions with or without 110 mM β-PMP-Glc (6) were slow cooled 1 °C/min to defined sub-zero temperatures and subsequently rapidly cooled and stored at -80 °C prior to thawing at 37 °C.

The results of being able to effectively reduce the β-pBrPh-Glc was significant as a cytotoxic effect was observed with a 55 mM solution of this compound in 15% glycerol when RBCs were incubated at room temperature up to one hour (figure 8.14). Immediately upon the addition of the 55 mM β-pBrPh-Glc cryo-solution 5% hemolysis was observed (95% RBC integrity at T=0 min). After incubation with this solution for 30 min or more, this hemolysis was increased to ~10% resulting in ~90% RBC integrity (T=30 and 60 min, figure 8.14). This toxic effect on the RBCs

was not observed with a 30 mM solution of β-pBrPh-Glc in 15% where even after 60 min incubation at room temperature RBC integrities were greater than 98% (figure 8.14).

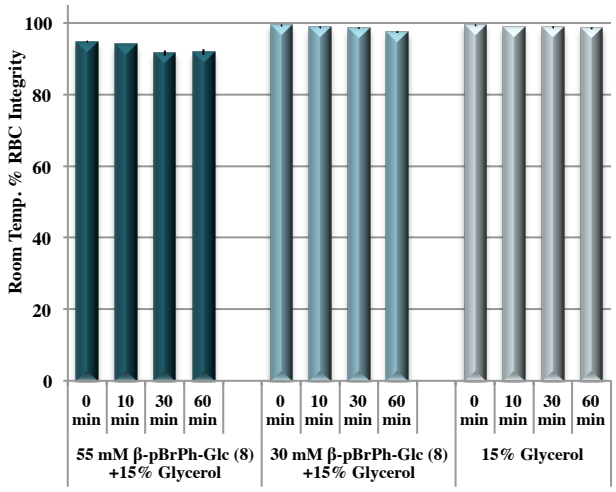

Figure 8.14 RBC integrities after room temperature incubation for indicated time period with 30 mM or 55 mM β-pBrPh-Glc (**8**) in 15% glycerol cryo-solutions without freezing.

As described previously, a reduction in glycerol concentration is highly desirable for RBC cryopreservation as it will result in decreased post-thaw deglycerolization processing times. Consequently, both the 55 mM and 30 mM solution of β-pBrPh-Glc (**8**) were next added to cryo-solutions containing 10% glycerol to explore whether the 15% glycerol solution could be further reduced while maintaining higher post-thaw RBC integrities. The results from these studies using the interrupted freezing protocol are shown in figure 8.15. Both the 30 mM and 55 mM β-pBrPh-Glc in 10% glycerol were able to increase post-thaw integrities relative to the 10% glycerol control alone. 10% glycerol resulted in ~10% post-thaw RBC integrity for both freezing conditions, and the addition of 110 mM β-PMP-Glc did not increase this value. However, 30 mM β-pBrPh-Glc (**8**) did increase this value to ~20% for both freezing conditions, whereas the 55 mM β-pBrPh-Glc resulted in the highest increase when added to 10% glycerol with ~35% post-thaw RBC integrity. Unfortunately, these results are not desirable since a significant amount of hemolysis is observed post-thaw with these cryo-solutions. Consequently, one of the most effective cryo-solutions discovered for effective RBC freezing with greatly reduced glycerol concentrations was the 30 mM β-pBrPh-Glc in 15% glycerol solution. Using freezing conditions that mimic the slow-cooling conditions employed for the high glycerol (>40%) method of RBC cryopreservation employed clinically in Canada and the United States,[4,113] post-thaw RBC integrities using 30 mM β-pBrPh-Glc in 15% glycerol were 65-70%, which is almost triple that observed with the 15% glycerol control solution alone (~25%).

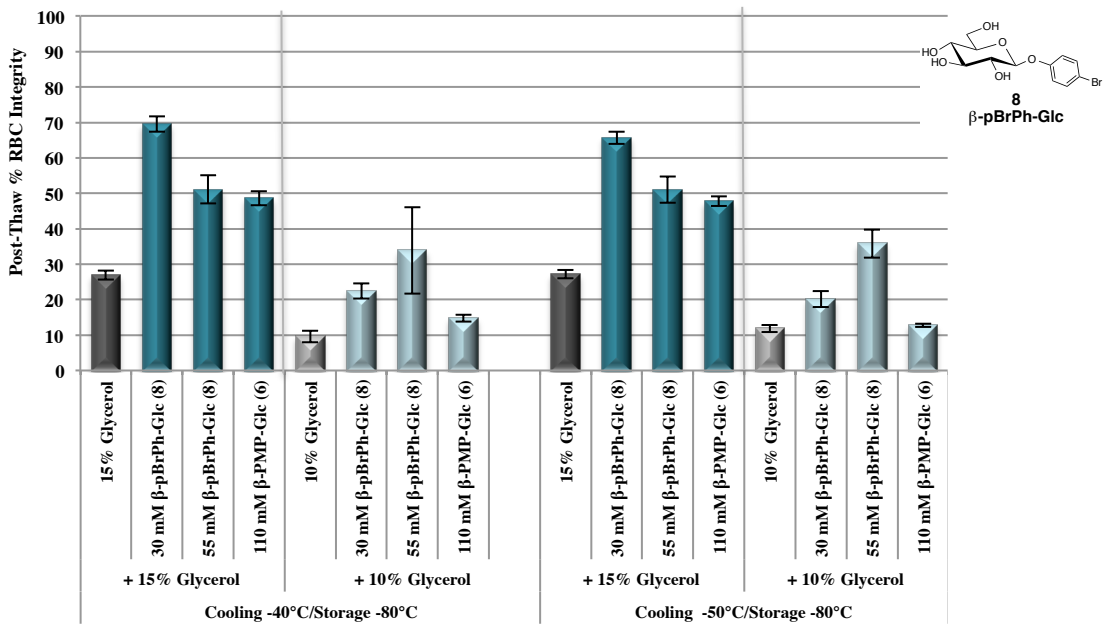

Figure 8.15 The effect of β-pBrPh-Glc (**8**) on post-thaw RBC integrity (100 - % hemolysis) using reduced concentrations of glycerol. RBC samples were slow cooled 1 °C/min to defined sub-zero temperatures and subsequently rapidly cooled and stored at -80 °C prior to thawing at 37 °C.

8.4.6 Initial Deglycerolization of RBCs in the Presence of Glycerol and Phenolic-Glucosides

Having discovered that IRI active phenolic-glucosides β-PMP-Glc (**6**) and β-pBrPh-Glc (**8**) could function as effective cryo-additives for the freezing of RBCs with significantly reduced glycerol concentrations, interest arose in exploring deglycerolization conditions post-freeze-thaw with these novel cryo-solutions. Current deglycerolization methods are time consuming due to limitations on how fast glycerol can be removed from RBCs without causing excessive damage.[122] The addition and removal of glycerol results in large osmotic gradients that can cause drastic changes in cell volumes that can be damaging. Human RBCs hemolyze if they swell beyond a maximal volume or if they are returned to isotonic conditions after shrinking below a minimal volume.[122,146,147] This is the major cause of intravascular hemolysis that occurs if glycerolized RBCs are transfused without removal of the glycerol from the RBCs, and is the reason why residual glycerol concentrations must be less than 1% after deglycerolization prior to transfusion.[4,111,113-115] The high glycerol concentrations (>40%) employed for the clinical cryopreservation of RBCs in Canada and the United States necessitates a multistep glycerol removal protocol to avoid hemolysis caused by drastic osmotic fluctuations and excessive cell volume changes. The typical deglycerolization method employed was developed by Meryman in 1972,[114] and it involves an initial wash with 12% saline, followed by a gradual gradient to an intermediate wash with 1.6% saline, and a final wash with isotonic saline (0.9% saline).[114,115,122,148]

The novel phenolic-glucoside containing cryo-solutions that resulted in increased post-thaw RBC integrities contained 15% glycerol. Thus, it was hypothesized that the more suitable washing conditions were those employed for the low glycerol/rapid freeze RBC cryopreservation method. The deglycerolization conditions employed for the low glycerol method involve an initial wash with 16% mannitol in 0.9% saline, followed by two washes of isotonic saline to reduce intracellular glycerol concentrations to less than 1%.[118] Mannitol was utilized as it stabilizes the cell membrane and it gradually reduces the osmolarity of the solution to prevent hypotonic hemolysis while removing glycerol from the RBCs. As stated in section 8.2.1 and 1.4.3, the low glycerol method is most effective when rapid freezing conditions are employed, and typically cooling rates greater than 100°C/min are required for high freeze-thaw-deglycerolized RBC recoveries.[118] The deglycerolization studies presented in this section are the first conducted with novel phenolic-glucoside IRIs as cryo-additives for RBC freezing. Consequently, we sought to ensure that immediate post-thaw hemolysis was low to afford the greatest quantity of RBCs proceeding through the deglycerolization process. As such, we examined post-thaw RBC integrities resulting from rapid cooling of the RBCs utilizing β-PMP-Glc (**6**) or β-pBrPh-Glc (**8**) as cryo-additives with low glycerol concentrations. These freezing conditions are not employed clinically in Canada for RBC cryopreservation. However, they were a logical starting point to optimize the deglycerolization protocols to ensure adequate glycerol removal first, prior to optimizing the glycerolization and slow-cooling freezing stage of the cryopreservation protocol.

The post-thaw integrities for the rapid-freezing experiments are shown in figure 8.16. For these experiments, 110 mM β-PMP-Glc (**6**), 55 mM β-pBrPh-Glc (**8**) or 30 mM β-pBrPh-Glc (**8**) were added to 10% or 15% glycerol solutions to examine the effect of the phenolic-glucosides with these freezing protocols. RBC samples suspended in cryo-solutions were then super-cooled at -5°C and then either nucleated and rapidly cooled to -80°C or -196°C by submersion in either dry ice or liquid nitrogen, or directly rapidly cooled from the -5°C holding temperature without nucleation. It is evident that the rapid freezing conditions are better for the low glycerol containing cryo-solution compared with the slow-cooling conditions. A 15% glycerol solution alone resulted in 75% RBC integrity post-thaw under the nucleated rapid freezing conditions to -80°C (figure 8.16) whereas only 25% RBC integrity was obtained with this solution under slow-cooling conditions (figure 8.15 and sections 8.4.2-8.4.5). With the nucleated rapid freezing conditions to -80°C, the addition of 110 mM β-PMP-Glc (**6**) to 15% glycerol did not increase post-thaw integrities relative to the 15% glycerol control (figure 8.16). However, when added to a 10% glycerol solution, β-PMP-Glc did increase post-thaw integrities from 26% (for 10%

glycerol alone) to 42%. In both instances when β-pBrPh-Glc was added to the glycerol solution and the samples were nucleated and rapidly cooled to -80°C post-thaw integrities were better than the glycerol controls (both 10% and 15%). Similar to what was observed with the slow-cooling conditions, 30 mM β-pBrPh-Glc solutions resulted in higher integrities than the 55 mM β-pBrPh-Glc solutions (figure 8.16). For the nucleated rapid freezing conditions to -80°C the overall best results were obtained with the 30 mM β-pBrPh-Glc in 15% glycerol cryo-solution, which provided 94% post-thaw RBC integrity.

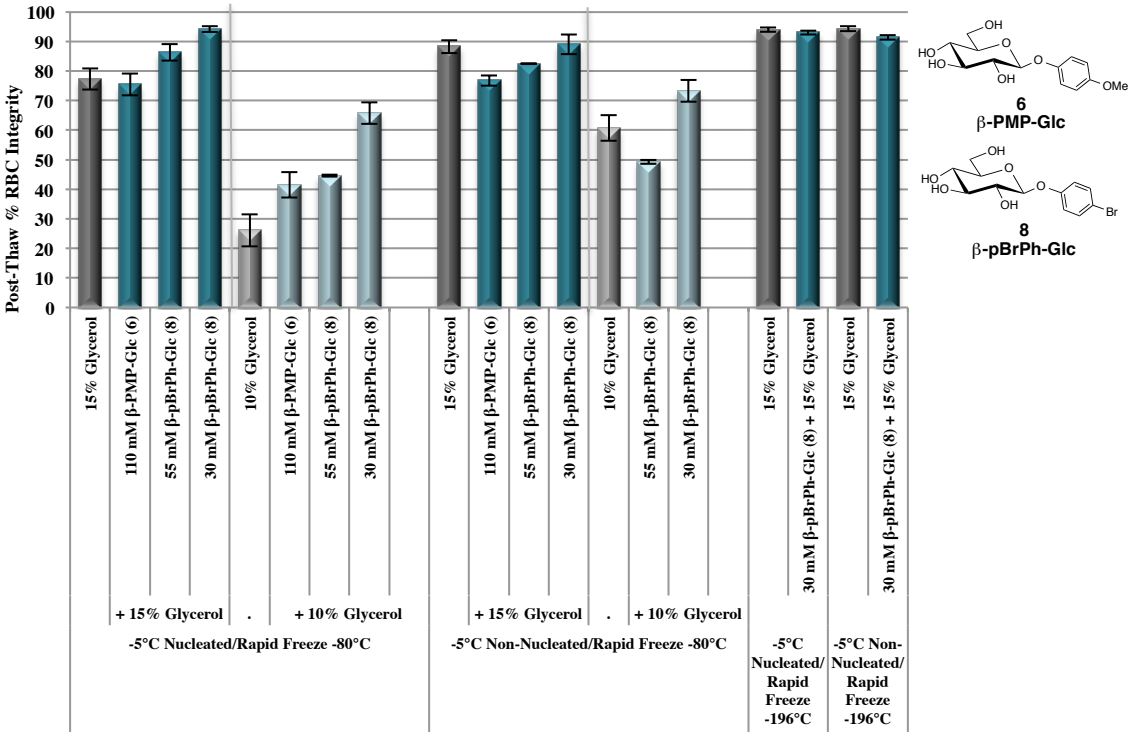

Figure 8.16 The effect of rapid freezing conditions on post-thaw RBC integrity using β-PMP-Glc (**6**) or β-pBrPh-Glc (**8**) in glycerol cryo-solutions. RBC samples were either nucleated at -5°C and then rapidly cooled to -80°C or -196°C, or rapidly cooled from -5°C to -80°C or -196°C without nucleation. All samples were thawed at 37 °C.

The non-nucleated conditions generally resulted in post-that integrities that were similar to or slightly better than the nucleated rapid freezing conditions. This suggests that controlling the point of ice nucleation for these cryo-solutions with rapid RBC freezing is not crucial for obtaining high post-thaw integrities. RBC samples rapidly frozen to -196°C had very high post-thaw RBC integrities, with 91-95% integrity obtained for the 15% glycerol cryo-solutions both with and without 30 mM β-pBrPh-Glc (figure 8.16). Thus, as expected post-thaw RBC integrities were significantly higher with the rapid freezing conditions compared with the slow-cooling conditions described in sections 8.4.2-8.4.5. Consequently, both rapid freezing protocols to -80°C and -196°C were utilized for the deglycerolization studies to ensure a high amount of intact RBCs

were subjected to the washing conditions to get an accurate representation of RBC recovery throughout this process.

RBC samples were frozen in 15% glycerol, 110 mM β-PMP-Glc + 15% glycerol or 30 mM β-pBrPh-Glc +15% glycerol cryo-solutions with the rapid freezing conditions to -80°C or -196°C. All cryo-solutions also contained 1.5% mannitol as this additive was used in the original deglycerolization method described by Rowe in 1968.[118] The deglycerolization protocols employed were also similar to that described for the low glycerol cryopreservation method.[118] After thawing at 42°C, samples were centrifuged and post-thaw supernatant containing excess glycerol was removed and the quantity of Hgb in this supernatant was measured spectrophotometrically using Drabkin's assay (see section 8.4.3). Following this, three washes were completed to remove glycerol, and after each wash the supernatant was removed and the amount of Hgb present in this supernatant was quantified. Wash 1 was a 16% mannitol in 0.9% saline solution, wash 3 was final 0.9% saline solution and after the wash 3 supernatant was removed the remaining RBCs were resuspended in an isotonic dextrose/saline solution (0.9% saline/0.2% dextrose). Wash 2 was varied and included the original 0.9% saline solution (condition A), as well as a 1.6% saline solution (condition B), a 10% mannitol in 0.9% saline solution (condition C), and a 10% mannitol in 1.6% saline solution (condition D). A summary of the wash conditions employed is provided in table 8.1. The amount of Hgb in the supernatants was used as an index of the extent of cellular damage incurred post-thaw and throughout each of the three washes. The results are presented as a percentage of Hgb lost in each step relative to the total Hgb measured for each RBC sample. The overall recovery (% RBC recovery) was calculated by the sum of total Hgb lost throughout each step of deglycerolization process compared to the total Hgb originally measured in the RBC sample.

Table 8.1 Summary of original deglycerolization wash conditions

Cryo-Solution	Wash 1 Conditions	Wash 2 Conditions	Wash 3 Conditions
15% Glycerol	16% Mannitol/0.9% Saline	0.9% Saline (Condition A)	0.9% Saline
		1.6% Saline (Condition B)	0.9% Saline
		10% Mannitol/0.9% Saline (Condition C)	0.9% Saline
		10% Mannitol/1.6% Saline (Condition D)	0.9% Saline
110 mM β-PMP-Glc 15% Glycerol	16% Mannitol/0.9% Saline	0.9% Saline (Condition A)	0.9% Saline
		1.6% Saline (Condition B)	0.9% Saline
		10% Mannitol/0.9% Saline (Condition C)	0.9% Saline
		10% Mannitol/1.6% Saline (Condition D)	0.9% Saline
110 mM β-PMP-Glc 15% Glycerol	16% Mannitol/0.9% Saline	0.9% Saline (Condition A)	0.9% Saline
		1.6% Saline (Condition B)	0.9% Saline
		10% Mannitol/0.9% Saline (Condition C)	0.9% Saline
		10% Mannitol/1.6% Saline (Condition D)	0.9% Saline

The percent Hgb lost in the post-thaw supernatants and wash 1 of the deglycerolization process are presented in figure 8.17. It is evident that the rapid freezing conditions to -80°C are detrimental for the 15% glycerol and the 110 mM β-PMP-Glc + 15% glycerol cryo-solutions as a significant amount of Hgb was lost in the post-thaw supernatant (figure 8.17A). 97% Hgb was lost in the post-thaw supernatant for the 15% glycerol solution, essentially indicating that all RBCs were hemolyzed with this cryo-solution, and the 110 mM β-PMP-Glc + 15% glycerol resulted in 67% Hgb lost in the post-thaw supernatant. These immediate post-thaw recoveries were significantly decreased compared to the post-thaw hemolysis values obtained with the rapid freezing conditions presented in figure 8.16. However, these results are not surprising as the sample volumes for each type of experiment were very different. The RBC freezing experiments presented earlier in figure 8.16 use a total volume of 300 μL, whereas the deglycerolization experiments were frozen with a total volume of 2 mL. Consequently, the freezing rate in the deglycerolization studies is likely slower than the original RBC freezing experiments and this is reflected by the different recoveries. As mentioned earlier, rapid freezing rates greater than 100°C/min are required for the low glycerol cryopreservation method, and so it is plausible that the larger volumes are not frozen to -80°C at an ideal rate.[118] However, further studies are required to determine the rate of freezing for these conditions using a thermocouple temperature probe, which would also provide valuable information to for optimizing the freezing protocol.

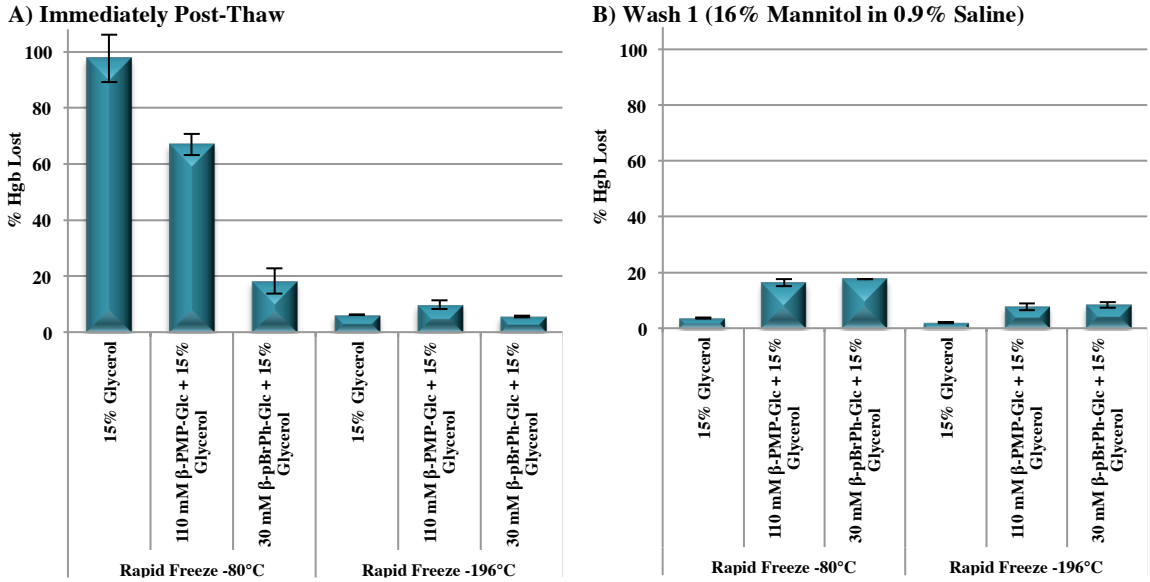

Figure 8.17 % Hgb lost in the deglycerolization process after rapid freezing to -80°C or -196°C with 15% glycerol, 110 mM β-PMP-Glc +15% glycerol, or 30 mM β-pBrPh-Glc +15% glycerol cryo-solutions. All cryo-solutions also contained a 1.5% mannitol additive. **A)** Immediate % Hgb lost in post-thaw supernatant. **B)** % Hgb lost after wash 1. Wash 1 solution consisted of a 16% mannitol in 0.9% saline solution.

The highly beneficial effect of the 30 mM β-pBrPh-Glc in a 15% glycerol solution is evident with the rapid freezing to -80°C conditions. The % Hgb lost immediately post-thaw was significantly less than the 15% glycerol control, and the β-pBrPh-Glc containing cryo-solution resulted in only 20% Hgb lost in the post-thaw supernatant (figure 8.17A). These results were approaching the immediate post-thaw recoveries of the samples rapidly frozen to -196°C. All samples subjected to the rapid freezing to -196°C conditions resulted in low % Hgb lost immediately post-thaw ranging from 6-10%, regardless of the cryo-solution used to protect the RBCs (figure 8.17A).

The effect of wash 1 (a 16% mannitol in 0.9% saline solution) on these thawed RBC samples is shown in figure 8.17B. Samples frozen to -80°C with either β-PMP-Glc additive or β-pBrPh-Glc additive resulted in a loss of ~17% Hgb. Less Hgb was lost for the same cryo-additives when the samples were rapidly frozen to -196°C (~8% Hgb lost in wash 1 supernatant). It is evident that this first wash condition is optimal for 15% glycerol rapidly frozen to -196°C as only 2% Hgb was lost at this step.

The most crucial step in the deglycerolization process is wash 2 as this typically involves moving from a solution of high osmolality (such as 16% mannitol or 12% saline) to a drastically lower osmolality (such as 1.6% or 0.9% saline).[114,118,122,148] Thus, we investigated various wash 2 conditions including the standard 0.9% saline wash (condition A), as well as a 1.6% saline wash (condition B), a 10% mannitol in 0.9% saline wash (condition C), and a 10% mannitol in 1.6% saline wash (condition D) as summarized in table 8.1. Mannitol was employed in conditions C and D to provide a more gradual gradient in osmolality changes between wash 1 and wash 3. All four conditions were subject to a final wash (wash 3) of 0.9% saline. The % Hgb lost in wash 2 is presented in figure 8.18A and the % Hgb lost in wash 3 is presented in figure 8.18B. The overall final % RBC recoveries after the deglycerolization process are shown in figure 8.18C. Following removal of the wash 3 supernatant the remaining RBCs were resuspended in an isotonic dextrose/saline solution (0.2% dextrose/0.9% saline).[118]

When β-PMP-Glc or β-pBrPh-Glc were used as additives in the cryo-solutions, a significant amount of cellular damaged is incurred when the second wash was either 0.9% or 1.6% saline (Figure 8.18A, conditions A and B). This wash results in ~20% Hgb lost when β-PMP-Glc was used to freeze RBCs, and for β-pBrPh-Glc the second wash results in a significant loss of ~40% when only the saline solutions are used. The addition of mannitol to the second wash solution prevents additional hemolysis at this step (conditions c and d). However, the third wash after the mannitol-containing wash 2 solutions again results in a significant loss of Hgb ranging from 20-45% for both β-PMP-Glc and β-pBrPh-Glc cryo-additives. These results are not observed with

the 15% glycerol solution alone, and this cryo-solution resulted in minimal Hgb loss and thus minimal cellular damage during both wash 2 and wash 3 (figure 8.18A and B). Thus, it is clear from the % Hgb lost in both wash 2 and wash 3 that when either β-PMP-Glc or β-pBrPh-Glc are utilized in the cryo-solutions, it is difficult to return the RBCs to isotonic conditions during deglycerolization without incurring a significant amount of cellular damage. This is in contrast to 15% glycerol, which behaves relatively well with all of the wash 2 conditions employed.

The overall percent RBC recoveries after the deglycerolization process are presented in figure 8.18C. As expected, the 15% glycerol solution alone resulted in high recoveries (80-90%) when rapid freezing conditions to -196°C were employed. When β-PMP-Glc or β-pBrPh-Glc were used in the cryo-solutions with these same freezing conditions, recoveries are drastically decreased. The β-PMP-Glc containing solutions had overall post-freeze-thaw-deglycerolization recoveries of 40-60%, whereas the β-pBrPh-Glc containing solution had recoveries of 10-40%. Thus, it is evident that these washing conditions are not suitable for the cryo-solutions containing these novel phenolic-glucoside cryo-additives. All of the samples rapidly frozen to -80°C had very poor RBC recovery regardless of the cryo-solution employed. The β-pBrPh-Glc cryo-solution when rapidly frozen to -80°C did result in a low amount of recovered RBCs after the deglycerolization process. However, analysis of the percent hemolysis obtained upon resuspension of the deglycerolized RBCs in dextrose/saline indicated that these recovered cells were not stable in isotonic solution. 40-60% hemolysis was measured immediately after the recovered RBCs were resuspended in isotonic dextrose/saline, thus when taking this into consideration the overall recoveries for the β-pBrPh-Glc containing cryo-solution frozen at -80°C would be less than 10%. Overall, the results from this deglycerolization study reveal that the routinely used deglycerolization protocol for low glycerol RBC cryopreservation methods do not translate to the novel cryo-solutions containing the potently IRI active phenolic-glucosides β-PMP-Glc or β-pBrPh-Glc.

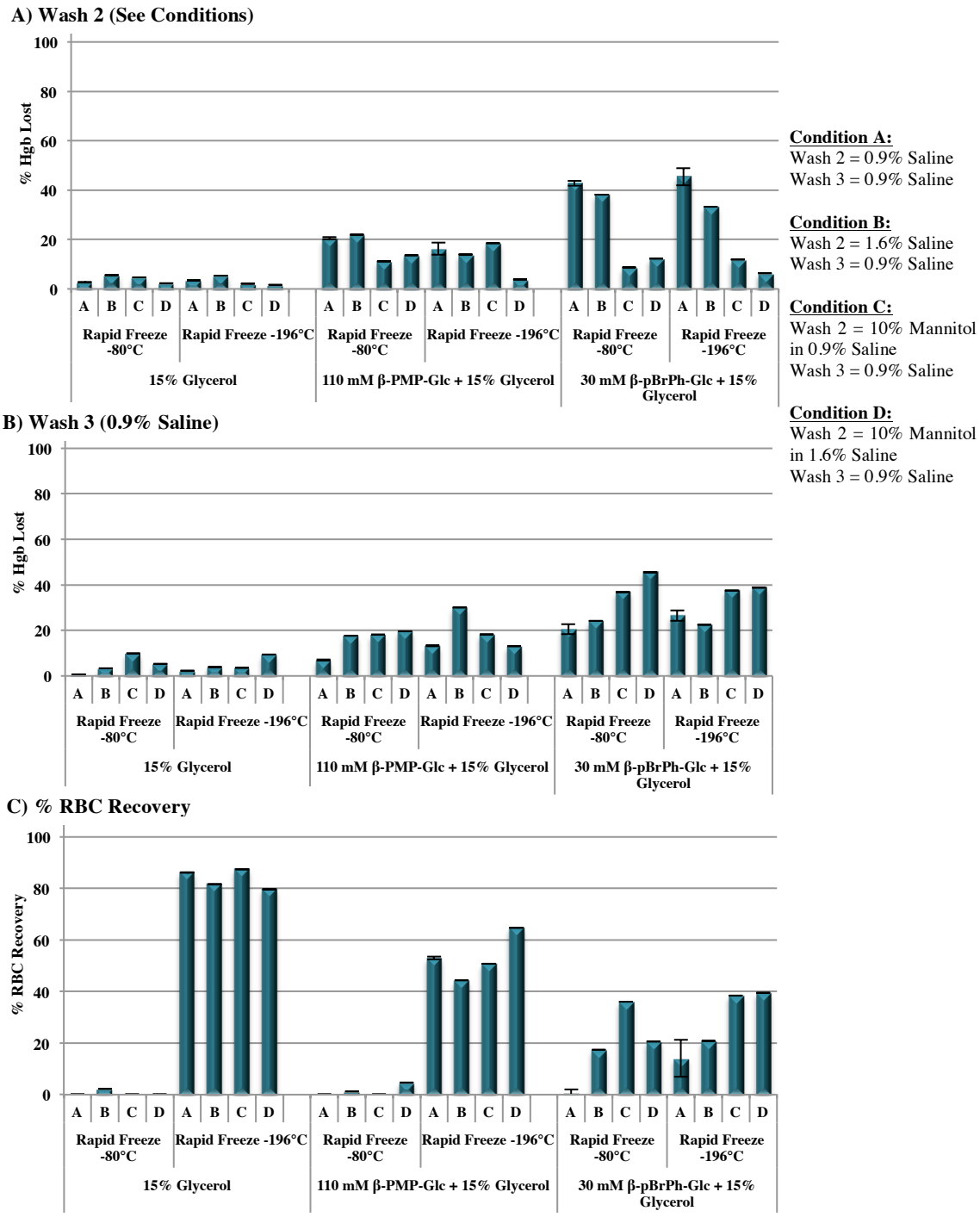

Figure 8.18 % Hgb lost in washes 2 and 3 and total % RBC recoveries after rapid freezing to -80°C or -196°C with 15% glycerol, 110 mM β-PMP-Glc +15% glycerol, or 30 mM β-pBrPh-Glc +15% glycerol cryo-solutions. All cryo-solutions also contained a 1.5% mannitol additive. **A)** % Hgb lost after wash 2. Wash 2 conditions are designated as follows: Condition A = 0.9% Saline; Condition B = 1.6% Saline; Condition C = 10% Mannitol in 0.9% Saline; Condition D = 10% Mannitol in 1.6% Saline. **B)** % Hgb lost after wash 3. Wash 3 solution consisted of a 0.9% saline solution after all wash 2 conditions. **C)** Total % RBC recoveries post-freeze-thaw and deglycerolization.

It is evident from the individual analysis of the percent Hgb lost in each wash step that the most cellular damage is occurring when low osmolality wash solutions (0.9% and 1.6% saline) are used immediately after solutions of high osmolalities (10% and 16% mannitol solutions) (figure 8.18A and B). Thus, the step-down in osmolality used in the previously described deglycerolization conditions is detrimental when the cryo-solutions contain β-PMP-Glc or β-pBrPh-Glc. The unloading of glycerol from RBCs is sensitive to large osmotic gradient fluctuations and excessive cell volume changes.[122,146,147] As such, we sought to examine the osmotic tolerance and mean cell volumes (MCV) of RBCs suspended in cryo-solution, as well as their osmotic tolerance and MCVs after each successive washing step. This would help determine the gradient steps of washing solutions that are well tolerated and can be used to deglycerolize the RBCs.

8.4.7 Osmotic Tolerance of RBCs after Treatment with Glycerol or Phenolic-Glucoside Solutions

The RBC osmotic tolerance experiments were conducted with a similar procedure to what has been described previously.[1,146] RBCs were first incubated at room temperature with the appropriate cryo-solution of either 15% glycerol, 110 mM β-PMP-Glc + 15% glycerol, 30 mM β-pBrPh-Glc +15% glycerol, or 20 mM β-pBrPh-Glc +15% glycerol. All cryo-solutions also contained a 1.5% mannitol additive as described previously in this section. A 20 mM β-pBrPh-Glc solution was examined in these studies to investigate if the lower β-pBrPh-Glc concentration was tolerated better with the osmolality changes in the wash solutions as 30 mM β-pBrPh-Glc was detrimental in the previous deglycerolization conditions (figures 8.17 and 8.18). In addition, a SAGM control (saline-adenine-glucose-mannitol) was also examined in the osmotic tolerance assay as this is the isotonic solution RBCs are typically stored in. Following incubation with these solutions, MCVs were measured on a hematology analyzer and samples were centrifuged, the supernatants were removed and osmolalities were measured using a micro-osmometer. The packed RBCs were resuspended in NaCl solutions ranging in concentration

Table 8.2 Measured osmolalities (mOsm/kg) of NaCl solutions. Osmolalities greater than 3000 mOsm/kg were not able to be accurately read and are recorded as NR (no reading).

% NaCl (w/v)	NaCl Conc. (g/L)	Osmolality (mOsm/kg)
0.1	1	30
0.2	2	61
0.3	3	95
0.35	3.5	112
0.4	4	125
0.5	5	157
0.55	5.5	173
0.6	6	189
0.65	6.5	206
0.75	7.5	234
0.9	9	280
1	10	309
1.5	15	424
2	20	618
2.5	25	692
3	30	906
3.5	35	1070
4	40	1203
4.5	45	1361
5	50	1507
5.5	55	1609
6	60	1805
6.5	65	1939
7	70	2025
7.5	75	2173
8	80	2308
8.5	85	2562
9	90	NR (>3000)
9.5	95	NR (>3000)
10	100	NR (>3000)

from 0-10% NaCl and the % hemolysis obtained from resuspension in these solutions was quantified spectrophotometrically. The osmolalities of the NaCl solutions are provided in table 8.2. Figure 8.19 shows the % hemolysis observed after resuspension in the NaCl solutions following incubation with each cryo-solution. Table 8.2 provides the MCVs and supernatant osmolalities after incubation with each cryo-solution.

Immediately following incubation, all four cryo-solutions assessed exhibited similar osmotic tolerance profiles (figure 8.19). The profiles indicate that after incubation with the cryo-solutions, the RBCs can be suspended in NaCl solutions ranging from 3.5-5.5% NaCl (35-55 g/L) without causing extensive hemolysis and damage to the RBCs. These NaCl concentrations correspond to osmolalities of 1070-1609 mOsm/kg (table 8.2). Interestingly, both β-pBrPh-Glc concentrations will not tolerate resuspension in NaCl solutions greater than 6% (>1800 mOsm/kg), and above these concentrations RBC hemolysis occurs. This same effect is not observed with 15% glycerol or the β-PMP-Glc cryo-solution, which can tolerate up to 10% NaCl for resuspension with minimal hemolysis observed. Thus, after thawing, it appears the RBC samples should be able to be successfully washed with NaCl solutions 3.5-5.5% without causing extensive cell damage resulting in hemolysis of the RBCs. When the RBCs were suspended in the cryo-solutions they swelled to a much larger volume than when they are suspended in isotonic SAGM storage solution (table 8.3). The MCV of RBCs suspended in SAGM was 93 fL, whereas suspension in 15% glycerol, 110 mM β-PMP-Glc +15% glycerol, or 20 mM β-pBrPh-Glc +15% glycerol resulted in MCVs of ~120 fL. Interestingly, while a 30 mM β-pBrPh-Glc +15% glycerol solution swelled RBCs, the MCVs were lower than that observed with the other cryo-solutions at ~108 fL. The RBC swelling observed with these cryo-solutions is consistent with the loading and internalization of glycerol.[1]

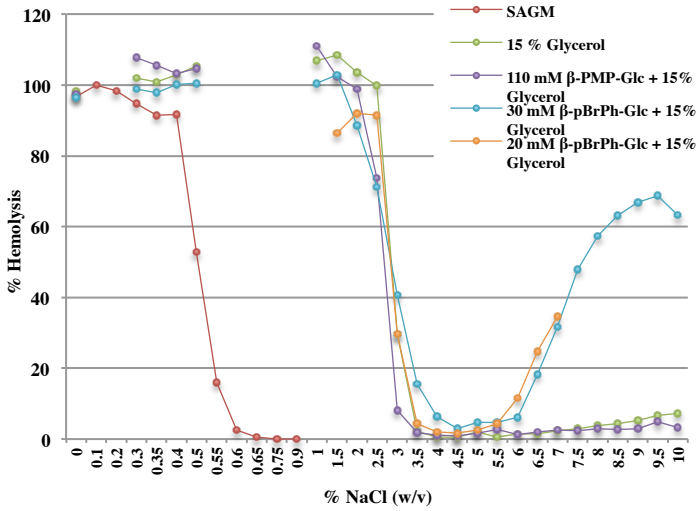

Figure 8.19 Osmotic tolerance of RBCs incubated with SAGM or cryo-solutions. After incubation with the indicated solution, packed RBCs were resuspended in various NaCl solutions and assessed for % hemolysis.

Table 8.3 Measured RBC MCVs and supernatant osmolalities (mOsm/kg) after incubation with cryo-solutions. Osmolalities greater than 3000 mOsm/kg are recorded as NR (no reading).

Solution	MCV (fL)	Supernatant Osmolality (mOsm/kg)
SAGM	93.2	360
15% Glycerol	120.1	NR (>3000)
110 mM β-PMP-Glc + 15% Glycerol	118.9	NR (>3000)
30 mM β-pBrPh-Glc + 15% Glycerol	108.4	NR (>3000)
20 mM β-pBrPh-Glc + 15% Glycerol	120	NR (>3000)

8.4.8 Osmotic Tolerance of RBCs after Cryo-Solution Incubation and Treatment with Wash 1

Having established that following incubation with the cryo-solutions the RBCs could be re-suspended in solutions ranging from 3.5-5.5% NaCl or 1070-1609 mOsm/kg, we next investigated the solution osmolalities that would be tolerated after wash 1. Following incubation with the cryo-solutions and removal of the supernatant, the packed RBCs were resuspended in wash 1 solutions. The wash 1 solutions had osmolalities that were 1400-1500 mOsm/kg as resuspension in these solutions resulted in minimal hemolysis (4.5-5% NaCl, figure 8.19). Thus, a 5% NaCl solution (50 g/L) was used as a wash 1 solution (W1-A condition). However, there was also interest in exploring a mannitol solution as wash 1 as mannitol is suggested to stabilize cell membranes a facilitate glycerol unloading from the RBCs.[118] Consequently, a 0.3 M mannitol solution in 4.98% NaCl (49.8 g/L NaCl) was also utilized as a wash 1 solution (W1-B condition) as this solution had an osmolality of 1396 mOsm/kg (table 8.4). The osmotic tolerance profiles following both wash 1 conditions are presented in figure 8.20 and the MCVs after wash 1 along with wash 1 supernatant osmolalities are provided in table 8.5.

Table 8.4 Osmolalities of wash 1 solutions.

Wash 1 Solution	Osmolality (mOsm/kg)
50 g/L NaCl	1507
0.3 M Mannitol, 49.8 g/L NaCl	1396

The osmotic tolerance profiles for each cryo-solution are quite different following wash 1. 15% glycerol could be resuspended directly into a 0.9% saline solution immediately following both wash 1 conditions and minimal hemolysis was observed (figure 8.20). With the β-PMP-Glc containing cryo-solution, an increase in hemolysis began when the RBCs were resuspended in NaCl solution less that 1.5%; however, higher saline concentrations were well tolerated and low

RBC hemolysis was obtained. These results indicate that following wash 1, both 15% glycerol and β-PMP-Glc can be resuspeded and washed in solutions that are close to isotonic conditions (0.9% saline). In contrast, the 30 mM β-pBrPh-Glc cryo-solution could only be resuspended in saline solutions greater than 900 mOsm/kg (3% NaCl, table 8.2), and lower osmolalities resulted in significant hemolysis (figure 8.20). Thus, RBCs suspended in the 30 mM β-pBrPh-Glc cryo-solution appear to be highly susceptible to hemolysis by large differences in solution osmolalities.

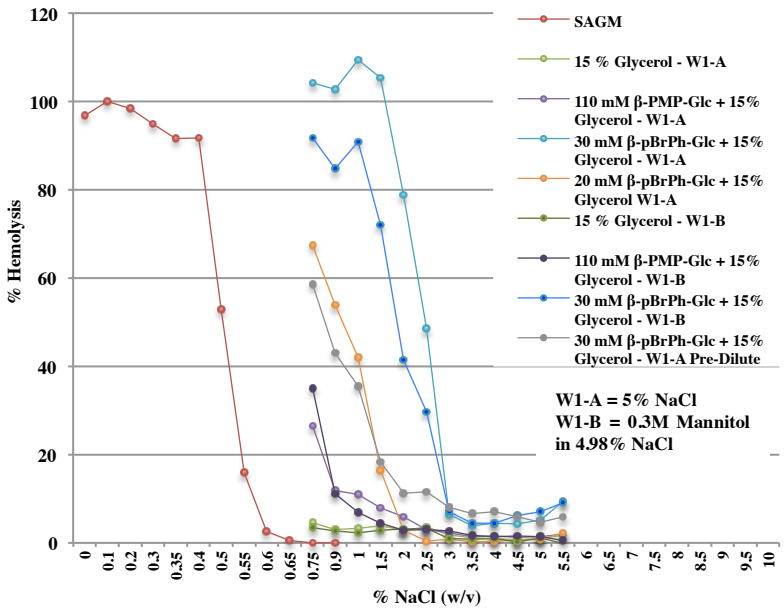

Figure 8.20 Osmotic tolerance of RBCs after wash 1. Following removal of cryo-solution supernatant, packed RBCs were resuspended in wash 1 solutions consisting of either 5% NaCl (W1-A) or 0.3M mannitol in 4.98% NaCl (W1-B). After incubation with wash 1, packed RBCs were resuspended in various NaCl solutions and assessed for % hemolysis.

Table 8.5 Measured RBC MCVs and supernatant osmolalities (mOsm/kg) after incubation with wash 1.

Cryo-Solution	Wash 1 Solution	MCV (fL)	Supernatant Osmolality (mOsm/kg)
15% Glycerol	50 g/L NaCl	96.6	1830
	0.3M Mannitol, 49.8 g/L NaCl	95.9	1727
110 mM β-PMP-Glc + 15% Glycerol	50 g/L NaCl	104.2	1905
	0.3M Mannitol, 49.8 g/L NaCl	103.1	1716
30 mM β-pBrPh-Glc + 15% Glycerol	50 g/L NaCl	76	1822
	0.3M Mannitol, 49.8 g/L NaCl	79.2	1761
20 mM β-pBrPh-Glc + 15% Glycerol	50 g/L NaCl	86.2	1841

Interestingly, this hemolysis can be mitigated by employing a wash 1 "pre-dilution" (see W1-A pre-dilute curve for 30 mM β-pBrPh-Glc in figure 8.20). This involves an initial addition of the wash 1 solution to the RBCs suspended in cryo-solution, and following removal of this pre-dilution supernatant, the packed RBCs are resuspended in the wash 1 solution. This provides a more gradual step-down from the high osmolality of the cryo-solution (>3000 mOsm/kg, table 8.3) to the significantly lower osmolality of wash 1 (1507 for 5% NaCl, table 8.4). By using a pre-dilution step prior to wash 1, the RBCs after wash 1 can be resuspended in 2% NaCl without significant hemolysis (W1-A pre-dilute curve), as opposed to 3% NaCl when no pre-dilution step is used (W1-A conditions for 30 mM β-pBrPh-Glc). A decrease in β-pBrPh-Glc concentration to 20 mM was also more beneficial for the washing of the RBCs compared with the 30 mM solution. The 20 mM β-pBrPh-Glc osmotic tolerance profile was similar to that obtained when a wash 1 pre-dilute was used with 30 mM β-pBrPh-Glc, where significant hemolysis was observed

after resuspension in NaCl concentrations less than 1.5% following wash 1 (figure 8.20). The results for the osmotic tolerance profiles from wash 1 indicated that osmolalities of the wash 2 solutions for 15% glycerol or β-PMP-Glc solutions should be approximately 400 mOsm/kg (1.5% NaCl, table 8.2), whereas for 30 mM β-pBrPh-Glc a higher solution osmolality is required of ~900 mOsm/ kg (3% NaCl, table 8.2).

The MCVs following wash 1 returned to normal physiological RBC volumes for both 15% glycerol and β-PMP-Glc solutions (table 8.5). The MCVs for these solutions following wash 1 were 96-104 fL in size, which is close to that obtained for the RBCs suspended in SAGM (93 fL, table 8.2). However, the MCVs from the β-pBrPh-Glc containing solution remained significantly smaller than regular RBC volumes, with both solutions having MCVs of 76-86 fL following wash 1 (table 8.5). Thus, a plausible explanation for the lower osmotic tolerance of the RBCs when β-pBrPh-Glc is present in the cryo-solution could be that following the first wash with a hypertonic NaCl solution, the RBCs remain shrunken. Upon resuspension in a solution that has a lower osmolality than the wash solution, the cells swell beyond their maximal cell volume, causing the RBCs to hemolyze.[1,122,146,147] While an explanation for why the β-pBrPh-Glc solutions excessively shrink the cells upon washing with a hypertonic saline solution is currently not known, it is evident that a more gradual decrease in solution osmolality is required for washing with these cryo-solutions.

8.4.9 Osmotic Tolerance of RBCs after Treatment with Wash 2

A similar analysis of osmotic tolerances for wash 2 was preformed for all cryo-solutions. Based of the osmotic tolerance profiles obtained from wash 1 (figure 8.20), the wash 2 conditions utilized were 1.5% saline (~400 mOsm/kg) for 15% glycerol and the β-PMP-Glc solution, and 3% saline (~900 mOsm/kg) for both β-pBrPh-Glc solutions. The osmotic tolerance profiles following wash 2 are presented in figure 8.21 and the MCVs and supernatant osmolalities after wash 2 are presented in table 8.6. Following wash 2 at 1.5% saline, RBCs initially treated with 15% glycerol and 110 mM β-PMP-Glc +15% glycerol solutions can be resuspended in an isotonic saline solution and minimal RBC hemolysis is observed. Interestingly, the curves for the β-pBrPh-Glc containing solutions after wash 2 did not shift from the curves obtained after wash 1. Both the 20 mM β-pBrPh-Glc solution and the 30 mM β-pBrPh-Glc that had a pre-dilution prior to wash 2 resulted in significant hemolysis after resuspension in less than 1.5% saline solutions (figure 8.21), which was similar to that obtained after wash 1 (figure 8.20). Moreover, the 30 mM β-pBrPh-Glc with no pre-dilution prior to wash 2 resulted in significant hemolysis when resuspended in 2% saline (figure 8.21), which is only slighter lower than wash 1 at 2.5%

saline (figure 8.20). Thus, it appears that the washing sequence employed for RBCs initially treated with 15% glycerol or 110 mM β-PMP-Glc +15% glycerol solutions can successfully be returned to an isotonic state after 2 washes. However, it appears that RBCs initially treated with β-pBrPh-Glc solutions are more susceptible to damage from decreasing solution osmolalities, and that returning the cells to an isotonic state may be challenging. Furthermore, the MCVs after wash 2 for RBCs initially treated with β-pBrPh-Glc were still smaller than physiological volumes (table 8.6), and in fact were similar to the MCVs observed after wash 1 (table 8.5) at approximately 83 fL. Thus, a second wash a lower osmolality than wash 1 (900 mOsm/kg *versus* 1500 mOsm/kg) was unable to swell the RBCs back to a normal cell volume. As described previously, this is possibly the reason for the significant hemolysis observed upon resuspension in solutions of lower osmolalities.[1,122,146,147]

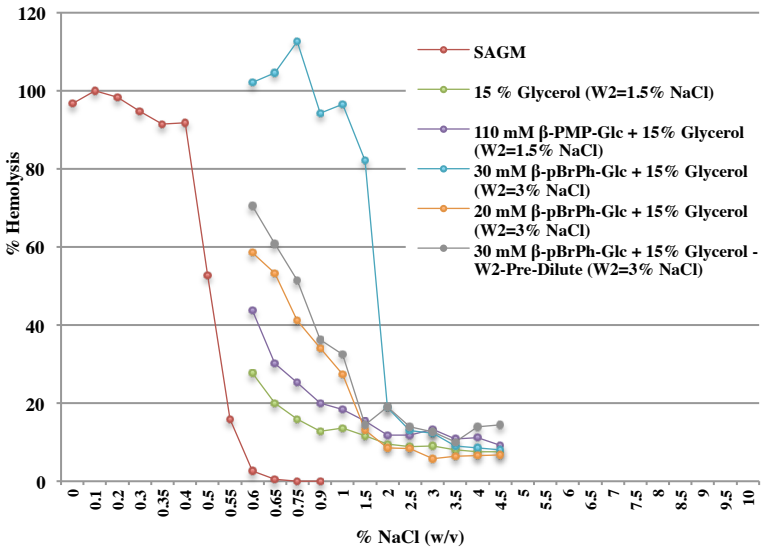

Table 8.6 Measured RBC MCVs and supernatant osmolalities (mOsm/kg) after incubation with wash 2.

Cryo-Solution	Wash 2 Solution	MCV (fL)	Supernatant Osmolality (mOsm/kg)
15% Glycerol	15 g/L NaCl	99.7	645
110 mM β-PMP-Glc + 15% Glycerol	15 g/L NaCl	104.4	654
30 mM β-pBrPh-Glc + 15% Glycerol	30 g/L NaCl	82.7	1103
20 mM β-pBrPh-Glc + 15% Glycerol	30 g/L NaCl	87.7	1040

Figure 8.21 Osmotic tolerance of RBCs after wash 2. RBCs were first incubated with cryo-solutions, then washed with a 5% NaCl wash 1 solution, and either a 1.5% or 3% NaCl solution for wash 2. After incubation with wash 2, packed RBCs were resuspended in various NaCl solutions and assessed for % hemolysis.

8.4.10 Osmotic Tolerance of RBCs after Treatment with Wash 3

The final step of the osmotic tolerance experiments was to ensure that after the final isotonic saline wash (wash 3 = 0.9% saline) the RBCs had returned to a normal physiological response to osmotic gradients. As such, the experiments were repeated after a final wash with 0.9% NaCl and hemolysis assessed after resuspension in hypotonic saline solutions to observe if the osmotic tolerance curves were similar to the SAGM control. Only RBCs initially treated with 15% glycerol or β-PMP-Glc were subjected to a final wash with isotonic saline as the previous

osmotic tolerance curves indicated that minimal hemolysis would occur (figure 8.21). RBCs initially treated with the 30 mM β-pBrPh-Glc solution were subjected to a third wash of 2% saline. The osmotic tolerance curves following wash 3 are presented in figure 8.22. The curves obtained following wash 3 of RBCs initially treated with 15% glycerol or 110 mM β-PMP-Glc + 15% glycerol solutions were similar to that of the SAGM control. This suggests that the RBCs have returned to a physological response to saline solutions after being subjected to the three step washing protocol (wash 1 = 5% NaCl; wash 2 = 1.5% NaCl; wash 3 = 0.9% NaCl). Unfortunately, after the third wash of 2% saline for RBCs treated with the 30 mM β-pBrPh-Glc +15% glycerol solution (figure 8.22) the osmotic profile was similar to that observed with wash 2 (figure 8.21). A significant amount of hemolysis was obtained upon resuspension in 1.5% saline following wash 3. Thus, it is evident that this washing protocol for β-pBrPh-Glc (wash 1 = 5% NaCl; wash 2 = 3% NaCl; wash 3 = 2% NaCl) is not ideal for the unloading glycerol from cells treated with the 30 mM β-pBrPh-Glc +15% glycerol cryo-solution.

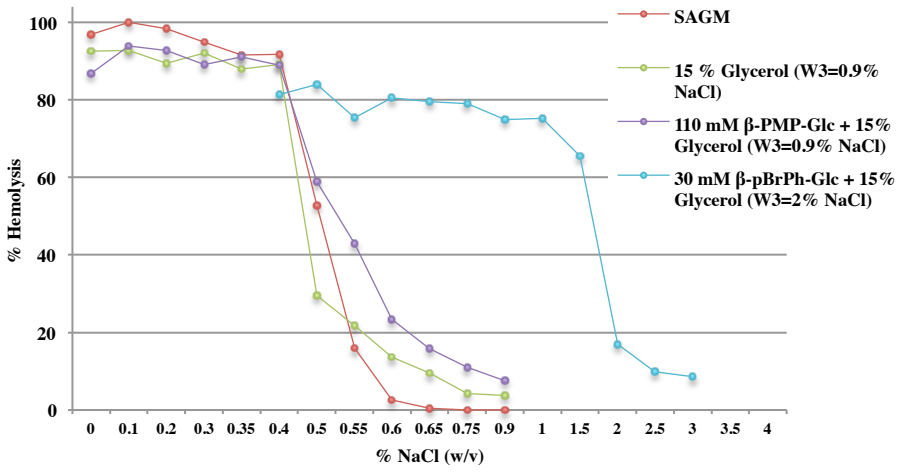

Figure 8.22 Osmotic tolerance of RBCs after wash 3. RBCs were first incubated with cryo-solutions, then washed with a 5% NaCl wash 1 solution, either a 1.5% (for glycerol and β-PMP-Glc) or 3% (for β-pBrPh-Glc) NaCl wash 2 solution. After incubation with wash 3, RBCs were resuspended in NaCl solutions and assessed for % hemolysis.

Overall, the osmotic tolerance studies following treatment of RBCs with either 15% glycerol, 110 mM β-PMP-Glc + 15% glycerol, 30 mM β-pBrPh-Glc +15% glycerol or 20 mM β-pBrPh-Glc +15% glycerol cryo-solutions have provided valuable information that can be translated to deglycerolization conditions to cause minimal damage to the RBCs. These studies have indicated that the ideal wash solutions for the 110 mM β-PMP-Glc + 15% glycerol solution are as follows: wash 1 = 5% NaCl (~1500 mOsm/kg); wash 2 = 1.5% NaCl (~400 mOsm/kg); wash 3 = 0.9% NaCl (isotonic saline). While the wash conditions employed in these studies for RBCs treated with the 30 mM β-pBrPh-Glc +15% glycerol solution were not ideal as the RBCs could not be returned to isotonic conditions, an interesting observation from the wash 1 conditions provided

potential deglycerolization washing conditions for this solution. It was observed that using a pre-dilution step prior to incubation with wash 1 resulted in the RBCs being more tolerable to resuspension in lower osmolality NaCl solutions (figure 8.20, W1-A pre-dilute for 30 mM β-pBrPh-Glc). This pre-dilution step involved the addition of the wash 1 solution into the RBC-cryo-solution mixture prior to centrifugation to gradually decrease the osmolality of the cryo-solution-RBC mixture closer to the osmolality of the wash 1 solution. With this step, the osmotic tolerance curve for RBCs treated with the 30 mM β-pBrPh-Glc solution indicated that minimal hemolysis is obtained when the RBCs are resuspended in 1.5% NaCl (figure 8.20). This suggests that the second wash condition could be similar to that utilized for β-PMP-Glc (1.5% NaCl) following a 5% NaCl wash 1 solution. Consequently, this pre-dilution step was employed prior to each wash step for RBCs cryopreserved with both β-PMP-Glc and β-pBrPh-Glc. This pre-dilution process also mimics more closely clinical deglycerolization conditions that are gradually reduced from a 12% saline wash to a 1.6% saline wash using continual centrifugation.[114,115,122,148]

8.4.11 Attempted Deglycerolization after Analysis of RBC Osmotic Tolerances

Having established optimal washing conditions from the osmotic tolerance experiments, these conditions were then applied for the deglycerolization of RBCs frozen with either 15% glycerol, 110 mM β-PMP-Glc + 15% glycerol, 30 mM β-pBrPh-Glc +15% glycerol or 20 mM β-pBrPh-Glc +15% glycerol cryo-solutions. As described previously, all cryo-solutions also contained 1.5% mannitol and all samples were frozen under rapid freezing conditions to -80°C or -196°C and thawed at 42°C (section 8.4.6).[118] The washing conditions employed for these deglycerolization experiments were selected based on the osmotic tolerance results described in sections 8.4.7 - 8.4.10 and were as follows: wash 1 = 5% NaCl (condition A) or 0.3 M mannitol in 4.98% saline (condition B) (osmolalities of 1507 mOsm/kg and 1396 mOsm/kg, respectively); wash 2 = 1.5% NaCl; wash 3 = 0.9% NaCl; resuspension in isotonic dextrose/saline (0.2%/0.9%). However, pre-dilutions were employed prior to the addition of each wash solution for a more gradual decrease in solution osmolalities and to mimic more closely deglycerolization conditions used clinically.[114,115,122,148] Prior to each wash, a pre-dilute was conducted on the solution before by adding an equal volume of wash solution as the previous step's supernatant (~500 μL). The wash 1 pre-dilute was thus added to the post-thaw cryo-solution/RBC mixture, and the sample was resuspended and centrifuged. The supernatant of the wash 1 pre-dilute was then removed and the quantity of Hgb present in this supernatant was quantified. This wash 1 pre-dilute would contain the Hgb lost from freezing and thawing, and the Hgb lost from the pre-dilution with the wash 1 solution. Subsequently, the packed RBCs were then resuspended and equilibrated with the wash 1

solution for 10 minutes, followed by the addition of the wash 2 solution (~500 μL) for the wash 2 pre-dilute. This process was repeated for all three washes, and the quantity of Hgb in each pre-dilute solution, which is a combination of Hgb lost in the wash step and the subsequent pre-dilute step, was measured spectrophotometrically using Drabkin's assay (see section 8.4.3). The overall recovery (% RBC recovery) was calculated by the sum of total Hgb lost throughout each pre-dilute supernatant and the final wash 3 of deglycerolization process, compared to the total Hgb originally measured in the RBC sample.[118]

The % Hgb lost in each wash pre-dilute and the final wash 3 is presented in figure 8.23. The wash 1 pre-dilute represents a combination of the % Hgb lost immediately post-thaw and the % Hgb lost upon the addition of 500 μL of W1 to the thawed cryo-solution/RBC mixture (figure 8.23A). Similar to that observed in section 8.4.6, a 15% glycerol solution with rapid freezing to -80°C resulted in significant damage to the RBCs as a high amount of Hgb is lost in the wash 1 pre-dilute supernatant. When β-PMP-Glc is added to the cryo-solution under the same freezing conditions, the % Hgb lost is less than that of 15% glycerol alone, but this value is still moderately high with ~40% Hgb lost in the wash 1 pre-dilute. However, when β-pBrPh-Glc is added to the cryo-solutions with rapid freezing to -80°C, the quantity of Hgb lost in the wash 1-pre-dilute is close to that of the -196°C rapid freezing conditions for both concentrations of β-pBrPh-Glc (figure 8.23A). Thus, immediately upon thawing and with the addition of 500 μL of either wash 1 solutions (conditions A or B), a large quantity of RBCs are still intact with the 20 mM and 30 mM β-pBrPh-Glc cryo-solutions. This highlights the beneficial effect of this cryo-additive for the freezing of RBCs, especially to the higher sub-zero temperature of -80°C (compared with -196°C).

For all cryo-solutions and freezing conditions assessed, it is evident that a significant amount of Hgb is lost in the wash 2 pre-dilute supernatant (figure 8.23B). This step resulted in 16-33% Hgb lost regardless of the freezing condition or the cryo-solution used. The wash 2 pre-dilute is a combination of the % Hgb lost in wash 1 and the % Hgb lost upon the addition of 500 μL of the wash 2 solution (1.5% NaCl). An analysis of the Hgb lost immediately following wash 1 (both conditions A and B) indicated that less than 4% Hgb was lost in the wash 1 supernatant (data not shown). Thus, the 16-33% Hgb lost in the wash 2 pre-dilute can be attributed to the addition of the lower osmolality wash 2 solution to the higher osmolality wash 1/RBC mixture, despite the more gradual gradient approach with the pre-dilution conditions. This is consistent with the second wash of the deglycerolization process being the most important wash solution that can result in the most damage to the RBCs during the unloading of glycerol.[114,118,122,148]

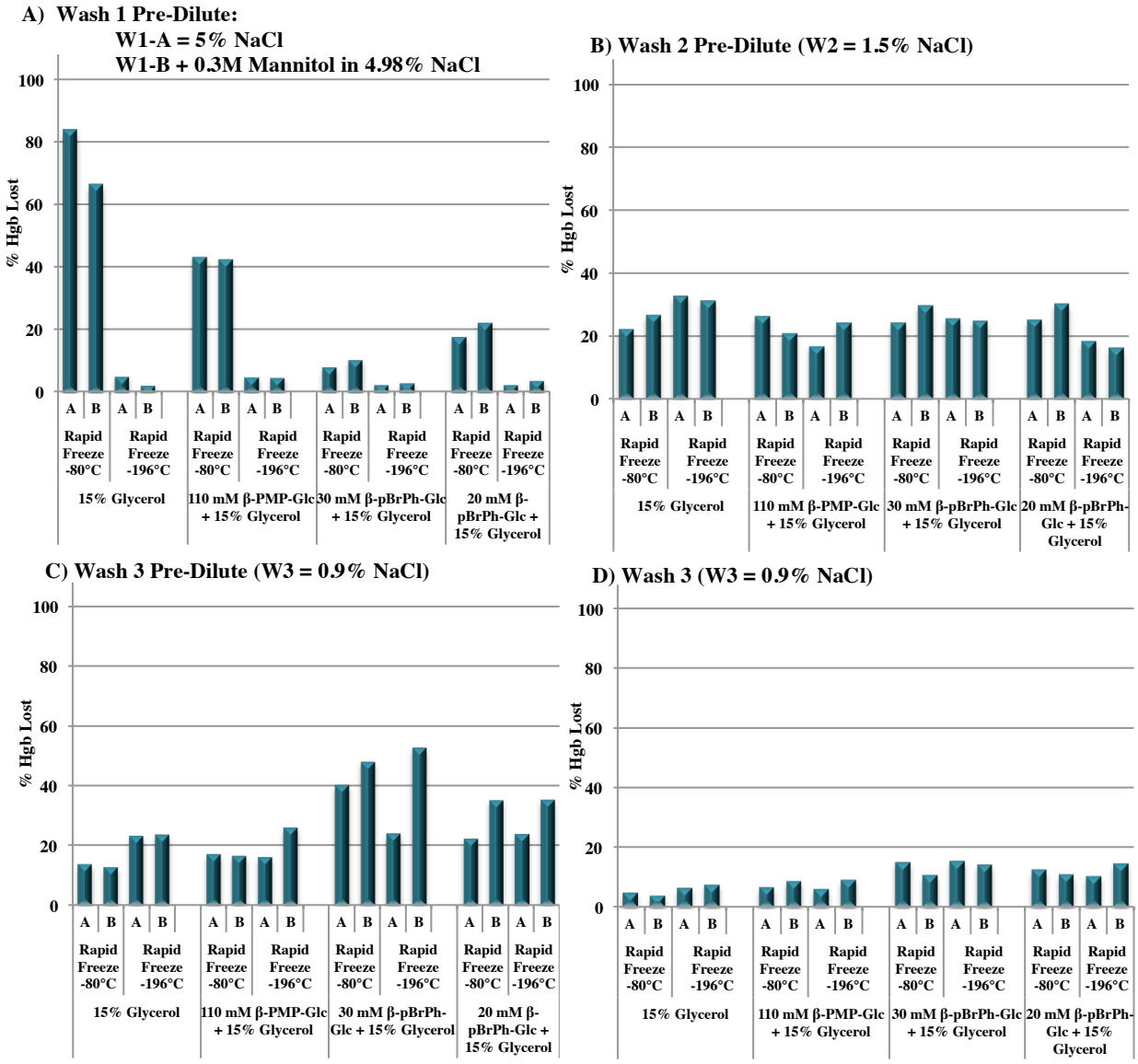

Figure 8.23 % Hgb lost in the deglycerolization process after rapid freezing to -80°C or -196°C with 15% glycerol, 110 mM β-PMP-Glc +15% glycerol, 30 mM β-pBrPh-Glc +15% glycerol, or 20 mM β-pBrPh-Glc +15% glycerol cryo-solutions. All cryo-solutions also contained a 1.5% mannitol additive. **A)** % Hgb lost after wash 1 pre-dilute. Wash 1 conditions are designated as follows: Condition A = 5% Saline; Condition B = 0.3M Mannitol in 4.98% Saline. **B)** % Hgb lost after wash 2 pre-dilute. Wash 2 solution consisted of a 1.5% saline solution after both wash 1 conditions. **C)** % Hgb lost after wash 3 pre-dilute. Wash 3 solution consisted of a 0.9% saline solution. **D)** % Hgb lost after wash 3 (0.9% saline solution).

A similar result was also obtained with the wash 3 pre-dilute (figure 8.23C). The % Hgb lost in the wash 3 pre-dilute supernatant ranged from 17-53%, with the highest amount of Hgb being lost when RBCs were frozen with the 30 mM β-pBrPh-Glc. The majority of the Hgb was actually lost in the wash 2 supernatant, which typically ranged from 20-40% Hgb depending on the cryo-solution used to freeze the RBCs (data not shown). Typically the addition of the wash 3 solution to the wash 2/RBC mixture for the wash 3 pre-dilute resulted in only 5% extra Hgb loss relative

to the wash 2 supernatant. Thus, it is evident that a significant amount of hemolysis is occurring in the step-down process from wash 1 to wash 2. This data suggests that the second wash solution is not ideal for RBCs frozen with these novel cryo-solution and that further optimization for this stage of the deglycerolization process is still required.

The final wash (wash 3) in this deglycerolization protocol was a 0.9% saline wash. The % Hgb lost during this wash is presented in figure 8.23D. Regardless of the freezing condition or cryo-solution used, the amount of Hgb lost at this stage was less than 15%. This indicates that the final step-down to the 0.9% saline solution is tolerable with the cryopreserved RBCs and that the cells can be returned to an isotonic solution without incurring significant damage. This is significant as the previously employed deglycerolization protocol described in section 8.4.6 resulted in a significant amount of Hgb lost at this stage, indicating that the RBCs were not able to return to isotonic solution at that stage.

The total post-freeze-thaw-deglycerolization % RBC recoveries for these washing solutions are presented in figure 8.24. Unfortunately, overall the RBC recoveries were quite low, with the highest value being 50%. It is evident that these washing procedures are not optimal for RBCs rapidly frozen to -196°C in 15% glycerol. Total recoveries were ~35% using this method, whereas in the original washing conditions utilized in section 8.4.6 total recoveries were 80-90% (figure 8.17C). A plausible explanation for this could be that a high mannitol concentration for the first wash is required for the RBCs frozen in 15% glycerol.[118] Additionally, this deglycerolization method involved an extensive amount of centrifugation for each wash step and pre-dilute wash step that can be damaging to the RBCs, resulting in excess hemolysis throughout this process. While recoveries with this deglycerolization method were low, they were significantly better than the recoveries obtained in section 8.4.6 when the RBCs were frozen with the β-PMP-Glc or β-pBrPh-Glc containing cryo-solutions to -80°C. The previously employed washing conditions resulted in negligible RBC recoveries for the -80°C freezing conditions, whereas the conditions described here resulted in 10-23% RBC recoveries. Furthermore, the deglycerolized RBCs were resuspended in an isotonic dextrose/saline solution with minimal hemolysis observed upon resuspension (10-15%). It is evident that for the phenolic-glucoside containing cryo-solutions, saline washes as opposed to mannitol washes are less damaging to the RBCs. Despite both wash 1 conditions having similar osmolalities, the mannitol (condition B) wash resulted overall in lower RBC recoveries than the saline wash (condition A). Overall, these deglycerolization results are promising and suggest that with further optimization of the washing conditions higher RBC recoveries can be obtained. In particular, the second wash step must be

revised as this is the stage where the greatest amount of cellular damage is caused (figure 8.23B and C), resulting in the highest loss of Hgb throughout the deglycerolization process.

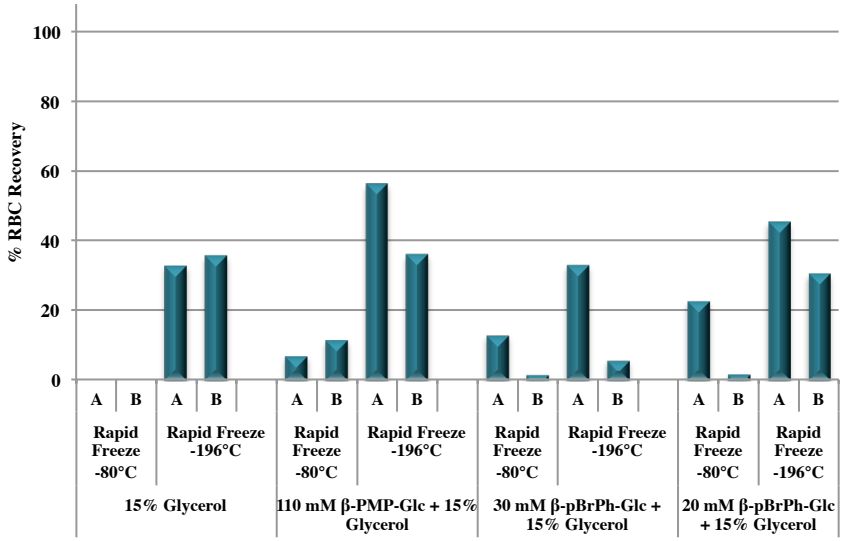

Figure 8.24 Total % RBC recoveries post-freeze-thaw-deglycerolization with 15% glycerol, 110 mM β-PMP-Glc +15% glycerol, 30 mM β-pBrPh-Glc +15% glycerol, or 20 mM β-pBrPh-Glc +15% glycerol cryo-solutions.

8.4.12 Summary and Conclusions for the Freezing of RBCs in the Presence of Phenolic-Glucoside IRIs with Reduced Glycerol Quantities

The RBC cryopreservation experiments described in section 8.4 have highlighted that small molecule IRIs can successfully be utilized for the freezing of RBCs in the presence of greatly reduced glycerol concentrations. Specifically, phenolic-glucosides can be beneficial cryo-additives for RBCs, resulting in greater RBC integrity (less hemolysis) relative to the glycerol control using slow-cooling conditions that are typically clinically employed in Canada and the United States for the high glycerol RBC cryopreservation method. In particular, a 110 mM β-PMP-Glc (**6**) solution in 15% glycerol resulted in double post-thaw integrities of the 15% glycerol solution alone (50% *vs*. 25%) when slow-cooling conditions were used. The best results were observed with a 30 mM β-pBrPh-Glc additive in 15% glycerol, where ~70% post-thaw RBC integrity was observed, which is almost triple that of the 15% glycerol cryo-solution alone. These results are highly significant as a reducing glycerol concentrations from the 40% solutions that are currently used for RBC cryopreservation can drastically reduce deglycerolization times allowing for faster access to cryopreserved RBC units for life-saving transfusions. While deglycerolization conditions for these novel RBC cryo-solutions containing β-PMP-Glc or β-pBrPh-Glc additives were explored, further optimization is still required to increase post-thaw

RBC recoveries. Initial optimization of wash solutions using RBC osmotic tolerance experiments provided successful osmotic step-down solutions that would cause the least amount of damage to the RBCs, in particular for the first wash in the deglycerolization process. However, the most crucial is the second wash in this process that decreases the high osmotic cryo-solution and wash 1 solution that the RBCs were suspended in, to a much lower osmotic environment closer to isotonic physiological conditions. As such, this second wash needs to be further optimized for each specific cryo-solution to enable to RBCs to return to isotonic conditions without undergoing significantly hemolysis. Once the RBCs can be successfully deglycerolized from the novel cryo-solutions, focus will then be on further optimizing the glycerolization stage and freezing stage of the cryopreservation protocol.

8.5 Summary and Conclusions for the Cryopreservation Potential of Carbohydrate-Based Small Molecule IRIs

Overall, this chapter has highlighted how potent small molecule ice recrystallization inhibitors can be successfully utilized as novel cryoprotectants or cryo-additives for the cryopreservation of various different cell lines. Many of these small molecules were found to be relatively non-toxic for a human liver cell line (HepG2 cells), in particular at and above concentrations where they were potently IRI active (section 8.2). The simple IRI active monosaccharide galactose and disaccharide sucrose were discovered to be beneficial for the cryopreservation of HSCs in UCB at high concentrations (220 mM). In particular, sucrose resulted in post-thaw $CD34^+$ (hematopoietic progenitor cells) cell viabilities of 50% without the addition of DMSO when slow-thaw conditions were employed (section 8.3). This is significant as there is a need to reduce or eliminate the used of the toxic CPA DMSO. The phenolic-glucosides were discovered to be beneficial cryo-additives for the freezing of human RBCs. The addition of β-PMP-Glc or β-pBrPh-Glc to reduced glycerol concentrations (15%) could significantly increase post-thaw RBC integrity (reduce post-thaw hemolysis) (section 8.4). Decreased glycerol concentrations are highly desirable for RBC cryopreservation as this could result in faster deglycerolization methods for quicker access to cryopreserved RBC units. Interestingly, the phenolic-glucosides that were successful for RBC freezing were detrimental for both HepG2 cryopreservation and UCB cryopreservation (sections 8.2 and 8.3). Moreover, both galactose and sucrose that were beneficial for UCB cryopreservation, failed to increase post-thaw integrities when utilized to freeze RBCs. This underscores the complexity of the cryopreservation process and suggests that while the inhibition of ice recrystallization is beneficial for a cryoprotectant, specific compounds are better suited as cryoprotectants for certain cell types. It also further demonstrates that the beneficial effect of a cryo-additive may not be transferable to all cell lines, and that because a

compound fails to protect one cell type does not indicate it will fail to protect all cell types during cryopreservation. Collectively, the results from this chapter have established that not only can small molecules be potent inhibitors of ice recrystallization, but these novel IRI active derivatives have tremendous potential for improving upon current cryopreservation protocols that are limited in terms of the commonly used CPAs, DMSO and glycerol.

8.6 Experimental Procedures for Chapter 8

All novel IRI active compounds (derivatives **1**-**16**) used in this chapter for cytotoxicity cryopreservation assays were prepared as described in the experimental sections of chapters 6 and 7. Cell culture protocols, MTT assay and cryopreservation protocols for HepG2 cells, UCB and RBCs are described below.

HepG2 Cell culture:

HepG2 (human liver hepatocellular carcinoma cells, ATCC, HB-8065) were cultured in Eagle's minimum essential media (MEM) supplemented with 10% FBS (fetal bovine serum), 1% non- essential amino acids, 1 mM sodium pyruvate and 1% penicillin–streptomycin in 75cm^2 Corning® flasks.[55] Cells were incubated in a 37°C incubator supplied with 5% CO_2. Passages 5–18 were used in this study. No evidence of overgrowth or morphological changes consistent with apoptosis was observed. All cells were removed from the plates using 3 mL Accutase solution for use in experiments.

MTT assay with HepG2 Cells:

The MTT assay was performed as described previously.[55,57,58] HepG2 cells were plated in 96-well plates and treated with 100 μL of MEM supplemented carbohydrate and incubated at 37°C for 16 h with 5% CO_2. Cells incubated with MEM without supplement were used as a negative control, and cells supplemented with 1% Triton-X were used as a positive control. Following incubation, the supplemented media was removed and 200 μL of fresh media and 50 μL of MTT solution (5 mg/mL) in HBSS (Hank's balanced salt solution) were added and the plates were incubated at 37°C with 5% CO_2 for 3 h. The plates were then centrifuged, the media aspirated and 200 μL of MTT solubilization solution (10% Triton X-100, 0.1 N HCl in isopropanol) was added to each well. The plates were incubated at room temperature in the dark for 2-4 h and the absorbance of each well was then read at a wavelength of 570 nm with a multiwell plate reader (AD 34°C Absorbance Detector, Beckman Coulter, Inc., Mississauga, ON). Viability was

reported as a percentage of the control. All experiments were repeated at least three times in 10 consecutive wells for each condition.

HepG2 Cryopreservation and Thawing:

HepG2 cells were cultured and detached as described above.[55] Cells were diluted with culture media and counted using a hemocytometer. Aliquots containing 1×10^6 cells were added to 1.5 mL Eppendorf tubes and cells were pelleted by centrifugation for 10 min at 580×g. The supernatant was removed and the cells were resuspended in 100 μL MEM supplemented with the desired carbohydrate and/or DMSO cryo-additives. Cell suspensions were transferred to 2 mL cryogenic vials and placed in a "Mr. Frosty" freezing container. The container was placed in a –80°C freezer for 16h to provide a cooling rate of 1°C/min. Samples were then stored in the vapor phase of liquid nitrogen (–196°C) for a minimum of 24 hours. Following storage, samples were rapidly thawed in a 37°C water bath with gentle agitation for flow cytometry analysis.

Post-Thaw HepG2 Flow Cytometry:

After cryopreservation and thawing, cell suspensions were diluted with 400 μL of 1X Annexin V binding buffer and 100 μL were transferred to polypropylene flow cytometry tubes. 5 μL of 7-AAD and 4 μL of Annexin V-PE were added and samples were vortexed and incubated for 15 min in the dark.[55] Following incubation, 10 μL of CountBright counting beads were added and samples were diluted to 500 μL with 1X Annexin V binding buffer. Flow cytometry analysis on 100,000 cells was carried out on a Beckman Coulter FC500 flow cytometer. Annexin V-PE was measured with 575nm optical filter (FL-2), while 7-AAD was measured with 675 nm optical filter (FL-4). Viability was determined by the total number of 7-AAD$^-$ cells detected. Apoptosis was determined by the number of 7-AAD$^-$ cells that were Annexin V$^+$. Cell recoveries were calculated from total cells counted and the sample volume analyzed, determined from the number of counting beads detected and the concentration of beads in the analyzed solution. Counting beads were measured with 610 nm optical filter (FL3). Time between thawing and analysis by flow cytometry was less than 1 h. All samples were tested in triplicate.

Collection and Processing of Cord Blood:

Umbilical cord blood was collected following healthy term delivery and informed consent from mothers, in accordance with institutional approval from the Research Ethics Board of The Ottawa Hospital. Cord Blood was processed as according to Rubinstein's method to obtain

leukocyte concentrates (LCs).[93] 10% pentastarch (Pentaspan) was added to the cord blood aliquoted into 50 mL Falcon tubes in the collection bag to obtain a final concentration of 2% and was incubated at room temperature for 10 min.[72] The cord blood was then centrifuged at 52 *g* at 10°C for 15-20 min depending upon the volume of cord blood. The buffy coat aliquoted into 50 mL Falcon tubes to removes this layer from the packed RBCs and this buffy coat layer was then centrifuged at 400 *g* for 10 min at 10°C. The plasma was removed and stored in a separate Falcon tube and the packed leukocytes were resuspended in 20 mL of plasma resulting in the leukocyte concentrate (LC). Total mononuclear cell counts and $CD34^+$ cell concentrations and viability were then determined by flow cytometry.

Cryopreservation of UCB and Thawing:

Cryopreservation of the LCs obtained from processed UCB was performed similarly to protocols described previously.[93] Aliquots of LCs containing 4×10^6 total mononuclear cells were added to 1.5 mL Eppendorf tubes and cells were pelleted by centrifugation for 10 min at 400 *g* and 10°C. The supernatant was removed and the cells were resuspended in 80 μL plasma. To this, 20 μL of cryo-solution supplemented with 5% (w/v) Dextran were added to afford a final concentration of cryo-solution as indicated in the text supplemented with 1% (w/v) Dextran. The cryo-solutions added (20 μL) were at 5 times the desired concentration as they were diluted to the appropriate amount when added to the mononuclear cells suspended in plasma (80 μL). Cell suspensions were transferred to 2 mL cryogenic vials and placed in a "Mr. Frosty" freezing container. The container was placed in a −80°C freezer for 16h to provide a cooling rate of 1°C/min. Samples were then stored in the vapor phase of liquid nitrogen (−196°C) for a minimum of 24 hours. Following storage, samples were either rapidly thawed in a 37°C water bath with gentle agitation or thawed slowly at room temperature for flow cytometry analysis.

Flow Cytometry of UCB:

Flow cytometric analysis of UCB was conducted as according to the ISHAGE guidelines.[97,98] After cryopreservation and thawing, cell suspensions were diluted with 900 μL of DPBS and 200 μL were transferred to polypropylene flow cytometry tubes. 8 μL of CD45-FITC and 8 μL of CD34-PE were added and the samples were vortexed and incubated in the dark for 10 min. 8 μL of 7-AAD was then added and the samples were vortexed and incubated in the dark for 5 min. Following incubation, 20 μL of CountBright counting beads were added and samples were diluted to 1 mL with 1X RBC lysing buffer. Flow cytometry analysis was carried out on a

Beckman Coulter FC500 flow cytometer. Data analysis and gating strategies were carried out as according to the ISHAGE guidelines.[97,98] Viability of $CD34^+$ cells was determined by the total number $CD45^+/CD34^+$ cells that were 7-AAD^-. Time between thawing and analysis by flow cytometry was less than 1 h. All samples were tested at least in duplicate.

RBC Blood Collection and Preparation:

Human whole blood was collected from healthy volunteers into vacutainer tubes containing EDTA anticoagulant using standard phlebotomy. The sample was centrifuged at 2200 g for 10 min at 4 °C. Plasma supernatant and buffy coat were removed and the RBC pellet was washed twice with 0.2%/0.9% dextrose/saline buffer. After the last wash, RBCs were resuspended in an equal volume of packed RBCs of 0.2%/0.9% dextrose/saline buffer to a final hematocrit (Hct) of 0.50 L/L. RBC samples in buffer solution were stored refrigerated (4–6 °C) for up to 1 week until needed.

RBC Freezing Experiments:

An equal volume of freezing solution in 0.2%/0.9% dextrose/saline buffer was added to 150 μL of leukoreduced RBCs in 0.2%/0.9% dextrose/saline buffer for a final volume of 300 μL. The final concentrations of all freezing solutions are as indicated in the text. RBC suspensions were transferred to cryo-tubes and incubated at room temperature for 10 min prior to immersion in a methanol bath and cooling to -5 °C. A thermocouple was inserted into a glycerol control sample for temperature measurements at 1 s intervals. Once the internal solution reached -5 °C, ice nucleation was induced by touching the cryo-tubes with pre-cooled (in liquid nitrogen) forceps. RBC samples were then held at -5 °C for 5 min. Samples were then slow-cooled at a rate of 1 °C/min to defined subzero temperatures (see text), then either thawed immediately from this temperature ("cooling" profiles) or plunged and stored into dry ice (-80 °C) or liquid nitrogen (-196 °C) for 30 min ("cooling/storage" profiles).

RBC Thawing and Post-Thaw Hemolysis:

All RBC samples were thawed under fast-thaw conditions in a 37 °C water bath. Post-thaw Hcts and percent hemolysis was determined for all freezing experiments by comparing the supernatant hemoglobin concentration to total hemoglobin concentration using the cyanmethemoglobin Drabkin's method.[134,135] Percent post-thaw RBC integrity was calculated using the measured percent hemolysis values according to the following equation: % post-thaw RBC integrity = 100 - % hemolysis.

Cryomicroscopy:

Cryomicroscopy was performed using a Linkam FDCS cryostage and temperature controllers that were fitted to a Nikon 80i microscope. A small volume (10 uL) of sample was added to a quartz crucible, placed on the cryostage and cooled at 25 °C/min to a pre-determined temperature that was 5 °C below the estimated freezing point for the sample. Ice was nucleated using a liquid nitrogen-cooled probe and the ice front was collected in real time using a Hamamatsu Photonics ORCA II camera and Nikon NIS-Elements software.

RBC Osmotic Tolerance:

RBC samples in buffer (500 μL) were suspended with cryo-solutions (500 μL) and incubated at room temperature for 10 mins. Following incubation, 10 μL of the RBC/cryo-solution mixture was added to 1 mL of saline solution (concentrations indicated in the text in figure 8.19) and the absorbance of the solution was measured at 540 nm. Hemolysis was calculated by comparing the ratio of the measured absorbance of the sample to the measured absorbance of a positive control for RBC hemolysis (SAGM/RBC solution added to 0% Saline (water)) that results in 100% hemolysis. For the osmotic tolerances after washes, following incubation with cryo-solution or wash solution, samples were centrifuged at 2200 RPM for 10 min at 4°C and the supernatant was removed. Packed RBCs were then resuspended in the desired wash solution (wash 1 after cryo-solution incubation; wash 2 after wash 1 incubation; wash 3 after wash 2 incubation) and incubated at room temperature for 10 min. Following incubation, 10 μL of the RBC/wash solution mixture was added to 1 mL of saline solution (concentrations indicated in the text in figures 8.20-8.22) and the absorbance of the solution was measured at 540 nm. Hemolysis was calculated as described above.

Deglycerolization Experiments:

All RBC samples for deglycerolization studies were frozen using rapid freeze conditions directly into dry ice (-80°C) or liquid nitrogen (-196°C). Total sample volumes were 1 mL treating 500 μL of RBCs in buffer with 500 μL of cryo-solutions. Thawing was conducted at 42°C.

Washing Conditions with no Pre-Dilutions: Following thawing of RBC samples, total Hgb content was measured using a hematology analyzed. RBC samples were then centrifuged at 2200 RPM for 10 min at 4°C and the cryo-solution containing supernatant was removed and assessed for the quantity of Hgb. Packed RBCs were then resuspended in wash 1 solution (as indicated in

the text) by adding an equal volume of the removed supernatant and were incubated for 10 min at room temperature. Samples were then centrifuged at 2200 RPM for 10 min at 4°C and the Wash 1 supernatant was removed and assessed for the quantity of Hgb. This process was repeated for wash 2 and wash 3. Following removal of wash 3, remaining packed RBCs were resuspended in a 0.9%/0.2% Saline/Dextrose solution and assessed for % hemolysis. The quantity of Hgb present in each supernatant and the final % hemolysis were quantified using Drabkin's assay.

Washing Conditions with Pre-Dilutions: Following thawing of RBC samples, total Hgb content was measured using a hematology analyzed. To this RBC/cryo-solution mixture was added 500 μL of wash 1 for the wash 1 pre-dilution and the samples were mixed and incubated for 10 min at room temperature. RBC samples were then centrifuged at 2200 RPM for 10 min at 4°C and the wash 1 pre-dilute supernatant was removed and assessed for the quantity of Hgb. Packed RBCs were then resuspended in wash 1 solution (as indicated in the text) to a final volume of 1 mL and were incubated for 10 min at room temperature. Samples were then centrifuged at 2200 RPM for 10 min at 4°C and 20 *u*L of the wash 1 supernatant was removed to assess for Hgb content. The samples were then resuspended in the remaining wash 1 supernatant and 500 μL of the wash 2 solution was added for the wash 2 pre-dilution. After incubation for 10 min the samples were centrifuged at 2200 RPM for 10 min at 4°C and the wash 2 pre-dilute supernatant was removed and assessed for the quantity of Hgb. This process was repeated for wash 2, wash 3 pre-dilution and wash 3. Following removal of wash 3, remaining packed RBCs were resuspended in a 0.9%/0.2% Saline/Dextrose solution and assessed for % hemolysis. The quantity of Hgb present in each supernatant and the final % hemolysis were quantified using Drabkin's assay.

8.7 References

1. Meryman, H.T. *Transfusion*. **2007**, *47*, 935-945.
2. Baust, J.G.; Gao, D.; Baust, J.M. *Organogenesis*. **2009**, *5*, 90-96.
3. Bakhach, J. *Organogenesis*. **2009**, *5*, 119-126.
4. Scott, K.L.; Lecak, J.; Acker, J.P. *Transfus. Med. Rev*. **2005**, *19*, 127-142.
5. Baust, J.M. *Cell Preserv. Technol*. **2002**, *1*, 17-31.
6. Jurisicova, A.; Varmuza, S.; Casper, R.F. *Hum. Reprod. Update*. **1995**, *1*, 558-566.
7. Mazur, P. Life in the Frozen State - Principles of Cryobiology (Boca Baton, FL: CRC Press; 2004.
8. Acker, J.P.; McGann, L.E. *Cell Transplant*. **2002**, *11*, 563-571.
9. Mazur, P.; Leibo, S.P.; Chu, E.H.Y. *Exp. Cell Res*. **1972**, *71*, 345-355.

10. Fowler, A.; Toner, M. *Ann. N.Y. Acad. Sci.* **2005**, *1066*, 119-135.

11. Hobbs, P.V. Ice Physics (1st ed.). Oxford: Oxford University Press, USA; 1975.

12. Pegg, D.E.; Diaper, M.P. *Cryobiology.* **1991**, *28*, 18-35.

13. Pegg, D.E.; Diaper, M.P. *Biophys. J.* **1988**, *54*, 471-488.

14. Lovelock, J.E. *Proc. R. Soc. Lond. B. Biol. Sci.* **1957**, *147*, 427-433.

15. Leibo, S.P.; Mazur, P. *Cryobiology.* **1971**, *8*, 447-452.

16. Mazur, P. *J. Gen. Physiol.* **1963**, *47*, 347-369.

17. Karlsson, J.O.; Cravalho, E.G.; Borel Rinkes, I.H.; Tompkins, R.G.Y., M. L.; Toner, M. *Biophys. J.* **1993**, *65*, 2524-2536.

18. Toner, M.; Caravalho, E.G.; Karel, M. *J. Appl. Phys.* **1990**, *67*, 1582-1593.

19. Muldrew, K.; McGann, L.E. *Biophys. J.* **1990**, *57*, 525-532.

20. Mazur, P. *Cell Biophys.* **1990**, *17*, 53-92.

21. Fowler, A.; Toner, M. *Ann. N.Y. Acad. Sci.* **1998**, *858*, 245-252.

22. Farrant, J.; Molyneux, P.; Hasted, J.B.; Peares, P.; Echlin, P. *Philos. Trans. R. Soc. London, Ser. B.* **1977**, *278*, 191-205.

23. McGann, L.E. *Cryobiology.* **1978**, *15*, 382-390.

24. Meryman, H.T. *Cryobiology.* **1971**, *8*, 173-183.

25. Lovelock, J.E. *Biochim. Biophys. Acta.* **1953**, *11*, 28-36.

26. Lovelock, J.E. *Biochem. J.* **1954**, *56*, 265-270.

27. Mazur, P.C. *Science.* **1970**, *168*, 939-949.

28. Meryman, H.T. *Annu. Rev. Biophys. Bioeng.* **1974**, *3*, 341-363.

29. Song, Y.C.; Khirabadi, B.S.; Lightfoot, F.; Brockbank, K.G.M.; Taylor, M.J. *Nat. Biotechnol.* **2000**, *18*, 296-299.

30. Scheinkonig, C.; Kappicht, S.; Kolb, H.J.; Schleuning, M. *Bone Marrow Transplant.* **2004**, *34*, 531-536.

31. Topacoglu, H.; Karcioglu, O.; Ozsarac, M.; Oray, D.; Niyazi Ozucelik, D.; Tuncok, Y. *Vet. Hum. Toxicol.* **2004**, *46*, 138-140.

32. Hallare, A.V.; Köhler, H.R.; Triebskorn, R. *Chemosphere.* **2004**, *56*, 659-666.

33. Mazur, P. *Am. J. Physiol. - Cell Physiol.* **1984**, *247*, C125-C142.

34. Rapatz, G.; Sullivan, J.J.; Luyet, B. *Cryobiology.* **1968**, *5*, 18-25.

35. Anchordoguy, T.J.; Rudolph, A.S.; Carpenter, J.F.; Crowe, J.H. *Cryobiology.* **1987**, *24*, 324-331.

36. Crowe, J.H.; Crowe, L.M.; Carpenter, J.F.; Rudolph, A.S.; Wistrom, C.A.; Spargo, B.J.; Anchordoguy, T.J. *Biochim. Biophys. Acta.* **1988**, *947*, 367-384.

37. Davis, J.; Rowley, S.; Braine, H.; Piantadosi, S.; Santos, G. *Blood.* **1990**, *75*, 781-786.

38. Berz, D.; McCormack, E.M.; Winer, E.S.; Colvin, G.A.; Quesenberry, P.J. *Am. J. Hematol.* **2007**, *82*, 463-472.

39. Galmes, A.; Gutiérrez, A.; Sampol, A.; Canaro, M.; Morey, M.; Iglesias, J.; Matamoros, N.; Duran, M.A.; Novo, A.; Bea, M.D.; Galán, P.; Balansat, J.; Martínez, J.; Bargay, J.; Besalduch, J. *Haematologica*. **2007**, *92*, 986-989.

40. Greco, N.J.; Seetharaman, S.; Kurtz, J.; Lee, W.R.; Moroff, G. *Stem Cells Dev*. **2006**, *15*, 124-135.

41. Shim, J.-S.; Cho, B.; Kim, M.; Park, G.-S.; Shin, J.-C.; Hwang, H.-K.; Kim, T.-G.; Oh, I.-H. *Br. J. Haematol*. **2006**, *135*, 210-213.

42. Palasz, A.T., Gustafasson, H., Rodriguez-Martinez, H., Gusta, L., Larsson, B., and Mapletoft, R. J. *Cryobiology*. **1995**, *32*, 572-572.

43. Naidenko, T. *Cryo-letters*. **1997**, *18*, 375-382.

44. Lagneaux, D.; Huhtinen, M.; Koskinen, E.; Palmer, E. *Equine Vet. J*. **1997**, *29*, 85-87.

45. Pegg, D.E. *Cryobiology*. **1992**, *29*, 774.

46. Rubinsky, B.; DeVries, A.L. *Cryobiology*. **1989**, *26*, 580.

47. Hansen, T.N.; Smith, K.M.; Brockbank, K.G.M. *Transplant. Proc*. **1993**, *25*, 3182-3184.

48. Wang, T.; Zhu, Q.; Yang, X.; Layne, J.R.; DeVries, A.L. *Cryobiology*. **1994**, *31*, 185-192.

49. Mugano, J.A.; Wang, T.; Layne, J.R., Jr.,; DeVries, A.L.; Lee, R.E. *Cryobiology*. **1995**, 556-557.

50. Larese, A.; Acker, J.; Muldrew, K.; Yang, H.Y.; McGann, L. *Cryo-letters*. **1996**, *17*, 172-182.

51. Wang, J.H.; Bian, H.W.; Huang, C.N.; Ge, J. G. *Acta Biol. Exp*. **1999**, *32*, 271-276.

52. Carpenter, J.F.; Hansen, T.N. *Proc. Natl. Acad. Sci. U. S. A*. **1992**, *89*, 8953-7.

53. Chao, H.; Davies, P.L.; Carpenter, J.F. *J. Exp. Biol*. **1996**, *199*, 2071-6.

54. Leclère, M.; Kwok, B.K.; Wu, L.K.; Allan, D.S.; Ben, R.N. *Bioconjugate Chem*. **2011**, *22*, 1804-1810.

55. Chaytor, J.L.; Tokarew, J.M.; Wu, L.K.; Leclère, M.; Tam, R.Y.; Capicciotti, C.J.; Guolla, L.; von Moos, E.; Findlay, C.S.; Allan, D.S.; Ben, R.N. *Glycobiology*. **2012**, *22*, 123-133.

56. Capicciotti, C.J.; Leclère, M.; Perras, F.A.; Bryce, D.L.; Paulin, H.; Harden, J.; Liu, Y.; Ben, R.N. *Chem. Sci*. **2012**, *3*, 1408-1416.

57. Mosmann, T. *J. Immunol. Methods*. **1983**, *65*, 55-63.

58. Liu, S.; Wang, W.; von, M.E.; Jackman, J.; Mealing, G.; Monette, R.; Ben, R.N. *Biomacromolecules*. **2007**, *8*, 1456-1462.

59. de Almeida, M.V.; Le Hyaric, M. *Mini-Rev. Org. Chem*. **2005**, *2*, 283-297.

60. Lorber, B.; Bishop, J.B.; DeLucas, L.J. *Biochim. Biophys. Acta*. **1990**, *1023*, 254-265.

61. Michel, H.; Oesterhelt, D. *Proc. Natl. Acad. Sci. U.S.A*. **1980**, *77*, 1283-1285.

62. Harvie, P.; Wong, F.M.P.; Bally, M.B. *Biophys. J*. **1998**, *75*, 1040-1051.

63. Hildreth, J.E. *Biochem. J*. **1982**, *207*, 363-366.

64. Baron, C.; Thompson, T.E. *Biochim. Biophys. Acta*. **1975**, *382*, 276-285.

65. Plusquellec, D.; Chevalier, G.; Talibart, R.; Wróblewski, H. *Anal. Biochem*. **1989**, *179*, 145-153.

66. Koopman, G.; Reutelingsperger, C.; Kuijten, G.; Keehnen, R.; Pals, S.; van Oers, M. *Blood*. **1994**, *84*, 1415-1420.

67. Vermes, I.; Haanen, C.; Steffens-Nakken, H.; Reutellingsperger, C. *J. Immunol. Methods*. **1995**, *184*, 39-51.

68. Latt, S.A. *Can. J. Genet. Cytol*. **1977**, *19*, 603-623.

69. Hunt, C.J.; Armitage, S.E.; Pegg, D.E. *Cryobiology*. **2003**, *46*, 76-87.

70. Hunt, C.J.; Armitage, S.E.; Pegg, D.E. *Cryobiology*. **2003**, *46*, 61-75.

71. Yang, H.; Zhao, H.; Acker, J.P.; Liu, J.Z.; Akabutu, J.; McGann, L.E. *Cryobiology*. **2005**, *51*, 165-175.

72. Yang, H.; Acker, J.P.; Abley, D.; McGann, L.E.; Akabutu, J. *Bone Marrow Transplant*. **2001**, *27*, 457-461.

73. Carvalho, K.A.T.; Cury, C.C.; Oliveira, L.; Cattaned, R.I.I.; Malvezzi, M.; Francisco, J.C.; Pachalok, A.; Olandoski, M.; Faria-Neto, J.R.; Guarita-Souza, L.C. *Transplant. Proc*. **2008**, *40*, 839-841.

74. Hunt, C.J. *Transfus. Med. Hemoth*. **2011**, *38*, 107-123.

75. Harris, D.T. *Br. J. Haematol*. **2009**, *147*, 177-184.

76. Gluckman, E. *Br. J. Haematol*. **2009**, *147*, 192-199.

77. Gluckman, E. *Blood Rev*. **2011**, *25*, 255-259.

78. Yang, H.; Acker, J.P.; Hannon, J.; Miszta-Lane, H.; Akabutu, J.J.; McGann, L.E. *Cytotherapy*. **2001**, *3*, 377-386.

79. Minegishi, M.; Itoh, T.; Fukawa, N.; Kitaura, T.; Miura, J.; Takahashi, H.; Suzuki, A.; Kudo, Y.; Narita, A.; Sato, Y.; Suzuki, M.; Watanabe, T.; Wada, Y.; Takeyama, Y.; Tsuchiya, S. *Int. J. Hematol*. **2007**, *85*, 78-84.

80. Galmés, A.; Besalduch, J.; Bargay, J.; Novo, A.; Morey, M.; Guerra, J.M.; Duran, M.A. *Transfusion*. **1999**, *39*, 70-73.

81. Halle, P.; Tournilhac, O.; Knopinska-Posluszny, W.; Kanold, J.; Gembara, P.; Boiret, N.; Rapatel, C.; Berger, M.; Travade, P.; Angielski, S.; Bonhomme, J.; Deméocq, F. *Transfusion*. **2001**, *41*, 667-673.

82. Bakken, A.M.; Bruserud, O.; Abrahamsen, J.F. *J. Hematother. Stem Cell Res*. **2003**, *12*, 351-358.

83. Nicoud, I.B.; Clarke, D.M.; Taber, G.; Stolowski, K.M.; Roberge, S.E.; Song, M.K.; Mathew, A.J.; Reems, J.-A. *Transfusion*. **2012**, *52*, 2055-2062.

84. Son, J.H.; Heo, Y.J.; Park, M.Y.; Kim, H.H.; Lee, K.S. *Cryobiology*. **2010**, *60*, 287-292.

85. Woods, E.J.; Liu, J.; Derrow, C.W.; Smith, F.O.; Williams, D.A.; Critser, J.K. *J. Hematother. Stem Cell Res*. **2000**, *9*, 161-173.

86. Katayama, Y.; Yano, T.; Bessho, A.; Deguchi, S.; Sunami, K.; Mahmut, N.; Shinagawa, K.; Omoto, E.; Makino, S.; Miyamoto, T.; Mizuno, S.; Fukuda, T.; Eto, T.; Fujisaki, T.; Ohno, Y.; Inaba, S.; Niho, Y.; Harada, M. *Bone Marrow Transplant*. **1997**, *19*, 283-287.

87. Rodrigues, J.P.; Paraguassú-Braga, F.H.; Carvalho, L.; Abdelhay, E.; Bouzas, L.F.; Porto, L.C. *Cryobiology*. **2008**, *56*, 144-151.

88. Buchanan, S.S.; Gross, S.A.; Acker, J.P.; Toner, M.; Carpenter, J.F.; Pyatt, D.W. *Stem Cells Dev*. **2004**, *13*, 295-305.

89. Motta, J.P.R.; Gomes, B.E.; Bouzas, L.F.; Paraguassú-Braga, F.H.; Porto, L.C. *Cryobiology*. **2010**, *60*, 301-307.

90. Sasnoor, L.M.; Kale, V.P.; Limaye, L.S. *J. Hematother. Stem Cell Res.* **2003**, *12*, 553-564.

91. Wu, L.K.; Tokarew, J.M.; Chaytor, J.L.; von Moos, E.; Li, Y.; Palii, C.; Ben, R.N.; Allan, D.S. *Carbohydr. Res.* **2011**, *346*, 86-93.

92. Balint, B.; Ivanović, Z.; Petakov, M.; Taseski, J.; Jovčić, G.; Stojanović, N.; Milenković, P. *Bone Marrow Transplant.* **1999**, *23*, 613-619.

93. Rubinstein, P.; Dobrila, L.; Rosenfield, R.E.; Adamson, J.W.; Migliaccio, G.; Migliaccio, A.R.; Taylor, P.E.; Stevens, C.E. *Proc. Natl. Acad. Sci. U.S.A.* **1995**, *92*, 10119-10122.

94. Yang, H.; Loutfy, M.R.; Mayerhofer, S.; Shuen, P. *Transfusion.* **2011**, *51*, 284-292.

95. Carpenter, J.F.; Hansen, T.N. *Proc. Natl. Acad. Sci. U.S.A.* **1992**, *89*, 8953-8957.

96. Matsumoto, S.; Matsusita, M.; Morita, T.; Kamachi, H.; Tsukiyama, S.; Furukawa, Y.; Koshida, S.; Tachibana, Y.; Nishimura, S.-i.; Todo, S. *Cryobiology.* **2006**, *52*, 90-98.

97. Sutherland, D.R.; Anderson, L.; Keeney, M.; Nayar, R.; Chin-Yee, I. *J. Hematother. Stem Cell Res.* **1996**, *5*, 213-226.

98. Keeney, M.; Chin-Yee, I.; Weir, K.; Popma, J.; Nayar, R.; Robert Sutherland, D. *Commun. Clin. Cytom.* **1998**, *34*, 61-70.

99. Venditti, A.; Battaglia, A.; Del Poeta, G.; Buccisano, F.; Maurillo, L.; Tamburini, A.; Del Moro, B.; Epiceno, A.M.; Martiradonna, M.; Caravita, T.; Santinelli, S.; Adorno, G.; Picardi, A.; Zinno, F.; Lanti, A.; Bruno, A.; Suppo, G.; Franchi, A.; Franconi, G.; Amadori, S. *Bone Marrow Transplant.* **1999**, *24*, 1019-1027.

100. Brocklebank, A.M.; Sparrow, R.L. *Cytometry.* **2001**, *44*, 254-261.

101. Gajkowska, A.; Oldak, T.; Jastrzewska, M.; Machaj, E.K.; Walewski, J.; Kraszewska, E.; Pojda, Z. *Folia Histochem. Cytobiol.* **2006**, *44*, 53-60.

102. Tam, R.Y.; Ferreira, S.S.; Czechura, P.; Chaytor, J.L.; Ben, R.N. *J. Am. Chem. Soc.* **2008**, *130*, 17494-17501.

103. Kanias, T.; Acker, J.P. *FEBS J.* **2010**, *277*, 343-356.

104. Ramsey, G. *Transfusion.* **2008**, *48*, 2053-2055.

105. Holovati, J.L.; Hannon, J.L.; Gyongyossy-Issa, M.I.C.; Acker, J.P. *Transfus. Med. Rev.* **2009**, *23*, 25-41.

106. Högman, C.F. *Vox Sang.* **1998**, *74*, 177-187.

107. Högman, C.F.; Meryman, H.T. *Transfus. Med. Rev.* **1999**, *13*, 275-296.

108. Weinberg, J.A.; McGwin, G.J.; Vandromme, M.J.; Marques, M.B.; Melton, S.M.; Reiff, D.A.; Kerby, J.D.; Rue, L.W.I. *J. Trauma.* **2010**, *69*, 1427-1432.

109. Spinella, P.; Carroll, C.; Staff, I.; Gross, R.; Mc Quay, J.; Keibel, L.; Wade, C.; Holcomb, J. *J. Crit. Care.* **2009**, *13*, R151.

110. Valeri, C.R. *Vox Sang.* **2002**, *83*, 193-196.

111. Hess, J.R. *Transfus. Med.* **2004**, *14*, 1-8.

112. Hess, J.R.; Greenwalt, T.G. *Transfus. Med. Rev.* **2002**, *16*, 283-295.

113. American Association of Blood Banks Technical Manual (Bethesda, MD: American Association of Blood Banks; 2006.

114. Meryman, H.T.; Hornblower, M. *Transfusion.* **1972**, *12*, 145-156.

115. Valeri, C.R.; Ragno, G.; Pivacek, L.E.; Srey, R.; Hess, J.R.; Lippert, L.E.; Mettille, F.; Fahie, R.; O'Neill, E.M.; Szymanski, I.O. *Transfusion*. **2001**, *41*, 933-939.

116. Lelkens, C.C.M.; Noorman, F.; Koning, J.G.; Truijens-de Lange, R.; Stekkinger, P.S.; Bakker, J.C.; Lagerberg, J.W.M.; Brand, A.; Verhoeven, A.J. *Transfusion*. **2003**, *43*, 157-164.

117. Bandarenko, N.; Cancelas, J.; Snyder, E.L.; Hay, S.N.; Rugg, N.; Corda, T.; Joines, A.D.; Gormas, J.F.; Pratt, G.P.; Kowalsky, R.; Rose, M.; Rose, L.; Foley, J.; Popovsky, M.A. *Transfusion*. **2007**, *47*, 680-686.

118. Rowe, A.W.; Eyster, E.; Kellner, A. *Cryobiology*. **1968**, *5*, 119-128.

119. Robert Valeri, C.; Pivacek, L.E.; Cassidy, G.P.; Ragno, G. *Transfusion*. **2000**, *40*, 1341-1345.

120. Robert Valeri, C.; Ragno, G.; Pivacek, L.; Mary O'Neill, E. *Transfusion*. **2001**, *41*, 928-932.

121. Valeri, C.R.; Zaroulis, C.G.; Vecchione, J.J.; Valeri, D.A.; Anastasi, J.; Pivacek, L.E.; Emerson, C.P. *Transfusion*. **1980**, *20*, 159-170.

122. Lusianti, R.E.; Benson, J.D.; Acker, J.P.; Higgins, A.Z. *Biotechnol. Progr*. **2013**, *29*, 609-620.

123. Valeri, C.R.; Ragno, G.; Popovsky, M.A. *Transfus. Med*. **2004**, *14*, 387-388.

124. Bloom, M.; AP, W.E.R.; Doebbler, G.; Cowley, C. *Bibl Haemat*. **1965**, *23*, 64245.

125. Knorpp, C.T.; Merchant, W.R.; Gikas, P.W.; Spencer, H.H.; Thompson, N.W. *Science*. **1967**, *157*, 1312-1313.

126. Williams, R.J. *Cryobiology*. **1983**, *20*, 521-526.

127. Stolzing, A.; Naaldijk, Y.; Fedorova, V.; Sethe, S. *Transfusion Apheresis Sci*. **2012**, *46*, 137-147.

128. Holovati, J.L.; Gyongyossy-Issa, M.I.C.; Acker, J.P. *Cryobiology*. **2009**, *58*, 75-83.

129. Stoll, C.; Holovati, J.L.; Acker, J.P.; Wolkers, W.F. *Biotechnol. Progr*. **2012**, *28*, 364-371.

130. Brumfiel, G. *Nature*. **2004**, *428*, 14-15.

131. Quan, G.B.; Han, Y.; Liu, M.X.; Fang, L.; Du, W.; Ren, S.P.; Wang, J.X.; Wang, Y. *Cryobiology*. **2011**, *62*, 135-144.

132. Capicciotti, C.J.; Kurach, J.D.R.; Turner, T.R.; Acker, J.P.; Ben, R.N. *Org. Biomol. Chem*. **2013**, *Submitted/Under Review September 2013*.

133. Farrant, J.; Walter, C.A.; Lee, H.; McGann, L.E. *Cryobiology*. **1977**, *14*, 273-286.

134. Drabkin, D.L. *Am. J. Med. Sci*. **1948**, *215*, 110-110.

135. Sowemimo-Coker, S.O. *Transfus. Med. Rev*. **2002**, *16*, 46-60.

136. Acker, J.P.; M. Croteau, I.; Yi, Q.-L. *Clin. Chim. Acta*. **2012**, *413*, 1746-1752.

137. Krijnen, H.W.; de Wit, J.J.F.M.; Kuivenhoven, A.C.J.; Loos, J.A.; Prins, H.K. *Vox Sang*. **1964**, *9*, 559-572.

138. Souzu, H.; Mazur, P. *Biophys. J*. **1978**, *23*, 89-100.

139. Carruthers, A.; DeZutter, J.; Ganguly, A.; Devaskar, S.U. *Am. J. Physiol. Endocrinol. Metab*. **2009**, *297*, E836-E848.

140. Concha, I.I.; Velásquez, F.V.; Martínez, J.M.; Angulo, C.; Droppelmann, A.; Reyes, A.M.; Slebe, J.C.; Vera, J.C.; Golde, D.W. *Blood*. **1997**, *89*, 4190-4195.

141. Barnett, J.E.; Holman, G.D.; Chalkley, R.A.; Munday, K.A. *Biochem. J.* **1975**, *145*, 417-429.

142. García-Álvarez, I.; Garrido, L.; Fernández-Mayoralas, A. *ChemMedChem*. **2007**, *2*, 496-504.

143. Baldwin, S.A. *Biochim. Biophys. Acta*. **1993**, *1154*, 17-49.

144. Moore, T.J. *J. Lipid Res*. **1968**, *9*, 642-646.

145. Mazur, P.; Miller, R.H. *Cryobiology*. **1976**, *13*, 507-522.

146. Parpart, A.K.; Lorenz, P.B.; Parpart, E.R.; Gregg, J.R.; Chase, A.M. *J. Clin. Invest*. **1947**, *26*, 636-640.

147. Meryman, H.T. *Nature*. **1968**, *218*, 333-336.

148. Meryman, H.T.; Hornblower, M. *Transfusion*. **1977**, *17*, 438-442.

Conclusions

The overall goal of this work was to elucidate structural features that are necessary for potent ice recrystallization inhibition and to identify novel small molecules that are potent ice recrystallization inhibitors (IRIs). Compounds that are potent IRIs have tremendous potential for applications in cryopreservation as novel cryoprotectants. As such, the overall objectives of this work were: (1) to elucidate the important structural features for the potent IRI activity of native synthetic AFGPs and AFGP analogues; (2) to determine the relationship between IRI, TH and cryopreservation ability of natural biological antifreezes, including AFPs and AFGPs; (3) to identify novel small molecule potent inhibitors of ice recrystallization and to elucidate the important structural features required for the IRI activity of these molecules and for simple carbohydrates; and (4) to explore the cryopreservation potential of small molecule ice recrystallization inhibitors to identify novel cryoprotectants that can improve upon current cryopreservation protocols.

The first part of this work involved the investigation of structural features that influence the IRI activity of natural and synthetic BAs and BA analogues as these are some of the most potent inhibitors known to date. A variety of synthetic AFGPs (synAFGPs) and AFGP analogues were prepared and assessed for both types of antifreeze specific activities, TH and IRI activity. The results from the synAFGPs consisting of an $(Ala\text{-}Thr\text{-}Ala)_n$ tripeptide repeat highlight the importance of glycopeptide size/length for both TH and IRI activity (chapter 3). This study also highlighted how minor variations in the amino acid sequence of AFGPs can have detrimental effects for both TH and IRI as native AFGP-8 with four repeats of $(Ala\text{-}Ala\text{-}Thr)_n$ exhibited both activities, whereas synAFGPs with four repeats of $(Ala\text{-}Thr\text{-}Ala)_n$ were inactive for both at equimolar concentration. While the synAFGPs were found to adopt a polyproline type II (PPII) helical structure in solution, this secondary structure was determined not to be a prerequisite for IRI or TH activity. HyP AFGP derivatives that also adopt this structure failed to exhibit either activity (chapter 3). While the TH activity of AFGPs has been extensively studied in the literature, these studies are the first reports that have examined the structural features that are important for the IRI activity of these biological antifreezes. Collectively, they indicate that even minor structure variations can have drastic effects on the potent IRI activity of AFGPs resulting in IRI inactive (glyco)peptides.

In addition to studying derivatives of AFGPs, this work also explored the relationship between IRI, TH and cryopreservation ability of natural AFGPs, AFPs and mutants of AFPs. The results of this study further validated previous reports that TH and IRI activity were not tightly correlated (chapter 4). This was achieved both by a comparison of the two activities between difference

classes of BAs, as well as within a single class of AFP and its mutants (the *Lp*AFP). The results from this study highlighted how TH and IRI activity can be modulated independently and are dependent upon the type of BA. Additionally, results from this study further demonstrated that BAs are ineffective as cryoprotectants, and revealed the potential influence of ice crystal shape and growth progression on cell survival during cryopreservation.

The most significant contribution of this work was the discovery that small carbohydrate-based molecules can be potent ice recrystallization inhibitors. Prior to this work, all reported small molecules were simple carbohydrate derivatives that exhibited only moderate IRI activity. This activity was attributed to their ability to disrupt or disorder the structure of bulk-water, which was ultimately correlated to hydration characteristics of these carbohydrates. The led to the hypothesis that molecules that are known to disrupt, alter and/or sequester the structure of bulk-water by self-assembling in solution may have unrealized potential as IRIs. As such, carbohydrate-based surfactants and hydrogelators were assessed for their ability to inhibit ice recrystallization. The most potent analogues discovered in each class were the pyranose-based surfactant β-octyl-Gal and the aldonamide-based hydrogelator NOGlc (chapter 6). β-Octyl-Gal exhibited potent IRI activity at 22 mM (21% MGS relative to PBS) whereas NOGlc was highly IRI active at a significantly lower concentration of 0.5 mM (12% MGS relative to PBS). These two derivatives were the first examples of potent small molecule IRIs and represent a tremendous advancement in the field of ice recrystallization inhibitors. Prior to this, all known ice recrystallization inhibitors were large peptides, glycopeptides or polymers.

The carbohydrate-based surfactants and hydrogelators are amphiphilic molecules. Structure-function studies on these derivatives indicated that the presence of hydrophobic moieties was essential for potent IRI activity (chapter 6). The importance of hydrophobic groups for activity has also been demonstrated by other analogues reported by our laboratory. However, these amphiphilic molecules all contained long alkyl chains and possessed surfactant-like characteristics, which can be detrimental to cells and can solubilize cell membranes. This led to the exploration of conjugating other hydrophobic moieties to carbohydrate residues such as an aryl ring.

An anomalous potent small molecule IRI was discovered, which was the glucopyranose derivative β-PMP-Glc (chapter 7). This derivative is the first glucopyranose-based derivative that exhibited potent IRI activity while the analogous galactopyranose-based derivative was IRI inactive. Extensive structure-function studies on β-PMP-Glc indicated that essentially all structural variations and modifications to this compound are highly detrimental for activity (chapter 7). Changes in the configuration of carbons bearing hydroxyl groups on the carbohydrate residue, glycosidic-linkage modifications, and changes in aryl group substituents

and their positions all resulted in a drastic decrease in IRI activity. The only modification to β-PMP-Glc that was tolerated and retained or increased the activity of this compound was replacing the *para*-methoxy substituent with a bromine (β-pBrPh-Glc), chlorine (β-pClPh-Glc) or fluorine (β-pFPh-Glc). Overall, these studies identified a number of highly IRI active phenolic-glycosides as a second class of small molecule ice recrystallization inhibitors.

Finally, this work also explored various IRI active small molecules for their cryopreservation potential with different cell types including a human liver cell line (HepG2), HSCs obtained from human UCB, and RBCs obtained from human peripheral blood. The most promising results were obtained with the phenolic-glucosides, which were discovered to be beneficial cryo-additives for the freezing of human RBCs. The addition of β-PMP-Glc or β-pBrPh-Glc to reduced glycerol concentrations (15%) could significantly increase post-thaw RBC integrity (reduce post-thaw hemolysis) (chapter 8). Decreased glycerol concentrations are highly desirable for RBC cryopreservation as this could result in faster deglycerolization methods for quicker access to cryopreserved RBC units. Interestingly, the phenolic-glucosides that were successful for RBC freezing were detrimental for both HepG2 cryopreservation and UCB cryopreservation (Chapter 8). This underscores the complexity of the cryopreservation process and suggests that while the inhibition of ice recrystallization is beneficial for a cryoprotectant, specific compounds are better suited as cryoprotectants for certain cell types. Overall, the results from the cryopreservation studies established that not only can small molecules be potent inhibitors of ice recrystallization, but these novel IRI active derivatives have tremendous potential for improving upon current cryopreservation protocols that are limited in terms of the commonly used cytotoxic cryoprotectants, DMSO and glycerol.

Contributions to Original Research

1. Analysis of the ice recrystallization inhibition (IRI) activity and thermal hysteresis (TH) activity of homogenous synthetic AFGPs, and hydroxyproline and *C*-linked AFGP analogues to elucidate key structural motifs important for potent IRI activity.
2. Investigating the relationship between IRI, TH and cryopreservation ability of natural biological antifreezes, including AFGPs, AFPs and recombinant WT and mutant AFPs.
3. Synthesis of C6 and C1 modified carbohydrate derivatives and disaccharides, and analysis of the IRI activity of derivatives **1-12**, **29-33**, and **35**-**56** as described in chapter 5.
4. Synthesis and analysis of IRI and TH activity of carbohydrate-based surfactants and hydrogelators and their derivatives.
5. Synthesis and analysis of IRI and TH activity of phenolic-glycosides, including mono-, di- and trisaccharide phenolic glycoside derivatives.
6. Analysis of cytotoxicity and cryopreservation potential of small molecule ice recrystallization inhibitors with a human liver cell line (HepG2 cells), HSCs obtained from UCB, and RBCs obtained from peripheral blood. Assessment of osmotic tolerance of RBCs treated with small molecule IRIs. Assessment of deglycerolization protocols post-freezing and thawing of RBCs with small molecule IRIs.

Publications and Patents Resulting from this Thesis

Publications:

1. **Capicciotti, C.J.**, Poisson, J, Boddy, C.N. and Ben, R.N. "Modulating Antifreeze Activity and the Effect Upon Post-Thaw Cell Viability." *Cryobiology*. Submitted/under review, December 2013.

2. **Capicciotti, C.J.**, Kurach, J.D.R., Turner, T.R., Acker, J.P. and Ben, R.N. "Small molecule inhibitors of ice recrystallization enable freezing of human red blood cells with greatly reduced quantities of glycerol." *Organic and Biomolecular Chemistry*. Submitted/under review, November 2013.

3. van der Wal, S., **Capicciotti, C.J.**, Rontogianni, S., Ben, R.N. and Liskamp, R.M. "Synthesis and evaluation of linear CuAAC-oligomerized antifreeze neo-glycopeptides." *ChemBioChem*. Submitted/under review, November 2013.

4. Trant, J.F., Biggs, R.A., **Capicciotti, C.J.** and Ben, R.N. "Developing highly active small molecule ice recrystallization inhibitors based upon *C*-linked antifreeze glycoprotein analogues." *RSC Advances*. **2013,** *3*, 26005-26009.

5. Corcilius, L., Santhakumar, G., Stone, R.S., **Capicciotti, C.J**., Joseph, S., Matthews, J.M., Ben, R.N. and Payne, R.J. "Synthesis of peptides and glycopeptides with polyproline II helical topology as potential antifreeze molecules." *Bioorganic and Medicinal Chemistry*. **2013**, 12, 3569-3581.

6. **Capicciotti, C.J.**, Doshi, M. and Ben, R.N. "Ice recrystallization inhibitors: from biological antifreezes to small molecules." Chapter in: Recent developments in the study of recrystallization. Ed. Wilson, P. **2013**, InTech, New York: 177-224.

7. **Capicciotti, C.J.**, Leclère, M., Perras, F.A., Bryce, D.L., Paulin, H., Harden, J., Liu, Y. and Ben, R.N. "Potent inhibition of ice recrystallization by low molecular weight carbohydrate-based surfactants and hydrogelators." *Chemical Science*. **2012**, *3*: 1408-1416. Article selected for the inside front cover art in the May 2012 issue of Chemical Science.

8. Wilkinson, B.L., Stone, R.S., **Capicciotti, C.J.**, Thaysen-Andersen, M., Matthews, J.M., Packer, N.H., Ben, R.N. and Payne, R.J. "Total synthesis of homogeneous antifreeze glycopeptides and glycoproteins." *Angewandte Chemie International Edition*. **2012**, *51*, 3606-3610.

9. Chaytor, J.L., Tokarew, J.M., Wu, L.K., Leclère, M., Tam, R.Y., **Capicciotti, C.J.**, Guolla, L., von Moos, E., Findlay, C.S., Allan, D.S. and Ben, R.N. "Inhibiting ice recrystallization and optimization of cell viability after cryopreservation." *Glycobiology*. **2012**, *22*, 123-133.

10. **Capicciotti, C.J.**, Trant, J.F., Leclère, M. and Ben, R.N. "Synthesis of *C*-linked triazole-containing AFGP analogues and their ability to inhibit ice recrystallization." *Bioconjugate Chemistry*. **2011**, *22*, 605-616.

Patents:

1. Ben, R.N and **Capicciotti, C.J.** "Small molecule ice recrystallization inhibitors and methods of use thereof." Patent publication Number: WO 2013/175299 A1. May 2013.